Midwest Geological Sequestration Consortium

An Assessment of Geological Carbon Sequestration Options in the Illinois Basin

Final Report

October 1,2003–September 30, 2005

Principal Investigator: Robert Finley
Illinois State Geological Survey
(217) 244-8389
finley@isgs.uiuc.edu

Report Issued: December 31, 2005

U.S. DOE Contract: DE-FC26-03NT41994

The Board of Trustees of the University of Illinois
K.L. Williams, Associate Director
c/o Grants & Contracts Office
1901 S. Research Park, Suite A
Champaign, IL 61820

Illinois State Geological Survey
with Team Members:
Kentucky Geological Survey
Indiana Geological Survey
Southern Illinois University
Brigham Young University
D.J. Nyman & Associates

Disclaimer

This report was prepared as an account of work sponsored by an agency of the United States Government. Neither the United States Government nor any agency thereof, nor any of their employees, makes any warranty, express or implied, or assumes any legal liability or responsibility for the accuracy, completeness, or usefulness of any information, apparatus, product, or process disclosed, or represents that its use would not infringe privately owned rights. Reference herein to any specific commercial product, process, or service by trade name, trademark, or manufacturer, or otherwise does not necessarily constitute or imply its endorsement, recommendation, or favoring by the United States Government or any agency thereof. The views and opinions of authors expressed herein do not necessarily state or reflect those of the United States Government or any agency thereof.

Contributors

Project director, Robert J. Finley of the Illinois State Geological Survey (ISGS), prepared the Executive Summary for An Assessment of Geological Carbon Sequestration Options in the Illinois Basin. Robert Finley and Scott Frailey, ISGS, conducted the technical review of this document.

Task coordinators (ISGS) for the Compilation of Available Base Data and Assessment of Data Needs chapter were Christopher Korose, Geographic Information Systems (GIS) data, and Damon Garner, database information.

The information for the Assessment of Coalbed Sinks and Methane Production Options chapter is a product of the work of many individuals. Task coordinators were John Rupp, Indiana Geological Survey (IGS), David Morse (ISGS), and Tom Moore (ISGS). ISGS contributors were Andrew Anderson, COMET modeling; Scott Frailey, COMET modeling and volumetrics; Keith Hackley (ISGS), isotopic characterization; Christopher Korose, GIS and volumetrics; and Dee Lund, GIS studies. IGS contributors were Maria Mastalerz, coal geology and laboratory experiments, and Agnieszka Drobniak, mapping. Laboratory experiments were conducted by Satya Harpalani, Southern Illinois University at Carbondale.

Task coordinator for the chapter titled CO_2 Sequestration and Enhanced Oil Recovery Potential in Illinois Basin Oil Reservoirs was Beverly Seyler (ISGS), petroleum geology and original-oil-in-place (OOIP) study. Other ISGS contributors were Scott Frailey, VIP compositional reservoir modeling and OOIP study; Damon Garner, OOIP study; Steve Gustison, John Grube, and Bryan Huff, petroleum geology and OOIP study; Rex Knepp, petroleum geology and geological modeling; Christopher Korose, GIS and mapping; and Donald Keefer and Sarah Rittenhouse, geostatistics. Additional contributors to the petroleum geology and OOIP study were John Rupp (IGS) and Brandon Nutall of the Kentucky Geological Survey (KGS).

Hannes Leetaru (ISGS) served as task coordinator for the chapter Saline Reservoirs as a Sequestration Target. ISGS contributors to the work described in the chapter were Robert Bauer, micro-seismicity, fractures, and structural mechanics; Scott Frailey, VIP compositional reservoir modeling; Donald Keefer, geostatistics; Dennis Kolata, geologic interpretation; Chris Korose, GIS and mapping; Hannes Leetaru, geologic interpretation and geophysics; David Morse, geologic interpretation; Edward Mehnert, groundwater hydrology; and Sarah Rittenhouse, geostatistics. From the KGS, contributions were made by James Drahovzal, geologic interpretation and deep structures; and Steve Fisher, geochemistry. John McBride, Brigham Young University (BYU), contributed geophysics information.

Hannes Leetaru (ISGS) and John McBride (BYU) provided geophysics information and prepared the Deep Faulting and Structural Reactivation beneath the Southern Illinois Basin chapter.

Geochemistry of the Mt. Simon Sandstone with Carbon Dioxide Sequestration was prepared by Steve Fisher (KGS), geochemistry.

Structure and Isopach Maps in the Kentucky Portion of the MGSC Study Area chapter was prepared by James Drahovzal (KGS).

Robert Finley (ISGS), project director, prepared the chapter Regulatory Framework for Geological Carbon Sequestration.

Damon Garner (ISGS), database, and Christopher Korose (ISGS), GIS, prepared Compilation of Results in Print and Digital Media.

The Teacher/Student Training Material section was prepared by Sallie Greenberg (ISGS).

Hannes Leetaru (ISGS) prepared the Education/Outreach Activities chapter.

Action Plan for Implementation of Technology Validation Field Testing was prepared by Robert Finley (ISGS), project director.

James Cokinos (ISGS) made the unit conversions for this report.

The capture/separation and source-sink optimization was prepared by Massoud Rostam-Abadi, Shiaoguo Chen, and Yongqi Lu (ISGS).

The unit and specific pipeline studies were done by Doug Nyman (Nyman and Associates) and Steve Dracos (Universal Ensco, Inc.).

Contents

Abstract

The Midwest Geological Sequestration Consortium (MGSC) has investigated the options for geological carbon dioxide (CO_2) sequestration in the 155,400-km^2 (60,000-mi^2) Illinois Basin. Within the Basin, underlying most of Illinois, western Indiana, and western Kentucky, are relatively deeper and/or thinner coal resources, numerous mature oil fields, and deep salt-water-bearing reservoirs that are potentially capable of storing CO_2. The objective of this Assessment was to determine the technical and economic feasibility of using these geological sinks for long-term storage to avoid atmospheric release of CO_2 from fossil fuel combustion and thereby avoid the potential for adverse climate change.

The MGSC is a consortium of the geological surveys of Illinois, Indiana, and Kentucky joined by six private corporations, five professional business associations, one interstate compact, two university researchers, two Illinois state agencies, and two consultants. The purpose of the Consortium is to assess carbon capture, transportation, and storage processes and their costs and viability in the three-state Illinois Basin region. The Illinois State Geological Survey serves as Lead Technical Contractor for the Consortium. The Illinois Basin region has annual emissions from stationary anthropogenic sources exceeding 276 million metric tonnes (304 million tons) of CO_2 (>70 million tonnes (77 million tons) carbon equivalent), primarily from coal-fired electric generation facilities, some of which burn almost 4.5 million tonnes (5 million tons) of coal per year. Assessing the options for capture, transportation, and storage of the CO_2 emissions within the region has been a 12-task, 2-year process that has assessed 3,600 million tonnes (3,968 million tons) of storage capacity in coal seams, 140 to 440 million tonnes (154 to 485 million tons) of capacity in mature oil reservoirs, 7,800 million tonnes (8,598 million tons) of capacity in saline reservoirs deep beneath geological structures, and 30,000 to 35,000 million tonnes (33,069 to 38,580 million tons) of capacity in saline reservoirs on a regional dip >1,219 m (4,000 ft) deep.

The major part of this effort assessed each of the three geological sinks: coals, oil reservoirs, and saline reservoirs. We linked and integrated options for capture, transportation, and geological storage with the environmental and regulatory framework to define sequestration scenarios and potential outcomes for the region. Extensive use of Geographic Information Systems (GIS) and visualization technology was made to convey results to project sponsors, other researchers, the business community, and the general public. An action plan for possible technology validation field tests involving CO_2 injection was included in a Phase II proposal (successfully funded) to the U.S. Department of Energy with cost sharing from Illinois Clean Coal Institute.

Executive Summary

The Midwest Geological Sequestration Consortium (MGSC) has investigated the options for geological carbon dioxide (CO_2) sequestration in the 155,400-km^2 (60,000-mi^2) Illinois Basin. Within the Basin, underlying most of Illinois, western Indiana, and western Kentucky, are relatively deeper and/or thinner coal resources, numerous mature oil fields, and deep saline reservoirs that are potentially capable of storing CO_2. Assessing the options for capture, transportation, and storage of the CO_2 emissions within the region has been a 12-task, 2-year process under Phase I of a U.S. Department of Energy (DOE)-funded Regional Carbon Sequestration Partnership with co-funding from the Illinois Office of Coal Development through the Illinois Clean Coal Institute (ICCI).

The Illinois Basin region has annual emissions exceeding 276 million metric tonnes (304 million tons) of CO_2 (>70 million tonnes (77 million tons) carbon equivalent) from fixed sources, primarily from 122 mostly coal-fired, electric generation facilities, some of which burn almost 4.5 million tonnes (5 million tons) of coal per year. The distribution of emissions from these plants is highly skewed. The 4 largest plants emit about 22% of total CO_2 emissions, the 13 largest plants emit >50% of total CO_2 emissions, and the 30 largest plants emit >80% of total CO_2 emissions. Carbon dioxide separation and capture from flue gases of various stationary sources can be described by either post-combustion or precombustion configurations. For pulverized coal (PC) plants, the post-combustion monoethanolamine (MEA) process is the most technically and economically viable process for CO_2 capture; however, this process carries substantial costs due to the parasitic load imposed on the plant. A techno-economic study conducted for a 533-MW (gross) Illinois-coal fired plant indicates an electricity cost of 52 mills/kWh without capture and 91 mills/kWh with MEA absorption. The cost of CO_2 avoidance was $54/tonne ($49/ton) for the PC+MEA plant and $36/tonne ($33/ton) for the oxygen-enriched coal combustion plant, both 533-MW (gross). The cost of electricity for a 533-MW Illinois-coal fired integrated gasification combined cycle (IGCC)+physical absorption (Selexol) plant is lower than for a PC+MEA plant at 64 mills/kWh. The cost of CO_2 avoidance is $17/tonne ($15/ton).

Transportation of CO_2 from capture sites to storage locations for other than limited duration pilot-scale and feasibility testing will be by pipeline. To assess the approximate costs of pipeline transportation in the Illinois Basin, a 321.87-km (200-mi) hypothetical pipeline length was selected from near Pekin, Illinois, to Edwards County, southeastern Illinois, in the geographical center of the Basin's projected CO_2 storage. For reference, the flow capacity of a 45.72-cm (18-inch)-diameter pipeline would be about 9.63 million m^3 (340 million standard cubic feet) per day (scf/day).

The opportunity to sequester CO_2 in coals that are currently considered unminable for the forseeable future was included in the assessment of these coals. With respect to defining unminable coal, no consideration is given to coals shallower than 152 m (500 ft) in depth. From 152 to 305 m (500 to 1,000 ft) in depth, coals from 0.46 to 1.1 m (1.5 to 3.5 ft) are considered sequestration targets. Highest values

exceed 1,000 tonnes of CO_2 per acre. Highest methane production potential exceeds 139,944 m^3 per hectare (2 million scf per acre) in the same area.

Enhanced oil recovery (EOR) offers the most important economic offset to the costs associated with carbon sequestration in the Illinois Basin. To assess this potential, a Basin-wide EOR estimate was made based on a new understanding of the original oil in place (OOIP) in the Basin, the CO_2 stored volume, the assessed EOR resource, the geographical distribution of EOR potential, the type of recovery mechanism (miscible vs. immiscible), and the daily EOR injection rate as a measure of CO_2 demand. The resource target for EOR is 137 to 207 million m^3 (860 to 1,300 million barrels (bbl)) recoverable with consequent sequestered volume of 140 to 440 million tonnes (154 to 485 million tons) of CO_2. The distribution of the unrecovered EOR resource has also been mapped by field. Larger fields holding multiple reservoirs constitute a larger target. With CO_2 EOR projects linked to sequestration, an understanding of CO_2 demand has also been modeled. Modeling of demand for "new" CO_2 for five of the Illinois Basin oil reservoir studies shows that demand falls off rapidly after 2 to 5 years for individual fields, assuming that CO_2 is recycled. Initial injection rate for immiscible floods may require 17.8 to 35.6 million m^3/day/m^3 (100 to 200 million scf/day/standard barrel (stb)) of OOIP and miscible floods may require 44.5 to 89.0 million m^3/day/m^3 (250 to 500 million scf/day/stb) of OOIP.

Three major salt water-filled, or saline, reservoirs in the Illinois Basin were reviewed as potential CO_2 storage reservoirs: the Ordovician St. Peter Sandstone and the Cambrian Ironton-Galesville and Mt. Simon Sandstones. The St. Peter Sandstone is widespread, porous, and permeable with good lateral continuity. Seals above the St. Peter include several hundred feet of dense limestone and dolostone overlain by 45.7 to 76.2 m (150 to 250 ft) of Maquoketa Shale. The Ironton and Galesville Sandstones are thin and are not present in the central and southern parts of the Basin, so further consideration of them in the context of Basin-wide sequestration potential is not appropriate. There are perhaps no more than 20 penetrations of the Mt. Simon in the southern part of the Illinois Basin; thus, reservoir quality data are limited. Extrapolating studies of natural gas storage reservoirs in the Mt. Simon over the Illinois Basin suggest a capacity of 5.9 billion tonnes (6.5 billion tons) in the Mt. Simon and 1.9 billion tonnes (2.1 billion tons) in the St. Peter in structural traps. An additional 28 to 33 billion tonnes (31 to 36 billion tons) may be trapped by dissolution below 1,219 m (4,000 ft) outside of structural traps and below deep natural gas storage, even in areas where no such geological structure is present.

An integrated study of capture and transportation costs was also carried out. The average cost of the sequestration process without by-product recovery is about $53/tonne ($48/ton) of CO_2 sequestered. The cost of capturing CO_2 from power plants contributes to about 90% of the total sequestration costs. The average transportation and injection costs are <2% and <8%, respectively, of the total sequestration cost. For example, when no by-product benefit is considered, the average transportation distance is only 21.9 km (13.6 mi) for a 10% of total Basin emission control level.

Finally, a module of six activities was developed for education and outreach on the topic of CO_2 sequestration. These activities will be piloted in a series of educator workshops to be held during Phase II. In collaboration with educators and Consortium members, the module will be refined and vetted for final publication and widespread use.

Experimental Methods

Experimental work was conducted by ISGS and subcontractors. Standard laboratory analyses were completed and are described in the coal section of this report. Methods and results can be reviewed in the expanded technical summaries. The list below summarizes the experiments and the organizations performing the work:

- isotopes, Keith Hackley, ISGS
- chromatographic, Gary Salmon, ISGS
- Langmuir isotherms, CO_2 flooding, and compressibility, Satya Harpalani, Southern Illinois University at Carbondale
- Langmuir isotherms, isotopes, John Rupp, Indiana Geological Survey

Project Summary

Objectives

The objectives of Phase I were to assess the technical and economic feasibility of using geological sinks for long-term storage to avoid atmospheric release of carbon dioxide (CO_2) from fossil fuel combustion and thereby avoid the potential for adverse climate change. Assessing the options for capture, transportation, and storage of the CO_2 emissions within the region was a 12-task, 2-year process under Phase I of a U.S. Department of Energy (DOE)-funded Regional Carbon Sequestration Partnership with co-funding from the Illinois Office of Coal Development through the Illinois Clean Coal Institute (ICCI).

Early Phase I work focused on database development and assessment of carbon capture and transportation options in the region. All available work on carbon capture technology and costs was compiled. Transportation focused on both truck and rail options for field tests and pipeline requirements for long-term sequestration. The primary effort under Phase I focused on three geological sinks: coals, oil reservoirs, and saline reservoirs. The enhanced coalbed methane (ECBM) and enhanced oil recovery (EOR) recoverable resources were assessed as were the CO_2 volumes that could be sequestered. Finally, links were created between capture, transportation, and geological storage to define sequestration scenarios and potential outcomes for the region. Extensive use of Geographic Information Systems (GIS) technology was made to develop results for project sponsors, other researchers, the business community, and the general public. Two project-sponsored conferences were held specifically to inform public stakeholders of project results as part of a program of education and outreach carried out by the Midwest Geological Sequestration Consortium (MGSC) members. Phase I results will flow directly into Phase II activities that have been designed to implement small-scale field testing of coal seam injectability, EOR processes, and the ability to inject into, and secure, small test volumes of CO_2 delivered to one of several potential saline reservoir targets.

Results and Discussion

The Consortium consists of the geological surveys of Illinois, Indiana, and Kentucky joined by six private corporations, five professional business associations, one interstate compact, two university researchers, two Illinois state agencies, and two consultants to assess carbon capture, transportation, and storage processes and their costs and viability in the three-state Illinois Basin region. The Illinois State Geological Survey served as Lead Technical Contractor for the Consortium.

The MGSC has investigated the options for geological CO_2 sequestration in the 155,400-km^2 (60,000-mi^2) Illinois Basin. Within the Basin, underlying most of Illinois, southwestern Indiana, and western

Kentucky, are relatively deeper and/or thinner coal resources, numerous mature oil fields, and deep saline reservoirs that are potentially capable of storing CO_2. The Illinois Basin region has annual emissions exceeding 276 million metric tonnes (304 million tons) of CO_2 (>70 million tonnes (77 million tons) carbon equivalent) from fixed sources, primarily from 122 mostly coal-fired, electric generation facilities, some of which burn almost 4.5 million tonnes (5 million tons) of coal per year. The MGSC has focused on the potential of deep coal seams that are currently judged unminable to adsorb gaseous CO_2, the ability to coax more oil from old fields by CO_2 flooding, and the injection of CO_2 into saline reservoirs some 2,134 to 2,743 m (7,000 to 9,000 ft) below the surface. Injection into deep coals may enhance methane (CH_4) production, thereby augmenting natural gas supplies. Injection into old oil fields will recover some of the approximately 10 billion barrels of oil remaining in Illinois Basin reservoirs. These activities will accomplish sequestration while also helping to meet the nation's need for fossil fuels. The integrity of the entire process of CO_2 injection will be scrutinized in detail to understand what contribution Illinois Basin geological sinks can make to national and international goals in accomplishing carbon sequestration and what technology developed here can be extrapolated to other regions.

Carbon Capture

About 90% of the CO_2 emissions from fixed sources in the Illinois Basin are derived from coal-fired power plants (Table S-1). Most of these plants are equipped with pulverized coal boilers and use a simple steam cycle. The flue gas from these plants contains about 14% CO_2. The distribution of emissions from these plants is highly skewed: the 4 largest plants emit about 22% of total CO_2 emissions, the 13 largest plants emit >50% of total CO_2 emissions, and the 30 largest plants emit >80% of total CO_2 emissions. The largest coal-fired power plant in the Illinois Basin is the Rockport plant in Spencer County, Indiana, which emits about 16 million tonnes (18 million tons) annually. The 10% of CO_2 emissions in the Illinois Basin from sources other than power generation include 5 refineries, 23 iron and steel plants, 8 cement plants, 1 lime plant, 2 aluminum plants, 1 ammonia plant, and 8 ethanol plants. Much of the ethanol plant production of CO_2 is captured for use in food and beverage products and for dry ice, and ethanol plants are a likely source for CO_2 for Phase II small-scale field demonstration testing. Because the gas stream from an ethanol plant is >90% CO_2, the cost of capture is relatively low and estimated to be about $15.34/tonne ($13.92/ton) for a plant with 379 million L/year (100 million gallons/year) production capacity.

Table S-1. CO_2 emissions in the United States and the Illinois Basin.

Sources	U.S. total (tonnes)	Illinois Basin (tonnes)	Basin to U.S. (%)	Industry (%) of Basin
Power generation	2,239,700,000	254,260,000	11.4	92.1
Coal	1,868,400,000	249,216,000	13.3	90.3
Natural gas	299,100,000	4,996,000	1.7	1.8
Oil	72,200,000	48,000	0.1	0.02
Industries				
Refinery	184,918,000	9,703,000	5.2	3.5
Iron and steel	54,411,000	3,857,000	7.1	1.4
Cement	42,898,000	3,245,000	7.6	1.2
Ammonia	17,652,000	214,000	1.2	0.1
Aluminum	4,223,000	820,000	19.4	0.3
Lime	12,304,000	273,000	2.2	0.1
Ethanol	8,383,000	3,734,000	44.5	1.4
Total	**2,564,489,000**	**276,106,000**		**100**

The separation and capture of CO_2 from flue gases of various stationary sources can be described by either post-combustion or precombustion configurations. Oxygen-enriched coal combustion can also be considered as a special case of the precombustion concept. For the power generation sector, the selection of a capture methodology mainly depends on the power generation process used; for most industrial emission sources, post-combustion capture is potentially the most suitable option. Techno-economic assessments were made for three power generation scenarios: post-combustion capture from a pulverized coal (PC) boiler with a monoethanolamine (MEA) absorption process, precombustion removal from an integrated gasification combined cycle (IGCC) process with a membrane reactor, and an oxygen-rich combustion process.

For PC plants, the post-combustion MEA process is the most technically and economically viable process for CO_2 capture; however, this process carries substantial costs due to the parasitic load imposed on the plant. A techno-economic study conducted for a 533-MW (gross) Illinois-coal fired plant indicates a cost of electricity of 52 mills/kWh without capture and 91 mills/kWh with MEA absorption. Burning coal in an oxygen-enriched atmosphere is a potentially attractive technology for producing a CO_2-enriched flue gas for sequestration. The cost of electricity was estimated to be 81 mills/kWh for a similarly sized oxygen-enriched coal combustion (oxy-combustion) power plant. The cost of CO_2 avoidance was $54/tonne ($49/ton) for the PC+MEA plant and $36/tonne ($33/ton) for the oxy-combustion plant, both 533-MW (gross). The cost of electricity for a 533-MW Illinois-coal fired IGCC+physical absorption (Selexol) plant is lower than for a PC+MEA plant at 64 mills/kWh. The cost of CO_2 avoidance is $17/tonne ($15/ton).

The cost of electricity for the PC+MEA plant and the oxy-combustion plant was determined to be independent of the type of coal used, either Illinois Herrin Coal or Powder River Basin (PRB). The CO_2

avoidance cost for the Illinois coal was slightly lower than for the PRB coal. An IGCC plant+Selexol process burning high-sulfur Illinois coal was more attractive than burning PRB coal because the elemental sulfur by-product is considered to be a salable commodity. Finally, the results of a sensitivity analysis demonstrated the impact on CO_2 avoidance cost of the heat of absorption of the MEA solvent and the energy consumption of the air separation unit (ASU) at an oxy-combustion plant. A 50% reduction in heat of adsorption for MEA and 50% lower energy consumption in the ASU of an oxy-combustion plant would result in 27% and 37% reductions, respectively, in CO_2 avoidance cost for these two processes.

Transportation of CO_2

Transportation of CO_2 from capture sites to storage locations will be by pipeline for long-term sequestration to lower long-term expenses. For pilot-scale testing, including field demonstration activities during Phase II, transportation will be by truck in combination with on-site storage in portable tanks in order to meet the injection schedule of the field test. An 18-wheel highway tank truck carries approximately 18 tonnes (20 tons) of liquid CO_2, whereas pipelines can be sized to deliver millions of tons per year of CO_2, as are the pipelines serving EOR projects in the Permian Basin of West Texas. To assess the approximate costs of pipeline transportation in the Illinois Basin, a 322-km (200-mi) hypothetical pipeline length was selected from near Pekin, Illinois, to Edwards County, southeastern Illinois, in the geographical center of the Basin's storage capacity. Considered were details of route selection and design, various capacity options, geohazards such as subsidence from coal mining, pipeline wall thickness requirements in populous areas, and pipeline diameter versus pump station requirements. Permits required, right-of-way type and dimensions, construction practices, land use and compensation requirements (e.g., crops lost during construction), and operating costs were assessed. For reference, the flow capacity of a 45.72-cm (18-inch)-diameter pipeline would be about 9.63 million m^3 per day (340 million standard cubic feet per day (scf/day)) without a pump.

Finally, pipeline operating costs will be nominal compared with installation costs, but it is still important to quantify those operating costs. If the inlet pressure were to be 17,237 kPa (2,500 psig) and the minimum delivery pressure were to be 10,342 kPa (1,500 psig), which would maintain a liquid-like state of CO_2, then intermediate compression would not be required for a 50.8-cm (20-inch) line in the sample case. Based on a recent 225-km (140-mi), 15.24-cm (6-inch) liquefied petroleum gas pipeline, operating costs are estimated to be $163.17/cm of diameter/km/year ($667/inch of diameter/mi/year). The resulting costs for different line capacities are noted in Tables S-2 to S-4.

Table S-2. Summary of costs per mile for an Illinois Basin CO_2 pipeline.

Diameter (inches)	Right-of-way ($)	Materials ($)	Construction ($/mile)	Services ($)	Total cost ($)
4	36,713	24,303	85,071	29,217	175,304
6	36,713	47,630	115,915	38,049	238,307
8	44,500	79,370	141,753	47,812	313,435
10	44,500	115,424	173,476	56,678	390,078
12	51,731	159,084	210,730	67,447	488,992
16	66,750	247,199	275,533	88,422	677,905
18	66,750	310,766	306,206	95,721	779,444
20	66,750	381,893	336,354	102,050	887,047
22	66,750	460,465	365,978	107,183	1,000,375
24	66,750	546,136	395,601	121,018	1,129,505

Table S-3. Cost per inch-diameter mile and total cost for the sample Illinois Basin pipeline.

Diameter (inches)	($/mile)	($/inch-diameter/mile)	($/200 miles)
4	175,304	43,826	35,000,000
6	238,307	39,718	48,000,000
8	313,435	39,179	63,000,000
10	390,078	39,008	78,000,000
12	488,992	40,749	98,000,000
16	677,905	42,369	136,000,000
18	779,444	43,302	156,000,000
20	887,047	44,352	177,000,000
22	1,000,375	45,472	200,000,000
24	1,129,505	47,063	226,000,000

Table S-4. Annual operating costs for the sample Illinois Basin pipeline.

Diameter (inches)	($/mile)	($/200 miles)
4	2,667	533,333
6	4,000	800,000
8	5,333	1,066,667
10	6,667	1,333,333
12	8,000	1,600,000
16	10,667	2,133,333
18	12,000	2,400,000
20	13,333	2,666,667
22	14,667	2,933,333
24	16,000	3,200,000

Costs for CO_2 delivered by truck are approximately $80 to $82/tonne ($72.57 to $74.38/ton) based on the experience at the Frio Brine Pilot, Houston, Texas, and the local market. Lower-cost options may be available in the Illinois Basin based on collaboration with new ethanol plants seeking markets for their CO_2 output, but would be outside of existing transportation arrangements for food-grade CO_2.

Coalbed Sinks and Methane Production Options

The Illinois Basin includes substantial coal resources, with the State of Illinois holding the largest bituminous coal resource of any state, 191 billion tonnes (211 billion tons) (Jacobson and Korose, 2003). Extraction techniques range from surface mines to room-and-pillar and longwall subsurface mining with most mining occurring around the margins of the Basin. Most of the Basin's remaining coal resources are moderate to high in sulfur content; therefore, market share has been lost to low-sulfur, western coal from the PRB, and Illinois coal production has declined by half since 1990. The opportunity to sequester CO_2 in coals currently considered to be unminable is based on both technical and economic considerations and could be supported by production of coalbed CH_4 displaced from these coals. With respect to defining unminable coal, no consideration is given to coals at depths <152 m (<500 ft). From 152 to 305 m (500 to 1,000 ft) in depth, coals from 0.48 to 1.1 m (1.5 to 3.5 ft) are considered sequestration targets. A seam <1.1 m (<3.5 ft) in thickness is currently not minable with existing equipment. It would be costly to develop new equipment relative to mining seams of greater thickness, which remain an abundant part of the resource base. Below 305 m (1,000 ft) in depth, all seams >1.1 m (>1.5 ft) in thickness are a sequestration target, given the abundance of shallower resources that will be cheaper to mine and more easily accessible for future mining.

Key characteristics of seven coals were mapped throughout the Illinois Basin, including thickness, depth, elevation, moisture content, ash content, heating value, temperature, and expected reservoir pressure. Most data were available for the Herrin and Springfield coals, the major coal seams in the Basin. High-volume bituminous coal samples were tested and compiled with existing data. Results suggest that the adsorption isotherms for CO_2 are up to about 4.5 times greater for CO_2 than for methane (CH_4). Gas contents for Illinois Basin coals are in the range of 3.12 to 4.68 m^3/tonne (100 to 150 scf/ton) for the better samples; CO_2 adsorption capacity can range from 14.1 to 21.9 m^3/tonne (450 to 700 scf/ton) at 2,068 kPa (300 psi). Permeability is an issue for Illinois Basin coals, and COMET simulator modeling shows distinctly different breakthrough patterns for CO_2 injection based on permeability alone. Typical initial conditions for simulator modeling were thickness of 1.097 m (3.6 ft), depth of 198.726 m (652 ft), total porosity of 3%, permeability of 0.0029608 μm^2 (3 md), and area of 10,117 m^2 (one-fourth of a 10-acre injection pattern). Output curves illustrated cumulative water production, cumulative CO_2 injection, cumulative CO_2 production after breakthrough, and cumulative CH_4 production for various sets of conditions used to define metric recovery and CO_2 storage factors. Maps and numerical assessments have been prepared of sequestration capacity by seam in tonnes per acre (Table S-5), and these maps generally reflect the configuration of the Basin with the deepest coals in southeastern Illinois in the area along the Indiana border. Highest values for CO_2 storage capacity exceed 1,000 tonnes (1,102 tons) CO_2 per acre. Highest potential for ECBM production exceeds 13.99 m^3/m^2 (2 million scf/acre) in the same area.

Table S-5. Methane recovery and sequestration storage potential for major coal seams in the Illinois Basin.

Illinois Basin seam	ECBM recoverable (billion scf)	CO_2 storage (trillion scf)	CO_2 storage (million tonnes)
Danville/Baker	807	8	440
Hymera/Jamestown/ Paradise	200	2	110
Herrin	902	10	518
Springfield	1,251	13	717
Survant	1,081	11	582
Colchester	1,274	13	667
Seelyville/Davis	1,163	11	602
Illinois Basin totals			
Illinois	6,032	62	3,300
Indiana	361	3	186
Kentucky	286	3	152
Total	**6,680**	**68**	**3,638**

Oil Reservoir Sinks and Oil Recovery Options

Enhanced oil recovery offers the most important economic offset to the costs associated with carbon sequestration in the Illinois Basin. To assess this potential, a Basin-wide EOR assessment was made based on a new understanding of the original oil in place (OOIP) in the Basin, the CO_2 storage capacity, the assessed EOR resource, the geographical distribution of EOR potential, the type of recovery mechanism (miscible vs. immiscible), and the daily EOR injection rate as a measure of CO_2 demand. The oil recovery factor (E_R) and CO_2 storage factor (E_S) can be applied to the OOIP volume to estimate storage potential and oil recovery potential. Important to the estimation of these key factors has been detailed geological and reservoir modeling using reservoir descriptions for three major reservoir types, reservoir pressure and temperature, and fluid properties of a generalized Illinois Basin crude oil. Also, general industry rules-of-thumb based on actual CO_2 injection and production response in West Texas have been applied to check results against field experience in the Permian Basin. A published estimate of 1.9 billion m^3 (12 billion bbls) OOIP has long been held for the Illinois Basin, but reassessment of that volume now suggests that OOIP is closer to 2.24 billion m^3 (14.1 billion bbls) (Table S-6).

Table S-6. Distribution of original oil in place assessed by field OOIP in the Illinois Basin. A total of 81 fields with OOIP of 25 million bbls or more would be major targets for CO_2 EOR.

OOIP million stb	Fields (no.)
>750	4
100–750	15
50–100	24
25–50	38
<25	>1,000
1,410	~1,500

With cumulative production for the Basin of about 0.67 billion m^3 (4.2 billion bbls), a nearly 1.5-billion m^3 (10-billion bbl) resource remains, primarily as unrecovered resources in known fields. To assess the recovery potential of a part of this resource and the concurrent stored CO_2 volumes, reservoir modeling and compositional reservoir simulation were carried out. Parts of nine fields were used to create generic geological models for the most prolific reservoirs in the Basin, the Aux Vases and Cypress Sandstones and the St. Genevieve Limestone. These models incorporated data from >1,000 total wells, 120 wells with core, >2,000 core points, 12,000 field acres, and 20 flow zones. Structure and isopach maps were developed deterministically from well logs, whereas porosity and permeability distributions were developed geostatistically from core analysis data for the reservoir simulator. Processes simulated were miscible and immiscible flooding, based on reservoir pressure and temperature, and both continuous and water-alternating-gas CO_2 injection. The nine study areas were parts of Dale, Griggs, Iola, Johnsonville, Mill Shoals, Olney, Sailor Springs, Wakefield, and Zeigler Fields. Deterministic reservoir description created necessary maps and cross sections, and geostatistical description created the three-dimensional descriptions of porosity and permeability required for geocellular modeling of primary, secondary, and tertiary (CO_2 EOR) recovery. E_R generally fit with the West Texas rules-of-thumb of 10% of OOIP or 25% of primary plus secondary (waterflood) recovery. Separate calculations were made for immiscible and miscible EOR conditions (Table S-7).

Table S-7. Oil recovery and CO_2 storage factors for the Illinois Basin derived from geological and reservoir modeling and compared with West Texas rules-of-thumb.

Oil recovery factors (bbl produced/bbl OOIP)			CO_2 net utilization (million scf stored CO_2/bbl oil produced)		
Zone	**1 mm**	**Miscible**	**Zone**	**1 mm**	**Miscible**
Cypress	4.5–5.9	8.6–11	Cypress	1.7–3.1	4.6–9.0
Aux Vases	5.6–7.1	11–15	Aux Vases	1.5–3.3	4.6–8.8
Ste. Genevieve	5.0–6.5	8.6–16	Ste. Genevieve	1.4–5.4	4.6–9.2
West Texas	4–10	8–16	West Texas	5–10	

Immiscible conditions are thought to prevail at depths <610 m (<2,000 ft), near miscible at 610 to 914 m (2,000 to 3,000 ft) depth, and miscible conditions at depths >914 m (>3,000 ft). Further detailed studies may define the immiscible-miscible boundary more clearly, but for this study the near-miscible category will be used. Pressure and temperature gradients have been found to vary sufficiently within the Basin such that general rules cannot always be applied. The distribution of OOIP by miscibility suggests 1.0 to 1.2 billion m^3 (6.4 to 7.5 billion standard barrels (stb)) of immiscible oil, 0.56 to 0.65 billion m^3 (3.5 to 4.1 billion stb) of near-miscible oil, and 0.33 to 0.40 billion m^3 (2.1 to 2.5 billion stb) of miscible oil. The resource target for all three categories of EOR is 137 to 207 million m^3 (860 to 1,300 million stb) recoverable with consequent sequestered volume of 140 to 440 million tonnes (154 to 485 million tons) of CO_2 (Table S-8). The distribution of the unrecovered EOR has also been mapped by field.

Larger fields hold multiple reservoirs and thereby comprise a larger target. Although preliminary, the immiscible models record about one-half the oil but required only one-half the CO_2 volume.

Table S-8. Recoverable oil target and sequestered CO_2 volume based on geological and reservoir modeling, Illinois Basin.

CO_2 EOR and CO_2 SV (Distribution)		
Condition	**CO_2 (million tonnes)**	**EOR (billion stb)**
Miscible	58–180	0.24–0.387
Near	53–153	0.28–0.40
Immiscible	29–110	0.34–0.49
Total	140–440	0.86–1.3

With CO_2 EOR projects linked to sequestration, an understanding of CO_2 demand has also been modeled. During EOR projects, as in West Texas, CO_2 is produced and recycled. If CO_2 is recycled, then the largest demand for CO_2 is early in the project, and reinjection capability will have a significant impact on the project economics and volumes actually sequestered. Modeling of the demand for "new" CO_2 for five of the Basin oil reservoir studies shows that demand falls after 2 to 5 years. Initial injection rate for immiscible floods may require 17.8 to 35.6 million m^3/day/m^3 (100 to 200 million scf/day/stb) of OOIP, and miscible floods may require 44.5 to 89 million m^3/day/m^3 (250 to 500 million scf/day/stb) of OOIP.

Deep Saline Reservoir Sinks

Three major salt water-filled, or saline, reservoirs in the Illinois Basin were reviewed as potential CO_2 storage reservoirs: the Ordovician St. Peter Sandstone and the Cambrian Ironton-Galesville and Mt. Simon Sandstones. In addition, data were collected on the potential seals for these reservoirs. The St. Peter Sandstone is a widespread, porous, and permeable quartz sandstone that is generally fine-grained and has good lateral continuity. It can vary in thickness across the Illinois Basin from 31 m (100 ft) to as much as 121 m (400 ft) in thickness. Seals above the St. Peter include several hundred feet of dense limestone and dolostone overlain by 46 to 76 m (150 to 250 ft) of Maquoketa Shale. The Ironton and Galesville Sandstones form a usable fresh water aquifer in northern Illinois and can have a combined thickness of over 61 m (200 ft). However, it was found that these units are thin or are not present in the central and southern parts of the Basin, so further consideration of them in the context of sequestration is not appropriate.

The Mt. Simon Sandstone is commonly used for natural gas storage in the Illinois Basin. The Mt. Simon has fair to good permeability and porosity, and the overlying strata contain impermeable limestone, dolomite, and shale intervals. The Mt. Simon should be an appropriate reservoir in which to test injection

of CO_2. The depth of the Mt. Simon ranges from <610 to >4,267 m (<2,000 to >14,000 ft) below the surface, and it is a fresh water aquifer in the northern part of the Illinois Basin. Areas of fresh water resource are to be avoided, as are areas where natural gas storage occurs; excluding these parts of the Basin still leaves approximately the southern half of the Basin where the reservoir is brine-filled and no oil or natural gas resources have been discovered in this unit. At its greatest thickness in the Illinois Basin, the Mt. Simon is over 793 m (2,600 ft) thick. The Mt. Simon does not crop out in Illinois, but correlative units are exposed in southern Wisconsin, southeastern Minnesota, and Missouri. The Mt. Simon exists in the subsurface throughout Indiana, Iowa, Michigan, and Ohio. Depending on the locality, the sandstone strata in the Mt. Simon can vary from fine to coarse grained. There also appear to be zones of predominantly finer-grained sandstone and coarser sandstone. Between some sandstone strata are thin beds of dark gray shale laminae and other lower reservoir quality deposits that would act as baffles to buoyant CO_2 and might disperse CO_2 injected relatively low in the reservoir. The Mt. Simon Sandstone was deposited on an unconformity, an irregular erosional surface on the Precambrian basement, that was filled in as Mt. Simon deposition proceeded, creating some risk that the Mt. Simon is thin or absent in otherwise structurally favorable CO_2 storage sites. Seismic data will be essential to evaluate Mt. Simon storage sites including Phase II assessments.

Mt. Simon reservoir quality is expected to decline with depth based on plots of porosity versus depth; although data are limited below 1,829 m (6,000 ft), Mt. Simon at the Manlove Gas Storage Field does show porosity of about 9% in the 1,829 to 1,981-m (6,000 to 6,500-ft) depth range. There are perhaps no more than 20 penetrations of the Mt. Simon in the southern part of the Illinois Basin; thus, reservoir quality data are limited. One well, the Texaco Johnson No. 1 well at Salem Field, has been studied. The top of the Mt. Simon in this well is at 2,560 m (8,400 ft), and the well penetrates about 259 m (850 ft) of Mt. Simon. Although the upper part of the sandstone shows negligible porosity, a lower 46-m (150-ft) interval has log porosities up to 14% and averages around 10%. Location of test sites and long-term sequestration sites must take into account both thickness variation and reservoir quality variation within the Mt. Simon Sandstone. Importantly, internal heterogeneity in this unit may help in the retention and dispersal of injected CO_2, which will be taken into account during further reservoir modeling as part of Phase II.

The approximately 52-km^2 (20-mi^2) Manlove Gas Storage Field is an excellent analog for structural trapping of CO_2 that may occur during the sequestration process and has been studied extensively to take advantage of the well logs, core, reservoir mineralogy, water chemistry, and other data available from the field operator. The Manlove data were used to develop estimates of CO_2 trapping capability assuming an analogous structure such as might be found below many of the major oil field structures in the Basin where EOR may take place. Stacking of these sinks is important with respect to cost offsets for pipeline delivery infrastructure and the possibility that stored CO_2 may be available for EOR as a commodity

as the EOR process is demonstrated and implemented. A Mt. Simon structure like Manlove would trap about 15 million tonnes (16.5 million tons) of CO_2 as free phase until water was displaced to spill point, leaving irreducible water saturation in the pore space. Potential capillary trapping of CO_2 in the transition zone below the free-phase contact is assessed at 7 million tonnes (7.7 million tons). Below the transition zone, CO_2 is projected to dissolve in the formation water trapping another 12 million tonnes (13.2 million tons) for a total of about 34 million tonnes (37.5 million tons) CO_2 trapping potential in an analogous structure. Extrapolating these mechanisms over the Illinois Basin suggest a capacity of 5.9 billion tonnes (6.5 billion tons) in the Mt. Simon and 1.9 billion tonnes (2.1 billion tons) in the St. Peter in structural traps. The capacity estimate for the St. Peter was based on the Hillsboro Gas Storage Field assuming structurally based CO_2 only. An additional 28 to 33 billion tonnes (31 to 36 billion tons) may be trapped by dissolution below 1,219 m (4,000 ft) outside of structural traps and below deep natural gas storage, even in areas where no such storage is present.

The abundant information from Manlove has allowed detailed compositional simulation (using Landmark Graphics VIP software) to assess disposition of CO_2 within the Mt. Simon. The Mt. Simon has often been described in terms of reservoir and seal, the latter represented by the overlying Eau Claire Shale, which is a correct concept only at a large scale of description. Detailed, two-dimensional modeling of a 68.58-m (225-ft)-thick Mt. Simon interval using 0.9144 m × 182.88 m (3 ft × 600 ft) cells shows that CO_2 disperses laterally based on internal heterogeneities that represent impediments to vertical flow. The Mt. Simon is not uniform internally and has a distinct zonation of reservoir quality that needs to be better understood. Clearly, this finding will have great importance during Phase II field testing and subsequent planning for any large-scale sequestration activities.

Finally, an assessment of deep fault structure and seismicity in the Illinois Basin was conducted to help evaluate the integrity of deep saline reservoirs like the Mt. Simon that may be underlain by a basement fault. An assessment was made of observable spatial associations between earthquake parameters and subsurface structure as deduced from geological and geophysical databases. Risks to sequestration storage sites would correlate to the degree to which faults with observable displacement propagate from the Precambrian basement up into Paleozoic strata and the proximity of the faults to known areas of seismicity. Based on Phase I work, the fold structures along the La Salle anticlinal trend may present some risk for release of CO_2 stored in the deep Mt. Simon Sandstone, which rests just above the basement-sedimentary cover contact, and this determination will need to be factored into storage site selection decisions.

Linked Capture, Transportation, and Storage Options

An integrated sequestration process includes capture, transportation, and CO_2 volume injection into geological reservoirs. The links between different emission sources and sinks, as well as different

transportation routes, impact the economic performance of the sequestration process. Assessment of such links was designed to optimize the integrated CO_2 sequestration process in the Illinois Basin by determining the most economical distribution of captured CO_2, at capture levels ranging from 10 to 50% of total stationary Basin emissions, among representative identified storage fields.

A commercial software package, LINGO, was used to optimize the integrated CO_2 sequestration system. All of the power plants and the 24 largest storage fields in the Basin were considered. The costs of CO_2 capture (90% reduction) from coal-fired power plants and pipeline transportation were obtained from a techno-economic study completed by the MGSC in October 2004. The CO_2 capture costs ($40 to $60/tonne ($36 to $54/ton)) were based on the MEA process. The loss of electricity capacity in the Basin due to the installation of MEA plants was not included in the optimization study. Sequestration costs were evaluated with and without by-product credits from EOR and ECBM. A 30-year life span was considered for pipelines and the MEA process.

Results from the optimization study are summarized in Tables S-9 and S-10. The average cost of the sequestration process without by-product recovery is about $53/tonne ($48/ton) of CO_2 sequestered. The cost of capturing CO_2 from power plants contributes to about 90% of the total sequestration costs. The average transportation and injection costs are <2% and <8%, respectively, of the total sequestration cost, depending on level of control. One of the reasons for the low cost of transportation is the rich geological storage structure in the Illinois Basin. The scattered geological fields in the Basin make the average transportation distance relatively short. For example, when no by-product benefit is considered, the average transportation distance is only 21.9 km (13.6 mi) for a 10% emission control level.

Table S-9. Summary of CO_2 sequestration cost without by-product credits.

Emission control level	50% (128.44 million tonnes/year)	25% (64.02 million tonnes/year)	10% (28.75 million tonnes/year)
Capture cost (million $/year)	6,055.8	3,018.4	1,506.6
Transportation cost (million $/year)	137.81	33.06	7.3
Injection cost (million $/year)	642.1	320.1	143.7
Total cost (million $/year)	6,835.8	3,371.5	1,426.3
Average cost CO_2 sequestered ($/tonne)	53.2	52.7	52.4

Table S-10. Summary of CO_2 sequestration cost with by-product credits.

Emission control level	50% (128.4 million tonnes/year)	25% (64.0 million tonnes/year)	10% (27.0 million tonnes/year)
Capture cost (million $/year)	6,055.8	3,018.4	1,275.2
Transportation cost (million $/year)	138.7	47.3	26.6
Injection cost (million $/year)	230.7	-91.3	-276.20
Total cost (million $/year)	6,425.3	2,974.3	1,025.7
Average cost CO_2 sequestered ($/tonne)	50.0	46.5	37.9

Due to the low cost of the pipeline transportation, the locations of power plants became less important than the scale of the plants. The storage of CO_2 emissions from the 20 largest power plants in the Basin provided the optimum sequestration cost. The economics of the sequestration process significantly improved ($38 to $50/tonne ($34 to $45/ton) of CO_2 sequestered) when the by-product credits from the EOR ($20/tonne ($18/ton) CO_2) and CBMR ($15/tonne ($14/ton) CO_2) were included, especially at a 10% emission control level (Table S-10).

Results from a sensitivity analysis revealed that the CO_2 capture cost had the most impact on the overall cost of the sequestration process. The impact of the CO_2 capture cost was more pronounced with increasing levels of CO_2 emissions control. At the 50% control level, there was a direct relationship between projected sequestration cost and percent reduction in capture cost, which indicated that future efforts to reduce the sequestration cost should be focused on developing more cost-effective capture technologies.

Education and Outreach

Consortium educational materials are focused on teaching the sequestration process. The materials developed reflect the specifics of the Illinois Basin region and are designed to mirror the research conducted in Phase I. The materials are designed to be used by all three states participating in the MGSC: Illinois, Indiana, and Kentucky. The MGSC materials illustrate connections between the concepts of climate change, physical geology, and sequestration. Middle school and high school students will learn and understand concepts such as greenhouse gases, climate change, geological structures, water quality, permeability, porosity, and the geology of the Illinois Basin and how to relate them to test geological sequestration in the MGSC region. The educator workshops conducted in Phase II will utilize the materials produced in Phase I and will also incorporate sequestration education materials from other partners in the MGSC, Keystone, and additional outside sources.

A module of six activities was developed and will be piloted in a series of educator workshops to be held during Phase II. In collaboration with educators and Consortium members, the module will be refined and vetted for final publication and widespread use. The Phase II workshop plan is a comprehensive effort to educate teachers throughout the Illinois Basin area. The materials are designed for use in any of the three states and are tied to specific state learning standards and to national learning standards in an easy-to-read matrix. The materials will be posted on the MGSC Web site and will be updated and refined as new information becomes available and feedback from workshop participants is incorporated. The major Phase I educational outreach goals of being ready to plan and conduct workshops and carry out educational information delivery at the beginning of Phase II have been met. In addition, demonstrations of EOR, the nature of CO_2, and other demonstrations modified from other

DOE-supported work were presented at a Project Advisory Group and two public meetings. These demonstrations were well received and served as an ice-breaker for the meetings.

Conclusions and Recommendations

Led by the geological surveys of Illinois, Indiana, and Kentucky, the MGSC-Illinois Basin developed a framework within which to assess geological storage of CO_2 in deep coal seams, mature oil fields, deep saline reservoir formations of the Illinois Basin. With major funding from the U.S. DOE and the Illinois Office of Coal Development, ICCI, the MGSC has focused on the potential of these types of reservoirs to serve as sinks for a portion of the 276 million tonnes (304 tons) of annual CO_2 emissions from fixed sources in the Illinois Basin. This assessment includes the potential of deep, unminable coal seams to adsorb gaseous CO_2, the ability to enhance oil recovery from old oil fields by CO_2 flooding, and the injection of CO_2 into saline reservoirs some 1,219 to 3,048 m (4,000 to 10,000 ft) below the surface. Injection into deep coals may help produce CH_4 to augment natural gas supplies. Injection into old oil fields will help recover some of the approximately 10 billion bbls of oil remaining in Illinois Basin reservoirs. These activities will accomplish sequestration as they help to meet the nation's need for fossil fuels.

During Phase I, existing data indicated that the geology of the Basin is favorable for CO_2 storage, or sequestration. In almost all of its oil fields, all three potential CO_2 sinks are vertically stacked. The Consortium has assessed and will continue to investigate the methods and economics of CO_2 capture at facilities such as coal-fired power plants and to examine the costs of transportation of large quantities of CO_2 via pipeline. The MGSC has focused on the properties of the rock units that control injectability of CO_2, the total capacity for storage near major CO_2 sources, and the safety of injection and storage processes. The distribution of the overlying rock units that act as seals for the reservoirs was also assessed. We will address these issues in Phase II in much more detail through a series of six actual field tests. The overall integrity of the storage and sealing rock units is critical for safety and the effectiveness in isolating CO_2 from the atmosphere and, thereby, avoiding the potential for adverse climate change. Each of the Phase II field tests will have an extensive monitoring program for air, shallow groundwater, oil and water produced from oil reservoirs, and salt water produced from deep reservoirs to understand the fate of injected CO_2 at each test site. The integrity of the entire process will be scrutinized to understand what contribution Illinois Basin geological sinks can make to national and international goals in accomplishing carbon sequestration and what technology developed here can be extrapolated to other regions.

Given that the OOIP in the Illinois Basin is now understood to be about 14.1 billion bbls, about 2 billion bbls greater than before Phase I MGSC Partnership studies, CO_2 flooding of mature oil reservoirs will

lead to both CO_2 storage and to incremental oil production. The value of the incremental production will help offset costs associated with the infrastructure development required to collect and deliver CO_2 to oil field operators. For unminable coal beds, the CH_4 produced (as CO_2 replaces the coalbed CH_4) adds to natural gas supplies and offsets costs. Coalbed CH_4 production in the Illinois Basin is in its infancy, however, and the most likely near-term economic benefits will come from EOR. Understanding of EOR processes is much further along than for ECBM production, and extrapolation of EOR performance parameters from West Texas to the Illinois Basin suggests that the Basin's EOR potential is substantial. Saline reservoirs offer the largest volume of storage capacity, and CO_2 verifiably sequestered in such reservoirs may represent tradable carbon credits in the future.

The MGSC Phase II Partnership will carry out extensive public outreach with regard to its activities and to carbon sequestration generally. The MGSC will arrange presentations to industry, government, and the general public to provide information on the progress of MGSC research and the importance of the Phase II field tests. The Consortium has 11 companies that have nominated 34 potential field test sites in the Basin for Phase II and 16 companies, trade associations, and government agencies from Illinois, Indiana, Kentucky, and across the nation that serve on the MGSC's Project Advisory Group. Additional sites have been nominated since the submittal of the Phase II proposal. The MGSC has a growing body of information on its Web site (www.sequestration.org) that will be maintained to keep sponsors, team members, and the general public informed of the progress of our continued studies.

Technical Reports

The following reports are specific to tasks and subtasks and may reference different parts of the Phase I chronology. Therefore, any reference to an inferred or implied date or time is with regards to the 2-year assessment project. Periodically, there are references to tasks and subtasks from the original proposal.

Compilation of Available Base Data and Assessment of Data Needs

The data assessment task and subtasks of this project (Task 1) were initiated simultaneously with subsequent tasks and continued through (1) assessment of carbon capture and transportation options from major point-sources (Tasks 2 and 3), and (2) mapping/assessment of geologic sinks (coal, petroleum, and saline reservoirs) (Tasks 4, 5, and 6). The first major step after project initiation was to conduct a data inventory and assess needs. A questionnaire was sent to all project participants asking for information about their data sets. Questions ranged from the general (e.g., contact information, intended use of data set, relative importance) to the specific (e.g., type, format, spatial extent of data, degree of documentation, proprietary issues). Additionally, questions included requests for new data sets that were desired or deemed critical to the project. Answers to this questionnaire (1) provided the basis for a descriptive summary of data inventory and needs, (2) helped identify key data sets and their inherent limitations, and (3) identified working relationships and/or contacts to be facilitated by project and task managers.

Following the data inventory and needs assessment, standards for transferring spatial data layers and tabular data were developed, and guidelines were developed to help organize and track the flow of data within the project among those who work hands-on with different data sets and share them. Data were transferred between project staff in .ZIP file format and routed through key project database staff so that data control information could be collected and a zipped snapshot of the data could be archived. In addition, basic documentation was included with the data in order to improve data sharing among project participants and to make any compilation or merging of data from different sources less prone to error.

Data Compilation

Most of the data used for this project were compiled from multiple sources spanning multiple states, agencies, and times. Two of the greatest data management challenges of the project were to achieve data consistency and to assess the quality of data from previous geologic interpretations. Data collected by different agencies over time can have consistency issues because of different purposes, instrumentation, methodology, terminology, measurement resolution, or timing. Differences in documentation and how the raw data were compiled and archived are issues also. The raw data from which previous interpretations were made are not always available for quality assessments.

Quality Control

All data sets were examined for consistency, completeness, and accuracy. Data quality was improved if possible. When data consistency issues arose—such as differences in measurement resolution or terminology—strategies were devised to make these data more comparable. Some existing data sets were incomplete and required alternative sources and/or methods for improving or estimating values of the missing data. Often, multiple data sources were used to compile the most accurate data set. Whenever possible, data sets were checked to determine numeric, positional, or temporal accuracy, and new data were collected as necessary for comparison to existing data in order to ensure accuracy.

Most of the quality control procedures were performed on tabular data using a Microsoft Access database to maintain data integrity among relational tables and ensure duplicates and orphan records were removed. Data quality analysis was performed using both Access queries and Microsoft Excel statistical functions. Access dynamic database queries were favored because of their automatic updates when new data are added.

Data Analysis, Archiving, and Dissemination

The geological surveys of Illinois, Indiana, and Kentucky use the same or similar software for Geographic Information Systems (GIS) and tabular data analysis and storage. These include ArcGIS and ArcInfo for GIS data manipulation and analysis; ArcSDE and ArcIMS for GIS data storage, archiving, and dissemination; Excel and Access for datafile transfer and manipulation; and SQL Server or Oracle databases for institutional storage and archiving of tabular data.

Included in the standards for transferring data among project participants were specific protocols for spatial data. Geographic coordinates (longitude and latitude, in decimal degrees; 1983 North American Datum) were preferred for the transfer of GIS spatial data layers or for tabular data containing coordinates. Specific coordinates helped standardize the input of spatial data into ArcGIS and allowed for the most accurate re-projection of data to measurable coordinate space. The standard file types for GIS spatial data layers are zipped shape files or personal geodatabase files. ArcGIS projection information files (*.prj files) were included with shape file data to enable and facilitate the ease of data re-projection. Also, a complete description of the reference coordinate system used (e.g., projection and datum) was included for tabular data not yet incorporated into GIS data layers.

Data were organized into project work areas and regularly backed up. Completed project analysis and data sets were loaded into institutional databases for archiving. Network access to these ArcSDE, Oracle, and SQL Server databases provided a robust connection that enables the simultaneous use of these data by many users. Important data layers for major CO_2 sources and geological reservoirs in the Illinois

Basin were loaded into active Internet map services, using ArcIMS software at the geological surveys of Illinois, Indiana, and Kentucky. These layers are currently being shared through the NATCARB Internet portal.

Working data sets that are evolving as new data or analyses were added for Phase II were stored in either institutional databases or Access. Access offers portability where complex and dynamic query analysis tools are being constructed rapidly for end users. Access is a convenient data “container” for data distribution because many data sets can be generated in many formats from a single file using a user-friendly interface. Access also interfaces well with Excel, which was used by those who were not familiar with database architecture and SQL language.

Assessment of Coalbed Sinks and Methane Production Options

Carbon dioxide (CO_2) emissions from stationary sources such as power plants and refineries in the Illinois Basin alone are estimated at 283,270,000 tonnes (312,248,521 tons) annually. Even larger volumes of this greenhouse gas are expected to be emitted in future years as energy demand increases. The United States aims to reduce greenhouse gas emissions by 18% by 2012. To meet this goal, various organizations are currently developing strategies to safely capture and remove some of these anthropogenic emissions. In order to reduce greenhouse gases, several measures are being implemented. Geological sequestration of CO_2 in coal seams that are currently unminable is one of the most promising options, and Illinois Basin coals could potentially store CO_2. Pennsylvanian-age coals in the Illinois Basin are widespread in southwestern Indiana, Illinois, and western Kentucky; some regions are less attractive to mining because of relative coal depth, greater or lesser thickness, or less desirable quality. These areas, however, could be attractive for CO_2 sequestration and are possible targets for enhanced coalbed methane (ECBM) production.

The objective of coalbed assessment (Task 4) is to evaluate the potential of deep, uneconomic coal seams in the Illinois Basin for both CO_2 sequestration and ECBM production. The latter potential hinges primarily on the suitability of Illinois Basin coals for CO_2 injection and adsorption, which displaces methane (CH_4) from the coals. In this task, existing data were compiled and new data generated that related to CO_2 sequestration and ECBM production.

Compilation of Coal Availability and Coal Quality Data (Subtask 4.1)

Compilation of the existing maps and their update by the addition of new data points was an initial phase of Task 4. The Illinois State Geological Survey and the Indiana and Kentucky Geological Surveys had extensive data and maps generated for previous studies; consequently, the first step was to conduct a data inventory to assess further needs. Gathering and merging existing coal data and generating Geographic Information Systems (GIS) layers for the entire Basin (or for each state) to obtain Basin-wide data sets were key in generating the necessary information to assess coalbed sinks and CH_4 production. All publicly available information was inventoried and compiled; in addition, data from confidential industry files, from completed and current project reports, and from unpublished information from all consortium partners have been added.

Tabular coal resource and quality data were reviewed, compiled, and standardized for Danville/Baker, Hymera/Jamestown/ Paradise, Herrin, Springfield, Survant, Colchester, and Seelyville/Davis/Dekoven, the seven major coalbeds in the Illinois Basin (Figure 1-1). All data sets were examined for consistency, completeness, and accuracy. Data quality was checked. Some existing data sets were incomplete; often,

multiple data sources were used to compile the most accurate data set. Whenever possible, new data were collected during this project in areas where information had been identified previously as being insufficient.

These tabular data were used for map generation and subsequent volumetric calculations in the estimation of potential ECBM production and CO_2 storage. Building on Basin-wide work for three coal

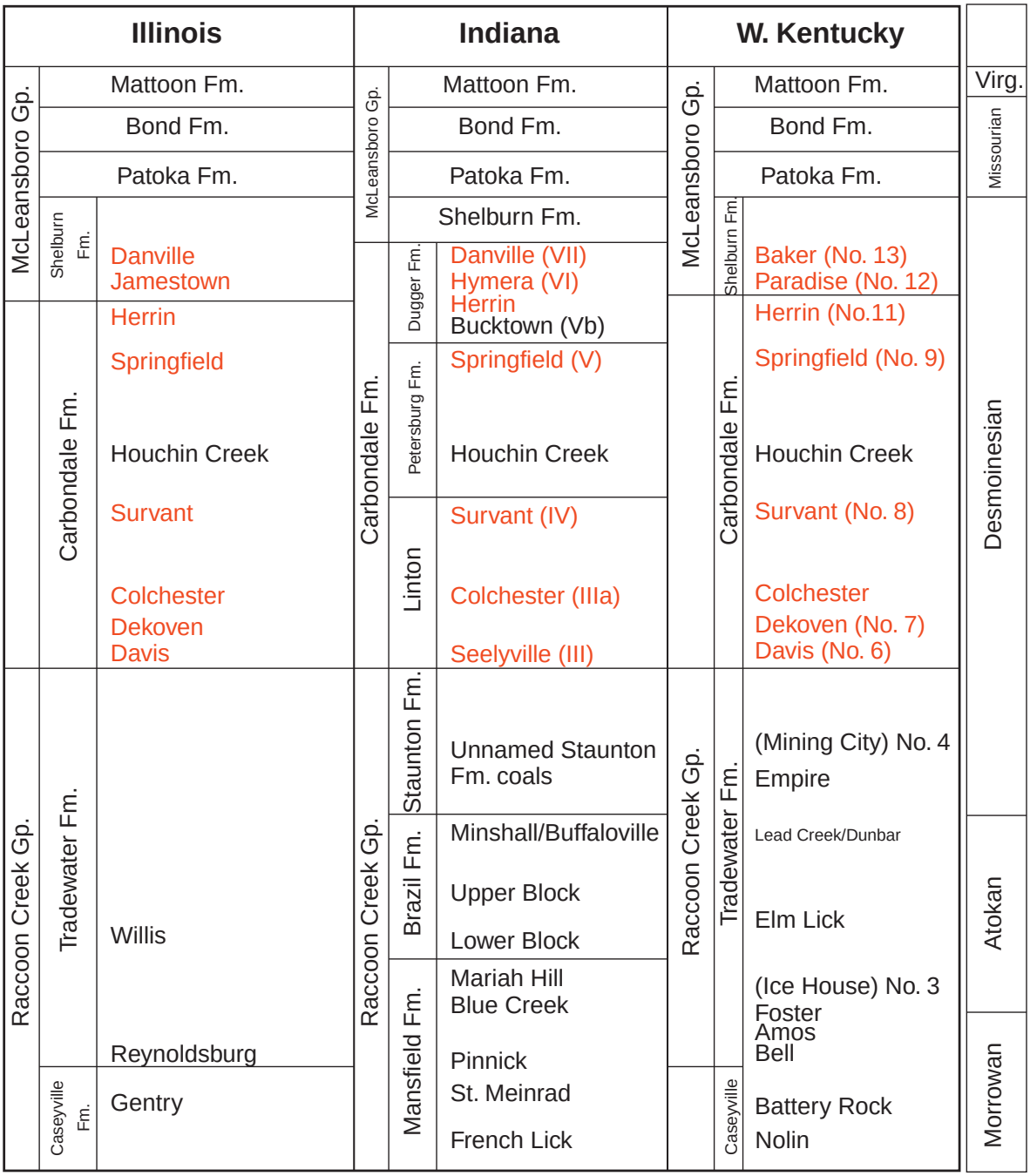

Figure 1-1 *Lithostratigraphy of the Pennsylvanian System in the Illinois Basin (modified from Mastalerz and Harper, 1998; Tri-State Committee on Correlation of the Pennsylvanian System in the Illinois Basin, 2001). The position of major coalbeds is shown. Those in red are considered for CO_2 sequestration in this study.*

seams (Springfield, Herrin, and Danville/Baker Coals) that had been completed as part of previous studies sponsored by the U.S. Geological Survey (USGS), four additional seams (Hymera/Jamestown/Paradise, Survant, Colchester, and Seelyville/Davis/Dekoven) were mapped at the Basin scale during this study. Based on the newly collected information, maps of areal extent, thickness, mined areas, depth, and elevation were generated (Appendix 2). Additional GIS layers of coal-quality parameters such as ash, moisture, sulfur content, heating value, and vitrinite reflectance (R_o), as well as reservoir parameters such as temperature and pressure, were mapped for this study and compiled for selected coalbeds (Appendix 3) for assessment and for potential use in GIS-based volumetric calculations.

The maps related to coal geometry (thickness and depth) are the basis for volumetric calculations of potentially injected CO_2, whereas the maps of coal-quality parameters help to evaluate variability in CO_2 ECBM and storage related to coal properties. Maps of reservoir temperature and pressure are critical to understanding phase properties of potentially stored CO_2.

Table 1-1 shows generated coal resource maps, and Table 1-2 contains information about coal-quality maps created for selected coalbeds. Some maps listed in Table 1-2 do not cover the entire Basin due to limited data availability.

Table 1-1. Coal resource maps compiled or generated for the purpose of the project (in alphabetical order).

Coalbed	Thickness maps	Depth maps	Structure maps
Colchester	x	x	x
Danville/Baker	x	x	x
Herrin	x	x	x
Hymera/ Jamestown/ Paradise	x	x	x
Seelyville/Davis/ Dekoven	x	x	x
Springfield	x	x	x
Survant	x	x	x

Table 1-2. Coal quality, temperature, and pressure maps generated for selected seams during the project.

Seam	Ash (dry)	Sulfur (dry)	Moisture (ar)	BTU (dry)	BTU (mai)	BTU (afmi)	BTU (daf)	R_o	T	P
Colchester	×	×	×							
Danville/ Baker	×	×	×							
Herrin	×	×	×	×	×	×	×	×		
Hymera/ Jamestown/ Paradise	×	×	×							
Seelyville/ Davis/ Dekoven	×	×	×					×		
Springfield	×	×	×	×	×	×	×	×	×	×
Survant	×	×	×							

Note: x, map generated; BTU, British Thermal Unit, a heating value; R_o, vitrinite reflectance; T, temperature (calculated); P, pressure (calculated); ar, as received; dry, dry basis; mai, moisture- and ash-included basis; afmi, ash-free, moisture-included basis; daf, dry, ash-free basis.

Setting of Criteria and Determination of Unminable Coal Seams (Subtask 4.2)

Setting sequestration criteria for coal seams that are less likely to be mined and determining their resources is important in addressing the CO_2 sequestration options. Because CO_2 sequestration is a long-term undertaking, both current and future minability criteria need to be considered. Economic and geological conditions influence coal minability and may be specific to individual coal basins. Changing economic conditions may result in changing thickness and depth criteria for clarifying coals as unminable. Consequently, by infusing coalbeds with CO_2, seams that might otherwise be minable at some future time may be considered unminable.

The criteria to designate areas of coal seams as "unminable" or less likely to be mined, were determined after a lengthy and multi-angle discussion. The Midwest Geological Sequestration Consortium (MGSC) definition of unminable considers current criteria and future mining trends for the Illinois Basin. The depth-based intervals of 152 to 274 m (500 to 900 ft) and >366 m (>1,200 ft) were used for the assessment of the input parameters for the modeling program COMET (Estimate Sink Capacity For Coal Seam Storage section of this report).

For sequestration "fairway" screening in the GIS evaluations, these criteria were slightly modified as follows:

1. 91 to 152 m (300 to 500 ft) deep—no CO_2 sequestration, CBM target only.
2. 152 to 305 m (500 to 1,000 ft) deep—sequestration/ECBM target in coals between 0.46 and 1.1 m (1.5 and 3.5 ft) thick. Coals >1.1 m (>3.5 ft) thick are considered minable.

3. >305 m (>1,000 ft) deep—sequestration target in coals >0.46 m (>1.5 ft) thick (all coals assumed to be unminable at this depth).

While establishing these criteria for CO_2 sequestration and ECBM production potential, these assumptions, among others, were considered:

1. The minimum thickness for identifying, perforating, and producing CH_4 from a coal seam is 0.46 m (1.5 ft), regardless of depth.
2. The current minimum minable thickness by underground coal equipment is 1.1 m (3.5 ft).

In support of the criteria used to define the relative minability of the Basin's coal resources, current coal mining production was compared to the resource that was defined indirectly as minable using the depths and thicknesses in Figure 1-17. The total coal resource identified in this study is 413 billion tonnes (455 billion tons) of which 142 billion tonnes (157 billion tons) (or 34.5%) meets the "minable" criteria of <305 m (<1,000 ft) deep and >1.1 m (>3.5 ft) thick. The 2004 coal production of the Basin was 90.4 million tonnes (99.6 million tons) (Energy Information Administration, 2005). If the coal rate was doubled to 181 million tonnes (200 million tons), it would take nearly 220 years to mine 25% of the coal designated as minable for this study.

Testing CO_2 Adsorption and CH_4 Desorption (Subtask 4.3)

Adsorption and desorption characteristics of selected coals were obtained in two ways at two laboratories:

1. The analysis of high-pressure adsorption isotherms was conducted at Marc Bustin's laboratory in Vancouver, British Columbia, Canada (RBM laboratory) (Table 1-3). At this laboratory, the sample was crushed to –20 mesh and placed in an equilibrium-moisture bath for 20 days. Equilibrium moisture and ash yield were determined on a 2-g split of the samples. The sample was then placed in a high-pressure vessel, and CH_4 and CO_2 adsorption analyses were carried out at 17ºC, which was thought to be the reservoir temperature. The CH_4 isotherms were run up to 11,032 kPa (1,600 pounds per square inch absolute (psia)), and CO_2 was run up to pressures where capillary condensation or the equation of state collapsed (usually above 4,137 kPa (600 psia)).

Table 1-3. Samples from the Indiana portion of the Illinois Basin and analyzed at RMB lab and arranged by increasing depth.

Sample	Coal	Location	County	Depth (ft)	In situ pressure (psi)
Spring WM	Springfield	Wabash m.	Gibson	150	65
MD-G Spr 184	Springfield	MD-G	Gibson	184	80
TH Seel	Seelyville	Dugger	Sullivan	352	152
Spring Sullivan	Springfield	Vic-1	Sullivan	373	162
Seel 33H8 448	Seelyville	33-H8 BB	Sullivan	448	194
Seel 33H 452	Seelyville	33-H8BB	Sullivan	452	196
Seel Sullivan	Seelyville	Vic-1	Sullivan	556	241
Knox Seel	Seelyville	Knox CBM	Sullivan	650	281

2. The sorption and CO_2 flooding studies were conducted at Dr. Harpalani's laboratory at Southern Illinois University (SIU laboratory). The primary objective was to determine the ability of Illinois Basin coals to hold CH_4 and CO_2 and to test the ability of CO_2 flooding to enhance the recovery of CH_4 from coalbed methane (CBM) reservoirs. A secondary objective was to determine the effect of injecting CO_2 on the microstructure of coal (e.g., to obtain estimates of the sorption-induced coal matrix strain).

In order to fulfill the project/task objectives, the work was divided into the following three tasks:

1. Sorption characterization. This task included establishing sorption isotherms for the coal samples to determine the ability of the coals to retain and release CH_4 and to store CO_2.
2. CO_2 flooding. The task involved injecting CO_2 during the desorption part of the CH_4 sorption cycle and measuring the amount of additional CH_4 released.
3. Sorption-induced volumetric strain. Cores of coal were exposed to different multi-gas environments, and the CH_4/ CO_2 sorption-induced matrix volumetric strain (shrinkage/ swelling) was measured for Illinois coals. Using the measured strains, matrix shrinkage/ swelling coefficients were calculated for desorption of CH_4 as well as CH_4 and CO_2 exchange.

Because of the different approaches used in the two laboratories, that work is described in the following two sections.

Carbon Dioxide and Methane Adsorption Capacity Inferred from High-pressure Adsorption Isotherms (RMB Laboratory)

Figure 1-2 presents all available CO_2 adsorption isotherms for Indiana coals. Eight of the 14 isotherms in this figure were generated during this project (Table 1-3). For all of the samples, CH_4 adsorption

isotherms are also available (Figure 1-3). The range of pressure for Indiana coal is from 448 to 1,937 kPa (65 to 281 psig), and for these conditions, the range of CO_2 adsorption capacities (on dry, ash-free [daf] basis) varies from close to 5.2 cubic meters per tonne (m^3/tonne)(200 standard cubic feet per ton (scf/ton)) for the lowest pressure to almost 18.0 m^3/tonne (700 scf/ton) for the highest pressures (Figure 1-2). Corresponding CH_4 adsorption capacities range from ~1.3 to 5.2 m^3/tonne (~50 to 200 scf/ton)(Figure 1-3).

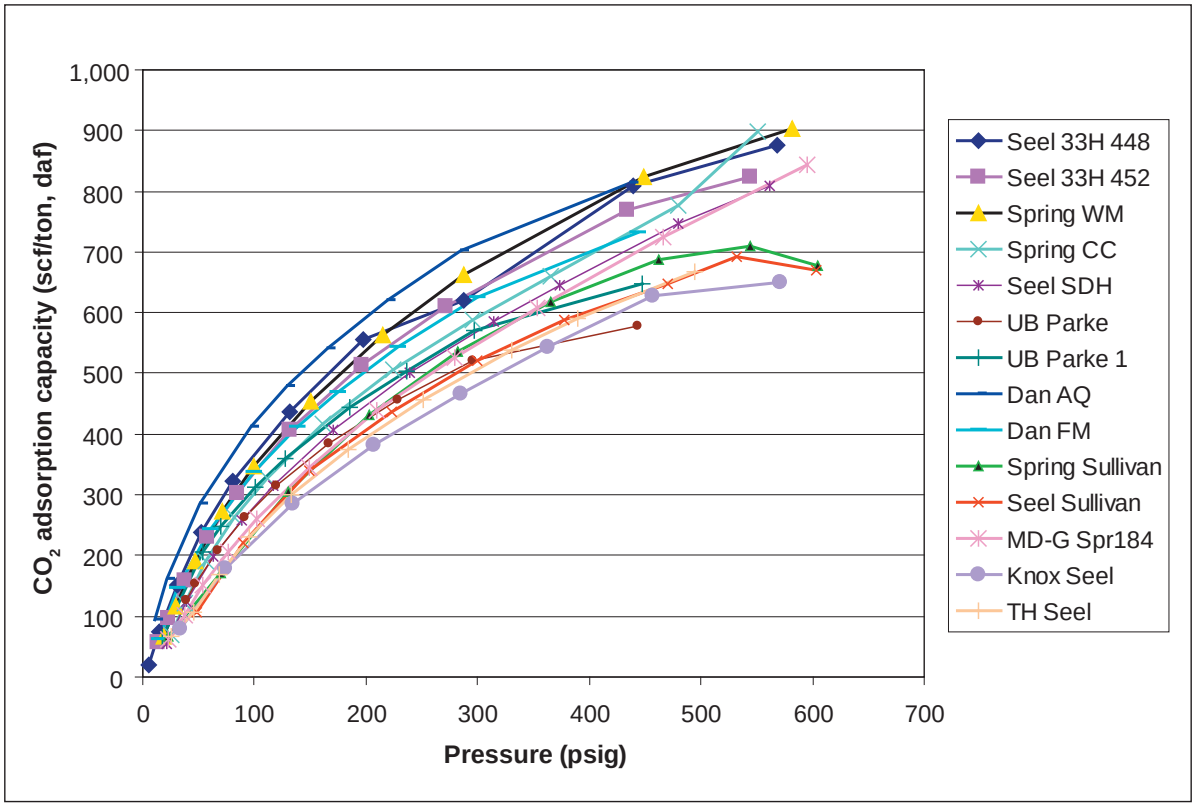

Figure 1-2 *Carbon dioxide adsorption capacity of Indiana coals. Eight of these samples (see Table 1-3) were analyzed during this project.*

The ratio of CO_2 to CH_4 adsorption capacities varies with pressure. At 2.07 MPa (300 psi), the CO_2/CH_4 ratio varies from 3.7 to 5.7 for the coals studied (Mastalerz et al., 2004). The Seelyville and Springfield coals have the highest ratio because of relatively low CH_4 sorption capacity.

Although no CO_2 adsorption isotherms at the RMB laboratory were available from Illinois and western Kentucky coals, the Indiana samples can be used to estimate adsorption capacities of the Illinois Basin coals. For the range of pressures of <689 kPa to >3,792 kPa (<100 psi to >550 psi), CO_2 adsorption capacities would range from 5.2 to 23.2 m^3/tonnes (200 to 900 scf/ton) (Figure 1-2). It needs to be emphasized that these isotherms were run at 17°C and, therefore, are valid exclusively for the areas where the reservoir temperature is 17°C. For coalbeds that have different reservoir temperatures, adsorption isotherms will be somewhat different. In general, adsorption decreases with temperature.

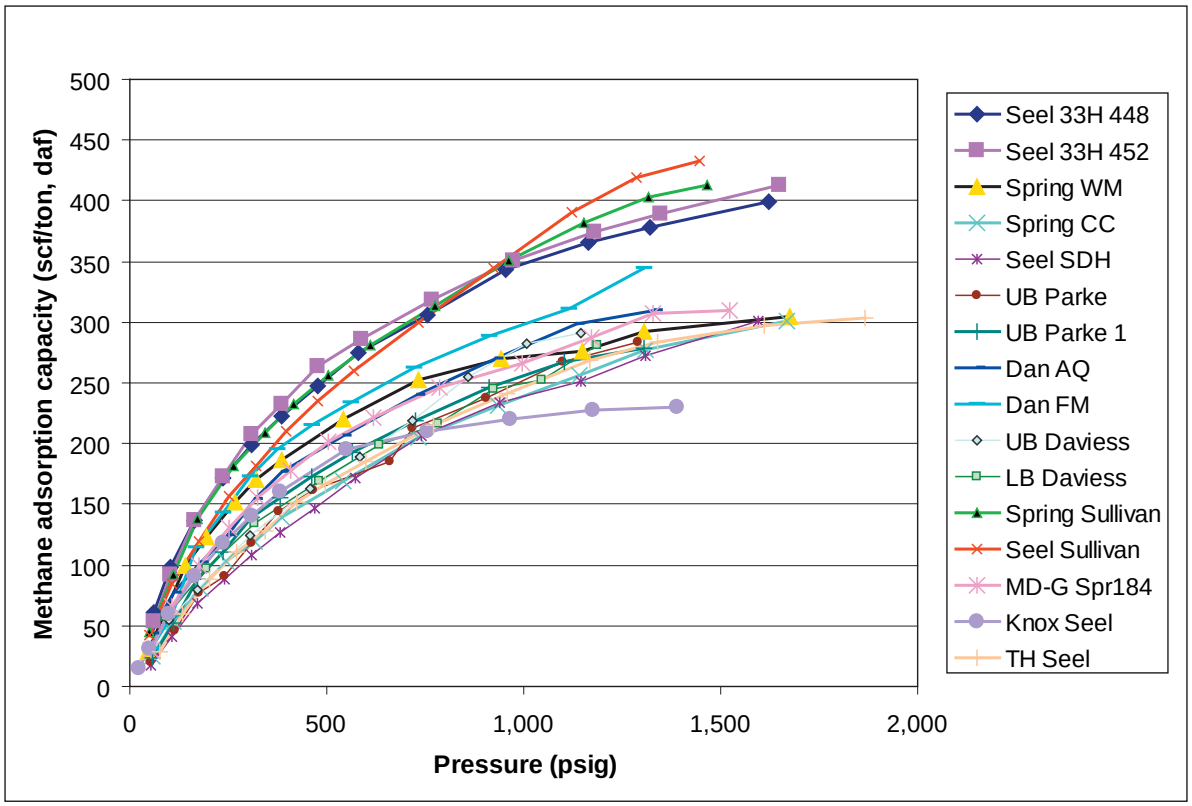

Figure 1-3 *Methane adsorption capacity of Indiana coals. Eight of these samples (see Table 1-3) were analyzed together with CO_2 isotherms during this project.*

Sorption and CO_2 Flooding Study of Coal Samples (SIU Laboratory)

Experimental Procedure

To date, no procedure has been standardized for establishing the sorption isotherms for coal. The DOE (Goodman, 2004) is currently working to do so by comparing the isotherms obtained from different laboratories worldwide using Argonne Premium coals. The most widely accepted method to develop isotherms for coal is the gas expansion technique using the Law of Mass Conservation and basic real gas laws.

Pulverized samples (40 to 100 mesh) were prepared from coal cores, 7.3 cm ($2^8/_9$ inches) in diameter, collected from the exploration program of the Illinois State Geological Survey. Samples from other parts of the Basin were provided by the Indiana and Kentucky Geological Surveys.

Prior to the sorption characterization experiments, ~80 g of the sample was placed in the environmental chamber, set at reservoir temperature and 96% relative humidity, for 24 to 36 hr for moisture equilibrium. Of the moisture-equilibrated sample, 1 g was used for moisture and ash analyses, and the remainder was used for the sorption experiment. Using the standard volumetric technique, based on the

mass balance procedure, sorption experiments were carried out for CH_4 and CO_2 up to a final maximum pressure of ~9,653 and ~5,171 kPa (~1,400 and ~750 psia), respectively. Once the maximum pressure for the adsorption isotherm was reached, the pressure was decreased to obtain the desorption characteristics.

For the CO_2 flooding experiments, the adsorption test was completed following the standard procedure. During the desorption part of the cycle, standard procedure was followed until the pressure decreased to a predetermined pressure between 1,379 and 3,447 kPa (200 and 500 psia) to best replicate the anticipated in situ conditions (Tom Moore, 2004, personal communication). Carbon dioxide was then injected into the sample, now only partially saturated with CH_4, at a pressure of ~3,447 kPa (~500 psia). After equilibrium was attained, which was determined by pressure remaining constant for 16 to 36 hr, gas composition was measured using a gas chromatograph. Using the measured molar composition and the principle of mass conservation, the partial pressure of each gas was calculated. This procedure allowed further calculation of the volume of each gas adsorbed and/or desorbed. The procedure was repeated until the partial pressure of CH_4 decreased to <689 kPa (<100 psia), which was assumed to be the abandonment pressure; at this pressure, the experiment was discontinued.

Sorption-induced Matrix Volumetric Strain

Cores of coal were obtained from the drilling program of the ISGS. These cores were stored in an environmental chamber under controlled conditions of temperature and humidity. Since the objective of these experiments was to measure the matrix properties, the cores with the fewest cleats were selected for experimental work in order to study the behavior of the coal matrix alone.

The experimental setup for this study was designed to enable measurement of volumetric strain due to changes in gas composition alone while keeping the total gas pressure constant. This design eliminated changes in matrix volume due to mechanical effects, such as compression or relaxation of the matrix grains. A schematic of the experimental setup is shown in Figure 1-4. The main components of the setup were pressure vessels that could withstand pressures up to 34,474 kPa (5,000 psi), a data acquisition system to monitor strain, and a gas chromatograph to measure the composition of gas mixtures in the vessels. Four pressure vessels enabled testing of four coal samples simultaneously. Because sorption is very sensitive to temperature, the pressure vessels were placed in a constant temperature bath. Strain gauges were affixed to the surface of each sample in order to monitor strains in the three orthogonal directions (x, y, and z). After attaching the gauges, leads were attached to each strain gauge. The entire assembly was then placed in the pressure vessel with the required gauge outlets connected to a data acquisition system. This procedure was repeated for all four test samples.

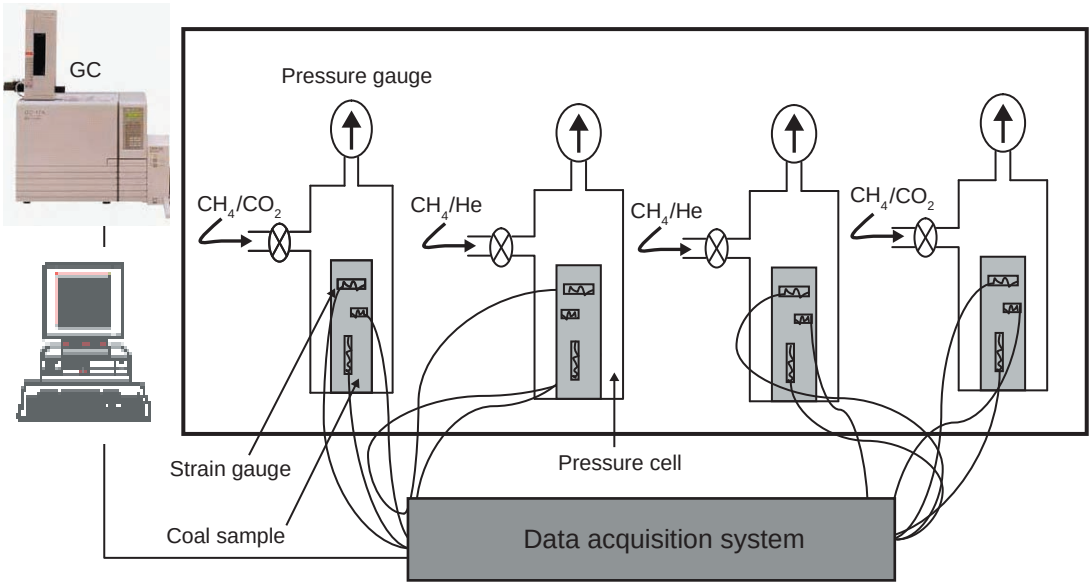

Figure 1-4 *Schematic of the experimental setup to measure the sorption-induced volumetric strain. GC, gas chromatograph.*

Results and Discussion

Sorption and Flooding Characterization: Illinois Coals

The CH_4 and CO_2 experimental sorption data were analyzed using the Langmuir isotherm equation [1]:

$$\frac{V}{V_L} = \frac{P}{P + P_L}, \qquad [1]$$

where V is the gas volume adsorbed at pressure P, and V_L and P_L are the Langmuir constants. Using the experimental results, the Langmuir constants were calculated and used to establish the isotherms. The Langmuir isotherms for CH_4 and CO_2 for Illinois coals are shown in Figure 1-5. The results show that the Herrin Coal has the highest sorption capacity, both for CH_4 and CO_2. The in situ gas content and mean initial pressure, measured by the ISGS for the location, were estimated to be 2.4 m^3/tonne and 2,586 kPa (93 scf/ton and 375 psi). The results show that all three coals adsorb more CO_2 than CH_4, thus exhibiting preferential adsorption for CO_2. Relative sorption ratios (CO_2/CH_4) were calculated for two different pressures, 689 kPa and 5,516 kPa (100 psia and 800 psia), based on the maximum anticipated injection pressure. The Langmuir constants and the relative sorption ratios for all Illinois samples are listed in Table 1-4.

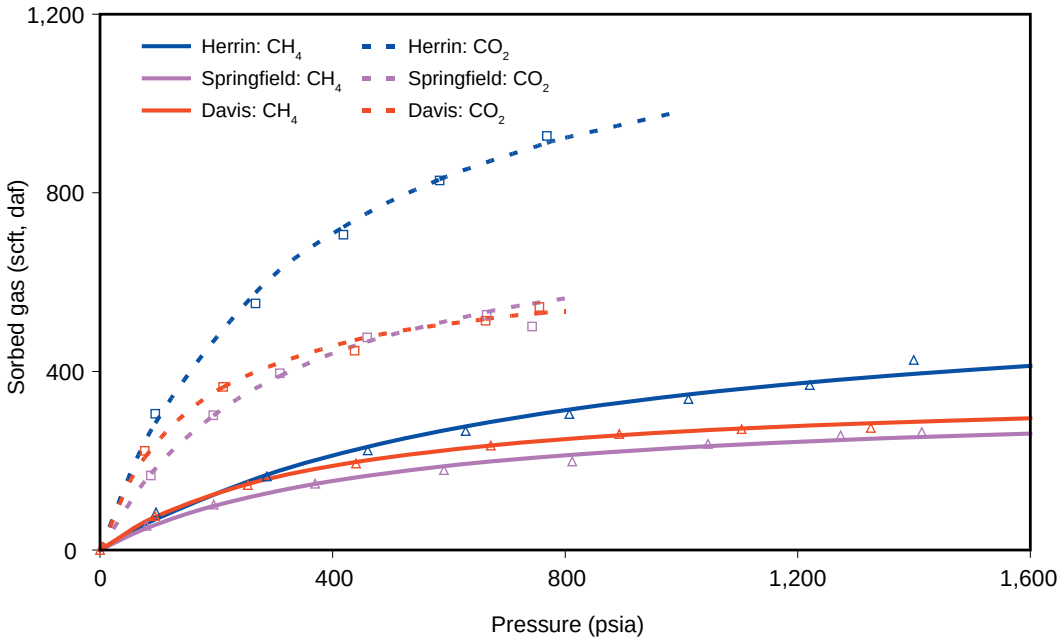

Figure 1-5 *Sorption isotherms for Illinois coals.*

Table 1-4. Langmuir constants for volume (V_L) and pressure (P_L) and relative sorption ratio for Illinois coals.[1]

Sample	CH_4		CO_2		Range and average relative sorption ratio at 100 and 800 psia (in situ pressure)
	V_L (scf/ton, daf)	P_L (psia)	V_L (scf/ton, daf)	P_L (psia)	
Herrin	603	740	1,324	347	4.1–2.9 (3.5)
Springfield	338	474	785	314	3.2–2.7 (2.7)
Davis	364	372	644	163	3.2–2.2 (2.3)

[1]All volumes are in standard cubic feet per ton (scf/ton), on a dry, ash-free (daf) basis. Measured ash and moisture contents and sample descriptions are given in Appendix 1, Table A1-1.

For CO_2 flooding, the CH_4 adsorption isotherm was first established for a maximum pressure of 8,687 kPa (1,260 psia), followed by a series of desorption steps until the CH_4 pressure decreased to 3,689 kPa (535 psia) (gas content: 6.81 m^3/tonne (264 scf/ton)). Although above the in situ pressure, 3,689 kPa (535 psia) is the maximum injection pressure, based on 15.38 kPa/m (0.68 psi/ft) of depth. At this point, CO_2 was injected in cycles into the sample at a constant pressure of ~3,792 kPa (~550 psia). A cycle included injecting CO_2, attaining equilibrium, measuring the gas composition using the gas chromatograph, and calculating the partial pressure of CH_4 and CO_2. After three cycles of injection, the experiment was stopped. The experimental results are shown in Table 1-5. The results show that, with three cycles of CO_2 injection, the sorbed CH_4 was resolved down from 6.81 m^3/tonne to 0.38 m^3/tonne (264 scf/ton to 15 scf/ton), a release of an additional 6.81 m^3/tonne (249 scf/ton) CH_4, or ~94% CBM recovery, while the total pressure was maintained relatively high throughout (~3,723 kPa (~540 psia)). The amount of additional CH_4 recovered was ~40% of the CH_4 sorption capacity of the coal sample.

Table 1-5. Results of CO_2 flooding into Herrin Coal.

Total gas pressure (psia)	Total pressure/partial pressure of CH_4 (psia)	Sorbed CH_4 (scf/ton, daf)	Remarks	Sorbed CO_2 (scf/ton, daf)
1,260	1,260	449	Pressure depletion	
1,068	1,068	403		
843	843	364		
635	675	285		
535	535	264		
539	232	212	injection 1	632
543	103	145	injection 2	1,078
541	54	15	injection 3	1,455

The sorbed CO_2 volume calculated from the CO_2 flooding experiment is substantially higher than the volume from the CO_2 Langmuir isotherm. This phenomenon has been seen in other laboratories. Presently, this phenomenon is not completely understood but is suspected to be related to the pressure-volume relationship between CO_2 and CH_4 mixtures or sorption of a gas in the presence of another sorptive gas in a multi-gas environment.

The sorbed CH_4 was plotted against the total gas pressure and partial pressure of CH_4 to determine the desorption behavior with CO_2 injection. Shown in Figures 1-6 and 1-7 are the time-independent amounts of gas sorbed. Figure 1-6 suggests that, with injection of CO_2, incremental sorbed CH_4 can be released while total pressure is maintained relatively high. A closer look at Figure 1-7, however, indicates that the rate of release of CH_4 with reduction in partial pressure of CH_4 (slope of line) was

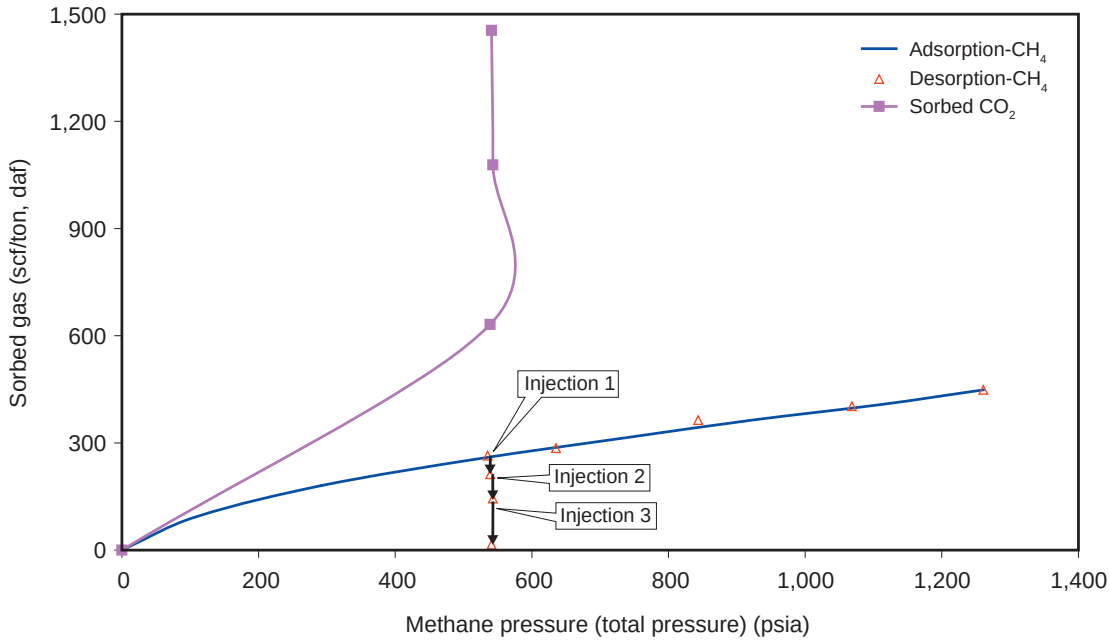

Figure 1-6 *Sorbed CH_4 and CO_2 as a function of total pressure (Herrin sample).*

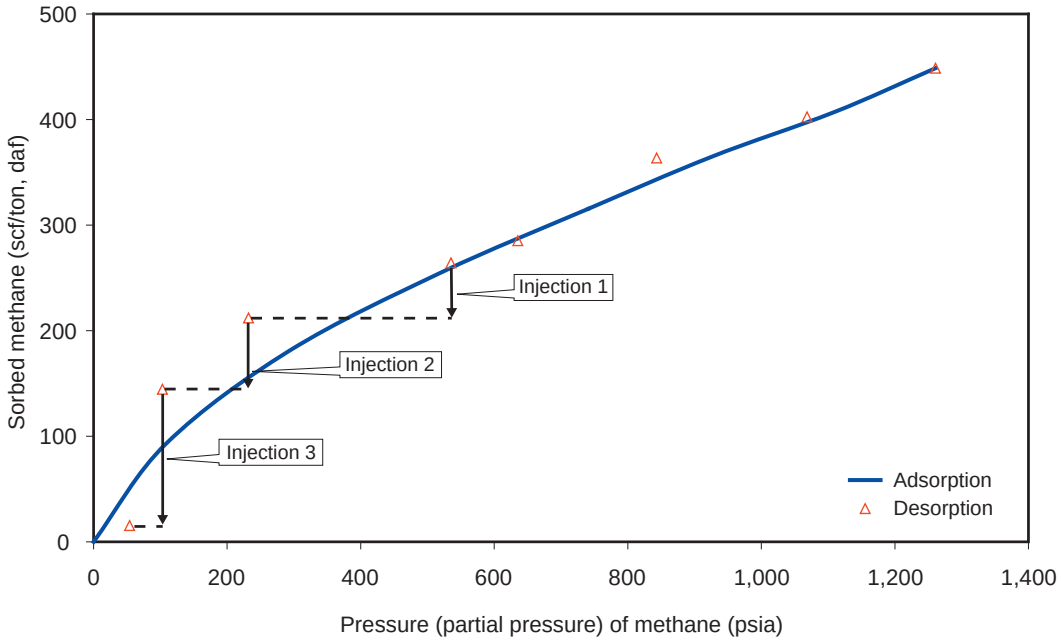

Figure 1-7 *Methane desorption isotherm with CO_2 flooding (Herrin sample).*

less initially, until the partial pressure of CH_4 decreased to ~689 kPa (~100 psia), after which most of the CH_4 was released. This result suggests that it is possible to recover most of the sorbed CH_4 by CO_2 injection only after the partial pressure of CH_4 is brought down significantly (at least ~689 kPa (~100 psia)) by continuous injection. Simultaneously with desorption of CH_4, a significant amount of CO_2 was adsorbed during these injections. The ratio of adsorbed CO_2 to desorbed CH_4 (which is important for the economics of the incremental CBM recovery) was calculated to be ~6:1. This suggests that for the aforementioned conditions, it would require six molecules of CO_2 to recover each incremental CH_4 molecule. Although this high ratio may be less favorable for CH_4 recovery, it is certainly encouraging for carbon sequestration since significant amounts of CO_2 can be sequestered in the Herrin seam. Also, this ratio is different from that estimated from the Langmuir isotherms for single gas components because of the complexity of adsorption of a gas in a multi-gas environment. This difference is less understood, and additional research in this area should be pursued.

Sorption and Flooding Characterization: Indiana Coals

The sorption isotherms for Indiana coals are presented in Table 1-6 and Figure 1-8. For the Indiana coal samples, Seelyville-I has the highest sorption capacity for both CH_4 and CO_2. The other two samples have similar sorption capacities. All of the samples exhibited preferential adsorption for CO_2 rather than CH_4. The relative sorption ratio for these samples varied between 3.8 and 2.4 at 689 and 5,516 kPa (100 and 800 psia), respectively.

Table 1-6. Langmuir constants and relative sorption ratio for Indiana coals.

Sample	CH_4		CO_2		Relative sorption ratio at 100 and 800 psia
	V_L (scf/ton, daf)	P_L (psia)	V_L (scf/ton, daf)	P_L (psia)	
Springfield	354	276	743	135	3.4–2.4
Seelyville-I	533	512	1,088	226	3.8–2.6
Seelyville-II	262	261	861	213	3.8–3.5

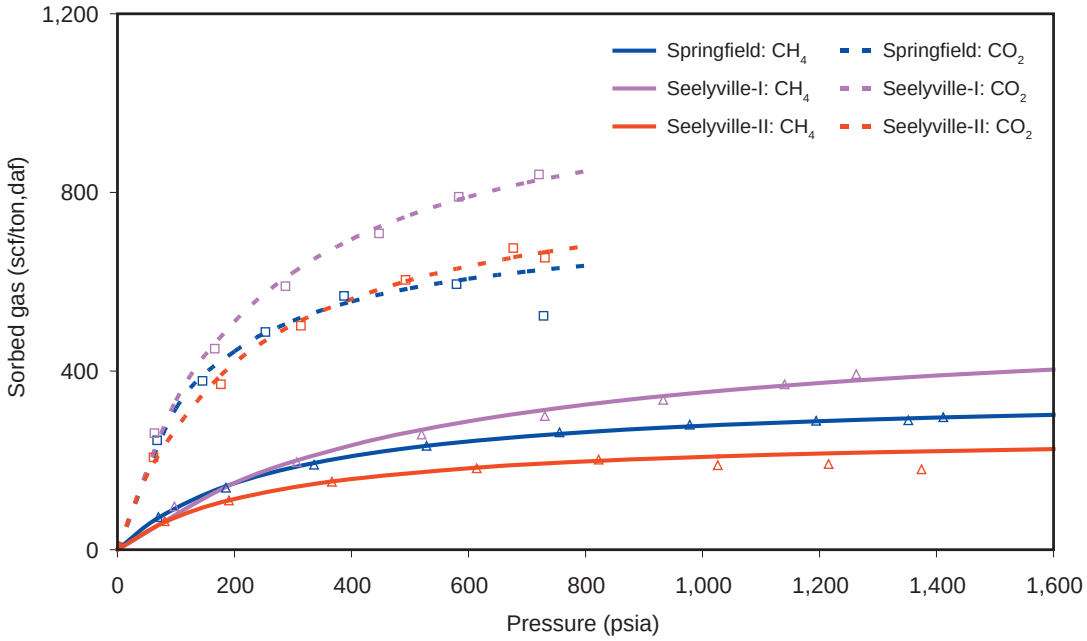

Figure 1-8 *Sorption isotherms for Indiana coals.*

The CO_2 flooding results for the Seelyville-I sample are shown in Figures 1-9 and 1-10 and presented in Table 1-7. After three injections, sorbed CH_4 in the coal sample was reduced from 6.26 to 2.81 m^3/tonne (243 to 109 scf/ton), an incremental release of 3.45 m^3/tonne (134 scf/ton), or 55% ECBM recovery. The additional CH_4 recovered was ~25% of the sorption capacity. Figure 1-9 suggests that the incremental CH_4 was recovered even when the total gas pressure remained high (~3,447 kPa (~500 psia)). However, Figure 1-10 shows that most of the incremental CH_4 was recovered by the first two injections and that the third injection resulted in little additional CH_4 recovery. At the end of the experiment, the ratio of the amount of adsorbed CO_2 to desorbed CH_4 was calculated to be ~8:1. The reason for this high ratio is that a considerable amount of CO_2 is adsorbed without releasing a proportional amount of CH_4 at lower pressures (<689 kPa (<100 psia)). The results suggest that CO_2 injection is capable of producing additional CH_4 and enhancing its recovery, along with considerable CO_2 sequestration potential. However, CO_2 injection can enhance the recovery of CH_4 only up to a limit, beyond which additional injection becomes ineffective, approximately 2.58 m^3/tonne (100 scf/ton) for this case.

Table 1-7. Results of CO_2 flooding into Seelyville-I coal.

Pressure/partial pressure of CH_4 (psia)	Total gas pressure (psia)	Sorbed CH_4 (scf/ton, daf)	Remarks	Sorbed CO_2 (scf/ton, daf)
1,437	1,437	385	Pressure depletion	
1,255	1,255	351		
1,022	1,022	330		
802	802	308		
577	577	262		
492	99	243		
496	218	150	Injection 1	600
496	94	113	Injection 2	940
497	40	109	Injection 3	1,090

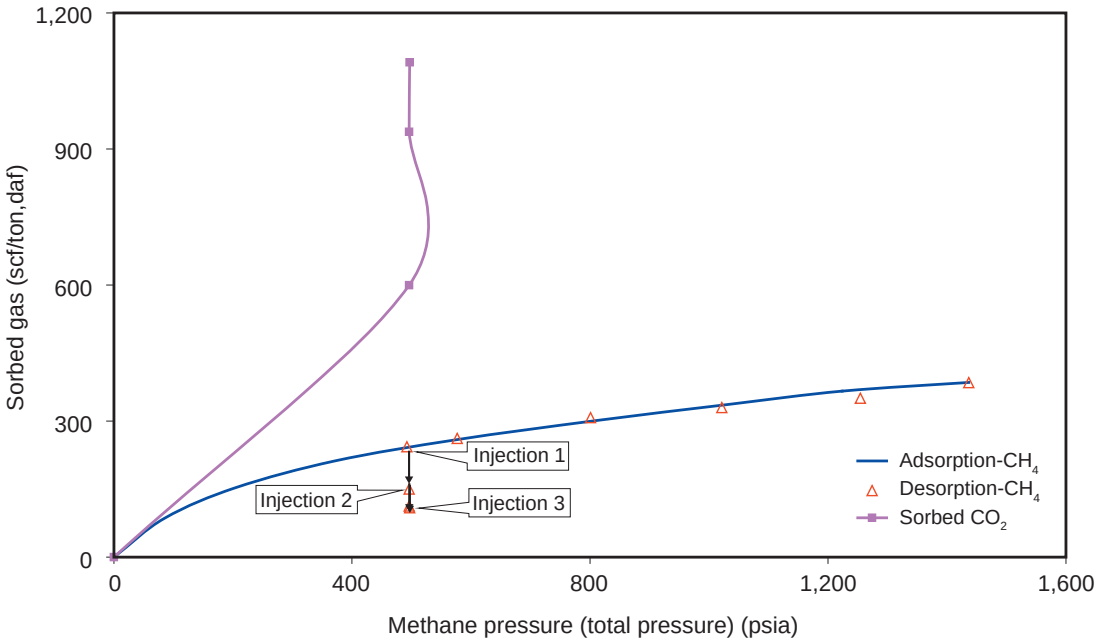

Figure 1-9 *Sorbed CH_4 and CO_2 as a function of total pressure (Seelyville-I coal).*

The sorbed CO_2 volume calculated from the CO_2 flooding experiment is substantially higher than the volume from the CO_2 Langmuir isotherm. This phenomenon has been seen in other laboratories. Presently, this phenomenon is not understood but is suspected to be related to the pressure-volume relationship between CO_2 and CH_4 mixtures or sorption of a gas in the presence of another sorptive gas in a multi-gas environment.

Sorption and Flooding Characterization: Kentucky Coals

The sorption isotherms for the three Kentucky samples tested are shown in Figure 1-11 and presented in Table 1-8. The results show that the Springfield sample has the highest sorption capacity for CH_4

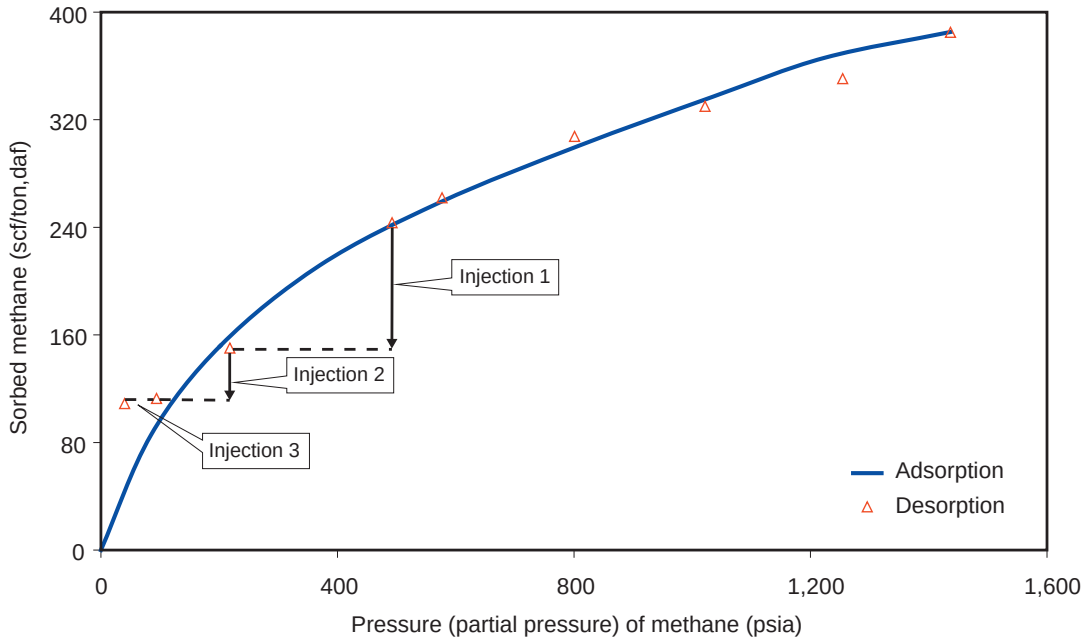

Figure 1-10 *Methane desorption isotherm with CO_2 flooding (Seelyville-I coal).*

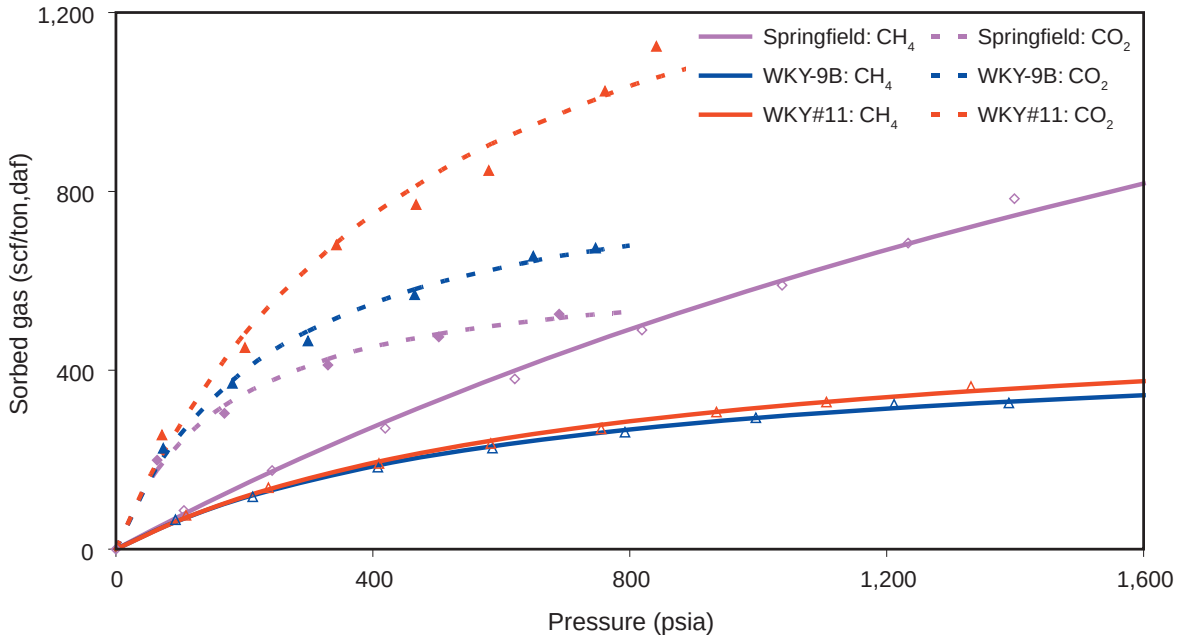

Figure 1-11 *Sorption isotherms for Kentucky coals.*

although the Langmuir fit is not very good for the sample. The other two samples have similar sorption capacities. The relative sorption ratio (CO_2/CH_4) at 689 and 5,516 kPa (100 and 800 psia), varied between 4.3 and 1 respectively. One surprising finding is that, for the Springfield sample, CH_4 sorption capacity (Langmuir constant for volume, V_L values) was greater than that for CO_2, although for pressure range of interest, the amount of sorbed CH_4 was always less than that of CO_2.

Table 1-8. Langmuir constants for volume (V_L) and pressure (P_L) and relative sorption ratio for Kentucky coals.

Sample	CH_4		CO_2		Relative sorption ratio at 100 and 800 psia
	V_L (scf/ton,daf)	P_L (psia)	V_L (scf/ton,daf)	P_L (psia)	
Springfield	2,434	3,164	644	170	3.3–1:1
WKY-9B	482	641	887	245	4.0–2.5:1
WKY#11	549	737	1,678	498	4.3–3.6

The results of the CO_2 flooding experiments for the Springfield sample are shown in Figures 1-12 and 1-13, and presented in Table 1-9. There was one important difference in the experimental procedure followed for the samples from Kentucky. Due to the anticipated low gas content in situ, as measured by canister tests, the usual desorption steps were carried out to ~1,379 kPa (~200 psi) prior to commencement of CO_2 injection. The results indicate that the first CO_2 injection led to considerable re-adsorption of free CH_4 in the sample container. After the second and third injection, however, most of the sorbed CH_4 was released. During these injections, while 4.37 m^3/tonne (170 scf/ton) of CH_4 was desorbed, 16.6 m^3/tonne (644 scf/ton) of CO_2 was adsorbed concomitantly. The CO_2/CH_4 exchange ratio was, therefore, ~ 4:1.

The sorbed CO_2 volume calculated from the CO_2 flooding experiment is substantially higher than the volume from the CO_2 Langmuir isotherm. This phenomenon has been seen in other laboratories.

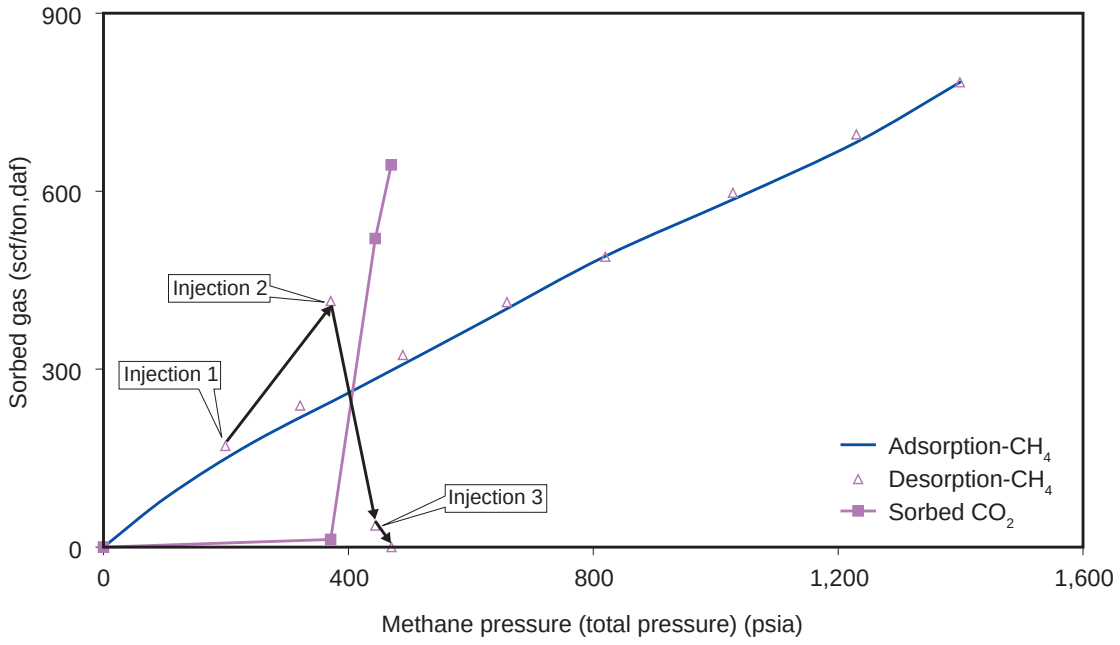

Figure 1-12 *Sorbed CH_4 and CO_2 as a function of total gas pressure (Springfield sample).*

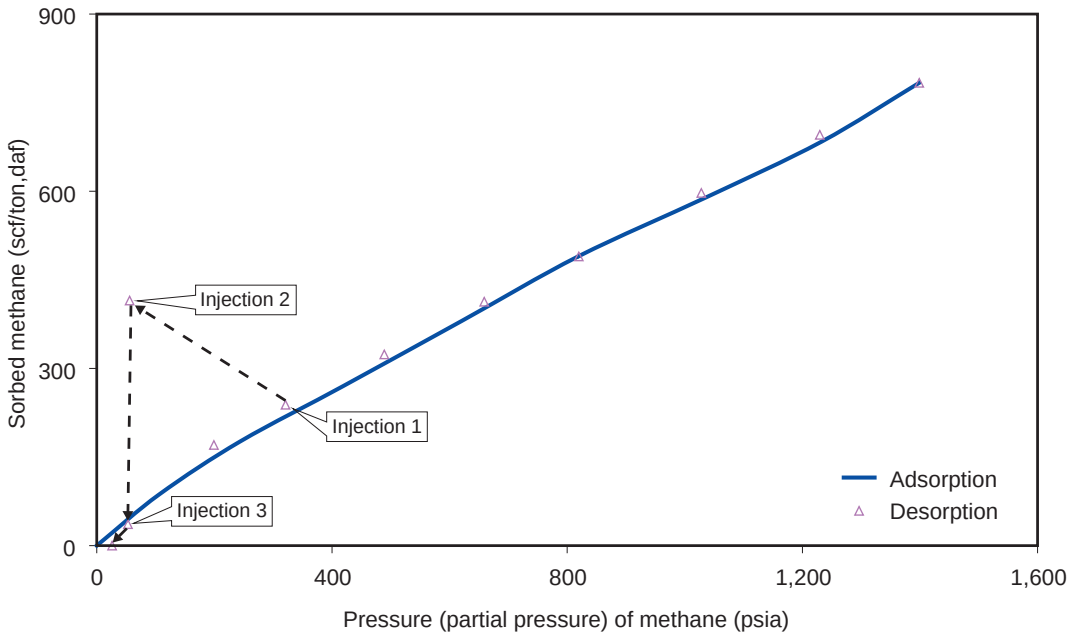

Figure 1-13 *Methane desorption isotherm with CO_2 flooding (Springfield sample).*

Presently, this phenomenon is not understood but is suspected to be related to the pressure-volume relationship between CO_2 and CH_4 mixtures or sorption of a gas in the presence of another sorptive gas in a multi-gas environment.

Table 1-9. Results of CO_2 injection into the Springfield sample.

Pressure/partial pressure of CH_4 (psia)	Total gas pressure (psia)	Sorbed CH_4 (scf/ton, daf)	Remarks	Sorbed CO_2 (scf/ton, daf)
1,399	1,399	784	Pressure depletion	
1,230	1,230	696		
1,028	1,028	597		
820	320	490		
659	659	413		
489	489	324		
321	321	239		
199	159	170		
56	371	415	Injection 1[1]	13
53	444	36	Injection 2	520
26	470	0	Injection 3	644

[1]Re-adsorption of CH_4 as a result of CO_2 injection.

The results for all samples from Kentucky exhibited the observed CH_4 re-adsorption behavior. It is not clear whether the observed difference is because CO_2 injection commenced at relatively lower CH_4 pressures, or whether the coal type is distinctly different from the other coals tested. It is suspected that the observed behavior, shown as the slight hump in Figure 1-13 is due to the low CH_4 pressure prior to

commencement of CO_2 injection. The results suggest that, with continued CO_2 injection, it is possible to recover incremental CH_4 even if there is, in fact, some re-adsorption of CH_4 initially.

Sorption-induced Volumetric Strain

Two samples each from the Herrin and Springfield seams (taken from the Wabash exploratory well drilled by the ISGS) were used for these experiments. Each sample was a split core, approximately 3.8 cm (1.5 inches) long. All four samples were first flooded with CH_4 at a pressure of 5,861 kPa (850 psi) as the volumetric strain was continuously monitored. The CH_4 injection phase was carried out in a single step to save time. This experimental study was aimed at estimating the coal matrix volumetric changes due to CH_4 desorption and CO_2 adsorption. The actual volumes of the two gases sorbed were not measured; rather, the concentrations of the two gases were monitored. Time required to achieve equilibrium was different for the two gases and coal types and was approximately 10 days for each injection step. After strain equilibrium at ~5,861 kPa (~850 psi) was attained, one sample each from the Herrin and Springfield seams was subjected to increasing concentration of CO_2 (gradual CO_2 flooding). Total pressure was maintained constant by bleeding gas every time CO_2 was injected, thus replicating ECBM conditions. The procedure was continued until the gas in the vessel was pure CO_2. At each equilibrium step, a sample of gas was analyzed using the gas chromatograph, and the gas mixture concentration was measured. The measured composition was used to determine the partial pressures of the individual gases for each injection step. The corresponding strain (change in volume/original volume, or $\Delta V/V$) was calculated for each injection step.

The other two samples were subjected to increasing helium pressure, while maintaining constant total pressure, to measure the strain due to desorption of CH_4, thus replicating the primary depletion technique. Helium was used to ensure that the mechanical conditions in and around the samples were the same throughout the experiment. Helium is also inert, that is, non-sorptive. At the end of the experiment, all four samples were, therefore, "saturated" either with helium or CO_2.

Volumetric strain results for CH_4 and CO_2 exchange due to increase of CO_2 pressure in the samples are shown in Figure 1-14. The volumetric strain due to CH_4/CO_2 exchange in the Springfield sample was twice that in the Herrin sample. The strain results for CH_4 desorption are shown in Figure 1-15. The path followed by *de*sorption-induced shrinkage exhibits some hysteresis, undergoing slightly more shrinkage than the *ad*sorption-induced swelling, since there is some residual strain at the end of the experiment. Because the two figures are for different samples, the results can be compared only qualitatively.

The results of the core matrix swelling and shrinkage experiments involving CO_2 flooding can be summarized as follows:

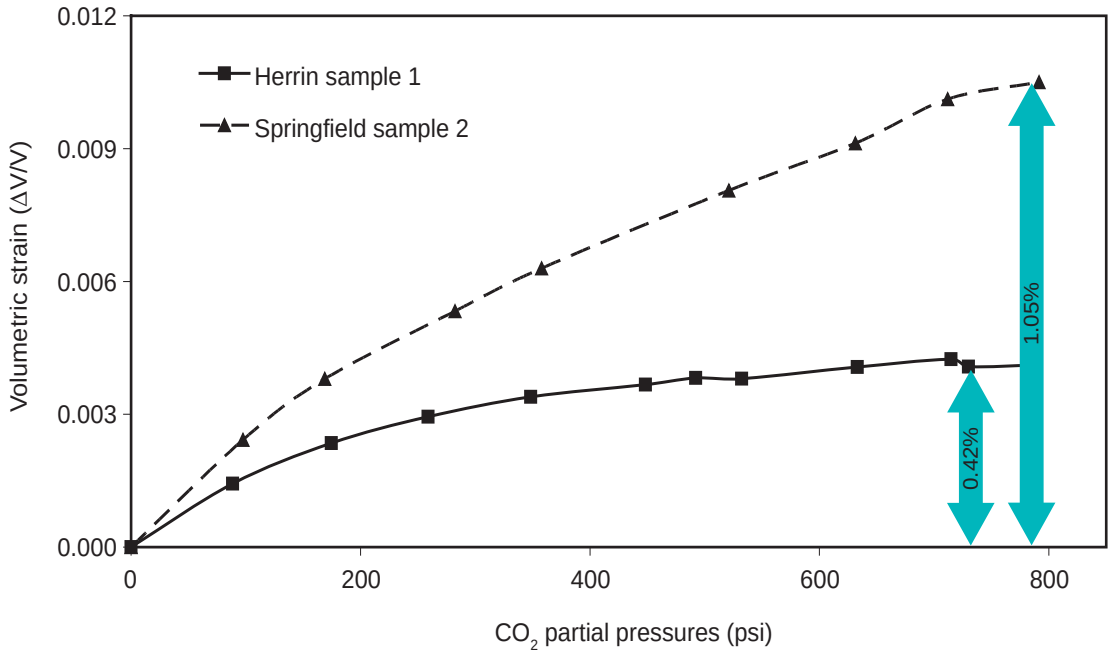

Figure 1-14 *Volumetric strain for CH_4 and CO_2 exchange.*

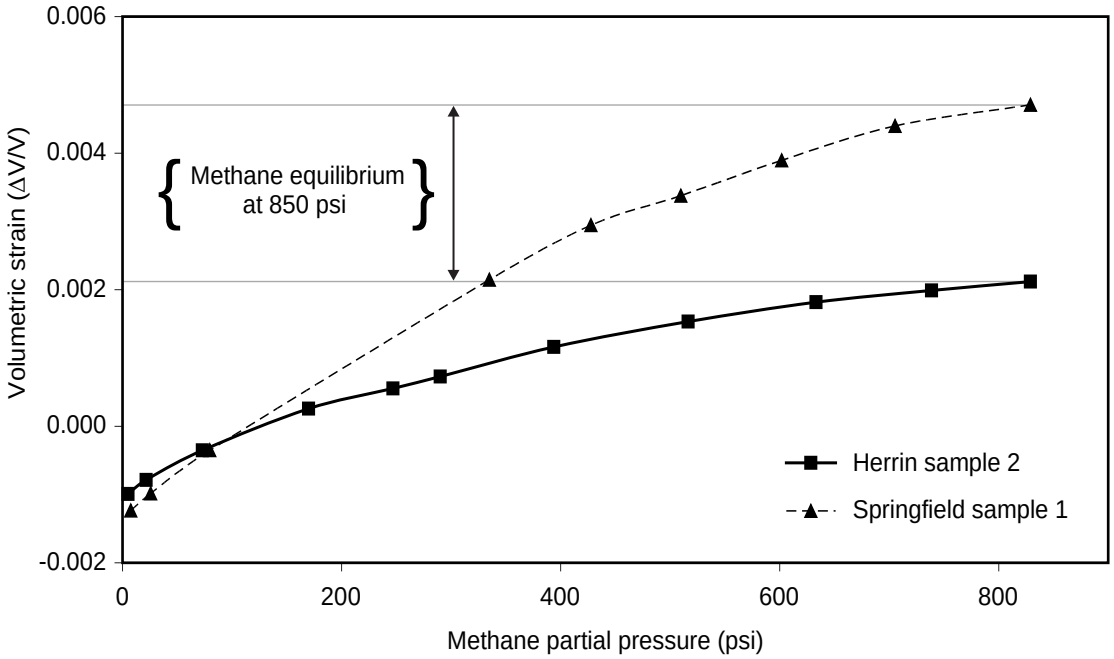

Figure 1-15 *Volumetric strain for CH_4 desorption steps.*

1. For CH_4 adsorption, the volume of the coal matrix increased by ~0.35%. Coefficient values for matrix swelling ranged from 1.76×10^{-5} kPa to 3.92×10^{-5} kPa (2.55×10^{6} psi^{-1} to 5.68×10^{6} psi^{-1}), with an average of 2.80×10^{-5} kPa (4.06×10^{6} psi^{-1}). Matrix shrinkage, $C^{\dagger}_{m}$, and swelling coefficients, C^{*}_{m}, are expressed as

$$C^{\dagger}_{m} \text{ or } C^{*}_{m} = \frac{1}{V_m}\left(\frac{\Delta V_m}{\Delta P}\right) \qquad [2]$$

where V_m is the matrix volume, and ΔP is the change in applied pressure at both internal and external surfaces.

2. Using the volumetric strain due to desorption of CH_4 (Figure 1-15), the calculated coefficient values for matrix shrinkage were 2.60×10^{-5} kPa (3.77×10^{6} psi^{-1}) for the Herrin core and 5.01×10^{-5} kPa (7.26×10^{6} psi^{-1}) for the Springfield core.

3. With CO_2 injection (CO_2 flooding), accompanied by release of CH_4, additional swelling was ~0.42% for the Herrin core and ~1.05% for the Springfield core (Figure 1-14). For the CH_4 and CO_2 exchange, the calculated differential swelling coefficient values were 3.56×10^{-5} kPa (5.17×10^{6} psi^{-1}) for the Herrin core and 9.10×10^{-5} kPa (13.2×10^{6} psi^{-1}) for the Springfield core.

Conclusions

The following conclusions are based on the experimental work completed:

1. The Herrin and Seelyville-I samples have the highest CO_2 sorption capacity. These coals, therefore, have the highest potential to retain CO_2. For the samples from Kentucky, although the Springfield sample has the highest CH_4 sorption capacity, its CO_2 sorption capacity is not the largest. Hence, higher CH_4 sorptive capacity does not universally translate to higher CO_2 capacity, and the two do not always go together.

2. Cyclic injection of CO_2 into coals after partial desorption of CH_4 leads to incremental recovery of CH_4. However, the pattern of release is not uniform but falls into three broad categories. In the first category, injection of CO_2 leads to immediate release of CH_4, and, with continued CO_2 injection, all of the sorbed CH_4 is released, which would be the most favorable condition for ECBM. In the second category, CO_2 injection leads to incremental desorption of CH_4, but only up to a certain limit, after which CO_2 becomes ineffective. This coal type would still serve well as CO_2 storage, although any ECBM plan must be carefully assessed prior to implementation. In the third category, where CO_2 injection was carried out only after the reservoir pressure was reduced considerably, initial injection led to re-adsorption of CH_4, although, with continued injection, incremental CH_4 is desorbed. This finding needs to

be investigated further to determine whether the observed results were due to the low CH_4 pressure or to the particular coal type.

3. Swelling and shrinkage of the coal matrix due to injection of CO_2 are considerable in Illinois coals. Hence, permeability damage with CO_2 injection is a real possibility. The extent of the damage, however, cannot be estimated at this time, nor can it be inferred based on the results obtained to date.

4. The coefficient for sorption-induced matrix shrinkage for Illinois coals is close to that reported for the San Juan Basin (SJB), where the phenomenon of matrix shrinkage is thought to have had a significant impact on CBM production (Table 1-10). However, SJB is much deeper and, therefore, more highly stressed than Illinois Basin coals. Furthermore, since the combined effect of matrix shrinkage and stressing is not known, it is difficult to extrapolate and infer whether the phenomenon would have a noticeable impact in the Illinois Basin. Finally, most of the producing reservoirs in SJB are saturated, with high gas content, and the amount of CH_4 desorbed is much higher than that expected in the Illinois Basin. Therefore, matrix strain, a direct consequence of the amount of gas desorbed, is prominent in the SJB coals. Based on the findings of this study, it is recommended that the coupled effect of stress and matrix strain be investigated further to determine its impact on coal permeability.

Table 1-10. Comparison of matrix swelling and shrinkage of Illinois coal with SJB coal.

	San Juan Basin[1]	Herrin Coal[1]	Springfield Coal[1]	Illinois (avg.)[1]
Swelling coefficient (CH_4 adsorption)	5.61×10^6 (Avg.)	3.09×10^6	5.04×10^6	4.06×10^6
Shrinkage coefficient (CH_4 desorption)	3.90×10^6	3.77×10^6	7.26×10^6	5.52×10^6
Swelling coefficient (CH_4/CO_2 exchange)	12.5×10^6	5.17×10^6	13.2×10^6	9.17×10^6
Swelling coefficient (CO_2 adsorption)	1.60×10^6	-	-	-

[1]Units are psi^{-1}.

Determination of Coal Characteristics Affecting Coal Adsorption and Desorption (Subtask 4.4)

Gas is retained in coals in the following ways: (1) *adsorption* upon internal surfaces (in micropores); (2) *absorption* into the molecular structure of coal; (3) *as free gas* in voids, cleats, and fractures; and (4) *as a solute* in groundwater present within the coal seam (Rice, 1993). Gas adsorption upon the internal surface area of the coal is considered to be, by far, the most important mechanism for gas retention.

Several parameters that influence gas adsorption were considered and mapped for individual coalbeds in the Illinois Basin. These include moisture content, ash and sulfur contents, heating value and vitrinite reflectance, and reservoir pressure and temperature. The influence and distribution of these parameters are discussed. Other parameters such as maceral composition, surface area and pore-size distribution, and cleat orientation and coal permeability are also very important for gas adsorption and are briefly addressed in the Other Parameters section. Presently, data are not sufficient to address these parameters in detail, but they will be investigated further in Phase II of the project.

Moisture Content

Moisture plays an important role in the sorption of gases on coal. Numerous studies show that moisture decreases sorption capacity, competing with gas for the same sites and blocking these sites (e.g., Seldon, 1934; Gunter, 1965; Mavor et al., 1990). For a given coal sample, the reduction of sorption capacity takes place only until critical moisture (equilibrium moisture) is reached (Joubert et al., 1973, 1974). Therefore, it is important to have equilibrium moisture values to represent in situ reservoir conditions and gas sorption capacity at these conditions. Clarkson and Bustin (2000) also demonstrated that, to a large extent, CO_2 selectivity over CH_4 is a function of moisture content, which stresses the necessity of accurate knowledge of in situ coal-matrix water content for the accurate prediction of gas adsorption.

Maps of the moisture content for the individual coalbeds are presented in Appendix 3. These moisture maps use both equilibrium moisture values (approximately representing in situ conditions) and as-received moisture values (not necessarily representing in situ conditions); therefore, these maps need to be interpreted with caution. These two different moisture bases were combined on one map to get better data coverage; using equilibrium moisture alone would give significantly fewer data points.

With everything else being equal, areas having relatively low-moisture contents would be more favorable for CO_2 sequestration. These low-moisture areas on most maps coincide with the deepest parts of the Illinois Basin.

Mineral Matter Content

There is a generally accepted idea that mineral matter acts as an inert dilutant with respect to gas sorption, which means that mineral matter does not contribute to the coal's gas sorption capacity and that the gas sorption takes place on the organic fraction of the coal (Gunther, 1965; Metcalfe et al., 1991; Mavor et al., 1991). Following this notion, the gas sorption should be higher in coal having lower mineral matter content. Mineral matter content (MM) can be obtained from the Parr formula (MM = 1.08A + 0.55S where A is ash and S is sulfur). Frequently, ash yield is used as an approximation for the mineral matter content.

Maps of the ash yield for individual coalbeds are presented in Appendix 3. These maps, especially those having a relatively more data points, show large variations in ash yield, which will contribute to variations in gas sorptions if these coalbeds become targets for CO_2 sequestration. With other things being equal, the areas of relatively low ash yield are more favorable for CO_2 sequestration. The maps were generated using ash values on a dry basis; for in situ reservoir conditions, ash values are somewhat lower because of moisture. Sulfur content maps are presented in Appendix 3. These maps are included because sulfur is an important component of mineral matter, which is very important for coal utilization.

Heating Value and Vitrinite Reflectance

Heating value maps and vitrinite reflectance maps for the Herrin and Springfield Coal Members have been generated primarily to show the coal rank distribution in the Illinois Basin. Vitrinite reflectance is a better parameter to determine coal rank because it is measured on relatively homogenous "woody" material. In contrast, heating value is determined on bulk coal, thus introducing variations related to coal petrographic composition. However, considerably fewer data are available for vitrinite reflectance than for heating value; therefore, both these parameters were generated so that they can be used jointly to look at rank variations.

Heating value, expressed in British Thermal Units (BTU) per pound, is mapped on four different bases: moisture- and ash-included bases; dry basis; ash-free, moisture-included basis; and dry, ash-free basis. For the purpose of studying variations in rank, heating value maps on ash-free, moisture-included basis are recommended for use in combination with vitrinite reflectance maps.

Table 1-11. Vitrinite reflectance ranges and coal ranks as defined by ASTM.

ASTM coal rank	Maximum vitrinite reflectance (%)
Sub-bituminous	<0.47
High-volatile bituminous C	0.47–0.57
High-volatile bituminous B	0.57–0.71
High-volatile bituminous A	0.71–1.10
Medium-volatile bituminous	1.10–1.50
Low-volatile bituminous	1.50–2.05
Semi-anthracite	2.05–3.00 (approximately)
Anthracite	>3.00 (approximately)

Coal rank is a very important parameter that greatly influences gas sorption. Generally, higher-rank coals have higher sorption capacity because of the increasing proportion of micropores, and, consequently, more adsorption sites than lower-rank coals. Illinois Basin coals are high-volatile bituminous C, B, and (sporadically) A rank (Table 1-11). In general, the highest rank occurs in the deepest part of the Basin in Illinois and tectonically engaged areas in western Kentucky, demonstrated

both by heating value maps (on ash-free, moisture-included basis) and vitrinite reflectance maps. With regard to coal rank, all other things being equal, the highest-rank areas would be the most favorable for CO_2 sorption.

Reservoir Pressure and Temperature

Sorption properties of gas at depth are a function of temperature and pressure. For CO_2 storage, in situ coal temperature and pressure are of special importance because of the uncertainty of temperature- and pressure-dependent phase changes of CO_2 (Figure 1-16). Accurate determination of the in situ coal temperature is critical for evaluating the potential sequestration capacity in coals; therefore, it is critical that adsorption isotherms (that provide us with adsorption capacity data) are performed at the temperature of in situ coal.

Illinois Basin coalbeds have reservoir temperatures ranging from less than 12.78°C (55°F) to more than 26.67°C (80°F) in isolated areas in Illinois, where geothermal anomalies are present with temperature gradients up to -16.44°C/30 m (2.4°F/100 ft). Higher temperatures favor more gas in the free phase than in the sorbed phase. Because the reservoir temperatures of the Illinois Basin coals are relatively low, however, this effect may not be distinct and likely occurs only locally.

Coal seam pressure ranges from <689 kPa (<100 psi) close to the margin of the Basin to >3,792 kPa (>550 psi) in deeper structural areas in western Kentucky. The sorption capacity increases with pressure, as demonstrated by adsorption isotherms, but the increase occurs at a decreasing rate. Therefore, areas of higher pressure could sequester more CO_2. However, with increasing depth, pressure and temperature increase and tend to have compensatory effects such that the net increase or decrease with depth is not clear. Coals under higher overburden pressure will have lower permeability, which inhibits sequestration. This range of pressures and temperatures places all coalbeds of the Illinois Basin under subcritical fluid conditions (gaseous phase) for CO_2 sequestration (Figure 1-16). However, adsorbed CO_2 may have an equivalent density higher than subcritical CO_2; further research is required.

Other Parameters

Maceral Composition

The literature data on the influence of maceral composition on CO_2 sorption are limited and inconclusive. Carroll and Pashin (2001) showed no clear relationships for the Black Warrior Basin coals, but their study did not split the vitrinite group into individual macerals. Clarkson and Bustin (1999) suggest that bright (vitrinite-rich) coal absorbs more CO_2 and CH_4 than dull (vitrinite-poor) coals. A preliminary study of Indiana coals suggests that maceral composition is important in determining CO_2 sorption

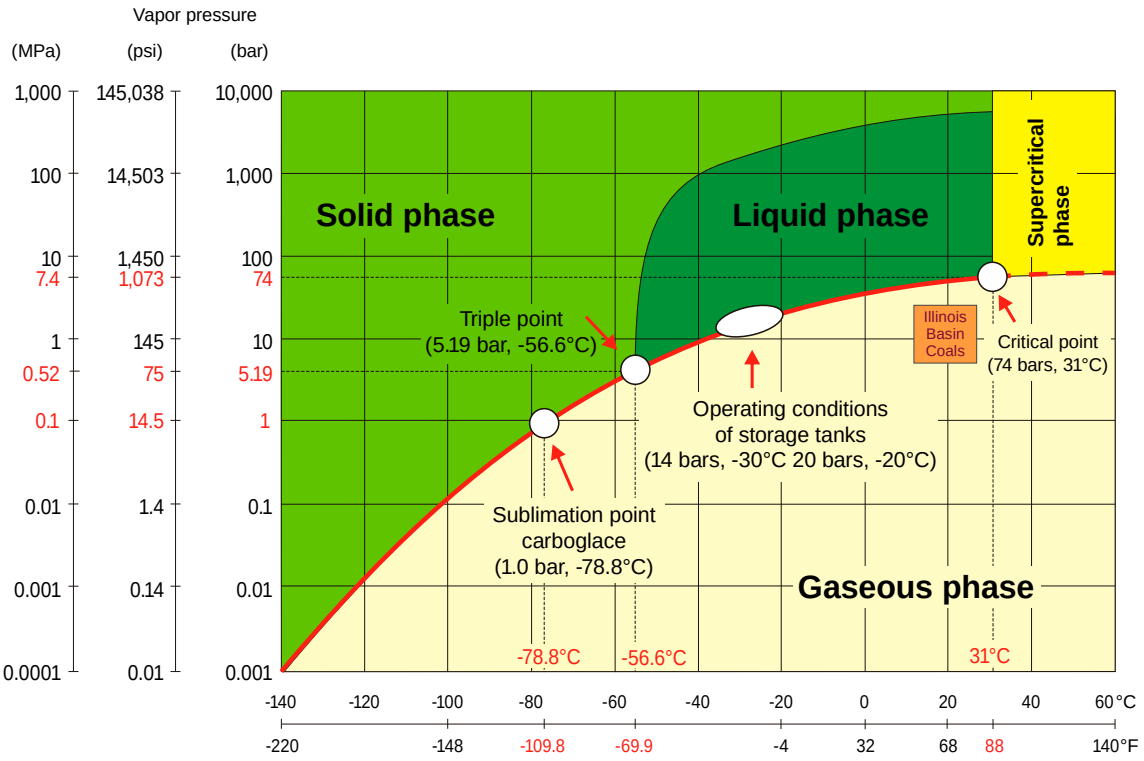

Figure 1-16 *Phase diagram for CO_2.*

capacity. Samples with higher CO_2 sorption generally have the highest vitrinite content. Collotelinite, a vitrinite maceral, appears to have the greatest influence on CO_2 sorption capacity of all macerals (Mastalerz et al., 2004). Additional samples are needed to test this relationship.

Surface Area and Pore-size Distribution

It has been frequently suggested that the micropore, and not the mesopore, volume is the main control on gas adsorption; therefore, coals with larger micropore volume are expected to have higher gas adsorption. However, this relationship appears to be neither universal nor exclusive. Bustin and Clarkson (1998) clearly demonstrate, for a suite of Canadian and Australian coals of similar rank and maceral composition, that coals with the highest micropore volume (isotherms performed on dry coals) do not necessarily have the highest CH_4 adsorption capacity (determined on moisture-equilibrated coals).

Undoubtedly, pore-size distribution must play a role in the selectivity of CO_2 over CH_4 because of the differences in the relative molecular sizes of CO_2 and CH_4. Carbon dioxide has a smaller half-width (0.289 nm vs. 0.310 nm for CH_4) and, therefore, can reach not only macropores and micropores but also ultramicropores (Cui et al., 2004). In addition to the relatively smaller kinetic diameter of CO_2, the adsorption energy of CO_2 is also greater than that of CH_4 for most pore sizes. Therefore, CO_2 can diffuse into the microporous coal matrix more easily than CH_4 can. According to Cui et al. (2004),

these differences in kinetic diameters and adsorption energies through pore-size ranges can explain the considerably higher diffusivity of CO_2 than CH_4 in the coal matrix. Coal has a heterogeneous, interconnected pore network. For example, if this network is constricted by ultramicropores with pore width <0.6 nm, as suggested by Cui et al. (2004), CO_2 (0.289 nm half-width) may penetrate, while CH_4 (0.310 nm half-width) may not.

Cleat and Fracture Permeability

Cleating and fracturing of coal have a large effect on coal permeability, and it has been known for a long time that coal can vary greatly in the nature and frequency of cleating. Yet there has not been a quantitative, reproducible measure of cleats in coal, which makes it difficult to find a relationship between the cleats and gas injection.

Estimation of Sink Capacity for Coal Seam Storage (Subtask 4.5)

Reservoir Model Description

The model used in the parametric and Basin-scale volumetric studies is a 80,937.46-m^2 (20-acre), one-quarter 5-spot model of a 324-km^2 (80-acre) injection pattern. The model contains an injector and producing well in diagonally opposite corners of the square model area. Use of a one-quarter 5-spot pattern reduces the area required to be modeled due to symmetrical flow between a pair of injection and production wells in a 5-spot pattern. Through reduction of the model area, computation time is reduced. This reduction enables greater resolution to be achieved through application of a finer model grid while maintaining an acceptable time for simulation completion. Symmetrical flow is observed because isotropic permeability is modeled (same permeability between face and butt cleats). The model is composed of a single layer (no vertical permeability) with constant thickness. The size of gridblocks increases distally from the wells with the largest gridblock occurring at the center of the model. Gridblocks range in size from 2.844 to 21.855 m (9.33 to 71.8 ft) with 625 cells used in the model. Gas storage and transport is characterized using a dual porosity/single permeability mechanism in which

> two-phase flow of gas and water occurs in the fracture or cleat system. The fracture system is assumed continuous and provides flow paths to producing wells. Gas flows via diffusion from the discontinuous matrix blocks into the fracture system. The two systems are coupled by use of a desorption isotherm at the matrix-cleat interface (COMET Manual, 2002).

Re-adsorption is permitted but limited to the available surface area.

Parameter descriptions for in situ coal in the Basin were partitioned into three depth divisions: 152 to 274 m (500 to 900 ft), 274 to 366 m (900 to 1,200 ft), and >366 m (>1,200 ft).

Depth intervals are measured from the surface. Surface elevation along the trend of a north-south cross section of the Illinois Basin decreases in the southern direction. Temperature and pressure gradients were obtained for each of the characteristic depth divisions based on regional data. The temperature gradient is extrapolated from surface temperature records. Carbon dioxide injection pressure is 4/5 the hydrostatic pressure of the reservoir at the depth of the coal seam.

Probability distributions of reservoir parameters were developed by examining data produced by the members of the Consortium and from the available literature. The data were partitioned into three subsets for each of the Basin depth divisions, and then data were statistically analyzed to create representative parameter distributions unique to each subset. Due to the addition of later data sets, manual skewing of populations, and other non-mathematically rigorous methods of data manipulation, these probability distributions should be considered in the more general categories of "low," "best," and "high." The use of these terms does not denote or imply specific probabilities.

Parametric Study Summary

Varying coal seam properties of CBM reservoirs were examined for their effects on ECBM production and CO_2 sequestration storage capacity from analysis of performance indicators obtained through flow modeling (COMET3).

Coal reservoir properties and the parameters necessary for understanding and defining the coal CO_2 sink were identified. The Illinois Basin was partitioned into three characteristic depth intervals (152 to 274 m, 274 to 366 m, and >366 m (500 to 900 ft, 900 to 1,200 ft, and >1,200 ft)). Parameter distributions were determined in each respective depth division. Depth intervals are measured from the surface. Temperature and pressure gradients were obtained for each of the characteristic depth divisions based on regional data. The temperature gradient is extrapolated from surface temperature records.

The distributions of coal properties were developed for the Illinois Basin from extensive databases compiled over decades by the Illinois State, Indiana, and Kentucky Geological Surveys. The coal properties examined in the parametric study included compressibility, cleat spacing, depth, gas concentration, initial pressure, CH_4 Langmuir volumes and pressures, permeability, porosity, relative permeability, temperature, and thickness.

Incorporated into this study are the results of gridblock sensitivity, which calculated the number and size of gridblocks needed to form a grid pattern. The incorporation of these results optimized computation time and removed model dependence on grid size and geometry. The resulting grid constrains the change in pore volume between adjacent cells to less than a factor of 2. The number of gridblocks was

optimized to reduce computation time while maintaining a high degree of accuracy in matching flow properties (rate and cumulative production). Additionally, the gridblock sensitivity was performed to remove model bias by eliminating the dependence of model results on the number of gridblocks used in the simulation.

Through reservoir simulation of ECBM, CH_4 recovery and CO_2 storage factors were estimated at various thermal conditions that included 50% CO_2 cut in produced gas and time at which breakthrough of CO_2 occurs at gas-producing wells. The results of reservoir simulations using the distributions of petrophysical and reservoir properties are applicable on a Basin-wide scale as indicators of performance for ECBM production and CO_2 storage. Results from this parametric study will be used to screen and prioritize laboratory experiments, locations for CO_2 sequestration, and ECBM developments in Phase II.

Performance Indicators (Recovery and Storage Factors)

Recovery and storage factors are calculated from the model output. The criterion with greatest importance was determined as a 50% CO_2 cut in the production gas stream. This criterion serves as a proxy for a possible economic limit although no economic analysis was performed.

The recovery factor (RF) is defined as

$$RF = \frac{G_{p(CH_4)}}{OGIP_{(CH_4)}} \qquad \text{Range } \{0–1\}$$

where RF is the ratio of CH_4 gas produced (G_p) to original gas (CH_4) in place ($OGIP_{CH_4}$).

The storage factor SF(OGIP) is defined as

$$SF(OGIP) = \frac{G_{inj(CO_2)} - G_{p(CO_2)}}{OGIP_{(CH_4)}} \qquad \text{Range } \{\text{all real numbers} > 0\}$$

where SF(OGIP) is a ratio of the volume of CO_2 injected into the reservoir (G_{ing}) divided by the original CH_4 gas in place (OGIP). The storage factor is defined such that any CO_2 existing as a free gas in the cleat and fracture system contributes to the sequestered gas volume, regardless of the storage mechanism (adsorbed free phase in cleats or dissolution in water).

The storage factor SF(G_s+PV) is defined with respect to the CO_2 Langmuir isotherm as

$$SF(G_s) = \frac{G_{inj\ (CO_2)} - G_{p(CO_2)}}{hA(1-\phi)G_{s(CO_2)}}$$ Range {0–1}; more precisely {0–1+ $V_{free\ gas}$)

where $SF(G_s)$ is the ratio of injected CO_2 to the total storage capacity of the coal. Due to the inclusion of any CO_2 existing in a free state, this ratio can be >1. Fracture and cleat porosity is low in most reservoirs; thus, the volume of gas that may exist in a free state within this pore volume is small, resulting in a ratio slightly >1. This condition can only occur if the coal matrix is completely saturated with CO_2.

The distributions of reservoir properties and parameters were divided into low, best, and high subsets for each depth interval. Exact probabilistic quartiles were not assigned due to the variability in data quality and availability of all necessary model input parameters. Thus, recovery and storage factors were calculated using low-, best-, and high-parameter estimates to produce simulations representing the low-, expected-, and high-member estimates. The recovery and storage factors are calculated for each of the three subdivisions using their respective distributions of reservoir properties. These performance indicators, when applied in the GIS to mapped coal seams of the Illinois Basin, enable Basin-scale calculations of recoverable ECBM and CO_2 storage capacity.

Previous Research Applied to Parametric Study

The results of previous investigations and experiments were applied to this parametric study. Volumetric equations (Appendix 1) for calculating GIP, derived to verify the internal calculations performed by the COMET model, an external method for validation of parametric study results, were applied in a GIS processing model for the Illinois Basin coals. Application of these equations to a GIS processing model enabled the calculation of ECBM gas reserves in the Illinois Basin. Utilizing recovery and storage factors calculated from the parametric study and applied to each generalized depth division, a Basin-wide estimate of recoverable ECBM gas reserves was calculated and CO_2 storage capacity was estimated. No primary CBM was assumed. Relative permeability curves were derived from analysis of data available from other productive CBM locations. Numerous methods for data conversion, analysis, and internal correctness of COMET input data were created. These included conversions to COMET input requirements (units and reporting basis), derivation of Langmuir isotherms, and internal correctness (e.g., V_L and P_L to G_{con}, degree of saturation to G_{con}, ash and moisture to pure coal densities and bulk volumes).

Parametric Study Conclusions

The parametric study is a comparison of software simulations with continuous CO_2 injection to a base case under primary production. In simulations using CO_2 ECBM recovery, injection is initialized from

the start of the simulation (no primary production). A simulation is composed entirely of values from the parameter distribution "best" estimate with a single parameter altered to the magnitude of its respective low or high distribution.

In the parametric study, the parameter with the largest effect on the magnitude (positive or negative) of RF, SF(OGIP), and SF(G_s+PV) are relative permeability, relative permeability, and absolute permeability, respectively. The parameters with the largest effect in the 152 to 274 m, 274 to 366 m, and >366 m (500 to 900 ft, 900 to 1,200 ft, and >1,200 ft) depth intervals are relative permeability, relative permeability, and co-maximums relative permeability and absolute permeability, respectively. Gas concentration is not included in the SF(OGIP) figures due to the bias introduced in the formula for calculating SF(OGIP). For example, a small initial gas concentration will result in a very large storage factor [SF(OGIP)] as this term is a ratio of sequestered CO_2 to CH_4 OGIP. A large SF(OGIP) value does not represent a greater ability to sequester CO_2, but is a result of a small initial gas concentration in the denominator (Table 1-12). A combination of relative permeability and absolute permeability is called effective permeability and is used in COMET. Indirectly both relative and absolute permeability have the same impact on SF.

Table 1-12. Results of COMET parametric study using Illinois Basin coal properties for the depth intervals of 500 to 900 ft, 900 to 1,200 ft, and >1,200 ft identifying the parameters with the greatest influence on the methane recovery factor (RF), storage facors based on initial gas in place, SF(G_p), and CO_2 storage capacity as defined by Langmuir isotherm, SF(G_s).

Parameter	500 to 900 ft		900 to 1,200 ft		>1,200 ft	
	Largest	2nd largest	Largest	2nd largest	Largest	2nd largest
RF	k_{rel}	G_c	k_{rel}	ϕ	k_{rel}, k_{abs}	ϕ
SF(G_p)	k_{rel}	pressure	k_{rel}	ϕ	k_{rel}, k_{abs}	C_p
SF(G_s)	k_{rel}	ϕ	k_{rel}	ϕ	k_{rel}, k_{abs}	C_p

The parameters with second largest impact after absolute and/or relative permeability were gas content (G_c), pressure, cleat porosity, and pore compressibility. An additional component of the study investigated the effect of changing the time during which CO_2 injection was initialized on the recovery factor. Increasing the duration of time the well produced during primary production, before CO_2 injection was commenced, increased the magnitude the recovery factor would achieve by the end of the simulation. The end of the simulations was set at a fixed time of 30 years.

Performance Indicators Applied to Basin-Scale Volumetric Calculations of ECBM and CO_2 Storage Capacity

Models were developed to produce low, best, and high estimates of recoverable CBM and CO_2 storage capacity in each of the three depth intervals. Low, best, and high simulation cases were created using only the input parameters from their respective parameter ranges. Thus, unlike the parametric study, the

simulations are composed of values from only one parameter range. Therefore, the previous performance indicators derived from the parametric study cannot be applied directly to the Basin-scale volumetric calculations.

The performance indicators obtained from the low, best, and high estimates from each of the three depth intervals are applied in a GIS processing model for the Illinois Basin coals to calculate Basin-scale volumetric estimates. For all depth intervals, recovery factor tended to increase for both primary and ECBM when a parameter's magnitude is changed from its "low" to "high" distribution. The incremental RF (total RF – primary RF) has an opposing trend. Only the deepest division (>366 m (>1,200 ft)) deviates slightly from this trend. Thus, from analysis of the incremental recovery results, it can be concluded that the greater the primary recovery, the less incremental benefit CO_2 injection will produce. According to model results, application of enhanced CO_2 recovery yields the maximum benefit when the predicted recovery under primary production is low.

The storage factors [SF(OGIP) and SF(G_s)] increase in magnitude as RF increases for all simulation depth intervals; there is a small deviation from the trend in the >366-m (>1,200-ft) depth interval. This result is expected when examining the volumes and gases adsorbed to the coal. As primary recovery increases, more of the OGIP is produced, effectively creating adsorption sites. This increases the volume available to sequester additional CO_2, thereby increasing the storage capacity and resultant storage factors.

In simulations of primary production, the average reservoir pressure decreases below the desorption pressure for the majority of the simulation. In simulations using CO_2 injection without a primary production period, the average reservoir pressure does not drop below the desorption pressure. Thus, there are two mechanisms utilized to produce gas. In simulations under primary production, gas desorption occurs by pressure reduction. In simulations using CO_2 injection, gas is desorbed through competitive absorption, whereby CO_2 is preferentially absorbed into the coal matrix, and CH_4 molecules that are adsorbed to the coal matrix are displaced.

Applications and Future Research

As production data become available, history matching field data from the Hon #9 CBM test well in northeastern White County, Illinois, with the COMET CBM simulator provides the opportunity to compare field data to simulator results from the statistical distribution of parameters and the test well specific data.

Volumetric equations for calculating OGIP, derived to verify the internal calculations performed by the COMET model, were applied to GIS models of the Illinois Basin, enabling a calculation of ECBM gas

reserves in the Illinois Basin. Using recovery and storage factors, calculated from the parametric study and applied to each generalized depth division, a Basin-wide estimate of recoverable ECBM gas reserves and CO_2 storage capacity was estimated.

Development of Individual Coal Sink Fairway Maps from Simulation Results Using GIS

Screening of Coalbeds for ECBM/CO_2 Consideration

Previous assessments of Illinois Basin coal resources demonstrate over 258 billion tonnes (284 billion tons) of remaining identified resources (Demir et al., 2004). For Illinois, the seven seams assessed in this study constitute almost 98% of the state's total remaining identified resources, and the percentage is likely the same for the entire Illinois Basin. If half of these resources were recovered, mining could proceed at double the current rate (2004) for more than the next 128 years. Thus, the deepest coal resources, which cost the most to mine, and thinnest resources, which are the least accessible to underground mining machinery, will be mined after shallower and thicker coals are mined, if at all. It is these economically and technically less attractive coal resources in the deep Basin fairway that were used in the volumetric estimations of recoverable ECBM and CO_2 storage potential and that were identified as potential ECBM field validation test sites.

Consequently, Basin-wide coal thickness and depth screening criteria were imposed on coal seam gas volume estimations (Figure 1-17). The actual sequestration-related screening criteria for designating

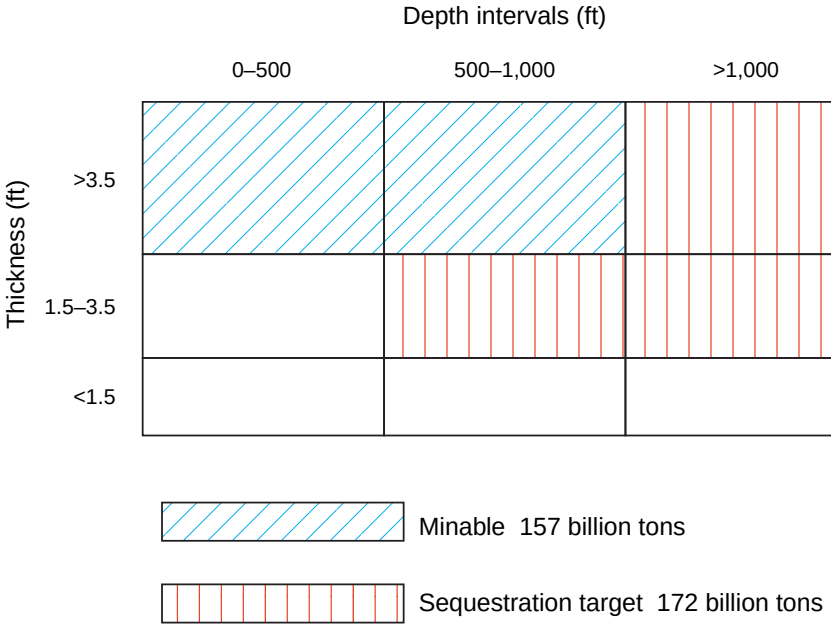

Figure 1-17 *Basin-wide coal thickness and depth screening criteria.*

certain areas of a coal seam as less desirable for mining, or "unminable," were determined after considering numerous options. In addition to those criteria related to the technical or economic limitations of mining, the implication is that, by infusing the coals with CO_2, seams that might otherwise be minable at some future time will be rendered unminable unless the CO_2 is later removed. Although shallower coals (<152 m (<500 ft)) may provide CH_4 gas production, these shallow coals were not used in the CO_2 sequestration estimations because of their future mining potential, and because of CO_2 migration-related or safety concerns. Although mines may operate at these depths or greater, coal seams >305 m (>1,000 ft) deep are considered the least amenable to underground mining for the purposes of this study. Coals that are too thin (<1.1 m (<3.5 ft) thick) likely will not be underground mined regardless of depth (Wood et al., 1983; Hatch and Affolter, 2002). Coals <0.46 m (<1.5 ft) thick were considered to be impractical sequestration targets because of operational reasons that preclude accurate perforating and stimulating. Therefore, coal seams <0.46 m (<1.5 ft) thick were not used for sequestration, regardless of depth. Coal seams <305 m (<1,000 ft) deep with thicknesses suitable for underground mining (>1.1 m (>3.5 ft)) were not considered as potential CO_2 sequestration targets.

Therefore, as summarized in the section Set Criteria And Determine Uneconomic Coal Seams, the criteria for sequestration fairway screening in the GIS evaluation were as follows:

1. 91 to 152 m (300 to 500 ft) deep—no CO_2 sequestration, CBM target.
2. 152 to 305 m (500 to 1,000 ft) deep—sequestration/ECBM target in coals between 0.46 and 1.1 m (1.5 and 3.5 ft) thick.
3. >305 m (>1,000 ft) deep—sequestration target in coals >0.46 m (>1.5 ft).

Due to differences between the state surveys' minimum coal thickness definitions in previous studies, 14 inches was used as the minimum thickness for some seams that were newly mapped at the Basin-wide scale.

GIS Methodology to Estimate Potential Gas Volumes

As stated in the previous section related to COMET modeling (Estimate Sink Capacity for Coal Seam Storage), three CO_2 storage mechanisms were identified for coalbeds: matrix adsorption, free-phase (vapor), and dissolution in water. The predominant mechanism is the adsorption of CO_2 to the coal matrix; secondary mechanisms are free-phase CO_2 (vapor) in the cleats and dissolved CO_2 in formation water present in the cleat system. Because the cleat system pore volume is relatively minor within Illinois Basin coals, any CO_2 stored in the cleat system is expected to be minor compared with that held by adsorption.

Because very few CO_2 ECBM projects exist in the world, no specific ECBM screening criteria were available to use for Basin-wide screening of coals. Furthermore, the CBM industry in the Illinois Basin is only beginning, so little CBM production experience is available for use in this assessment. However, the Illinois Basin has a historically active coal mining industry so that coal resource and coal bulk volume studies exist. As such, to estimate ECBM and CO_2 storage capacity in the Illinois Basin, volumetric estimates were made from previous coal resource studies or from coal resources newly mapped for this assessment. Because the volume of ECBM and CO_2 storage is dependent on the OGIP, a volumetric OGIP study was conducted as part of this study. All of the OGIP is not recoverable, and the entire coal bulk volume cannot sequester CO_2 at saturated conditions, so the volumetric estimate was discounted for recovery and storage efficiency as determined by the COMET modeling.

Coal resource (thickness) map data were the principal component in the GIS analysis, and data were input as GIS layers of average thickness ranges defined for the areal extent of each coal seam studied. To approximate a continuous surface, coal elevation contours were used in the calculation of finely gridded coal depth maps to aid GIS-based depth screening and the assignment of parameters classified by depth range for spatial calculation. The distribution of data for ash content was deemed adequate for mapping and was used with the coal area and thickness GIS layers for each coal seam. In addition, coal density, moisture content, adsorptive capacity, and degree of saturation were required to estimate GIP and storage capacity; however, these parameters were spatially inadequate for mapping, so average values were used for all coal seams.

Seam-specific calculations for the estimation of CBM OGIP, recoverable ECBM, and CO_2 storage capacity were performed at the one-acre, two-dimensional grid cell level using ArcGIS ModelBuilder with raster (GRID) tools and functions. Based on the input data required for COMET modeling, GIS calculations were performed using grouped sets of average input parameters based on three subdivisions of depth range within the coals. The calculations were performed for three trials based on low, best, and high estimates of the input data, which were used, respectively, as an aid in calculating potential gas volumes. Specific details regarding the input data, assumptions or limitations, and equations used can be found in the section that follows or are listed in Appendix 1.

The final results indicate ranges of 1.6 to 4.6 billion tonnes (1.8 to 5.1 billion tons) of CO_2 potentially sequesterable in coals and 0.085 to 0.309 trillion m^3 (3.0 to 10.9 trillion scf) of CH_4 recoverable as a result of CO_2 sequestration. Best estimates are 3.6 billion tonnes (4 billion tons) and 0.19 trillion m^3 (6.7 trillion scf), respectively (Table 1-13).

GIS Detailed Methodology

Component Data Sets Input into GIS Calculations

Basin-wide polygon layers for coal resources and coal quality were sourced from previous mapping studies or from data newly compiled, merged, and mapped under Subtask 4.1 of this study; tabular data on CBM/CO_2-related parameters were utilized as average data for coal depth-range subdivisions. A two-dimensional grid of surface elevation was also used as part of the calculations, and the original USGS 90-m digital elevation model (DEM) files were merged for the Illinois Basin regional area and reprocessed to approximately 1-km cells by the Kentucky Geological Survey as part of a previous study.

Develop GIS Processing Model

A GIS processing model in ArcMap ModelBuilder was developed, tested, and implemented based on the Langmuir gas content-related calculations (Estimate Sink Capacity For Coal Seam Storage section), to be run for individual coal seams. An example GIS flow chart is shown in Figure 1-18. Calculations were

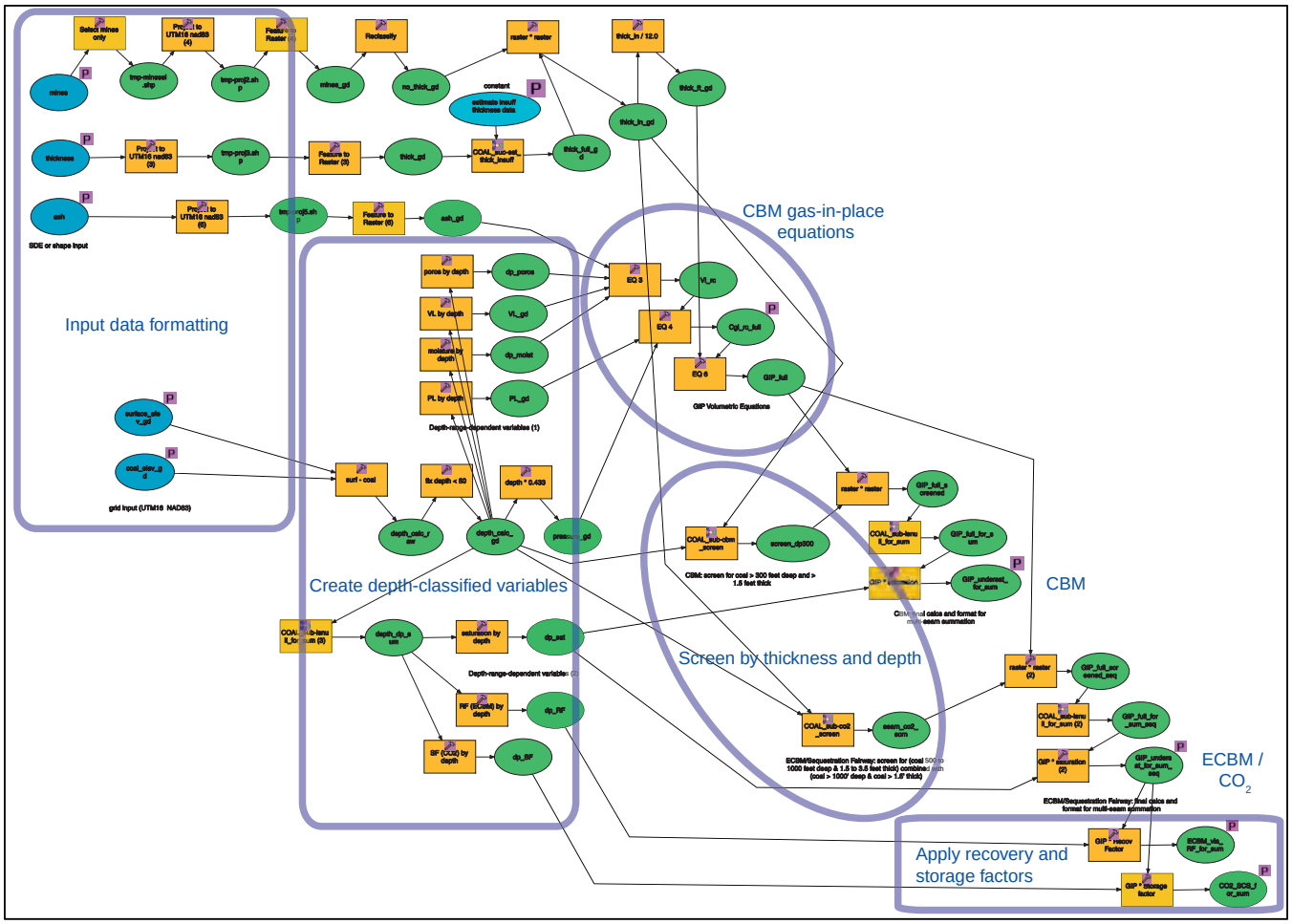

Figure 1-18 *MGSC coal screening and gas calculations GIS model.*

performed spatially for specific depth-range subdivisions, based on parameters necessary for modeling in COMET, for the low, best, and high estimates. These depth-classified, average data values were used spatially in the GIS calculations along with two-dimensional grid data. All data parameters were incorporated as input variables to the model, and the model was replicated for each seam. Data were input specifically for each seam, and all seams were run in succession via a second batch-processing model—once for each of the low-, best-, and high-estimate scenarios.

Grid Calculations Implemented in the GIS Processing Model

All input polygons or grids were re-projected to a common working coordinate system in ArcMap (UTM Zone 16, NAD83). Coal elevation contour lines were converted to a continuous-surface grid using ArcMap's Topo-to-Grid tool; the resultant coal elevation grid was subtracted from surface elevation to get a finely gridded coal depth map. Other polygon layers (e.g., coal thickness, ash content, mined areas) were converted to grids, and mined areas (equal to 0 coal thickness remaining) were subtracted from the thickness grids. Using approximately seam mean thickness minus one standard deviation, coal thickness was estimated for areas of known or inferred coal yet with insufficient thickness data available.

Depth-dependent variables were incorporated into the GIS calculations via a reclassification of the depth grid map to create other maps such as porosity. These depth-classified variables were changed in the GIS processing model for each particular estimation (low, best, high). The formulas for GIP calculations were added to the processing model, and GIS polygon and grid components were inserted into the formulas within the processing model interface; spatial calculations were performed per 4,046.873-m^2 (one-acre) grid cell, and then the result was screened by coal thickness and depth considerations to select for sequestration fairway coal areas. The CO_2 storage factors (from COMET modeling) were applied to the calculated GIP by depth classification to obtain potential CO_2 storage. Similarly, ECBM recovery factors were also applied to the calculated GIP to obtain the potential recoverable ECBM from CO_2 sequestration.

Tabulations and Final Data Results

Seam-specific grid results were saved and tabulated in ArcMap to obtain Basin and state totals; grid results for all seams were spatially summed to obtain total Basin and state totals for coal. For final formatting, grids were converted to polygons, and individual grid cell values were dissolved into average value per acre ranges to simplify polygons. A descriptive legend data field was added to the data layer attributes to supplement the integer values. The GIS calculation process and files were documented, and metadata were created. Final layers were re-projected to Geographic Decimal Degree NAD83 for archiving into ArcSDE, and shapefiles were exported from ArcSDE for data transfer.

Additional Discussion Regarding GIS Methodology

As just stated, coal thickness was estimated for certain areas where coal resource information is sparse but where the coals were known or thought to be present, based on previous structural mapping studies, and identification on electronic logs. Simply omitting these areas, as is done in mapping calculations for remaining *identified* coal resources, would underestimate the potential GIP. To incorporate the potential additional gas in these areas, a conservative low estimate of coal thickness for these areas was included in the calculations. Where available, seam mean thickness minus one standard deviation was obtained from the seam's raw thickness data points and assessed Basin-wide; if no thickness data points were readily available, the mode of the averaged thickness ranges from the grid cells was used. Further drilling is warranted in these areas to verify the minimum estimated coal thickness.

Additionally, new resources were preliminarily mapped under this study for the Hymera/Jamestown/Paradise, Survant, Colchester, and Seelyville/Davis/Dekoven seams. For coals >91 m (>300 ft), areas of estimated thickness plus the newly mapped coal resources were estimated to add approximately 15% to the published bulk coal resource; however, thickness and depth screening criteria applied in the delineation of the CO_2 sequestration fairway coals ultimately decreased the assessed coal resources for CO_2/ECBM consideration to approximately 60% of the previously published coal-resource tonnage (284 billion tonnes) for the Illinois Basin. Comparatively, the bulk volumes of coal available for CBM production and CO_2 sequestration and ECBM recovery as assessed in this study are approximately 298 and 156 billion tonnes (329 and 172 billion tons), regardless.

In select local areas in northwestern Illinois, ECBM/CO_2 results may be based on coal that, in the drillhole data, is actually less than 152 m (500 ft) deep (minimum depth for CO_2 sequestration potential) due to limited regional drillhole information in this area. This contributed a very small amount to the gas resource.

Results

The final results indicate ranges of 1.6 to 4.6 billion tonnes (1.8 to 5.1 billion tons) of CO_2 potentially sequesterable in coals and 0.07 to 0.28 trillion m^3 (3.0 to 10.9 trillion scf) of CH_4 potentially recoverable as a result of CO_2 sequestration (Table 1-13). The best estimate case shows that coals in the Illinois Basin are estimated to potentially store about 3.6 billion tonnes (4 billion tons) of CO_2 and produce about 0.17 trillion m^3 (6.7 trillion scf) of ECBM, of which the seam-specific components are shown in Table 1-14. Figure 1-19 shows the total CO_2 storage potential, and Figure 1-20 shows ECBM gas values.

Table 1-13. Low-to-high estimates for enhanced CH_4 production and CO_2 storage potentials in Illinois Basin coals.

Illinois Basin estimates	ECBM recoverable (billion scf)	CO_2 storage (billion scf)	CO_2 storage (million tonnes)
Low	3,041	30,315	1,608
Best	6,680	68,550	3,637
High	10,892	86,066	4,566

Table 1-14. Best estimates for enhanced CH_4 production and CO_2 storage potential in Illinois Basin coals.

Illinois Basin seam	ECBM recoverable (billion scf)	CO_2 storage (billion scf)	CO_2 storage (million tonnes)
Danville/Baker	807	8,299	440
Hymera/Jamestown/Paradise	200	2,073	110
Herrin	903	9,758	518
Springfield	1,252	13,511	717
Survant	1,081	10,978	582
Colchester	1,274	12,583	668
Seelyville/Davis/Dekoven	1,163	11,349	602
Illinois Basin total	6,680	68,550	3,637

The ECBM recoverable and CO_2 storage potentials for the coals in total are shown to be greater (on average, per acre) toward the deeper, center area of the Basin where a higher number of seams are stratigraphically present, and thus where the total coal thickness is the greatest (Figure 1-21). Seam-specific ECBM and CO_2 storage potential maps exhibit a strong visual correlation to fairway areas screened by coal thickness and depth criteria, and to the inherent spatial data utilized in the gas-content calculations (Appendix 1).

Discussion and Comparison to Previous Results

Previous Illinois Basin CBM estimates ranged from 0.14 to 0.71 trillion m^3 (5 to 25 trillion scf) (Archer and Kirr, 1984; Demir et al., 2004); the present study approximated the OGIP as 0.626 trillion m^3 (22.1 trillion scf), of which 41% is considered an ECBM target. The MGSC-updated OGIP for the Illinois Basin coals compares well with previous rigorous estimates. The MGSC study overall added new coal volume to previously mapped coal seams for the assessment of OGIP while observing a minimum coal depth of 91 m (300 ft). The gas recovery factor (CBM produced compared to the original CBM in place) for our best estimate case using typical coal properties ranged from approximately 70 to 78% as applied to the seam depth partitions; the storage factor (CO_2 in place compared to the original CBM in place) for the same case was approximately 0.18 to 0.21 billion m^3 (7.0 to 8.2 billion scf) (CO_2) per 0.0283 billion m^3 (1.0 billion scf) CBM, which corresponds to approximately 88 to 90% of the CO_2-saturated gas concentration. The value of these storage factors is very high compared to the Langmuir isotherm CO_2/CH_4 ratio; however, when compared to the undersaturated gas content, the values compare well.

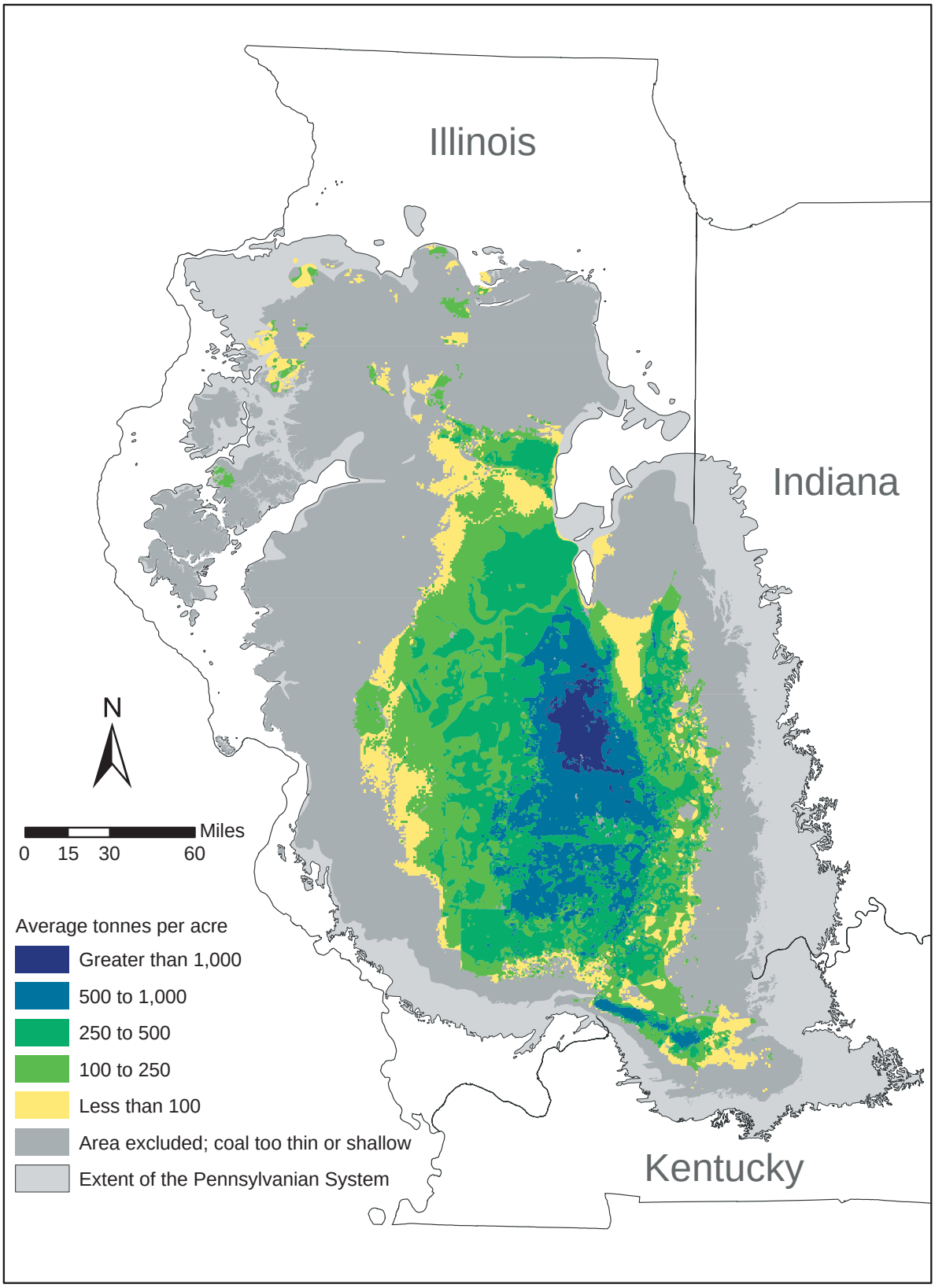

Figure 1-19 *Total CO_2 storage potential for all coals included in this study.*

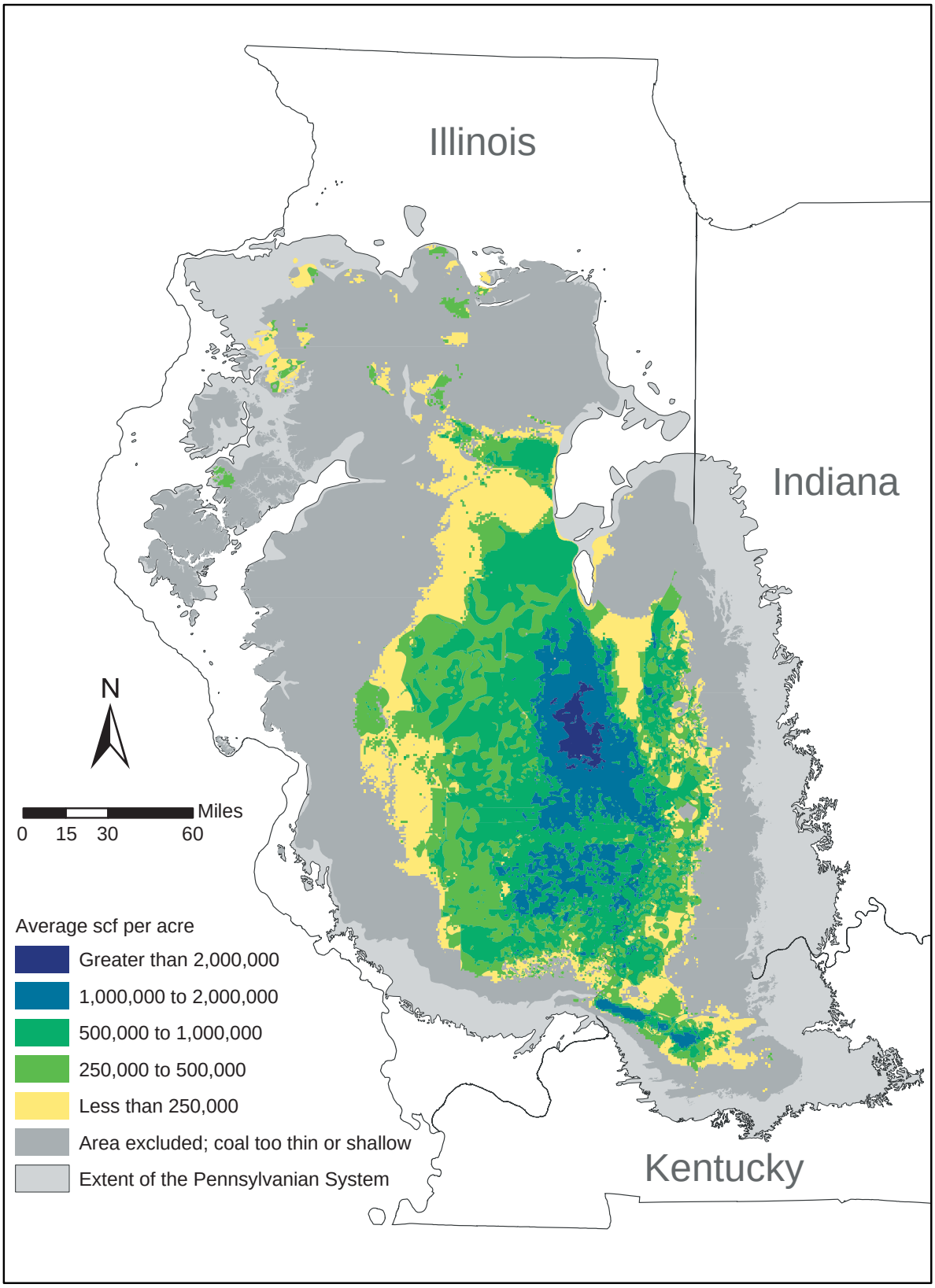

Figure 1-20 *Total potential ECBM recovery for all coals included in this study.*

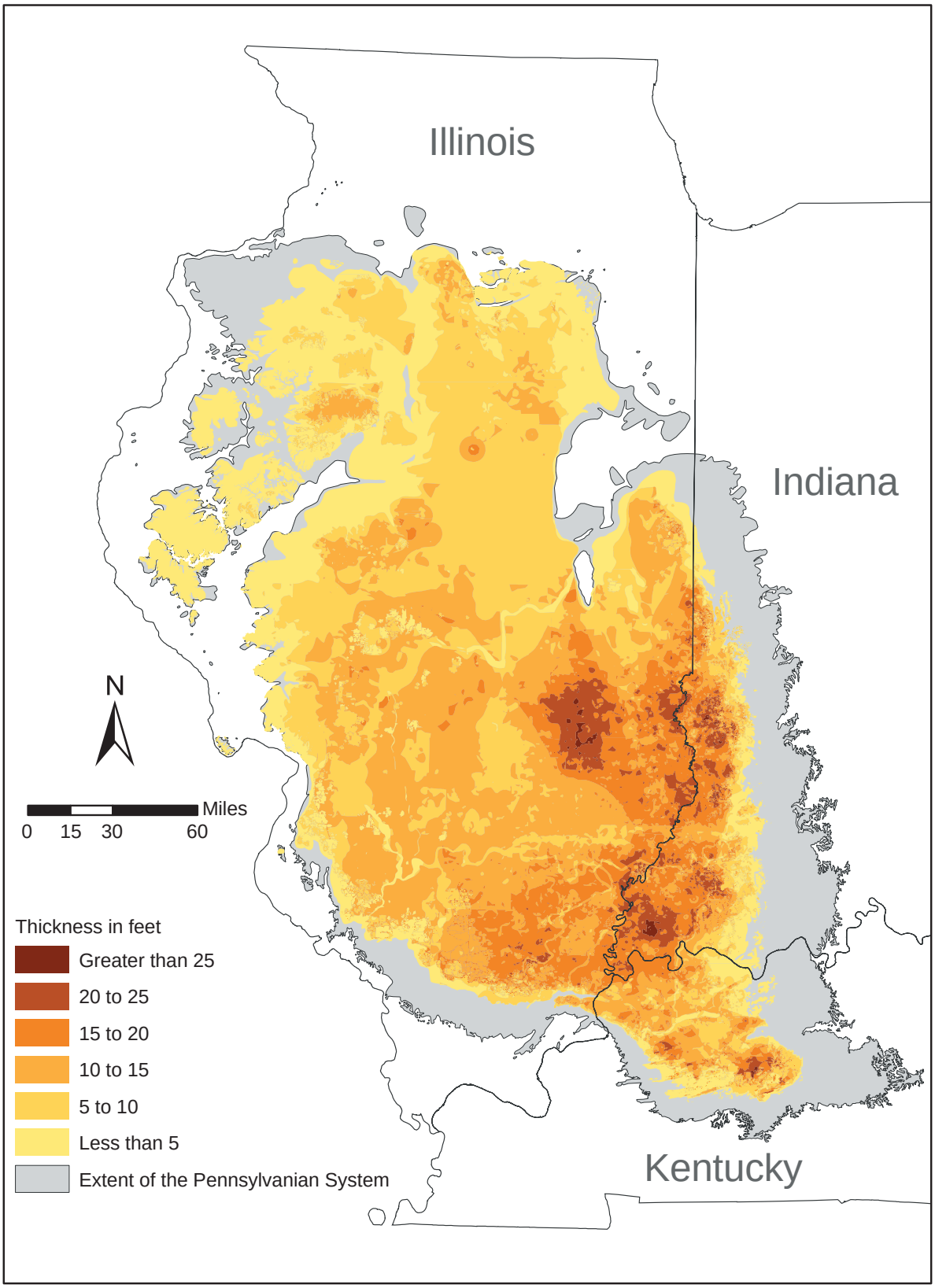

Figure 1-21 *Cumulative average thickness of all coals included in this study.*

The methodology used in the previous MIDCARB project for estimating CO_2 storage potential in coal assumes that all of the coal is 100% saturated with CO_2 and that no free-phase or aqueous dissolved CO_2 exists in the cleat system. The MGSC estimate includes all storage mechanisms and recovery and storage efficiency terms. Using the MIDCARB formulations, an estimate of 3.9 billion tonnes (4.3 billion tons) of CO_2 storage capacity is made, which coincidentally compares well with the MGSC estimate because the bulk coal volumes are substantially higher for the MGSC study.

Isotopical Characterization of In-place CO_2 (Subtask 4.8)

Isotope Geochemistry: Background

Isotopes are atoms of the same element that have a different number of neutrons in the nucleus. The stable carbon isotopes, ^{12}C and ^{13}C, and the radioactive isotope, ^{14}C, can be used to characterize and monitor CO_2 injected into the subsurface. The carbon isotopic composition of the injected CO_2 (depending on the source) should be significantly different from dissolved CO_2 in the subsurface deposits of the chosen site. The isotopic composition of a formation fluid depends on its geochemical history, such as the extent of carbonate equilibrium, CH_4 formation, and redox reactions associated with buried organic matter.

The half-life of ^{14}C is about 5,730 years, and the isotope can be used to date carbon material to about 45,000 to 50,000 years old. Material that is millions of years old such as oil, coal, and natural gas (associated with petroleum generation) should consist of no detectable ^{14}C. In geochemical studies, ^{14}C is often reported as percent modern carbon (pMC). The amount of ^{14}C naturally present in the atmosphere in 1950, prior to atmosphere testing of nuclear devices, is defined as 100 pMC. As groundwater moves down through the soil zone, away from atmospheric equilibrium and into the subsurface geology, rocks such as limestone and dolomite, which are millions of years old, begin to dissolve, diluting the ^{14}C content and changing the stable carbon isotope composition of the dissolved inorganic carbon (DIC). Other geochemical reactions, such as oxidation of old, buried organic matter and CH_4 generation will also dilute the ^{14}C content and alter the ^{13}C and ^{12}C composition of the DIC.

The stable carbon isotopes are measured as ratios of the least abundant isotope (^{13}C) to the most abundant isotope (^{12}C) in the sample and compared to the same isotope ratio in the international standard material, PeeDee Belemnite (PDB). The results are reported in the delta (δ) notation as per mill (parts per thousand, ‰) differences to the standard material:

$$\delta\,^{13}C = ([(^{13}C/^{12}C)_{sa} - (^{13}C/^{12}C)_{std}] / (^{13}C/^{12}C)_{std})1{,}000.$$

Thus, the results can be either negative or positive values depending on whether the sample has less or more of the heavier isotope ^{13}C compared with PDB.

Certain processes in nature fractionate, or partition, isotopes differently between compounds. For example, processes that produce CH_4 and CO_2, such as microbial methanogenesis, result in the CH_4 containing significantly more of the ^{12}C isotope while the CO_2 contains more of the ^{13}C isotope. Thus, the CO_2 will have a more positive $\delta^{13}C$ value while the CH_4 will have a more negative value. Photosynthesis also causes isotopic fractionation of CO_2, resulting in the plants having more negative $\delta^{13}C$ values than found in atmospheric CO_2. Thus, the $\delta^{13}C$ of different types of organic or inorganic carbon in the subsurface may have very different values. During Phase I, the isotopic composition of many different sources of CO_2 was measured.

Isotopic CO_2 Characterization from Various Sources

The isotopic characterization of CO_2 from several different sources, including coal seams, a refinery, ethanol manufacturers, fossil-fuel-burning power plants, and groundwater were completed. The results showed significant differences in the stable carbon isotopes ($\delta^{13}C$) and ^{14}C activity of each source. The isotopic composition of CO_2 from the refinery and from the combustion of natural gas showed the greatest separation compared with the range of isotopic compositions for DIC of groundwater and the expected values for soil CO_2. The refinery and natural gas combustion CO_2 sources had the most negative $\delta^{13}C$ values and very little ^{14}C activity. The isotopic composition of the CO_2 from the ethanol manufacturing plants was very different from the fossil-fuel sources of CO_2 but had composition similar to the range of values expected for soil CO_2 and had $\delta^{13}C$ values similar to that observed in the DIC of groundwater. The DIC of groundwater has a wide range of ^{14}C activity and $\delta^{13}C$ values, depending on the age of the water and its geochemical history. The CO_2 released from the pores of coal seams had ^{14}C concentrations <20 pMC and relatively positive $\delta^{13}C$ values; the CO_2 from the combustion of coal had very low ^{14}C activity (~ 1 pMC) and relatively negative $\delta^{13}C$ values. Following is a more detailed description of the isotopic results obtained from the different sources of CO_2 sampled. New samples of dissolved CO_2 associated with crude oil or deep brines from the Illinois Basin were not available. However, $\delta^{13}C$ and ^{14}C data of DIC in brines from the Michigan Basin and a few $\delta^{13}C$ values from Illinois Basin brines sampled in southern Illinois and one for CO_2 collected from a brine well in central Illinois were included.

The CO_2 released from the pores of coal-seam samples contained variable isotopic compositions. Gases from core samples representing five different coal seams obtained from two drill holes were collected; one located in White County and the other four in Jasper County, Illinois. The depths of the coal seams sampled in Jasper County were significantly deeper than those in White County (Table 1-15). Samples

of the cores from each coal seam were placed into aluminum canisters and sealed (Demir et al., 2004). The gases released from the coal samples were collected and analyzed on a gas chromatograph, and the CO_2 was separated and purified for isotopic measurements. The $\delta^{13}C$ and ^{14}C of the CO_2 fraction were analyzed. The $\delta^{13}C$ ranged from +7.4 to –1.2‰, with one outlier that had a –11.1‰ value. The ^{14}C activity ranged from 3.8 to 9.7 pMC, with one outlier that had an activity of 18.5 pMC. The following are the isotopic results for each of the coal seams measured. The ^{14}C activities are greater than expected and may be an artifact of the sampling/handling process. The canisters contained air before the core samples were placed inside, and the tubing leading from the valves on the canisters also contain air prior to releasing the gas from the canisters. Thus, some atmospheric CO_2 contamination probably occurred in each sample.

Table 1-15. Isotopic composition of CO_2 released from samples of coal.

Sample ID	County	Depth (m)	% CO_2	^{13}C CO_2	^{14}C (pMC)
Danville-coal-gas	White	118.0	2.15	1.6	13
Herrin-coal-gas	White	137.5	2.12	4.9	8.31
Springfield-coal-gas	White	162.5	1.31	0.7	9.66
Davis-coal-gas	White	248.7	1.13	-11.1	18.5
Excello Shale	White	183.2	0.25	NA[1]	NA[1]
Danville-coal-gas	Jasper	362.1	2.24	-1.21	3.8
Herrin-coal-gas	Jasper	374.9	2.6	1.36	5.78
Seelyville-coal-gas	Jasper	456.3	2.23	7.35	5.98

[1]NA, not analyzed due to insufficient CO_2 concentration.

The CO_2 collected from the refinery exhibited the lowest ^{14}C concentration. This source was expected to exhibit very little if any ^{14}C since the source of carbon is oil, which is typically many millions of years old. The very small amount of ^{14}C detected in this sample probably reflects contamination of the sample by a small fraction of air that either penetrated the manufacturing process or leaked into the sample container during sample collection/handling. The results of the isotopic measurements for the CO_2 from the refinery plant are shown in Table 1-16.

Table 1-16. Isotopic composition of CO_2 from a refinery plant using crude oil.

Sample ID	County	% CO_2	^{13}C CO_2	^{14}C (pMC)
Refinery Plant (3/17/05)	Madison, IL	81.05	-36.4	0.19

The $\delta^{13}C$ values obtained for the power-plant stack gases were typical of different fuel sources (Table 1-17). Because the power plants burned fossil fuels, very little ^{14}C detection for the CO_2 collected from the stack gases was expected. However, approximately 1 pMC was detected in the CO_2 of the coal-burning power-plant stack gases, which probably represents contribution of atmospheric CO_2 from the air used

for combustion of the fossil fuel and/or some air contamination introduced during the sampling/handling process. The ^{14}C activity of the natural-gas-burning power plant was larger than that observed for the coal-burning power plants, possibly because of less CO_2 concentration in the natural-gas-burning stack gases, resulting in a larger contribution of atmospheric CO_2 contamination and, thus, greater ^{14}C activity.

Table 1-17. Isotopic composition of CO_2 from fossil fuel power plants.

Sample ID	County	Fuel	% CO_2	^{13}C CO_2	^{14}C (pMC)
051905 Meredosia	Morgan, IL	Sub-bituminous coal	12	-24.6	1.06
063005 Meredosia	Morgan, IL	Bituminous coal	9.1	-25.9	0.92
080205 Kinmundy	Marion, IL	Natural gas	2.7	-39.6	4.92

The isotopic composition of the CO_2 from the combustion of coal is quite different from that of the CO_2 released from the pores of the coal-seam samples discussed earlier (Table 1-15). Typically a significant amount of CH_4 is associated with buried coal seams, and during CH_4 production, CO_2 is also generated. As mentioned in the section Isotope Geochemistry: Background, stable isotopes are fractionated in different proportions during CH_4 generation. The light carbon isotope (^{12}C) is concentrated in the CH_4, resulting in a more negative isotopic composition and causing the heavier carbon isotope to be concentrated in the associated CO_2, which explains the relatively positive $\delta^{13}C$ values observed for the CO_2 with the coal-seam gas samples. In addition to the possible contamination with atmospheric CO_2 discussed earlier, the CO_2 present in the in situ coal-seam pore spaces would be in equilibrium with the DIC of the surrounding groundwater, which also helps explain why greater ^{14}C activity for the coal gas CO_2 compared to the very low ^{14}C activity of the CO_2 associated with the combustion of coal was observed (Table 1-17).

The isotopic results for CO_2 produced at the ethanol manufacturing plants were quite distinct from the CO_2 from coal seams or that produced from refineries and the fossil-fuel power plants. As expected, the CO_2 from the two ethanol plants had isotopic results that were typical of CO_2 produced from recently harvested corn. The results of the isotopic measurements for the CO_2 from the ethanol plants are shown in Table 1-18.

Table 1-18. Isotopic composition of CO_2 from fermentation plants producing ethanol.

Sample ID	County	% CO_2	^{13}C CO_2	^{14}C (pMC)
080404- CO_2	Tazewell, IL	93.82	-10.5	105.2
033005- CO_2	Daviess, IN	85.05	-10	105.8

Groundwater was sampled from residential water wells located in west-central Illinois, one of which contained excessive amounts of CO_2. There was a problem of copper corrosion at the house that was

apparently caused by the elevated CO_2 in the well water, which caused the water to be acidic, resulting in pipe corrosion problems. Because this type of problem could have an impact on subsurface CO_2 sequestration activities, the $\delta^{13}C$ and ^{14}C composition of the DIC was measured. The $\delta^{13}C$ and ^{14}C results for the DIC in two residential water wells, one with excessive CO_2 levels (072304-1), are shown in Table 1-19. The isotopic composition of the DIC in the groundwater from these wells is similar to that of other relatively shallow groundwater from central Illinois.

Table 1-19. Isotopic composition of DIC from groundwater in west-central Illinois.

Sample ID	County	Producing depth (ft)	CO_2 (atm)	$^{13}C_{DIC}$ (‰)	$^{14}C_{DIC}$ (pMC)
072304-1	Henry	155–302	0.081	-8.69	64.2
072304-2	Henry	~200–250	0.031	-7.52	50.7

Isotopic Characterization Summary

The results obtained in this reconnaissance study indicate that isotope characterization will be quite useful for distinguishing sources of CO_2 collected in the vicinity of Phase II injection pilots and in the future for a CO_2 sequestration industry. The isotopic composition of CO_2 from the different sources sampled show good separation when these data are plotted on a graph of ^{14}C versus $\delta^{13}C$ (Figure 1-21).

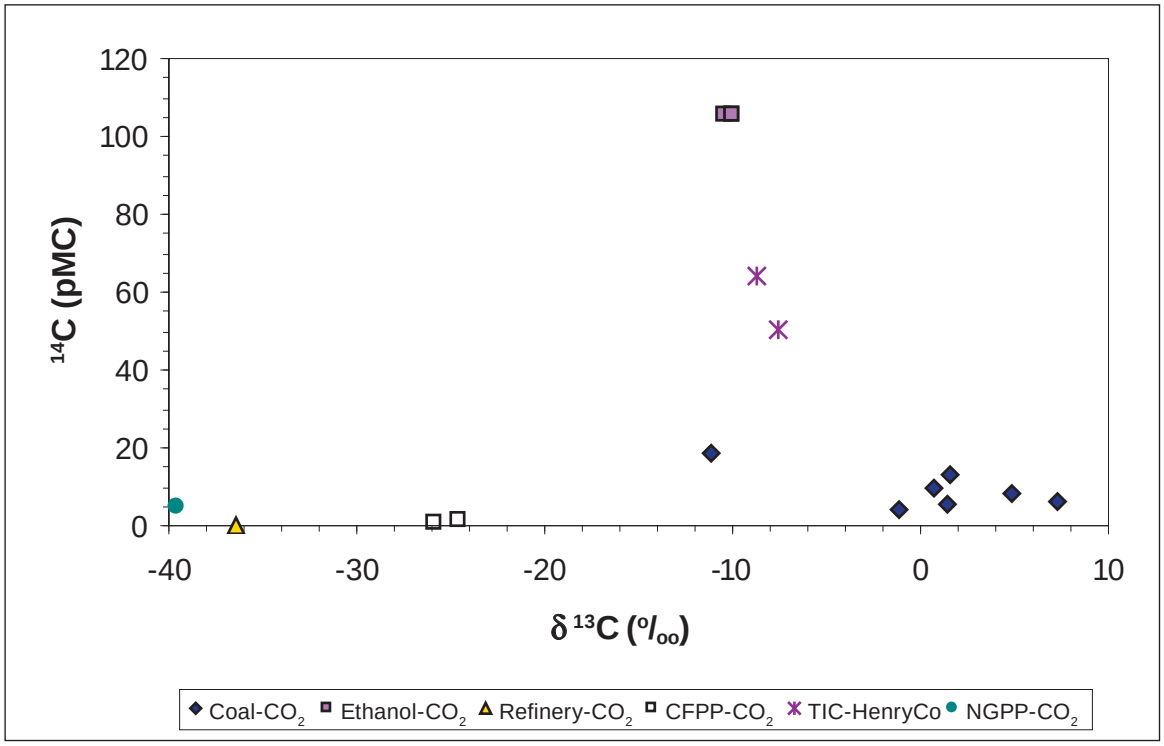

Figure 1-21. *Plot of $\delta^{13}C$ and ^{14}C for different sources of CO_2 sampled. Coal-CO_2, CO_2 released from coal seams; ethanol-CO_2, CO_2 from ethanol manufacturing plant; Refinery-CO_2, CO_2 from petroleum refinery plant; CFPP-CO_2, coal-fired power plant; TIC-HenryCo, total inorganic carbon from groundwater in Henry County, Illinois; NGPP-CO_2, natural-gas-fired power plant).*

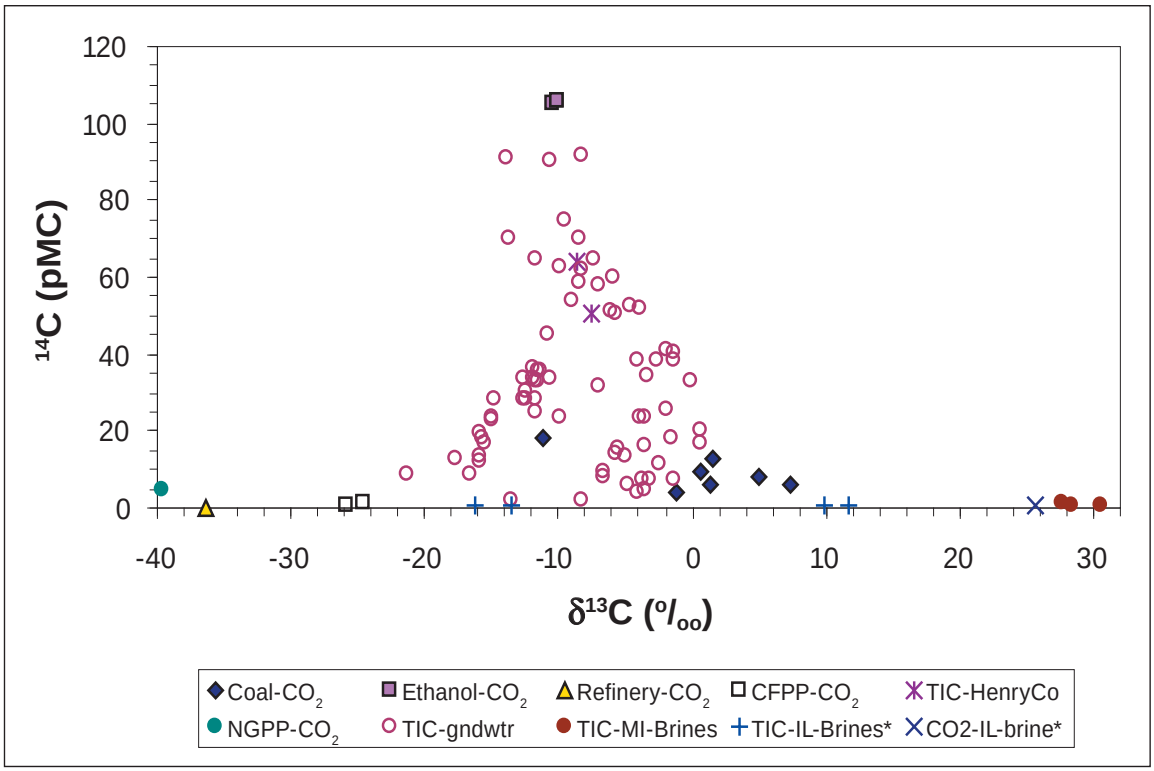

Figure 1-22. *Plot of $\delta^{13}C$ and ^{14}C for various sources of CO_2, total DIC of groundwater (Hackley, 2002), total inorganic carbon (TIC) for Michigan brines (MI-Brines) (Walter et al., 1996), TIC for Illinois brines (IL-Brines) (Hwang, 1996), and typical ranges expected for the different sources discussed in text. Asterisk indicates the ^{14}C values are estimated. CFPP, coal-fired power plant; NGPP, natural gas power plant.*

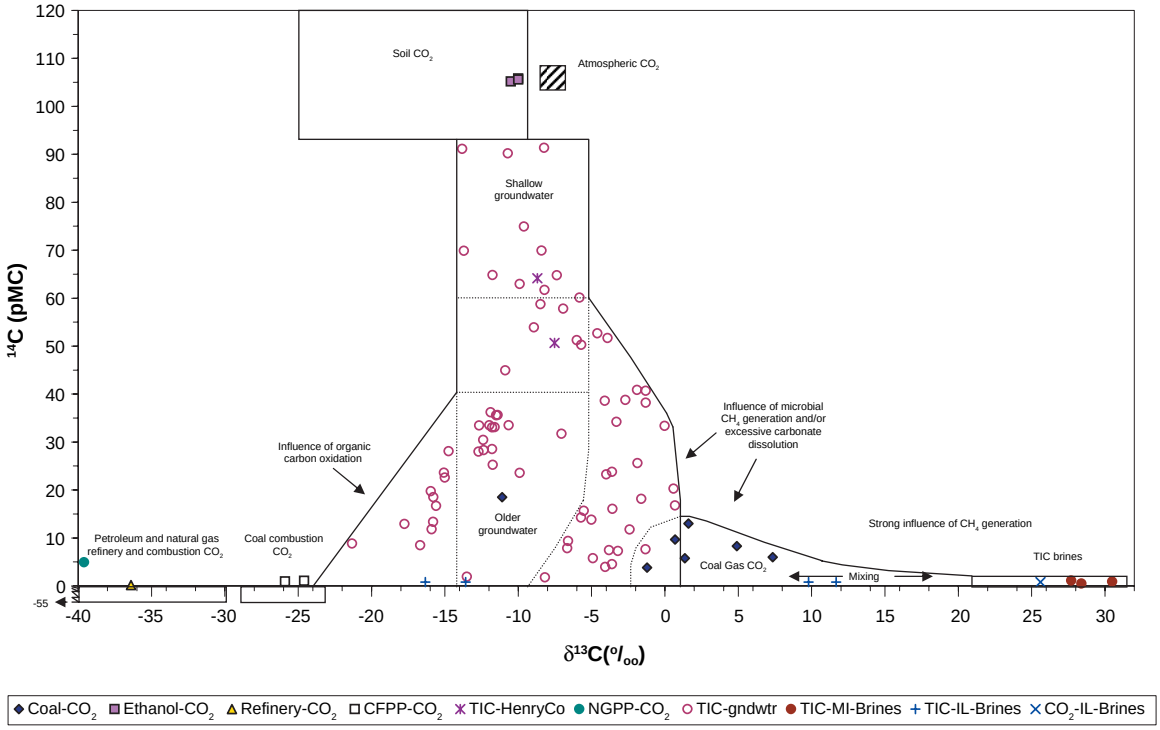

Figure 1-23. *Plot of $\delta^{13}C$ and ^{14}C for various sources of CO_2 (from Figure 1-18). Descriptions help define different regions of the figure, depending on the sources of CO_2 or total DIC (TIC) involved.*

The isotopic composition of the CO_2 from the ethanol-manufacturing process is quite different from that of CO_2 produced from fossil-fuel combustion and that adsorbed to the coal samples. The results fall within the ranges expected for the different types of samples collected (Figures 1-22 and 1-23). Included in Figures 1-22 and 1-23 are additional data for total DIC from groundwater (Hackley, 2002) in central Illinois and data for total DIC in brines from the Antrim Shale in the Michigan Basin (Walter et al., 1996). These Michigan brines were associated with extensive amounts of microbial CH_4 that had quite negative $\delta^{13}C$ values, explaining the very positive $\delta^{13}C$ values of the DIC (Walter et al., 1996). New samples of brines from the Illinois Basin were not available for ^{14}C and $\delta^{13}C$ testing; however, four $\delta^{13}C$ measurements were included from brines in southern Illinois (Hwang, 1996) and one $\delta^{13}C$ value from CO_2 associated with brine in central Illinois (unpublished data). The average ^{14}C activity of the brines measured in the Michigan Basin was included to have available $\delta^{13}C$ data for Illinois Basin brines on the plot in Figures 1-22 and 1-23. The negative $\delta^{13}C$ values of the DIC for the Illinois Basin brines from southern Illinois are probably due to oxidation of buried organic matter, which would decrease the $\delta^{13}C$ values. The $\delta^{13}C$ results for the groundwater samples showed a large range of values depending on the age of the water and the geochemical processes influencing the water chemistry.

The isotopic results of the brine and groundwater samples emphasize the importance of characterizing the DIC in the formation waters surrounding the specific sites chosen for geological CO_2 sequestration testing. Although the CO_2 collected from the ethanol process is quite different from that from older groundwater samples, it is similar to what is expected in the soil horizons and shallow groundwater (Figures 1-22 and 1-23). The CO_2 produced by the refinery manufacturing process, which uses petroleum products as a source of carbon, and the stack gas CO_2 from natural gas combustion show the largest separation compared to groundwater DIC, soil CO_2, and the other natural sources of CO_2 sampled (Figures 1-22 and 1-23).

Influence of CO_2 Adsorption on CO_2 Isotopic Composition

During this project, no demonstration-scale CO_2 injection was carried out, and therefore CO_2 could not be characterized at in situ reservoir conditions. Therefore, only limited data were obtained, and these come from laboratory-scale experiments performed at Indiana University using a custom-made system to study gas sorption (Figure 1-24) at reservoir pressure and temperature conditions.

The main part of the instrumentation is a pressure vessel that accommodates a coal core that is about 0.30 m (1 ft) long and 7.6 cm (3 inches) in diameter (Figure 1-25). Coal in this pressure vessel will adsorb, desorb, and transmit CO_2, CH_4, and mixed CO_2/CH_4 gas (Figure 1-25) under a range of reservoir gas pressures of up to 10,342 kPa (1,500 psi) and temperatures from 15.56°C to 60°C (60°F to 140°F). A metered flux of CO_2 and CH_4 (commercially available gases from cylinders) is fed into the pressure

Figure 1-24. *Part of a system to study gas sorption. The high pressure vessel is on the left, and the ISCO pump is on the right.*

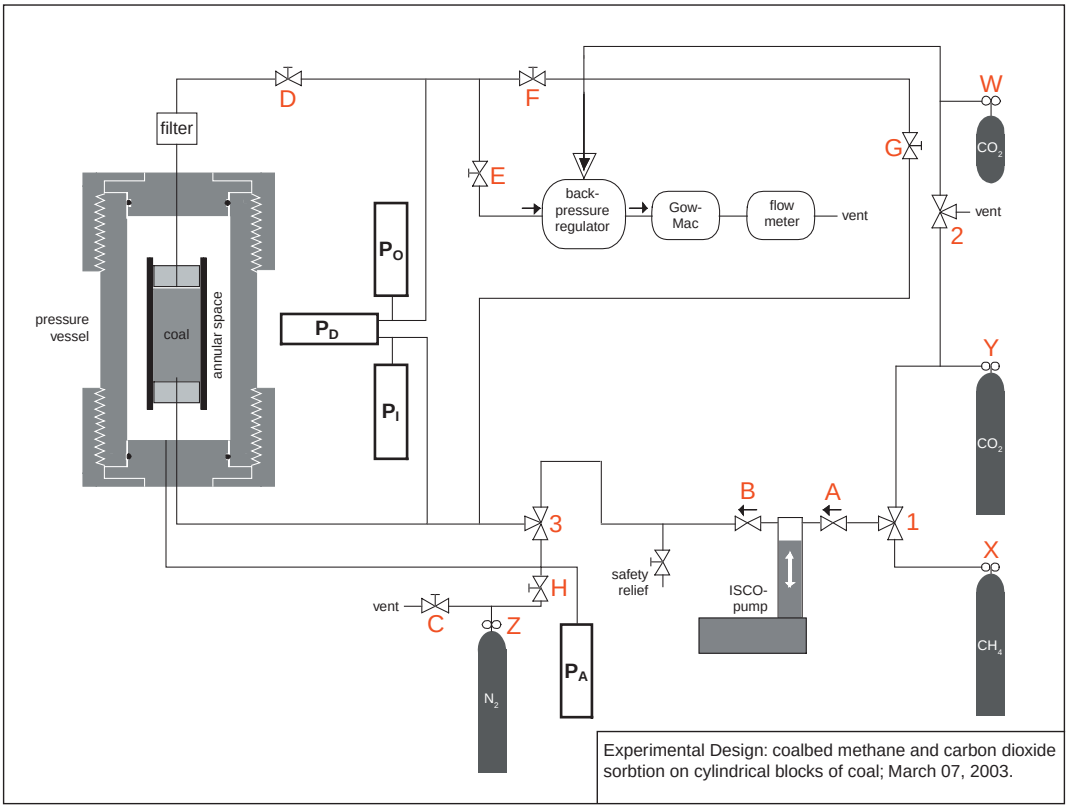

Figure 1-25. *Schematics of the system to study gas sorption.*

vessel at a given pressure and temperature. Pressure transducers (Figure 1-25) continuously and automatically monitor pressures at various points in the system. Currently four pressure transducers are being used—one differential pressure transducer and three non-differential pressure transducers—in addition to mechanical gauges for pressure monitoring and control. An ISCO pump with 100-mL (0.0264 gallons) capacity per stroke is designed to meter gas flow at high pressure into the reactor. After going through the coal, the gas can be compositionally analyzed, and its CH_4/CO_2 ratio can be monitored with a Binary Gas Analyzer GOW-MAC 20 (Figure 1-25), which is a dual-pass unit with a thermal conductivity detector (TCD). The total volume of the gas is measured with a volumetric flow meter (FUL-1600). A Keithley data logger is used to collect data from the sensors and enter it into a spreadsheet on a computer. The data collection frequency can be chosen to reflect intervals from seconds to hours.

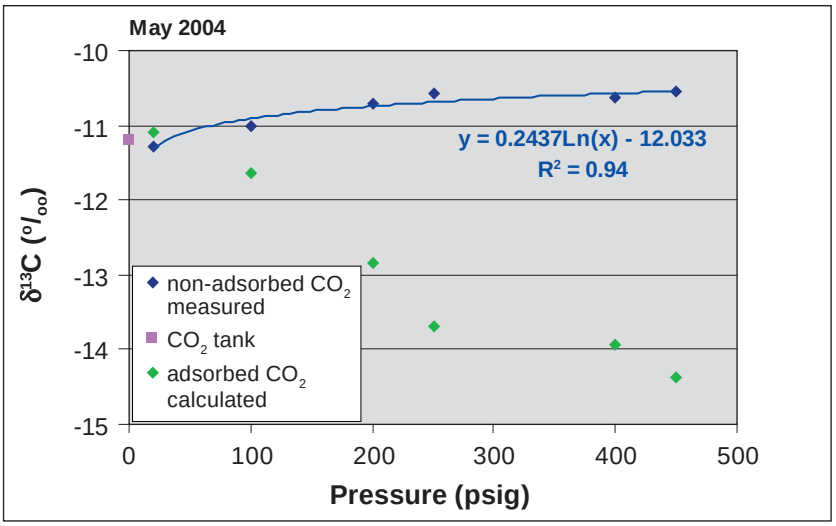

Figure 1-26. *Experiment 1: Changes in $\delta^{13}C$ of CO_2 with pressure.*

In order to understand the isotopic behavior of CO_2 due to adsorption and desorption, three runs were made (Figures 1-26 through 1-28), during which samples of the gas in the vessel were collected during desorption, after sufficient data were gathered to define the adsorption isotherms. A sample of the injected CO_2 gas (from the tank) was also collected to indicate the isotopic value of the system at equilibrium. The results are presented in Figure 1-29.

These preliminary data suggest that, during injection of small amounts of CO_2 at low pressure, a significant portion of CO_2 penetrates the coal freely, being adsorbed (Figure 1-29), and no isotopic effect of preferential adsorption is observed. When pressure is increased, the ratio of adsorbed to injected CO_2 decreases, diffusion into the micropore structure of coal becomes more competitive, with lighter molecules ($^{12}CO_2$) having an advantage over the heavier ones ($^{13}CO_2$) as a result of kinetic isotopic effect. At pressures above 1,724 kPa (250 psig), the ratio of adsorbed to injected gas stabilizes,

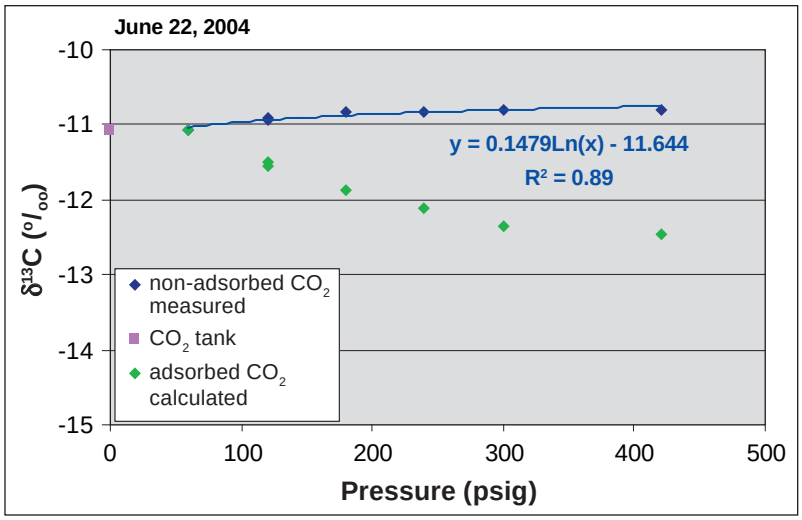

Figure 1-27. *Experiment 2: Changes in $\delta^{13}C$ of CO_2 with pressure.*

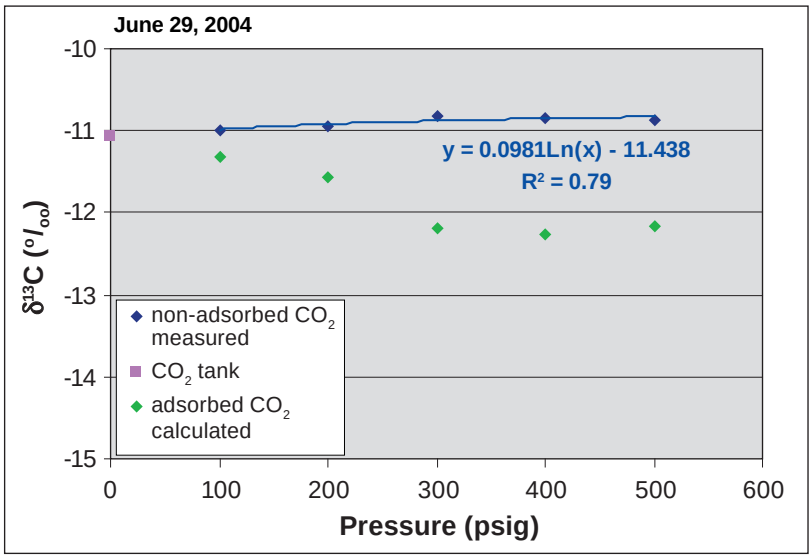

Figure 1-28. *Experiment 3: Changes in $\delta^{13}C$ of CO_2 with pressure.*

and reaches equilibrium at about 0.17. Additionally, the isotopic difference between injected tank CO_2 and non-adsorbed gas stabilizes at about 0.37/mill ($^0/_{00}$) on average (0.61, 0.28, and 0.24‰ for separate experiments), which suggests that this value is the equilibrium isotopic difference for this system. This equilibrium averages at about 2/$^0/_{00}$ if expressed as a difference in $\delta^{13}C$ between adsorbed and non-adsorbed portions of CO_2. From 1,724 to 3,447 kPa (250 to 500 psi) (and also likely at higher pressure), this equilibrium is sustained only when the competitiveness remains at the same level; that is, if the adsorbed/injected CO_2 ratio remains at about 0.17.

Our experiments suggest that, at pressures above 1,724 kPa (250 psi), the ratio of adsorbed CO_2 to injected CO_2 is relatively constant (~0.17, Figure 1-29). Thus, the remaining fraction (0.83) of CO_2 will

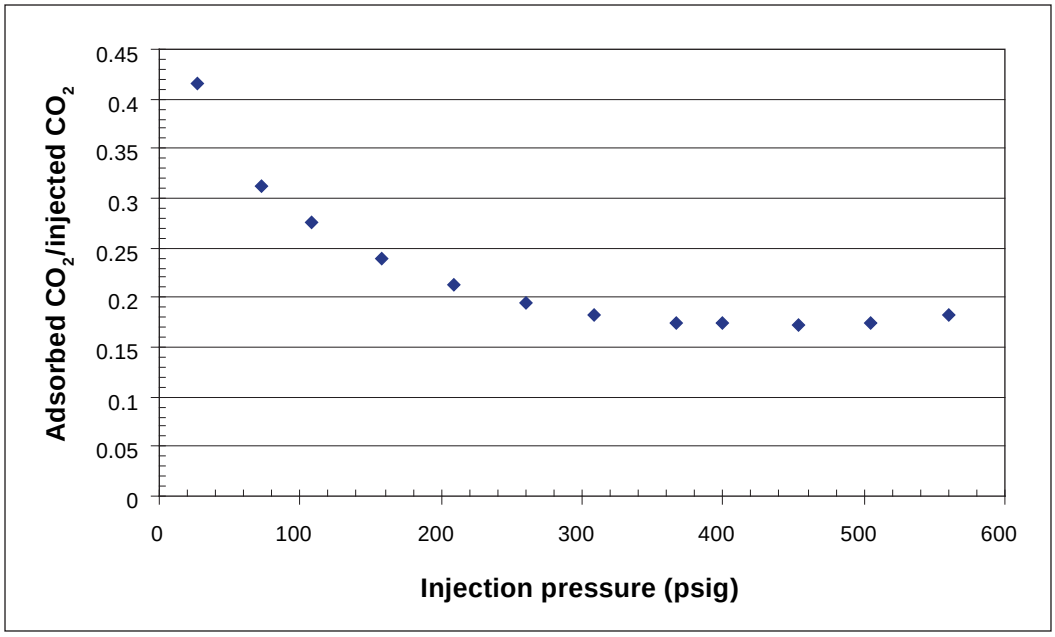

Figure 1-29. *Change in ratio of adsorbed to injected CO_2 with pressure.*

migrate further to the nearest available adsorption site. This diffusion into the coal is competitive isotopically because only 17% of injected CO_2 molecules will be adsorbed at a given site, and the rest will migrate further via fractures and macropores. That competitive diffusion into coal will give preference to isotopically lighter $^{12}CO_2$ molecules, as demonstrated by our experimental examples. $^{12}CO_2$ will be continuously outcompeting $^{13}CO_2$ in diffusion and occupation of the competitive micropore adsorption sites. Therefore, ^{13}C-enriched CO_2 will migrate further along fractures and interconnected macropore networks and will be accompanied by losses of $^{12}CO_2$ molecules due to their preferential diffusion.

These preliminary results are encouraging, and the observed isotopic changes may be used as helpful tracers. Monitoring the isotopic composition of atmospheric CO_2 near the surface in surrounding areas could possibly help to detect leaks of injected CO_2 to the surface via fault zones, fractures, or sandy erosional channels. Additionally, the injected CO_2 could be isotopically labeled to be easily discriminated from the regular atmospheric CO_2 of the area. Sampling of the monitoring wells around the injection site could also be helpful in tracking the spreading of the CO_2 plume in the coalbed and as a control for its isotopic composition at a particular site.

These are very limited data and preliminary suggestions, and more samples need to be analyzed to study changes in gas isotopic behavior during CO_2 sequestration. Because these preliminary data show the potential importance, both laboratory and field scale isotopic effects will be further investigated in Phase II of the project.

Appendix 1: COMET Modeling

Table A1-1. Sample details.

Sample	State	ID	Moisture (%)	Ash (%)
Herrin	Illinois	Hon #9	10	3
Springfield		Wabash	8.7	9.7
Davis		Wabash	8.6	20
Springfield	Indiana	02/2004 V-3 Sullivan County	7.5	5.7
Seelyville-I		02/2004 III-3 Sullivan County	7.3	9.1
Seelyville-II		Knox #26	9.6	10.2
Springfield	Kentucky	DC-04-09-WKY 9C Peabody	2.8	15.5
WKY-9B		DC-04-09-WKY 9B Peabody	3.9	11.8
WKY#11		WKY#11- Can 21	4.8	11.5

Table A1-2. COMET input parameters and data origin.

Reservoir parameter	Data origin	Reservoir parameter	Data origin
Cleat spacing, ft	measured	$P_{initial,}$ psi	calculated
Compressibility, psi^{-1}	estimated	PL_{CH4}	measured
Depth, ft (midpoint)	calculated	PL_{CO2}	estimated
$Gc_{initial,}$ scf/ton (bulk rock)	calculated	Porosity, %	estimated
Gs, scf/ton (bulk rock)	calculated	Sg_{free}	observed
$h_{net,}$ ft (coal)	measured	Sorption time, days	calculated
k, bed-scale, md	measured	Sw	observed
k, butt, md	calculated	Temperature, °F	calculated
k, face, md	calculated	$VL_{CH4,}$ scf/ton (bulk rock)	measured
k, relative, krg/krw	estimated	$VL_{CO2,}$ scf/ton (bulk rock)	estimated

Table A1-3. COMET model configuration for calculation of performance indicators (RF and SF) for GIS Basin-scale volumetric calculations.

Model input	500 to 900 ft			900 to 1,200 ft			>1,200 ft		
	Low estimate	Best estimate	High estimate	Low estimate	Best estimate	High estimate	Low estimate	Best estimate	High estimate
Cleat spacing, ft	0.00328	0.03937	0.11483	0.00328	0.03937	0.11483	0.00328	0.03937	0.11483
Compressibility, psi^{-1}	10^{-5}	10^{-4}	10^{-4}	10^{-5}	10^{-4}	10^{-4}	10^{-5}	10^{-4}	10^{-4}
Depth, ft (midpoint)	540	700	860	930	1,050	1,115	1,220	1,300	1,400
$Gc_{initial,}$ calculated scf/cu ft (rock)	1.47	2.86	3.68	1.46	2.63	3.36	2.63	3.43	4.23
$h_{net,}$ ft	1.5	4.2	5.6	1.5	3.6	5.4	1.5	3.8	5.6
k, bed-scale, md	3	30	50	1	10	30	0.5	5	30
$P_{initial,}$ psi	233.82	303.1	372.38	402.69	454.65	482.795	528.26	562.9	606.2
PL_{CH4}	796	577	523	796	577	523	796	577	370
PL_{CO2}	442	306	170	442	306	170	442	306	170
Porosity, %	0.05	0.03	0.01	0.03	0.02	0.01	0.03	0.01	0.005
Sorption time, days	90	20	5	90	20	5	90	20	5
Temperature, °F	58.26	67.1	77.8	64.2	73.4	83.1	68.7	77.9	89
$VL_{CH4,}$ scf/ft^3 (rock)	10.78	15.97	20.13	9.46	13.86	17.48	11.23	14.63	18.45
$VL_{CO2,}$ scf/ft^3 (rock)	24.86	42.89	50.46	21.59	37.25	43.81	22.78	39.30	46.23

Table A1-4. Parametric study COMET input data.

	500 to 900 ft			900 to 1,200 ft			>1,200 ft		
	Low case	Best case	High case	Low case	Best case	High case	Low case	Best case	High case
Depth, ft	540	700	860	930	1,050	1,115	1,220	1,300	1,400
$h_{net,}$ ft	1.5	4.2	5.6	1.5	3.6	5.4	1.5	3.8	5.6
$Gc_{initial,}$ calculated scf/ton (rock)	47.07	91.61	118.04	46.81	84.18	107.54	84.22	109.83	135.47
Gs, calculated scf/ton (rock)	78.44	176.17	268.27	101.77	195.76	268.85	143.46	231.47	366.96
Degree of saturation, assumed %	0.6	0.52	0.44	0.46	0.43	0.4	0.59	0.47	0.37
$VL_{CH_4,}$ scf/ton	308	456	575	311	456	575	350	456	575
PL_{CH_4}	796	577	523	796	577	523	796	577	370
$VL_{CO_2,}$ scf/ton	710	1,225	1,441	710	1,225	1,441	710	1,225	1,441
PL_{CO_2}	442	306	170	442	306	170	442	306	170
$P_{initial,}$ psi	233.82	303.1	372.38	402.69	454.65	482.795	528.26	562.9	606.2
Pressure gradient, psi/ft	0.433	0.433	0.433	0.433	0.433	0.433	0.433	0.433	0.433
Temperature, °F	58.26	67.1	77.8	64.2	73.4	83.1	68.7	77.9	89
Sorption time, days	90	20	5	90	20	5	90	20	5
Porosity, %	0.05	0.03	0.01	0.03	0.02	0.01	0.03	0.01	0.005
Compressibility, psi^{-1}	10^{-5}	10^{-4}	10^{-4}	10^{-5}	10^{-4}	10^{-4}	10^{-5}	10^{-4}	10^{-4}
Cleat spacing, ft	0.0033	0.0394	0.1148	0.0033	0.0394	0.1148	0.0033	0.0394	0.1148
k, bed-scale, md	3	30	50	1	10	30	0.5	5	30

Derivation of Volumetric Equations

Zuber (1996) stated, "Desorption is the process by which methane molecules detach from the micropore surfaces of the coal matrix and enter the cleat system where they exist as free gas. The desorption isotherm defines the relationship between the absorbed gas concentration in the coal matrix and the free gas pressure in the coal cleat system."

The Langmuir equation (Equations [2] and [3]) calculates the nonlinear relationship between matrix gas concentration (storage capacity) and pressure. This equation estimates the adsorbed gas content in the coal matrix based on the units of the Langmuir volume, which can be standard cubic feet per ton or standard cubic feet per cubic feet. The units of standard cubic feet per ton are converted to standard cubic feet per cubic feet using a 0.0312 conversion factor. In addition to mass or volume basis, the Langmuir volume can be used on these bases: pure; in situ; dry, ash-free; or dry, mineral-matter-free.

Langmuir equations:

$$C_m = \frac{V_L p}{p_L + p}(0.031\rho_b) \qquad [2]$$

$$C_g(p) = \frac{V_L p}{(p_L + p)} \qquad [3]$$

Equation [3] is the general case of the Langmuir equation, as it lacks a conversion factor.

The curve generated by the Langmuir equation, the Langmuir isotherm, describes desorption under saturated conditions. When in situ reservoir conditions are undersaturated (initial pressure and gas content plot below the isotherm or capacity of the coal), the reservoir produces only water. Water production (dewatering) is the primary method for pressure reduction as the cleat and fracture system is initially saturated with water. When coal pressure is decreased such that the reservoir pressure conditions intersects the desorption isotherm, gas desorption is initiated. In CBM, desorption is the mechanism by which adsorbed gas moves from the secondary permeability controlled by diffusion effects (Fick's Law) to the primary (dominant) permeability composed of the cleat and natural fracture system (where Darcian flow dominates).

Equation [4] corrects the Langmuir volume (found in Equation [3]) from dry, ash-free (daf) to bulk "rock" coal (in situ) conditions using average ash content and equilibrium moisture. The equation also converts the Langmuir volume from standard cubic feet per ton to standard cubic feet per cubic feet, and its derivation is

$$\left(\left[\frac{1\ lbs}{453.59\ g}\right]\left[\frac{1\ ton}{2{,}000\ lbs}\right]\left[\frac{2.54\ cm}{1\ in}\right]^3\left[\frac{12\ in}{1\ ft}\right]^3\right) = 0.0312\ \left[\frac{(\text{ton})(\text{cm}^3)}{(\text{g})(\text{ft}^3)}\right]$$

$$V_{L-rc}\left[\frac{scf}{ft^3}\right] = V_{L-daf}\left[\frac{scf}{ton}\right] 0.0312\left[\frac{(ton)(cm^3)}{(g)(ft^3)}\right]\rho_c\left[\frac{g}{c}\right](1-f_a-f_m)$$

$$V_{L-rc} = 0.0312 V_{L-daf}\,\rho_c\,(1-f_a-f_m) \qquad [4]$$

Equation [5] is a specific case of Equation [3] that accounts for the degree of saturation (S_g) of the coal, which ranges from 0 to 1.0.

$$C_b = C_{gi-rc} = \frac{V_{L-rc} P_i}{(P_L + P_i)} S_g \qquad [5]$$

Equation [6] is, according to Zuber (1996), the "volumetric gas-in-place equation for coalbed methane reservoirs. This equation includes the appropriate terms for estimating the free gas in the coal interconnected fracture system and the adsorbed gas in the coal matrix. Gas dissolved in the water is almost always negligible and has not been included in [this equation]."

GIP equation:

$$G_i = Ah\left[\frac{43560\phi_f(1-S_{wfi})}{B_{gi}} + 1.359 C_{gi}\,\rho_c\,(1-f_a-f_m)\right] \qquad [6]$$

GIP "rock" coal equation (Equation [6] modified):

$$G_i = (43.560)\,Ah(1-\phi)C_{gi-rc} \qquad [7]$$

S_{wfi} is an estimate of irreducible water saturation in the interconnected coal fracture system as seen in the GIP equation (Equation [6]). In an example with water completely saturating the cleats and natural fractures, the first term on the right side of Equation [6]

$$\frac{43560\phi_f(1-S_{wfi})}{B_{gi}}$$

is negligible because interconnected fracture water saturation fraction S_{wfi} = 1, causing the term to be 0. In other words, there is no free gas saturation (1–S_{wfi}) in the cleat system. Consequently, this term is not included in Equation [6].

The GIP "rock" coal equation (Equation [7]) does not have a "daf" correction as in the second term of Equation [5]:

$1.359 C_{gi}\, \rho_c\, (1 - f_a - f_m)$.

The correction is not present in Equation [7] because the gas concentration ($C_{gi–rc}$) used in this equation is corrected from "daf" to "rock" coal by Equation [4].

Three steps are required to find GIP "rock" coal:

1. Find $V_{L–rc}$ using Equation [4].
2. Find $C_{gi–rc}$ using Equation [5] with $V_{L–rc}$.
3. Find GIP using Equation [7] with $C_{gi–rc}$.

Taking unaltered input data and creating one equation opposed to the previously described stepwise process, the GIP equation becomes

$$G_i = (4{,}3560) Ah \left[S_g \frac{\left[0.0312 V_{L–daf}\, \rho_c\, (1 - f_a - f_m)(1 - \phi)\right] P_i}{(P_L + P_i)} \right]$$

Gridblock Sensitivity

To optimize simulation time while maintaining the accuracy of model results, standard gridblock patterns of different dimensions were tested. The number of gridblocks per side in the square test patterns were 15, 20, 35, 50, 65, and 85. The model area is a quarter 5-spot of a 324-km^2 (80-acre) pattern. A quarter 5-spot pattern can be assumed to be representative of the reservoir if the reservoir properties are homogeneous and isotropic throughout the reservoir or have quadrilateral symmetry about the producing well in the region being modeled. From a fluid dynamics perspective, this method can be applied because the axes of symmetry coincide with the no-flow boundaries in a developed well pattern with surrounding wells.

Analysis of the output from these simulations using standard gridding reveals a trend showing the dependency of model results on the number of gridblocks. Flow rates and the difference between flow

rates from separate simulations decreased as the number of gridblocks in the test pattern increases. Based on this observation, a study was preformed to extrapolate the minimum number of gridblocks necessary for the gas rate plots to converge and remove the model's dependency on the number of gridblocks. This occurred at approximately 120 to 125 gridblocks per side.

Table A1-5. Description of variables for the GIP equation.

Variable	Description	Units
	Matrix gas concentration	[*scf/ft*^{3}]
	Initial gas concentration	[*scf/ft*^{3}]
	Initial gas concentration (rock)	[*scf/ft*^{3}]
	Gas concentration (bulk = rock)	[*scf/ft*^{3}]
	Langmuir volume	[*scf/ft*^{3}]
	Langmuir pressure	[*psia*]
p_i	Initial pressure	[*psia*]
p	Pressure	[*psia*]
V_{L-daf}	Langmuir volume (daf)	[*scf/ft*^{3}]
	Langmuir volume (rock)	[*scf/ft*^{3}]
	Pure coal density	[*g/c*]
	Bulk coal density	[*g/c*]
f_a	Ash weight fraction	Fraction
	Moisture weight fraction	Fraction
G_i	Gas in place	[*Mscf*]
	Conversion factor	$\left[\frac{(ton)(cm^3)}{(g)(ft^3)}\right]$
43,560	Conversion factor	[*ft*^{2}*/ac*]
1.359	Conversion factor	$\left[\frac{(Mscf)(ton)(cm^3)}{(ac\text{–}ft)(scf)(g)}\right]$
A	Well spacing/drainage area	[*acres*]
h	Coal seam thickness	[*f*]
	Porosity	Fraction
	Interconnected fracture (effective) porosity	Fraction
	Interconnected fracture water saturation	Fraction
	Gas formation volume factor at P_i	[*rcf/Mscf*]

To further optimize computation time, hybrid gridblock patterns were developed using gridblocks of varying sizes, which enables high resolution of flow properties around the well locations through a reduction of gridblock size. To optimize computation time, the size of the gridblocks increases distally from the well locations to reduce the overall number of gridblocks in the pattern (computationally, simulation time is dependent on the number of gridblocks, not their size). Because irregular grids cannot be defined, the resulting pattern contains small gridblocks at the four corners of the grid despite only needing high resolution in two diagonal corners. The hybrid grid is created such that the smallest gridblock in the hybrid grid is equal to the size of the gridblocks in the standard grid to which emulation

is sought. This hybrid grid drastically reduced computation time while still maintaining a high degree of accuracy in comparison to the data produced by the finely gridded patterns.

The hybrid gridblock pattern was further refined by maximizing the difference in size between each adjacent cell, allowing for an exponential increase in gridblock size with increasing distance from the well locations resulting in smaller computation times. Exponential growth in gridblock size results in the exponential growth in the total pore volume contained within each gridblock. The maximum difference between pore volumes in adjacent gridblocks is approximately 10%, which does not violate the "commonly accepted factor-of-2 difference" modeling convention.

In simulations that utilize large numbers of gridblocks, COMET must change the algorithm it uses to solve the simulation. COMET switches to the Preconditioned Generalized Conjugate Gradient (PGCG) solver from the Block D4 solver. The PGCG solver is used when the hybrid gridblock pattern is applied due to the large number of gridblocks around the production and injection wells. Thus, to optimize computation time, an effort to reduce the number of PGCG iterations was also undertaken. It is important to note, however, that, by reducing the number of PGCG iterations by loosening tolerances such as RESTOL, the precision of the simulation decreases. Therefore, this method is used sparingly.

Relative Permeability

The literature was reviewed for available relative permeability data because such data are unavailable for Illinois Basin coals. The relative permeability data was divided into two categories: (1) laboratory experiments using coal core samples and (2) history-matched data from gas and water production data of productive CBM fields. These data sets were digitized and statistically analyzed to produce low, best, and high estimates that were applied to all depth subsets in the Basin.

The literature and COMET model regard CH_4 and CO_2 as a single gas phase, which is represented with one relative permeability curve. Therefore, two components, gas and water, adequately describe the multiphase flow of the modeled relative permeability curves.

Three relative permeability curves were calculated for gas and water phases using the Cory Exponent equations representing low, best, and high estimates. A sensitivity study was performed to see the effects of the three relative permeability sets and the probability estimate “best” was chosen for use in future modeling. Relative permeability in reservoir models could have been based on “Tiffany”- or “Allison”-like history-matched relative permeability curves, but the use of the calculated relative permeability curves was chosen to encompass the range of both laboratory- and field-acquired relative permeability data. If Illinois Basin coal relative permeability data were available, this process would not be necessary.

The generic relative permeability set curves were created using the Cory exponent equations (Willhite, 1986):

$$S_{wD} = \frac{(S_w - S_{iw})}{(1 - S_{or} - S_{iw})} \quad [7]$$

$$k_{rg} = \alpha_1 (1 - S_{wD})^{B_1} \quad [8]$$

$$k_{rw} = \alpha_2 S_{wD}^{B_2} \quad [9]$$

The variables are described in Table A1-6.

Table A1-6. Variables used in the Corey exponent equations.

Variable	
S_{wD}	Normalized water saturation
S_w	Water saturation fraction
S_{iw}	Initial water saturation fraction
S_{or}	Trapped gas saturation fraction
k_{rg}	Gas relative permeability
k_{rw}	Water relative permeability
α_1, α_2	Constants
B_1, B_2	Constants

Model Sensitivity Versus Reservoir Sensitivity (Absolute Sensitivity)

Model parameter distributions encapsulate the range variability of reservoir parameters in the Illinois Basin. It is important to note that the results from these reservoir simulations may not be applicable to other reservoirs.

Model sensitivity to reservoir parameters is biased by the ranges of values that are contained within the parameter distributions. The magnitude of parameters used in the study are representative of the ranges of values expected in the Illinois Basin and do not represent the maximum and minimum theoretical values. Hypothetically, the parameter that causes the greatest change in the performance indicators may not be the parameter to which the specific reservoir model is most sensitive. The modeled reservoir may have greater sensitivity to a different parameter; however, if this parameter's distribution has low dispersion (tightly controlled due to good data and/or limited regional variability), then the effect on

the performance indicators may be less than a parameter with lower “absolute” sensitivity but greater dispersion.

It may be possible to eliminate this bias by normalizing the range of parameters to the maximum range of theoretical values (e.g., a 2% change in the theoretical range of a parameter may correspond to a 17% change in the recovery factor). Attempting to make this correction is further complicated by parameters that have an infinite range (e.g., permeability $\{0 \rightarrow +\infty\}$). This method may be developed and applied in future studies.

Therefore, the reservoir sensitivity to a parameter represents the resultant change on performance indicators by varying the parameter within the range specified by its probability distribution. Care must be taken when applying these results to different and dissimilar reservoirs.

Appendix 2: Coal Resources

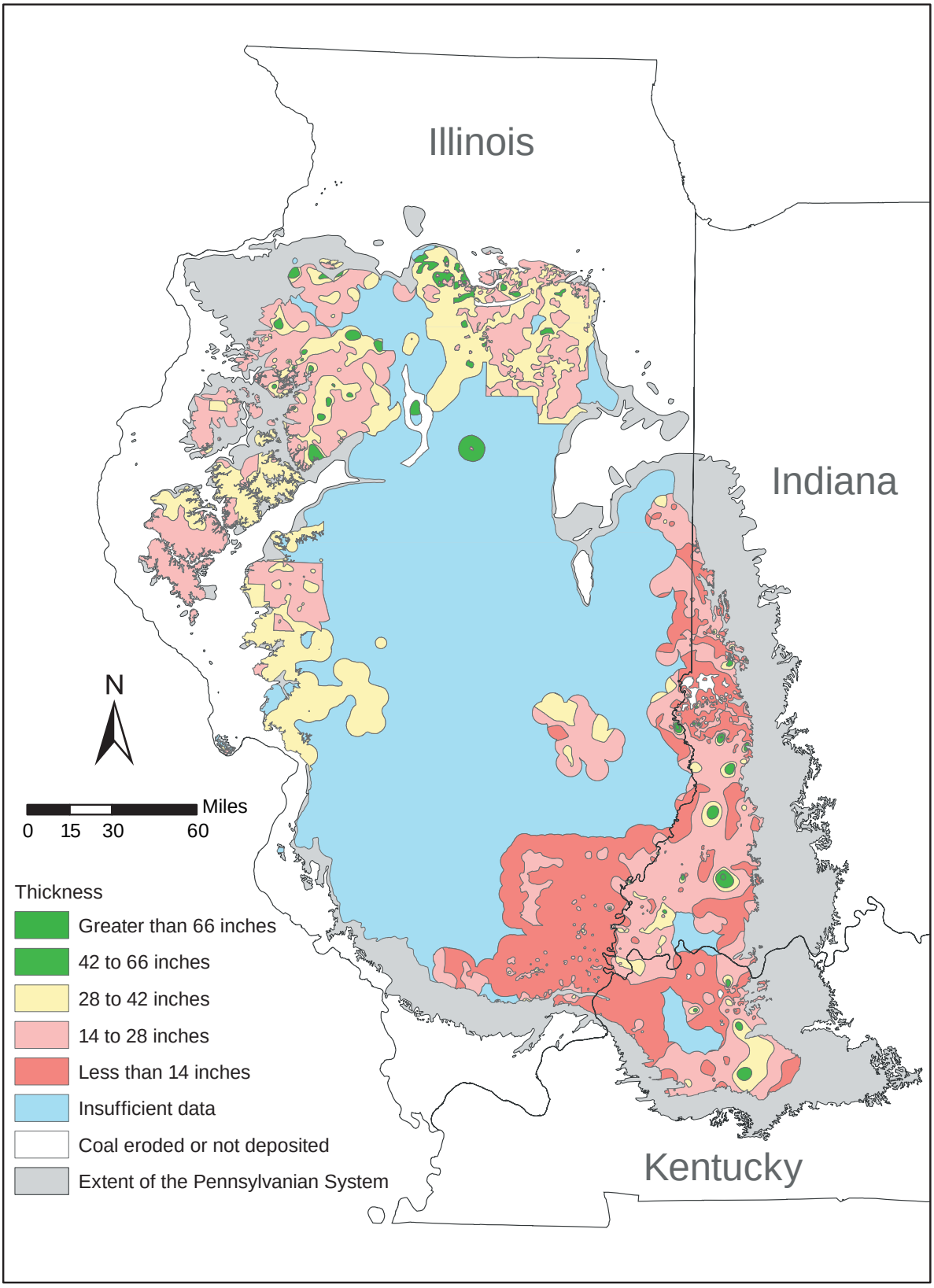

Figure A2-1 *Thickness of the Colchester Coal in the Illinois Basin.*

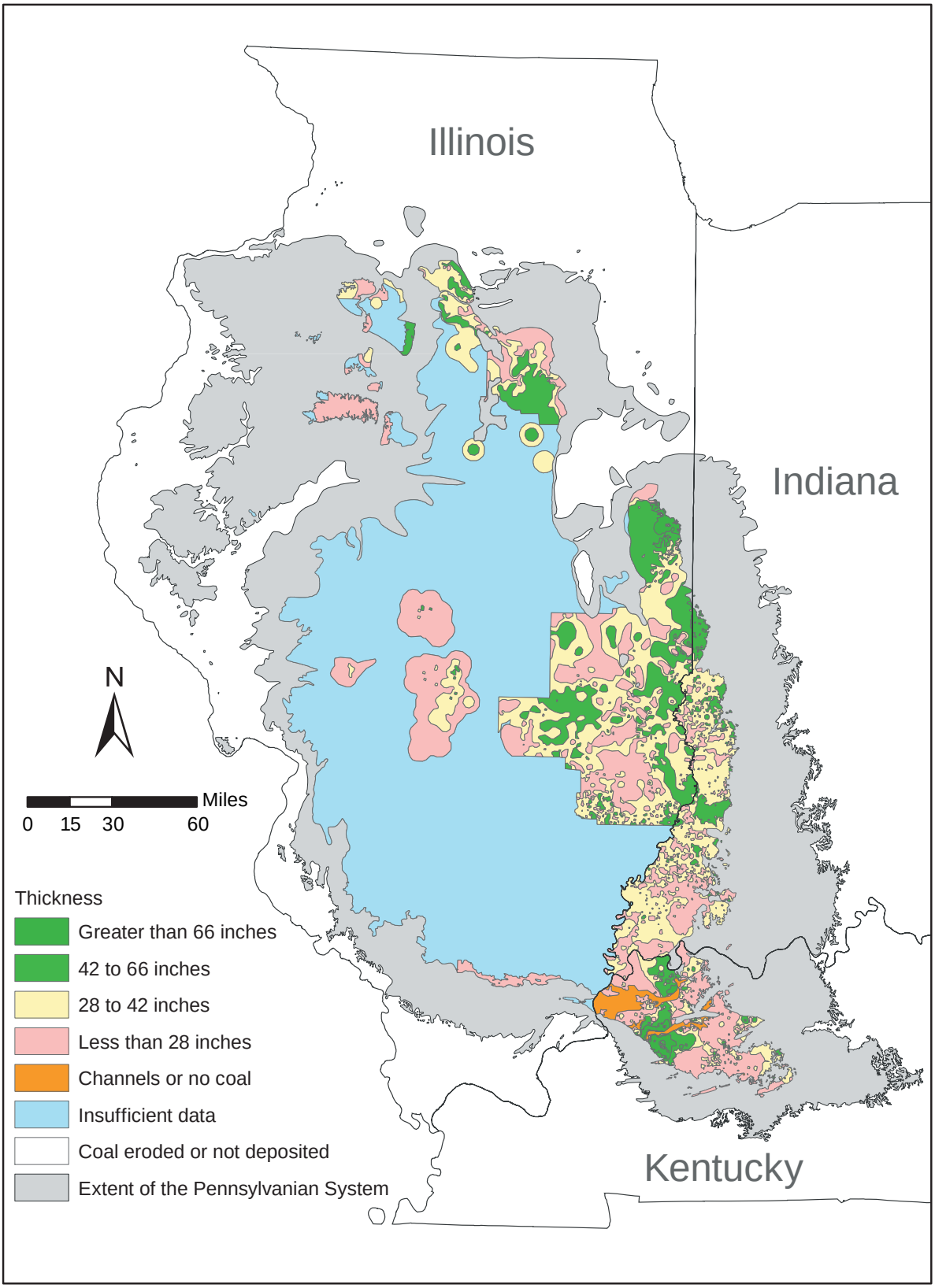

Figure A2-2 *Thickness of the Danville/Baker Coal in the Illinois Basin.*

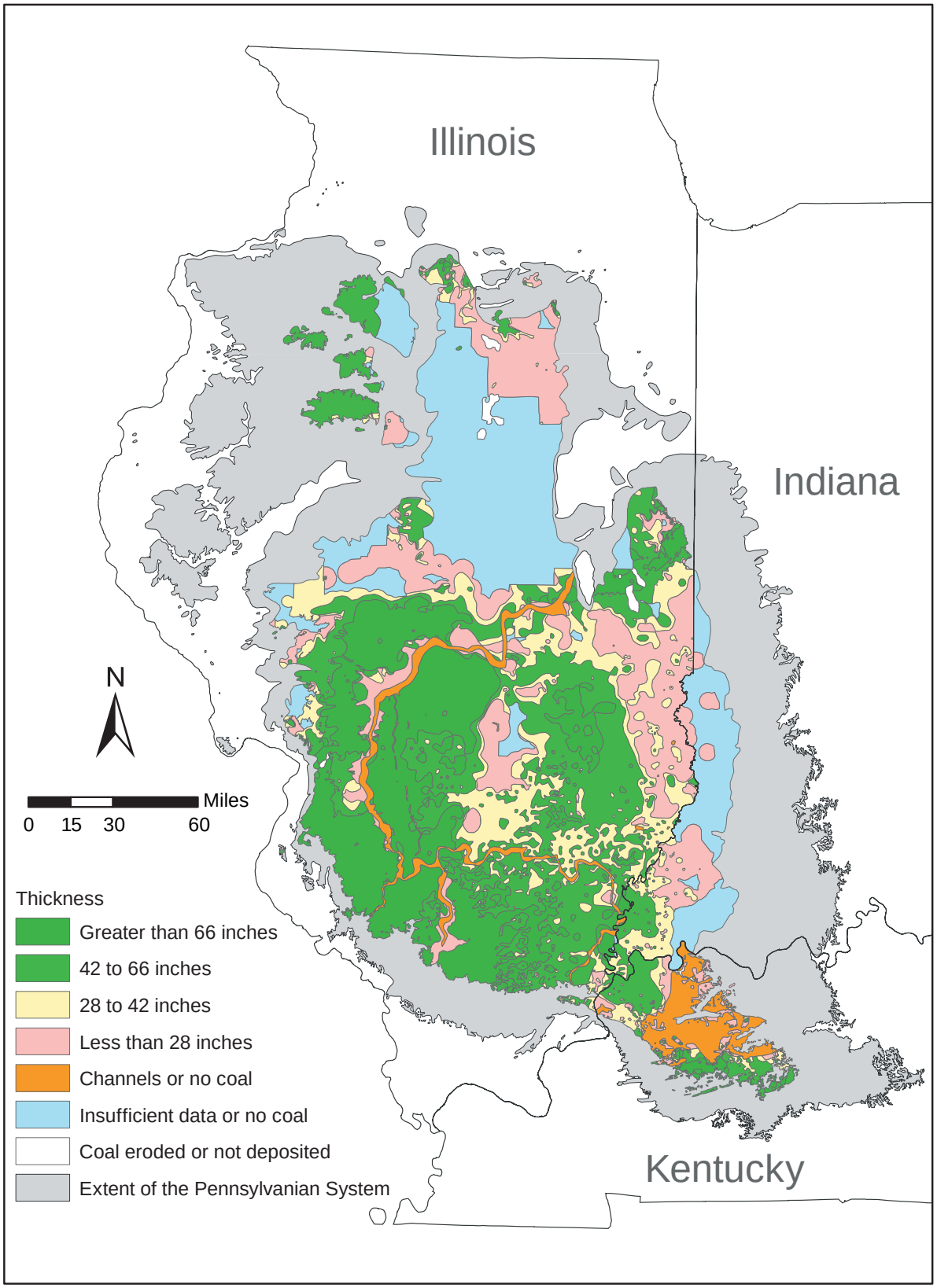

Figure A2-3 *Thickness of the Herrin Coal in the Illinois Basin.*

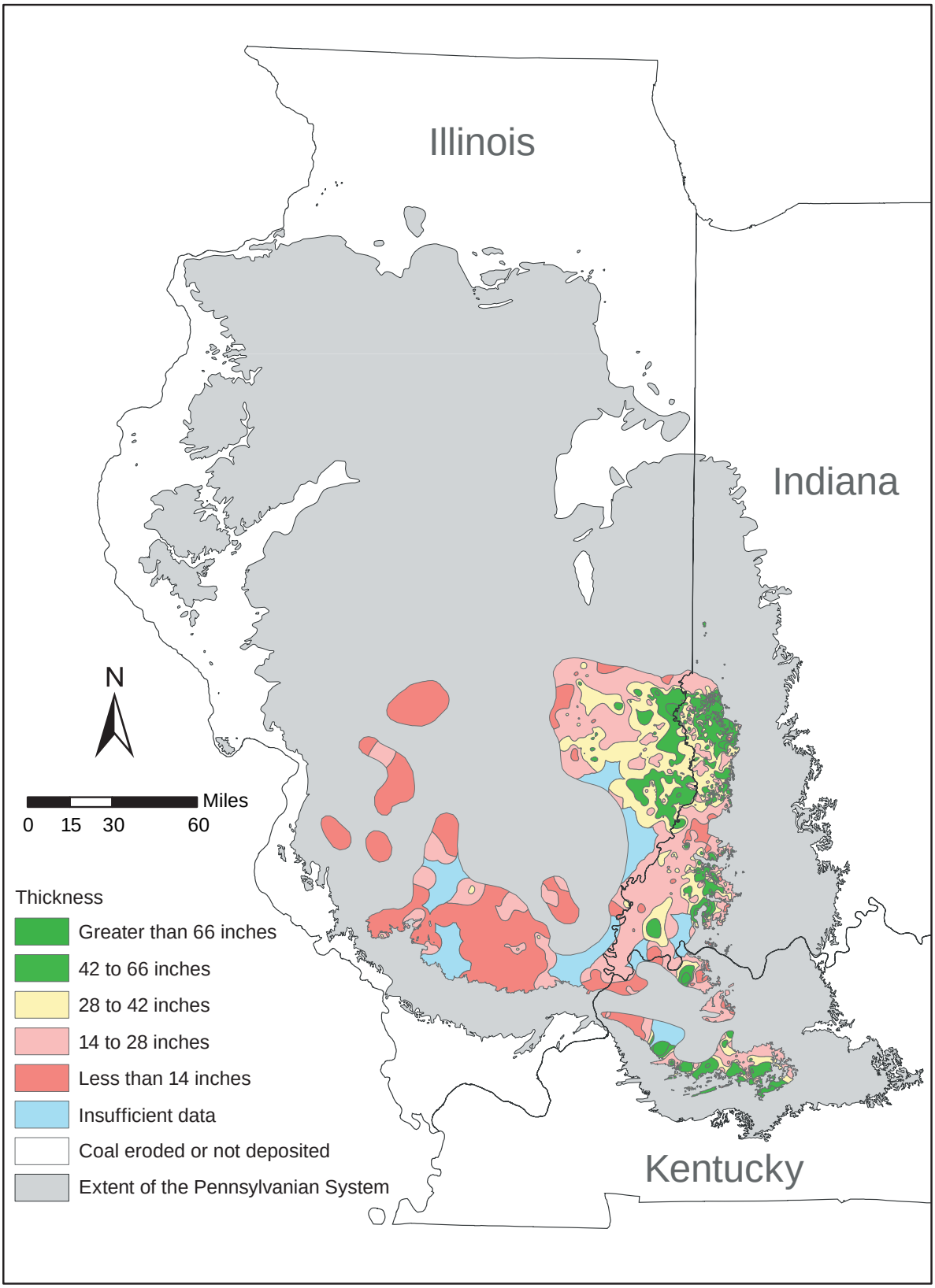

Figure A2-4 *Thickness of the Hymera/Jamestown/Paradise Coal in the Illinois Basin.*

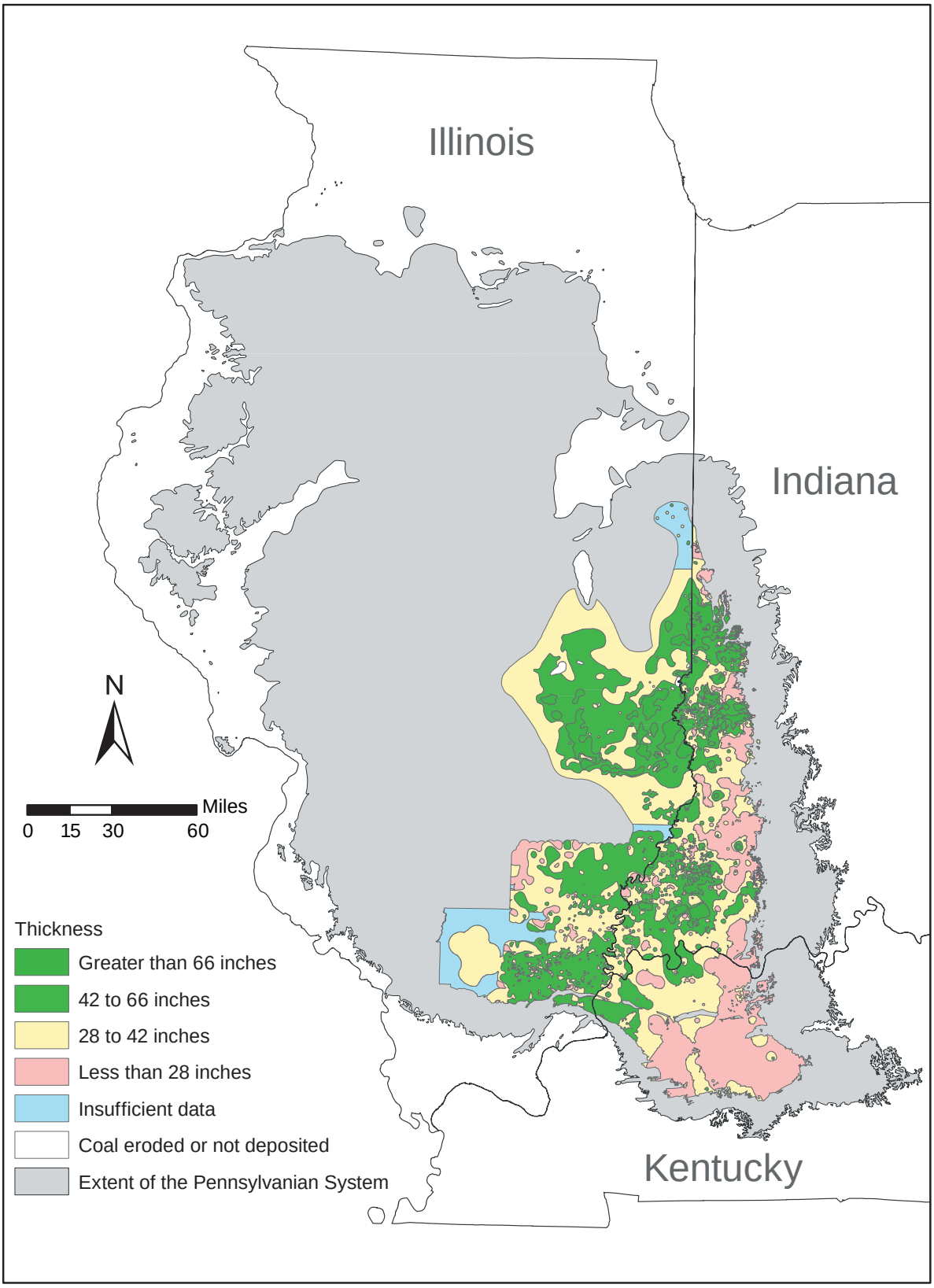

Figure A2-5 *Thickness of the Seelyville/Davis/Dekoven Coal in the Illinois Basin.*

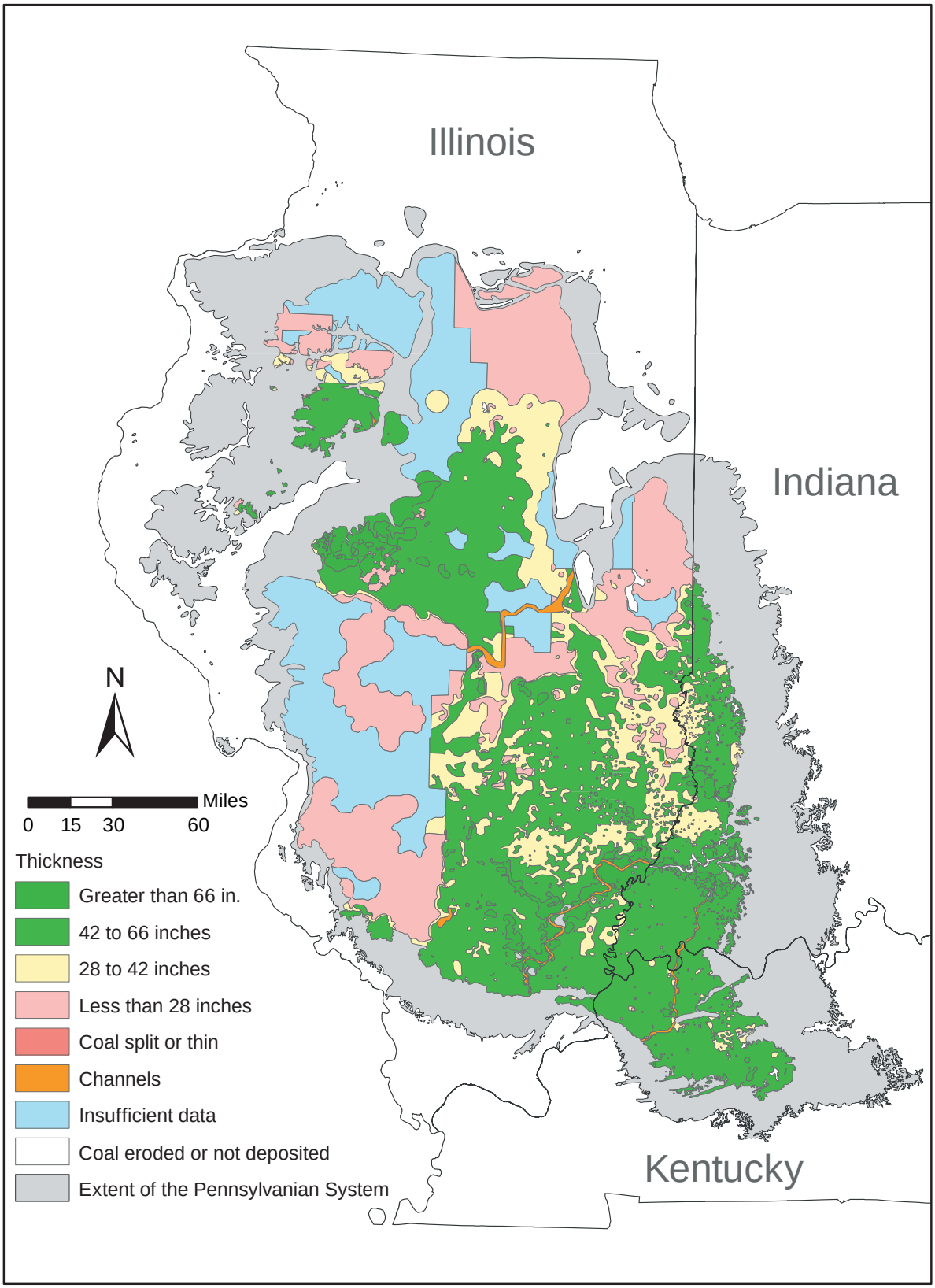

Figure A2-6 *Thickness of the Springfield Coal in the Illinois Basin.*

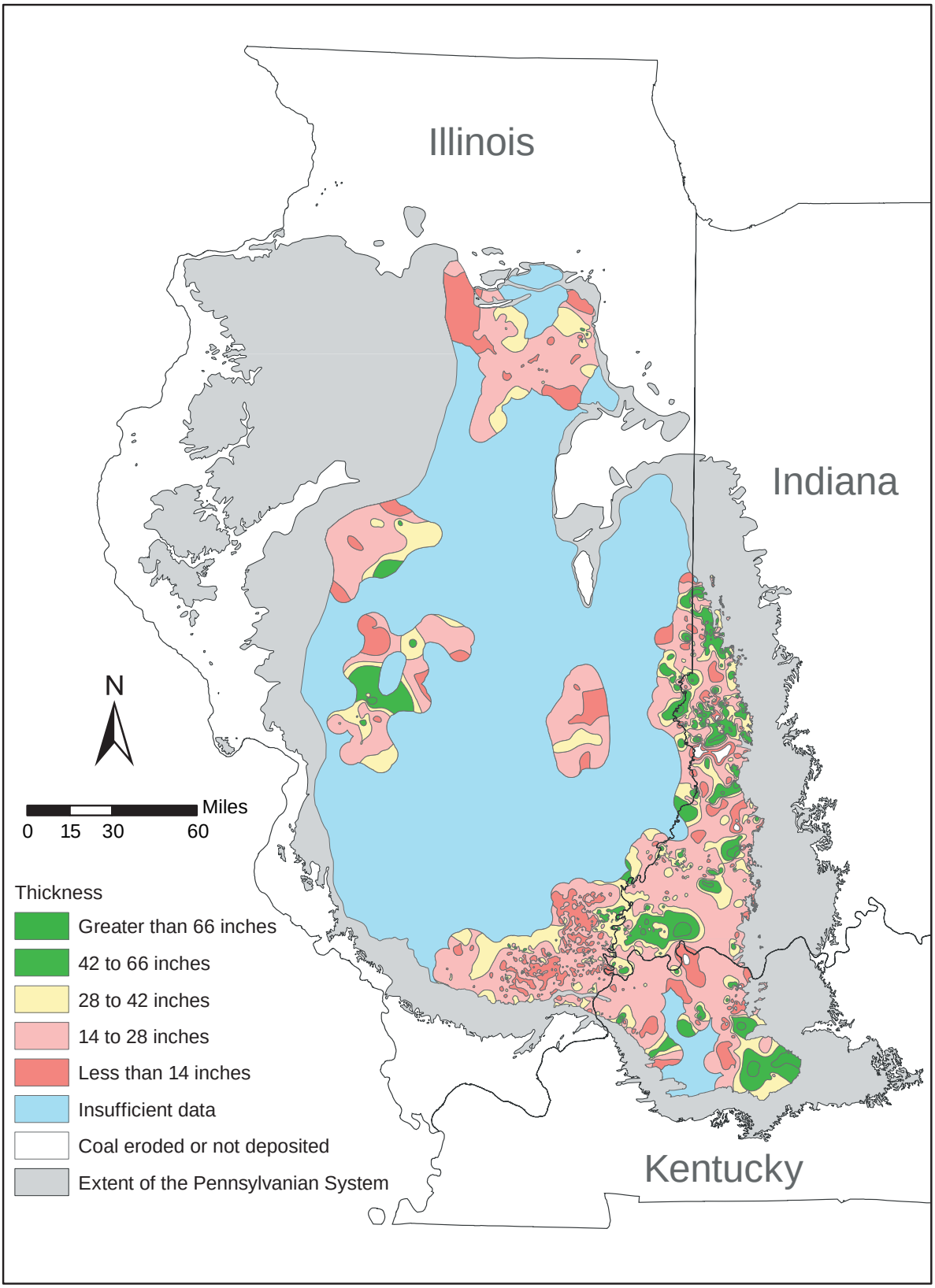

Figure A2-7 *Thickness of the Survant Coal in the Illinois Basin.*

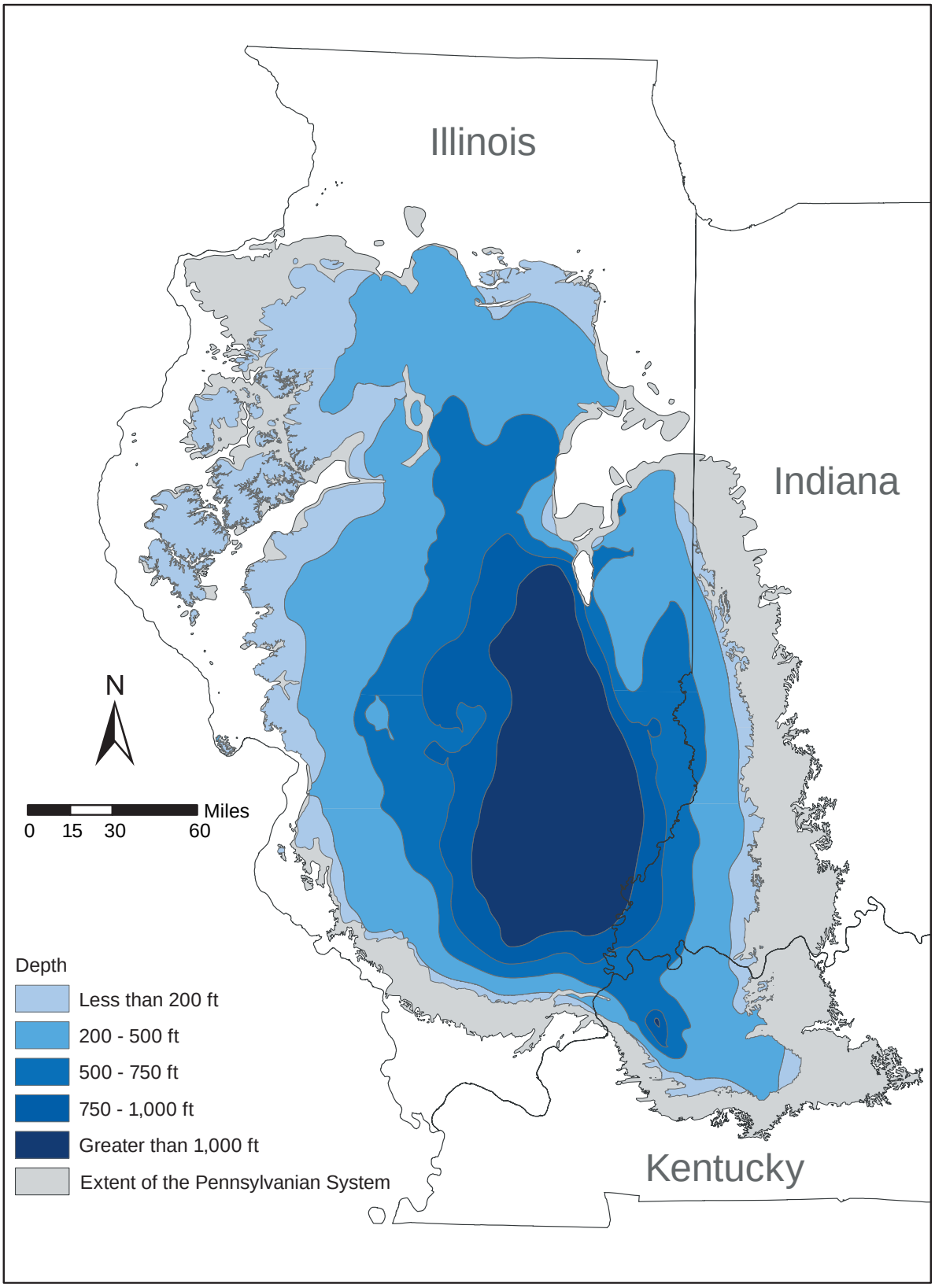

Figure A2-8 *Depth of the Colchester Coal in the Illinois Basin.*

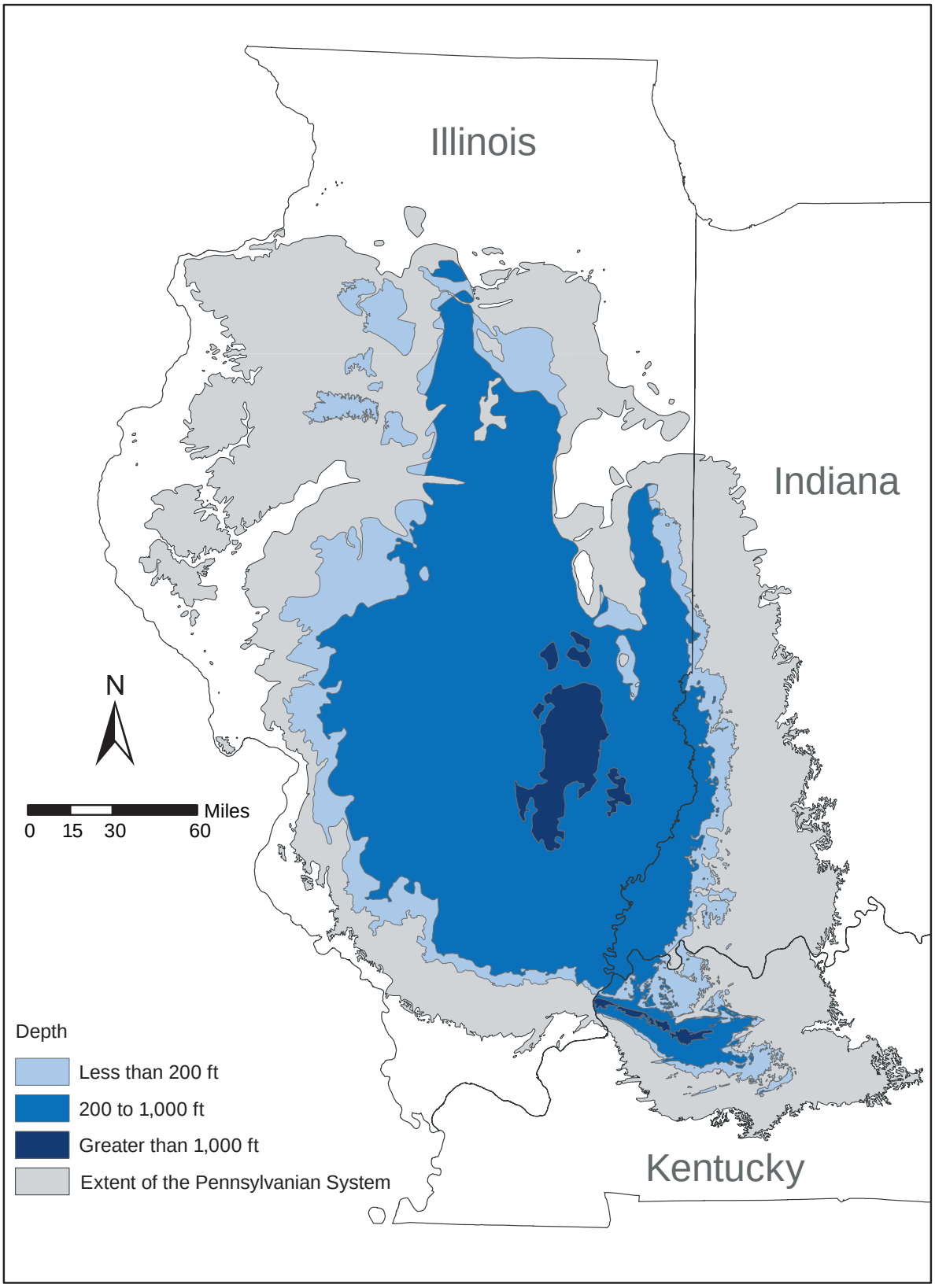

Figure A2-9 *Depth of the Danville/Baker Coal in the Illinois Basin.*

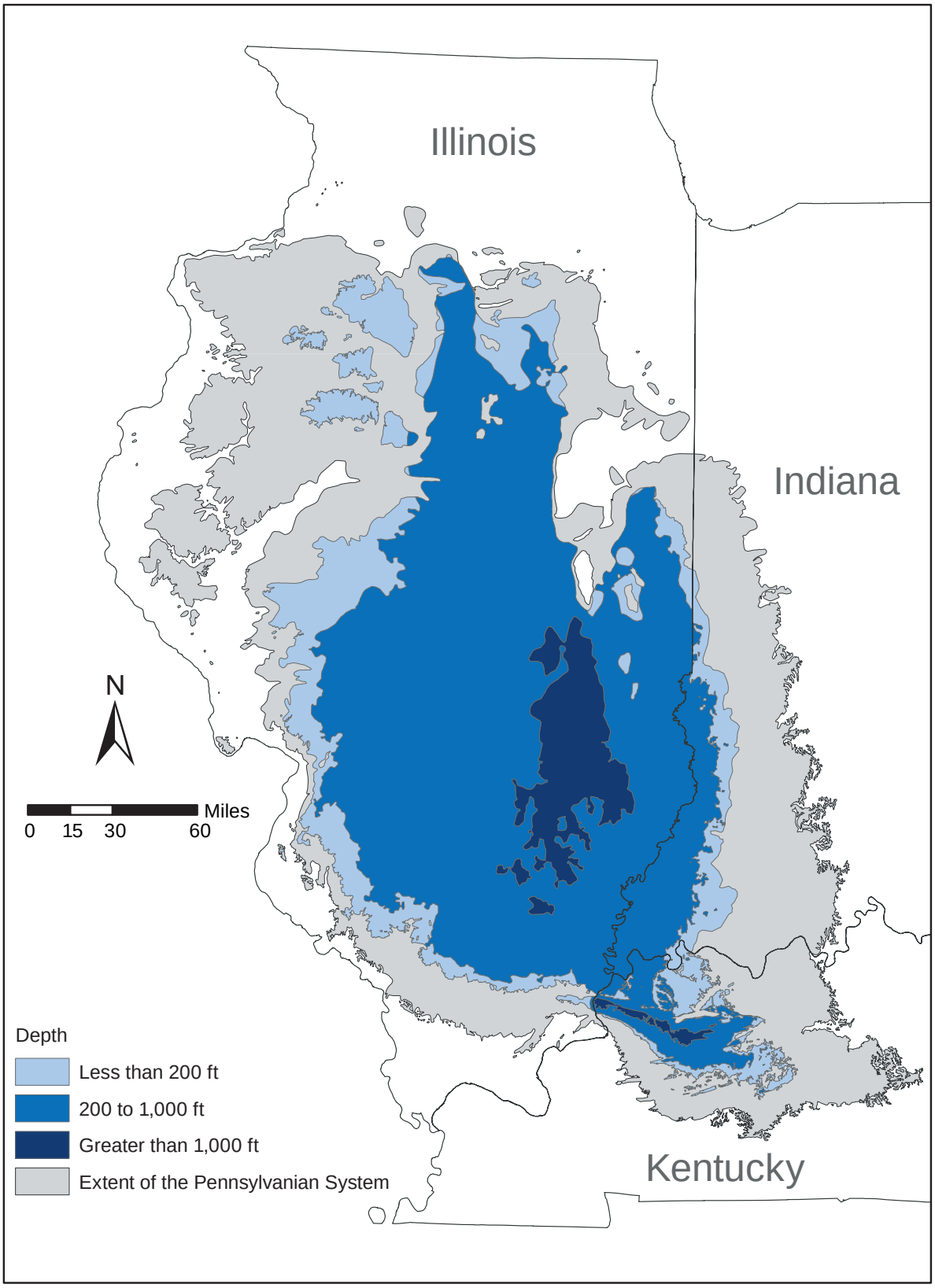

Figure A2-10 *Depth of the Herrin Coal in the Illinois Basin.*

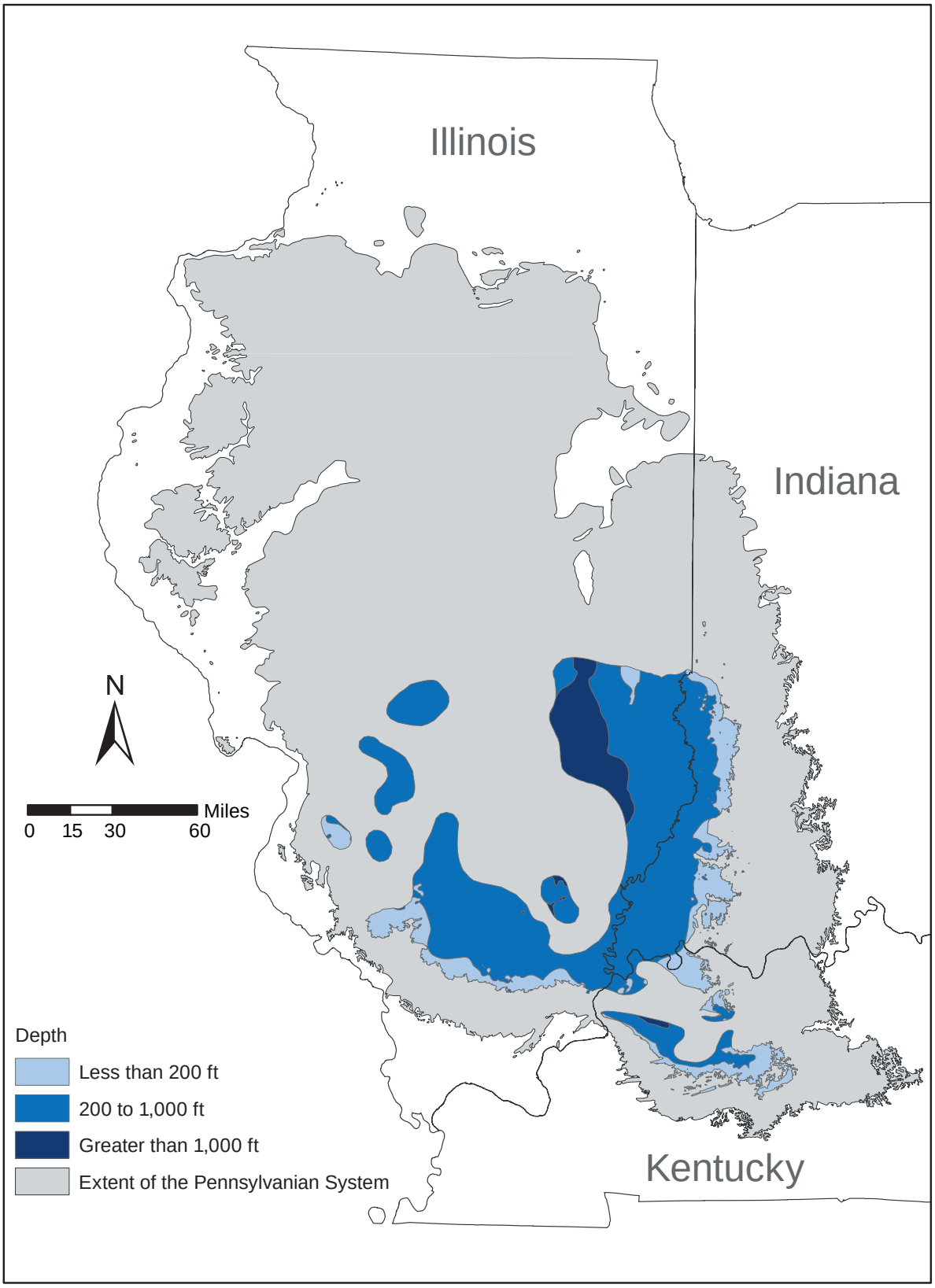

Figure A2-11 *Depth of the Hymera/Jamestown/Paradise Coal in the Illinois Basin.*

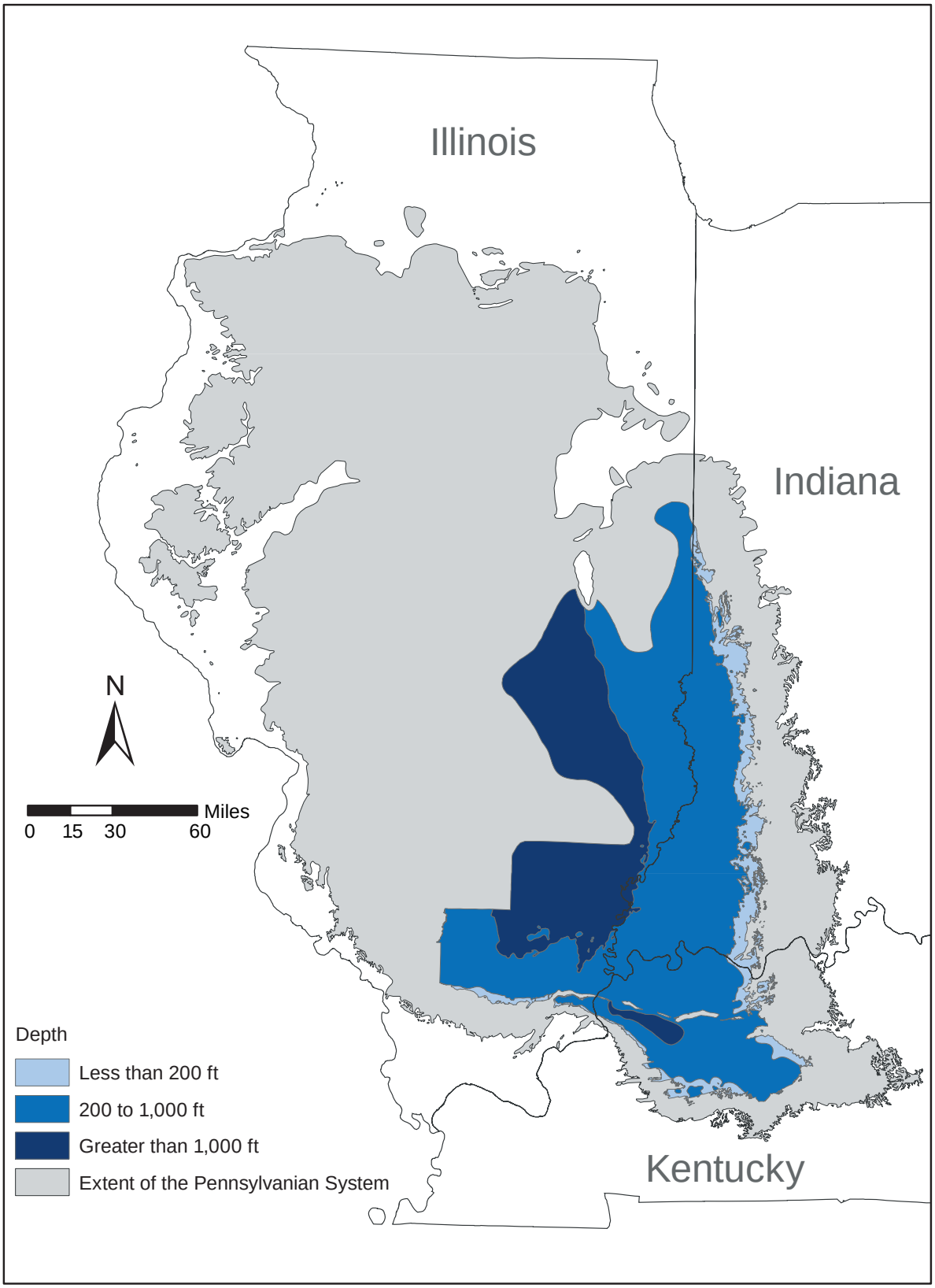

Figure A2-12 *Depth of the Seelyville/Davis/Dekoven Coal in the Illinois Basin.*

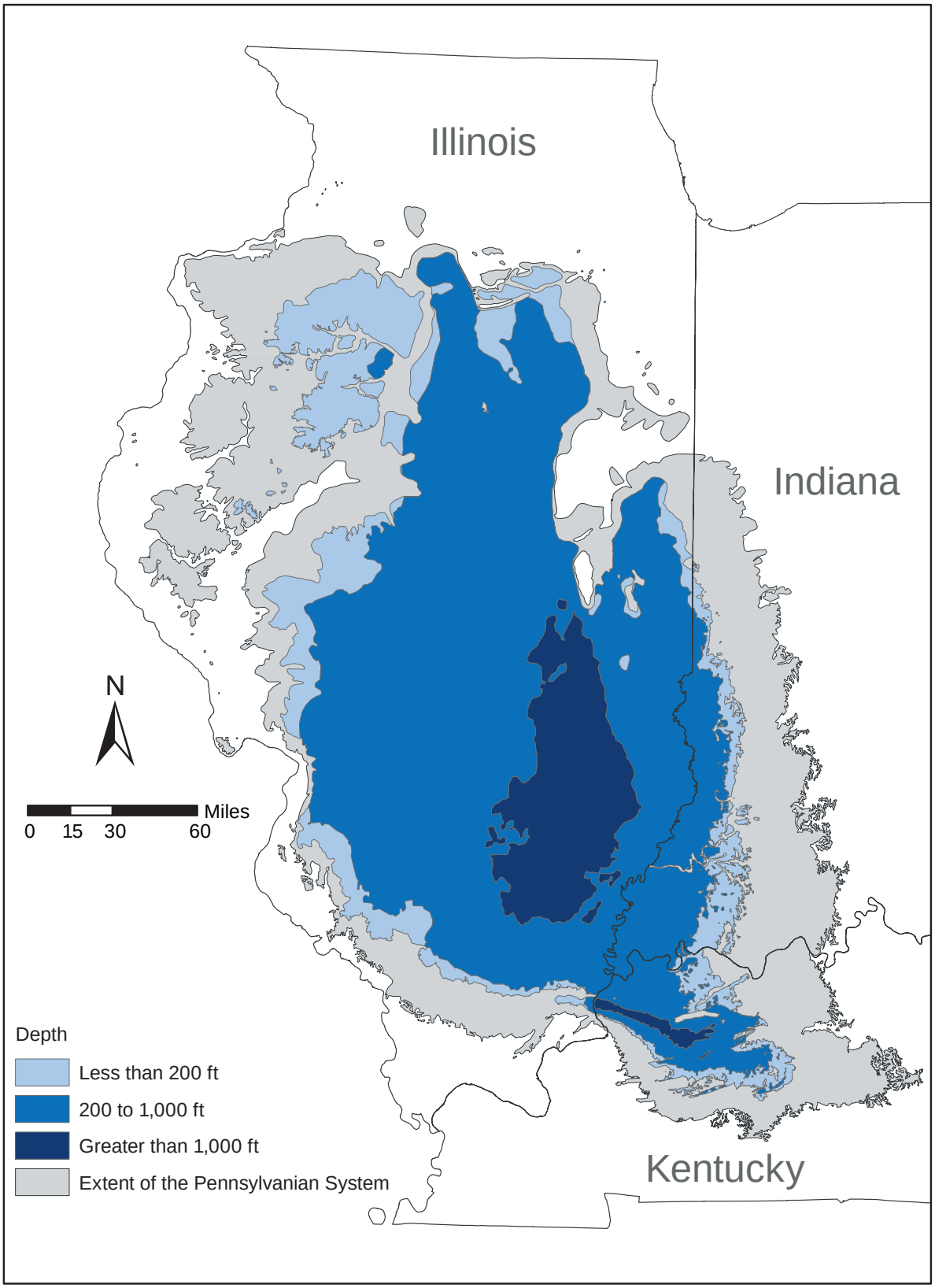

Figure A2-13 *Depth of the Springfield Coal in the Illinois Basin.*

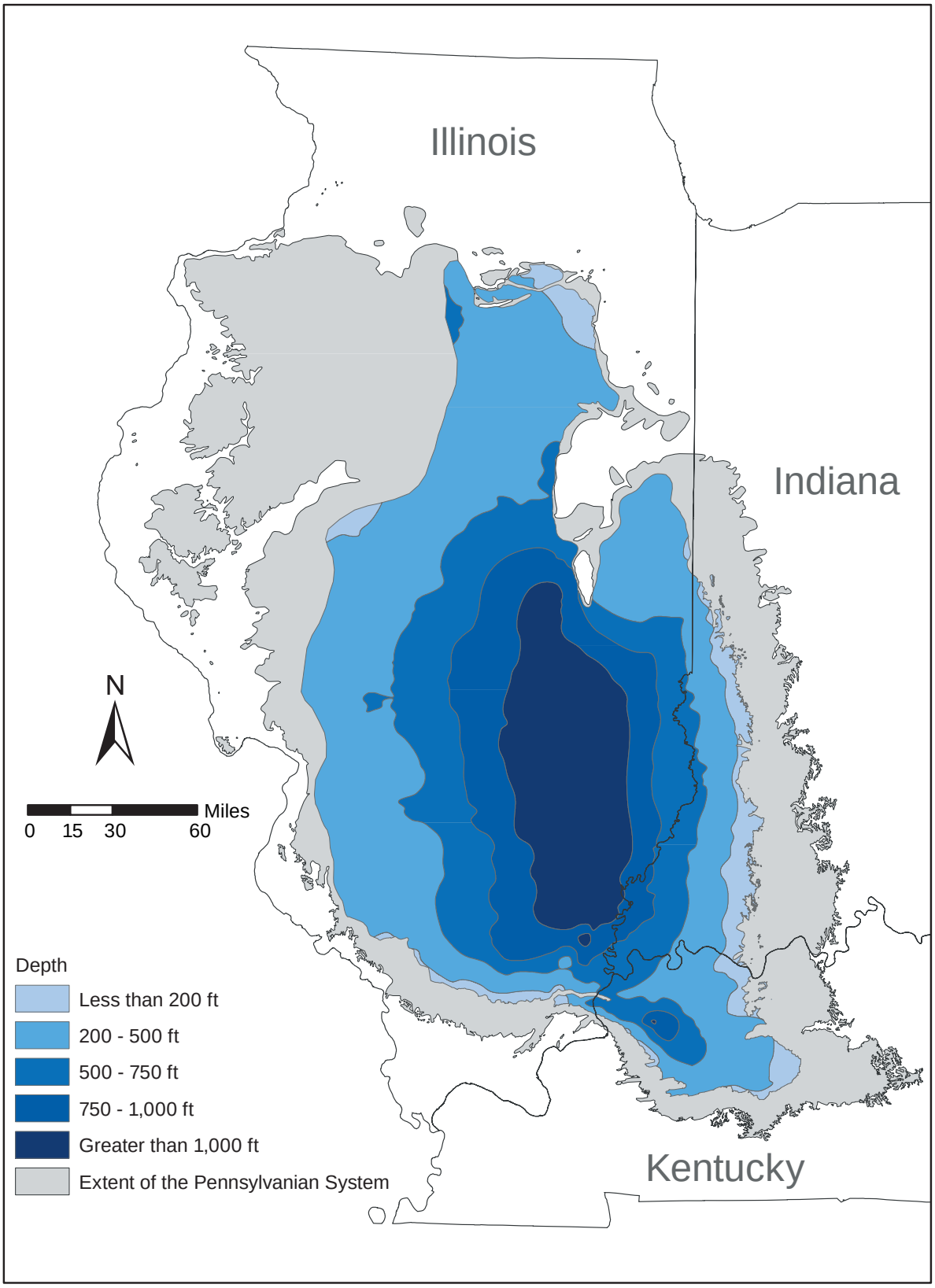

Figure A2-14 *Depth of the Survant Coal in the Illinois Basin.*

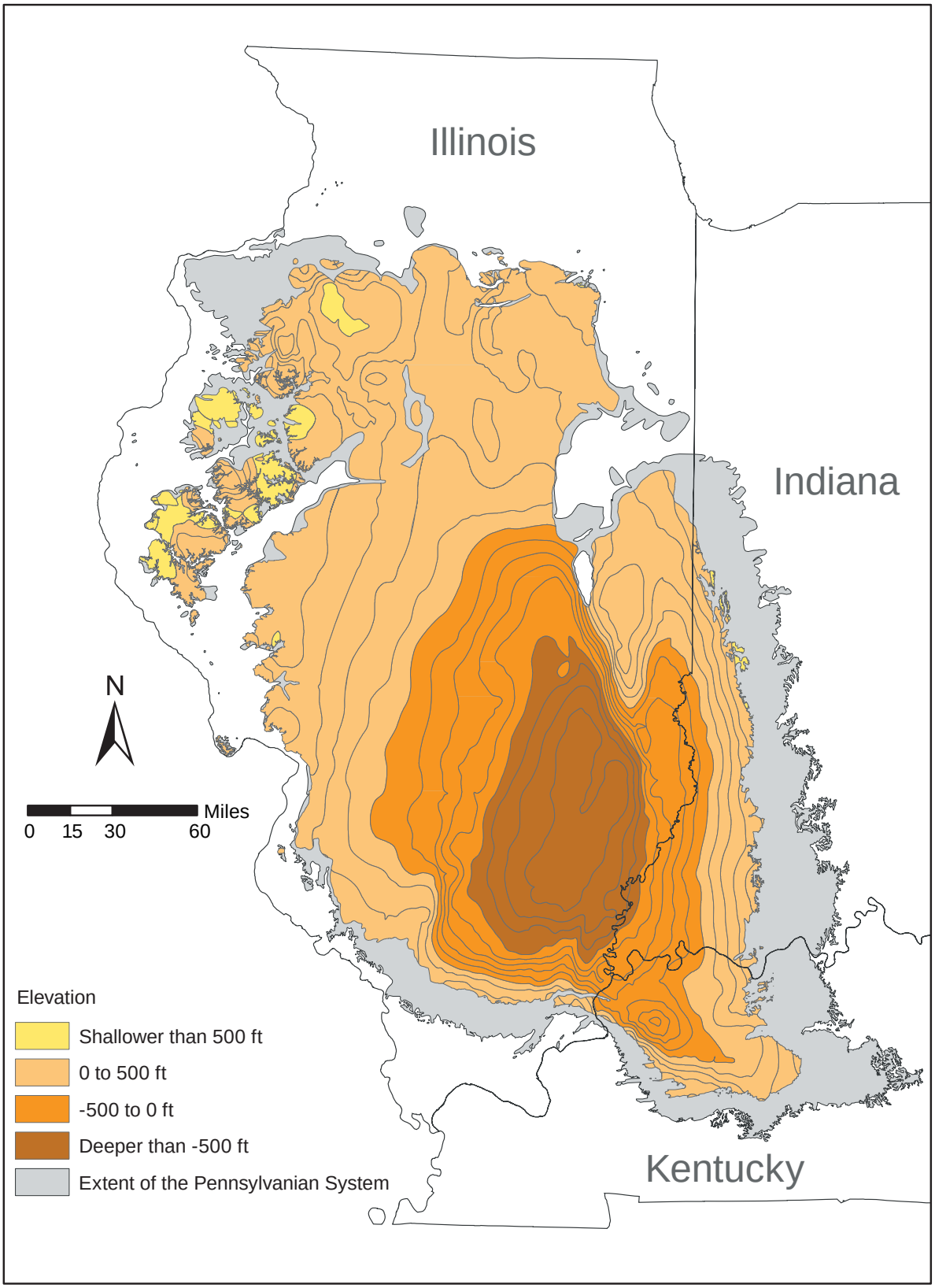

Figure A2-15 *Elevation of the Colchester Coal in the Illinois Basin.*

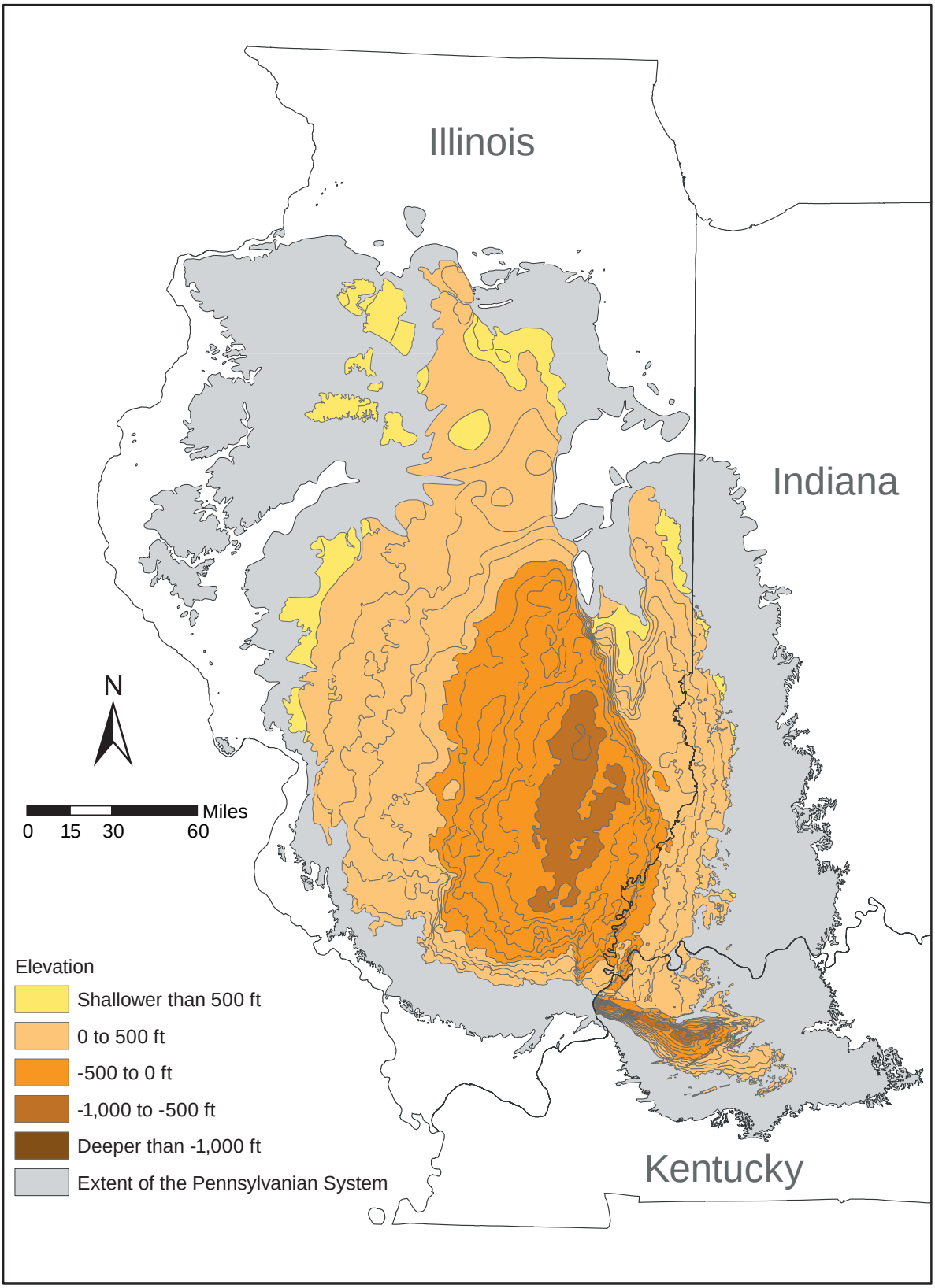

Figure A2-16 *Elevation of the Danville/Baker Coal in the Illinois Basin.*

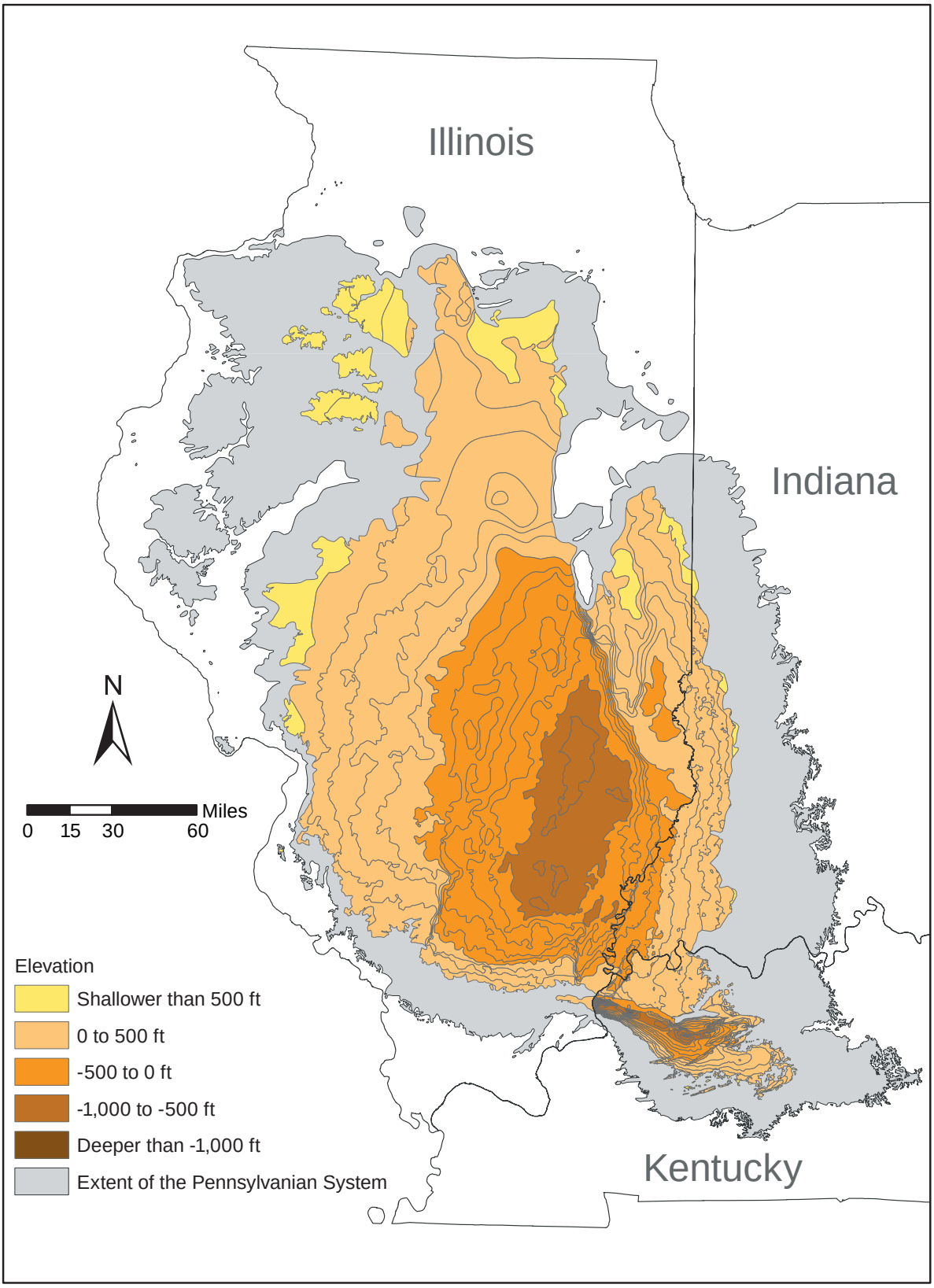

Figure A2-17 *Elevation of the Herrin Coal in the Illinois Basin.*

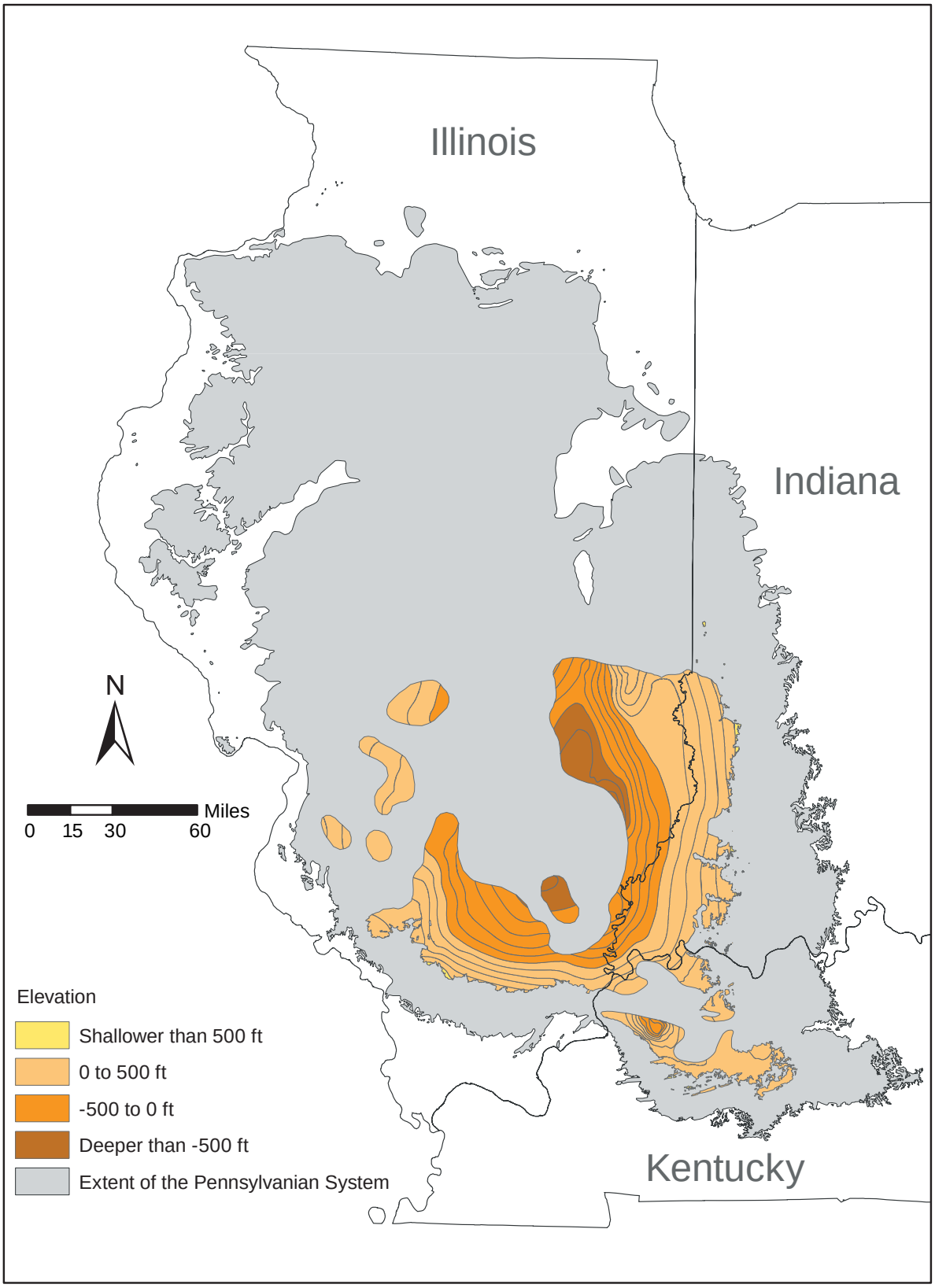

Figure A2-18 *Elevation of the Hymera/Jamestown/Paradise Coal in the Illinois Basin.*

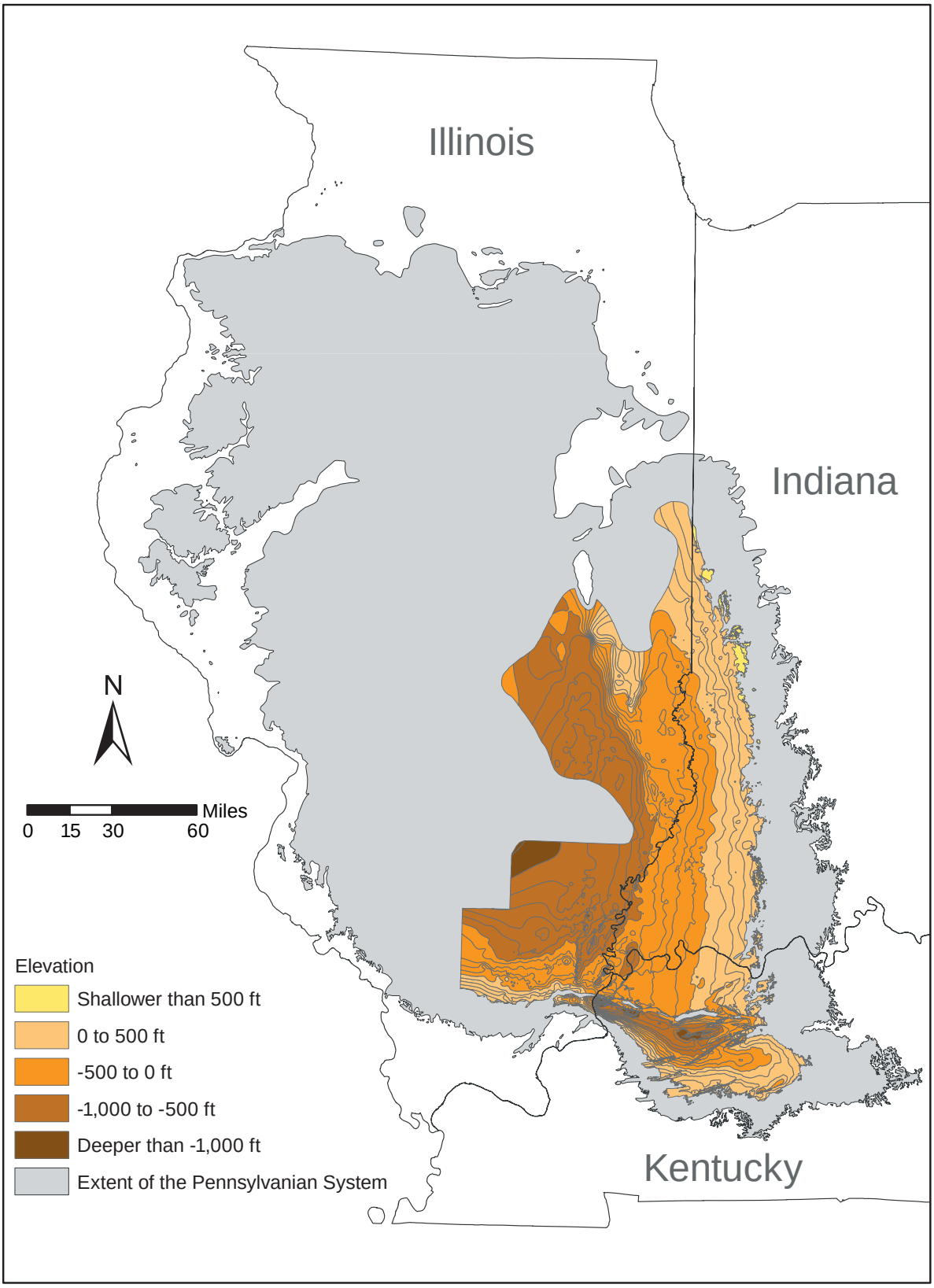

Figure A2-19 *Elevation of the Seelyville/Davis/Dekoven Coal in the Illinois Basin.*

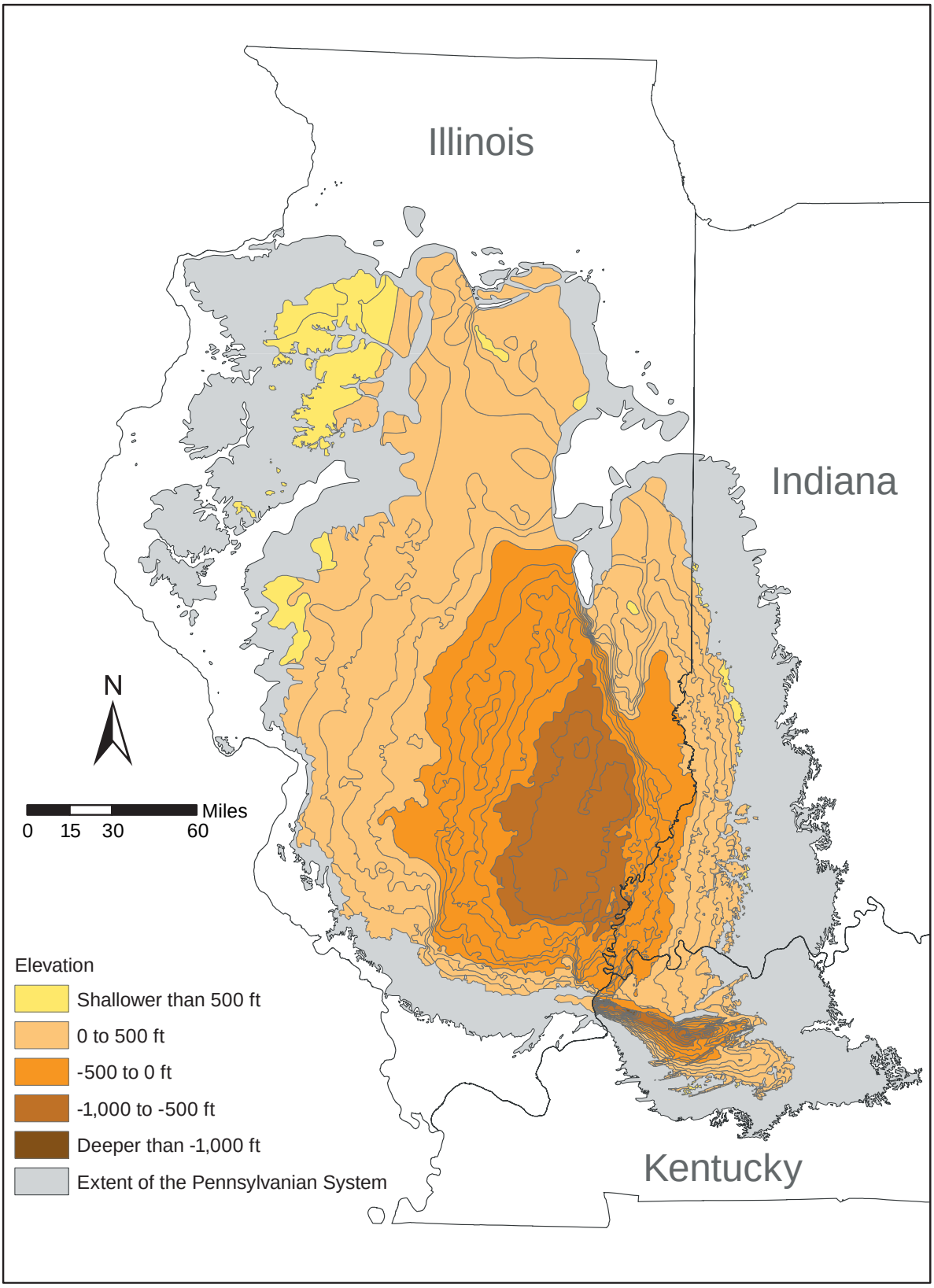

Figure A2-20 *Elevation of the Springfield Coal in the Illinois Basin.*

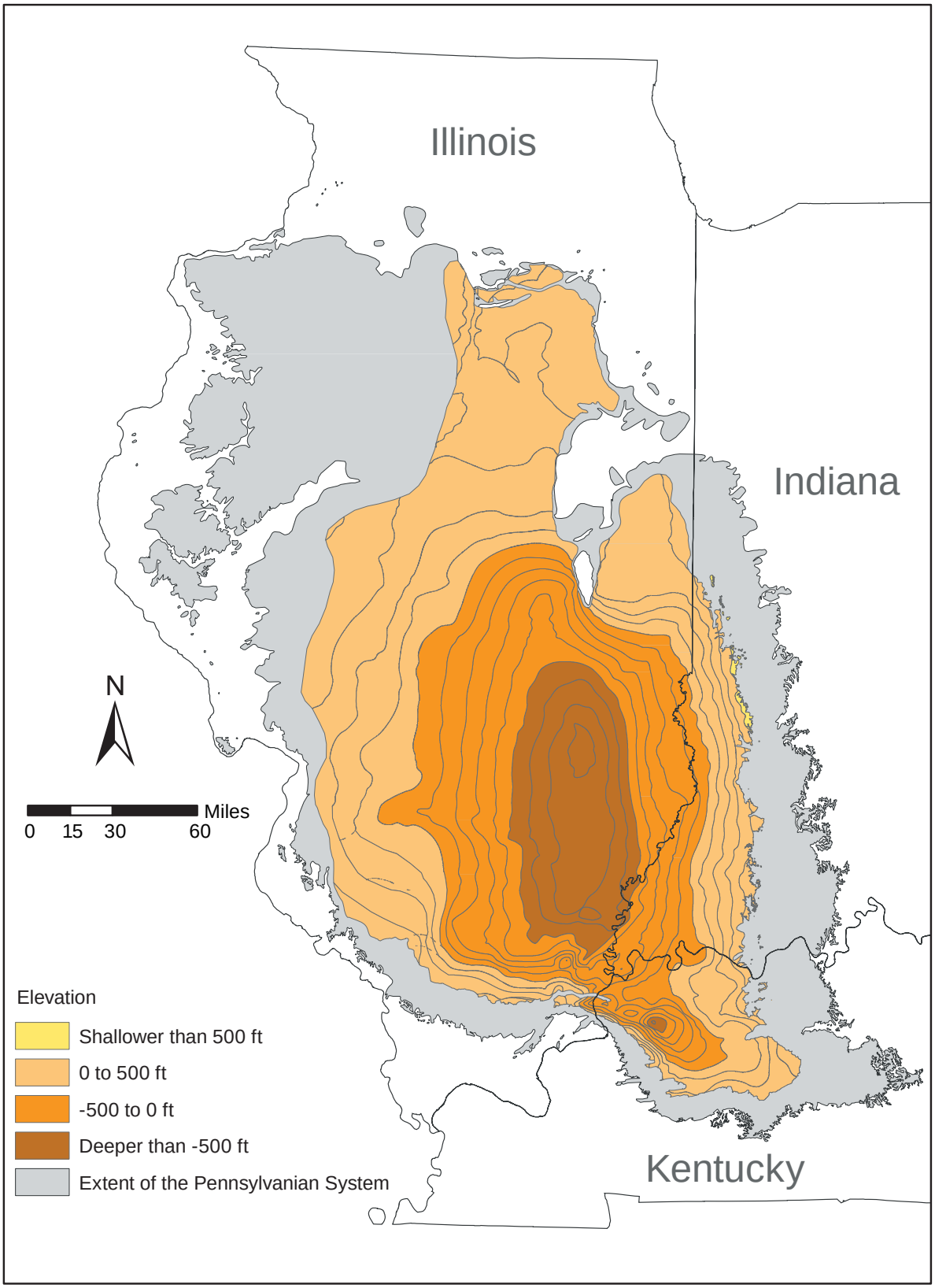

Figure A2-21 *Elevation of the Survant Coal in the Illinois Basin.*

Appendix 3: Coal Quality

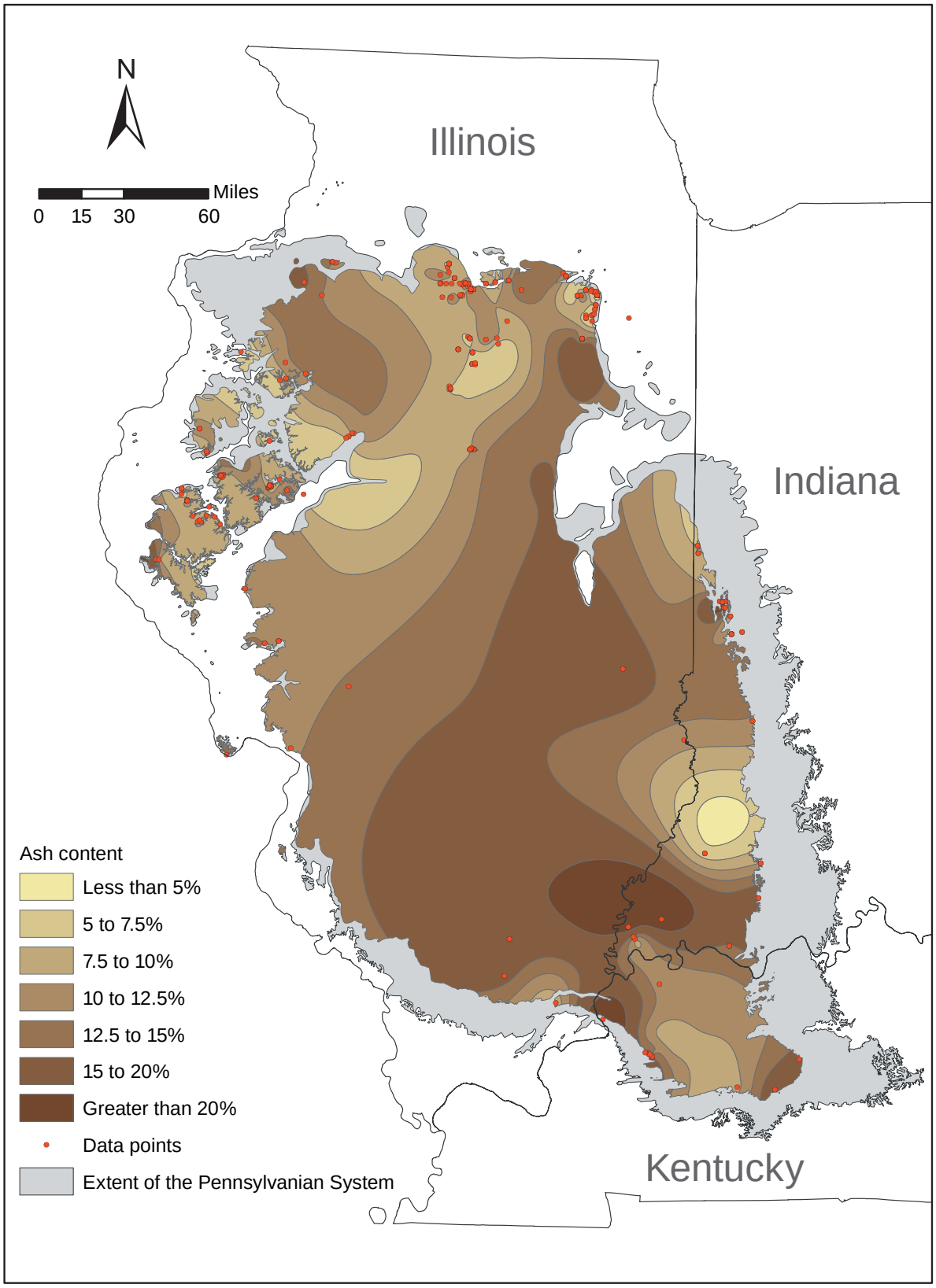

Figure A3-1 *Ash content (dry basis) of the Colchester Coal in the Illinois Basin.*

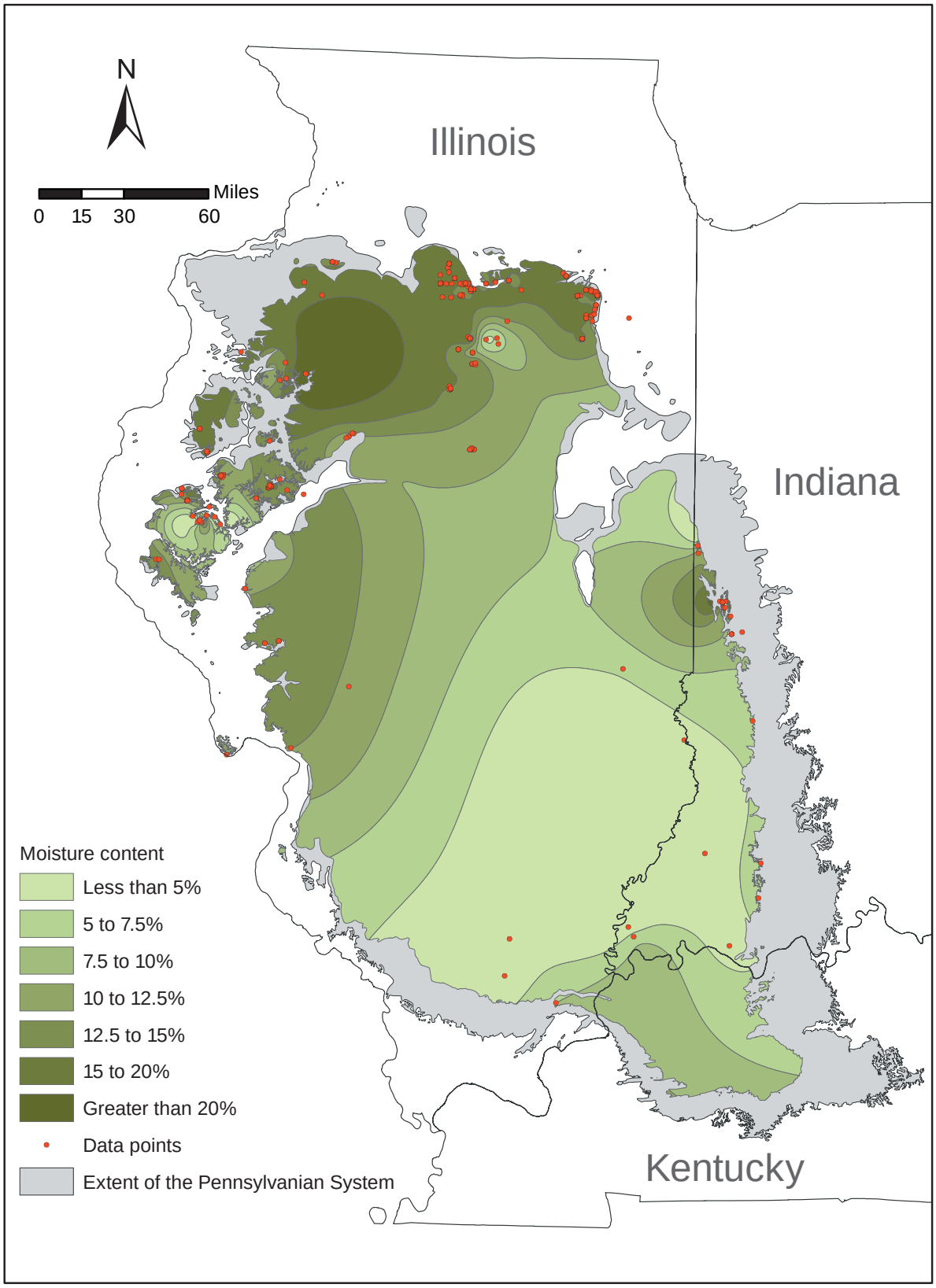

Figure A3-2 *Moisture content of the Colchester Coal in the Illinois Basin.*

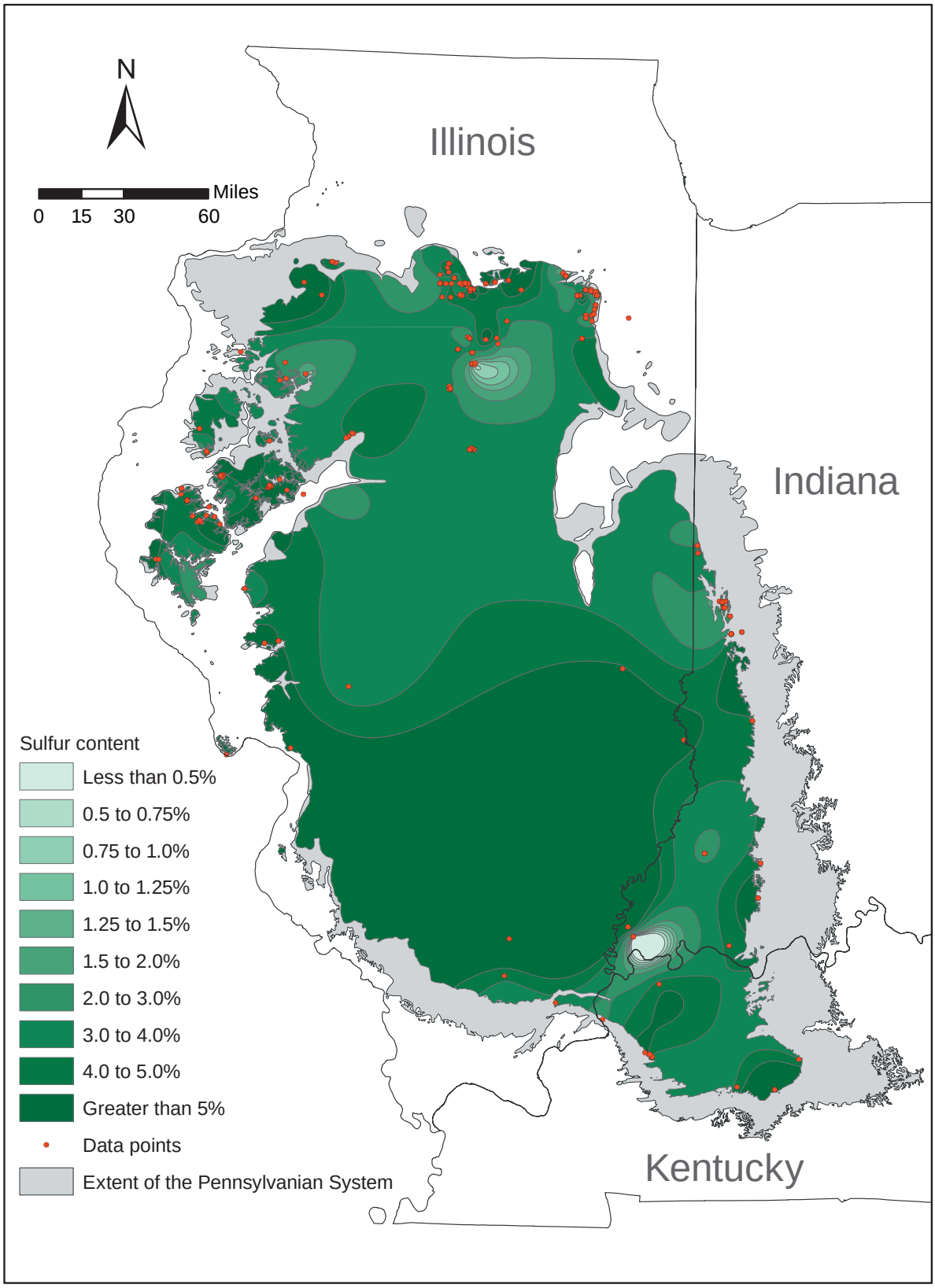

Figure A3-3 *Sulfer content (total, dry basis) of the Colchester Coal in the Illinois Basin.*

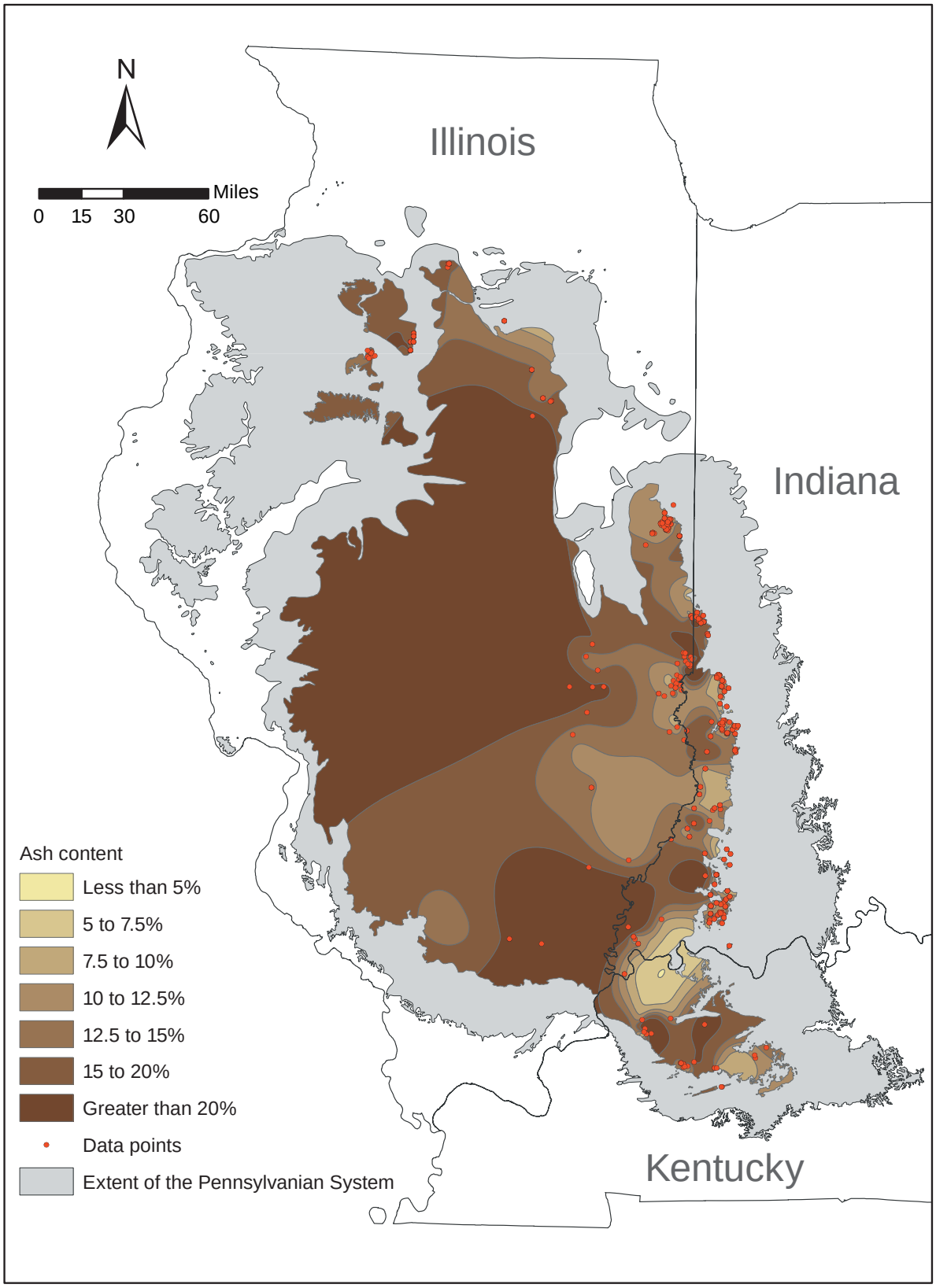

Figure A3-4 *Ash content (dry basis) of the Danville/Baker Coal in the Illinois Basin.*

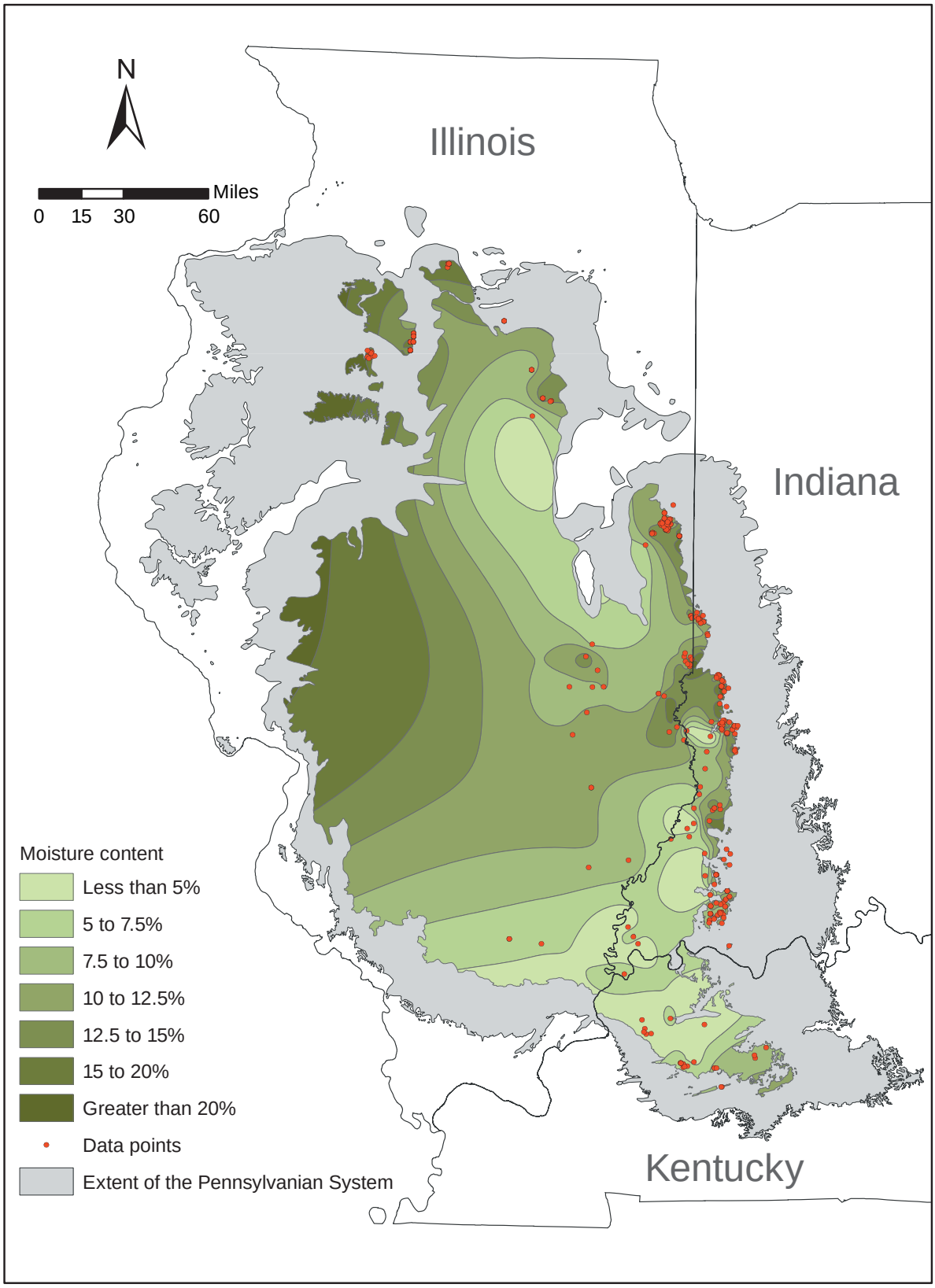

Figure A3-5 *Moisture content of the Danville/Baker Coal in the Illinois Basin.*

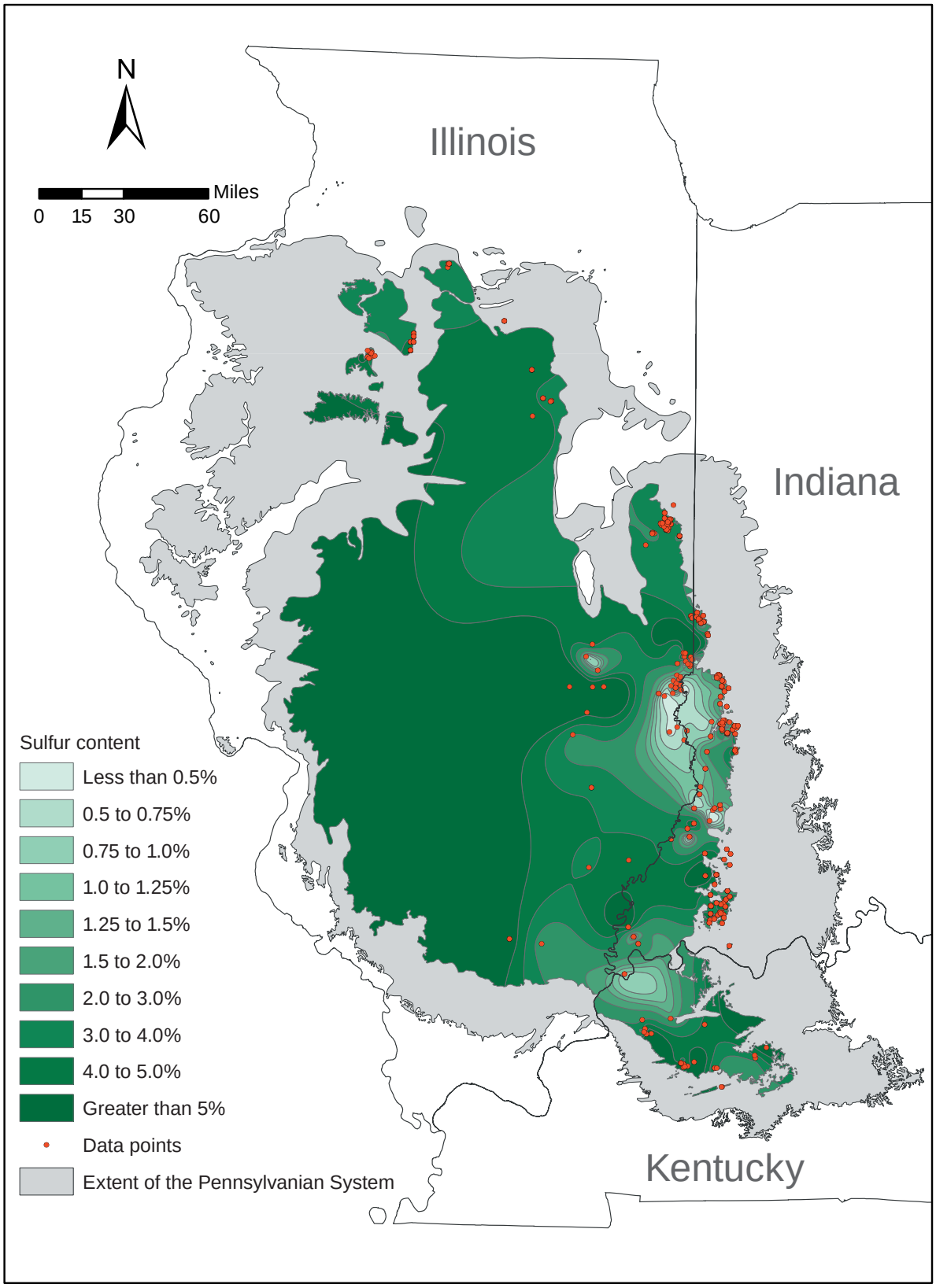

Figure A3-6 *Sulfer content (total, dry basis) of the Danville/Baker Coal in the Illinois Basin.*

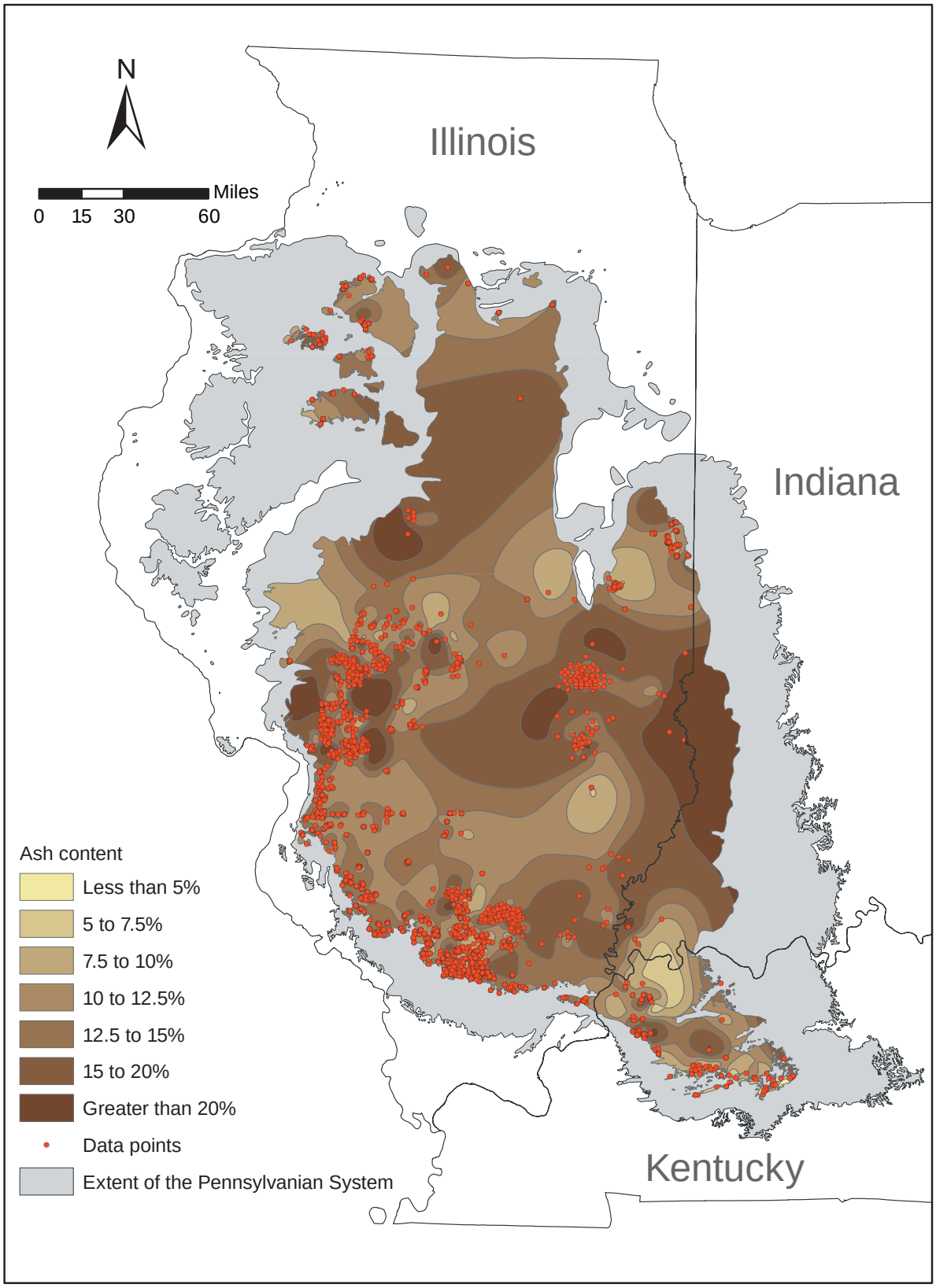

Figure A3-7 *Ash content (dry basis) of the Herrin Coal in the Illinois Basin.*

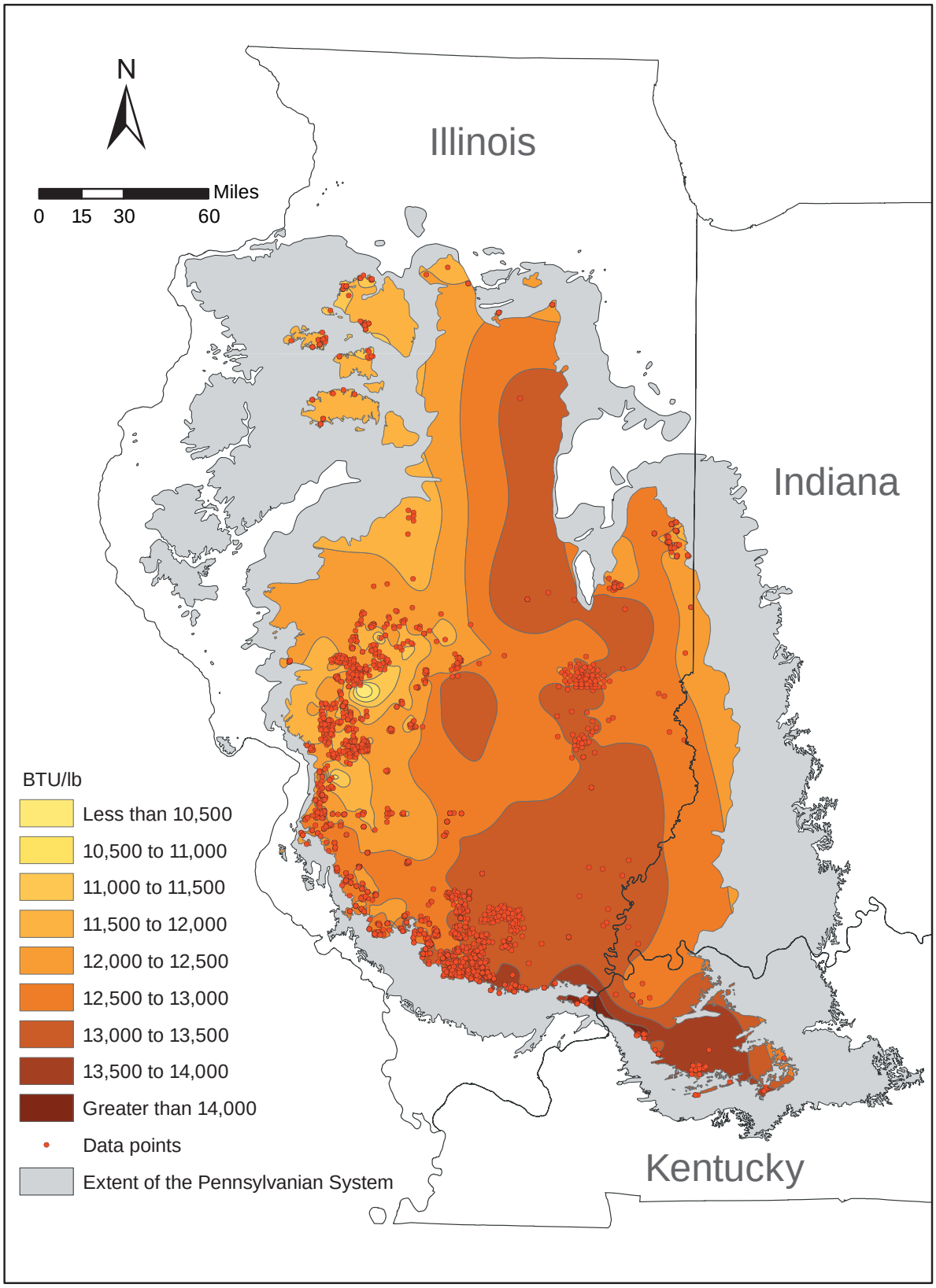

Figure A3-8 *Heating value (ash free, moisture included basis) of the Herrin Coal in the Illinois Basin.*

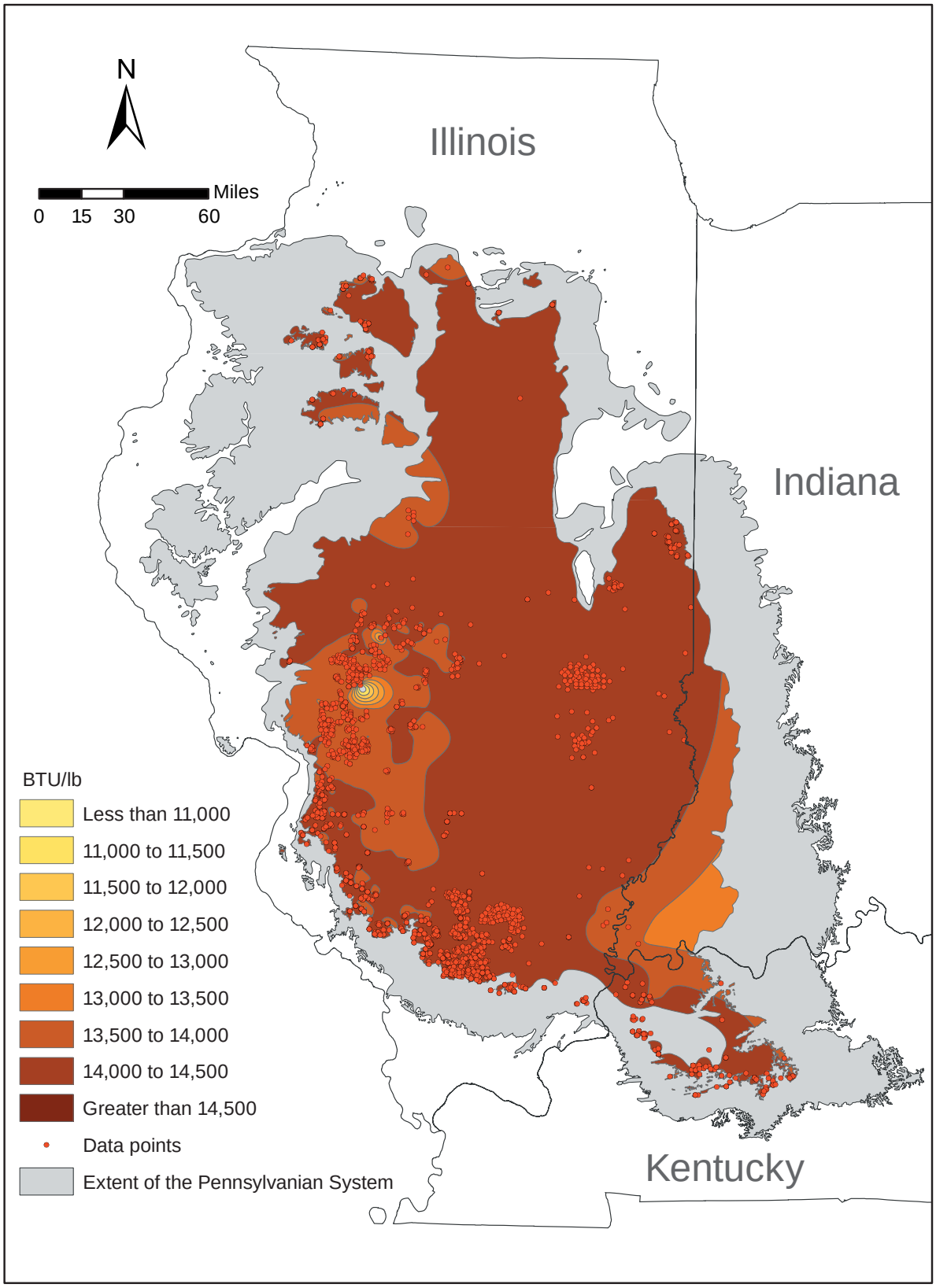

Figure A3-9 *Heating value (dry, ash free basis) of the Herrin Coal in the Illinois Basin.*

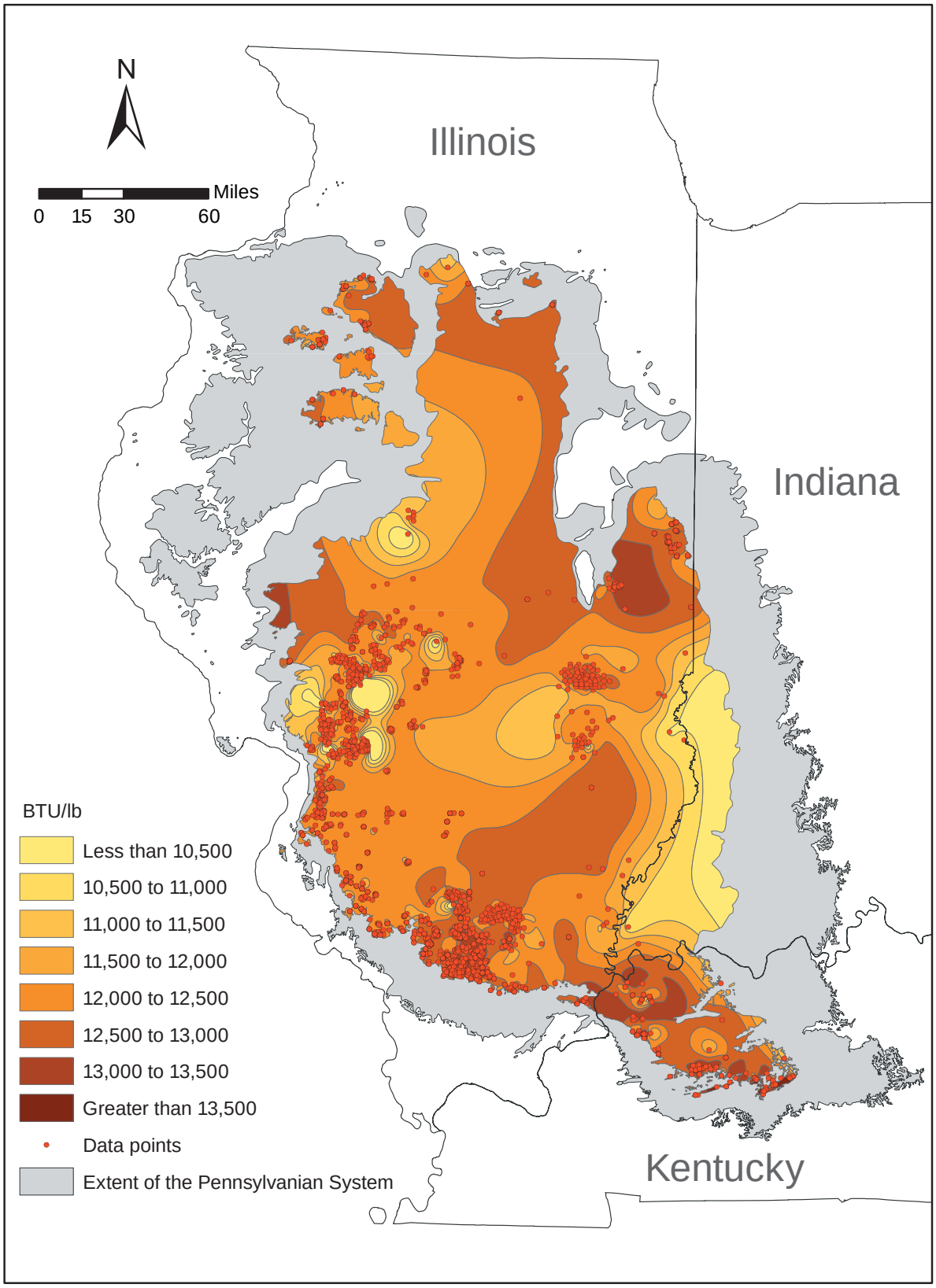

Figure A3-10 *Heating value (dry basis) of the Herrin Coal in the Illinois Basin.*

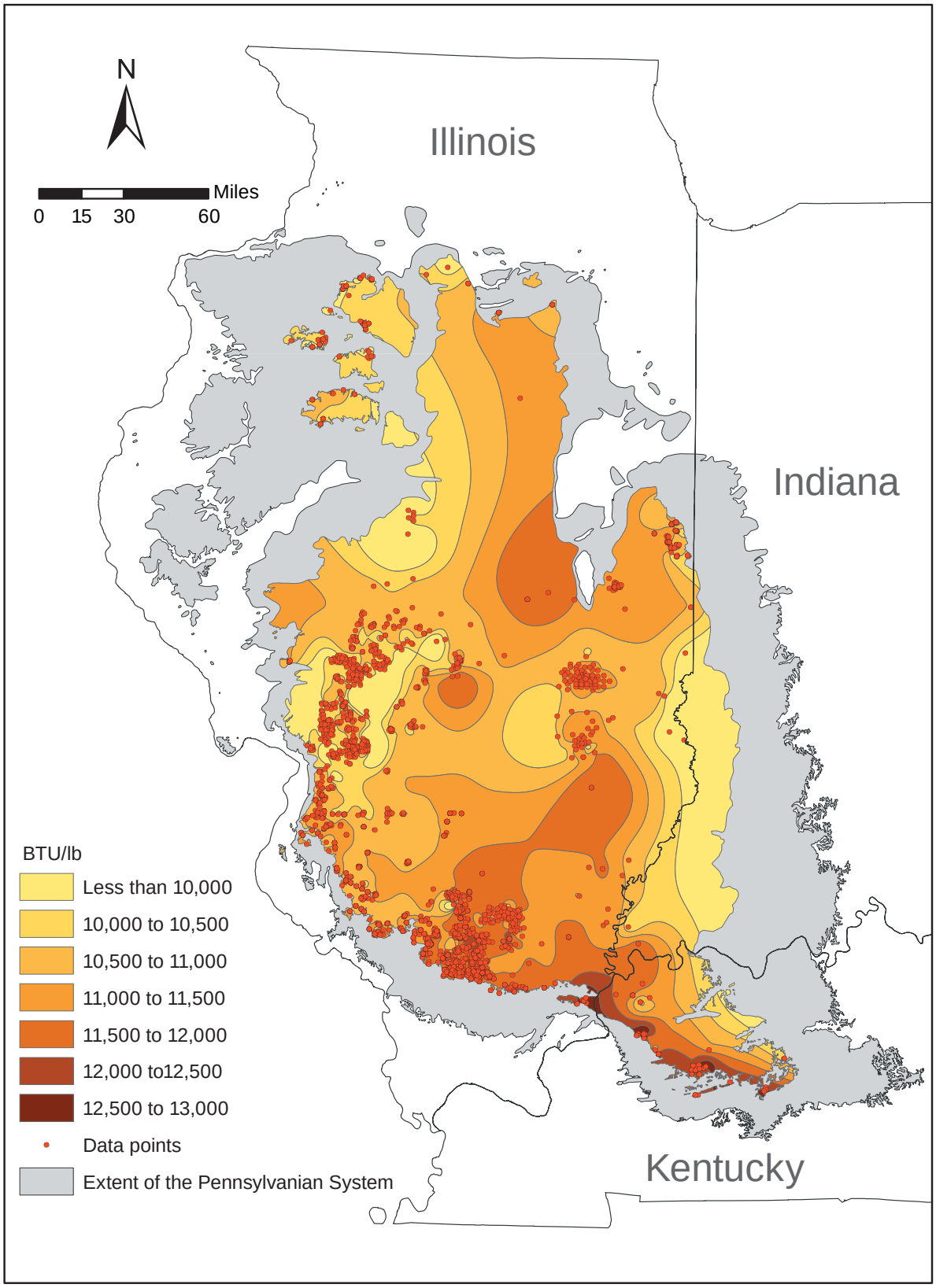

Figure A3-11 *Heating value (moisture and ash included basis) of the Herrin Coal in the Illinois Basin.*

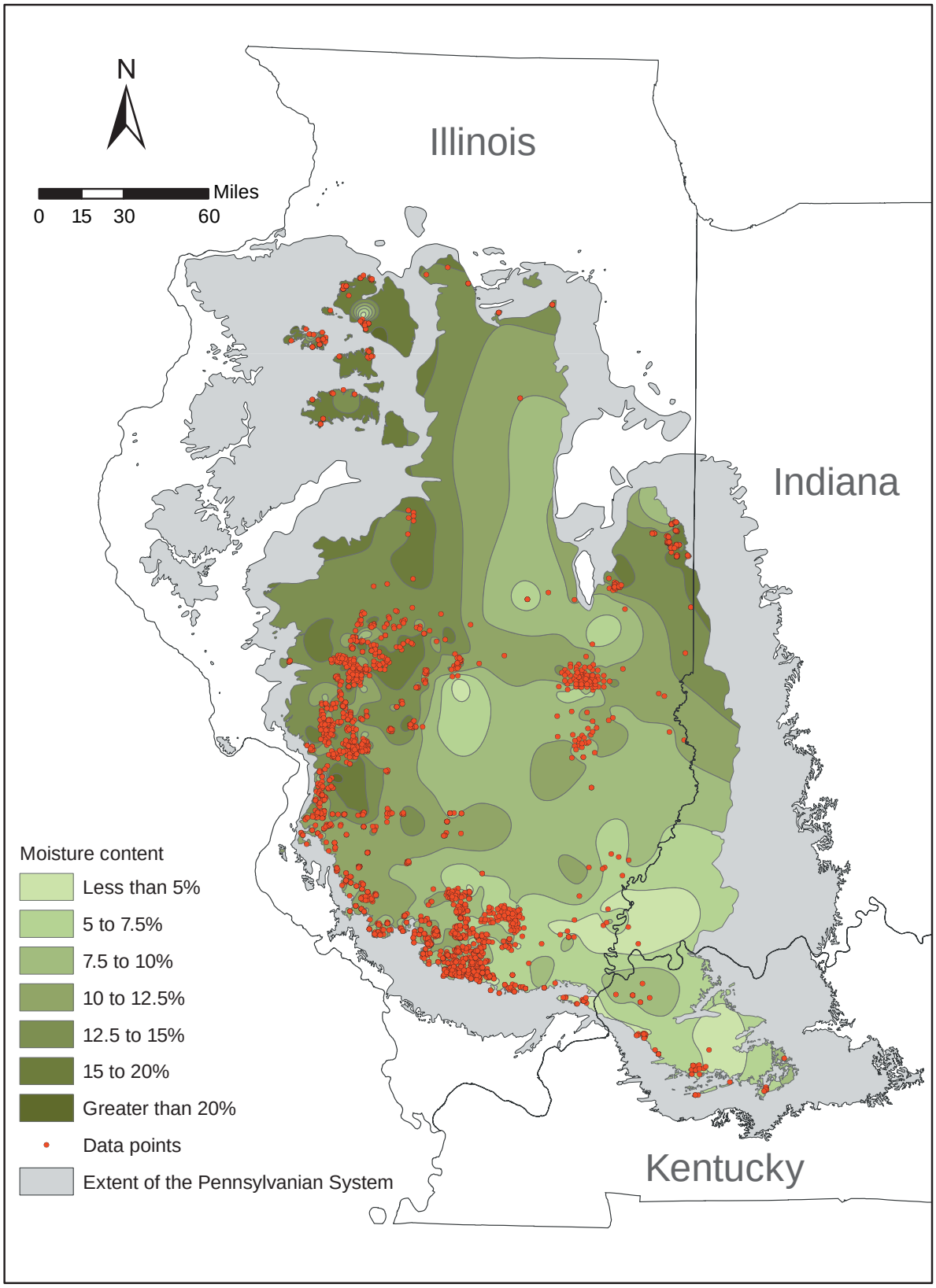

Figure A3-12 *Moisture content of the Herrin Coal in the Illinois Basin.*

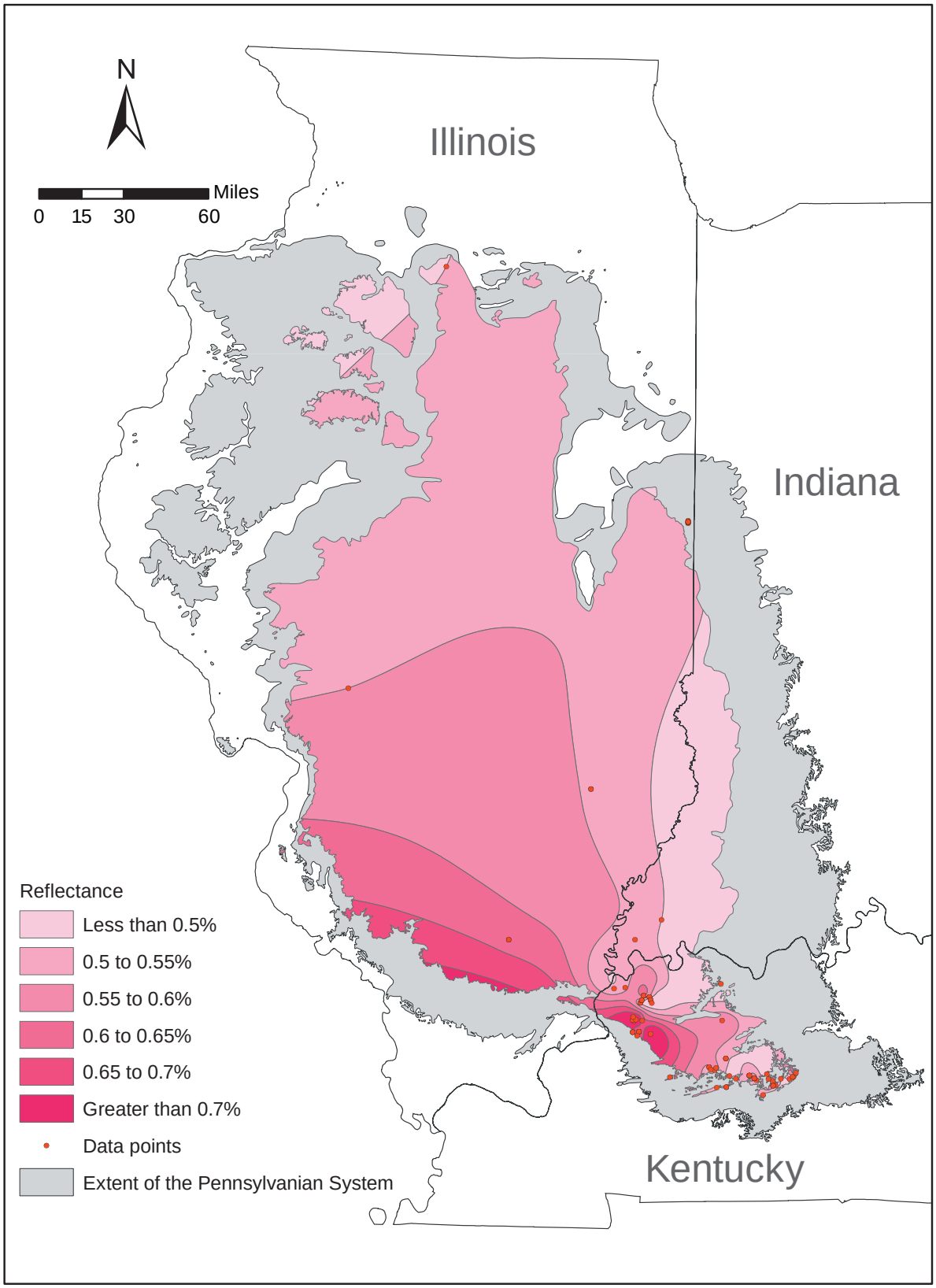

Figure A3-13 *Vitrinite reflectance of the Herrin Coal in the Illinois Basin.*

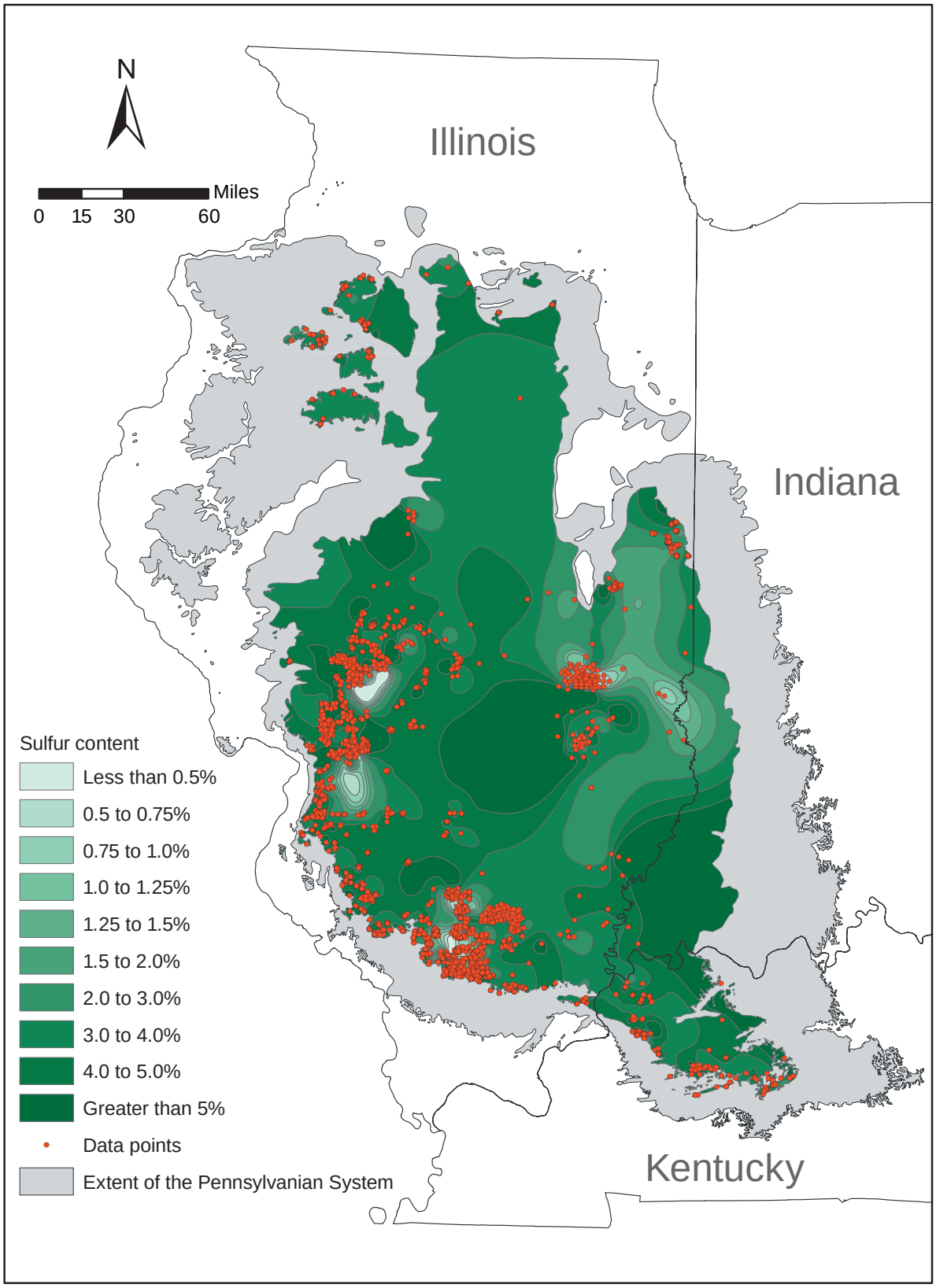

Figure A3-14 *Sulfur content (total, dry basis) of the Herrin Coal in the Illinois Basin.*

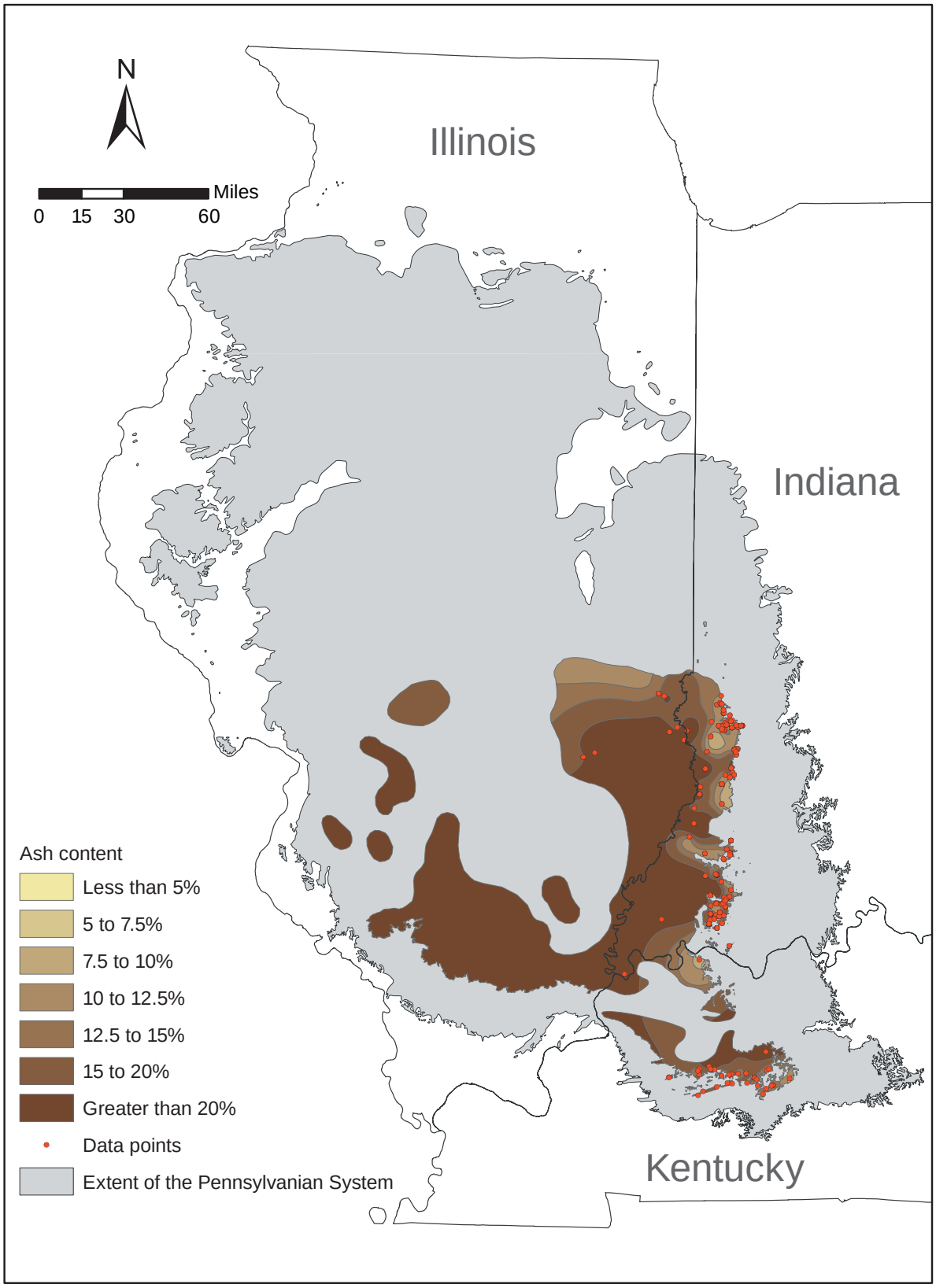

Figure A3-15 *Ash content (dry basis) of the Hymera/Jamestown/Paradise Coal in the Illinois Basin.*

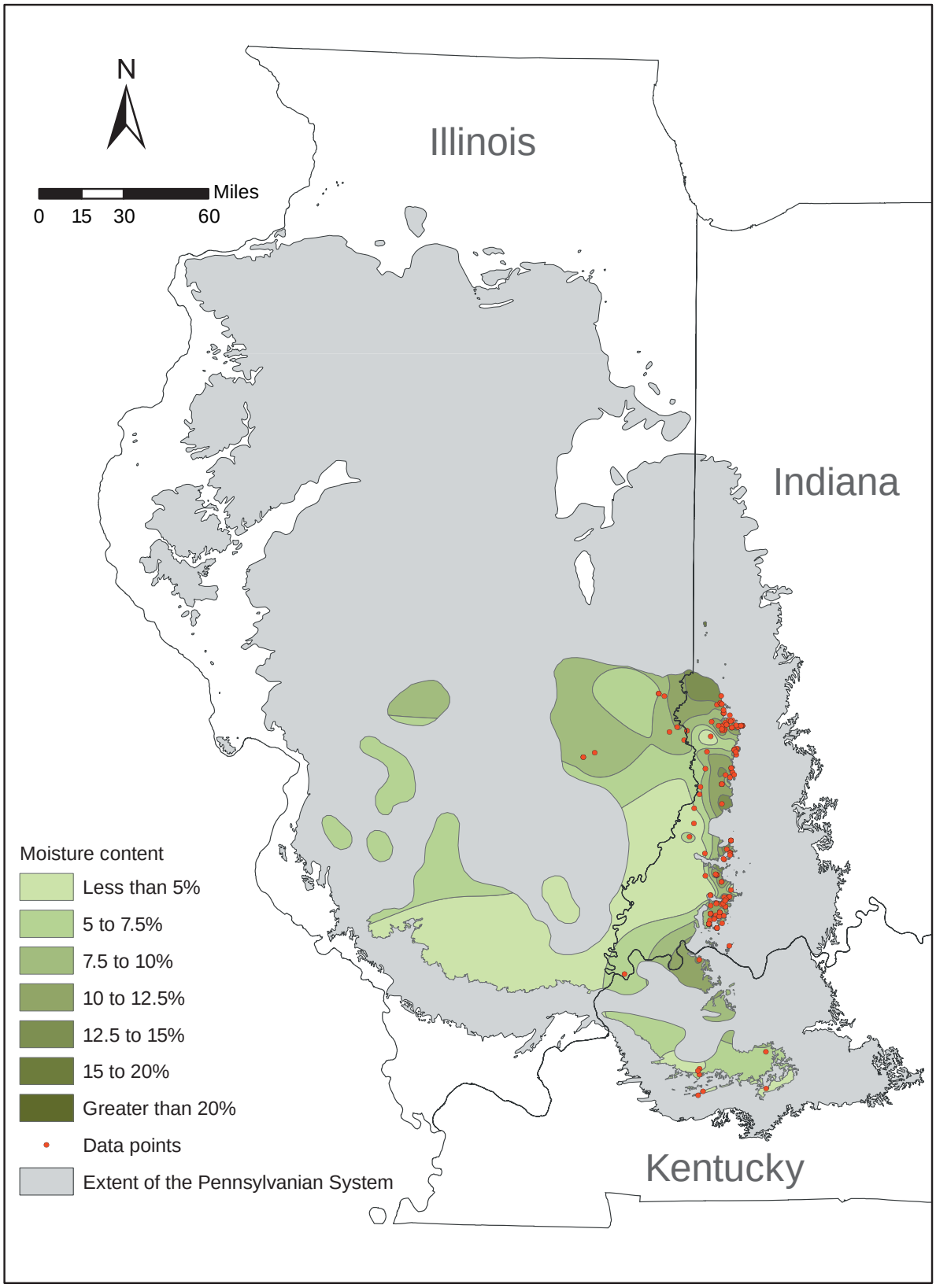

Figure A3-16 *Moisture content of the Hymera/Jamestown/Paradise Coal in the Illinois Basin.*

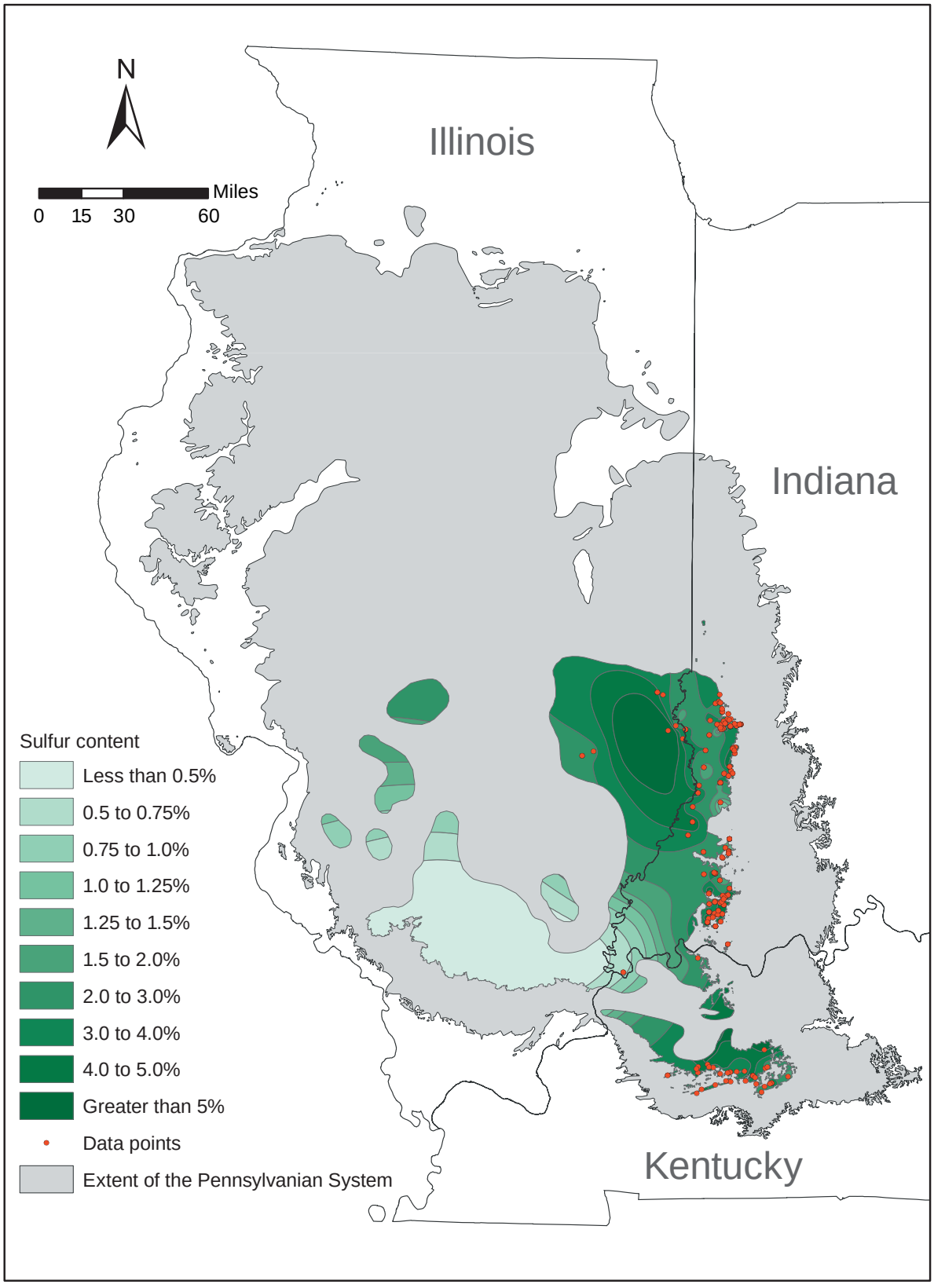

Figure A3-17 *Sulfur content (total, dry basis) of the Hymera/Jamestown/Paradise Coal in the Illinois Basin.*

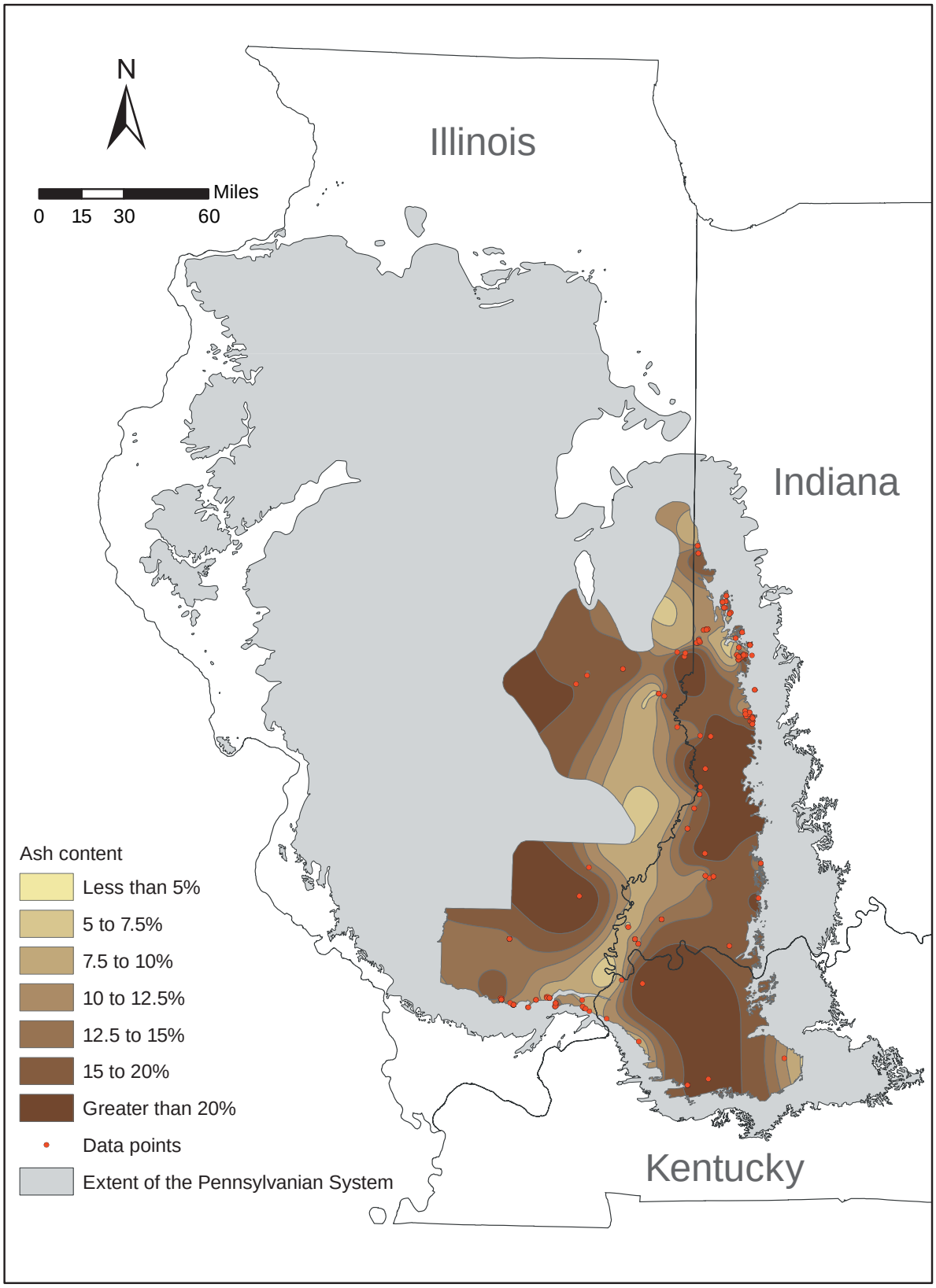

Figure A3-18 *Ash content (dry basis) of the Seelyville/Davis/Dekoven Coal in the Illinois Basin.*

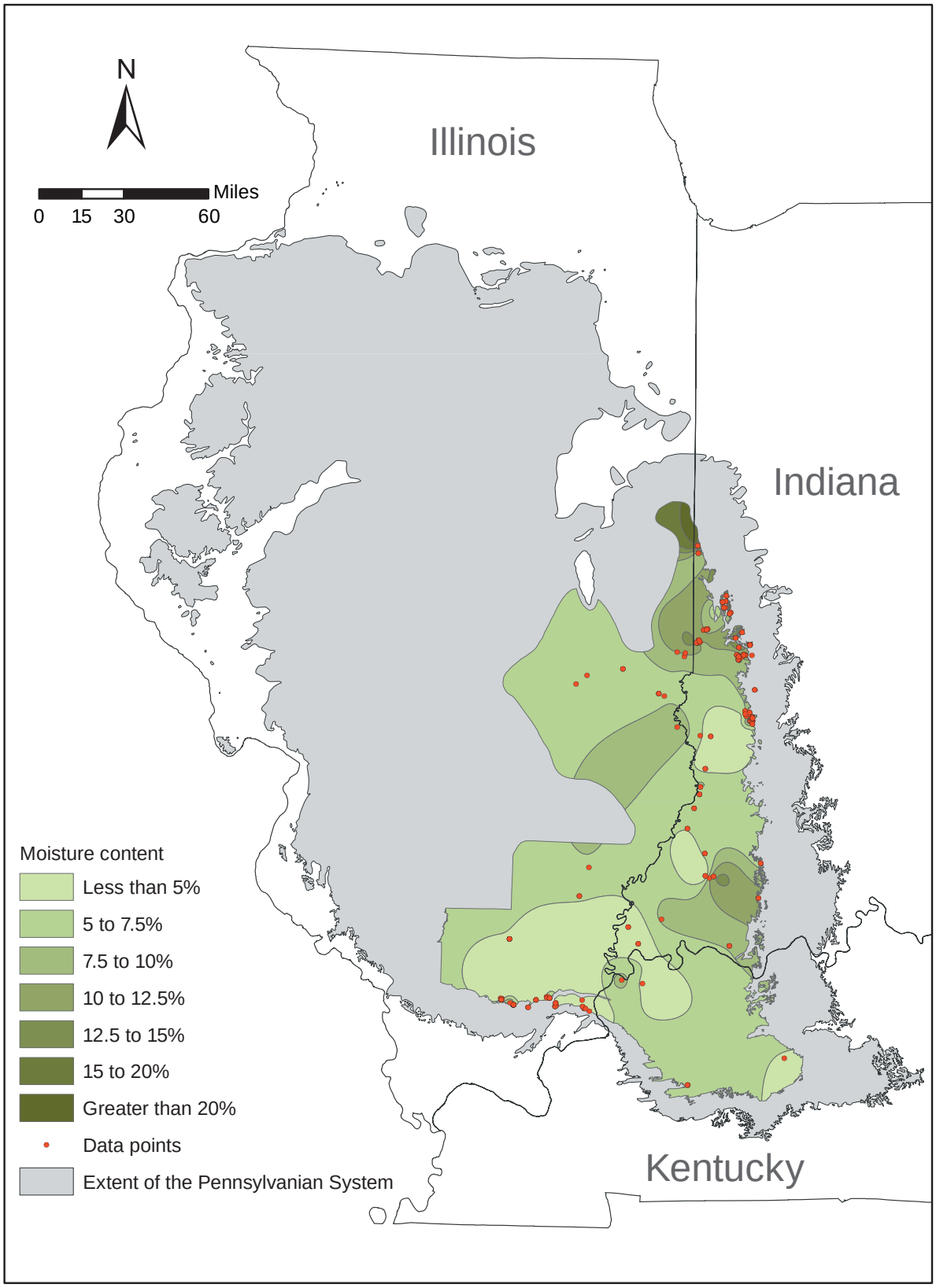

Figure A3-19 *Moisture content of the Seelyville/Davis/Dekoven Coal in the Illinois Basin.*

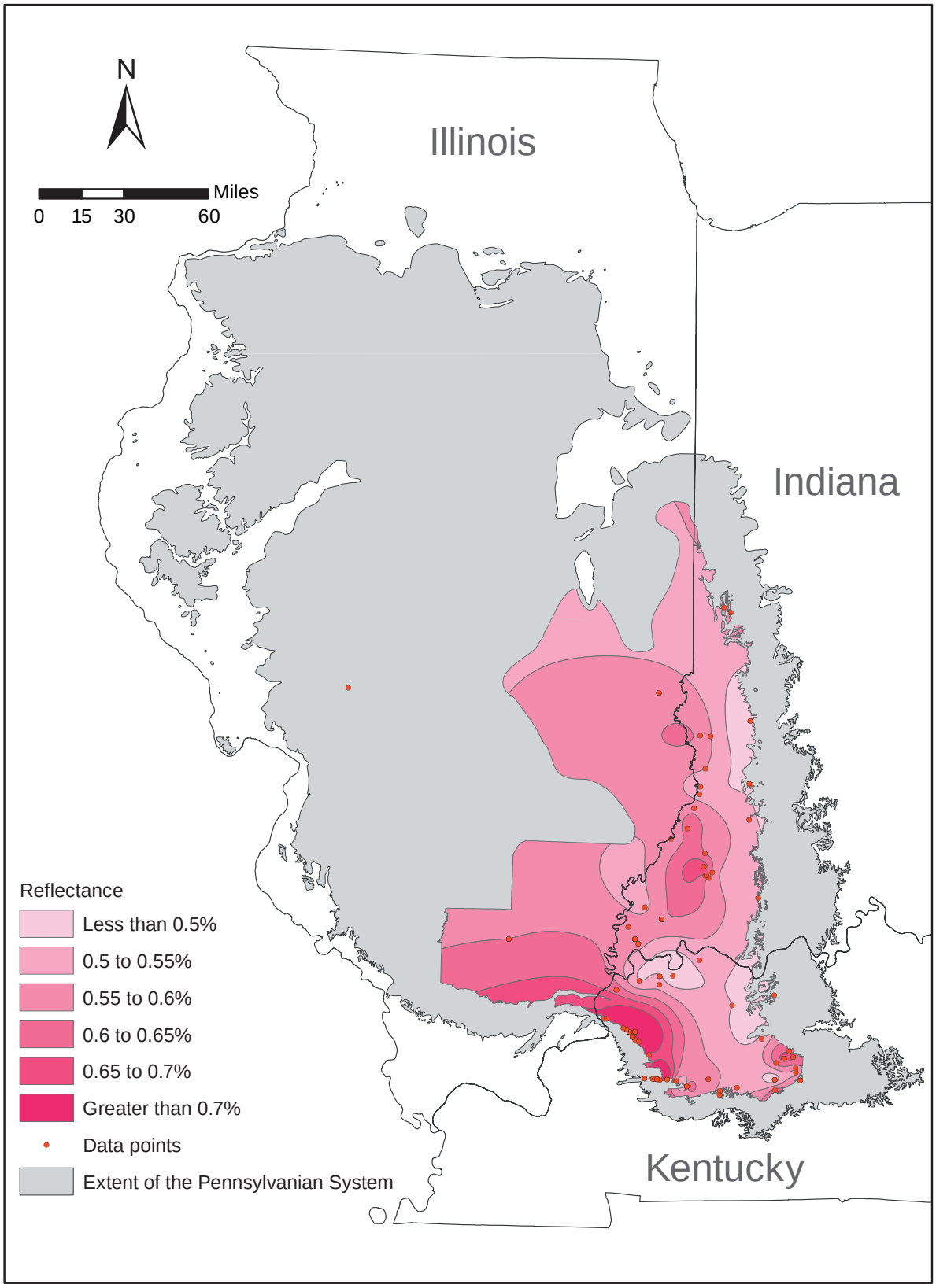

Figure A3-20 *Vitrinite reflectance of the Seelyville/Davis/Dekoven Coal in the Illinois Basin.*

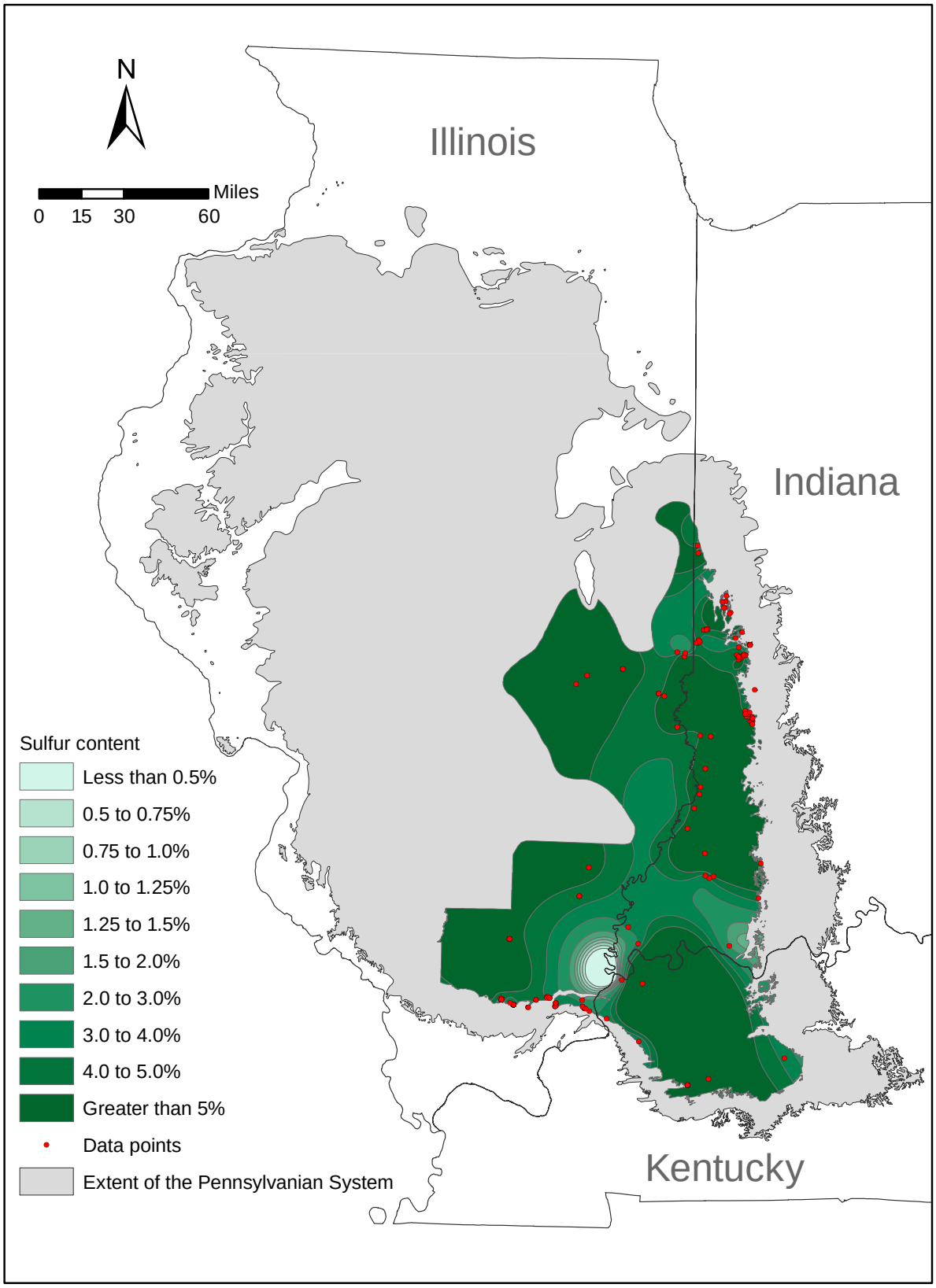

Figure A3-21 *Sulfur content (total, dry basis) of the Seelyville/Davis/Dekoven Coal in the Illinois Basin.*

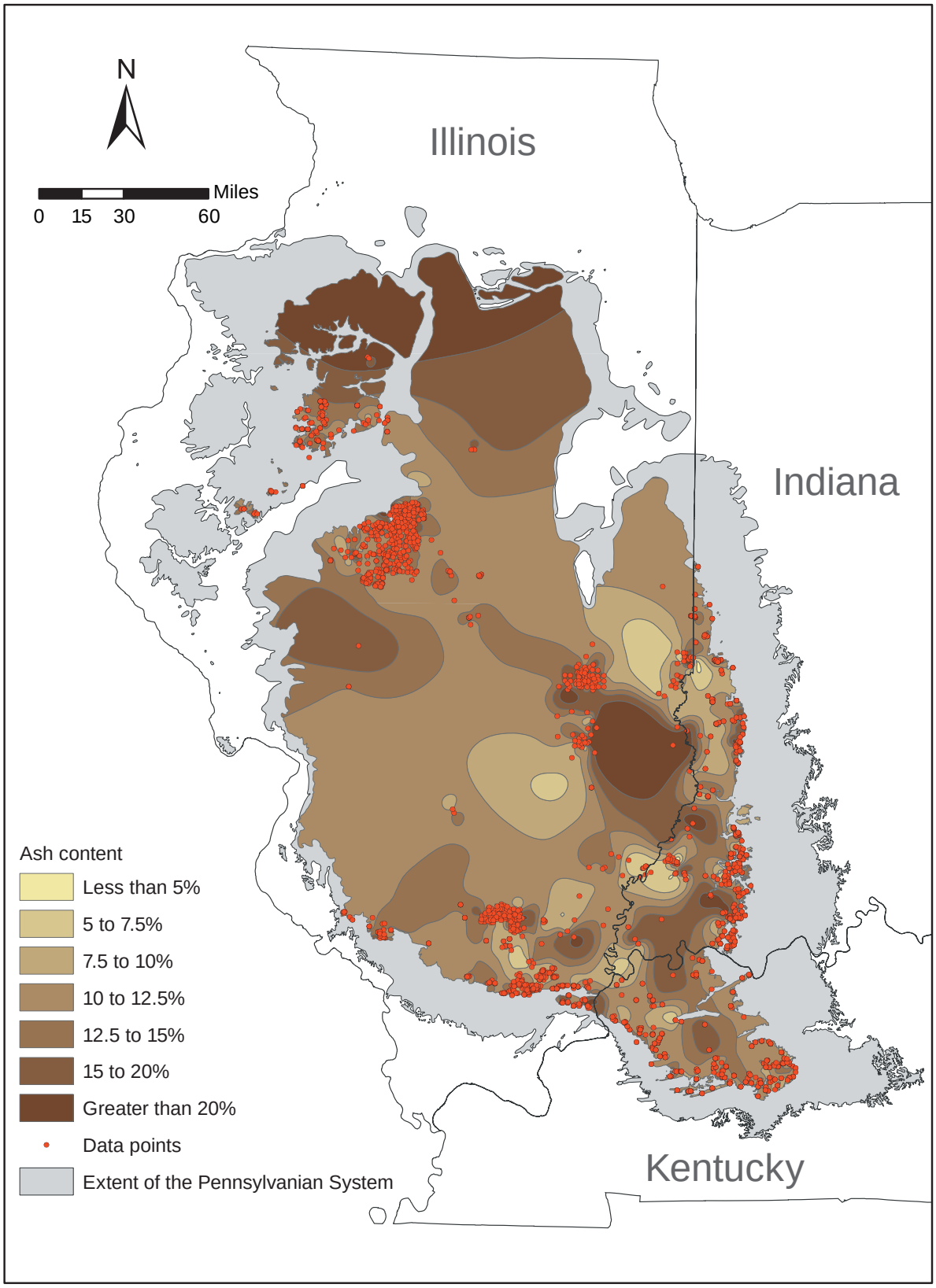

Figure A3-22 *Ash content (dry basis) of the Springfield Coal in the Illinois Basin.*

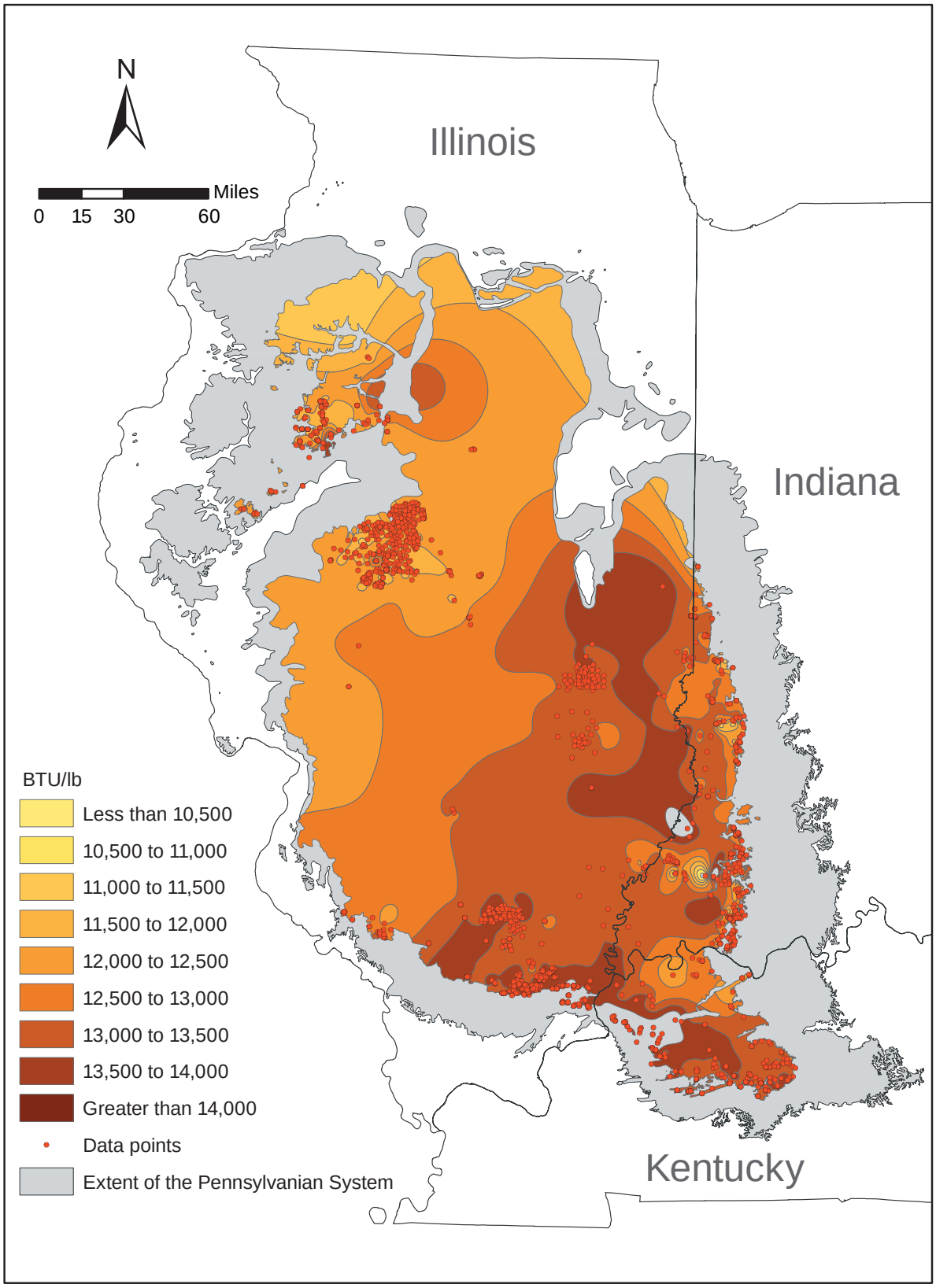

Figure A3-23 *Heating value (ash free, moisture included basis) of the Springfield Coal in the Illinois Basin.*

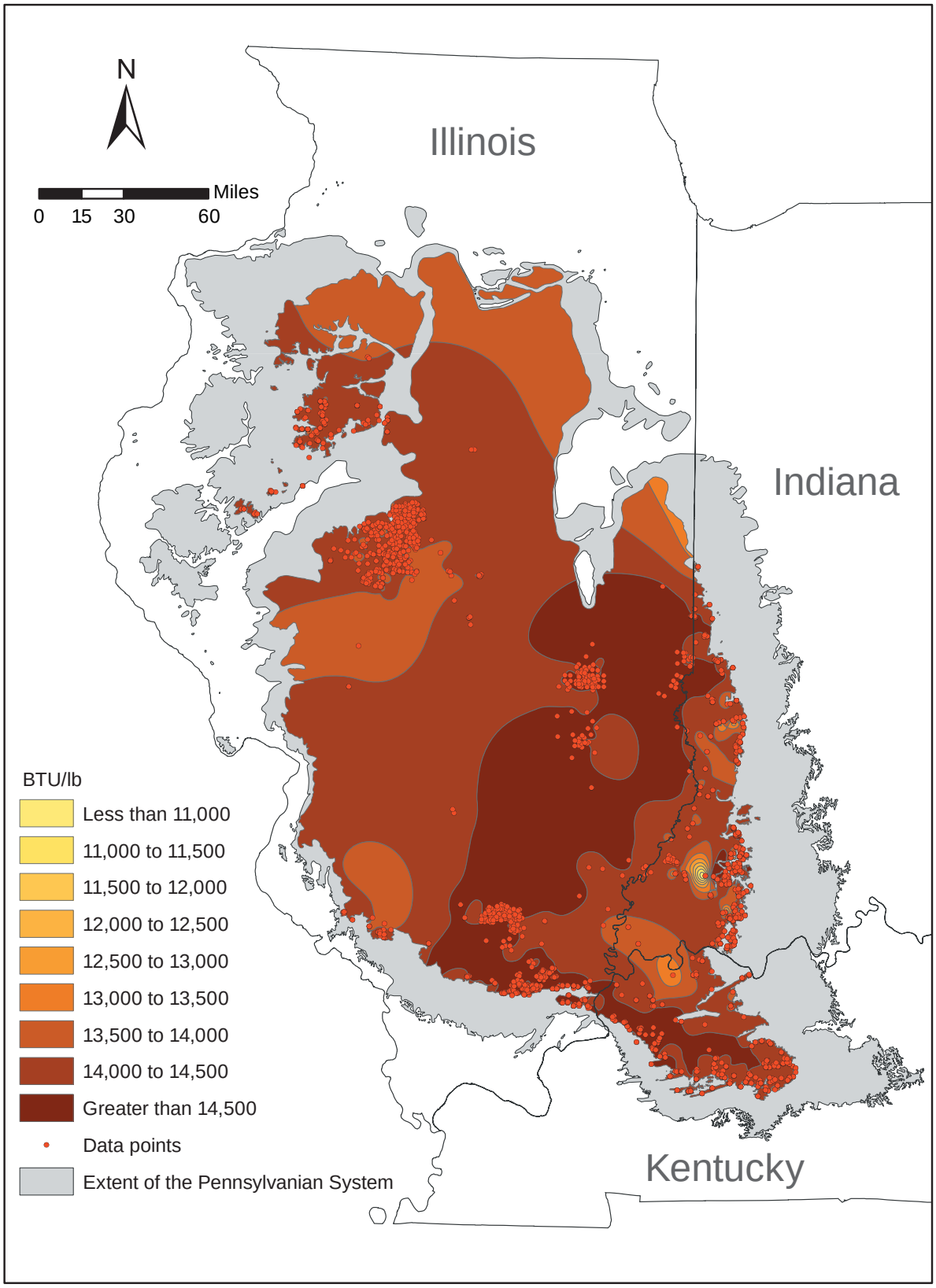

Figure A3-24 *Heating value (dry, ash free basis) of the Springfield Coal in the Illinois Basin.*

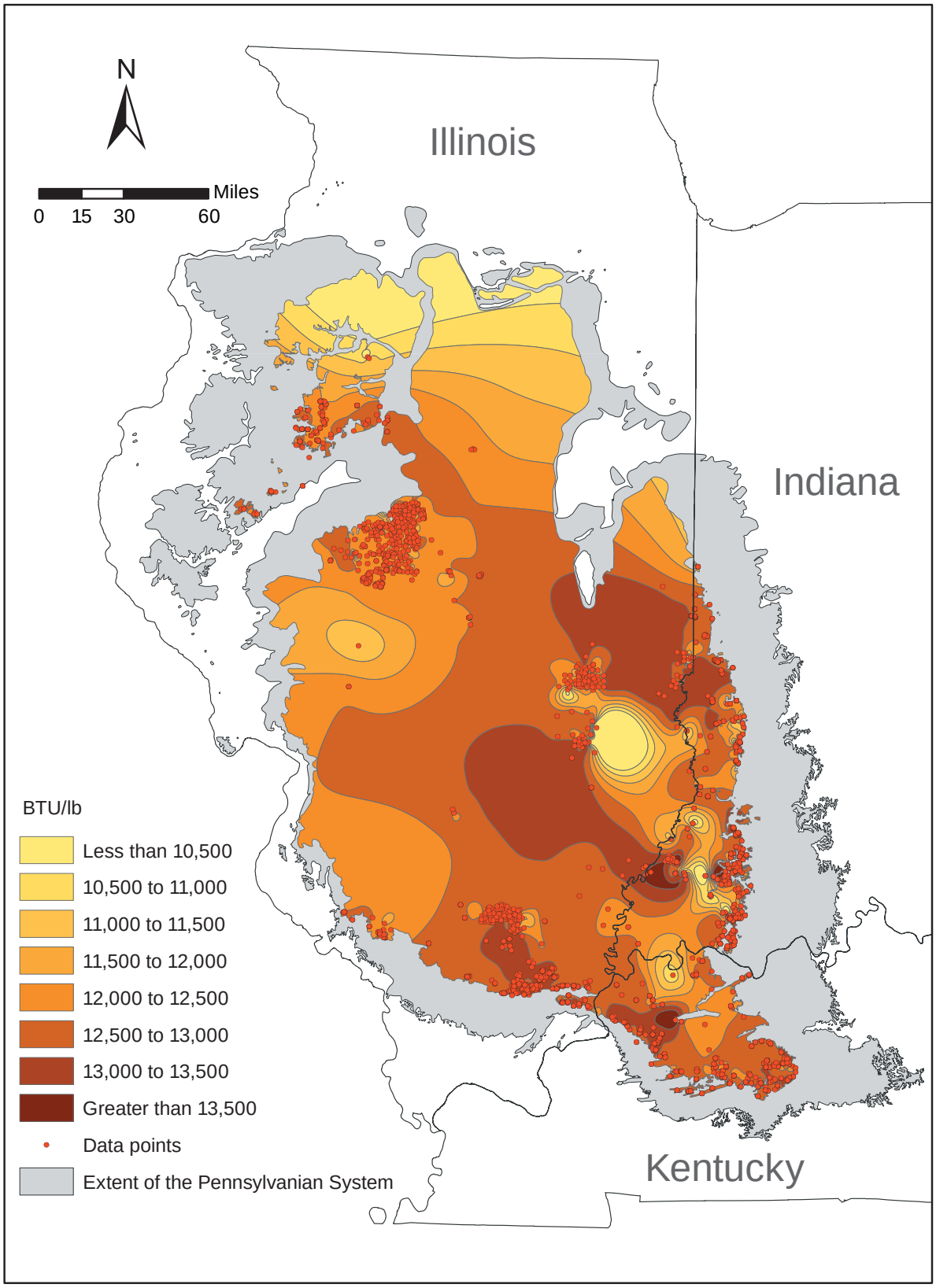

Figure A3-25 *Heating value (dry basis) of the Springfield Coal in the Illinois Basin.*

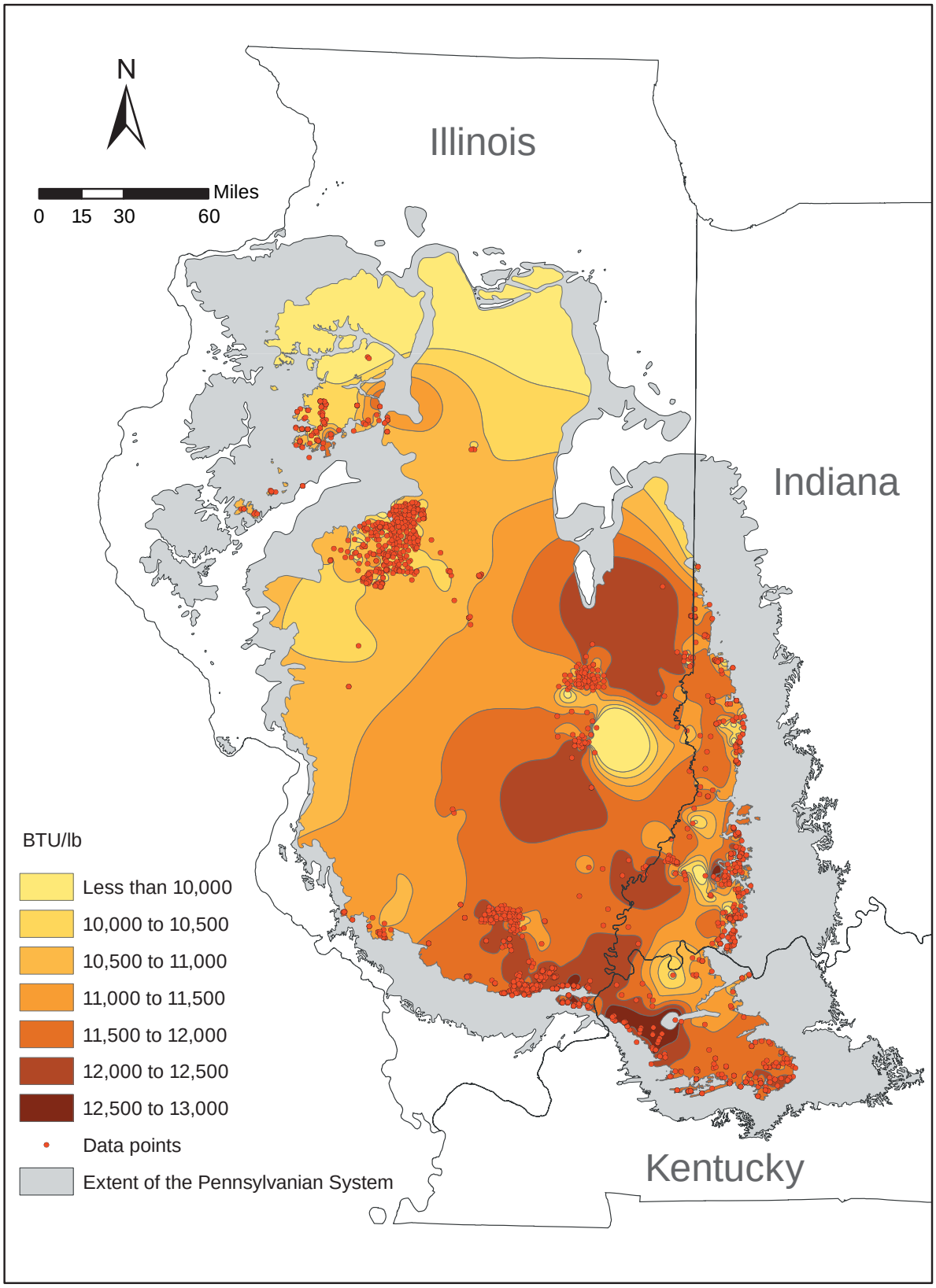

Figure A3-26 *Heating value (moisture and ash included basis) of the Springfield Coal in the Illinois Basin.*

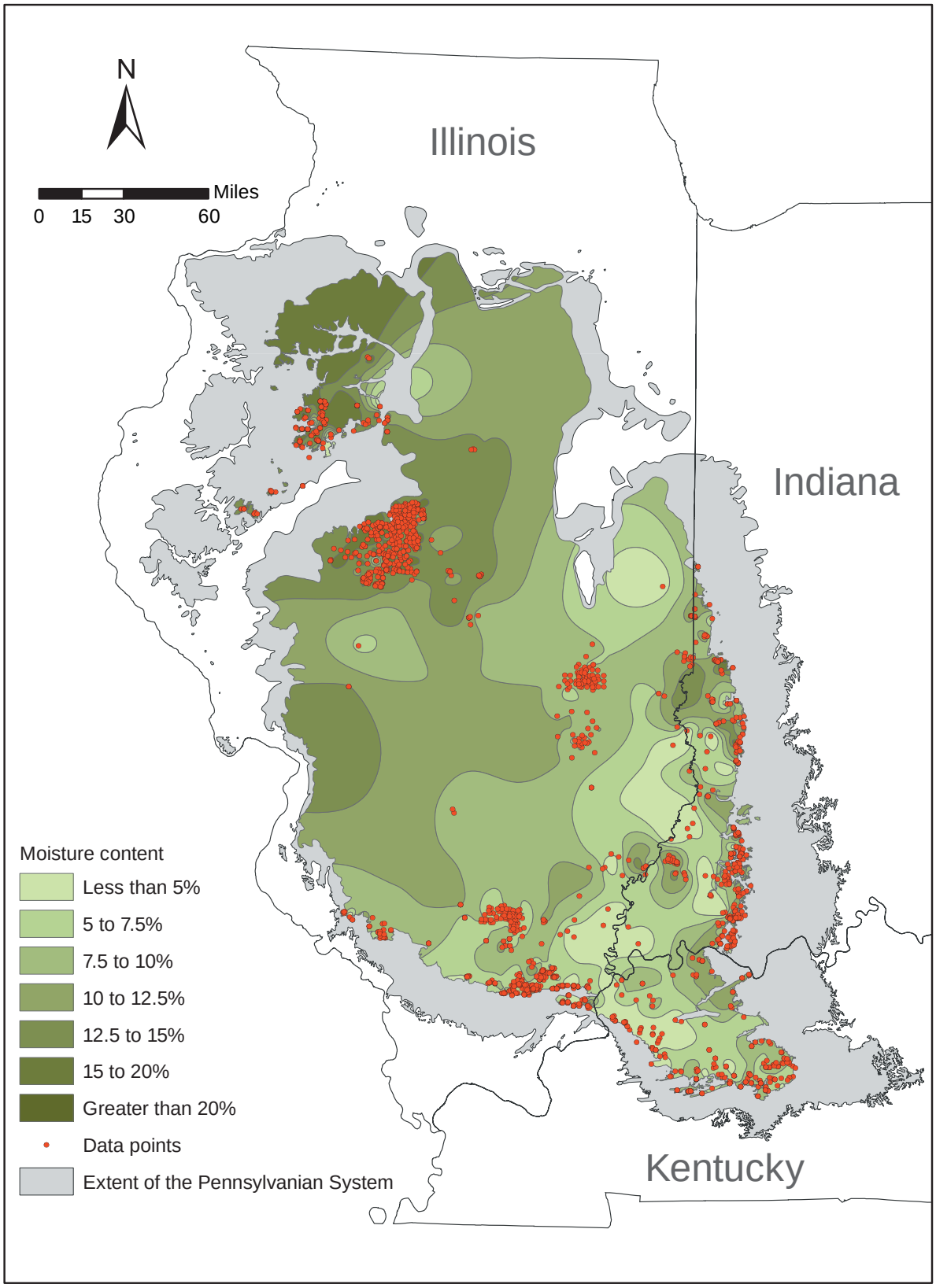

Figure A3-27 *Moisture content of the Springfield Coal in the Illinois Basin.*

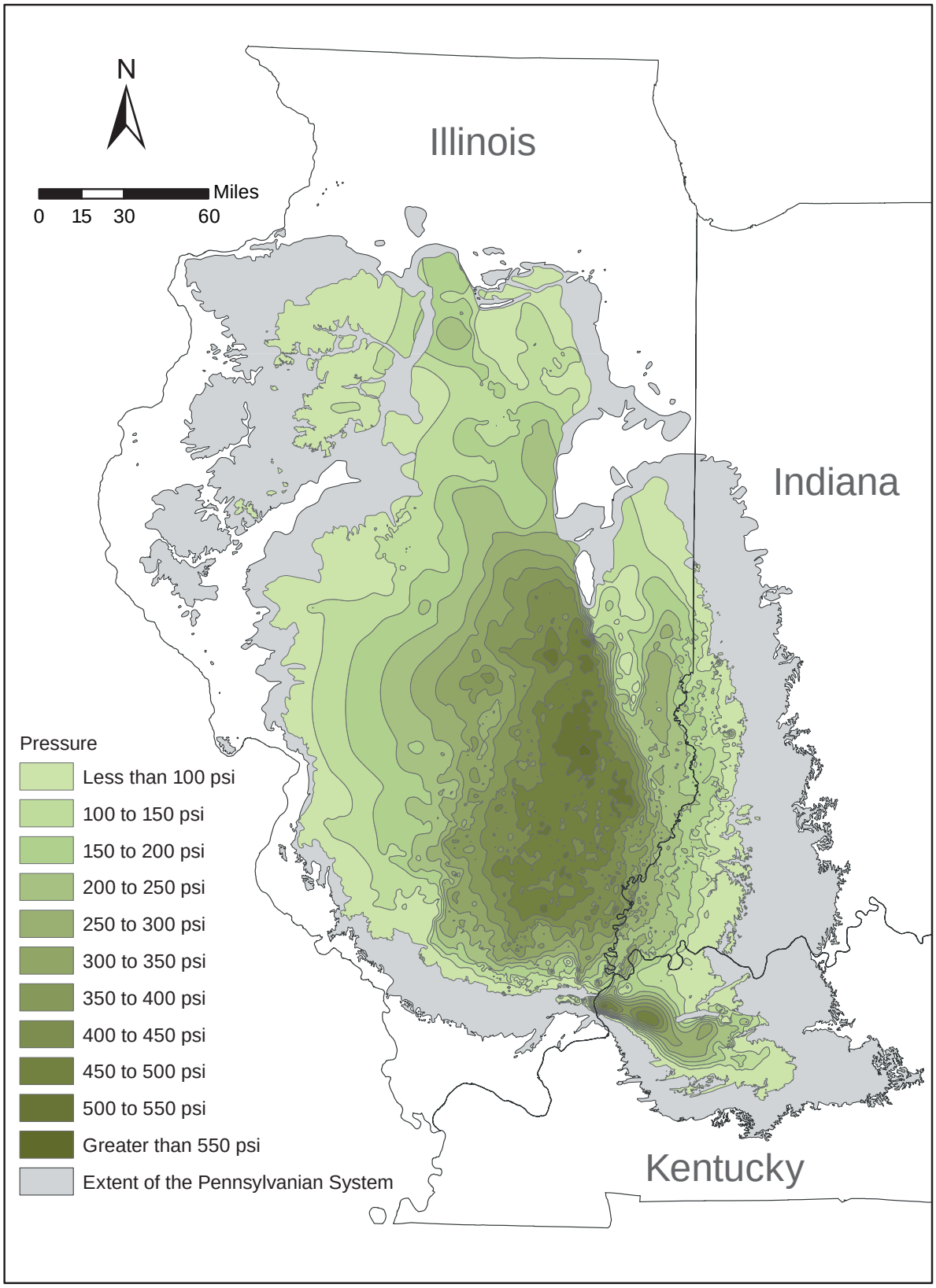

Figure A3-28 *Pressure of the Springfield Coal in the Illinois Basin.*

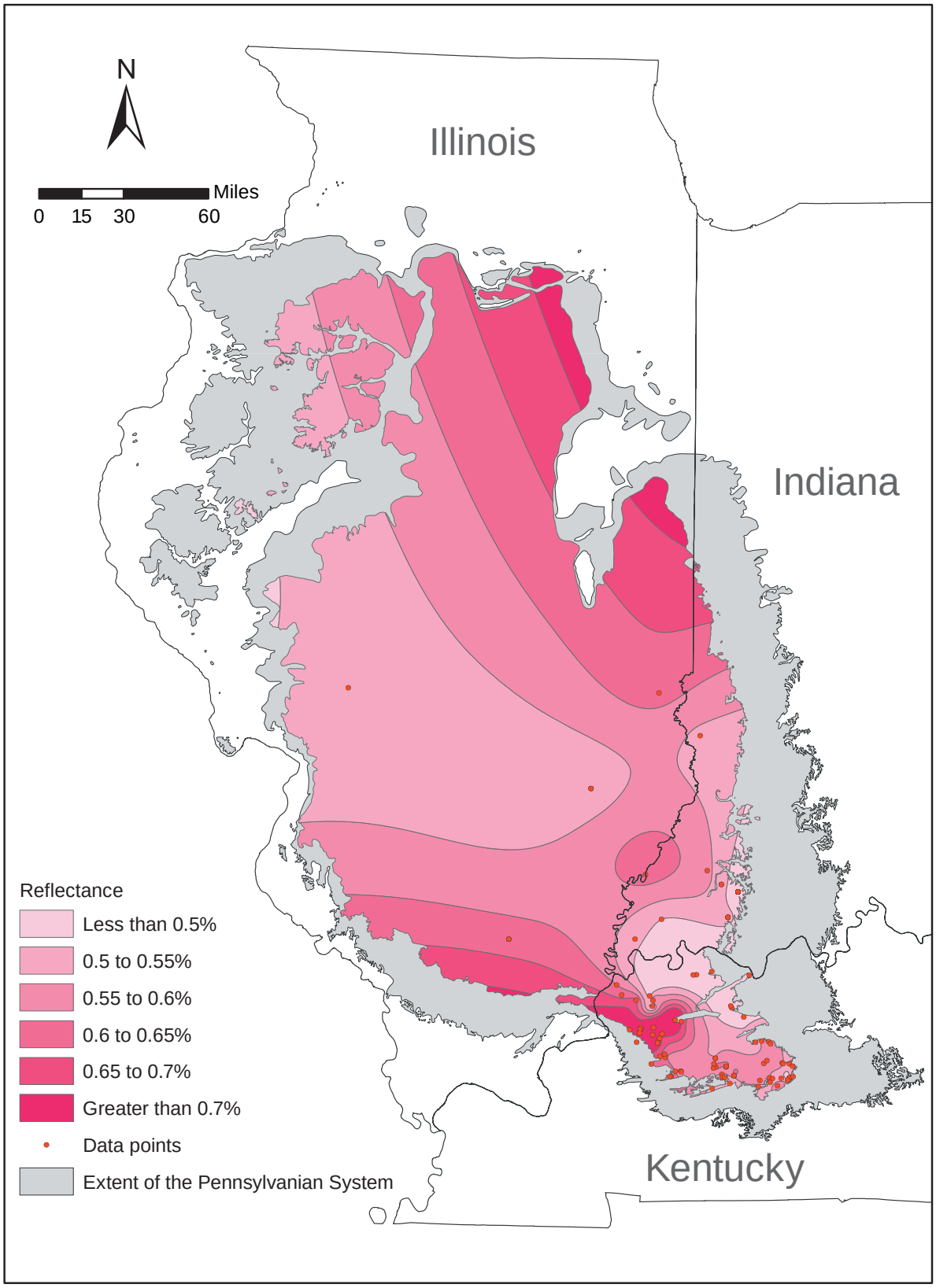

Figure A3-29 *Vitrinite reflectance of the Springfield Coal in the Illinois Basin.*

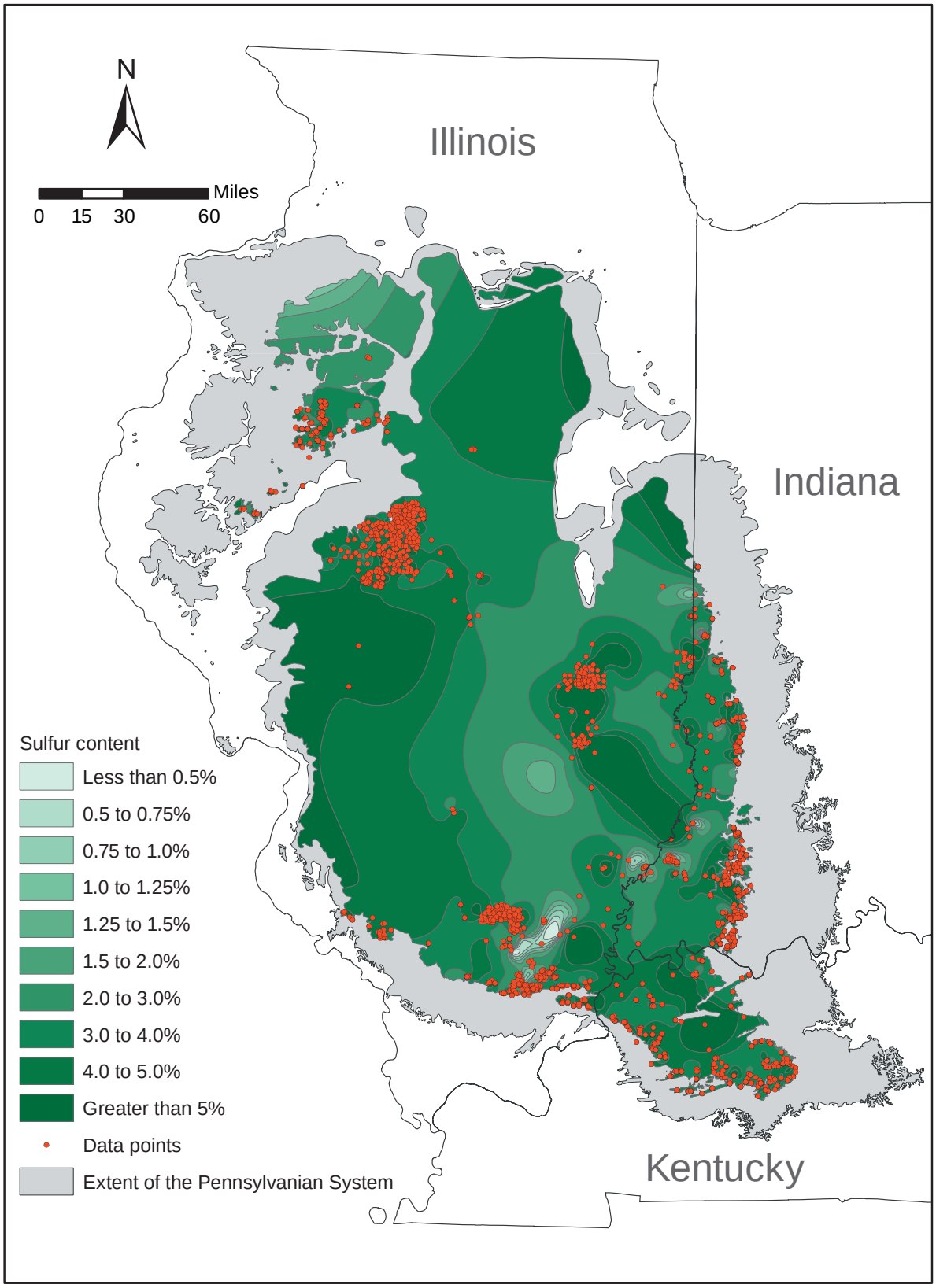

Figure A3-30 *Sulfur content (total, dry basis) of the Springfield Coal in the Illinois Basin.*

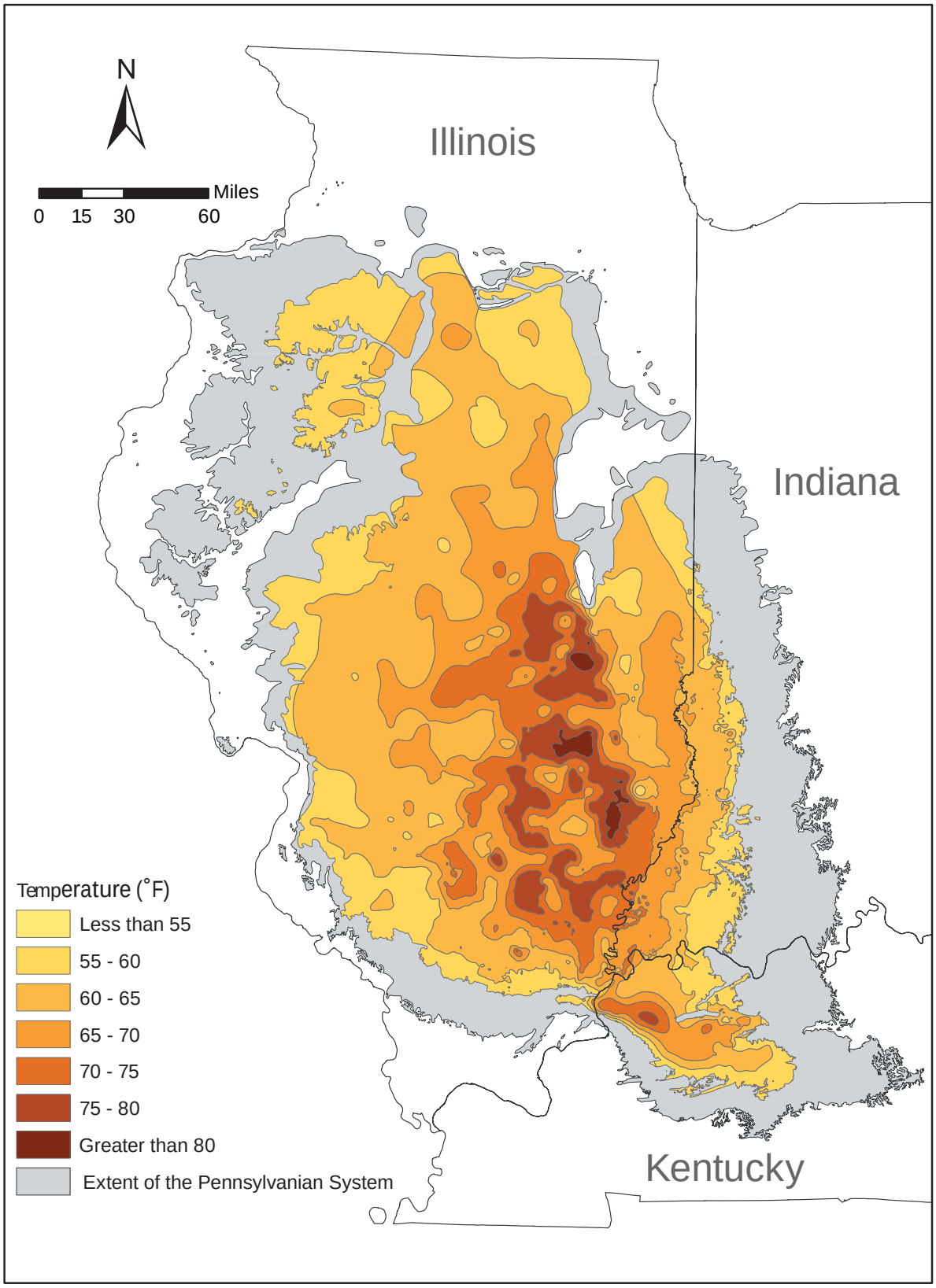

Figure A3-31 *Temperature of the Springfield Coal in the Illinois Basin.*

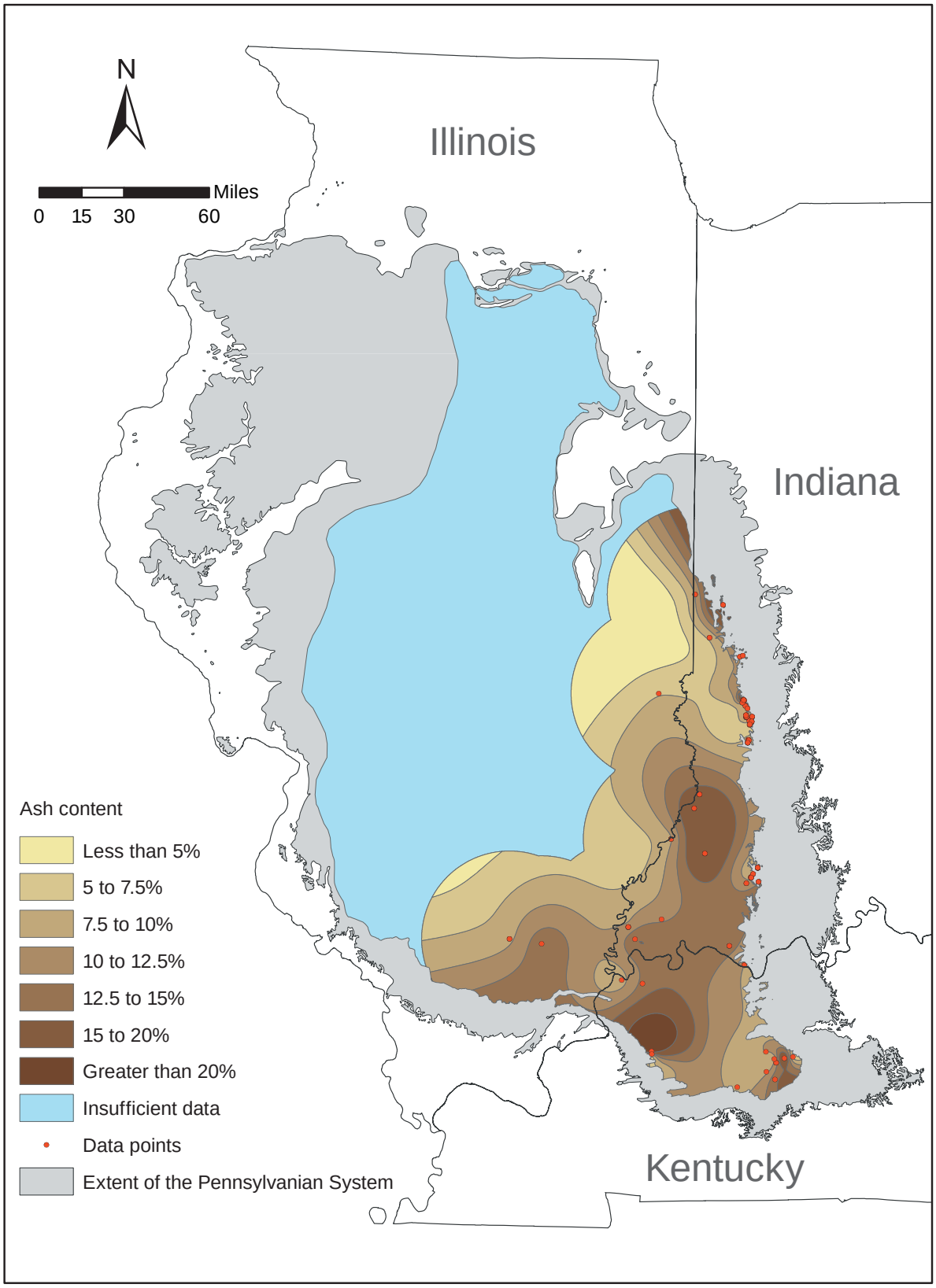

Figure A3-32 *Ash content (dry basis) of the Survant Coal in the Illinois Basin.*

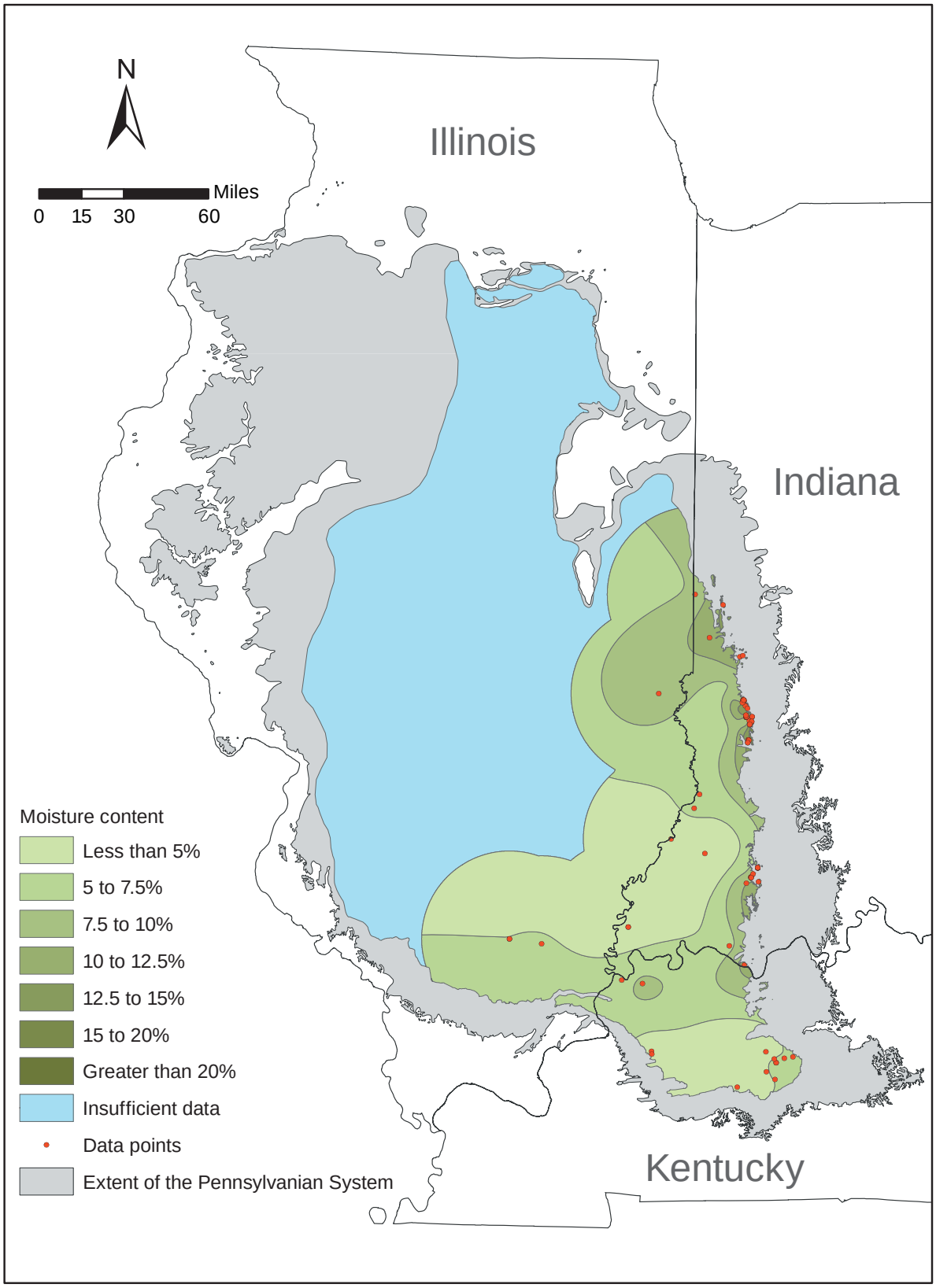

Figure A3-33 *Moisture content of the Survant Coal in the Illinois Basin.*

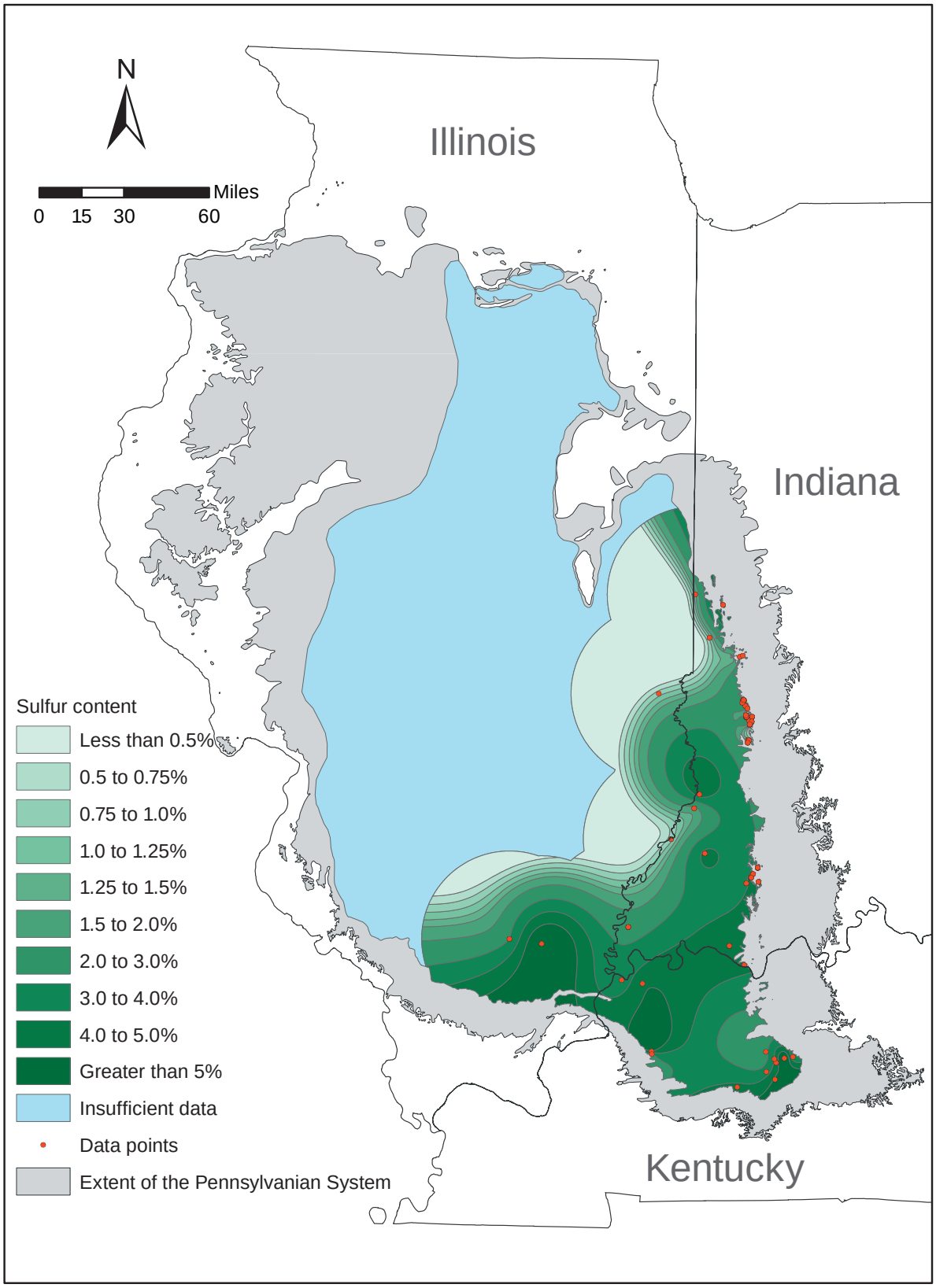

Figure A3-34 *Sulfur content (total, dry basis) of the Survant Coal in the Illinois Basin.*

Appendix 4: GIS Calculations of Potential Gas Volumes

The following series of maps represent intermediate GIS layers used to estimate the total coal volume's CO_2 ECBM and storage capacity. The maps are based on the GIS source layers, data values, and equations listed herein. Gas content calculations and areal screening were performed for each coal seam, based on each seam's specific thickness and depth distribution in the Illinois Basin. These intermediate data layers were based on combined data as sourced from (1) seam-specific average properties and (2) properties averaged from all major coals considered as a whole. A detailed volumetric assessment utilizing solely seam-specific input data and COMET modeling would be required to visualize any potential gas volumetric results on a per-seam basis.

The parameters specific to each coal seam are thickness, depth, and ash content. Parameters that were unavailable by seam include degree of saturation, Langmuir isotherm, coal density, moisture content, porosity, initial pressure, and COMET-derived CH_4 recovery and CO_2 storage factors. The following listing shows data values and calculations used in the GIS processing steps.

Listing of Source Data and Equations for GIS Processing Model Grid-based Calculations

Source data

A. GIS map (SDE polygon) layers, converted to GRIDS:

Thickness (ft)

Mined areas

Ash content (%)

Coal elevation (100-ft contours)

B. GRID source data:

Surface elevation (ft) grid (approx. 1-km cell size).

C. Intermediate, or calculated data

Coal depth calculated grid = surface elevation grid – coal elevation grid

Pressure gradient for coals = 0.433 psi/ft depth; used in pressure grid calculation; depreciated

D. Constants

Pure coal density = 1.28 g/cm^3

Thickness-estimated value; seam-specific value used to estimate insufficient thickness data areas in maps

E. Depth-range-dependent, constant values (Table A4-1):

1. one value for each coal depth interval: 152 to 274 m, 274 to 366 m, >366 m (500 to 900 ft, 900 to 1,200 ft, >1,200 ft)
2. different values used for each of low, best, and high estimates for:

VL: Langmuir volume (scf/ton, daf)

PL: Langmuir pressure (psi)

Pressure, initial (psi)

Moisture (%)

Porosity, fraction

Saturation, percentage

RF: MGSC ECBM recovery factor

SF: MGSC CO_2 storage factor

Table A4-1. Depth-range–dependent constants.

	Depth-range subdivisions		
	500 to 900 ft	900 to 1,200 ft	>1,200 ft
Low estimate			
VL	308	311	350
PL	796	796	796
Moisture	14.6	15.0	12.5
Pressure	234	403	528
Porosity	0.05	0.03	0.03
Saturation	60	46	59
RF	0.657	0.603	0.639
SF	6.116	7.261	4.86
Best estimate			
VL	456	456	456
PL	577	577	577
Moisture	10.3	10.3	8.7
Pressure	303	455	563
Porosity	0.03	0.02	0.01
Saturation	52	43	47
RF	0.74	0.7	0.778
SF	7.052	8.183	7.086
High estimate			
VL	575	575	575
PL	523	523	370
Moisture	5.9	6	5.9
Pressure	372	483	606
Porosity	0.01	0.01	0.005
Saturation	0.44	0.40	0.37
RF	0.887	0.858	0.846
SF	8.609	8.712	7.721

Gas Content Calculations

For documentation, the calculation steps below use the following notations:

“Equation variable”
[grid]
CONSTANT

[constant_d]: use reclassified depth grid to obtain three depth-dependent, average-value constants

Three steps are required to find GIP for “rock” coal:

1. Find Langmuir volume of “rock” coal “Vl_rc” using

"Vl_rc" = 0.0312[VL_D]PURE_COAL_DENSITY(1 – [ash] – [moisture_d])(1 – [porosity_d])

2. Use "Vl_rc" to find concentration "C_g" using

$$C_g = \left[\frac{(Vl\_rc)\,[pressure\_d]}{[PL\_d] + [pressure\_d]}\right][saturation\_d]$$

where [depth_calculated] used for depth-dependent-constants = ([surface_elevation] – [coal_elevation]), and depth categories are assessed for each seam.

3. Use Vl_rc to find GIP using

GIP = 43,560(1-acre grid cell)[thickness]C_g

ECBM recovery factors and CO_2 storage factors obtained from the COMET modeling were then applied to the GIP volumes for each seam for the coal areas identified by the application sequestration fairway screening criteria for coal thickness and depth as described herein.

An early trial calculation in this study used a coal elevation surface (grid) in the spatial calculation of gas concentration. However, this method was discontinued because of the stepwise nature of the other input data applied for specific depth intervals and because Langmuir values relate to the constant temperature for which they were measured. Thus, a constant representative pressure was applied in the calculations for respective depth ranges that were consistent with the other parameter distributions (listed above). Other trial calculations assessed different combinations of mapped versus constant-value input data before arriving at the final methodology as detailed above.

As a final check, gas volumes were calculated for the coals using average values obtained directly from measured gas content data to compare against those obtained by the formulas given herein. A best-fit curve through the measured data followed a pattern similar to the gas contents calculated for each depth-range. Total coal results were the same, with best estimates rounding to 3.6 billion tonnes (4 billion tons) and 0.19 trillion m^3 (6.7 trillion scf) of potentially sequesterable CO_2 and recoverable CH_4, respectively.

Modeling of ECBM Recovery

The coal reservoir properties and the parameters necessary for understanding the coal CO_2 sink were identified, and those having the greatest effect on coal-seam reservoir simulations (COMET3) are currently being tested for their relative sensitivity in controlling CO_2 sequestration and CH_4 recovery performance. Coal characteristics for use in the reservoir models were identified, and probabilistic

ranges of the input parameters were made. The set of possible values was first made for the COMET3 simulator input parameters on a Basin-wide basis. Then more restricted distributions were made for depth-partitioned subsets (152 to 274 m, 274 to 366 m, >366 m (500 to 900 ft, 900 to 1,200 ft, >1,200 ft), and the relatively deep grabens of western Kentucky). Values from each of these subsets will be used in a parametric study to test the sensitivity of the critical input parameters on the modeled CO_2 storage and CH_4 recovery volumes. Gas samples from coal core canister desorption tests have been characterized in terms of their isotopic composition. That and any such new data will be compared to gases from likely CO_2 sources for a geological sequestration demonstration to distinguish the native from injected CO_2. This work is ongoing at the end of Year 1.

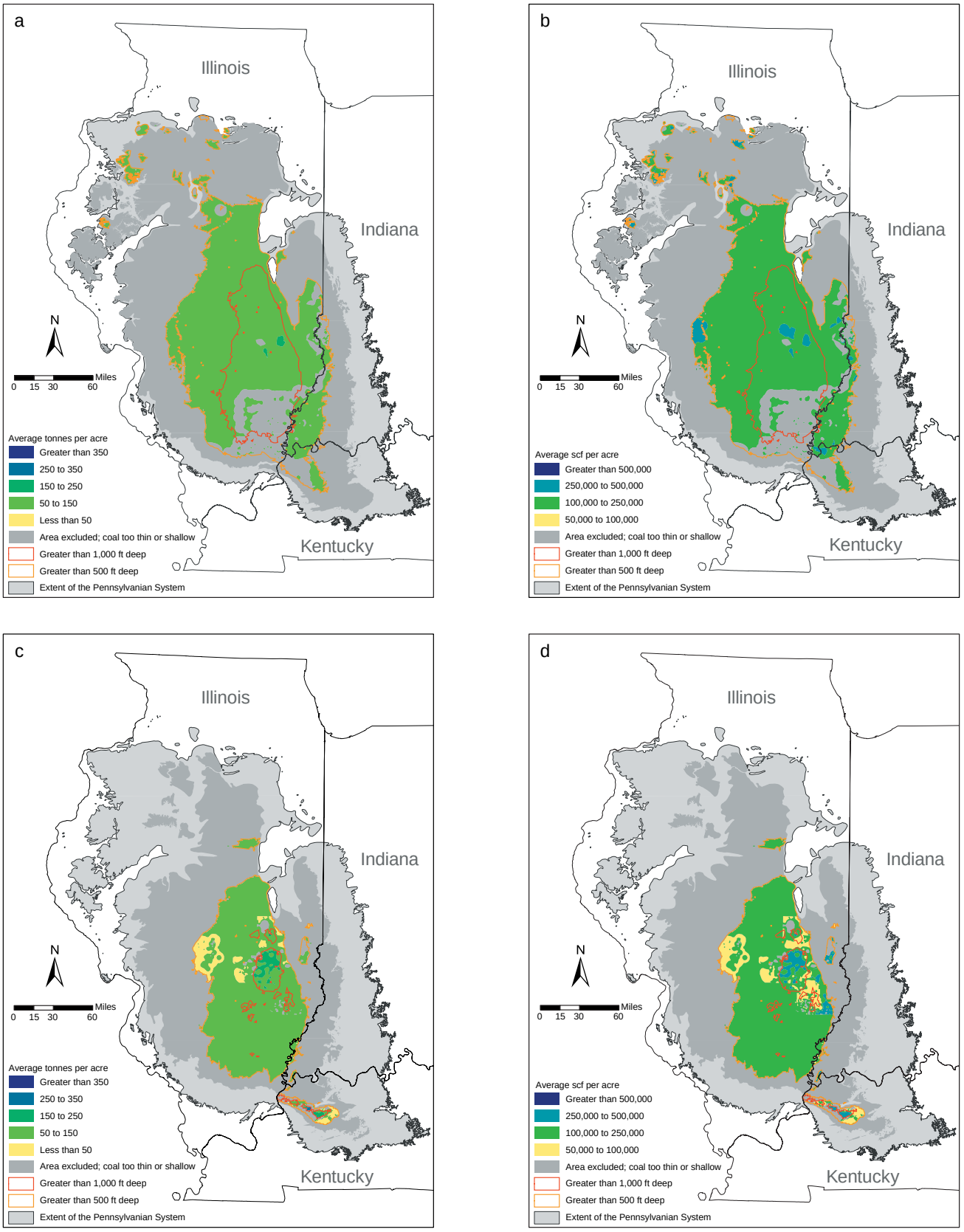

Figure A4-1 *Potential for (a) CO_2 storage and (b) ECBM recovery in the Colchester Coal and potential for (c) CO_2 storage and (d) ECBM recovery in the Danville/Baker Coals in the Illinois Basin.*

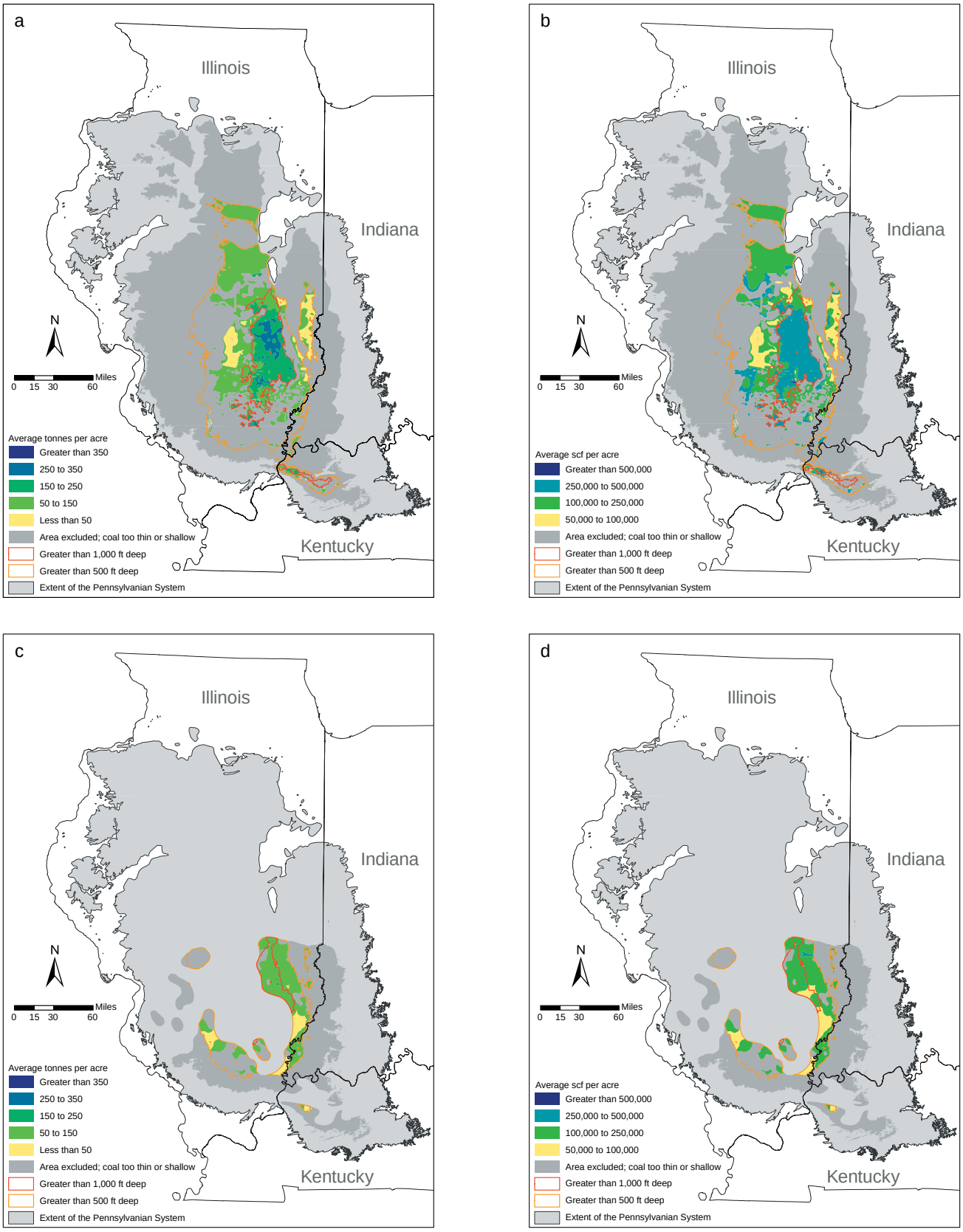

Figure A4-2 *Potential for (a) CO_2 storage and (b) ECBM recovery in the Herrin Coal and potential for (c) CO_2 storage and (d) ECBM recovery in the Hymera/Jamestown/Paradise Coals in the Illinois Basin.*

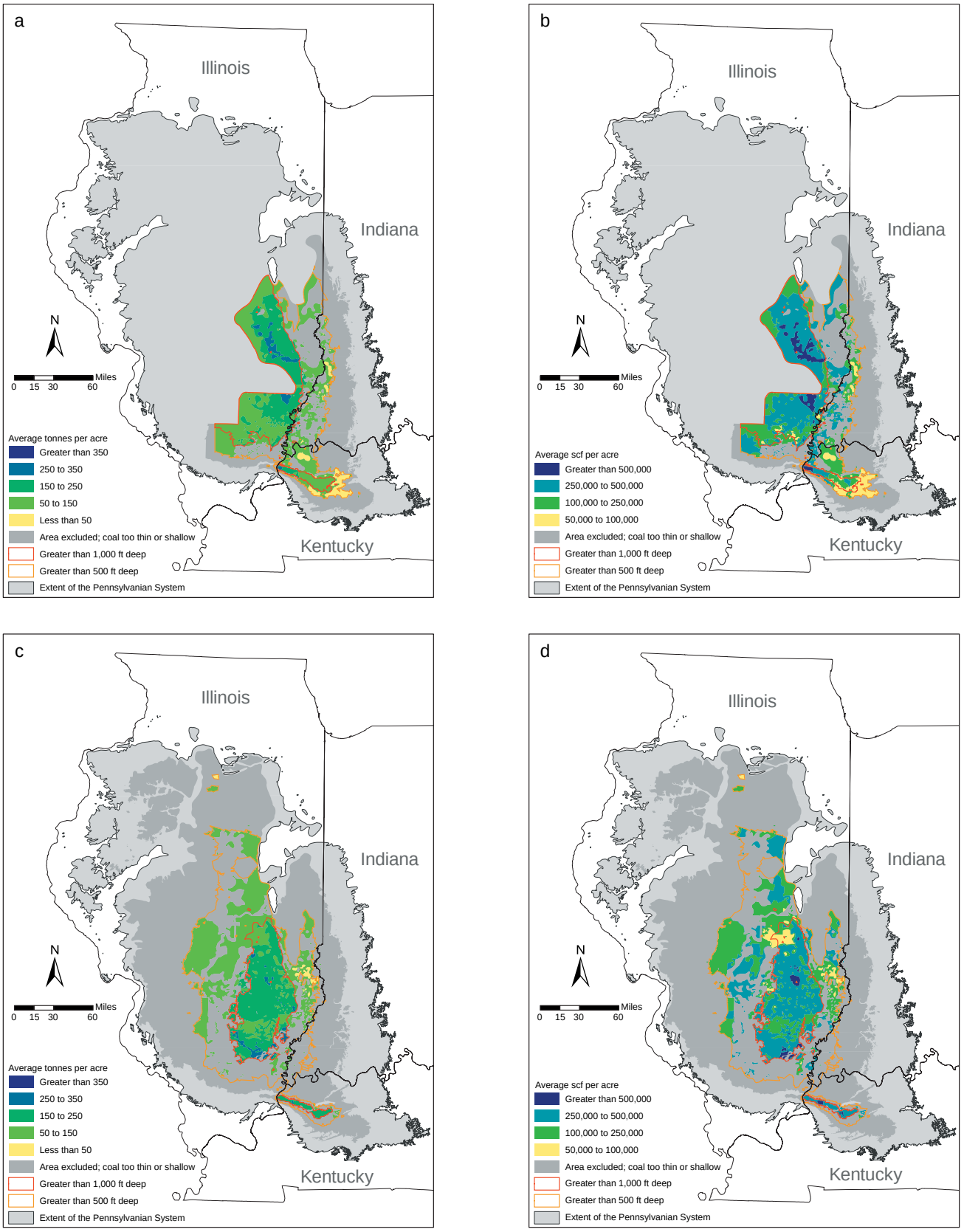

Figure A4-3 *Potential for (a) CO_2 storage and (b) ECBM recovery in the Seelyville/Davis/Dekoven Coals and potential for (c) CO_2 storage and (d) ECBM recovery in the Springfield Coal in the Illinois Basin.*

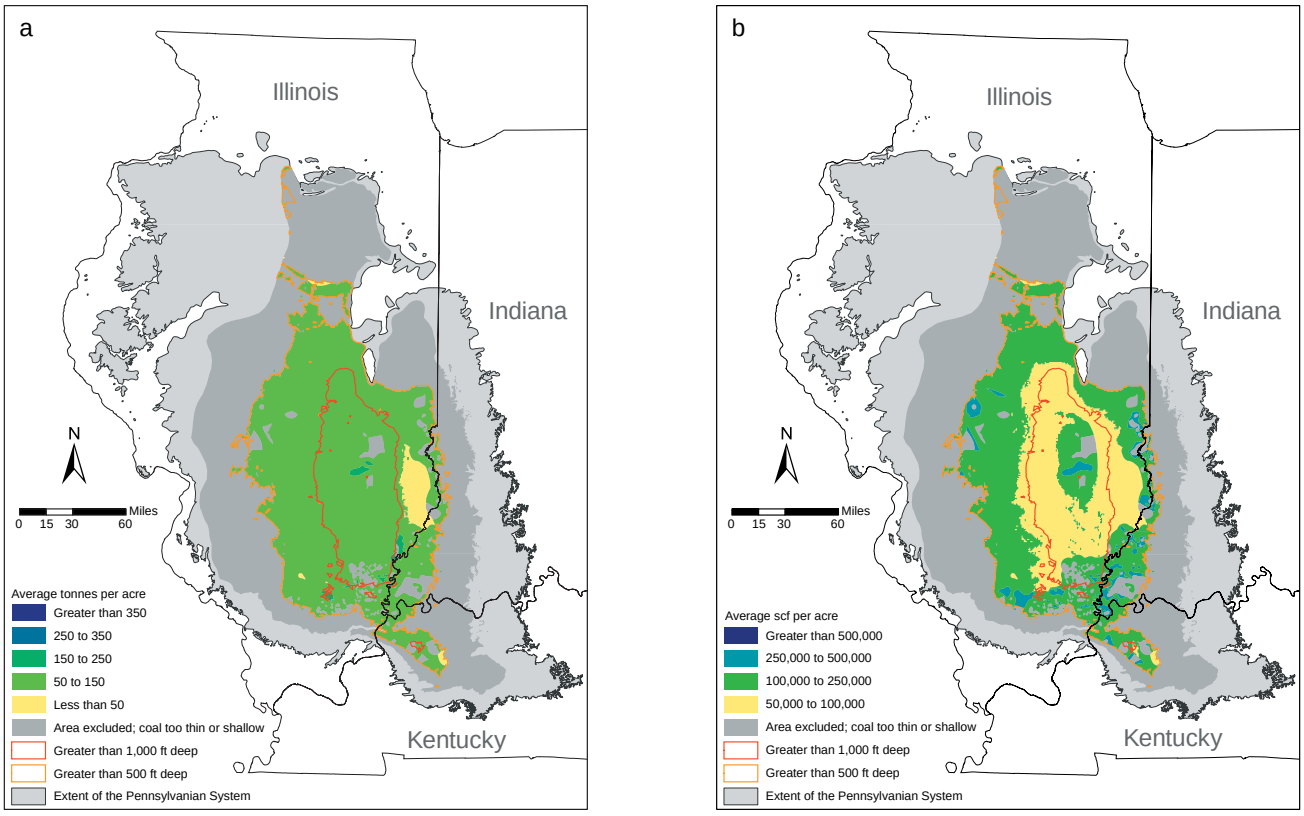

Figure A4-4 *Potential for (a) CO_2 storage and (b) ECBM recovery in the Survant Coal in the Illinois Basin.*

CO_2 Sequestration and Enhanced Oil Recovery Potential in Illinois Basin Oil Reservoirs

Introduction

The use of crude oil-bearing strata as a geologic sink for the sequestration of carbon dioxide (CO_2) includes a value-added component, that of recovering new oil from existing oil fields that have undergone primary and/or waterflood production. CO_2 has been used for enhanced oil recovery for more than two decades in the Permian Basin of West Texas. CO_2 experience in West Texas suggests that following waterflooding by a CO_2 flood can produce an additional 10% of original oil in place (OOIP) or an additional 25% beyond the total oil produced during the primary and waterflooding phases.

The Illinois Basin of Illinois, Indiana, and Kentucky has been an active oil basin for more than a century, to date yielding a cumulative production of >0.68 billion m^3 (>4.3 billion barrels) of crude oil. More than 2,000 waterflood units and areas exist in the Basin. Only one brief test of CO_2 flooding, however, has been undertaken within the boundaries of the Basin as of this date.

This study focuses on four major topics regarding the potential of CO_2 flooding in Illinois Basin fields. The first is an estimation of potential additional hydrocarbon that might be recovered by CO_2 flooding, which required an updated estimate of the Basin-wide OOIP. The second is the establishment of selection criteria for likely candidate fields, drawing on analogs with the West Texas CO_2 experience and the geologic setting of the Illinois Basin. The third is a test and validation of the oil recovery estimates employing geologic, geostatistical, and reservoir models built for specific geologic settings. The final task is a calculation of the volume of carbon that could be sequestered by such programs and of the volume of additional hydrocarbon recovery that might reasonably be expected.

Stratigraphy

The stratigraphic relationship of Cypress, Aux Vases, Ste. Genevieve, and other rock units in the Illinois Basin are shown in Figure 2-1 (Howard and Whitaker, 1990). Middle Mississippian Chesterian units account for 66% of oil produced to date in the Illinois Basin. Fields in this study were selected from the three most prolific producing horizons in the Basin, the Cypress Sandstone, the Aux Vases Sandstone, and the carbonate reservoirs in the Ste. Genevieve Limestone. All of these units have been placed in the Chesterian or Valmeyeran Series. Most Chesterian cycles are composed primarily of siliciclastic intervals overlain by thin, widespread carbonates. There are 12 Chesterian cycles in most areas of the Illinois Basin. The Cypress Sandstone and the overlying Beech Creek (Barlow) Limestone represent the most widespread and most oil-productive Chesterian cycle. The Cypress Sandstone is typically made

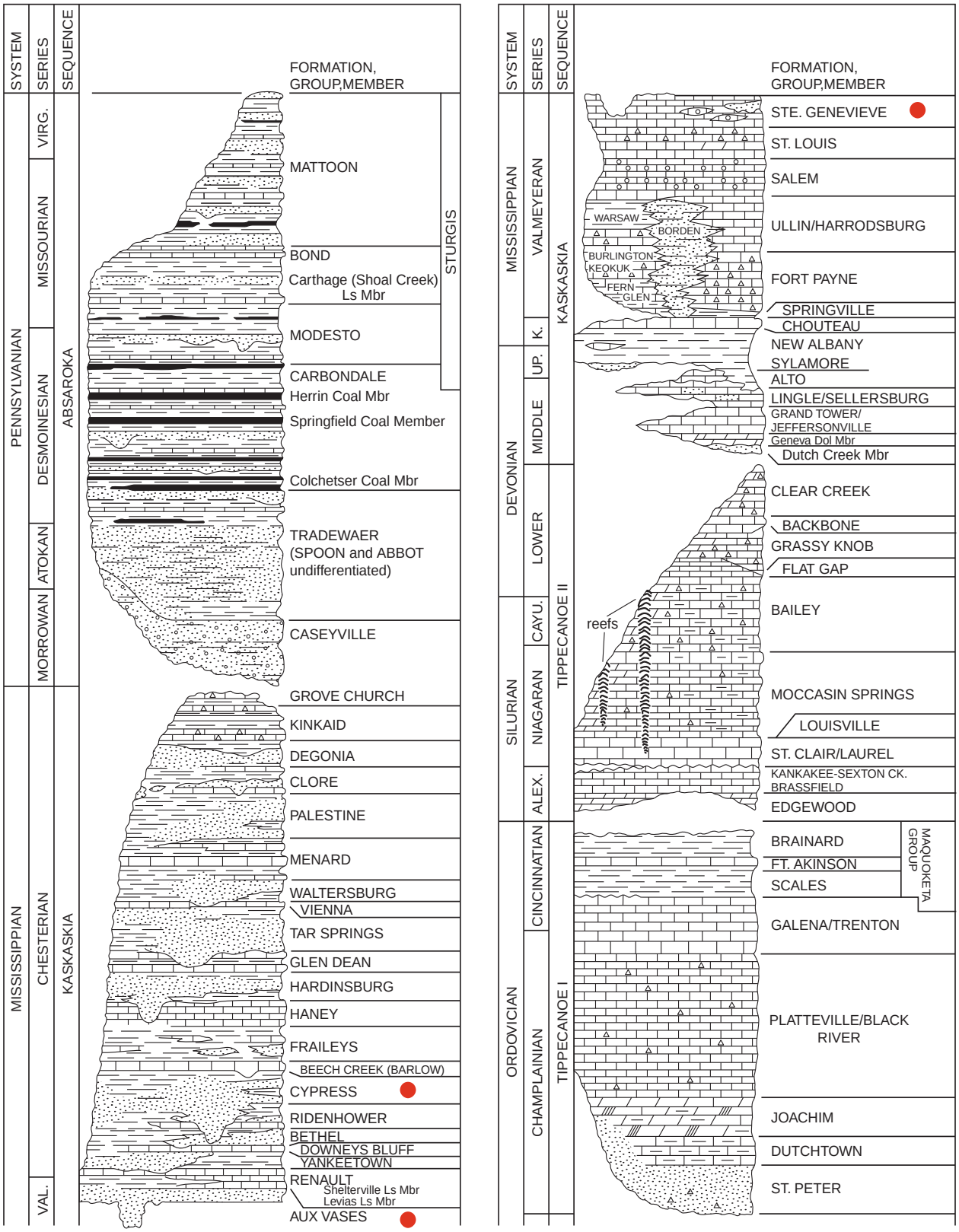

Figure 2-1 *Generalized stratigraphic column of the Illinois Basin depicting the most prolific hydrocarbon-producing horizons (marked by red dots). The chart beneath displays the approximate portion of hydrocarbons produced within the Basin that are attributable to each zone (Howard and Whitaker, 1990).*

up of a relatively thick middle sandstone overlain by a shale-rich interval containing one or more thin, localized upper sandstone units.

The stratigraphic record of Chesterian rocks such as the Cypress sandstone indicate that the Basin had a low-gradient, southward dipping sea floor and a low subsidence rate relative to rates of sedimentation. Accommodation space was thin, forcing siliciclastic and carbonate sand material entering the Basin to spread laterally rather than vertically. Water depths were shallow in this slowly subsiding cratonic sea. Widespread tidal features observed within the sediments indicate that tidal currents significantly influenced sediment movement within the Basin. The embayed geometry of the entire Basin, combined with regional embayments resulting from the dynamics of prograding delta systems, likely induced a high tidal range in some regions or possibly across the entire Basin. The thin accommodation space combined with shallow water depths and active currents (including tidal and storm) caused prograding sediments to be actively reworked and spread out. Thin, discontinuous and stacked deposits are characteristic of this setting.

Along the central, active portions of prograding deltas, thick estuarine deltas and probably tidal bayhead deltas to fluvial sands were deposited. These deltas prograded from the northeast and down-dip to the southwest and south. Swann (1963) identified this fluvial-deltaic system and titled it the "Michigan River System." Unlike the classic Mississippi River bird-foot constructive delta, the Cypress deltas were likely influenced by destructive, sediment-spreading tidal currents.

Linear, thin, stacked sandstones that show a dominant northeast-southwest to north-south trend are very common and widespread in both the upper and lower Cypress. These features are very similar to tidal current ridges that form in modern coastal areas where tidal currents are strong and where vertical tidal ranges are large.

The stratigraphic relationships of the lower and middle Cypress were greatly complicated by a significant drop in relative sea level that is recorded in Cypress sediments. Although minor sea level fluctuations were common during deposition of the Cypress, they are difficult to document on a regional scale. An interval that contains thin red, green, or variegated beds (interpreted as remnant, ancient soil horizons) and a thin coal (interpreted as a swamp deposit) is commonly found above and near the top of the middle Cypress sandstone and below the upper sandstones. Sea level dropped at the depth where the red beds occur and subaerial exposure of most, if not the entire Basin, which resulted in erosion and valley incisement. As sea level rose, thick sand packages filled portions of these eroded valleys. These transgressive sands, located in the lower and middle Cypress intervals, are juxtaposed against older and unrelated regressive Cypress sands.

The Aux Vases Sandstone directly overlies the Ste. Genevieve Limestone; both units are middle Mississippian in age. The Illinois Basin lies within the interior of the North American craton. During deposition of Ste. Genevieve carbonates and Aux Vases and younger Chesterian siliciclastics, the Illinois Basin was a shallow embayment open to deeper marine conditions in the region of the Pascola Arch. The depositional paleoslope was gentle, and shallow marine depositional environments were widespread. By the end of the middle Mississippian Valmeyeran time, active subsidence in the Michigan Basin had stopped (Craig and Varnes, 1979), leaving an unimpeded fairway for influx of sediment from the Canadian Shield into Illinois and further south during Chesterian time.

Three broad, regional facies belts in the Aux Vases Sandstone have been identified across the Basin. Medium- to fine-grained sandstones on the west flank of the Basin are the thickest, commonly 100 ft or greater. Aux Vases Sandstone units in the most oil-productive part of the Basin usually reach a maximum of 6.1 to 14 m (20 to 45 ft) thick (Seyler, 1998). These units are very fine grained and may be associated with interbedded shale and siltstone or limestones. Along the eastern margin of Illinois and into Indiana, the Aux Vases is more carbonate-rich, and sandstones in the formation become more isolated, finer grained, and thinner.

The primary reservoir facies in the Aux Vases Sandstone is composed of isolated bodies of fine-grained, friable, bidirectionally cross-bedded, brown, oil-stained sandstone. These sandstone bodies commonly have a convex-upward geometry relative to datum and have been interpreted as sandstone bars in Zeigler Field (Seyler, 1998). Low- to high-angle cross-bedding composed of dark, coarser-grained, porous lamina alternating with lighter, finer-grained, less porous laminae. Porosity of the reservoir facies ranges between 17 and 30%, and permeability ranges between 0.025 and 0.790 μm^2 (25 and 800 millidarcies (md)).

The Ste. Genevieve Limestone consists of the Karnak, Spar Mountain, and Fredonia Members (not shown) in descending order. Oolite lenses in the Fredonia Limestone Member are the most prolific petroleum reservoirs in the Ste. Genevieve. McClosky oolite is an informal drillers' term applied to thin, lenticular oolite reservoirs in the Fredonia Member. Specific pays within McClosky zones are further subdivided into McClosky A, B, C, and D zones. The Fredonia Limestone is typically made up of beds of dense, fine-grained or bioclastic limestone alternating with zones of very oolitic limestone. Some units are dolomitic. The porosity and permeability of the oolitic zones range from excellent to poor, depending on the amount of preserved intergranular porosity. When later stage interstitial calcite cements intergranular pores, porosity and permeability are poor.

The oolitic zones are not continuous over long distances. Some can be traced over a distance of a few miles, but most pinch out or grade laterally into dense units within a short distance. The oolite facies

in the Ste. Genevieve are widespread, but are very lenticular. Oolite lenses may be stacked, and several zones may be productive in an area. Oolitic sand bar lenses tend to be elongate, flat-bottomed, convex-upward lenses from 0.8 km (0.5 mi to several miles) in length, 0.2 to 1.2 km (0.125 to 0.75 mi) in width, and <6 m (<20 ft) thick (Cluff and Lineback, 1981; Choquette and Steinen, 1980; Carr, 1973). The bars commonly occur as swarms of subparallel bars that have relatively uniform spacing and a northeast-southwest orientation. The geometric relationships and depositional facies indicate deposition by tidal processes (Cluff, 1986). Modern examples of similar oolitic tidal-bar belts are found on the Great Bahamas Bank, Bahamas, where high tidal currents have oriented individual tidal bars that are similar in size and shape to those found in the Ste. Genevieve Limestone (Gibson, 2001).

Reservoirs Suitable For Miscible and Immiscible CO_2 Enhanced Oil Recovery (Subtasks 5.1 and 5.2)

Oil Field Miscibility Classification

Defining plays of oil reservoirs as miscible or immiscible is important in determining the potential for enhanced oil recovery (EOR) during CO_2 sequestration. "Miscible" describes CO_2 and crude oil that become a single mixture under certain temperature and pressure conditions via the mass transfer of intermediate hydrocarbons (C_5 to C_{12}) from the crude oil to the CO_2 phase. "Immiscible" describes CO_2 and crude oil under conditions where separation of the two fluids is distinct and identifiable. Mass transfer exists in immiscible CO_2 flooding of the oil reservoir; however, there is a CO_2-rich phase and a crude oil-rich phase.

The critical pressure (7,398 kPa (1,073 psia)) and temperature (31°C (87.8°F)) of CO_2 are important to determining miscible and immiscible potential of oil reservoirs. For miscibility to occur, CO_2 must exist as a critical fluid (i.e., dense-phase, liquid-like, supercritical CO_2); this condition is only possible for reservoir temperatures exceeding the critical temperature of CO_2 and the crude oil's minimum miscibility pressure (MMP). The MMP of a crude oil increases with temperature, is at least equal to the critical pressure of CO_2, and is generally thought to exceed the original bubble-point pressure of the crude oil.

Immiscible conditions exist at reservoir temperature and pressure generally less than the critical temperature of CO_2 and temperatures above the critical temperature when reservoir pressure is less than the MMP pressure. Under immiscible conditions, liquid or gas-like phases of CO_2 are possible.

Determining Conditions of Immiscibility and Miscibility

Because of the uncertainty due to lack of data availability for temperature and pressure conditions within reservoirs in the Illinois Basin, oil fields were assigned a CO_2 miscibility classification of miscible, near miscible, or immiscible based on temperature and pressure conditions that were calculated at the bulk volume-weighted depth of each field (Equation [1]). Bulk volume is the area and the thickness product of each reservoir. The criteria used to assess miscibility conditions at depth were based on temperature and pressure "windows" around the critical point of CO_2. These "windows" were defined as 31.11±1.11°C (88±2°F) for temperature and 6,894.757±689.476 kPa (1,000±100 psia) for pressure. The relative importance of temperature and pressure conditions were evaluated based on four scenarios using maximum and minimum temperature and pressure gradients. The combinations of temperature and pressures creating the largest near-miscible range were used as criteria for assigning miscibility classes to oil fields (Figure 2-2).

Reservoir temperature depends on both reservoir depth and the local geothermal gradient, for which there are few reliable and available sources. Based on maps published by the American Association of Petroleum Geologists and unpublished estimates of geothermal gradient used by logging companies within the Basin, the general geothermal gradient is estimated to lie between -17.2°C/30 m (1.0°F/100 ft) and -17.1°C/30 m (1.2°F/100 ft). Few modern logs in the Basin have recorded bottom-hole temperatures; a survey of those available falls within a few hundredths of a degree per foot of this range.

Calculation of reservoir pressure is straightforward because hydrostatic pressure can be directly related to depth. For testing purposes, a minimum pressure gradient of 9.795 kPa/m (0.433 psi/ft) was assumed, as was a maximum gradient of 22.621 kPa/m (1.0 psi/ft), the accepted fracture gradient in the Basin. A third test was run at 18.096 kPa/m (0.8psi/ft), the maximum waterflooding injection pressure allowed in Illinois and Indiana.

The purpose of the oil field miscibility classification is Basin-wide screening for EOR potential. Many of the oil fields are composed of multiple reservoirs at varying depths such that all miscibility classes may be present, but the oil field classification is designed to reflect the predominate miscibility class. The bulk volume-weighted depth of each oil field was calculated to compare to the depth ranges were CO_2 is miscible, near miscible, or immiscible using Equation [1]:

$$D_f = \frac{\sum D_{ri} h_i A_i}{\sum h_i A_i} \qquad [1]$$

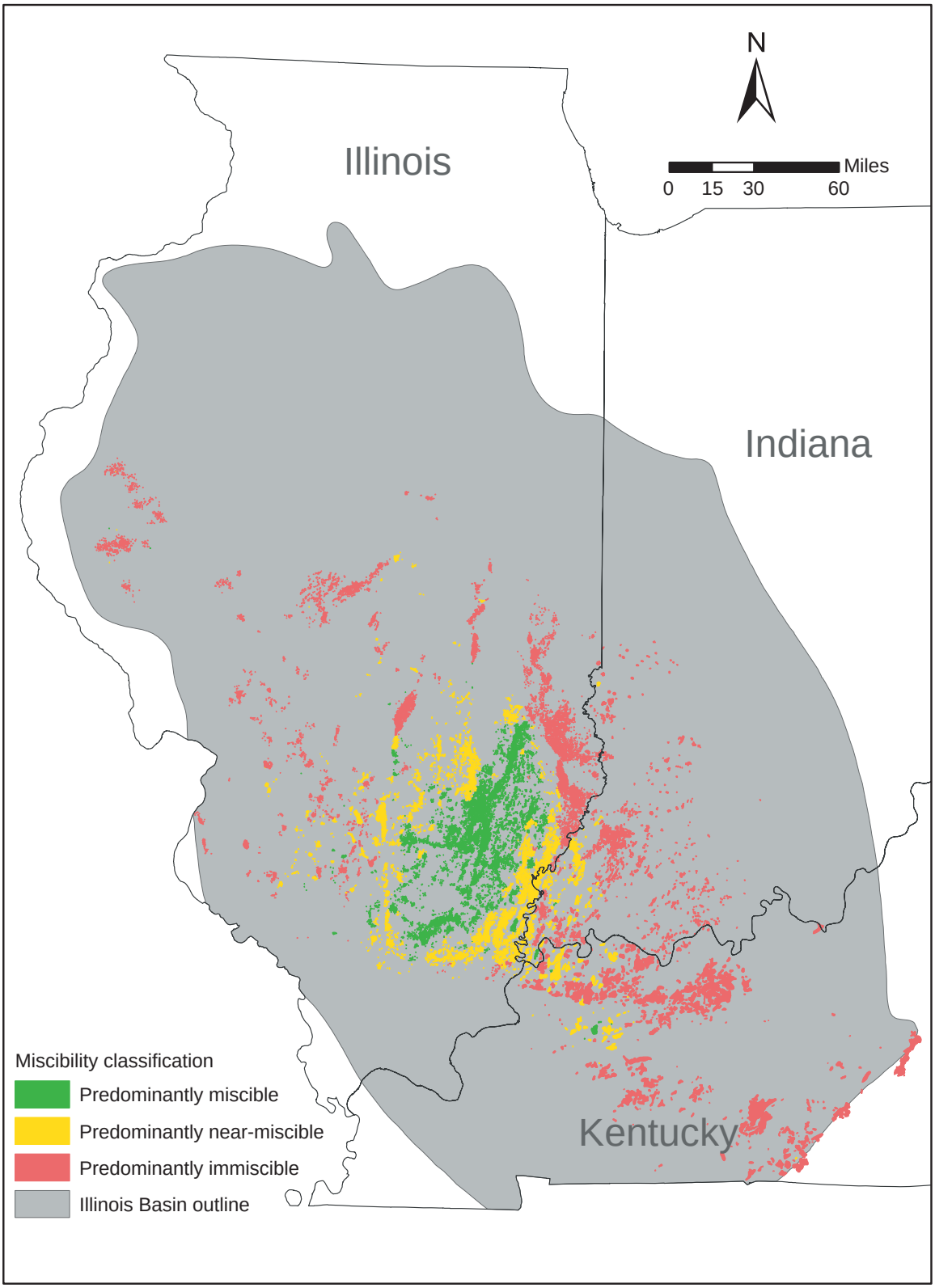

Figure 2-2 *EOR miscibility classification for oil fields in the Illinois Basin.*

where

D_f, is bulk volume weighted depth of each field;
D_{ri}, is top average depth of each reservoir i;
h_i, is average thickness of each reservoir i; and
A_i, is cumulative area of each reservoir i.

Since insufficient data were available, temperature, pressure, and minimum and maximum gradients were assumed based on Basin history and the equations were solved for depth to define the depth ranges of our classification categories.

Critical depth ranges based on two temperature gradients (G_T) were evaluated using Equation [2]:

$$D_{Tc} = \left(\frac{(T_c - 62)}{G_T}\right) + 100\ ft \qquad [2]$$

Equation [2] assumes the gradient is constant starting from 62°F at 100 ft. Tables 2-1 and 2-2 have depth ranges calculated from the various combinations of pressure and temperature gradients.

Table 2-1. Depth ranges of each miscibility class calculated based on a temperature ±2°F of the critical temperature (86 to 90°F) and two temperature gradients.

Condition	Classification	Criteria	Gradient (°F/ft)	Depth range (ft)
1	immiscible	T_c < 86 °F	1.0 °F/100	< 2,500
	near miscible	86°F ≤ T_c < 90°F	1.0 °F/100	2,500 ≤ D < 2,900
	miscible	T_c ≥ 90°F	1.0 °F/100	≥ 2,900
2	immiscible	T_c < 86°F	1.2 °F/100	< 2,100
	near miscible	86°F ≤ T_c < 90°F	1.2 °F/100	2,100 ≤ D < 2,433
	miscible	T_c ≥ 90°F	1.2 °F/100	≥ 2,433

Critical depth ranges (D_{pc}) are based on two pressure gradients: $D_{pc} = P_c/G_p$.

Table 2-2. Depth ranges of each miscibility class calculated based on pressures roughly ±100 psia of the critical pressure (P_c=1,000 to 1,200 psia) and two pressure gradients.

Condition	Classification	Criteria	Gradient (psia/ft)	Depth range (ft)
3	immiscible	P_c < 1,000 psia	0.433	D < 2,310
	near miscible	1,000 psia ≤ P_c < 1,200 psia	0.433	2,310 ≤ D < 2,770
	miscible	P_c ≥ 1,200 psia	0.433	D ≥ 2,770
4	immiscible	P_c < 1,000 psia	0.800	D < 1,250
	near miscible	1,000 psia ≤ P_c < 1,200 psia	0.800	1,250 ≤ D < 1,500
	miscible	P_c ≥ 1,200 psia	0.800	D ≥ 1,500

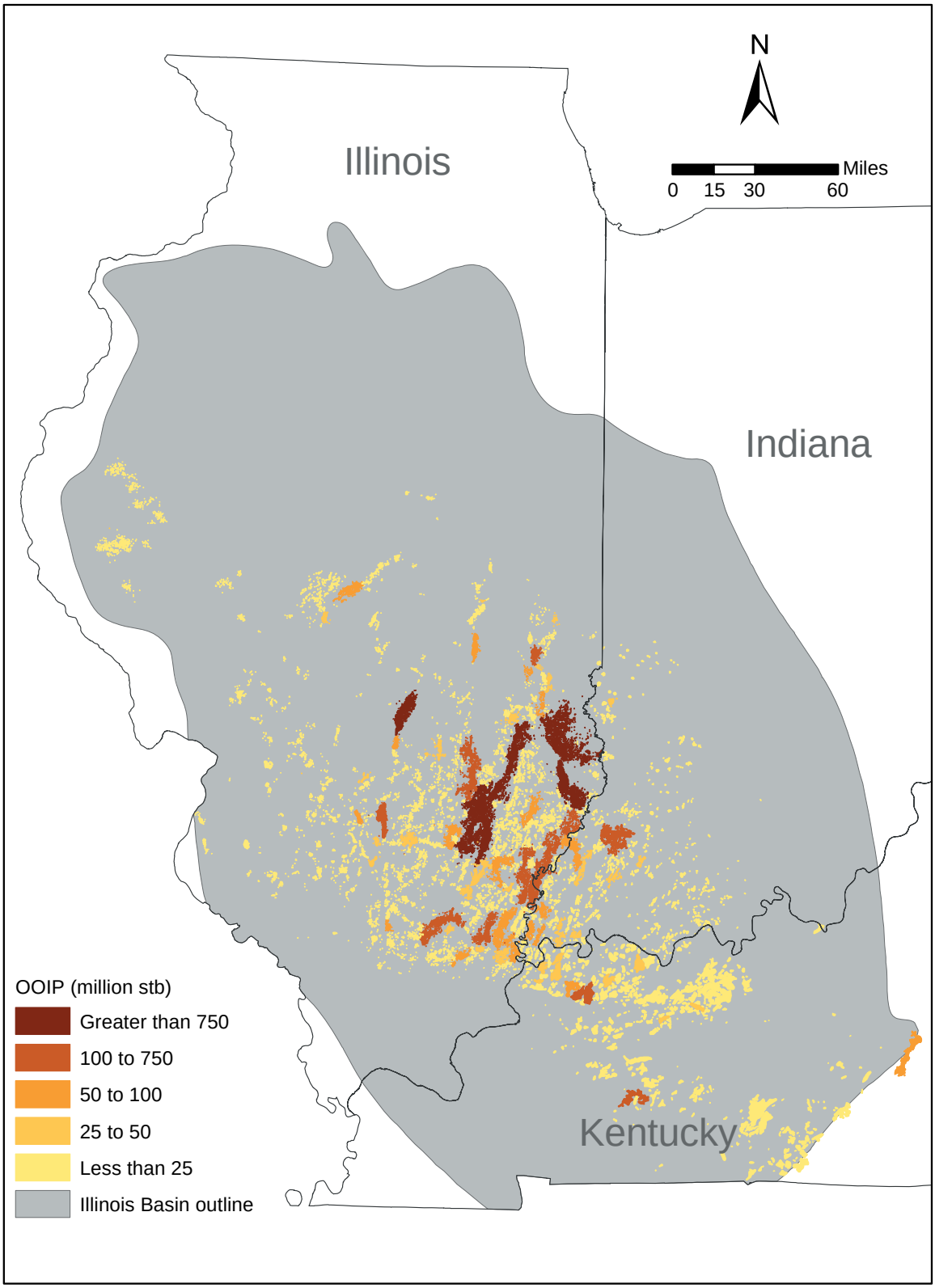

Figure 2-3 *OOIP per oil field in the Illinois Basin.*

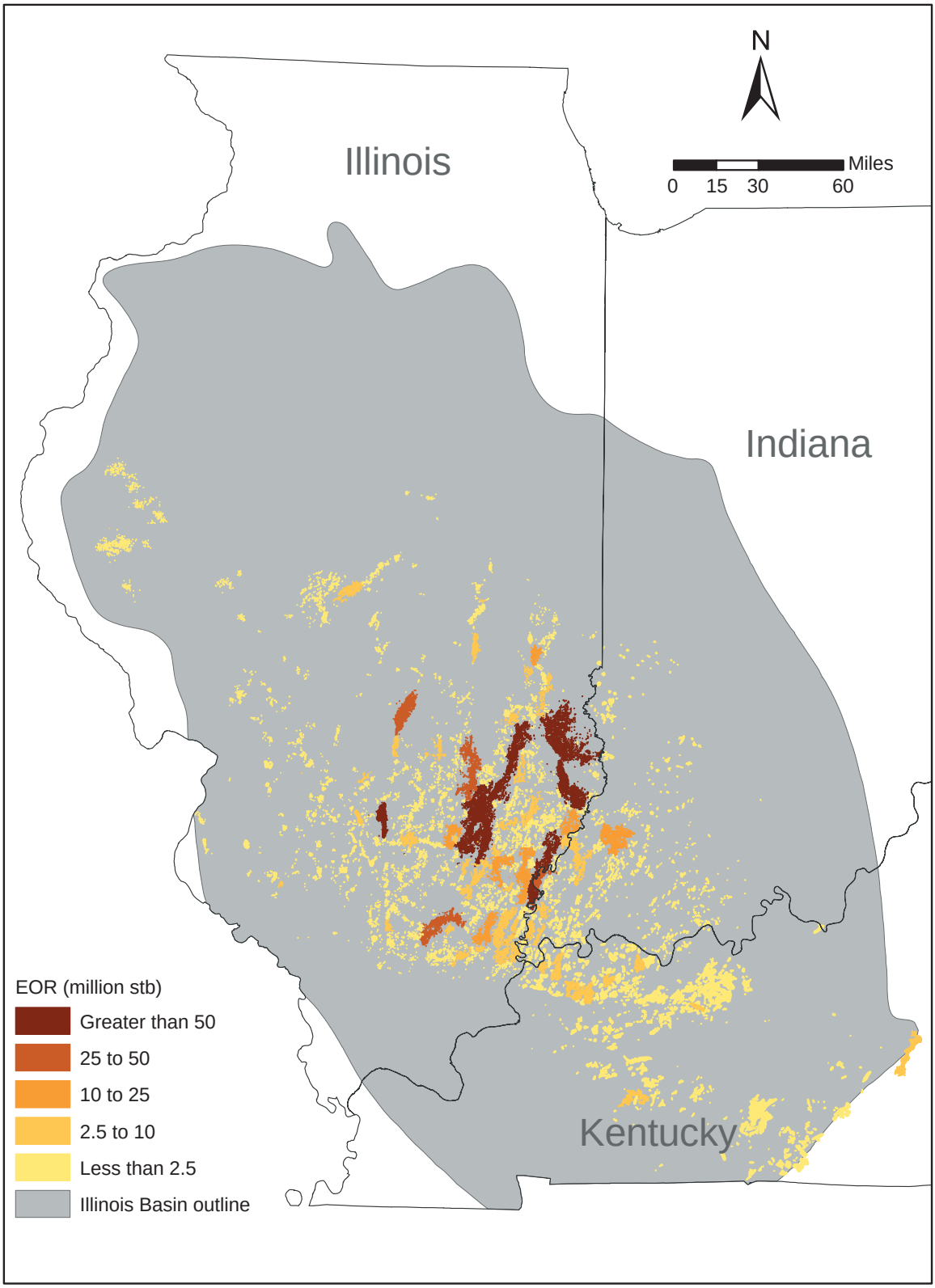

Figure 2-4 *Potential enhanced oil recovery per oil field in the Illinois Basin.*

Reservoir Classification

The combinations of temperature and pressure creating the largest near-miscible range were used as criteria for assigning miscibility classes to oil fields. When comparing the minimum depths at which temperature and pressure are sufficient for CO_2 to transition from the immiscible to the near-miscible state (gas or liquid phase into the supercritical state), minimum depth is 640 m (2,100 ft), assuming a temperature gradient of -17.22°C/30 m (1.0°F/100 ft). Similarly, when comparing the maximum depths at which temperature and pressure are sufficient for CO_2 to transition from the near-miscible to the miscible state, maximum depth is 884 m (2,900 ft), assuming a temperature gradient of -17.22°C/30 m (1.0°F/100 ft). It was concluded that temperature was the controlling factor determining CO_2 miscibility in reservoirs in the Illinois Basin. For Basin-wide categorizing of the oil fields, <640 m (<2,100 ft) was immiscible, 640 to 884 m (2,100 to 2,900 ft) was near-miscible, and >884 m (>2,900 ft) was miscible.

To display the results of the oil field miscibility classification, oil field boundaries within the Illinois Basin were mapped as polygons and colorized based on miscibility class using GIS techniques (Figure 2-2). The CO_2 miscibility criteria were then overlaid with other criteria such as OOIP (Figure 2-3) to determined the best areas to study further for EOR potential (Figure 2-4).

Quantification of Key Reservoir Parameters for Major Plays (Subtask 5.3)

Original OOIP Calculation

Based on industry experience with CO_2 flooding for tertiary recovery, operators using the technique in the Illinois Basin might reasonably expect to recover 10% of OOIP beyond the volume already yielded by primary and waterflood recovery. A recent estimation of Basin OOIP was approximately 1.91 billion m^3 (12.0 billion stb); estimated average recovery potential was 36% (Mast and Howard, 1991) when primary and secondary production were combined. To date, about 0.68 billion m^3 (4.3 billion stb) have been produced, and production continues at a level of approximately 1.91 m^3 (12.0 billion stb) annually. Production comes from over 50 different horizons in the Basin. An estimated 78% of cumulative production has come from reservoirs in middle Mississippian Chesterian sandstones and the Ste. Genevieve Limestone. This study focused on examples from the three most prolific producing formations in the Illinois Basin: the Cypress and Aux Vases Sandstones and the Ste. Genevieve Limestone.

ArcGIS and Access databases were used to obtain a more up-to-date estimate of Basin OOIP (Figure 2-3). The analysis uses the standard OOIP (stb) formula, which is expressed as

$$OOIP = Ah\varphi(1-S_w)/B_o \qquad [3]$$

where

A is reservoir area. The area of each reservoir in each oil field was calculated using area buffers around each well completed in a given reservoir. Because well location and associated reservoir level data were not available for each well in the Illinois Basin, average reservoir area within each oil field could not be estimated using the same methodology across the Basin. Each state applied different methods or different parameters to evaluate reservoir area. The Illinois State Geological Survey (ISGS) estimates were based on GIS-generated radial or circular well buffers equal to 72,843.714 m^2 (18 acres) and hand-generated rectangular well buffers. The Indiana Geological Survey (IGS) also applied a GIS-based radial or circular buffer to each well. The Kentucky Geological Survey (KGS) estimated reservoir area by multiplying the number of producing and abandoned wells by one of three well spacings (16,187.49; 40,468.73; or 80,937.46 m^2 (4, 10, or 20 acres)). To identify anomalous area values, the ratio of reservoir area to the number of wells per reservoir was calculated and compared with a theoretical maximum.

h is average reservoir thickness. Average reservoir thickness data for oil fields were formerly derived from statistical compilations of annual reports of the petroleum industry in Illinois, the waterflood database, geophysical logs, and core analysis data. The ISGS data are primarily from statistical compilations in annual reports of the petroleum industry; however, sub-sampling of the waterflood database and geophysical logs for large reservoirs improved these data. The IGS estimates of thickness were based on reports using geophysical logs and core data. The KGS stored thickness values from geophysical logs and completion intervals from well completion reports separately in its database. The KGS thickness values were based on geophysical logs, when available, and well completion reports if no geophysical data were available. The overall distribution of thickness across the Illinois Basin is lognormal with mode thickness class between 1.524 to 3.048 m (5 and 10 ft).

ϕ is average reservoir porosity. Core plug or geophysical analysis were the primary sources of data used to estimate the average or mode reservoir porosity within an oil field for each formation in which a reservoir was present. The ISGS used a base data set from a previously published report (Mast and Howard, 1991) and analyzed data from core plug data to derive mode porosity values for reservoirs consisting of sandstones (18%) and carbonates (12%). The IGS and KGS calculated porosity from ongoing databases. Frequency histograms of porosity classes across the Illinois Basin indicate that porosity values are multimodal, reflecting the diverse range of formations from which oil is produced (Figures 2-5, 2-6, and 2-7).

S_w is water saturation. Saturation of any given fluid in a pore space is the volume of fluid to the total pore space volume. Water saturation is based on porosity, permeability, and capillarity of the rock.

Water saturation values applied in the OOIP analysis were 45% for Illinois and 35% for Invdiana and Kentucky based on general observations (Seyler et al., 2004).

B_o is oil formation volume factor. Oil formation volume factor is dependent on pressure, temperature, and crude oil composition. Within the Illinois Basin, a very narrow range of values, 1.1 to 1.2 reservoir barrels (rb)/stb, is common (Moore et al., 2004). Because of this narrow range of values, a conservative value of 1.15 was applied. Any error introduced by the oil formation volume factor would have little impact on OOIP estimate.

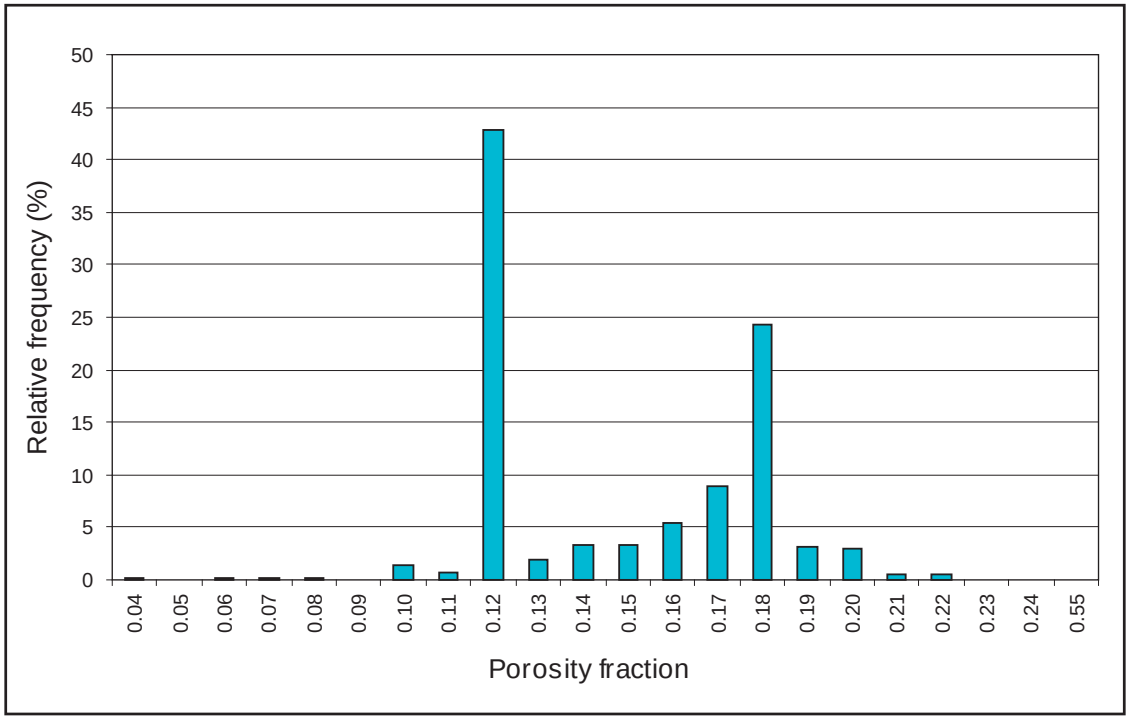

Figure 2-5 *Average porosity of Illinois reservoirs.*

Cumulative oil production data are not available at the reservoir level due to co-mingling at the well bore and stock tanks. The primary source of these field-level data are pipeline inventory reports. The cumulative oil production totals for Kentucky counties in the Illinois Basin were based on tax records because they are generally more accurate than pipeline inventory reports.

Reservoir drainage areas were calculated using a variety of spatial and non-spatial methods depending on the state. Values for both reservoir thickness and average reservoir porosity were obtained from databases maintained by the three state geological surveys, and average water saturation was estimated from observations of the surveys. Formation volume factor, which is dependent on crude composition

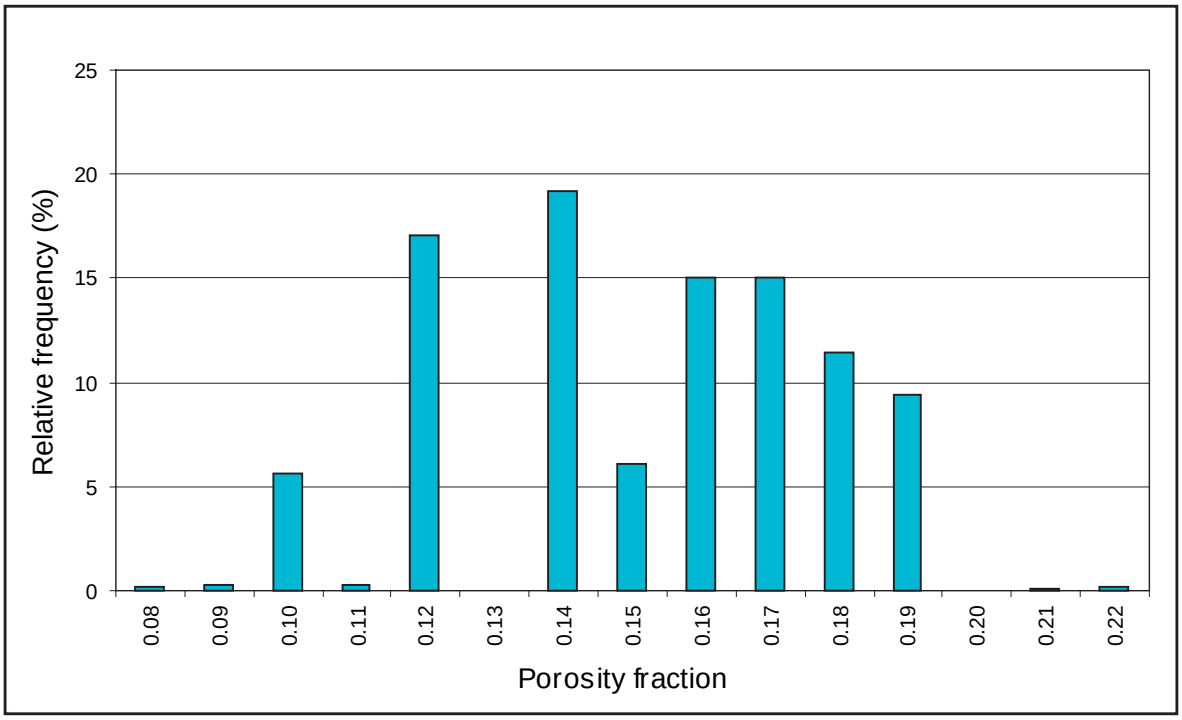

Figure 2-6 *Average porosity of Indiana reservoirs.*

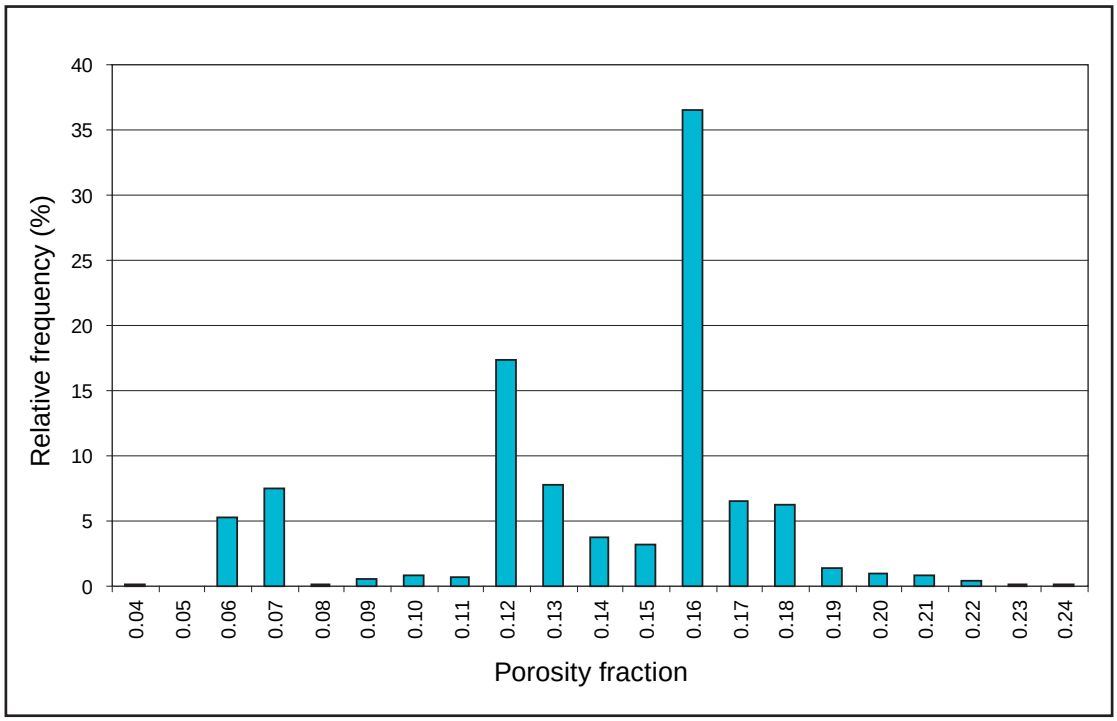

Figure 2-7 *Average porosity of Kentucky reservoirs.*

and pressure-temperature regime, was assigned a value of 1.15 rb/stb, based on an operator's comments. OOIP estimates were made for all fields in the Basin.

Calculated OOIP for the fields was compared with cumulative production as a validity check, using the 36% recovery factor of Mast and Howard (1991) for the mean value. For a subset of larger fields with superior historical production data, a decline-curve analysis was used as a secondary validation.

Using these methods, a revised estimate of Basin-wide OOIP is 2.24 billion m^3 (14.1 billion stb), an increase of 17.5% over the previous estimate of 1.91 billion m^3 (12.0 billion stb) (Figure 2-3).

In an effort to determine whether sufficient unrecovered immobile oil exists such that CO_2 EOR infrastructure would have economic potential, the OOIP for the Illinois Basin was calculated, and cumulative oil production subtracted to derive an estimate of unrecovered-oil-in-place (UOIP). The amount of OOIP for each reservoir was calculated using representative values for reservoir area, average net thickness, average porosity, water saturation, and oil formation factor. Cumulative oil production was available at the field level for the Illinois Basin (Figure 2-8). Cumulative oil production data are not available at the reservoir level due to co-mingling at the well bore and stock tanks.

Decline Curves

Background

Decline curves, a completely independent, production-based method, was used to validate the OOIP estimated from volumetrics. Decline curves methodology is a empirical rate-time relationship loosely based on Darcy's equation and can be described as either exponential or hyperbolic depending on the reservoir drive mechanisms causing the production decline. The primary use of decline curves is to forecast rate that can be used to calculate remaining production, abandonment time, and OOIP. To calculate each of these, peripheral information such as an economic abandonment rate or recovery factory is required.

For this study, exponential decline was used because it is simple to implement in graphical form using semilog coordinates. Additionally, production trends that behave exponentially exhibit a linear trend on semilog coordinates with rate on the logarithm scale. All fields studied appeared to behave exponentially. Equation [4] for exponential decline follows:

$$q = q_i e^{-Dt} \qquad [4]$$

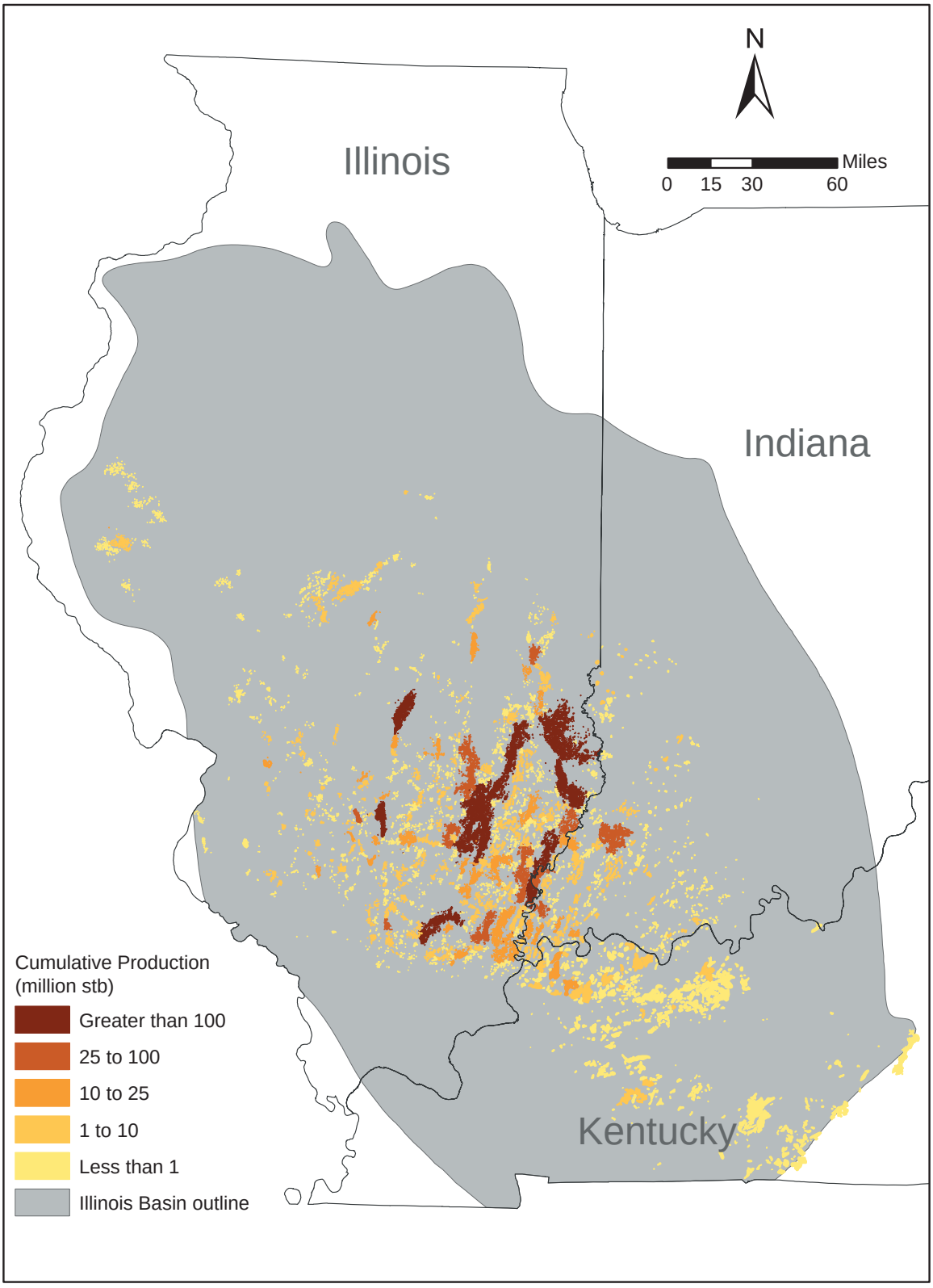

Figure 2-8 *Cumulative production per oil field in the Illinois Basin.*

where q_i is the initial rate in stock tank barrels per year, D is the nominal decline coefficient in units of reciprocal years, t is time in years, and q is a forecasted rate in stock barrels per year at time t based on decline (D). The initial rate is not necessarily the rate at discovery but the rate at the beginning of the exponential trend of data. When q_i is not the initial rate, which almost always is the case, the cumulative production prior to the exponential decline must be included in subsequent analysis.

The cumulative oil (N_p) for the period of exponential decline (including the forecast) is calculated directly using the formula in Equation [5]:

$$N_p = \frac{q_i - q}{D} \qquad [5]$$

Rate q is less than q_i such that N_p would be the cumulative oil production between rates q_i and q that have exponential decline D. For the application using decline curves to approximate OOIP, q is selected as the abandonment rate. Abandonment rate for a field is a very involved and subjective analysis and is well beyond the scope of this validation of volumetric OOIP. Fortunately, the OOIP estimate is very insensitive to the value of the abandonment rate as the lower rates in future years add inconsequential cumulative oil production compared with the earliest years of peak production of oil fields. (Conversely, when using decline curves to estimate remaining field life or abandonment time, the abandonment rate is critical.) An abandonment field rate of 159 m^3/yr (1,000 stb/yr) was used.

Comparison to Volumetric OOIP

Decline curves were only applied to the Illinois oil fields because annual production is not available for Indiana and Kentucky. The production data up to 1988 is from Huff (1988) and was augmented to 2004 by Huff (2004). It is well known that relatively less attention was given to production records from some of the early oil production from the older oil fields. Consequently, the decline curve OOIP estimated for the earliest fields will be too low. Where recent annual rate deviations from the linear, exponential trend occurred, the most representative line was adjusted to fit the general trend of the historical data.

Annual oil production from 40 Illinois oil fields were selected (Table 2-3); this section represents nearly 60% of the Basin's 2.24 billion m^3 (14.1 billion stb) OOIP. An oil recovery of 36% was used to estimate OOIP from decline curves. The average relative error between the volumetric and decline curve OOIP estimates is 38%. This relative error is modest and is strongly influenced by the assumption of assigning all oil fields the same recovery factor and by the underreported oil production of the earlier oil fields. The relative error is <30% when six of the fields with the larger relative error are dropped. Figure 2-9 shows this relationship graphically on logarithmic coordinates, which shows the general trend and good agreement between decline curves and volumetric OOIP estimates.

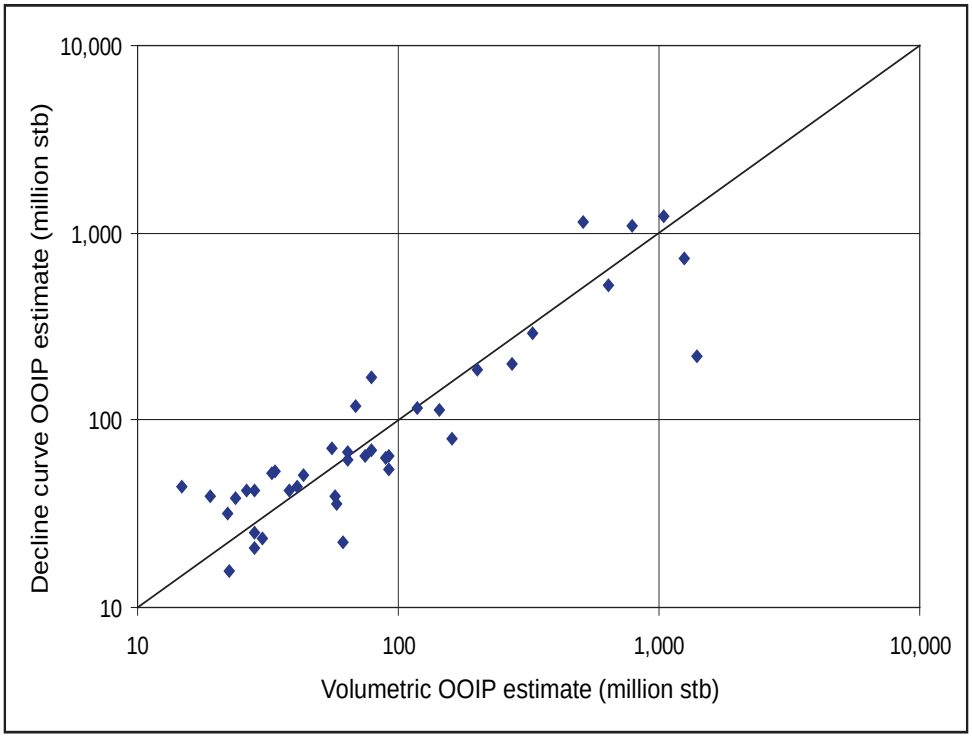

Figure 2-9 *Comparison of volumetric and decline curve OOIP estimates for 40 Illinois Basin oil fields. Some of the earliest oil fields are known to have oil production that is underreported; consequently, the decline curve estimate falls below the unit slope. Decline curve estimate assumes 36% oil recovery. The line through the data is a unit slope; it is not a regression line.*

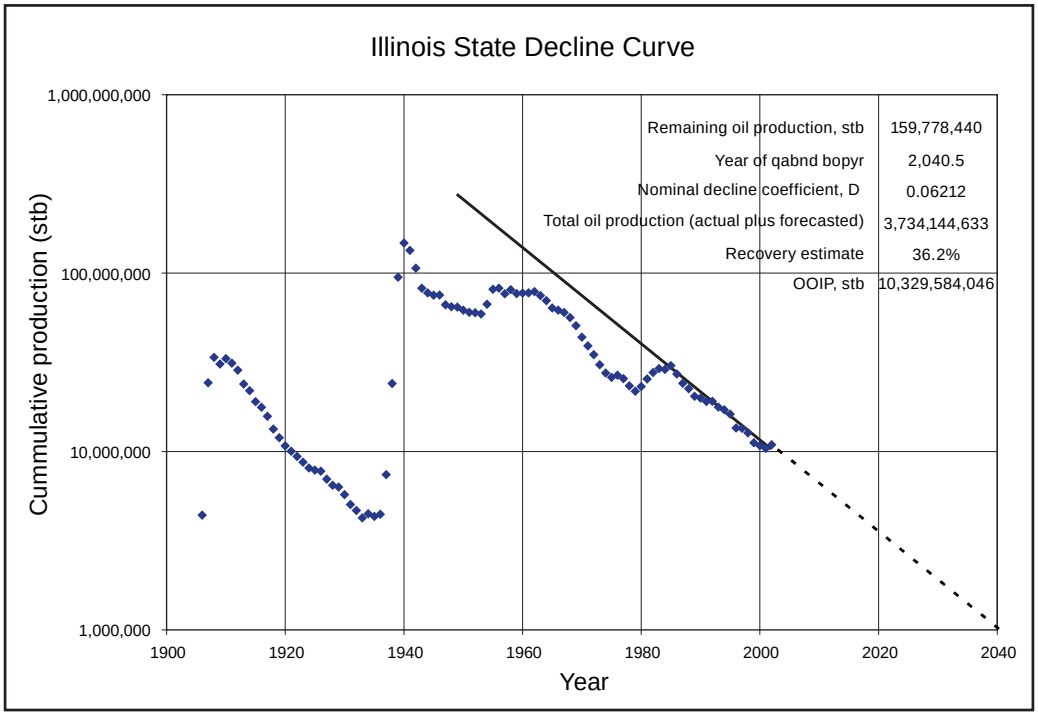

Figure 2-10 *Decline curve OOIP estimate for the State of Illinois. Illinois represents approximately 10.3 billion stb (74%) of the Basin's 14.1 billion stb OOIP. An oil recovery factor of 36.2% was required to match the decline curve OOIP estimate of 10.3 billion stb.*

Decline curves were also applied for the entire State of Illinois oil production (Figure 2-10). Of the 2.24 billion m^3 (14.1 billion stb) volumetric estimate, 1.64 billion m^3 (10.3 billion stb) of OOIP underlies Illinois. Using the historical oil production from the State, an oil recovery factor of 36.2% was required to match the 1.64 billion m^3 (10.3 billion stb) OOIP. This oil recovery factor is consistent with the Howard and Mast (1991) estimate of 36%.

Overall decline curve OOIP supports the OOIP estimate of 2.24 billion m^3 (14.1 billion stb) derived from volumetrics. The total State production matched much better than the field by field comparison.

West Texas-based Oil Recovery and CO_2 Storage Factors

To estimate the potential CO_2 EOR and CO_2 storage in oil reservoirs for the Illinois Basin, a methodology was devised that had Basin-wide applicability. An ideal but impractical method is to conduct a reservoir study of each reservoir within each field in the Basin. OOIP or cumulative oil production by field or reservoir provides a common basis for assessment of all fields within the Basin. For CO_2 oil recovery, a West Texas rule-of-thumb exists on an OOIP basis. Although a rule-of-thumb for a CO_2 storage factor is unavailable, CO_2 gross and net utilization rules-of-thumb are available; however, CO_2 utilization is on a produced barrel of oil basis.

Oil recovery is defined as the oil produced in stock tank barrels compared with the OOIP in stock tank barrels and is typically reported as a fraction or percentage. The value of oil recovery is specified for a particular drive mechanism (primary or waterflood oil recovery factor) or period of time in the life of an oil reservoir (ultimate oil recovery).

CO_2 utilization is defined as the volume of CO_2 injected to produce a stock tank barrel of oil. The use of gross and net utilization takes into account the amount CO_2 that is produced and recycled. In other words, gross utilization is the total CO_2 injected compared with the incremental oil production as a consequence of CO_2 injected. Net utilization is the total CO_2 injected minus the CO_2 produced compared with the incremental oil production as a consequence of CO_2 injected. Because the net utilization represents the difference between injected and produced, it accounts for the CO_2 remaining in the reservoir, which could be trapped or mobile-free phase and/or dissolved in oil or water.

Table 2-3. OOIP comparison between volumetric OOIP and decline curve OOIP using 36 and 48% oil recovery.

Field	Volumetric OOIP (million stb)	OOIP with 48% oil recovery (million stb)	48% relative error (%)	OOIP with 36% oil recovery (million stb)	36% relative error (%)	Total oil (actual plus forecasted) (million stb)
Aden	19	29	43	39	69	14
Albion	144	84	52	112	25	40
Allendale	161	60	92	80	68	29
Assumption	22	24	7	32	36	11
Barnhill	30	18	53	23	25	8
Benton	69	89	25	119	53	43
Boyd	26	32	20	43	48	15
Bungay	41	33	23	44	6	16
Centerville East	28	19	39	25	11	9
Centrailia	92	41	77	54	52	20
Clay City	1,249	553	77	737	52	265
Dale	329	218	41	290	12	105
Eldorado	58	27	74	36	48	13
Goldengate	89	47	62	63	35	23
Herald	92	48	63	64	36	23
Inman East	64	51	23	67	6	24
Iola	43	39	12	51	17	18
Johnsonville	79	128	47	171	73	62
Lawrence	1,046	923	13	1,230	16	443
Main	1,403	165	158	221	146	79
Marine	24	29	20	39	48	14
Mattoon	74	48	43	64	15	23
Maunie	22	12	62	16	35	6
Mill Shoals	33	39	17	52	45	19
Mt Auburn	61	17	113	23	92	8
Mt Carmel	64	46	34	61	6	22
New Harmony	643	396	48	528	20	190
Omaha	28	16	56	21	29	8
Parkersburg	57	29	64	39	37	14
Patoka	28	31	12	42	40	15
Phillipstown	118	88	29	117	0	42
Roland	202	140	37	186	8	67
Sailor Springs	274	149	59	199	32	72
Salem	512	850	50	1,133	75	408
St James	56	54	4	71	24	26
Storms	78	52	40	69	12	25
Tonti	15	33	76	44	99	16
Woodlawn	34	40	17	53	45	19
Total	**8,231**	**5,551**	**45**	**7,401**	**38**	**2,664**

The CO_2 storage factor (*SF*) is the volume (or mass) of CO_2 stored per stock tank barrel (*stb*) of OOIP, which can be derived from the oil recovery factor (*RF*) and CO_2 net utilization (U_N):

$$SF\left[\frac{Mscf - CO_2\ stored}{stb - OOIP}\right] = RF\left[\frac{stb - oil\ produced}{stb - OOIP}\right] U_N\left[\frac{Mscf - CO_2\ stored}{stb - oil\ produced}\right] \quad [6]$$

West Texas CO_2 floods have historically been considered successful only as a consequence of achieving miscible conditions between in situ crude oil and injected CO_2; consequently, rules-of-thumb and field observations based on West Texas are representative of miscible CO_2 floods and not immiscible CO_2 floods.

Two simple rules-of-thumb for CO_2 oil recovery are 10% of OOIP or 25% of primary plus waterflood oil recovery (Fox and Avasthi, 2004). Applying these rules-of-thumb to the Illinois Basin's historically accepted OOIP of 1.91 billion m^3 (12.0 billion stb) and cumulative oil production of 0.68 billion m^3 (4.3 billion stb) yields 0.19 billion m^3 (1.2 billion stb) and 0.17 billion m^3 (1.1 billion stb), respectively (0.22 billion m^3 (1.4 billion stb) for the 2.24 billion m^3 (14.1 billion stb) of OOIP estimated for this study). For estimating the CO_2 requirement, Fox and Avasthi recommended 40% of the hydrocarbon pore volume (HCPV). This recommendation can be applied on a reservoir-by-reservoir basis by assuming pressure and temperature gradients to estimate the oil formation volume factor and that net CO_2 is one half of gross CO_2 requirements. Applying this rule-of-thumb to the 2.24 billion m^3 (14.1 billion stb) gives an estimate of 350 million tonnes (386 million tons) of CO_2 stored as a consequence of CO_2 EOR in all of the known oil reservoirs in the Basin.

Brock and Bryan (1990) reported selected data on 23 field-scale or pilot CO_2 floods; oil recovery ranged from 7.1 to 22% with an arithmetic average of 12.7%. Those authors also reported net CO_2 utilization of 0.43 to 2.24 thousand m^3/m^3 (2.4 to 12.6 thousand standard cubic feet (scf)/stb) with an arithmetic average of 1.22 thousand m^3/m^3 (6.87 thousand scf/stb).

For this work, West Texas-based oil recovery for miscible conditions was used as 10 to 16%, and immiscible oil recovery factor was used as 4 to 8% (Melzer, 2004). Net utilization for miscible and immiscible oil recovery was used as 0.89 to 1.8 thousand m^3/m^3 (5 to 10 thousand scf/stb) (Brock and Bryan, 1990), which is equal to 0.265 to 0.530 tonnes of CO_2/stb (18.850 thousand scf = 1 tonne).

Applying the West Texas-based oil recovery and CO_2 storage factors Basin-wide to the new OOIP from this study resulted in 0.16 to 0.19 billion m^3 (1.0 to 1.2 billion stb) EOR and 310 to 620 million tonnes (342 to 683 million tons) of CO_2 stored. The distribution by miscible, immiscible, and near miscible are shown in Table 2-4.

Table 2-4. The distribution by miscible, immiscible, and near miscible using West Texas rules-of-thumb.

Attribute	Immiscible	Near miscible	Miscible	Total
CO_2 storage (million tonnes)	140–280	79–160	92–180	310–620
CO_2 EOR (million stb)	450–530	250–300	300–350	1,000–1,200

Previous CO_2 Studies in Illinois: Mattoon Field CO_2 Project, 1992–1994

Work was performed from 1992 through 1994 under a cost-shared cooperative Agreement No. DE-FC22-93BC 14955 between the U.S. Department of Energy (DOE) and American Oil Recovery, Inc. (Decatur, Illinois) titled, *Applications of Advanced Petroleum Production Technology and Water Alternating Gas Injection For Enhanced Oil Recovery—Mattoon Oil Field, Illinois*. The following information is a synopsis of the Final Report submitted to DOE in March 1995.

This project was part of a DOE program designed to recover bypassed oil from fluvial deltaic Class 1 reservoirs. Cypress Sandstone fluvial deltaic reservoirs in Mattoon Field, Coles County, Illinois, were selected for demonstration of CO_2 utilization in improved oil recovery from a partially depleted mature field. The design and scope of this project included CO_2 injectivity testing in the Pinnell and Sawyer units, well stimulation treatments with CO_2 in the Strong unit, and infill well drilling, completion, and oil production. The field activities were supported by extensive CO_2-oil-water coreflood experiments, CO_2-oil phase interaction experiments, and integrated geologic modeling and reservoir simulations.

A comprehensive reservoir characterization study of the Cypress Sandstone within Mattoon Field identified five layers (A, B, C, D, E) within the study area. Three-dimensional geologic models created from well data were used to interpret the location, size, and continuity of the productive intervals. CO_2 injectivity tests were performed in the A interval in the Pinnell unit, E interval in the Sawyer unit, and D interval in the Strong unit.

Poor inter-well communication and limited areal extent of the Cypress Sandstone A interval at the Pinnell unit were confirmed by CO_2 injectivity tests and reservoir simulation. Inefficient displacement of reservoir crude oil by injected CO_2 was caused by reservoir heterogeneity and attendant gas channeling.

Injectivity tests in the Sawyer unit showed good inter-well communication. An infill well, the AOR/Seaman No. 15, was drilled, cored, completed, and produced. Results of core sample analysis from the project infill well verified the isolation of the target E sandstone interval from the extensively waterflooded lower B and C sandstone intervals. Reservoir simulation results indicated that a significant

amount of additional oil may be recovered by the implementation of a water-alternating gas (WAG) injection program.

Injectivity tests in the Strong unit consisted of "huff-and-puff" treatments with CO_2 in two wells. Initial results from one of the wells were very encouraging. No significant response was obtained from the other. Simulated results of huff-and-puff treatments with CO_2 in the Cypress Sandstone demonstrated that rule-of-thumb volume of 18 tonnes (20 tons) of CO_2 per perforated foot of pay constituted over treatment. Slug sizes of 5% HCPV and 10% HCPV improve simulated oil production rates above the decline curve while 18 tonnes (20 tons) per perforated foot (73% HCPV) reduced oil production rates below pre-injection levels. The injectivity tests in the Strong unit demonstrated that single well huff-and-puff well treatments may be the most cost-effective in mature fields like the Mattoon Field where well integrity is questionable and where well re-completion costs are high.

Laboratory experiments and data collected and described in the final report include compositional analysis and minimum miscibility pressure (MMP) of Mattoon stock tank oil, pressure-volume-temperature phase behavior of CO_2 and crude oil mixtures, determination of relative permeability from unsteady displacements, compatibility of Cypress Sandstone with water (from various water sources) to be used in WAG demonstration tests, advanced analyses of Cypress Sandstone core samples from the AOR-Seaman No. 15 well, and reservoir characterization maps and data of Mattoon Field.

Table 2-5 summarizes the oil production results. All pilots showed an increase in oil production except for the Strong unit, No. 6 well, which had no post-CO_2 injection change in oil production. For the huff-and-puff-type injection scheme, this well had the largest volume of CO_2 injected. It is likely that this large volume displaced the oil too far from the well so that on the "puff" the oil was too far to return to the well.

Table 2-5. Summary of Mattoon Field, Coles County, Illinois, CO_2 pilot.

Unit/well	Sand	CO_2 (ton)	Type	CO_2 injection duration (days)	Oil rate pre-CO_2 (stb/day)	Oil rate post-CO_2 (stb/day)	Time of increased oil rate (mo)
Pinnell unit							
No. 1	A	2,800	Continuous	31	3	60	3
No. 14 Uphoff	A	184	Huff-and-puff	12	3	6	3+
Sawyer unit	E	2,000	Continuous	41	9	45	5+
Strong unit							
No. 8	D	243	Huff-and-puff	25	0.5	3	4+
No. 6	D	1,001	Huff-and-puff	25	0.5	0.5	–

Investigation of Specific Reservoirs to Verify Play-based Conclusions and Selection Criteria for CO_2/EOR Study Examples (Subtask 5.4)

Industry experience has shown that the efficacy of CO_2 flooding is strongly influenced by pressure and temperature. In settings where pressure and temperature conditions allow miscibility of CO_2 in crude oil, recovery is superior to that in sites where CO_2 remains immiscible. Given the relatively shallow depth of oil reservoirs in much of the Basin, limits on the maximum pressure and temperature exist. Consequently, reservoir depth is critical to both CO_2 storage potential and the volume of hydrocarbons recovered. For this reason, the miscibility condition (miscible, near-miscible, and immiscible) was designated a primary criterion in the selection of potential EOR sites.

Using the techniques outlined in Subtask 5.1, each field in the Illinois Basin was classified as miscible, near miscible, or immiscible based on bulk volume-weighted depth and mapped using ArcGIS to screen for CO_2/EOR potential. In the example maps provided, each oil field is color coded based on its miscibility classification: the relatively shallow, predominantly immiscible reservoirs are colored red, the relatively deeper predominantly miscible reservoirs are coded green, and reservoirs in which estimated reservoir pressure and temperature are too close to the critical pressure and temperature of CO_2 to be clearly classified as miscible or immiscible are coded yellow (Figures 2-3, 2-3, 2-4, 2-8, and 2-11). The miscible oil fields have the greatest potential for the largest EOR volume.

In addition to oil reservoir depth to production, other criteria are important for selecting suitable fields for CO_2 flooding. Accessibility to CO_2 sources and to current and future transportation facilities (pipelines, rail lines, and major highways) make up one class of selection criteria. A second variable is quality of well cementation and completions. As a general rule, fields developed after implementation of increased regulatory oversight of cementation and plugging techniques (ca. 1942) are more desirable than older fields.

Field Modeling

In addition to meeting the general selection criteria just outlined, fields chosen for reservoir modeling and simulation also require sufficient data. Of some 190,000 wells in the Illinois portion of the Basin, wireline logs are available for about half. Only 12,000 have any form of porosity log. Most wells in the Basin are represented only by an “electrical log,” with spontaneous potential (SP) and resistivity tracks.

For reservoir modeling purposes, the critical data source proved to be core analysis. As modern porosity logs are rare in the Basin, especially within the older, waterflooded sections of fields, core analyses were the most dependable source of porosity data. The three target formations are represented by some 3,100 analyzed cores: 600 in the Ste. Genevieve and about 1,250 each in the Aux Vases and Cypress. Many

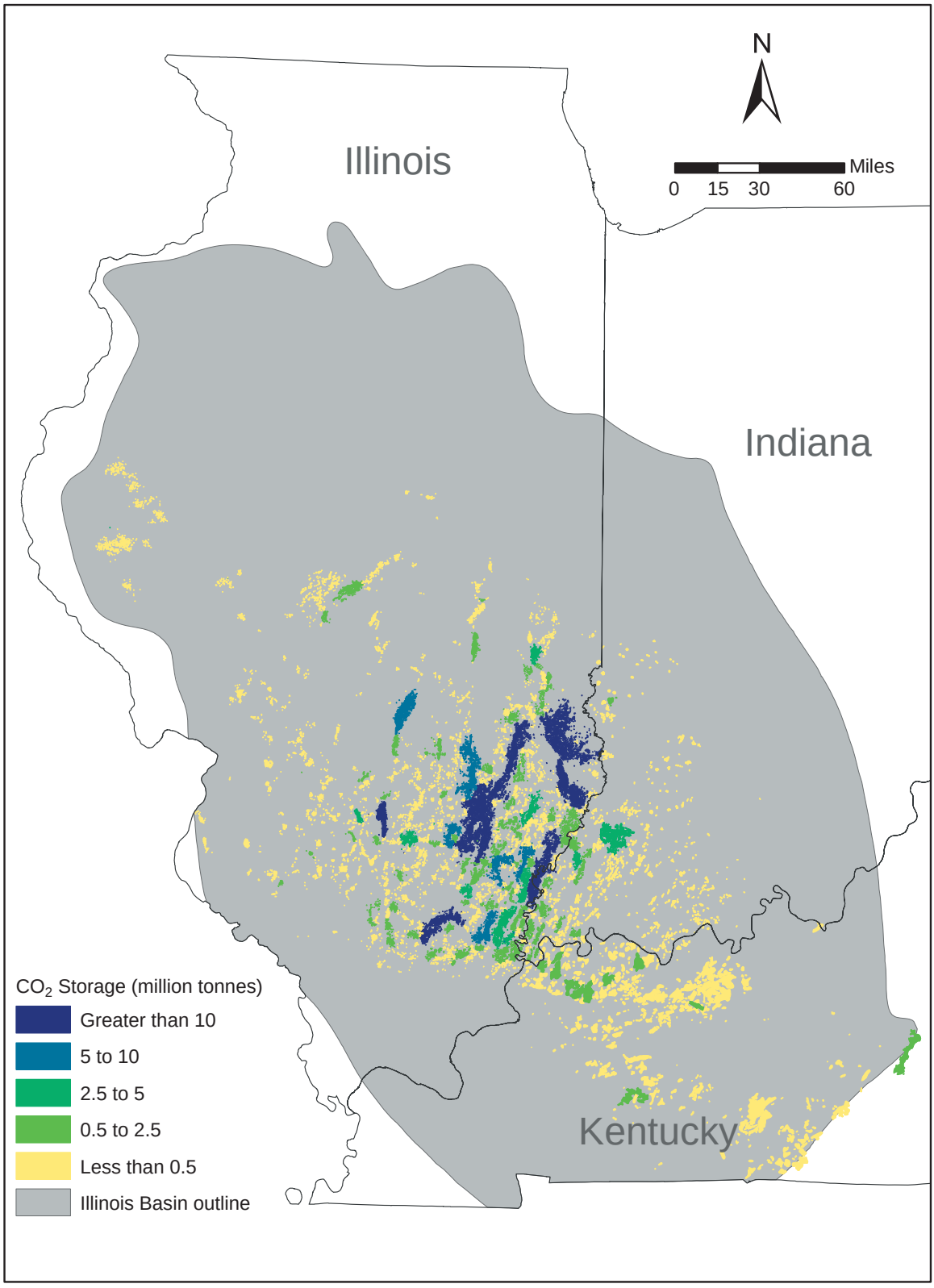

Figure 2-11 *CO_2 storage potential per oil field in the Illinois Basin.*

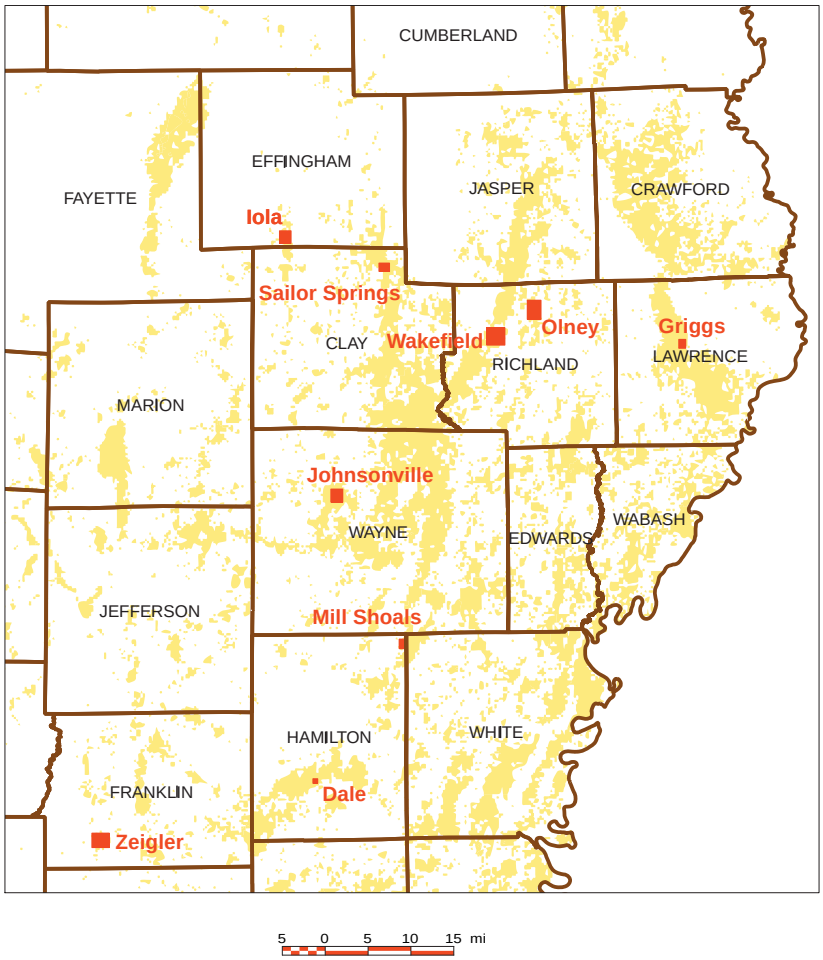

Figure 2-12 *Index map of southeastern Illinois depicting locations of the geologic and reservoir performance studies, with all oil fields (yellow) displayed in the background. The red blocks are proportional to the area of the studies.*

analyses in the ISGS files include permeability measurements as well as porosity. To use this data to its best advantage, the small-scale studies were sited on clusters of cored wells in the target formations.

Nine fields, three from each geologic unit, were identified using the general criteria for selection: two from each of the target formations (Figure 2-12 and Table 2-6) yielded six possible target fields. These nine reservoirs were investigated in detail using geological, geostatistical, and reservoir modeling techniques.

Geological Modeling

Landmark Graphics Corporation's GeoGraphix Suite of applications was used for geological modeling. This suite includes well-log analysis, cross-section building and display, and gridding and contouring packages. In the absence of production and drill-stem testing, log- and core-based zones were identified in the producing formations by comparing log traces through the cored interval to the discrete core

measurements. For each zone, maps of structure and thickness were generated in GeoGraphix and used as constraints to geostatistical modeling on permeability and porosity zonation.

Table 2-6. Fields identified for geologic and reservoir studies to be used to estimate oil recovery and CO_2 storage factors for the Basin-wide assessment of CO_2 EOR and storage capacity.

Aux Vases	Cypress	Ste. Genevieve
Iola Cons.	Clay City Cons., Wakefield Unit	Dale Cons.
Mill Shoals	Lawrence, Griggs Unit	Johnsonville Cons.
Zeigler	Sailor Springs Cons.	Olney Cons.

Geostatistical Modeling

The effort employed Isatis geostatistical modeling software, using stochastic techniques to produce three-dimensional representations of porosity and permeability distribution for each individual field. Using the structure maps generated for each study's geologic models as spatial constraints, variograms were constructed and modeled to reflect both regional and local geological trends. Each simulation effort comprised some 30 visualizations, of which those that "passed" the "most likely" test for porosity and permeability models were used in the reservoir flow model simulations.

Reservoir Modeling

The Landmark program VIP, a compositional reservoir simulation model, was used to approximate CO_2 EOR using the deterministically and geostatistically generated models. The reservoir model grid selection was coordinated with the geologic model development so that the reservoir model reflected the petrophysical trends found in the geologic models. This minimized post-geostatistical model upscaling. A three-component Peng-Robinson equation of state was used to simulate the general fluid properties observed historically in the Basin. Because oil recovery and CO_2 storage factors were desired to reflect only geologic features, not well placement or completions, blanket 5-spot patterns were placed across the model.

Geologic Models

Griggs Lease at Lawrence Field Geologic Model of Cypress Sandstone Reservoir

Deterministic Model

Lawrence Field occupies approximately 162 km^2 (62.5 mi^2) in Lawrence County, Illinois, and has produced over 64 million m^3 (400 million stb) of oil from 23 separate horizons since its discovery in 1906. The Cypress (Mississippian) and the Bridgeport (Pennsylvanian) sandstones are the most prolific

horizons in the field. It is estimated that the Cypress sandstones have yielded about 41 million m^3 (260 million stb) of oil from over 4,000 wells. Currently, about 39.5% of estimated OOIP has been produced; the water cut exceeds 97% after nearly 40 years of waterflooding. The Griggs lease (located in Section 32, T4N, R12W) that was selected to represent the Cypress reservoir section was chosen on the basis of the availability of core analyses, whole core, and a recent log suite. The Griggs unit offered a Cypress reservoir section that represents one of several depositional environments in the Basin as well as a Cypress reservoir section that is typical of the Basin.

Lawrence Field is located on the southern end of the south-southeast–trending La Salle Anticlinal Belt. Two closed structures separated by a saddle define the field. Section 32 is positioned along the crest of the northern structure. Approximately 107 m (350 ft) of closure is indicated on the Barlow structure map for the northern anticline. Depth to the top of the reservoir in the study area starts at 411 m (-259 m MSL) (1,350 ft (-850 ft MSL)). Cypress reservoirs along the crest of the anticline lie entirely within the oil column and, although oil accumulation is controlled by structure, stratigraphy is a significant factor that affects the ultimate recovery.

In the Lawrence Field area, the Cypress Formation consists predominantly of sandstone and shale. Where present, the reservoir sandstones are generally found about 12 m (40 ft) below the base of the Beech Creek (Barlow) Limestone. The intervening interval consists of shale, siltstone, and shaly or calcareous sandstone. In some cases, a red and green variegated to mottled mudstone immediately overlies the reservoir sandstone. The reservoir sandstones in Lawrence Field are equivalent to the middle sandstones of the Cypress. Many fields produce from thin, lenticular sandstones in the upper portion of the Cypress.

Variegated, mottled, laminated to structureless mudstones that cap the sandstones appear to be marsh/mudflat sediments that were at times subjected to subaerial exposure, suggesting that the underlying sandstones were deposited in a shallow marine, nearshore setting. A low-stand, sequence stratigraphic boundary is now recognized at this horizon throughout the Basin. The paleographic setting indicated in the stratigraphic record of the reservoirs at Lawrence Field appears to be that of a large, tidally influenced, marine embayment that formed during the regressive phase of the Cypress depositional cycle.

The reservoir sandstones can be absent or develop to as much as 14 m (45 ft) in thickness. Based on electric log response, particularly the SP character, core observations, and permeability values, the sandstones that make up the reservoir interval were divided into five zones, A through E in ascending order (Figures 2-13 through 2-23). All zones are not necessarily present in any particular area. Zone A is commonly tight and separated from the others by shale. Zone A does not appear to contribute

significantly to production. Zones B through E, the primary reservoir, appear cyclical in nature, particularly on logs, and are separated from each other by thin, low-permeability shaly sandstones, shales, or calcareous beds. Thickness of these individual zones is generally less than 3 m (10 ft). Isopach maps of these zones show very similar geometric characteristics. Elongate, sheet-like sandstones that form with thick, northeast-southwest–trending ridges are common to all four zones.

For the Griggs geologic model, net thickness estimation from the SP logs was possible due to the abundance of core and SP log availability. Net sandstone thickness maps were constructed for each of the Cypress intervals in the Griggs area. Because porosity logs that best define the thickness of effective reservoir rock are limited in the area, thickness data were acquired from normalized SP logs. An effective reservoir for the Cypress Sandstone in the Griggs area was determined from core and porosity logs to be sandstone with porosity ≥15%. A porosity value of ≥15% corresponds to a value of ≥50% clean sandstone response of the SP log, which is calibrated on a log-by-log basis where the 0% clean sandstone point is established by a shale baseline. The shale baseline corresponds to where the SP log is responding to shale beds. The 100% clean sandstone point is established where the SP log is responding to a consistently clean, reservoir quality sandstone, where porosity is in the maximum range, commonly with values up to 25% or greater. The percentage of clean sandstone is then a simple calibrated linear measure from the shale point, 0% clean sandstone, to the 100% clean sandstone point, and the 50% or greater reservoir clean sandstone is defined by any portion of the SP curve that is equal to or greater than half the measured distance from the 0% point to the 100% point on the SP response curve.

Environmental indicators observed in the Lawrence Field Cypress cores are evidence for deposition in a marine setting. Supporting this interpretation is the widespread, elongated, parallel-ridged, sheet-like geometry of the Cypress sandstones. The thin planar bedding combined with wavy and ripple laminations and wispy to continuous clay laminations are indicative of deposition by moderate currents with slack periods. Tidal currents influenced sedimentation, as tidal couplets and flaser bedding can be observed in most cores. Scattered carbonaceous material was most likely derived from the woody effluents of a nearby delta.

Variegated, mottled, laminated to structureless mudstones that cap the sandstones appear to be marsh/mudflat sediments that were periodically subjected to subaerial exposure, suggesting that the underlying sandstones were deposited in a shallow marine, nearshore setting. A low-stand, sequence stratigraphic boundary is now recognized at this horizon throughout the Basin. The paleographic setting indicated in the stratigraphic record of the reservoirs at Lawrence Field appears to be that of a large, tidally influenced, marine embayment that formed during the regressive phase of the Cypress depositional cycle.
Porosity and permeability values measured from core and used in the model of the Griggs area are summarized in Table 2-7. Porosity values measured from core in this area range from 10% to 30% and permeability values range from 9.8×10^{-5} μm^2 to 0.395 μm^2 (0.1 md to >400 md).

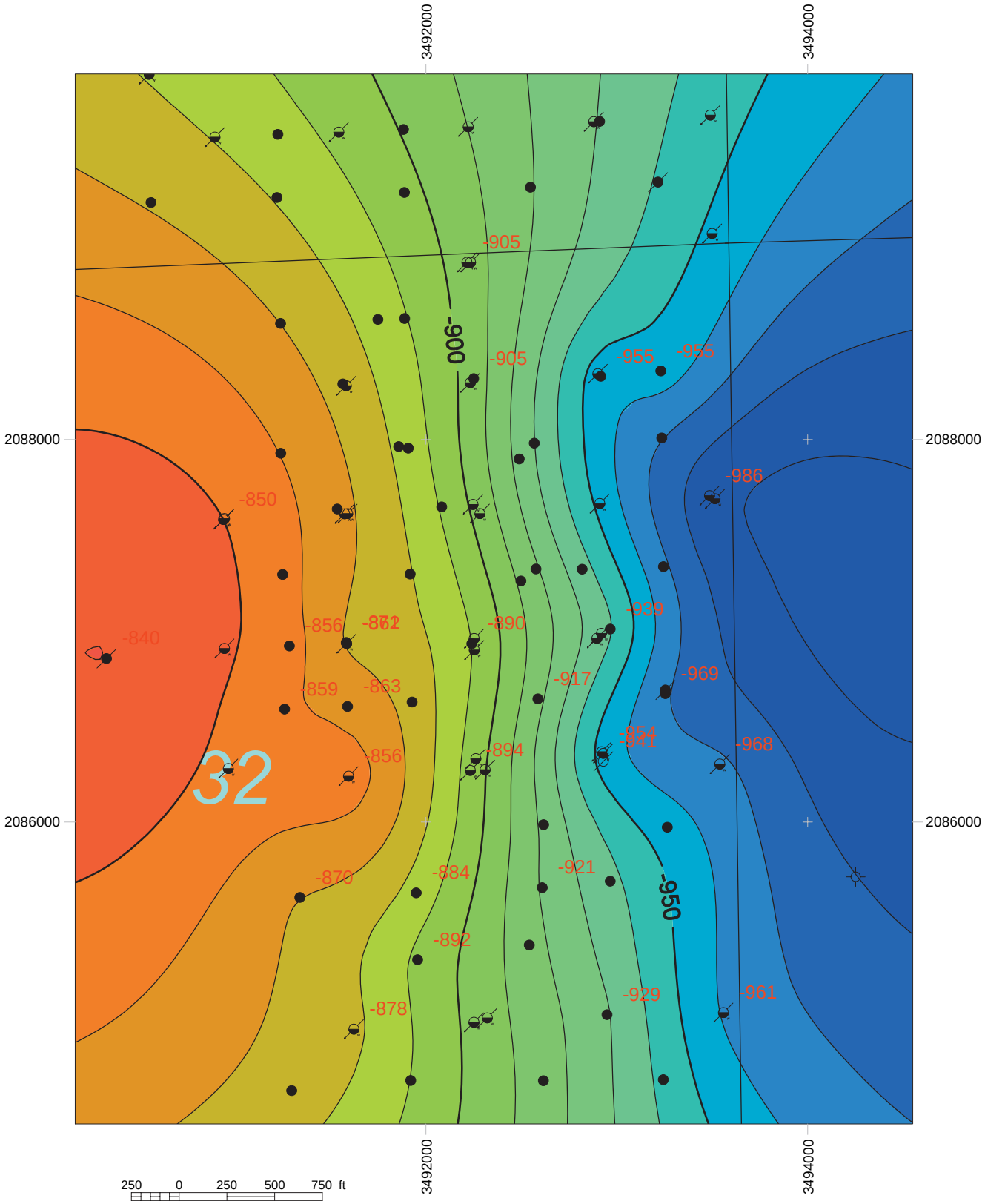

Figure 2-13 *Depth structure map on top of Cypress Sandstone, Griggs study, Lawrence Field. Datum = MSL; contour interval = 10 ft.*

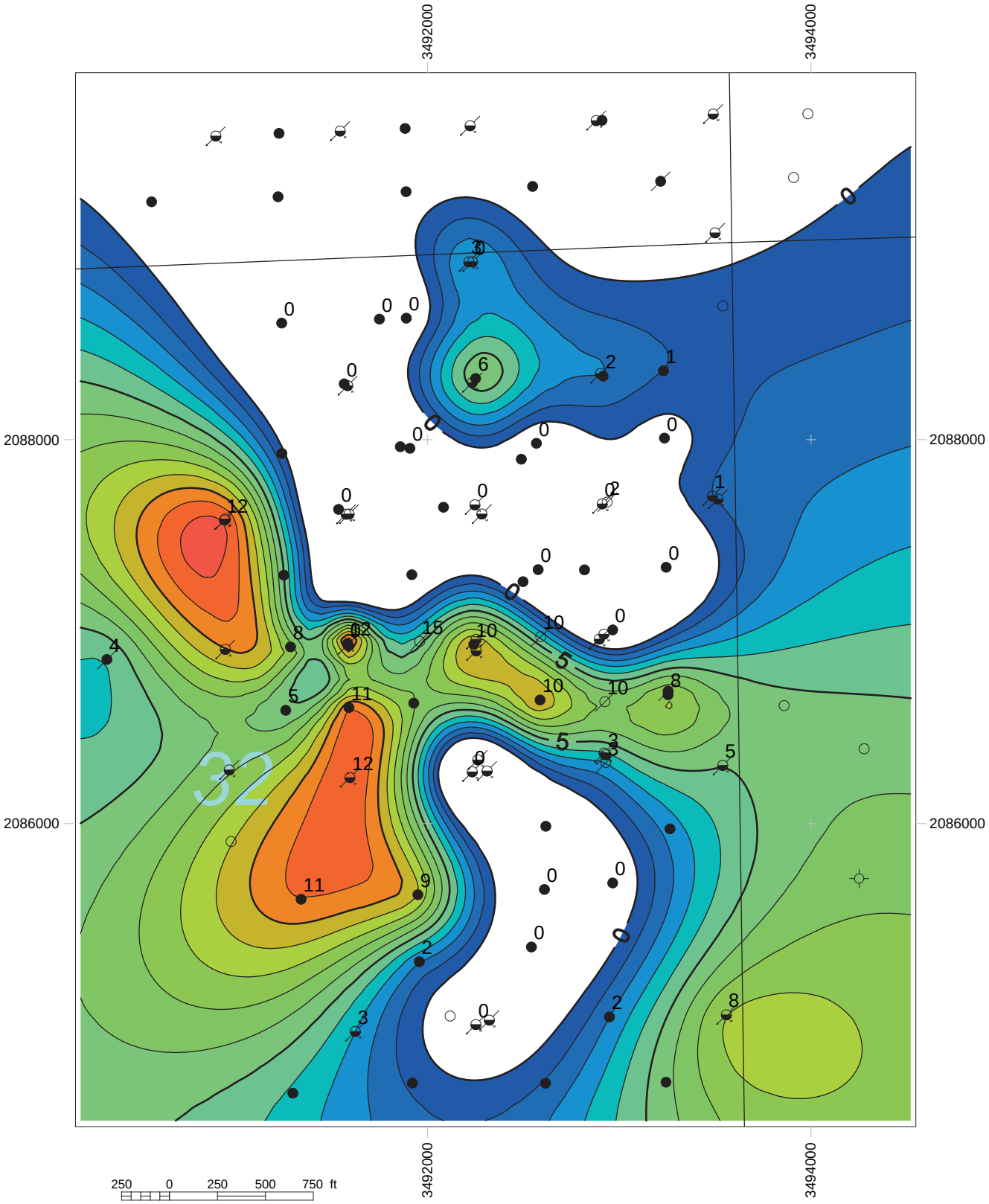

Figure 2-14 *Net sand isopach, Cypress Zone E, Griggs study, Lawrence Field. Contour interval = 1 ft.*

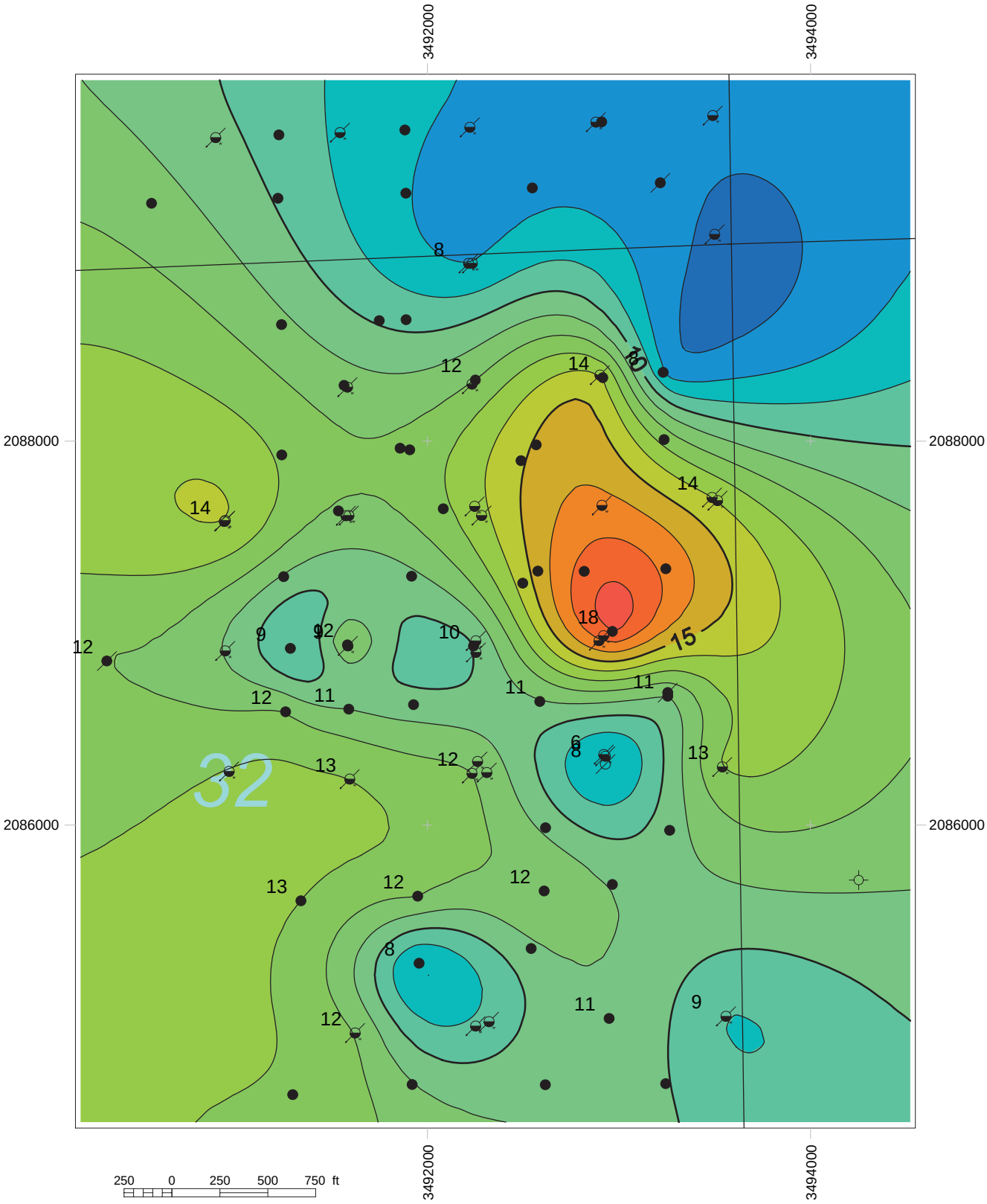

Figure 2-15 *Gross sand isopach, Cypress Zone E, Griggs study, Lawrence Field. Contour interval = 1 ft.*

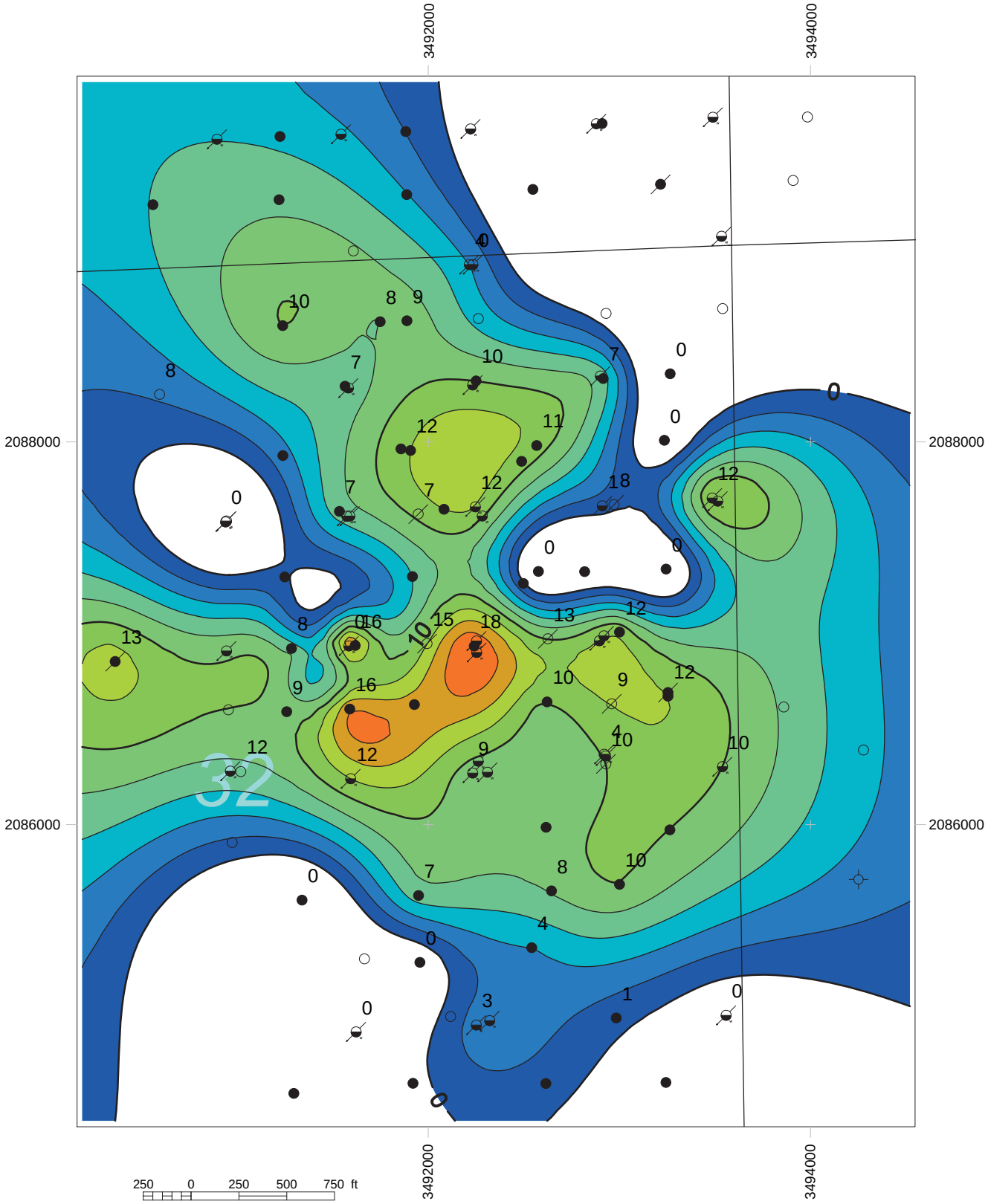

Figure 2-16 *Net sand isopach, Cypress Zone D, Griggs study, Lawrence Field. Contour interval = 2 ft.*

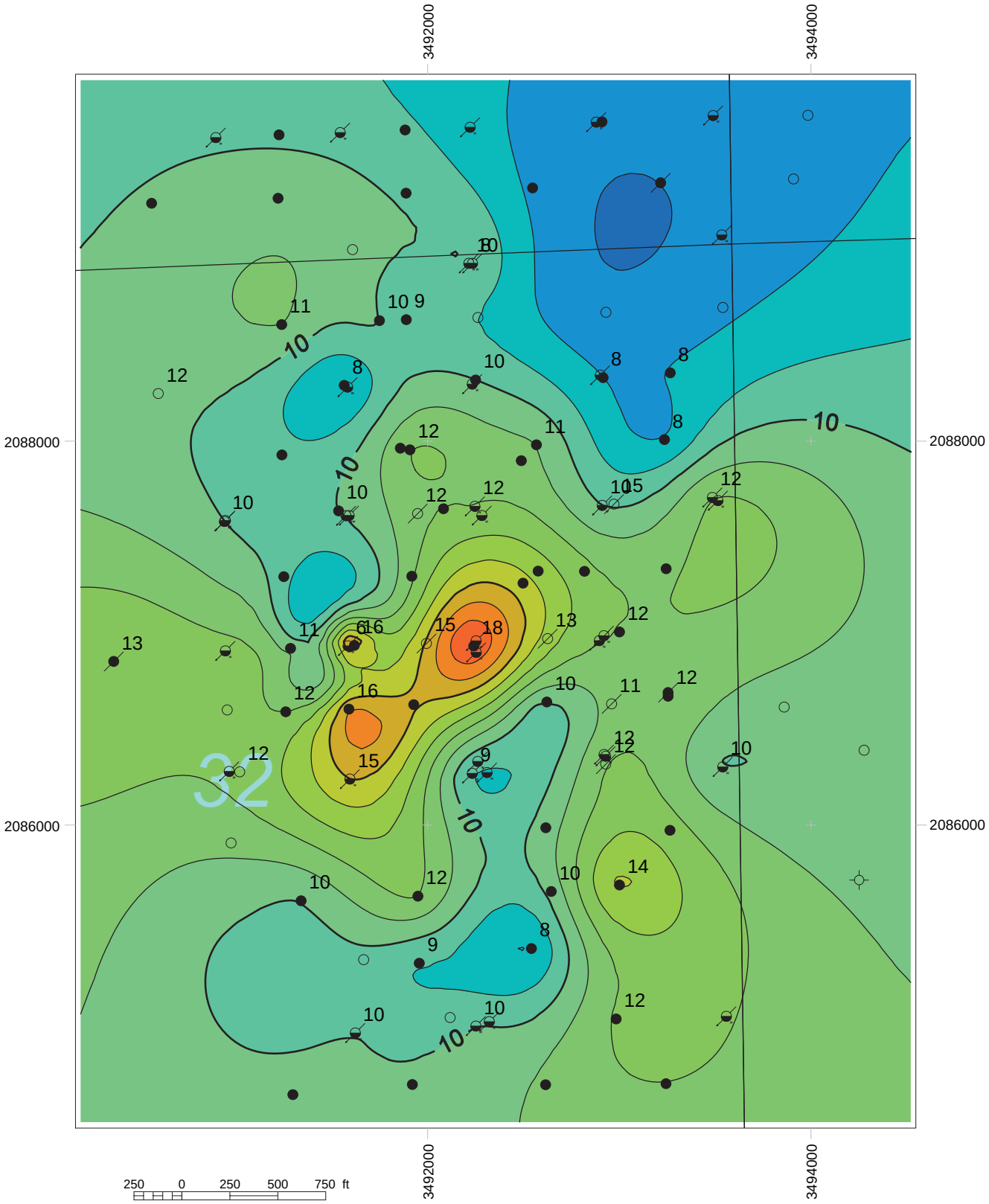

Figure 2-17 *Gross sand isopach, Cypress Zone D, Griggs study, Lawrence Field. Contour interval = 1 ft.*

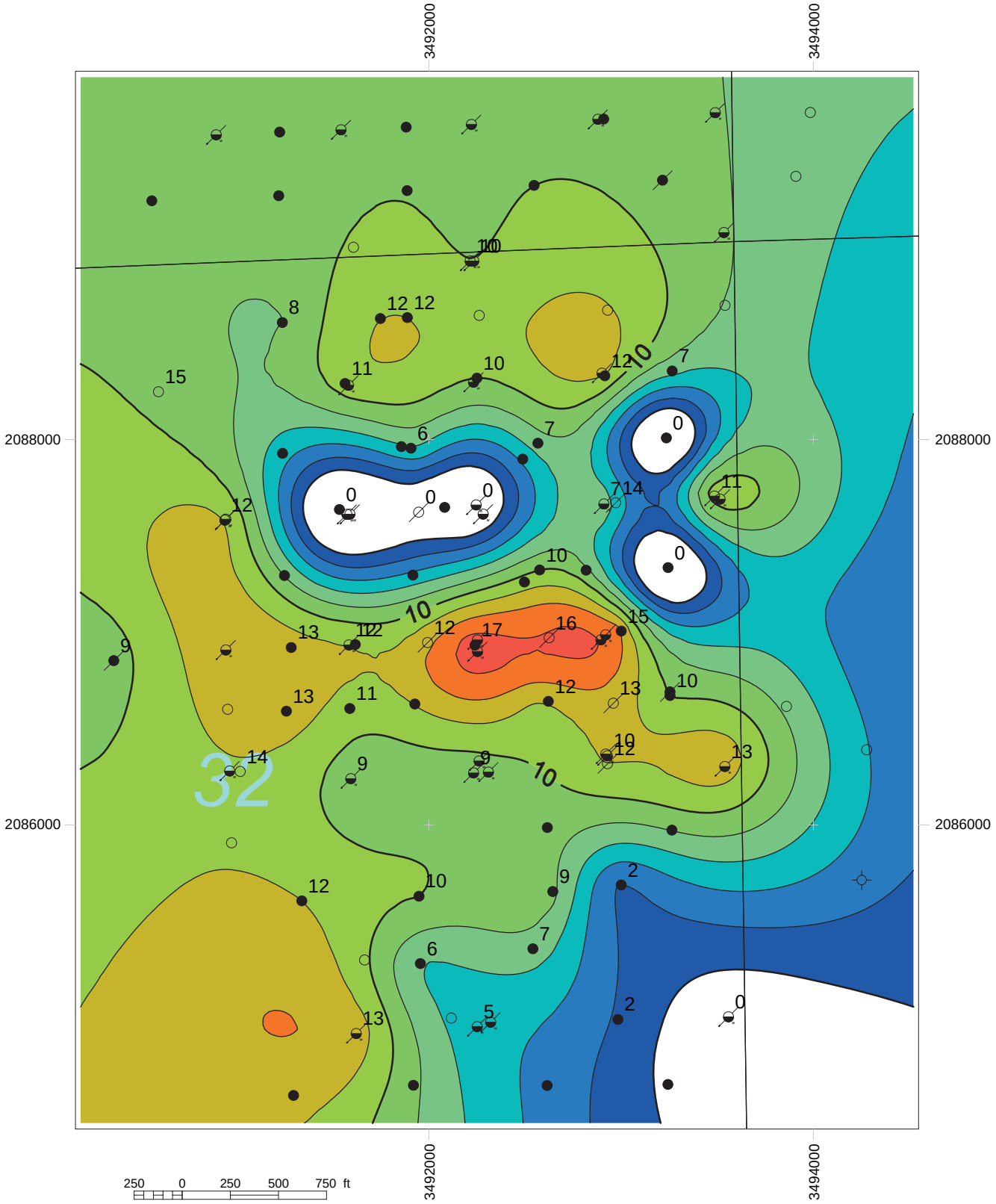

Figure 2-18 *Net sand isopach, Cypress Zone C, Griggs study, Lawrence Field. Contour interval = 1 ft.*

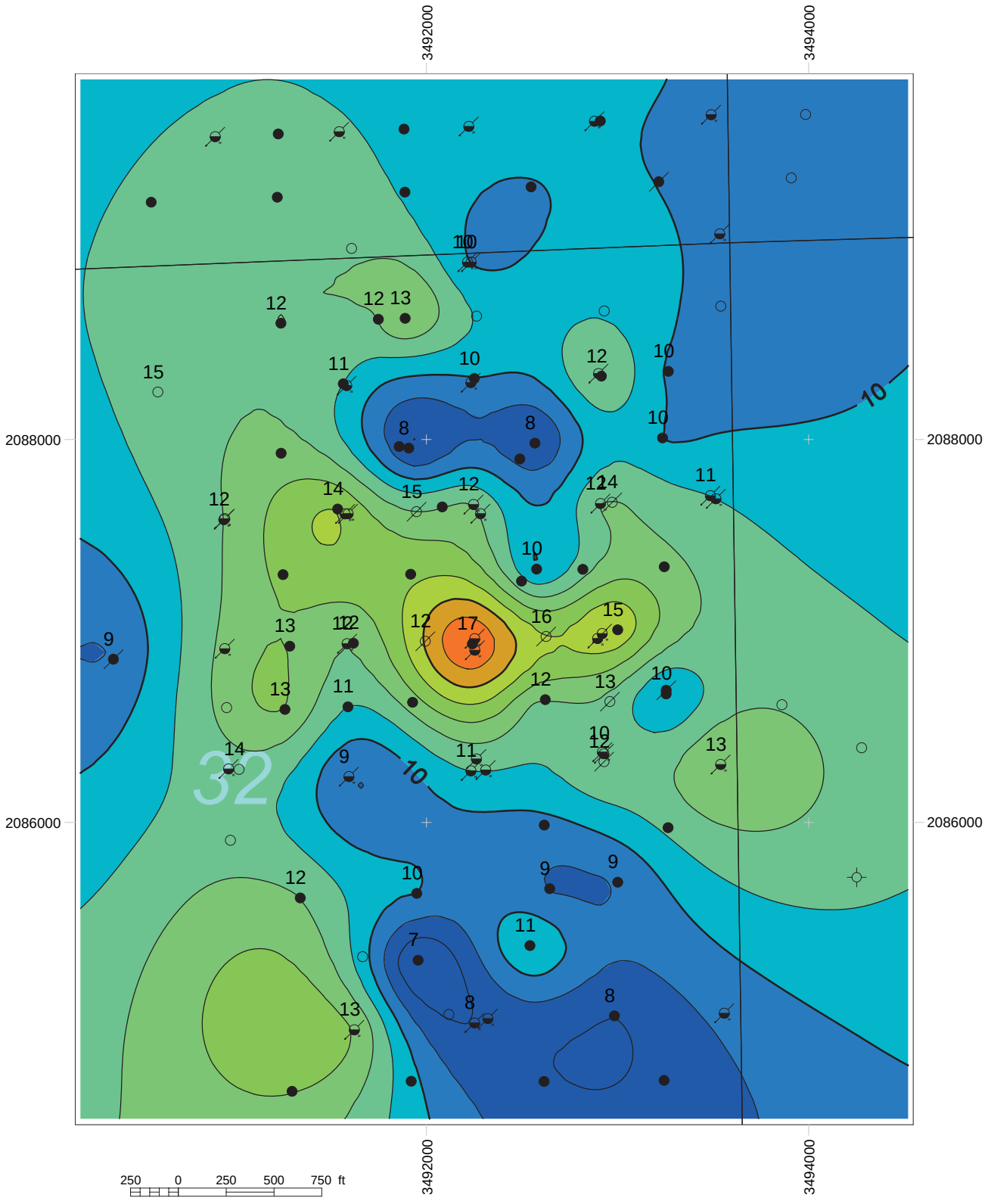

Figure 2-19 *Gross sand isopach, Cypress Zone C, Griggs study, Lawrence Field. Contour interval = 1 ft.*

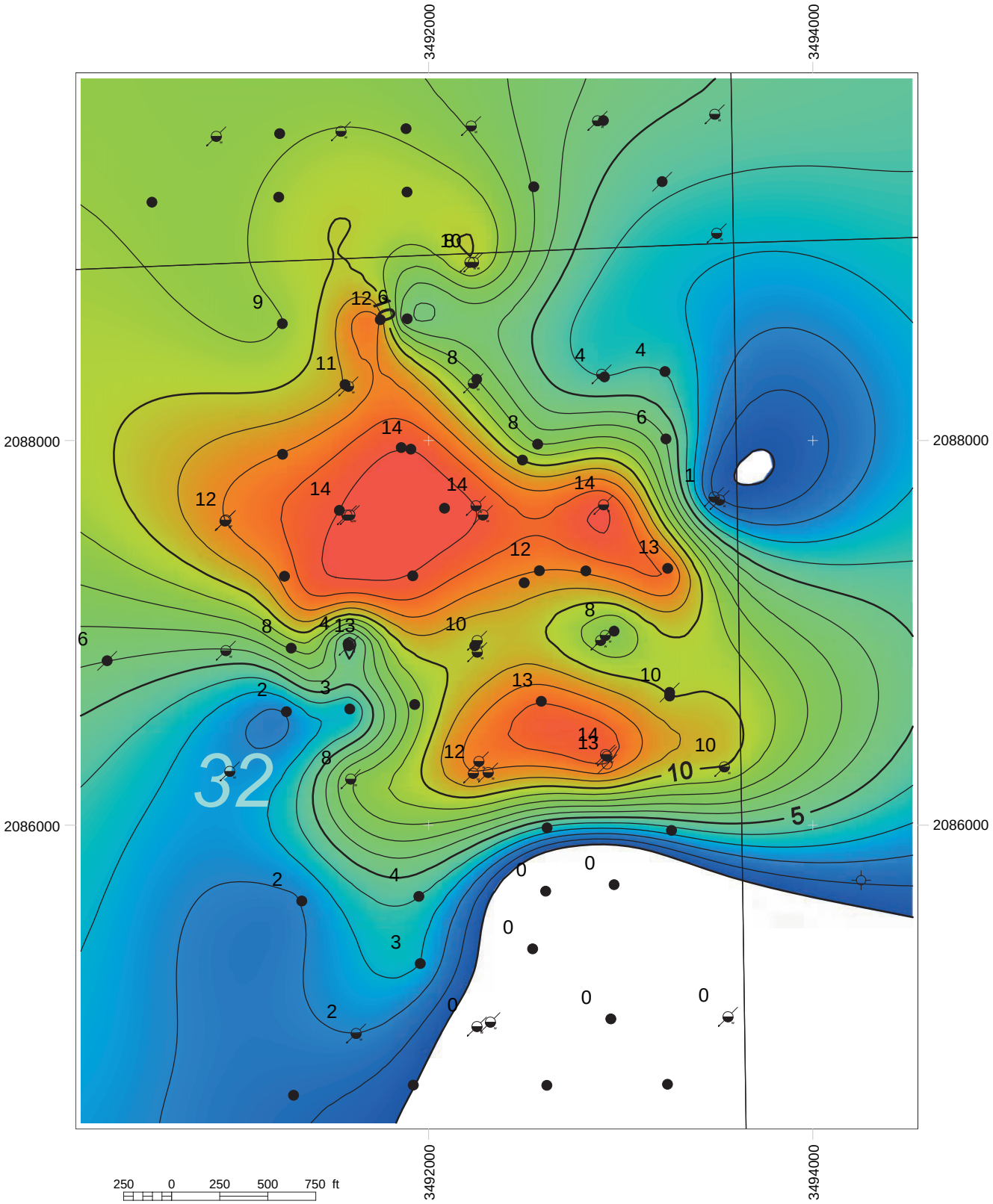

Figure 2-20 *Net sand isopach, Cypress Zone B, Griggs study, Lawrence Field. Contour interval = 1 ft.*

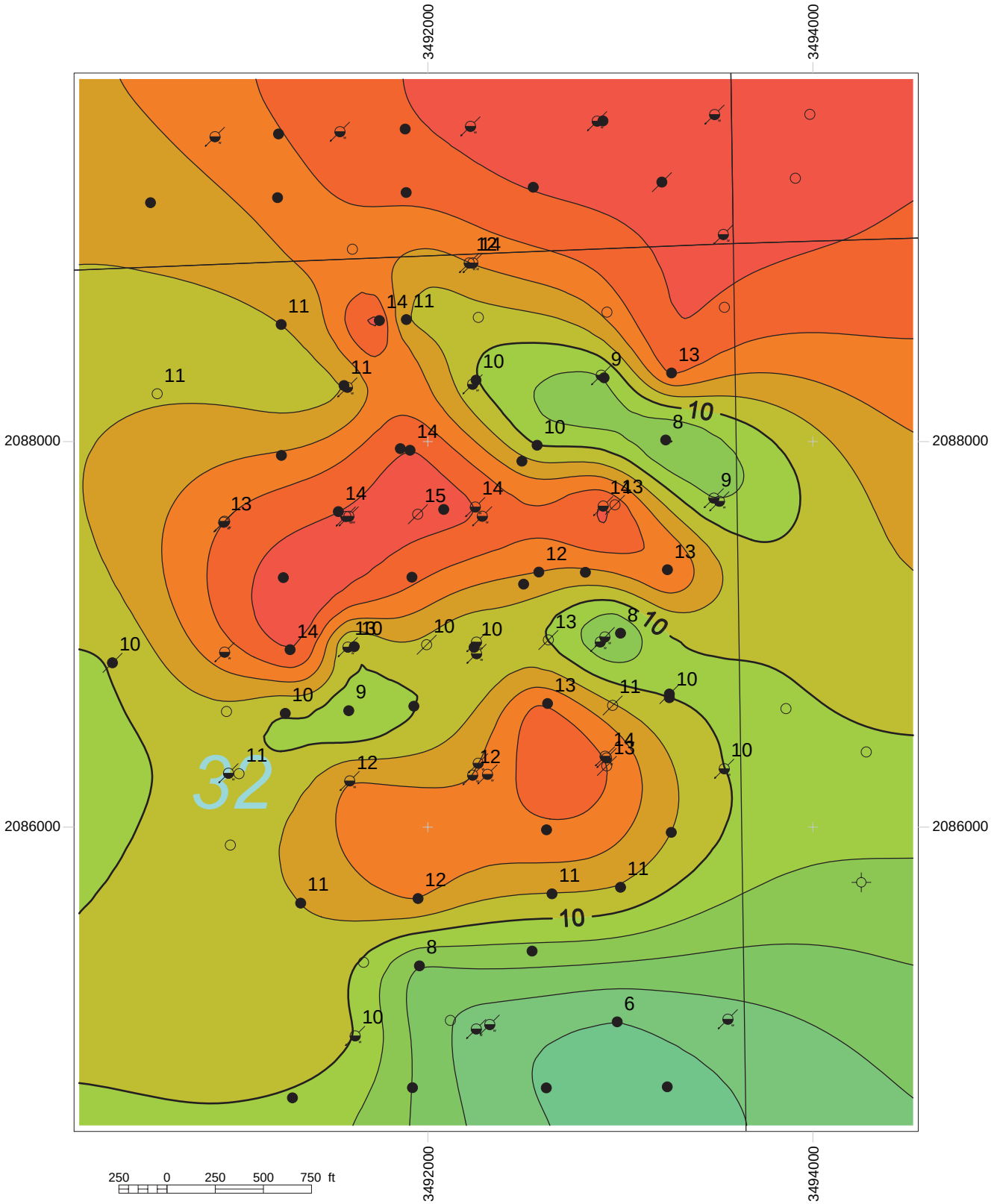

Figure 2-21 *Gross sand isopach, Cypress Zone B, Griggs study, Lawrence Field. Contour interval = 1 ft.*

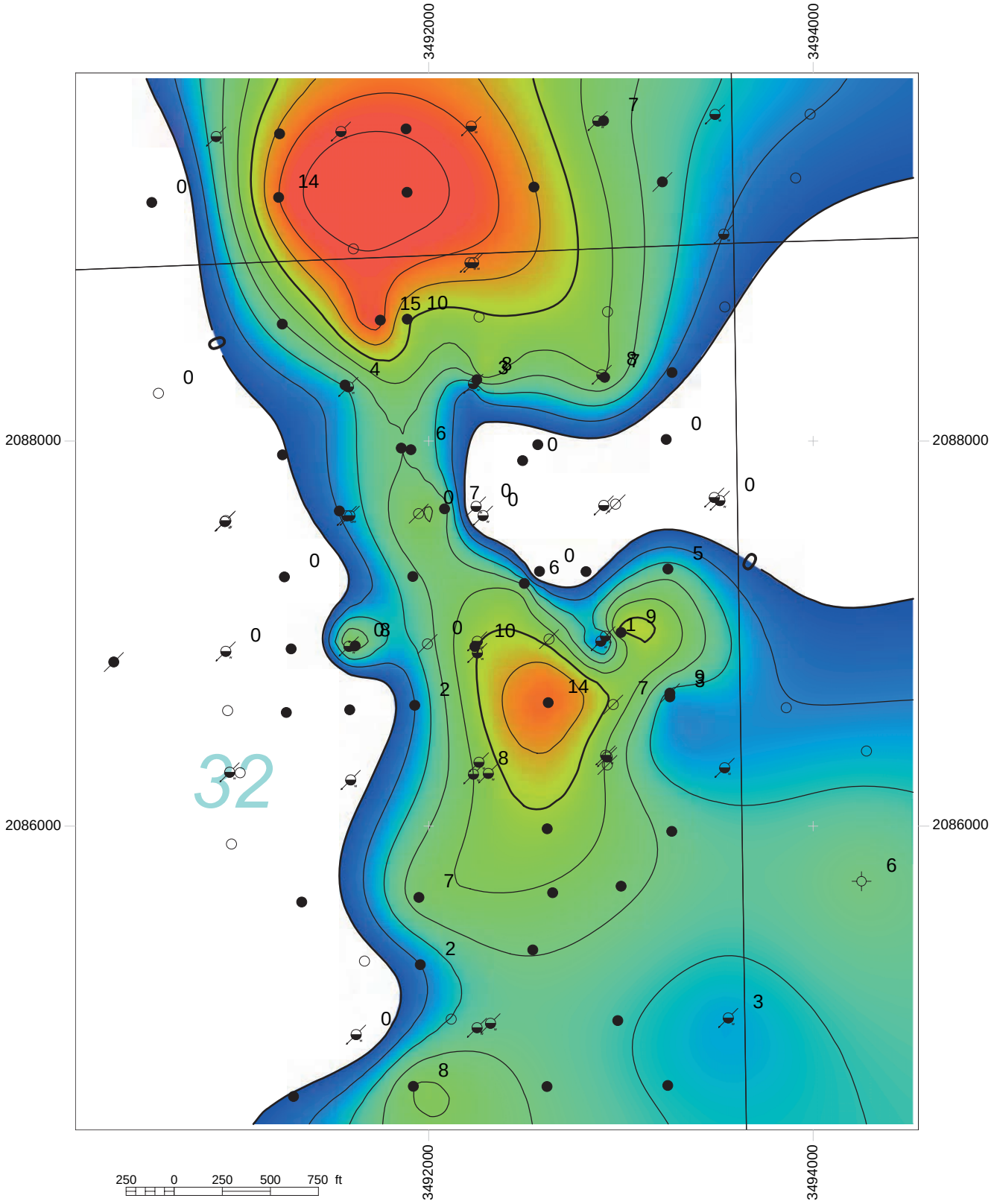

Figure 2-22 *Net sand isopach, Cypress Zone A, Griggs study, Lawrence Field. Contour interval = 1 ft.*

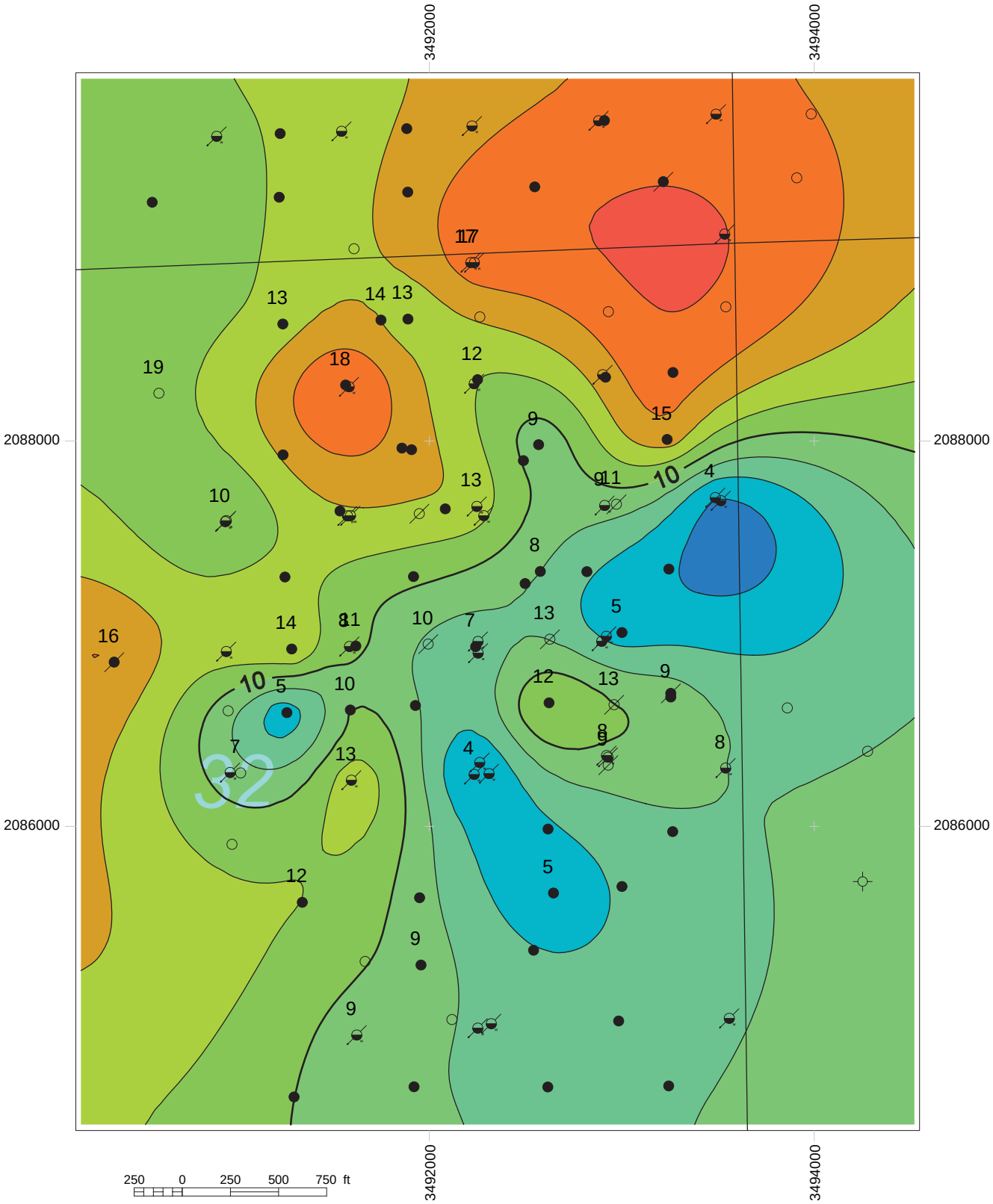

Figure 2-23 *Gross sand isopach, Cypress Zone A, Griggs study, Lawrence Field. Contour interval = 2 ft.*

Geostatistical Model

For the Griggs unit, a three-dimensional geostatistical porosity model was built using collocated co-simulation, which was conditioned by the geological model of thickness within the various flow zones. Thickness trends also provided constraints on the model where there were insufficient data to build the conceptual model. Variograms based on a spherical model were constructed with the trends observed in the thickness data. The simulation was repeated for 70 to 100 realizations and then post-processed to determine the most likely representation of the study area (Figure 2-24).

The most likely realization of the porosity model was used to construct a permeability model that followed a collocated co-simulation approach. A variogram (spatial variance vs. distance) of the simulated porosity model based on a spherical curve-fit model was used to produce 100 realizations of the permeability model within the study area. Statistical post-processing was used to determine the most probable representation within the study site (Figure 2-25).

Sailor Springs Field Geologic Model of Cypress Sandstone Reservoir

Deterministic Model

The Sailor Springs study covers approximately 3,075,623 m^2 (760 acres (3.1 km^2 (1.2 mi^2))) in Clay County, Illinois, a part of Sailor Springs Consolidated Field. The study area lies in and adjacent to a pair of waterflood units in Section 15, T5N, R7E. Production in the study area comes mainly from the Chesterian Cypress Sandstone; smaller amounts come from the Valmeyeran Aux Vases Sandstone and Ste. Genevieve Limestone.

Eighty-seven wells penetrate the Cypress in the area, of which 14 are cored through some part of the formation. Core analysis, including porosity and horizontal permeability, are available for 151 core samples taken throughout the cores; porosity is available only for an additional 24 samples. Core and log analyses indicate that in the study area the Cypress Sandstone comprises thin, fine-grained sandstones with interbedded shale units. Three persistent sandstone units were identified, of which the lowermost is not productive. The two upper units (Zones 1 and 2) are relatively thin compared with the massive lower layer; maximum thicknesses in the study area were 9.1 m (30 ft) (Zone 1) and 7.9 m (26 ft) (Zone 2) compared with a thickness of 37.5 m (123 ft) for Zone 3, which is typically 100% water saturated in this portion of the Illinois Basin. The three zones are hydraulically isolated, with intervening shale layers averaging 9.1 m (30 ft) in thickness (Figures 2-26, 2-27, and 2-28).

Table 2-7. Reservoir properties for each study.

Reservoir	Average porosity (%)	Average permeability (md)	High permeability (md)	Average thickness (ft)	Reservoir	Average porosity (%)	Average permeability (md)	High permeability (md)	Average thickness (ft)
Small Griggs[1]					**Zeigler**				
Zone 1, layer 1	12.89	34.32	476.31	7	Zone 1	19.91	141.52	641.54	0.94
Zone 1, layer 2	19.45	83.4	484.48	15	Zone 2	19.38	191.97	660.7	1.41
Zone 2, layer 1	17.62	70.51	484	14	NX = 33 (330 ft), NY = 27 (330 ft), NZ = 50 (1 ft)				
Zone 2, layer 2	17.97	75.07	484.48	11	Total area = 10,890 ft × 8,910 ft × 50 ft = 2,227.50 acres (surface)				
NX = 120 (10 ft), NY = 110 (10 ft), NZ = 60 (1 ft)									
Total area = 1,200 ft × 1,100 ft × 60 ft = 30.30 acres (surface)									
Large Griggs[1]					**Iola**				
Zone A-5	12.13	31.65	139.15	17	Brown	13.38	19.19	1,016.46	10.21
Zone B-4	19.61	63.41	270.99	11	Green	18.16	12.48	276.63	15
Zone C-3	19.31	106.35	404	14	NX = 64 (115 ft), NY = 70 (115 ft), NZ = 38 (2 ft)				
Zone D-2	18.21	31.50	171.25	15	Total area = 7,360 ft × 8,050 ft × 76 ft = 1,360.15 acres (surface)				
Zone E-1	13.97	11.37	95.46	7					
NX = 63 (69.7 ft), NY = 79 (69.7 ft), NZ = 60 (1 ft)									
Total area = 4,391.1 ft × 5,506.3 ft × 60 ft = 555.07 acres (surface)									
Sailor Springs					**Olney**				
Zone 1, layer 1	17.01	74.11	432	15.37	Zone 1	10.78	74.35	492.65	9.8
Zone 1, layer 2	17.61	71.12	430	15.37	Zone 2	9.1	13.25	404.92	5.1
Zone 2, layer 1	17.76	60.16	482	14.89	NX = 52 (167.29 ft), NY = 71 (168.71 ft), NZ = 109 (1 ft)				
Zone 2, layer 2	17.92	52.50	432.43	14.76	Total area = 8,699.08 ft × 11, 978.41 ft × 109 ft = 2,392.13 acres (surface)				
NX = 67 (98.69 ft), NY = 54 (97.98 ft), NZ = 86 (1 ft)									
Total area = 6,612.23 ft × 5,290.92 ft × 86 ft = 803.14 acres (surface)									
Wakefield					**Johnsonville**				
SB1	18.17	89.85	595.7	9.21	Zone 1	15.15	487.30	3,600	8.37
SB2	17.37	133.25	595	6.24	Zone 2	15.25	527.68	3,603	8.31
UC Zone 1	15.36	166.01	596.29	13.49	NX = 65 (115 ft), NY = 70 (115 ft), NZ = 140 (1 ft)				
UC Zone 2	15.15	122.38	595.7	12.89	Total area = 7,475 ft × 8,050 ft × 140 ft = 1,381.40 acres (surface)				
NX = 28 (400 ft), NY = 28 (400 ft), NZ = 68 (1 ft)									
Total area = 11,200 ft × 11,200 ft × 68 ft = 2,879.71 acres (surface)									
Mill Shoals[2]					**Dale**				
Zone 1, layer 1	10.45	25.4	278.99	19.79	Zone 1, layer 1	12.34	59.38	1,100.4	4.69
Zone 1, layer 2	10.04	23.10	282.164	19.80	Zone 1, layer 2	13.16	42.67	685.7	4.68
Zone 2, layer 1	17.33	29.96	330	13.08	Zone 2, layer 1	15.49	146.27	1,282.92	5.92
Zone 2, layer 2	12.07	18.39	330.19	12.60	Zone 2, layer 2	15.32	135.62	1,391.44	5.92
NX = 52 (86.15 ft), NY = 70 (86.21 ft), NZ = 65 (1 ft)					NX = 42 (50 ft), NY = 45 (50 ft), NZ = 65 (1 ft)				
Total area = 4,479.8 ft × 6,034.7 ft × 65 ft = 620.62 acres (surface)					Total area = 2,100 ft × 2,250 ft × 65 ft = 108.47 acres (surface)				

[1] Thickness measurements for Small Griggs and Large Griggs are constant thickness rather than average thickness.
[2] Mill Shoals reservoir properties shown here are from core measurements, which include all facies of the Aux Vases.

Both of the two oil productive zones (1 and 2) demonstrate porosity of 19 to 22% and permeability of 0.197 to 0.296 μm^2 (200 to 300 md). A maximum of 0.426 μm^2 (432 md) was observed in one core sample. Shale layers have porosity of approximately 9 to 10%, and most have horizontal permeability of less than 2.96×10^{-3} μm^2 (3 md). Occasional thin sand stringers raise permeability in the shale interval

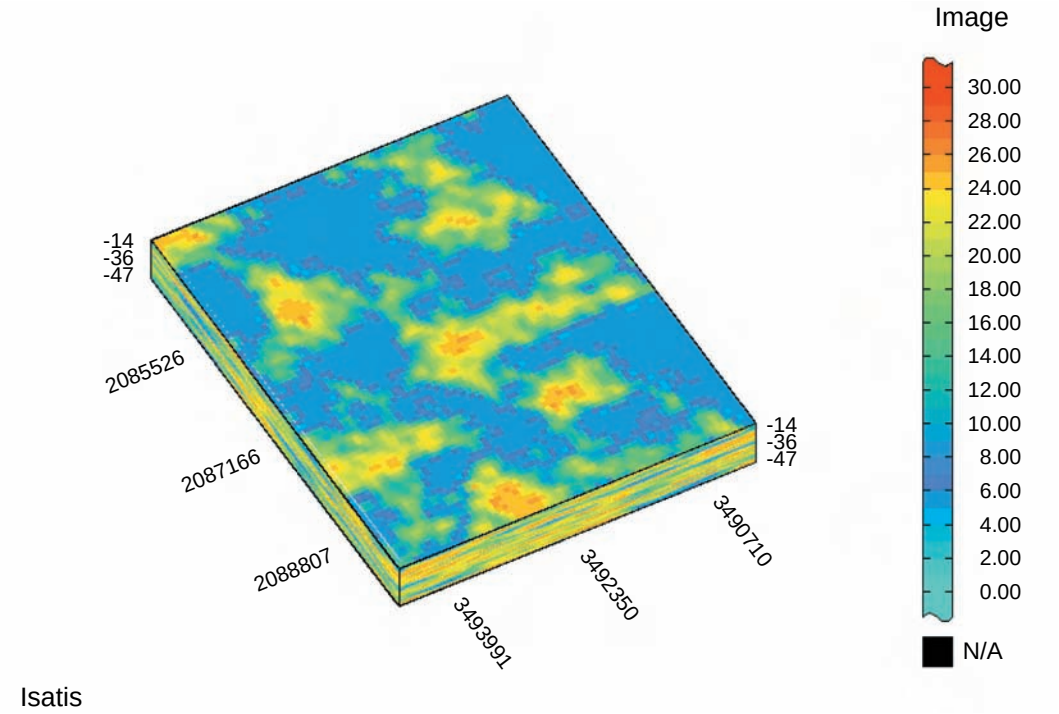

Figure 2-24 *Three-dimensional visualization of the Griggs lease study area. This core-derived porosity model was produced using turning bands simulation. The display shown is the "most likely" realization of a set of 30 simulations. The anisotropic variogram used in the scenario was a nested nugget and spherical combination.*

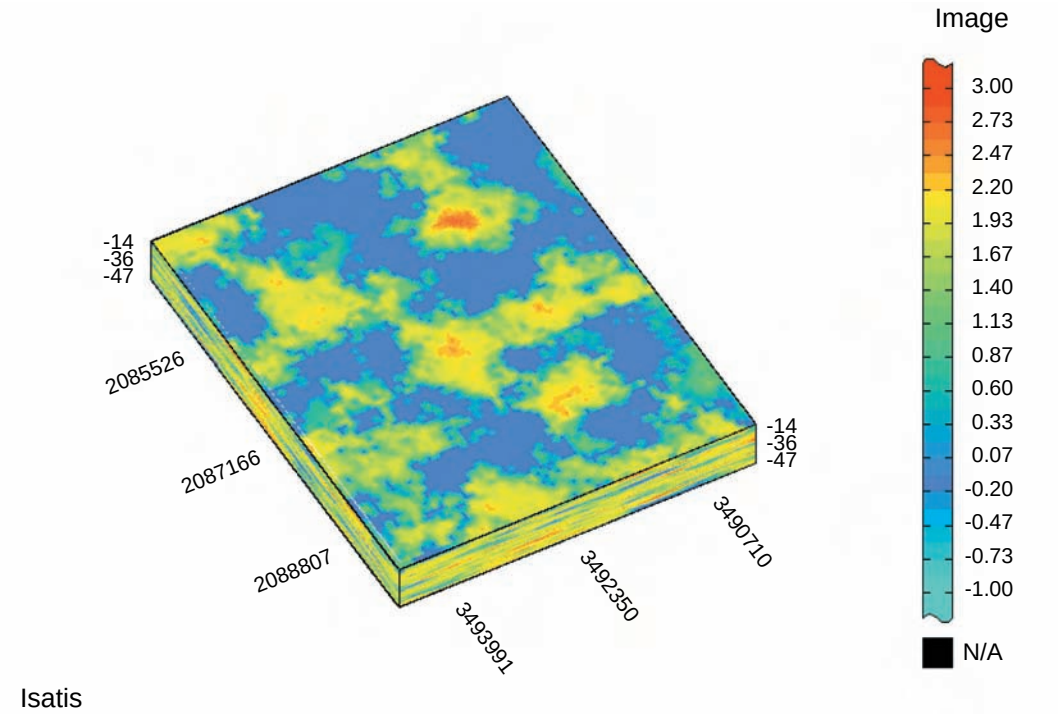

Figure 2-25 *Three-dimensional visualization for the Griggs lease study area. This log_{10} core-derived horizontal permeability model was produced using collocated co-simulation employing the Markov-Bayes assumption. The display shown is the "most likely" realization of a set of 30 simulations. The variogram used in the scenario was similar to the variogram used in the porosity model.*

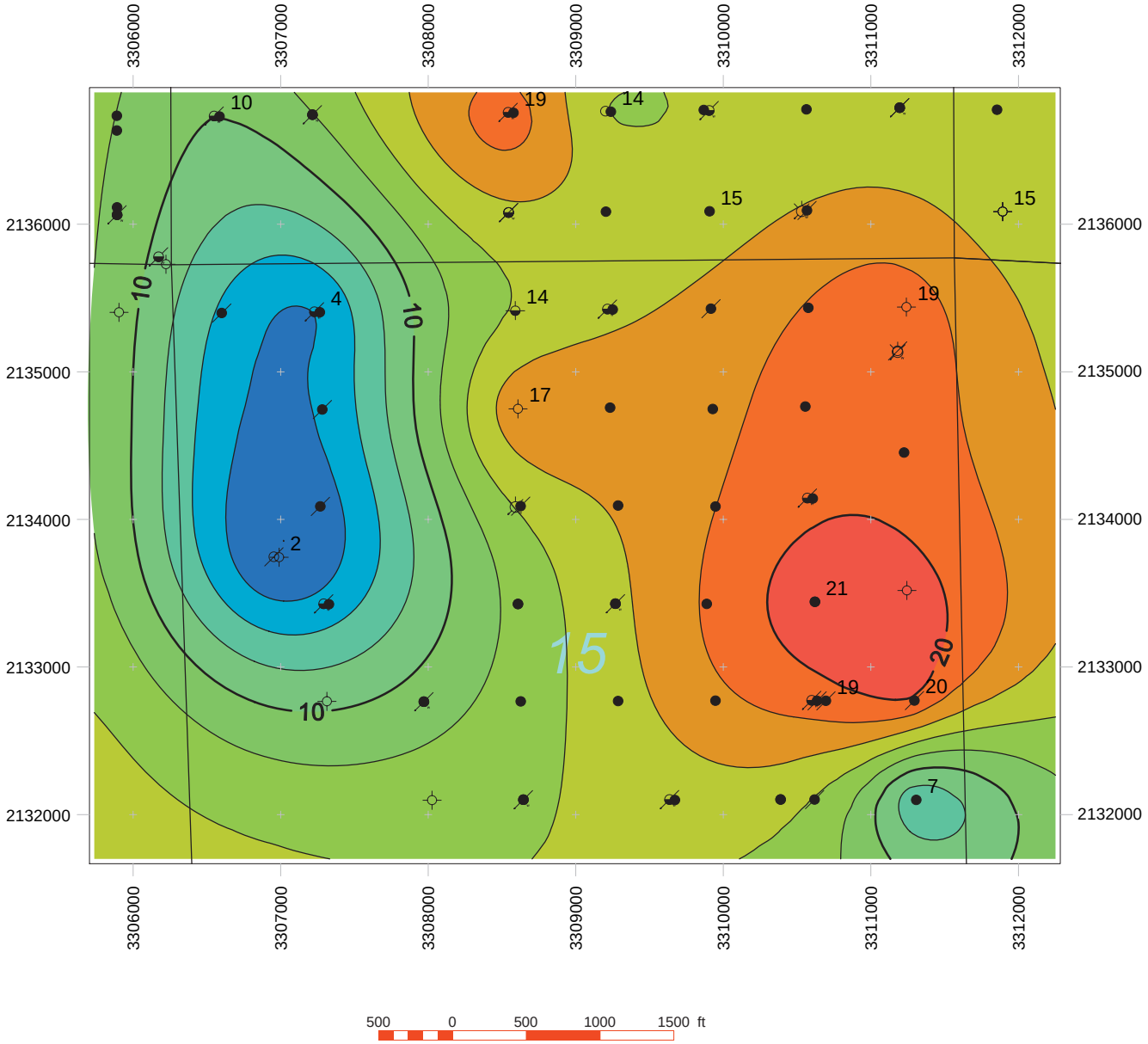

Figure 2-26 *Gross isopach map, Cypress Sandstone Zone 2, Sailor Springs study of Clay City Consolidated Field. Contour interval = 2 ft.*

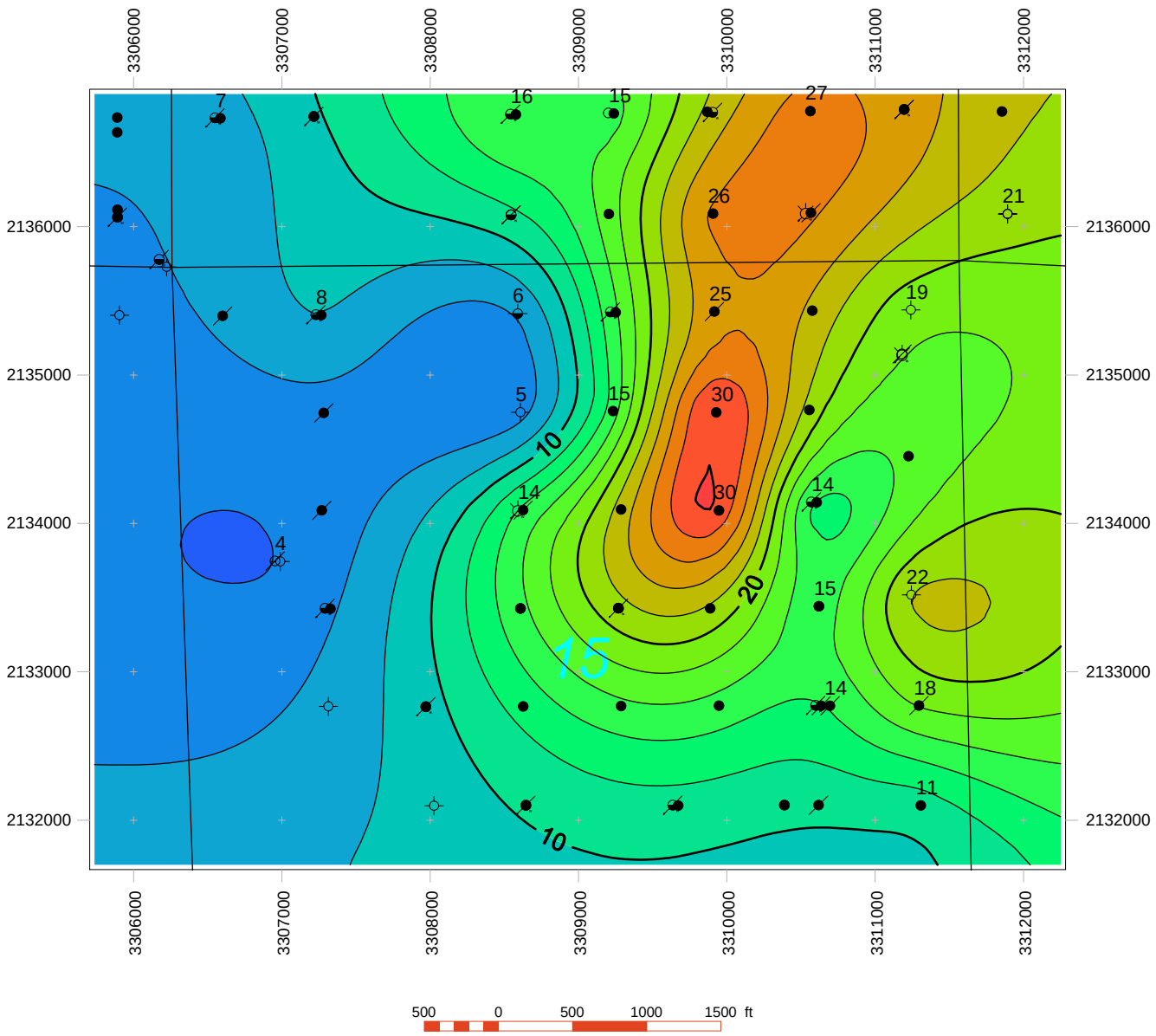

Figure 2-27 *Gross isopach map, Cypress Sandstone Zone 1, Sailor Springs study of Clay City Consolidated Field. Contour interval = 2 ft.*

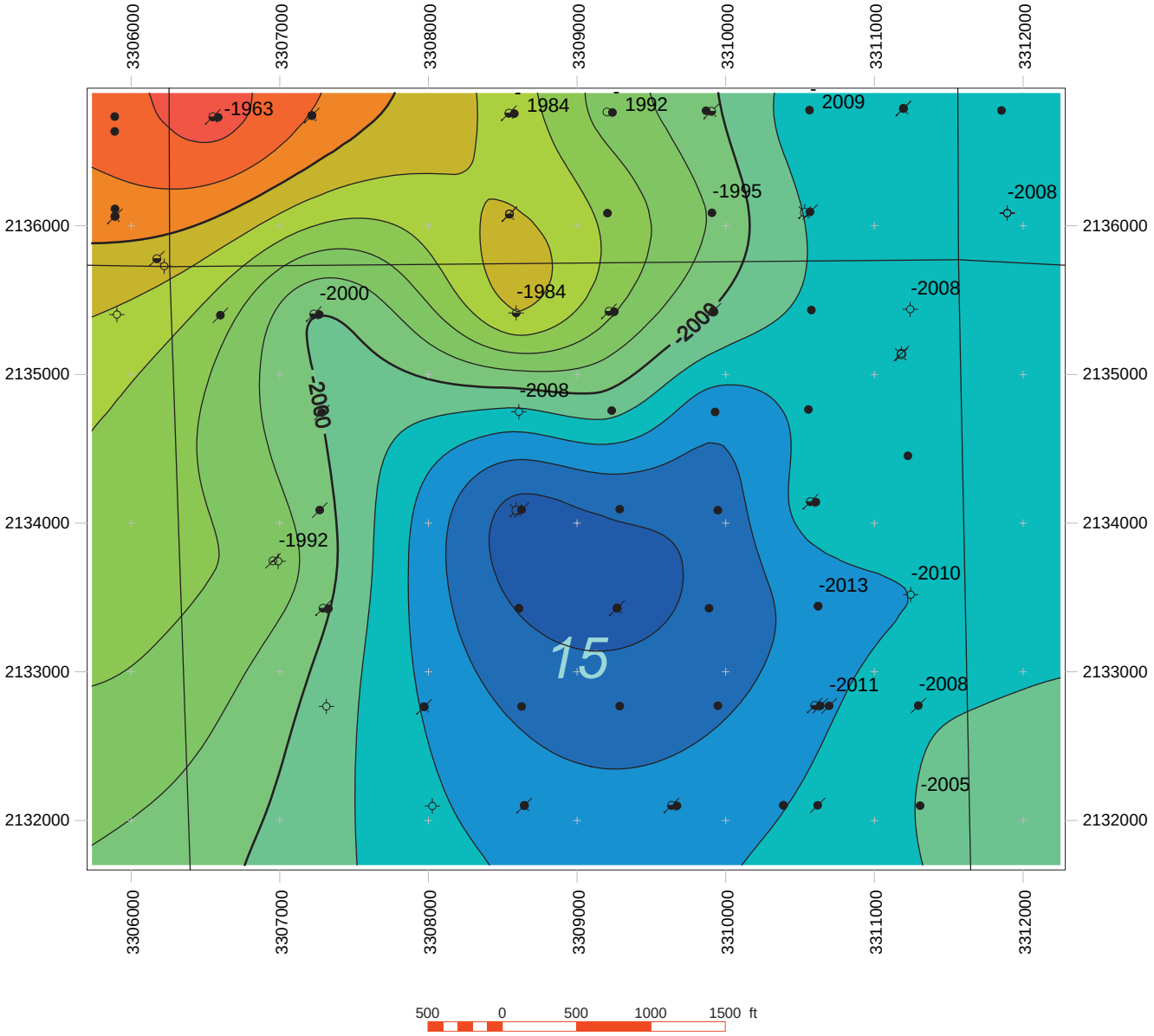

Figure 2-28 *Depth structure map on the top Cypress Sandstone Zone 2, Sailor Springs study of Clay City Field. Datum = MSL; contour interval = 5 ft.*

to the order of 9.86×10^{-3} μm^2 (10 md), but these sand bodies can rarely be correlated between adjacent wells (Figures 2-26, 2-27, and 2-28).

Sailor Springs

Geostatistical Model

Three-dimensional geostatistical models of both porosity and permeability were built in the Sailor Springs study. Porosity was modeled using the turning bands method for stochastic simulation. This approach employs the core data in conjunction with histograms and variograms derived from that data to interpolate values at sites where core data were not available. An isotropic spherical variogram was used at Sailor Springs to capture the spatial horizontal and vertical continuity of the data. Thirty distinct realizations of the resulting porosity model were produced, all of which honored both the core data and the variogram calculated from that data. These realizations were post-processed to determine the most statistically probable simulation and compared with known data as a final check (Figure 2-29).

A horizontal permeability model was produced using a collocated co-simulation approach with the "most likely" three-dimensional porosity model. Although permeability data were scarce and scattered relative to porosity data, the correlation between porosity and permeability was deemed sufficient to allow use of the porosity model to condition permeability, particularly in those locations lacking permeability data. A variogram derived from the porosity model was used to inform the less populated horizontal permeability data set. The variogram used for permeability simulations was an anisotropic spherical model. This simulation effort also yielded 30 realizations, which were statistically post-processed to determine which realization was the most probable to represent the geologic trends within the site (Figure 2-30) based on ISGS staff experience.

Clay City Consolidated Wakefield Unit
Geologic Model of Cypress Sandstone Reservoir

Deterministic Model

The Wakefield study is centered on the Wakefield unit, covering slightly more than four sections (10,590,667 m^2 (2,617 acres)) within the portion of Clay City Consolidated Field lying in Richland County, Illinois. The most important productive intervals in the immediate area of the study include the Tar Springs, Cypress, and Aux Vases Sandstones and the Ste. Genevieve and Salem Limestones. The Clay City model concentrated on the upper portion of the Cypress Sandstone, which in the study area represents shallow marine deposition. Two discontinuous "stringer" sandstones and an underlying thicker reservoir interval that covers the entire area were identified from log signatures and core data. The stringers lie within a mixed sand-shale interval some 9.1 to 12 m (30 to 40 ft) thick below the Barlow Lime and above the more continuous interval, here called upper Cypress. Isopach maps of the

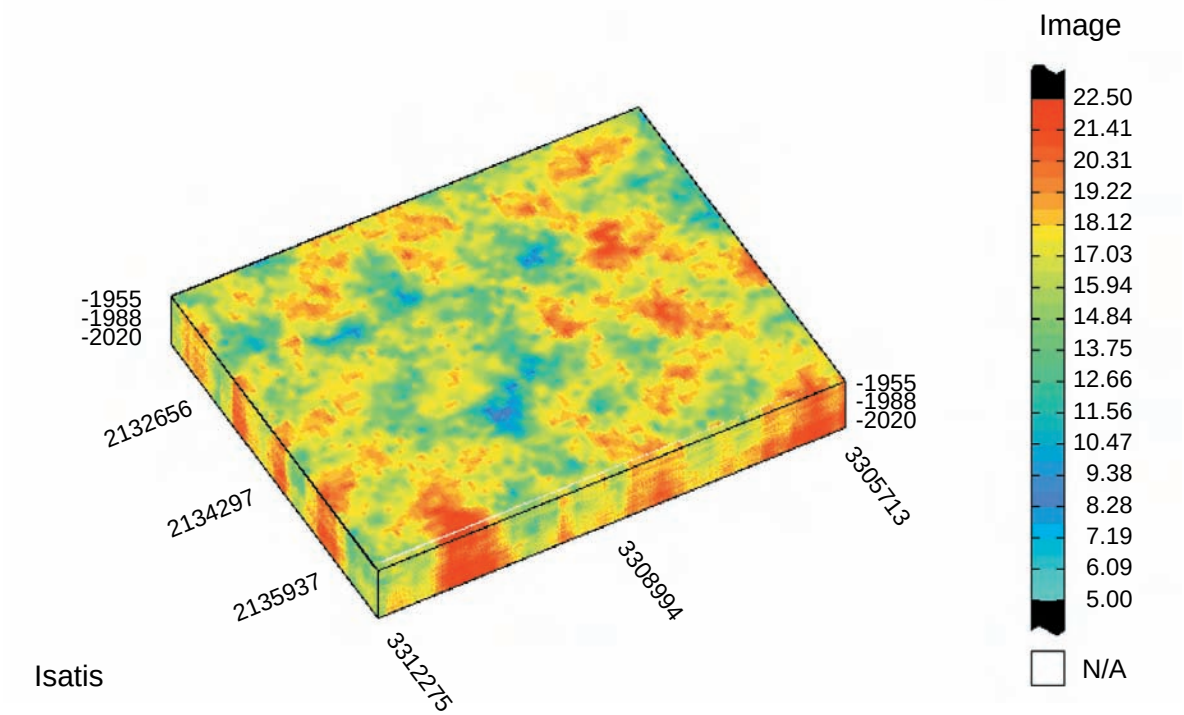

Figure 2-29 *Three-dimensional visualization of the Sailor Springs Field study area. This core-derived porosity model was produced using turning bands simulation. The display shown is the "most likely" realization of a set of 30 simulations. The anisotropic variogram used in the scenario was a nested nugget and spherical combination.*

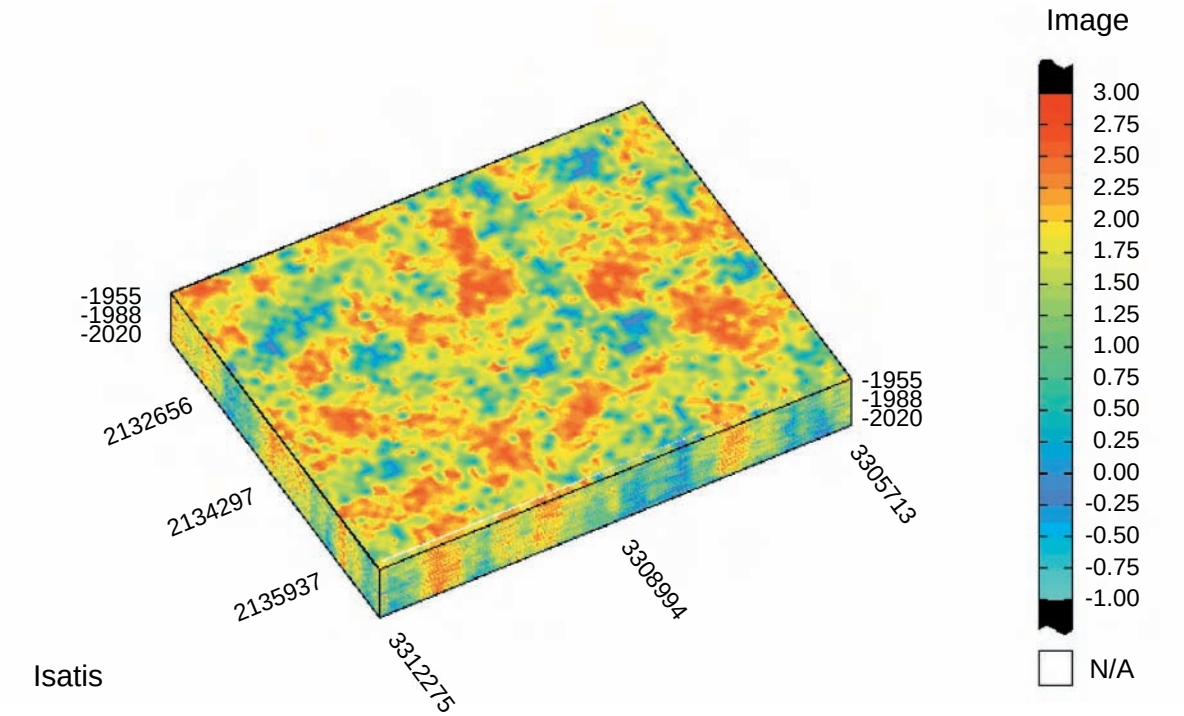

Figure 2-30 *Three-dimensional visualization for the Sailor Springs Field study area. This $\log_{10}$ core-derived horizontal permeability model was produced using collocated co-simulation employing the Markov-Bayes assumption. The display shown is the "most likely" realization of a set of 30 simulations. The variogram used in the scenario was similar to the variogram used in the porosity model.*

two stringer sands display a persistent thin that lies east and south of the crest of the structure; the same thin may be present but is less clear-cut in the upper Cypress. The upper stringer is present over most of the area, and the lower stringer covers about 50% of the study area.

The three sand bodies are hydraulically isolated by shale bodies. Thicknesses of the three units reach 5.5 m (18 ft) in the upper stringer, 3.7 m (12 ft) in the middle stringer, and 16.5 m (54 ft) in the upper Cypress. All three intervals have been perforated within the study area, with a maximum initial production value near 111 m^3/day (700 stb/day) coming from the upper stringer, although 13 to 19 m^3/day (80 to 120 stb/day) initial production is more common.

Nineteen wells in the study area were cored. Laboratory studies yielded >300 porosity and horizontal permeability measurements and 30 vertical permeability measurements. With the exception of one well, core permeability in the reservoir intervals are ≥0.0987 μm^2 (≥100 md); a maximum is about 0.789 μm^2 (800 md). Porosity in the reservoir interval ranges from 16 to 21%. Permeability measured in one well (the Storer 1) is suspect as values are from 10 to 100 times those measured in all other wells, although porosity remains unchanged. Non-reservoir intervals have permeability values <0.0197 μm^2 (<20 md) and porosity of ≤14%. Vertical permeabilities measured in the Correll 1-B and Secrest 1-B wells were the same order of magnitude as horizontal permeability in all but two samples (Figures 2-31 to 2-35).

Geostatistical Model

A three-dimensional geostatistical porosity model of the Wakefield unit was constructed using collocated co-simulation, which was conditioned by the deterministically modeled thicknesses of the individual flow zones. Choice of this approach was based on the assumption that porosity is a function of thickness and in general increases proportional to thickness. Flow unit isopach trends were also used to constrain the model in any areas with insufficient data to construct a conceptual model. Variograms based on a spherical model were constructed consistent with the trends in thickness. The simulation was repeated for 50 to 100 realizations and post-processed statistically to determine the most likely representation of the study area (Figure 2-36).

A permeability model was created from the porosity model's most probable realization, using the same collocated co-simulation approach employed to build the porosity model. A variogram of the simulated porosity model based on a spherical model was used to produce 100 realizations of the permeability model within the study area. Post-processing was used to determine statistically the most probable representation within the study site (Figure 2-37).

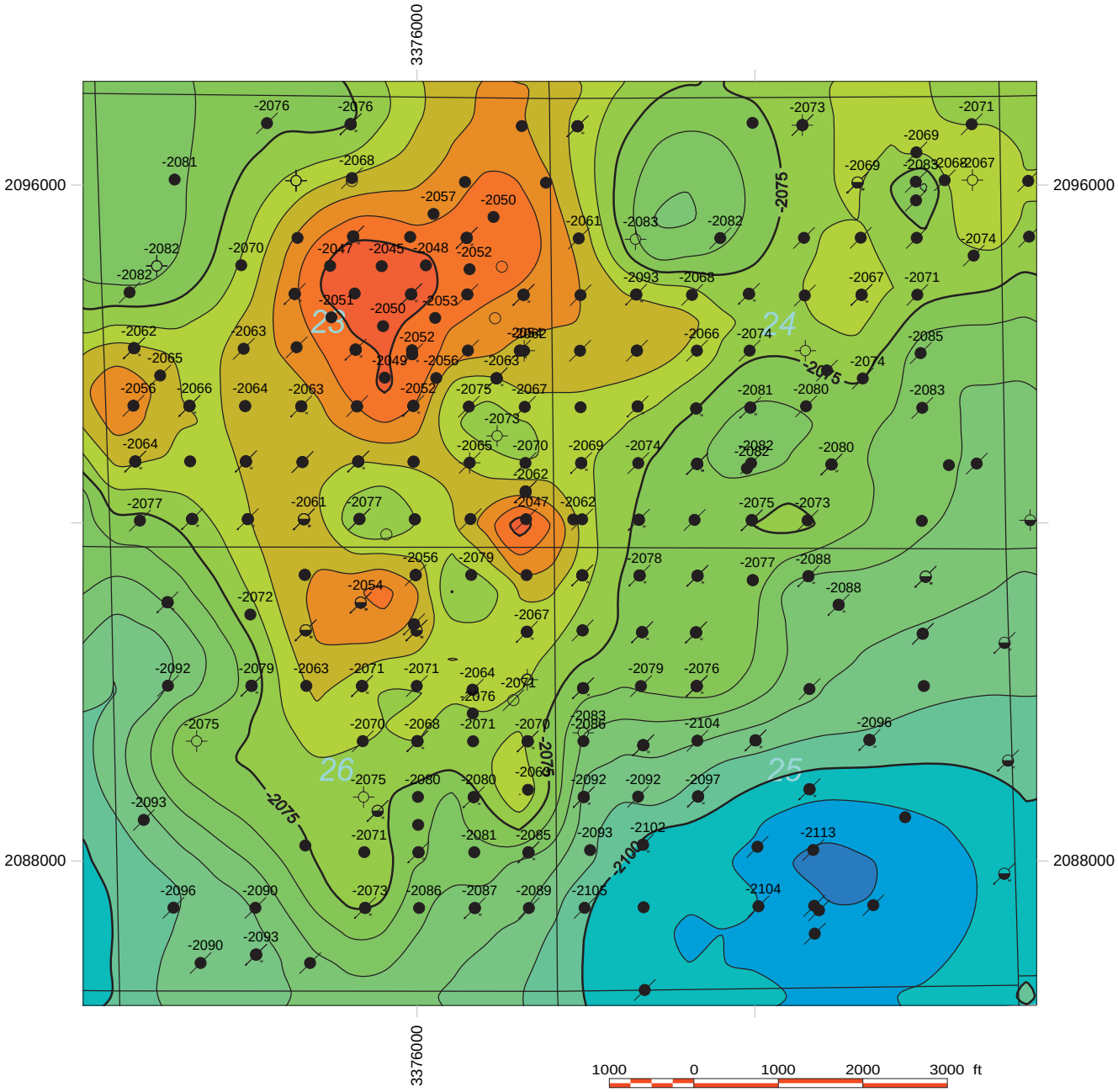

Figure 2-31 *Depth structure map on the upper Cypress Sandstone, Wakefield study in Clay City Consolidated Field. Datum = MSL; contour interval = 5 ft.*

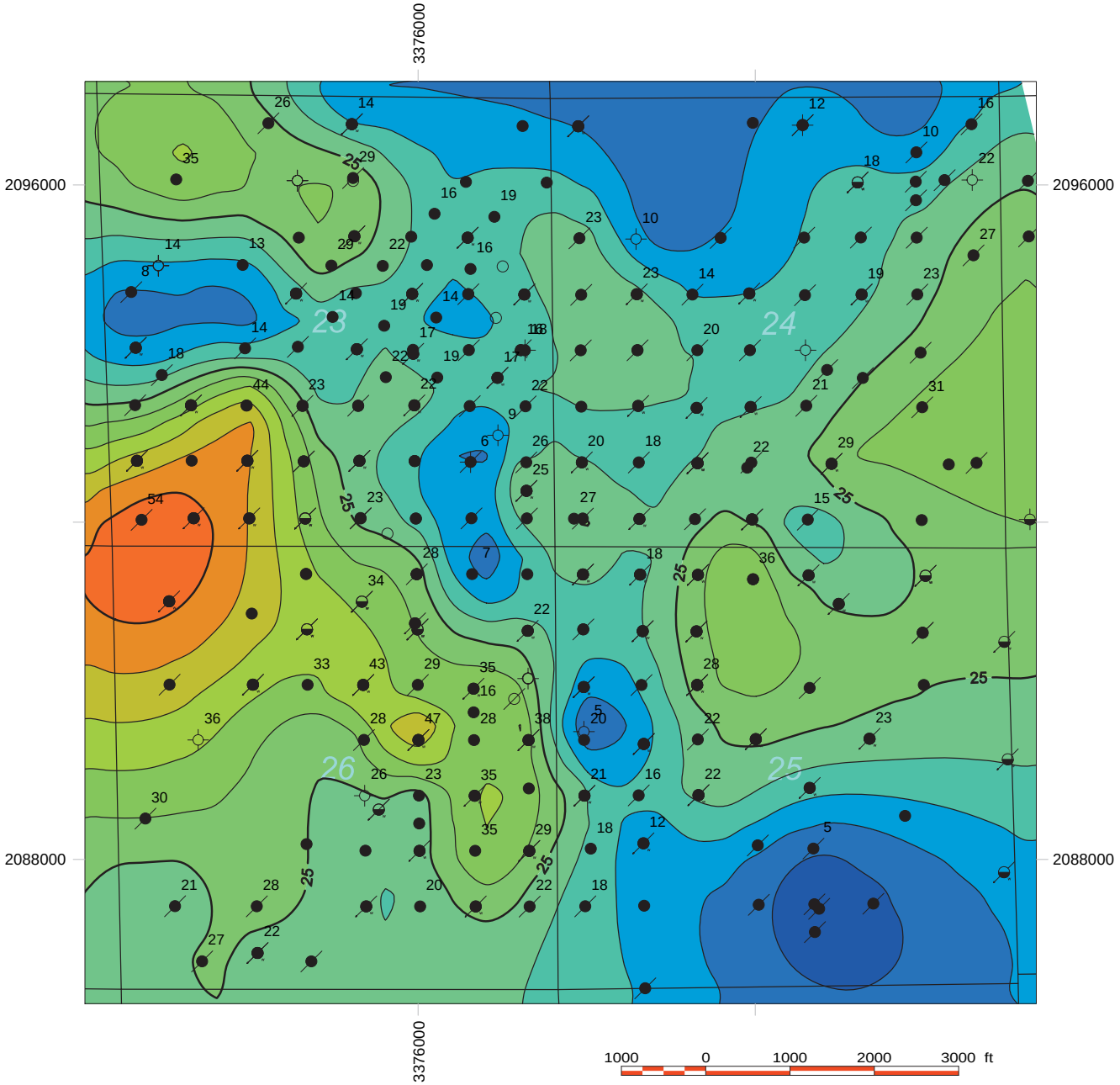

Figure 2-32 *Gross isopach map of the upper Cypress Sandstone, Wakefield study in Clay City Consolidated Field. Contour interval = 5 ft.*

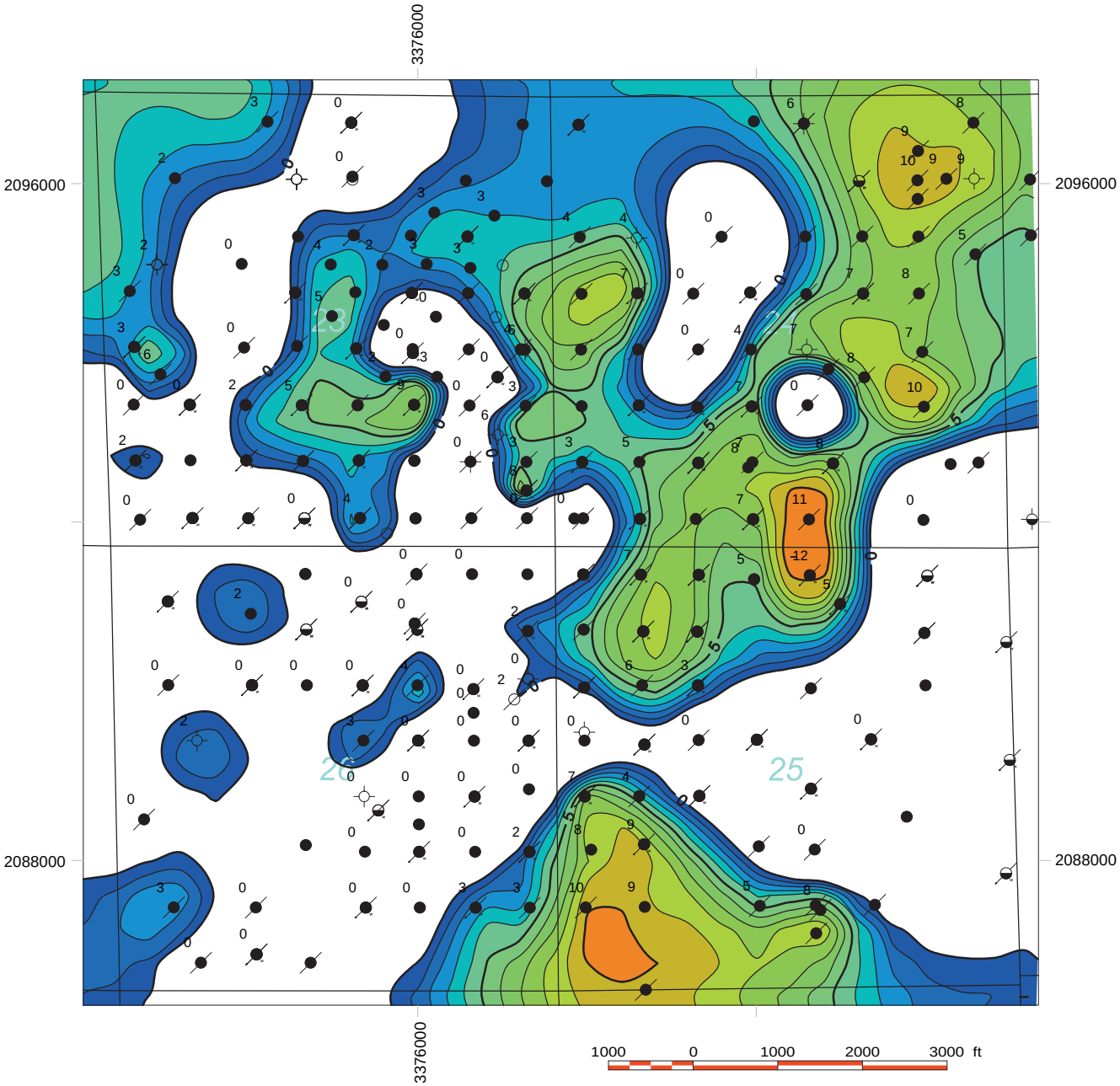

Figure 2-33 *Gross isopach map of the sub-Barlow stringer II, Cypress Sandstone, Wakefield study in Clay City Consolidated Field. Contour interval = 1 ft.*

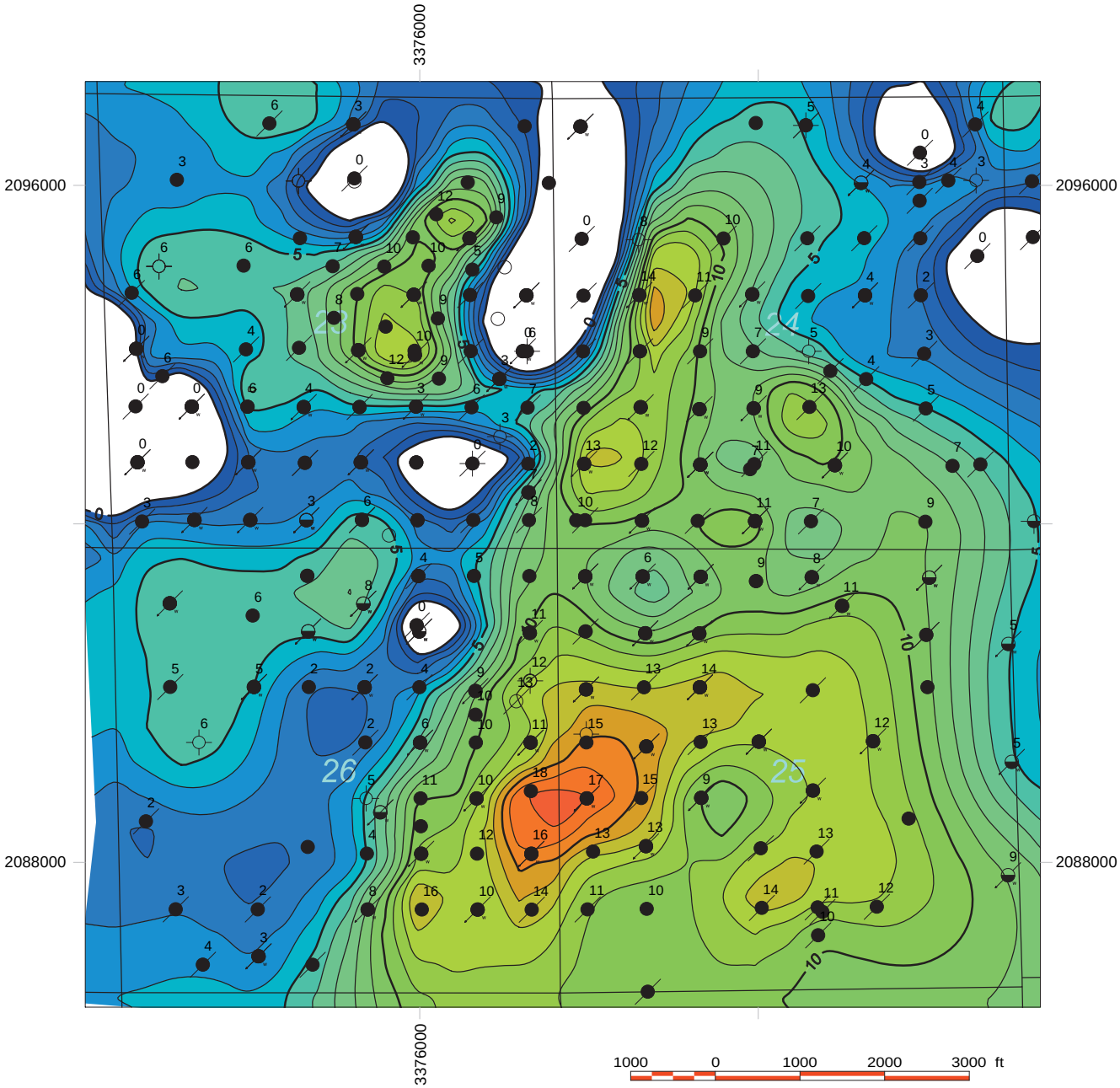

Figure 2-34 *Gross isopach map of the sub-Barlow stringer I, Cypress Sandstone, Wakefield study in Clay City Consolidated Field. Contour interval = 1 ft.*

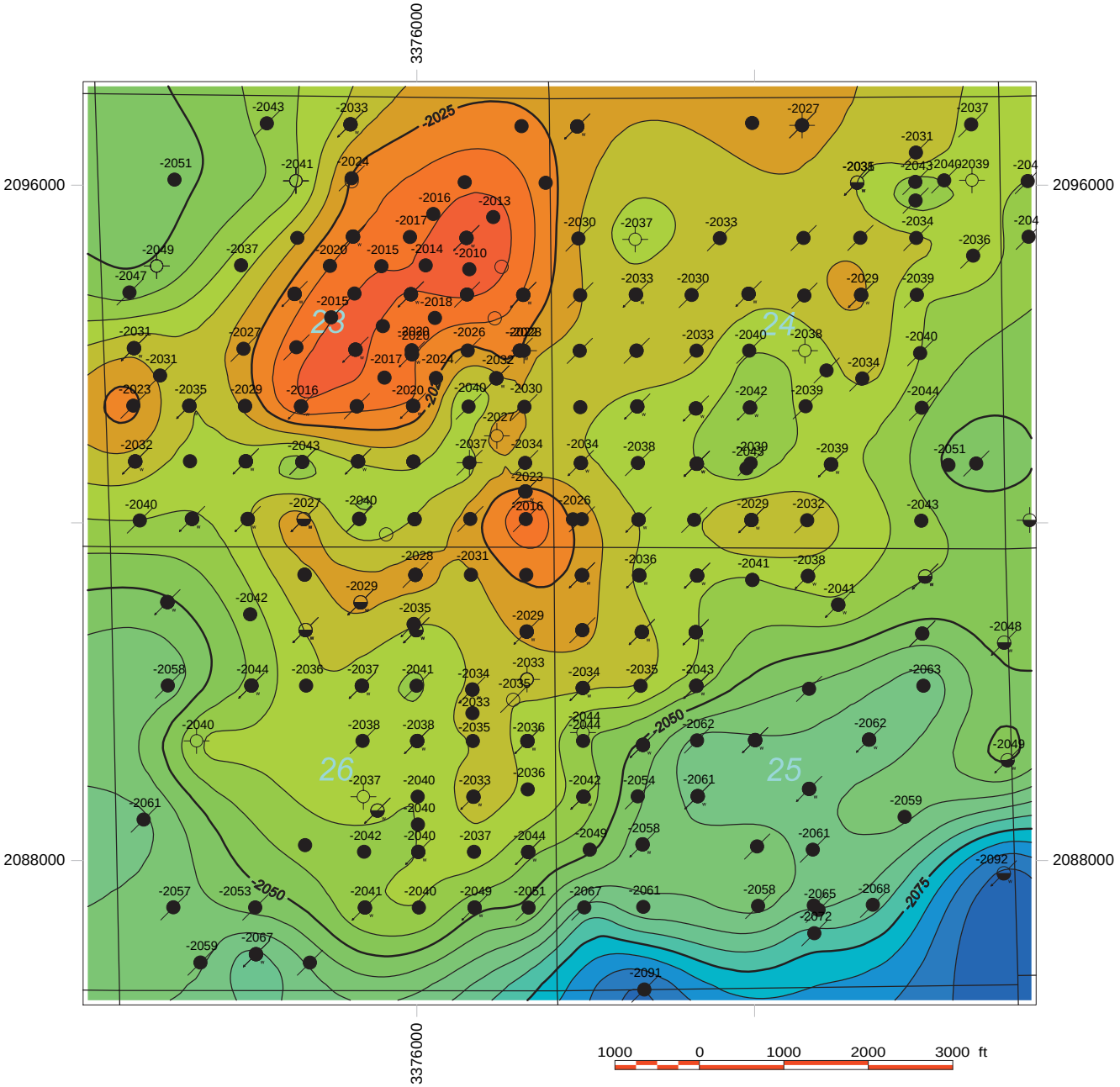

Figure 2-35 *Depth structure map on the base of the Barlow Lime, Wakefield study in Clay City Consolidated Field. Datum = MSL; contour interval = 5 ft.*

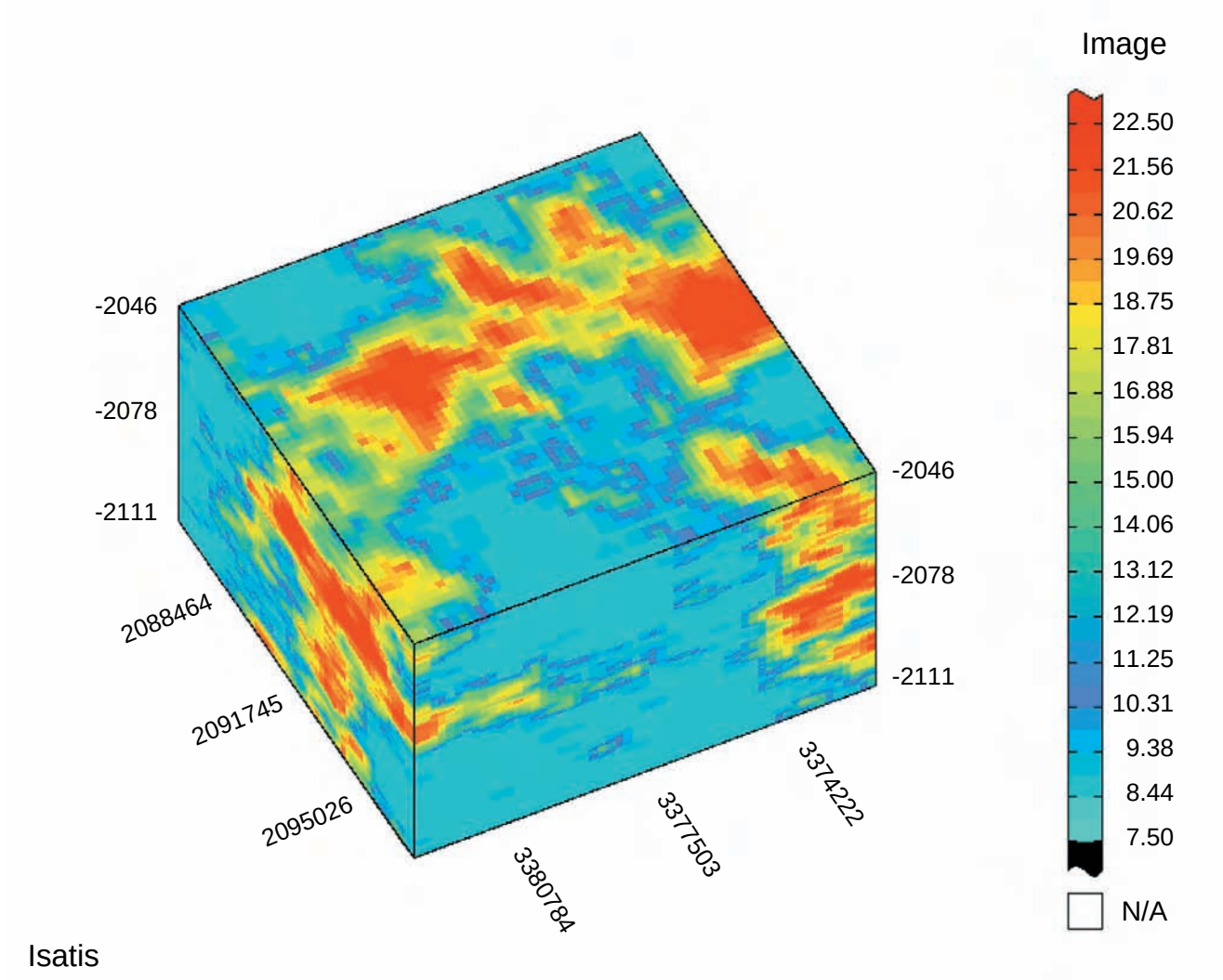

Figure 2-36 *Three-dimensional visualization of the Wakefield study area. This core-derived porosity model was produced using turning bands simulation. The display shown is the "most likely" realization of a set of 30 simulations. The anisotropic variogram used in the scenario was a nested nugget and spherical combination.*

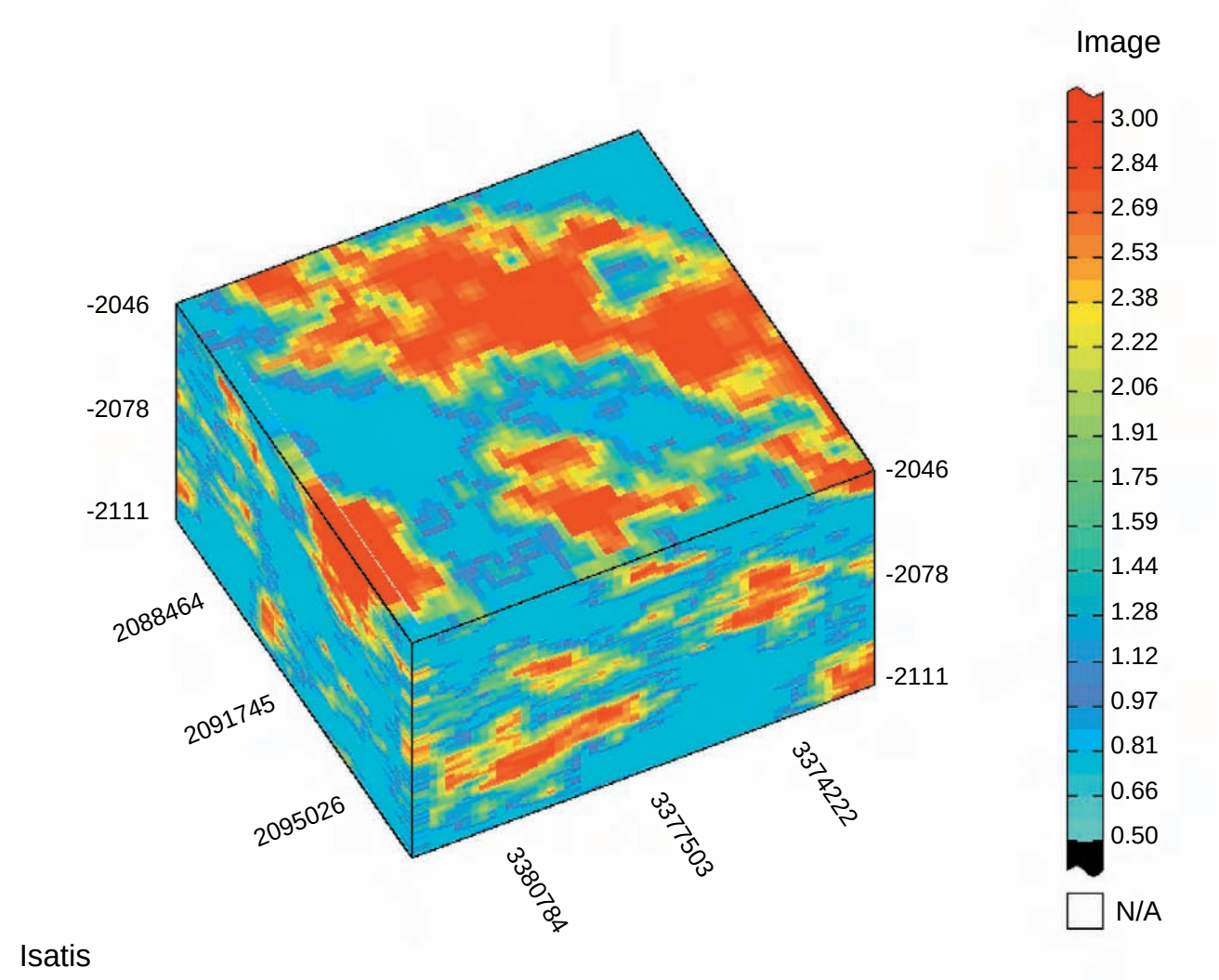

Figure 2-37 *Three-dimensional visualization for the Wakefield study area. This log_{10} core-derived horizontal permeability model was produced using collocated co-simulation employing the Markov-Bayes assumption. The display shown is the "most likely" realization of a set of 30 simulations. The variogram used in the scenario was similar to the variogram used in the porosity model.*

Mill Shoals Field Geologic Model of Aux Vases Sandstone Reservoir

Deterministic Model

Mill Shoals Field occupies approximately 31 km^2 (12 mi^2) at the intersection of Wayne, Hamilton, and White Counties, Illinois, and has produced over 2.4 million m^3 (15 million stb) of oil from nine separate horizons since its discovery in 1939. The Mississippian Aux Vases Sandstone and carbonates of the Ste. Genevieve Limestone are the most prolific horizons in the field. The area that was selected to model this field is located in Sections 24 and 25, T3S, R7E, in Hamilton County. The area was chosen because of the presence of an Aux Vases reservoir section that is typical of the Basin and on the basis of the availability of recent log suites and whole core with core analyses.

Mill Shoals Field is located along a northeast-trending anticlinal structure in the Fairfield Basin, the central, lowest region of the Illinois Basin. The modeled area is a recently discovered step-out along the western flank of the anticline. Depth to the top of the reservoir in the study area starts at about –869 m (–2,850 ft) MSL (Figures 2-38 and 2-39). Oil accumulation in the Aux Vases is controlled by stratigraphically discrete sandstone bodies that form along the crest and flanks of the anticlinal structure.

In the Mill Shoals area, the Aux Vases consists predominantly of sandstone, shale, and some carbonate. Two sandstone reservoir horizons, a lower (Zone 2) and an upper (Zone 1) horizon, have been identified within the Aux Vases. Sandstone facies within these horizons are interpreted to have been deposited in tidal flat and tidal channel environments, with the channel facies being the productive facies. Reservoir-quality sandstones are very fine to fine grained and commonly display tabular cross-bedded, duneform beds. Tidal currents influenced sedimentation and are readily apparent in the tidal flat facies as tidal couplets and flaser bedding. Marine trace fossils are common in the tidal flat sandstones and shales, and calcite-cemented burrows are common in the upper beds of the cross-bedded reservoir sandstones. Thickness maps of Aux Vases reservoirs commonly show discrete, pod-like geometries and are 202,344 to 404,687 m^2 (50 to 100 acres) in aerial extent. Individual reservoir sandstones generally attain a thickness of 3.0 to 7.6 m (10 to 25 ft) (Figures 2-40 and 2-41). These facies have been identified in other Aux Vases reservoirs across the Basin.

Porosity and permeability values measured from core and used in the model of the Mill Shoals area are summarized in Table 2-7. Porosity of just the reservoir facies ranges from 16 to 28%, and permeability ranges from 0.0247 to 0.493 μm^2 (25 to 500 md). Historically, Aux Vases reservoirs yield approximately 40% recovery from primary production and waterflooding.

Step-out drilling in Mill Shoals Field located additional productive “pods” several decades after the original portion of the field was waterflooded. Core photos in Figure 2-42 are from the Hamilton Oil V. Fyie No. 35-25, one of newer wells at the western margin of the field. Figure 2-43 shows porosity and permeability analysis plots.

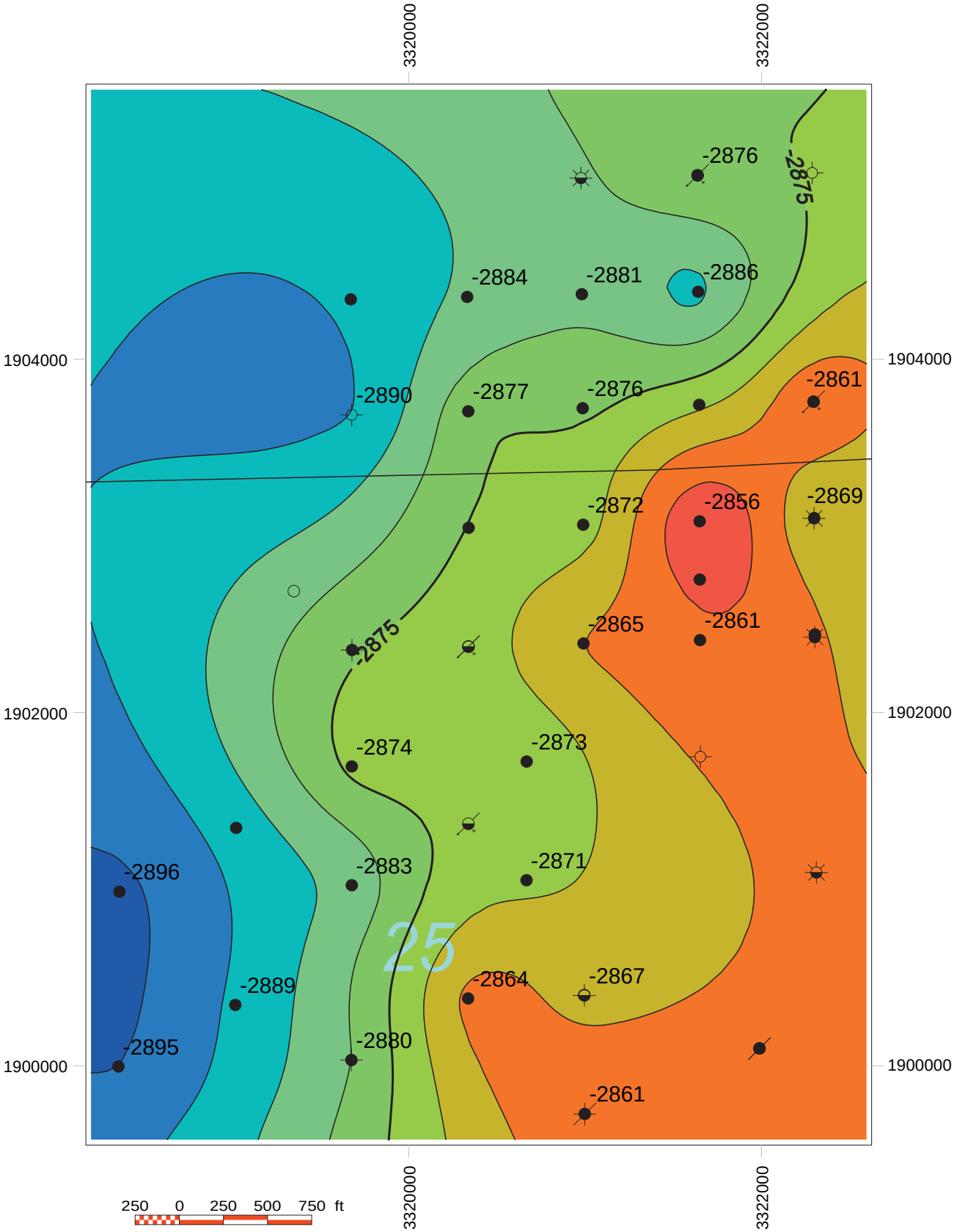

Figure 2-38 *Depth structure map on top of Zone 2, Aux Vases Sandstone, Mill Shoals Field study. Datum = MSL; contour interval = 5 ft.*

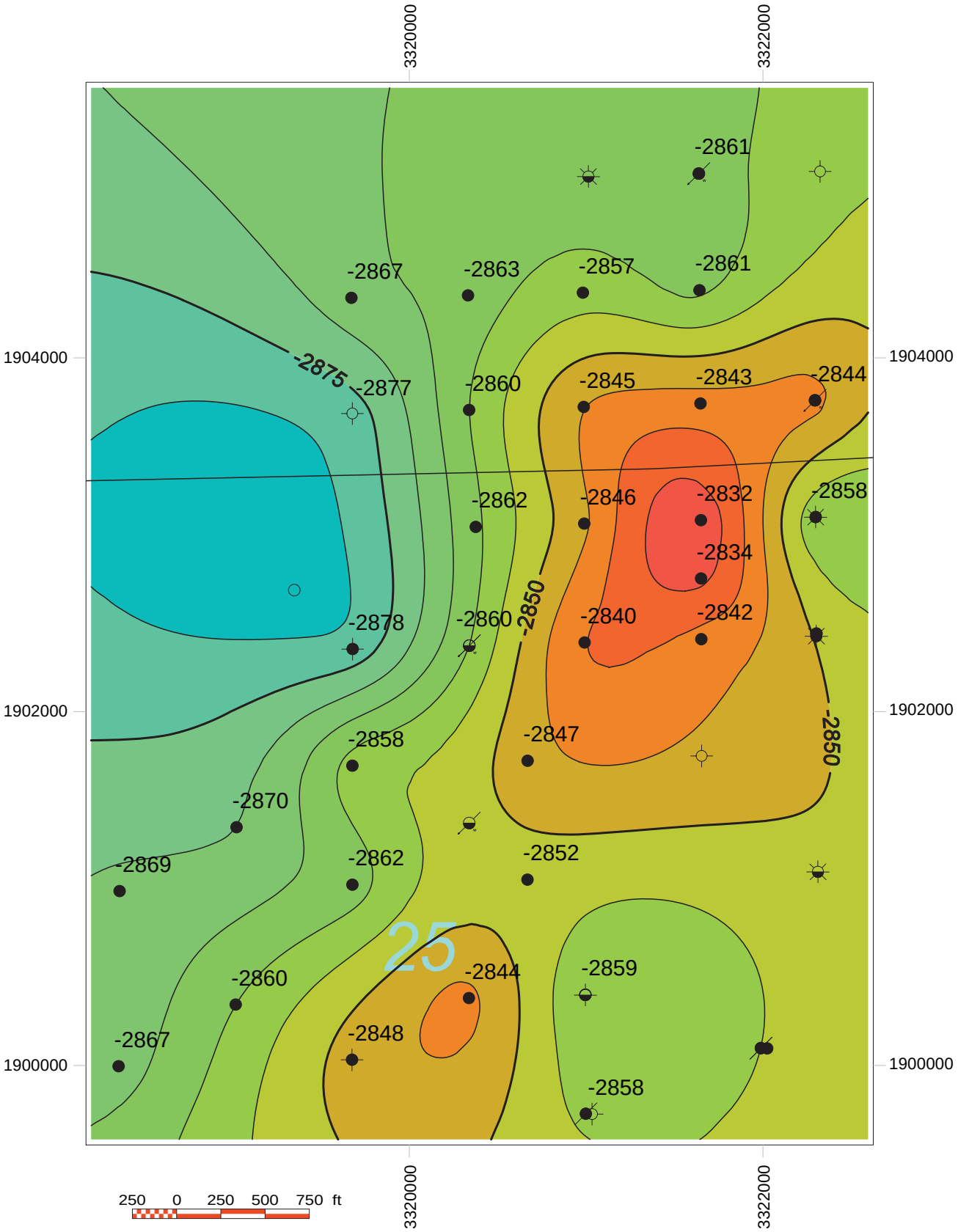

Figure 2-39 *Depth structure map on top of Zone 1, Aux Vases Sandstone, Mill Shoals Field study. Datum = MSL; contour interval = 5 ft.*

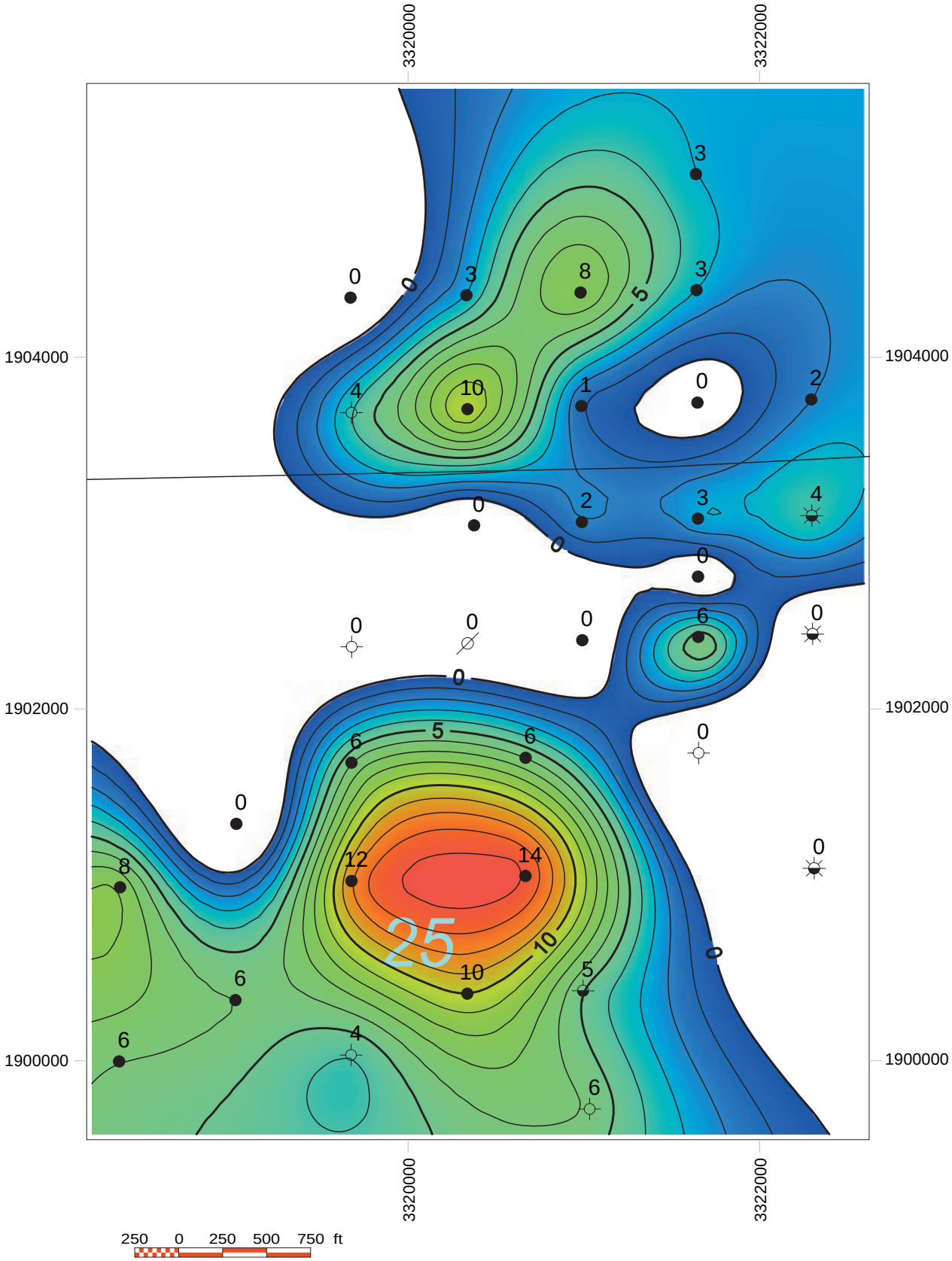

Figure 2-40 *Based on net sandstone isopach map of Zone 2, Aux Vases Sandstone, Mill Shoals Field study. Contour interval = 1 ft.*

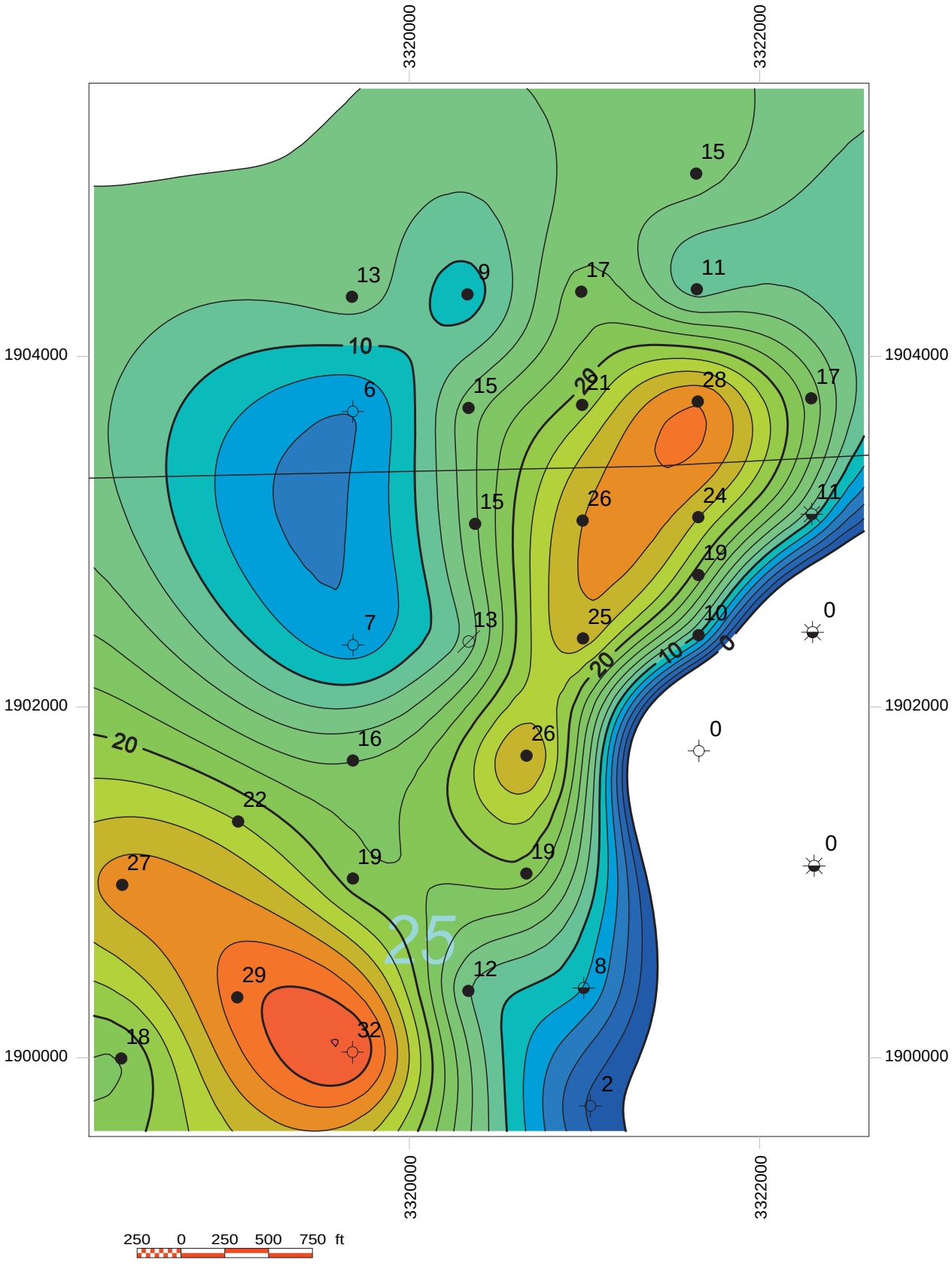

Figure 2-41 *Based on net sandstone isopach map of Zone 1, Aux Vases Sandstone, Mill Shoals Field study. Contour interval = 2 ft.*

Figure 2-42 *Composite core photograph of Hamilton Oil V. Fyie No. 35-25 (marked by a blue star on the maps). The Headington Oil V. Fyie No. 35-25 exhibits the two reservoir and one non-reservoir facies commonly found in Aux Vases sandstone reservoirs. These sandstones were deposited by tidal processes in mid-sand flat, tidal dune, tidal channel, and tidal flat environments. Sand grains in the reservoir facies are loosely cemented with large amounts of intergranular porosity. Highly porous and permeable reservoir facies are underlain by non-reservoir facies with low permeability and porosity. Grains in the green ripple-bedded facies are tightly cemented with little to no intergranular porosity. 1, burrowed, fine-grained crossbedding in a tidal sand flat environment (Zone 1 facies). 2, fine-grained sandstone representing tidal channel and tidal sand flat environments (Zone 1). 3, non-reservoir rock, very fine-grained sandstone and siltstone with ripple and flaser bedding representing a lower energy mid-flat environment (Zone 2).*

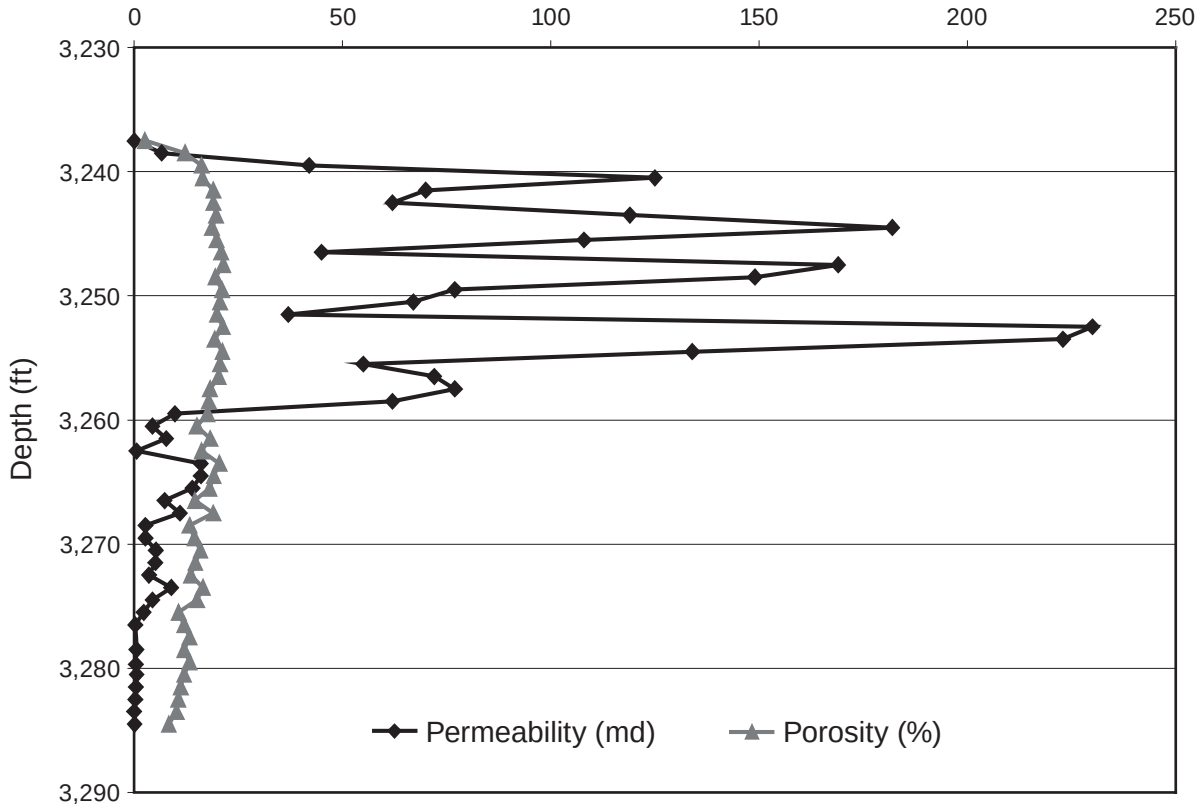

Figure 2-43 *Core analysis curves for porosity and permeability, V. Fyie No. 35-25 well.*

Geostatistical Model

Three-dimensional geostatistical models of porosity and permeability were built at Mill Shoals. Porosity was modeled using the turning bands method for stochastic simulation. This approach employs core data in conjunction with histograms and variograms derived from these data to interpolate values at sites where core data were not available. At Mill Shoals an isotropic spherical variogram was used to capture the spatial horizontal and vertical continuity of the data. Thirty distinct realizations of the resulting porosity model were produced, all of which honored both the core data and the variogram calculated from that data. These realizations were post-processed to determine the most statistically probable simulation and compared with known data as a final check (Figure 2-44).

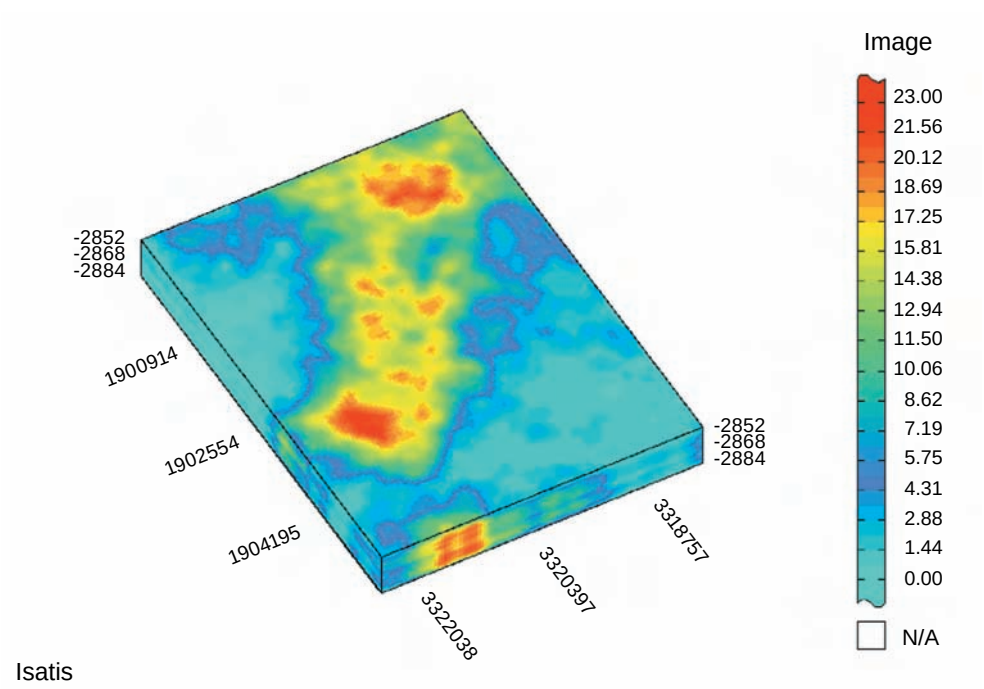

Figure 2-44 *Three-dimensional visualization of the Mill Shoals study area. This core-derived porosity model was produced using turning bands simulation. The display shown is the "most likely" realization of a set of 30 simulations. The anisotropic variogram used in the scenario was a nested nugget and spherical combination.*

A horizontal permeability model was produced using a collocated co-simulation approach with the "most likely" three-dimensional porosity model. Although permeability data were scarce and scattered relative to porosity data, the correlation between porosity and permeability was deemed sufficient to allow use of the porosity model to condition permeability, particularly in those locations lacking permeability data. A variogram derived from the porosity model was used to inform the less populated horizontal permeability data set. The variogram used for permeability simulations was an anisotropic spherical model. This simulation effort also yielded 30 realizations, which were statistically post-processed to determine which realization was the most probable to represent the geologic trends within the site (Figure 2-45).

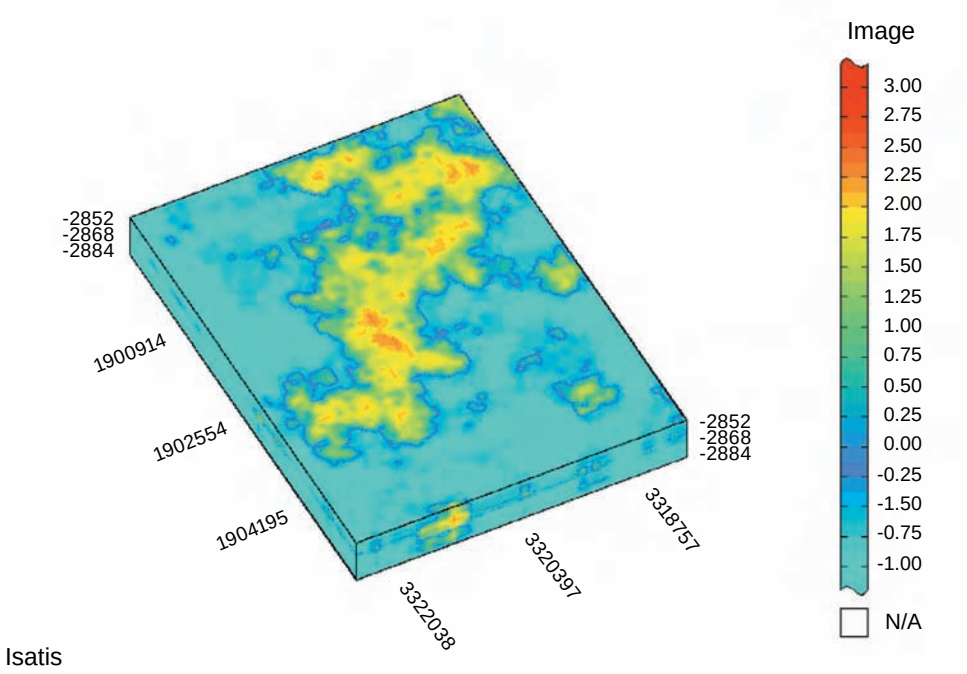

Figure 2-45 *Three-dimensional visualization for the Mill Shoals study area. This log_{10} core-derived horizontal permeability model was produced using collocated co-simulation employing the Markov-Bayes assumption. The display shown is the "most likely" realization of a set of 30 simulations. The variogram used in the scenario was similar to the variogram used in the porosity model.*

Zeigler Field Geological Model of Aux Vases Sandstone Reservoir

Deterministic Model

Zeigler Field is a typical sandstone reservoir in the Aux Vases, and because of an abundance of available geologic and engineering data, the field is ideal for detailed reservoir characterization. The Aux Vases Formation at Zeigler Field was deposited by tidal processes in a shallow marine, mixed siliciclastic-carbonate environment. Cross-bedded reservoir sandstones are interpreted to be tidal sand bars deposited in a shallow marine environment. A depositional model developed using core, geophysical log, and outcrop data shows tidal mud-flat and sand-flat deposits associated with reservoir sandbar facies. Reservoir sandstones are overlain by tidal-flat siltstones and shales and are underlain by sediments deposited in a lower energy regime. Very fine-grained, ripple-bedded, nonporous and impermeable sandstones are sealed laterally by impermeable tidal-flat and interbar deposits.

One isolated, two narrowly connected, and two slightly overlapping sandstone bars were identified in Zeigler Field. These bars are isolated by lateral facies changes from porous cross-bedded sandstone to nonporous shaley sandstone or mudstone deposits (Figures 2-46 to 2-49). The existence and magnitude of permeability barriers that separate three of the sandstone bars in the main body of the field were more readily determined using pressure data than using correlations of electric logs or core descriptions (Seyler, 1998). Variations in pressure data documented the existence of a permeability barrier that

separates the east part of the field from the west part. Pressure data showed a less complete permeability barrier separating the north part of the Plumfield lease from the south part of the lease. In this instance, fluid communication between the bars slowed through a narrow constriction via pressure data. In Zeigler Field, four sandstone bars were identified that were deposited, separated, narrowly connected, and slightly overlapping.

Zeigler Field is primarily a stratigraphic trap with no structural closure on the Ste. Genevieve or Barlow Limestone contoured structure maps. The field is located a few miles north of the Cottage Grove

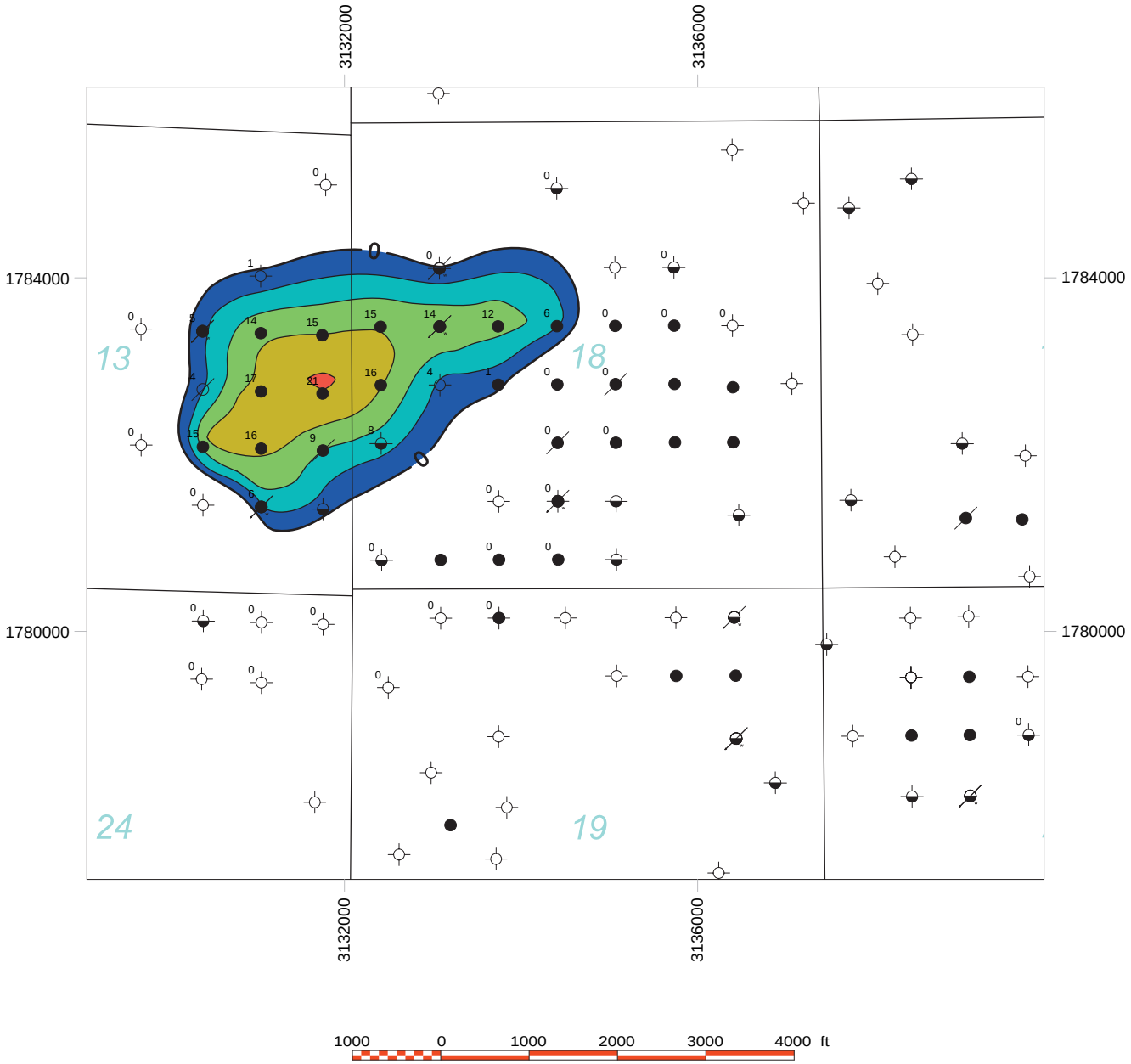

Figure 2-46 *Gross isopach map of the West Plumfield Zone of the Aux Vases Sandstone, Zeigler Field study. Contour interval = 5 ft.*

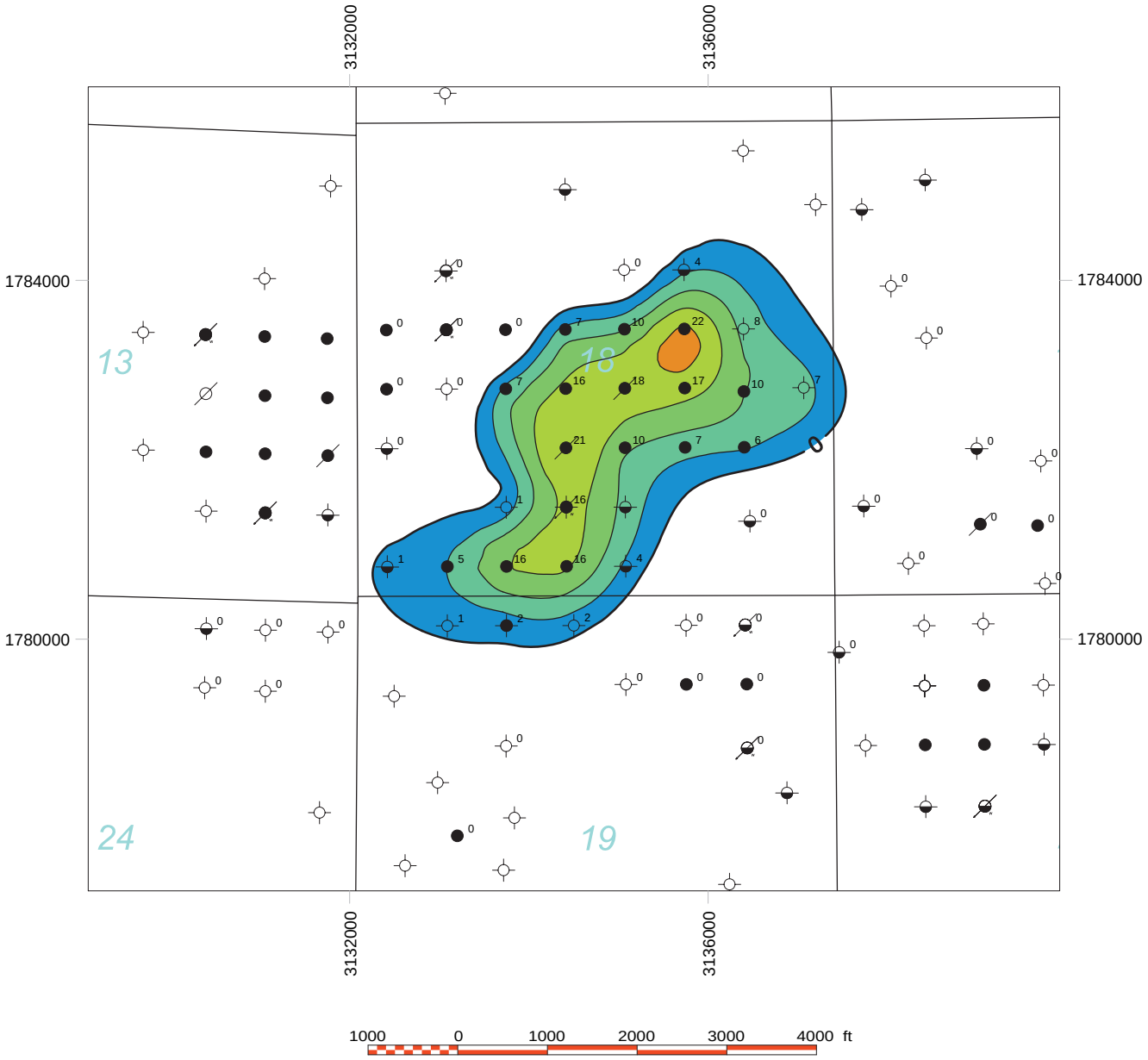

Figure 2-47 *Gross isopach map of the Plumfield Zone of the Aux Vases Sandstone, Zeigler Field study. Contour interval = 5 ft.*

Fault System; therefore, a natural fracture system of vertical fractures observed in the underlying Ste. Genevieve Limestone is likely to project into Aux Vases Sandstone bars. A natural fracture system oriented subparallel to maximum horizontal compressive stresses likely exists at Zeigler Field.

Reservoir fluids are confined to the limited lateral extent of clean reservoir sandstone bars that are encased in nonporous and impermeable facies. As a result, the sandbars were systematically produced, and waterflooded fluids were banked against the edges of sandbars. Wells located at bar margins that contain thinner, less porous, and less permeable reservoir intervals have produced twice as much oil as

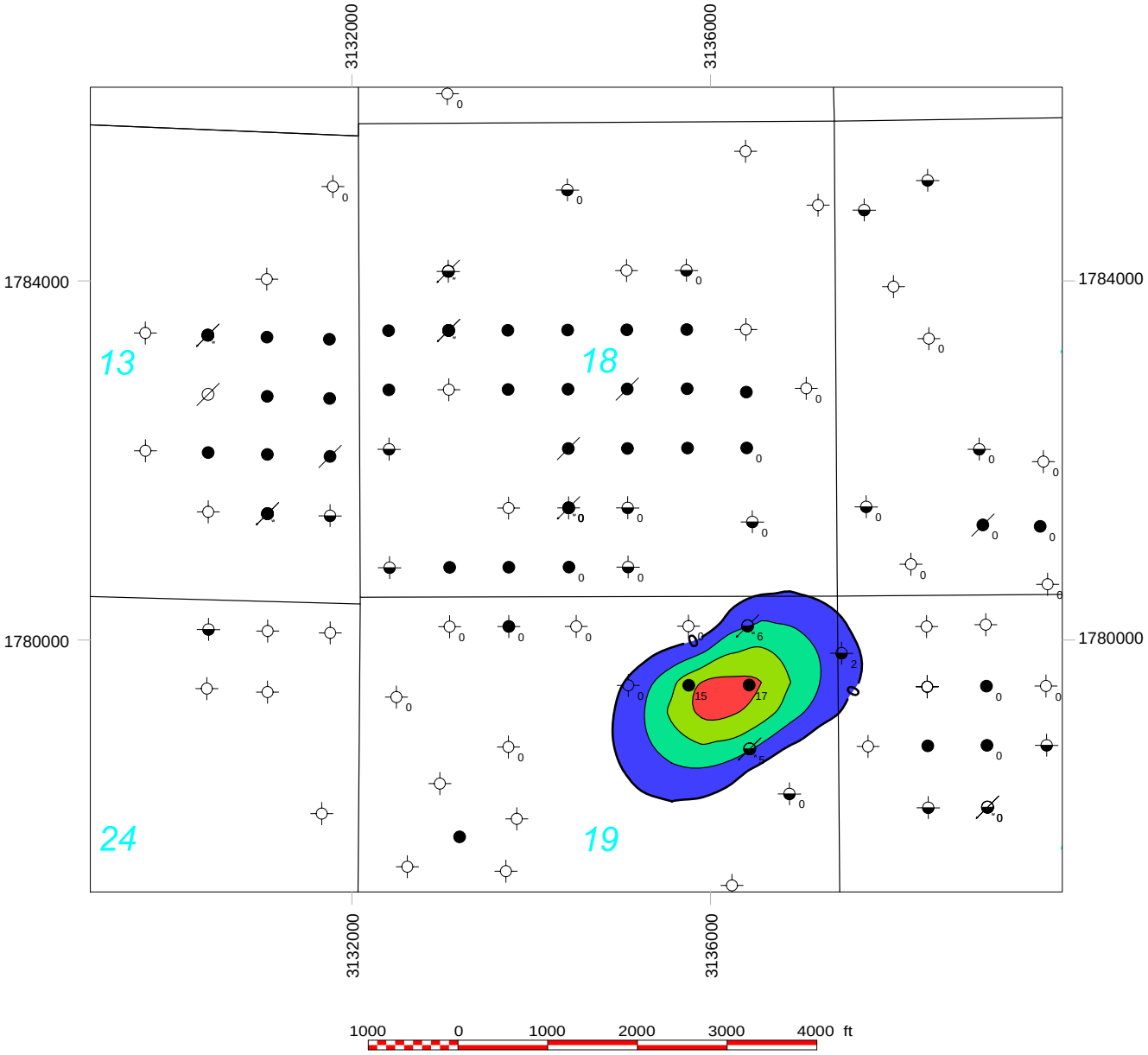

Figure 2-48 *Gross isopach map of the South Plumfield Zone of the Aux Vases Sandstone, Zeigler Field study. Contour interval = 5 ft.*

offsetting wells with thicker, more porous and more permeable reservoir intervals due to this waterflood "banking" effect.

Diagenetic alterations have played a major role in preserving and enhancing porosity and permeability. A thin layer of diagenetic clay minerals coats virtually every sand grain in the reservoir sandbar facies. These clay minerals have prevented the precipitation of porosity-occluding quartz overgrowths and preserved porosities as high as 30% in the reservoir facies. Pore-lining diagenetic clay minerals cause the sandstone to be loosely cemented and friable. They are also responsible for problems during

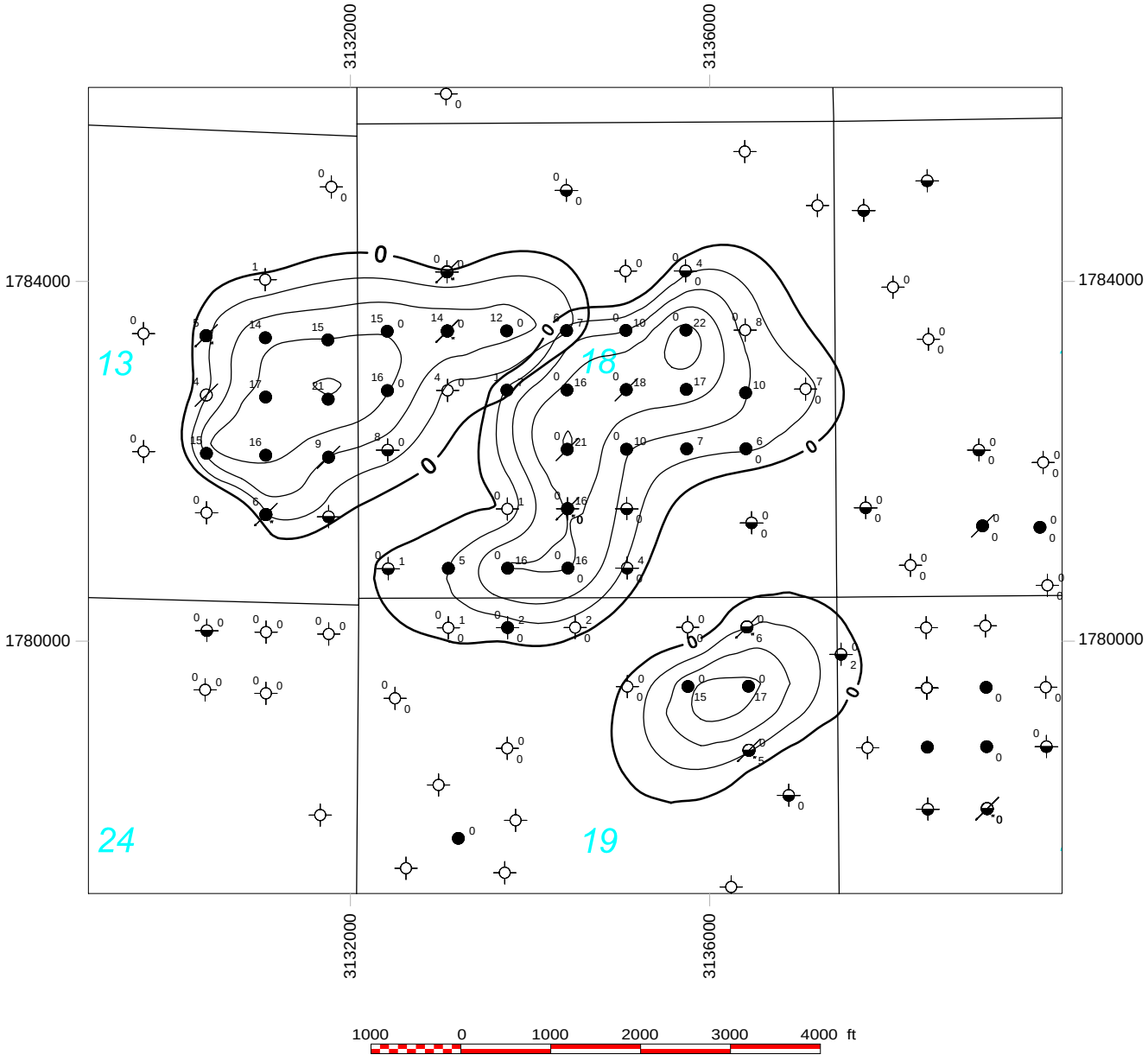

Figure 2-49 *Map comparing gross isopach thicknesses of the three productive sands within the Aux Vases Sandstone, Zeigler Field study. Contour interval = 5 ft.*

reservoir evaluation and during design of drilling, completion, and recovery programs. Low resistivities (2 ohm-meter resistivity log deflections) in reservoir sandstone intervals are very common at Zeigler and other Aux Vases Sandstone reservoirs as a result of pore-lining diagenetic clay minerals.

Recovery efficiencies for sandstone bars in Zeigler Field are greater than the industry norm of 30% to 40% after primary and secondary operations. In the main body of the field, the three sandbars for which historical production data are available have an average recovery efficiency of 48% (calculated using an average porosity of 21%, a formation volume factor of 1.068 rb/stb, and an oil saturation of 65%).

The West Plumfield sandstone bar had a recovery efficiency of 45%, and the combined Plumfield and South Plumfield sandstone bars had a recovery of 51%. The greater recovery efficiency of the Plumfield and South Plumfield bars was attributed to the greater sweep efficiency and longer duration of the waterflood. The reservoir management program undertaken at Zeigler Field resulted in that much higher than average recoveries with an early and effective program of pressure monitoring and maintenance (Figures 2-46 to 2-49).

Geostatistical Model

A three-dimensional geostatistical porosity model was constructed for the Zeigler study using collocated co-simulation conditioned by the geological model of thickness within each flow zone. The choice of this approach was based on the assumption that porosity is a function of thickness and, in general, increases in proportion to thickness. Unit isopach trends also were used to constrain the model in areas lacking sufficient data to represent a conceptual model fully. Variograms based on a spherical model were constructed consistent with trends observed in the thickness data. The simulation was repeated for 50 to 100 realizations and then post-processed to determine the most likely representation (or P50) of the study area (Figure 2-50).

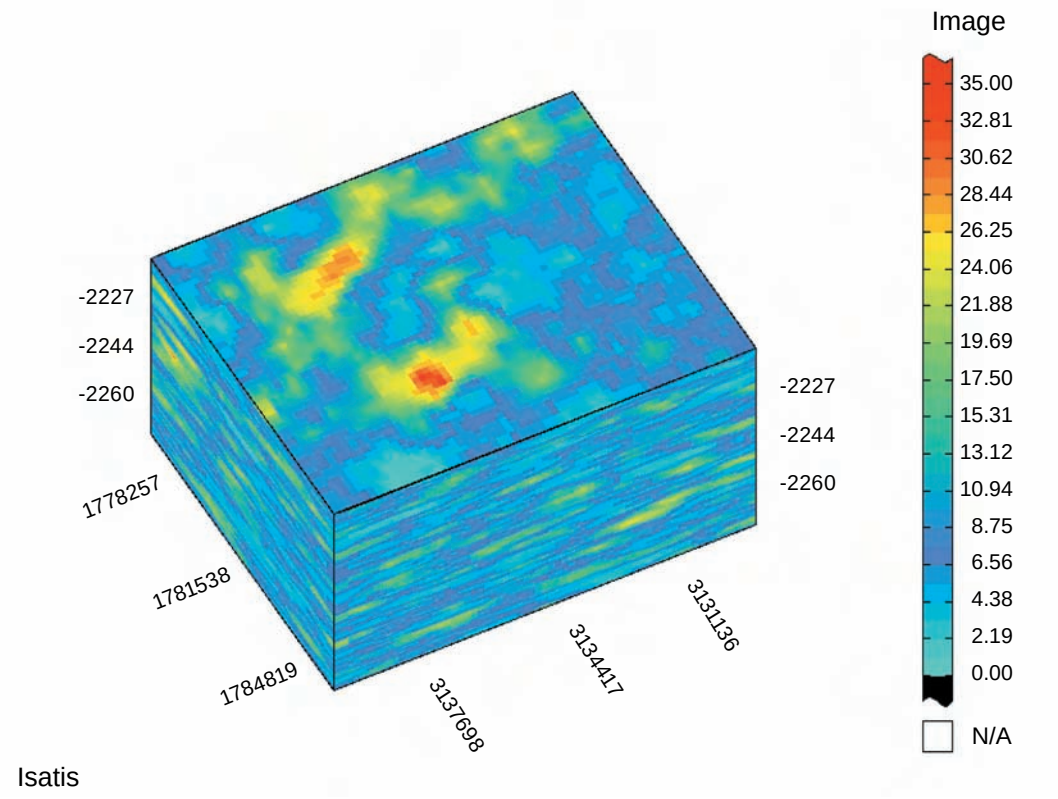

Figure 2-50 *Three-dimensional visualization of the Zeigler study area. This core-derived porosity model was produced using turning bands simulation. The display shown is the "most likely"realization of a set of 30 simulations. The anisotropic variogram used in the scenario was a nested nugget and spherical combination.*

Using the most likely realization of the porosity model, a permeability model was created using the same collocated co-simulation approach. A variogram of the simulated porosity model, using a spherical model, was used to produce 50 to 100 realizations of the permeability model within the study area. Post-processing was used to determine the most probable representation within the study site (Figure 2-51).

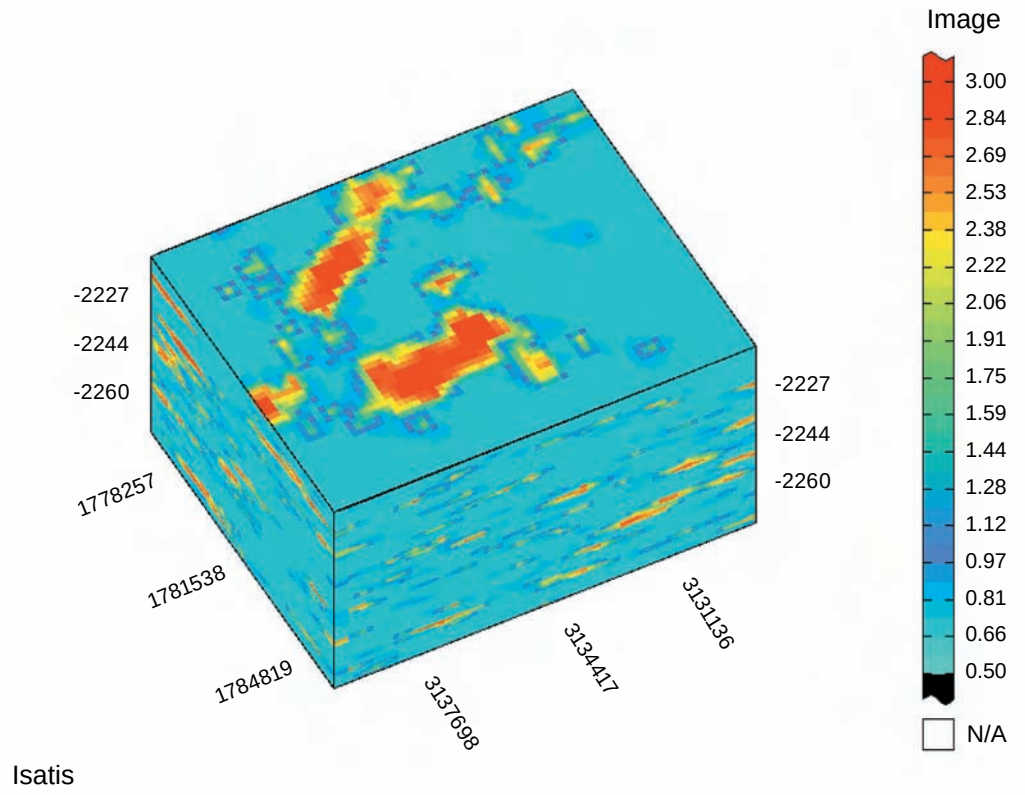

Figure 2-51 *Three-dimensional visualization for the Zeigler study area. This log_{10} core-derived horizontal permeability model was produced using collocated co-simulation employing the Markov-Bayes assumption. The display shown is the "most likely" realization of a set of 30 simulations. The variogram used in the scenario was similar to the variogram used in the porosity model.*

Iola Field Geologic Model of Aux Vases Sandstone Reservoir

Iola Field (2.89 million m^3 (18.2 million stb), cumulative) produces chiefly from the Chesterian Bethel and Aux Vases Sandstones and the Ste. Genevieve Limestone. The field straddles the Clay-Effingham County line in south-central Illinois, where it occupies a north-south–trending string of structural closures separated by small saddles. The study area covers approximately 5.2 km^2 (2 mi^2 (1,244 acres)) atop one such closure at the southern edge of Clay County. This closure comprises the South Mason waterflood unit. Of 170 wells in the study area, 8 were cored, resulting in 60 porosity and permeability measurements.

Wireline log and core analysis of the Aux Vases in the study area allow the Aux Vases to be separated into three flow units. Porosity and permeability of the upper two, termed Green and Brown, respectively, were modeled, and these models and geological models were then submitted for reservoir simulation. A third, lowermost flow unit (Blue) was present only over the eastern portion of the study area, and not in any of the cored wells. The Blue unit was not productive within the limits of the study. The modeled units are in vertical contact over the southern and western portions of the study area and are separated by a shale unit of up to 1.5 m (5 ft) thick elsewhere.

Blue and Green flow units display isopach trends and log responses that are consistent with nearshore marine deposition, typical of the Aux Vases Sandstone in this portion of the Illinois Basin (Figures 2-52 to 2-55). No core samples or photographs are available for more definitive analysis of depositional setting. Core analyses of the productive interval indicate porosities in the range of 14 to 26%; porosities in the Green interval are lower. Permeability is on the order of 0.0493 to 0.0987 μm^2 (50 to 100 md) with a maximum of 0.247 μm^2 (250 md) in a single sample. The shales above, below, and between the modeled layers have porosities of 7 to 10% and permeabilities below 4.93×10^{-3} μm^2 (5 md) (Figures 2-52 to 2-55).

Geostatistical Model

Three-dimensional geostatistical models of both porosity and permeability were built at Iola. Porosity was modeled using a turning bands method of stochastic simulation. This method uses the core data in conjunction with histograms and variograms derived from that data to calculate values at sites where no core data are available. For the Iola study, an isotropic spherical variogram was used to capture the spatial horizontal and vertical continuity of the data for the conceptual model. Thirty distinct realizations of the porosity model were produced, all of which honored both core measurements and the variogram calculated from the data. These realizations were post-processed to determine the most statistically probable simulation and compared with known data as a final check (Figure 2-56).

A horizontal permeability model was produced using a collocated co-simulation approach with the "most likely" three-dimensional porosity model. Although permeability data was scarce and scattered relative to porosity data, the correlation between porosity and permeability was deemed sufficient to allow use of the porosity model to condition permeability, particularly in those locations lacking permeability data. A variogram derived from the porosity model was used to inform the less populated horizontal permeability data set. The variogram used for permeability simulations was an anisotropic spherical model. This simulation effort also yielded 30 realizations, which were post-processed to determine which realization was the most probable to represent the geologic trends within the site (Figure 2-57).

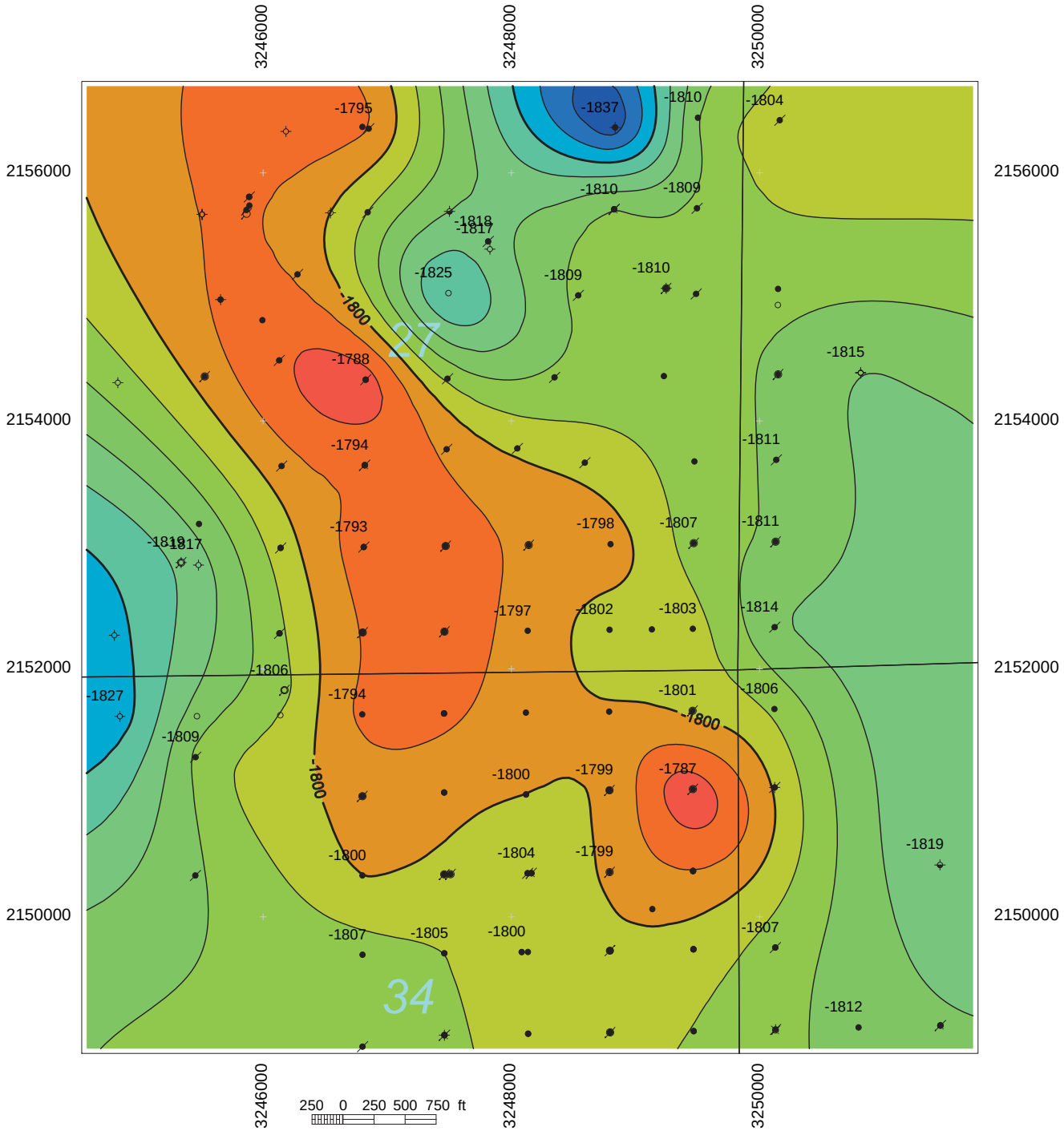

Figure 2-52 *Depth structure map on top of Green zone of Aux Vases Sandstone, Iola Field study. Datum = MSL; contour interval = 5 ft.*

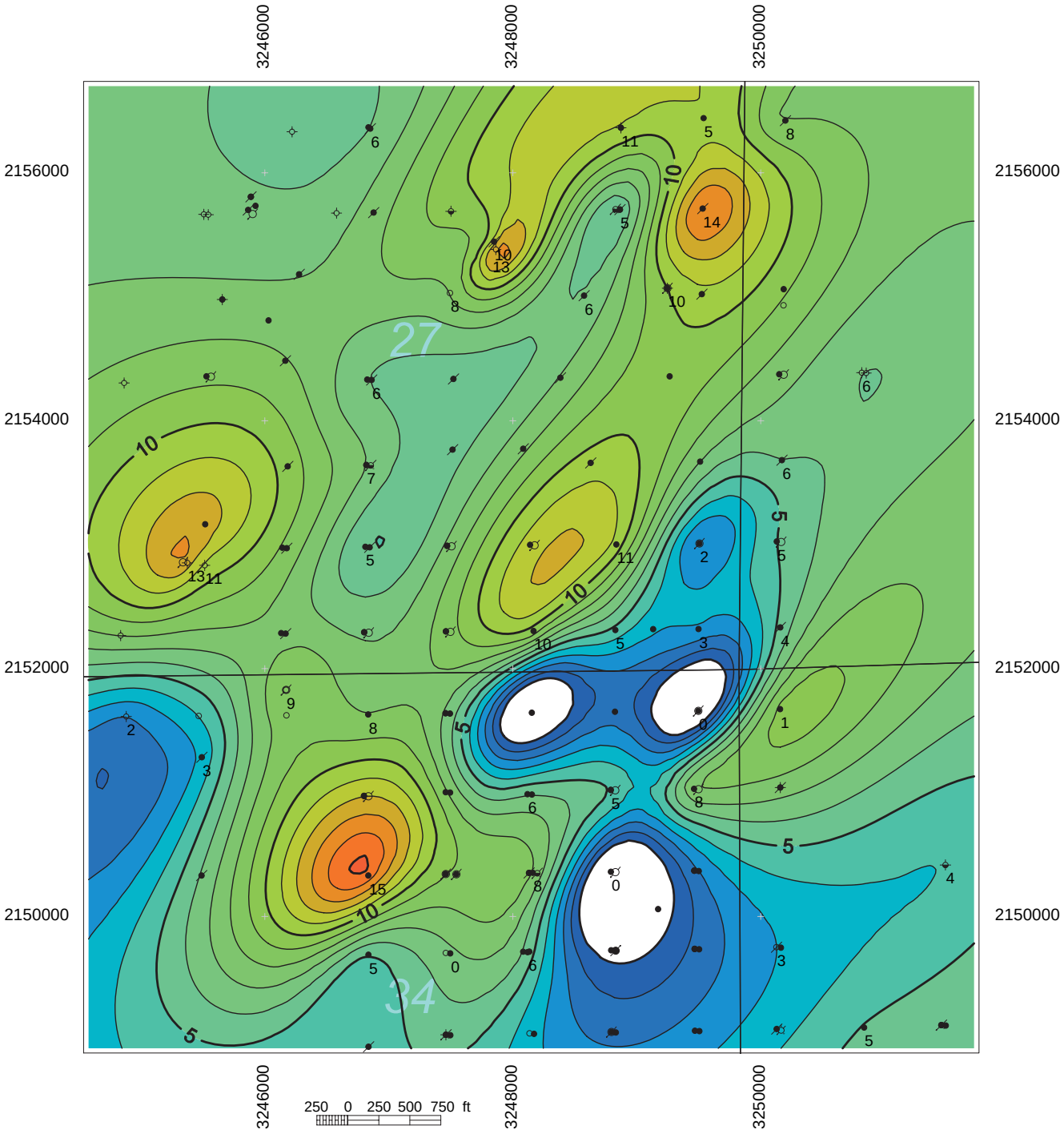

Figure 2-53 *Gross isopach map of Green zone in Aux Vases sandstone, Iola Field study. Contour interval = 1 ft.*

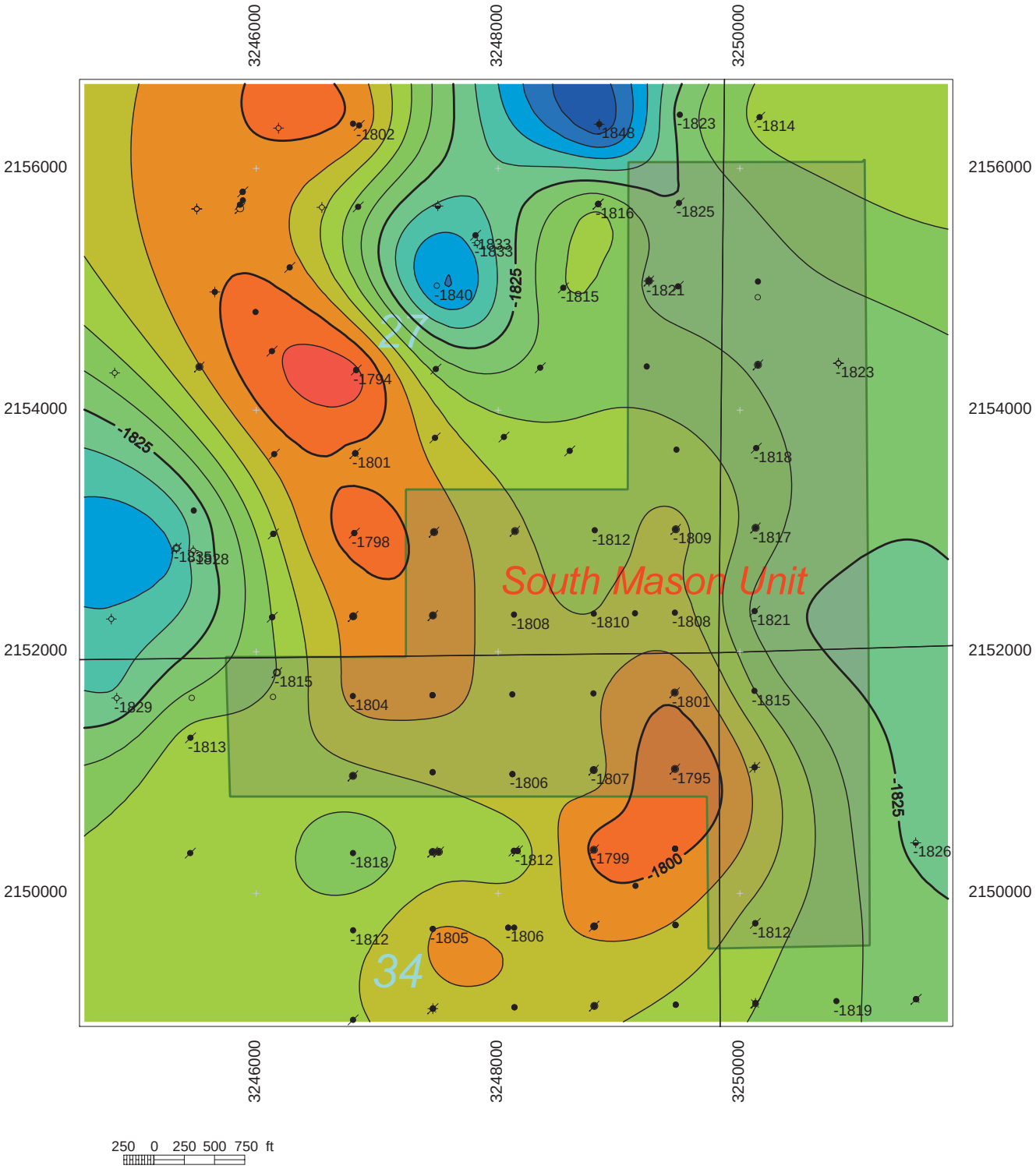

Figure 2-54 *Depth structure map on top of Brown zone of Aux Vases Sandstone, Iola Field study. Datum = MSL; contour interval = 5 ft.*

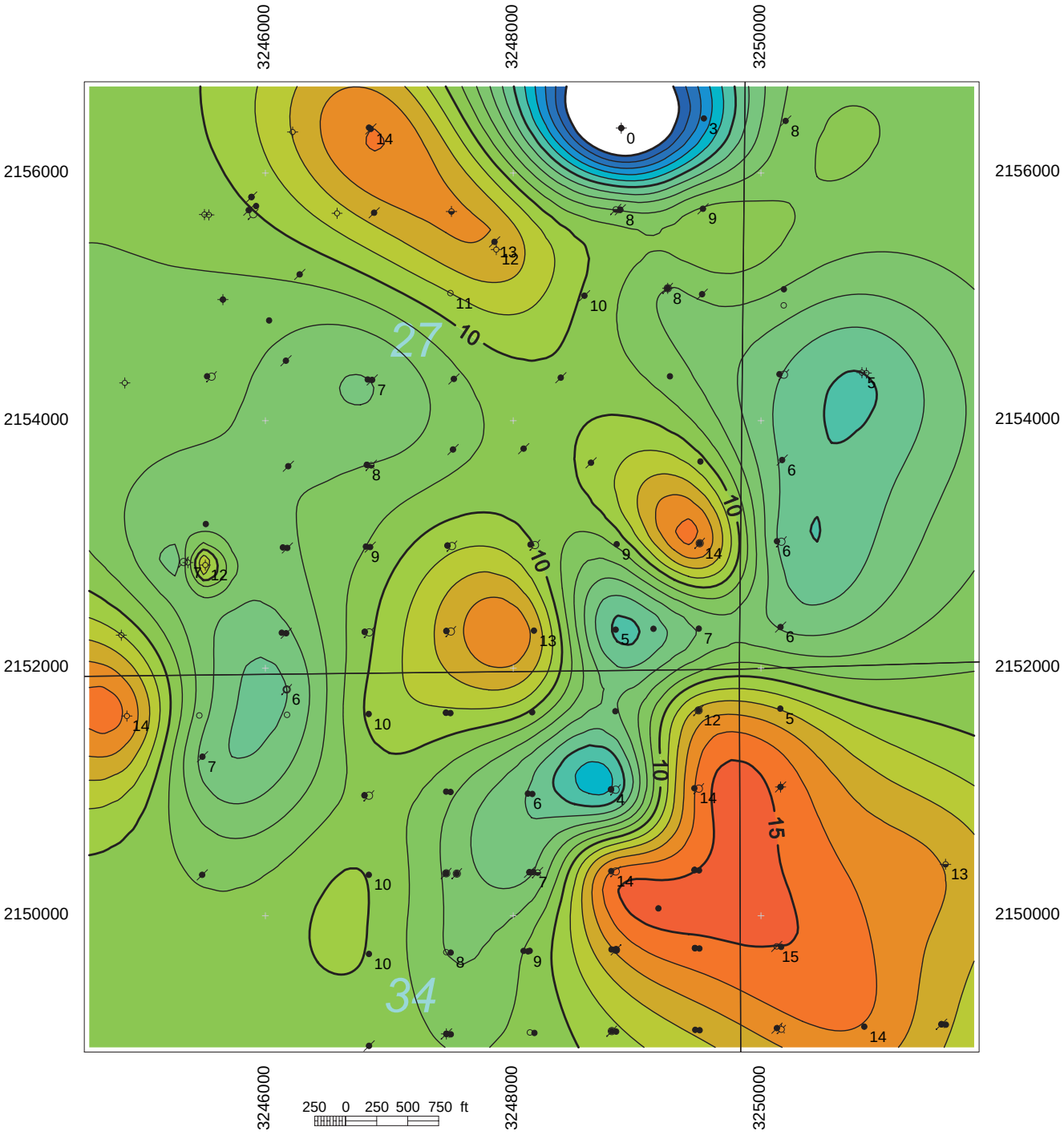

Figure 2-55 *Gross isopach map of Brown zone in Aux Vases sandstone, Iola Field study. Contour interval = 1 ft.*

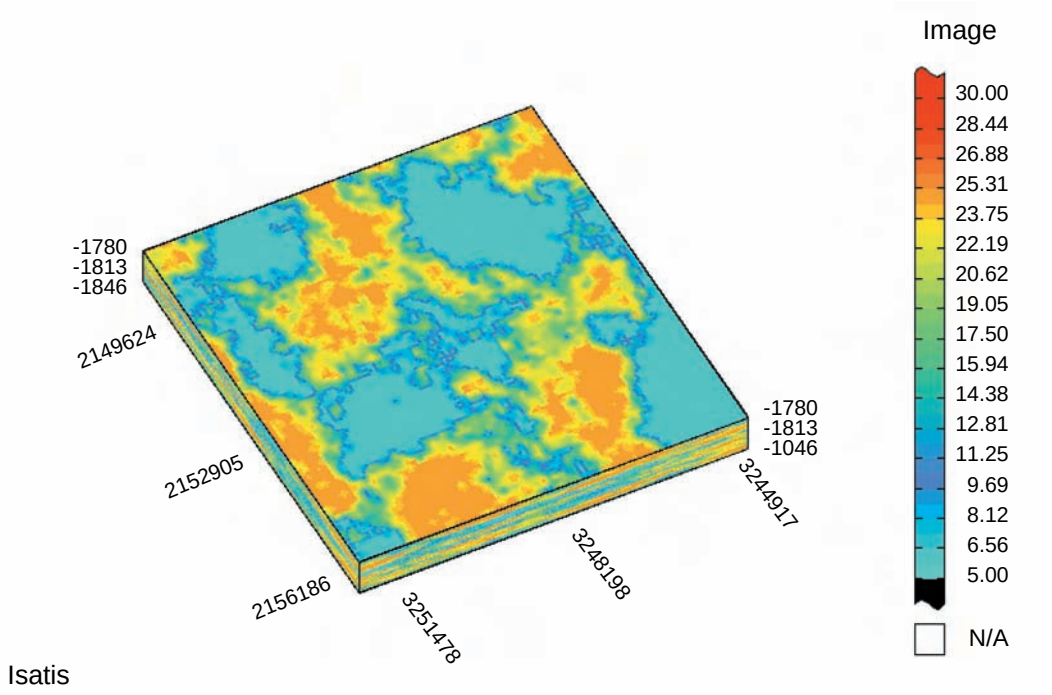

Figure 2-56 *Three-dimensional visualization of the Iola study area. This core-derived porosity model was produced using turning bands simulation. The display shown is the "most likely" realization of a set of 30 simulations. The anisotropic variogram used in the scenario was a nested nugget and spherical combination.*

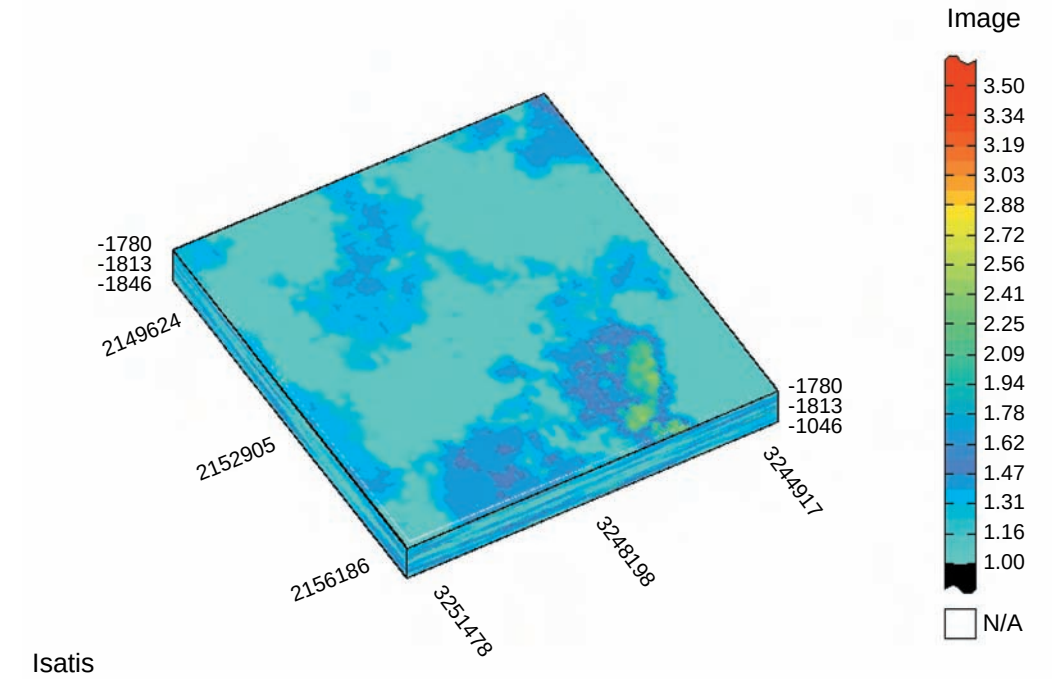

Figure 2-57 *Three-dimensional visualization for the Iola study area. This log_{10} core-derived horizontal permeability model was produced using collocated co-simulation employing the Markov-Bayes assumption. The display shown is the "most likely" realization of a set of 30 simulations. The variogram used in the scenario was similar to the variogram used in the porosity model.*

Olney Field Geologic Model of the Ste. Genevieve Limestone (McClosky Oolite) Reservoir

Reservoirs in this study area are typical of the McClosky member of the Ste. Genevieve Limestone (Mississippian) in the Illinois Basin, wherein production is from elongate oolite shoals arranged *en echelon*. These homogeneous bodies generally reach a thickness of 10 to 15 ft and have an areal extent of approximately 0.40 km (0.25 mi) wide by 3.2 km (2 mi) long. These shoals often are stacked one above another, and productive intervals have been known to coalesce both laterally and vertically. Such shoals are characterized by abundant intergranular porosity accompanied by permeability of as much as 4 darcies (d). The shoals drain well and through primary production and waterflooding often produce up to 50% of OOIP.

The Olney study covers some 9,360,417 m^2 (2,313 acres) in Richland County, Illinois, a portion of the Olney Consolidated Oil Field. Seventy wells penetrate the Ste. Genevieve Limestone within the study area, of which 27 are dry holes and 29 are productive (the remainder are injectors and disposal wells). Five wells were cored in the 1950s; laboratory analysis of the recovered cores yielded 26 porosity and 17 horizontal permeability measurements. Of the five cored wells, four were also logged, although no modern log suites are available.

Based on available wireline logs, sample descriptions, and perforation intervals, two separate oolite shoals were identified within the study area. Where penetrated by wells, the two are everywhere isolated from each other but may well come in contact in the interwell spaces as the minimum separation is <0.61 m (<2 ft). The upper shoal, which has a maximum thickness of slightly >3 m (>10 ft), trends northeast across the northern portion of the study area. The lower shoal is present only along the western edge of the study area. Four wells penetrate both reservoir bodies.

Based on core analyses, porosity in the shoals averages about 17% with a maximum of 20%. Permeability is low compared with other Ste. Genevieve fields studied, reaching a maximum of 0.553 μm^2 (560 md). Non-reservoir limestones encasing the shoals have permeabilities of $<9.86 \times 10^{-3}$ μm^2 (<10 md) and porosities in the range of 9 to 12% (Figures 2-58 to 2-60).

Geostatistical Model

Three-dimensional geostatistical models of both porosity and permeability were built for the Olney study. Porosity was modeled using the turning bands method for stochastic simulation. This approach employs core data in conjunction with histograms and variograms derived from that data to interpolate values at sites where core data were not available. An isotropic spherical variogram was used at Olney to capture the spatial horizontal and vertical continuity of the data. Thirty distinct realizations of the resulting porosity model were produced, all of which honored both the core data and the variogram

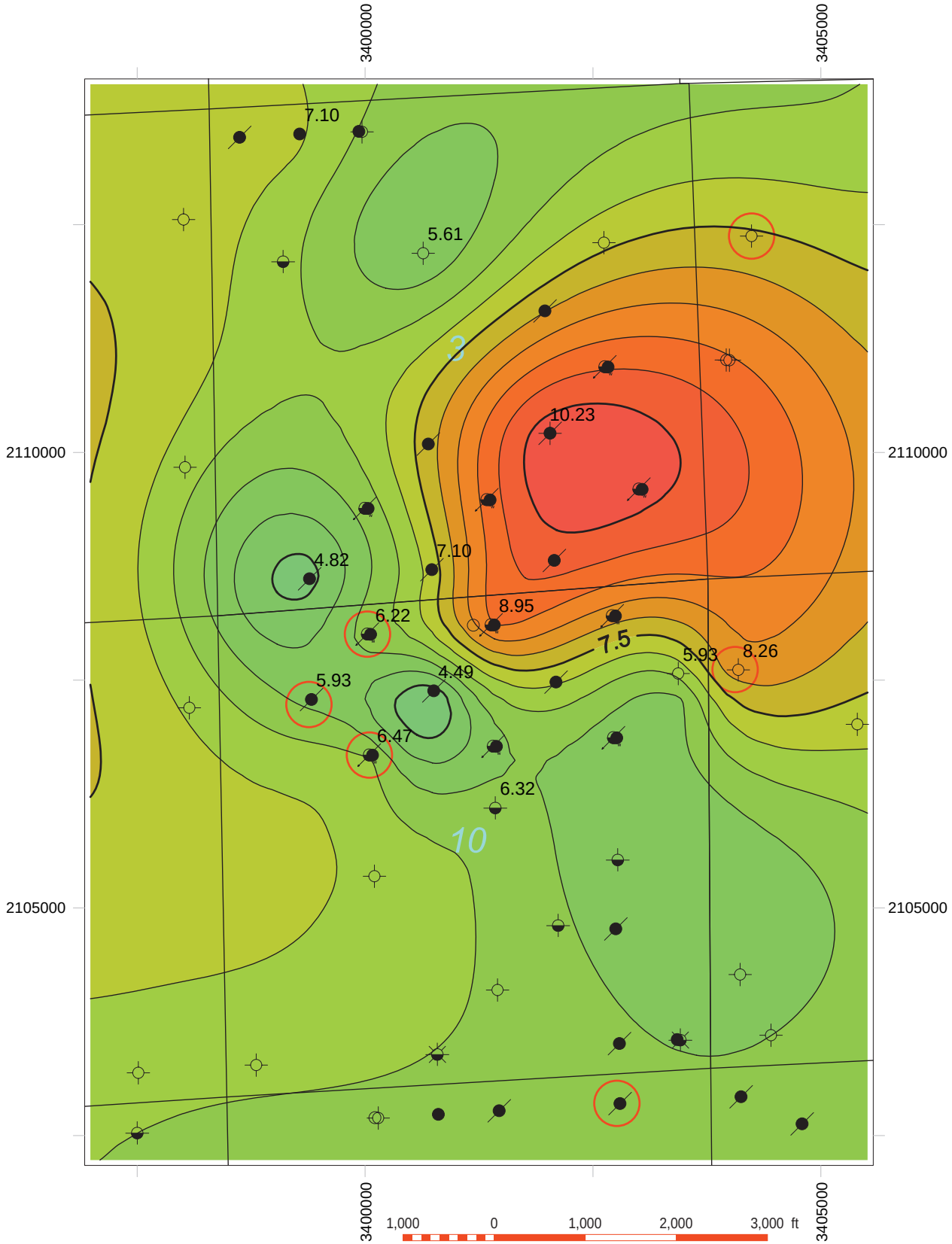

Figure 2-58 *Gross isopach map of upper porosity zone in Ste. Genevieve Limestone, Olney Field study. Contour interval = 0.5 ft. Red circles are cored wells with porosity and permeability measurements.*

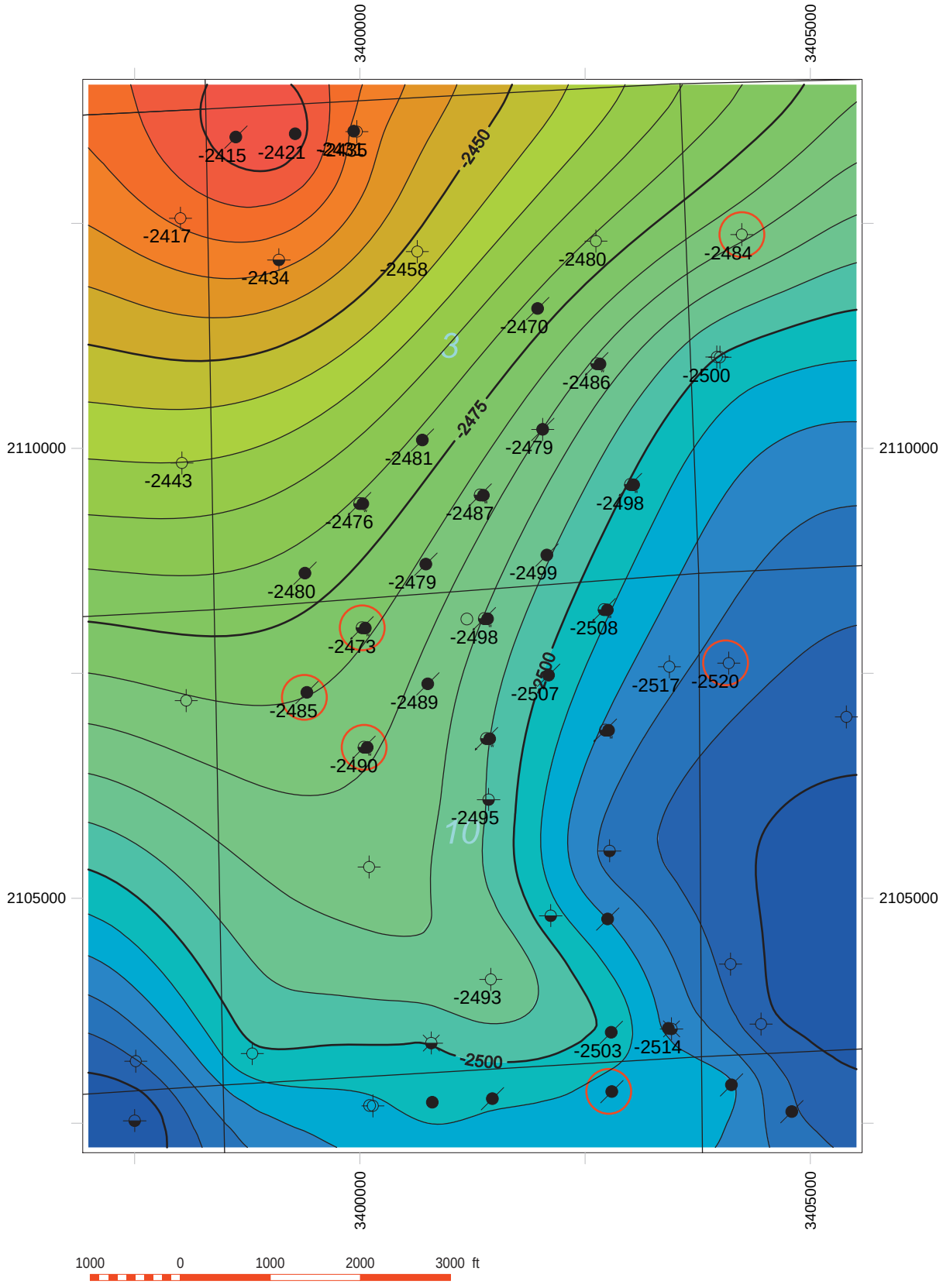

Figure 2-59 *Depth structure map on the top of the Ste. Genevieve Limestone, Olney Field study. Contour interval = 5 ft.*

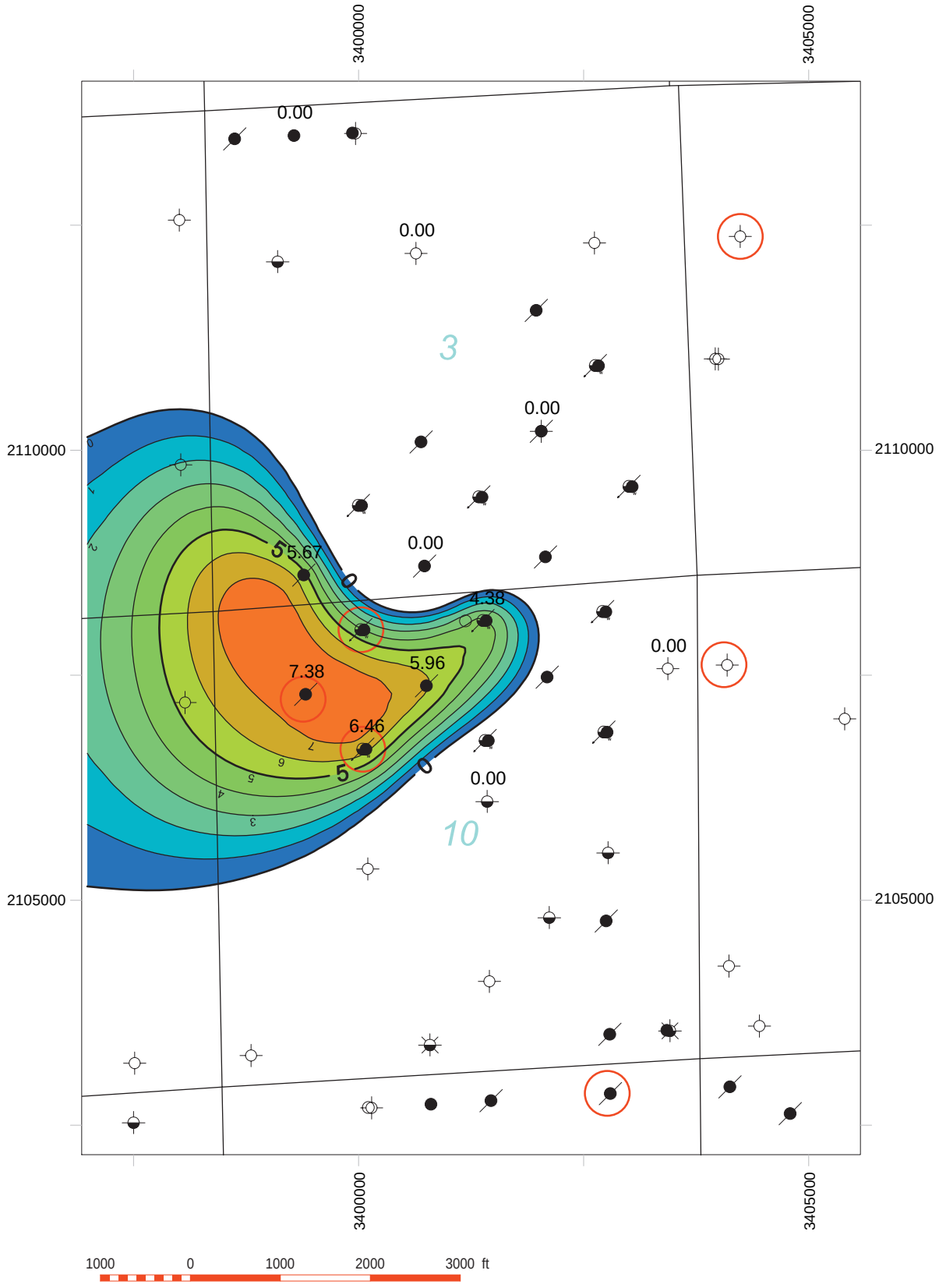

Figure 2-60 *Gross isopach map of lower pososity zone in Ste. Genevieve Limestone, Olney Field study. Contour interval = 1 ft.*

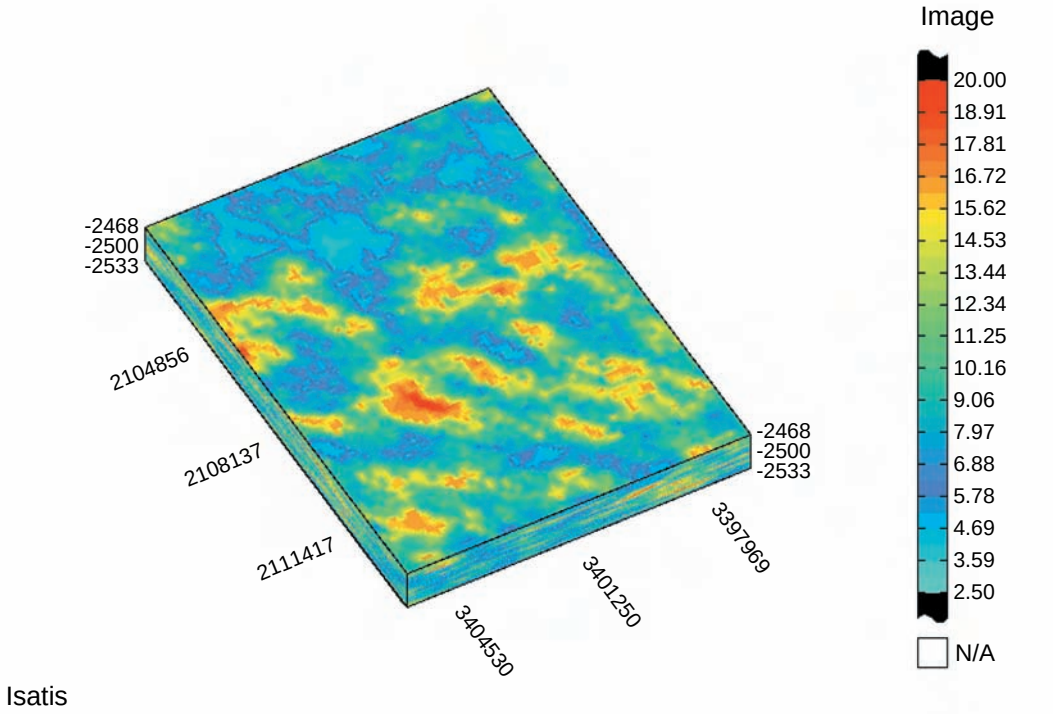

Figure 2-61 *Three-dimensional visualization of the Olney study area. This core-derived porosity model was produced using turning bands simulation. The display shown is the "most likely" realization of a set of 30 simulations. The anisotropic variogram used in the scenario was a nested nugget and spherical combination.*

calculated from that data. These realizations were post-processed to determine the most statistically probable simulation and compared with known data as a final check (Figure 2-61).

A horizontal permeability model was produced using a collocated co-simulation approach with the "most likely" three-dimensional porosity model. Although permeability data were scarce and scattered relative to porosity data, the correlation between porosity and permeability was deemed sufficient to allow use of the porosity model to condition permeability, particularly in those locations lacking permeability data. A variogram derived from the porosity model was used to inform the less populated horizontal permeability data set. The variogram used for permeability simulations was an anisotropic spherical model. This simulation effort also yielded 30 realizations, which were post-processed to determine which realization was the most probable to represent the geologic trends within the site (Figure 2-62).

Johnsonville Field Geologic Model of the Ste. Genevieve Limestone (McClosky Oolite) Reservoir

Reservoirs in this study area are typical of the McClosky member of the Ste. Genevieve Limestone (Mississippian) in the Illinois Basin. Production comes from a series of *en echelon* oolite shoals. These homogeneous elongate bodies usually reach a maximum of 3.0 to 4.6 m (10 to 15 ft) in thickness, with

an areal extent of approximately 0.40 km (0.25 mi) in width by 3.2 km (2 mi) in length along their axes. The shoals are often stacked one above another, and reservoirs occasionally coalesce. Such shoals are characterized by abundant intergranular porosity and high permeability, exceeding 3.948 μm^2 (4 d) in some sections. The shoals drain well and, after primary production and waterflooding, often produce up to 50% of OOIP.

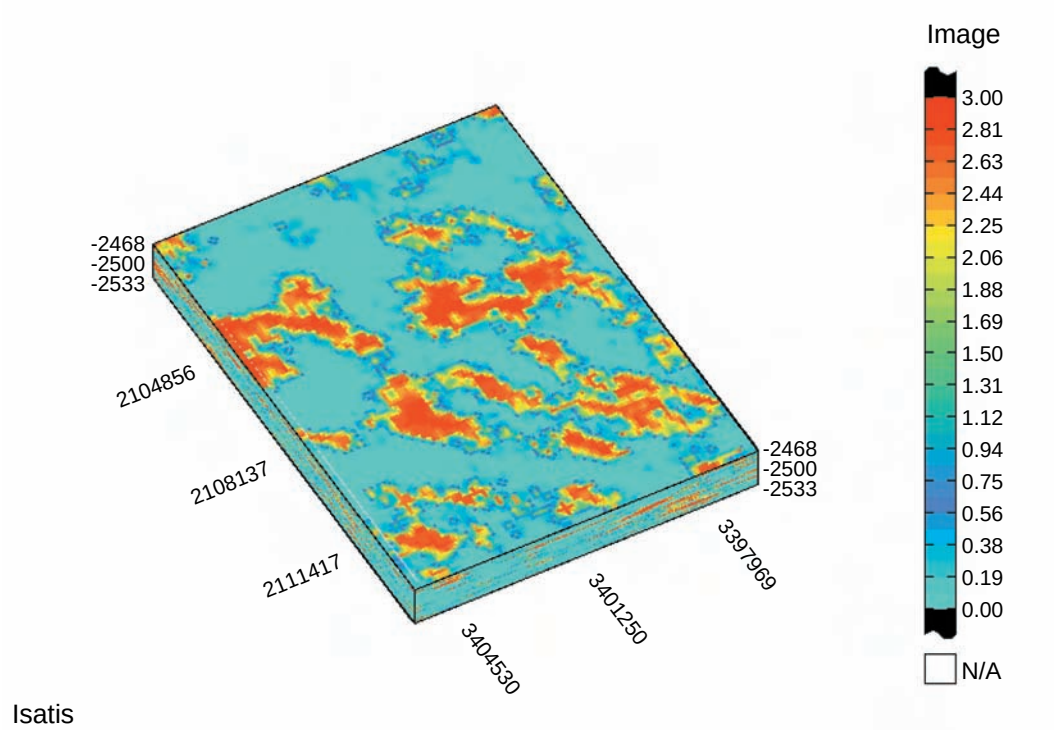

Figure 2-62 *Three-dimensional visualization for the Olney study area. This log_{10} core-derived horizontal permeability model was produced using collocated co-simulation employing the Markov-Bayes assumption. The display shown is the "most likely" realization of a set of 30 simulations. The variogram used in the scenario was similar to the variogram used in the porosity model.*

The study area covers slightly more than two sections (5,301,404 m^2 (1,310 acres)) in Johnsonville Field, Wayne County, Illinois, an area penetrated by 213 wells. Fifteen of the wells are cored, although laboratory studies of the cores have yielded 67 porosity and horizontal permeability measurements. A few of the cored wells also have 1950s-vintage wireline logs, as do approximately 40% of all other wells, although correlation of reservoir intervals from these logs is generally difficult. Core descriptions with detailed lithologic information are available for several of the cores.

The modeled reservoir body is the uppermost shoal in a series of stacked shoals that are encased in relatively impermeable limestone. The relatively large lateral extent of this feature argues for lateral coalescence of two shoals, although no clear-cut boundary is visible in isopach trends based on log picks (Figures 2-63 and 2-64). Measured core permeability in the reservoir interval reach as high as 5.625

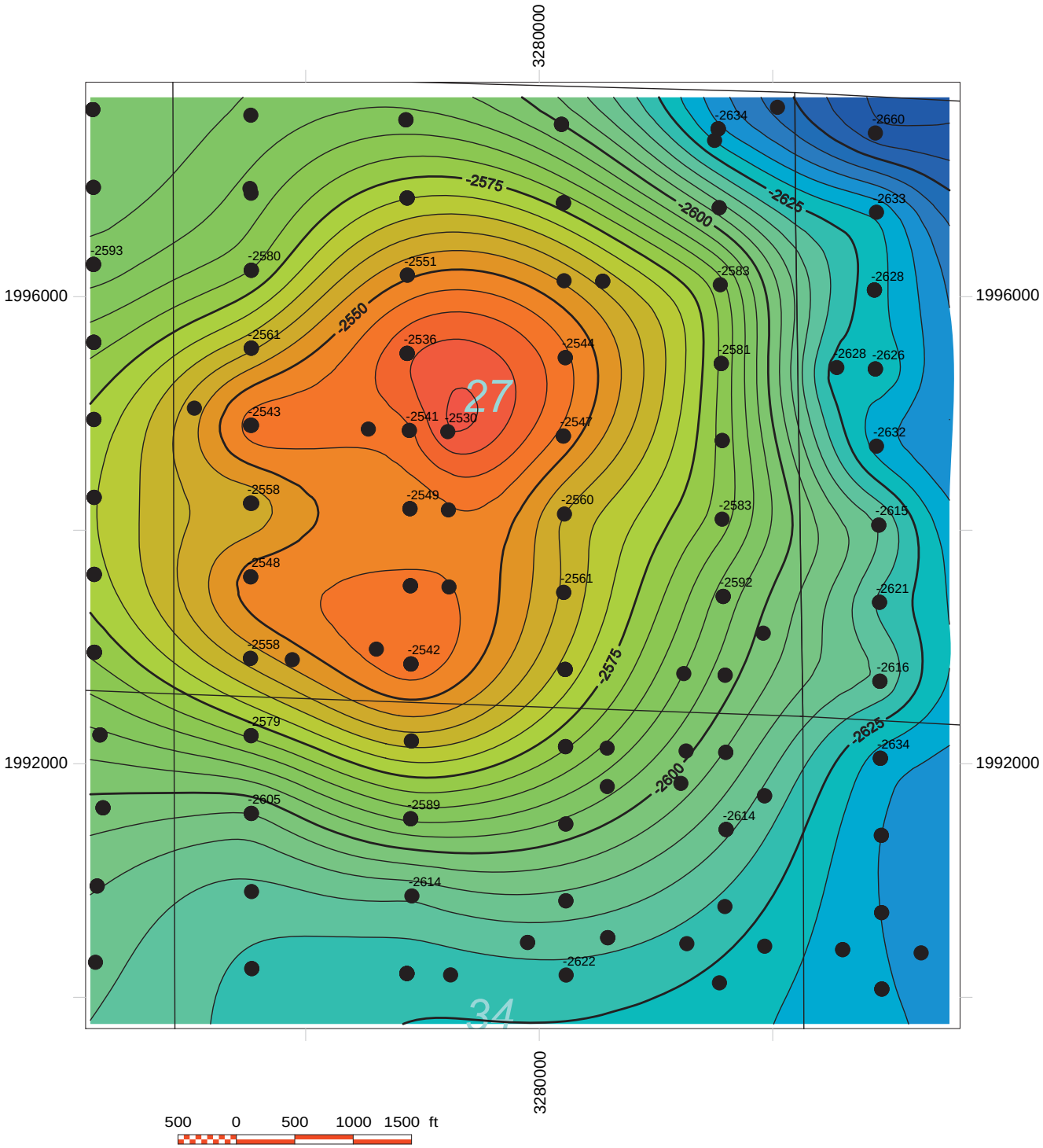

Figure 2-63 *Depth structure map on top of productive zone of Ste. Genevieve Limestone, Johnsonville Field study. Datum = MSL; contour interval = 5 ft.*

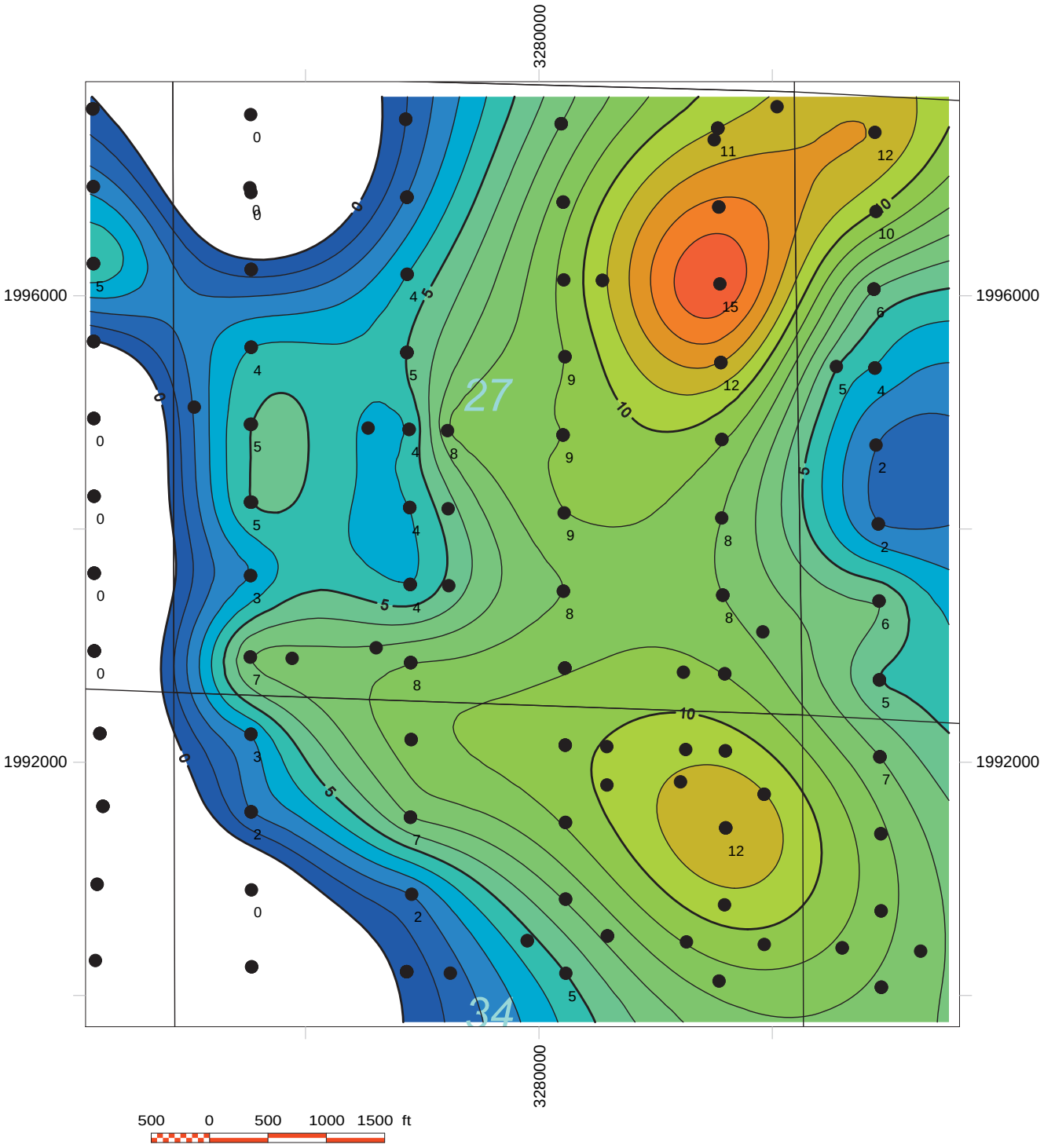

Figure 2-64 *Gross isopach map of the productive zone in the Ste. Genevieve Limestone, Johnsonville Field study. Contour interval = 1 ft.*

μm² (5.7 d) with several individual measurements of >3.948 μm² (>4 d). Measured core porosity reaches a maximum of 22% and averages approximately 20% in high-permeability zones. Non-reservoir facies display permeabilities ranging from $<9.86 \times 10^{-4}$ to 0.0296 μm² (<1 to 30 md) and porosities of 9 to 15%.

Geostatistical Model

For the Johnsonville study, collocated co-simulation was used to construct a three-dimensional geostatistical porosity. This model was conditioned by the modeled thickness within the various flow zones. Co-simulation with isochore was selected based on the observation that porosity varies directly with thickness. Isochore trends also provided a constraint on the model where data were not sufficient to build a conceptual model. Variograms based on a spherical model were constructed with the trends observed in the thickness data. The simulation was repeated for 70 to 100 realizations and then statistically post-processed to determine the most likely representation of the study area (Figure 2-65).

The most likely realization of the porosity model was used to construct a permeability model, following a collocated co-simulation approach. A variogram of the simulated porosity model based on a spherical model was used to produce 100 realizations of the permeability model within the study area. Post-processing was used to determine the most probable representation within the study site (Figure 2-66).

Dale Field Geologic Model of Ste. Genevieve Oolitic Reservoir

Deterministic Model

The reservoir in the study area is typical of production from the McClosky member of the Ste. Genevieve Limestone (Mississippian) in the Illinois Basin. Reservoirs are homogeneous oolite shoals, oriented en echelon and forming stacked reservoirs that occasionally coalesce. These oolite bodies are generally <3 m (<10 ft) thick, 0.4 km (0.25 mi) wide, and their axes 3.2 km (2 mi) long. The shoals are characterized by abundant intergranular porosity and high permeability, reaching 1.579 μm² (2 d) in some sections. The shoals drain well and, after primary production and waterflooding, can produce up to 50% of OOIP.

The Dale Field study area covers an area of 809,375 m² (200 acres), which includes nine wells. Five wells have 50 m (165 ft) of core. Laboratory studies have yielded 165 porosity and horizontal permeability measurements. All cored wells and two uncored wells also have 1950s-vintage wireline logs. Rigorous correlation of reservoir intervals using these logs requires special attention to reservoir geometry.

Two reservoir-quality shoal bodies (upper and lower) that are separated by a relatively impermeable limestone have been identified from the cores (Figures 2-67 to 2-69). Permeabilities in the reservoir interval reach 1.579 μm² (1.6 d), although porosity rarely exceeds 20%.

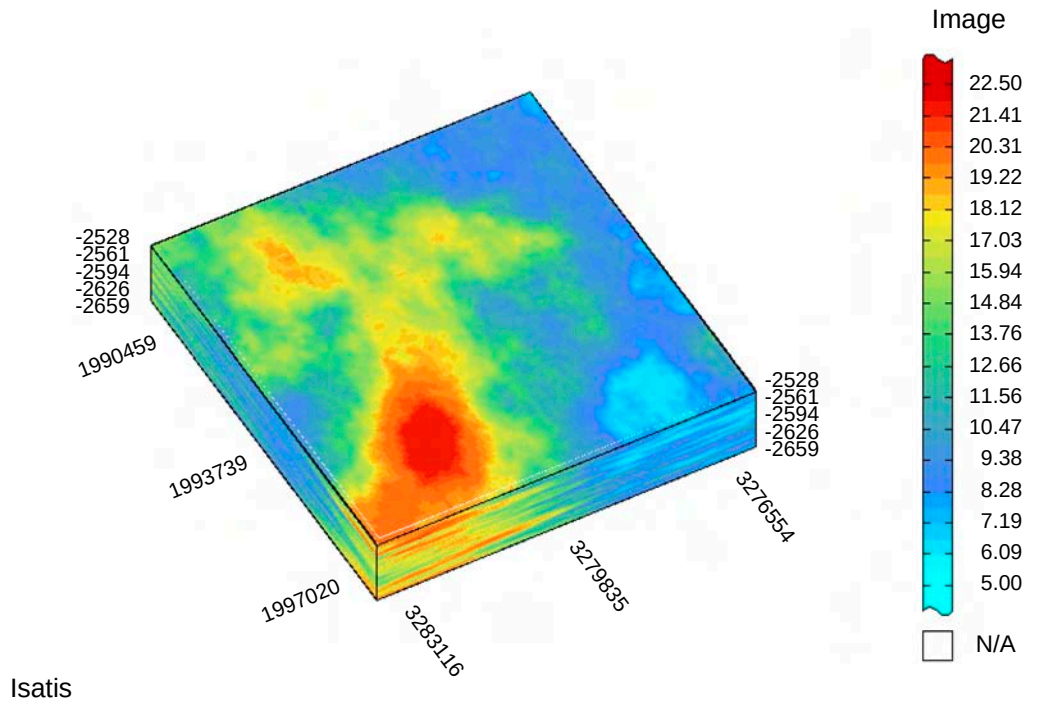

Figure 2-65 *Three-dimensional visualization of the Johnsonville study area. This core-derived porosity model was produced using turning bands simulation. The display shown is the "most likely" realization of a set of 30 simulations. The anisotropic variogram used in the scenario was a nested nugget and spherical combination.*

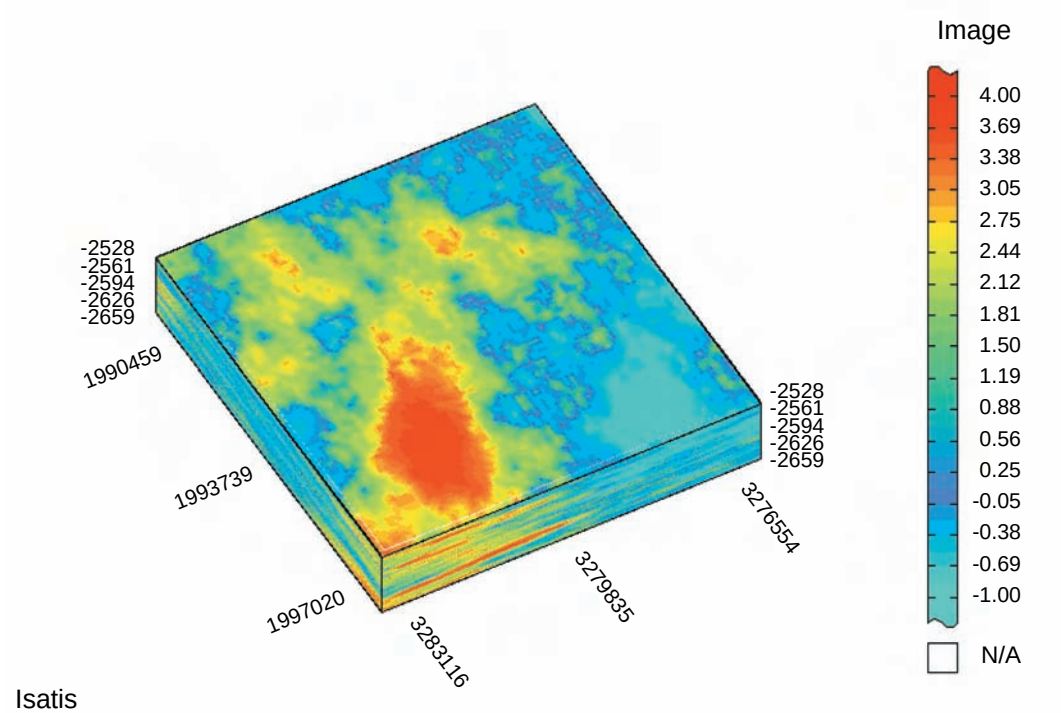

Figure 2-66 *Three-dimensional visualization for the Johnsonville study area. This log_{10} core-derived horizontal permeability model was produced using collocated co-simulation employing the Markov-Bayes assumption. The display shown is the "most likely" realization of a set of 30 simulations. The variogram used in the scenario was similar to the variogram used in the porosity model.*

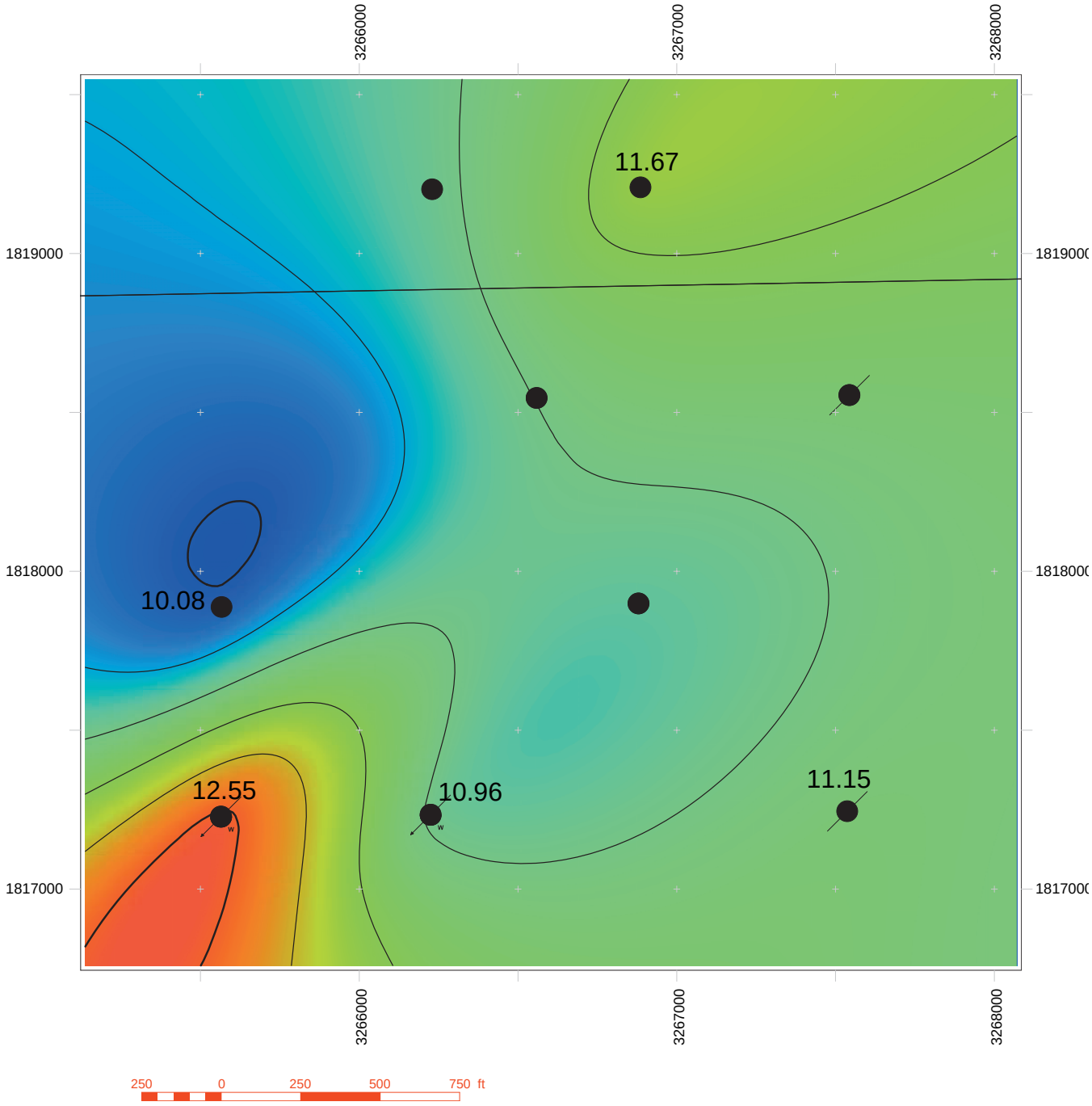

Figure 2-67 *Gross isopach map of the upper porosity zone, Ste. Genevieve Limestone, Dale Field study. Contour interval = 0.5 ft.*

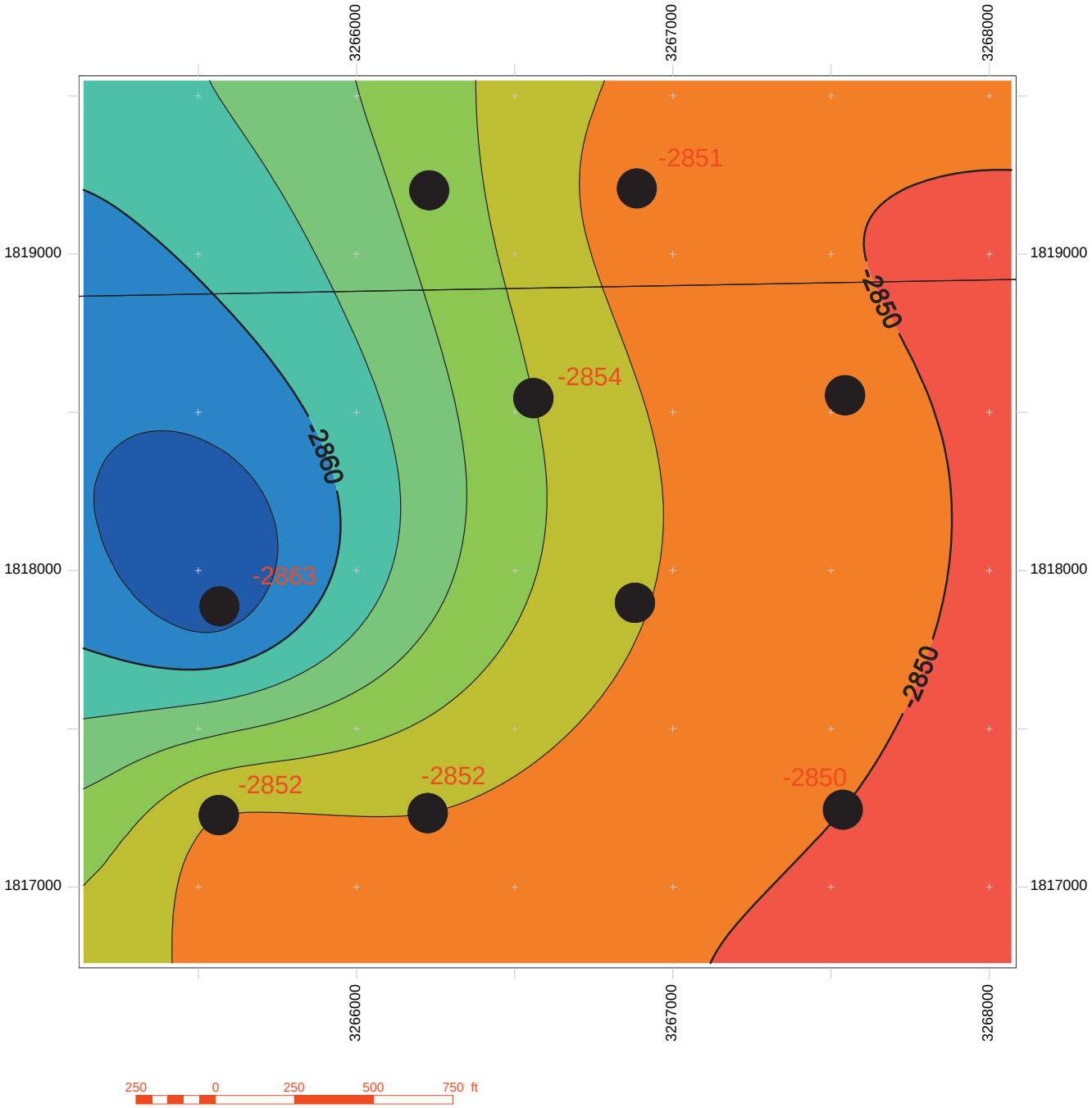

Figure 2-68 *Depth structure map on Ste. Genevieve Limestone, Dale Field study. Datum = MSL; contour interval = 2 ft.*

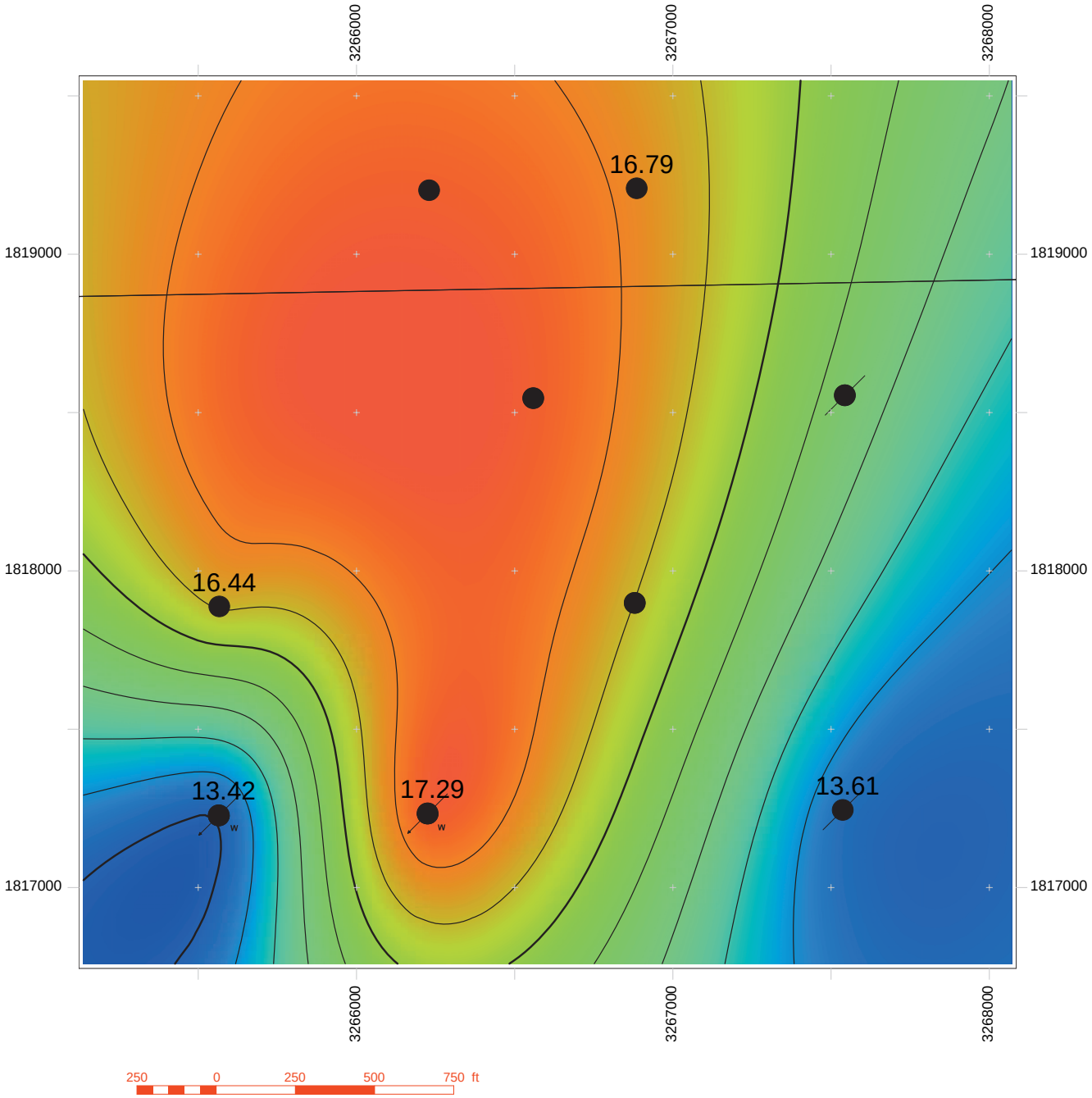

Figure 2-69 *Gross isopach map of the lower porosity zone, Ste. Genevieve Limestone, Dale Field study. Contour interval = 0.5 ft.*

Geostatistical Model

Three-dimensional models were produced for porosity and permeability using a geostatistical approach. Porosity was modeled using a turning bands method of stochastic simulation. This method uses the core data in conjunction with histograms and variograms derived from those data to calculate values at sites where core data were unavailable. In the Dale study, the constructed variogram comprised a nested anisotropic nugget and spherical combination, all calculated based on based on trends observed in the geological model. Thirty distinct realizations of the porosity model were produced, all of which honored both the measured data from cores and the calculated variogram. The combined realizations were then post-processed to determine the most statistically probable simulation and were compared with known data as a final check (Figure 2-70).

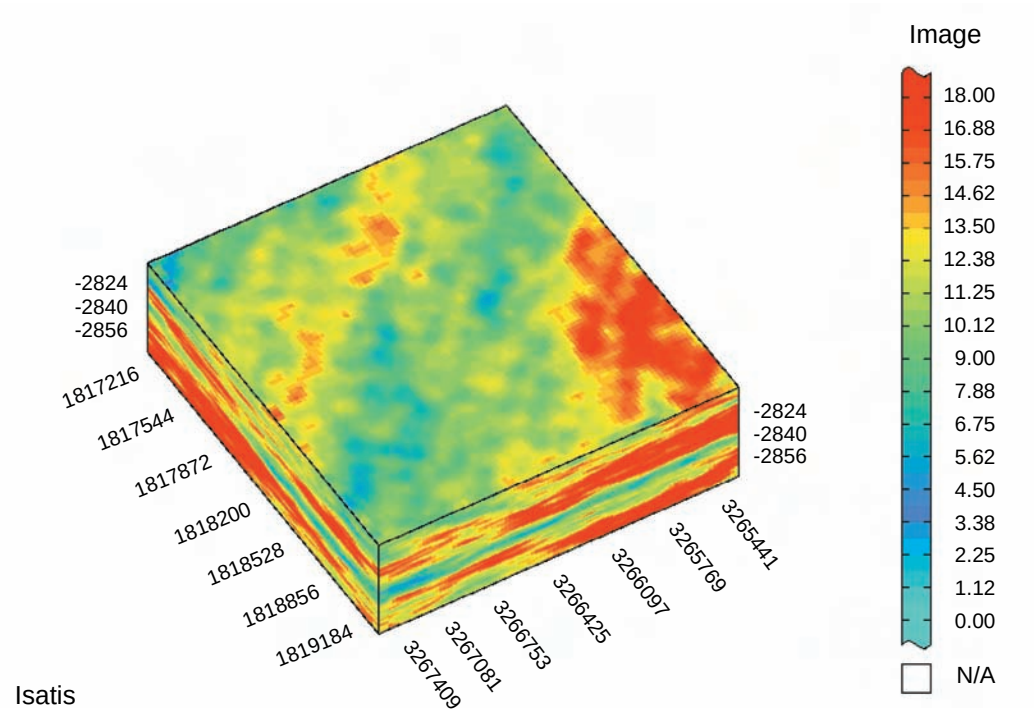

Figure 2-70 *Three-dimensional visualization of the Dale field study area. This core-derived porosity model was produced using turning bands simulation. The display shown is the "most likely" realization of a set of 30 simulations. The anisotropic variogram used in the scenario was a nested nugget and spherical combination.*

A horizontal permeability model was produced using a collocated co-simulation approach with the "most likely" three-dimensional porosity model. The correlation between porosity and permeability was deemed sufficient to allow use of the porosity model to condition permeability, particularly in those locations lacking permeability data. A variogram derived from the porosity model was used to inform the less populated horizontal permeability data set. The variogram used for permeability simulations was an anisotropic spherical model. This simulation effort also yielded 30 realizations that were post-processed statistically to determine which realization was the most probable to represent the geologic trends within the site (Figure 2-71).

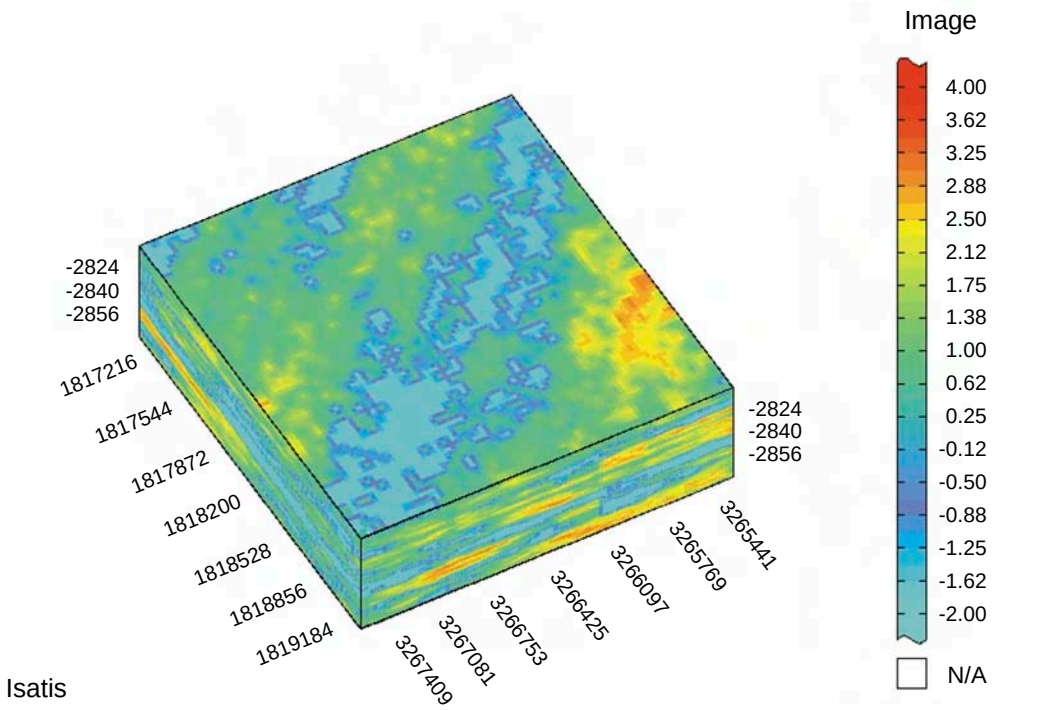

Figure 2-71 *Three-dimensional visualization for the Dale field study area. This log_{10} core-derived horizontal permeability model was produced using collocated co-simulation employing the Markov-Bayes assumption. The display shown is the "most likely" realization of a set of 30 simulations. The variogram used in the scenario was similar to the variogram used in the porosity model.*

Reservoir Simulation Methodology (Subtask 5.5 and 5.6)

The purpose of the geologic and reservoir modeling is to provide estimates of oil recovery and CO_2 storage factors as a consequence of CO_2 EOR. General rules-of-thumb for these factors are available based on West Texas historical observations. An improvement to these rules-of-thumb was desired by modeling specific geologic oil bearing formations in the Illinois Basin to attain recovery and storage factors.

Upscaling

Upscaling techniques were used in this project to calculate effective reservoir properties for a coarse grid scale used in reservoir flow modeling that had blocks several times larger than the fine scale in which the geologic and geostatistical descriptions were generated (Kelkar and Perez, 2002). The grid used to generate the geostatistical models was at a small scale in order to capture variations observed in the cores, logs, and seismic data. However, the resolution of models needed for flow simulation is much coarser due to limitations of time and computer resources.

The approach used to upscale the static property of porosity was the arithmetic averaging technique based on the principle that the pore volume for the coarse grid equals the sum of the pore volumes of the fine grid's cells that fall inside the coarse grid (Kelkar and Perez, 2002). This averaging was done for the three-dimensional geostatistical grid using upScale (a program made by the ISGS staff and students). It produced upscaled two-dimensional layers that could then be imported by Landmark's Gridgen pre-processor to VIP, the reservoir simulation program.

Upscaling the dynamic property of horizontal permeability depended on the relative spatial arrangement of the fine-scale permeability grid as well as anisotropy. Although it is known that none of the reservoirs used in this study are ideal cases, harmonic averaging was used to upscale permeability. Harmonic averaging provides the effective permeability for the case in which the permeability is arranged in series, and it changes only perpendicular to the direction of flow (Kelkar and Perez, 2002). Harmonic averaging of the three-dimensional geostatistical model was also computed using upScale software and then used for flow modeling.

Reservoir Model

West Texas rules-of-thumb for oil recovery and CO_2 utilization (CO_2 storage factors) are specific to historical observations of predominantly miscible CO_2 flooding of the pervasive carbonates of the Permian Basin. The oil reservoirs in the Illinois Basin are dominated by sandstones and are at relatively shallower depths, such that as much as 50% of the OOIP may be considered immiscible to mixing in situ with CO_2.

An improvement from applying the West Texas rules-of-thumb to the Illinois Basin where CO_2 EOR has been found would be to have geologic and reservoir models based on Illinois Basin geology and crude oil properties. The purpose of the reservoir simulations was to obtain CO_2 oil recovery and storage factors as a fraction of the volume of OOIP using geologic models based on the most prolific Illinois Basin oil-producing reservoirs.

For almost all of the reservoirs, actual well locations were used. Wells were omitted when they were too close; these wells were likely redrills or twinned wells. Also, if relatively large areas were void of wells, new wells were located in these areas of the reservoir models. Injection 5-spot patterns were approximated for all of the models with more injectors at the model (no-flow) boundaries where possible so that the pressure at the model edges was relatively higher. In a few instances, existing wells were relocated to complete 5-spots that otherwise resulted in very poor areal sweep efficiency.

The reservoir simulations were designed to reflect general operations and were not specific to any field's production history. As such, the production and development history of all reservoir models was 25 years of primary production (solution gas drive), 40 years of waterflooding, followed by 20 years of CO_2 flooding. The purpose of simulating the primary and waterflooding periods was to create "initial" model conditions to CO_2 flooding in terms of the magnitude and distribution of oil saturation and reservoir pressure.

Each geologic model was simulated at pressures assumed to be immiscible (3,447 kPa (500 psia)) and miscible (10,342 kPa (1,500 psia)) at a reservoir temperature of 32.22°C (90°F). Continuous CO_2 injection and WAG CO_2 injection were modeled for miscible and immiscible floods. As a result, four values of recovery and storage factor were based on a single geologic model.

To ascertain oil-saturated geologic reservoirs only, the GOC and WOC contacts were designated outside of the modeled region. Capillary pressure was not used in these models, as such a constant, initial saturation (35%) was used.

Relative Permeability

The depth, net thickness, porosity, and permeability for each model were included in the geologic model. Net thickness was assumed to be equal to gross thickness. Relative permeability was the only rock property added to the reservoir model. The end points of the oil-water and gas-oil relative permeability curve were selected based on general Basin observations and published waterflooding information.

Irreducible water saturation of 35% was selected based on historical observations from state survey staff. Residual oil saturation to gas and water of 18 and 25%, respectively, was selected based on numerous relative permeability data sets from Honarpour et al. (1986). The residual or trapped gas saturation of 10% was based on Craig's (1993) data collection of minimum or trapped gas saturation in the presence of a waterflood. Craig's reported trapped gas saturation data ranged from about 2 to 20%.

Very little relative permeability data were available. Moreover, there was no obvious way to find a set of relative permeability to represent each geologic formation. Wetability of the predominantly sandstone

formations was expected to be water-wet, so relative permeability data were synthetically generated to mimic water-wet conditions.

The relative permeability to oil at irreducible water was selected as 0.8, and the relative permeability to water at residual oil was selected as 0.3. The gas relative permeability at the irreducible water saturation was 0.9. These relative permeability values use the absolute permeability as a base. A Corey exponent of 3.0 was used for each of the relative permeability data sets.

Fluid Properties

Crude oil, associated (hydrocarbon) gas, CO_2, and water properties were required. The water properties are constant. The water density, viscosity, and formation volume factors were 1.1 g/cm^3 (69 lbm/ft^3), 0.8 mPa · s, and 1.01 rb/stb, respectively. Water and rock compressibility of 2.1×10^{-5} and 3.4×10^{-5} kPa (3×10^{-6} and 5×10^{-6} psi^{-1}), respectively, were used.

The crude oil, associated (hydrocarbon) gas, and CO_2 properties were defined using a five-component Peng-Robinson equation of state. No specific PVT data were available for this study. As such, three oil field operators and engineers were contacted and asked about their historical observations in the Basin with regards to oil viscosity, solution gas-oil ratio, oil formation volume factor, and bubble point pressure (Aman, 2004; Gallagher, 2004; Moore, 2004). The general observation was that oil viscosity was 2 to 4 mPa · s, solution gas oil ratio was near 26.7 up to 62.3 m^3/m^3 (150 up to 350 scf/stb), oil formation volume factor was 1.05 to 1.15 rb/stb, and bubble point pressure was 1,379 to 5,515 kPa (200 to 800 psia). There were notable exceptions to each of these values, which represented generalization of PVT properties of Illinois crude oils. Published data supported these ranges (Sims, 1993).

A four-component Peng-Robinson equation of state was first attempted (Phillips, 2004) to simulate a medium API gravity crude oil using the Lohrenz, Bray, and Clark oil viscosity correlation (Lohrenz et al., 1964). The components were CO_2, methane, hexane, and octadecane. The mole fraction of each was changed to match the observed PVT properties without drastically changing the respective mole fraction of each pseudo-component too much from that expected of a medium-gravity crude oil. However, oil viscosity in the observed range was not achievable, so a fourth hydrocarbon pseudo component (ethane) was added, and the Pederson oil viscosity correlation was used. Mole fractions for CO_2, methane, ethane, hexane, and octadecane of 0.01, 0.08, 0.12, 0.13, and 0.66, respectively, were used to give PVT properties in the desired range of historical observed values, including a bubble point pressure near 3,447 kPa (500 psia).

Well Configuration

Wells were simulated as constant rate with a bottom-hole flowing pressure constraint as such wells attempted to produce or inject the specified concentrate while honoring the specified bottom-hole flowing pressure. For producers, if the bottom-hole flowing pressure fell below the specified bottom-hole flowing pressure, the wells' production rate fell below the specified production rate. For injectors, if the bottom-hole injection pressure moved above the specified bottom-hole injection pressure, the wells' injection rate fell below the specified injection rate.

For oil producers, a total liquid rate was used that represented the pumping capability of a pumping unit; 40 m^3 (250 stb) of liquid per day was used with a 345 kPa (50 psia) bottom-hole flowing pressure. For water injection during the waterflood, 5,516 and 16,547 kPa (800 and 2,400 psia) were used for the immiscible and miscible cases, respectively. A maximum rate of 79 m^3 (500 barrels) of water per day injected was used.

During CO_2 injection, the same bottom-hole pressure constraints of the waterflood were used and 14.2 million m^3/day (500 million standard cubic feet per day (million scf/day)). Because of the mathematical stability of the simulation runs and to decrease the time of a simulation, a gas production rate of 12.7 million m^3/day (450 million scf/day) was imposed. (This rate was 90% of the maximum rate of 14.2 million m^3/day (500 million scf/day) and was intended to reduce the cycling of gas and maintain a reservoir pressure in the desired classification of miscible on immiscible.) All wells were perforated/completed in all model layers, regardless of their status as a producer or injector.

Simulation Settings

Most models were attempted with IMPES (implicit pressure, explicit saturation). The full implicit method was used when IMPES was unsuccessful or was projected to have lengthy model run times. A minimum time step of 0.01 days was allowed; maximum was 100 days. The pressure maximum of 3,447 kPa (500 psia) was used for fully implicit, and 2,068 kPa (300 psia) was used for IMPES. Maximum saturation and composition changes of 0.1 were used. Defaults of other required VIP numerical solution variables were used.

Reservoir Simulation Results

Primary and Waterflooding Oil Recovery

No specific history matching was attempted for any of the nine geologic models. However, because of the pressure and rate constraints at wells, general Basin observations on rate were modeled. No effort was made to optimize primary oil recovery separately from waterflood oil recovery, because the purpose of modeling the primary and waterflooding periods preceding the CO_2 floods was to provide "initial"

conditions to the CO_2 flood with respect to volume of oil in place and the distribution of the oil. Mast and Howard (1991) approximated the total oil recovery from those oil reservoirs that were waterflooded as 48%.

The SIMRESULTS post-processing module of VIP directly provided the value of total primary and waterflooding oil recovery. The lower pressure cases (for immiscible CO_2) gave total primary and waterflooding oil recovery of 42%, and the higher pressure (for miscible CO_2) cases gave 45% total primary and waterflooding oil recovery. For the lower pressure simulations, the Aux Vases, Cypress, and St. Genevieve recoveries were 40, 42, and 45%, respectively. For the higher pressure simulations, the Aux Vases, Cypress, and St. Genevieve recoveries were 43, 45, and 46%, respectively. The differences between the lower and higher pressure cases are inconsequential and show only that the models' total oil recovery was not in excess of Basin observations.

CO_2 Enhanced Oil Recovery

CO_2 injection immediately followed the waterflood. Two CO_2 injection schemes were simulated: continuous CO_2 injection and WAG. Continuous CO_2 was uninterrupted CO_2 injection, whereas WAG was injected on an annual basis with CO_2 injection the first year and water injection the second year, alternating each year until the last year of simulated 20 years of CO_2 injection. Each of these injection schemes was studied for immiscible and miscible CO_2 flooding (500 and 1,500 psia, respectively).

The CO_2 oil recovery factor was given directly via the SIMRESULTS module of VIP for each geologic model. The immiscible simulated CO_2 flood incremental oil recovery ranged from 4.5 to 7.1%, and the miscible floods ranged from 8.6 to 16% incremental oil recovery. The arithmetic averages by formation are shown in Table 2-8. The average for all nine models was 5.9 and 12% (11.5) for immiscible and miscible, respectively. When averaged, there was very little difference between continuous and WAG CO_2; however, a general observation was made that WAG had higher oil recovery when injector/producer patterns were more uniform; conversely, continuous CO_2 had higher oil recovery with irregularly arranged injection/producer patterns. In general, the modeled oil recovery was highest for the Ste. Genevieve models. The Cypress models gave the lowest oil recovery regardless of miscibility type or injection scheme.

CO_2 Storage

The CO_2 storage factor was not available directly from VIP post-processing programs but was calculated from gas and oil production results. The storage factor (SF) was mathematically defined as

$$SF = (RF)(U_N) \qquad [7]$$

Table 2-8. CO_2 oil recovery and storage factors estimated from VIP compositional simulation. Each recovery factor is the arithmetic average of the three geologic models simulated for each formation type. Net utilization is given also.

Geologic formation	Miscibility type	Injection scheme	CO_2 oil recovery factor (%)	CO_2 net utilization, (thousand scf/stb[1])	CO_2 storage factor (tonnes/thousand stb[2])
Aux Vases	Immiscible	Continuous	6.6	2.7	9.6
		Wag	6.2	1.7	5.7
	Miscible	Continuous	12	8.4	55
		Wag	12	4.9	30
Cypress	Immiscible	Continuous	5.4	2.9	8.3
		Wag	5.1	1.8	5.0
	Miscible	Continuous	9.9	8.5	45
		Wag	9.8	5.0	26
St. Genevieve	Immiscible	Continuous	6.1	3.4	11
		Wag	5.8	1.5	4.7
	Miscible	Continuous	14	7.6	56
		Wag	11	5.0	30
Average	Immiscible	Continuous	6.0	3.0	9.6
		Wag	5.7	1.7	5.1
	Miscible	Continuous	12	8.2	52
		Wag	11	5.0	29

[1] stb, produced barrel of oil.
[2] stb, barrel of original oil in place.

The oil recovery factor (RF) was direct output from SIMRESULTS (described in the previous section). Net utilization (U_N) was defined as the ratio of CO_2 injected to incremental oil produced; however, the CO_2 injected term was modified to reflect any produced CO_2. Cumulative CO_2 injection was given directly from the JOB STATUS window of the main VIP module. Produced CO_2 was not an output; consequently, the incremental cumulative total gas production was used (cumulative total gas produced at the end of CO_2 less the cumulative total gas produced at the end of waterflooding). This assumed that associated gas was very low compared to CO_2 production; hydrocarbon gas production is very low due to the naturally low solution gas-oil ratios of Illinois Basin crude oils. Moreover, after 25 years of primary depletion, very little gas remained in the modeled reservoirs.

The numerator of the net utilization is the difference between the cumulative CO_2 injected and the incremental total gas produced. The denominator of the net utilization is the cumulative oil production at the end of the CO_2 flood minus the cumulative oil produced following the simulated waterflood. The immiscible flood net utilizations (0.25 to 0.96 m^3/m^3 (1.4 to 5.4 thousand scf/stb)) were less than those for miscible flooding (0.82 to 1.6 m^3/m^3 (4.6 to 9.2 thousand scf/stb)). Table 2-8 has the average net utilization and storage factors. Continuous CO_2 stored nearly twice the CO_2 as the WAG process, which is consistent with the fact that the WAG process injects CO_2 for about half the time of the continuous CO_2 injection process.

A preliminary, but substantial finding is that while immiscible flooding recovers one third to one half the oil volume compared with recovery from miscible flooding, it may take as little as 15% of the CO_2 that the miscible flooding requires to produce a stock tank barrel of oil. The field pilots for Phase II will be designed to substantiate this computational finding.

Comparison to West Texas Rules-of-Thumb

The Illinois Basin geologic modeling-based miscible CO_2 oil recovery factors were validated with the two rules-of-thumb for CO_2 oil recovery factor, 10% of OOIP and 25% of primary plus waterflooding production. The miscible recovery factors averaged 11.5% compared with 10% for the West Texas rule-of-thumb. The ratio of CO_2 oil recovery to the sum of primary and waterflooding oil production ranged from 22 to 31%, arithmetic average was 25%, which is identical to the West Texas rule-of-thumb.

The Illinois Basin geologic modeling-based immiscible CO_2 oil recovery factors were much lower than the rules-of-thumb; these rules-of-thumb are based on miscible flooding, not immiscible flooding. The average ratio of CO_2 oil recovery to the sum of primary and waterflooding oil production was 14%, which is consistent with the lower oil production of immiscible flooding.

The storage factors corresponding to the recovery and utilization numbers are shown in Table 2-8. A CO_2 specific density of 18.850 thousand scf/tonne was used to convert from standard volume (scf) to mass (tonne).

Basin-wide Assessment

This study focuses on the potential utility of CO_2 flooding for EOR in the Illinois Basin. Specifically, the study addresses calculation of the amount of CO_2 that could be removed from the environment and stored in mature oil fields and the quantity of additional hydrocarbons potentially recovered through CO_2 flooding.

As a starting point, total OOIP for the Illinois Basin was calculated using computer-based volumetric calculations. This new methodology yielded a revised estimate for OOIP of 2.24 billion m^3 (14.1 billion stb), an increase of 0.33 billion m^3 (2.1 billion stb) (17.5%) beyond previous estimates. Of that total, geographic and geologic analyses indicate that 46% of the reservoir volume in the basin falls within or near the miscible pressure-temperature regime for CO_2 (Figures 2-2 to 2-3).

Presentations (Subtask 5.7)

Frailey, S. 2005. Oil reservoirs: CO_2 storage and EOR. MGSC PAG meeting, September 13, Urbana, IL.

Knepp, R., D. Garner, S. Frailey, B. Seyler, J. Grube, D. Keefer, and S. Rittenhouse. 2005. Sequestration of carbon emissions in geologic formations: Enhanced oil recovery. 4th Annual Conference on Carbon Capture and Sequestration, May 2005, Alexandria, VA.

Leetaru, H., S. Rittenhouse, S. Frailey, D. Keefer, D. Morse, R. Finley, and J. McBride. 2005. Sequestration of carbon emissions in geologic formations: Saline aquifers. 4th Annual Conference on Carbon Capture and Sequestration, May 2005, Alexandria, VA.

From the reservoir modeling, an oil recovery attainable through use of CO_2 flooding ranges from 0.14 to 0.21 billion m^3 (0.86 to 1.3 billion stb) (Table 2-9). Based on the net utilization estimated from the reservoir models, 140 to 440 million tonnes (154 to 485 million tons) can be sequestered as a consequence of CO_2 EOR in the Illinois Basin. West Texas-based rules-of-thumb gave 0.16 to 0.19 billion m^3 (1.0 to 1.2 billion stb) for EOR and 310 to 620 million tonnes (342 to 683 million tons) for CO_2 storage estimates. Overall, the geologic and reservoir modeling gave results consistent with the historical bases West Texas rules-of-thumb. Figures 2-4 and 2-11 show the geographical distribution of CO_2 and EOR and storage in the Basin.

Table 2-9. Basin assessment of CO_2 storage and EOR ascertained via the oil recovery and CO_2 storage factors by miscibility type. Factors were applied by field using the updated value of 14.1 billion stb OOIP using the miscibility type designated.

Condition	CO_2 storage (million tonnes)	EOR (billion stb)
Miscible	58–180	0.24–0.38
Near miscible	53–153	0.28–0.40
Immiscible	29–110	0.34–0.49
Total	140–440	0.86–1.3

Saline Reservoirs as a Sequestration Target

Introduction

The Illinois Basin offers diverse opportunities for the geologic sequestration of carbon dioxide (CO_2). This report contains a synthesis and reinterpretation of the existing well and seismic data that apply directly to sequestration potential in coal beds, oil reservoirs, and deep saline formations. The lessons derived from the study of analogs in natural gas storage for carbon sequestration is particularly important with respect to geologic risk, storage, validation, and prediction of reservoir distribution and performance.

The Illinois Basin has numerous, vertically stacked, geologic formations that could be good CO_2 sequestration sinks. In addition, there are numerous geologic formations (seals) that would vertically impede or stop vertical flow of CO_2 into shallow, near-surface aquifers or the atmosphere.

The Pennsylvanian coal beds in the Illinois Basin are continuous across large areas of the Basin. These beds are currently an active exploration target for coal bed methane. CO_2 can be sequestered in coal strata as part of a coal bed methane CO_2 sequestration project, potentially enhancing the methane recovery rate. Because CO_2 is readily adsorbed by coal, the coal beds could also be considered an important secondary seal, trapping any CO_2 that might escape the primary reservoir and seal.

The Mississippian age oil reservoirs are the most prolific Basin oil reservoirs and contribute 80% of Illinois, Indiana, and Kentucky's oil production. Carbon dioxide could be sequestered in oil reservoirs as part of an enhanced oil recovery program. Because the seals within these Mississippian age oil reservoirs have trapped oil and gas for approximately 260 million years, they should be good seals for CO_2. Carbon dioxide can be sequestered not only in the oil reservoirs but also in the saline water-bearing parts beneath the reservoir. Mississippian age oil fields have been successfully used for natural gas storage in Illinois, Indiana, and Kentucky for more than 50 years (Griffith and Rinehart, 1971; Buschbach and Bond, 1973).

The deep saline reservoirs offer the greatest potential for sequestration of CO_2. The three most important are the Ordovician age St. Peter Sandstone and Cambrian age Ironton-Galesville Sandstone and Mt. Simon Sandstone reservoirs (Figure 3-1). The St. Peter Sandstone is an important aquifer in northern Illinois. It is porous and permeable across most of Illinois but rapidly pinches out in Indiana and Kentucky. The St. Peter has been used for natural gas storage and could be used for CO_2 sequestration in the south-central part of the Basin where the formation fluid is saline. The Ironton-Galesville is present only in the northern part of Illinois and would not be a good reservoir in which to inject CO_2 because of its importance as a source of potable freshwater.

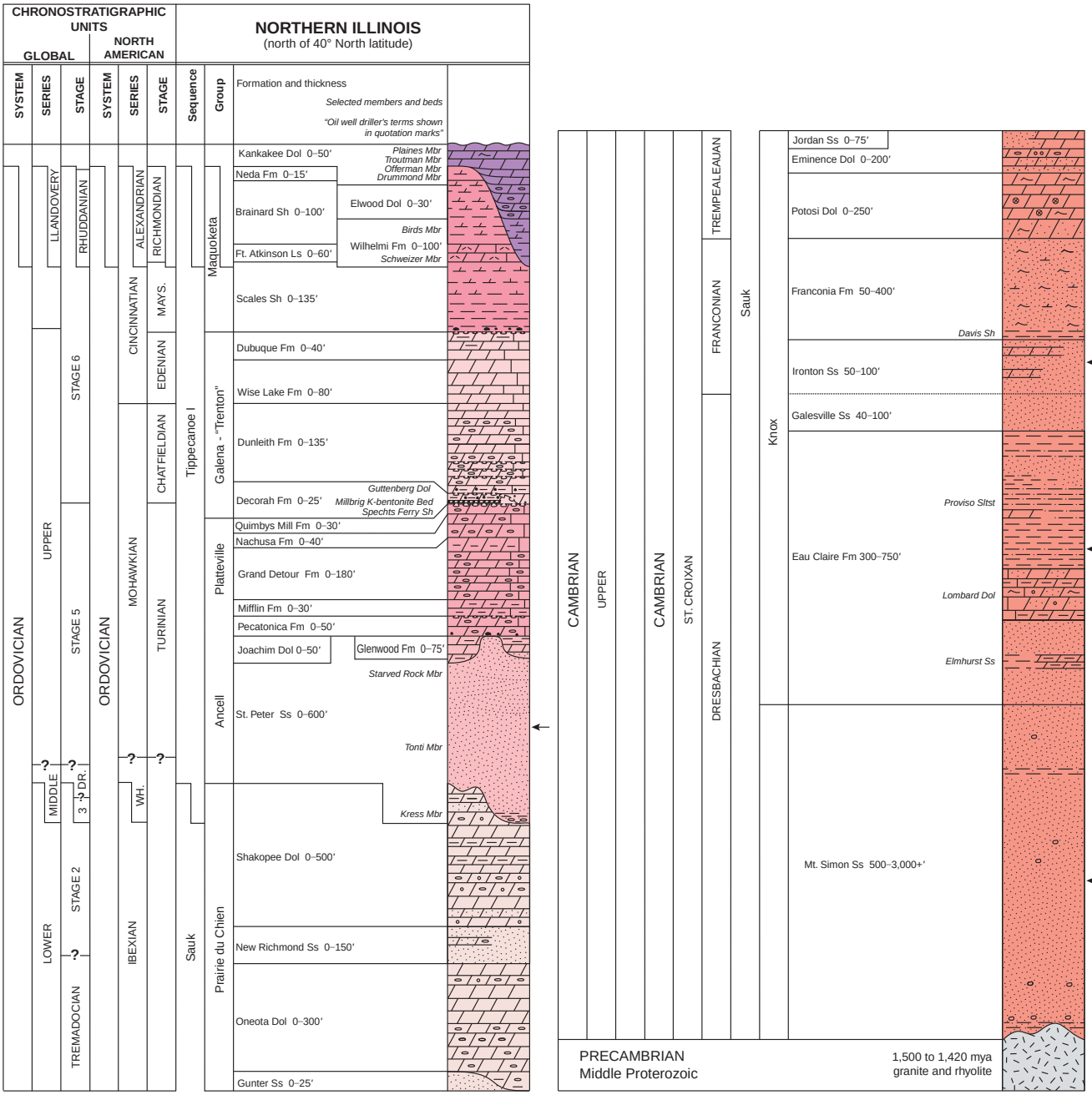

Figure 3-1 *Stratigraphic column of Ordovician through Precambrian rocks in northern Illinois (Kolata, 2005). Arrows point to the formations discussed in this report. Dr., Darriwillian; Dol, dolomite; Fm, formation; Ls, limestone; MAYS., Maysvillian; Mbr, Member; Sh, shale; WH., Whiterockian; Mya, million years ago; Ss, sandstone; Silts, siltstone.*

The Mt. Simon Sandstone underlies all of the Illinois Basin except in local areas where it failed to cover paleohighs on the Precambrian surface. The Mt. Simon attains a maximum thickness of 792 m (2,600 ft) in east-central Illinois and west-central Indiana and is an ideal target for sequestration. The Eau Claire Formation, directly overlying the Mt. Simon, provides the primary seal that will prevent CO_2 migration into shallower formations.

The Illinois Basin has the largest number of saline natural gas storage fields in the United States (Figure 3-2). These gas storage fields provide important analogs that can be used to analyze the potential for CO_2 sequestration. These analogs illustrate seal integrity, injection capability, storage capacity, and reservoir continuity. The long history (almost 50 years) of successful natural gas storage in the Mt. Simon and St. Peter formations demonstrates that these two saline reservoirs could provide successful containment of CO_2 sequestration and that further detailed evaluation is warranted.

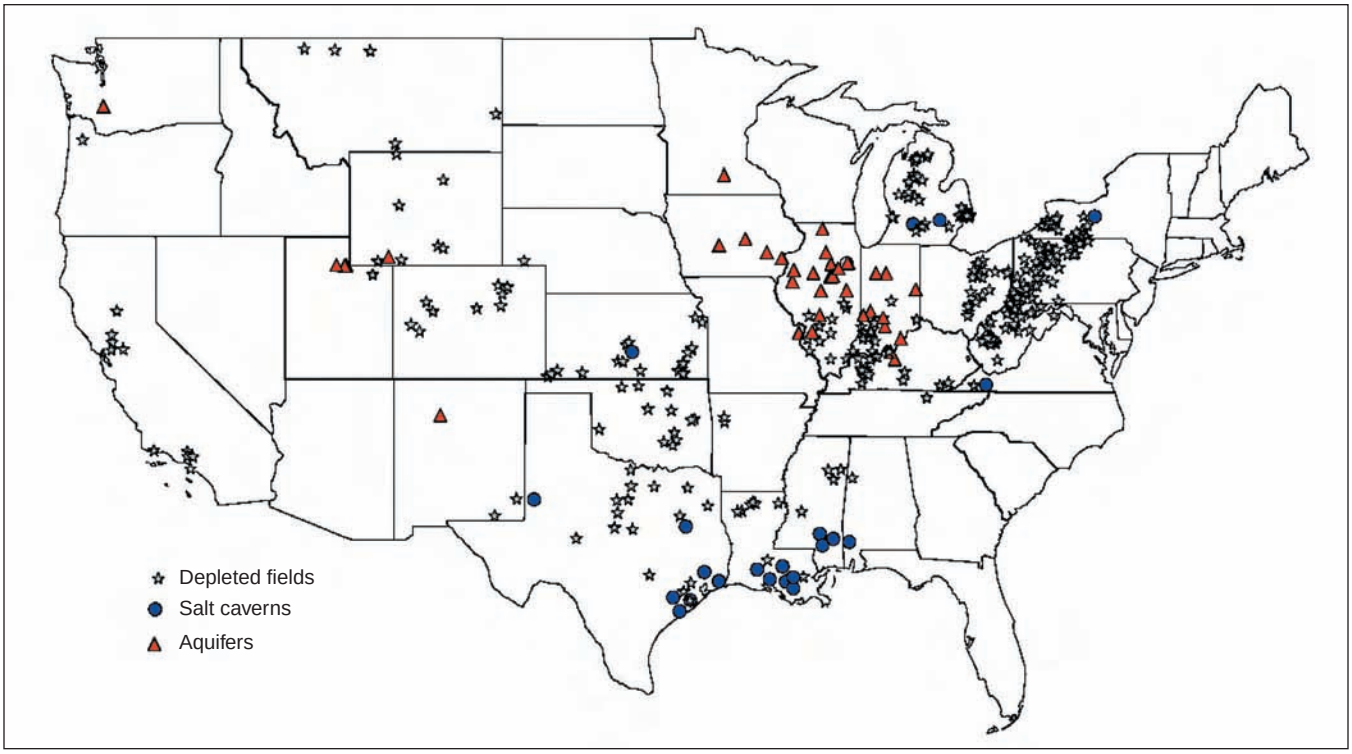

Figure 3-2 *Location of underground natural gas storage facilities in the United States (EIA, 2004).*

Regional Structure

The Illinois Basin covers an area of approximately 349,648 km^2 (135,000 mi^2) and includes parts of three states—Illinois, Indiana, and Kentucky. The Basin is bounded by the Wisconsin Arch to the north, the Kankakee Arch to the northeast, the Cincinnati Arch to the east, the Pascola Arch to the south, the Ozark Dome to the southwest, and the Mississippi River Arch to the northwest (Figure 3-3). Some of these arches and domes, such as the Ozark Dome, have been persistent high areas since at least Ordovician time and may have been paleohighs in the Cambrian (Bell et al., 1964). The Kankakee Arch is a broad structure that differentiates the Illinois and Michigan Basins and connects the Wisconsin Arch to the northwest with the Cincinnati Arch to the southwest.

The La Salle Anticlinal Belt is a series of en echelon folds that extend from Lawrence County in the southeastern part of Illinois to Lee County, Illinois, to the north. Significant fault systems occurring in the Illinois Basin are the Cottage Grove, Wabash Valley Fault System (WVFS), the Rough Creek-Shawneetown Fault System, and the Du Quoin Monocline (Figure 3-4).

Recent reflection seismic lines show the Du Quoin Monocline to be formed by deep-seated faulting occurring below the New Albany; above the New Albany, the strata are folded. The Du Quoin Monocline and related structural features are >96.6 km (>60 mi) in length.

The Cottage Grove Fault System is a strike-slip series of faults that extends over 120 km (75 mi) in an east-west direction across southern Illinois and Kentucky. There may be as much as 61 m (200 ft) of vertical displacement (Nelson, 1981; Duchek et al., 2004), and the fault zone is commonly 6.4 to 8 km (4 to 5 mi) wide. The Cottage Grove Fault System appears to be a demarcation between oil-producing strata to the north and non-hydrocarbon–containing strata to the south of the fault system (Figure 3-5). No sequestration test projects are likely to be located south of the Cottage Grove Fault System.

The WVFS lies in southeastern Illinois along the boundary between the states of Illinois and Indiana (Figure 3-4). The system is about 96.6 km (60 mi) long and 24 km (15 mi) wide, and individual faults can have up to 146 m (480 ft) of vertical displacement (Nelson, 1981). The Wabash Valley is an active area for recent faulting, as documented by the earthquakes epicenters (Figure 3-6).

The Rough Creek-Shawneetown Fault Zone is south of the potential areas for sequestration but is important because the faults in this zone have vertical displacements of up to 1,066 m (3,500 ft).

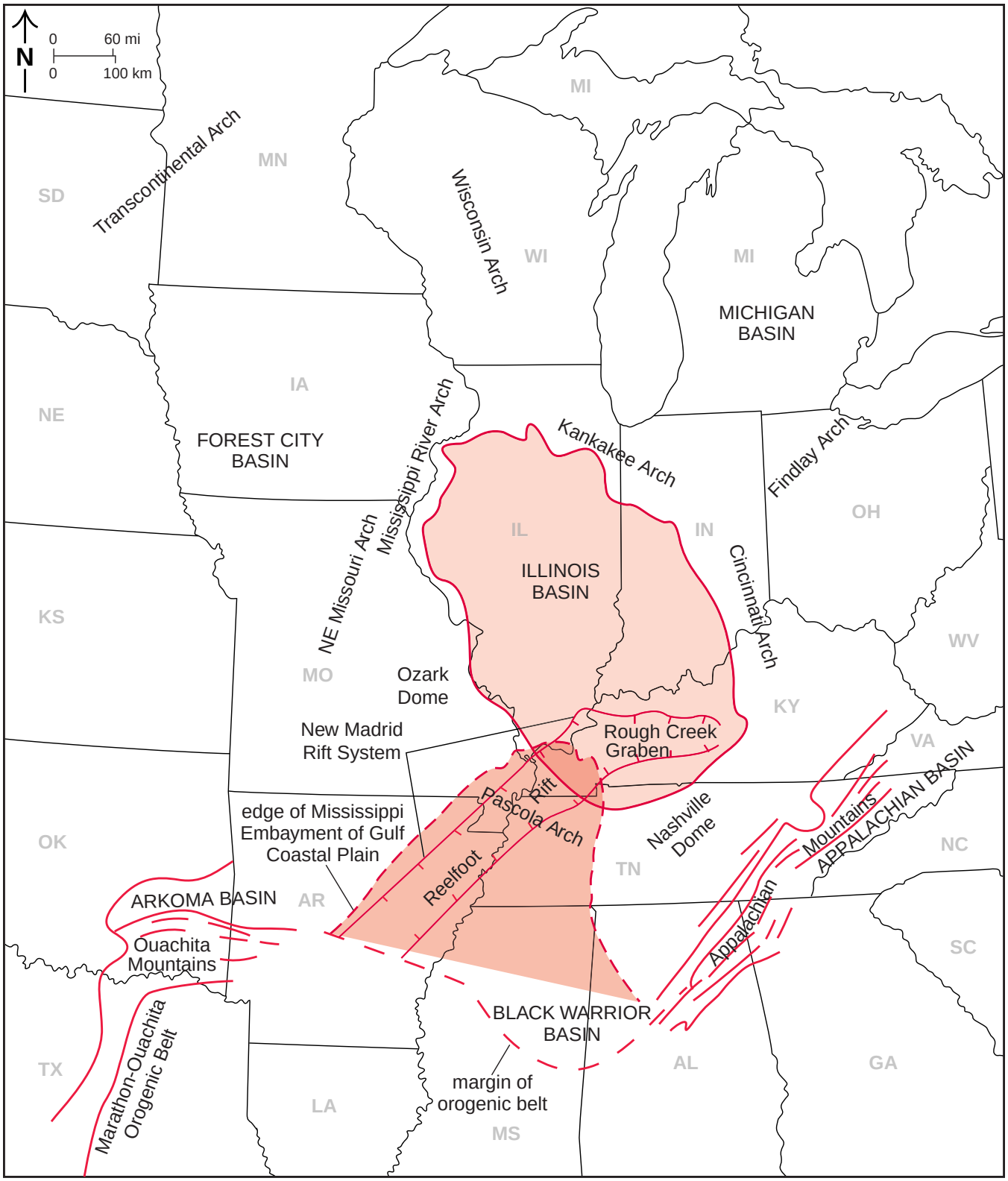

Figure 3-3 *Regional map of the central United States showing the major tectonic features surrounding the Illinois Basin (Kolata, unpublished).*

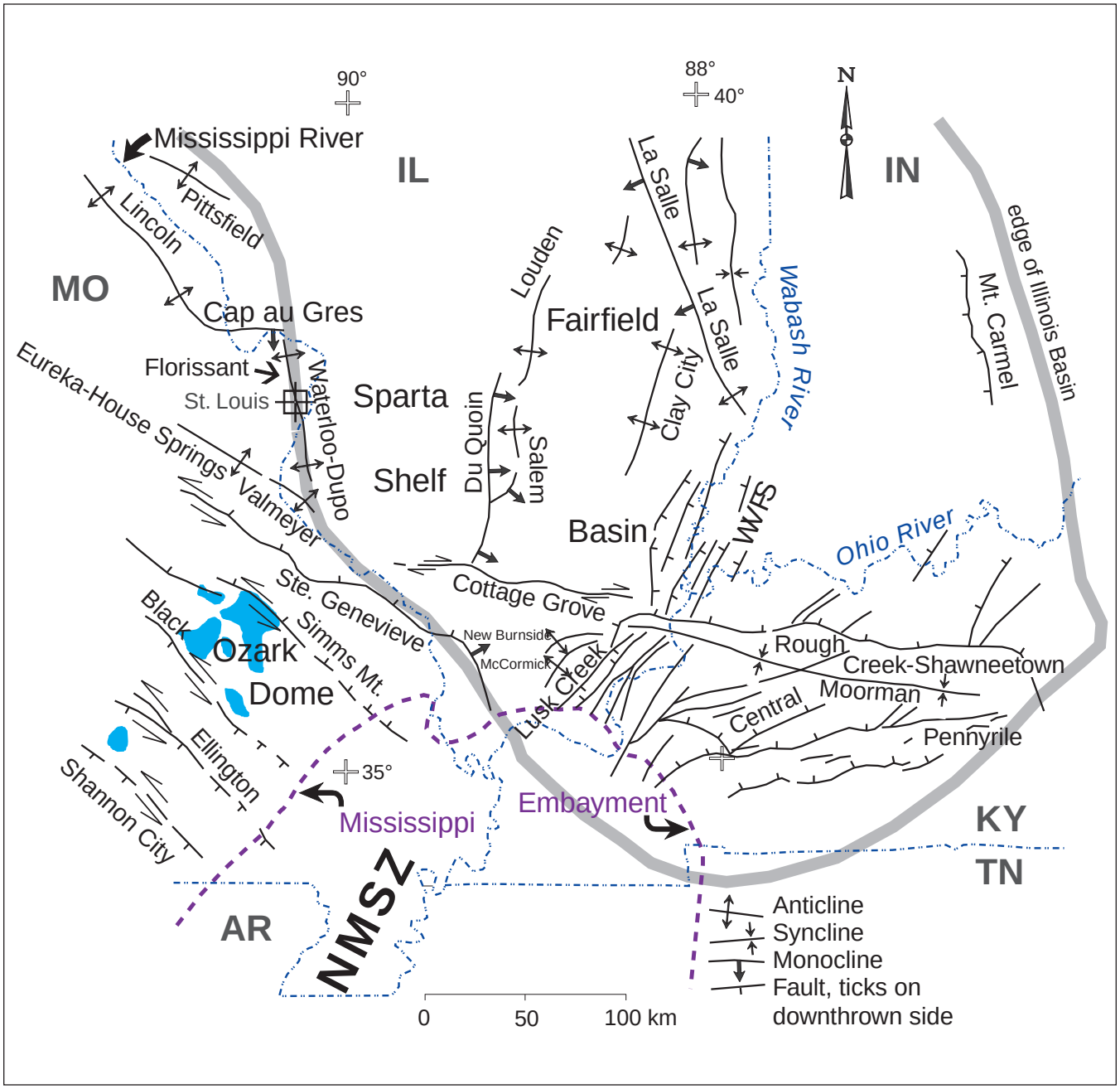

Figure 3-4 *Map of the major structural features in the southern portion of the Illinois Basin (McBride and Nelson, 1999). WVFS, Wabash Valley Fault System; NMSZ, New Madrid Seismic Zone.*

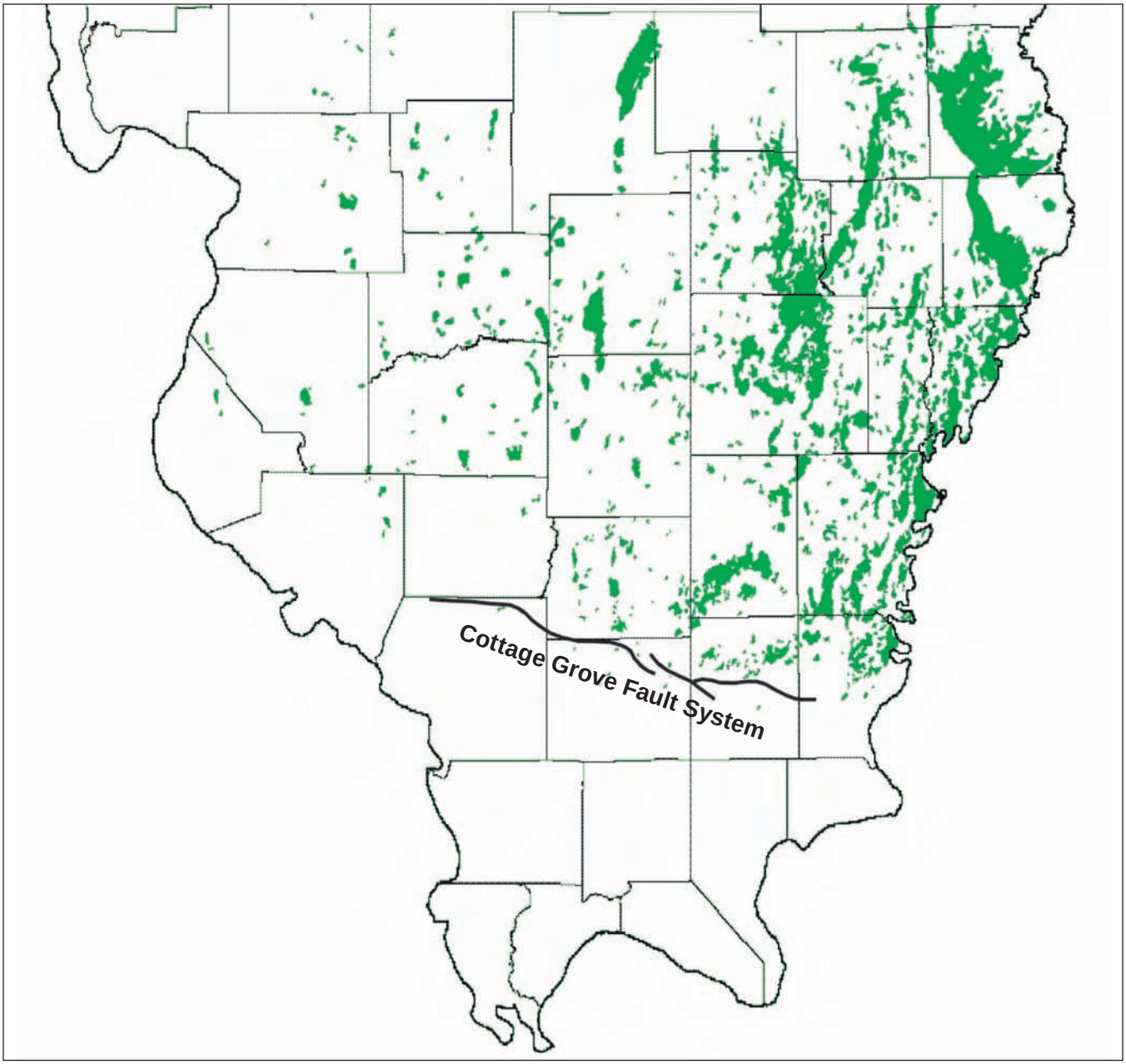

Figure 3-5 *Map of the Cottage Grove Fault System and oil production in Illinois. Oil production is relatively minor south of this fault system.*

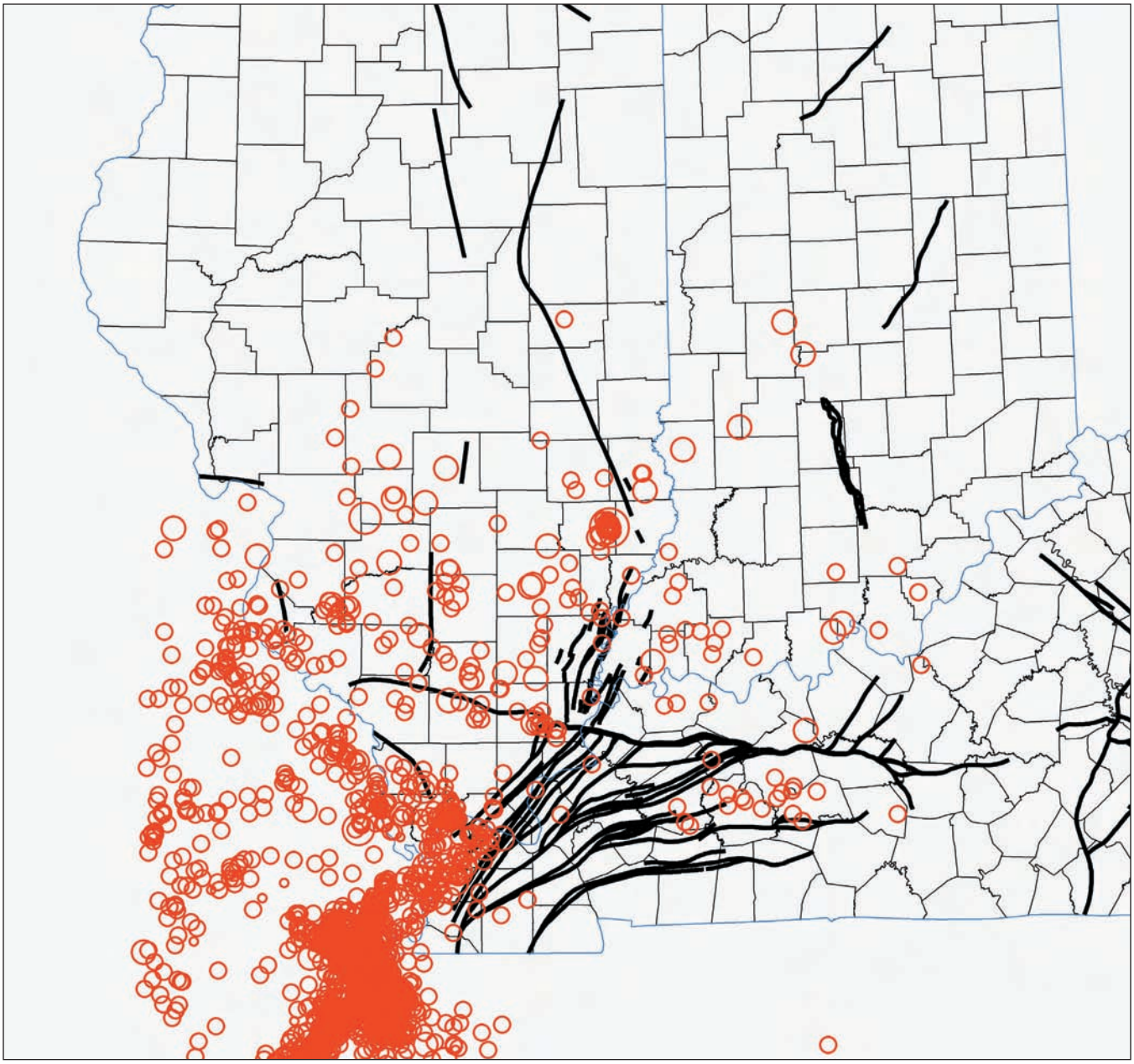

Figure 3-6 *Map of the major faults in the Illinois Basin and the distribution of earthquakes.*

Significant Seals

An important issue relating to the use of saline reservoirs as injection zones for CO_2 is the presence or absence of hydrologic seals to stop upward fluid movement. The three major, thick shale units that form significant seals are the Devonian age New Albany Shale, Ordovician age Maquoketa Formation, and the Cambrian age Eau Claire Formation. There are many minor, thinner Mississippian and Pennsylvanian age shale beds that form seals for hydrocarbon traps that will provide additional barriers to CO_2 migration to the surface.

New Albany

The New Albany Shale Group (Middle Devonian through Kinderhookian, lower Mississippian in age) is a continuous black to gray, organic-rich shale that occurs throughout most of the Illinois Basin. The New Albany Shale is considered as the most significant source rock for all of the oil generated in the Illinois Basin.

The maximum thickness of the New Albany is >140 m (460 ft) in southeastern Illinois and northwestern Kentucky (Figure 3-7). A second area of thick New Albany occurs in southeastern Iowa (not shown) and west-central Illinois, where the New Albany Shale is >90 m (300 ft) thick.

Maquoketa

The Maquoketa Group (Upper Ordovician) strata are composed primarily of relatively thick gray shale with <10% limestone. The Maquoketa ranges from 30 m (100 ft) in thickness near the Mississippi River to >30 m (800 ft) at the eastern edge of the Basin (Figure 3-8). In northeast Illinois the Maquoketa has been partially eroded by a pre-Silurian uplift event and the group is abnormally thin to nonexistent in a few areas. Unless eroded, the Maquoketa or its equivalent is found over the entire Illinois Basin and extends into parts of Michigan and Iowa.

Eau Claire

The Cambrian age Eau Claire Formation is composed primarily of a silty, argillaceous dolomitic sandstone or sandy dolomite in northern Illinois and becomes a siltstone or shale in the central part of the Illinois Basin (Willman et al., 1975). In the southern part of the Basin, the Eau Claire is a mixture of dolomite and limestone with some fine-grained siliciclastics. The regional cross sections in the central part of Illinois show that the Eau Claire is a persistent shale interval above the Mt. Simon that is expected to provide a good seal (Figure 3-9). The Eau Claire ranges from 91 m (300 ft) thick in the western and northern part of Illinois to >305 m (1,000 ft) in the southern part of the Basin.

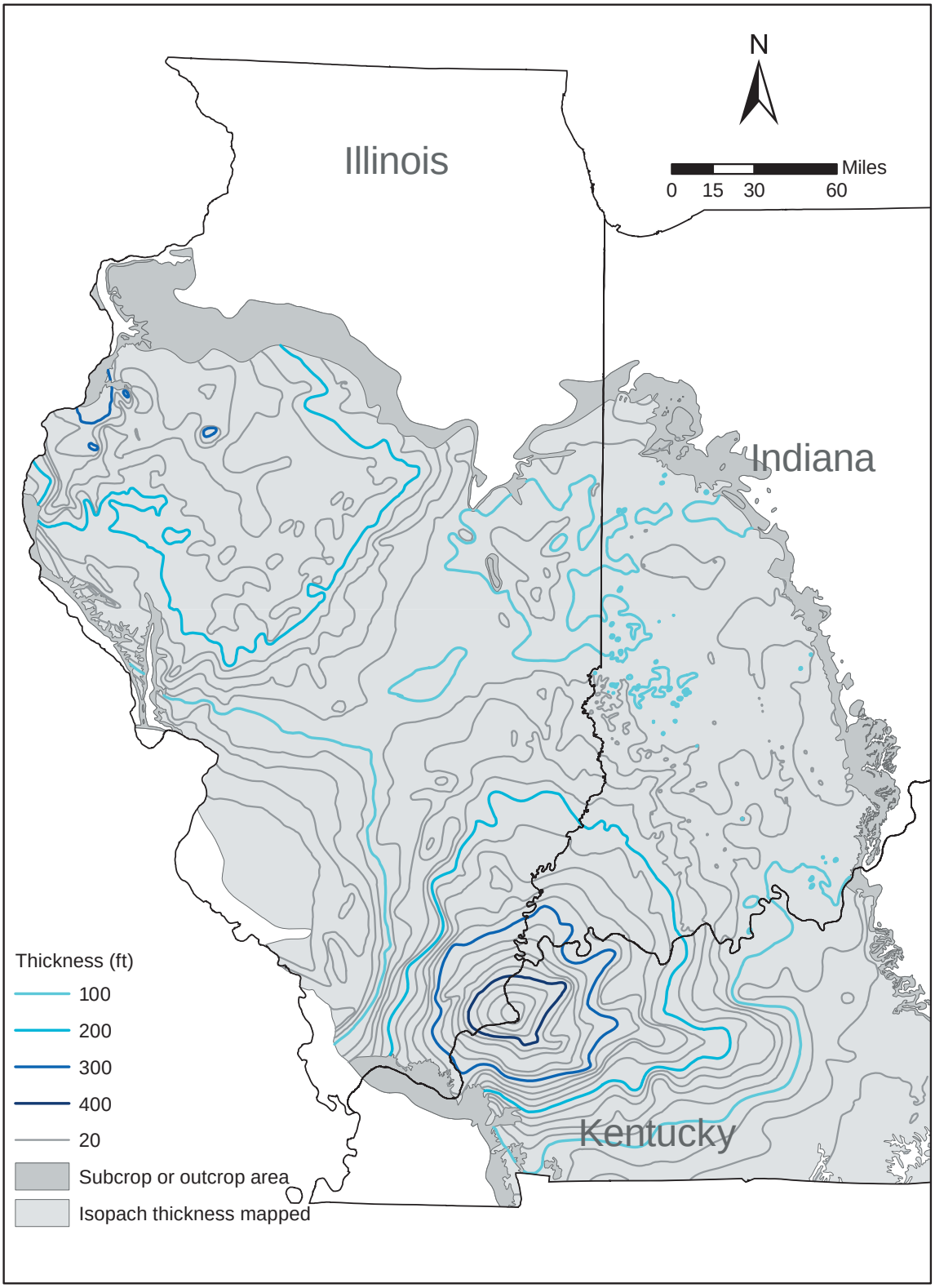

Figure 3-7 *Isopach of the New Albany Shale in the Illinois Basin and surrounding areas (Hasenmueller and Comer, 2000).*

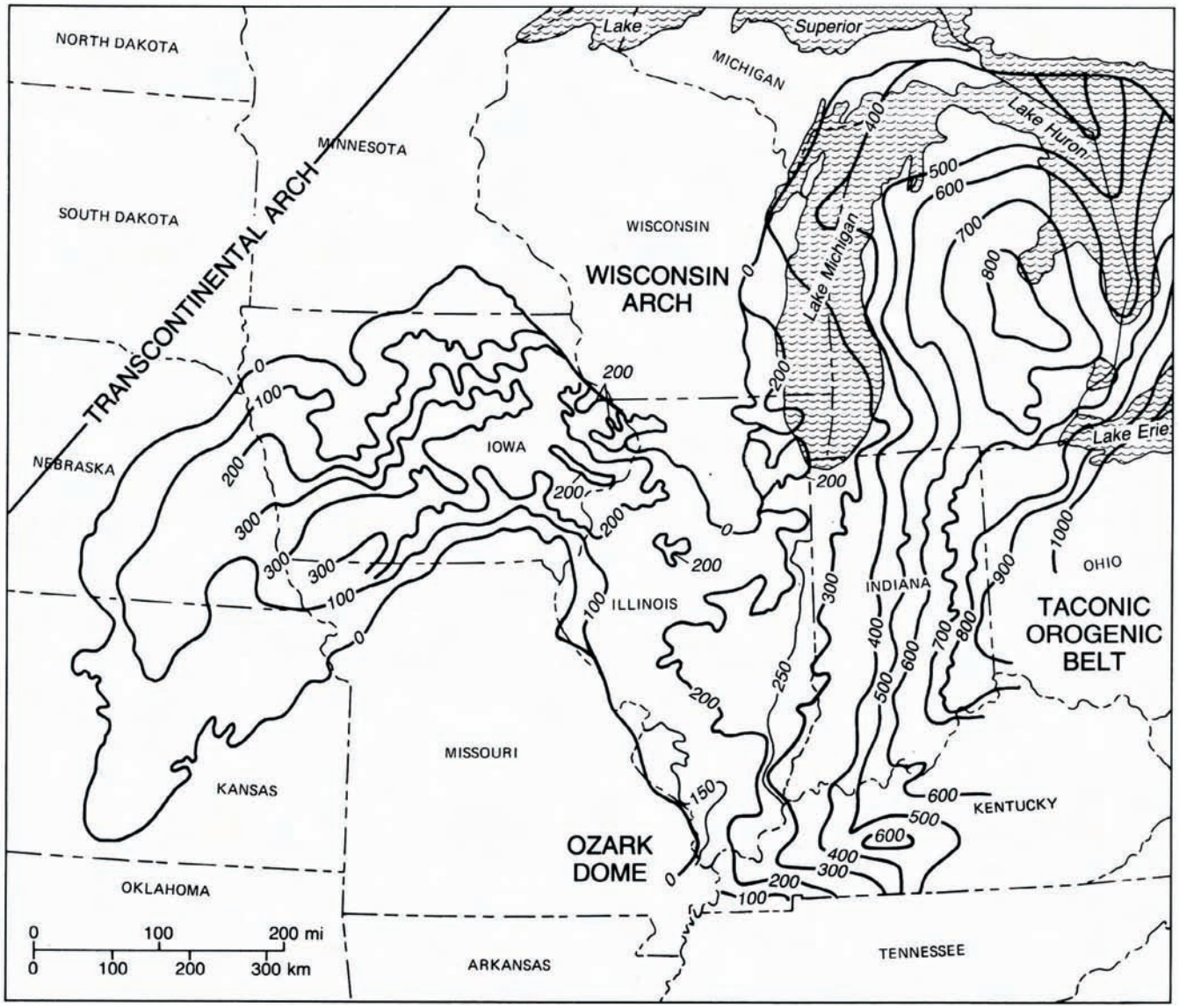

Figure 3-8 *Isopach of the Maquoketa Shale in the Illinois Basin and surrounding areas (Kolata and Graese, 1983). Contour interval = 100 ft.*

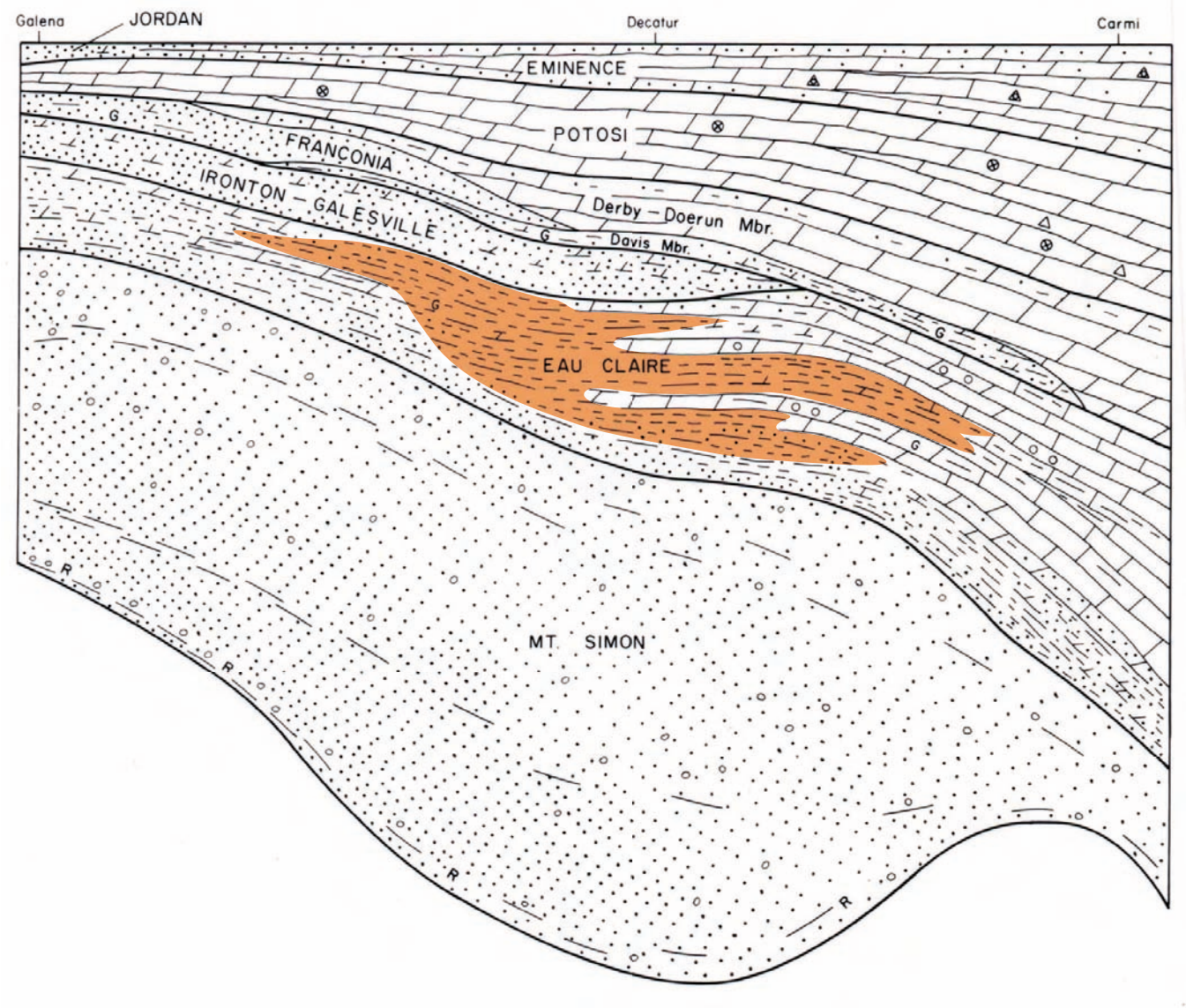

Figure 3-9 *Diagrammatic cross section of the Cambrian System from northwestern to southeastern Illinois. The orange color shows the areas where the Eau Claire Formation is primarily shale and should be a good seal. Uncolored areas may behave as seals, but there is an enhanced risk for leakage because of fracturing (modified after Willman et al., 1975).*

Sinks

The St. Peter Sandstone, Ironton-Galesville Sandstone, and Mt. Simon Sandstone (Figure 3-1) are all deep, porous, and permeable saline reservoirs in Illinois and are potential sequestration sinks. Where they are shallow along their outcrop on the margin of the Illinois Basin, they are also freshwater aquifers. Areas of potable water (<10,000 mg/L [ppm] total dissolved solids) were mapped and considered as possible sites for sequestration.

St. Peter Sandstone

The Ordovician age St. Peter Sandstone is a widespread, porous and permeable sandstone. It is generally fine grained, but local zones within the St. Peter are medium to coarse grained. The sandstone beds have good lateral continuity, but their thickness is variable. The sandstone thickens and thins, filling depressions in the underlying paleotopography. In areas where there are local irregularities in the underlying unconformity surface, the St. Peter can exceed 183 m (600 ft) in thickness (Buschbach, 1964). In general, the St. Peter is 61 to 122 m (200 to 400 ft) thick in northern Illinois and Indiana, is 30 to 61 m (100 to 200 ft) thick over most of the central portion of the Illinois Basin, and thins eastward into central Indiana (Figure 3-10) (Gutstadt, 1958). The St. Peter reservoir has been used successfully for natural gas storage (e.g., Hillsboro gas project). There are a couple of hundred feet of dense limestone and dolostone above the St. Peter that provide seals. Above these carbonate rocks lies the Maquoketa Shale, a widespread sealing horizon that is commonly 46 to 76 m (150 to 250 ft) thick.

Ironton-Galesville Sandstone

The unconformity between the Knox and the overlying St. Peter is the sub-Tippecanoe unconformity. The Cambrian age Ironton and Galesville Sandstones are two of the most important aquifers in northern Illinois and have a combined thickness of >61 m (200 ft) (Figure 3-11). Directly overlying the Ironton-Galesville are the predominantly dolomite formations of the Knox (Lower Ordovician to Upper Cambrian age). These Knox formations above the Ironton are the Shakopee Dolomite, New Richmond Sandstone, Oneota Dolomite, Gunter Sandstone, Eminence Dolomite, Potosi Dolomite, and Franconia Formations (Figure 3-1). There is a considerable unconformity on top of the Knox. It is difficult to differentiate these formations from wireline log data. The Knox thickens to the south where it may exceed 1,371 m (4,500 ft). The Knox thins northward due to erosion, thinning, and facies changes from dolomite to siliciclastics strata. There are no consistent, thick shales in the Knox that could form effective seals to fluid movement from the Ironton-Galesville Sandstones.

The Ironton and Galesville Sandstones are considered in this report as one unit because they occur as a single aquifer in the northern part of Illinois, and neither unit occurs in southern Illinois. These two sandstones are difficult to differentiate from each other using wireline logs. The Ironton is a relatively poorly sorted, fine- to coarse-grained dolomitic sandstone that averages about 30 m (100 ft) thick in northern Illinois. The underlying Galesville Sandstone is fine grained, well sorted, and has no shale beds. The Galesville averages about 12 m (40 ft) thick in northern Illinois. The Galesville is relatively better sorted, finer grained, and has better porosity than the overlying Ironton. Neither sandstone bed is present in the central and southern portion of the Illinois Basin, where the sandstone grades into a non-sandy dolomite.

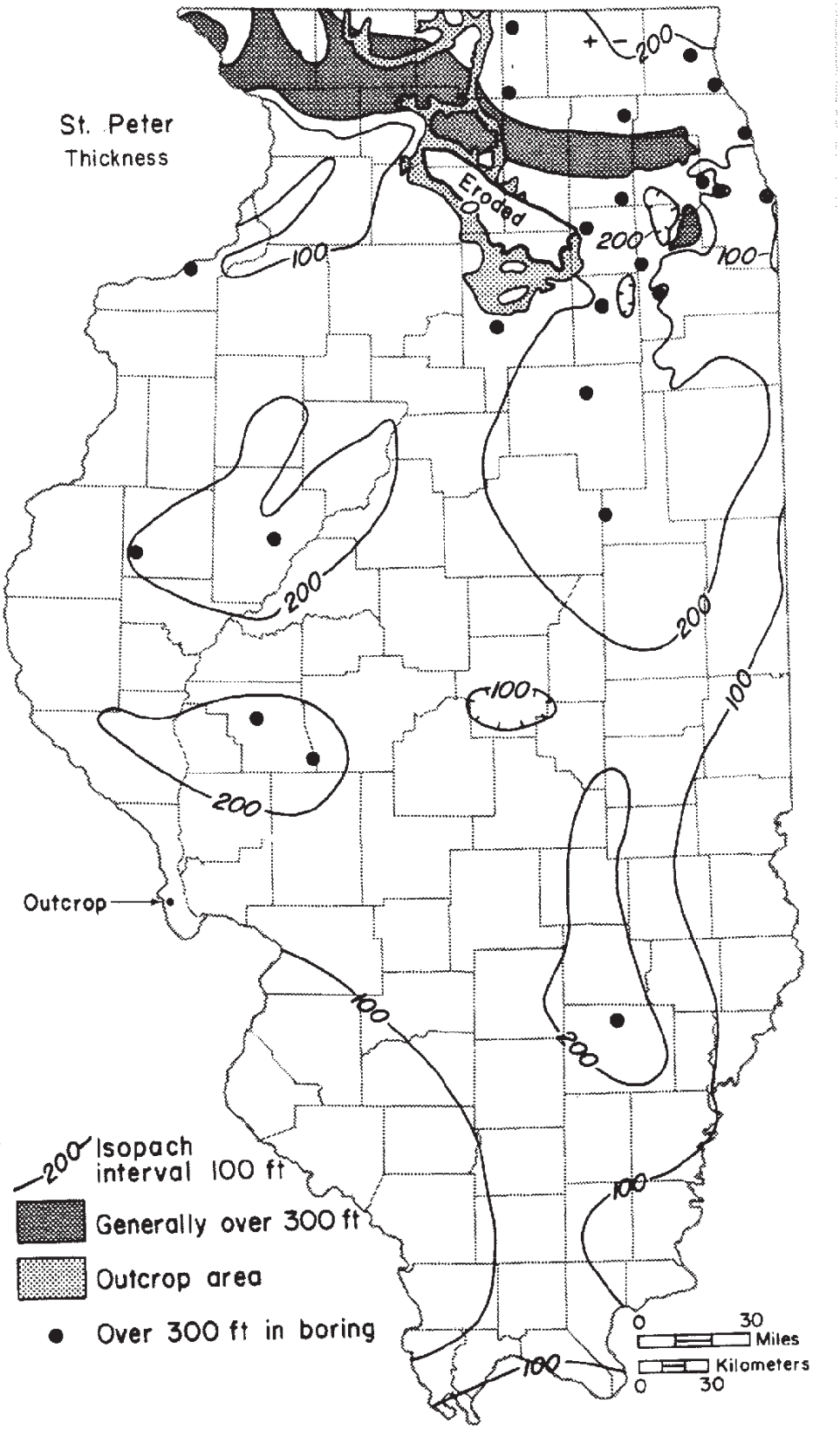

Figure 3-10 *Isopach of the St. Peter Sandstone in the Illinois Basin (Willman et al., 1975). The St. Peter pinches out in Indiana and Kentucky.*

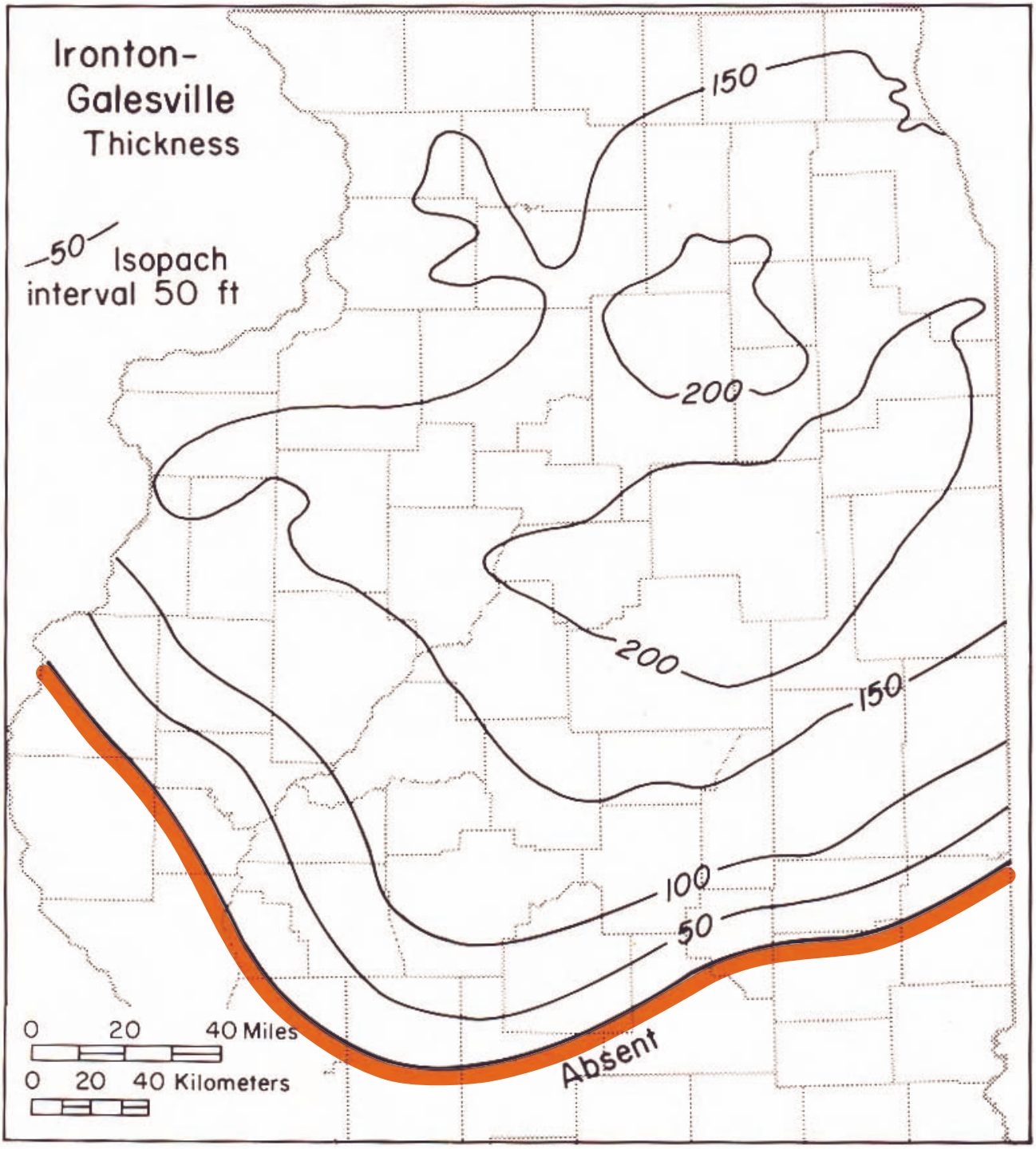

Figure 3-11 *Isopach of the Ironton-Galesville Sandstone in Illinois. The orange line signifies the southern limit of the formation. There are no sandstone facies south of this line (Willman et al., 1975).*

Mt. Simon

The Mt. Simon Sandstone is commonly used for natural gas storage in the Illinois Basin. Data from natural gas storage reservoirs suggest that the Mt. Simon should be an excellent reservoir in which to test injection of CO_2. The depth of the Mt. Simon ranges from <600 m (2,000 ft) to >4,300 m (14,000 ft) below the surface (Figure 3-12).

Because of the paucity of well penetrations into the Mt. Simon in the southern and central parts of the Basin, the Mt. Simon structure map is projected conformably from the Galena structural surface.

In the Illinois Basin, the Mt. Simon Sandstone is Upper Cambrian in age and lies unconformably on Precambrian basement rocks that are composed of granite or granodiorite in the north (Atekwana, 1996) and granite or rhyolite in the south (Bradbury and Atherton, 1965). In the Illinois Basin, there are fewer than 25 wells that have penetrated through the entire Mt. Simon Sandstone interval to the Precambrian basement (Figure 3-13). Much of the Precambrian basement formed between 1.48 and 1.38 billion years ago and is part of the eastern granite-rhyolite province (Bickford et al., 1986). In east-central Illinois, the Mt. Simon may be resting on a Precambrian unit with up to 3,600 m (12,000 ft) of rocks called the Centralia Sequence. On seismic lines, these sub-Mt. Simon strata display coherent reflectors suggestive of a sedimentary succession (McBride et al., 2003).

At its thickest point in the Illinois Basin, the Mt. Simon is >790 m (2,600 ft) thick (Figure 3-14). The Mt. Simon does not crop out in Illinois, but correlative units are exposed in southern Wisconsin, southeastern Minnesota, and Missouri. The Mt. Simon is known in the subsurface throughout Indiana, Iowa, Michigan, and Ohio. To the southwest, the Mt. Simon has been correlated with the Lamotte Sandstone of Missouri (Workman and Bell, 1948, p. 2043; Houseknecht and Ethridge, 1978). The Mt. Simon may correlate to equivalents in the Bayfield Sandstone of northern Wisconsin, the Jacobsville Sandstone of northern Michigan, and the Fond du Lac Sandstone of Minnesota (Buschbach, 1964). The Mt. Simon comprises the lower part of the Sauk Sequence of Sloss (1963). The regional relationships of the lower Sauk were summarized by Sargent (1991). The Mt. Simon is the basal sandstone of the Potsdam Sandstone Megagroup (obsolete nomenclature) of Swann and Willman (1961) and Willman et al. (1975).

Depending on the locality, the sandstone strata in the Mt. Simon can vary from fine to coarse grained. There also appear to be zones of predominantly finer-grained sandstone and coarser sandstone. Between some sandstone strata are thin beds of dark gray shale laminae. At the bases of some coarser sandstone strata, the Mt. Simon is conglomeratic with pebbles 2 to 4 mm (0.07 to 0.15 inches) in diameter. The principal cementing material is quartz in the form of overgrowths. The Mt. Simon commonly has a basal arkose-rich interval that is 6 to 12 m (20 to 40 ft) thick but can range up to 122 m (400 ft).

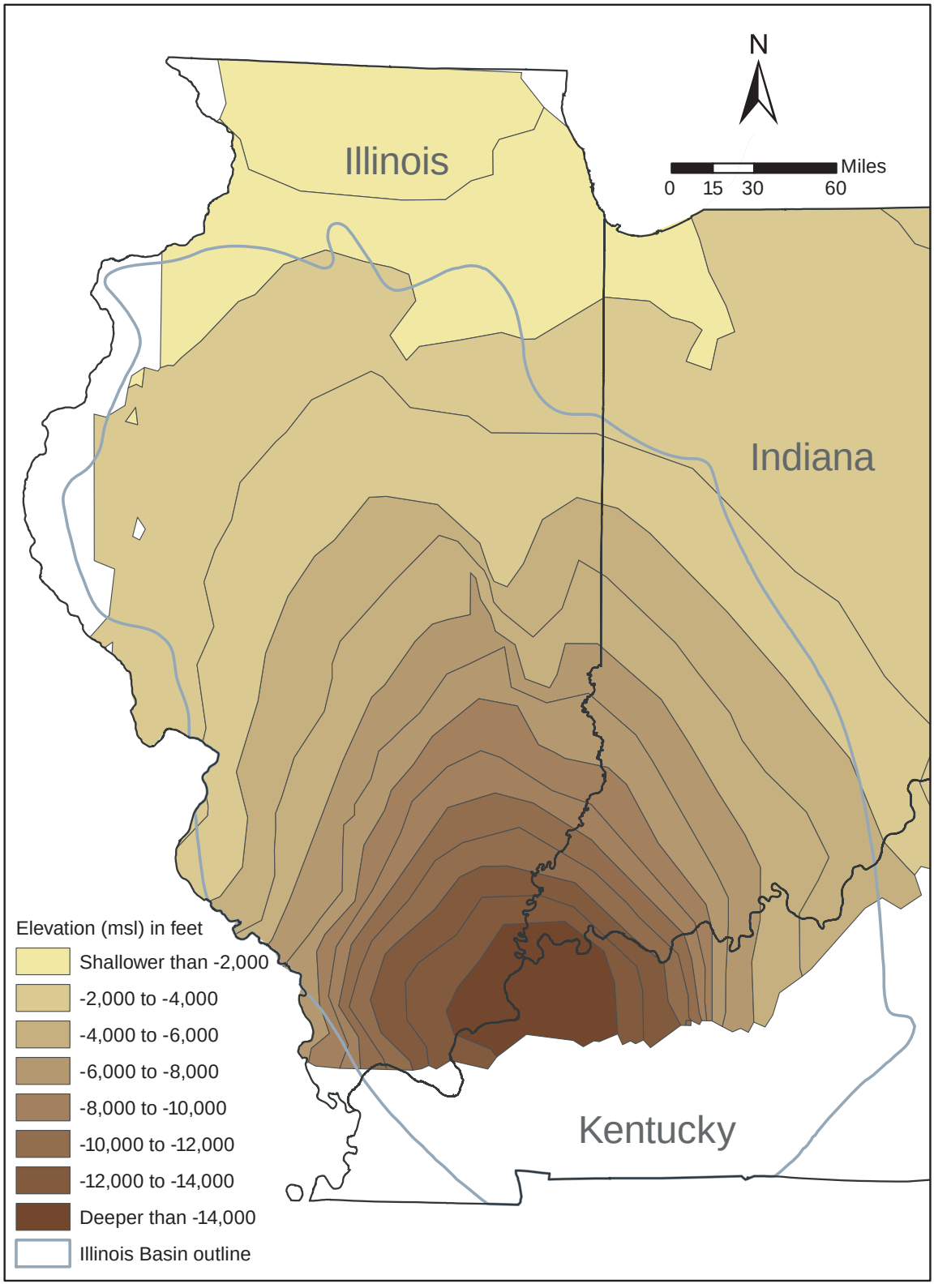

Figure 3-12 *Structure on top of the Mt. Simon Sandstone in the Illinois Basin. The structure is based on conformable mapping from the Galena (Trenton) structure. The southernmost portion of the Basin is thought to be devoid of the Mt. Simon Sandstone due to no sandstone signature or available well loss (see Figure 3-13 for well locations).*

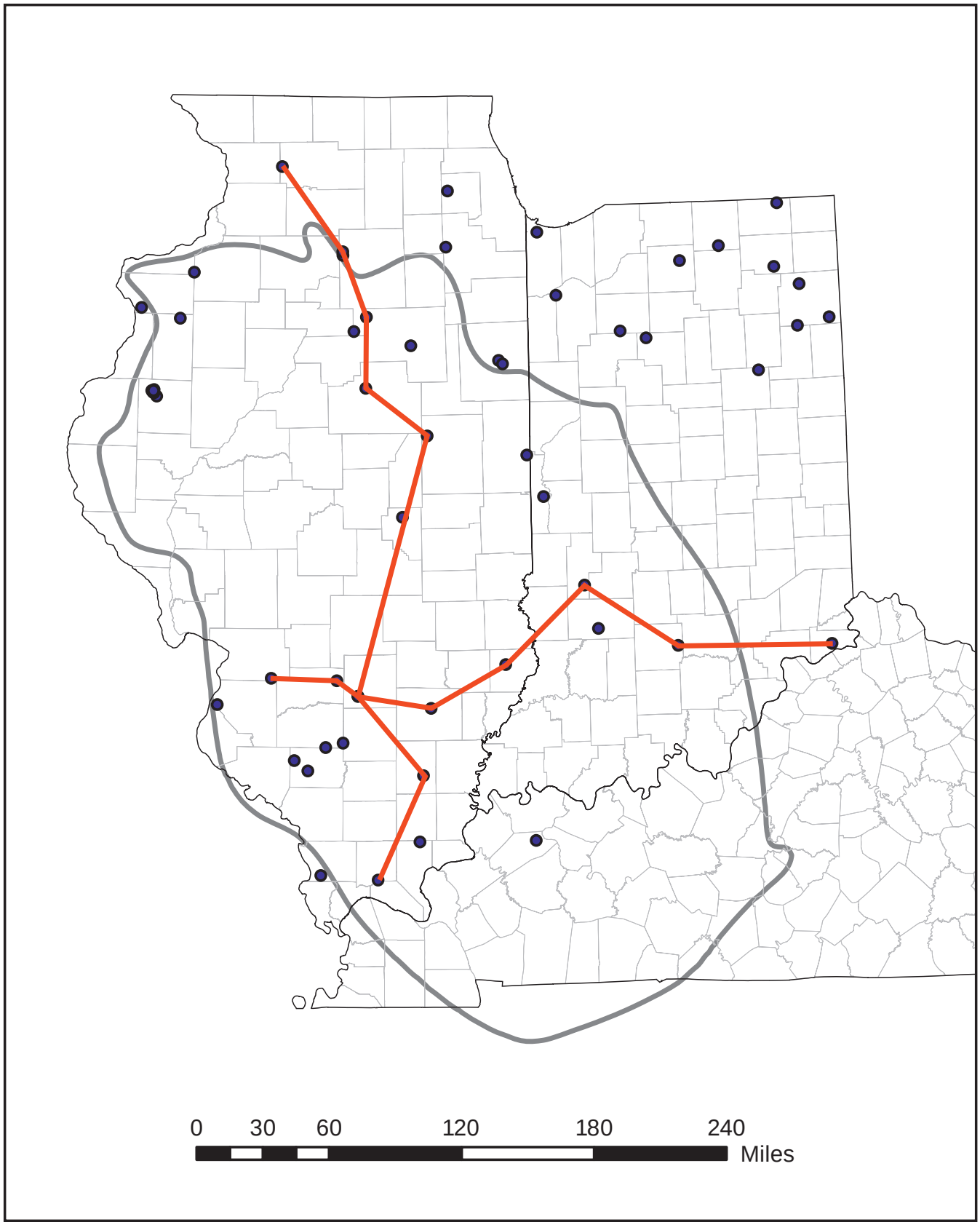

Figure 3-13 *Well locations of wireline logs with Mt. Simon penetration.*

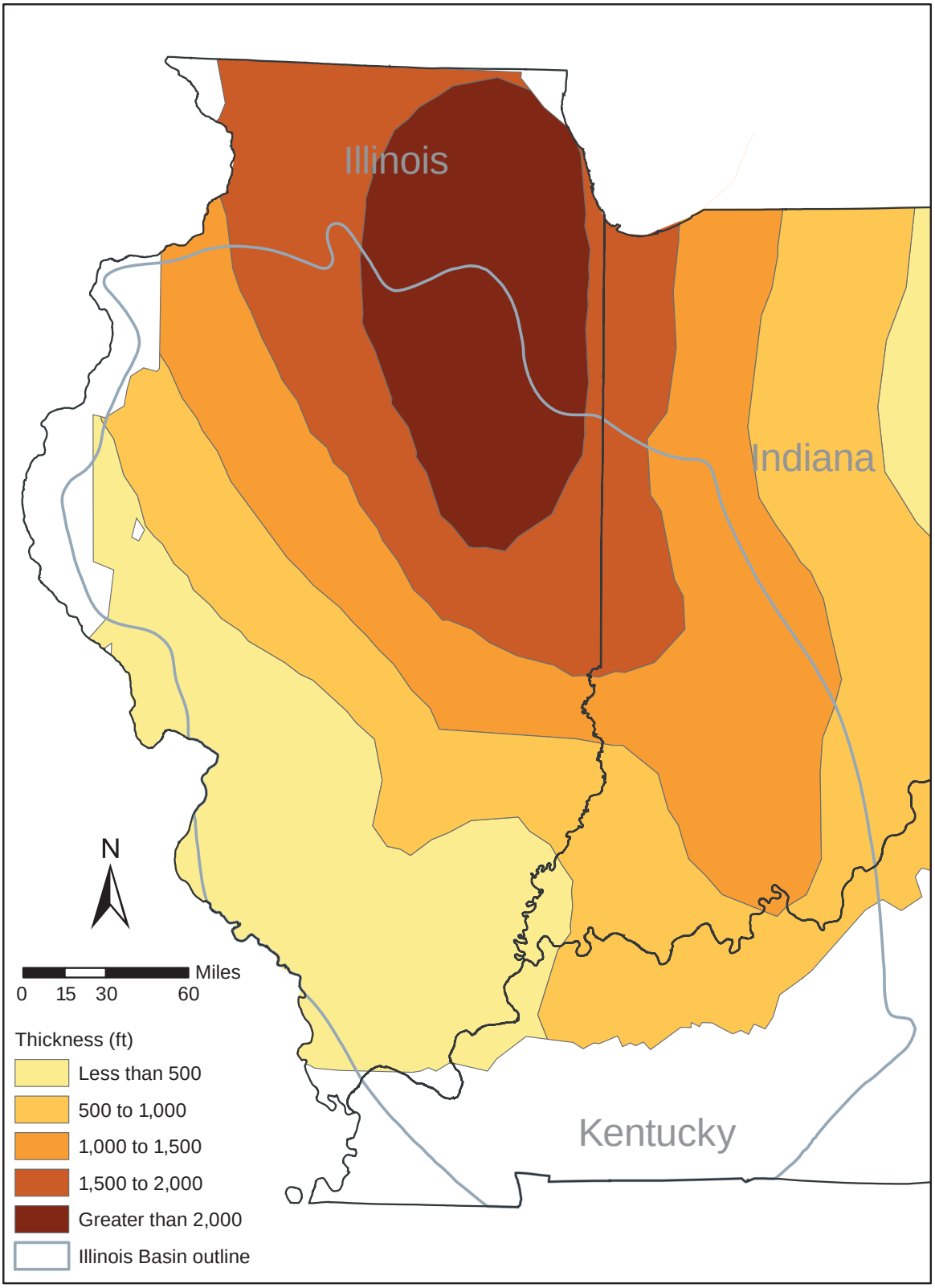

Figure 3-14 *Contour map of the thickness of the Cambrian Mt. Simon Sandstone within the Illinois Basin based on all available drill-hole data. Well locations are shown in Figure 3-13.*

Most very fine-grained Late Cambrian and Early Ordovician sandstones and coarse siltstones, including the Mt. Simon, in the Upper Mississippi Valley contain large amounts of detrital and authigenic K-feldspar (Odom, 1978, 1975). In the Mt. Simon, the feldspar-rich intervals occur in strata with a grain size <0.125 mm (0.005 in). Coarser-grained sandstones contain little to no feldspar. Approximately 27% of the feldspar in the finer strata is authigenic. These authigenic feldspars occur as euhedral overgrowths that surround ditrital K-feldspar grains. Radiometric age determinations (Odom, 1978) suggest that the detrital feldspar was derived from Middle Precambrian to Late Precambrian rock that underlies the Mt. Simon.

The Canadian Shield has been considered as the primary source of the Mt. Simon sediment. Paleocurrents flowed from the north and northeast of the Illinois Basin (Ojakangas, 1963). The Ozark dome at the St. Francois Mountains was a secondary source for these sandstones (Houseknecht and Ethridge, 1978). In the St. Francois Mountains of Missouri, the Mt. Simon was deposited as alluvial fans and braided fluvial systems surrounding paleohigh areas. The relief of the paleotopography of the Precambrian surface has been documented to be up to 550 m (1,800 ft) in this area of Missouri. The Precambrian age rock in the Illinois Basin is composed of a medium- to coarse-grained granite or rhyolite and is between 1.1 to 1.4 billion years old (Bickford et al., 1986). The Precambrian age strata occur at depths of from 610 m (2,000 ft) in the northernmost part of Illinois to >4,300 m (14,000 ft) below the surface in the southern part of the Illinois Basin. The unconformity between the overlying Mt. Simon (also known as the sub-Sauk unconformity) is estimated to span 600 to 900 million years (Willman et al., 1975).

There is considerable paleorelief on the Precambrian surface that may exceed 300 m (1,000 ft) in southwestern Illinois (Atherton, 1971). The Mt. Simon over these paleohigh areas is thin or not present at all. Exposed Precambrian highlands existed locally through Eau Claire deposition because the Eau Claire may also be absent in these high areas. Near the Missouri border the Eau Claire becomes a relatively pure dolomite, and in Missouri the equivalent stratigraphic interval is referred to as the Bonneterre Dolomite (Bell et al., 1964). The Bonneterre Dolomite (Eau Claire Formation) in Missouri contains igneous rock fragments, suggesting that there were Precambrian paleohigh areas that were islands during the deposition of these carbonates (Houseknecht and Ethridge, 1978).

Depositional Environments

Mt. Simon Facies

The Mt. Simon in northern Illinois has been divided into seven members based on alternation of relatively coarse sand and granule-rich intervals with relatively fine-grained intervals (Templeton, 1950). Only the upper three members have not been traced to northeastern Illinois (Buschbach, 1964). From the base upward, these three consist of the Lacey, Gunn, and Charter Members. Gas storage in north-central Illinois is typically confined, by limits of structural closure, to the upper 61 m (200 ft) of the

formation, presumably in the Charter Member, although the present study made no attempt to recognize the members. Well-log derived electrofacies were used to define the different Mt. Simon units.

Regional cross sections (Figures 3-15 and 3-16) across the northern portion of Illinois suggest that the Mt. Simon can be subdivided into three distinct electrofacies. The normalized gamma-ray (shale volume or V_{shale}) curve is used to infer grain size. (In some cases, it is appropriate to assume that the shale index [I_{shale}] is equivalent to V_{shale}.) The gamma-ray log measures the amount of naturally occurring radioactivity in a formation. The finer-grained sandstones commonly have more abundant clay minerals, which contain radioactive elements. The coarser-grained rocks contain less feldspar and clay minerals. The stratigraphic datum on both the north-south (Figure 3-15) and east-west (Figure 3-16) cross sections is the Mt. Simon.

The uppermost Mt. Simon Sandstone electrofacies unit (Figure 3-15) is composed of thin (3.0 to 6.1 m (10 to 20 ft)) sandstone beds that are interbedded with thin (<0.3 m (1 ft)) shale and siltstone beds. The uppermost Mt. Simon unit is used for gas storage at Manlove Gas Storage Field, Champaign County, Illinois. Interpretation of core through the upper Mt. Simon at Manlove suggests a nearshore, tidally influenced depositional system.

The middle Mt. Simon electrofacies unit has thicker sandstone beds than the upper unit. It also has a finer-grained interval in the middle with coarsening both upward and downward. No core of this unit was available, and the interpretation was based on electrofacies.

The lowermost Mt. Simon electrofacies unit has thick-bedded sandstone with some beds being ≥30 m (≥100 ft) in thickness. There are also high gamma-ray intervals that do not have a typical neutron log response for shale but that have core data and sample description that suggest an arkose.

The east-west cross section (Figure 3-16) illustrates some of the problems of studying the Mt. Simon Sandstone. Most of the wells penetrate only the upper 61 m (200 ft) of Mt. Simon and never have a chance to encounter the middle and lower Mt. Simon facies. The two most western wells in the cross sections did not encounter Mt. Simon and instead drilled through a thin Eau Claire Formation into granite. These features were topographic high areas during the Eau Claire and Mt. Simon deposition. Observed from both well control and seismic, the paleohigh areas are common in southwestern and south-central Illinois.

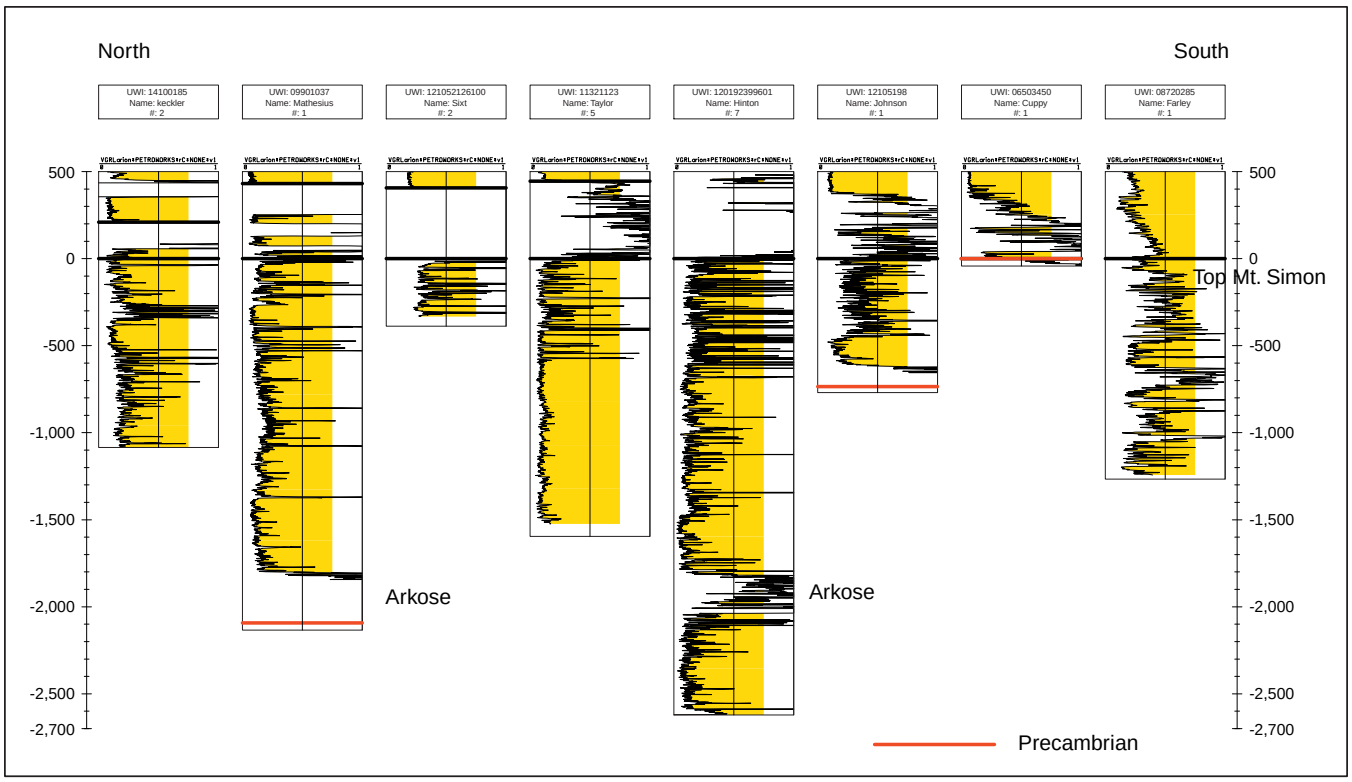

Figure 3-15 *North-south cross section of the Eau Claire and Mt. Simon across the Illinois Basin illustrating the stratigraphic and structural relationships.*

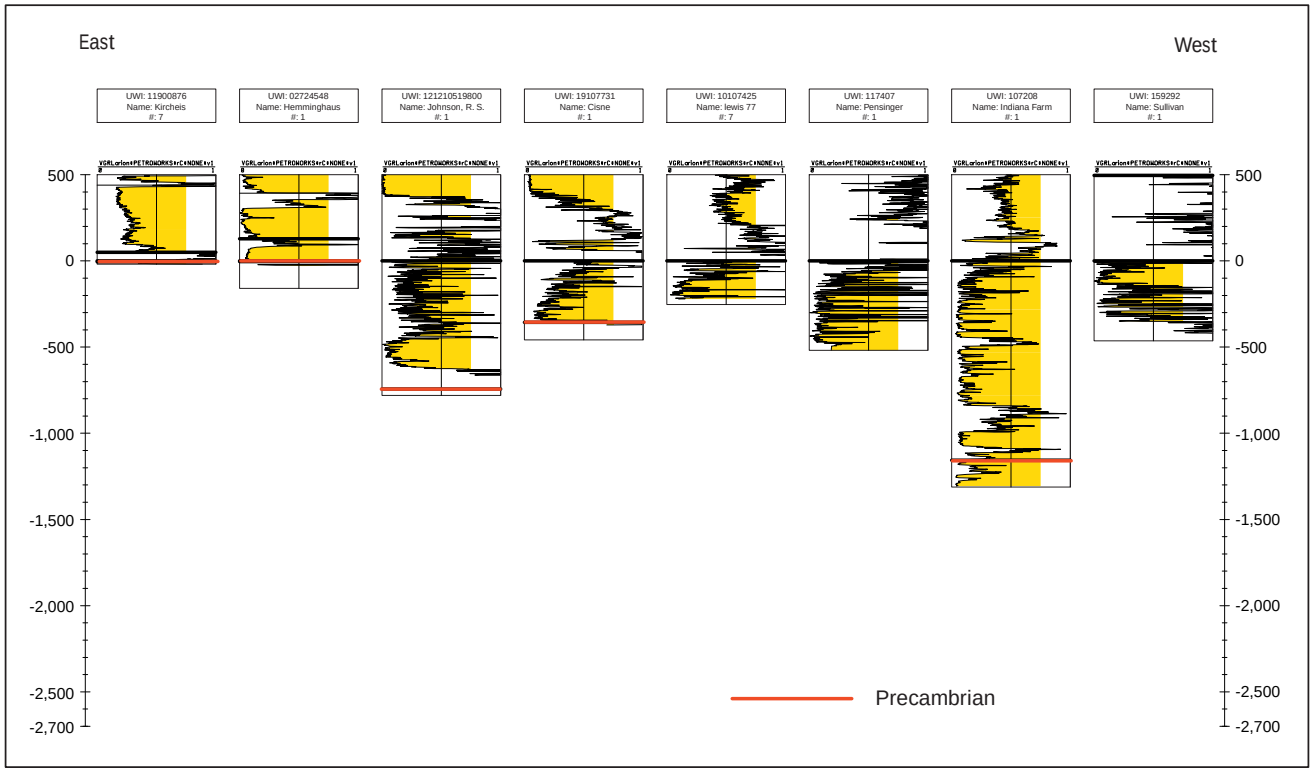

Figure 3-16 *East-west cross section of the Eau Clare and Mt. Simon across the Illinois Basin illustrating the stratigraphic relationship (datum is the top of the Mt. Simon Sandstone).*

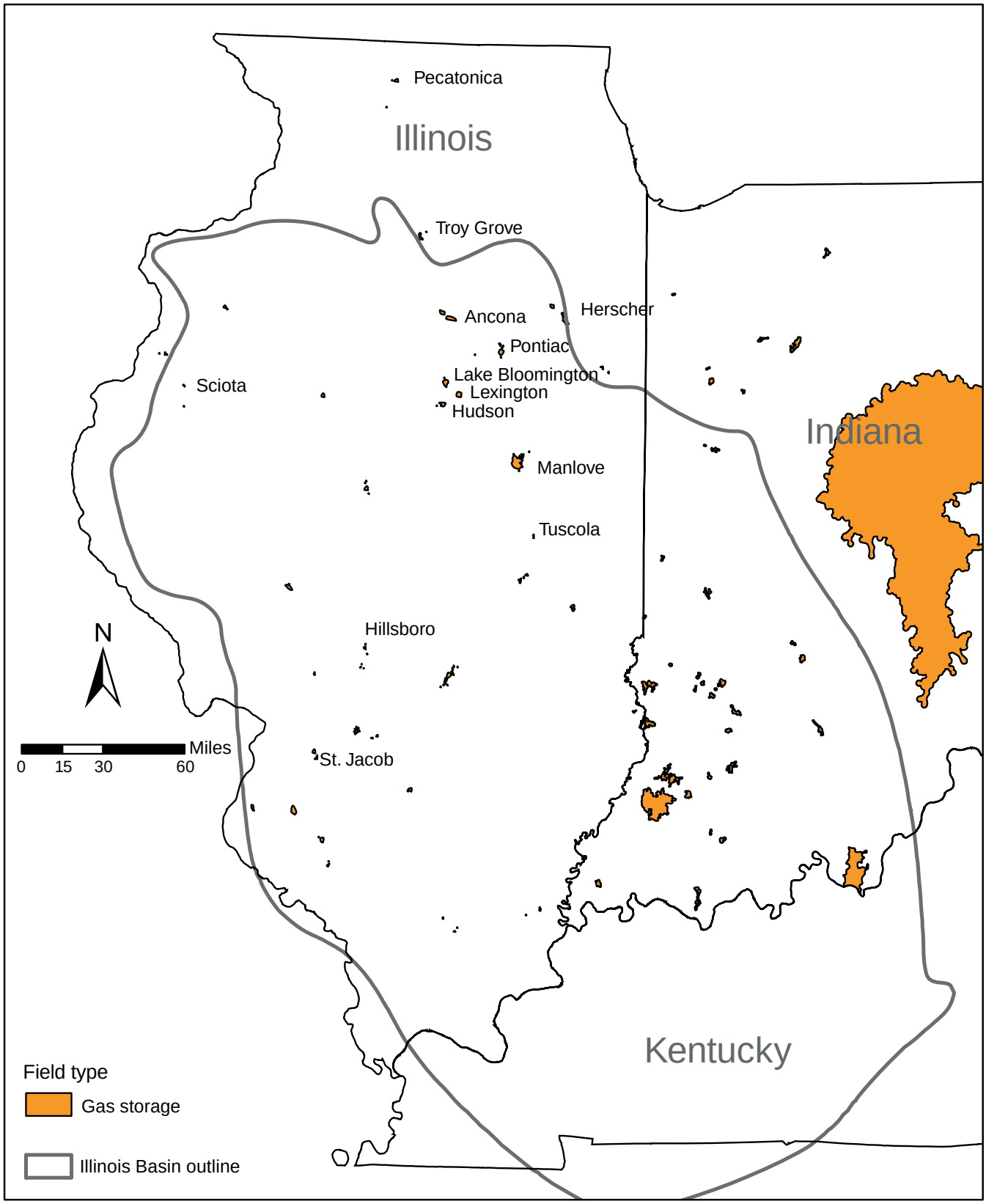

Figure 3-17 *Location of all gas storage projects in Indiana and Illinois.*

Gas Storage Project Analogs

The most likely sites for CO_2 sequestration are anticlines because they are known to have the necessary structural closure for storage and containment of hydrocarbons and natural gas. Natural gas utilities are currently using many of the anticlines in the northern part of Illinois and Indiana for natural gas storage. These gas utilities inject natural gas during the low demand summer cooling season and produce the gas and sell it to their customers during the winter heating season. Deeper reservoirs in the present gas storage anticlines are considered unacceptable for CO_2 sequestration because migration into the gas storage zone(s) would dilute the stored natural gas. Although all gas storage anticlines were eliminated as potential sites for CO_2 sequestration research, they provide the best analogs for CO_2 storage in similar reservoirs elsewhere.

Natural gas was first successfully stored in subsurface formations in 1915 in Welland County, Ontario, Canada. The first successful underground storage in the United States was in 1916 at Zoar Field, near Buffalo, New York. By 1919, there was an active gas storage project at Menfie Field in Kentucky. The first gas storage project in Illinois was in 1941 into the Pennsylvanian age sandstone aquifer at New Harmony. The operators were able to successfully inject gas into the sandstone, but recovery of the natural gas was not commercial because of saltwater disposal problems. The first commercial gas storage project in Illinois was at Waterton Anticline in 1950. Another early project was at Herscher anticline (Buschbach and Bond, 1973).

The Mt. Simon Sandstone is commonly used for storage because it has good permeability and porosity, and the overlying Eau Claire Formation provides impermeable seals of limestone, dolomite, and shale. Because of its demonstrated ability to hold natural gas, the Mt. Simon will be an excellent reservoir in which to test injection of CO_2.

The upper 60 m (200 ft) of the Mt. Simon are composed of multiple sandstone beds that are commonly no more than 6 m (20 ft) thick and are separated from each other by thin zones of laterally discontinuous shale or low permeability siltstone. Three-dimensional reservoir modeling of the upper Mt. Simon demonstrates the lack of laterally extensive correlative low permeability barriers that would vertically compartmentalize the reservoir; instead, the low permeability zones behave as baffles that restrict but do not stop reservoir communication. Wireline logs suggest that below the upper Mt. Simon there are additional porous reservoir sandstones with potentially stacked reservoir strata hundreds of feet thick. Gas storage projects in the Illinois Basin all confirm that the Eau Claire Formation is an effective seal in the northern and central portions of the Basin. The lack of wells penetrating the Mt. Simon in the southern portion of the Basin makes it difficult to evaluate the Eau Claire in this area. From limited well data, the Eau Claire in southern Illinois is predominantly a carbonate with less shale.

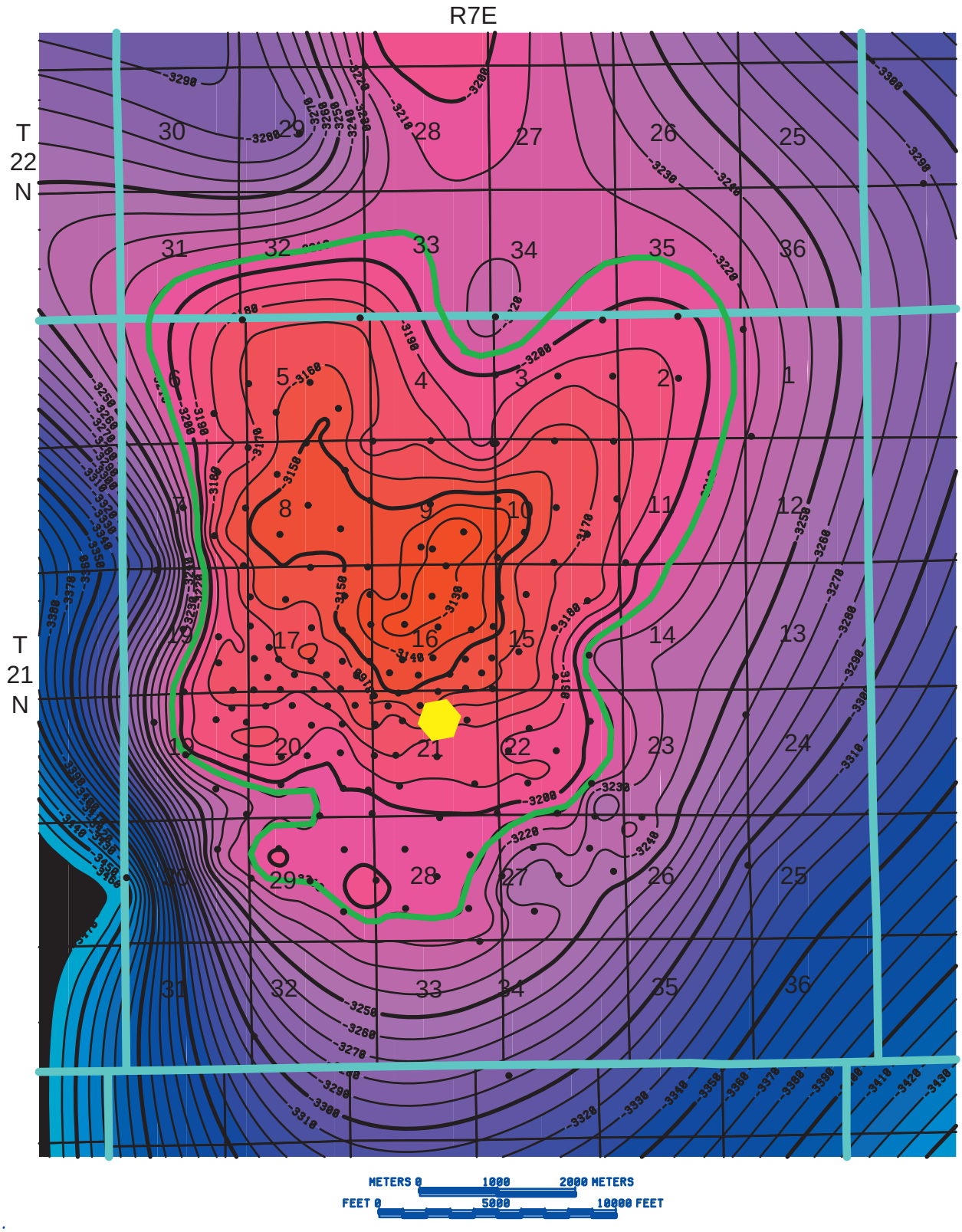

Figure 3-18 *Structure map of the top of the Mt. Simon Sandstone at Manlove Field showing individual wells with Mt. Simon structural tops. The contour "-3,210 ft" (green line) defines the area of closure for the Manlove structure. The yellow hexagon is the location of the Hinton No. 7 well.*

Manlove Field

Manlove Field, a 4.33 billion m^3 (153 billion scf) aquifer gas storage field, including cushion gas, is located in Champaign County, Illinois, and is operated by Peoples Energy Corporation (Figure 3-17). The field is formed by a north-south–trending, closed anticline 16 km (10 mi) long and 10 km (6 mi) wide with about 27 m (90 ft) of structural closure (Figure 3-18). The reservoir is in the Upper Cambrian Mt. Simon Sandstone, with a sealing caprock formed by about 30 m (100 ft) of dense shale in the overlying Cambrian Eau Claire Formation. The field has a steep west flank and a gentle east flank (Figure 3-18). The spill point lies in the northeastern part of the field. The field covers approximately 73 km^2 (28 mi^2). The Mt. Simon is about 1,200 m (4,000 ft) deep in this field and has an average porosity of 12% and an average permeability of 0.099 μm^2 (100 millidarcies (md)).

The field, located about 210 km (130 mi) south of Chicago, began withdrawals in 1966 after initial injection in 1964. Maximum daily withdrawal capacity is approximately 0.028 billion m^3 (1 billion scf); maximum annual withdrawal (maximum working gas) is about 1.2 billion m^3 (44 billion scf) (Anonymous, 1994, p. 47). Gas is transported to the Chicago market via two large-diameter, company-owned pipelines.

The field was originally drilled as a St. Peter Sandstone gas storage field (488 m (1,600 ft) deep), but, after initial injection in 1961, leaking gas was discovered in the glacial drift above the field. Injection was halted in August 1961, but the source of the leak could not be determined. Gas was then injected into the underlying Galesville Sandstone (975 m (3,200 ft) deep) in 1963, which also appeared to leak. Later tests of the even deeper Mt. Simon Sandstone indicated that the Eau Claire Formation provided a proper seal and that porosity and permeability in the reservoir were sufficient to store and deliver gas effectively. Gas was initially injected into the Mt. Simon aquifer in 1964, and the project became operational in 1966.

The Manlove gas storage study shows the upper Mt. Simon unit to be composed of thick sandstone beds separated by discontinuous low permeability shale and siltstone layers that are thought to behave as baffles to the vertical flow of natural gas. Some of these low permeability layers appear to be laterally correlative across the field. The low permeability zones are, in some areas, composed of shale-rich zones that can range up to a few feet thick. In other areas, these zones are fine-grained sandstones where the pores have been cemented by silica cement and feldspar cement.

The Mt. Simon Sandstone at Manlove Field is not a homogeneous reservoir. The Mt. Simon Sandstone consists of stacked clean sandstone units capped with thin interbeds of fine sandstone, siltstone, and shale. Gamma-ray logs indicate that many thin shaley interbeds separate sandstones in the Mt. Simon, but most of these shaley strata cannot be correlated widely (Figure 3-19). Examination of core from the J.

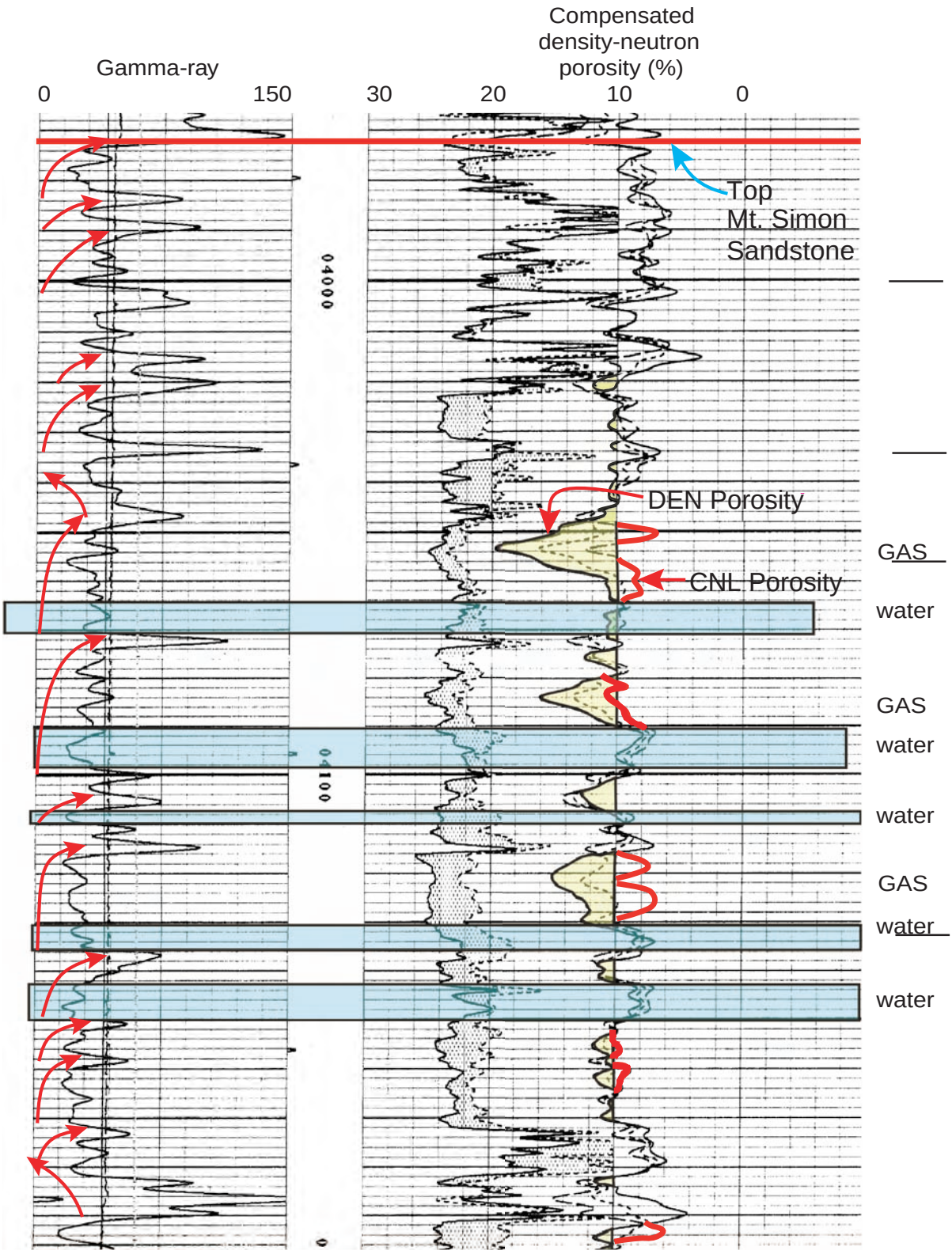

Figure 3-19 *Wireline log of the Mt. Simon Sandstone J. Williams No. 4 well, Manlove Field. Injected gas is identified where density (DEN) porosity and neutron porosity (CNL) values show divergence (yellow). Discrete intervals show "gas effect" density and neutron log separation in several clean sandstones. Individual gas-bearing sandstones appear to have basal water sands (blue) where the density and neutron porosities have similar values, suggesting that individual gas sands may be compartmentalized. Contour interval = 10 ft.*

Williams No. 4 well in the field indicated that the shale beds that caused these spikes in the gamma-ray logs are clusters of thin beds or laminae of shale, ranging from a few millimeters to a few centimeters in thickness, but with natural radioactivity sufficient to generate high gamma-ray values (Figure 3-18). These interbeds produce the high radioactivity observed in the I_{shale} gamma-ray curves. The shaley interbeds could not be readily correlated between neighboring wells just 200 m (660 ft) apart. Thus, the interbeds could not be used to finely subdivide the reservoir. The only good correlative shaley marker within the Mt. Simon, called the L120 bed, was located approximately 67 m (220 ft) below the top of the Mt. Simon Sandstone. The L120 is at approximately 1,270 to 1,280 m (4,180 to 4,190 ft).

The structure map and the three-dimensional models of the Manlove area illustrate the north-south–oriented, asymmetrical, doubly plunging anticline. Gas is stored at a depth of about 994 m (3,260 ft), filling a vertical closure of approximately 46 m (150 ft). At this depth, the area under closure is approximately 73 km^2 (28 mi^2) (Buschbach and Bond, 1974, p. 51)

Three-dimensional Deterministic Porosity Model

The porosity values derived from wireline logs were used to generate a deterministic three-dimensional model of the reservoir porosity of the Mt. Simon reservoir at Manlove Field. The grid used to generate the model had x and y increments of 76 m (250 ft). The vertical cell dimension was about 0.6 m (2 ft) but varied across the field because the model assumed a proportional thickening and thinning of grid cells in the interval between the top of the Mt. Simon and the L120 shale marker bed (Morse and Leetaru, 2005).

A three-dimensional diagram view of this model is shown in Figure 3-20. Porosity values have been lumped in 2.5% intervals for color contrast. Horizontal slice maps of the porosity model were prepared to determine lateral geometry and continuity of sandstone and shale bodies. A vertical slice from the far northeastern part of the model and a small plot of the gamma-ray log for the J. Williams No. 4 well are shown in their proper location for reference in Figure 3-20. These maps plot the average porosity of an approximately 61- to 91-cm (2- to 3-ft)-thick grid interval proportionally spaced from the top of Mt. Simon Sandstone at 1,211 m (3,972 ft) to the correlated shale (L120) located about 65 m (215 ft) below the top of the Mt. Simon.

The abundant core and modern wireline logs at Manlove Field provided the opportunity for an accurate three-dimensional porosity model of the Mt. Simon gas storage reservoir. Porosity was calculated using traditional neutron-density porosity cross plot. Neutron logs from several older wells with a “gas effect” could not be used in the modeling.

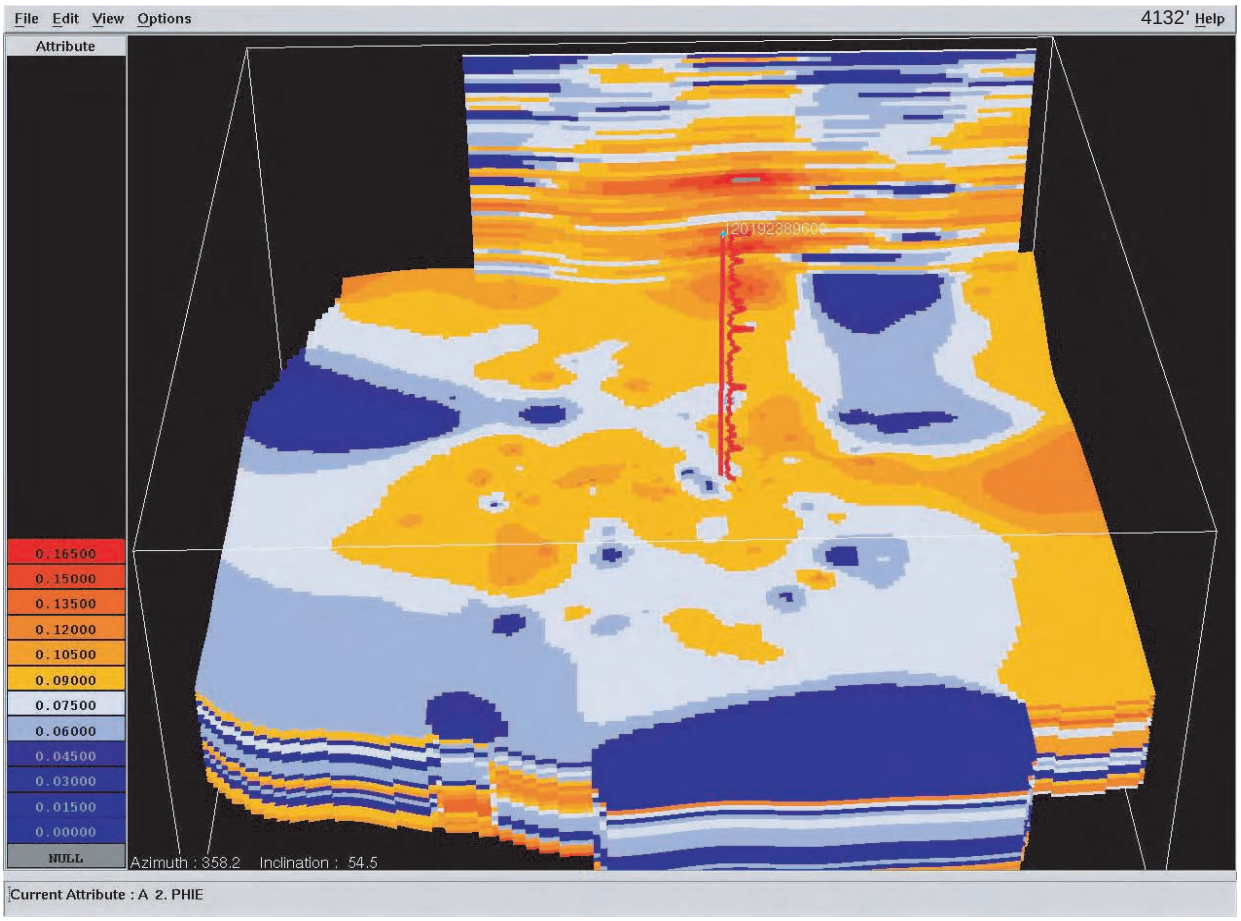

Figure 3-20 *Horizontal slice map of Manlove Field porosity model, 1,260 m (4,132 ft). An east-to-west–oriented, sinuous, high-porosity sand body crosses the center of the field just to the south of the reference well and is interpreted to be a tidal channel deposit. This sand body is jointed by a channel or remnant barrier island of sand from the north. To the east another barrier island may exist. View is toward the north.*

Reservoir characterization at Manlove Field provided a three-dimensional visualization showing porous sandstones in a series of stacked east-west–trending tidal channels and north-south–trending bars (Figure 3-20). The tidal channel sandstones are oriented west to east, approximately 300 m (1,000 ft) wide, and typically 2 to 3 m (6 to 10 ft) thick. The bar sandstones are about 1.6 km (1 mi) wide and up to 6.1 m (20 ft) thick. Natural gas is primarily stored in the bar facies that occur at depths >23 m (75 ft) below the top of the Mt. Simon.

Three-dimensional Geostatistical Model

A model was produced for the Manlove Field to provide insights as to the heterogeneity of the Mt. Simon Sandstone. Deterministic models inherently provide a general representation of regional trends and features of the formation. Stochastic modeling honors both the variogram and the histogram of the

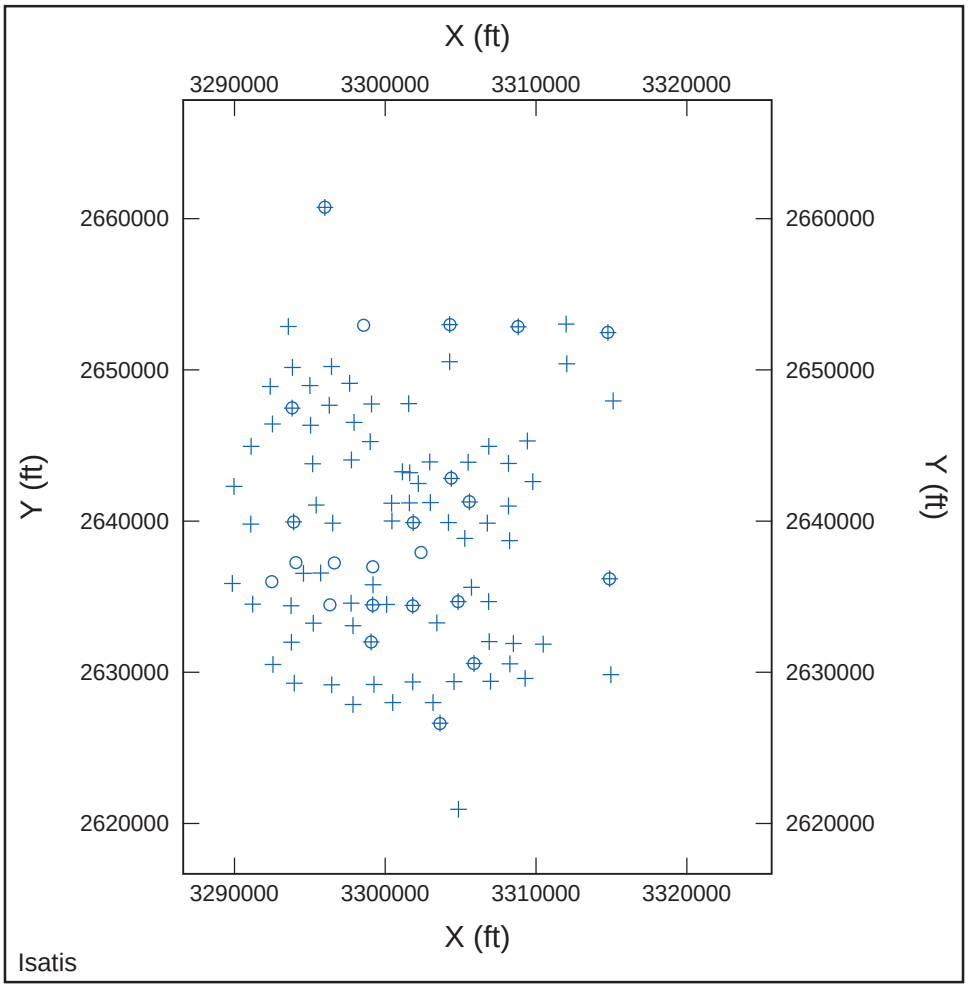

Figure 3-21 *Base map showing locations of core and wireline data used in modeling the Mt. Simon reservoir at Manlove Field. Spatial distribution is represented by crosses (wireline data) and circles (core data).*

original data set, but it also adds in a degree of statistically plausible "randomness." It is this feature that provides a potentially more realistic model for fluid flow simulation.

In addition to a deterministic porosity model of the Manlove Field, geostatistical analysis was used to study the spatial distribution and characteristics of porosity and permeability of the Mt. Simon at this field. Porosity was estimated from 35 cored wells and 98 wireline logs (Figure 3-21). The average Mt. Simon porosity was 11.1% (Figure 3-22), and the average permeability was 0.029 μm^2 (29.7 md) (Figure 3-23).

The three-dimensional experimental variograms analyzing the spatial correlation of porosity (Figure 3-24) are represented by two thin red lines (solid and dashed). A nugget and spherical combination model (thin, solid red line on Figures 3-24 and 3-25), which captures geologic continuity and range, was used to

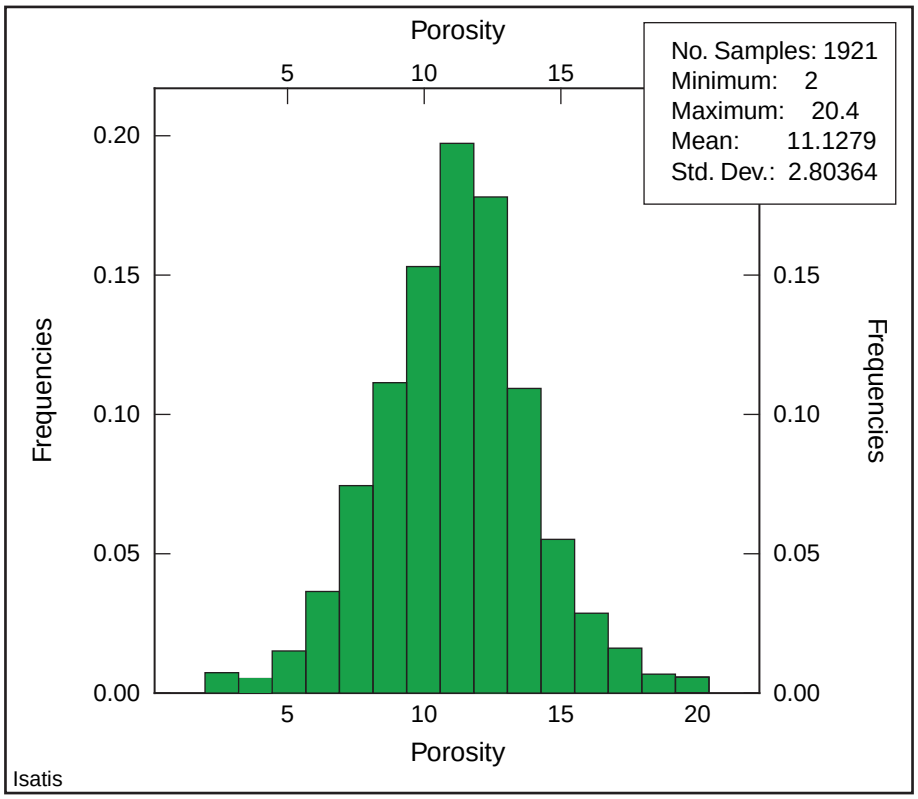

Figure 3-22 *Histogram showing the distribution of porosity from core and the corresponding statistics for the Mt. Simon reservoir at Manlove Field.*

fit the experimental variogram. This procedure enables the simulation effort to capture both horizontal and vertical continuity that is reflected in the core and wireline data.

The isotropic variogram model (Figure 3-24) shows a sill of 0.85, which is the variance (y-axis) where the model variogram has a zero slope. This is where the data become statistically stable over some distance. Figure 3-24 shows that the bodies of higher porosity have a general length of 1,524 m (5,000 ft), a width of 610 m (2,000 ft), and a depth of 3 m (10 ft) that is illustrated by the value of distance (x-axis) where the respective curve has a zero slope. A spherical model is applied (the thick yellow line) to preserve the positive definiteness with a known mathematical function. A nugget (y-intercept) is used to compensate for human errors in sampling which would cause small-scale fluctuation in the variogram, as well as the uneven distribution of data. The nugget intersects the variance at 0.3 in this model. The spherical component of this model follows the general trend of the variogram to preserve this feature in the model.

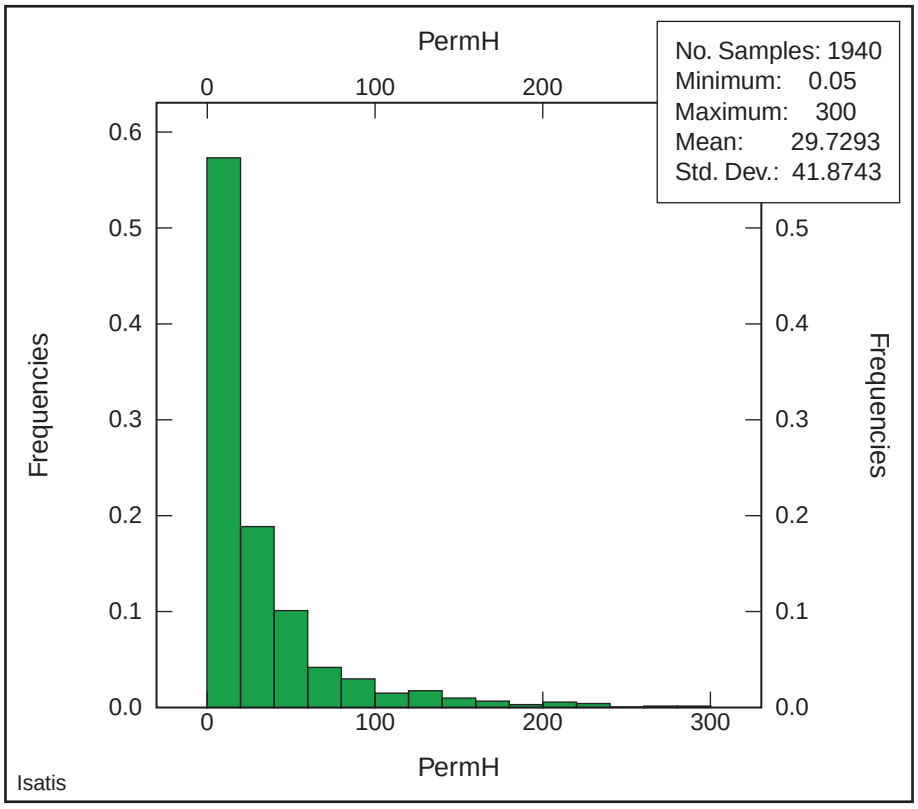

Figure 3-23 *Histogram showing the distribution of horizontal permeability (PermH) from core and corresponding statistics for the Mt. Simon reservoir at Manlove Field.*

Grid Characteristics

The grid used to generate the model had x and y increments of 91.4 m (300 ft). The vertical interval was 0.9 m (3 ft). The model assumed a constant thickness, which was calculated down from a datum consisting of the top structure map of the Mt. Simon Sandstone.

Simulation Results

Thirty simulations were performed for porosity and horizontal permeability models. From these simulations, the most statistically and geologically reasonable realizations were picked by a post-processing sequence. All simulations were compared statistically to one another to reveal which portions of the model were the most uncertain. A sophisticated statistical ranking system was used to determine which realizations were the most statistically probable of the 30. This ranking system looked at every grid node and compared all models to one another. The models that varied the most were considered outliers (or the 10th and 90th percentiles, P_{10} and P_{90}), and the model that fell in the middle (the 50th percentile or P_{50}) was considered to be the most probable. Several different maps were produced, such as probability and standard deviation maps, to demonstrate visually the uncertainty of the model. After all

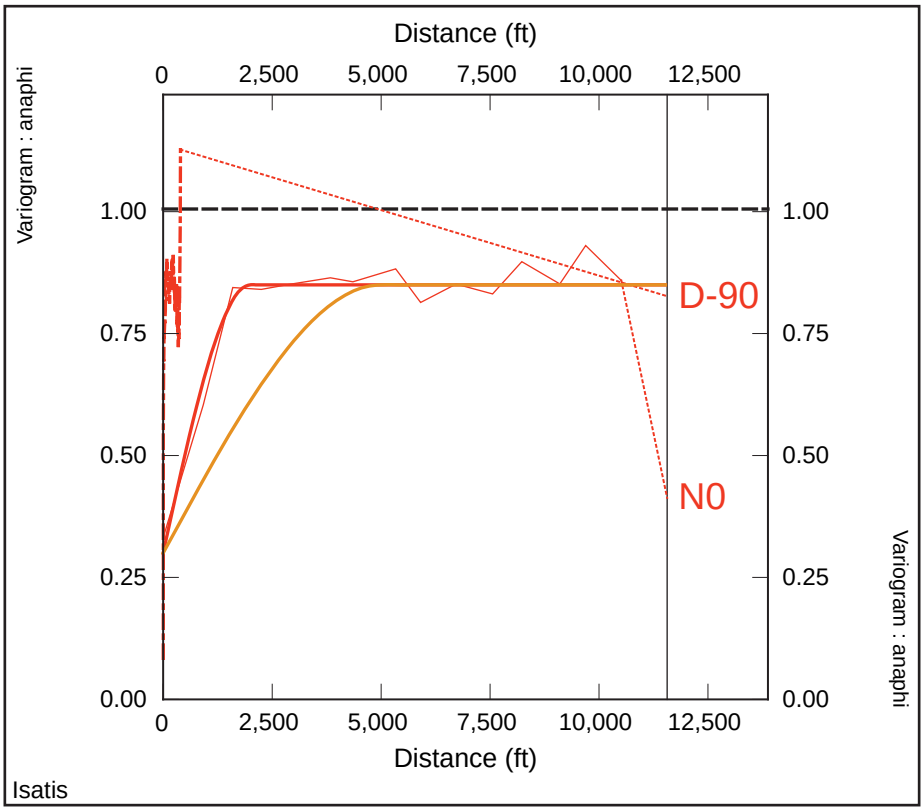

Figure 3-24 *Experimental variogram for Mt. Simon core porosity is shown here as two red lines (dashed and solid). The spherical modeled variogram structure is shown as a yellow line.*

realizations were analyzed, the most probable (or P_{50}) was picked from each variable to produce the final porosity and permeability models.

A three-dimensional diagram of the final porosity model is shown in Figure 3-26. Porosity values have been binned in 2 to 3% intervals for color contrast. A three-dimensional diagram of the final permeability model is shown in Figure 3-27. Horizontal permeability values have been displayed in logarithmic intervals for color contrast. These methods are described in detail in Appendix 1.

A three-dimensional diagram of the final permeability model is shown in Figure 3-25. Horizontal permeability values have been displayed in logarithmic intervals for color contrast. The geologic stochastic model distributed horizontal (Figure 3-25) and vertical (Figure 3-26) permeability throughout the three-dimensional model used for flow simulation. In both Figures 3-25 and 3-26, the blue colors are the highest permeability values, and the yellows and reds are low permeability. Although the colors in the figures for vertical and horizontal permeability are the same, the values are not. Vertical permeability ranges up to 0.148 μm^2 (150 md), whereas the horizontal permeability is almost 0.79 μm^2 (800 md). These lower vertical permeability layers have lateral dimensions that can be 610 m (2,000 ft) or more

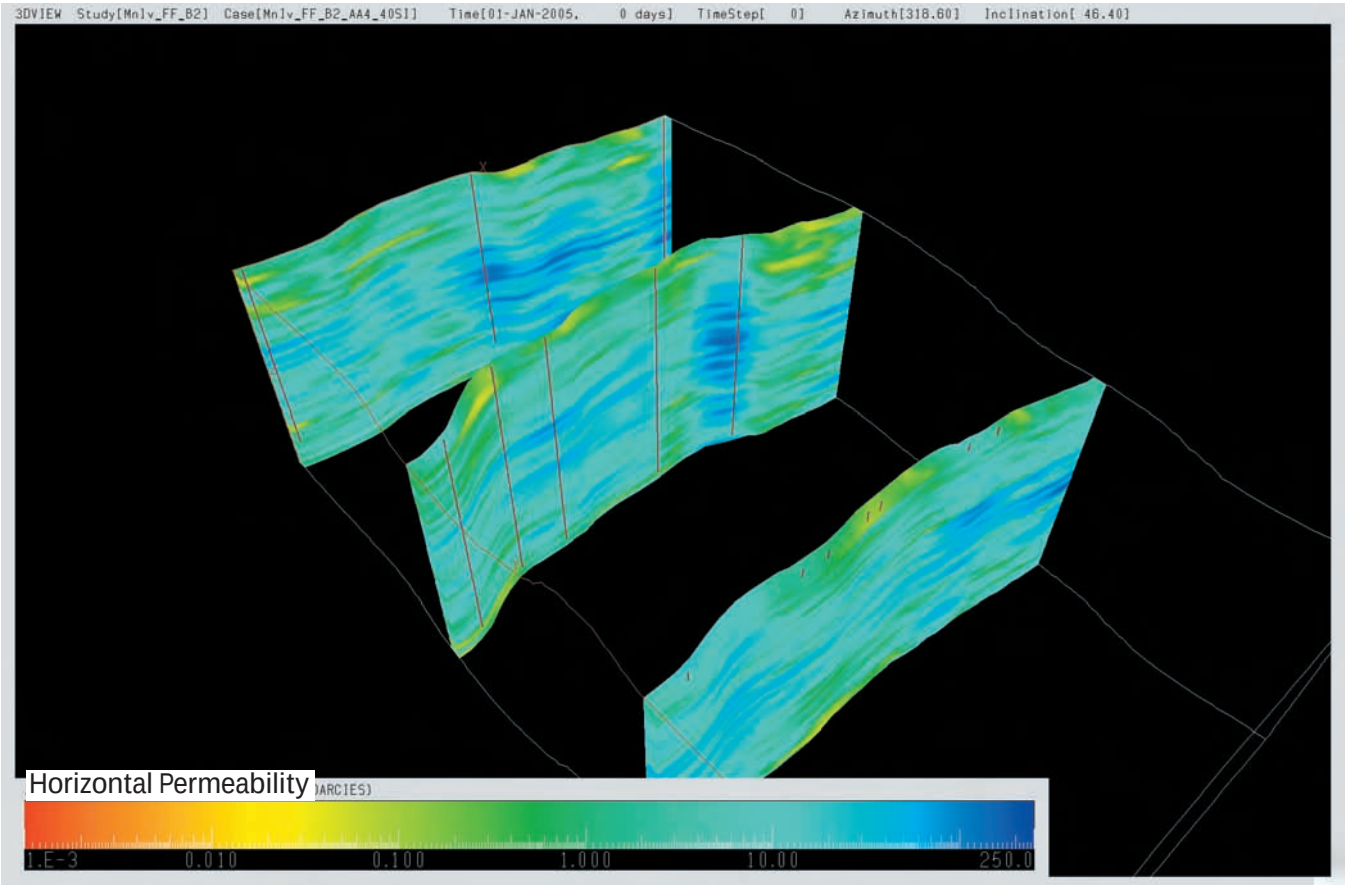

Figure 3-25 *Most probable realization of horizontal permeability of the Mt. Simon at Manlove Field. Values for horizontal permeability are displayed on a log scale ranging from 0.01 md (blue) to over 300 md (red).*

in length but are most commonly at least 300 m (1,000 ft) wide. The upper 23 m (75 ft) of Manlove Mt. Simon reservoir is composed of relatively impermeable siltstones that form a partial impediment to vertical CO_2 movement.

Published Field Studies on Mt. Simon Gas Storage Projects

Herscher and Herscher NW Fields

The Herscher and Herscher NW Anticlines (Figure 3-17) located in the southwest corner of Kankakee County, Illinois, produced oil from the Galena Group ("Trenton limestone") in the early 1900s. The field was abandoned for more than 40 years until the late 1950s, when it was converted into a natural gas storage facility for peak demand delivery in the Chicago metropolitan area. Most of this natural gas is stored in the Upper Cambrian Mt. Simon Sandstone, but additional storage occurs in the Cambrian Galesville Sandstone and Elmhurst Sandstone Member of the Eau Claire Formation (Benesh et al., 1956; Morse and Leetaru, 2005).

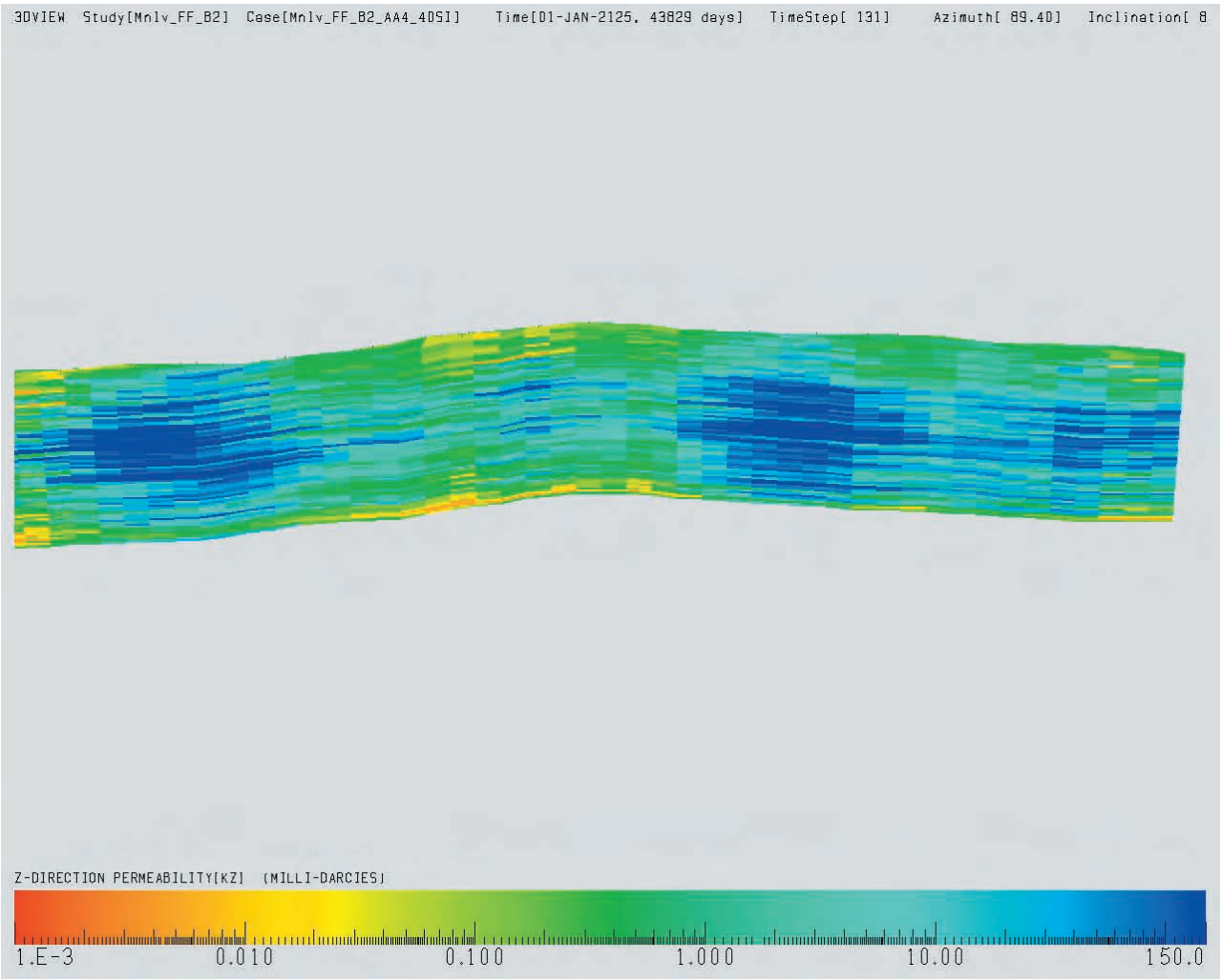

Figure 3-26 *Cross section through the central part of the Manlove structure showing the variation in vertical permeability as extrapolated from core.*

The Herscher area has two anticlinal domes, Herscher and Herscher NW (Figure 3-28). These two structures are separated by a structurally lower area or saddle. The crest of the Mt. Simon at the Herscher structure is 30 m (100 ft) lower than the crest at Herscher NW. There are 23 m (75 ft) of Mt. Simon structural closure at the Herscher structure, but <15 m (50 ft) of Mt. Simon closure at the Herscher NW structure.

In the Herscher area, the Mt. Simon is >760 m (2,500 ft) thick (Buschbach, 1964, p. 40). It is composed of fine- to coarse-grained sandstone with localized conglomerates and thin beds of shale and siltstone (Willman et al., 1975). The contact with the overlying Eau Claire Formation is conformable. A three-dimensional model of the porosity distribution at Herscher area was available and based on log and core porosity data and surface grids of the elevation of the top of the Elmhurst Sandstone Member of the Eau Claire Formation, the top of the Mt. Simon Sandstone, and two Mt. Simon shale marker beds (Morse and Leetaru, 2005). The fence diagram of this porosity model (Figure 3-29) shows that the upper part of

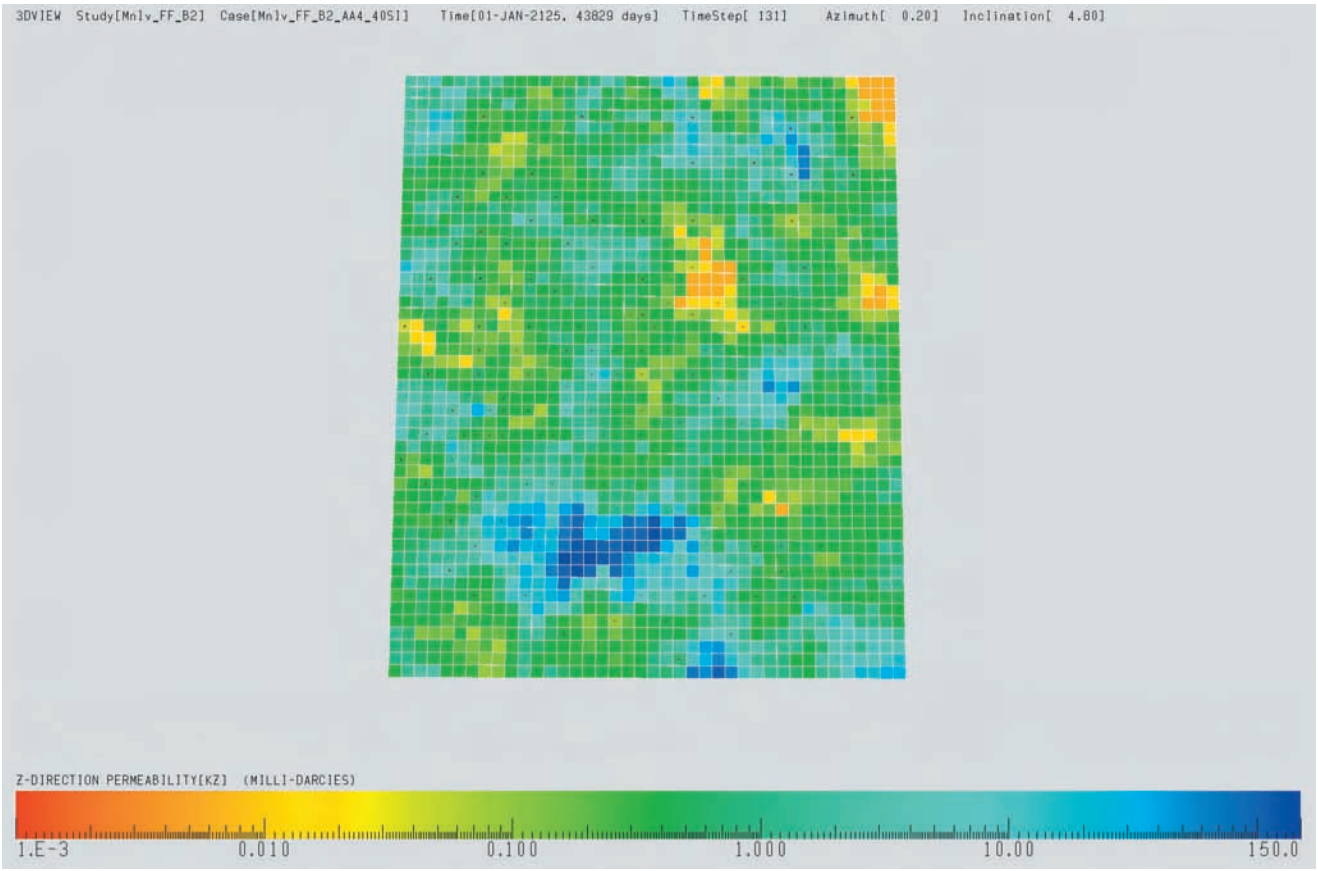

Figure 3-27 *Map of the Manlove grid values for layer 3 showing lateral variation in vertical permeability.*

the Mt. Simon in the southeastern part of the field area is not as porous as that in the northwestern area (Hersher NW). Shale beds, colored green, are discontinuous and may form baffles to gas flow.

The Eau Claire Formation is composed of alternating layers of dolomite, limestone, sandstone, shale, and siltstone. At Herscher Field, the middle of the Eau Claire Formation consists predominantly of shale beds that form an effective seal preventing gas from migrating from the Mt. Simon into overlying formations, such as the aquifers of the Galesville or St. Peter Sandstone. The basal member of the Eau Claire Formation, the Elmhurst Sandstone, is used for gas storage in Herscher NW Field. The Elmhurst Sandstone is <30 m (100 ft) thick in the Herscher area and appears to gradationally overlie the Mt. Simon Sandstone, which is the main gas reservoir.

The Eau Claire is conformably overlain by clean, porous, unfossiliferous Galesville Sandstone (Buschbach, 1964). The Galesville is used for gas storage at Herscher, but this reservoir does not appear to have an adequate seal separating it from the shallower freshwater aquifers. The first mapping of the Herscher structure was based on the St. Peter Sandstone (Athy, 1928). In 1952, the Natural Gas Storage Company of Illinois undertook extensive drilling of >100 wells to the Galena Group to further

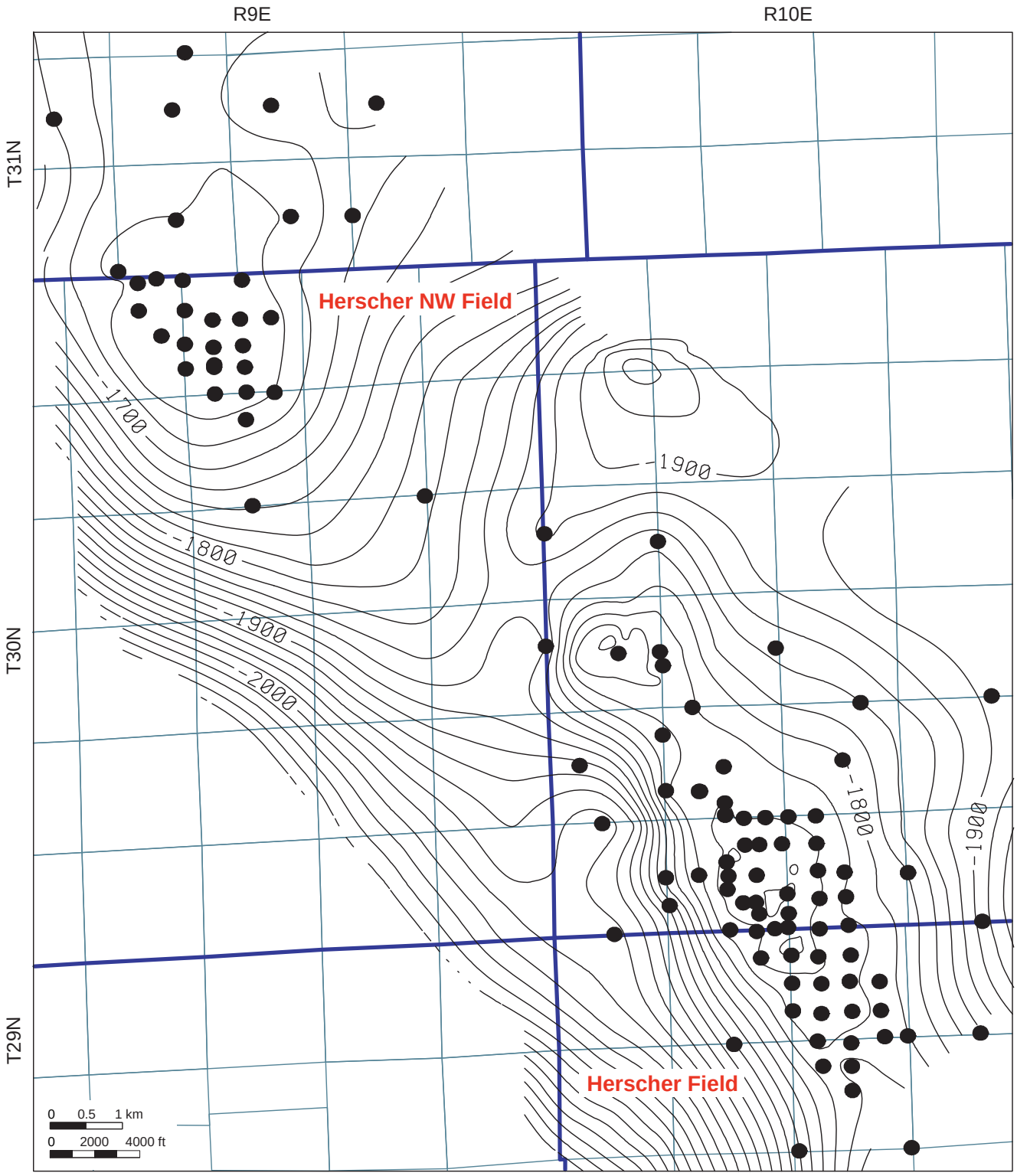

Figure 3-28 *Structure on the top of the Mt. Simon Sandstone at Herscher and Herscher NW Fields (Morse and Leetaru, 2005). Only wells that penetrated the Mt. Simon surface are shown in this figure. Contour interval = 20 ft.*

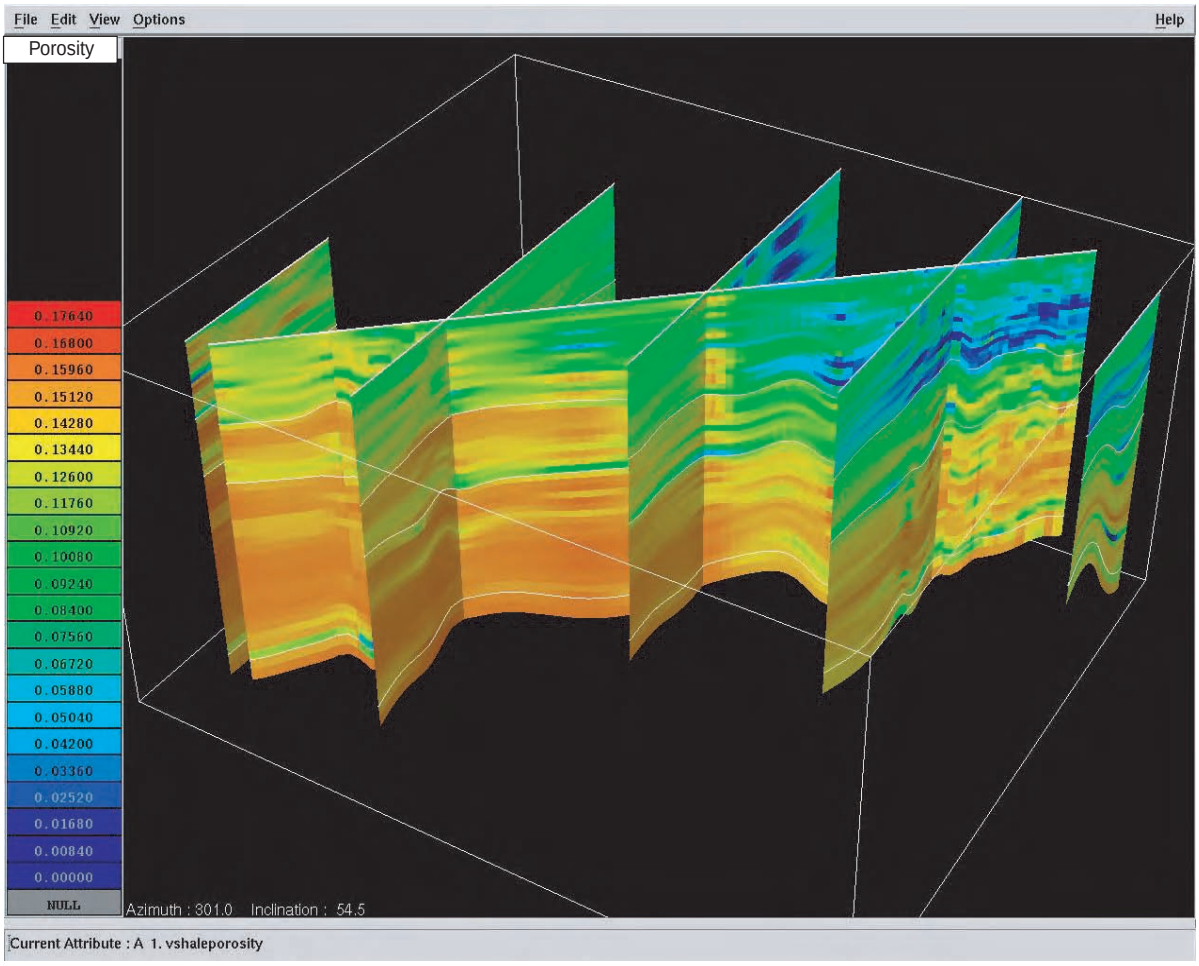

Figure 3-29 *Three-dimensional visualization of the porosity distribution of the Mt. Simon at Herscher Field. View is from the northwest (left) to the southeast (right).*

map the structural relief and areal extent of the Herscher anticlines (Buschbach and Bond, 1974). After these structure test wells were drilled, the company drilled four additional test wells to the Galesville Sandstone. In April 1953, the company began injecting gas into the Galesville Sandstone for gas storage. However, within 4 months after injection commenced, 33 shallow water wells directly above the Herscher structure began to bubble gas (Benesh et al., 1956). Gas injection into the Galesville Sandstone was immediately stopped. Although the source of the leak was never resolved, Buschbach and Bond (1974) and Benesh et al. (1956) attributed the problem to (1) a possible hole in a well's casing, (2) a possible structural fault, or (3) a poor seal. It is suspected that the lack of an adequate seal above the Galesville was the most probable cause for the leak since there are other fields with similar leaks from these Cambrian sandstone reservoirs (Buschbach and Bond, 1974).

In 1956, Natural Gas Pipeline Company of America recommenced injection of gas into the Galesville reservoir, taking some measures to control the gas. They kept the reservoir pressure of the Galesville

constant by withdrawing water from the periphery of the gas bubble and re-injecting it into the overlying Potosi dolomite. They also recycled gas from vent wells in the overlying Galena Limestone and St. Peter Sandstone back into the Galesville. In 1972, the annual withdrawal from the Galesville was >21 million m^3 (>742 million cubic ft (21 billion scf)). The base gas volume was >37 million m^3 (>1,300 million cubic ft (38 billion scf)) at the end of that withdrawal season (Buschbach and Bond, 1974). These practices are still in use today at Herscher Field.

In 1957, after testing showed the Eau Claire Formation to be a good seal, the operator began storing natural gas into the underlying Mt. Simon Sandstone in the Herscher Anticline. Throughout the early 1960s, the Natural Gas Pipeline Company drilled additional Mt. Simon wells and simultaneously continued gas injection into the Mt. Simon reservoir. This reservoir provides a second, important storage unit for the field. In 1972, the annual withdrawal from the Mt. Simon was 13.7 million m^3 (482 million scf). The Mt. Simon base gas volume was >56 million m^3 (>1,960 million scf) at the end of the 1972 withdrawal season (Buschbach and Bond, 1974).

Published Studies on Mt. Simon and St. Peter Gas Storage Projects

The following discussions of gas storage projects (Figure 3-17) are modified from Buschbach and Bond's 1974 publication of underground storage of natural gas in Illinois. For the Mt. Simon gas storage, the average reservoir properties stated are for the upper interval only.

Ancona Project

The Ancona gas storage project is located on an anticline 16 km (10 mi) long and 6.4 km (4 mi) wide, with a northwest trend in Livingston County, Illinois. The Mt. Simon Sandstone, the storage reservoir, has an average porosity of 12.3% and average permeability of 0.113 μm^2 (114 md). There are 88 m (290 ft) of closure at the top of the Mt. Simon reservoir. The Mt. Simon occurs at a depth of 657 m (2,154 ft). The original pressure tests showed no pressure communication of the Mt. Simon with overlying Ironton-Galesville and St. Peter Sandstones indicating that the Eau Claire is a good seal in this area. Ancona was developed in 1965 and remains an active gas storage field today.

Hillsboro Project

The Hillsboro gas storage project is located on a structural dome with 30 m (100 ft) of closure on top of the St. Peter Sandstone in south-central Illinois. The reservoir has an average porosity of 16% and an average permeability of 0.247 μm^2 (250 md). At Hillsboro, the St. Peter is 960 m (3,150 ft) below the surface and ranges from 30 to 49 m (100 to 160 ft) in thickness. Directly overlying the St. Peter reservoir is the Joachim limestone. Pressure tests of the St. Peter reservoir showed the Joachim Formation to be

a poor seal. The overlying Maquoketa shale is the sealing formation, and no porous intervals above this seal are in pressure communication with the underlying St. Peter.

Hudson Project

The Hudson gas storage project has 49 m (160 ft) of structural closure at the top of the Mt. Simon reservoir. The Mt. Simon reservoir at Hudson has an average porosity of 11%, has an average permeability of 0.044 μm^2 (45 md), and is about 1,158 m (3,800 ft) below the surface. Water pumping tests showed no evidence of pressure communication with any zones above the Eau Claire formation, confirming the effectiveness of this seal.

Lake Bloomington Project

The Lake Bloomington gas storage field is on a north-south–trending anticline about 7 km (4.5 mi) long and 4.4 km (2.75 mi) wide. There is about 30 m (100 ft) of closure on the top of the Mt. Simon reservoir. The Mt. Simon has an average porosity of 11%, average permeability of 0.011 μm^2 (11 md), and an average depth of 1,074 m (3,525 ft). There have been no published reports of leaks from the Mt. Simon at Lake Bloomington.

Lexington Project

The Lexington gas storage field lies on an anticline and has 30 m (100 ft) of closure at the Mt. Simon level, and the Mt. Simon reservoir has an average porosity of 11% and permeability of 0.037 μm^2 (37 md). The reservoir occurs 1,128 m (3,700 ft) below the surface. Initial pressure tests showed the Eau Claire to be a good seal, stopping fluid flow from the Mt. Simon to overlying formations.

Pecatonica Project

The Pecatonica gas storage field lies on an anticline in northern Illinois. It is one of the shallowest gas storage projects in Illinois at an average depth of 244 m (800 ft) below the surface. The gas is stored in a sandstone bed within the Eau Claire Formation. The reservoir has an average porosity of 18.6% and permeability of 0.549 μm^2 (556 md). The field has about 9 m (30 ft) of closure on top of the reservoir sandstone. The field is important because there are strong indications that groundwater movement has created a tilted gas-water interface that has increased the storage capacity of the field. The overlying Eau Clair strata provide an effective seal for this project.

Pontiac Project

The Pontiac gas storage project lies on an anticline that is 4.8 km (3 mi) wide and 8 km (5 mi) long. The Mt. Simon reservoir has an average porosity of 10% and permeability of 0.025 μm^2 (25 md) at a depth of 914 m (3,000 ft). Pressure tests indicate that the Mt. Simon is not in pressure communication with overlying formations. Pressure testing of the overlying St. Peter Sandstone suggests that this reservoir did not have an effective seal to the overlying formations; therefore, no injection was attempted into this formation.

St. Jacob Project

Natural gas is stored in the St. Peter Sandstone in the St. Jacob anticline. The anticline has 30 m (100 ft) of closure. The reservoir has an average porosity of 14%, has permeability of 0.395 μm^2 (400 md), and occurs at 872 m (2,860 ft) below the surface. There appears to be no pressure communication with the overlying Galena (Trenton) Formation, a producing oil field.

Sciota Project

The Sciota Anticline located in northeastern Illinois has 21 m (70 ft) of closure at the top of the Mt. Simon, which is 792 m (2,600 ft) deep. The Mt. Simon has an average porosity of 12% and an average permeability of 0.039 μm^2 (39.2 md). Pressure tests suggest that the Eau Claire provides a good seal between the Mt. Simon and overlying formations.

The Trenton was tested as a potential storage reservoir during early development of the field. Pumping tests suggested that the Maquoketa Shale may not be an effective seal because it is only 9 m (30 ft) thick and, therefore, too thin.

Troy Grove Project

The Troy Grove anticline is 8 km (5 mi) long and 5 km (3 mi) wide. The Mt. Simon reservoir has an average porosity of 17%, and an average permeability of 0.148 μm^2 (150 md), at a subsurface depth of 1,219 m (4,000 ft). The structure is cut by at least four faults, one of which has 55 m (180 ft) of vertical displacement. There is some evidence that the faults may have breached the Eau Claire seal, as there has been some migration of natural gas to overlying formations.

Tuscola Project

The Tuscola Anticline has >213 m (700 ft) of closure. The Mt. Simon reservoir has an average porosity of 8.5% and a permeability of 0.022 μm^2 (22 md) at a depth of 1,219 m (4,000 ft). The field has been abandoned and is no longer used for gas storage.

Hazardous Waste Disposal Projects Analogs

Sequestration of CO_2 in deep, saline aquifers is similar to the injection of industrial waste into deep, saline aquifers. In the Illinois Basin, hazardous and nonhazardous wastes have been injected into deep, saline aquifers via injection wells since the 1950s. The U.S. Environmental Protection Agency (USEPA) regulates the injection of waste into the subsurface. A well used to permanently dispose of waste in deep, saline aquifers is considered a Class I underground injection well. Class I wells are only permitted to inject waste into a saline aquifer where total dissolved solids (TDS) in water exceed 10,000 mg/L (ppm). Additional information about Class I injection wells is available (USEPA, 2001; Brower et al. 1989; Mehnert et al., 1990). Sixteen Class I underground injection wells are currently active in or near the Illinois Basin, and 33 wells have operated in the past (Table 3-1). Many of these wells inject into the Mt. Simon formation, which is vertically overlain by the Eau Claire shale. No Class I wells have been permitted to operate in the western Kentucky portion of the Illinois Basin.

Table 3-1. Class I underground injection wells in the Illinois Basin.[1]

State	County	Injection zone	Upper confining layer	Currently active
IL	Clark	Devonian	New Albany	N[2]
IL	Clark	Salem	Pennsylvanian	N[2]
IL	Douglas	Eminence-Potosi	Prairie du Chien	N[2]
IL	Douglas (3 wells)	Eminence-Potosi	Prairie du Chien	Y
IL	Fayette	Salem (Mississipian)	St. Louis	N[3]
IL	Kankakee	Mt. Simon	Eau Claire	N[3]
IL	Putnam	Elmhurst-Mt. Simon	Eau Claire	Y
IL	Vermilion	Potosi	Prairie du Chien	N[2]
IN	Elkhart	Mt. Simon	Eau Claire	N[2]
IN	Lake	Mt. Simon	Eau Claire	Y
IN	Lake (3 wells)	Mt. Simon	Eau Claire	N[2]
IN	LaPorte (3 wells)	Mt. Simon	Eau Claire	Y
IN	LaPorte (2 wells)	Devonian	New Albany	N[2]
IN	Porter (8 wells)	Mt. Simon	Eau Claire	Y
IN	Posey	Tar Springs (Mississipian)		N[2]
IN	Posey (2 wells)	Bethel (Mississipian)		N[2]
IN	Vanderburgh	Unknown (well depth = 2,500 ft)		N[2]
IN	Vermillion	Mt. Simon	Eau Claire	N[2]

[1](Brower et al., 1989; USEPA, 2003).
[2]Well plugged.
[3]Well switched from Class I to Class II injection well.

These wells are valuable for the assessment of CO_2 sequestration potential for several reasons. First, they demonstrate the concept that liquids can be safely placed and stored in the subsurface in the same reservoir formation as is being considered for CO_2 sequestration. In fact, operators of Class I underground injection wells must demonstrate, typically through flow modeling, that the waste will remain in the subsurface for at least 10,000 years. These wells also provide extensive geologic data

in areas that otherwise would not have such data at greater depths. These data include basic geologic data, such as lithology and stratigraphy, and hydrogeologic data, such as porosity and permeability. These wells have been used to inject millions of gallons of liquid waste into several formations—Mt. Simon, Eminence-Potosi, and Devonian and Salem carbonates (Table 3-1)—several of which are potential storage targets for CO_2 sequestration. Finally, the operational history of these underground injection wells should provide useful information on the operation and testing of injection wells for CO_2 sequestration.

The USEPA (2001) reviewed Class I underground injection wells nationwide to evaluate the risk of these wells to human health and the environment. Only four cases of significant wastewater migration from these wells were documented; none of these leaks affected a drinking water source. These leaks occurred in Florida (3 cases) and Ohio (1 case). USEPA (2001) concluded that Class I underground injection wells for wastewater disposal provide an extremely low risk to an underground drinking water source.

Groundwater Movement

In this discussion, groundwater is inclusive of fresh groundwater in the Mt. Simon in northern Illinois and brine in the southern part of the state. Groundwater flow in the deeper part of the Illinois Basin is not well understood because few wells penetrate deep formations such as the Mt. Simon Sandstone. However, based on limited field data and numerical modeling, some information on groundwater flow is available.

Within the Mt. Simon Sandstone aquifer, Bond (1972) determined that groundwater flows from west to east beneath the northern third of Illinois. Bond (1972) also noted that groundwater flows to the south in the deeper part of the Illinois Basin, but some data supporting this conclusion were questionable. In some areas, the available data indicate that the flow direction appears to be random. Groundwater flow in the Mt. Simon Sandstone is generally very slow, on the order of inches per year. Finally, Bond (1972) noted that in some areas groundwater flows upward from the Mt. Simon aquifer to the Ironton-Galesville in the Chicago area, where pumpage has lowered pressures in the Ironton-Galesville.

Gupta and Bair (1997) used a steady-state, variable density, groundwater flow model to evaluate flow in the Mt. Simon sandstone in the Midwest (Ohio, Indiana, and parts of Illinois, Wisconsin, Michigan, Pennsylvania, West Virginia, and Kentucky), including the eastern portion of the Illinois Basin. Results from this modeling indicated that flow in the shallow layers, such as the Pennsylvanian bedrock, follows topographic-driving forces—recharge in upland areas and discharge in topographic lows such as river valleys. For deeper layers, such as the Mt. Simon Sandstone, that may be potential CO_2 sequestration

reservoirs in the Illinois Basin, the flow patterns are influenced by the geologic structure with flow away from arches, such as the Kankakee Arch and toward the deeper parts of the Illinois Basin (Figure 3-31). The model also indicated that groundwater flows upward from the Mt. Simon to the Eau Claire and downward from the Ironton-Galesville into the Eau Claire (Figure 3-30), but these vertical velocities are very small (<0.25 cm/year (<0.01 inch/year)). Gupta and Bair (1997) estimated that 17% of the water entering the Mt. Simon exits via upward leakage into the upper confining layer, and the remaining 83% flows laterally.

These modeling results agree with a hypothesis described by Bredehoeft et al. (1963) to explain the high brine concentrations (three to six times higher than present seawater) found in some deep basins including the Illinois Basin. Bredehoeft et al. (1963) argued that confining layers such as the Eau Claire act as semi-permeable membranes, allowing water to pass out of permeable formations such as the Mt. Simon while retarding the passage of charged salt particles. The clay minerals in the confining layer have a net negative charge that retards the anions in the water. These anions then retard the movement of the cations (positive charge) via electrical attraction. This process happens very slowly, over hundreds of thousands of years.

This information reflects our current understanding of groundwater flow in the Illinois Basin. This understanding is based on very limited data and may change as additional information becomes available.

Fractures and Structural Mechanics

Because there is no fracture or structural mechanics data specific to CO_2 injection in the Illinois Basin, the experiences from the pressure cycling process associated with underground natural gas storage in the Basin were used. There are key mechanical properties of the reservoir and caprock materials required to assess formation geomechanical response to pressure cycling associated with injections. Safe operation pressures for a reservoir depend on three primary geomechanical factors: (1) mechanical properties of the reservoir and overburden, (2) the natural state of stress in the reservoir and overburden, and (3) the stress changes induced in the reservoir and overburden by gas pressure cycling.

To evaluate stresses in the reservoir and caprock induced by pressure cycling, a geomechanical model can be used to evaluate shearing at the interface of the caprock with the reservoir and horizontal stresses from lateral expansion and contraction of the gas storage zone. The stresses are best analyzed with one of several numerical models, such as finite element, finite difference, or boundary and discrete element models. The accuracy of any model depends on the accuracy and availability of material properties and boundary conditions.

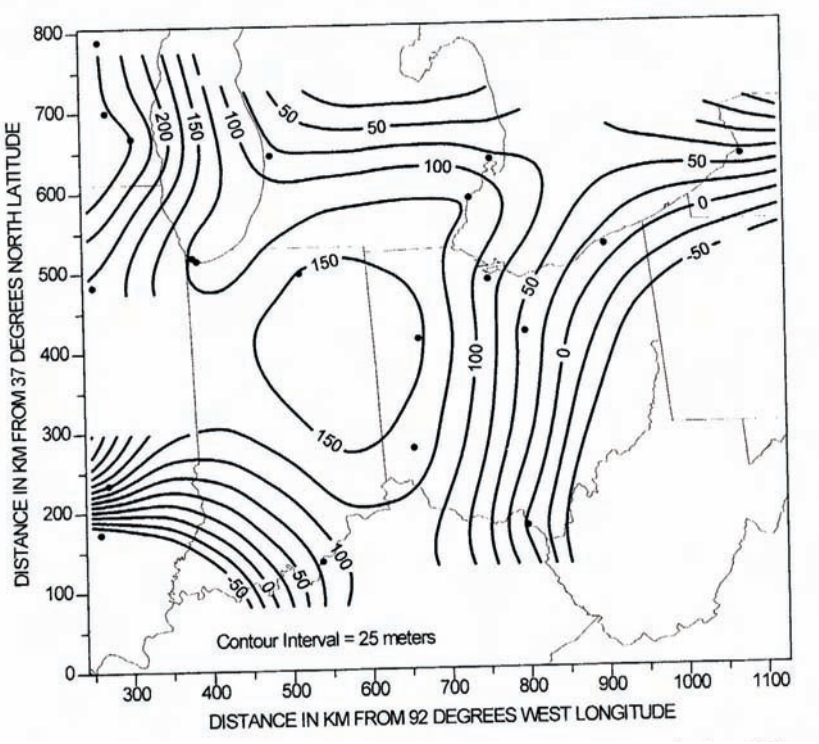

Figure 3-31 *Observed variable-density head in the Mt. Simon sandstone (from Gupta and Bair, 1997). Groundwater flows from areas of higher head to lower head, along lines perpendicular to the head lines. Contour interval = 25 m.*

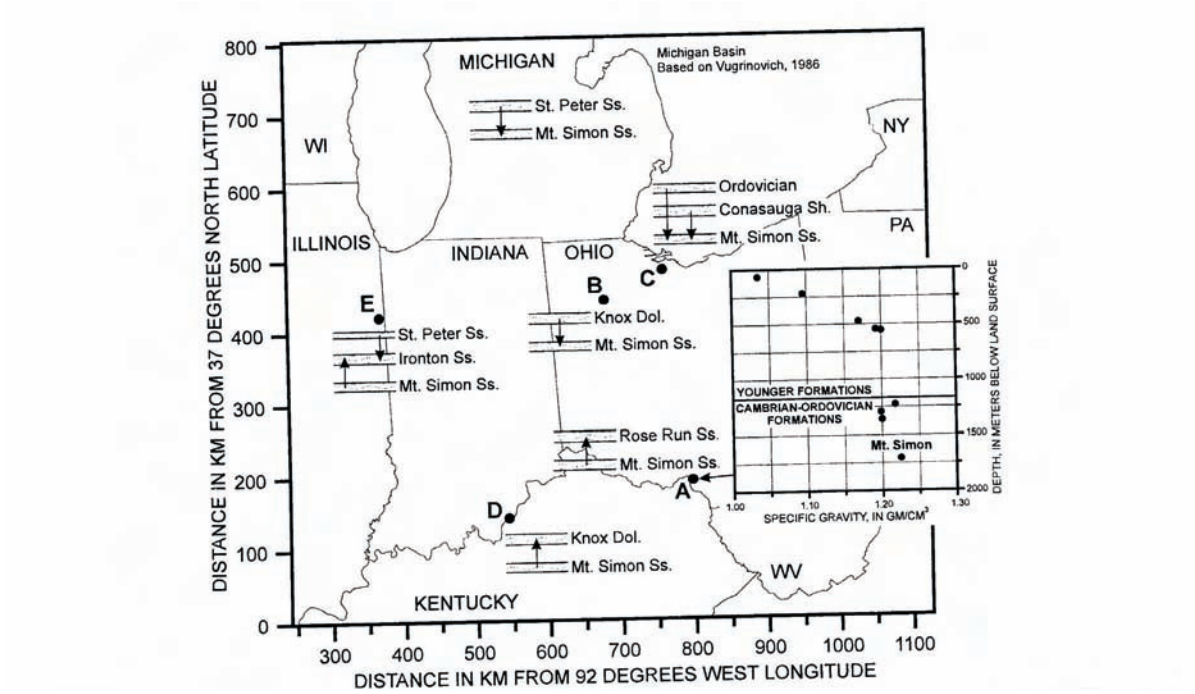

Figure 3-30 *Observed vertical flow components in the Mt. Simon Sandstone around the Upper Midwest (from Gupta and Bair, 1997). Michigan Basin based on Vugrinovich (1986).*

Faults and Earthquakes

Illinois is susceptible to earthquakes ranging from minor magnitude (<2) events to large earthquakes >5.0. Illinois earthquakes occur primarily in the southern part of the state, and most of the earthquakes are concentrated in a few areas south of the most likely sequestration sites. The primary concern is that movement on faults could create migration pathways along which CO_2 might escape to shallower zones or to the surface. Although the presence of multimillion-year stable trapping of oil and gas in porous and permeable reservoirs in Illinois suggests that migration of fluids is not an important issue, tectonically active areas were eliminated as potential sequestration sites.

There are two possible relationships between earthquakes and underground sequestration reservoirs: one is induced seismicity from the operation of underground CO_2 storage reservoirs, and the second is the effects of earthquakes on the reservoirs.

Reservoir-Induced Seismicity

Underground gas storage facilities may produce seismicity through two possible scenarios: changing stress conditions across pre-existing fractures/faults or through expansion and contraction of the reservoir during cycling of gas storage. The first condition reduces the normal stresses on fractures or faults by increasing fluid pressures within the fault plane. This change pushes the sides of the fault or fracture plane apart, reducing the friction forces and allowing slippage of the two sides past each other at lower stresses in the region. The second condition of expansion and contraction of the reservoir raises and lowers the caprock and overburden, which causes sliding or shearing between the layers of rock above the reservoir, producing microseismic activity. Microseismic activity can also be produced through the expansion/contraction movements that cause tensile fractures in the rock layers themselves under conditions of excessive bending and low tensile strength of the rock.

According to Kisslinger (1976), there are only a few documented examples of tectonic movements induced by fluid injection through boreholes: Rocky Mountain Arsenal well, Denver, Colorado (Healy et al., 1968), and the controlled experiment at the Rangely Oil Field (Raleigh et al., 1976) in Rangely, Colorado. In 1967, in the Rocky Mountain Arsenal, Colorado, a magnitude 5.5 earthquake was attributed to high-pressure (38,900 kPa (389 bars) or 12,000 kPa (120 bars) above the original reservoir pressure) fluid injection into a 3.8-km (2.4-mi)-deep well (Healy et al., 1968). This magnitude earthquake would be considered large for the central United States. This magnitude equals that of the largest earthquake in the central United States during the last century, which caused damage to buildings up to 177 km (110 mi) away. This magnitude is fairly extreme compared with most found in literature associated with fluid injection/withdrawal.

Raleigh et al. (1976) reports on the Rangely, Colorado, experiment where fluid was injected into a sandstone reservoir where faults run through it. The authors were able to closely predict the pressure needed to induce seismicity by measuring the in situ stresses of the area, knowing the orientations of fault planes, and measuring the frictional properties of the reservoir rocks. Knowing the original reservoir pressures is also very useful in assessing pressures for safe fluid injection pressures. Nagelhout and Roest (1997) reviewed a similar problem for a reservoir in salt and found that faults running through the reservoir may have slippage due to pressure changes from normal operations associated with cycling of pressures. Evans et al. (2005) reviewed microseismicity associated with a 3-km (1.9-mi)-deep, massive fluid injection into granite in France that contained interconnected shear zones. Small seismicity was produced when fluid pressure was 50 to 90 bars above original formation pressures.

Other examples of fractures and injection pressures below the least principal stress are presented by Baisch and Harjes (2003) following injection experiments in a highly characterized 9.1-km (5.7-mi)-deep borehole in Germany. During the experiments, elevated pore fluid pressure remained well below the least principal stress and thus was too small to cause hydraulic opening of existing fractures. Those authors thought that the detected seismicity was the result of lowering the effective normal stress across fractures and that fracture permeability exhibits large spatial and directional variations. These variations control fluid migration paths and associated propagation of elevated fluid pressure during fluid injection. The highly permeable branches of this fracture network strongly affect the propagation of fluid pressure and prohibit the concept of a smooth "pressure front." The observed seismicity was associated with fractures that allowed large volumes of fluid flow.

McClain (1970) suggests several conditions that must be satisfied if injection of fluids is to result in inducing earthquakes:

1. The regional tectonic stress state is near to the breaking strength of the rocks before injection is started. This state implies that the injection well is located in an area of at least moderate tectonic activity and that the reservoir formation is at a considerable depth—several thousand feet deep.

2. Reservoir formation should accept the waste fluids into its porosity, but its permeability needs to be low enough that pore-pressure buildup is possible. The reservoir formation type that best fits this requirement is one where the porosity results from an existing fracture system in crystalline rocks that otherwise are nonporous and have low permeability. A formation with porosity from intergranular spaces, such as in sandstone, could also meet this requirement if permeability is low and/or injection pressure is high.

3. Fluid injection must be at rates and pressures such that the formation pore pressures are significantly increased over a wide area.

A much lower level of seismic activity is the microseismicity associated with changes in gas reservoir volume. Zoback and Zinke (2002) showed that different stress regimes exist above the top of a reservoir than at the edge of two different reservoirs. These regimes changed with changes in volume of the reservoir, and microseismic activity was recorded in the top of the reservoir and in the shale caprock. Enough shearing had taken place to cause casing failures in both fields. Knoll (1992) showed that fluid-induced seismic events occur even for quickly decreasing primary fluid pressure in low permeability materials. Upon gas or fluid withdrawal, the fast decrease in primary fluid pressure near the well bore releases pressures and in situ stress near the bore, but distant low permeability zones away from the bore can maintain high secondary pore pressures. This situation reduces the shear strength of the small weakness zones by reducing the local normal stress and triggering small local fluid-induced seismic events.

In order to detect and accurately locate the epicenter of these microseismic events, multiple geophones need to be installed fairly closely to the events. White et al. (2004) presented the general layout of seismic monitoring equipment in vertical boreholes about 200 m (656 ft) above the Weyburn Field, Saskatchewan reservoir, to monitor this microseismicity. The consortium will evaluate the use of microseismicity in the Phase II extension of this project.

Earthquake Effects on Reservoirs

Another point of interest concerning earthquakes is the effect they might have on the reservoirs themselves. Without published experiences of the effects of earthquakes on gas storage facilities, one way to investigate the effects is to look at how other underground reservoirs are affected. Los Alamos laboratory has been working on seismic stimulation of oil reservoirs for enhanced production. Roberts (1997) cited that very little proof-of-concept existed and that anecdotal stories related that low-frequency (1 to 500 Hz) seismic stress waves had been observed to enhance oil production from depleted reservoirs. The project focused on (1) laboratory core flow experiments, (2) field seismic monitoring of downhole stimulation tests, and (3) theoretical modeling of the coupled stress/flow phenomenon. One field test at Lost Hills, California, had seismic stimulation increase oil production by approximately 20%, which was similar to an increase observed in this field after the magnitude 7.1 Hector Mine earthquake. Jackson (2001) also presented advances in seismic stimulation technologies under the Petroleum Technology Transfer Council work.

Storage Volume and Mechanisms

Water Salinities

Chemistry data are sparse for the water in the Mt. Simon Sandstone in the Illinois Basin, especially in areas other than the natural gas storage fields that use the Mt. Simon sandstone as a reservoir. A map of

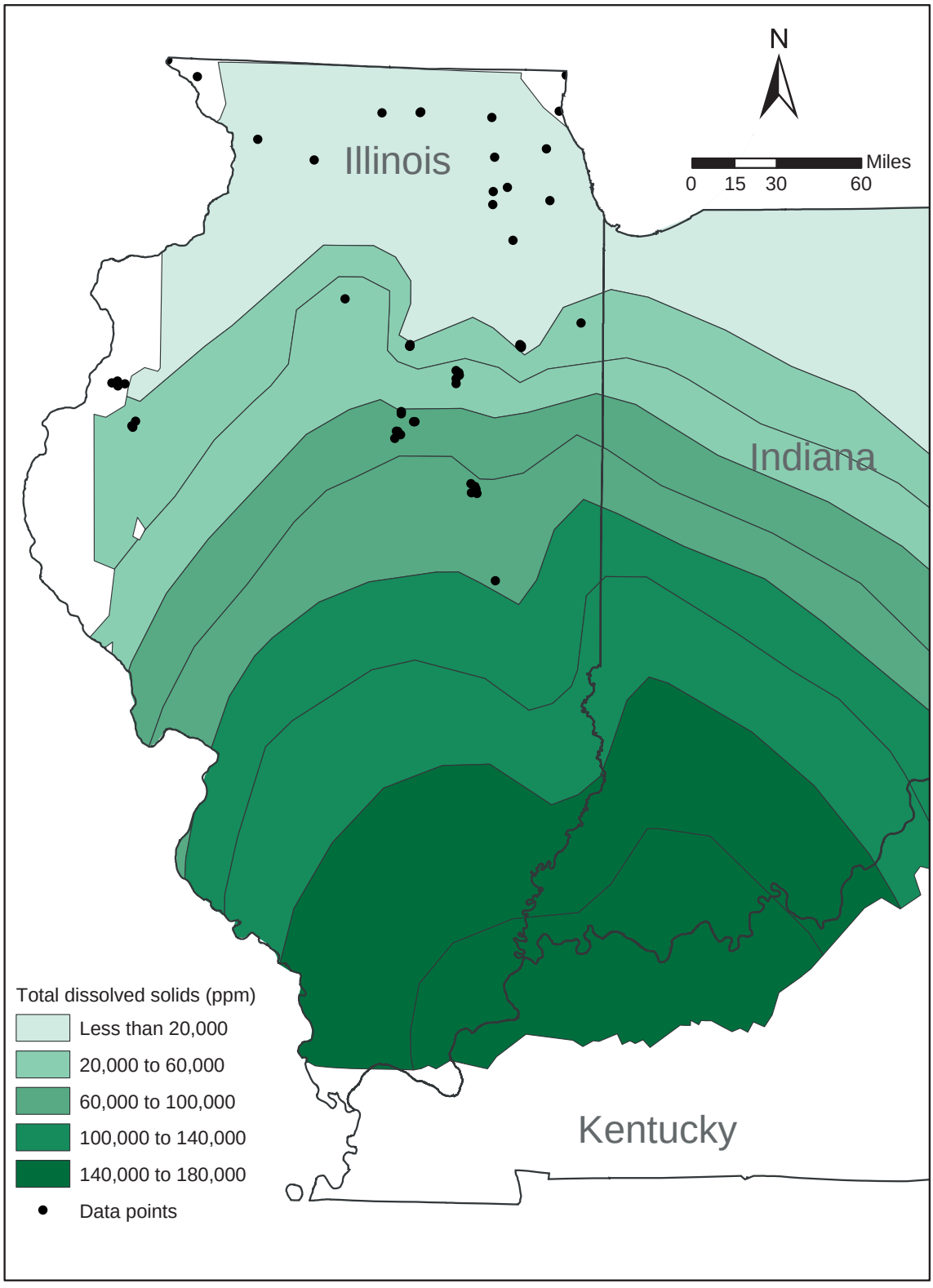

Figure 3-32 *Regional salinity map of the Mt. Simon Sandstone formation waters.*

the variations in salinity (TDS) of the water in the upper Mt. Simon Sandstone is shown in Figure 3-32. The salinity of the water in the Mt. Simon Sandstone increases with depth from the north and northwest to south and southeast. The total dissolved solids increase from 235 mg/L (235 ppm) to as much as over 180,000 mg/L (180,000 ppm) along this trend. In northern Illinois, the Mt. Simon is a freshwater aquifer and contains potable water. The surface recharge area of the Mt. Simon lies to the north in Wisconsin where the formation outcrops.

In general, CO_2 solubility in water

- increases with an increase in pressure,
- decreases with an increase in temperature, and
- decreases with an increase in salinity.

To estimate the change in CO_2 solubility with depth, a combination of all three effects (pressure, temperature, and salinity increase with depth) occurs. Figure 3-33 shows a trend of CO_2 solubility with depth using a constant pressure (9.795 kPa/m (0.433 psi/ft)) and temperature gradient (–17.22°C/30.48 m from 16.67°C at 30.48 m (1°F/100 ft from 62°F at 100 ft)) with four assumed salinity gradients. The salinity gradients were based on a TDS of 85,000 ppm at 1,372 m (4,500 ft) (Manlove Field) to assumed values of 100,000, 150,000, and 250,000 ppm at 3,048 m (10,000 ft); freshwater was the fourth "gradient." Between 1,372 and 3,048 m (4,500 and 10,000 ft), the salinity gradients were 2.73, 11.8, and 30.0 ppm/ft, respectively.

The freshwater gradient shows that CO_2 solubility increases with depth because the increase in CO_2 solubility as a result of increasing pressure dominates compared with the decrease in CO_2 solubility as a result of increasing temperature. However, when salinity is considered, the 2.73 ppm/ft gradient causes nearly constant CO_2 solubility with depth. Gradients exceeding this level decrease CO_2 solubility with depth. This relationship is a very important aspect in assessing CO_2 sequestration storage potential in the deep, untested saline formations around the world.

Temperature and Pressure Dependence of CO_2 Density

Density changes nonlinearly with pressure (constant temperature) and nonlinearly with temperature (constant pressure) primarily due to phase changes and at subcritical temperature and pressure. Moreover, an increase in temperature decreases density, whereas an increase in pressure increases CO_2 density. Assuming pressure and temperature gradients of 9.795 kPa/m (0.433 psi/ft) and -17.22°C/30 m (1°F/100 ft), respectively, the net result of the simultaneous increase in pressure and temperature with depth on density is nearly linear (Figure 3-34) and approximately constant from 1,200 to 2,400 m (4,000 to 8,000 ft) at 0.732 to 0.772 g/cm^3 (45.7 to 48.2 pound mass [lbm]/ft^3). This linearity occurs at depths greater than about 2,800 ft where supercritical CO_2 is expected using this pressure and temperature gradient.

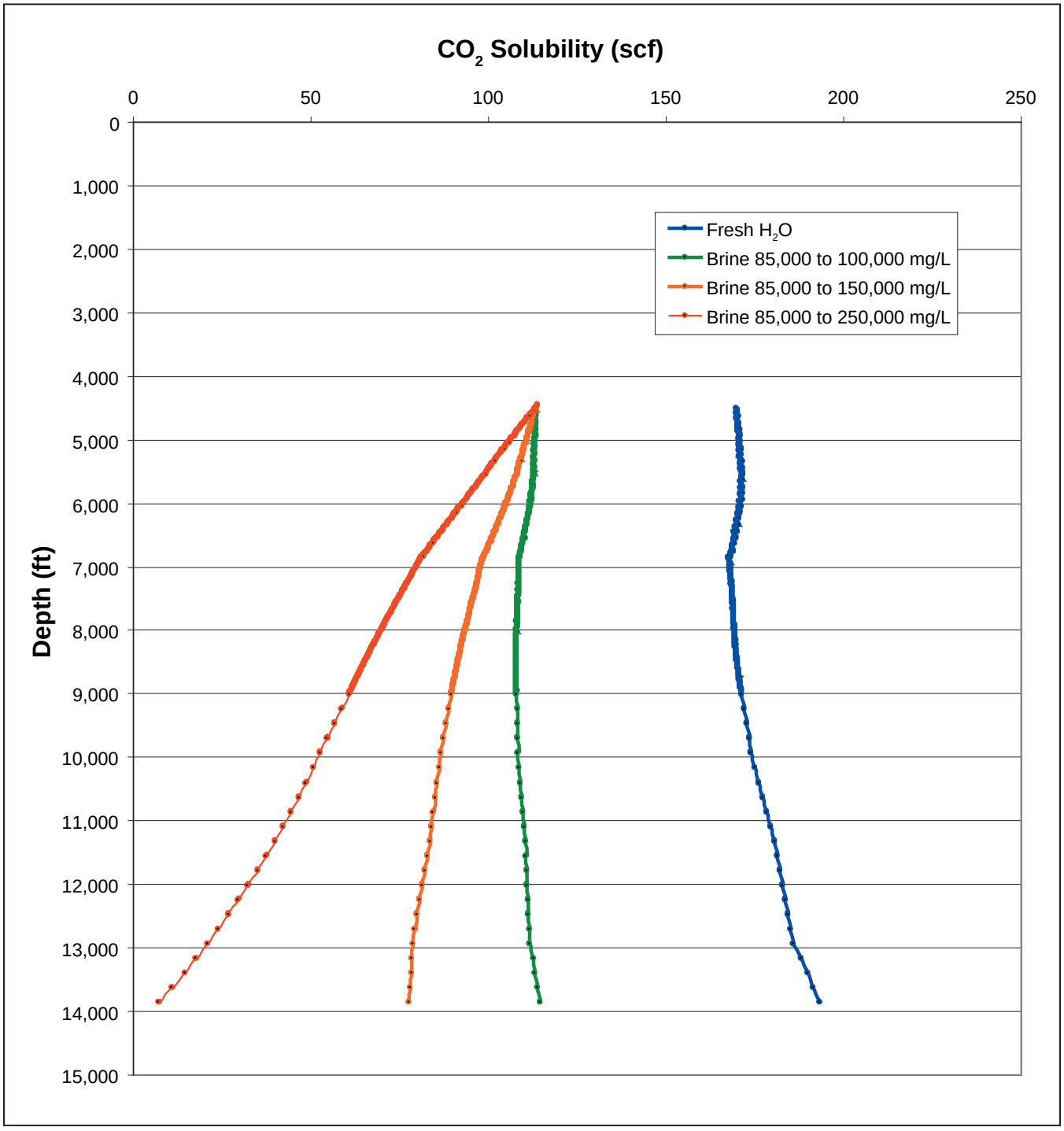

Figure 3-33 *Relationship of CO_2 solubility with depth for freshwater and brine (Chang, 1998).*

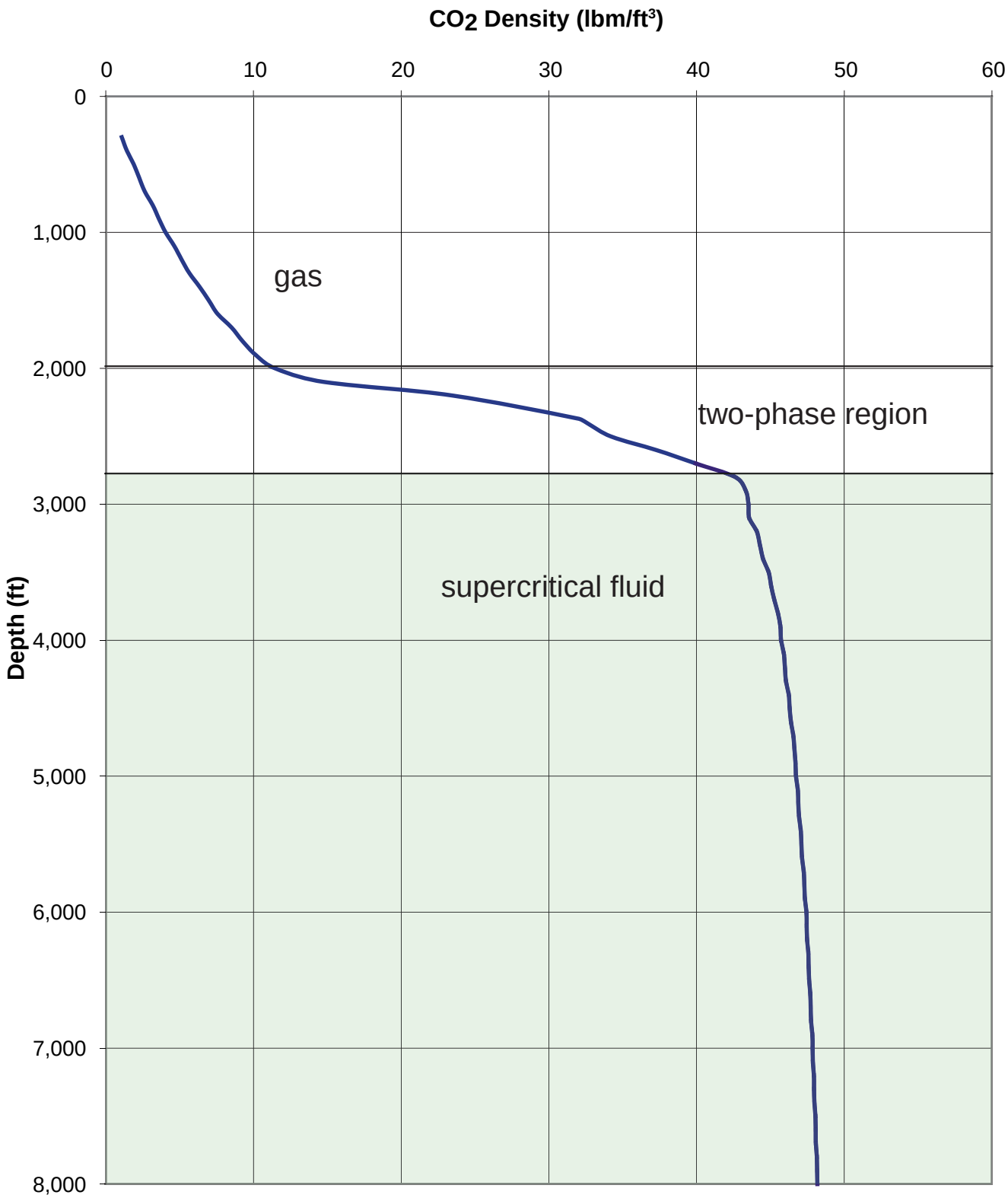

Figure 3-34 *Relationship of CO_2 density with changes in depth (Chang, 1998). This relationship with depth assumes 0.433 psi/ft pressure gradient and 10°F/100 ft (datum: 62°F at 100 ft).*

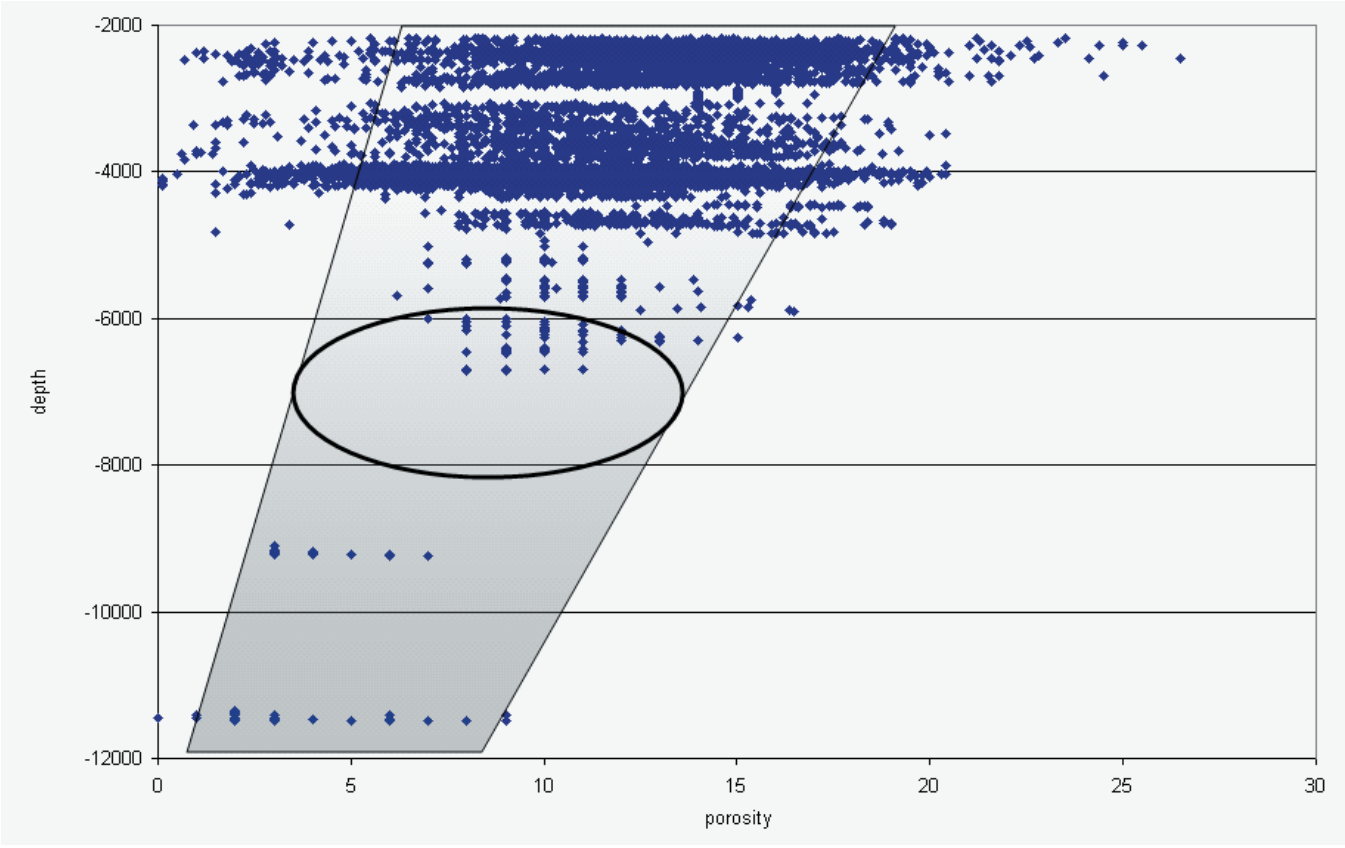

Figure 3-35 *Relationship of the Mt. Simon reservoir porosity with measured depth below the surface.*

Mt. Simon Porosity with Depth

Core analysis data were compiled from reports and well data donated to the ISGS, primarily by the gas storage operators. The core data came from 56 wells and included about 8,400 values from tested samples that ranged in depth from 661 m (2,168 ft) to 1,799 m (5,900 ft). These data were supplemented with 610 porosity values calculated from geophysical logs (density or density-neutron cross plots) of deep, sandstone-rich Mt. Simon Sandstone intervals that ranged in depths from 1,372 m (4,500 ft) to 455 m (1,492 ft) from five deep Illinois wells (Figure 3-35).

There are not enough data to evaluate the relationship of Mt. Simon porosity with depth. In general, there should be a reduction in porosity with depth because of compaction. However, variation in sedimentary facies complicate this interpretation. From gamma-ray logs, the upper portion of the Mt. Simon appears to be composed mostly of thin-bedded sandstone bodies with a high percentage of clay minerals. These thin-bedded facies appear to be significantly different from the thick-bodied sandstones found in the deeper Mt. Simon as shown in both the Hinton No. 7 (Figure 3-36) and the Johnson No. 1 (Figure 3-37) wells. The lower facies show excellent porosity.

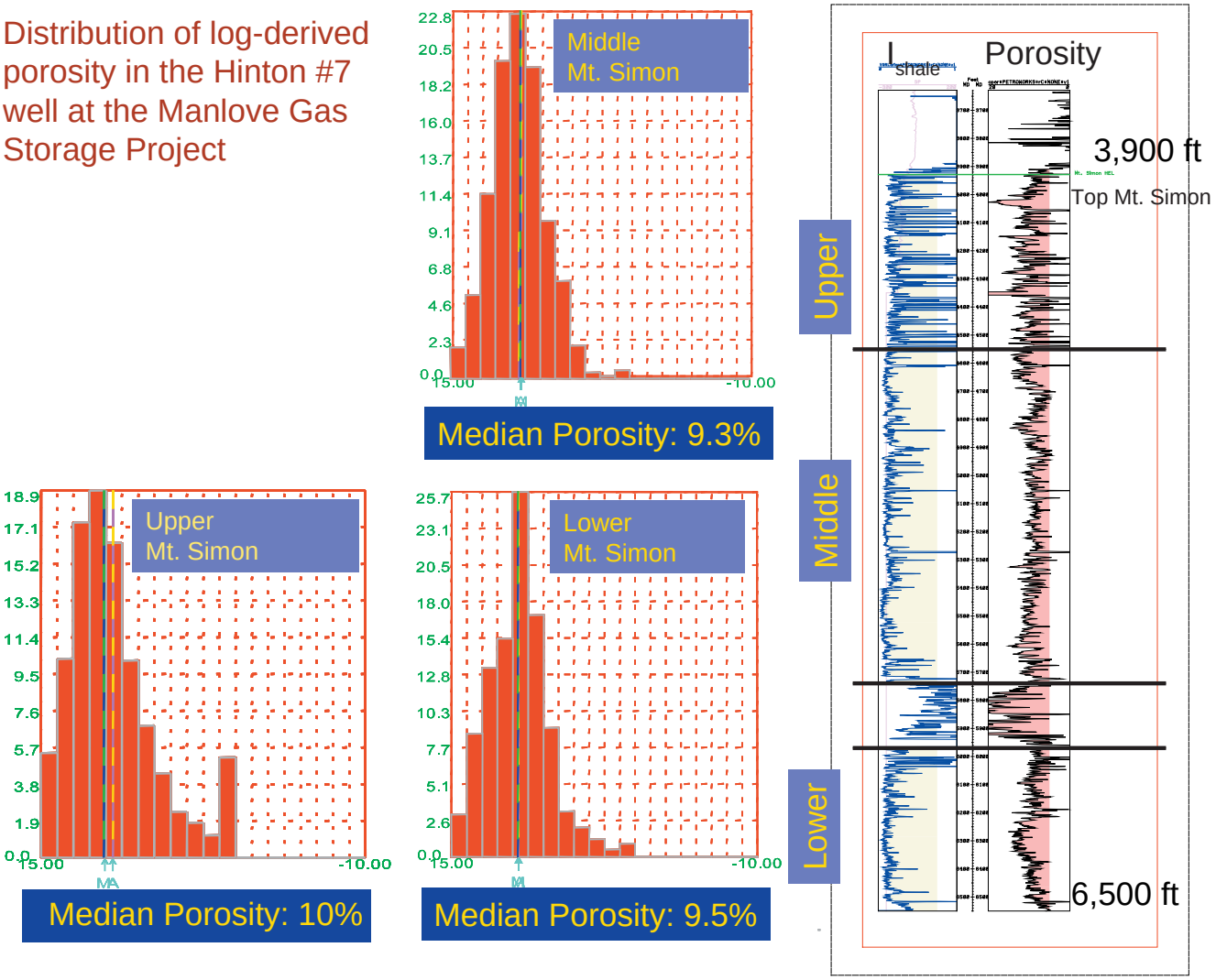

Figure 3-36 *Wireline log of the Peoples Gas Hinton No. 7 well, Champaign County, Illinois. The histograms of porosity variation show no appreciable drop in porosity across the entire 609.6 m (2,000 ft) of Mt. Simon reservoir.*

Porosity logs in the Hinton No. 7, the deepest well located in the Manlove Gas Storage Field in Champaign County, Illinois, allow the examination of changes in porosity with depth. This deep well has modern logs and penetrates approximately 600 m (2,000 ft) of Mt. Simon without reaching the Precambrian basement. The Hinton No. 7 well encountered upper, middle, and lower Mt. Simon intervals (Figure 3-36). There is a 46-m (150-ft) arkose zone that separates the middle and lower units. Porosity in this well was derived from a cross plot of the neutron and density wireline log data. There is a shale volume correction on the derived porosity. The calculated porosity values show that Mt. Simon porosity changes little with depth over the 600-m (2,000-ft) interval. Porosity histograms show about the median porosity 10% in the upper zone, 9.3% in the middle, and 9.5% in the lower Mt. Simon zone.

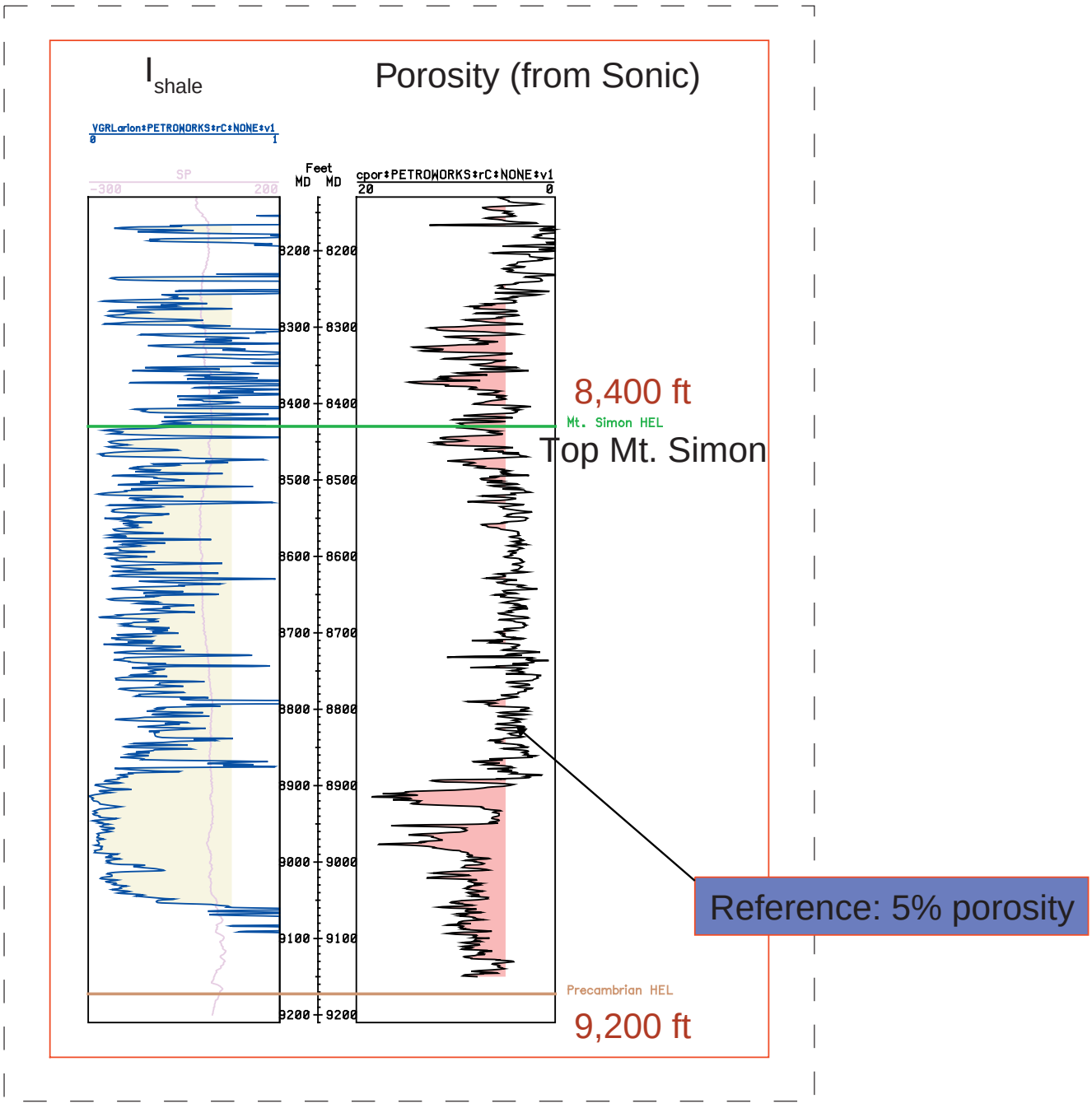

Figure 3-37 *Wireline log of the Texaco Johnson No. 1 well, Marion County, Illinois. The porosity curve computed from the sonic log shows that the best porosity is near the base of the Mt. Simon.*

For the Texaco R.S. Johnson No. 1 in Salem Field, porosity was calculated from the sonic wireline log (Figure 3-37). The top of the Mt. Simon is at 2,600 m (8,400 ft), and the formation is about 260 m (850 ft) thick. The well penetrated the Precambrian basement at 2,800 m (9,200 ft). There is a 46-m (150-ft) interval between the basal sandstone and the Precambrian that is interpreted to be an arkose sandstone. Natural radioactive potassium in the feldspar gives it an elevated gamma-ray value similar to shale. However, the sonic log suggests that the unit is not a shale. A similar zone in the Hinton No. 7 well (Figure 3-36) between 1,750 m (5,730 ft) and 1,820 m (5,960 ft) had elevated gamma-ray values, but core samples showed the zone to be an arkose with high-porosity and permeability values.

The upper 122 m (400 ft) of Mt. Simon in the Johnson well is interpreted to be equivalent to the upper Mt. Simon in the Hinton No. 7, but, unlike the more northerly Hinton well, the Johnson well encountered negligible calculated porosity in the upper 50% of the Mt. Simon. However, the lower 46 m (150 ft) of Mt. Simon in the Johnson well has intervals with calculated porosity up to 14% and average log porosity of about 10%. This zone would be a good target for sequestration.

Using Oil Fields to Calculate St. Peter and Mt. Simon CO_2 Storage Volumes

No direct data are available to approximate the volume of CO_2 that can be stored in undrilled and untested geologic structures; consequently, this lack of data requires either estimating using gross approximation or by using geologic structures defined by oil fields. In the case of a CO_2 sequestration industry, the only-large scale, field-tested storage (natural gas) in the Basin is in geologic structures where a buoyant fluid is injected at the top of a structure and displaces the in situ water downward and laterally out of the structure. As such, the assessment of CO_2 storage is presented as storage in "structures only" and "structures plus off-structure" storage.

The Manlove Gas Storage project has abundant Mt. Simon reservoir property data. The bulk volume of the Mt. Simon to the structure's spillpoint was available in a previous geologic study. A volumetric approach was used to estimate pore volume available for CO_2 sequestration potential for Manlove so that this volume could be used to estimate CO_2 storage of other structures in the Basin. The Hillsboro Gas Project was used as the basis for estimating the CO_2 storage of the St. Peter formation in the Basin. A rigorous geologic study was not available, so the reported Hillsboro natural gas storage volume was converted to equivalent CO_2, assuming that the natural gas was 100% methane.

Carbon dioxide can be sequestered as a free phase, as a trapped phase by capillary forces, and by dissolution into the water (Table 3-2). The total of storage capacity is the sum of all three trapping mechanisms. The Manlove volumetric model used assumed that the geologic structure was filled to its

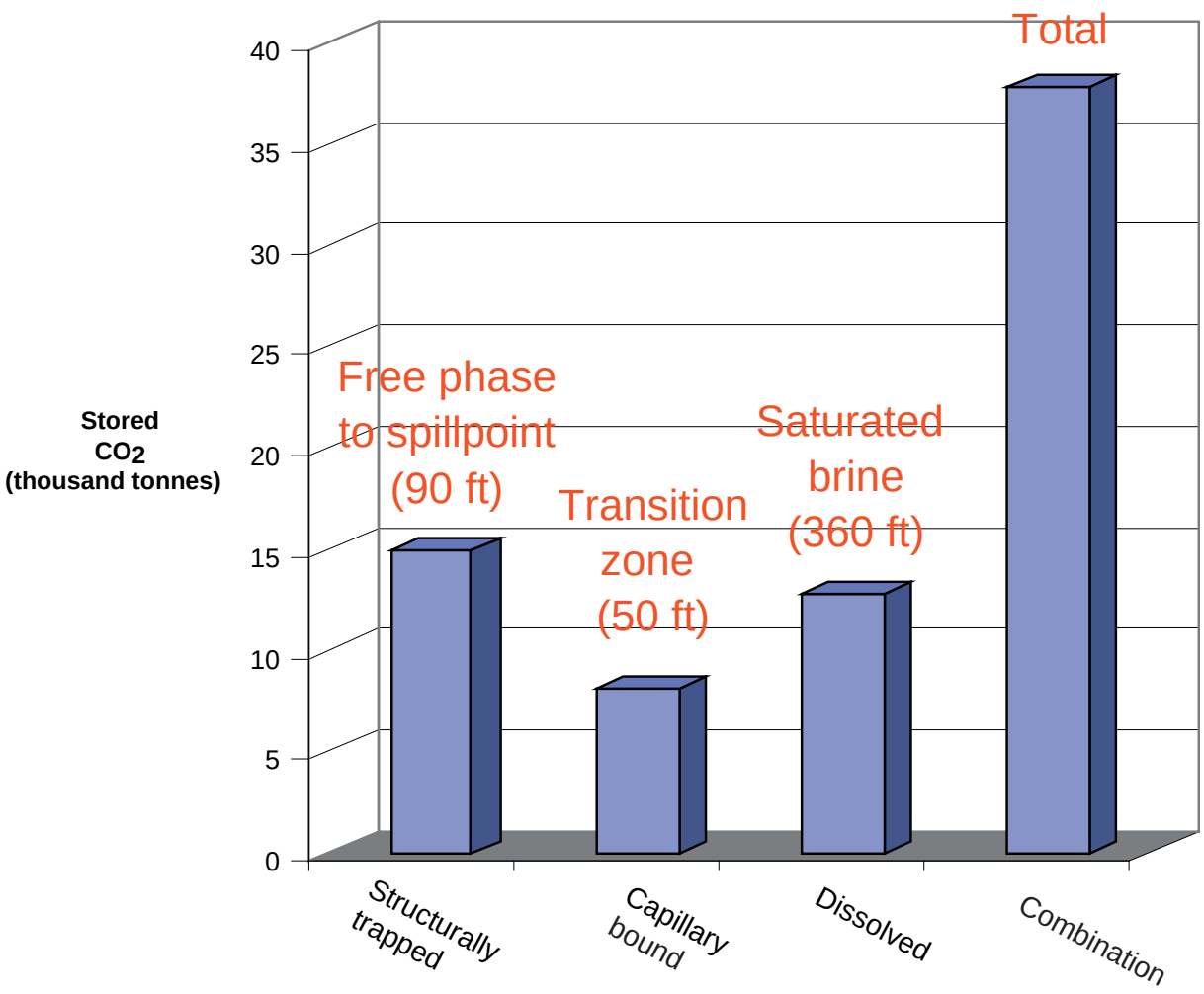

Figure 3-38 *CO_2 storage capacity by storage mechanism at Manlove Field assuming the field is being used for CO_2 sequestration instead of natural gas.*

spillpoint with CO_2 at irreducible water saturation of 30%. To account for observed low permeability layers, the vertical thickness of the formation was assumed to be 80% of the gross interval. Immediately below the spillpoint, a 15-m (50-ft) capillary transition zone was assumed, which was underlain by 110 m (360 ft) of CO_2-saturated brine water. These numbers were based on general observation of a previous study (Morse and Leetaru, 2005).

The structurally trapped free phase to spillpoint was calculated to be slightly under 15 thousand tonnes of stored CO_2 (Figure 3-38). The free phase displaced water out of the pores until water was at irreducible water saturation. This type of situation is likely to occur immediately below the caprock or vertical flow barrier; however, a macroscopic or volumetric displacement efficiency would decrease this volume. The irreducible water is assumed to be saturated with CO_2.

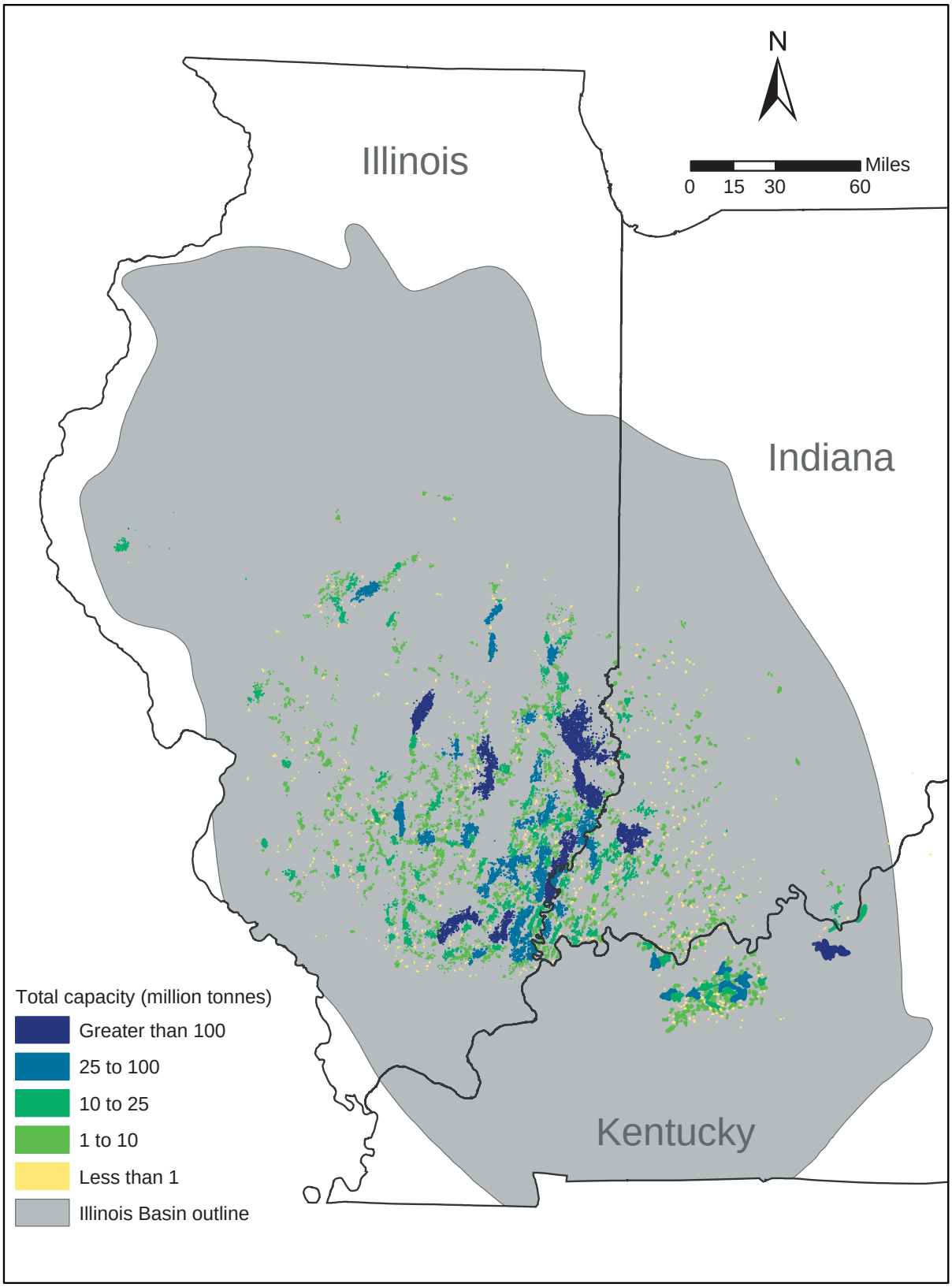

Figure 3-39 *Map showing potential CO_2 storage volumes for the Mt. Simon and St. Peter in the Illinois Basin as defined by the outline of the existing oil fields.*

Table 3-2. Storage capacity equations

M_{CO_2} =	$19.76Ah\phi\rho_{CO_2}(1 - S_{wirr})E_{Vm}$	Mobile, free phase (structurally trapped)
	$3.519Ah\phi\rho_{CO_2std}R_{sCO_2/w}S_{wirr}E_{Vm}$	CO_2 saturated brine, swept to S_{wirr}
	$19.76Ah\phi\rho_{CO_2}S_{CO_2irr}E_{Virr}$	Immobile, free phase (capillary bound)
	$3.519Ah\phi\rho_{CO_2std}R_{sCO_2/w}(1 - S_{CO_2irr})E_{Virr}$	CO_2 saturated brine, swept to $1 - S_{CO_2irr}$
	$3.519Ah\phi\rho_{CO_2std}R_{sCO_2/w}(1 - E_{Vm} - E_{Virr})$	CO_2 saturated brine, unswept
Equation variables and constants		
M_{CO_2}	Mass, tonne	
19.76	Constant (conversion from lbm to tonne)	
3.519	Constant (conversion to tonne)	
A	Area, acres	
h	Thickness, ft	
ϕ	Porosity, fraction	
ρ_{CO_2}	Density, lbm/ft^3	
ρ_{CO_2std}	Density, lbm/ft^3	
S_{wirr}	Irreducible water saturation, fraction	
S_{CO_2irr}	Irreducible water saturation, fraction	
E_{Vm}	Displacement efficiency, fraction	
E_{Virr}	Displacement efficiency, fraction	
$R_{sCO_2/w}$	CO_2 dissolved in water, scf/ft^3	

The capillary-bound CO_2 is assumed to occur within a transition zone of 15 m (50 ft) below the free-phase contact (Figure 3-38). Approximately 7 thousand tonnes of trapped free phase CO_2 could be stored within this zone. This immobile (trapped) CO_2 was formed when injected CO_2 buoyed upward due to CO_2 and water density differences or was "pulled" downward due to capillary forces. Some CO_2 remained trapped within the pore space. The water surrounding the trapped CO_2 was assumed to be saturated with CO_2.

Below the CO_2/water transition zone, a dissolved CO_2 zone is assumed to occur. The dissolved CO_2 zone contains 110 m (360 ft) of CO_2 saturated brine containing about 12,000 tonnes (13,000 tons) of stored CO_2 (Figure 3-38). The water near the base of the structure does not have free-phase CO_2, but is assumed to contain dissolved CO_2 only. Depending on the mechanism of the water contact with CO_2, the water may or may not be 100% saturated with CO_2.

The CO_2 storage potential combined from all three types of storage mechanism is approximately 38,000 tonnes (42,000 tons). The Manlove bulk volume with the ratio of the oil field area to the Manlove Field area was used to estimate the bulk volume of undrilled Mt. Simon underlying the oil fields. Using the assumed Manlove storage mechanism distribution and the bulk volume of the Mt. Simon, CO_2 storage was estimated. Figure 3-39 indicates the relative storage capacity of these fields. The total Basin storage capacity for the Mt. Simon only within anticlines is 2.8 billion tonnes (3.1 billion tons) for the mobile phase, 1.2 billion tonnes (1.3 billion tons) for the immobile phase, and 1.9 billion tonnes (2.1 billion tons)

for the dissolved phase. The total volume of CO_2 storage available within geologic structural storage in anticlines is 5.9 billion tonnes (6.5 billion tons) of CO_2. The St. Peter is a relatively thin reservoir compared with the Mt. Simon, and only the mobile, free phase CO_2 storage is considered applicable. The St. Peter has 1.9 billion tonnes (2.1 billion tons) of storage capacity.

If the entire Mt. Simon, including non-structure pore volume, could accommodate and effectively store CO_2, the total saline-water–bearing formation CO_2 storage in the Basin is approximately 75 billion tonnes (83 billion tons).

Fluid Flow Models

CO_2 Movement through a Saline Reservoir

The CO_2 injection rate into a reservoir is limited by the potential of unintentionally hydraulically fracturing the caprock by injecting at a subsurface pressure that exceeds the parting or fracture-propagation pressure of the formation. During the initial injection, the CO_2 will follow the higher permeability zones within the rock and bypass low permeability zones, which will result in fingering of the CO_2 and an areal distribution that may be considerably greater than initial predictions. The complex distribution pattern of CO_2 is important because it may pass beyond the spillpoint of the anticline and enter the general fluid flow pattern of the basin without adequately filling the structure. Furthermore, the storage capacity of a given geologic structure may be significantly reduced if off-structure channeling of CO_2 occurs.

In a gas storage reservoir, the base of the gas cap is not necessarily a flat plane, but instead can have major undulations, even after several years of injection (Chaumet et al., 1966). This irregular base of the gas/water interface will reduce the amount of storage capacity because the spillpoint may be reached before the system equalizes. The cause of this gas/water interface undulation has not been evaluated but may be due to changes in rock facies (grain sizes) and corresponding changes in capillary pressure.

Examples from oil and gas reservoirs suggest that hydraulic fracturing occurs when injection pressures are >15.8 to 22.6 kPa/m (>0.7 to 1.0 psi/ft). Injection pressures of 12.44 kPa/m (0.55 psi/ft) are commonly used in natural gas storage fields, but, in some areas, injection pressures as high as 15.8 kPa/m (0.7 psi/ft) have been used. In Illinois and Indiana, an injection pressure gradient is regulated at 18.1 kPa/m (0.8 psi/ft). Kentucky's is at 16.58 kPa/m (0.733 psi/ft). A fracture gradient commonly used in the Illinois Basin by fracture stimulation companies is 22.6 kPa/m (1.0 psi/ft).

An Eau Claire sandstone reservoir at Pecatonica gas storage project in northern Illinois has a hydrodynamic gradient due to natural water movement in the sandstone reservoir (Burnett, 1967). The Pecatonica project is one of the closest gas storage projects located to the Eau Claire–Mt. Simon outcrop

recharge areas. The result of the groundwater movement is that the natural gas bubble has a tilted gas/water contact with a net result of increased storage capacity.

Water Displacement

Water displacement by injected CO_2 is a design concern in any major carbon sequestration injection program. For example, if there is a chance the CO_2 injected into a formation might migrate where the formation outcrops at the surface, effort should be made to minimize this possibility. Another potential problem could occur if CO_2 would leak into overlying formation outcrops or part of the local freshwater aquifer system. In terms of outer boundary flow conditions, there are two types of reservoirs: closed and open.

Closed System Injection

In a closed system, where there is no pressure communication with surrounding geologic formations, free-phase CO_2 storage capacity would be available from the water and pore compressibility. With increasing pressure, the water contracts, and the pore volume expands. Additional storage capacity is through dissolution of CO_2 into reservoir water. During the injection, storage capacity of a closed system will decrease as distance from the project site increases. Post-injection should see a relaxation in the pressure disturbance, and CO_2 should be distributed more evenly. Water has low compressibility compared with that of CO_2, but the possible Mt. Simon thickness of 610 m (2,000 ft) available for injection would generate significant pore volume available for sequestration. There would also be a slight increase in pore and bulk volume due to pore expansion due to injection pressures.

Manlove reservoir properties were used to study this relationship. A simple analog model of "closed" Manlove Field using only 0.028 billion m^3 (1 billion scf) of reservoir pore volume assuming 27 m (90 ft) of closure, 10% porosity, and 0.8 net to gross thickness. The water and pore compressibility was assumed to be 10×10^{-6} and 3.0×10^{-6} psi^{-1}, respectively. A 10% increase in pore pressure above the initial reservoir pressure would result in a 600,000-tonne (661,000-ton) increase in storage capacity at this field (Figure 3-40).

Open System Injection

In an open system, the reservoir is connected to the outcrop belt and pressure changes due to CO_2 injection in one area would affect the entire aquifer system. In an open system compressibility is only important around wellbores during injection and not the reservoir as a whole post-injection. Three simple piston-like displacement volumetric models were evaluated to estimate velocity and distance the water displaced from CO_2 injection moves. The model assumed 30 m (100 ft) of CO_2 saturated thickness,

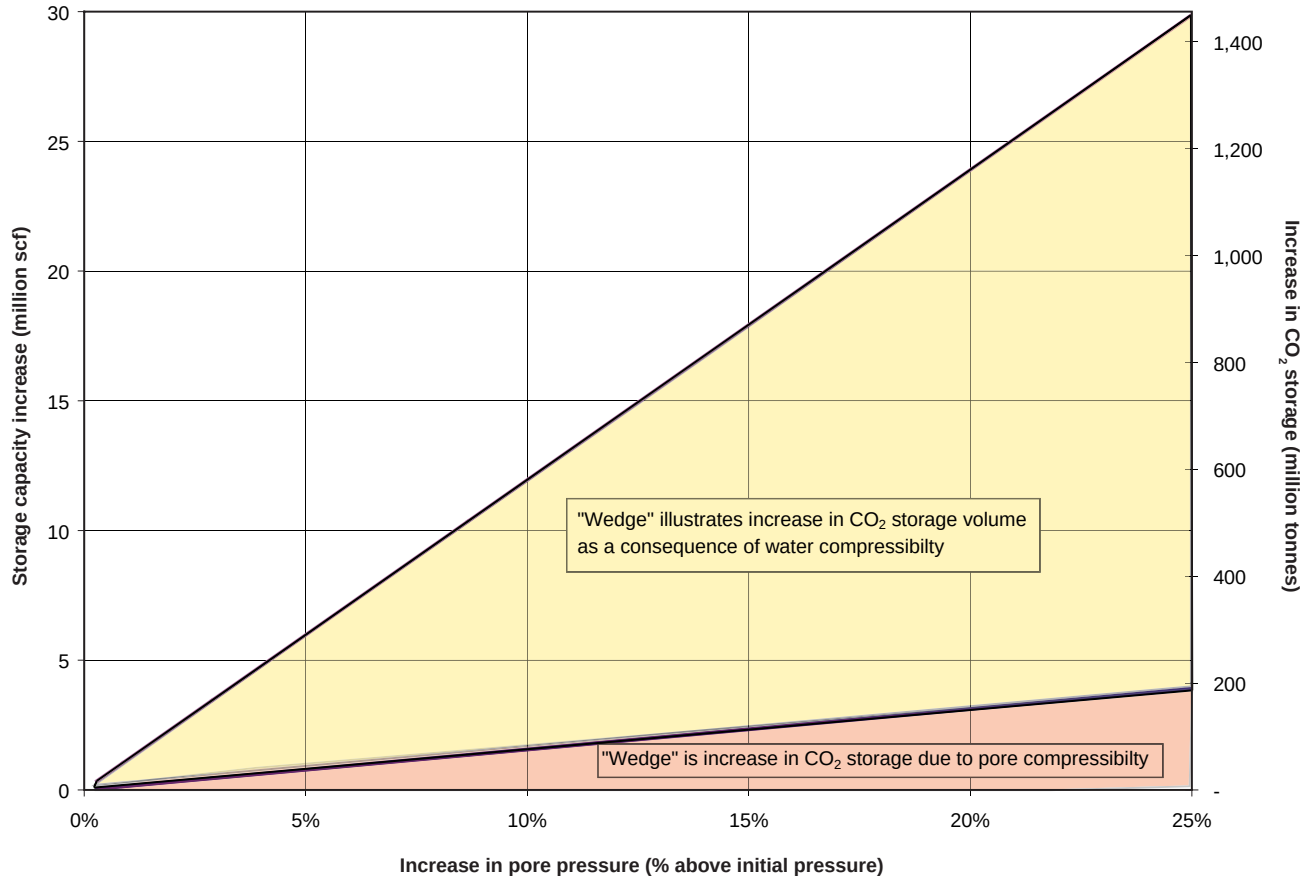

Figure 3-40 *Pore space available for CO_2 storage increases due to pore, bulk volume, and water compressibility. Manlove underground storage analogy: 1.0 billion scf reservoir pore volume under a structure with a four-way closure of 90 ft (10% porosity and 0.80 net to gross ratio). Water and pore compressibility are 10×10^{-6} and 3.0×10^{-6}/psi, respectively. Depth of 8,000 ft is assumed.*

10% porosity, 30% irreducible water saturation, 9.795 kPa/m (0.433 psi/ft) pressure gradient, temperature gradient of -17.22°C/30 m (1°F/100 ft), with injection commencing at a depth of 1,800 m (6,000 ft). The three scenarios (1,000 tonnes/yr (1,102 tons/yr), Figure 3-41; 10,000 tonnes/yr (11,023 tons/yr), Figure 3-42; 30,000 tonnes/yr (33,069 tons/yr), Figure 3-43) were all assumed to be from one well. Similar results are expected if the injection is from multiple wells within the same anticline.

These simple sensitivity models show that, after decades of continuous injection, the injection of large volumes of CO_2 has an inconsequential effect on the position of a distant freshwater-salt water interface. However, only one injection point is considered, and the effect will be different when a larger number of injection wells are distributed at multiple anticlines throughout the Basin. The results also show that the rate of water movement is minimal 80 km (50 mi) away from the injection site (Table 3-3).

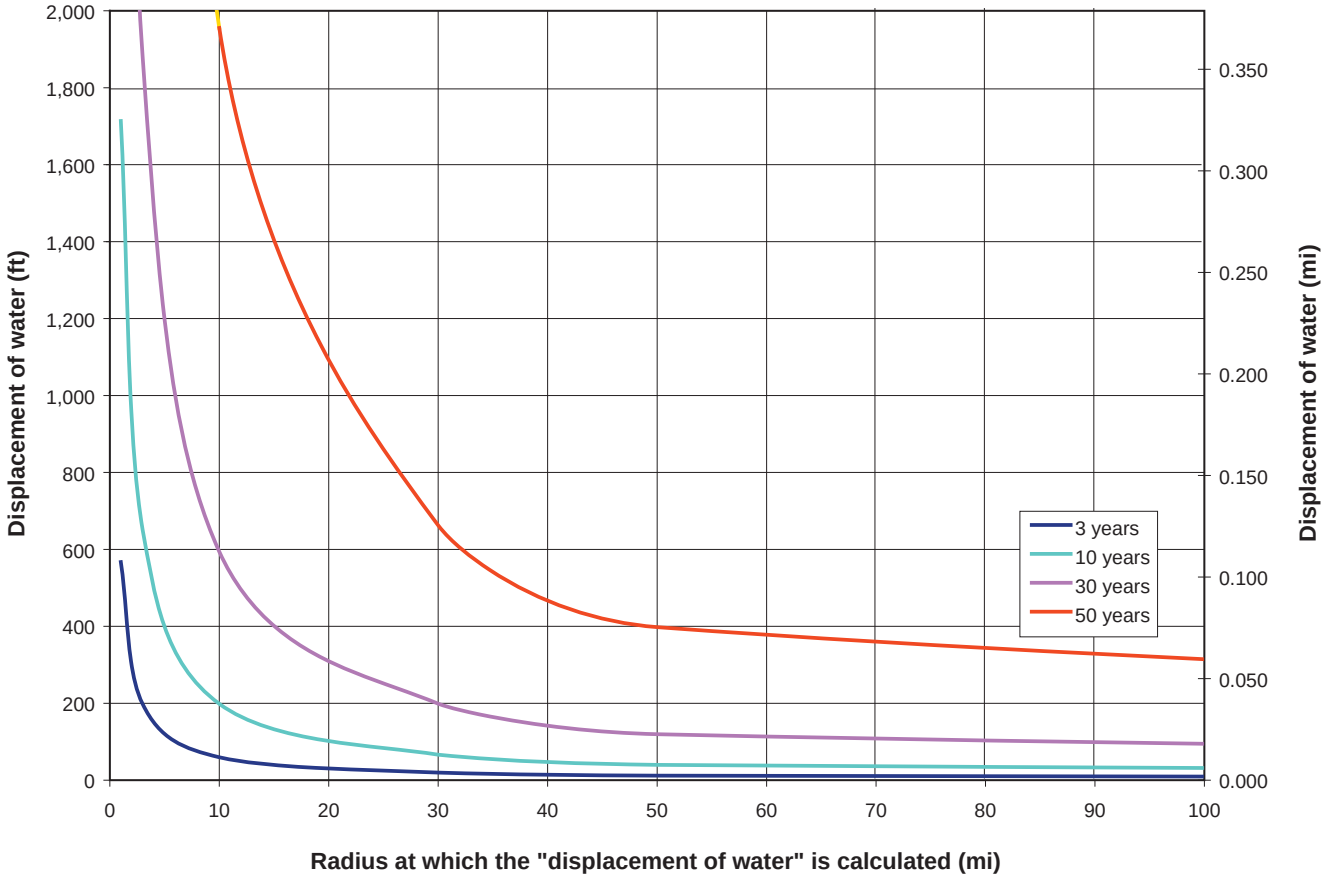

Figure 3-41 *Simple right cylinder piston-like displacement of water by CO_2 injection without dissolution assuming 1 thousand tonnes per year of injection. Assumed properties: 1 thousand tonnes per year of CO_2 injection, 100 ft CO_2 saturated thickness, 10% porosity, 6,000 ft deep, 30% irreducible water saturation, 0.433 psi/ft, 1°F/100 ft.*

Table 3-3. Velocity of water movement at 10, 30, and 50 mi from the CO_2 injection site.

Injection rate (thousand tonnes/year)	Water movement (ft/day)		
	At 10 mi	At 30 mi	At 50 mi
1	0.0181	0.0109	0.00182
10	0.178	0.108	0.0182
30	0.515	0.320	0.0545

In response to the movement of the freshwater-salt water interface, the dynamics of the freshwater part of the flow system will change, which is important to consider in the evaluation of the long-term effects of CO_2 sequestration in deep saline aquifers, since these formations are used as water supplies in large metropolitan areas at the margins of the Basin. Before any possible interference with freshwater areas, water could be pumped from monitoring wells near the spillpoint that could balance the displaced water with the CO_2 stored.

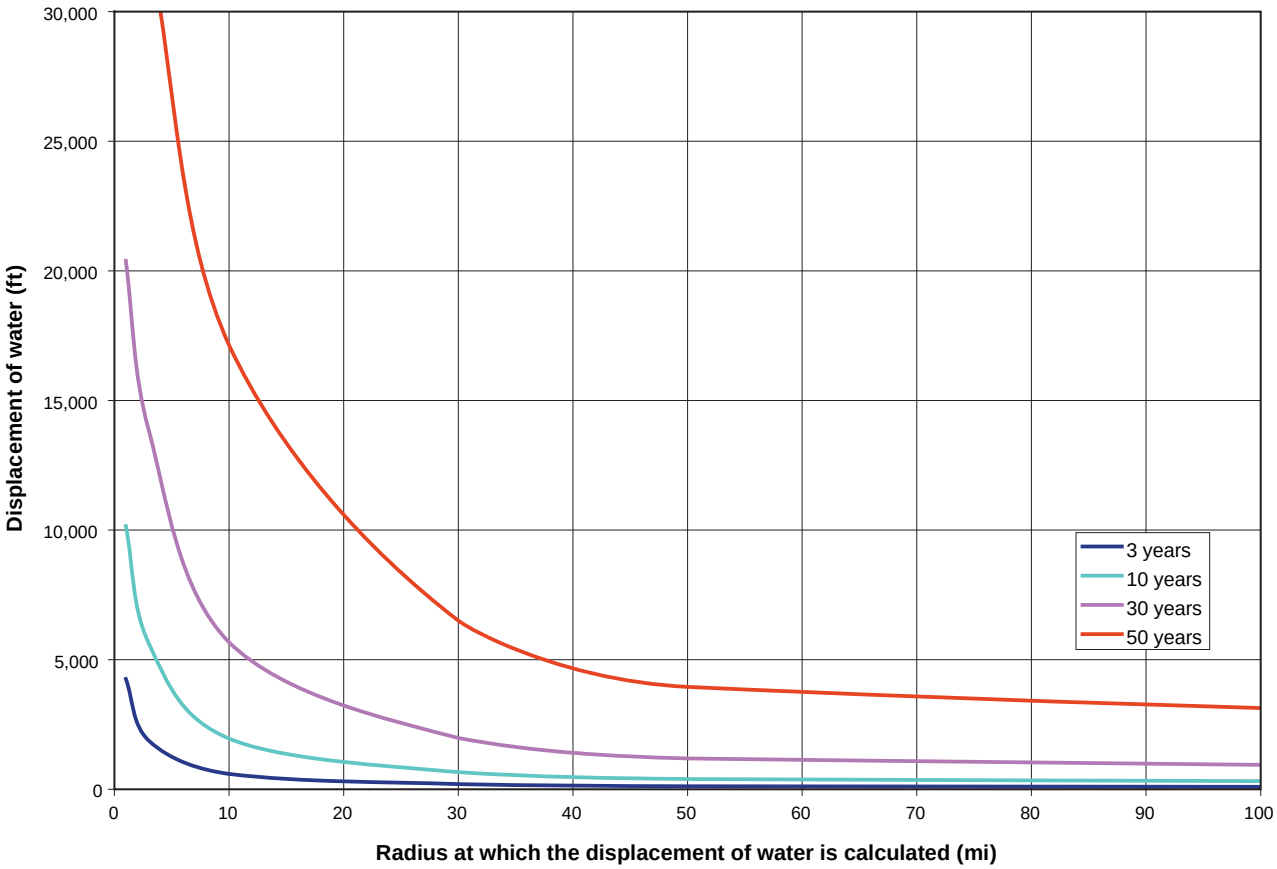

Figure 3-42 *Simple right cylinder piston-like displacement of water by CO_2 injection without dissolution assuming 10 thousand tonnes per year of injection. Assumed properties: 10 thousand tonnes per year CO_2 injection, 100 ft CO_2 saturated thickness, 10% porosity, 6,000 ft deep, 30% irreducible water saturation, 0.433 psi/ft.*

Simulated CO_2 Movement in a Reservoir

To understand the influence of laterally discontinuous vertical barriers (shale) to flow, a simple single-well reservoir model with average rock and fluid properties of the Mt. Simon was generated using Landmark's VIP compositional reservoir simulation program. The base model had no vertical barriers, whereas the model with shales had impermeable layers every 18 m (60 ft). These shale layers had a lateral continuity of approximately 305 by 305 m (1,000 ft by 1,000 ft) surrounding the wells. In both models, the vertical permeability of the reservoir (non-shale) was 0.001 μm^2 (1 md), horizontal permeability of 0.010 μm^2 (10 md), and porosity was 8%. Depth was assumed to be 1,829 m (6,000 ft) with an initial pressure of 16,547 kPa (2,400 psia). The system was assumed to be open with only modest pressure increases, and the injection was at the base of a 305-m (1,000-ft) interval. An open system was simulated by using corner "wells" to reduce pressure buildup of the aquifer due to CO_2 injection.

Thirty years of continuous injection followed by 100 years of shut-in was simulated; each model had the same CO_2 volume injected. A comparison of the two CO_2 flow simulation models (Figure 3-44)

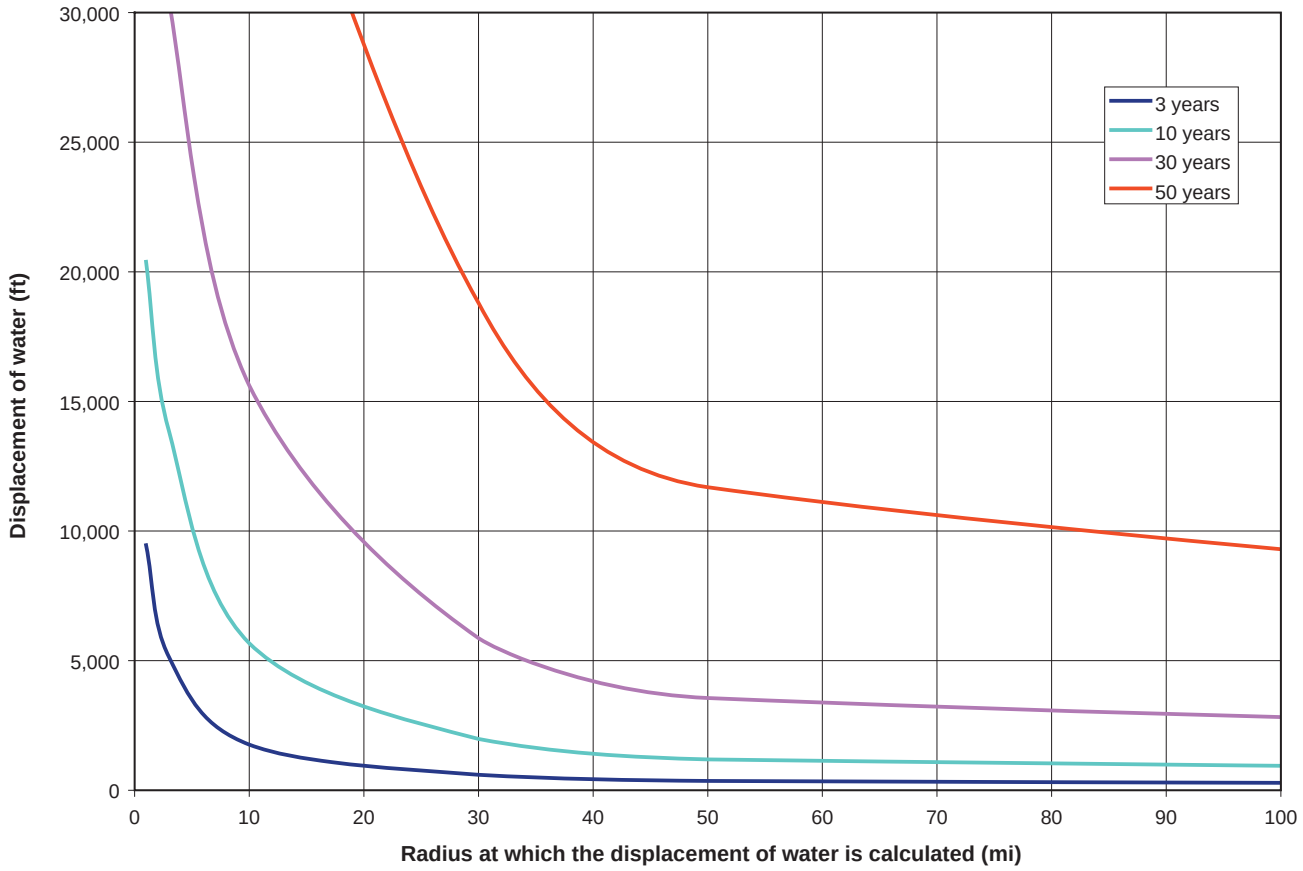

Figure 3-43 *Simple right cylinder piston-like displacement of water by CO_2 injection without dissolution assuming 30 thousand tonnes per year of injection. Assumed properties: 30 thousand tonnes per year CO_2 injection, 100 ft CO_2 saturated thickness, 10% porosity, 6,000 ft deep, 30% irreducible water saturation, 0.433 psi/ft.*

illustrates that the shale barriers are important in increasing the lateral extent of the CO_2 storage capacity and dramatically decreasing the vertical extent of the CO_2 storage. No-flow vertical barriers such as non-reservoir siltstones and shales allowed free-phase CO_2 saturation buildup below the shale and reduce vertical migration rates. Additionally, this increases the free phase CO_2 saturation but reduces the contribution of dissolution to total storage. This drop in dissolution is caused by the reduced contact of CO_2 with water when the shale barrier impedes vertical flow. The decrease in the volume of CO_2 dissolved in water is only temporary and will increase with time.

Geologic and reservoir models were developed based on the Manlove gas storage field using the three-dimensional stochastic reservoir model as the geologic framework. This reservoir model has 75 layers with a 0.94-m (3-ft) thickness. The later extent of the model was 40 × 80 cells in x and y directions, respectively, or about 183-m (600-ft) cell dimensions. The model assumed a single well injection completed in 15 m (48 ft) out of a total 69 m (225 ft). The injected interval was 9.4 m (30 ft) from the bottom of the model. The injected well was assumed to have continuous CO_2 injection of 398 tonnes/day

or 145 thousand tonnes/yr (7.5 million scf/day). The cumulative CO_2 injection over the 80-year period was 6.2 billion m^3 (219 billion scf (10.5 million tonnes (11.6 million tons))), which would be equivalent to 3.5 billion m^3 (124 billion scf) of methane. (Manlove is reported to have 4.3 billion m^3 (153.1 billion scf) of methane gas in place.) Toward the end of the 80-year simulated period, the model indicated that an insignificant mass of CO_2 may have left the structure via vent wells that surrounded the model edges. The vent wells were used to release the model pressure to simulate an infinite acting reservoir.

During the simulation, >15.9 million m^3 (>100 million stb) of water was displaced by CO_2. The average pressure increased by 3,447 kPa (500 psi) (9,653 to 13,100 kPa (1,400 to 1,900 psi)) during the 80 years of injection. During the 40 years of shut-in after injection, pressure decreased by 2,758 kPa (400 psi) (13,100 down to 10,342 kPa (1,900 down to 1,500 psi)).

The model assumed a gross thickness of the reservoir to be 69 m (225 ft), irreducible water saturation at 35%, and trapped CO_2 saturation at 18%.

The geologic model suggests laterally extensive areas with little to no vertical permeability that would impede the vertical flow of CO_2 (Figure 3-27) similar to those that were observed in the simple geologic model (Figure 3-44). The vertical permeability visualization of layer 43 (Figure 3-27) shows that these layers have zones where vertical permeability is high enough to allow for vertical migration of CO_2.

The compositional flow simulation model showed the CO_2 injection from a single well rapidly migrates vertically upward until it encounters the top 23 m (75 ft) of Mt. Simon lower vertical permeability zones (Figure 3-45 and 3-46). The CO_2 migrated laterally under areas of low vertical permeability until it encounters a high vertical permeability zone, and continues the upward migration. The seal for this model is the impermeable shales of the Eau Claire Formation, which was modeled as a single no-flow boundary at the top of the model (not shown).

Site Selection

The presence of structural closure is one of the most important criteria in the selection of a CO_2 sequestration test site. Structural closure will decrease the probability of CO_2 leaking updip and into the freshwater aquifer systems. Structural closure will also enable easier monitoring and verification of the injection site because the CO_2 will be trapped in a small known area. Most oil fields in the Illinois Basin have a structural component; therefore, the most likely sequestration site will be located beneath an existing oil field. Oil wells into the overlying oil field may provide inexpensive observation wells for a deeper CO_2 sequestration interval.

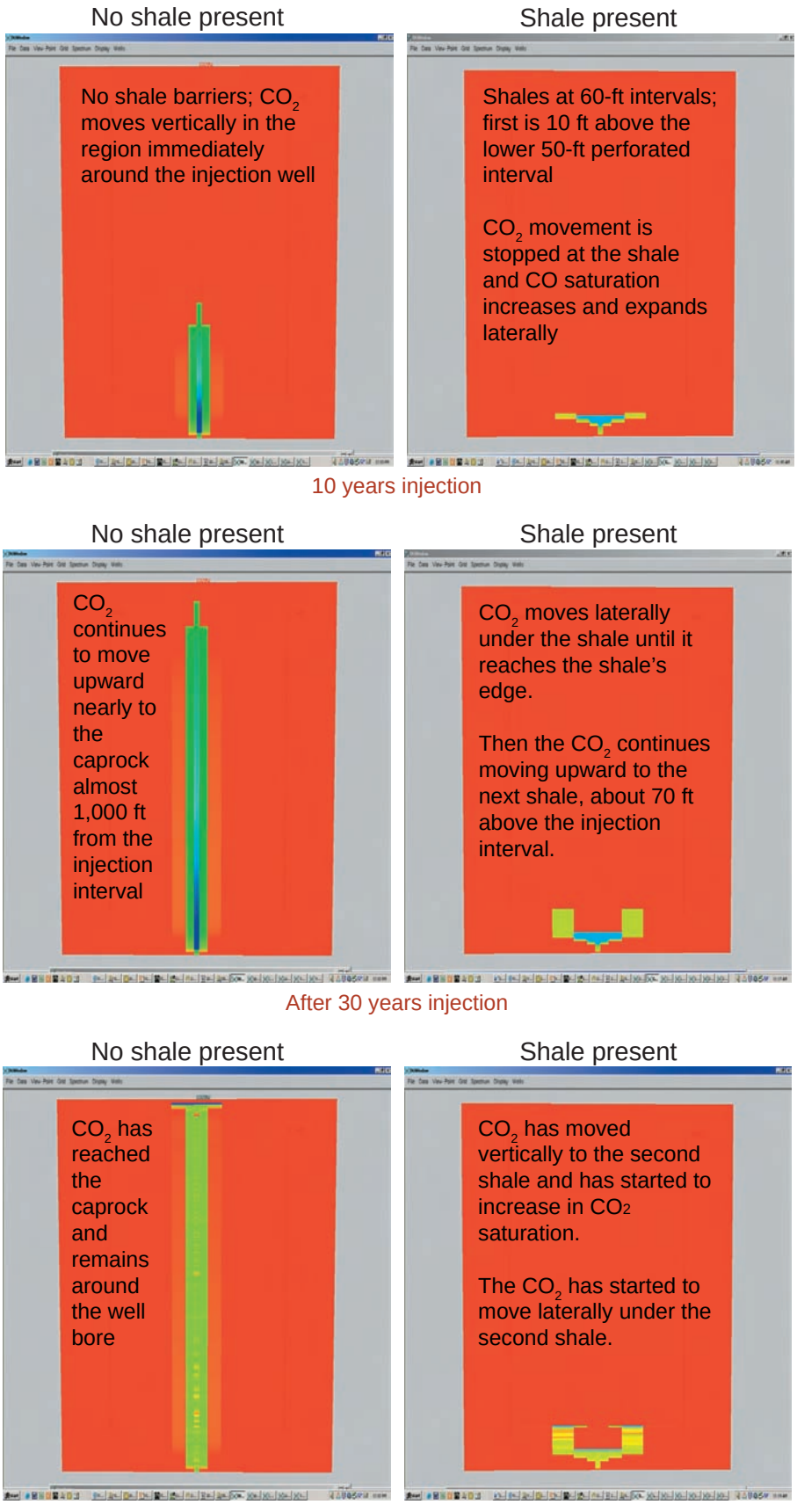

Figure 3-44 *Compositional flow simulation results of CO_2 movement through a reservoir with shale layers (right column) and no layers (left column).*

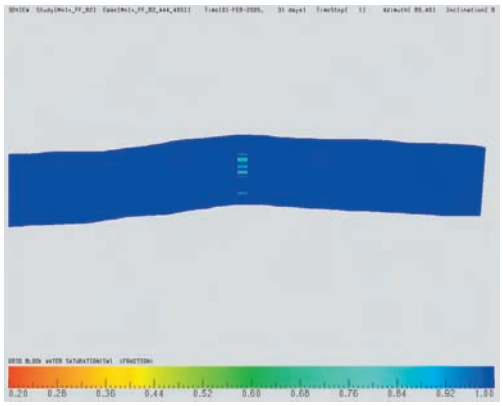

a. 1 month

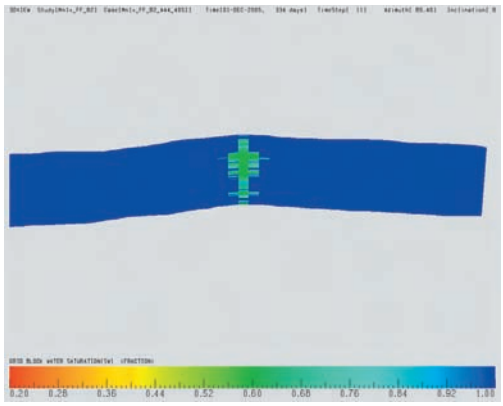

b. 12 months

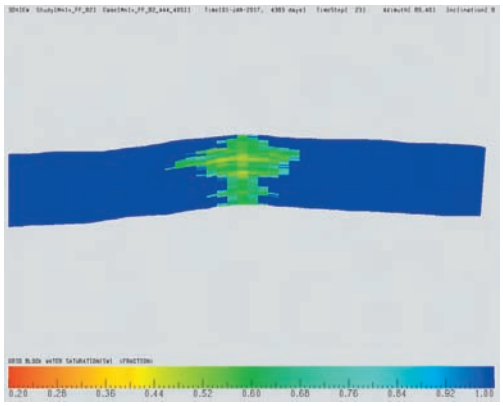

c. 12 years

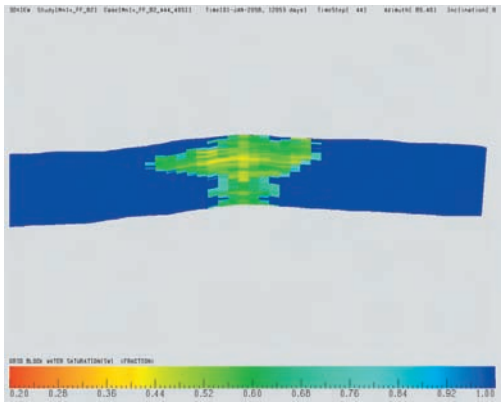

d. 33 years

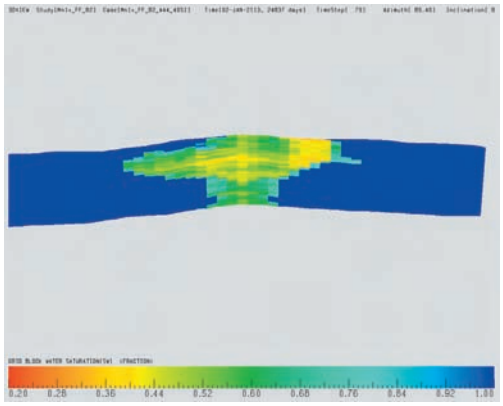

e. 69 years

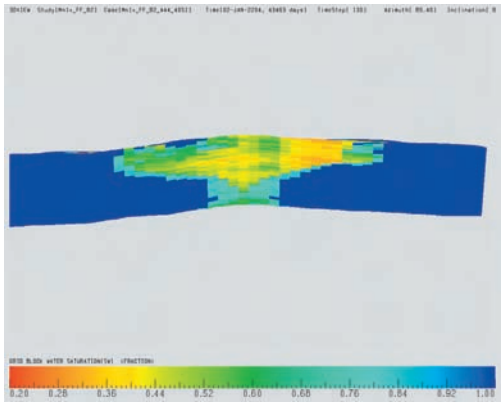

f. 120 years

Figure 3-45 *Cross section time slices showing the movement of CO_2 through the Manlove Mt. Simon reservoir. The color indicates water saturation. Dark blue is 100% water saturation.*

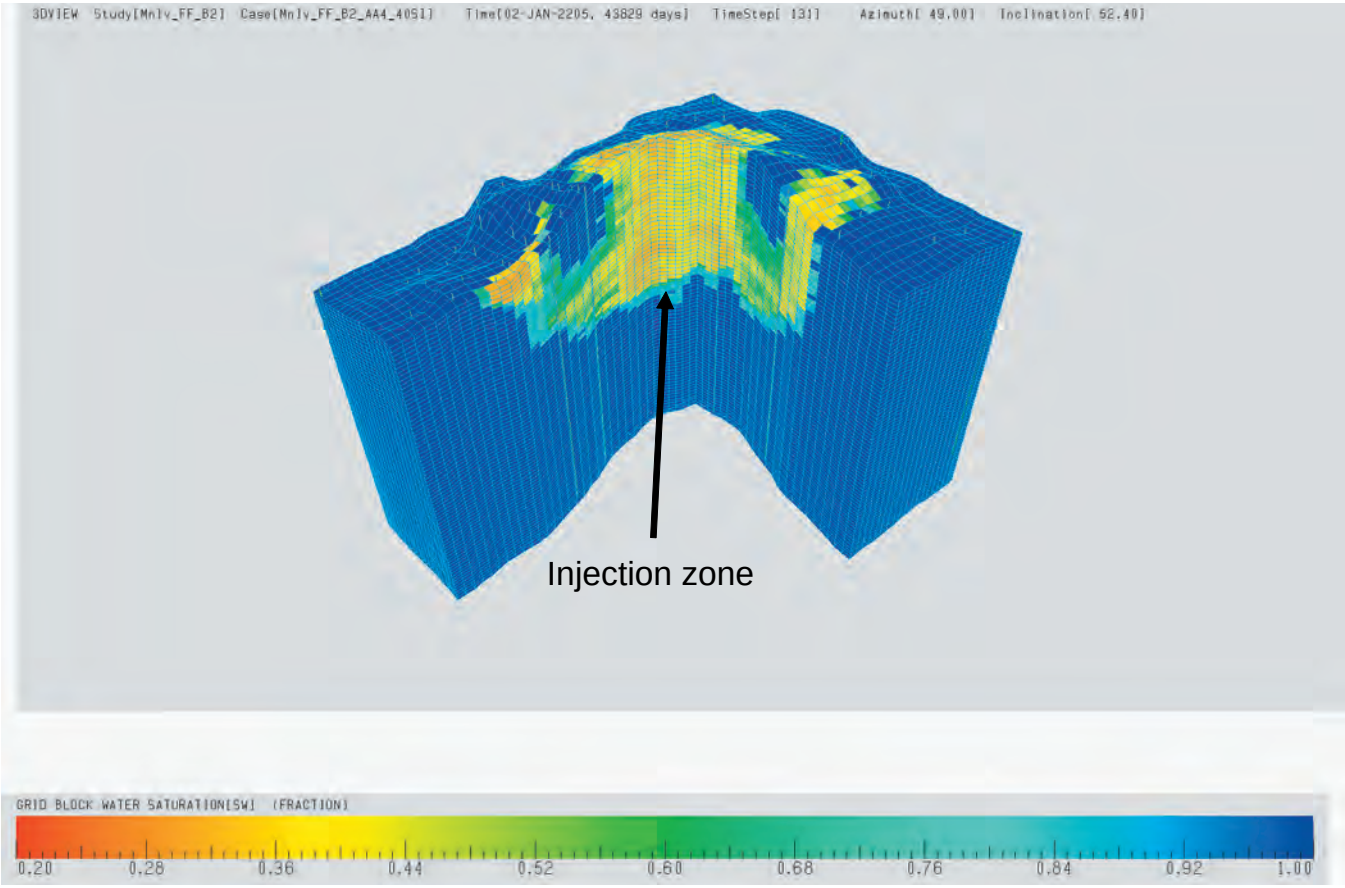

Figure 3-46 *Cross section time slice showing the movement of CO_2 through the Manlove Mt. Simon reservoir at Manlove Gas Storage Field.*

The presence of an anticlinal structure is only one of the site selection criteria for CO_2 sequestration research. Not all of the strata in Illinois have the proper reservoir attributes to be good targets for storage of CO_2. For example, an optimum depth might range from 850 to 2,100 m (2,800 to 7,000 ft). There are two reasons for this depth range. Between 850 and 900 m (2,800 and 3,000 ft), CO_2 changes from a gas phase to a liquid-like phase. The liquid-like phase has a higher density, and greater mass of CO_2 would be able to be injected into any pore space. The upper limit of 2,100 m (7,000 ft) is somewhat arbitrary, but deeper wells are more expensive to drill, complete, and inject CO_2 into; however, depth will vary with specific project economics.

Based on limited and sparse well data and subsequent modeling, Gupta and Bair (1997) made observations that vertical flow from the Mt. Simon is possible. Combining the lithology change with the vertical flow possibility merits Phase II work that includes out-of-zone monitoring to investigate the vertical flow possibility.

The Illinois Basin Consortium has a good understanding of some of the geologic risks in deep saline reservoirs because of the number of deep wells, 6,437 km (4,000 mi) of reflection seismic data, and numerous natural gas storage projects in multiple saline reservoirs.

The base of the Mt. Simon overlies the Precambrian unconformity. This unconformity may represent over 500 million years of erosion, and in southwestern Illinois and Missouri there may be more than 300 m (1,000 ft) of paleotopography. There is strong evidence from the existing seismic control, well logs, and outcrops that the Mt. Simon sandstone thins or is not present on Precambrian high areas. This lack of sandstone represents a significant geologic risk when planning a sequestration project in the Mt. Simon Sandstone. However, these paleohigh areas can be resolved using reflection seismic data. The Precambrian highs have a diagnostic onlap and termination of seismic reflectors at the Eau Claire and Mt. Simon levels.

The ISGS acquired new two-dimensional reflection seismic profiles across the Tonti Field in Marion County, Illinois, and Boyd Field in Jefferson County, Illinois. Tonti Field produces from Devonian age oil reservoirs. This field was selected as a good location for testing sequestration because it apparently had a small structure with a well-defined closure at the Devonian horizon. The seismic profile showed that the well-defined structure at the Devonian was not as distinct in the deeper horizons (Figure 3-47) and that the Devonian structure was partially a result of the reef buildup and is stratigraphic not tectonic in origin. The termination of seismic reflectors on the flank of the Tonti structure at the Precambrian suggest that the Precambrian was a topographic high during Mt. Simon deposition; therefore, the Mt. Simon is likely either thin or absent at the Tonti area.

Sequestration sites should not have faults that penetrate potential injection zones. As previously discussed, the injection of high-pressure fluids into a fault plane could reactivate the fault zone. The Tonti two-dimensional seismic profile does show apparent faulting across the flank of the structure.

The better reservoir facies may not necessarily be located at the top of the Mt. Simon formation. As shown on the Johnson well (Figure 3-37), the best reservoir sandstone was near the base of the Mt. Simon. In general, the upper part of the Mt. Simon appears to be more heterogeneous and has been interpreted to be a tidally influenced deposit that gradually becomes finer grained to the south. The basal Mt. Simon may have been deposited as part of an alluvial fan and braided fluvial system. These depositional environments produce coarser-grained, massive sandstone strata than the overlying tidal deposits. The coarser strata appear to retain their porosity better than the finer-grained units.

Another important issue with these saline reservoirs is the presence or absence of seals to fluid movement. At the southernmost tip of Illinois and in northwestern Kentucky, the Eau Claire becomes

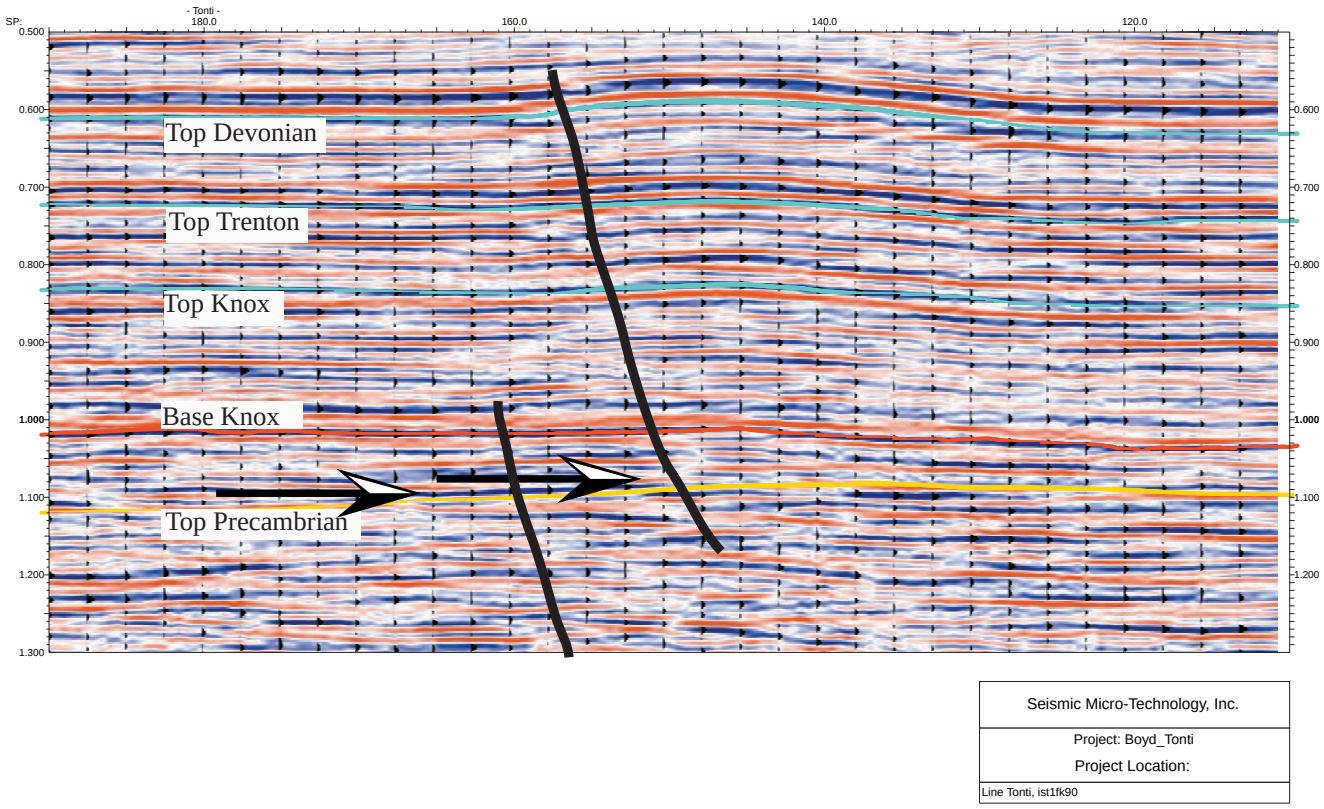

Figure 3-47 *North-south reflection seismic profile across Tonti Field in Marion County, Illinois.*

predominantly a carbonate and may not be as effective a seal as the Eau Claire in the northern part of the Basin.

The St. Peter Sandstone is also a viable target for sequestration. The St. Peter is directly overlain by dense nonporous carbonates that may form a good seal, but carbonates are brittle and may have fractures. These fractures could form conduits to release CO_2 into shallower horizons. However, the presence of the Maquoketa shale a couple of hundred feet above the St. Peter should provide a 46- to 76-m (150- to 250-ft)-thick seal in the case that the carbonates cannot fully contain the CO_2. The St. Peter has been successfully used as a natural gas storage reservoir in Jacobs Field and Hillsboro Field but leaked in other gas storage fields. Although leaks have occurred in the case of the Galesville at Hillsboro Gas Storage Field, proper reservoir monitoring and surveillance have prevented the recurrence of leakage.

Summary of Selection Criteria

Seven significant criteria were used for evaluating CO_2 sequestration sites in Illinois:

1. geologic structural closure,
2. subsurface depth of the target reservoir,
3. faults and earthquake hazards,
4. paleotopography on the Precambrian,
5. lateral proximity of the target reservoir to its equivalent freshwater interval,
6. reservoirs with adequate porosity and permeability for storage and injection of CO_2, and
7. the quality and thickness of the reservoir seal.

Deep Faulting and Structural Reactivation Beneath the Southern Illinois Basin

Introduction

The Illinois Basin in the central United States exemplifies an intra-cratonic basin within a relatively stable continental interior. The structure and stratigraphy of the Basin's thick Paleozoic sedimentary section has been thoroughly investigated using petroleum industry borehole information and limited seismic reflection profiles (Kolata and Nelson, 1991; McBride and Nelson, 1999). The seismic stratigraphy and shallow basement composition of the Precambrian upper crust has also been well-characterized, especially for the southern part of the Basin (Pratt et al., 1992; Van Schmus et al., 1996; Potter et al., 1997; McBride and Kolata, 1999; McBride et al., 2003). The deeper tectonic structure underpinning the Basin, however, remains poorly known. The crustal trends of deep-seated fault zones (e.g., the Reelfoot Rift and the Rough Creek Graben) (Figures 4-1 and 4-2) are based largely on inferences from geopotential field data without the benefit of seismic reflection imaging (e.g., Braile et al., 1997).

In general, the seismogenic frameworks for tectonically active zones along plate boundaries or within major rifts are relatively well understood. Intra-plate regions, such as the Illinois Basin, generally receive lesser attention. The New Madrid Seismic Zone (NMSZ), which dominates seismic hazard assessments in the upper Mississippi River valley of the central United States (Figure 4-3), is perhaps the world's best studied zone of intra-plate seismicity (Schweig and Ellis, 1994). Even though the underlying cause remains controversial, the epicenter patterns, focal mechanism solutions, and hypocenter depths between 4 and 15 km (2.5 and 9.3 mi) clearly reveal a northeast-trending dextral strike-slip zone interrupted by a left-stepping restraining bend where events represent thrust mechanisms (Chiu et al., 1992) (Figures 4-1, 4-3, and 4-4). The seismogenesis of the NMSZ is accordingly relatively well-characterized. This well-defined pattern is in contrast to the diffuse distribution of epicenters just to the northeast of the NMSZ beginning in the southernmost Illinois Basin (McBride, 1998) (Figure 4-3). Although the diffuse pattern is likely due in part to the poorer seismograph coverage beyond the NMSZ (Mitchell et al., 1991), no strong linear patterns, analogous to the NMSZ, have been recognized in the Basin (e.g., Amorèse, 2003). Furthermore, although focal mechanism solutions of the larger events in the diffuse zone are consistent with a northeast-trending dextral strike-slip strain, the actual seismogenic source north of the NMSZ has remained poorly understood, despite the fact that the largest twentieth century U.S. earthquakes between the Appalachians and the Rockies (Figures 4-1, 4-3, 4-4, and 4-5) have occurred within the diffuse zone of the southern Illinois Basin in Illinois and Indiana and not in the NMSZ proper (Figures 4-1, 4-3, and 4-4).

This study documents the first case of a major deformation zone in the Precambrian crust bene ath the Paleozoic depocenter of the southern Illinois Basin and demonstrates the reactivation of a pre-existing fault structure by moderate-magnitude contemporary seismicity. This study integrates an unprecedented amount of information for the U.S. interior derived from hundreds of petroleum industry borehole logs (Figure 4-6), reprocessed industry seismic reflection profiles (Figure 4-5), geopotential field data, and deformation parameters from relatively well-located earthquakes in the study area (Figures 4-1, 4-3, 4-4, and 4-5). The value of associating an earthquake event with an image of a pre-existing deformation zone in the seismogenic crust would be to improve the assessment of seismic hazard (by pinpointing buried potentially hazardous faults) and to assess the integrity of a stratigraphic formation, underlain by a basement fault, that is under consideration as a target for carbon dioxide (CO_2) sequestration.

Objectives of This Study

- Procure seismic reflection data from industry sources for the study area.
- Produce high-quality, high-resolution scans of large-format paper seismic reflection records and archive them on CDs and DVDs.
- Produce scanned and vectorized versions of selected, critical seismic reflection paper records, which converts a paper record into a digital SEG-Y format file that can be digitally processed further.
- Perform further processing of vectorized records and output to SEG-Y data.
- Produce an active database of digital seismic reflection profile data integrated with Geographic Information Systems (GIS) registered map data using Seismic Micro-Technology's KINGDOM software and transfer the created project to the Illinois State Geological Survey (ISGS). This database can be readily amended in the future as additional seismic data and map information become available.
- Devise a strategy for integrating subsurface geological and geophysical information with information from historical and instrumental earthquake records.
- Provide an in-depth assessment of observable spatial associations between earthquake parameters (e.g., hypocenter location and focal mechanism) and subsurface structure as deduced from the geological and geophysical databases.
- Provide an analysis of the assessment results in a written report.

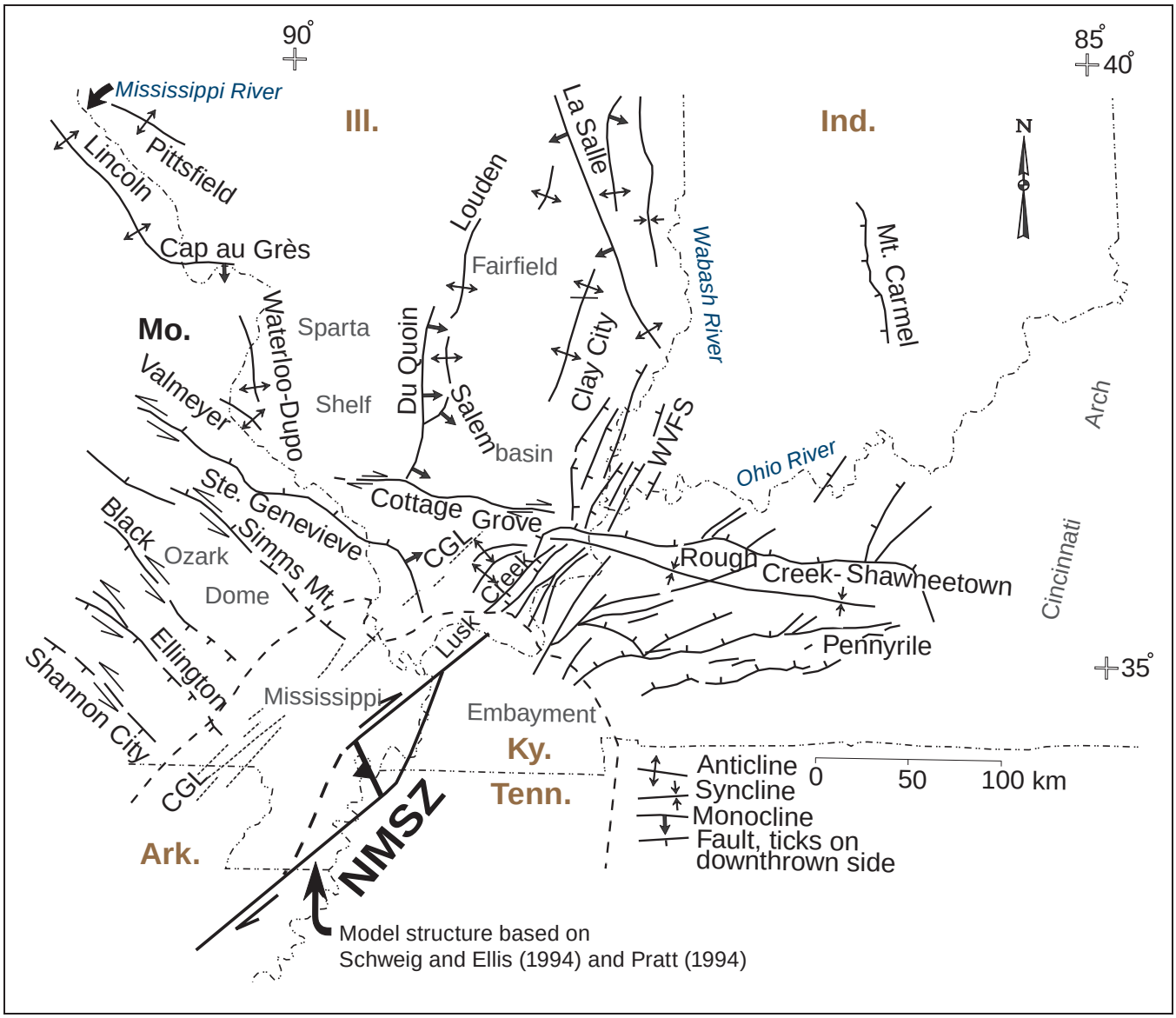

Figure 4-1 *Structural setting for the Illinois Basin. WVFS, Wabash Valley Fault System; NMSZ, New Madrid Seismic Zone; CGL, Commerce Geophysical Lineament.*

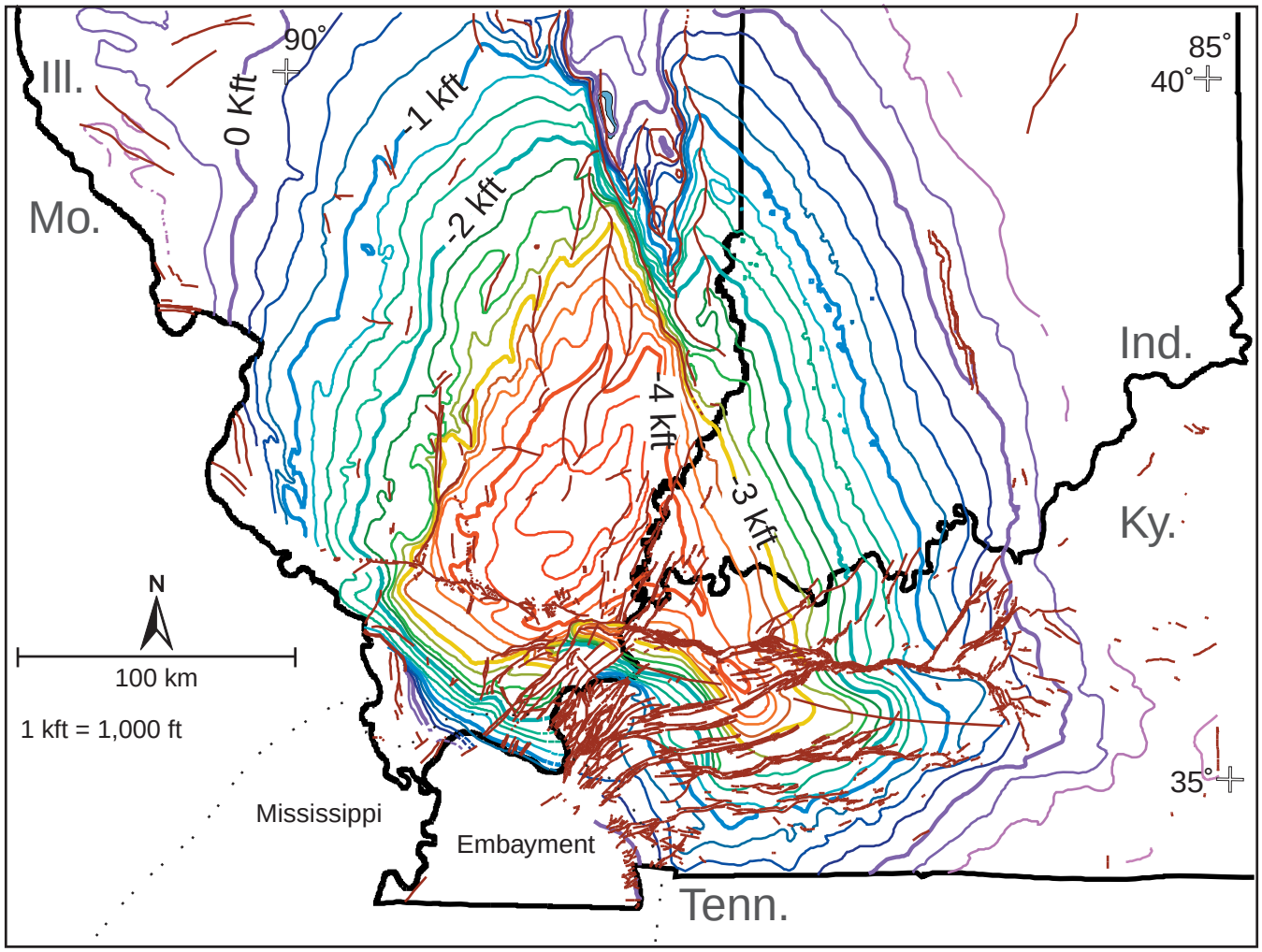

Figure 4-2 *Structural configuration of the southern Illinois Basin shown by contours representing the depth to the base of the Upper Devonian New Albany Shale (contour interval = 250 feet below sea level; original units) and by structural axes (faults and folds). Source of information is the Gas Research Institute, Chicago, Illinois.*

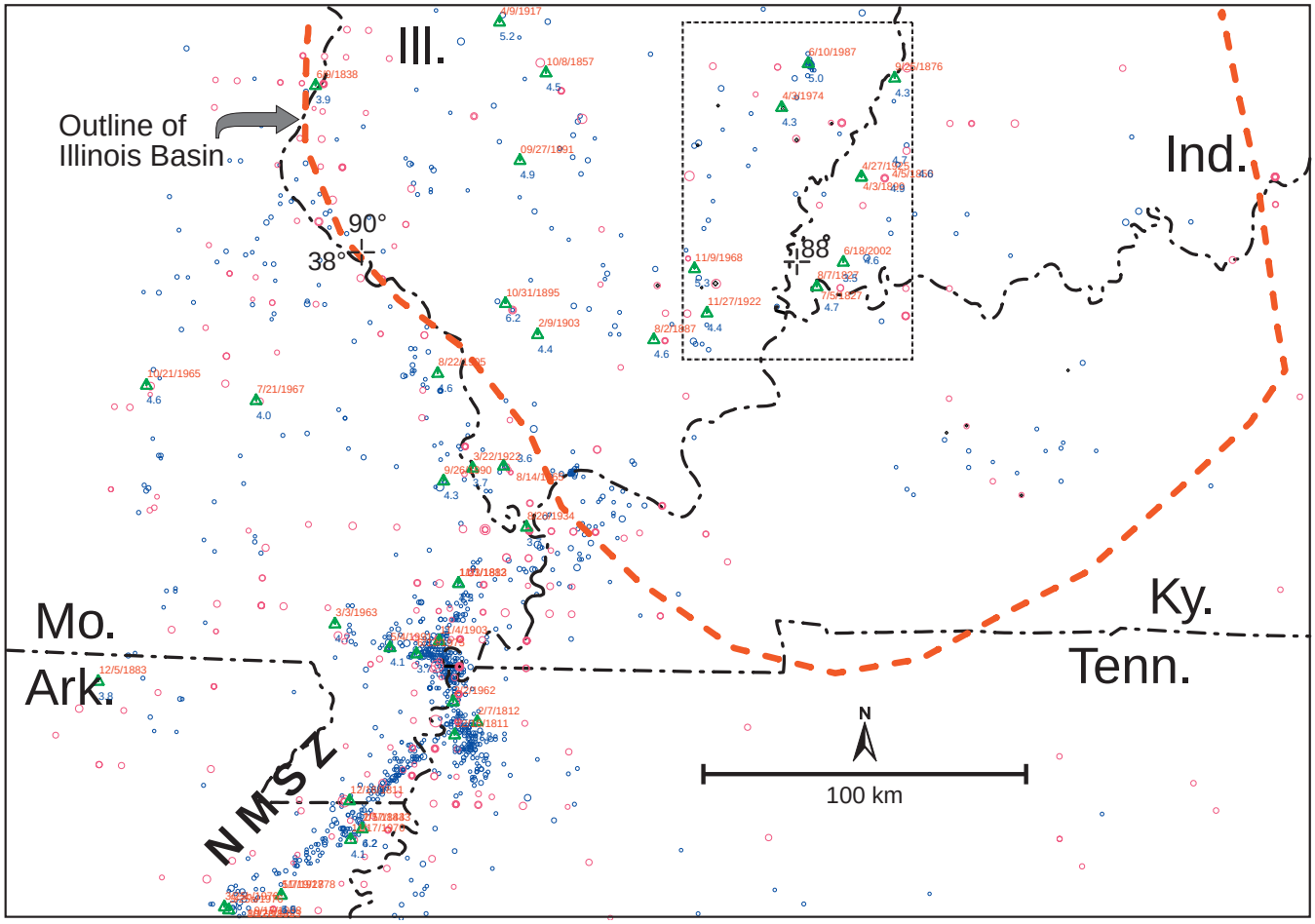

Figure 4-3 *Central U.S. earthquakes through 2004. Sources: (1) the* Catalog of Central US Earthquakes, 1810–1980 *(Nuttli and Brill, 1981) (with body wave magnitude of at least 2.4; 1811–1973); (2) instrumental data from the Center for Earthquake Research and Information (with body wave magnitude of at least 2; 1974–2004). These two databases are represented by red and blue circles, respectively; circle size provides a relative measure of magnitude (see original sources for actual magnitudes). The labeled black diamonds show the epicenters for events relocated by the U.S. Geological Survey for the Wabash Valley Fault System region (Gordon, 1988). Green triangles are from the database of relocated events by Bakun and Hopper (2004) (date and moment magnitude are given). Dotted rectangle gives area of map in Figure 4-5.*

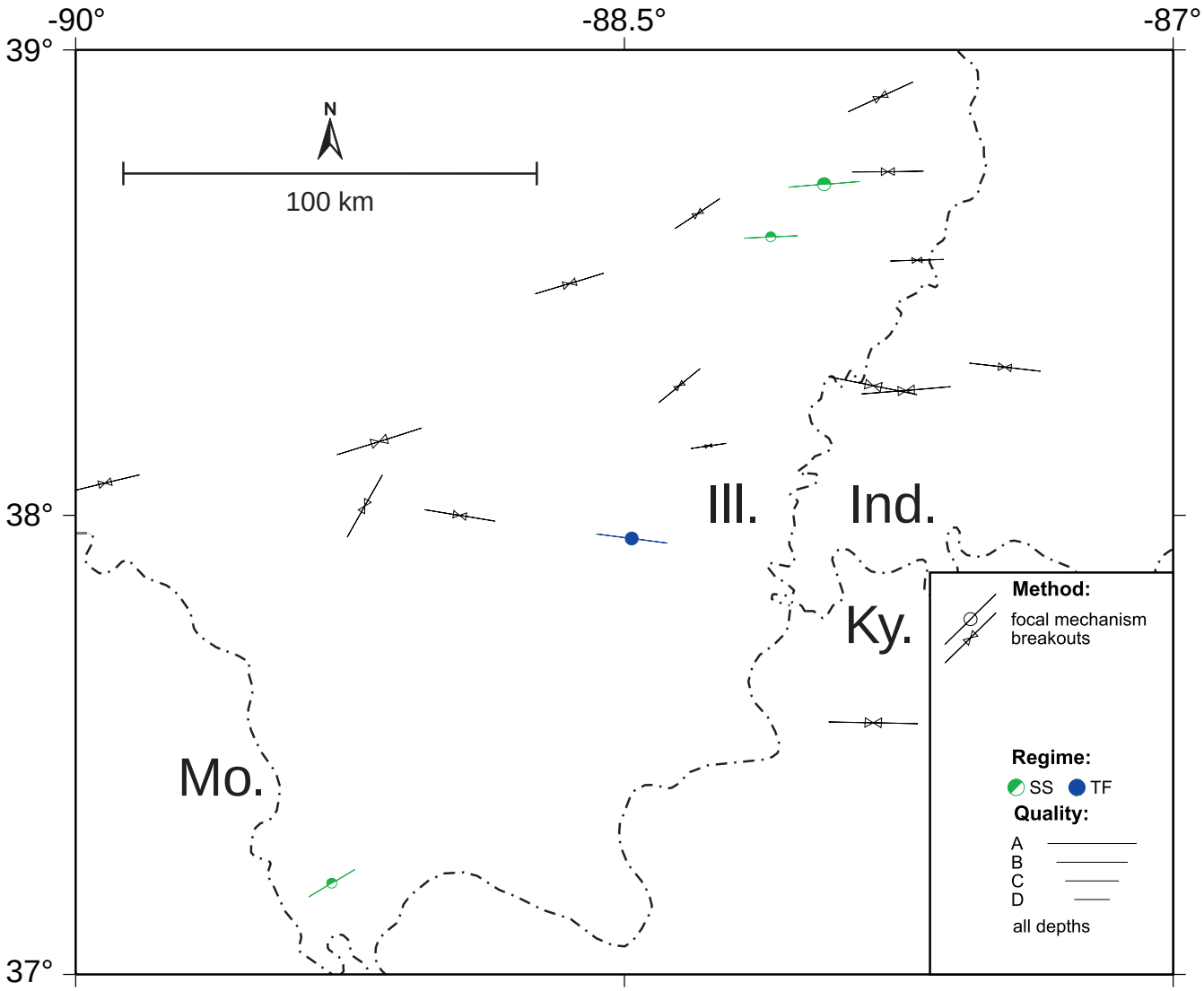

Figure 4-4 *Map of available stress information for the southern Illinois Basin (Reinecker et al., 2004).*

Regional Geological and Geophysical Setting

Geological Setting of Basement Beneath the Illinois Basin

The roughly oval-shaped Illinois Basin overlying parts of Illinois, Indiana, western Kentucky, and southeastern Missouri, contains as much as 7,000 m (22,970 ft) of Cambrian through Pennsylvanian age sedimentary rocks (Buschbach and Kolata, 1991). An areally extensive granite-rhyolite terrane (eastern granite-rhyolite province, 1.48 to 1.45 billion years ago) is thought to lie beneath the Paleozoic strata of the Basin and the surrounding region on the basis of outcrops of rhyolite, dacite, and related granitic plutons in the St. Francois Mountains of southeastern Missouri and a few scattered basement drill holes in Basin areas (Buschbach and Kolata, 1991; Rudman and Rupp, 1993; Lidiak, 1996; Van Schmus et al., 1996). This province is part of a vast igneous belt stretching from northern Mexico to eastern Québec (Lidiak, 1996; Karlstrom et al., 1999). The thickness of these rocks is unknown but is thought to represent either a thin veneer (a few kilometers thick) or isolated igneous intrusions within an otherwise unknown basement (Bickford et al., 1986).

Geophysical Setting

The study area is a region where two important Illinois Basin earthquakes occurred (1974 and 1987) (Figure 4-5) relatively close to one another (and to nearby reflection profiles), along the western flank of the La Salle Anticlinorium (LSA) and the Wabash Valley Fault System (WVFS) (Figures 4-1 and 4-5). These two events have been a focus of study in the literature and have very similar parameters of body-wave magnitude (1974, m_b = 4.7; 1987, m_b = 5.2), depth (10 to 15 km (6.2 to 9.3 mi)), mode of faulting (dominantly strike slip), and nodal plane orientations consistent with the known regional stress direction of east-northeast (Langer and Bollinger, 1991) (Figure 4-4). This area lies approximately 76 km (47 mi) north of the epicenter of the largest twentieth century U.S. earthquake between the Appalachians and the Rocky Mountains. That November 9, 1968, magnitude 5.4 event nucleated at ~21-km (~13-mi) depth (Gordon, 1988) along a north-northeast–striking thrust fault. Previous geophysical exploration studies of this event (McBride et al., 1997, 2002) concluded that the hypocenter corresponded to a prominent west-dipping reflector zone interpreted as a blind thrust. The LSA and WVFS are major structural trends that form a “spine” down the length of the Illinois Basin (Figure 4-1) and have long been suspected as influencing the nucleation of earthquakes (Hamburger and Rupp, 1988) but without a specific causal explanation. The area surrounding the juncture of the northwest-trending LSA and the northeast-trending WVFS, which represents an “abutting” of a contractional and an extensional regime, respectively, is one of the most structurally complex areas of the midcontinent (Nelson, 1991; Hamburger and Rupp, 1988). This area also corresponds to the eastern flank of the Fairfield sub-basin, which leads southward into the deepest part of the Illinois Basin outside of the Reelfoot Rift-Rough Creek Graben system (Figure 4-1).

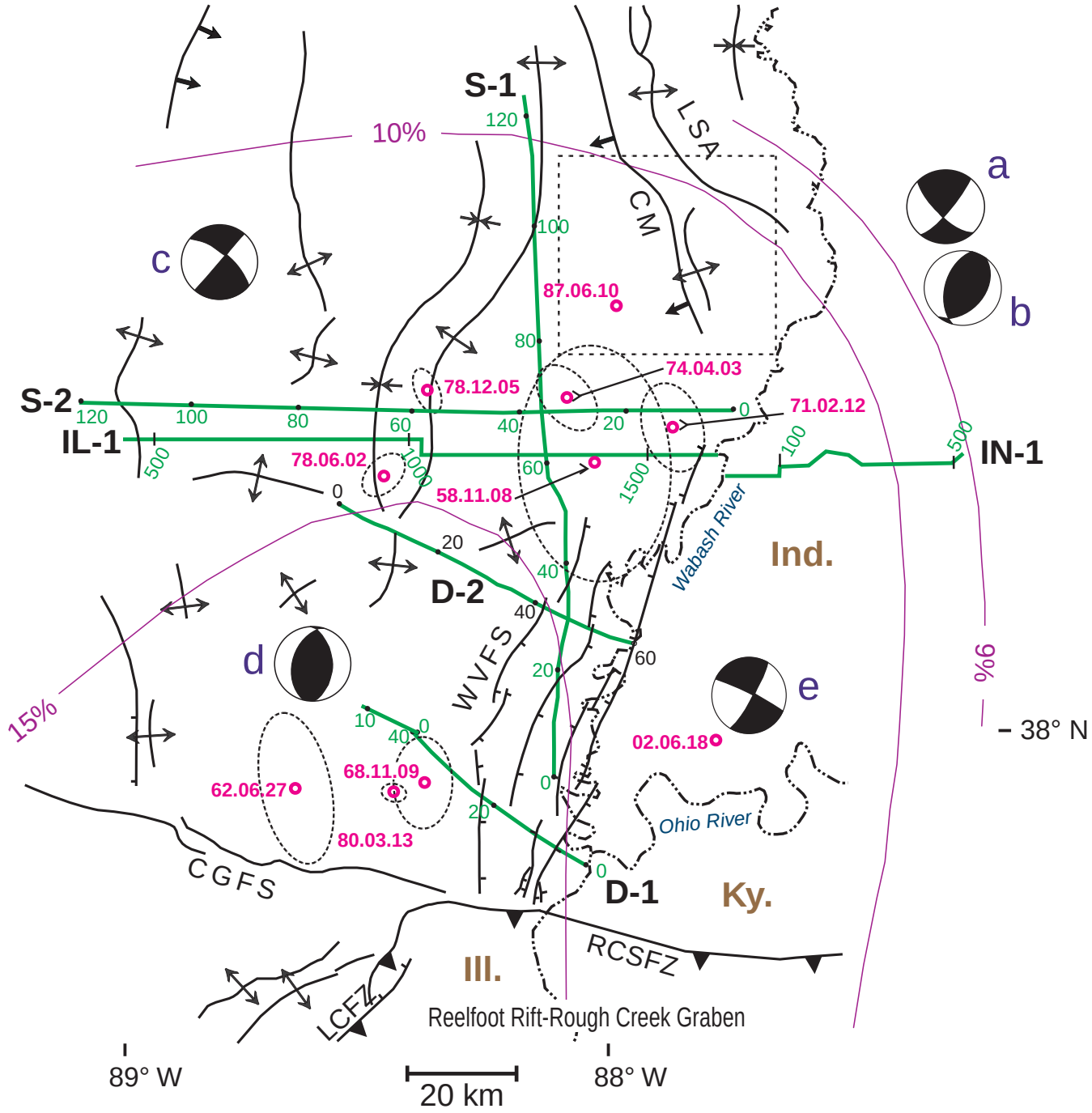

Figure 4-5 *Map of the south-central Illinois Basin and Wabash Valley Fault System (WVFS); known fold axes, faults, and other structures (Nelson, 1995); and revised, instrumentally recorded epicenters ($m_{bLg} \geq 3.0$) with nominal 95% confidence ellipses from Gordon (1988) and Langer and Bollinger (1991). CM, Charleston Monocline; LSA, LaSalle Anticlinorium; CGFS, Cottage Grove Fault System; m_{bLg}, body-wave magnitude using Lg wave. Simplified contours show the seismic hazard surrounding the NMSZ as peak acceleration (%g) with a 10% probability of exceedance in 50 years (site: NEHRP B–C boundary) (Frankel, 1995). Seismic reflection profiles used in this study are also shown. All but IL-1 and IN-1 are proprietary and are depicted in a general way only with locations marked every 20 km. Dashed box indicates area of a loose network of proprietary profiles (~140 km of line, total), which cannot be shown due to confidentiality agreements. Earthquake focal mechanisms are plotted from Taylor et al. (1989) and Langer and Bollinger (1991): (a) main shock of 1987 event, (b) typical reverse-fault aftershock of 1987 event, (c) main shock of 1974 event, and (d) main shock of 1968 event.*

Most earthquake research in the midcontinent has been focused on the NMSZ (Figures 4-1, 4-3, and 4-4); the Illinois Basin seismic zones have remained largely neglected. More recently, reanalyses of historical and instrumentally recorded events suggest the association of larger events with the major geological structures in the Basin along trend alignments of epicenters. Historical epicenter relocation studies by the U.S. Geological Survey (USGS), based on the method of Bakun and Wentworth (1997), have in several instances repositioned moderate-to-large magnitude earthquakes over or near major structural axes (e.g., Du Quoin Monocline, Cottage Grove Fault System) (Bakun et al., 2003; Bakun and Hopper, 2004) (Figure 5). Bakun and Hopper (2004) used their results to make tentative associations between a historical earthquake and a specific causative fault, which they explained as reactivation of pre-existing fault zones by contemporary seismicity. McBride (1997, 1998), McBride and Nelson (1999), and Duchek et al. (2004) have shown that many of the major deformation zones of the Basin, including those noted in Bakun and Hopper's (2004) study, are penetrated by faults that propagate up from Paleozoic basement and, thus, could potentially represent a seismic source zone (Figure 4-7). Langenheim et al. (1997) presented evidence that the Commerce Geophysical Lineament (Figure 4-1), defined as a linear trend of potential field anomalies cutting diagonally across the southern Illinois Basin, correlates to a sparse linear trend of epicenters and thus may be a reactivated seismic source zone with the Precambrian basement. A statistical analysis of regional epicenter trends for the NMSZ, Illinois Basin, and the surrounding area (Amorèse, 2003) recognized distinct linear bands that matched in a general way with some of the structural trends in the Basin (Figure 4-8). In summary, evidence is evolving that supports a seismogenic source or sources beneath the Illinois Basin beyond the better-studied realm of the NMSZ, but cases relating specific structures to a particular event or group of events have lagged behind.

Data and Methodology

The study area of this project represents one of the largest concentrations in the midcontinent of logged petroleum industry boreholes and available digital industry seismic reflection profiles (Figure 4-6), which surround the three Illinois Basin earthquake epicenters (Figure 4-5). Although both paper and digital records of the seismic data were analyzed for this study, the results presented herein are based on the high-quality digital data, which were processed, visualized, and mapped digitally. Seismic records were stratigraphically correlated using established reflector-stratal associations (Heigold and Oltz, 1991; Potter et al., 1997; Drahovzal, 1997; McBride and Kolata, 1999) and synthetic seismograms (Figure 4-9). Reprocessing of seismic reflection data procured from industry sources for this study includes (1) extending Vibroseis records through recorrelation of the original field records (Okaya and Jarchow, 1989; McBride et al., 2003), (2) post-stack migration, and (3) cosmetic filtering (to reduce noise) of previously processed records. Additional profiles, available only as paper sections, were scanned and vectorized

in order to create digital SEG-Y records, followed by migration and cosmetic filtering. More detailed discussion of seismic data acquisition and processing parameters representative of the data for this study can be found in McBride (1997), McBride and Kolata (1999), and McBride et al. (2002, 2003).

For this study, 43,568 borehole logs from the ISGS database (Figure 4-6) were used to calculate depths to the Beech Creek Formation (Barlow Formation surface, Mississippian) and to create contour maps showing the structure of the deeper sedimentary part of the Basin based on the data (Figure 4-10a). First-derivative ("slope") maps, which show areas of prominent sloping strata (Figure 4-10b), were computed

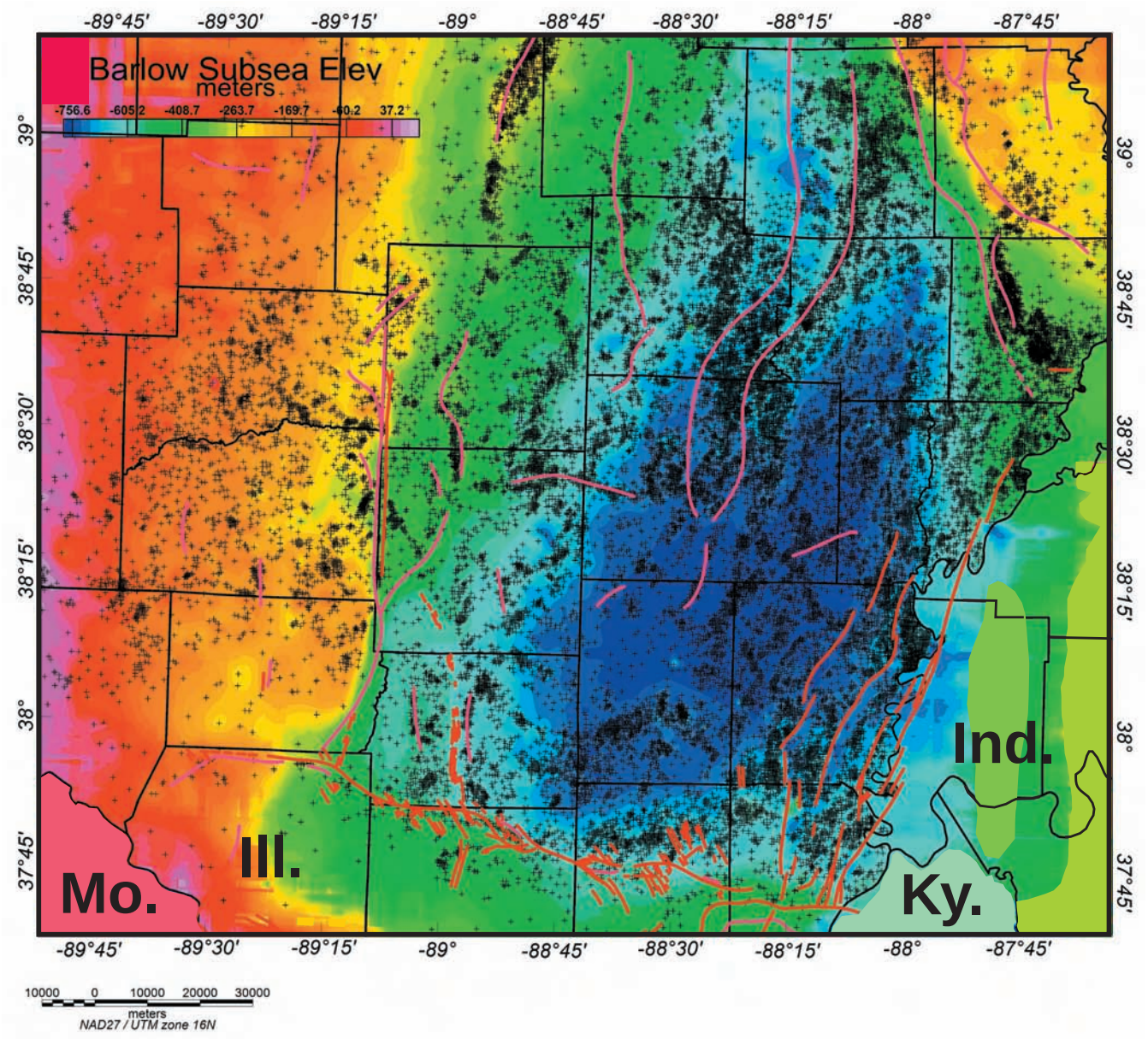

Figure 4-6 *Map showing location of boreholes from the databases of the Illinois State Geological Survey superimposed over a gridded version of the Barlow surface and structural axes (Nelson, 1995).*

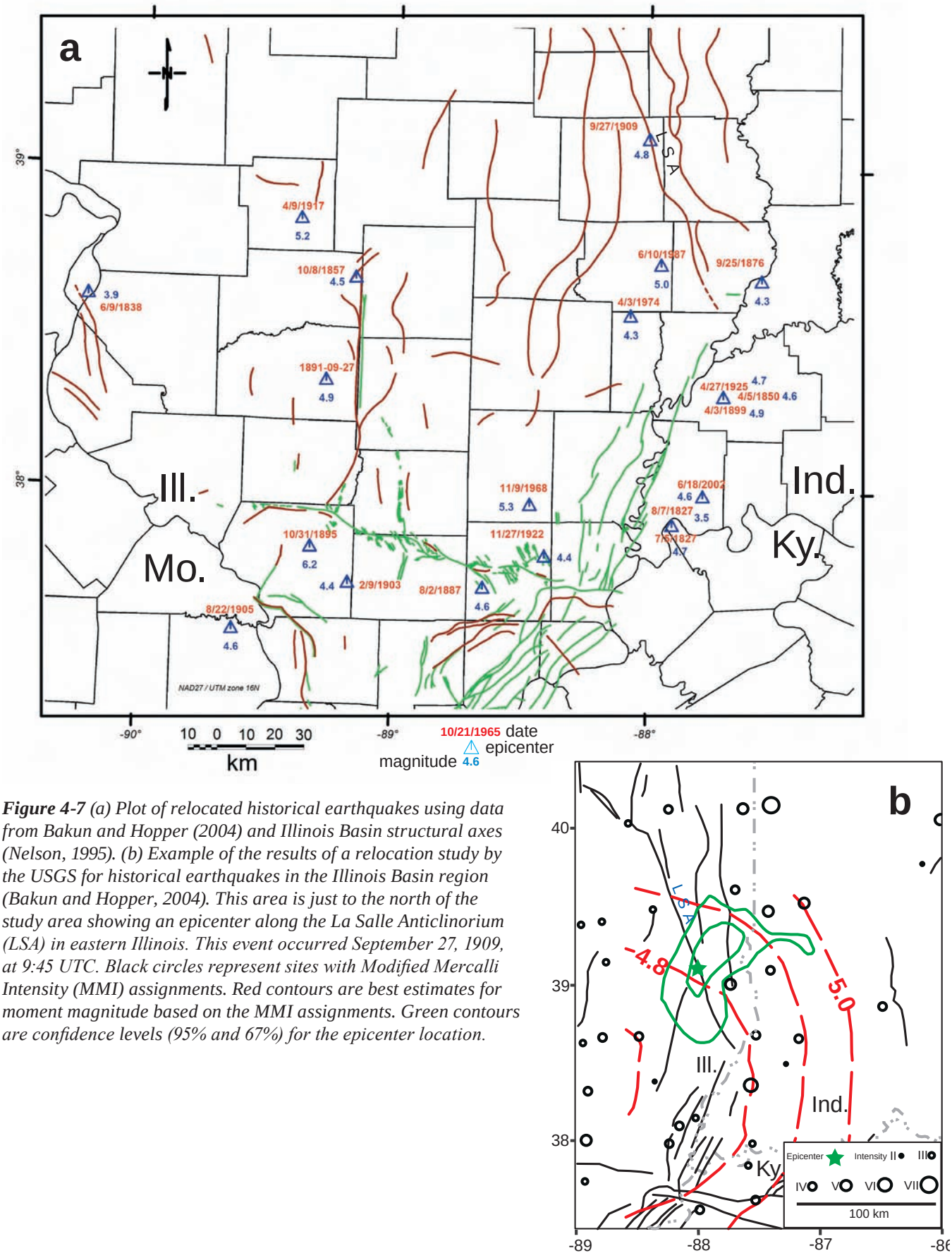

Figure 4-7 *(a) Plot of relocated historical earthquakes using data from Bakun and Hopper (2004) and Illinois Basin structural axes (Nelson, 1995). (b) Example of the results of a relocation study by the USGS for historical earthquakes in the Illinois Basin region (Bakun and Hopper, 2004). This area is just to the north of the study area showing an epicenter along the La Salle Anticlinorium (LSA) in eastern Illinois. This event occurred September 27, 1909, at 9:45 UTC. Black circles represent sites with Modified Mercalli Intensity (MMI) assignments. Red contours are best estimates for moment magnitude based on the MMI assignments. Green contours are confidence levels (95% and 67%) for the epicenter location.*

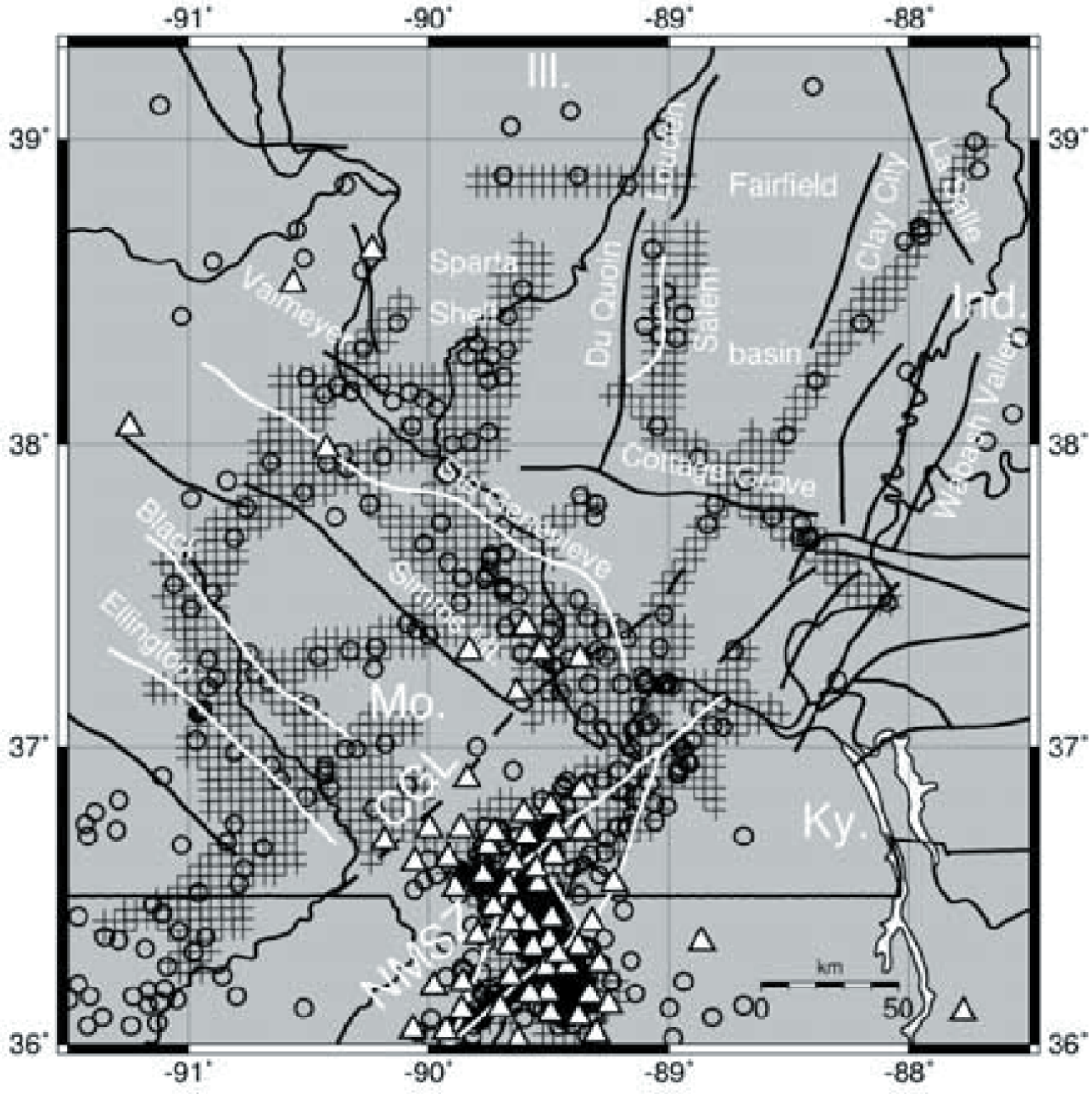

Figure 4-8 *Results of a statistical trend analysis by Amorèse (2003) for earthquakes north of the New Madrid Seismic Zone (NMSZ) in the Illinois Basin. CGL, Commerce Geophysical Lineament.*

using the Barlow Formation surface. The slope maps (red areas, Figure 4-10b) are an innovation, not previously used in the Illinois Basin, that allowed us to identify subtle linear trends in deep stratigraphic units otherwise not visible on conventional structure maps. These maps were computed especially for this study using the ESRI product ArcMap (Spatial Analyst) from the Beech Creek unit. The top of the Beech Creek is a limestone marker that can be correlated and occurs across most of the Illinois Basin.

Four earthquake catalogs have been used for this study, sub-sampled to the study area: the Otto Nuttli historical catalog for 1811 to 1973, the Center for Earthquake Research and Information (CERI)-Saint Louis University instrumental catalog for 1974 to 2004, the USGS database of relocated events for the Wabash Valley and surrounding area (Gordon, 1988), and relocated historical events from Bakun and Hopper (2004). On the maps in this report, these three catalogs are distinguished by differing symbologies or colors (Figures 4-3 and 4-7b).

In order to independently indicate the general structural configuration of the Illinois Basin in the study area and to track deformation zones (e.g., faults and folds mapped from reflection profiles), seismic records on the base of the Cambro-Ordovician Knox Supergroup were correlated and displayed as maps (Figure 4-11). These maps can be compared with those generated from borehole logs on the top of the Mississippian Beech Creek surface (Figure 4-10). Although no standardized stratigraphy exists for the deeply buried Precambrian seismic sequences (Centralia Sequence, Pratt et al., 1992) visible on the longer records (McBride and Kolata, 1999), individual seismic stratal markers used to find and map deeper horizon offsets and other deformation were locally identified (Figure 4-12). These markers can correlate within deformation tracked and intersecting seismic profiles and closely spaced, non-intersecting seismic profiles (e.g., Figure 4-13).

Observations and Interpretation

Subsurface Mapping and Fault Zones

The strategy for portraying the results is to sequentially construct the subsurface for the study area and then to superimpose dynamic deformation derived from earthquakes. In this way, the critical issue of structural reactivation by the contemporary stress system is addressed (Figure 4-4). The Beech Creek subsurface contour map (Figure 4-10a) indicates a gently southwest-plunging synclinal surface within the shallower portion of the Paleozoic basin. This synclinal surface is an expression of the northern flank of the Fairfield sub-basin (Nelson, 1991). The eastern flank of the syncline is steepest, is most clearly delineated, and defines the southwest-dipping limb of the LSA (Nelson, 1991; Marshak and Paulsen, 1997; McBride, 1997).

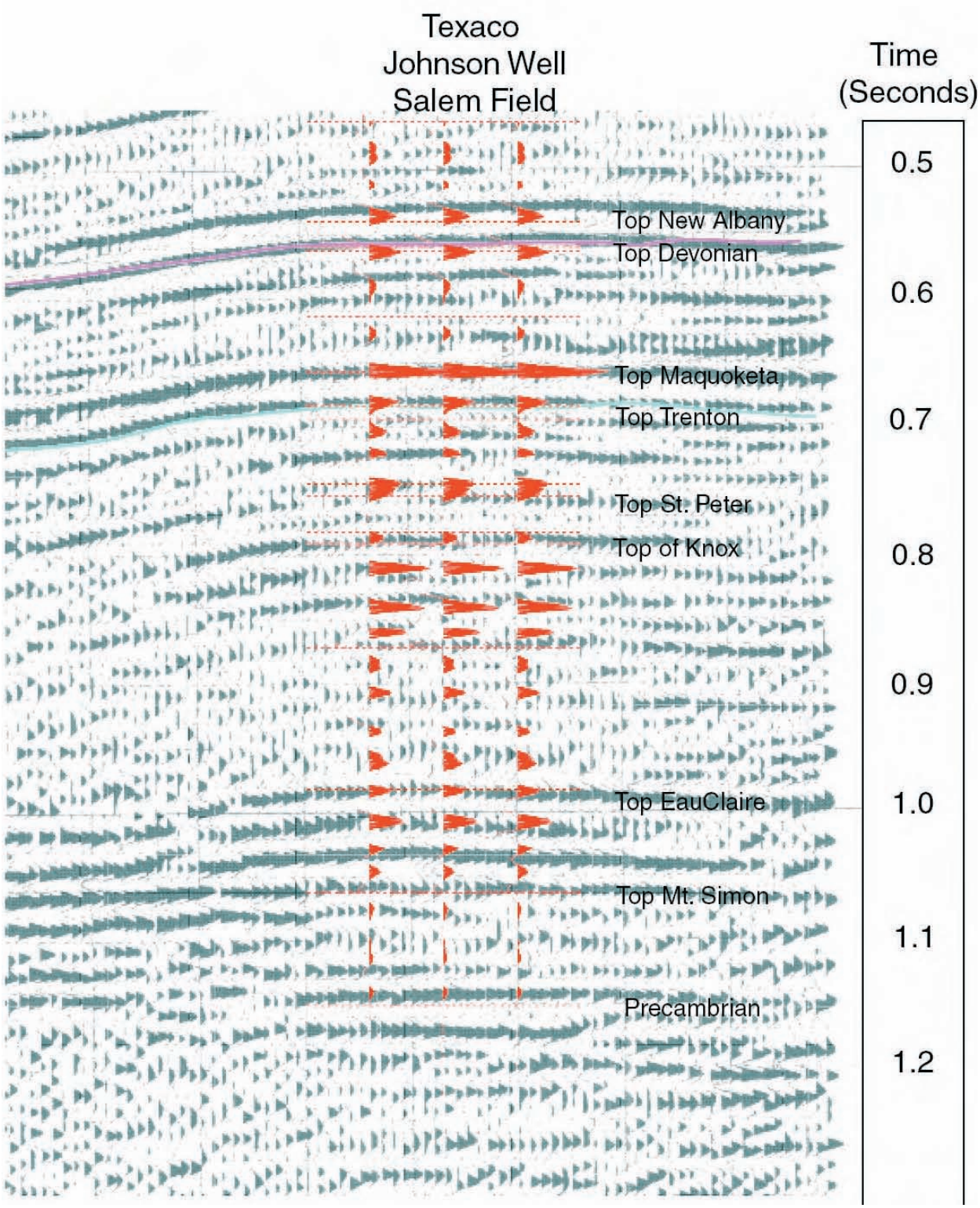

Figure 4-9 *Results of a synthetic seismogram modeled from the R.S. Johnson well drilled in the southern Illinois Basin and comparison with the nearest available proprietary industry seismic reflection profile available in the database of the ISGS. Drill hole location is latitude 38.552106, longitude 89.022413.*

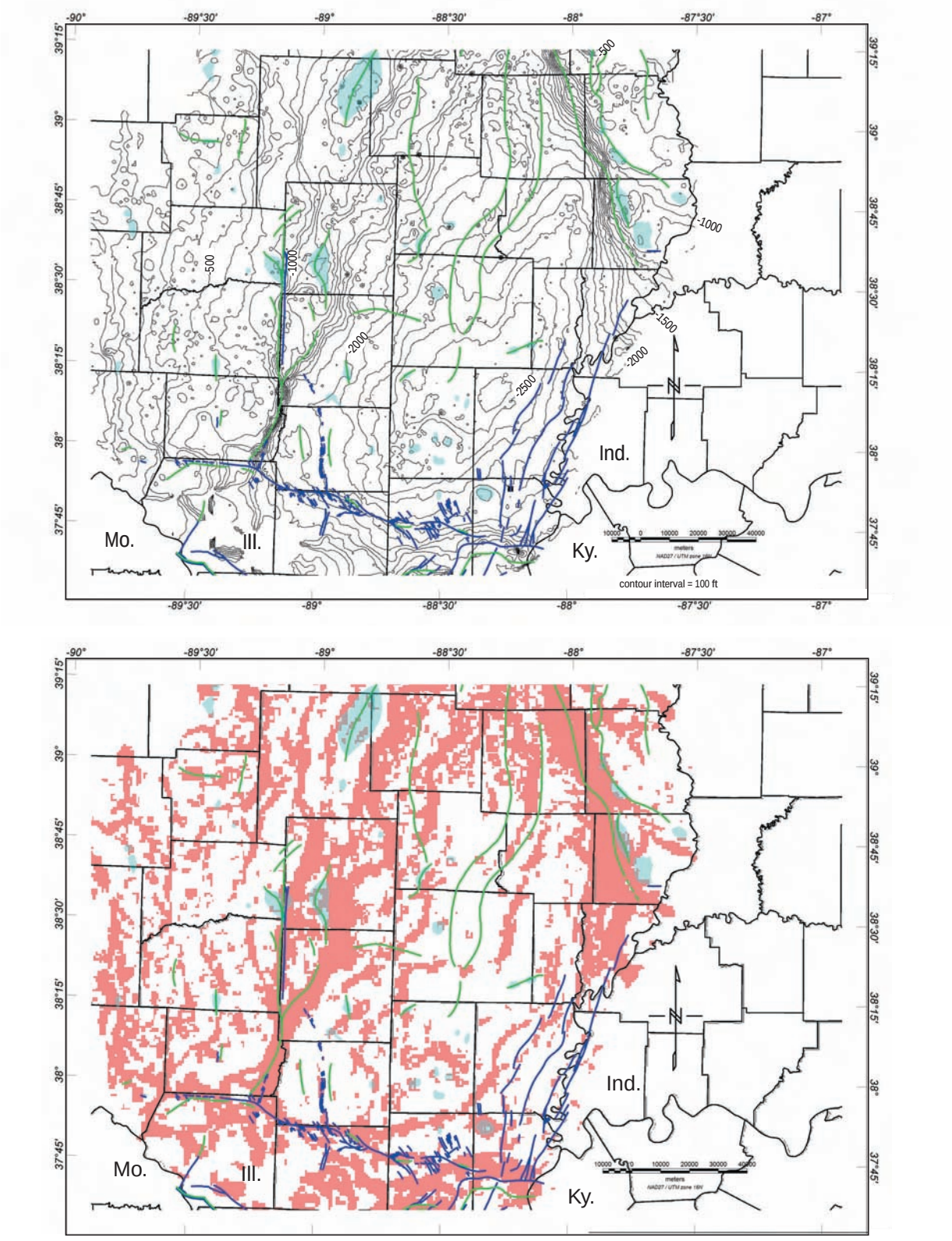

Figure 4-10 *(a) Structural contour map for the top of the Beech Creek Formation (Barlow Formation surface, Mississippian) (units are feet below sea level) constructed from the ISGS database (Figure 4-6). (b) First-derivative ("slope") maps were computed using the Barlow Formation surface. The red areas are zones that have a high-angle slope and may be potential deep-seated faults. Green and blue lines depict structural axes and faults, respectively, and blue polygons represent known structural closures (from ISGS, 2005).*

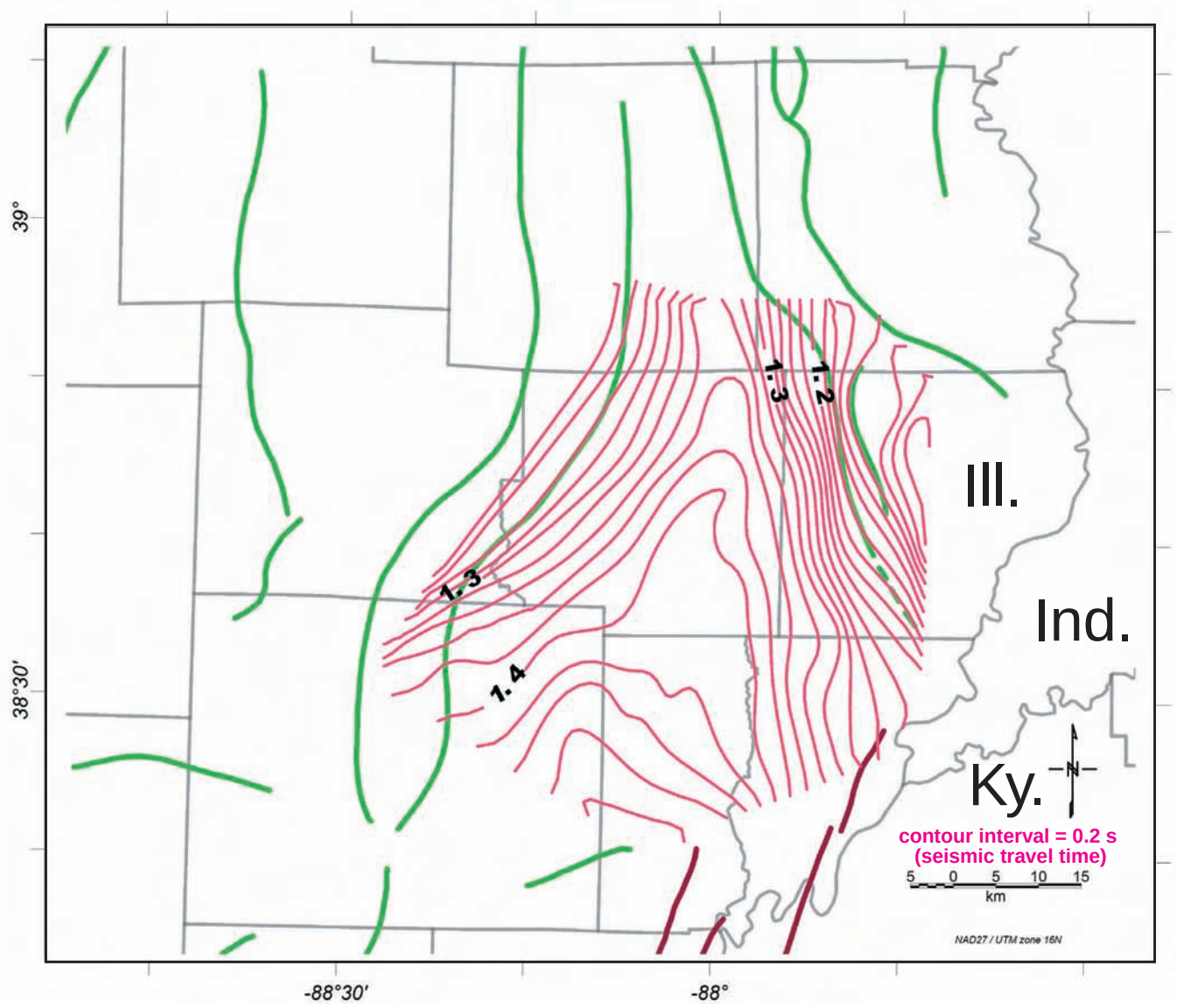

Figure 4-11 *Structural contour map for base of the Knox Supergroup based on correlated seismic reflection profiles (Figure 4-6) (units are seconds, two-way travel time).*

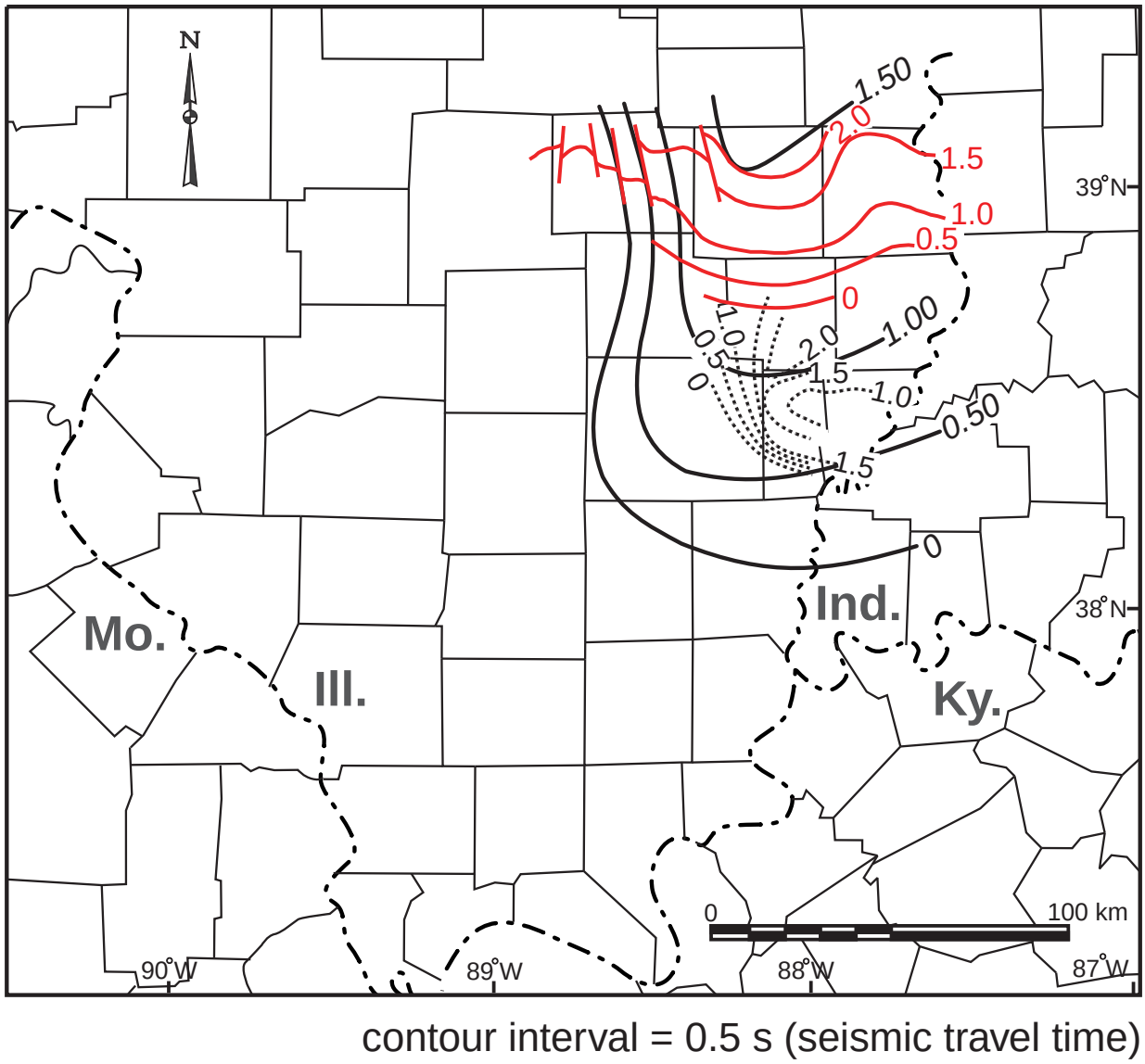

Figure 4-12 *Iso-travel time structural contour maps of Precambrian surfaces based on reprocessed and COCORP deep seismic reflection profiles (Figure 4-6) from McBride et al. (2003). Solid black line is travel time isopach map for the interval between the base of the Mt. Simon Sandstone and the base of the Enterprise subsequence (E in Figure 4-13) (McBride and Kolata, 1999). Contour interval is 500 ms. Travel time isopach map for the northern and southern sub-Centralia sequences (red and dashed black lines, respectively) (B and C, respectively in Figure 4-13). Contour interval is 500 ms. Sequence C corresponds to the faulted zone shown in Figures 4-14, 4-15, and 4-16. See McBride et al. (2003) and text for more information.*

A subsurface contour map (Figure 4-11) was also constructed in travel time from the seismic profiles for the base of the Knox Supergroup because drill-hole penetrations are usually unavailable. The results of this map generally confirm those of the shallower Beech Creek surface, but with a more focused structure, as shown by the steeper Knox contours on the eastern flank. The slope map emphasizes linear trends in the structure of the Mississippian strata as depicted by the prominent northeast-, north-, and northwest-striking trends. As expected, these trends match the flanks of the synclinal sub-basin.

The key seismic reflection profile for this area is S-1 (Figure 4-13), which trends north-south for a distance of 139 km and was reprocessed to 16 s for this study to increase the depth interval. This profile cuts through the western flank of the synclinal sub-basin. The full length of the profile is shown to 10 s in the form of a skeletonized section (Figure 4-13) in order to provide a regional structure context for the study area. The section vividly displays the coherent and highly structured Precambrian upper crust, which includes three previously mapped seismic stratigraphic sequences (McBride and Kolata, 1999; McBride et al., 2003). The origin of these sequences remains unknown, but it has been proposed to be layering within the granite-rhyolite igneous province that is known to underlie at least the uppermost part of the crust beneath the Illinois Basin, part of an extensive sedimentary rift basin, or the remains of a large collapsed Proterozoic rhyolitic caldera complex analogous to the caldera complexes exposed in the nearby St. Francois Mountains in southeastern Missouri (Pratt et al., 1992; McBride et al., 2003).

An immediate observation from the S-1 profile (labeled as C in Figure 4-13) is that an area appears between km 56 and 91 where the Precambrian reflectivity is interrupted by offsets, lateral truncations, and abrupt changes in dip. This 35-km (22-mi)-wide zone stands out as unique along the entire 139-km (86-mi) transect (Figure 4-13). In fact, such an intensely disrupted zone is not observed elsewhere on any seismic profiles in the Basin that are publicly available or available in the proprietary ISGS seismic database (McBride et al., 1997, 2003; Potter et al., 1997; McBride and Kolata, 1999; McBride and Nelson, 1999). On a higher-resolution (i.e., color amplitude) raster display of a portion of the S-1 profile (Figure 4-14a), more intricate details of the disrupted zone are apparent. This zone, which is apparently confined to the Precambrian section (i.e., below ~1.7 s locally), is interpreted as a region of intense faulting and deformation. The steeply dipping faults are defined by at least two reflectors being synthetically displaced. Further, the edges of offset reflectors are in places marked by diffractions, a finding that supports a fault interpretation. The attitude of the offset reflectors is consistent with a normal sense of faulting. Three principal fault zones can be mapped on S-1 (Figure 4-14a). A possible continuation of faults A and B to the northeast (Figures 4-15 and 4-16) is based on the network of seismic profiles shown in Figure 4-5. For example, Figure 4-17a shows a profile that intercepts fault A, which is expressed as a normal sense, down-to-the-south offset of basement reflectors. This fault propagates upward into a gentle down-to-the-south flexure of Paleozoic stratal reflectors.

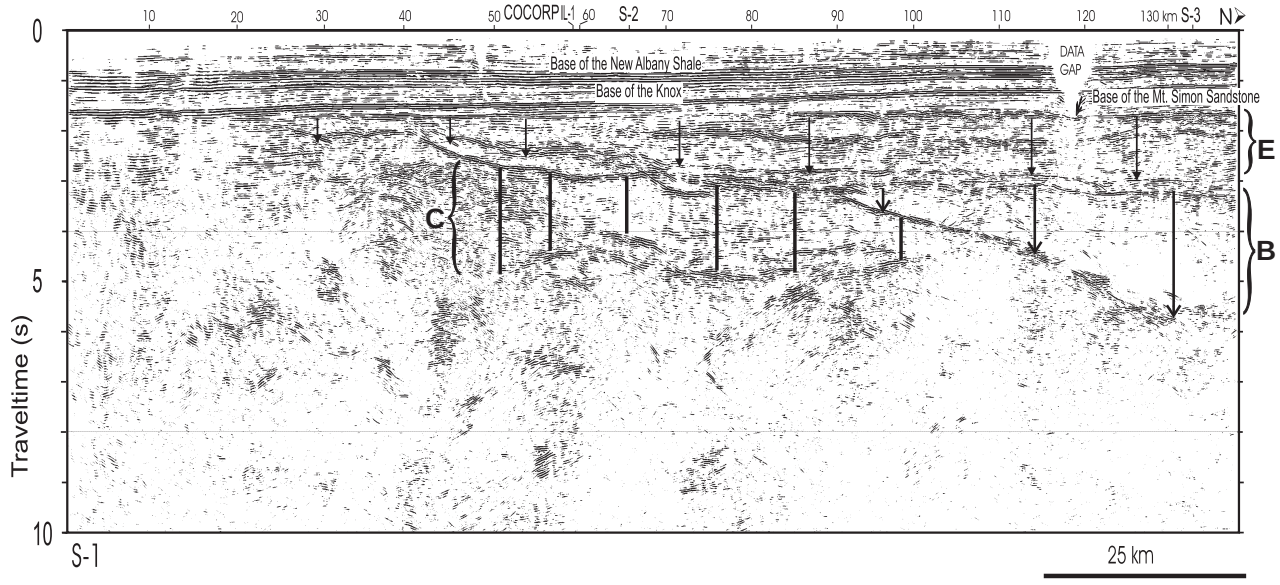

Figure 4-13 *Regional seismic reflection profile S-1. This profile has been reprocessed from the original uncorrelated Vibroseis records (see McBride et al., 2003, for details of acquisition and reprocessing) and then coherency filtered using a skeletonization procedure (see Cook and Vasudevan, 2003, for procedure) for this study. The skeletonization allows the portrayal of the principal reflectivity for very small-scale representations of the data such as used here. E, B, and C refer to three sequences recognized within the Precambrian Centralia Sequence (McBride et al., 2003). See Figure 4-12 for map view of these sequences.*

Some 2.5-D control (intersecting two-dimensional seismic lines) is available from two nearby intersecting east-west seismic profiles, S-2 and IL-1 (Figure 4-5). Profile S-2 (Figure 4-14b) reveals a zone of offset and disrupted reflectors very similar in style to that appearing on profile S-1 (Figure 4-14a), but showing a different set of orientations. Correlation of faulted offsets was made from the key north-south S-1 profile (Figure 4-14a) onto the cross profiles by following stratal reflectors and the character of the offset (e.g., similar number of offset reflectors, similarly tilted reflectors). In this way, the three fault zones are recognized as part of an array of northeast-striking faults that gradually change strike in a northeast-reaching "fan" orientation (Figures 4-15 and 4-16). The middle fault is distinguished by having the clearest expression on the seismic profiles and the largest offset (labeled B on Figure 4-14a). The entire fault zone appears to "underpin" the sub-basin, as shown by the sub-parallelism between the fault trends (A, B, and C) and the structural contours for the Mississippian and for the Cambro-Ordovician stratal markers (Figures 4-15 and 4-16). Fault A closely follows a prominent slope trend for Mississippian strata (Figure 4-15).

Figure 4-14 *(opposite page) (a) High-resolution (i.e., color amplitude) raster display of an excerpt of the S-1 profile showing the area of intense disruption within the Precambrian section. (b) Same as in Figure 4-14a, but showing S-2 profile for the area of intense disruption within the Precambrian section oriented perpendicular to the S-1 profile.*

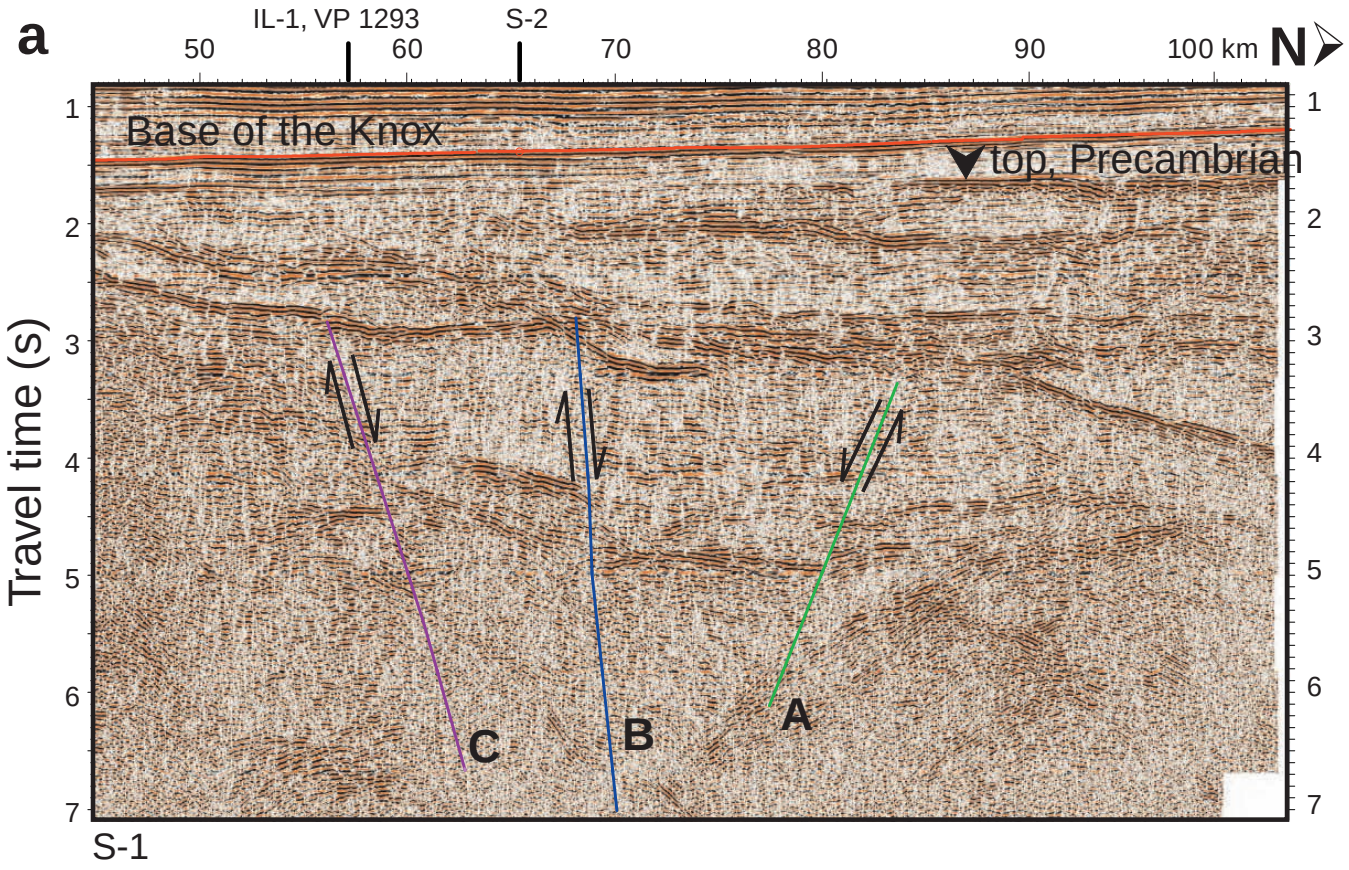
a
IL-1, VP 1293
S-2
50
60
70
80
90
100 km
N
Base of the Knox
top, Precambrian
Travel time (s)
1
2
3
4
5
6
7
C
B
A
S-1

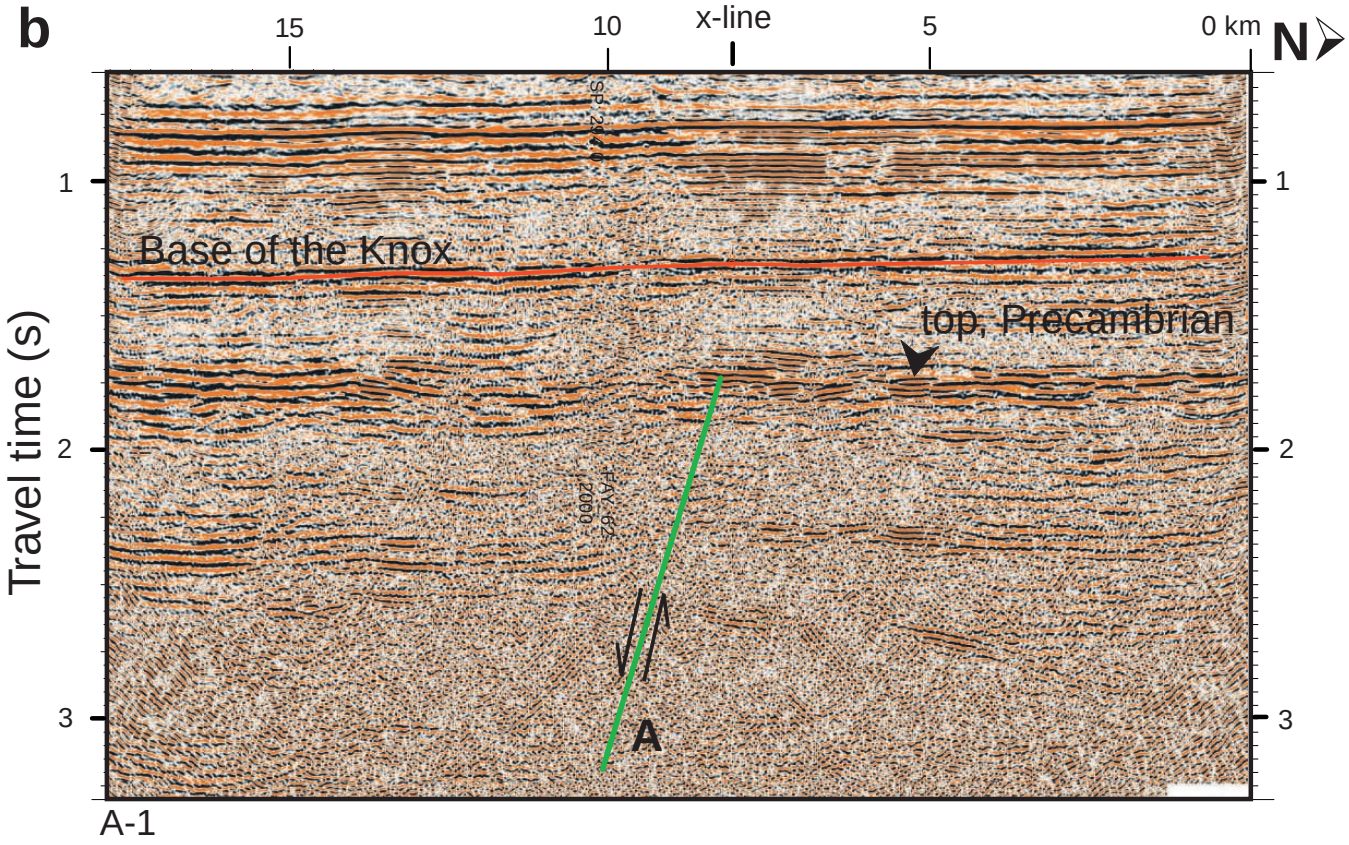
b
15
10
x-line
5
0 km
N
SP-2400
Base of the Knox
top, Precambrian
Travel time (s)
1
2
3
PAY-62
I-2000
A
A-1

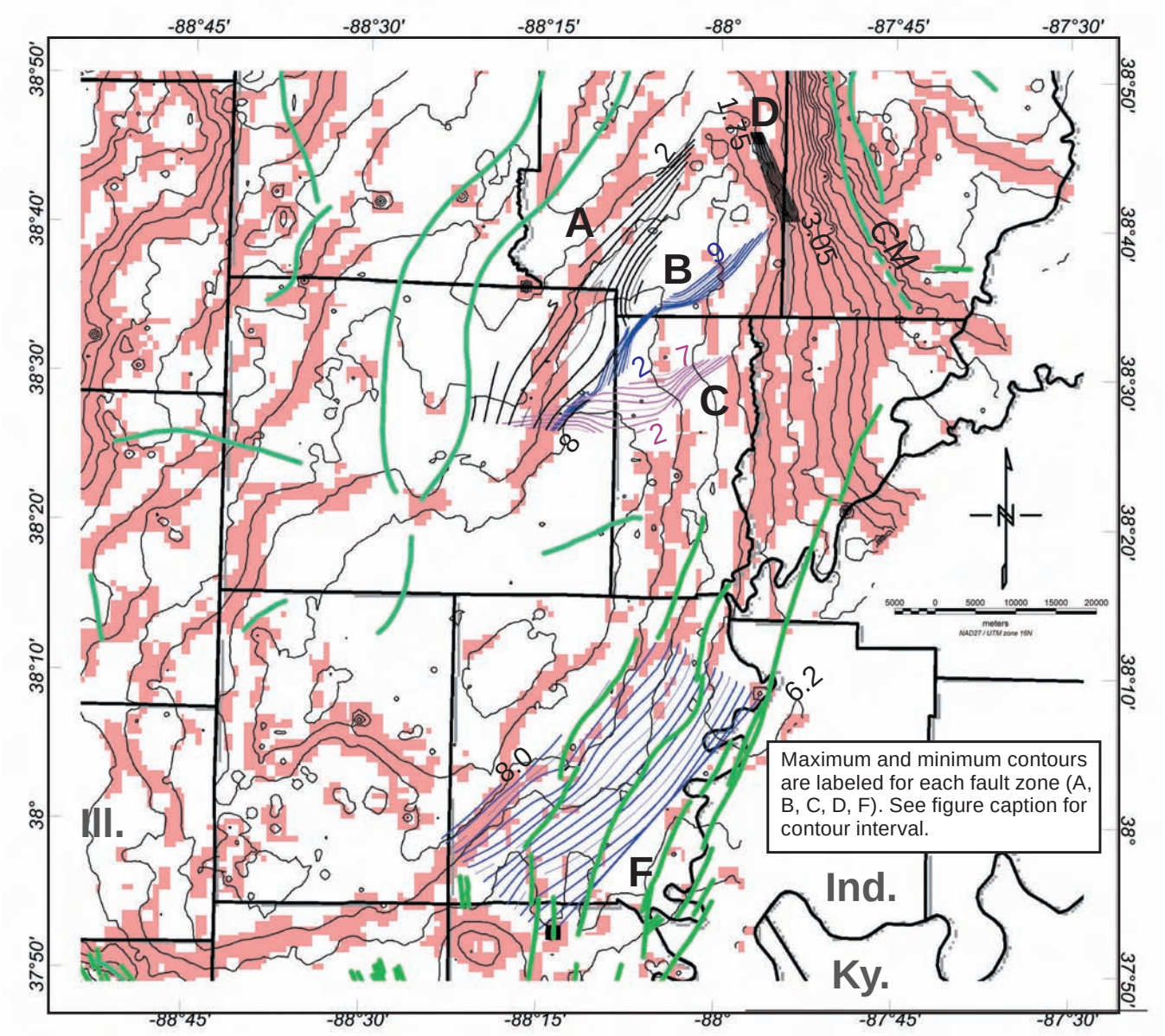

Figure 4-15 *Map of study area with contours of fault zones A (contour interval = 1 s), B (contour interval = 1 s), C (contour interval = 0.5 s), and D (contour interval = 0.5 s) (as labeled, seconds, travel time) as mapped from the seismic reflection profiles (Figure 4-6) projected onto a base map with county and state lines. Also shown are contour lines for a fault zone mapped near the 1968 event (F, contour interval = 0.1 s). Seismically defined fault contours are annotated with maximum and minimum values (s). Barlow Formation surface contours (thin black lines, feet, depth below sea level) are as shown in Figure 4-10b.*

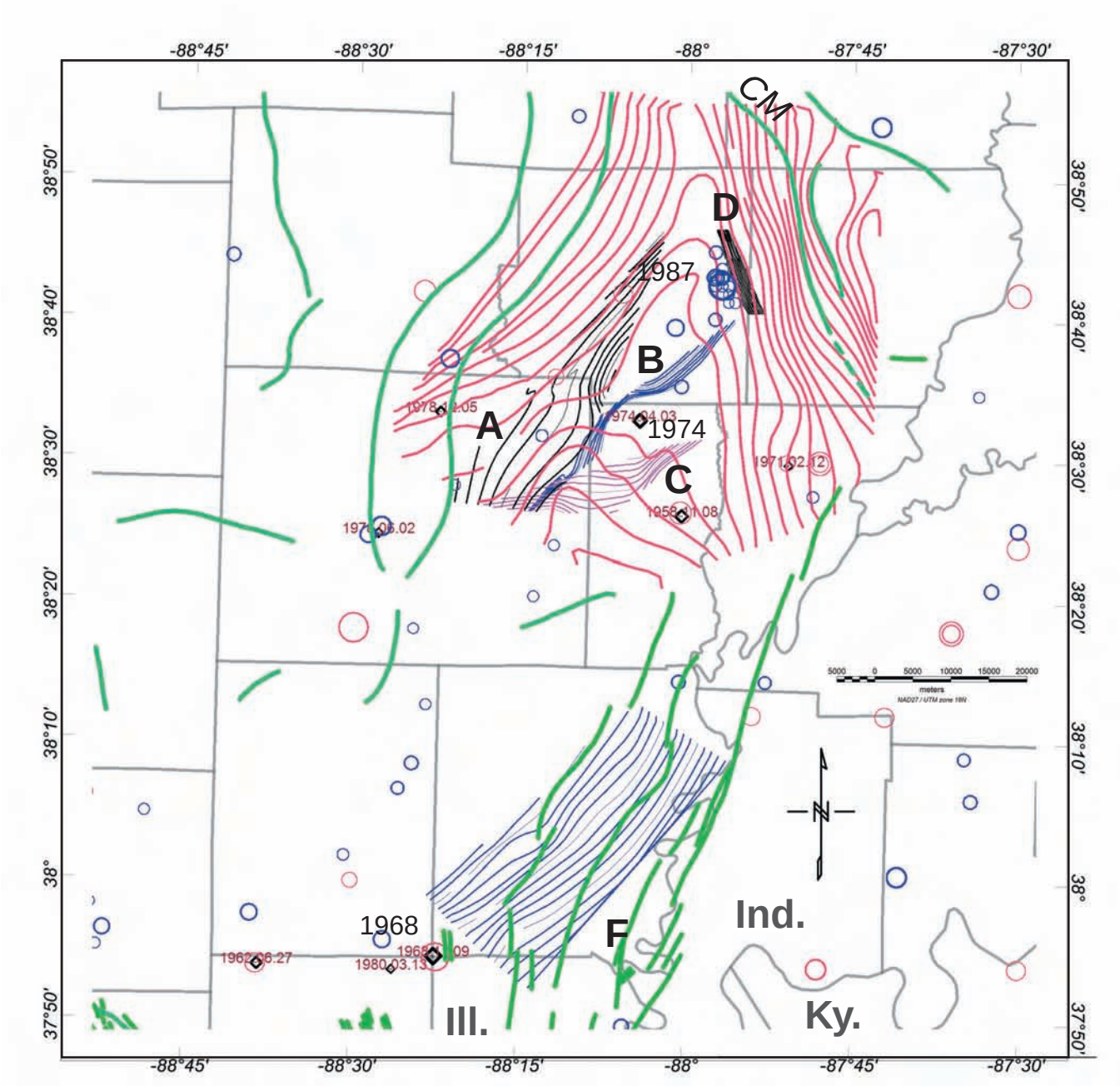

Figure 4-16 *Map of study area with contours of fault zones (see Figure 4-15) and of seismically mapped base of the Knox Group horizon (thick red lines, seconds, travel time). Superimposed on the contours are the epicenters from the three earthquake catalogs discussed in the text (blue is CERI catalog, red is Nuttli catalog, and black is from Gordon's (1988) relocation study. Green lines represent faults and structural axes. CM, Charleston Monocline axis (Nelson, 1995). Contour annotations have been omitted in order to simplify the display.*

On the eastern flank of the sub-basin, a narrow zone of faulting (cm) from seismic profiles that cross folded Paleozoic strata about 9 km (5.6 mi) west of the axis of the Charleston Monocline were mapped (Figures 4-1, 4-15, and 4-16). This fault zone closely follows structural contours based on the two Paleozoic markers and also mimics the trend of the Charleston Monocline axial trace (Figures 4-15 and 4-16). Interpretation of the seismic profiles west of the monocline (e.g., Figure 4-17b) follows a fault-propagation fold model in order to infer a fault as previously shown for this part of the Illinois Basin by McBride (1997). Specifically, the mapping of the fault is based on small breaks in the basement-cover contact and in overlying Paleozoic reflectors and on the abrupt bending of Paleozoic reflectors across the forward hinge point of the monocline (Figure 4-17b). As shown in general from seismic profiles and integrated borehole data for the Illinois Basin (Nelson, 1991; McBride and Nelson, 1999), a steep reverse fault that cuts the basement-cover contact is frequently expressed higher in the Basin sediments as a fault-propagation fold with a Laramide structural style.

In summary, two fault zones were mapped from the seismic profiles (Figures 4-15 and 4-16). The western zone consists of an array of faults that profoundly affects the Precambrian reflectivity sequences (Centralia Sequence) without apparently influencing the overlying Paleozoic strata. The eastern zone is relatively narrow and discrete and is defined by subtle offsets and bends in the top basement and Paleozoic reflectors. Both fault zones follow trends in the structure of Paleozoic strata, as depicted by the structural contour and the slope maps. Because the faults are defined by the available seismic profiles, they are shown cut off on their ends where no data are available.

Earthquake Distributions and Relation to Structure

As has been emphasized previously (McBride et al., 1997), epicenters in the study area show little direct spatial correlation to published locations of shallow subsurface information (e.g., as represented by structural axes) (Nelson, 1995): the 1974 and 1987 events are located between two major structural axes (Clay City Anticline, west of fault zone A, and Charleston Monocline) (Figure 4-16). Epicenter locations from the three catalogs are plotted superimposed over the structural contour and fault map as shown in Figure 4-16 (open circles).

1974 Event

Using the USGS-relocated earthquake database from Gordon (1988), the mb = 4.7, 1974 event plots within the center of the fault array on the western flank of the sub-basin. This event is characteristic of the stress system within the southern Illinois Basin, north of the NMSZ (Langer and Bollinger, 1991) (Figure 4-4). This stress system is dominated by northeast-striking dextral strike slip. The steep northeast-trending nodal plane focused at a depth of 15 km (9.3 mi) (Herrmann, 1979; Taylor et al., 1989) (or 2.5 to 3.0 s travel time, assuming 6 or 5 km/s (3.7 or 3.1 mi/s) seismic velocity, respectively) is

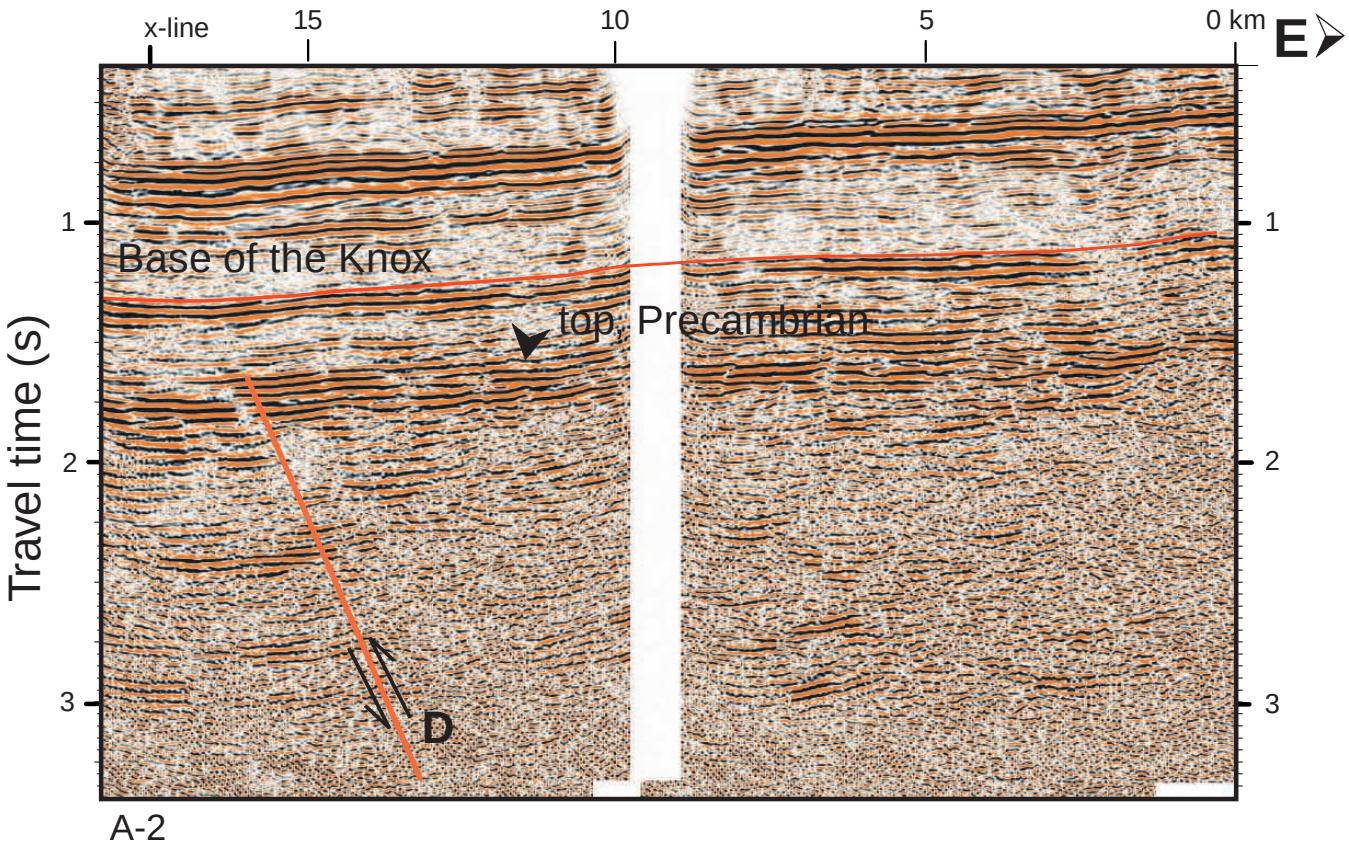

Figure 4-17 *Excerpts of two seismic reflection profiles located just off the western flank of the Charleston Monocline: (a) High-resolution (i.e., color amplitude) raster display of a north-south profile showing the possible continuation of fault A (Figure 4-16). Note the normal sense of the fault cutting through Precambrian rock. (b) An excerpt of an east-west profile showing the area of folded Paleozoic strata located basin-ward (i.e., to the west) of the Charleston Monocline (Figure 4-1) and the interpretation of a basement fault that facilitates the folding above.*

consistent with the observed steep fault zone mapped from the seismic reflection profiles. The location accuracy of this event (Gordon, 1988) does not permit the precise correlation of the hypocenter with an exact spot on the seismic sections. But, within the area of the 95% confidence ellipse (Figure 4-5), the hypocenter could be nucleating also the center fault (B) of the array as shown by projecting the hypocenter on the seismic section (Figure 4-14a) for an east-west distance of about 5 km (3.1 mi). Further, the fact that the hypocenter is definitely somewhere within the array suggests a correspondence with a pattern of faulting. This correspondence indicates strike-slip reactivation of a pre-existing array of normal-slip faults.

Nearby events in the southern Illinois Basin have mechanisms that are either similar to the 1974 event (e.g., the nearby 1987 event, located 21 km (13 mi) to the northeast, Figure 4-5) (Hamburger and Rupp, 1988; Langer and Bollinger, 1991) or consistent with a transpressional stress system in general (e.g., the 1968 event, located 76 km (47 mi) to the southwest) (Taylor et al., 1989; McBride et al., 1997).

1987 Event

The June 10, 1987, m_b = 5.2 event (Figure 4-5) is one of the best characterized earthquakes in the study area, and it included the recording of numerous aftershocks and detailed analyses of both the main shock and the aftershocks (Taylor et al., 1989; Langer and Bollinger, 1991). The depth of the main shock focus was in the range of 7 to 11 km (4.4 to 6.8 mi) (Hamburger and Rupp, 1988) or about 2.3 to 3.7 s equivalent reflection travel time, which corresponds to basement depths for the seismic profiles (for a conversion velocity of 6.0 km/s (3.73 mi/s)). The aftershock foci were in the depth range of 9 to 12 km (5.6 to 7.5 mi) (Langer and Bollinger, 1991). The main shock focal depth reported by Taylor et al. (1989) was 10 ± 1 km (6.2 ± 0.62 mi), and the strike and dip of the northwest-trending nodal plane were reported by Langer and Bollinger (1991) to be 312° and 80°SW, respectively. Focal mechanisms are a combination of strike-slip and reverse fault, although the former is dominant (Langer and Bollinger, 1991). Both Taylor et al. (1989) and Langer and Bollinger (1991) report a steep, northeast dip to the fault plane based on the aftershock foci. Although Taylor et al. (1989) showed no preferred alignment of the aftershock epicenters, and Langer and Bollinger (1991) indicated a north-northeast alignment, the CERI catalog showed 14 events around the main shock with a clear northwest trend, which closely follows the fault zone mapped from the reflection profiles and the structural contours of Paleozoic markers (Figures 4-16 and 4-17a, b). Seven of these events were recorded during the period of aftershocks several days after the main shock (from June 10, 1987, to June 23, 1987) (Figure 4-18), and the remaining six were recorded at various times before and after the main shock (1983 to 1990). A narrow zone of reverse faulting associated with a fault-propagation fold is mapped from the reflection profiles across the western flank of the LSA (locally, Charleston Monocline, Figures 4-16 and 4-17). The alignment of epicenters within ~500 m (~1,640 ft) of the tip of the reverse fault is striking parallel to the fault zone (Figures 4-17b and 4-18) and indicates a zone of steep, northeast-dipping recent faulting located immediately in front of and mimicking the fault zone mapped from the reflection data. Bakun and Hopper's (2004) study of relocated historical earthquakes includes a moment magnitude 4.8 event (September 27, 1909) with an epicenter located about 44 km (27 mi) north of the 1987 epicenter that is over the axis of the LSA (Figure 4-7b). Although no further parameters are available for this event, the location of this and other events (Figure 4-7a) along the trend of the LSA may suggest reactivation of basement faults underpinning the structure in Paleozoic strata. In summary, the fault parameters of a steep, northwest-striking and northeast-dipping plane, based on the 1987 earthquakes, are consistent with the fault pattern interpreted from the reflection profiles.

1968 Event

The November 9, 1968, m_b = 5.5 southern Illinois event was the largest magnitude and one of the deepest twentieth century U.S. earthquakes between the Appalachians and the Rocky Mountains (Langer and Bollinger, 1991). This event had a focal depth of 21.2 ± 5.4 km (13.2 ± 3.4 mi) (Gordon, 1988; see also Langer and Bollinger, 1991; Wheeler and Johnston, 1992) and was originally interpreted to have

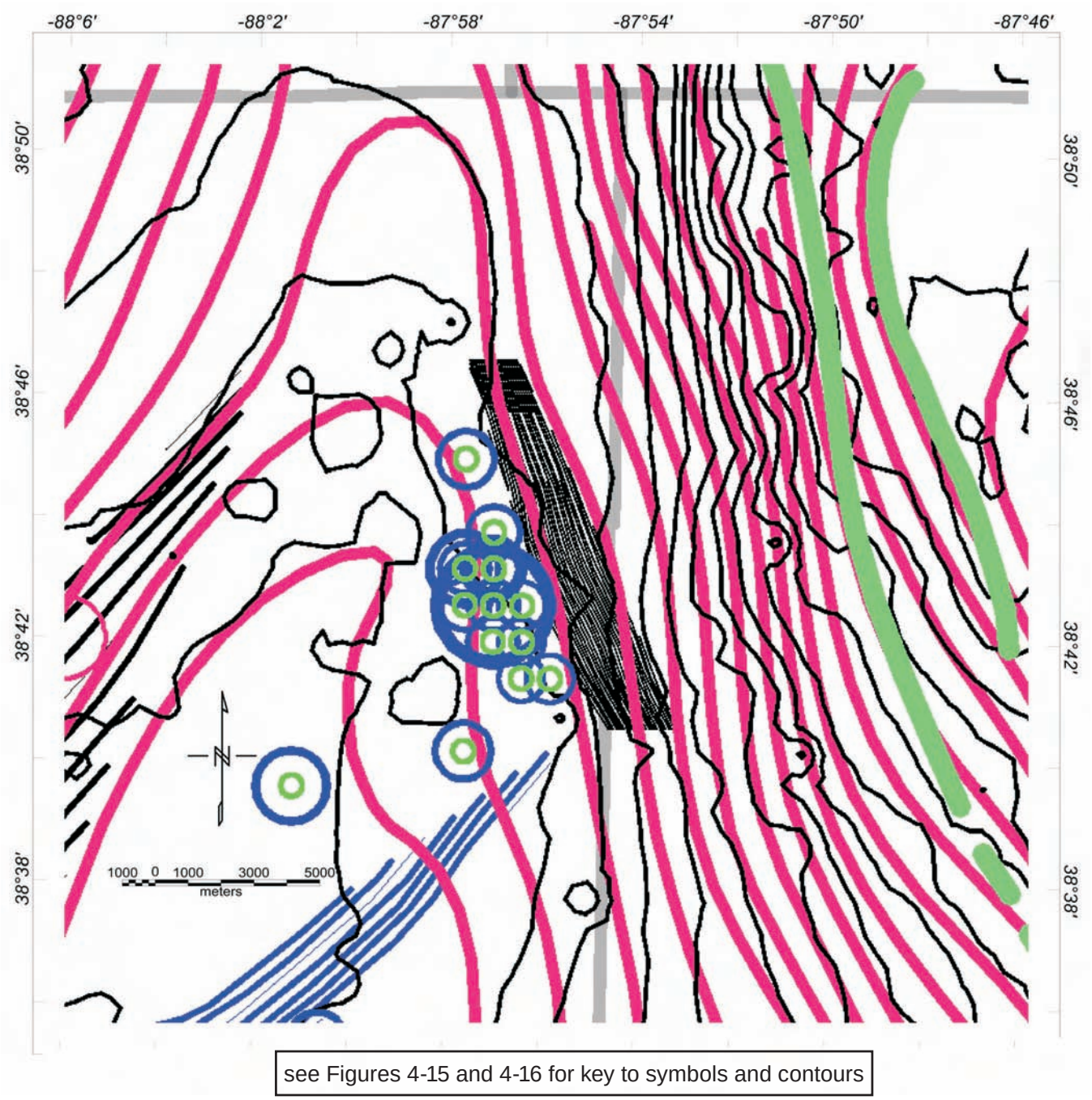

Figure 4-18 *Excerpted enlargement of map in Figure 4-16 showing distinct northwest trend of epicenters associated with the June 6, 1987, event (small bold green circles; see text for details). Symbology is the same as for Figure 4-16.*

nucleated along a west-dipping reverse fault striking at N15°E and dipping at about 45° (Stauder and Nuttli, 1970). After the 1978 seismograph network installation, three better-located events (June 2, 1978; December 5, 1978; March 13, 1980) (Figure 4-5) in the study area occurred with focal depths in the 20- to 25-km (12- to 16-mi) depth range (Gordon, 1988). The most accurately located of these is the 1980 event with a computed focal depth of 20.3 ± 1.8 km (12.6 ± 1.1 mi) and mbLg = 3.0 (Gordon, 1988; Langer and Bollinger, 1991). The epicenter is within a few kilometers of the 1968 event, and the two hypocenter depths are almost indistinguishable. Five aftershocks of the 1968 event, were recorded in the epicentral region of $m_b \leq 4$ at about the same depths as the main shock (Stauder and Pitt, 1970). In a previously published structural analysis of this event, based on a nearby deep seismic reflection profile (the epicenter was 4.9 km (3.0 mi) southwest of the profile, Figure 4-19), it was shown (McBride et al., 1997; McBride et al., 2003) that the hypocenter correlated spatially with a west-dipping (in the plane of the section) reflector sequence that was interpreted as a blind thrust reactivated by the earthquake and its associated aftershocks (Gordon, 1988). Using two previously published reprocessed deep reflection profiles (labeled D-1 and D-2 on Figure 4-5) (McBride et al., 2002), a possible surface can be drawn for the reflector as a northeast-striking plane (labeled F on Figure 4-16) that is parallel to the reflection-mapped fault (middle fault B in Figure 4-15) associated with the 1974 event located to the northeast.

Integration with Reprocessed Geopotential Field Data

These results were integrated with reprocessed potential field data (originally gridded data sets available from the USGS) in order to extend the scope of this interpretation by trends in potential field

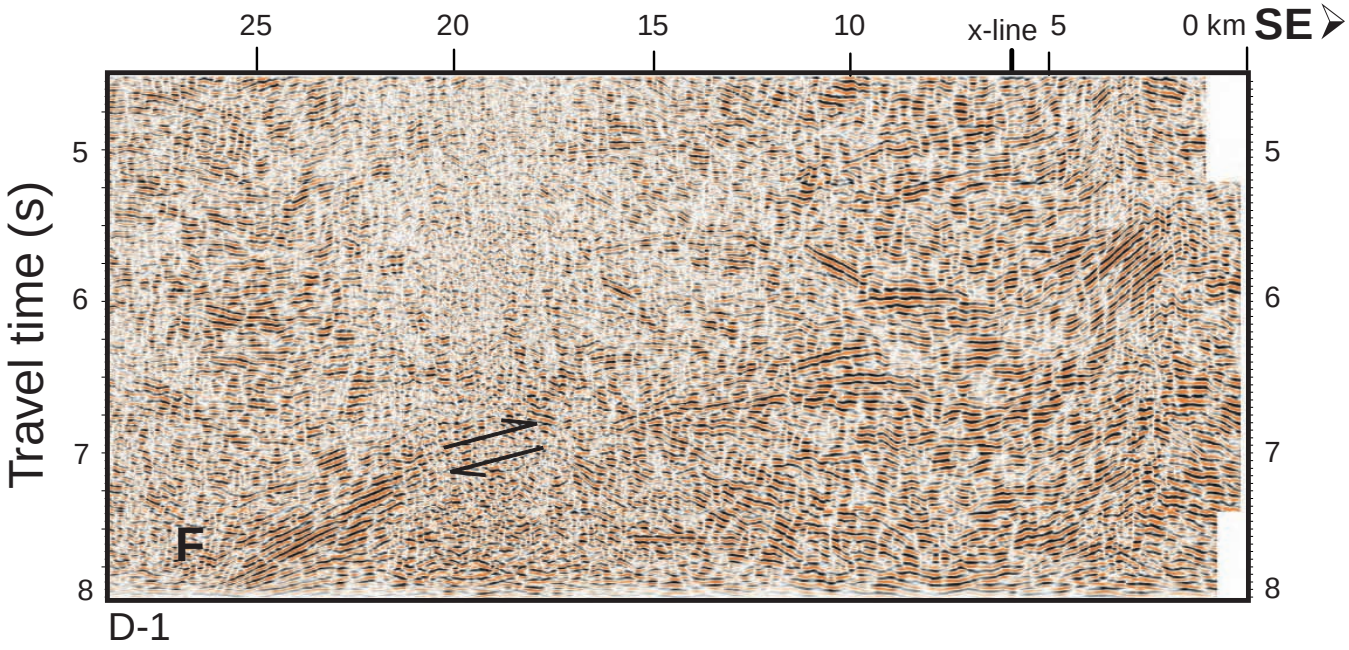

Figure 4-19 *Excerpt of seismic reflection profile near the 1968 event (see Figure 4-6 for approximate location). This figure is based on that by McBride (1998).*

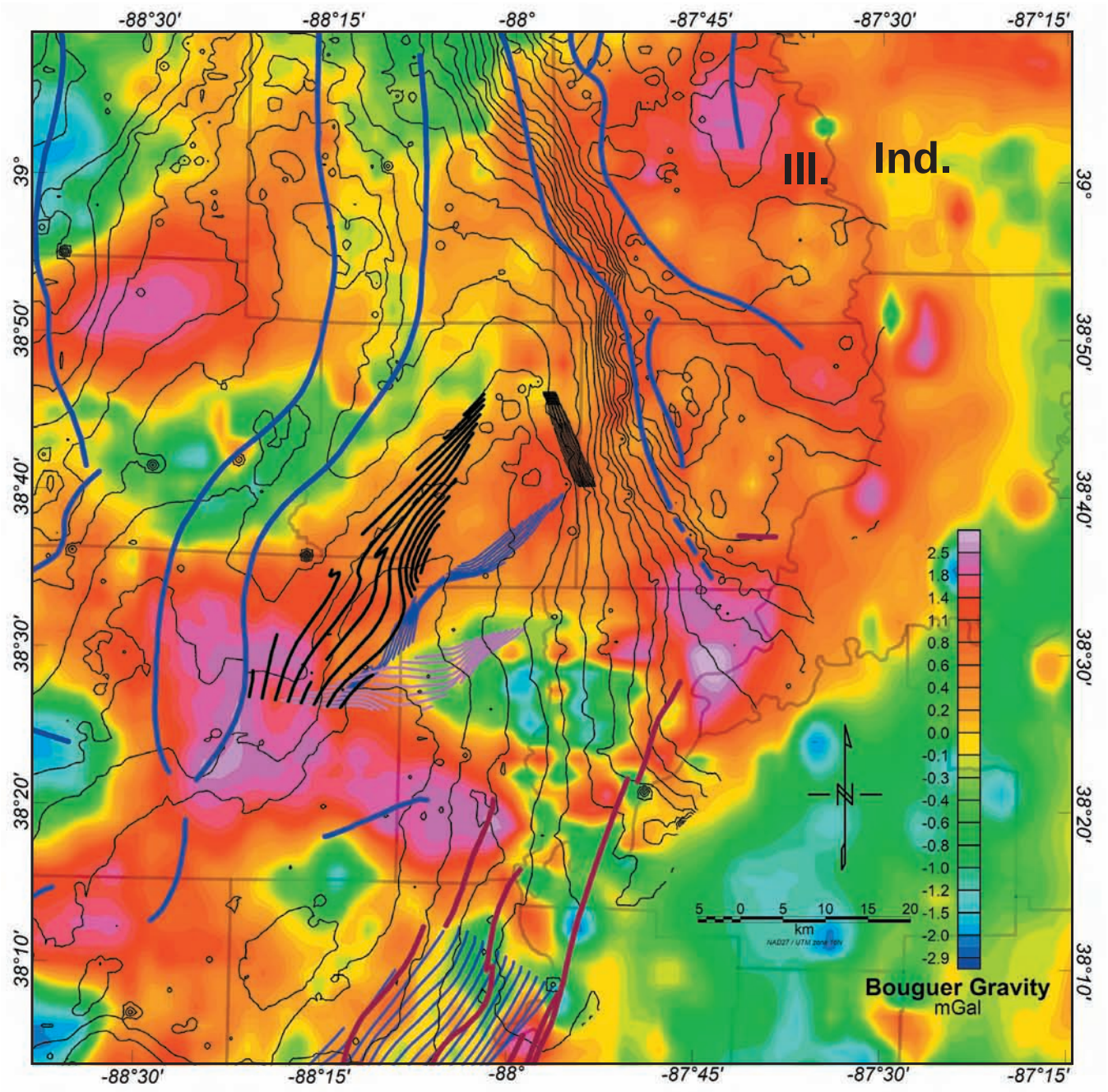

Figure 4-20 *Bouguer gravity residual anomaly map for the study area. The Barlow Formation surface contours map (Figure 4-10a) and fault zone contours (Figure 4-15) are also shown.*

patterns with those mapped from other geophysical data. The reprocessing techniques are discussed fully elsewhere (McBride et al., 2003). The residualized magnetic intensity map (Figure 4-20) shows a prominent low-intensity area corresponding to the head of the sub-basin. An exception, associated with the 1987 event, is fault zone D, which borders the northeastern edge of a localized high. The low intensities may represent a region of thicker sediments or volcaniclastic sediments within the Precambrian section, such as those imaged on the reflection profiles or a marked lateral change in basement magnetic susceptibility. Both the central northeast-trending fault zone near the 1974 epicenter and the northwest-trending fault zone near the 1987 epicenter show a parallelism with trends on the residualized map. Especially marked is a zone of low-to-medium intensity that encompasses the array of faults on the western flank of the sub-basin.

On a Bouguer gravity residual anomaly map (Figure 4-20), a similar pattern appears. To a first order, the gravity pattern represents varying depths to basement (Hildenbrand et al., 2002). Interestingly, the trend of northwest-aligned events around the 1987 main shock are situated over the eastern flank of a gravity high, which corresponds to a more restricted magnetic high (Figure 4-21). The spatial correspondence of gravity and magnetic highs suggests a mafic plutonic igneous source (Lidiak et al., 1985). In summary, the geopotential field data display trends that mimic the structural trends from the reflection profiles and the earthquake information, which suggests that the mapped fault zones correspond in a general way to gross lateral lithologic changes and thus supports their role as major geologic features.

Discussion and Conclusions

The control of earthquakes by pre-existing structure has been well-documented for plate boundary environments such as subduction zones and transform faults. In contrast, for intra-plate settings, very few constraints have been available for independently interpreting earthquake source parameters due mainly to the lack of appropriately located seismic reflection profiles. Making the case for reactivation of "old" geological structures by contemporary stress has thus been hindered for intra-plate environments. In fact, even with the extensively studied and thoroughly instrumented plate boundaries (e.g., San Andreas fault in central California), the exact correlation between contemporary instrumentally located events and specific faults is not always clear (Zoback et al., 1999).

This work is the first reported case for the U.S. midcontinent and one of the first studies for intra-plate settings, in general, of the spatial association of specific earthquakes and patterns of earthquakes with pre-existing basement structures at seismogenic depths. This work has been possible only because of the abundant geophysical and geological databases at the ISGS and the new imperative to analyze these data in support of understanding the overall safety and viability of CO_2 sequestration in deep saline reservoirs. Three separate cases of earthquake and pre-existing basement structure relationships

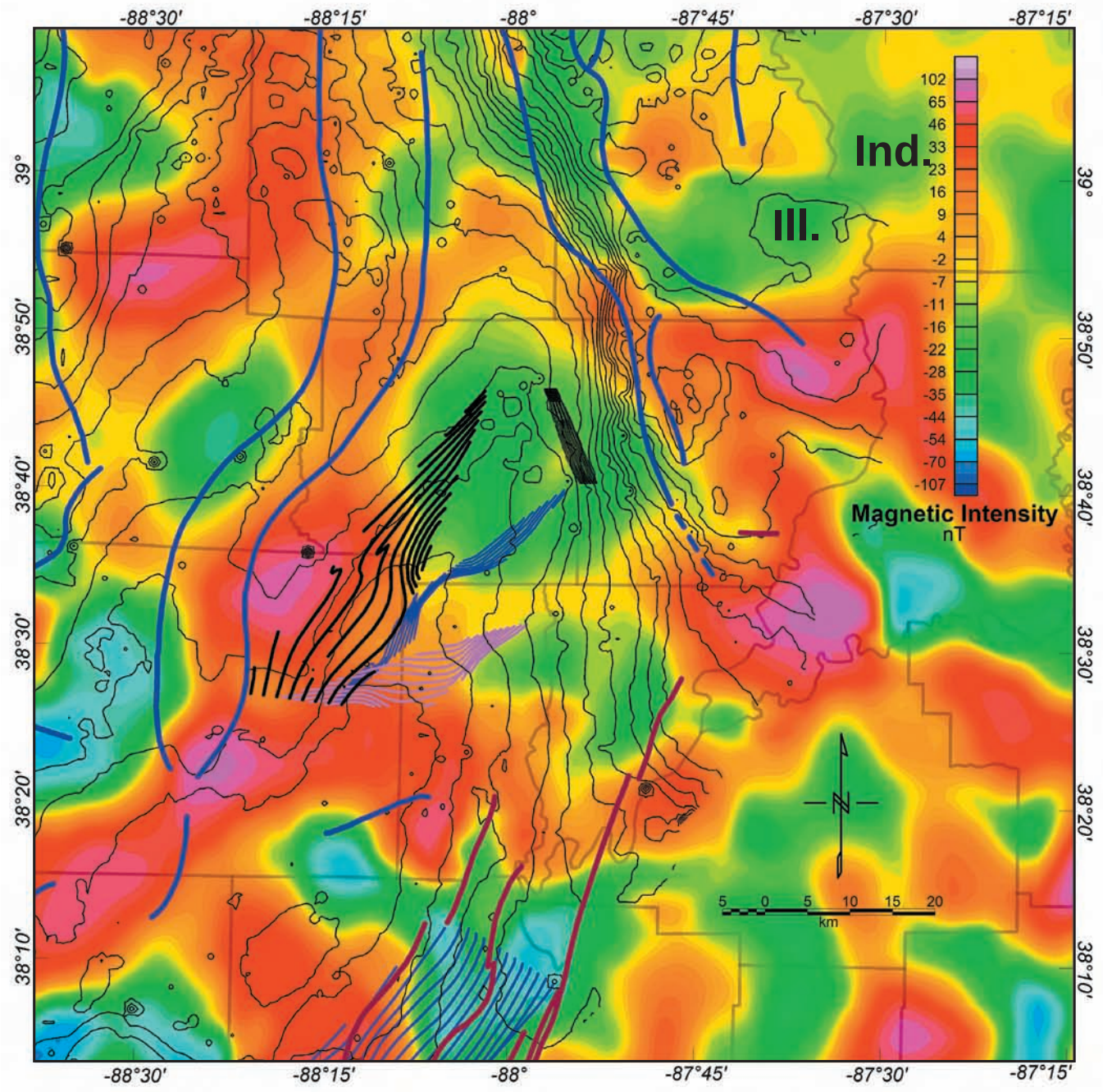

Figure 4-21 *Magnetic intensity map for the study area residualized by computing a 2-km upward continuation that is subtracted from the input data. The Barlow Formation surface contour map (Figure 4-10a) and the fault zone contours (Figure 4-15) are also shown.*

are presented. All three earthquake events, although tectonically and spatially distinct, represent the contemporary maximum horizontal compressive stress that trends just north of east in southern Illinois and Indiana (Zoback and Zoback, 1981; Nelson and Bauer, 1987; Ault, 1988; Hamburger and Rupp, 1988; Ellis, 1994; Bauer and Nelson, 2005) (Figure 4-4).

The association of a near-vertical nodal plane for the 1974 strike-slip event and an array of steep, geophysically defined faults at seismogenic depths suggests structural reactivation of a pre-existing surface by the contemporary stress field. The structural setting for the 1974 event is interpreted to be a graben complex (defined by faults A, B, and C) in Precambrian crust related to an episode of rift faulting localized beneath the depocenter of the Fairfield sub-basin (Figures 4-15 and 4-22). Both the location and trend of the graben complex mimic the structure of overlying Paleozoic structural trends (Figure 4-15). Therefore, the graben complex may have influenced the subsidence of this part of the Illinois Basin and may represent a long-lived zone of weakness in the seismogenic crust—one that has been subject to occasional reactivation by contemporary stress. Well-documented cases of contemporary earthquakes nucleating within and being controlled by crustal rifts within continental crust include the site of the January 26, 2001, earthquake in the Kachchh rift basin (India) and the rift complex that underlies the NMSZ (Braile et al., 1997; Schweig and Ellis, 1994; Mandal et al., 2004; Mishra et al., 2005). For example, the causative fault for the Bhuj event has been interpreted to be a combination of reverse and strike-slip faulting that reactivated pre-existing Mesozoic rift normal faults (Mandal et al., 2004).

The 1987 event nucleated along a steep northeast-dipping plane that faulted the basement immediately in front of the frontal fault of the LSA. This frontal fault is associated with an asymmetric Laramide-style fold in the Paleozoic section and is mimicked by the structural parameters of the earthquake-defined rupture. The northwest trend of local epicenters and the steep rupture plane are consistent with the basement fault defined from the seismic reflection profiles that contains the monocline flexure with the basin sediments. From the map pattern of interpreted faults (A, B, C, and D) in Figure 4-16, there is the possibility of complex fault and earthquake-related interactions. Given the overall northeast-trending dextral strike-slip strain for the area north of the NMSZ, the relative orientation between the northeast-trending graben faults (A, B, and C) and the northwest-trending fault pattern in front of the LSA (D) could be expected to produce a local restraining bend or jog where the two patterns meet (Figure 4-22). Although the paucity of information on earthquake distributions in the area precludes a detailed analysis, if strain interaction were occurring between the two fault patterns, then it would be reasonable to expect the restriction of rupturing during a major earthquake to limited portions of the larger faults (e.g., Muller and Aydin, 2004). According to a model proposed by Talwani (1988; 1999), intersecting faults can create a locked volume of rock where distant stress induces localized deformation. In this way, stress applied to one fault segment can temporarily lock another segment, which generates higher stresses that are necessary for rupture. Stresses can analogously be concentrated by faults interacting with

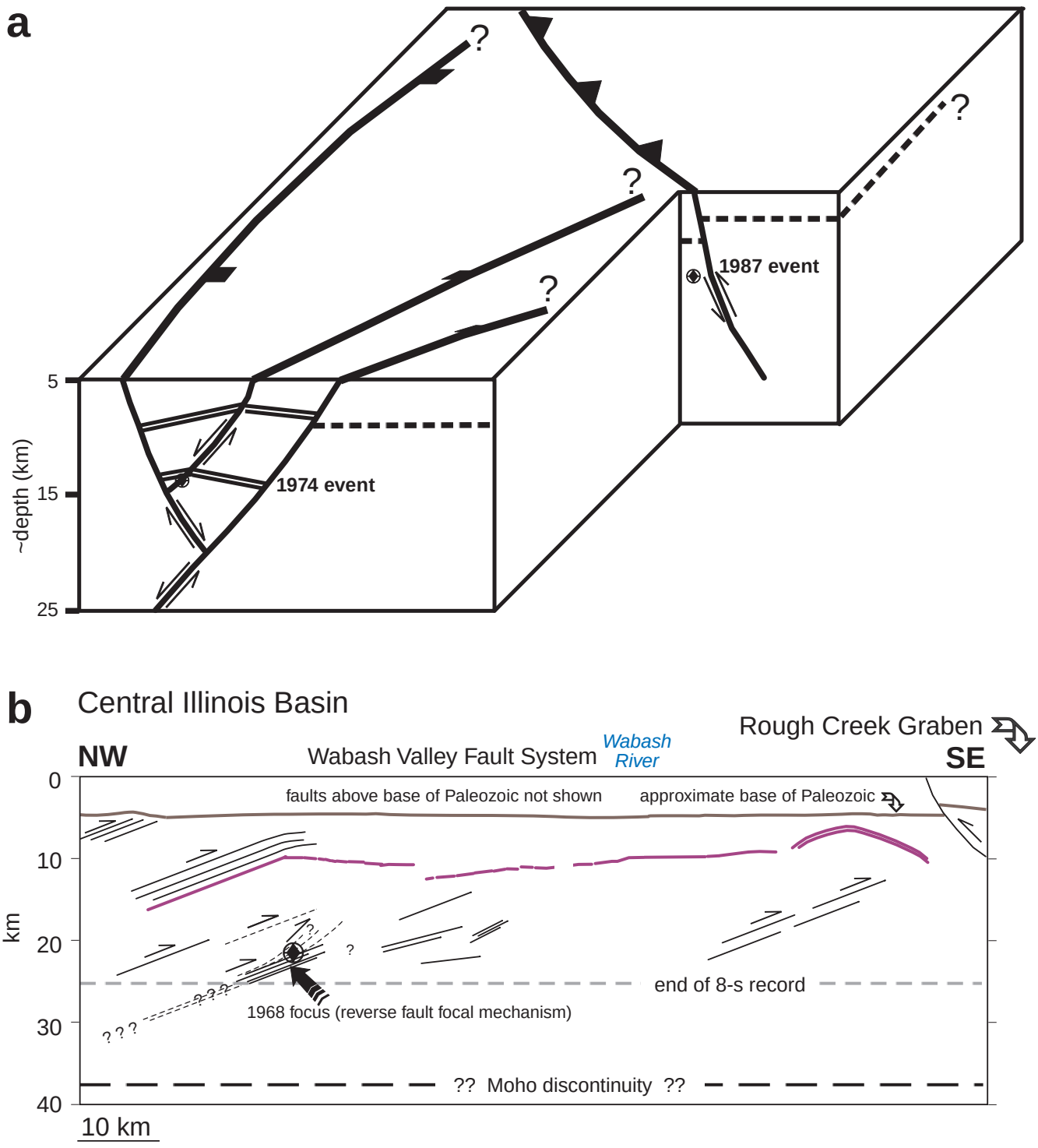

Figure 4-22 *(a) Diagram of basement structure for the interpreted zone of rifting beneath the Fairfield sub-basin and zone of faulting just west of the frontal thrust of the LSA (locally, Charleston Monocline). (b) Interpretive cross-section through the region of the 1968 earthquake (modified from McBride et al., 2002). Dashed lines are speculative. Interpretation of Rough Creek Graben, whose main Cambrian normal fault was reactivated during later compression, is from Kolata and Nelson (1997). Moho discontinuity is estimated from Allenby and Schnetzler (1983).*

pluton boundaries, such as shown by Hildenbrand et al. (2001) for igneous intrusions near the NMSZ as inferred from gravity and magnetic data. Such an explanation may be appropriate for explaining the orientation of faults B and D, which approximately outline the southeastern and northwestern confines of a gravity magnetic high (Figures 4-20 and 4-21).

One of the nodal planes of the 1968 event corresponds to a prominent zone of dipping middle crustal reflections, immediately west of the WVFS. The focal mechanism (moderately dipping reverse fault) of this earthquake is consistent with observed west-dipping reflectors. The earthquake parameters and the reflection profiles together suggest a "blind" thrust. The dipping reflector patterns associated with the 1968 event in the deep Precambrian crust are not collinear with fault surfaces updip in the Paleozoic sedimentary section. This finding indicates that shallow Paleozoic structures are effectively "decoupled" from deeper, possibly seismogenic structure, which suggests that understanding Paleozoic structure is not the key to understanding the earthquake source (McBride et al., 2002). From a re-analysis of aftershocks and stress changes associated with the 1811–1812 New Madrid earthquakes, the 1968 event can be interpreted to be a long-lived aftershock of this earthquake sequence located 200 km to the northeast of the area of the main shocks (Mueller et al., 2004). This event may represent the northernmost extent of a major deformation system, which could explain the relatively great depth of the hypocenter and its reactivation of a major pre-existing blind-thrust structure (Figure 4-22).

These three events and their relationship to pre-existing structure make the case for structural reactivation by earthquakes in an intra-plate setting. The amount of slip associated with the main shock of the 1987 event was modeled as having a fault length equal to a width of 2.3 km (1.4 mi) (Taylor et al., 1989). For the 1968 event, this value is ~2.9 km (~1.8 mi) (McBride et al., 2002). For both events, the modeled amount of average displacement is <50 cm (19.7 inches). Thus, the fault zones investigated in this study are major dynamic features, but the individual amounts of displacement (i.e., for just one event) are relatively minor. Only in one case (1987) could a relationship between deformation in the basement be associated with deformation within the overlying Paleozoic section.

Implications for CO_2 Sequestration in the Illinois Basin

The correlation between mapped faults and known historical and instrumental seismicity presents a risk for CO_2 sequestration in the Illinois Basin. Two possible relationships can be envisaged for earthquakes and underground reservoirs: (1) induced seismicity from injection of gas into underground storage reservoirs and (2) the effects of earthquakes on the reservoirs (Bauer, 2005).

CO_2 injection may produce seismicity through two possible scenarios: changing stress conditions across pre-existing fractures/faults or through expansion and contraction of the reservoir during cycling of

gas storage. The first condition locally reduces the normal stresses on fractures or faults by increasing gas pressures within the fault zone, allowing slippage of the two sides past each other at lower stresses. The second condition of expansion and contraction of the reservoir raises and lowers the caprock and overburden, which causes sliding or shearing to occur between the layers of rock above the reservoir, producing microseismic activity (Bauer, 2005).

Only a few documented examples exist of tectonic movements induced by fluid injection through boreholes (Kisslinger, 1976; Bauer, 2005): Rocky Mountain Arsenal well, Denver, Colorado (Healy et al., 1968), and the controlled experiment at the Rangely oil field (Raleigh et al., 1976) in Rangely, Colorado. A magnitude 5.5 earthquake was attributed to high pressure (38,900 or 12,000 kPa (389 or 120 bars) above the original reservoir pressure) fluid injection into a 3.8-km (2.4-mi)-deep well in 1967 in the Rocky Mountain Arsenal, Colorado (Healy et al., 1968). More recent studies of fluid-induced seismicity are presented by Evans et al. (2005) and Baisch and Harjes (2003) for sites in western Europe. For the U.S. continental interior, hydrocarbon recovery and waste-water injection into underground reservoirs have been suggested as causes of unexpected low-to-moderate magnitude earthquakes (e.g., Gomberg and Wolf, 1999); however, such studies are based partly on circumstantial evidence without a clear mechanism being defined. McClain (1970) suggested several conditions that must be satisfied if injection of fluids is to result in inducing earthquakes, relating to regional tectonic stress, porosity and permeability, and the rates and pressures of fluid injection.

A less understood issue concerns the effects, if any, of earthquakes on the reservoirs used for sequestration. Some evidence comes from studies of seismic stimulation of oil reservoirs for enhanced production. Experiments by Los Alamos National Laboratory (Roberts, 1997) find that low-frequency seismic stress waves have been observed to enhance oil production from depleted reservoirs by decreases in the fluid pressure drop. One field test at Lost Hills, California, had seismic stimulation increase oil production by approximately 20%, which was similar to the increase observed in this field after the magnitude 7.1 Hector Mine earthquake.

This study, based on exploration geological and geophysical data, provides a means for establishing geologic structures that can be used to constrain the risk from storage or sequestration of CO_2 in underground reservoirs. This risk is correlated to the degree to which faults with observable displacement propagate from Precambrian basement up into Paleozoic strata and the proximity of the faults to areas of known seismicity. This risk is clarified and enhanced by the possibility of seismicity induced by injection of CO_2 into underground reservoirs and by the effects of earthquakes on the reservoirs themselves. For this study, the fold structures along the LSA and the WVFS may present a risk of the release of CO_2 that is stored or sequestered within the deep Mt. Simon Sandstone (Cambrian), which rests immediately above the Precambrian basement (Figures 4-1, 4-3, and 4-4). In cases where

Paleozoic structures are decoupled from deeper seismogenic structures, however, the risk of sequestered gas escape is minimal.

Acknowledgments

This research was supported, in part, by a sub-contract between Brigham Young University and the Illinois State Geological Survey (University of Illinois at Urbana-Champaign): "Assessment of Geological Carbon Sequestration Options in the Illinois Basin" funded by the U.S. Department of Energy. The views and conclusions contained in this document are those of the authors and should not be interpreted as necessarily representing the official policies, either expressed or implied, of the U.S. Government. This work was also supported in part by a grant from the National Science Foundation under Award Number EAR-0307539. We also acknowledge the support of this research by Landmark Graphics via the Landmark University Grant Program at Brigham Young University and the University of Illinois at Urbana-Champaign. Data processing for this study was performed using Landmark's ProMAX 2D™. The authors also express appreciation to Seismic Micro-Technology (KINGDOM Suite™), who kindly provided a University Grant of their visualization and mapping software. The authors gratefully acknowledge reviews by R.J. Finley, which greatly improved the final version of the paper. This project was made possible in part by the kind release of seismic reflection data to the Illinois State Geological Survey by Amoco Production Company and Seismic Exchange, Inc.

Geochemistry of the Mt. Simon Sandstone with Carbon Dioxide Sequestration

Introduction

This preliminary report summarizes the results of geochemical modeling to predict carbon sequestration in the Mt. Simon Sandstone based on data from Manlove Gas Storage Field, Illinois. Results of this preliminary work serve to establish a methodology, provide initial estimates of sequestration effectiveness, and show where additional information is needed to refine the calculations.

Geochemical modeling was used to estimate the effects of injecting supercritical carbon dioxide (CO_2) into a saline formation to reduce the amount of CO_2 released to the atmosphere. Carbon sequestration in saline formations is attractive because geologic formations filled with saline formation water are volumetrically large, and the probability that a suitable formation will be located near a source of CO_2 is reasonably high. Candidate formations generally must be deeper than about 792 m (2,600 ft), and the water salinity of the formation must be more than approximately 10,000 mg/L (Gunter et al., 2000). These criteria ensure that the formation will not be used as a source of drinking water and that CO_2 will exist as a supercritical fluid after injection.

Injection of CO_2 into a saline formation triggers a series of processes and reactions. Physical processes are dominated by multiphase flow in heterogeneous media. The major processes include displacement of the formation water that initially filled pore spaces, formation of a CO_2 plume that does not dissolve in water and is less dense than water, vertical migration of the plume in response to buoyancy, lateral migration of the plume in response to the regional hydrologic gradient, and dispersion and diffusion in response to the porosity and permeability structure of the host formation. Chemical processes involve multiple, kinetically controlled geochemical reactions in heterogeneous media. The major reactions are those between supercritical CO_2 and formation water and then between intraplume formation water and the host formation framework.

Two general processes contribute to geochemical sequestration in saline formations. Solubility trapping refers to the dissolution of CO_2 in formation water. This aqueous carbon then becomes part of the formation water system and moves in response to local and regional hydrologic gradients. The amount of CO_2 that can dissolve in formation water depends primarily on pressure, temperature, and salinity conditions. More permanent sequestration occurs when carbon is removed from solution and precipitated as minerals (mineral trapping), which generally occurs as silicate minerals that contain calcium, magnesium, or iron dissolve, and carbonate minerals precipitate (e.g., Gunter et al., 2000).

Conceptual Model

The geochemical modeling simulations are based on a conceptual model of the rock system at Manlove Field, Illinois, which consists of the Mt. Simon Sandstone, intra-sandstone shale interbeds, and the overlying Eau Claire Formation. The fluid system consists of Mt. Simon formation water, the injected plume of supercritical CO_2, and irreducible water within the CO_2 plume.

The scenario modeled in this report is injection of supercritical CO_2 into a porous, permeable zone near the base of the Mt. Simon Sandstone. Because supercritical CO_2 is immiscible with and less dense than water, the plume will displace all but an unknown amount of irreducible water surrounding the sandstone matrix and will rise upward from the injection zone. The plume will also expand and migrate away from the injection zone because of diffusion, dispersion, and the regional hydrologic gradient, the pressure gradient due to injection. When injection ceases, the plume will continue to rise until it encounters the Mt. Simon and Eau Claire interface. The ultimate size and shape of the plume and the lithologies contacted by the plume and intraplume irreducible water will be determined by the porosity and permeability structure of the Mt. Simon Sandstone in the vicinity of the injection well and by the regional hydrologic gradient. Figure 8-1 presents a conceptual model of the CO_2 plume/water/rock system during injection relatively low in the well.

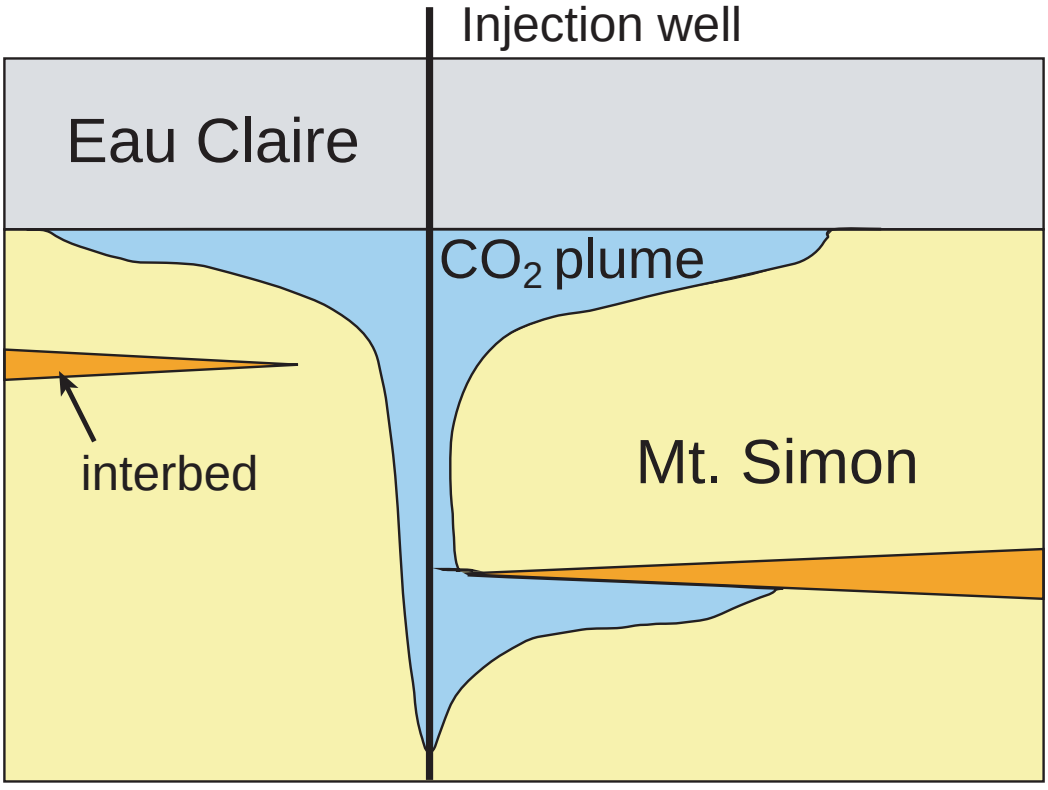

Figure 8-1 *Conceptual model of the Mt. Simon and Eau Claire interval selected for CO_2 injection.*

Four potential reaction environments exist: (1) The injected supercritical CO_2 will first react with the irreducible water that remains within the plume. (2) That irreducible water will in turn react with minerals in the Mt. Simon Sandstone. (3) The resulting water may react with shale interbeds within the Mt. Simon Sandstone, and (4) it will ultimately react with the overlying Eau Claire Formation.

These reactions were geochemically modeled:

1. Initial composition of Mt. Simon formation water. The available analyses lack data for two critical aqueous species. These concentrations are estimated by assuming chemical equilibrium with minerals in the Mt. Simon Sandstone. This formation water is designated Fluid 1.
2. Plume water. The plume of supercritical CO_2 will displace Mt. Simon formation water, leaving irreducible water within the plume. The Mt. Simon formation water will equilibrate with the CO_2 plume and will have a chemical composition significantly different from that of the formation water prior to CO_2 injection. The resulting water is termed Fluid 2 in the modeling simulations.
3. Water (sandstone). Fluid 2 will contact and react with the Mt. Simon Sandstone, producing Fluid 3.
4. Water (shale). Fluid 3 may contact and react with shale interbeds within the Mt. Simon Sandstone, resulting in Fluid 4.
5. Water (seal). Fluid 3 will ultimately reach and react with the Eau Claire sealing formation, resulting in Fluid 5.

Approach and Data Sources

Geochemical Modeling Software

The geochemical modeling software package, The Geochemist's Workbench® (GWB), Release 5.0 (Bethke, 2004), was used to simulate geochemical reactions. The thermodynamic data contained in the file *thermo.dat* was used in all calculations because it is the most complete data set available and because it supports activity coefficients calculated by an extended form of the Debye-Hückel equation (B-dot equation). Activity coefficients computed by this method are the most appropriate, generally available coefficients for the salinity, temperature, and chemical composition of Mt. Simon formation water.

In this initial study, no revisions or modifications were made to the thermodynamic data, mineral compositions, or equations used in GWB. All simulations were performed as equilibrium calculations rather than incorporating kinetic reaction rates because information regarding the dynamic development

and movement of the CO_2 plume is not yet available. As additional information is developed, both kinetic reaction rates and physical transport simulations can be added to the model used in this report.

Mt. Simon Sandstone Mineralogy

Petrographic (point-count) and X-ray diffraction results provided by the Illinois State Geological Survey (ISGS) were summarized to yield a representative composition of the Mt. Simon Sandstone. Petrographic examination showed the sandstone to be nearly pure quartz with minor amounts of potassium feldspar. X-ray diffraction analysis showed the feldspar to be predominantly microcline; however, other potassium feldspar minerals, probably overgrowths on detrital grains, are also present. Small amounts of detrital and authigenic clay were reported in a few samples but are not volumetrically significant. For modeling purposes, quartz and microcline are the dominant constituents. The median reported porosity value was 6%; however, a value of 10% was assumed to be more likely for the injection zone. Table 8-1 shows the sandstone composition used for modeling.

Table 8-1. Mt. Simon Sandstone composition used in geochemical modeling.

Item	(bulk vol %)
Quartz (grains and cement)	85
K-feldspar (microcline)	5
Porosity	10

Mt. Simon Formation Water Composition

ISGS staff provided a large number of chemical analyses of Mt. Simon formation water from various locations. For modeling simulations, median concentration values from 335 analyses of water from the Mt. Simon Sandstone at Manlove Field were used. Two critical constituents, dissolved potassium and aluminum, were not reported and had to be estimated. Dissolved aluminum is typically low in formation water and is difficult to measure accurately. When measured, values are generally in the 1-µg/L range. For geochemical modeling, dissolved aluminum is commonly assumed to be 10^{-6} molal, controlled by the solubility of aluminosilicate constituents (e.g., Garrels and Christ, 1965). The dissolved aluminum concentration was set to 10^{-6} molal, and GWB calculated the potassium concentration that would result from equilibrium between formation water and microcline. Pressure was estimated by using a hydrostatic gradient of 9.795 kPa/m (0.433 psi/ft) and a representative depth of 1,219 m (4,000 ft). The resulting formation water composition is shown in Table 8-2.

Table 8-2. Composition of Mt. Simon formation water.

Temperature (°C)	**22**
Pressure (atm)	**120**
pH	**6.3**
Concentrations (mg/kg H_20)	
Al	0.027
Ca	6,450
Cl	49,200
CO_3	0
Fe	48
HCO_3	414.8
K	0.319
Mg	1,340
Mn	5
Na	23,000
SiO_2	11.2
SO_4	1,600
Total dissolved solids	**84,200**

Shale Interbeds in Mt. Simon Sandstone

Two samples of shale interbeds from the Mt. Simon Sandstone were analyzed for mineral and chemical composition, and the results were provided by the ISGS. The samples were taken from the Peoples Gas Light and Coke, # 5 Hazen Well in Champaign County, Illinois. X-ray diffraction analysis results of whole-rock and clay-size fractions are listed in Table 8-3.

Eau Claire Formation

Four samples of the Eau Claire Formation were analyzed for mineralogy and chemical composition, and the results were provided by the ISGS. The samples were taken from the Jones and Laughlin, #1 Waste Disposal Well in Putnam County, Illinois. X-ray diffraction analysis results of whole-rock and clay-size fractions are listed in Table 8-4. One sample, from the 863.5-m (2,833-ft) depth, described as a silty shale, is the best representation of a seal rock. The others, described as sandy siltstone or silty claystones, are assumed to be coarser grained and more permeable than the silty shale and, therefore, not good analogs for a caprock.

Table 8-3. Mineralogy of Mt. Simon interbeds determined from X-ray diffraction analyses.

Depth (ft)	4,128	4,186.5
Description	**Dark gray shale**	**Dark gray shale**
Whole-rock sample (vol%)		
Quartz	17.89	23.99
K-feldspar	20.21	19.23
Plagioclase	1.18	2.51
Calcite	0.74	2.41
Dolomite	1.19	3.37
Hornblende	0.38	0.48
Pyrite	0.14	0.45
Marcasite	0.47	0.08
Expandable clays	1.43	0.96
Illite	41.30	35.92
Kaolinite	7.39	4.95
Chlorite	4.09	1.98
Clay-size fraction (vol%)		
Expandable clays	1.10	1.61
Illite	82.23	82.85
Kaolinite	10.05	10.36
Chlorite	6.61	5.18

Table 8-4. Mineralogy of Eau Claire Formation determined from X-ray diffraction analyses.

Depth (ft)	2,833	2,844	2,847	2,851
Description	**Silty shale**	**Sandy siltstone**	**Silty claystone**	**Silty claystone**
Whole-rock sample (vol%)				
Quartz	20.23	25.81	33.00	10.30
K-feldspar	26.44	31.68	37.31	20.72
Plagioclase	0.99	0.82	3.28	1.37
Calcite	1.49	0.72	1.97	1.09
Dolomite	3.86	26.33	6.89	3.58
Hornblende	0.22	0.30	0.27	0.44
Pyrite	0.00	0.73	1.71	0.39
Marcasite	1.09	3.16	1.71	0.59
Expandable clays	2.79	0.30	0.43	3.18
Illite	33.43	3.92	5.49	51.36
Kaolinite	1.46	0.25	0.36	1.44
Chlorite	3.40	0.46	0.68	1.84
Clay-size fraction				
Expandable clays	2.61	1.11	2.34	2.61
Illite	89.43	57.00	88.93	90.69
Kaolinite	1.45	3.01	2.30	1.91
Chlorite	6.52	38.88	6.43	4.79

Modeling Results

Reaction between Mt. Simon Formation Water and Injected CO_2

Injected supercritical CO_2 will initially displace pore water in the part of the Mt. Simon Sandstone that is occupied by the plume. However, some irreducible water will remain around the sandstone grains. This water will equilibrate with CO_2 under the pressure and temperature conditions of the Mt. Simon Sandstone at Manlove Field. CO_2 will dissolve and react with the water, resulting in a drop in pH and an increase in total carbon dissolved in the formation water.

The general reactions are

$$CO_2(\text{supercritical}) \leftrightarrow CO_2(\text{aqueous}) \qquad [1]$$

$$CO_2(\text{aqueous}) + H_2O \leftrightarrow CO_3^{-2} + 2H^+ \qquad [2]$$

The GWB module REACT was used to calculate the equilibration composition of Mt. Simon formation water (Table 8-2) with CO_2 at a fixed fugacity of 12,159 kPa (120 atm). Changes in formation water composition are listed in Table 8-5.

Table 8-5. Changes in formation water composition as a result of equilibrating with CO_2.

	Initial (Fluid 1)	Final (Fluid 2)
pH	6.30	3.44
Dissolved carbon (mg/kg H_2O)	81.85	4.42×10^4

Reaction Between Intraplume Waterand Mt. Simon Sandstone

After reacting with the injected CO_2, the resulting water (Fluid 2) will react with the Mt. Simon Sandstone. Because the Mt. Simon Sandstone is nearly pure quartz, with minor potassium feldspar and only traces of other constituents (Table 8-1), and because laboratory experiments elsewhere have shown that quartz is relatively resistant to attack by low-pH water (Krumhansl et al., 2003), this step was modeled as a reaction between Fluid 2 and microcline. The GWB module REACT was used to calculate changes in water composition as Fluid 2 progressively reacts with microcline until equilibrium is attained. Equilibrium between microcline and Fluid 2 is reached after 215 cm^3 (550 g) of microcline has dissolved per 1,000 g of water. The pH increases to 4.95, and total carbon decreases slightly as a small amount of dawsonite ($NaAlCO_3(OH)_2$) precipitates. Pore space is reduced by a net 10.9 cm^3/1,000 g of water, or from 10% to approximately 9.9%. Changes in pH, amounts of minerals precipitated, and dissolved carbon as the reaction progresses are shown in Figures 8-2, 8-3, and 8-4, respectively.

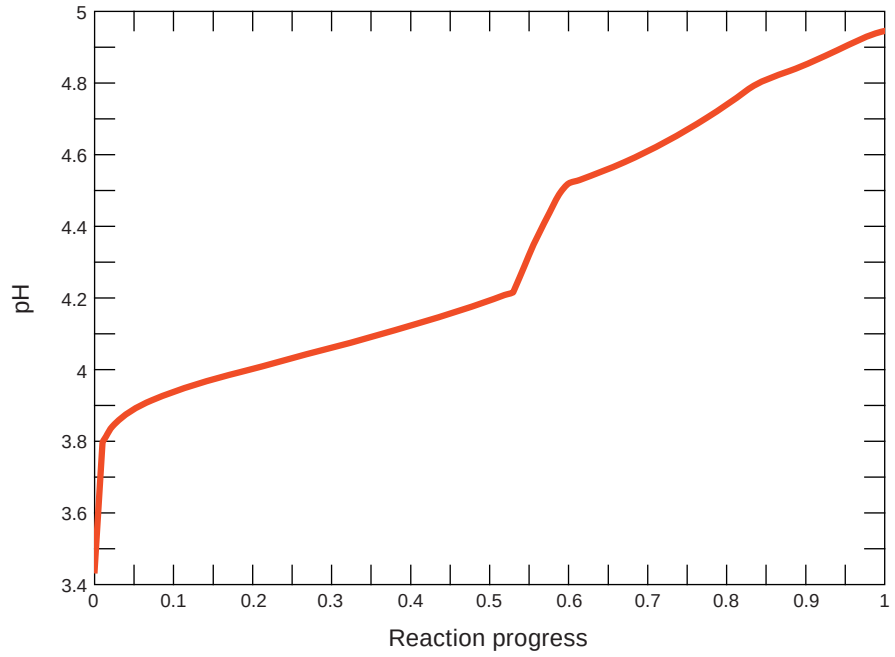

Figure 8-2 *Change in pH as reaction between Fluid 2 and microcline progresses.*

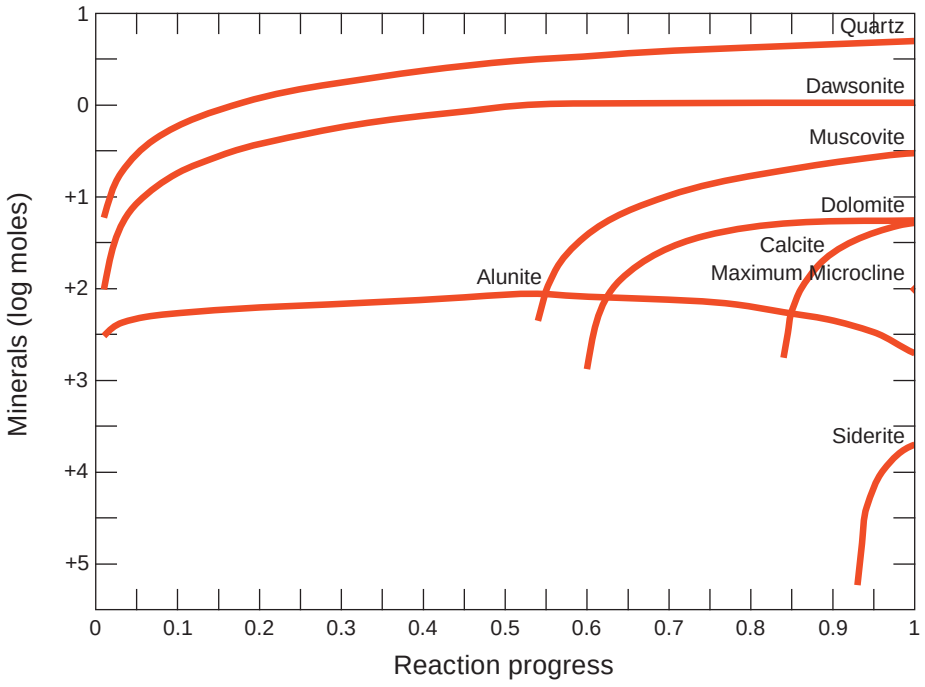

Figure 8-3 *Amounts of minerals precipitated as reaction between Fluid 2 and microcline progresses.*

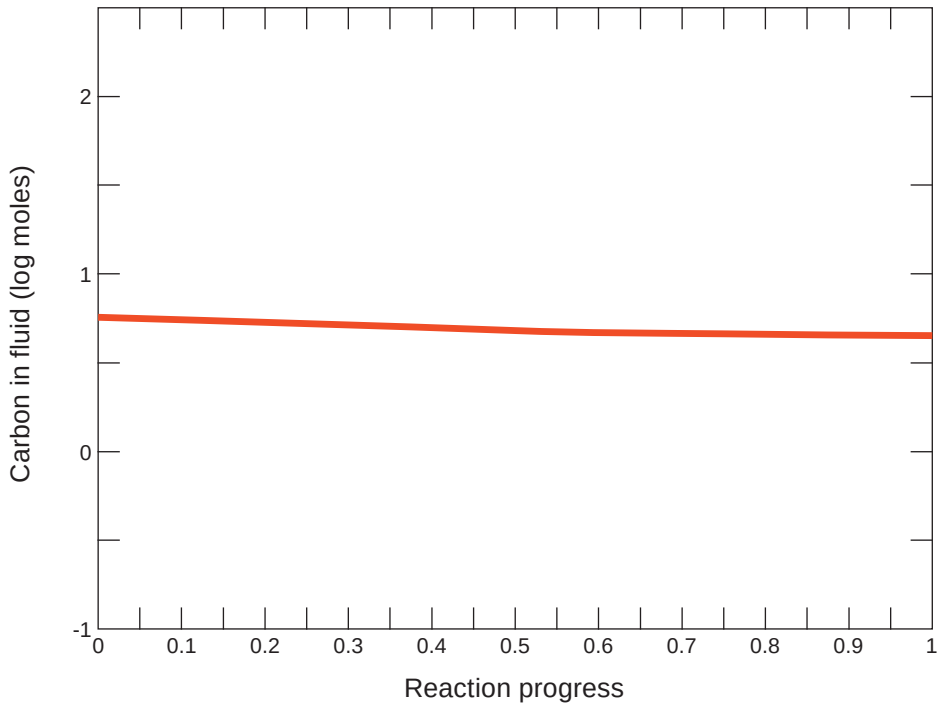

Figure 8-4 *Change in dissolved carbon as reaction between Fluid 2 and microcline progresses.*

Reaction Between Intraplume Water and Mt. Simon Interbeds

Following the proposed scenario, after intraplume formation water reacts with the sandstone matrix it may then contact and react with shale interbeds in the Mt. Simon Sandstone. Only two analyses of Mt. Simon shale interbeds were available (Table 8-3). Those results showed an average of 49% clay in the whole-rock sample; the clay-size fraction was dominated by illite. The clay-size fraction was assumed to be more readily reactive than silt-size or larger mineral grains. Therefore, a significant reaction occurred between the intraplume formation water and illite.

REACT was used to calculate the equilibrium conditions that would result from this reaction. As the reaction progresses, pH ultimately increases to 6.7 (Figure 8-5), several minerals precipitate (Figure 8-6), and the amount of carbon in solution decreases dramatically (Figure 8-7). Mineral precipitation slightly exceeds illite dissolution, resulting in a net reduction in porosity from 10% to approximately 9.3%. (An increasing trend represents precipitation, and a decreasing trend represents dissolution.)

Reaction Between Intraplume Water and the Eau Claire Formation

The CO_2 plume will ultimately rise until it encounters the Eau Claire caprock and spreads out along the Mt. Simon and Eau Claire interface. It is here that plume and rock will have the longest time to react; therefore, the physical, chemical, and mineralogical environment at this interface will have the greatest role in carbon sequestration by mineral precipitation.

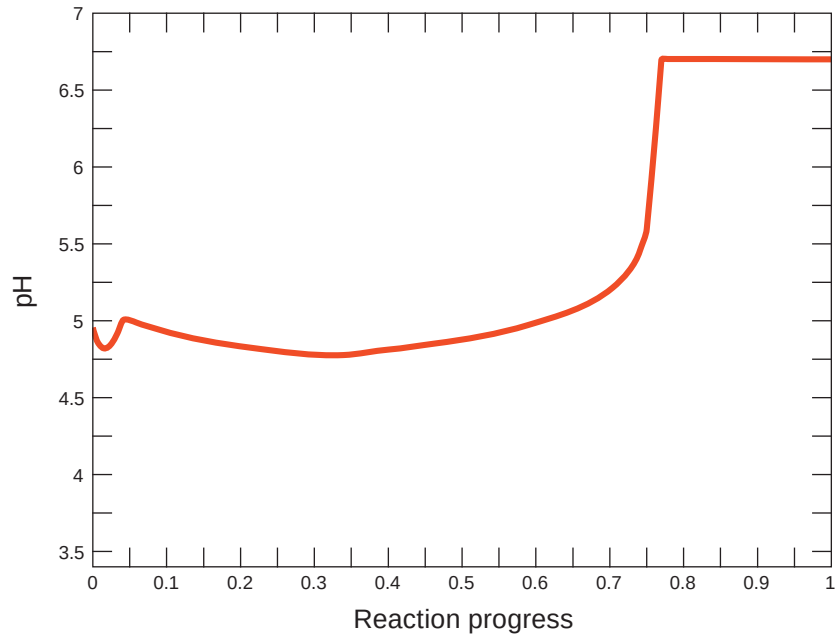

Figure 8-5 *Change in pH as reaction with illite progresses.*

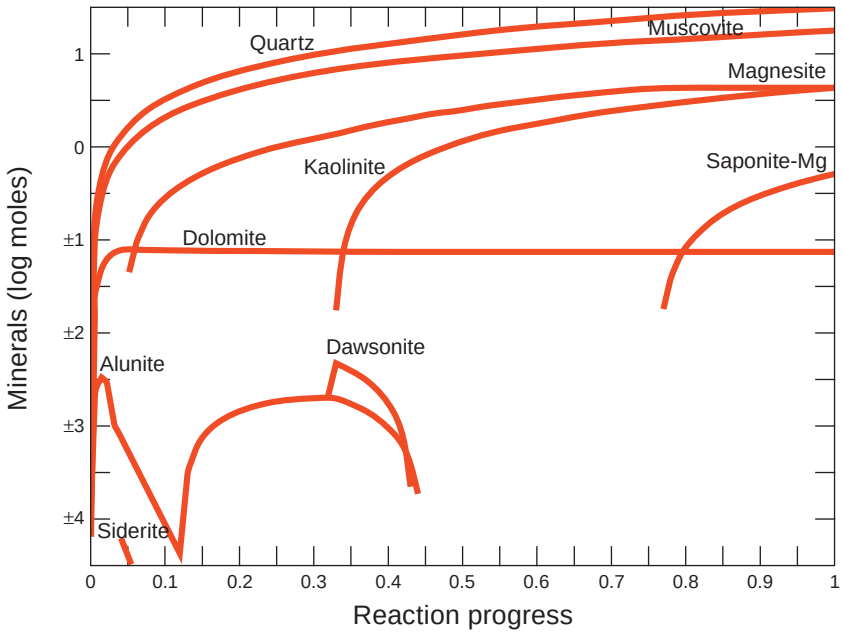

Figure 8-6 *Change in amounts of mineral constituents that precipitate as reaction with illite progresses.*

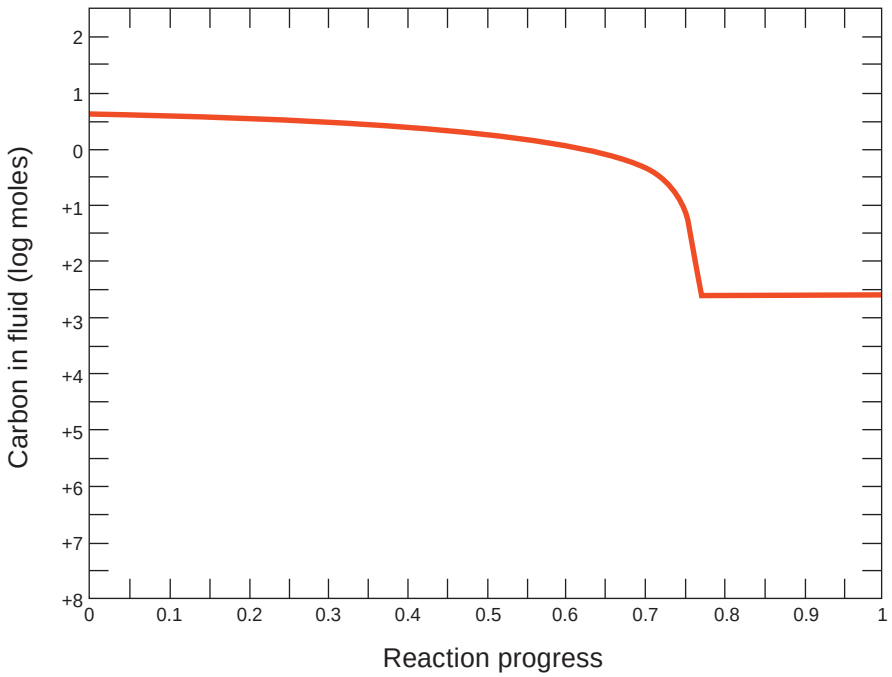

Figure 8-7 *Change in total amount of carbon in solution as reaction with illite progresses.*

Analyses of four Eau Claire samples are currently available (Table 8-4), although none of these samples are from the Manlove Field. The sample described as a silty shale is the best analog for a low-permeability seal. X-ray diffraction analysis of the silty shale showed approximately 40% of the whole rock to be clay minerals, and 89% of the clay-size fraction to be illite (Table 8-4). This sample is mineralogically similar to the shale interbeds in the Mt. Simon Sandstone and will have essentially the same capacity for carbon sequestration by mineral precipitation as shale interbeds in the Mt. Simon Sandstone.

Chlorite is reported to be present in small amounts in both Mt. Simon shale interbeds and in the Eau Claire Formation. The clay-size fraction of one sample from the Eau Claire Formation (sandy siltstone, Table 8-4) is nearly 40% chlorite. Chlorite is a magnesium-rich mineral and is potentially the most important constituent that can influence carbon sequestration by mineral precipitation in the Mt. Simon/ Eau Claire system. Because the composition of the Eau Claire cap rock has not been determined at the Manlove Field, it was decided to investigate the sequestration potential of a chlorite-rich cap rock. The same conditions as for Mt. Simon shale interbeds (10% porosity, chlorite = 40% of the whole rock) were assumed and the GWB module REACT was used to simulate results of reaction to equilibrium with Mt. Simon intraplume formation water.

Results (Figures 8-8, 8-9, and 8-10) show that magnesium-containing chlorite is a much more effective reactant than illite for carbon sequestration. The pH reaches a final value of 8.2 after only 594 cm^3

of chlorite have reacted (reaction progress variable equal to about 0.15 in Figure 8-8). Formation of magnesite ($MgCO_3$) is the primary carbon sink (Figure 8-9), and essentially all dissolved carbon is removed (Figure 8-10). Porosity is reduced from an initial 10% to approximately 9.2%.

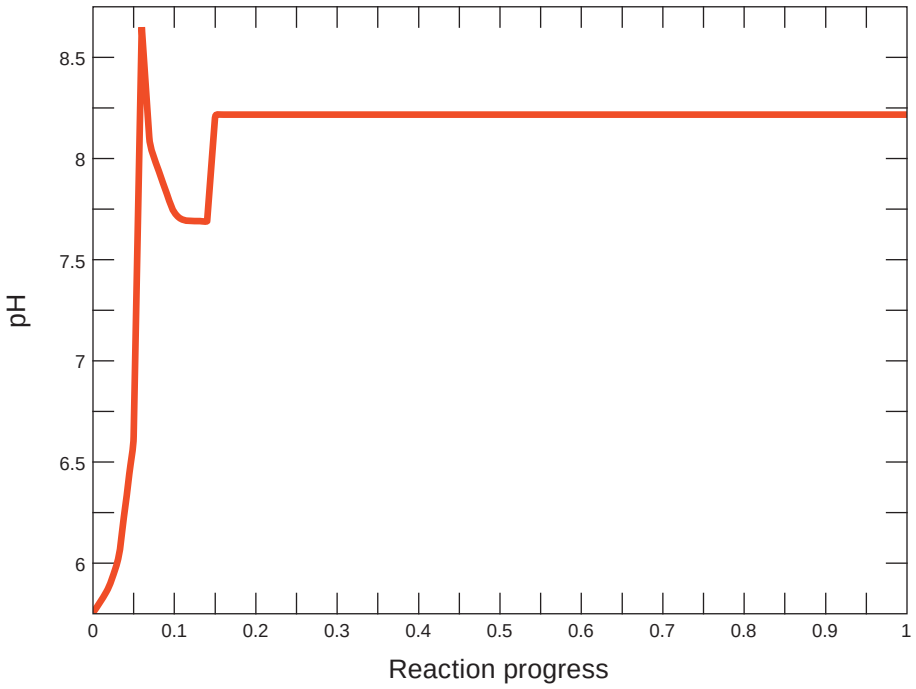

Figure 8-8 *Change in pH as reaction with chlorite progresses.*

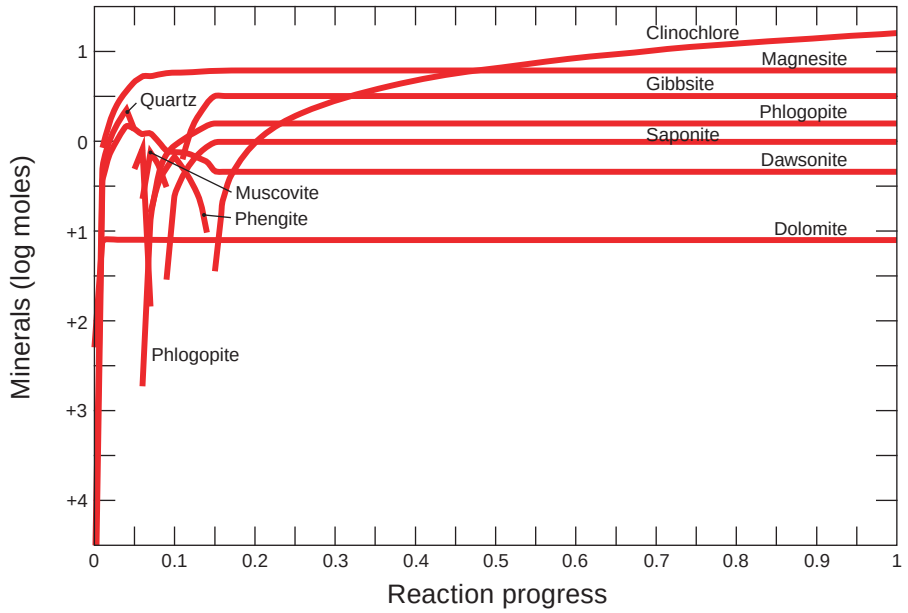

Figure 8-9 *Change in amounts of mineral phases that precipitate as reaction with chlorite progresses.*

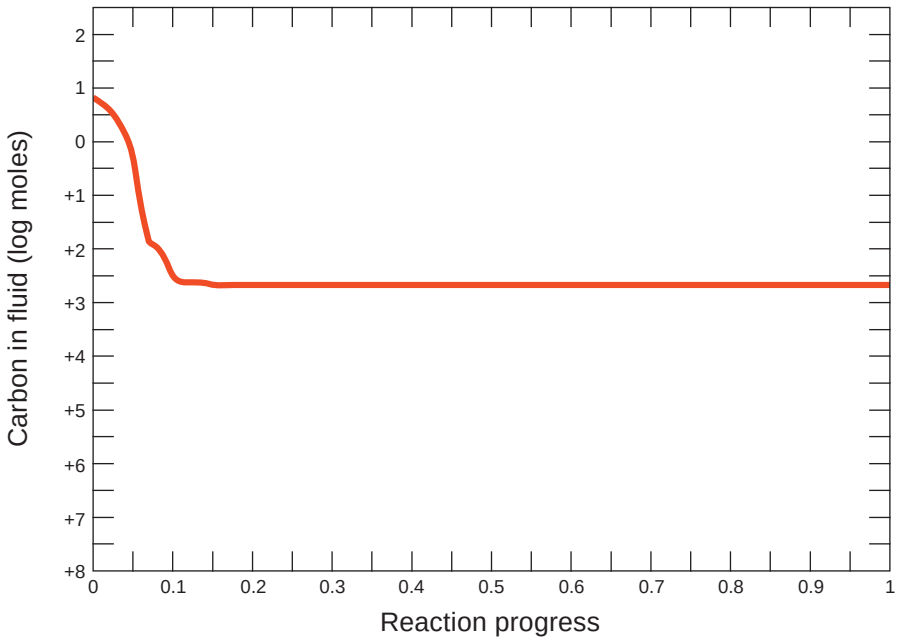

Figure 8-10 *Change in total amount of carbon in solution as reaction with chlorite progresses.*

Results Summary

Results of geochemical modeling indicate that approximately 44 g (1.6 oz) of carbon can dissolve per kilogram (2.2 lb) of water after CO_2 injection into the Mt. Simon Sandstone at Manlove Field. The pH will drop from 6.3 to about 3.4 as a result of the added CO_2. Reaction with the Mt. Simon Sandstone will increase pH to about 4.9, consume a negligible amount of carbon, and reduce porosity from about 10% to about 9.9%. Reaction with shale interbeds in the Mt. Simon can result in an increase in pH to about 6.7, consume nearly all dissolved carbon, and reduce porosity from 10% to approximately 9.3%. The mineralogy of the Eau Claire Formation at Manlove Field is not known. The available data show the Eau Claire Formation elsewhere to be mineralogically similar to shales in the Mt. Simon Sandstone at Manlove Field; therefore, reactions between intraplume formation water and the Eau Claire cap rock will be essentially the same as between formation water and shale interbeds. One sample of the Eau Claire Formation is relatively rich in chlorite. If the Eau Claire Formation above the injection zone at Manlove Field is similarly chlorite-rich, mineral trapping can be much more effective. The pH could rise to 8.2, all dissolved carbon could be precipitated as magnesite, and porosity could be reduced from an initial 10% to about 9.2%. Results are summarized in Table 8-6.

Table 8-6. Results of geochemical modeling.

	pH	Dissolved carbon (mg/kg H_2O)	Porosity (%)
Mt. Simon formation water	6.3	81	10
After CO_2 injection	3.4	4.4×10^4	10
After reaction with sandstone	4.9	4.4×10^4	9.9
After reaction with shale	6.7	24	9.3
After reaction with chlorite	8.2	18	9.2

These simulations show some potentially important features of carbon sequestration of the Mt. Simon:

1. Despite relatively high salinity, the solubility of CO_2 in formation water is large enough that both solubility trapping and mineral trapping are possible, but no reaction times were included in this study.
2. Porosity reduction adjacent to an injection well in the Mt. Simon Sandstone will be negligible; therefore, mineral precipitation should not reduce injection efficiency.
3. Mineral trapping by reactions between intraplume formation water and shale interbeds in the Mt. Simon Sandstone is potentially very significant. Shale interbeds near the injection zone can both increase the volume of the CO_2 plume and remove large amounts of dissolved carbon.
4. Mineral trapping by reactions between intraplume formation water and the Eau Claire Formation are also potentially very significant. To the extent that the Eau Claire Formation is chlorite-rich above the injection zone, essentially all dissolved carbon can be removed by precipitation as magnesite.

Discussion

A geochemical system consisting of supercritical CO_2, saline formation water, and heterogeneous geologic media is very complex (e.g., Johnson et al., 2001; Pruess et al., 2001; Xu et al., 2004). Predicting reactions and processes in such a system using currently available software and geochemical information requires making a number of assumptions, many of which are not apparent but importantly control the results. Some of the more critical assumptions used in the present study follow:

1. The thermodynamic properties describing reactions between supercritical CO_2 and aqueous carbon species (Equation [1]) are not precisely known. CO_2 fugacity was set equal to reservoir pressure, which could result in an overestimate of the amount of CO_2 that can dissolve in formation water.
2. Activity coefficients of aqueous species in CO_2-saturated, saline water are an area of current study. The GWB thermodynamic data and equations for calculating activity coefficients

were used without modification. Other approaches, if justified, could be run, and the results could be compared to those presented here.

3. All geochemical calculations are made on the basis of 1 kg (2.2 lb) of solvent water. The amount of rock volume involved in the reaction is determined from porosity estimates. All porosity was assumed to be filled with water. However, supercritical CO_2 will occupy some fraction of the total pore space, and some porosity may not be in effective communication with intraplume formation water. This uncertainty probably does not affect the calculations in any important way.
4. All simulations were run as equilibrium reactions. However, the system will be dynamic; the plume will move through the host formation, and reactions will occur over time, not instantaneously. Incorporating kinetic reaction rates is possible but of limited value until the dynamics of plume migration can be estimated. Krumhansl et al. (2003) suggest that equilibrium calculations overestimate the volumes of phases involved on the basis of comparing results produced by equilibrium models versus kinetic models. However, how well the reaction kinetics incorporated in software packages represent actual conditions is a question that could be addressed by laboratory experiments.
5. The model predicts dissolution and precipitation of a number of silicate phases, some of which have complex chemical compositions and crystal structure and might not react significantly over the time scale of CO_2 injection and plume migration. No phases in this study were suppressed. It was assumed that a solid phase of similar composition and volume, if not crystal structure, would react. If this is not correct, the predicted changes in porosity would be affected.

Structure and Isopach Maps in the Kentucky Portion of the Midwest Geologic Sequestration Consortium Study Area

Introduction

As part of the Phase I project of the Midwest Geologic Sequestration Consortium, a series of structure and isopach maps were constructed for various horizons and intervals in western Kentucky (Figures A5-1 to A5-18). These horizons are of specific interest to CO_2 geologic sequestration due to their relative depth and the thickness of their caprocks (seals). These maps will be critical in examining future possible geologic carbon sequestration targets in the Illinois Basin. Characteristics of these maps are discussed briefly and are shown in Table A5-1. The Precambrian surface exhibits the greatest structural relief and, therefore, has had a significant influence on the geometries of all shallower horizons and intervals. Because understanding of the Precambrian surface is critical to the mapping of each of the overlying units and intervals, it is discussed in somewhat greater detail.

Geologic Formations

Precambrian Surface

The Precambrian surface in western Kentucky is unconformable and separates overlying Paleozoic rocks from underlying Late to Middle Proterozoic rocks (Drahovzal and Harris, 1998; Stark et al. 1999; Drahovzal, 2000; Drahovzal and Harris, 2004). The underlying rocks can be parallel or angular to the overlying Paleozoic rocks (Shrake et al., 1990; Drahovzal, 1997; Stark, 1997). Composition of the Precambrian rocks beneath the unconformity ranges from sedimentary to igneous (Drahovzal et al., 1992).

Because there are only six basement wells in the Kentucky portion of the Midwest Geologic Sequestration Consortium project area, most of the data used in mapping the Precambrian surface are from published or proprietary seismic reflection data that were calibrated by well data where possible. The published data used in constructing the map include that of Hester (1988), Bertagne and Leising (1991), Goetz et al. (1992), Pratt et al. (1992), Drahovzal (1994), Potter et al. (1995, 1997), Bear et al. (1996), Drahovzal (1997), and Wheeler et al. (1997). The resulting basement map shown here is an update and expansion of an earlier map for a part of western Kentucky lying between long 87 and 89° W and including adjacent parts of Illinois and Indiana (Wheeler et al., 1997). The earlier map did not include data from seismic profiles lying to the east of long 87° W, and these additional data have resulted in changing the interpretation of basement in the eastern part of the earlier map.

In constructing the map, seismic reflection interpretations were made for the top of the Precambrian, top of the Eau Claire Formation, and top of the Knox Group. The interpreted two-way travel times in seconds were converted to approximate true depth in feet below sea level. The interval velocities used in making these conversions were based on correlation to nearby wells and interpretation of sonic log data. The specific velocities used in the conversion ranged from 5,486 to 5,700 m/s (18,000 to 18,700 ft/s) for the Eau Clair interval, 6,096 to 6,523 m/s (20,000 to 21,400 ft/s) for the Knox interval, and 4,200 to 5,029 m/s (13,780 to 16,500 ft/s) for the post-Knox interval. When summed together and corrected for the datum of each seismic profile, elevations at key points along each seismic reflection profile formed the basis for creating a grid on which the basement contour map was constructed.

Because of its profound influence on subsequently shallower horizons, the Precambrian surface structure contour map was constructed first. Once constructed, the shallower maps were completed in stratigraphic order from the deeper horizons upward. The seismic methodology used for the Precambrian maps was used for complementing the well data for the post-Knox unconformity and Eau Claire maps. Faults found from seismic and surface (outcrop) interpretations enhanced all of the maps of the shallower formations.

The western Kentucky, Precambrian surface is dominated by the deep asymmetrical graben referred to as the Rough Creek Graben. In general, the Rough Creek Graben is a fault-bounded, east-west–oriented half graben that is deep along the northern edge and shallow along the southern edge; it shallows from west to east. The graben is segmented lengthwise into at least three deep basins separated by northeast-oriented faults and a horst zone. One basinal area is centered in Webster County where the Precambrian surface exceeds 9,144 m (30,000 ft) in depth, a second lies in western Ohio County where it is more than 7,925 m (26,000 ft) deep, and a third in western Grayson County where the basement is up to 8,230 m (27,000 ft) deep. The northern boundary fault, the Rough Creek Fault Zone, is the major down-to-south fault along which the graben was downdropped during the Cambrian. In the vicinity of Webster County, where the graben is at its deepest, the throw on the Rough Creek Fault Zone is >4,572 m (>15,000 ft). Several lower-throw fault zones to the south define the southern extent of the graben. Throws are less east and west of this area and diminish to nearly zero eastward in Green and Taylor Counties. To the west, the graben is cut by the Fluorspar Area Fault Complex that transects the graben with major northeast-oriented faults. In this area also, the Rough Creek Graben grades into the northeast-oriented Reelfoot Rift, a somewhat more symmetrical graben feature.

During the Alleghany Orogeny, northwesterly compression in western Kentucky resulted in the reversing of the Rough Creek Fault Zone and the development of arching on the south side of the fault zone (Kolata and Nelson, 1991). During this episode, the southern boundary faults apparently were largely impassive. With the development of the Atlantic Ocean and the opening of the Gulf of Mexico

in Triassic and Jurassic times, extensional forces reversed the motion again on the northern faults and reactivated the southern boundary faults, resulting in extensive normal fault movement throughout western Kentucky and the development of the shallower Moorman Syncline (Strunk, 1984; Bertagne and Leising, 1991; Kolata and Nelson, 1991).

North of the Rough Creek Graben, the Precambrian surface dips westward off of the Cincinnati Arch. Near the arch, it is at a depth of about –762 m (–2,500 ft), but is deeper than –4,572 m (–15,000 ft) in Union County. The west dipping surface is interrupted by northwest-oriented, high-angle faults that create local broadly folded structures.

The eastern limit of the Rough Creek graben is poorly known, but a downwarp extends east-southeastward toward the Grenville Front in the vicinity of the Cumberland Saddle in south-central Kentucky where it may be semi-continuous with the graben structures of the Cambrian Rome Trough to the east (Harris, 1975; Thomas, 1991). The details of the relationship, however, are equivocal.

Mount Simon Sandstone

Seven wells penetrate the Mount Simon Sandstone in western Kentucky. Available seismic reflection data were used to augment well data in areas where the latter was sparse. The southern boundary of the Mount Simon is defined by the Rough Creek Fault System. Recently reevaluated seismic reflection data in Hart, Larue, Grayson, and Hardin Counties suggest that the Mount Simon may extend slightly south of the Rough Creek Fault System, possibly as a series of submarine fans. The isopach map of the Mount Simon shows an increase from approximately 107 m (350 ft) in central Kentucky to 244 m (800 ft) in western Kentucky (Webster County). The apparent thickening of the Mount Simon to the west may be attributed to the extremely limited well control and the complex faulting along the Rough Creek Fault System. To make the Mt. Simon structure map, it was assumed that the surface of the Mount Simon parallels the Precambrian surface fairly uniformly in western Kentucky. The surface ranges from –4,267 m (–14,000 ft) in Union County to –1,219 m (–4,000 ft) in central Kentucky.

Eau Claire Formation

Well control for the Eau Claire Formation is poor. Seismic data control was used to help define the top of the Eau Claire surface in Kentucky where well data were not present. In addition, the isopach interval from the Precambrian surface to the top of the Eau Clair south of the Rough Creek Fault System and the interval from the Mt. Simon to the top of the Eau Claire north of the fault system were used to further develop the map of the Eau Claire surface. The thickness of the Eau Claire changes drastically across the Rough Creek Fault System. In Ohio County, the thickness changes from <30m (<100 ft) north of the fault

to >5,791 m (>19,000 ft) on the south side. The Eau Claire top mirrors the Precambrian top, although fault offsets and folds show less relief.

Copper Ridge Dolomite

Well coverage for the Copper Ridge Dolomite is fairly sparse. The Copper Ridge was not picked in the reflection seismic data set. Therefore, an isopach for the Copper Ridge was created based solely on well data. The thickness of the Copper Ridge ranges from 457 to 2,134 m (1,500 to 7,000 ft). The greatest thickness occurs south of the Rough Creek Fault System. The isopach for the interval between the top of the Eau Claire to the top Copper Ridge was added to the Eau Claire top to construct the Copper Ridge surface. The top of the Copper Ridge, in general, parallels the top of the Eau Claire Formation. The Copper Ridge top ranges from –457 to –3,505 m (–1,500 to –11,500 ft).

Rose Run Sandstone

The Rose Run Sandstone overlies the Copper Ridge Dolomite. Due to the lack of well data, a generalized isopach map for the Rose Run was created to approximate the top of the Rose Run. The Rose Run is approximately 30 m (100 ft) in central Kentucky and pinches out to the west. Faulting in the Rough Creek Graben apparently does not effect thickness distribution. The top of the Rose Run ranges from –457 to –1,295 m (–1,500 ft to –4,250 ft). The deepest elevations occur in the graben.

Post-Knox Unconformity

Both well and seismic reflection data were used to create the surface of the post-Knox unconformity. The interval of the surface of the Copper Ridge/Rose Run to the surface of the post-Knox unconformity ranges in thickness from approximately 305 to 1,067 m (1,000 ft to 3,500 ft). The greatest thickness occurs in the Rough Creek Graben, suggesting synsedimentary faulting. The surface ranges from –183 m (–600 ft) in central Kentucky to –2,743 m (–9,000 ft) in the Rough Creek Graben of western Kentucky (Union County).

St. Peter Sandstone

The St. Peter Sandstone isopach was created using limited well data. The formation is relatively thin, pinching out in central Kentucky and to the south. The southern pinch out may be an effect of the Pennyrile Fault System. The maximum thickness is 30 m (100 ft) in Webster County. Isopach values were added to the post-Knox unconformity map to create the top of St. Peter structure contour map. The surface ranges from – 305 to –2,515 m (–1,000 to –8,250 ft); the lowest elevations are in the graben.

High Bridge Group

The High Bridge Group ranges in thickness from 152 to 305 m (500 to 1,000 ft). The thickest part of the formation is in Caldwell County, Kentucky; however, there is very little well control in far western Kentucky. The surface of the top of the High Bridge Group ranges from 0 to >–2,137 m (> –7,000 ft). The south side of the Rough Creek Fault System is upthrown approximately 500 ft at the High Bridge horizon, which indicates reverse motion along this fault system.

Trenton Limestone

The structural surface and isopach interval of the Trenton Limestone were mapped primarily from well logs. To minimize the influence of the deeper structure, the top of Trenton Limestone was contoured independent of the underlying High Bridge Group. The maximum thickness of the Trenton is 53 m (175 ft) in Grayson County. The Trenton pinches out to the west where the Sebree Trough surpressed carbonate deposition. The surface of the Trenton ranges from 140 m (460 ft) in central Kentucky to –1,280 m (–4,200 ft) in the Rough Creek Graben.

Maquoketa Shale

The maximum known thickness of the Maquoketa Shale is 171 m (560 ft). In Ohio County, the distribution of thickness suggests some fault control. The minimum known thickness is 58 m (190 ft) in Ballard County. The known surface elevations range from –193 m (–633 ft) south of the Pennyrile Fault System to –1,773 m (–5,816 ft) within the Rough Creek Graben.

Table A5-1. List of surfaces contoured, isopach intervals, and purpose.

Surface	Isopach interval	Purpose
Maquoketa Shale	Maquoketa Shale	Seal
Trenton Limestone	Trenton Limestone	Seal/Sink
High Bridge Group	High Bridge Group	Seal/Sink
Saint Peter Sandstone	Saint Peter Sandstone	Sink
Post-Knox unconformity	Post-Knox unconformity - Rose Run Sandstone/Copper Ridge Dolomite	Seal/Sink
Rose Run Sandstone	Rose Run Sandstone-Copper Ridge Dolomite	Sink
Copper Ridge Dolomite	Copper Ridge Dolomite-Eau Claire Formation	Seal/Sink
Eau Claire Formation	Eau Claire Formation- Mount Simon Sandstone/Precambrian	Seal
Mount Simon Sandstone	Mount Simon Sandstone-Precambrian	Base
Precambrian		

Conclusions

Based on these maps, a number of possible sink and seal combinations are present for CO_2 sequestration. Seismic interpretation of the Precambrian, post-Knox unconformity, and Eau Claire was used effectively to enhance and complement sparse well data in order to make structure and isopach maps for these and shallower formations. Some of the faults identified from seismic and surface studies were assumed to cross most of the geologic formation maps. For this assessment, conformity assumptions between geologic formations were required due to the limited well coverage; actual storage potential will be determined as additional well data become available through more drilling and testing.

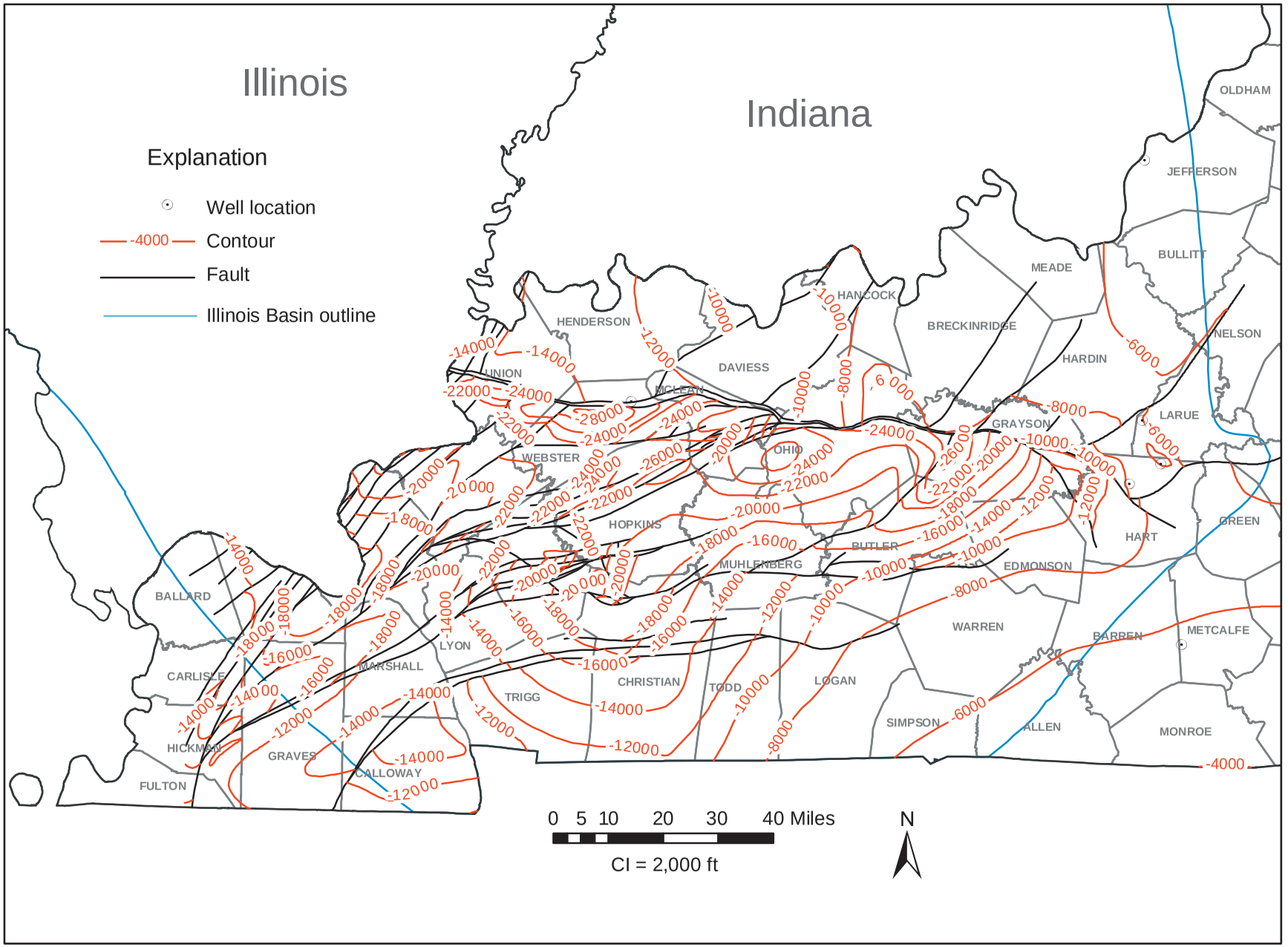

Figure A5-1 *Structure contours drawn on the Precambrian unconformity, Illinois Basin, western Kentucky.*

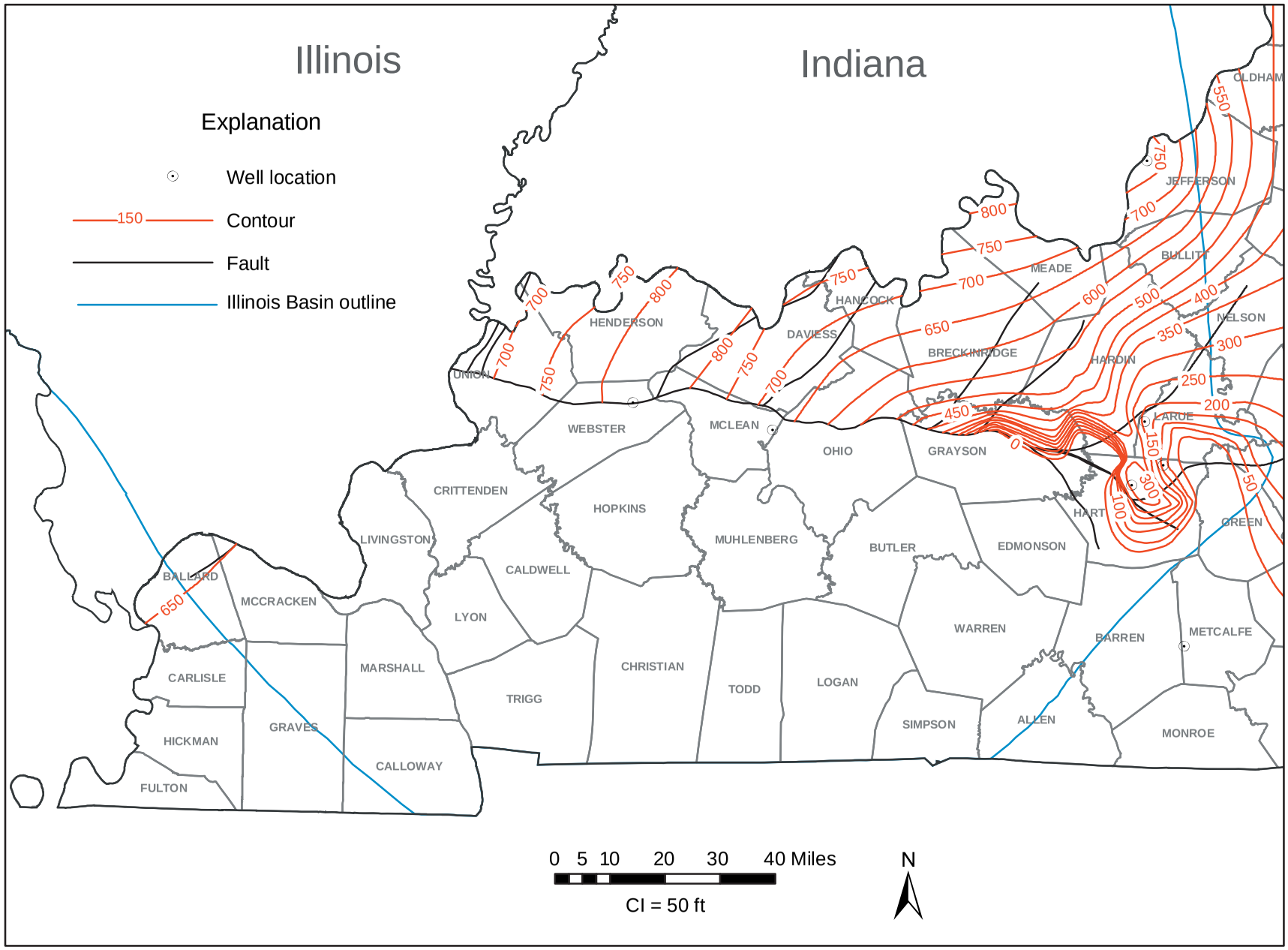

Figure A5-2 *Isopach contours of the Mt. Simon Sandstone, Illinois Basin, western Kentucky.*

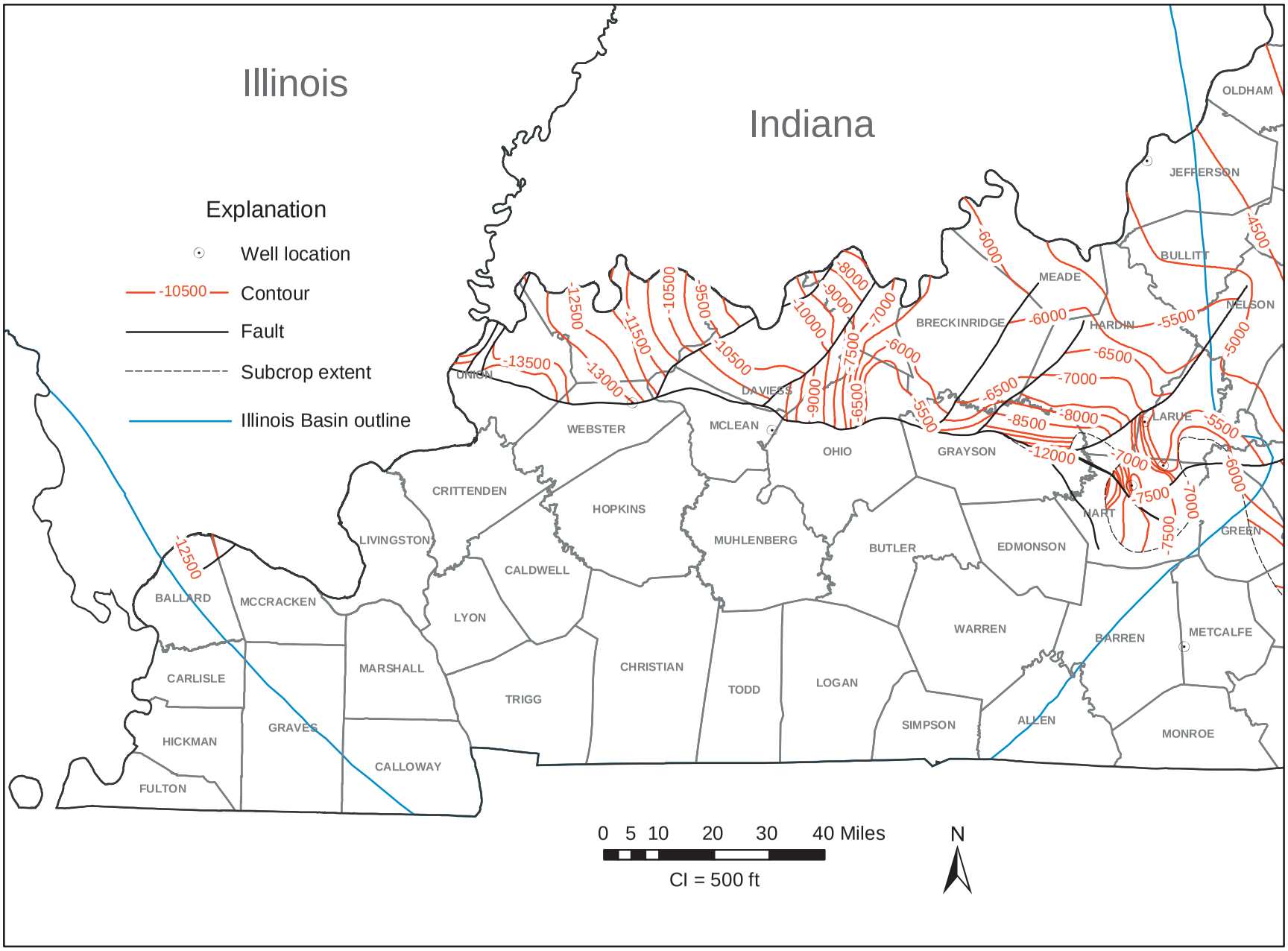

Figure A5-3 *Structure contours drawn on the top of the Mt. Simon Sandstone, Illinois Basin, western Kentucky.*

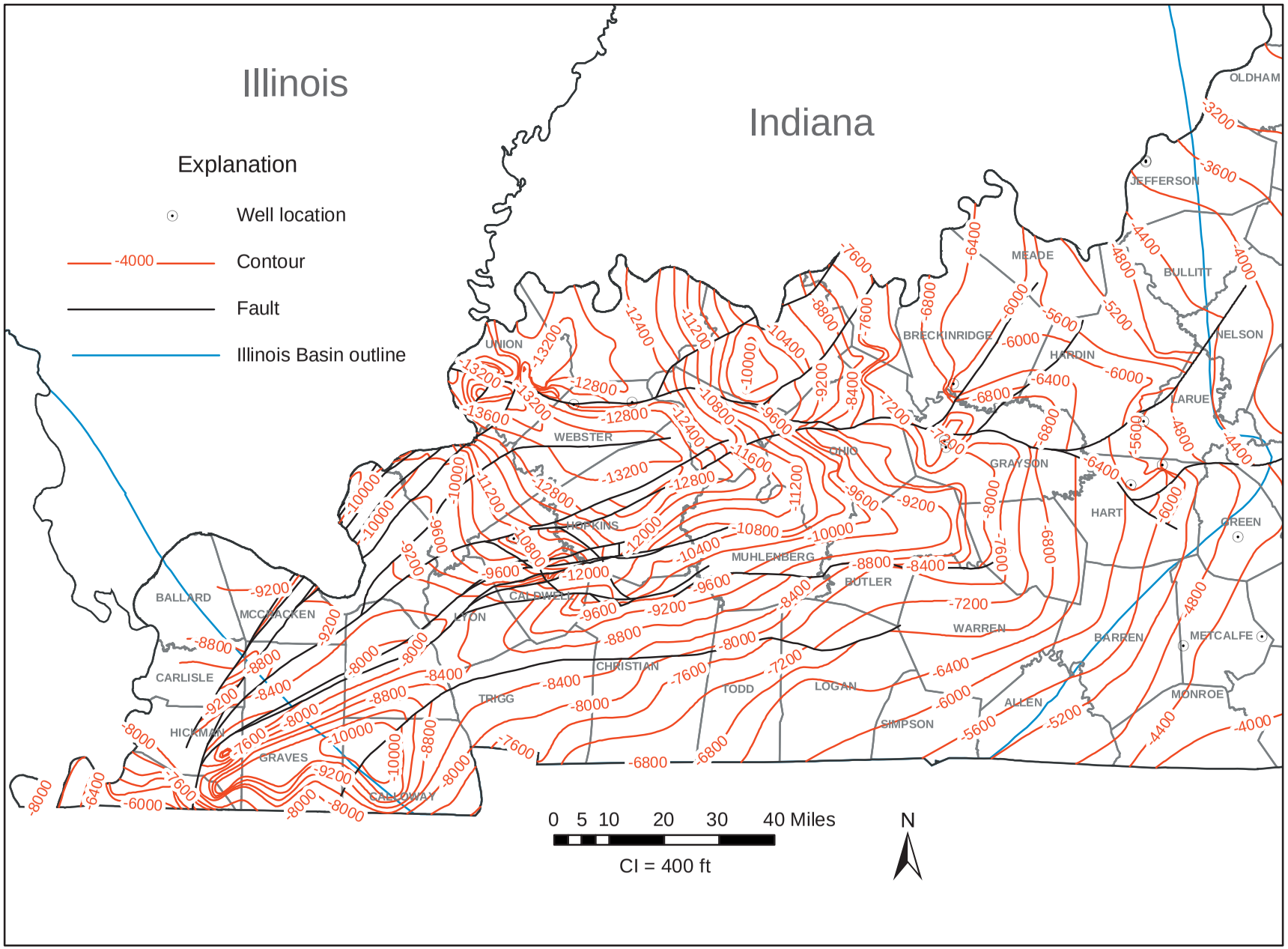

Figure A5-4 *Structure contours drawn on the top of the Eau Claire Formation, Illinois Basin, western Kentucky.*

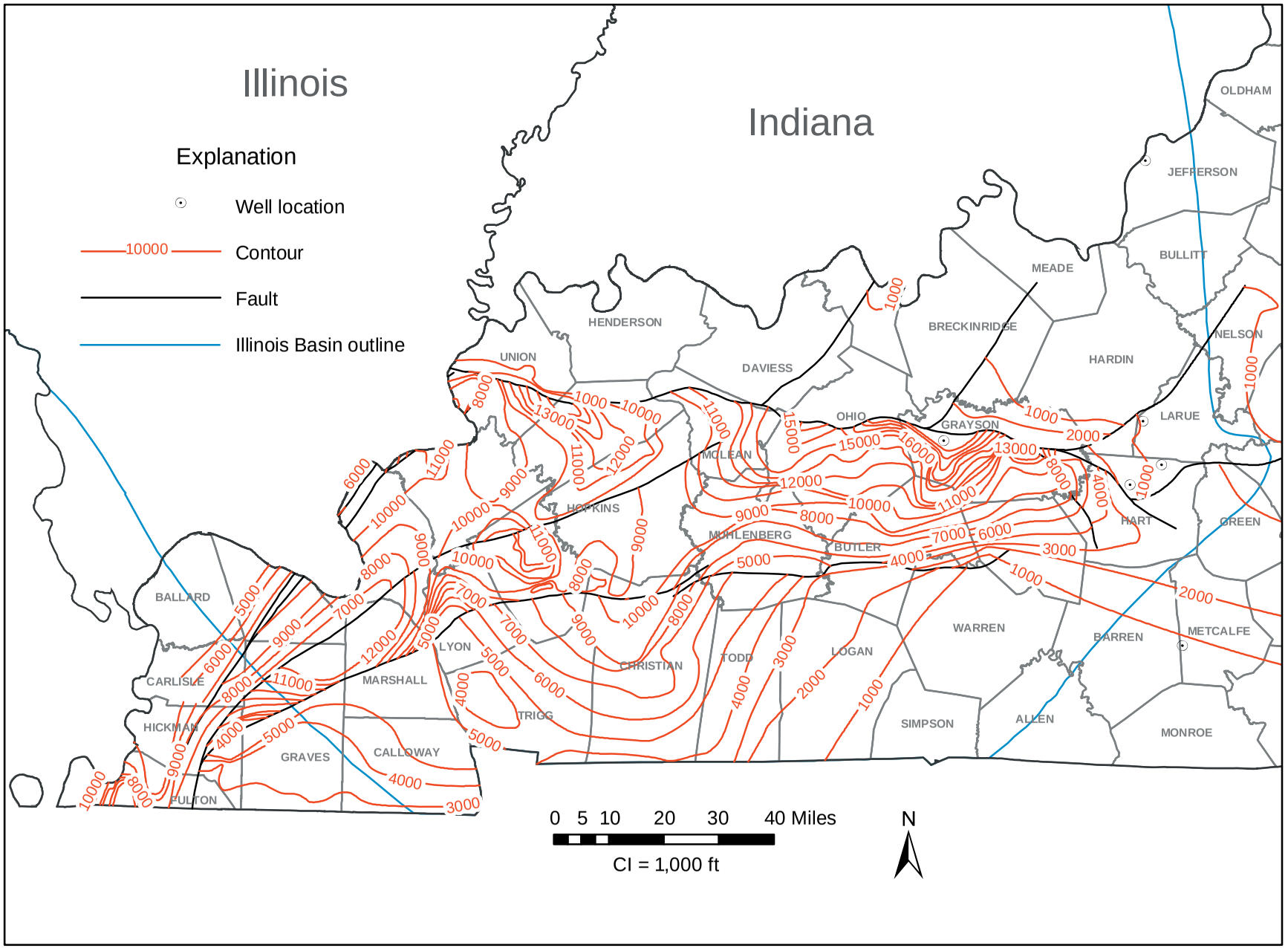

Figure A5-5 *Isopach contours of the interval between Precambrian unconformity/top f Mt. Simon to the top of Eau Claire Formation, Illinois Basin, western Kentucky.*

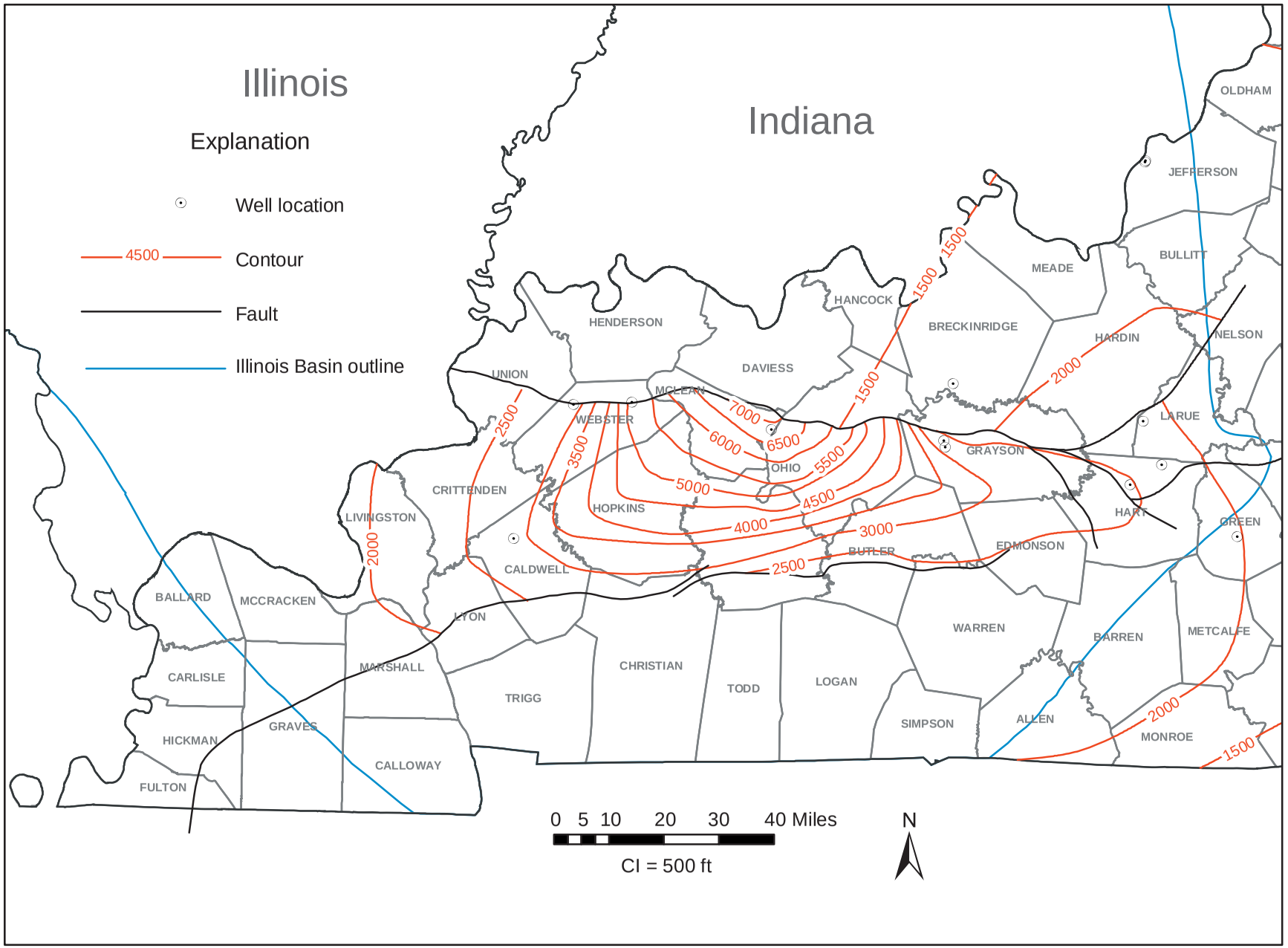

Figure A5-6 *Isopach contours of the interval between the top of Eau Claire Formation to the top of Copper Ridge Dolomite, Illinois Basin, western Kentucky.*

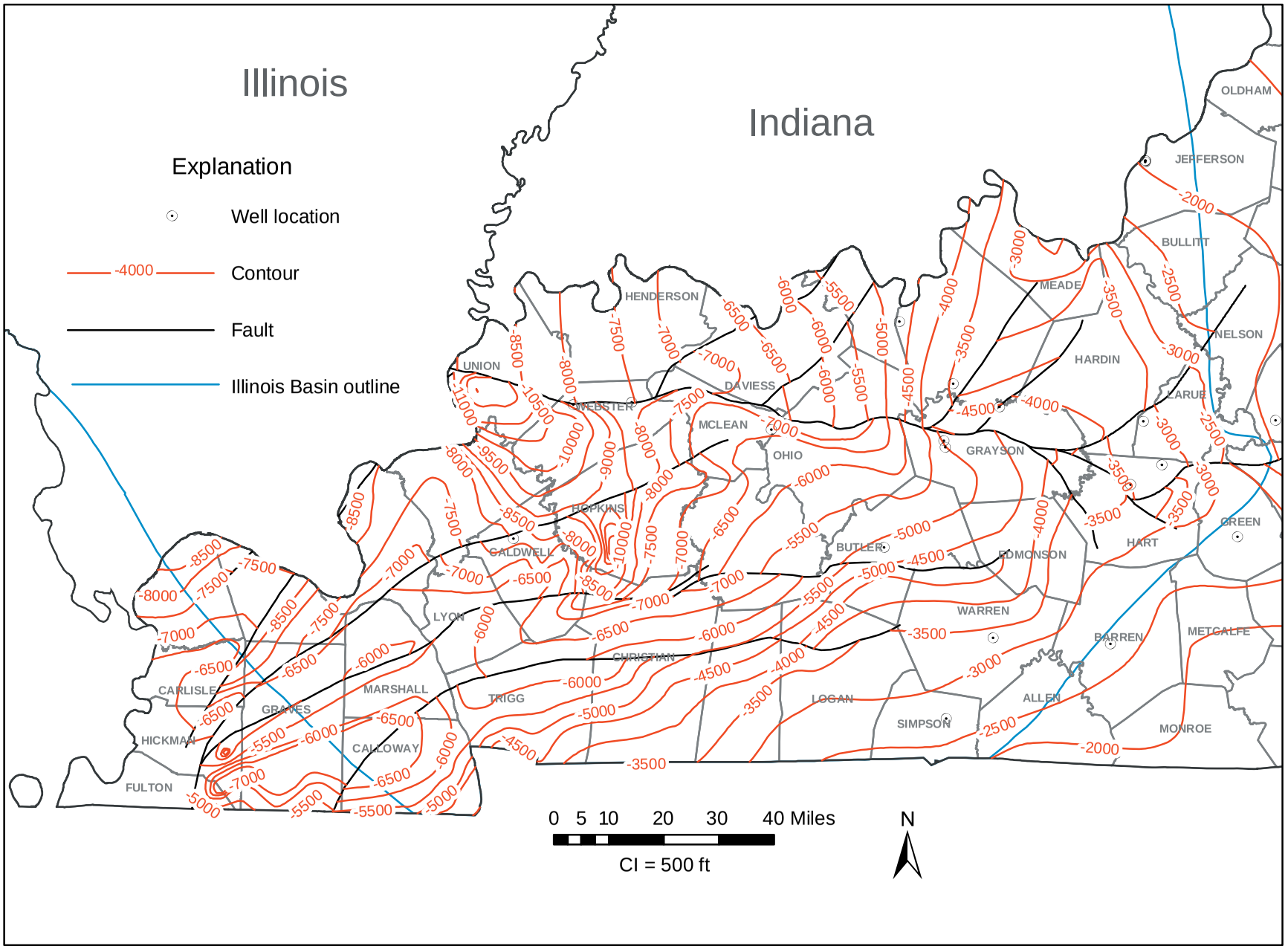

Figure A5-7 *Structure contours drawn on the top of the Copper Ridge Dolomite, Illinois Basin, western Kentucky.*

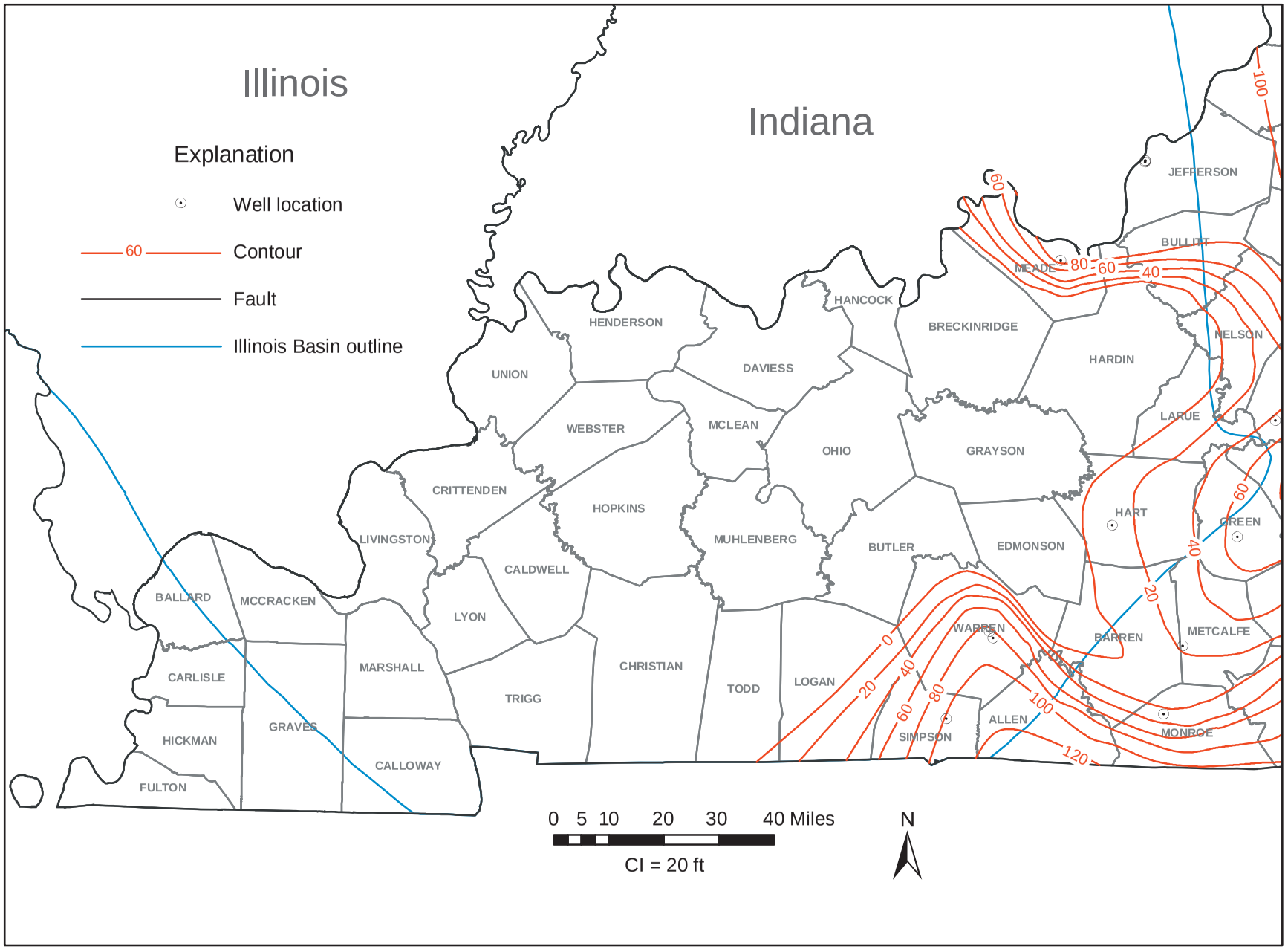

Figure A5-8 *Isopach contours of the interval between the top of Copper Ridge Dolomite to the top of Rose Run Sandstone, Illinois Basin, western Kentucky.*

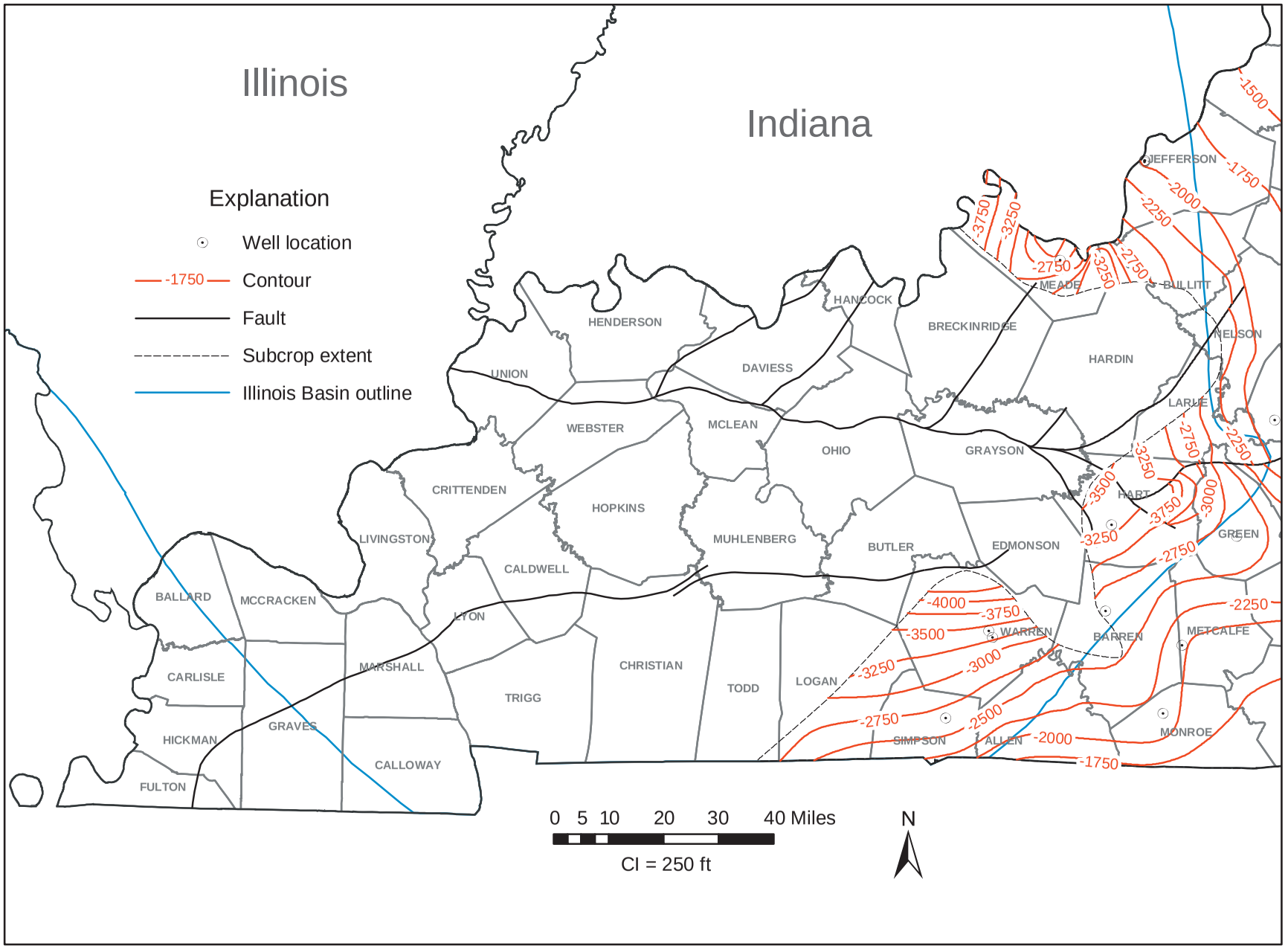

Figure A5-9 *Structure contours drawn on the top of the Rose Run Sandstone, Illinois Basin, western Kentucky.*

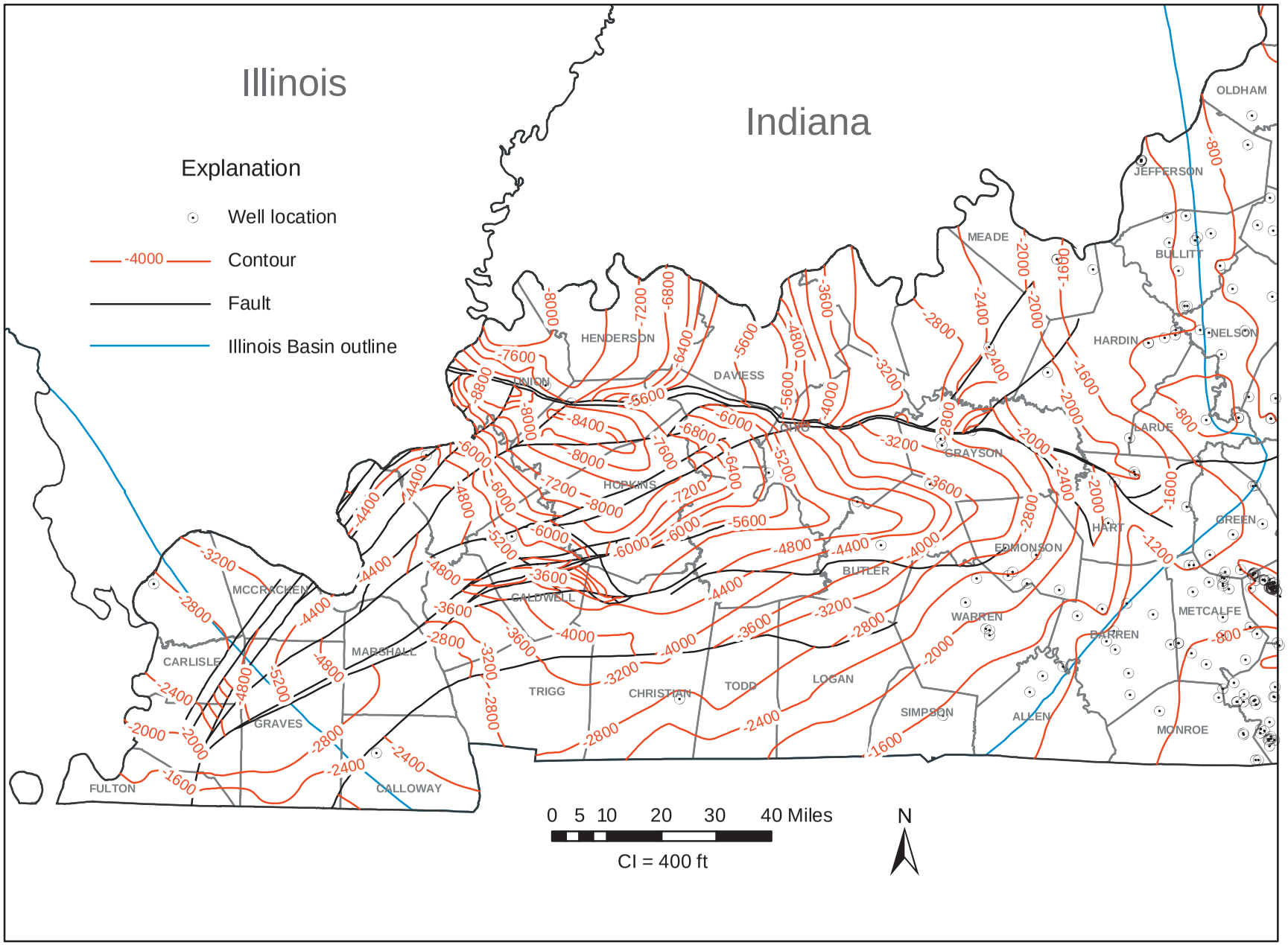

Figure A5-10 *Structure contours drawn on the top of the post-Knox unconformity, Illinois Basin, western Kentucky.*

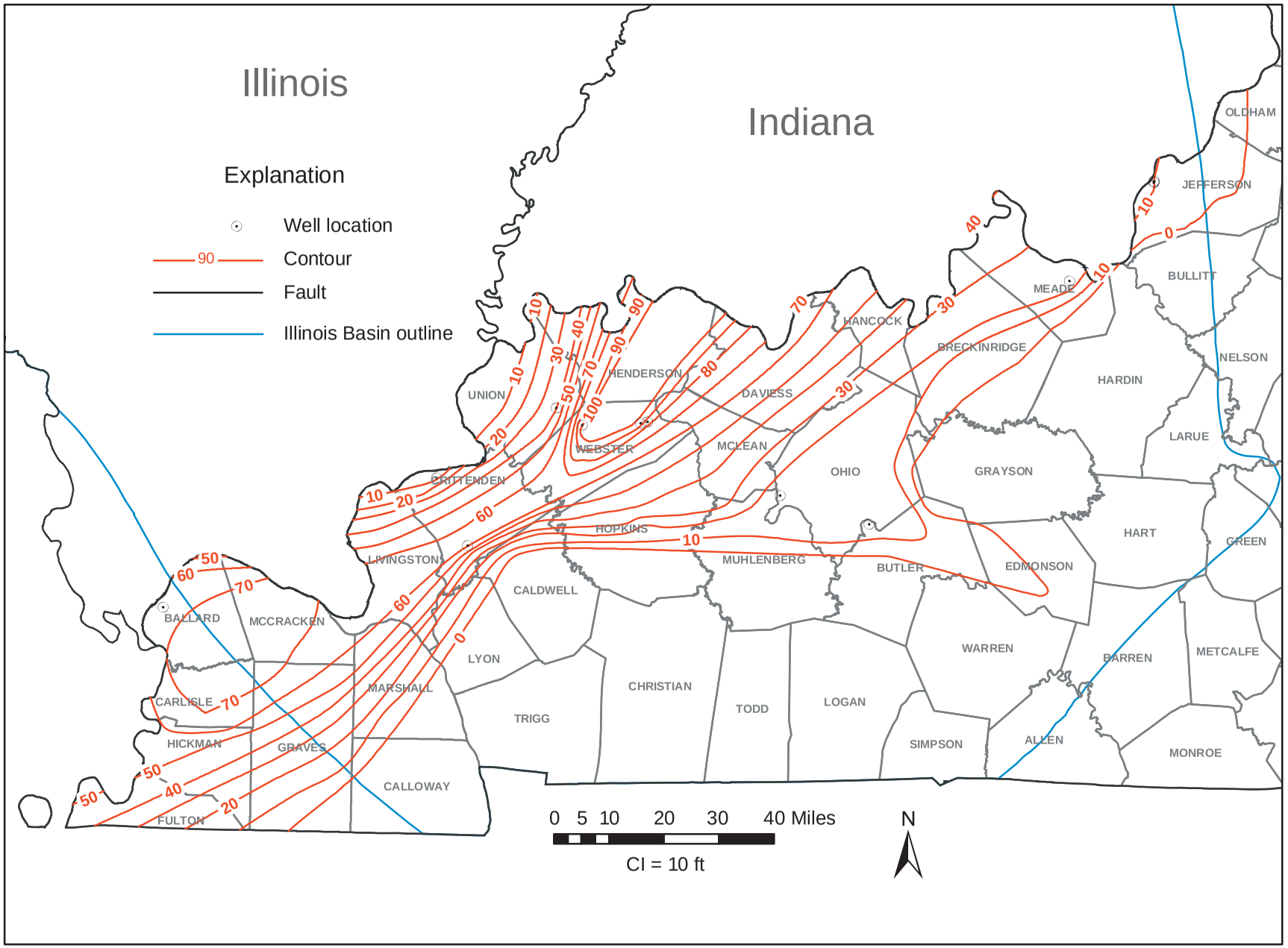

Figure A5-11 *Isopach contours for the St. Peter Sandstone, Illinois Basin, western Kentucky.*

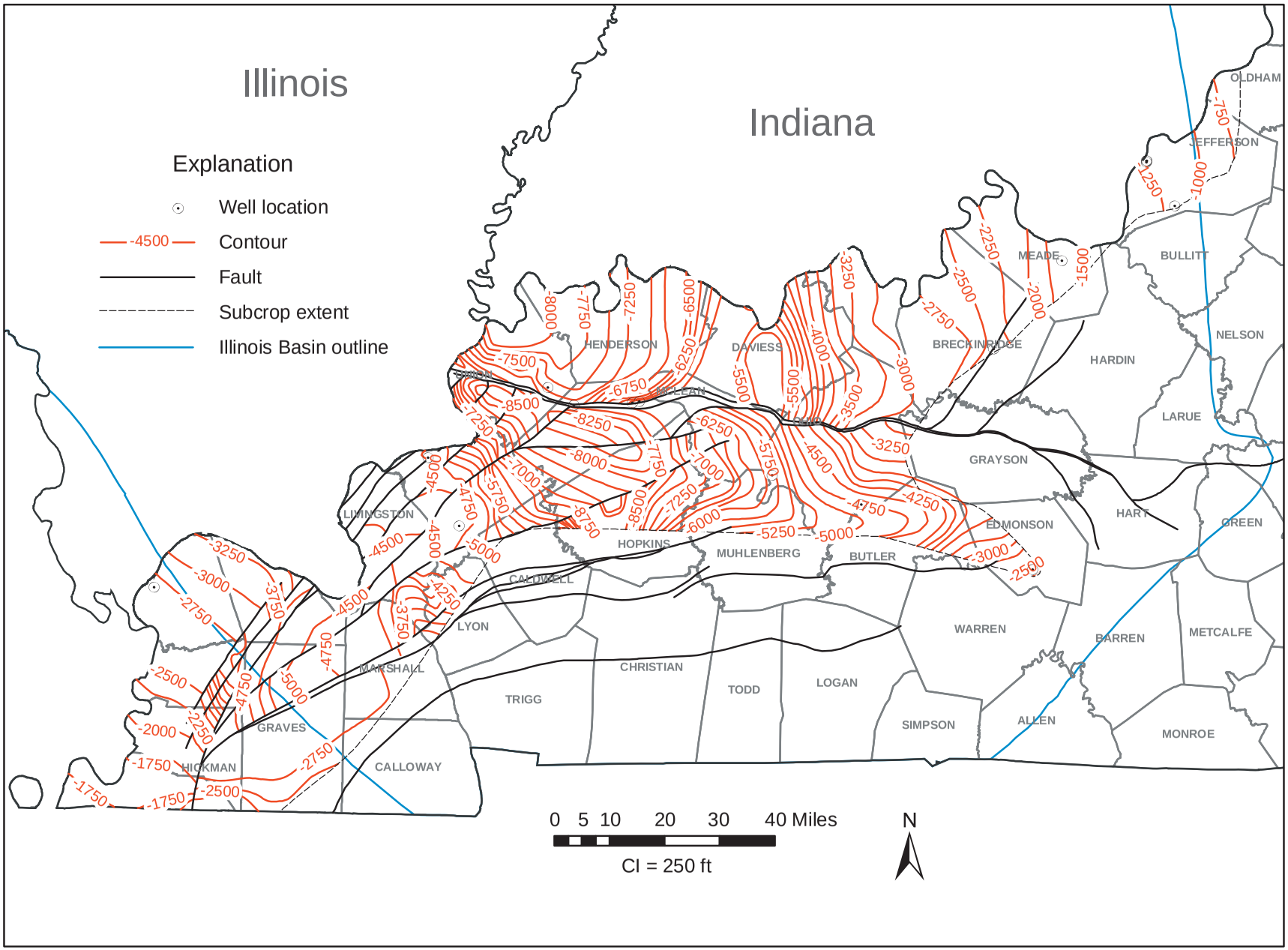

Figure A5-12 *Structure contours drawn on the surface of the St. Peter Sandstone, Illinois Basin, western Kentucky.*

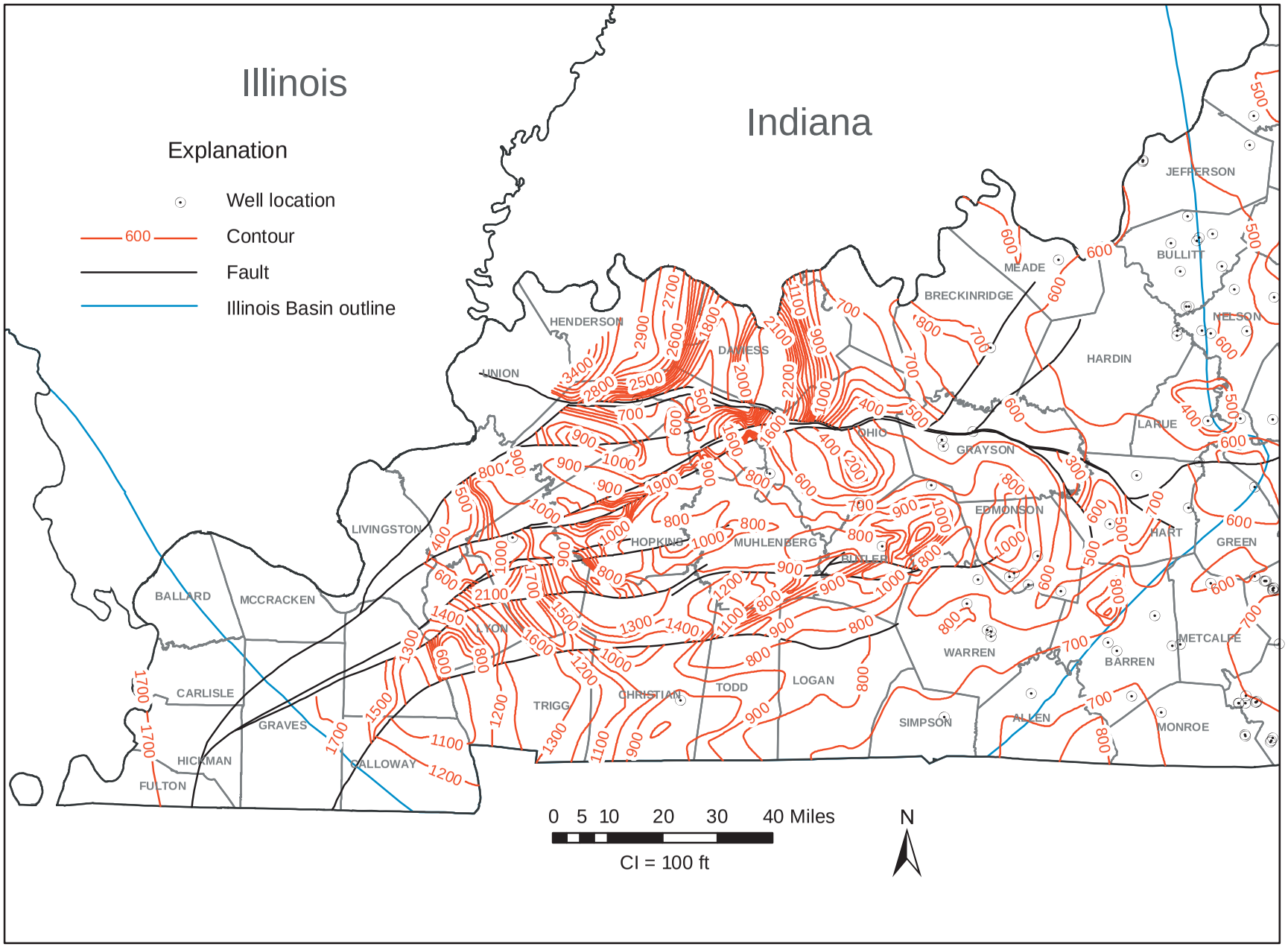

Figure A5-13 *Isopach contours of the High Bridge Group, Illinois Basin, western Kentucky.*

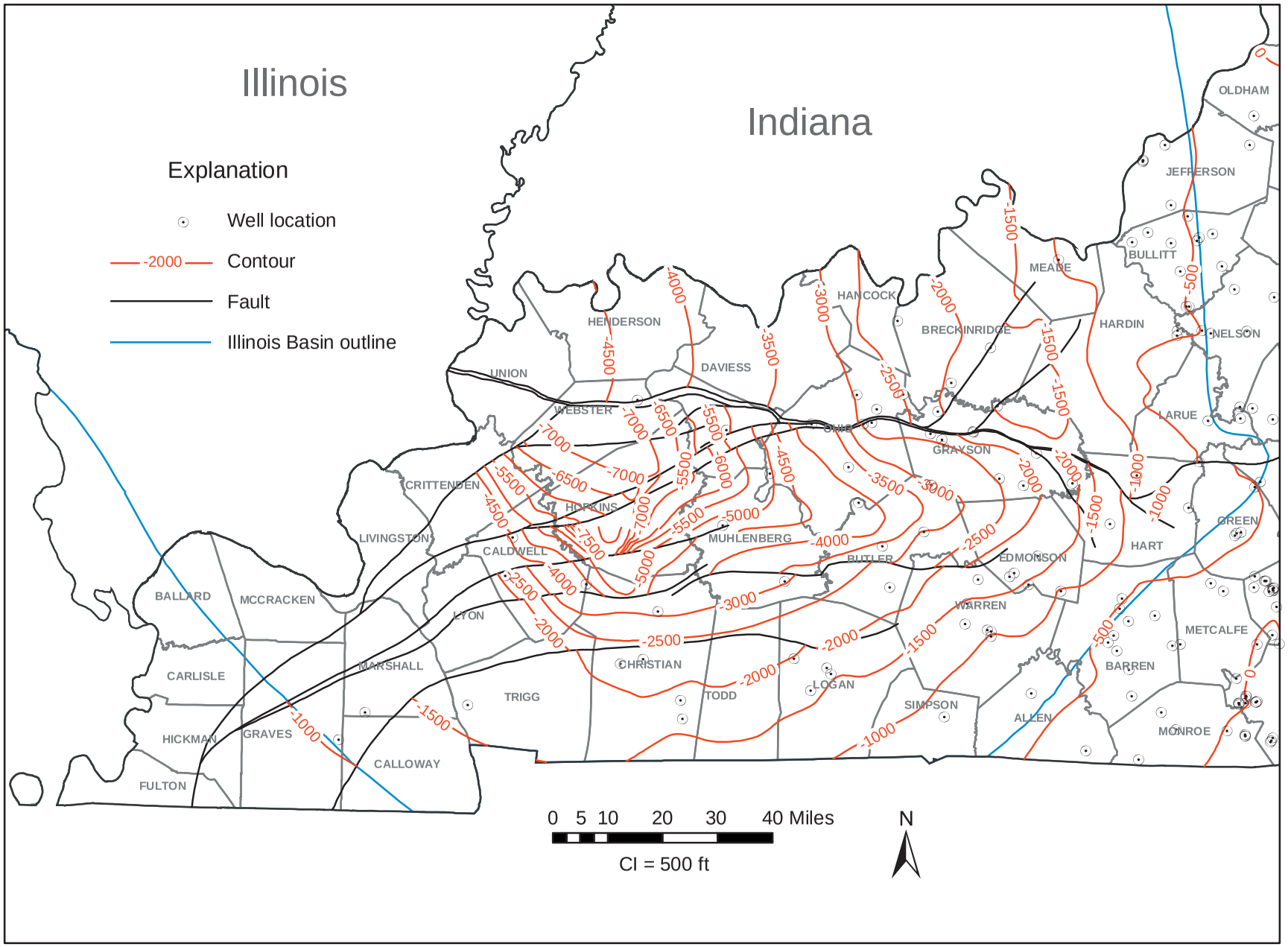

Figure A5-14 *Structure contours drawn on the top of the High Bridge Group, Illinois Basin, western Kentucky.*

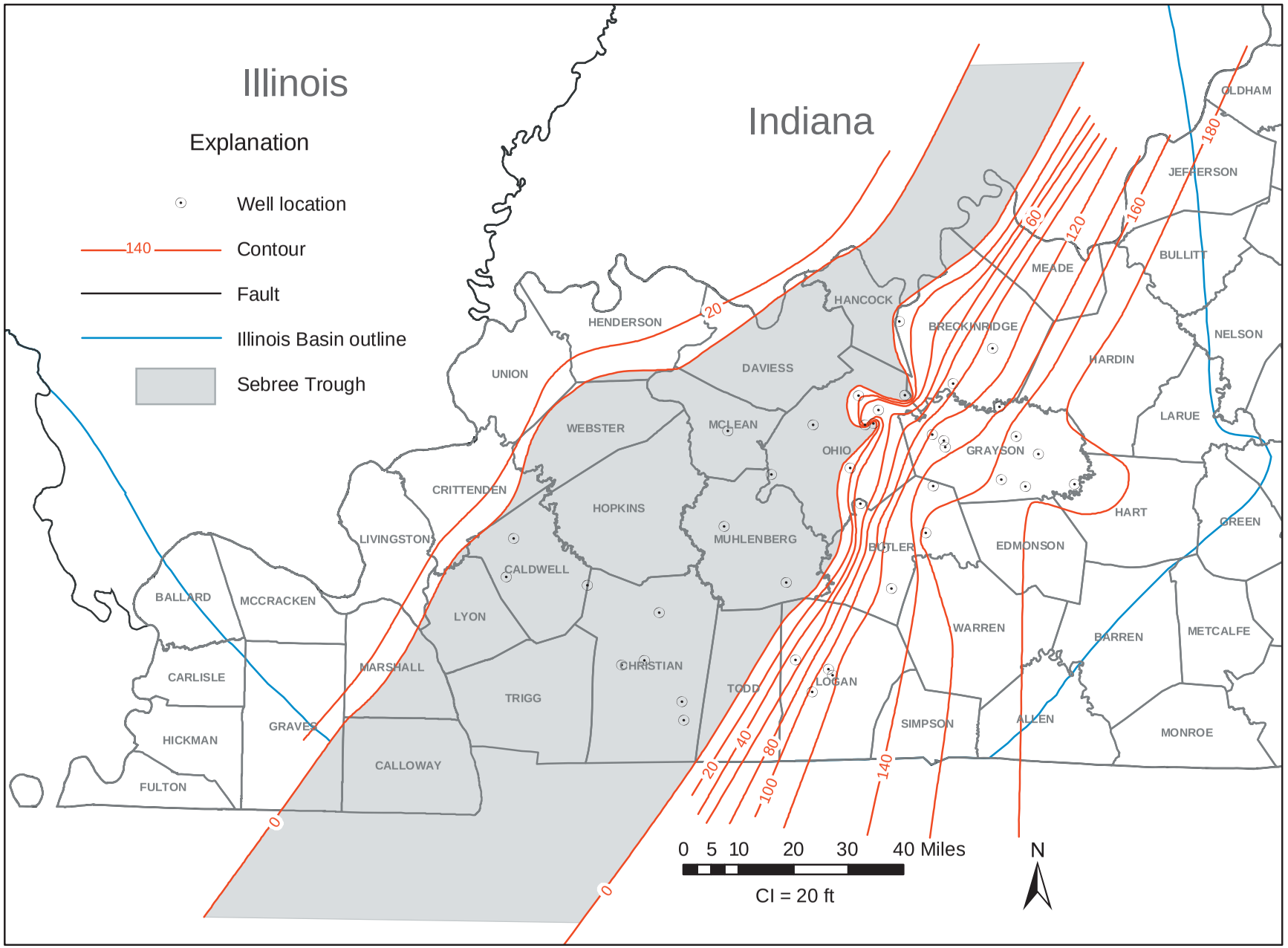

Figure A5-15 *Isopach contours of the Trenton Limestone, Illinois Basin, western Kentucky.*

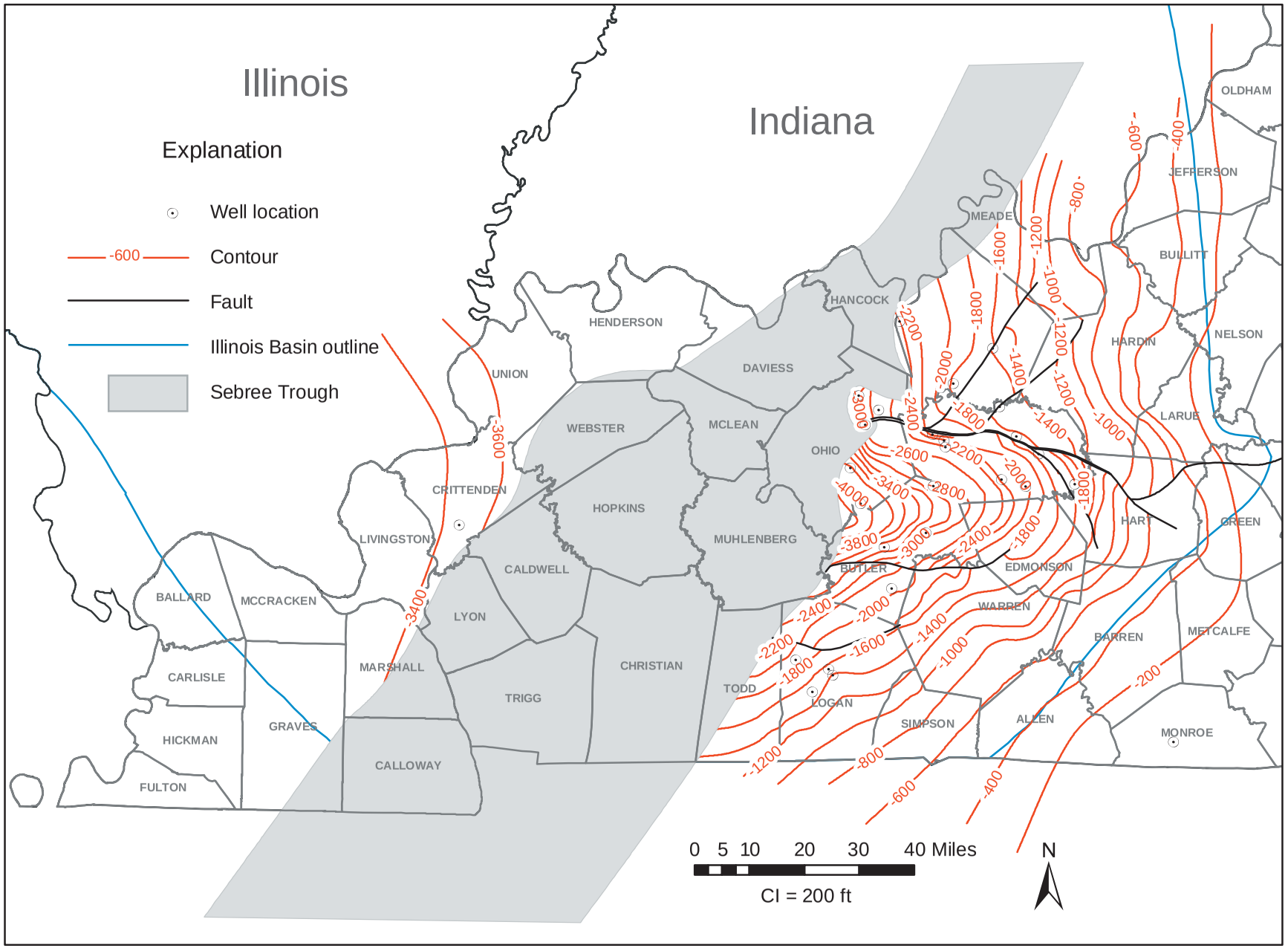

Figure A5-16 *Structure contours drawn on the top of the Trenton Limestone, Illinois Basin, western Kentucky.*

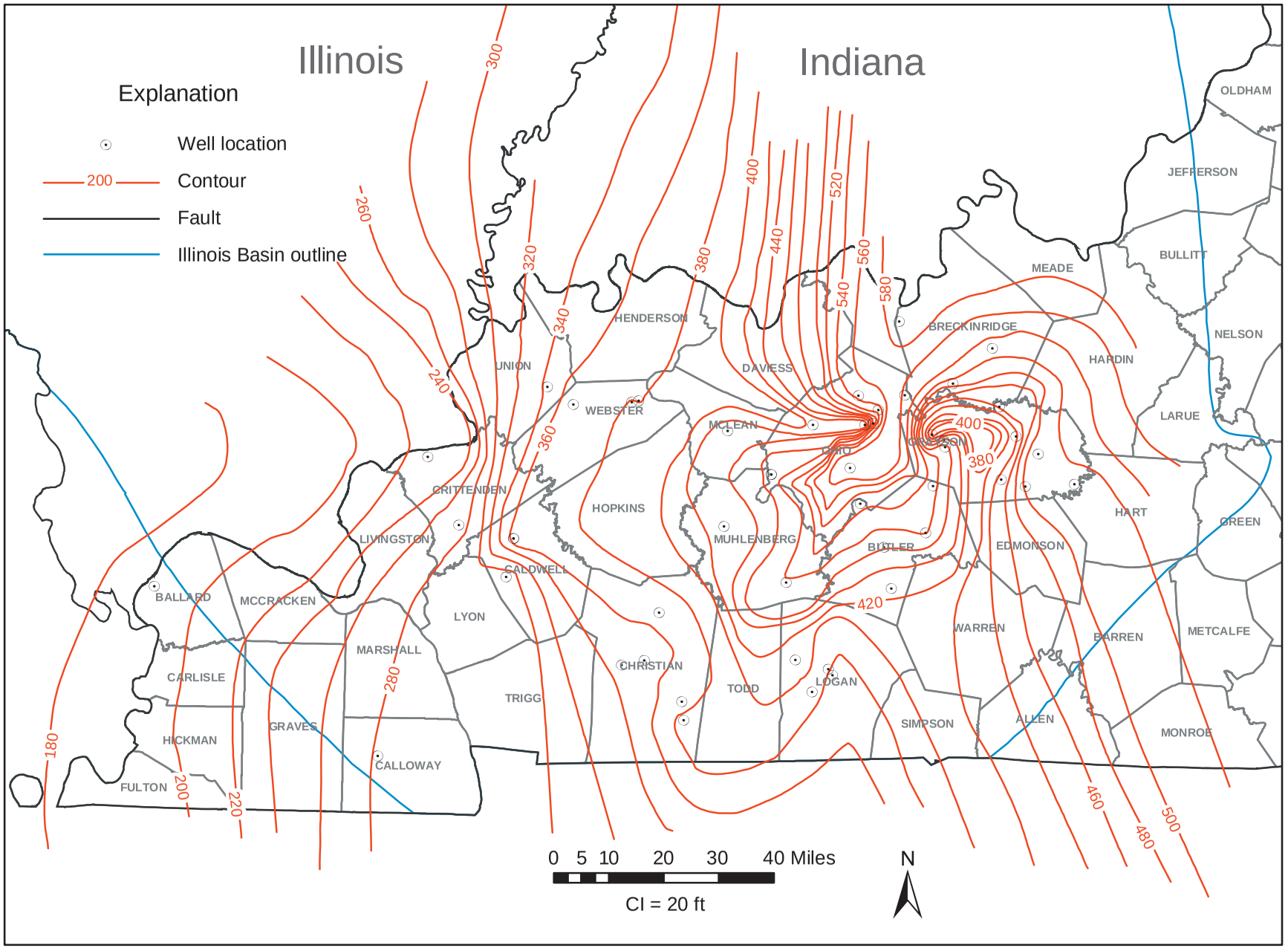

Figure A5-17 *Isopach contours of the Maquoketa Shale, Illinois Basin, western Kentucky.*

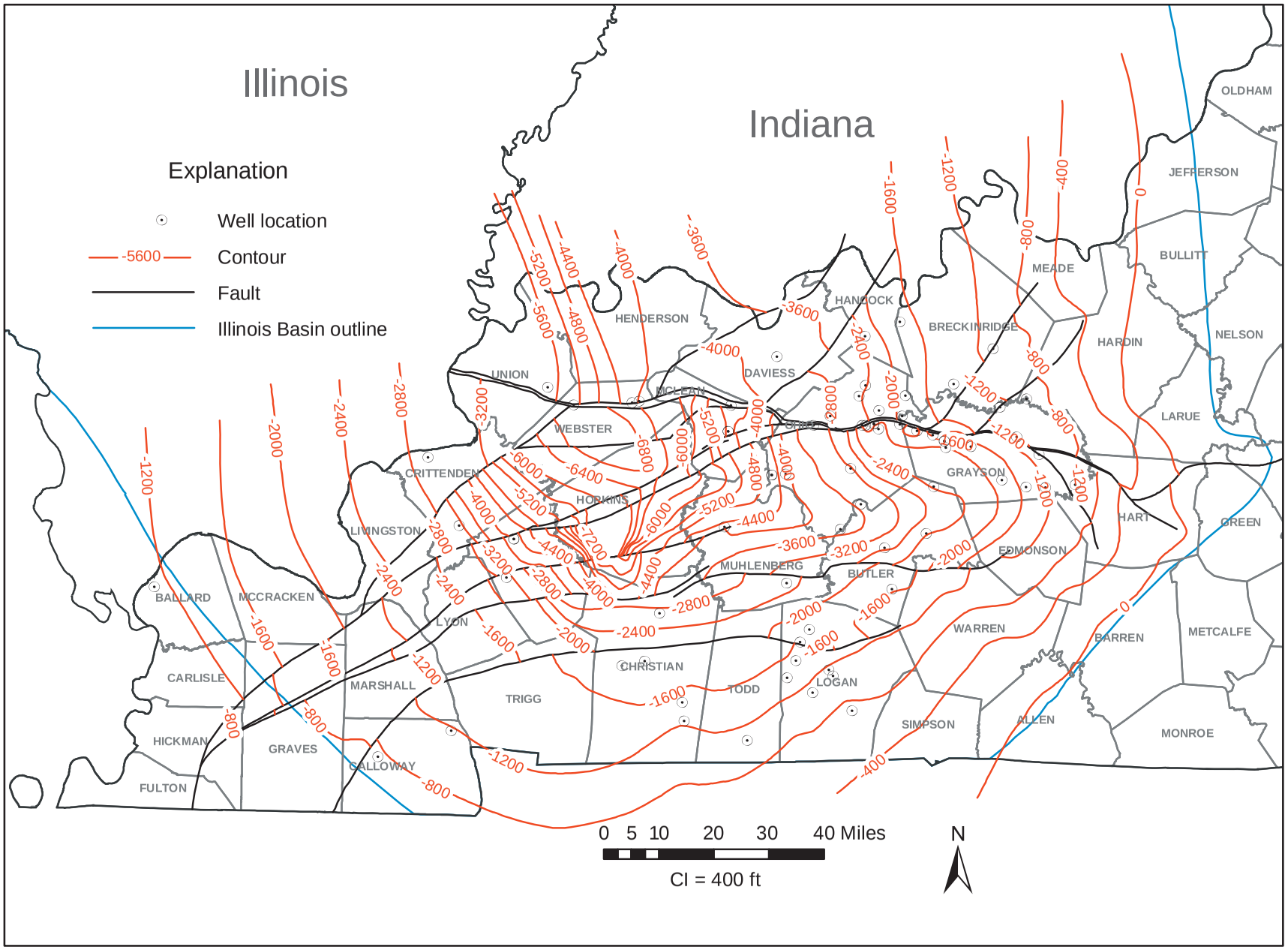

Figure A5-18 *Structure contours drawn on the top of the Maquoketa Shale, Illinois Basin, western Kentucky.*

Regulatory Framework for Geological Carbon Sequestration

The controversy over whether carbon dioxide (CO_2) is an air pollutant under the Clean Air Act (CAA) remains in contention between government and private sector groups that think emissions of CO_2 should be regulated. Currently, U.S. Environmental Protection Agency (USEPA) regulations do not define CO_2 as a pollutant, although CAA provisions are cited to support opposing positions on federal regulation of CO_2 emissions. Some states meanwhile, notably California and a group of northeastern states, have pressed forward with plans for automobile CO_2 emissions reductions or the development of a cap-and-trade scheme for CO_2. These positions are taken with a view toward the role of CO_2 as a heat-trapping gas within the atmosphere and therefore a cause for global climate change associated with combustion of fossil fuels. The process of CO_2 geological sequestration—consisting of capture, transportation, and storage of CO_2 in subsurface reservoirs called "sinks"—deals with a gas whose regulatory status is not well defined but may evolve rapidly in the near future.

Consequently, the development of a regulatory framework for handling CO_2 (not the same as mandating reductions in emissions from a given source or sources) must consider that CO_2 is currently not classified as a pollutant, waste, or contaminant. It therefore can be viewed as a *commodity* to be handled in a way that ensures public safety and that may be used to provide an economic offset to costs of sequestration should geological sequestration become desirable on a wide scale (Interstate Oil and Gas Compact Commission, 2005). Desirability of sequestration depends on proof of its safety, effectiveness in isolating CO_2, and cost relative to other options within future emissions controls strategy.

The broad national strategy as to how CO_2 will be viewed is currently being discussed. In July 2005, a three-judge federal court panel voted 2-1 to sustain the USEPA's denial of a petition by several environmental groups and states to regulate emissions of CO_2 from automobiles. One of the judges in the majority indicated that the USEPA had properly exercised its policy judgment by citing uncertainty in the effects of greenhouse gas emissions and concerns that CAA regulations may not be the best approach to addressing climate change. The dissenting judge indicated that the USEPA has the authority to regulate emissions of greenhouse gases and any air pollutant that may endanger welfare. Thus, the framework in which CO_2 may be considered an air pollutant subject to regulation as a pollutant rather than a commodity remains unsettled and will be subject to further review and interpretation.

The Underground Injection Control Framework

Underground injection of fluids for the production of oil and natural gas are regulated under the Safe Drinking Water Act, Underground Injection Control (UIC) Program. States cooperate with the USEPA under UIC regulations and may have primary enforcement responsibility ("primacy") for UIC

programs that meet minimum federal requirements. In the Illinois Basin, Illinois has primacy for UIC enforcement; in Indiana, enforcement is shared between the state and the USEPA; and, in Kentucky, the USEPA (Region 4) has responsibility for the program. The UIC program has established classes of injection wells that apply to two of the three geological sink options because these sinks are sources of either natural gas (coalbed methane) or oil. Injection wells that are designed for the enhanced recovery of oil or natural gas are designated UIC Class II wells, and there is ample precedent for these well designations in multiple states, especially in Texas and New Mexico, both of which have state primacy. We would anticipate that injection of CO_2 for enhanced oil recovery (EOR) or enhanced coalbed methane (ECBM) recovery from coal seams would meet UIC Class II requirements for well construction and siting, monitoring and testing, and recordkeeping and reporting. Informal discussion with Illinois officials at the Illinois Department of Natural Resources, Office of Mines and Minerals, Division of Oil and Gas, suggests that field pilot demonstrations of CO_2 EOR and ECBM in Illinois could be readily permitted as Class II wells, as would wider use of these techniques in a way analogous to their application in the Permian Basin of West Texas.

The permitting of CO_2 injection into a saline reservoir remains undefined with respect to UIC regulations. No recovery of hydrocarbons is involved, so a Class II designation is not applicable. In Texas, the Frio Brine Pilot injection well was judged to fall under UIC Class V, which was developed to handle the injection of nonhazardous fluids, where consideration was also given to the research character of the pilot test. The Interstate Oil and Gas Compact Commission (IOGCC) (2005) task force has recommended that, should USEPA regulate CO_2 injection for non-hydrocarbon recovery purposes under the UIC program, either a subclass of Class II be developed or a new classification be established. USEPA officials have indicated that some guidance may be sent to their regional office by the end of 2005 that may place pilot or field demonstration wells under a Class V permit, at least initially, perhaps following on the actions in Texas with respect to the Frio project. The distinction with respect to the saline reservoirs certainly pertains to the objective of the CO_2 remaining in the formation with little deliberate prospect of its recovery. It should be noted that, although EOR projects strive to operate using the minimum amount of CO_2 per barrel of oil, EOR with sequestration operations may have the additional objective of enhancing CO_2 retention in the reservoir once economic and/or technical limits to incremental oil recovery have been reached. Recovery of CO_2 at the conclusion of a given EOR project will depend on possibilities for future CO_2 use versus the cost of additional "new" CO_2, ease of transfer of recycled CO_2 to new project areas, and other considerations that may ultimately include the value of any carbon credits for the volume of sequestered CO_2 contained.

Current State Regulations Relevant to Sequestration

The IOGCC (2005) identified state statutes relevant to pipeline and natural gas storage regulation. Although these regulations are not likely to come into play during sequestration pilot testing, some aspects are of interest related to state regulation. In Illinois, the Illinois Gas Pipeline Safety Act (220 ILCS 20/) applies to "natural gas, flammable gas, or gas which is toxic or corrosive" and makes reference, as most state laws do, to the federal Natural Gas Pipeline Safety Act. No specific mention of CO_2 is made, and, as the IOGCC (2005) reported, no Illinois Basin state is considering any new laws related to a regulatory framework for CO_2. Whether CO_2 would be considered "toxic" because of its health effects at high ambient concentrations is unclear and was not discussed by IOGCC. In most situations, CO_2 is not considered toxic. Also in Illinois, the Gas Storage Act (220 ILCS 15/) applies to "the distribution, transportation, or storage of natural gas or manufactured gas." As it deals in detail with eminent domain for storage projects, this act also addresses the right to use geological stratum below 152 m (500 ft) for storage, implying that shallower formations could not be used for gas storage. This provision is highly unlikely to be a limitation on CO_2 sequestration, but it could indicate the state's interest in setting a depth criterion if saline reservoir CO_2 storage were to be addressed in future legislation. This is the sole geological reference in the act, and there are no references to the effectiveness of geological seals, an issue that may come up in the future, given that at least one natural gas storage facility in Illinois has known leakage issues.

The IOGCC (2005) identified parallel regulations in Indiana under IC 8-1 for pipelines and IC 14-37 for natural gas storage; however, IC 14-37 is more applicable to UIC Class II wells than the similarly named Illinois statute on gas storage facilities. An additional Indiana law, IC 14-38-2, dealing with test hole pollution and waste control, may apply to test drilling for CO_2 sequestration in saline reservoirs. This law provides for the permitting of test holes, exclusive of oil and natural gas drilling and coal exploration, that may be used for obtaining subsurface information to determine "the feasibility of an area for fluid disposal" and for "expanding the store of scientific knowledge of the geology of an area." IC 14-38-2 makes no reference to fluid injection, however, so it is likely that a permit under this law as well as some type of UIC permit would be required to carry out a sequestration pilot in Indiana. Unfortunately, Kentucky provided no response to the IOGCC survey of applicable state regulations.

Pipeline Permitting

Any test of CO_2 sequestration that would require development of pipelines for a larger-scale test, such as may occur for a one million tonne/year test injection under a Phase III project, would require additional permitting and the submission of a number of plans related to construction activities in Illinois. The Illinois Department of Natural Resources issues permits related to crossing or impacting rivers, lakes, and streams. Drilling under some of these features may be required to avoid impacts on riparian

environments. The Illinois Environmental Protection Agency (IEPA) issues National Pollution Discharge Elimination System (NPDES) permits related to impacts of siltation on streams or other discharge to streams during construction (e.g., water pumped from excavations). The IEPA requires a construction storm water permit for runoff from the right-of-way during pipeline construction. A county land use permit and a county site development (erosion control) permit would also be required. Although not necessarily required, an Agriculture Mitigation Agreement with the Illinois Department of Agriculture may be appropriate and may facilitate other permitting. Various plans would be required to deal with pollution prevention, spill prevention, inadvertent release of drilling mud, and unanticipated discoveries of historic artifacts or human remains. Similar permitting would be required in Indiana and Kentucky since NPDES permitting is part of a federal program.

Compilation of Results in Print and Digital Media

Some of the important Geographic Information Systems (GIS) maps included in this final project report are available as a suite of 1:1,000,000-scale PDF maps on the project CD and are planned for the Midwest Geological Sequestration Consortium (MGSC) project Web site. These larger maps represent select intermediate GIS layers and project results. Tabular project results from Phase I have been archived, and working project data files will be held for use in Phase II.

After final formatting and documentation, the resultant GIS data sets from Phase I will be shared through the NATCARB Internet portal, an interactive map service that allows users to browse, display, and query GIS layers and related data tables. Important GIS layers and data for major CO_2 sources and geological reservoirs in the Illinois Basin have been loaded into the NATCARB Internet portal by the geological surveys of Illinois, Indiana, and Kentucky (e.g., Figure 6-1). GIS layers are provided to NATCARB after the layers are deemed complete and have been formatted and documented appropriately.

At the time of this report, MGSC is actively sharing at least 42 regional and/or Illinois Basin-specific GIS layers (Table 6-1) and associated metadata through the NATCARB Internet portal (Figure 6-2).

Table 6-1. Tabulation of Illinois Basin GIS layers shared via the NATCARB Internet portal, by current layer grouping within the portal, at the time of this report.

GIS Layer[1]	Number
Aquifer	4
CO_2 sources	1
Coal	27 (30 to 49)
Geology	6
Oil	4 (4 to 12)
Sequestration layer	3 (4 to 8)

[1]Layers specific for each state are not included here. Additional MGSC layers potentially available to NATCARB are estimated in parentheses.

Table 6-1 is a "snapshot" of data dissemination work in progress at the time of this report. Numerous additional layers have the potential to be shared through NATCARB, although some discretion should be used so as to not overload the Internet portal with an abundance of data layers simply because they have been created in detail for MGSC project work (e.g., CO_2 storage for each of seven coal seams, compared with the summation of seam-specific results presented once).

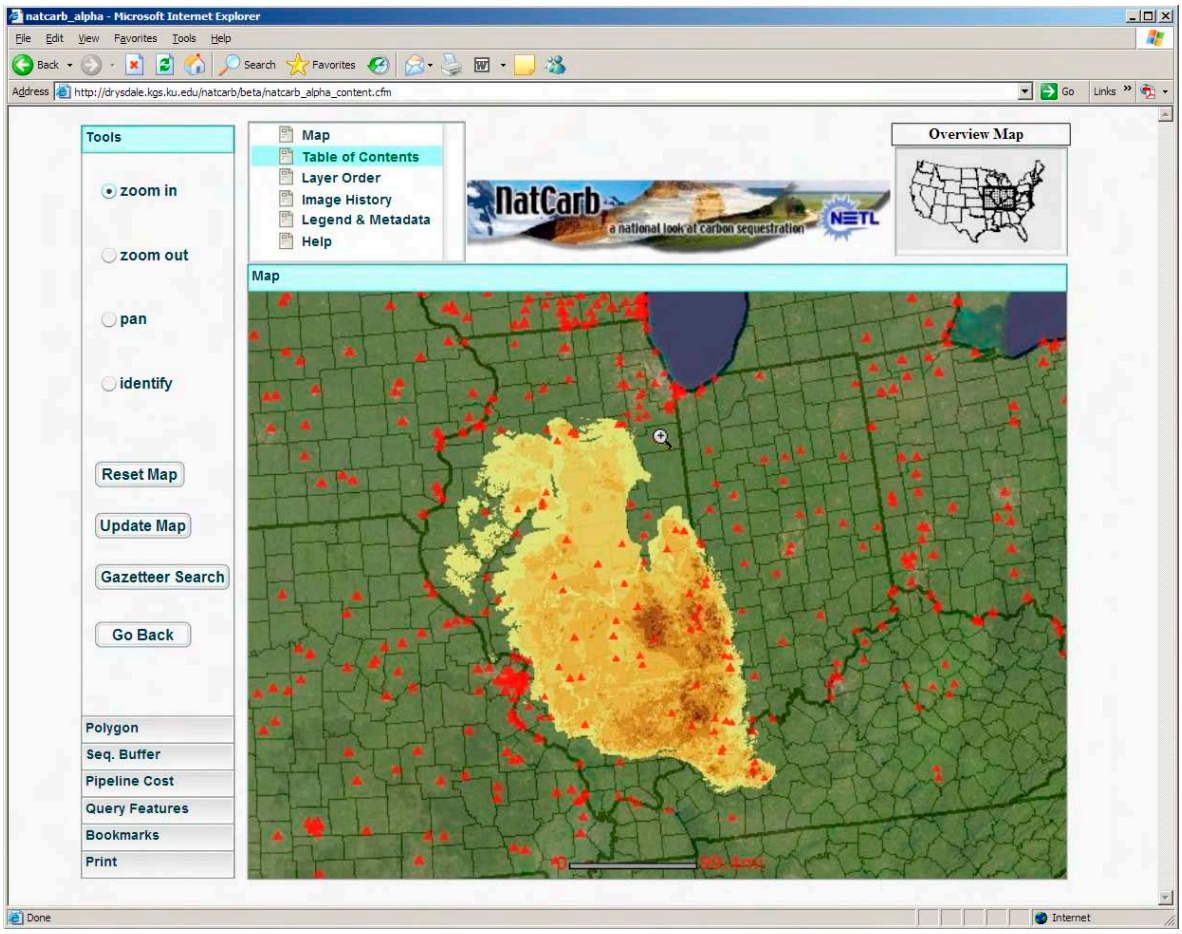

Figure 6-1 *Example of GIS layer display in the NATCARB Internet map portal. Shown is the cumulative average coal thickness layer for the Illinois Basin, where darker colors (browns) indicate areas of thicker coal, for the seven seams studied in Phase I. Overlain on this layer are the major CO_2 point-sources (in red triangles), as displayed for all partnerships.*

The descriptive "short list" of MGSC GIS shapefiles and tabular data that are planned to be made available for the Illinois Basin include the following:

1. locations and select emissions for major electric generators and industrial sources of CO_2 in tabular database and GIS layer format;
2. results of source/sink optimization study for integrated emissions capture, transport, and storage (tabular/GIS);
3. oil reservoir- and field-level properties and field-level results, including miscibility classification, cumulative production, original oil-in-place, and EOR and CO_2 storage results (tabular/GIS);
4. regional Mt. Simon and St. Peter Sandstone maps (GIS), saline reservoir properties data points (tabular/GIS), and CO_2 storage results (tabular/GIS);

Figure 6-2 *Example of GIS layers added to the NATCARB Internet map portal from a server machine in Illinois. Layers are added to a locally running Interactive Map Service (IMS) to enable a software/database connection with NATCARB. The layers are then activated for public interaction via the NATCARB's Web portal administrative interface.*

5. coal resource and coal quality properties base data points (tabular) and regional maps (GIS), and enhanced coalbed methane (ECBM)/CO_2-storage results for seven coal seams and cumulative coal (tabular/GIS);
6. additional shale/limestone/sandstone maps by formation, for the Illinois Basin region or for individual statewide extents (GIS); and
7. other miscellaneous reference geology or location base map layers (GIS).

In accordance with DOE direction on the public release and dissemination of data from all partnerships, the MGSC Phase I completed GIS layers will be available as fully documented shapefiles through the NATCARB and/or the MGSC Web sites.

Teacher/Student Training Materials for Geological Survey Workshops Offered to Educators for Grades 4 to 12

In fulfillment of subtask 10.2, the following educational materials have been designed to highlight the various aspects of geologic sequestration examined by the Midwest Geological Sequestration Consortium (MGSC) during Phase I of the carbon sequestration project. There are six individual activities focusing on climate change, geologic structure, petroleum uses, coalbed methane, saline reservoirs, and geologic sequestration. Each activity is divided into sections: (a) grade level, (b) learning standard assignment, (c) objectives, (d) background, (e) procedure, (f) references, (g) materials needed, and (h) student worksheets.

The educational materials submitted here for fulfillment of the Phase I deliverables are designed to be used in a series of workshops to be conducted during Phase II. At the time of this report, the materials have not yet had significant testing with students and teachers. The Phase I education deliverables will be tested and improved upon through workshops and contact with individual teachers during the first year of Phase II. Input from teachers and external reviewers will be incorporated, and the materials will be released in *GeoActivities Notebook* format (e.g., Treworgy, 2000) when completely vetted. Further external review is being sought from practicing educators and external reviewers. State Learning Standard assessments and age appropriateness will be tested and verified during the testing phase as well.

Phase I of the sequestration project was the development phase for educational materials and demonstrations. Phase II educational efforts focus on broadening and deepening the quality of the educational outreach effort. These materials and workshop opportunities provide an opportunity to educate teachers about climate change. The MGSC's goal is to reach teachers throughout the three partnership states, Illinois, Indiana, and Kentucky. Most science teachers in the tri-state area address climate change issues in their classrooms, which presents a tremendous opportunity to conduct more workshops than originally intended and to seek a broader audience. The first three workshops using the Phase I activities are planned for summer 2006.

The workshops are content driven, with activities developed to demonstrate difficult-to-understand concepts and address commonly held misconceptions about climate change (Greenberg, 2005). All of the educational materials developed in Phase I will be utilized in the workshops. In addition, pre-existing materials from other sources, such as the *Keystone Center Global Climate Change* curriculum (Keystone Center, 2005), will be incorporated into the workshop format. The goal is to provide a well-rounded, 2-day informational teacher workshop focused on global warming, climate change, the greenhouse effect, sequestration of carbon dioxide (CO_2), and related topics.

In addition to the scheduled workshops and provided educational materials, MGSC's work on these products will continue throughout Phase II. As work with teachers progresses, new inputs refine how materials are taught and which materials are used. Research will be conducted on how to support teachers after their participation in workshops and receipt of educational materials. Additional materials will likely be designed and tested during the initial workshop testing period. Continued development through Phase II is important as new data become available. Submitted with the educational materials is an outline of the workshop format and a sample schedule of the workshop subjects. These materials were developed by Sallie E. Greenberg at the Illinois State Geological Survey. For further information, contact greenberg@isgs.uiuc.edu.

Climate Change Issues, Carbon Storage Options, and Our Future Geologic Sequestration Workshop Description

Workshop Details:

- 20 to 25 participants per workshop

- 2 testing workshops Year 1 of Phase II; 4 to 5 workshops per year (or more) for duration of Phase II

- Location options:
  - Illinois State Geological Survey
  - Partnership locations
  - Rock Island Regional Office of Education (ROE)
  - Other state ROEs
  - Carbondale Science Center
  - Consortium venues

- Give participants as many educational materials and tools to support use of modules in the classroom as possible.

  - Suggested ISGS materials:
    - GeoActivities Notebook
    - Supplemental CD with activities (in development)
    - Fossil posters
    - Bedrock geology map
    - Carbon poster
    - Geoscience Education Series 15: Illinois Fossil Guide
    - Geoscience Education Series 16: Illinois Rock and Mineral Guide

        - Geoscience Education Series 17: Groundwater
        - Geoscience Education Series 18: Land-Use Decisions and Geology
        - Block model templates
        - Kits for conducting activities
    - Resources and educational materials from Consortium members
        - Illinois Office of Coal Development
        - Indiana Geological Survey
        - Kentucky Geological Survey
        - Oil and Gas Company and Association Literature
        - Ameren
        - Illinois Corn Growers

- Obtain invaluable input into curriculum changes and testing from teachers.

- Tie activities to National Learning Standards and consortium states of Illinois, Indiana, and Kentucky.
- Define audience:
    - Teachers throughout Illinois, Indiana, and Kentucky will be targeted.

    - These workshops will have broad-based appeal to teachers outside of the "test area."

- Estimate potential impact:
    - These workshops have the potential, by educating teachers, to impact thousands of students in Illinois and the Consortium States each year:

1 teacher with 25 students/year for 20 years	= 500 students impacted/teacher/career
25 teachers/workshop	= 12,500 students impacted/workshop
10 workshops	= 48,000 students impacted/workshop/year

- Build stronger partnerships:
    - Incorporate Keystone activities in workshops
    - Add Gulf Coast Carbon Center activities by Hovorka et al. (2005)

Climate Change Issues, Carbon Storage Options, and Our Future
Geologic Sequestration Workshop

Sample Schedule

Workshop Leaders
Sallie Greenberg and Bob Vaiden
Illinois State Geological Survey

Workshop Budget Schedule (Day 1)

Thursday Evening, June 15	Time
Registration/Introduction	**4:00 – 6:00 p.m.**
Workshop objectives and goals	
College credit information and paperwork	
Icebreaker Dinner	**6:00 – 7:00 p.m.**
Climate Change Keynote Speaker Presentation	**7:00 – 9:00 p.m.**

Workshop Schedule (Day 2)

Friday Morning, June 16

Geology of the Ice Age through the Present	**8:30 – 10:00 a.m.**
ACTIVITY: [To be determined.]	
DEMONSTRATION: Geologic Time Line	
An Overview of Quaternary Geology through the Present Day	
Climate Change and What We Can Do About It	
ACTIVITY: Is Our Climate Changing?	
ACTIVITY: Pollen Time	
Morning break	**10:00 – 10:15 a.m.**

Carbon Cycle **10:15 a.m. – 12:00 p.m.**

Short-term Carbon Cycle

Long-term Carbon Cycle

DEMONSTRATION: [To be determined.]

ACTIVITY: [To be determined.]

Carbon Sequestration

DEMONSTRATION: [To be determined.]

ACTIVITY: [To be determined.]

Lunch. Box lunch provided. **12:00 – 12:45 p.m.**

Friday Afternoon, June 16

Geologic History of the Illinois Basin **12:45 – 1:30 p.m.**

Build Illinois Presentation

DEMONSTRATION: Block Model

Groundwater Resources of the Illinois Basin **1:30 – 2:00 p.m.**

Groundwater, wells, and water contamination

DEMONSTRATION: Groundwater in a Jar

Groundwater in Action (Model)

Water resources across Illinois

ACTIVITY: A Groundwater Problem

Afternoon break **2:00 – 2:15 p.m.**

Saline Reservoirs **2:15 – 2:45 p.m.**

What are saline reservoirs, where can they be found?

How do they relate to CO_2 storage

ACTIVITY: [To be determined.]

Enhanced Oil Recovery and Storage **2:45 – 3:30 p.m.**

Illinois Basin Oil Industry, oil wells, drilling for oil, resources, and reserves

ACTIVITY: Petroleum All around Us

ACTIVITY: Keystone Enhanced Oil Recovery Demonstration

Coalbed Methane Recovery and Storage **3:30 – 4:15 p.m.**

Coal: The Illinois Basin fuel, coal usage, the ins and outs of coalbed methane

Carbon Comes Full Cycle—Workshop Wrap-up **4:15 – 4:30 p.m.**

APPLICATION TO LEARNING STANDARDS

Evaluation Forms

Workshop Conclusion

Petroleum in Our Daily Lives

Grade Level: 4 to 8

Authors: Sallie E. Greenberg and Robert C. Vaiden

Illinois Learning Standards: See Learning Standards Matrix

11.A. 1a, b, 2a, 3d, 4a-c
12.C. 1a, 2a, 3b, 5a
12.E. 1c, 2c, 3c
13.B. 1d, e, 2a–f, 4c, d, 5c, d

Objective:

- To explore and discuss the many ways petroleum is used in our daily lives and how it contributes to our quality of life.

Background:

The term *petroleum* comes from the Latin, *petr-*, "rock," and *oleum*, "oil." It literally means oil produced from rock. Petroleum is formed from organic matter, primarily microscopic phytoplankton and bacteria, trapped in marine sediments. The organic matter trapped with clay becomes the sedimentary rock called shale. During this rock-forming process, the carbon from the organic matter turns into oil and natural gas. The petroleum is lighter (less dense) than water, so it migrates upward through porous rocks, such as sandstone, until it reaches an impermeable rock and is trapped within geologic structures, such as an anticline. Petroleum is recovered by drilling wells and pumping the petroleum from the ground.

Petroleum currently is a very important resource in the technological society of the United States. In 2000, 40% of the total U.S. energy consumed was petroleum; 97% of this was used for transportation. (The remaining 60% energy usage was 25% natural gas, 23% coal, and 12% nuclear, hydroelectric, geothermal, and others). In addition to being our major source of fuel and electricity generation, petroleum is also used for many other purposes, such as starting material for plastics and synthetic fibers, dyes, adhesives, alcohols, explosives, fertilizers, weed killers, insecticides, insect repellents, solvents, industrial greases and waxes, refrigerants, synthetic rubber, polystyrene, polyethylene, and asphalt. All of the plastic in our lives comes from petroleum. We walk on petroleum (in our shoes), we wear petroleum (in our clothes), we live in petroleum (in our houses), we sit on petroleum (in our chairs,

cars, and sofas), and we use petroleum to cure illness (in our medicines). Our roads are made from asphalt, which is made from petroleum.

Petroleum, however, is a finite natural resource. Current estimated reserves are 0.37 to 0.48 trillion m^3 (2.3 to 3 trillion recoverable barrels). At our present (2000) consumption rate of 11 L (3 gallons) per day per person, and an expected 1.2% increase annually, petroleum reserves worldwide will eventually run out. How will our lives change when this happens? What steps can we take now to prevent major changes in our lives?

Using petroleum has risks, as well as benefits; burning petroleum and other fossil fuels creates carbon dioxide, a greenhouse gas, which is emitted to the atmosphere.

Materials:

2 plastic tubs
2 large labels
A variety of common items made from petroleum
A variety of common items not made from petroleum

Procedure:

This activity is an introductory demonstration, designed to be a jumping-off point for discussions about petroleum and about natural resources in our everyday lives and our dependence upon them.

Collect a variety of items from your home or classroom using the attached list of common household items made from petroleum (based on information from the American Petroleum Institute). Have each student bring in a small item from their home. To maintain an element of surprise in the activity, when you ask the students to bring an item, do not tell them the full nature of the demonstration.

The following day, place two tubs in the front of the classroom. Label one tub: Made from Petroleum. Label one tub: Not Made from Petroleum. Ask the students to deposit their items in the appropriate tub when they enter the classroom. The activity may be enhanced and discussion may be facilitated if some items are placed in the tubs prior to the student input. Choose items that you would be surprised to learn are made from petroleum, such as mascara or medicine capsules. These surprise items will add interest to the activity discussion.

After all of the items have been placed in tubs, go through each item as a group and discuss whether the items are made from petroleum or not. Were any items incorrectly placed? Were there items that

surprised the class? Which tub had the most items? How many common household items are made from petroleum? What will we do if we run out of petroleum? Which items could we do without? This activity may be used as a starting point for a discussion about dependency on a limited natural resource or international politics.

References:

Albrandt, T. S., and P. J. McCabe, 2002. Global petroleum resources: A view to the future. Geotimes, v. 47, no. 11, p. 11–18.

Kopaska-Merkel et al. 2005. Why do we need petroleum? www.beloit.edu

The Paleontological Research Institution www.priweb.org

Purdue University www.chemed.chem.purdue.edu

Skinner, B. J., and S. C. Porter, 1992. The Dynamic Earth, 2nd edition. John Wiley & Sons, Inc. New York, NY.

U.S. Department of Energy www.eia.doe.gov/neic/infosheets/petroleumproducts.htm

Contributed by Sallie E. Greenberg and Robert C. Vaiden, modified from Kopaska-Merkel et al. (2005).

Home Products Containing Petroleum
(Based on information from American Petroleum Institute)

Adhesive tape
Air conditioners
Ammonia
Antihistamines
Asphalt paving
Asphalt roofing
Aspirin
Astroturf
Audio cassette tapes
Automobile bumpers
Automobile safety seats
Awnings
Badminton birdies
Bandages
Baseboards
Bathtubs
Blankets
Blenders
Board games
Bookcases
Bubble gum
Building adhesives
Buttons
Cabinets
Cable housings
Cameras
Candles
Car tires
Carpets
Cat toys
Caulk
Ceiling tiles
Clocks
Clothing
Coffee makers
Cold cream
Compact disks
Combs and hair brushes
Computers
Contact lenses
Cortisone
Cosmetic cases
Countertops
Crayons
Credit cards
Dentures
Deodorant
Detergents
Dishes
Dishwashing liquids
Dolls
Door mats
Doors
Eyeglasses
Eye shadow
Fabric softeners
Fertilizer
Fishing poles
Flashlights
Flavoring
Flea collars
Floor polish
Flower pots
Food containers
Food preservatives
Frisbees
Furniture
Garage doors
Gasoline
Gloves
Hair curlers
Hair dryers
Hair dyes
Hearing aids
Home heating oil
Hoses
Ice chests
Ink
Insecticides
Insulation
Laundry baskets
Life jackets
Light housings
Linoleum tiles
Lipstick
Lubricants
Luggage
Lunch boxes
Mascara
Mattress stuffing
Molded window frames
Mops and brooms
Motion picture film
Nail polish
Natural gas
Nylon rope
Outlet covers
Paint
Paint brushes
Pan handles and lids
Pantyhose
Perfumes
Pet kennels
Petroleum jelly
Phonograph records
Photographs
Picture frames
Pillows
Ping-pong paddles
Plastic dog bones
Plastic fencing
Plexiglas
Plumbing fixtures
Plywood
Purses
Rain gutters
Raincoats
Recycling containers
Refrigerants
Refrigerator liners
Roller-skate wheels
Rubber cement
Shampoo
Shaving cream
Shingles
Shoe polish
Shoes
Shopping bags
Shower curtains
Showers
Skis
Sleeping bags
Sneakers
Solvents
Sports headgear
Stereos
Sulfa drugs
Telephones
Televisions
Tennis balls
Tents
Toasters
Toilet seats
Tool boxes
Toothbrushes
Toothpaste
Trash bags
Umbrellas
Upholstery
Videotapes
Vitamin capsules
Waste containers
Wheelbarrows
Winter jackets
Zippers

Some of these items may be replaced with items not made with petroleum. Find the items which can be made with natural materials, such as wood or paper instead of plastic or synthetic fibers. Where do the alternative resources come from? What materials can you replace each item with? **Why don't we?**

Climate Change throughout Geologic Time

Grade Level: 4 to 12
Authors: Sallie E. Greenberg and Robert C. Vaiden
Learning Standards: See Learning Standards Matrix

Objectives:

- To visually portray the magnitude of geologic time since the Earth's formation and to correlate the climate changes that have occurred throughout geologic time.

- To help understand the relative chronology of certain "milepost" events.

- To discuss geologic history (e.g., when dinosaurs lived and past climate changes).

Background:

The earth is like a history book that writes its story in the layers of rock. Geologists read those stories like pages in a book and piece together the geologic history of our planet. We discover periods that had climates vastly different from our present climate, periods of huge oceans and massive swamps, shifting tectonic plates, and repositioning of continents. We discover that many species lived and have died out, there were mass extinctions, and innumerable other events occurred. Clues to these past environments are left behind, recorded in rocks.

Over millions of years, the planet has seen every climatic condition imaginable, from the coldest to the hottest. There have been radical changes in climate—from about 6°C (42.8°F) colder than the global average 475 to 425 million years ago to 10°C (50°F) higher than global average in the Permian period (300 to 250 million years ago). Presently, we are well below the long-term global average temperature for the last 550 million years. Long-term severe changes in climate are nothing new on planet Earth. However, climate changes that occur on a human time scale (the last 10,000 years) could seriously affect our ability to live on the planet.

Climate change and global warming are currently being debated by scientists, governments, and individuals. Is our climate changing? Is the world heating up, or is it cooling down as some scientists have suggested? Are we affecting climate change and/or global warming by burning fossil fuels? Many questions exist and although there are few confirmed answers, continuing research is being done.

We do know that greenhouse gases such as carbon dioxide (CO_2), methane, and water vapor are being released into the atmosphere at greater rates than ever before. Millions of years worth of carbon stored in the earth in the form of oil, gas, and coal is being combusted to provide energy so we can drive our cars, heat our homes, and manufacture the goods we depend upon for our quality of life. Reducing the amount of CO_2 released into the atmosphere may slow global warming trends observed in the last decade to 15 years. As we understand the potential for global climate change due to the burning of fossil fuels and the resulting release of CO_2, it makes sense to research the ways in which we can isolate CO_2 from the atmosphere. Carbon sequestration is the isolation of carbon dioxide (CO_2) from the Earths atmosphere. Sequestration can play a significant role in preventing continued CO_2 buildup in the atmosphere.

Materials:

2 white or light-colored ropes, 7.0-m (23-ft) long
Black marking pen
2 sets of placards mounted on poster board or laminated measuring tape or stick
Stuffed animals: 4 flamingos (tropical), 3 penguins (arctic), and 2 robins (temperate)
Tags

Preparation:

The entire 7.0-m (23-ft)-long rope corresponds to all of geologic time from the formation of the planet until the present (4.6 billion years). Use the marking pen to mark the rope for each event. Tie a small tag to the rope at that spot. Ten placard or poster boards are used to make signs for specific geologic events in Earth's history. These placards are numbered so that the events are in chronological order (optional), and corresponding numbers are written on tags tied to the rope at specified lengths. Students may illustrate the placards.

Rope length	Geologic event	Calendar comparison	Millions of years ago
0 ft	Origin of planet Earth	00:00:01 on January 1	4,600
4 ft	Oldest rocks found at surface	mid-March	3,800
5 ft 6 in	Earliest sea life	early May	3,500
20 ft 3.6 in	Beginning of Paleozoic Era	late November	540
21 ft 6 in	Coal deposits formed	early December	300
21 ft 9 in	Beginning of Mesozoic Era	about December 10	245
22 ft	Dinosaurs become dominant	about December 15	190
22 ft 8 in	Beginning of Cenozoic Era	December 26	65
22 ft 11.5 in	"Ice Age"	1 min 15 sec before midnight on December 31	2.5
23 ft	All recorded human history	about 11:59:45 until midnight on December 31	6,000–0 yrs

Climate Change Symbols:

Purchase the birds or ask students to draw them, bring them from home, or otherwise create them. The birds represent the "climate conditions" in a given time period. The flamingo represents very hot climates, the robin represents temperate climates, and the penguin represents very cold climates. Other symbols can be used, so you may want to ask your students to come up with their own scheme.

Prepare the climate change indicators by attaching a tag to the animal indicating the time period it represents: penguins (cold periods), flamingos (hot periods), and robins (warm periods). Use the following chart to make specific time tags for each bird:

Bird	Climate conditions	Geologic time (millions of years)
Flamingo	Hot	500–475
Penguin	Cold	460–400
Robin	Warm	400–375
Flamingo	Hot	375–350
Penguin	Cold	350–300
Flamingo	Hot	300–200
Robin	Warm	200–125
Flamingo	Hot	100–50
Penguin	Cold	50 to Present

Procedure:

Ask for 10 volunteers to come to the front of the room (or hall outside the room) and give each one a placard. Spread out the 7.0-m (23-ft) length of rope and ask the volunteers to help hold up the rope at the location corresponding to their placard (numbers are on the rope and on the back of each placard).

Congestion will occur in the area of the rope representing the more recent geological record (Paleozoic Era to the present). This congestion is part of the visual impact showing how these major Earth events have all occurred in the relatively "recent" time of Earth's history. The person with the youngest placard (No. 10, All recorded human history) is told to just place a finger against the end of the rope.

Once all of the volunteers are in position, the instructor(s) can go to each position and briefly discuss the geologic event. Mention that it was the science of geology that first presented the evidence for the age of the Earth and provided the interpretation of the chronology of events in this history. Mention that it would take four or five additional ropes of this length to record all time back to the formation of the universe (about 16 billion years ago). Discussion could possibly include how we know the timing of the event and what factors may have caused the event (e.g., Mesozoic-Cenozoic transition). Use this activity to field questions related to geologic time.

Ask for an additional 9 volunteers, and give each one a tagged bird. Have the students spread themselves out along the rope according to the time range their bird represents. Mention that the climate on Earth has changed significantly over time. Ask students to make connections between the climate of the time with the events that were occurring at that time (e.g., 300 million years ago coal swamps were being deposited and the climate was hot). Ask the students whether the climate conditions help them understand the events occurring at that time. Mention also that climate change is a natural occurrence. Ask the students what they expect to happen if our climate changes again. Is this bad for the Earth? Is this bad for humans?

Alternate designs:

Numerous variations on this design are possible. For example, additional placards could be made to highlight additional events in Earth's history. Or a rope could be made showing only geologic time since the beginning of the Paleozoic Era, or only for the Cenozoic Era. Other time line activities may be found on the Kentucky Geological Survey Web site: http://www.uky.edu/KGS/.

Geologic eras:

Cenozoic (recent life): 65 million years ago to present time
Mesozoic (middle life): 245 million years ago until 65 million years ago
Paleozoic (ancient life): 540 million years ago until 245 million years ago
Precambrian: All geologic time before the Paleozoic

Adapted by Sallie E. Greenberg and Robert C. Vaiden, from Michael J. Chrzastowski.

Seeing Underground

Grade Level: 6 to 12
Authors: Sallie E. Greenberg and Robert C. Vaiden
Learning Standards: See Learning Standards Matrix

Objective:

- To examine and interpret the relationship between surface patterns of rock units and how they translate to geologic structures beneath the Earth's surface.

Terms:

Cross section, basin

Background:

Geologic maps show the bedrock surface below soils and glacial deposits. Observing the patterns created by the rock units on a geologic map can often lead to interpretation of underlying geologic structures, such as basins, domes, anticlines, and synclines. Observed patterns are the geologist's first clue that structure exists beneath the surface sediments.

Illinois, Indiana, and Kentucky contain a "hidden" structure known as the Illinois Basin. This Basin began forming more than 500 million years ago when the area was covered by an ancient ocean. As the land subsided, the center filled with sediments and organic material from marine animals and plants. For millions and millions of years, the basin continued to sink and fill with ocean sediments. By the Pennsylvanian age, 325 to 286 million years ago, the deep ocean had receded, and Illinois, Indiana, and Kentucky were a great, swampy, river delta. More sediments were deposited into the Illinois Basin, many came from terrestrial plants and animals. With time and pressure, these organic Pennsylvanian deposits became the coal we use for fuel today.

Using maps to understand the underlying geology is a major tool in the geologist's tool box. This activity helps students make the connection between what they see on a map surface and what lies underground. Two stratigraphic principles are assumed when interpreting geologic history from rock layers:

1. The Principle of Original Horizontality—sediments are generally deposited as essentially horizontal beds. If we find tilted or folded rock layers, tectonic forces have acted upon them.

2. The Principle of Superposition—each layer of sedimentary rock in an undisturbed section is younger than the layer beneath it and older than the one above it.

Materials:

Geologic map handout of Illinois Basin
Worksheet
Pencil

Procedure:

Discuss with the students about geologic maps and what they are used for—"to see underground," that is, to show the bedrock surface below the unconsolidated material at the Earth's surface. You can use the *Fossils of Illinois* poster to discuss with students what they see when looking at the geologic map of Illinois or you can use the geologic map handout of the Illinois Basin. Work with students to recognize that patterns, such as a bull's-eye, can be observed on the map. Familiarize students with the stratigraphic principles of original horizontality and superposition. These principles can be difficult to visualize when actually looking at maps. This exercise is designed to help students answer the question, How does the map help us know what it looks like underground?

Pass out the worksheet. Instruct students that they are going to learn to translate what the map of the surface tells them about the sub-surface of a slice of the Earth. A cross section shows what a vertical slice would look like if we could take one.

Students will connect the rock units on the worksheet. When connected properly, the outline of the rock units will show a basin. Instruct students to connect the contacts between each rock unit with its counterpart on the other side of the diagram. Draw a line between the two end segments. Is it a straight line? A curved line? If you are having difficulty visualizing the underground structure, draw the layers exactly as they are shown in the key and then connect the edges of each unit with those at the surface. The basin structure will appear.

This diagram of the geology of the Illinois Basin is very generalized. A more detailed cross section can be seen on the Bedrock Geology Map of Illinois or in the GeoActivity Missing Pages.

This diagram illustrates the pattern that 3 geological formations (or strata) have formed on the landscape surface. The strata are color-coded as shown in the legend in the lower left. If we "slice" the landscape, what pattern would we see on the face of the slice? This "slice"—or cross section—would show the underground structure that produces the surface pattern. On the face of the slice, draw the underground structure of the 3 strata layers to create a cross section.

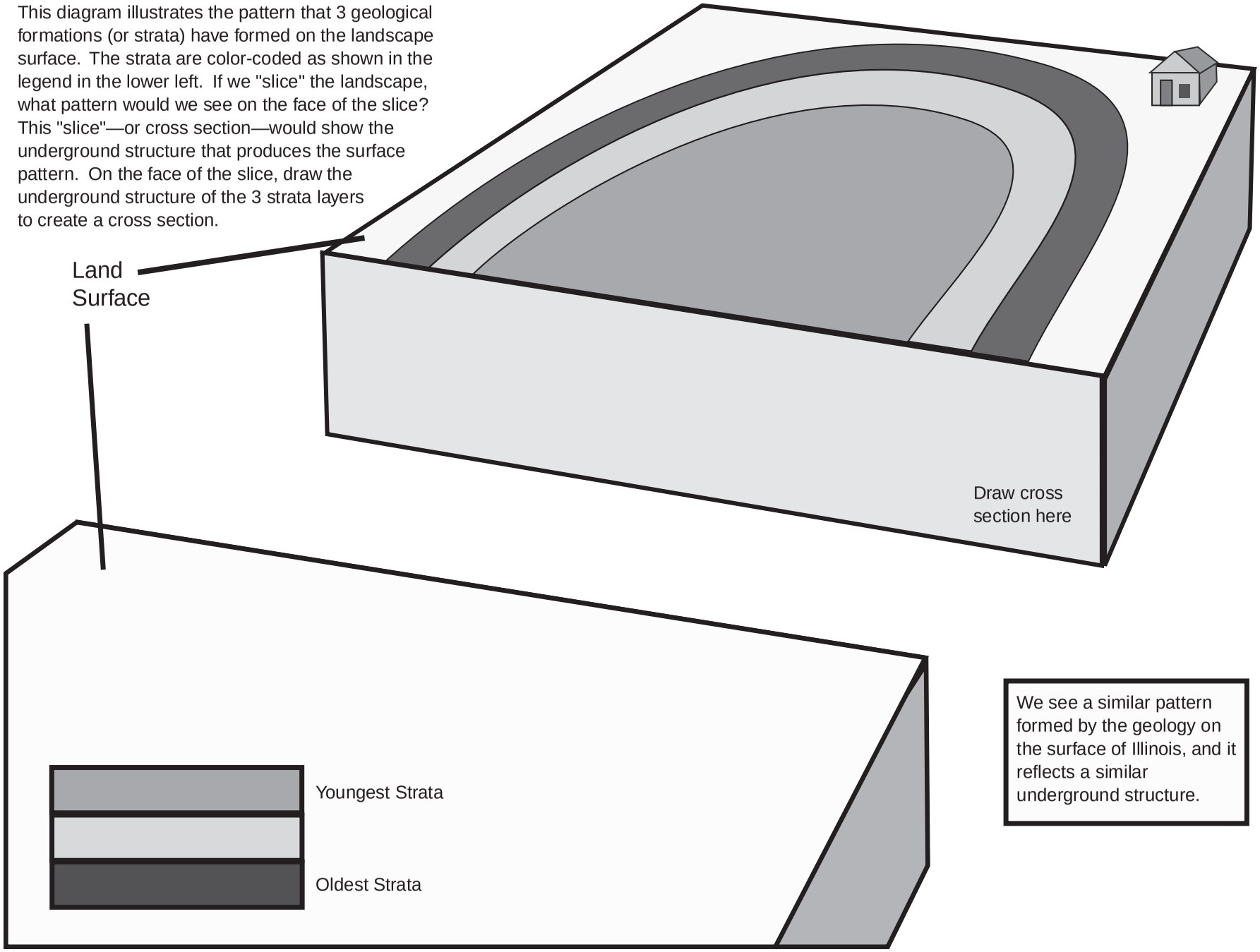

We see a similar pattern formed by the geology on the surface of Illinois, and it reflects a similar underground structure.

Answer Key

This diagram illustrates the pattern that 3 geological formations (or strata) have formed on the landscape surface. The strata are color-coded as shown in the legend in the lower left. If we "slice" the landscape, what pattern would we see on the face of the slice? This "slice"—or cross section—would show the underground structure that produces the surface pattern. On the face of the slice, draw the underground structure of the strata layers to create a cross section.

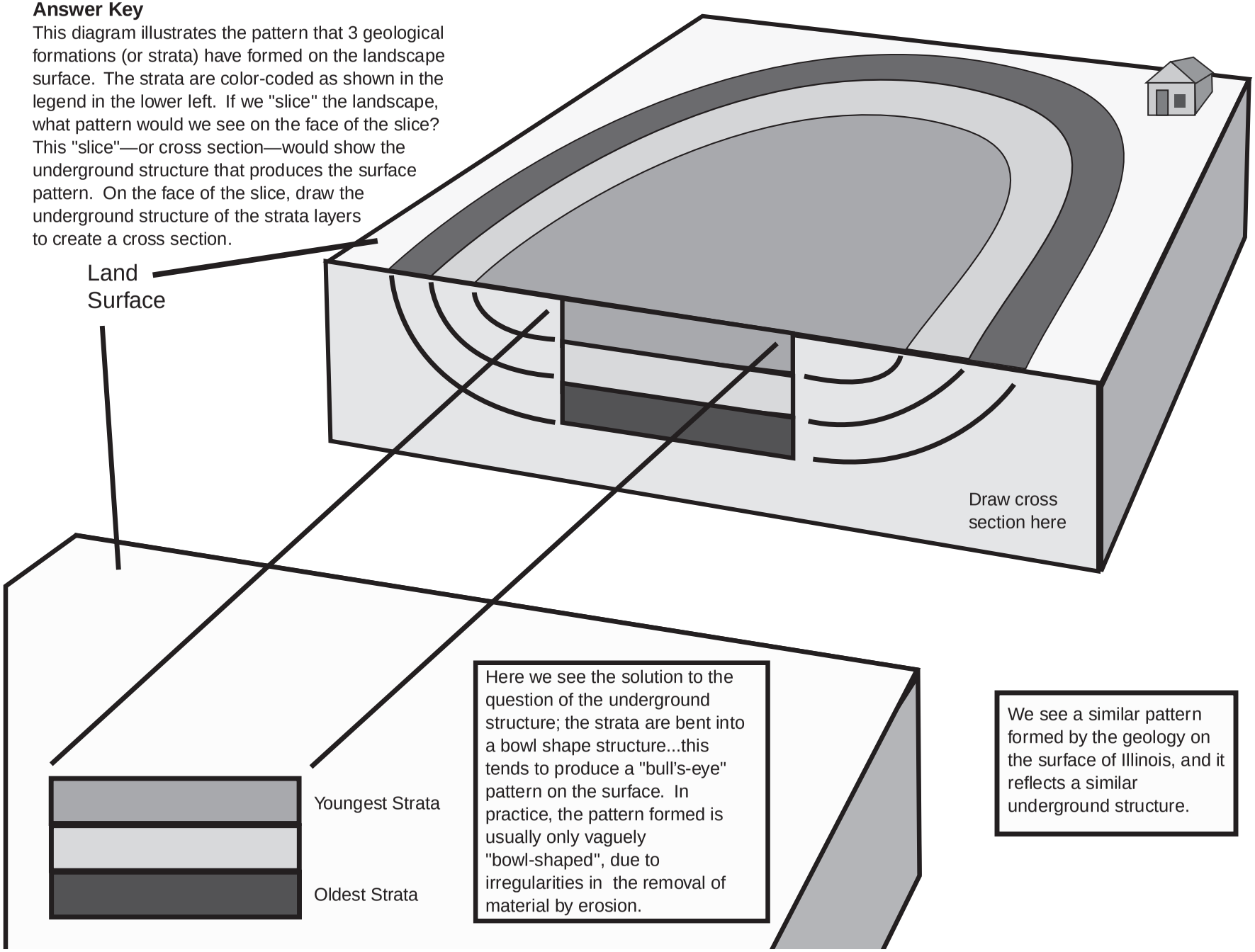

Here we see the solution to the question of the underground structure; the strata are bent into a bowl shape structure...this tends to produce a "bull's-eye" pattern on the surface. In practice, the pattern formed is usually only vaguely "bowl-shaped", due to irregularities in the removal of material by erosion.

We see a similar pattern formed by the geology on the surface of Illinois, and it reflects a similar underground structure.

Storing CO_2 Underground in Saline Reservoirs

Grade Level: 6 to 12
Authors: Sallie E. Greenberg and Robert C. Vaiden
Learning Standards: See Learning Standards Matrix

Objectives:

- Understand characteristics of saline reservoirs and water quality.

- Use maps and interpret data to determine geologic factors that make a formation good for geologic carbon storage.

Terms:

Sequestration, saline reservoir, total dissolved solids (TDS), water quality, potable, caprock, aquifer, porosity, permeability.

Background:

Greenhouse gases such as carbon dioxide (CO_2), methane (CH_4), and water vapor are being released into the atmosphere at greater rates than ever before. Millions of years worth of carbon stored in the Earth in the form of oil, gas, and coal is being combusted to provide energy so we can drive our cars, heat our homes, and manufacture the goods we depend on for our quality of life. Reducing the amount of CO_2 released into the atmosphere may slow the global warming trends that have been most clearly observed during the last 15 years. Carbon sequestration is the isolation of CO_2 from the Earth's atmosphere. Sequestration can play a significant role in preventing continued CO_2 atmospheric buildup. Geological CO_2 storage (or sequestration) in saline reservoirs is one possible way to reduce the amount of CO_2 emitted into the atmosphere. As we continue to better understand the potential for global climate change related to the burning of fossil fuels and the resulting release of CO_2, we look to science to discover ways to isolate CO_2 from the atmosphere.

Geological CO_2 sequestration involves storing CO_2 deep underground in rock formations that can retain large quantities of CO_2 for long periods of time. The CO_2 would be held in the small pore spaces that are present in rocks. These pore spaces have held saline waters, oil, and natural gas for millions of years. It is predicted that CO_2 injection into coal seams and mature oil fields could assist in the extraction of coalbed methane or oil that would otherwise be left in the ground, which could help offset the costs of

storing CO_2. Saline reservoirs that are currently filled with very salty water are also likely geological CO_2 storage sites.

Water salinity is measured in milligrams of total dissolved solids (TDS) per liter of water. Saline reservoirs are bodies of rock with pore spaces containing water with high amounts of TDS, especially salts. The TDS concentration in reservoirs can make the water too salty for human consumption, but water with low TDS may still be used for many agricultural and industrial uses.

Listed below are the USEPA guidelines (USEPA, 2006) on TDS in water. In some places, water with TDS up to 1,000 mg/L is consumed, but it is not always the best tasting water. Water containing up to 3,000 mg of TDS/L can be consumed by livestock or used for agricultural irrigation. According to the EPA, TDS in usable quality water ranges from 3,000 to 10,000 mg/L.

Drinking water	0–1,000 mg/L
Agricultural and industrial uses	3,000–10,000 mg/L
Brine/saltwater	>10,000 mg/L
Sea water	~35,000 mg/L

Saline reservoirs often occur at great depths, and TDS generally increases with depth. In the Illinois Basin, the rocks of the same geologic unit are deeper in the center of the Basin than at the edges. Sandstones near the surface in the north may be more than a mile deep at the Basin center. The increased depth usually corresponds to high concentrations of TDS. The Mt. Simon Sandstone, which is a drinkable water source in the northern part of Illinois, quickly becomes undrinkable (non-potable) in the central part of the Basin where the reservoir depth increases.

Many factors contribute to the suitability of a saline reservoir as a CO_2 storage site: percentage porosity, permeability, caprock, geological structures, rock type, faulting, and monitoring capacity. Porosity is a measure of the percentage of pore space in a rock or sediment. The higher the porosity is, the more oil, natural gas, water, or CO_2 can be stored in a rock. Permeability, the relative connectedness of the pore spaces, is an important factor in fluid movement through reservoirs and plays a role in recovering oil. Sandstone is a good example of a rock with high porosity and permeability. A good, impermeable, caprock, such as shale, has properties opposite those of the reservoir rock—low porosity and low permeability. The caprock acts as a barrier, or "lid," trapping oil, natural gas, water, or CO_2 in the reservoir rock. Anticlines and faults are geologic structures that also act as traps for oil, natural gas, and CO_2.

The ideal saline reservoir shares characteristics with the best oil-producing rocks. The reservoir should be sediments with high porosity (percentage of open pore spaces) and permeability (connectivity of open pore space) that has a geologic structure, such as an anticline or a fault that traps oil and natural gas. Directly above the reservoir should be a caprock unit of very low porosity and permeability, such as shale. The depth of the reservoir is also important. A saline reservoir should be well below drinking water units and still be economically viable for drilling. Also, the volume of the potential storage space must be great enough to justify the expense of drilling a well and recovering oil and natural gas or storing CO_2.

Monitoring CO_2 stored in saline reservoirs is important. Existing oil wells in sandstone units above the sequestration unit can be an effective way of monitoring (if the oil field has no CO_2 injected). Water brought up with oil can be monitored for changes in pH, which might indicate whether CO_2 is leaking into the rock units above the storage area. Soil gases will also be monitored for changes in chemistry and composition. Siting saline reservoirs is best done by considering all of these mentioned factors and determining the best possible location.

Materials:

Bedrock Geology of Illinois map
Cross section of Illinois (either from the bedrock map or handout)
Handout with Mt. Simon TDS data
Pencil

Procedure:

Begin this activity with a discussion of the Illinois Basin geology, saline reservoirs, and characteristics of saline reservoirs that make for a good sequestration site. Saline reservoirs typically have good porosity (such as that found in a sandstone), have a good impermeable, low-porosity caprock in the unit above (such as shale), and are relatively thick and high in TDS, making the water unusable for any other purpose.

Using the bedrock geology map, the stratigraphic column, and the cross section (Paleontology section of *Geoactivities Notebook*), guide the students to find thick, high porosity units (sandstone) overlain by low porosity units (shale). The largest is the Mt. Simon Sandstone near the bottom of the stratigraphic column. The Mt. Simon is overlain by the Eau Claire shale, which would form the “lid,” or caprock.

Give the students the map of the tri-state area with data points for TDS of the Mt. Simon Sandstone. Students will draw a contour line at 500, 1000, 10,000, 25,000, 50,000 and 100,000 mg/L.

Instruct students to apply USEPA guidelines for water usage to the map. Using the key as a guideline, have students color the range 0 to 1,000 mg/L TDS light blue. This range represents the drinkable water in the Mt. Simon sandstone. Use darker blue to color the water available for agricultural and industrial uses (3,000 to 10,000 mg/L TDS), and color the brines (>10,000 mg/L TDS) green.

The contour map of the salinity of the Mt. Simon sandstone reservoir demonstrates that throughout most of the Illinois Basin the Mt. Simon is too saline and too deep to be used as an aquifer and is a likely sequestration site. Furthermore, in much of the state, the Mt. Simon water is several times more saline than ocean water.

Discussion Questions:

Where would you be likely to use the Mt. Simon Sandstone as a source for your drinking water?

If you lived in Springfield, Illinois what might you use water from the Mt. Simon Sandstone for?

Where in the Illinois Basin would be good locations for Mt. Simon carbon sequestration?

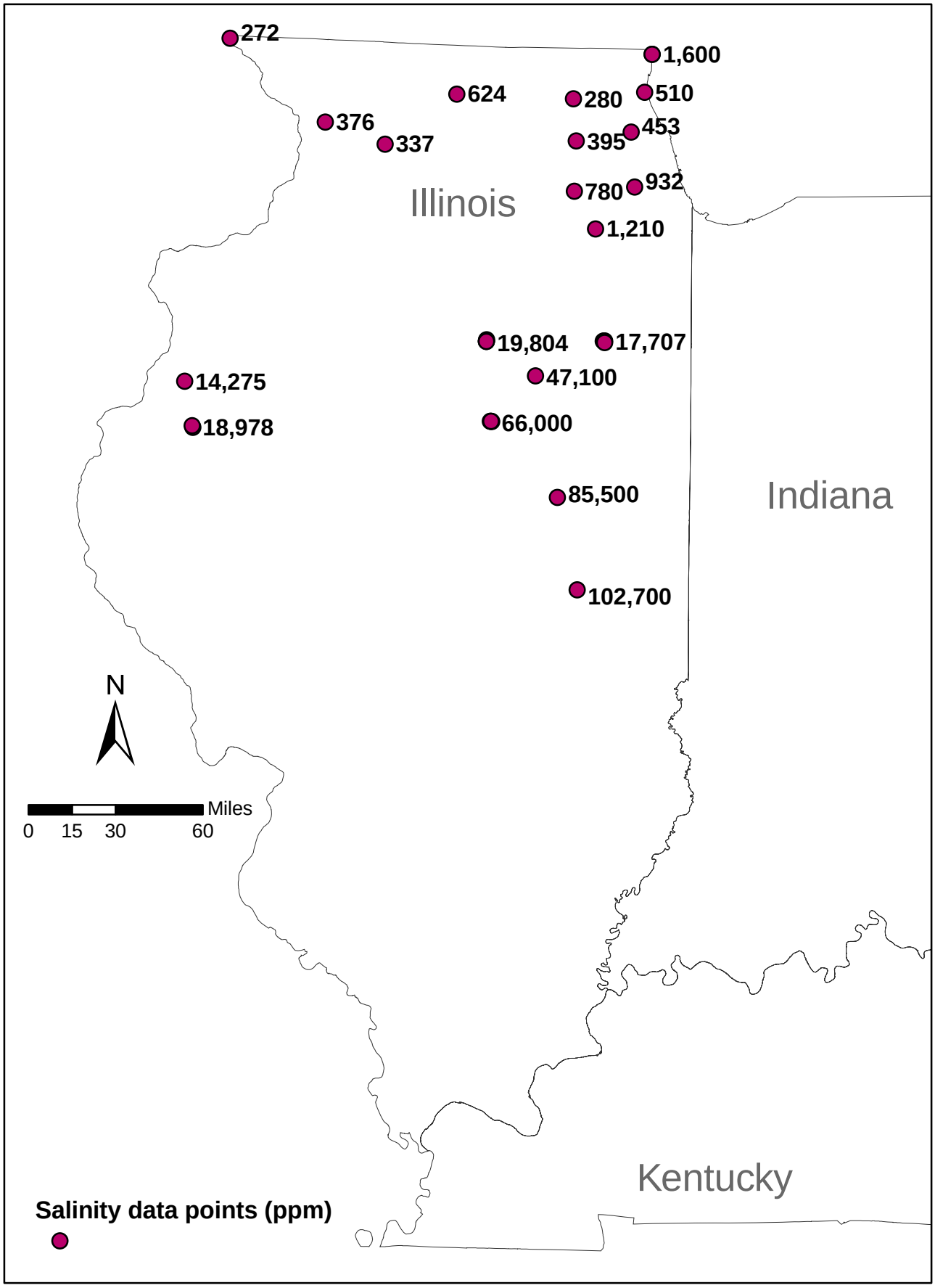
272
1,600
624
280
510
376
453
337
395
Illinois
780
932
1,210
19,804
17,707
14,275
47,100
18,978
66,000
85,500
Indiana
102,700
N
Miles
0 15 30 60
Kentucky
Salinity data points (ppm)

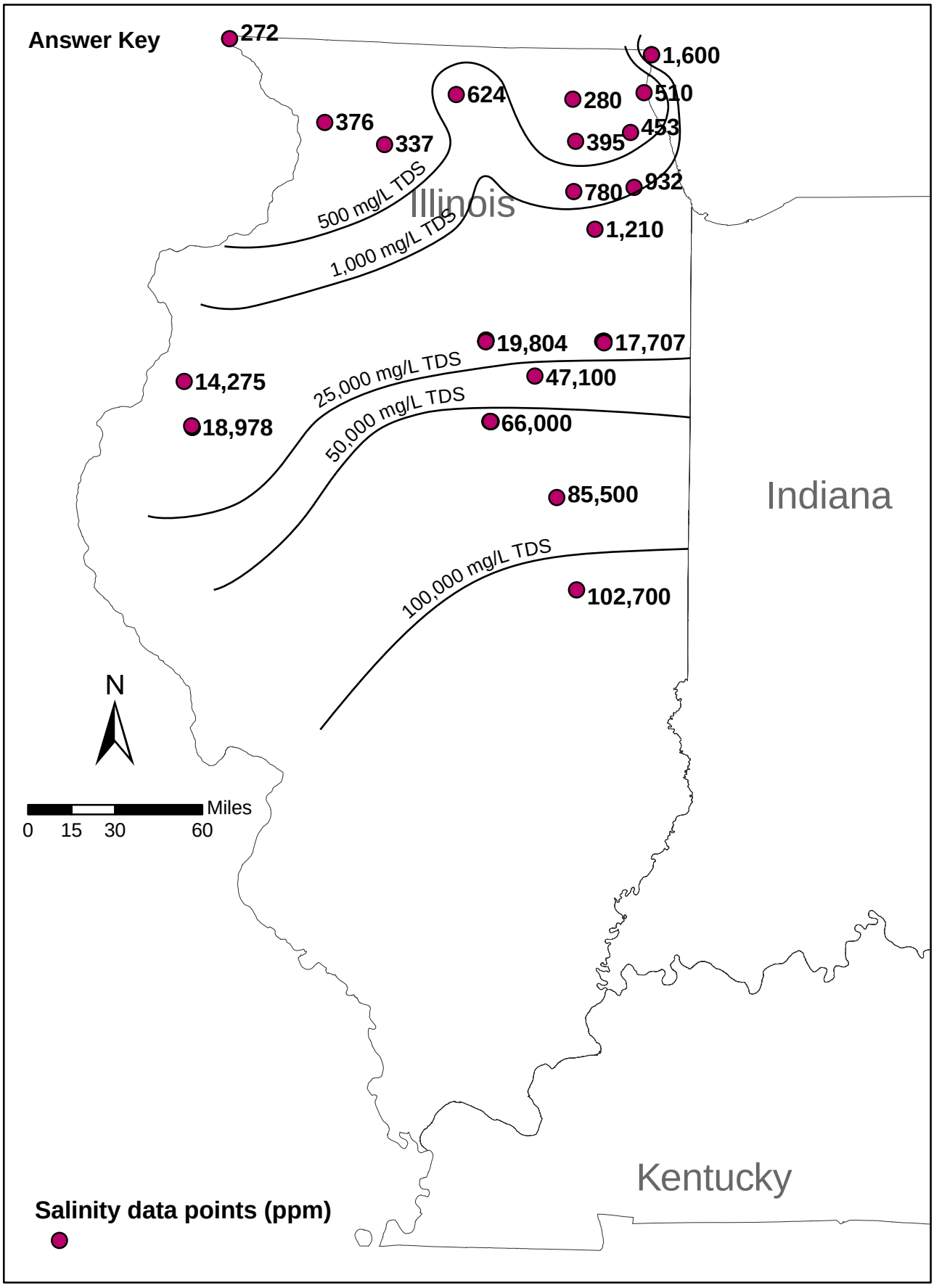
Answer Key
272
1,600
624
280
510
376
453
337
395
500 mg/L TDS
780
932
Illinois
1,000 mg/L TDS
1,210
19,804
17,707
25,000 mg/L TDS
14,275
47,100
50,000 mg/L TDS
18,978
66,000
85,500
Indiana
100,000 mg/L TDS
102,700
N
Miles
0 15 30 60
Kentucky
Salinity data points (ppm)

Tapping Our Underground Resources—Coal Bed Methane and CO_2 Sequestration

Grade Level: 6 to 12
Authors: Sallie E. Greenberg and Robert C. Vaiden
Learning Standards: See Learning Standards Matrix

Objectives:

- To illustrate where coal is found in the Illinois Basin.
- To determine where coal is economically minable.
- To use maps and data interpretation to determine the best place to achieve the combined goals of storing CO_2 in the Illinois Basin and recovering coal bed methane.

Terms:

coal bed methane, porosity, cleat, sequestration

Background:

Abundant coal resources exist in the Illinois Basin. Coal began forming during the Pennsylvanian period when Illinois, Indiana, and Kentucky were part of a tropical swamp near the equator. Plants and animals lived and died by the billions and were buried. Over time, with added heat and pressure, the organic material became the rock coal. Coal when burned gives off energy. During combustion, oxygen combines with carbon from the coal and forms CO_2, a greenhouse gas that is thought to trap heat from the Sun's rays in the Earth's atmosphere. Due to increasing demands for energy, greenhouse gases such as CO_2, CH_4, and water vapor are being released into the atmosphere at greater rates than ever before. Millions of years worth of carbon stored in the Earth is being combusted in the form of oil, gas, and coal to provide the energy we need to drive our cars, heat our homes, and manufacture the goods we depend upon for our quality of life. Reducing the amount of CO_2 released into the atmosphere may slow the global warming trends that have been observed in recent years.

Storage of CO_2 in unminable coal beds (sequestration) is one possible way to reduce the amount of CO_2 emitted into the atmosphere. If a viable method of CO_2 sequestration can be found, Illinois will be able to produce enough coal to supply energy for approximately the next 250 years—enough time to develop alternative energy options. If successful sequestration technologies are developed, we could continue to use coal resources during the transition to new fuels over a period of decades while avoiding further release of CO_2 into the atmosphere.

Coal beds hold methane (CH_4, a natural gas), which can be recovered from coal beds as the result of sequestration. Natural gas accounts for about 24% of U.S. energy consumption (Natural Gas Supply Association, 2006) and is used for a variety of residential and commercial energy needs, such as cooking and heating. Using coal beds as storage for CO_2 provides an opportunity to extract additional methane previously unproducible. CH_4 is adsorbed onto the internal surface area of coal, but is easily replaced by CO_2, which has a higher sorption affinity and a higher adsorption capacity than CH_4. Coal beds can adsorb approximately twice the amount of CO_2 as CH_4. So, even if we burned all of the natural gas harvested from the coal beds, the net effect is the removal of CO_2 from the atmosphere. The adsorption/desorption of gases on coal is dependent on temperature, pressure, and coal composition.

The thickness of a coal and its depth from the surface determine how economically viable it is to mine a coal seam. Two coal units in the Illinois Basin, the Herrin and Springfield Coals, are particularly important seams and provide 70% of the coal mined in Illinois. Because mining costs increase with depth, coals of any thickness >305 m (>1,000 ft) deep are considered "unminable" because they are likely too expensive to mine compared with abundant, available shallower coals. Coals at these great depths, however, are an excellent choice for CO_2 sequestration. Thinner coal beds (0.3 to 1.1 m (1 to 3.5 ft) thick) found between 152 and 305 m (500 and 1,000 ft) are also possible sequestration choices. Coal beds must be greater than 1.1 m (3.5 ft) thick to be mined using currently available equipment.

The Illinois Basin is a major geological structure of the tri-state area of Illinois, Indiana, and Kentucky. The Pennsylvanian period rocks (Late Carboniferous age), roughly 33 million years worth of coal swamp deposits, comprise the coal-bearing rocks of the Illinois Basin. The Illinois Basin rocks are layered below the surface and formed a bowl-like structure during deposition, with the oldest and generally thickest rocks at the center. These layers form a roughly concentric oval pattern where they intersect the surface, as can be seen on a geologic map. Storing CO_2 in coals deeper than 305 m (1,000 ft) and thicker than 1.1 m (3.5 ft) does not render the coals unminable. It simply means that any CO_2 stored therein will be released upon mining. If coal becomes very valuable, or very scarce, or both in the future, then it may become economical to mine these coals.

Coal bed porosity and permeability is also a factor in determining the viability of a coal seam for sequestration. There are two types of porosity in coals: matrix and fracture. The fracture pattern and connectivity are essential to being able to extract CH_4 from coal beds, much like being able to draw water from an aquifer.

Key Points:

- The Illinois Basin states hold significant coal resources.

- Burning coal emits a lot of CO_2, a heat-trapping gas; if CO_2 can be stored, we can use coal as a transition fuel while new fuel technologies and options are being explored.

- Using coal holds economic advantages for the Illinois Basin states by creating jobs, providing economic stability, and producing additional fuel resources such as recovered methane.

Materials:

Overhead map
Overhead projector
Colored erasable pens
Photocopied maps for each group or student

Procedure:

Students will create a map that identifies the ideal locations for sequestering (storing) CO_2 in coal beds and extracting CH_4. One overhead transparency or tracing papaer will be used to trace and transfer information from three maps containing different data already in map form.

1. Use the geologic map to determine which rock sequences in Illinois, Indiana, and Kentucky have coal-bearing rocks. Prior to this first step, discuss where coal is found and how it forms. Highlight the point that coal in the Illinois basin is found in Pennsylvanian rocks. When students transfer their first piece of information, they want to draw a line around the area where Pennsylvanian rocks are present in the Basin.

2. Use depth to determine sequestration possibilities. Maps are provided showing the depth from the surface to the Herrin and Springfield Coals. Discuss with the students that the depth to the coal is an important factor in determining which coal beds are economically minable. If a coal bed is very deep, the cost to mine it will be too high for profitability. It costs a lot more money to mine deep coals than shallow coals. In general, coals of any depth greater than 305 m (1,000 ft) are currently considered too deep for mining and therefore, good CO_2 storage possibilities. On their overhead map, have the students draw a line around the perimeter of the coals at depths >305 m (>1,000 ft). It will become clear when viewing the coal depth map that there are separate regions of the Illinois Basin that allow maximum mining potential and CO_2 storage potential.

3. Narrow down sequestration sites even further by understanding the differences in coal thickness in specific areas. Coal thickness can be used to narrow down which coal beds can be used for mining, which can be used for CO_2 storage, and where overlap occurs. At depths >305 m (>1,000 ft), coals >1.1 m (>3.5 ft) thick can be mined and coals <1.1 m (<3.5 ft) thick can be used for storing CO_2. There are some coals that can't be mined because they are too deep or too thin. There are also coal beds that are too thin to be useful for storing CO_2.

Coal <1.1 m (<3.5 ft) thick in the intermediate depth range of 152 to 305 m (500 to 1,000 ft) is generally not minable. It can, however, be used to store CO_2. Any coal beds >1.1 m (>3.5 ft) thick between 152 to 305 m (500 to 1,000 ft) deep are still potential mining sites.

On their overhead map, have the students draw a line around the perimeter of the areas of Herrin and Springfield Coals that are possible for storing CO_2 (areas where coal is 106.7 cm (42 inches) or less). Note that areas where no coal is present are not suitable for storage, nor are exceptionally thin coal beds.

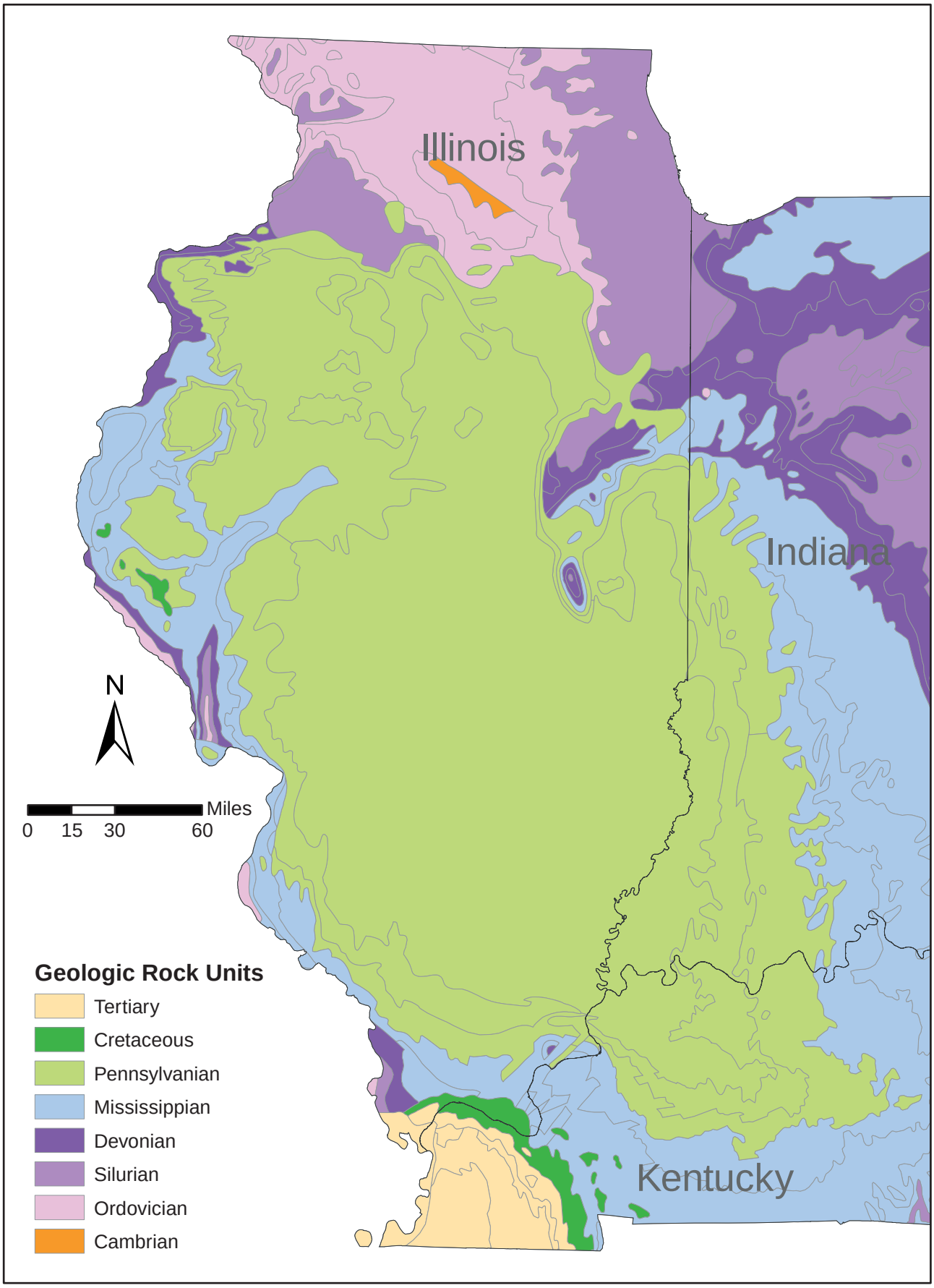
Illinois
Indiana
Kentucky
N
Miles
0 15 30 60
Geologic Rock Units
Tertiary
Cretaceous
Pennsylvanian
Mississippian
Devonian
Silurian
Ordovician
Cambrian

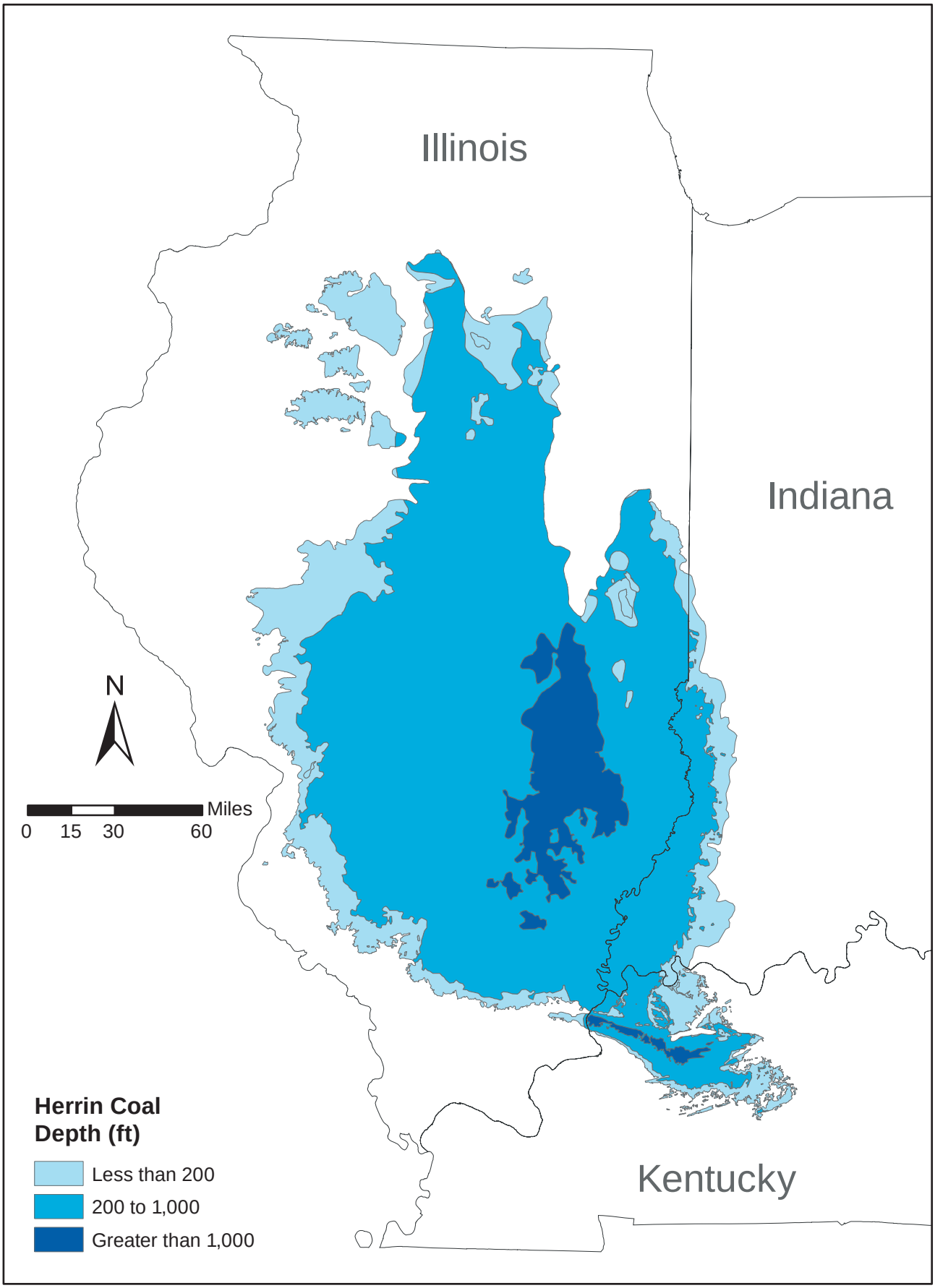
Illinois
Indiana
Kentucky
N
Miles
0 15 30 60
Herrin Coal
Depth (ft)
Less than 200
200 to 1,000
Greater than 1,000

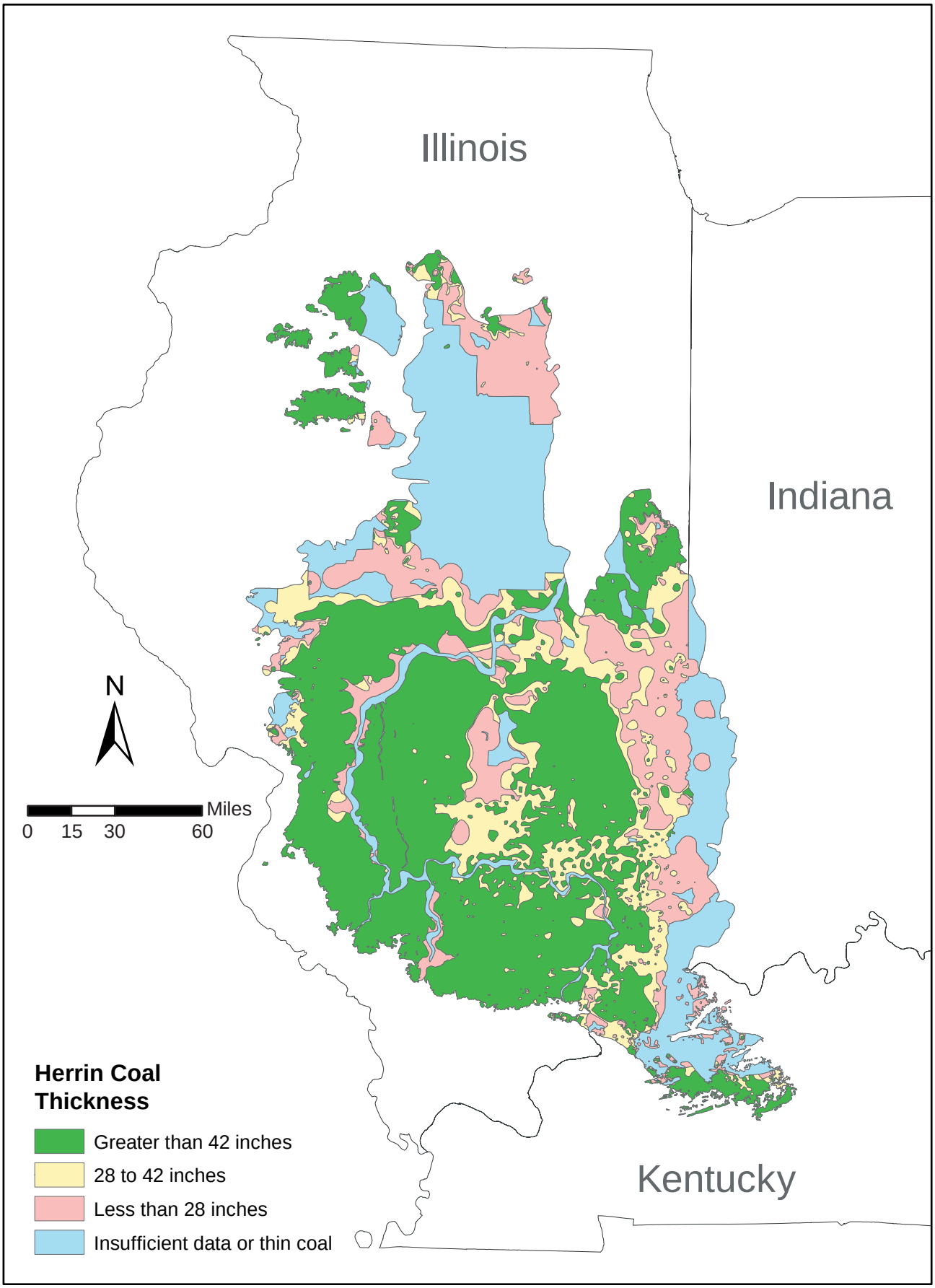
Illinois
Indiana
Kentucky
N
Miles
0 15 30 60
Herrin Coal Thickness
Greater than 42 inches
28 to 42 inches
Less than 28 inches
Insufficient data or thin coal

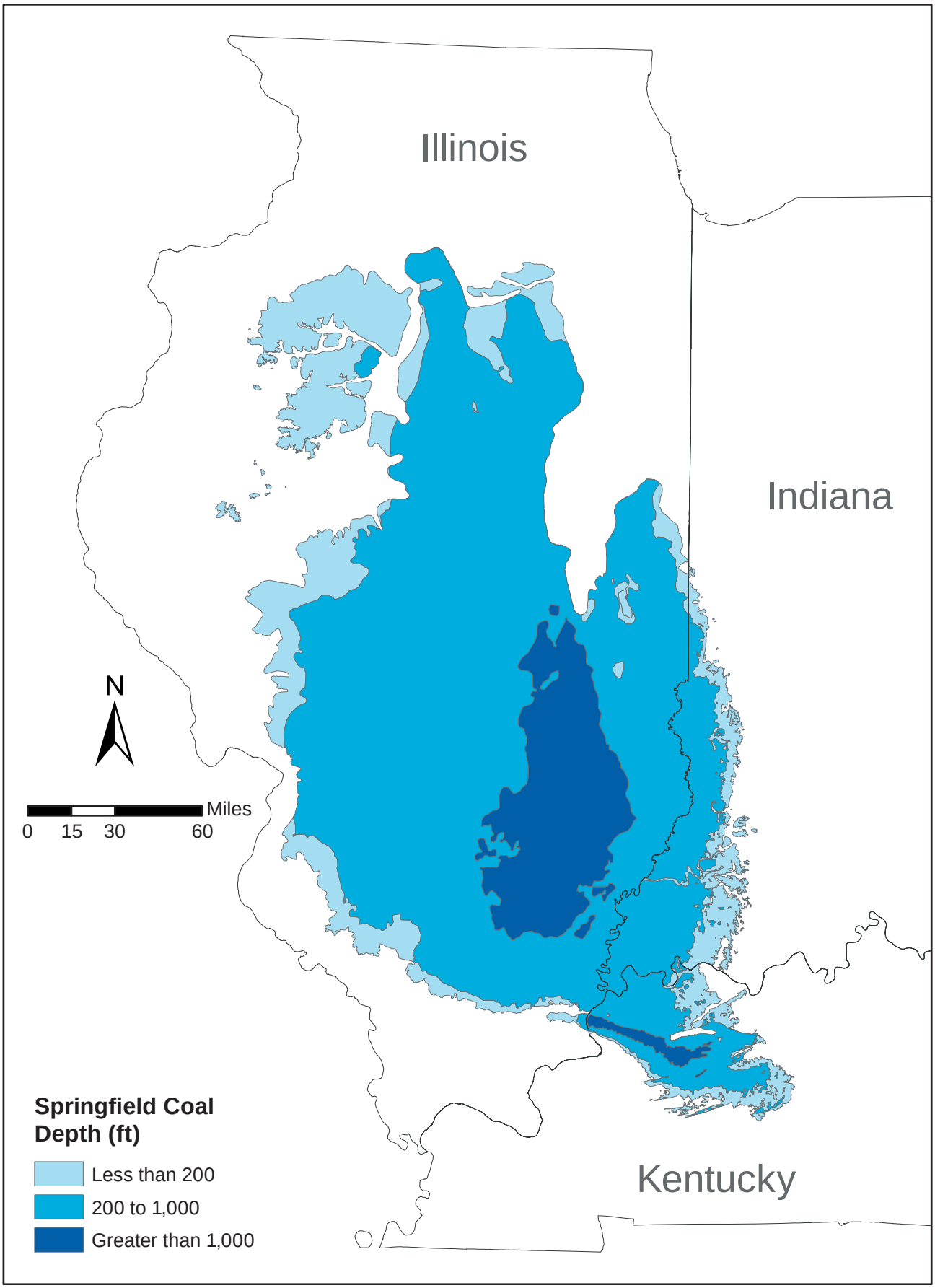
Illinois
Indiana
Kentucky
N
Miles
0 15 30 60
Springfield Coal Depth (ft)
Less than 200
200 to 1,000
Greater than 1,000

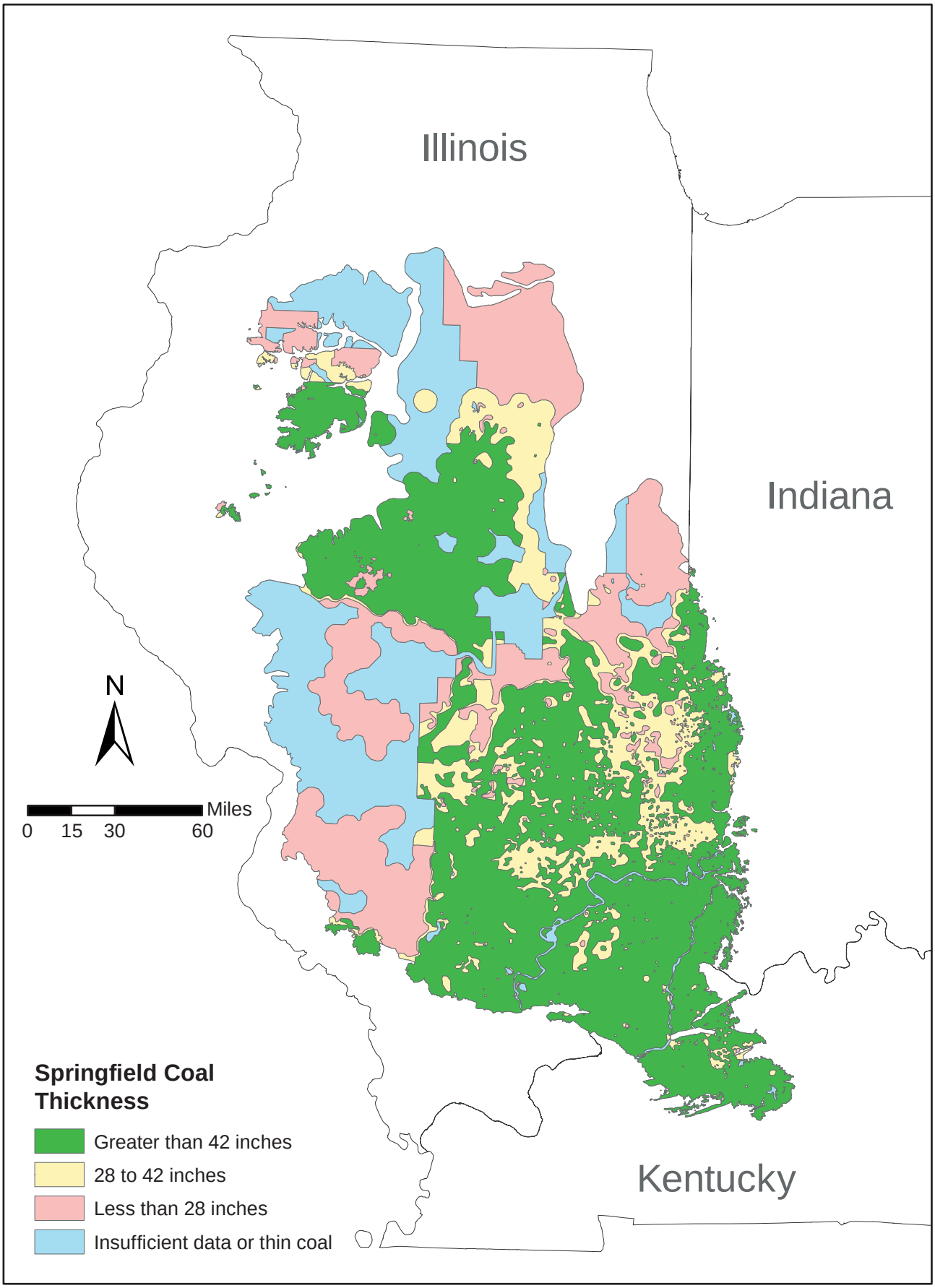
Illinois
Indiana
Kentucky
N
Miles
0 15 30 60
Springfield Coal Thickness
Greater than 42 inches
28 to 42 inches
Less than 28 inches
Insufficient data or thin coal

Putting Our Carbon Back into the Ground

Grade Level: 4 to 12
Authors: Sallie E. Greenberg and Robert C. Vaiden
Learning Standards: See Learning Standards Matrix

Objectives:

- To understand and integrate the three types of geologic carbon sequestration: enhanced oil recovery, coalbed methane, and saline reservoirs.

- To determine the best locations for each type of geologic carbon sequestration, where the locations overlap, and which locations are important for drinking water and other use.

Terms:

carbon sequestration, coalbed methane, enhanced oil recovery, saline reservoir, drinking water

Background:

Greenhouse gases such as carbon dioxide (CO_2), methane (CH_4), and water vapor are being released into the atmosphere at greater rates than ever before. Millions of years worth of carbon stored in the Earth in the form of oil, gas, and coal is being combusted to provide energy so we can drive our cars, heat our homes, and manufacture the goods we depend upon for our quality of life. Reducing the amount of CO_2 released into the atmosphere may slow the global warming trends that have been observed in recent years. As we continue to better understand the potential for global climate change due to the burning of fossil fuels and the resulting release of CO_2, we can look for ways to isolate CO_2 from the atmosphere. Geologic sequestration of carbon is the isolation of CO_2 from the Earth's atmosphere by storing it underground. Sequestration can play a significant role in slowing CO_2 buildup in the atmosphere.

Three types of geologic carbon sequestration are being explored in the Illinois Basin: enhanced oil recovery, coalbed methane, and saline reservoir. These storage types may provide us with the time needed to discover new technologies and create alternative fuel options, while decreasing the amount of CO_2 emitted into the atmosphere and helping our regional economy through the use of fossil fuels found in the Illinois Basin. If a viable method of CO_2 sequestration can be found, Illinois will be able to produce enough coal to supply energy for approximately the next 250 years, which may be enough time to develop alternative energy options. Our oil reserves produced via CO_2 injection may also become

economically viable as prices rise. If successful sequestration technologies are developed, coal, oil, and natural gas resources could continue to be used as a major transition to new fuels over a period of decades, while avoiding further release of CO_2 into the atmosphere.

Enhanced oil recovery uses CO_2 to recover the oil left behind after oil has been pumped out of a reservoir. Oil does not always move easily through sandstone reservoirs, and much oil is left behind after an oil field produces under typical methods. There comes a point at which it is no longer cost-effective to continue pumping oil from the ground in some fields. CO_2 is already being used as a recovery agent in oil fields in other basins. Using CO_2 for EOR becomes a more economical alternative when oil prices rise. A central well is used to inject CO_2, and surrounding wells are used to recover the oil. Liquid-like CO_2 under pressure is injected into a central well and moves the oil toward the outer wells, which are used to pump the oil out. Using this method for storing CO_2 is simply the next step in the process. The CO_2 would be held in small pore spaces present in rocks. These pore spaces have held saline waters, oil, and natural gas for millions of years.

Storage of CO_2 in unminable coal beds (sequestration) is another way to reduce the amount of CO_2 emitted into the atmosphere. Coal beds hold methane (CH_4, natural gas) that can be recovered as the result of CO_2 sequestration. Using coal beds as CO_2 storage sites provides an opportunity to extract CH_4 that was previously unrecoverable. The CH_4 is adsorbed onto the internal surface area of the coal matrix, but is easily replaced by CO_2, which has a higher sorption affinity and a higher adsorption capacity than does CH_4. Some coal beds can adsorb two to five times the amount of CO_2 as CH_4. So, even if we burned all of the natural gas recovered from the coal beds, the net effect is still the removal of CO_2 from the atmosphere.

Saline reservoirs are bodies of rock with pore spaces containing water with high amounts of total dissolved solids (TDS), especially salts. The concentration of TDS in deep saline reservoirs make the water too salty for human consumption or for many agricultural and industrial uses. Saline reservoirs occur deep underground in rock formations that are expected to retain large quantities of the CO_2 for long periods of time. The CO_2 would be held in small pore spaces present in rocks. The ideal saline reservoir for carbon sequestration shares characteristics with the best oil-producing rocks. It should be sedimentary rock with high porosity (percentage of open pore spaces) and permeability (connectivity of open pore space) that has a geologic structure, such as an anticline or a fault that traps oil and natural gas. Directly above it should be a caprock unit of very low porosity and permeability, such as shale. The caprock layer acts as a lid or a cover for the saline reservoir. The depth of the reservoir is also important. A saline reservoir should be well below drinking water geologic units, not too deep, and economically viable to drill into. Also, the volume of the potential storage space must be great enough to justify the expense of drilling a well and recovering oil and natural gas or storing CO_2.

It is predicted that CO_2 injection into coal seams and mature oil fields could assist in the extraction of coalbed methane or oil that would otherwise be left in the ground, which could help offset the costs of storing CO_2. Saline reservoirs, which are often the source rock of oil and natural gas fields, are likely natural storage sites.

Materials:

Worksheet
Pencil

Procedure:

This activity is designed as a summary activity to a unit on geologic carbon sequestration and climate change. This worksheet combines these three carbon sequestration methods and gives students an opportunity to summarize and use the information they have learned in other activities to determine which sites are best for which use: pumping drinking water, enhanced oil recovery, coaled methane recovery, or CO_2 storage in saline reservoirs.

1. This activity may be done individually or in small groups.
2. Discuss the three methods of geologic sequestration with students.
3. Students should read through the scenario on the worksheet and, using the diagram, decide what each location can be used for: drinking water, enhanced oil recovery, coaled methane recovery, or CO_2 storage in saline reservoirs. Also, ask students to identify places where more than one usage is possible.
4. Discuss the answers with the entire class.

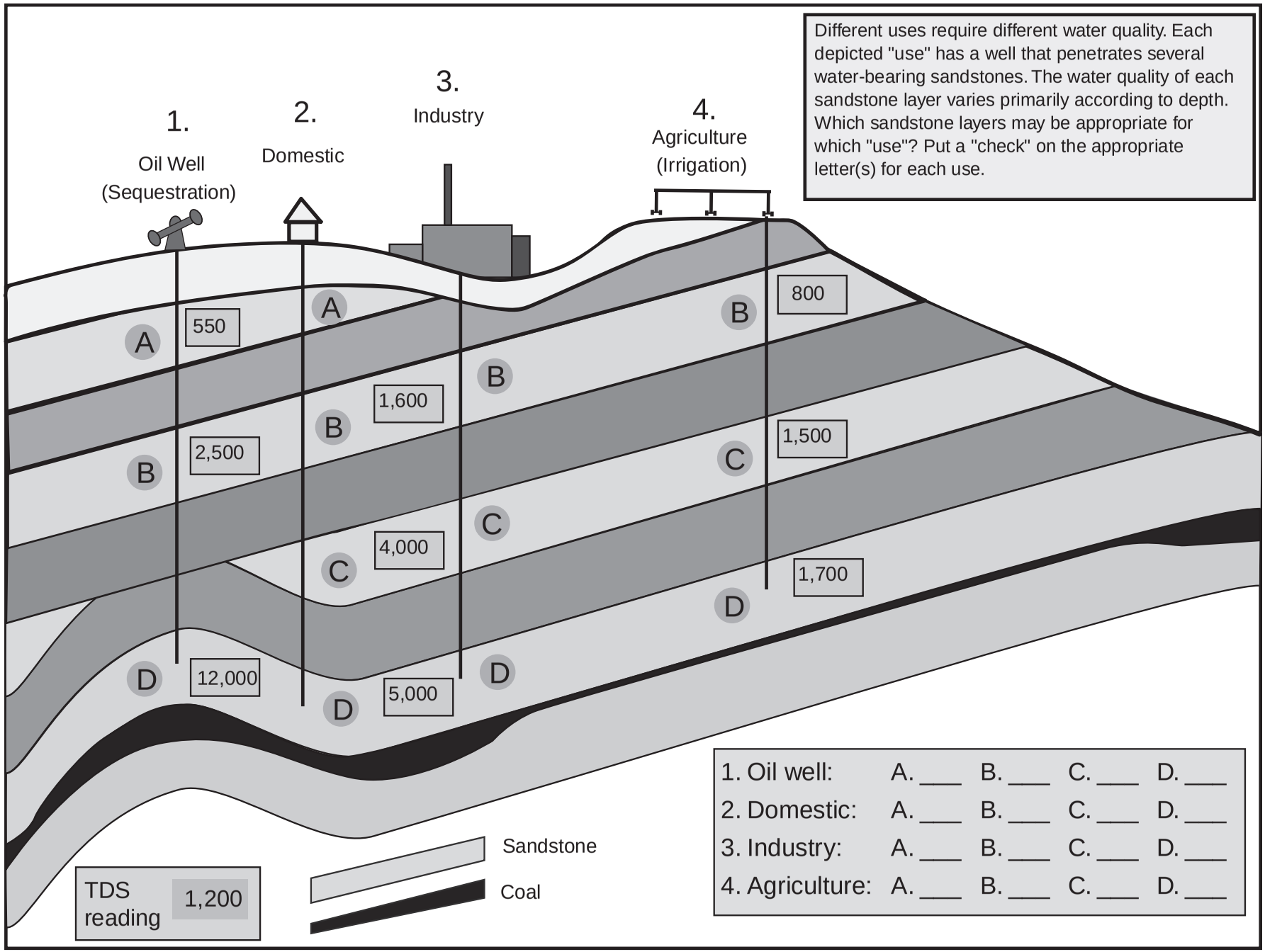
Different uses require different water quality. Each depicted "use" has a well that penetrates several water-bearing sandstones. The water quality of each sandstone layer varies primarily according to depth. Which sandstone layers may be appropriate for which "use"? Put a "check" on the appropriate letter(s) for each use.
1.
Oil Well
(Sequestration)
2.
Domestic
3.
Industry
4.
Agriculture
(Irrigation)
A
550
A
B
2,500
B
1,600
B
C
4,000
C
D
12,000
D
5,000
D
800
B
1,500
C
1,700
D
TDS reading
1,200
Sandstone
Coal
1. Oil well: A. ___ B. ___ C. ___ D. ___
2. Domestic: A. ___ B. ___ C. ___ D. ___
3. Industry: A. ___ B. ___ C. ___ D. ___
4. Agriculture: A. ___ B. ___ C. ___ D. ___

Answer key

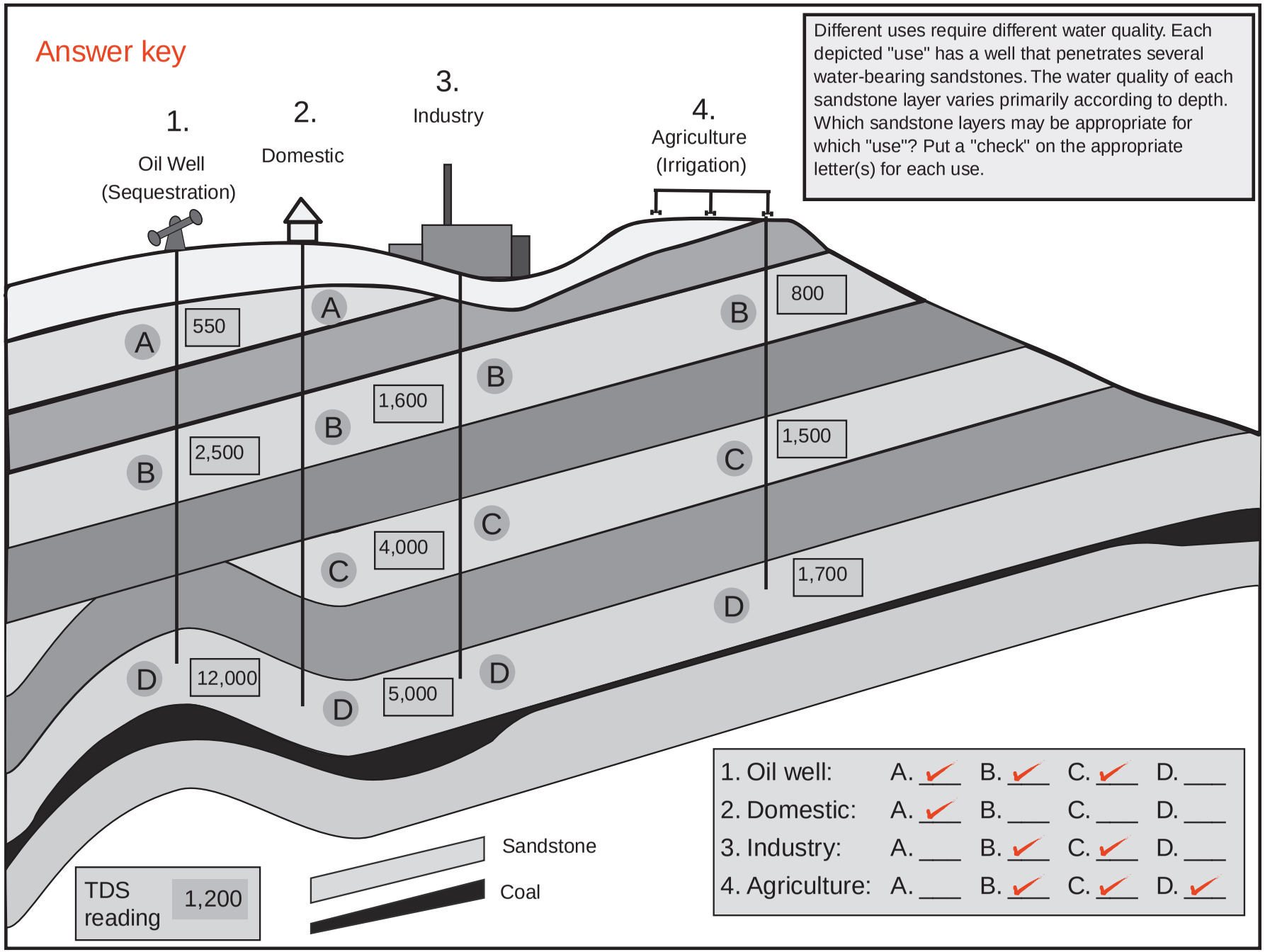

Different uses require different water quality. Each depicted "use" has a well that penetrates several water-bearing sandstones. The water quality of each sandstone layer varies primarily according to depth. Which sandstone layers may be appropriate for which "use"? Put a "check" on the appropriate letter(s) for each use.

1. Oil well:	A. ✓	B. ✓	C. ✓	D. ___
2. Domestic:	A. ✓	B. ___	C. ___	D. ___
3. Industry:	A. ___	B. ✓	C. ✓	D. ___
4. Agriculture:	A. ___	B. ✓	C. ✓	D. ✓

Illinois Learning Standards Matrix										
Activity Number and Title	**11A**	**11B**	**12A**	**12B**	**12C**	**12D**	**12E**	**12F**	**13A**	**13B**
Carbon Sequestration										
Petroleum in Our Daily Lives	X		X		X		X			X
Climate Change throughout Geologic Time	X						X			X
Seeing Underground	X						X			X
Storing CO2 Underground in Saline Reservoirs	X						X			X
Tapping Our Underground Resources	X						X			X
Putting Our Carbon Back into the Ground	X						X			X

X = Emphasis in Content

National Science Education Standards Matrix									
Please see the key to the content standards at the bottom of this page.									
Activity Number and Title	Suggested Grade Level		Content tandards						
	5-8	9-12	A	B	C	D	E	F	G
Geologic Sequestration									
Petroleum in Our Daily Lives	X		X			X		X,Y	X
Climate Change throughout Geologic Time	X	Y	X			X,Y		X,Y	X
Seeing Underground	X		X			X		X,Y	X
Storing CO_2 Underground in Saline Reservoirs	X	Y	X,Y			X,Y		X,Y	X
Tapping Our Underground Resources	X	Y	X,Y			X,Y		X,Y	X,Y
Putting Our Carbon Back into the Ground	X	Y	X,Y			X,Y		X,Y	X

A = Science as Inquiry B = Physical Science C = Life Science D = Earth and Space Science E = Science and Technology F = Science in Personal and Social Perspectives G = History and Nature of Science X = Emphasis in Content for 5-8 Y = Emphasis in Content for 9-12

Education/Outreach Activities

Two public conferences, titled “Carbon Sequestration in the Illinois Basin: What We Have Found, Where We Are Going, and How this Relates to Economic Development in the Southern Illinois Basin,” were held in Springfield, Illinois, on September 27, and in Evansville, Indiana, on September 28, 2005. These two seminars provided an overview of results of the current MGSC's Illinois Basin carbon sequestration studies to industry, government, and non-governmental organizations in Illinois, Kentucky, and Indiana. These presentations focused on the potential of carbon dioxide (CO_2) to enhance oil recovery and help produce methane as it is stored in deep saline reservoirs to avoid its release to the atmosphere.

On September 27, 2005, from 10 a.m. to noon, an overview of the program was given that described geological CO_2 storage options; it was held at the Hilton Hotel, 700 East Adams in Springfield, Illinois. We included an outlook for the program over the next four years. On September 28, 2005, from 1 to 5 p.m. at the Evansville Airport Marriott, 7101 U.S. Hwy 41 North, Evansville, Indiana, the same overview and outlook were presented, but more detailed information was added on our studies of CO_2 enhanced oil recovery potential in the Basin, our assessments of coalbed methane recovery potential, the data products and maps we expect to produce, and the work being carried out on shale gas production/sequestration potential. Both seminars included presentations and posters with an opportunity to ask questions, and there was no fee for these events. Feedback from conference attendees is presented in Tables 7-1 and 7-2.

We used the prepared teacher/student training materials (Task 10) for educators in grades 4 to 12 in demonstrations at three meetings during Phase I: The Partnership Advisory Group meeting in Champaign, Illinois, on September 13, 2005, and two informational meetings held in Springfield, Illinois, and Evansville, Indiana, on September 28 and 29, respectively.

Regional and national meetings offer the best opportunities to present research and receive peer review and feedback. More than 25 presentations, publications, and abstracts were produced during the course of the project. Because of the scope of the project, additional publications based on our research are expected to be completed as part of the Phase II U.S. Department of Energy-funded research.

Table 7-1. Summary of written feedback from conference attendees at the Springfield, Illinois, meeting.

MGSC Questionnaire—Springfield, IL
September 27, 2005

	Not familiar		Somewhat familiar		Knew a great deal	Total
	1	2	3	4	5	
1. How familiar were you with geologic sequestration prior to coming to today's meeting?	1	3		3		7

	Little or nothing		A fair amount		A great deal	
	1	2	3	4	5	
2. Overall, how much did you get out of this meeting?			4	2	1	7
3. How much did you get out of the demonstrations?			2	4	1	7
4. How much did you get out of the explanatory talks?			3	3	1	7

5. What brought you to the meeting today?
   - Regulatory job and potential for this to impact my job in the future.
   - Nearby
   - Opportunity to learn more about sequestration
   - Applicability to my job
   - CO_2 sequestration is critical to the future of Illinois coal. I wanted to learn more about this project.
   - DCEO
   - Potential/regulatory impact

6. What aspect of the meeting proved most and least useful for you?
   - Most
     - The demonstrations
     - Overview
     - Rob's overviews were the most helpful to us.
       I don't have background.
     - Hannes' discussion; slide presentations/explanation
     - Formal presentation
   - Least
     - Posters—always hard to get the impact of these
     - Geology
     - Terminology still not completely familiar

7. What, if any, concerns do you have about geologic carbon sequestration?
   - Breaking out of old oil wells that may/may not be properly plugged.
   - Leakage into shallow formations
   - Logistics of sequestration on a large scale
   - None. Great potential for Illinois

8. What additional information would you like to have about geologic carbon sequestration?
   - Just a suggestion—If these presentations go to the general public (non-engineer), include a definition cheat sheet.

Table 7-2. Summary of written feedback from conference attendees at the Evansville, Indiana, meeting.

MGSC Questionnaire—Evansville, IN
September 28, 2005

	Not familiar		Somewhat familiar		Knew a great deal	Total
	1	2	3	4	5	
1. How familiar were you with geologic sequestration prior to coming to today's meeting?	3	1	16	2	1	23

	Little or nothing		A fair amount		A great deal	
	1	2	3	4	5	
2. Overall, how much did you get out of this meeting?			8	11	4	23
3. How much did you get out of the demonstrations?		1	12	7	2	22
4. How much did you get out of the explanatory talks?			6	13	4	23

5. What brought you to the meeting today?
   - Letter and topic
   - To see how this might affect oil and CBM production
   - Past experience in Permian Basin CO_2 flooding
   - Interest in CO_2 and geologic sequestration
   - To learn!
   - Habit and desire to learn more
   - Learn more about EOR
   - To find out what is in the future for us in the energy business
   - Meeting notice
   - CO_2 sequestration
   - Wanting update
   - Interest in the project and how Phase I was doing
   - New Albany Shale information
   - I remembered
   - Find out timetable of project
   - DCEO
   - Possible field demonstration
   - Curiosity
   - Future development

6. What aspect of the meeting proved most and least useful for you?
   - Most
     - CO_2 EOR
     - GIS information/EOR
     - Presentations GIS data availability
     - CO_2 EOR
     - Talk on shales
     - Overall discussion of CO_2 sequestration
     - Volumetrics/engineering
     - Brought together experts at the Surveys

Time frame—potential oil recovery
Overview of project and current status of Phase I
All useful
EOR
Talks

Least
CBM resources and recovery
Trying to hear Scott and Chris who whispered to front 2 rows
Specific drilling of Devonian Shale
Deep saline reservoir information
Time frame—too little
Filling out this form
Displays

7. What, if any, concerns do you have about geologic carbon sequestration?
Corrosion!
Economic feasibility due to smaller field sites than conventional CO_2 flooded basins.
Recycling facilities would be costly and would be required to keep CO_2 from being flared.
The same forces pushing CO_2 sequestration (by law, etc.) are trying to eliminate drilling and production due to environmental.
It may be interesting as to which force is greater?
How to use CO_2 in flooding old oil fields
No concerns at this time
Low rate of return
Poison of aquifers?
Equipment needs—corrosion studies may be needed. Capturing and recycling for CO_2 floods
Timing

8. What additional information would you like to have about geologic carbon sequestration?
Sources and costs of CO_2 for EOR and update on government programs/tax credits
Update on projects. Access to raw reservoir production data used in study.
Have at this time.
CO_2, oil, gas operations
Newsletter

Action Plan for Implementation of Technology Validation Field Testing

Based on the Phase I work reported herein, the Midwest Geological Sequestration Consortium (MGSC) proposes field validation tests that will be carried out in Phase II that are based on assessments of potential storage reservoirs and seals throughout the Illinois Basin. Targeted geologic sinks for carbon dioxide (CO_2) sequestration include, from shallowest to deepest: deepest, less minable coal seams; mature oil reservoirs potentially amenable to enhanced oil recovery (EOR); and major saline reservoirs (the Mt. Simon and St. Peter Sandstones). Additionally, assessment of the New Albany Shale, an organic-rich shale, will be considered both as a sink and as a backup seal to these sandstones.

Mapping of coals and subsequent spatial analysis have defined a north-south "fairway" underlain by seven coals at depths up to 457.2 m (1,500 ft) in southeastern Illinois. In Indiana and Illinois, commercial production of coalbed methane has been established in two of these coals, the Seelyville and Davis/Dekovan, in Indiana and Illinois within the last 2 years, even though the upper end of gas content is generally about 4.68 to 5.31 m^3/tonne (150 to 170 standard cubic feet (scf)/ton). Results from the San Juan Basin, New Mexico, Tiffany Unit, demonstrate the applicability of CO_2 injection and adsorption for enhanced coalbed methane (ECBM) production. Understanding potential coal swelling remains an issue, and tests to date on Illinois Basin coals show that coal swells considerably with adsorption of CO_2. However, a part of the CO_2-induced swelling is compensated for by the shrinkage associated with desorption of methane (CH_4). Both of these factors are expected to have a significant impact on permeability and need to be evaluated for the ECBM plot. Additionally, the details of which types of coals are chemically best suited for CO_2 adsorption has not been determined. Assessments of Illinois Basin coal resources demonstrate 413 billion tonnes (455 billion tons) of resources. If just half of these resources were recovered, mining could proceed at double the current rate (2004) for more than the next 200 years. Generally, deeper coal seams are more costly to mine, especially deep seams <106.7 cm (<42 inches) thick (not accessible with presently available mining machinery). As such, these coals are deemed unminable. It is these economically and technically least-accessible resources in the deep basin fairway that have been identified as potential ECBM field validation test sites.

The CO_2 EOR processes in mature oil reservoirs can be divided into CO_2 floods that are likely to be immiscible or miscible. Miscible floods typically have higher oil recovery and depend on the dissolution of CO_2 in the oil in the reservoir to make the oil swell and reduce its viscosity. Miscibility depends upon temperature, pressure, and the chemical character of the oil. Immiscible CO_2 flooding depends on gaseous CO_2 re-pressurizing oil to the wellbore and will have less effect on reducing residual oil in the reservoir. Detailed comparison of key reservoir properties for West Texas miscible floods and reservoir properties for potential miscible floods in the Illinois Basin suggest favorable conditions for CO_2 EOR in

the Illinois Basin. A critical screening parameter for field validation tests that has emerged from Phase I, however, is to give priority to those fields that are under waterflood. Waterflooding maintains reservoir pressure, demonstrates effective connectivity between wells, has been implemented by remediating any obvious leaks at the wellhead or to the surface, and usually involves the creation of an operating unit over which a single company has control (by itself or through an operating agreement). These characteristics, when screened in comparison to sequestration capacity and the target oil resource in the waterflood unit, will help in the selection of favorable field validation tests. Most importantly, substantial Phase II costs can be avoided because less CO_2 will be required to test sequestration potential and EOR in a waterflood unit compared to a pressure-depleted oil reservoir still on primary production. However, an immiscible pilot may be investigated.

Organic-rich shales in the Illinois Basin will be assessed from two perspectives. The Devonian New Albany Shale in the Illinois Basin is commercially productive of CH_4 in the same way as the stratigraphically equivalent Antrim Shale in the Michigan Basin, a play that currently supports over 7,600 producing wells. New Albany reservoirs exist in Indiana and Kentucky, and samples are currently being tested for their CO_2 adsorption capacity as part of a separate U.S. Department of Energy (DOE)-funded study at the Kentucky Geological Survey. The organic carbon content of the shale is directly related to CO_2 adsorption capacity. Injection of CO_2 into the organic shales may result in adsorption of CO_2 and possibly associated enhanced production of CH_4, similar to that in coalbeds. The New Albany may provide a secondary seal for sequestration in any deeper Paleozoic reservoirs, such as the Mt. Simon and St. Peter Sandstones, because of its adsorption potential. Organic-rich shales may add to sequestration potential in the Illinois Basin, and they will be assessed as opportunities for collaboration with operators may arise.

The Cambrian Mt. Simon Sandstone is a saline reservoir that underlies most of the Illinois Basin at depths from 305 m to >4,877 m (1,000 ft to >16,000 ft). The Mt. Simon is overlain by shales of the Eau Claire Formation and is underlain by Precambrian granites. The Mt. Simon reservoir sandstone has porosity up to 14% and permeability of over 0.0987 μm^2 (100 millidarcies (md)) in some areas. Illinois Basin Mt. Simon gas storage fields indicate that the Eau Claire is an effective seal for gas containment. The upper 61 m (200 ft) of the Mt. Simon is composed of sandstone beds that are commonly <6.1 m (<20 ft) thick and separated from each other by thin zones of discontinuous shale or low permeability siltstone. Three-dimensional reservoir modeling of the upper Mt. Simon demonstrates the lack of laterally extensive correlative shale barriers that would vertically compartmentalize the reservoir; instead, the shales behave as baffles that impede and redirect migrating CO_2 but do not stop reservoir communication. Wireline logs suggest that below the upper Mt. Simon there are additional porous reservoir sandstones with potentially stacked reservoir strata hundreds of feet thick that might be the sequestration targets.

The long history (almost 50 years) of successful natural gas storage in the Mt. Simon indicates that this saline reservoir could provide successful containment for CO_2 sequestration. Two other Paleozoic sandstone reservoirs, the Ironton-Galesville and St. Peter Sandstones, were assessed for CO_2 storage potential. The St. Peter is particularly attractive because it is generally a clean, well-sorted sandstone with good porosity.

Implementation Plan for Five Sites

The Phase I proposal called for the designation of five sites for field validation testing. During the course of Phase I studies it became clear that these "sites" were indeed not specific locations in the Illinois Basin suitable for immediate drilling. Rather, these sites were trends in the major sink types that showed favorable characteristics with a good probability of yielding a specific location suitable for a field test. The five sites have been designated and are discussed in rank order; two trends have received a rank of 1 because both have a similar balance of risk versus advantages.

Rank 1: Miscible EOR Trend

Miscible CO_2 EOR processes, similar to nearly all of the EOR projects in the Permian Basin of West Texas, was ranked 1 because productive Illinois Basin field locations are well developed; hence, CO_2EOR development risk is low, and the processes of miscible EOR are also well known in the oil industry. More than 2,000 waterflood units or areas exist in the large Illinois Basin. However, composition and minimum miscibility pressures are not well known for Illinois Basin crude oils, and such data will be needed. Substantial incremental oil recovery is expected through the efficiency of the miscible process. Waterflooding to date helps define reservoir continuity and wellbore integrity. Seals are implicitly present based on oil trapping.

Rank 1: Saline Reservoirs in Defined Structures

The Mt. Simon Sandstone and the St. Peter Sandstone are major saline reservoirs that extend across much of the Illinois Basin and occur over anticlinal geologic structures in which injected CO_2 would be trapped by buoyant forces. Injection into these formations would not provide hydrocarbon recovery, but their large areal extent and much greater thickness of tens up to 610 m (hundreds to up to 2,000 ft) and depth offers very large volumes of storage potential at conditions under which the CO_2 can be monitored in formations above the structure and near the spillpoint of the structure. The primary concern in defining these features is the possibility that the Mt. Simon may be thin or absent above the Precambrian basement highs that may control the structures; hence, intensive seismic investigation is necessary before drilling. Geologic seals for these formations are present based on containment of natural gas at gas storage facilities constructed under sufficient overburden in shallower parts of the Basin.

Rank 2: Immiscible EOR Trend

Immiscible EOR and the use of liquid CO_2 at near-miscible conditions offer substantial oil resources and sequestration potential with low development risk. These processes may recover large volumes of oil but not have as high oil recovery as miscible flooding; however, preliminary results of compositional simulations suggest that immiscible CO_2 flooding may take 50% of the CO_2 per incremental barrel of oil, which compensates for the lower recovery. Waterflooding to date helps define reservoir continuity and wellbore integrity. Seals are implicitly present based on oil trapping.

Rank 3: Coal and ECBM Recovery in the Deep Basin Fairway

ECBM as a pilot process has been applied successfully in the San Juan Basin of New Mexico but not in the Illinois Basin. Illinois Basin coals deemed suitable for sequestration testing are shallower than western coals, and commercial CBM production has been established mainly from one coal in southwestern Indiana. Potential response of in situ Illinois Basin coal seams to CO_2 injection is not known, as are the bulk permeability and the hydrology of the seams; hence, development risk for sequestration is judged to be moderate to high. Seal risk is higher than for oil reservoirs due to shallower depths and greater risk of flow in fractures.

Rank 4: Saline Reservoirs on Regional Dip with No Local Structure

This opportunity ranks lowest at this time because as yet there is no experience injecting CO_2 (or any gas) off-structure into Illinois Basin saline reservoirs; hence, to place CO_2 reservoirs on unconfined regional dip would likely facilitate immediate migration of the CO_2 and limit opportunities for monitoring and understanding the fate of the CO_2. We do not propose testing of this option during Phase II. The advantages of this option include large storage capacity over greater areas. Migration toward natural gas storage facilities or potable water in the same formation would have to be assessed. Seals are present based on containment of natural gas at gas storage facilities constructed under sufficient overburden, but shallow areas in the northern part of the Basin should be avoided.

Phase II Pilot Nominations

Implementing geologic sequestration options in the Illinois Basin centers on successful Phase II field validation tests that demonstrate safe and successful surface operations, successful injection and production (oil and coal seam reservoirs) of CO_2, and monitoring of all aspects of geologic and operational risk. Thus far, 35 potential field test sites based on discussions with 10 oil field operators and one utility in the Illinois Basin (Table 9-1) have been identified. Year 1 of Phase II will involve detailed assessment and ranking of these test site opportunities available through these potential partners.

Table 9-1. Portfolio of potential field validation test sites in the Illinois Basin.

Site	Field name	Discovery date	Wells (no.)	Depth (ft)	CO_2 Sink Type	Unitized	Producing formation	Producing lithology
	Ameren Corporation							
1	Newton Plant, Jasper Co, IL			1,600	single-well (ECBM)	no	Carbondale Fm.	coal
2	Hutsonville, Crawford Co., IL			1,200	single-well (ECBM)	no	Carbondale Fm.	coal
	Bretagne GP							
3	Euterpe Field, Henderson Co., KY	1958	10	1,900	immiscible	no	Cypress	sandstone
	Continental Resources of Illinois							
4	Dale Consolidated Field, Thompsonville Unit, McCullum flood, IL	1940	3	2,750	miscible oil	yes	Aux Vases	sandstone
5	Omaha Dome Field, Gallatin Co., IL	from Exxon pre-1968	2	550–630	single-well injection	yes	Curlew Sand	sandstone
6	N. Benton Field, West City Unit, Franklin Co., IL	1941	30	2,800–2,900	miscible oil	yes	Aux Vases	sandstone
7	Spring Garden Field, Spring Garden Unit, Jefferson Co., IL	1977	20	3,100	miscible oil	yes	McClosky oolite bars (pair)	carbonate
8	Johnsonville Field, West Jeff Unit, Wayne Co., IL	1940		3,150	miscible oil	yes	McClosky oolite bars (pair)	carbonate
9	Patoka Field (dropped lease), Mt. Simon, St. Peter, Marion Co., IL,	1937		8,500	deep saline reservoir		none	
10	Ford South Field, Posey Co., IN	2004	1	1,859	single-well injection	no	Waltersburg	sandstone
11	Roland Cons. Field, White Co., IL	2004	1	2,236	single-well injection	yes	Tar Springs	sandstone
35	Citation Oil & Gas Corp							
	Salem Field, Marion Co., IL	pre-1963	>200, 1 to Mt. Simon	8,400	deep saline	yes	Mt. Simon, St. Peter	sandstone
	Covington Oil & Gas							
34	Mattoon Field, Coles Co., IL	1939	20	8,000	deep saline	no	Cypress, Carper	sandstone
	Gallagher Drilling							
12	Griffin Bald Unit, Posey Co., IN	1974	10	1,800	immiscible (liquid)	yes	Clore Sand	sandstone
13	Sugar Creek Field, Jackson Sandstone Unit, Hopkins Co., KY	1965	7	1,800	immiscible (liquid)	yes	Jackson Sand	sandstone
14	Owensville Consol. Cynthiana N Unit, Gibson Co., IN	1985	8	1,800–2,500	immiscible/ miscible	yes	Cypress	sandstone
15	Princeton E, Gibson Co., IN	1987	3	1,900	immiscible	yes	Benoist	sandstone

(continued)

Table 9-1 (continued). Portfolio of potential field validation test sites in the Illinois Basin.

Site	Field name	Discovery date	Wells (no.)	Depth (ft)	CO_2 Sink Type	Unitized	Producing formation	Producing lithology
	Howard Energy							
16	E. Mt. Carmel, Gibson Co., IN	1977	68	2,818–2,855	miscible oil	yes	Salem Limestone	carbonate
17	Albion Unit, Edwards Co., IL	1940	17	3,050–3,130	miscible oil	yes	Aux Vases, O'Hare (Ste. Genevieve)	sandstone, carbonate
18	So. Albion Unit, Edwards Co., IL	1940	9	2,900	miscible oil	yes	Benoist/Aux Vases	sandstone(s)
	Murvin Oil Company							
19	Glover-Kissner Unit, Massilon Field, Wayne County, IL	1987	6	3,270	miscible oil	yes	O'Hara (Ste. Gen)	carbonate
	Oelze Production							
20	Boyd Field, Mt. Simon, St. Peter, Jefferson Co., IL	1944	46	9,500	deep saline reservoir	yes	Benoist, Aux Vases	sandstone(s)
21	Beaucoup North, Washington Co., IL	1951	12	3,050	miscible oil	yes	Clear Creek	dolomite
22	Beaucoup South, Washington Co., IL	1951	17	1,430	immiscible	yes	Bethel	sandstone
23	Nashville North, Washington Co., IL	1979	58	2,740	immiscible	yes	Clear Creek	dolomite
	Podolsky Oil							
24	Black Oak School Unit, Wayne Co., IL	1937	19	3,100	miscible oil	yes	Aux Vases	sandstone
25	Zif-Feller Consolidated Unit, Wayne Co., IL	1937	9	2,940	miscible oil	yes	Aux Vases	sandstone
26	Bayley Unit, Gallatin/White Co., IL	1940	2	2,250	immiscible (liquid)	yes	Waltersburg	sandstone
27	Forsyth Field, Macon Co., IL	1963	40	2,122	immiscible (liquid)	yes	Silurian	dolomite
	Shakespeare Oil							
28	Assumption Central, Christian Co., IL	1984		1,200	immiscible	yes	Benoist	sandstone
29	Tonti Field, Mt. Simon, St. Peter, Lower Devonian, Trenton, Marion Co., IL	1939		9,500	deep saline	yes	Geneva	carbonate
	Team Energy							
30	Griffin Field, Posey Co., IN	1940	32	2,700–2,800	miscible oil	yes	Benoist, Aux Vases	sandstone(s)
31	Cooper-Dunn, Gibson Co., IN	1930	11	2,500	immiscible (liquid)	no	Cypress	sandstone
32	Welborn Field, Posey Co., IN	1943	22	2,800	miscible oil	partially	Aux Vases	sandstone
33	Rapture South, Posey Co., IN	1981	17	2,100	immiscible	yes	Waltersburg	sandstone

Coalbeds

The two ECBM test sites (1 and 2, Table 8-1) are in the MGSC coalbed sequestration fairway. Initial suitability will be determined based on test wells funded outside of the Phase I effort by the Illinois Office of Coal Development. Assessment of these sites will utilize results from the COMET coalbed CH_4 reservoir simulator, input from Phase I regional coalbed mapping and parameter quantification (e.g., depth, thickness, rank, ash content), and local mapping based on data from surrounding oil wells. Completion techniques and details of which coal seams to test will be determined by chemical and petrological assessment. Initial well configuration will involve a pressure observation well and an injection/soak/production well operated as a micropilot modeled after the Fenn-Big Valley (Canada) test by the Alberta Research Council (Mavor and Gunter, 2003; Law et al., 2002). Proportions of produced CH_4 and CO_2 will be determined by gas sampling, and the gas stream will be flared if necessary. The producing well will be air-drilled, if possible, to minimize formation damage by fines. Injectivity will be first tested with water in a pressure transient test followed by a short-term nitrogen injection test and then a CO_2 micropilot to assess coal swelling and permeability reduction.

Mature Oil Fields

CO_2 EOR test sites that met general screening criteria were nominated by operators (Table 8-1) interested in assessing the incremental oil production achievable through CO_2 miscible flooding, immiscible flooding, and injection/soak/production (also called "huff-and-puff") for heavy oil. Collectively, these sites are representative of the major reservoir types in the Illinois Basin necessary to test the technical and economic feasibility of CO_2 EOR. Given that natural CO_2 sources are unknown in the Basin, CO_2 from power plants, refineries, coal gasification facilities, and ethanol plants are the sources for future development of EOR. Sequestration as a consequence of an operational EOR project would occur when a project reaches an economic limit and a net volume of CO_2 remains in the reservoir.

For all EOR processes, injected CO_2 will be both lost to the reservoir (thereby sequestered) and produced with oil; normally, produced CO_2 would be recovered and reinjected, but costs for dehydration and compression may not be justified during a field validation test. Injection/soak/production in an oil reservoir has an unknown potential for net CO_2 storage that is to be assessed. If virtually all the CO_2 returns to the surface with the oil produced, then little effective sequestration is taking place. It is anticipated that a short-term, single-well pilot will evaluate the CO_2 storage of a huff-and-puff test.

Miscible flooding tests will be a major focus of the Phase II effort because of the efficiency and potential economic return that would support sequestration. One initial miscible test site might involve two producers and one injector (converted from a water injector) within a reservoir of limited extent, which would allow maximum control on volumes injected and produced. Larger field tests will involve drilling

one or two wells to optimally place an injector(s) within a field pattern. Current waterflooding processes, pulse/interference testing, or tracer tests will be used to validate hydraulic connectivity between wells. Ideally, surrounding water injectors or stratigraphic boundaries would contain the CO_2 within the test pattern.

Immiscible flooding below the minimum miscibility pressure (MMP) also has oil recovery and sequestration potential. Although the CO_2 and oil do not form a single phase as under the pressure-temperature conditions of miscibility, the CO_2-induced swelling will increase oil saturation, making the oil more amenable to displacement by water (Jarrell et al., 2002). Reservoirs of interest for immiscible flooding will also be under waterflood because, as in the miscible case, we will be able to judge the suitability (reservoir continuity, absence of unexplained fluid losses, absence of leaky casing) of the reservoir for testing based on material balance of water injected compared to water produced. Even if the pressure of the reservoir is below the thermodynamic MMP, CO_2 is known to somewhat reduce the residual oil saturation through increased vaporization. Also, injection of CO_2 near the top of a reservoir can assist gravity drainage (Jarrell et al., 2002).

Permitting of new wells and conversion of existing wells from producers to injectors will be handled by the collaborating lease operator under state regulations governing Underground Injection Control Class II wells. Assessments in advance of developing an injection test will be based on material balance calculations and use of Landmark Corporation's VIP compositional oil reservoir simulator. Waterflooded leases will typically have water supply wells that support the flooding operations, usually from formations shallower than the producing oil reservoir but deeper than domestic water supply wells that can be monitored for any CO_2 leakage.

Saline Reservoirs

MGSC Phase I activities involved evaluation of three potential saline reservoirs for sequestration in the Illinois Basin: the Ironton-Galesville, the St. Peter Sandstone, and the Mt. Simon Sandstone. Initial assessments of all three have been completed. The Ironton-Galesville is an excellent porous and permeable aquifer containing potable water resources in the northern part of the Basin, but it changes to a less favorable facies for injection and storage. The southern edge of the unit is not easily defined because of a lack of well control. At this time, the Ironton-Galesville does not appear to be a candidate for field test consideration for Phase II in the deeper part of the Basin.

The St. Peter Sandstone is generally a fine- to medium-grained, well-rounded, well-sorted sandstone. Some zones within the St. Peter are medium to coarse grained. Individual sandstone beds have good lateral continuity, but their thickness may be variable. The sandstone thickens and thins due to the

filling-in of underlying paleotopography, where local relief can exceed 61 m (200 ft). In general, the St. Peter is 61 to 122 m (200 to 400 ft) thick in the northern part of Illinois and Indiana, 30 to 61 m (100 to 200 ft) thick over most of the central portion of the Illinois Basin, and thins out near the eastern Basin margin. The St. Peter reservoir has been used successfully for natural gas storage, but at least one case of natural gas leakage from shallow St. Peter Sandstone is known in northern Illinois. There are a several hundred feet of dense limestone and dolostone above the St. Peter that provide seals, but the potential for any fracturing in these units must be assessed. Above these carbonate rocks lies the Maquoketa Shale, a widespread horizon that is commonly 46 to 76 m (150 to 250 ft) thick and that would be expected to act as an excellent seal. At Tonti Field (Site 29, Table 9-1), the St. Peter is 30 m (100 ft) of sandstone with an average porosity of 9 to 10% and would be an important saline reservoir for sequestration testing.

The Mt. Simon Sandstone is a freshwater aquifer in the northern part of the Illinois Basin and is used extensively for natural gas storage to the south of its zone of potable water, such as at depths of 1,280 m (4,200 ft) in Champaign County, Illinois, where salinities are approximately 80,000 mg/L (80,000 ppm). The Mt. Simon has good permeability and porosity, and the overlying Eau Claire Formation consists of impermeable limestone, dolomite, and shale seals. Because of its demonstrated ability to contain natural gas, the Mt. Simon would also be an excellent reservoir in which to test injection of CO_2. The upper Mt. Simon is composed of sandstone beds separated by thin zones of discontinuous shale or low-permeability siltstone. Three-dimensional analysis of data obtained from several natural gas storage facilities shows that these low-permeability barriers are not laterally continuous at field scale and may help increase storage capacity. Lower, thicker Mt. Simon sandstones may be the most favorable for injection because of their better reservoir quality. The overlying, more heterogeneous lithologies within the Mt. Simon would tend to increase solubility trapping and residual gas trapping before any mobile supercritical CO_2 migrated to the Eau Claire Shale, the seal of the top of the Mt. Simon.

Gas storage projects in the Illinois Basin all suggest that the Eau Claire Shale is a good seal in the northern and central parts of the Basin. It will be important to recover Eau Claire in core, in addition to core of the Mt. Simon, to understand its varying mineralogy and role as a reservoir seal. However, Phase I work has suggested that, although the Mt. Simon Sandstone is a regionally favorable sequestration target, major Basin-scale structural uplifts must be carefully assessed for faults and fractures and may, in fact, be areas to avoid for initial testing until deep structural conditions are better understood.

Saline reservoir sinks do not offer the economic benefits of EOR or ECBM recovery but do offer large storage capacity. If saline reservoir sinks prove viable with respect to injectability, capacity, and seal integrity, they may be the most suitable for long-term sequestration credits. Saline reservoirs may also be suitable for a CO_2 "bank" where CO_2 may be both injected and recovered, as needed, for EOR or ECBM processes. Phase II research will help to understand the scheduling of CO_2 injection during EOR, since

EOR flooding often involves alternating volumes of water and CO_2 as a means of improving vertical and areal sweep efficiency. Water/alternating gas (WAG) ratios will change during the life of an EOR project, but CO_2 streams from multiple large fixed sources, such as base-load power plants of 1,000 MW and more, will require millions of tons more storage capacity than even multiple EOR projects require. Such large-scale storage would need to target Illinois Basin saline reservoirs. Thus, MGSC Phase II must assess staged and combined development of EOR and saline reservoir storage in the Illinois Basin as a prelude to understanding the scope of storage capacity and transportation requirements needed to serve sequestration at million-tonne annual levels. The MGSC will investigate the use of several sink types in order to assess what might be the most viable sequestration strategy for the Illinois Basin.

Technical Data Needs and Site Evaluation

For the coal seam injection test, attempts will be made to assess injectability through pressure transient testing prior to CO_2 injection. Few data are available in the Basin on this parameter, and nitrogen injection in advance of CO_2 injection may be used if nitrogen can be obtained more readily and at lower cost prior to the CO_2 injection. For EOR testing, given that there are almost 30 sites to choose from for the four pilots, attempts will be made to select a test site where the reservoir can be well characterized with available data. Particularly, a well-documented waterflood that indicates good material balance is expected to be an effective flood without losing CO_2 to unknown parts of the reservoir. For both the ECBM and EOR tests there is no anticipated need for seismic data. However, for the saline reservoir test, two-dimensional surface seismic data and then a three-dimensional seismic data volume must be acquired to ensure that the Mt. Simon is not thinning or absent over the Precambrian basement high that would control structural closure over the selected test site. Seismic two-dimensional data were acquired over the Boyd and Tonti sites (sites 20 and 29, Table 9-1) in 2005 during Phase I, and indications of thinning were found for the Mt. Simon at Tonti, which suggested that the Mt. Simon may be a higher risk. No such thinning was seen at Boyd, but the Mt. Simon may be deeper than anticipated, and, thus, more costly to test. These results are preliminary.

References

Allenby, R.J., and C.C. Schnetzler. 1983. "United States crustal thickness." Tectonophysics, vol. 93, no. 1/2, pp. 13–31.

Aman, B. 2004. Personal communication.

Amorèse, D. 2003. "A new approach for associating earthquakes with geological structures: Application to epicenters in southern Illinois and southeastern Missouri." Geophysical Research Letters, vol. 30, no. 13, pp. 1689, doi:10.1029/2003GL017247.

Anderson, A.C., S.M. Frailey, H.E. Leetaru, and A. Lawal. 2005. "Volumetric equations for CO_2 storage in coalbeds, oil and gas reservoirs, and saline formations." Paper presented at the Fourth Annual Conference on Carbon Capture and Sequestration, May 2–5, Alexandria, VA.

Anderson, A.C., T.R. Moore, S.M. Frailey, J.A. Rupp, and C.F. Eble. 2005. "Identification of Favorable Reservoir Properties for CO_2 Sequestration and Enhanced Coalbed Methane Production in the Illinois Basin." Poster presented at the Fourth Annual Conference on Carbon Capture and Sequestration, May 2–5, Alexandria, VA.

Anonymous. 1994. Pipeline report, U.S. underground natural gas storage fields. Oil and Gas Journal, Sept. 12, Special Issue, p. 47.

Archer, P.L., and J.N. Kirr. 1984. "Pennsylvanian geology, coal, and coalbed methane resources of the Illinois Basin—Illinois, Indiana, and Kentucky," in C.T. Rightmire, G.E. Eddy, and J.N. Kirr, eds., Methane Resources of the United States. American Association of Petroleum Geologists, Studies in Geology, vol. 17, pp. 105–134.

Atekwana, E.A. 1996. "Precambrian basement beneath the central Midcontinent United States as interpreted from potential field imagery," in B.A. van der Pluijm and P.A. Catacosinos, eds., Basement and Basins of Eastern North America. Boulder, Colorado, Geological Society of America, Special Paper 308, pp. 33–44.

Atherton, E. 1971. "Tectonic development of the eastern interior region of the United States," in D.C. Bond, Background Materials for Symposium on Future Petroleum Potential of NPC Region 9 (Illinois Basin, Cincinnati Arch, and Northern Part of Mississippi Embayment). Illinois State Geological Survey, Illinois Petroleum 96, pp. 29–43.

Athy, L.F. 1928. "Geology and mineral resources of the Herscher quadrangle." Illinois State Geological Survey, Bulletin 55, 120 pp.

Ault, C.H. 1988. "The Wabash Valley fault system in Indiana and Kentucky," in C.W. Zuppann, B.D. Keith, and S.J. Keller, eds., Geology and petroleum production of the Illinois Basin; Volume 2. Mt. Vernon, Illinois, Illinois and Indiana-Kentucky Geological Societies, p. 21.

Baisch, S., and H.-P. Harjes. 2003. "A model for fluid-injection-induced seismicity at the KTB, Germany." Geophysics Journal International, vol. 152, pp. 160–170.

Bakun, W.H., and M.G. Hopper. 2004. “Catalog of significant historical earthquakes in the central United States.” U.S. Geological Survey, Open File Report 2004-1086, 142 pp.

Bakun, W.H., A.C. Johnston, and M.G. Hopper. 2003. “Estimating locations and magnitudes of earthquakes in eastern North America from modified Mercalli intensities.” Bulletin of the Seismological Society of America, vol. 93, pp. 190–202.

Bakun, W.H., and C.M. Wentworth. 1997. “Estimating earthquake location and magnitude from seismic intensity data.” Bulletin of the Seismological Society of America, vol. 87, pp. 1502–1521.

Bauer, R.A. 2005. “Earthquakes/microseismic activity and underground gas storage reservoirs,” ms.

Bauer, R.A., and J. Nelson. 2005. “Compilation of In Situ Stress Measurements in Illinois.” Illinois State Geological Survey, unpublished manuscript files, 11 pp.

Bear, G.W., A.J. Rudman, and J.A. Rupp. 1996. “Faulting and sediment distribution in the Wabash Valley and southern Indiana: implications for the tectonic history of the Illinois Basin.” Seismological Research Letters, vol. 67, p. 32.

Beaverson, S.K., and R.J. Finley. 2005. “Fact Sheet, Midwest Geological Sequestration Consortium.” http://sequestration.org/publish/mgsc_fact1.doc Accessd March, 2006. 2 pp.

Bell, A.H., E. Atherton, T.C. Buschbach, and D.H. Swann. 1964. “Deep oil possibilities of the Illinois Basin.” Illinois State Geological Survey, Circular 368, 38 pp.

Benesh, M.E., C.M. Clark, W.R. Clark, E.G. Hammerschmidt, D.L. Katz, J.D. Parent, O.S. Seim, and R.D. Sickafoose. 1956. “A study of the Herscher Storage Reservoir.” Unpublished Report located at the Illinois State Geological Survey library, 74 pp.

Bertagne, A.J., and T.C. Leising. 1991. “Interpretation of seismic data from the Rough Creek Graben of western Kentucky and southern Illinois,” *in* M.W. Leighton, D.R. Kolata, D.F. Oltz, and J.J. Eidel, eds., Interior cratonic basins. American Association of Petroleum Geologists, Memoir 51, pp. 199–208.

Bethke, C.M. 2004. “The Geochemist’s Workbench.” Rockware, Golden, CO.

Bickford, M.E., W.R. Van Schmus, and I. Zietz. 1986. “Proterozoic history of the midcontinent region of North America.” Geology, vol. 14, no. 6, pp. 492–496.

Bond, D.C. 1972. “Hydrodynamics in deep aquifer of the Illinois Basin.” Illinois State Geological Survey, Circular 470, 72 pp.

Bradbury, J.C., and E. Atherton. 1965. “The Precambrian basement of Illinois.” Illinois State Geological Survey, Circular 382, 13 pp.

Braile, L.W., W.J. Hinze, and G.R. Keller. 1997. "New Madrid seismicity, gravity anomalies, and interpreted ancient rift structures." Seismological Research Letters, vol. 68, no. 4, pp. 599–610.

Bredehoeft, J.D., C.R. Blyth, W.A. White, and G.B. Maxey. 1963. "Possible mechanism for concentration of brines in subsurface formations." American Association of Petroleum Geologists Bulletin, vol. 47, no. 2, pp. 257–269.

Brock, W.R., and L.A. Bryan. 1990. "Summary Results of CO_2 EOR Field Tests 1972–1987." Paper SPE 18977 presented at the 1990 SPE/DOE Symposium on Enhanced Oil Recovery, Tulsa, OK, April 22–25.

Brower, R.D., A.P. Visocky, I.G. Krapac, B.R. Hensel, G.R. Peyton, J.S. Nealon, and M. Guthrie. 1989. "Evaluation of underground injection of industrial waste in Illinois." Illinois Scientific Surveys Joint Report 2, 89 pp.

Burnett, P. 1967. Illinois Commerce Commission Docket No. 53338, Exhibit No. 20, p. 4.

Buschbach, T.C. 1964. "Cambrian and Ordovician strata of northeastern Illinois." Illinois State Geological Survey, Report of Investigations 218, 90 pp.

Buschbach, T.C., and D.C. Bond. 1974. "Underground storage of natural gas in Illinois—1973." Illinois State Geological Survey, Illinois Petroleum 101, 71 pp.

Buschbach, T.C., and D.R. Kolata. 1991. "Regional setting of the Illinois Basin," in M.W. Leighton, D.R. Kolata, D.F. Oltz, and J.J. Eidel, eds., Interior Cratonic Basins. Tulsa, Oklahoma, American Association of Petroleum Geologists, Memoir 51, pp. 29–55.

Bustin, R.M., and C.R. Clarkson. 1998. "Geological controls on coalbed methane reservoir capacity and gas content." International Journal of Coal Geology, vol. 38, pp. 3–26.

Byers, C.W. 1978. "Depositional environments of fine-grained upper Cambrian lithofacies," in E. Odom, ed., Lithostratigraphy, petrology, and sedimentation of Late Cambrian-Early Ordovician rocks near Madison, Wisconsin. Society of Economic Paleontologists and Mineralogists, Great Lakes Section, Field Trip Guidebook No. 3, pp. 67–82.

Carr, D.D. 1973. "Geometry and origin of oolite bodies in the Ste. Genevieve Limestone (Mississippian) in the Illinois Basin." Indiana Geological Survey, Bulletin 48.

Carroll, R.E., and J.C. Pashin. 2001. "Carbon sequestration potential of coalbed methane reservoirs in the Black Warrior Basin—relationship of sorption capacity to coal quality." Abstracts and Program, vol. 18, Eighteenth Annual Meeting of the Society for Organic Petrology, Houston, TX, p. 23.

Chang, Y.B. 1998. "A compositional model for CO_2 floods including CO_2 solubility in water." SPE Reservoir Evaluation and Engineering, pp. 155–160.

Chaumet, P., R. Croissant, and J. Colonna. 1966. "Stockage souterrain de gas naturel en aqifere: Dynamizue de l'interface eau-gaz (Underground aquifer natural gas storage: Dynamics of the water-gas interface)." Inst. Francais petrole Rev. et Annales combustibles liquids, vol. 21, no. 9, pp. 1255–1270.

Chiu, J.M., A.C. Johnston, and Y.T. Yang. 1992. “Imaging the active faults of the central New Madrid seismic zone using PANDA array data.” Seismological Research Letters, vol. 63, no. 3, pp. 375–393.

Choquette, P.W., and R.P. Steinen. 1980. “Mississippian non-supratidal dolomite, Ste. Genevieve Limestone, Illinois Basin: evidence for mixed-water dolomitization,” *in* D.H. Zenger, J.B. Dunham, and R.L. Ethington, eds., Concepts and Models of Dolomitization-A Symposium. SEPM Special Publication 28.

Clarkson, C.R., and R.M. Bustin. 1999. “The effect of pore structure and gas pressure upon the transport properties of coal: a laboratory and modeling study—1. Isotherms and pore volume distributions.” Fuel, vol. 78, pp. 1333–1344.

Clarkson, C.R., and R.M. Bustin. 2000. “Binary gas adsorption/desorption isotherms—effect of moisture and coal composition upon carbon dioxide selectivity over methane.” International Journal of Coal Geology, vol. 42, pp. 241–271.

Cluff, R.M. 1986. “Application of Modern Carbonate Sand Models to Oil and Gas Exploration, Mississippian Ste. Genevieve Limestone, Illinois Basin,” *in* B. Seyler, ed., Aux Vases and Ste. Genevieve Formations: A Core Workshop and Field Trip Guidebook. Illinois Geological Society and Illinois State Geological Survey.

Cluff, R.M., and J.A. Lineback. 1981. “Middle Mississippian carbonates of the Illinois Basin.” Illinois Geological Society.

Cluff, R.M., M.L. Reinbold, and J.A. Lineback. 1981. “The New Albany Shale Group of Illinois.” Illinois State Geological Survey, Circular 518, 83 pp.

Connolly, C. 2001. “The availability of the Seelyville Coal Member for mining in Indiana.” Indiana Geological Survey Open-File Study 01-8, Indiana Geological Survey, Bloomington, 52 pp.

Connolly, C.L., and A. Zlotin. 1999. “The availability of the Springfield Coal Member for mining in Indiana.” Indiana Geological Survey Open-File Study 99-7, Indiana Geological Survey, Bloomington, 49 pp.

Connolly, C.L., and A. Zlotin. 2000. “The availability of the Danville Coal Member for mining in Indiana.” Indiana Geological Survey Open-File Study 2000-1, Indiana Geological Survey, Bloomington, 47 pp.

Cook, F.A., and K. Vasudevan. 2003. “Are there relict crustal fragments beneath the Moho?” Tectonics, vol. 22, no. 3, 1026 2004-014282.

Craig, Jr., F.F. 1993. “The Reservoir Aspects of Waterflooding.” SPE Monograph Series, vol. 3, 4th edition.

Craig, L.C., and K.L. Varnes. 1979. “History of the Mississippian System—an interpretive summary.” Geological Survey Professional Paper 1010-R, pp. 371–406.

Cui, X., R.M. Bustin, and G. Dipple. 2004. “Selective transport of CO_2, CH_4, and N_2 in coals—insights from modeling of experimental gas adsorption data.” Fuel, vol. 83, pp. 293–303.

Dapples, E.C. 1955. “General lithofacies relationships of St. Peter Sandstone and Simpson Group.” American Association of Petroleum Geologists Bulletin, vol. 39, pp. 444–467.

Demir, I., D.G. Morse, S.D. Elrick, and C.A. Chenoweth. 2004. "Delineation of the Coalbed methane resources of Illinois." Illinois State Geological Survey, Circular 564, CD-ROM.

Drahovzal, J.A. 1994. "Basin-floor fan complexes: A new exploration strategy for the Rough Creek Graben," *in* J.L. Ridgley, J.A. Drahovzal, B.D. Keith, and D.R. Kolata, eds., Proceedings of the Illinois Basin Energy and Mineral Resources Workshop. Kentucky Geological Survey, Open-file Report 94-12 (Illinois State Geological Survey, Open-file report 94-4; Indiana Geological Survey, Open-File Report 94-2; U.S. Geological Survey, Open-File Report 94-298), pp. 7–8.

Drahovzal, J.A. 1997. "Proterozoic sequences and their implications for Precambrian and Cambrian geologic evolution of western Kentucky: evidence from seismic-reflection data." Seismological Research Letters, vol. 68, no. 4, pp. 553–566.

Drahovzal, J.A. 2000. "Alternating extension and contraction in the Proterozoic of the Eastern Midcontinent [abs.]." American Association of Petroleum Geologists Bulletin, vol. 84, no. 9, p. 1382.

Drahovzal, J.A., and D.C. Harris. 1998. "The East Continent Rift Basin: Its age and genesis [abs.]." American Association of Petroleum Geologists, vol. 82, no. 9, pp. 1766–1767.

Drahovzal, J.A., and D.C. Harris. 2004. "Potential Reservoirs for Geologic Sequestration in the East Continent Rift Basin." http://www.midcarb.org/Documents/Potential%20Reservoirs%20for%20Geologic%20Sequestration%20in%20the%20Eas%85.pdf Accessed March 6, 2006. 6 pp.

Drahovzal, J.A., L.H. Wickstrom, D. Walker, M.T. Baranoski, B.D. Keith, and L.C. Furer. 1992. "The East Continent Rift Basin: A new discovery." Kentucky Geological Survey, Series XI, Special Publication 18, 25 pp.

Driese, S.G., C.W. Byers, and R.H. Dott. 1981. "Tidal deposition in the basal Upper Cambrian Mt. Simon Formation in Wisconsin." Journal of Sedimentary Petrology, vol. 51, no. 2, pp. 367–381.

Drobniak, A., C.P. Korose, M. Mastalerz, A.C. Anderson, T.R. Moore, and J.A. Rupp. 2005. "Sequestration Potential in the Illinois Basin Coal Beds; Facts and Uncertainties." Poster presented at the Fourth Annual Conference on Carbon Capture and Sequestration, May 2–5, Alexandria, VA.

Drobniak, A., C.P. Korose, M. Mastalerz, A.C. Anderson, T.R. Moore, and J.A. Rupp. 2005. "Sequestration Potential in the Illinois Basin Coal Beds." Poster presented at Twenty-Second Annual Meeting of the Society for Organic Petrology, September 11–14, Louisville, KY; Eastern Section American Association of Petroleum Geologist Meeting, September 18–20, Morgantown WV; Fifty-Seventh Annual Meeting of the International Committee for Coal and Organic Petrology, September 18–23, Patras, Greece.

Drobniak, A., M. Mastalerz, C.F. Eble, C.P. Korose, and S.D. Elrick. 2004. "Illinois Basin Coal GIS Datasets for Coalbed Methane, Carbon Sequestration, and Coal Resource Studies." Poster presented at Midwest PTTC First Annual Illinois Basin Coalbed Symposium, November 16–17, Evansville, IN; 18th Annual Surface Mined Land Reclamation Technology Transfer Seminar, December 6–7, Jasper, IN.

Duchek, A.B., J.H. McBride, W.J. Nelson, and H.E. Leetaru. 2004. "The Cottage Grove fault system (Illinois Basin): Late Paleozoic transpression along a Precambrian crustal boundary." Geological Society of America Bulletin, vol. 116, no. 11, pp. 1465–1484.

Ellis, W.L. 1994. "Summary and discussion of crustal stress data in the region of the New Madrid seismic zone," in K.M. Shedlock and A.C. Johnston, eds., Investigations of the New Madrid Seismic Zone. U.S. Geological Survey, Professional Paper 1538-B, pp. B1–B13.

Energy Information Administration. 2004. Subject: Underground natural gas storage. http://www.eia.doe.gov/pub/oil_gas/natural_gas/analysis_publications/storagebasics/storagebasics.pdf Accessed Feb. 16, 2006.

Energy Information Administration. 2005. Annual Coal Report 2004, Table ES2: U.S. Coal Production by Coal-Producing Region and State, 2003-2004. http://www.eia.doe.gov/cneaf/coal/page/acr/acr_sum.html Accessed March 20, 2006.

Enick, R.M., and S.M. Klara. 1992. "Effects of CO_2 solubility in brine on the compositional simulation of CO_2 floods." SPE Reservoir Engineering, pp. 253–258.

Evans, K.F., H. Moriya, H. Niitsuma, R.H. Jones, W.S. Phillips, A. Genter, J. Sausse, R. Jung, and R. Baria. 2005. "Microseismicity and permeability enhancement of hydrogeologic structures during massive fluid injections into granite at 3 km depth at the Soultz HDR site." Geophysical Journal International, vol. 160, pp. 388–412.

Finley R.J. 2004. "Assessment of Geological Carbon Sequestration Options in the Illinois Basin." Presentation made at U.S. Department of Energy Kickoff Meeting, November 3, Pittsburg, PA.

Finley, R.J., S.R. Gustison, and H.E. Leetaru. 2004. "Geological Consideration for CO_2 Sequestration in a Cratonic Basin: An Assessment of Options in the Illinois Basin, USA." Paper presented at the Seventh International Conference on Greenhouse Gas Control Technologies, September 5–9, Vancouver BC, Canada.

Frailey, S.M., H.E. Leetaru, R.J. Finley, S.R. Gustison, C.P. Korose, D.A. Garner, J. Rupp, and J. Drahovzal. 2004. "Illinois Basin Screening Criteria for Geologic CO_2 Sequestration." Poster presented at the Third Annual Conference on Carbon Capture and Sequestration, May 3–6, Alexandria, VA.

Frailey, S.M., H.E Leetaru, E. Mehnert, M.A. Person, and V. Bense. 2005. "Basinwide implications of large CO_2 injected volumes to deep saline formations." Paper presented at the Fourth Annual Conference on Carbon Capture and Sequestration, May 2–5, Alexandria, VA.

Frankel, A. 1995. "Mapping seismic hazard in the Central and Eastern United States." Seismological Research Letters, vol. 66, pp. 8–21.

Fox, C., and S.M. Avasthi. 2004. "Practical Aspects of CO_2 Flooding and sequestration." SPE Short Course, at the 2004 SPE/DOE Symposium on Enhanced Oil Recovery, Tulsa, April 18–21.

Gallagher, M. 2004. Personal communication.

Garrels, R.M., and C.L. Christ. 1965. “Solutions, Minerals, and Equilibria.” Freeman, Cooper, and Company. San Francisco, CA. 450 pp.

Gibson, A.C. 2001. “Three-Dimensional Geometries and Porosity Trends of Subsurface Ooid Shoal Hydrocarbon Reservoirs in the Mississippian Ste. Genevieve Formation of the Illinois Basin, USA.” M.S. thesis. University of Illinois.

Goetz, L.K., J.G. Tylor, R.L. Macarevich, D. Brewster, and J. Sonnad. 1992. “Deep gas play probed along Rough Creek Graben in Kentucky part of southern Illinois Basin.” Oil and Gas Journal, vol. 90, no. 38, pp. 97–107.

Gomberg, J., and L. Wolf. 1999. “Possible cause for an improbable earthquake: The 1997 M_w 4.9 southern Alabama earthquake and hydrocarbon recovery.” Geology, vol. 27, no. 4, pp. 367–370.

Goodman, A.L., A. Busch, G.J. Duffy, J.E. Fitzgerald, K.A.M. Gasem, Y. Gensterblum, B.M. Krooss, J. Levy, E. Ozdemir, et al. 2004. “An Inter-laboratory Comparison of CO2 Isotherms Measured on Argonne Premium Coal Samples.” Energy and Fuels, vol. 18, pp. 1175–1182.

Gordon, D.W. 1988. “Revised instrumental hypocenters and correlation of earthquake locations and tectonics in the Central United States.” U.S. Geological Survey, Professional Paper 1364, 69 pp.

Greenberg, S.E. 2005. “Is Our Climate Changing? Perceptions and Misconceptions.” University of Illinois.

Griffith, H.D., Jr. and R.D. Rinehart. 1971. “Early planning for gas storage pays off—A case history of Kentucky’s largest gas field.” Society of Petroleum Engineers Annual Meeting, New Orleans Louisiana, SPE paper 3434.

Gunter, J. 1965. “Etude de la Liaison gaz-charbon.” Revue de l’Industrie Minerale, vol. 47, pp. 693–708.

Gunter, W.D., E.H. Perkins, and I. Hutcheon. 2000. “Aquifer disposal of acid gases: modelling of water-rock reactions for trapping of acid wastes.” Applied Geochemistry, vol. 15, no. 8, pp. 1085–1095.

Gupta, N., and E.S. Bair. 1997. “Variable-density flow in the midcontinent basins and arches region of the United States.” Water Resources Research, vol. 33, no. 8, pp. 1785–1802.

Gutstadt, A.M. 1958. “Cambrian and Ordovician stratigraphy and oil and gas possibilities in Indiana.” Indiana Geological Survey, Bulletin 14, 103 pp.

Hackley, K.C. 2002. “A chemical and isotopic investigation of the groundwater in the Mahomet Bedrock Valley aquifer—Age, recharge and geochemical evolution of the groundwater.” Urbana-Champaign, Illinois, University of Illinois, Ph.D. dissertation.

Hamburger, M.W., and J.A. Rupp. 1988. “The June 1987 southeastern Illinois earthquake: possible tectonism associated with the La Salle Anticlinal belt.” Seismological Research Letters, vol. 59, pp. 151–157.

Harris, L.D. 1975. “Oil and gas data from the Lower Ordovician and Cambrian rocks of the Appalachian basin.” U.S. Geological Survey, Miscellaneous Investigations Series, Map I-917 D.

Hasenmueller, N.R., and J.B. Comer, eds. 2000. GIS Compilation of Gas Potential of the New Albany Shale. Indiana Geological Survey, Illinois Basin Consortium, Gas Research Institute, CD-ROM, GRI-00/0068.

Hatch, J.R., and R.H. Affolter, eds. 2002. "Resource Assessment of the Springfield, Herrin, Danville, and Baker Coals in the Illinois Basin." U.S. Geological Survey, Professional Paper 1625-D, CD-ROM.

Healy, J.H., W.W. Rubey, D.T. Griggs, and C.B. Raleigh. 1968. "The Denver earthquakes." Science, vol. 161, no. 3848, pp. 1301–1310.

Heigold, P.C., and D.F. Oltz. 1991. "Seismic expression of the stratigraphic succession," in M.W. Leighton, D.R. Kolata, D.F. Oltz, and J.J. Eidel, eds., Interior Cratonic Basins. Tulsa, Oklahoma, American Association of Petroleum Geologists, Memoir 51, pp. 169–178.

Herrmann, R.B. 1979. "Surface wave focal mechanisms for eastern North American earthquakes with tectonic implications." Journal of Geophysical Research, vol. 84, no. B7, pp. 3543–3552.

Hester, N.C. 1988. "Seismic stratigraphy and structure of the Moorman Trough," in C.W. Zuppann, and B.D. Keith, eds., Geology and petroleum production of the Illinois Basin, vol. 2. Bloomington, Indiana, Indiana Geological Survey, p. 13.

Hildenbrand, T.G., J.H. McBride, D. Ravat. 2002. "The Commerce geophysical lineament and its possible relation to Proterozoic igneous complexes and large earthquakes in the south-central Illinois Basin." Seismological Research Letters, vol. 73, pp. 640–659.

Hildenbrand, T.G., W.D. Stuart, and P. Talwani. 2001. "Geologic structures related to New Madrid earthquakes near Memphis, Tennessee, based on gravity and magnetic interpretations." Engineering Geology, vol. 62, no. 1/3, pp. 105–121.

Honarpour, M., L.F. Koederitz, and A.H. Harvey. 1986. Relative Permeability of Petroleum Reservoirs. CRC Press.

Houseknecht, D.W., and F.G. Ethridge. 1978. "Depositional history of the Lamotte Sandstone of southeast Missouri." Journal of Sedimentary Petrography, vol. 48, pp. 575–586.

Hovorka, S.D., R. Hotinski, and S.J. Friedmann. 2005. "Audience-Pleasing Physical Models to Support CO_2 Outreach." Fourth Annual Conference on Carbon Capture and Sequestration, May 2–5. Alexandria, VA.

Howard, R.H. 1991. "Hydrocarbon Reservoir Distribution in the Illinois Basin," *in* M.W. Leighton, D.R. Kolata, D.F. Oltz, and J.J. Eidel, eds., Interior Cratonic Basins. American Association of Petroleum Geologists, Memoir 51, pp. 299–327.

Howard, R.H., and S.T. Whitaker. 1990. "Fluvial-estuarine valley fill at the Mississippian-Pennsylvanian unconformity, Main Consolidated field, Illinois," in J.H. Barwis, J.G. McPherson, and J.R.J. Studlick, eds., Petroleum reservoirs. New York, Springer-Verlag, pp. 319–341.

Huber, M.E. 1975. "A paleoenvironmental interpretation of the Upper Cambrian Eau Clair Formation of west-central Wisconsin." Madison, University of Wisconsin-Madison, M.S. thesis, 110 pp.

Huff, B. 1998. “Oil and Gas Development in Illinois.” Illinois State Geological Survey, Illinois Petroleum 154.

Huff, B. 2004. Personal communication.

Hwang, H.-H. 1996. “Source of saline groundwater in basal Pennsylvanian sandstones, southwestern Illinois—Implications for fluid mixing and water-rock interactions.” Urbana-Champaign, Illinois, University of Illinois, Ph.D. dissertation.

Interstate Oil and Gas Compact Commission. 2005. “Carbon capture and storage: A regulatory framework for states.” Oklahoma City, OK, 80 p.

ISGS. 2005. Subject: Geospatial data. http://www.isgs.uiuc.edu/nsdihome/ISGSindex.html Accessed Jan. 30, 2006.

Jackson, S. 2001. Advances in seismic stimulation technologies. PTTC Network News, 2nd Quarter.

Jacobson, R.J., and C.P. Korose. 2003. “Coal Geology of Illinois,” in 2003 Keystone Coal Industry Manual, Coal Age. PRIMEDIA Business Magazines and Media. Chicago, IL, p. 508.

Jarrell, P.M., C.E. Fox, M.H. Stein, and S.L. Webb. 2002. “Practical Aspects of CO_2 Flooding.” SPE Monograph, vol. 22, Henry L. Doherty Memorial Fund of AIME, Society of Petroleum Engineers Inc., 220 pp.

Johnson, J.W., J.J. Nitao, C.I. Steefel, and K.G. Knauss. 2001. “Reactive transport modeling of geologic CO_2 sequestration in saline aquifers: the influence of intra-aquifer shales and the relative effectiveness of structural, solubility, and mineral trapping during prograde and retrograde sequestration.” 1st Annual Conference on Carbon Sequestration Proceedings, Washington, DC.

Joubert, J.I., C.T. Grein, and D. Bienstock. 1973. “Sorption of methane in moist coal.” Fuel, vol. 52, pp. 181–185.

Joubert, J.I., C.T. Grein, and D. Bienstock. 1974. “Effect of moisture on the methane capacity of American coals.” Fuel, vol. 53, pp. 186–191.

Karlstrom, K.E., S.S. Harlan, M.L. Williams, J. McLelland, J.W. Geissman, and K.-I. Åhäll. 1999. “Refining Rodinia: Geologic Evidence for the Australia–Western U.S. connection in the Proterozoic.” GSA Today, vol. 9, no. 10, pp. 1–7.

Katz, D.L., and K.H. Coats. 1968. “Underground storage of fluids.” Ann Arbor, MI. Ulrich’s Books, Inc., 575 pp.

Kelkar, M., and G. Perez. 2002. “Applied Geostatistics for Reservoir Characterization.” Society of Petroleum Engineers, Inc. Richardson, Texas.

The Keystone Center. 2005. “Global Climate Change: An Interdisciplinary Curriculum Module.” Keystone, CO.

Kisslinger, C. 1976. “A review of theories of mechanisms of induced seismicity,” in W.G. Milne, ed., Induced Seismicity. Engineering Geology, vol. 10, no. 2/4, pp. 85–98.

Knepp, R., D.A. Garner, S.M. Frailey, B. Seyler, C.P. Korose, J.P. Grube, D.A. Keefer, and S.C. Rittenhouse. 2005. "CO_2 Sequestration and Enhanced Oil Recovery Potential in Illinois Basin Oil Reservoirs." Poster presented at the Fourth Annual Conference on Carbon Capture and Sequestration, May 2–5, Alexandria, VA.

Knoll, P. 1992. "The dynamic excess pore pressure concept—A new possible fracture mechanism for fluid-induced seismic events," *in* P. Knoll, ed., Induced Seismicity. A.A. Balkema Publishers, pp. 275–286.

Kolata, D.R. 1991. "Illinois Basin geometry," in M.W. Leighton, D.R. Kolata, D.F. Oltz, and J.J. Eidel, eds., Interior cratonic basins. American Association of Petroleum Geologists, Memoir 51, p. 197

Kolata, D.R. 2005. Bedrock Geology Map of Illinois. Illinois State Geological Survey. Scale 1:500,000.

Kolata, D.R., T.C. Buschbach, and J.D. Treworgy. 1978. "The Sandwich Fault Zone of northern Illinois." Illinois State Geological Survey, Circular 505, 26 p.

Kolata, D.R., and A.M. Graese. 1983. "Lithostratigraphy and depositional environments of the Maquoketa Group (Ordovician) in Northern Illinois." Illinois State Geological Survey, Circular 528, 49 p.

Kolata, D.R., and W.J. Nelson. 1991. "Tectonic history of the Illinois Basin," in M.W. Leighton, D.R. Kolata, D.F. Oltz, and J.J. Eidel, eds., Interior Cratonic Basins. Tulsa, Oklahoma, American Association of Petroleum Geologists, Memoir 51, pp. 263–285.

Kolata, D.R., and W.J. Nelson. 1997. "Role of the Reelfoot Rift/Rough Creek Graben in the evolution of the Illinois Basin," in R.W. Ojakangas, A.B. Dickas, and J.C. Green, eds., Middle Proterozoic to Cambrian rifting, central North America. Boulder, Colorado, Geological Society of America, Special Paper 312, pp. 287–298.

Kolata, D.R., D.F. Oltz, and J.J. Eidel. 1990. "Interior Cratonic Basins." Tulsa, Oklahoma, American Association of Petroleum Geologists, Memoir 51.

Korose, C.P., D.A. Garner, A.L. Luther, S.M. Frailey, and B.J. Seyler. 2004. "Oil Field Screening Study for CO_2 Sequestration and Enhanced Oil Recovery in the Illinois Basin." Poster presented at the Twenty-Fifth International ESRI User Conference, August 9–13, San Diego, CA.

Korose, C.P., and H.E. Leetaru. 2005. "Geological Sequestration of Carbon Dioxide in the Illinois Basin, Midwest Geological Sequestration Consortium." http://sequestration.org/publish/MGSC_outreach1.pdf Accessed March 7, 2006. 1 p.

Krumhansl, J.L., H.R. Westrich, and C. Jove-Colon. 2003. "Geochemical implications of CO_2 sequestration in arkosic sandstone reservoirs." 2nd Annual Conference on Carbon Sequestration Proceedings, Washington, DC.

Langenheim, V.E., and T.G. Hildenbrand. 1997. "Commerce geophysical lineament—its source, geometry, and relation to the Reelfoot Rift and New Madrid seismic zone." Geological Society of America Bulletin, vol. 109, no. 5, pp. 580–595.

Langer, C.J., and G.A. Bollinger. 1991. “The southeastern Illinois earthquake of 10 June 1987: the later aftershocks.” Bulletin of the Seismological Society of America, vol. 81, no. 2, pp. 423–445.

Law, D.H.S., L.G.H. Van der Meer, and W.D. Gunter. 2002. “Numerical simulator comparison study for enhanced coalbed methane recovery processes, part I: pure carbon dioxide injection.” SPE 75669, SPE Gas Technology Symposium, Calgary, AB, 14 pp.

Leetaru, H.E. 2005. “Geological traps to sequester CO_2 from the atmosphere.” Paper presented at the Association of Engineering Geologists, North Central Section Meeting, April 19th, Lombard, IL.

Leetaru, H.E. 2005. “Midwest Geological Sequestration Consortium Overview: Carbon Sequestration Leadership Forum (CSLF) Stakeholder Briefing.” Paper presented at the Fourth Annual Conference on Carbon Capture and Sequestration, May 2–5, Alexandria, VA.

Leetaru, H.E., S.M. Frailey, D.G. Morse, R.J. Finley, C.P. Korose, and J.H. McBride. 2005. “Site selection for carbon sequestration in saline reservoirs.” Paper presented at the Eastern Section of the American Association of Petroleum Geologists Annual Meeting, September 18–20, Morgantown, WV.

Leetaru, H.E., D.G. Morse, S.M. Frailey, J. Drahovzal, J.H. McBride, D.A. Keefer, C.P. Korose., S.C. Rittenhouse, R.A. Bauer, E. Mehnert, D.R. Kolata, and S. Fisher. 2005. “The Deep Geological Option: Saline Reservoirs.” Paper presented at the Public Outreach Meeting, September 27, Springfield, IL and September 28th, Evansville, IN and at the Regional Carbon Sequestration Partnership Review Meeting, October 12–14, Pittsburgh, PA.

Leetaru, H.E., D.G. Morse, S.M. Frailey, J. Drahovzal, J.H. McBride, D.A. Keefer, C.P. Korose., S.C. Rittenhouse, R.A. Bauer, E. Mehnert, D.R. Kolata, and S. Fisher. 2005. “Final Report, Task 6, Saline Reservoirs.” Paper presented at Producer Advisory Group Meeting, September 13, Champaign-Urbana, IL.

Leetaru, H.E., D.G. Morse, S.M. Frailey, R.J. Finley. 2005. “Mt. Simon Sandstone as a carbon sequestration sink in the Illinois Basin.” Paper presented at the 2005 Annual meeting of the American Association of Petroleum Geologists, June 19–22, Calgary AB, Canada.

Leetaru, H.E., D.G. Morse, S.M. Frailey, D.A. Keefer, E. Mehnert, J. Drahovzal, S. Fisher, S.C. Rittenhouse, and J.H. McBride. 2004. “Saline Reservoirs in the Illinois Basin.” Paper presented at the US DOE Regional Carbon Sequestration Partnerships Annual Program Review Meeting, November 16–17, Pittsburg, PA.

Leetaru, H.E., S.C. Rittenhouse, S.M. Frailey, D.A. Keefer, D.G. Morse, R.J. Finley, and J.H. McBride. 2005. “Deep saline reservoirs as a carbon sequestration target in the Illinois Basin.” Paper presented at the Fourth Annual Conference on Carbon Capture and Sequestration, May 2–5, Alexandria, VA.

Lidiak, E.G. 1996. “Geochemistry of subsurface Proterozoic rocks in the eastern Midcontinent of the United States: Further evidence for a within-plate tectonic setting,” in B.A. van der Pluijm and P.A. Catacosinos, eds., Basement and basins of eastern North America. Boulder, Colorado, Geological Society of America, Special Paper 308, pp. 45–66.

Lidiak, E.G., W.J. Hinze, G.R. Keller, J.E. Reed, L.W. Braile, and R.W. Johnson. 1985. "Geologic significance of regional gravity and magnetic anomalies in the east-central Midcontinent," in W.J. Hinze, ed., The Utility of Regional Gravity and Magnetic Anomaly Maps: Tulsa, Oklahoma, Society of Exploration Geophysicists, pp. 287–307.

Lohrenz, J., B.G. Bray, and C.R. Clark. 1964. "Calculating Viscosities of Reservoir Fluids from Their Compositions." Journal of Petroleum Technology, vol. 16, pp. 1171–1176.

Mandal, P., B.K. Rastogi, H.V.S. Satyanaraya, M. Kousalya, R. Vijayraghavan, C. Satyamurty, I.P. Raju, A.N.S. Sarma, and N. Kumar. 2004. "Characterization of the causative fault system for the 2001 Bhuj earthquake of M_w 7.7." Tectonophysics, vol. 378, no. 1/2, pp. 105–121.

Marshak, S., and T. Paulsen. 1997. "Structural style, regional distribution, and seismic implications of midcontinent fault-and-fold zones, United States." Seismological Research Letters, vol. 68, no. 4, pp. 511–520.

Mast, R.F., and R.H. Howard. 1991. "Oil and Gas Production Recovery Estimates in the Illinois Basin," in M.W. Leighton, D.R. Kolata, D.F. Oltz, and J.J. Eidel, eds., Interior Cratonic Basins. American Association of Petroleum Geologists, Memoir 51, pp. 295–298.

Mastalerz, M., H. Gluskoter, and J. Rupp. 2004. "Carbon dioxide and methane sorption in high volatile bituminous coals from Indiana, USA." International Journal of Coal Geology, vol. 60, pp. 43–55.

Mastalerz, M., and D. Harper. 1998. "Coal in Indiana—a geological overview." Indiana Geological Survey, Special Report 60, 45 pp.

Mavor, M.J., J.C. Close, and T.J. Pratt. 1991. "Summary of the completion, optimization, and assessment laboratory (COAL) site." GRI 91/0377, Gas Research Institute.

Mavor, M.J., and W.D. Gunter. 2003. "Alberta multiwell micro-pilot for CBM storage properties, enhanced methane recovery, and CO_2 storage potential." International Coalbed Methane Symposium, May 3–7, 2004, Tuscaloosa, AL, Paper 0412, 10 pp., 5 tbl., 10 fig., 1 CD-ROM.

Mavor, M.J., L.B. Owen, and T.J. Pratt. 1990. "Measurement and evaluation of isotherm data." Proceedings of the 65th Annual Technical Conference and Exhibition of the Society of Petroleum Engineers, SPE 20728, pp. 157–170.

McBride, J.H. 1997. "Variable deep structure of a midcontinent fault and fold zone from seismic reflection: La Salle deformation belt, Illinois basin." Geological Society of America Bulletin, vol. 109, no. 11, pp. 1502–1513.

McBride, J.H. 1998. "Understanding basement tectonics of an interior cratonic basin: southern Illinois Basin, USA." Tectonophysics, vol. 293, no. 1/2, pp. 1–20.

McBride, J.H., T.G. Hildenbrand, W.J. Stephenson, and C.J. Potter. 2002. "Interpreting the earthquake source of the Wabash Valley seismic zone (Illinois, Indiana, and Kentucky) from seismic-reflection, gravity and magnetic-intensity data." Seismological Research Letters, vol. 73, pp. 660–686.

McBride, J.H., and D.R. Kolata. 1999. “Upper crust beneath the central Illinois basin, United States.” Geological Society of America Bulletin, vol. 111, no. 3, pp. 375–394.

McBride, J.H., D.R. Kolata, T.G. Hildenbrand. 2003. “Geophysical constraints on understanding the origin of the Illinois Basin and its underlying crust.” Tectonophysics, vol. 363, no. 1/2, pp. 45–78.

McBride, J.H., H.E. Leetaru, and B.E. Tingey. 2004. “Structural Characterization of Faulting and Folding of Deep Reservoirs Beneath the Illinois Basin and Relation to Contemporary Seismicity.” Paper presented at the Annual Meeting of the Geological Society of America, Session on Assessment and Characterization of Geologic Formations for Long-Term CO_2 Storage (Sequestration), November 10, Denver, CO.

McBride, J.H., and W.J. Nelson. 1999. “Style and origin of Mid-Carboniferous deformation in the Illinois Basin, USA—Ancestral Rockies deformation?” Tectonophysics, vol. 305, no. 1/3, pp. 249–273.

McBride, J.H., M.L. Sargent, and C.J. Potter. 1997. “Investigating possible earthquake-related structure beneath the southern Illinois Basin from seismic reflection.” Seismological Research Letters, vol. 68, no. 4, pp. 641–649.

McClain, W.C. 1970. “On earthquakes produced by underground fluid injection.” Oak Ridge National Laboratory, Tennessee, ORNL-TM-3154.

Mehnert, E., C.R. Gendron, and R.D. Brower. 1990. “Investigation of the hydraulic effects of deep-well injection of industrial wastes.” Illinois State Geological Survey, Environmental Geology 135, and the Hazardous Waste Research and Information Center, Research Report 51, 100 pp.

Melzer, Steven. 2004. Personal communication.

Metcalfe, R.S., D. Yee, J.P. Seidle, and R. Puri. 1991. “Review of research efforts in coalbed methane recovery.” SPE 23025, SPE Asia-Pacific Conference, Perth, Western Australia, November 4–7.

Mishra, D.C., D.V. Chandrasekhar, and B. Singh. 2005. “Tectonics and crustal structures related to Bhuj earthquake of January 26, 2001: based on gravity and magnetic surveys constrained from seismic and seismological studies.” Tectonophysics, vol. 396, no. 3/4, pp. 195–207.

Mitchell, B.J., O.W. Nuttli, R.B. Herrmann, and W. Stauder. 1991. “Seismotectonics of the central United States,” in D.B. Slemmons, E.R. Engdahl, M.D. Zoback, and D.D. Blackwell, eds., Neotectonics of North America. Boulder, Colorado, Geological Society of America, Decade Map, vol. 1, pp. 245–260.

Moore, L., and M. Gallagher. 2004. Personal communication.

Moore, T. 2004. Personal communication.

Morse, D.G., and H.E. Leetaru, 2005, Reservoir characterization and three-dimensional models of Mt. Simon gas storage fields in the Illinois Basin: Illinois State Geological Survey, Circular 567, 72 pp.

Mueller, K., S.E. Hough, and R. Bilham. 2004. “Analysing the 1811–1812 New Madrid earthquakes with recent instrumentally recorded aftershocks.” Nature, vol. 429, no. 6989, pp. 284–288.

Muller, J.R., and A. Aydin. 2004. “Rupture progression along discontinuous oblique fault sets: implications for the Karadere rupture segment of the 1999 Izmit earthquake, and future rupture in the Sea of Marmara.” Tectonophysics, vol. 391, no. 1/4, pp. 283–302.

Nagelhout, A.C.G., and J.P.A. Roest, 1997, Investigating fault slip in a model of an underground gas storage facility: International Journal of Rock Mechanics and Mining Science, vol. 34, no. 3-4, paper no. 212.

Natural Gas Supply Association. 2006. Subject: Uses of natural gas. http://naturalgas.org/overview/uses.asp Accessed Feb. 22, 2006.

Nelson, W.J. 1981. “Faults and their effect on coal mining in Illinois.” Illinois State Geological Survey, Circular 523, 38 pp.

Nelson, W.J. 1991. “Structural styles of the Illinois Basin,” in M.W. Leighton, D.R. Kolata, D.F. Oltz, and J.J. Eidel, eds., Interior Cratonic Basins. Tulsa, Oklahoma, American Association of Petroleum Geologists, Memoir 51, pp. 209–243.

Nelson, W.J. 1995. “Structural Features in Illinois.” Illinois State Geological Survey, Bulletin 100, 144 pp.

Nelson, W.J., and R.A. Bauer. 1987. “Thrust faults in southern Illinois basin—Result of contemporary stress?” Geological Society of America Bulletin, vol. 98, no. 3, pp. 302–307.

Nuttall, B.C., J.A. Drahovzal, C.F. Eble, and R.M. Bustin. “Analyses of Devonian Black Shale in Kentucky for Potential Carbon Dioxide Sequestration and Enhanced Natural Gas Production.” http://sequestration.org/publish/ghgt7_poster.ppt Accessed March 7, 2006.

Nuttli, O., and K.G. Brill. 1981. “Earthquake source zones in the central US determined from historical seismicity,” in N. Barstow, K.G. Brill, O.W. Nuttli, and P.W. Pomeroy, eds., Approach to seismic zonation for siting nuclear electric power generating facilities in the eastern US. USNRC Report NUREG/CR 1577, pp. 98–143.

Odom, I.E. 1975. “Feldspar-grain size relations in Cambrian arenites, Upper Mississippi Valley.” Journal of Sedimentary Petrology, vol. 45, no. 3, pp. 636–650.

Odom, I.E. 1978. “Mineralogy of late Cambrian and early Ordovician sandstones, Upper Mississippi Valley,” in M.E. Ostrom, ed., Stratigraphic relationships of lower Paleozoic rocks of Wisconsin: in Lithostratigraphy, petrology, and sedimentology of late Cambrian-early Ordovician rocks near Madison, Wisconsin. Prepared for Eighth Annual Meeting Great Lakes Section, Society of Economic Paleontologists and Mineralogists, Madison, Wisconsin. Published by University of Wisconsin-Extension, Geological and Natural History Survey, Field Trip Guide Book No. 3, pp. 46–51.

Ojakangas, R.W. 1963. “Petrology and sedimentation of the upper Cambrian Lamotte sandstone in Missouri.” Journal of Sedimentary Petrology, vol. 33, no. 4, pp. 860–873.

Okaya, D.A., and C.M. Jarchow. 1989. “Extraction of deep crustal reflections from shallow Vibroseis data using extended correlation.” Geophysics, vol. 54, no. 5, pp. 555–562.

Ostrom, M.E. 1978. “Stratigraphic relationships of lower Paleozoic rocks of Wisconsin,” in Lithostratigraphy, petrology, and sedimentology of late Cambrian-early Ordovician rocks near Madison, Wisconsin. Prepared for Eighth Annual Meeting Great Lakes Section, Society of Economic Paleontologists and Mineralogists, Madison, Wisconsin. Published by University of Wisconsin-Extension, Geological and Natural History Survey, Field Trip Guide Book No. 3, pp. 3–22.

Phillips, W. 2004. Personal communication.

Potter, C.J., J.A. Drahovzal, M.L. Sargent, and J.H. McBride. 1997. “Proterozoic structure, Cambrian rifting, and younger faulting as revealed by a regional seismic reflection network in the southern Illinois basin.” Seismological Research Letters, vol. 68, no. 4, pp. 537–552.

Potter, C.J., M.B. Goldhaber, P.C. Heigold, and J.A. Drahovzal. 1995. “Structure of the Reelfoot-Rough Creek Rift System, Fluorspar Area Fault Complex, and Hicks Dome, southern Illinois and western Kentucky—New constraints from regional seismic reflection data.” U.S. Geological Survey, Prof. Paper 1538-Q, 19 pp.

Pratt, T.L. 1994. “How old is the New Madrid seismic zone?” Seismological Research Letters, vol. 65, pp. 172–179.

Pratt, T.L., E.C. Hauser, and K.D. Nelson. 1992. “Widespread buried Precambrian layered sequences in the U.S. Mid-continent: Evidence for large Proterozoic depositional basins.” American Association of Petroleum Geologists Bulletin, vol. 76, no. 9, pp. 1384–1401.

Pruess, K., T. Xu, J. Apps, and J. Garcia. 2001. “Numerical modeling of aquifer disposal of CO_2.” Society of Petroleum Engineers. Proceedings, SPE 66537, Exploration and Production Environmental Conference, February 26–28. San Antonio, TX. Unpaginated.

Raleigh, C.B., J.H. Healy, and J.D. Bredehoeft. 1976. “An experiment in earthquake control at Rangely, Colorado.” Science, vol. 191, no. 4233, pp. 1230–1237.

Reinecker, J., O. Heidbach, M. Tingay, P. Connolly, and B. Müller. 2004. The 2004 release of the World Stress Map. http://www-wsm.physik.uni-karlsruhe.de/pub/stress_data/stress_data_frame.html Accessed Jan. 31, 2006.

Rice, D.D. 1993. “Composition and origins of coalbed gas,” in B.E. Law and D.D. Rice, eds., Hydrocarbons from Coal. American Association of Petroleum Geologists, Studies in Geology no. 38, pp. 159–185.

Roberts, P. 1997. “Seismic Stimulation for Enhanced Production of Oil Reservoirs, Los Alamos National Laboratory.” http://www.ees.lanl.gov/Publications/Articles/97seismic_169.shtml Accessed Nov. 11, 2005.

Rostam-Abadi, M., S. Chen and Y. Lu. 2005. “Assessment of Carbon Capture Options for Power Plants.” Poster presented at the Fourth Annual Conference on Carbon Capture and Sequestration, May 2–5, Alexandria, VA.

Rudman, A.J., and J.A. Rupp. 1993. “Geophysical properties of the basement rocks of Indiana.” Indiana Geological Survey, Special Report 55, 16 pp.

Sargent, M.L. 1991. “Sauk Sequence, Cambrian System through Lower Ordovician Series,” in M.W. Leighton, D.R. Kolata, D.F. Oltz, and J.J. Eidel, eds., Interior cratonic basins. American Association of Petroleum Geologists, Memoir 51, pp. 75–85.

Schweig, E.S., and M.A. Ellis. 1994. “Reconciling short recurrence intervals with minor deformation in the New Madrid seismic zone.” Science, vol. 264, no. 5163, pp. 1308–1311.

Seldon, R.F. 1934. “The occurrence of gases in coal.” PI 3233, U.S. Bureau of Mines.

Seyler, B. 1998. “Geologic and Engineering Controls on Aux Vases Sandstone Reservoirs in Zeigler Field, Illinois: A Comprehensive Study of A Well Managed Oil Field.” Illinois State Geological Survey, Illinois Petroleum 153.

Seyler, B., J. Grube, and J. Huff. 2004. Personal communication.

Shrake, D.L., P.J. Wolfe, B.H. Richard, E.M. Swinford, L.H. Wickstrom, P.E. Potter, and G.W. Sitler. 1990. “Lithologic and geophysical description of a continuously cored hole in Warren County, Ohio, including description of the Middle Run Formation (Precambrian?) and a seismic profile across core site.” Ohio Geological Survey, Information Circular 56, 11 pp.

Sims, S.K. 1993. “Pressure-Volume-Temperature Correlations for Crude Oils from the Illinois Basin.” Illinois State Geological Survey, Illinois Petroleum 140.

Sloss, L.L. 1963. “Sequences in the cratonic interior of North America.” Geological Society of America Bulletin, v. 74, pp. 93–114.

Solano-Acosta, W., P.K. Radhakrishnan, and J.A. Rupp. 2004. “An Assessment of Potential Carbon Sequestration Volumes in Indiana’s Petroleum Fields, Aquifers, Unminable Coal Seams, and Shales.” Poster presented at the Third Annual Conference on Carbon Capture and Sequestration, May 3–6, Alexandria, VA.

Solano-Acosta, W., J.A. Rupp, M. Mastalerz, and A. Schimmelmann. 2004. “Enhanced Coalbed Methane Recovery and CO_2 Sequestration Options in Indiana Coals.” Poster presented at Thirty-Second International Geological Congress, August 20–28, Florence, Italy.

Stauder, W., and O.W. Nuttli. 1970. “Seismic studies: south central Illinois earthquake of November 9, 1968.” Bulletin of the Seismological Society of America, vol. 60, no. 3, pp. 973–981.

Stauder, W., and A.M. Pitt. 1970. “Note on an aftershock study, south central Illinois earthquake of November 9, 1968.” Bulletin of the Seismological Society of America, vol. 60, no. 3, pp. 983–986.

Stark, T.J. 1997. “The East Continent Rift Complex: Evidence and conclusions,” *in* R.W. Ojakangas, A.B. Dickas, and J.C. Green, eds., Middle Proterozoic to Cambrian rifting, central North America: Geological Society of America, Special Paper 312, pp. 253–266.

Stark, T.J., S.H. Rowley, C.K. Steffensen, J.A. Drahovzal, L.E. Schultz, G.W. Bear, and S. Bergman. 1999. “The English Graben: a seismic study of the relationship between a Proterozoic rift segment and subsequent Paleozoic structure and strata [abs.].” American Association of Petroleum Geologists Bulletin, vol. 83, no. 8, pp. 1373–1374.

Stevenson, D.L. 1969. Oil Production from the Ste. Genevieve Limestone in the Exchange Area, Marion County, Illinois. Illinois State Geological Survey, Circular 436, 23 pp.

Strunk, K.L. 1984. “Structural relationships of the Cottage Grove and Shawneetown fault systems near Equality, Illinois, as inferred from geophysical data.” Unpublished thesis, Carbondale, Southern Illinois University, 72 pp.

Swann, D.H. 1963. Classification of Genevievian and Chesterian (Late Mississippian) rocks of Illinois: Illinois State Geological Survey, Report of Investigation 216.

Swann, D.H., and H.B. Willman. 1961. “Megagroups in Illinois.” American Association of Petroleum Geologists Bulletin, vol. 45, no. 4, pp. 471–483.

Talwani, P. 1988. “The intersection model for intraplate earthquakes.” Seismological Research Letters, vol. 59, pp. 305–310.

Talwani, P. 1999. “Fault geometry and earthquakes in continental interiors.” Tectonophysics, vol. 305, no. 1/3, pp. 371–379.

Taylor, K.B., R.B. Herrmann, M.W. Hamburger, G.L. Pavlis, A. Johnston, C. Langer, and C. Lam. 1989. “The southeastern Illinois earthquake of 10 June 1987.” Seismological Research Letters, vol. 60, pp. 101–110.

Templeton, J.S., 1950, The Mt. Simon Sandstone of northern Illinois: Illinois Academy of Science Transactions, vol. 43, pp. 151–159.

Thomas, W.A. 1991. “The Appalachian-Ouachita rifted margin of southeastern North America.” Geological Society of America Bulletin, vol. 103, pp. 415–431.

Treworgy, J.D., ed. 2000. “Geological Activities and Other Resources for Teaching.” Illinois State Geological Survey. GeoActivities Series.

The Tri-State Committee on Correlation of the Pennsylvanian System in the Illinois Basin. 2001. “Toward a more uniform stratigraphic nomenclature for rock units (Formations and Groups) of the Pennsylvanian System in the Illinois Basin.” Illinois State Geological Survey, Indiana Geological Survey, and Kentucky Geological Survey, Illinois Basin Consortium Study 5, 26 p.

United States Environmental Protection Agency. 2001. “Class I Underground Injection Control Program: Study of Risks Associated with Class I Underground Injection Wells.” Office of Water, EPA 816-R-01-007, Washington, DC, 43 pp.

United States Environmental Protection Agency. 2003. Subject: Class I underground injection wells in Region 5. http://www.epa.gov/region5/water/uic/cl1sites.htm#il_active Accessed Feb. 16, 2006.

United States Environmental Protection Agency. 2006. Subject: TDS ranges. http://www.epa.gov Accessed Feb. 14, 2006.

Van Schmus, W.R., M.E. Bickford, A. Turek. 1996. "Proterozoic geology of the east-central Midcontinent basement," in B.A. van der Pluijm, and P.A. Catacosinos, eds., Basement and basins of eastern North America. Boulder, Colorado, Geological Society of America, Special Paper 308, pp. 7–32.

Vugrinovich, R. 1986. "Patterns of regional subsurface fluid movement in the Michigan basin." Michigan Geological Survey, Open File Report OFR 86-6, 27 pp.

Wade, S., H.E. Leetaru, J. Bradbury, P. Tomski, J. Dobbs, M. Krebs. 2005. "Building public acceptance for the regional carbon sequestration partnerships." Paper presented at the Fourth Annual Conference on Carbon Capture and Sequestration, May 2–5, Alexandria, VA.

Walter, L.M., J.M. Budai, L.M. Abriola, C.H. Stearns, A.M. Martini, and T.C.W. Ku. 1996. "Hydrogeochemistry of the Antrim Shale northern Michigan Basin." Department of Geological Sciences, University of Michigan, Annual Report, vol. 1, Gas Research Institute, GRI-95/0251.

Wheeler, R.L., and A.C. Johnston. 1992. "Geologic implications of earthquake source parameters in central and eastern North America." Seismological Research Letters, vol. 63, no. 4, pp. 491–514.

Wheeler, R.L., S. Rhea, S.F. Diehl, J.A. Drahovzal, G.W. Bear, and M.L. Sargent. 1997. "Seismotectonic map showing faults, igneous rocks, and geophysical and neotectonic features in the vicinity of the lower Wabash Valley, Illinois, Indiana, and Kentucky." U.S. Geological Survey, Geologic Investigations Series I-2583-D, scale 1:250,000.

White, D.J., G. Burrowes, T. Davis, Z. Hajnal, K. Hirsche, I. Hutcheon, E. Majer, B. Rostron, and S. Whittaker. 2004. "Greenhouse gas sequestration in abandoned oil reservoirs: The International Energy Agency Weyburn pilot project." GSA Today, vol. 14, no. 7, pp. 4–10.

Willhite, P.G. 1986. "Waterflooding." SPE textbook series, vol. 3, pp. 66, 67.

Willman, H.B., E. Atherton, T.C. Buschbach, C. Collinson, J.C. Frye, M.E. Hopkins, J.A. Lineback, and J.A. Simon. 1975. "Handbook of Illinois Stratigraphy." Illinois State Geological Survey, Bulletin 95, 261 pp.

Wood, G.H., Jr., T.M. Kehn, M.D. Carter, and W.C. Culbertson. 1983. "Coal Resource classification System of the U.S. Geological Survey." U.S. Geological Survey, Circular 891, 65 pp.

Workman, L.E., and A.H. Bell. 1948. "Deep drilling and deeper oil possibilities in Illinois." American Association of Petroleum Geologists Bulletin, vol. 32, no. 11, pp. 2041–2062.

Xu, T., J.A. Apps, and K. Pruess. 2004. "Numerical simulation of CO_2 disposal by mineral trapping in deep aquifers." Applied Geochemistry, vol. 19, no. 6, pp. 917–936.

Zoback, M.L., R.C. Jachens, and J.A. Olson. 1999. “Abrupt along-strike change in tectonic style: San Andreas fault zone, San Francisco Peninsula.” Journal of Geophysical Research, vol. 104, no. B5, pp. 10719–10742.

Zoback, M.D., and J.C. Zinke. 2002. “Production-induced normal faulting in the Valhall and Ekofisk Oil Fields.” Pure and Applied Geophysics, vol. 159, pp. 403–420.

Zoback, M.D., and M.L. Zoback. 1981. “State of stress and intraplate earthquakes in the United States.” Science, vol. 213, no. 4503, pp. 96–104.

Topical Reports

Assess Carbon Dioxide Capture Options for Illinois Basin Carbon Dioxide Sources

Topical Report

M. Rostam-Abadi
S.S. Chen
Y. Lu
Illinois State Geological Survey

Assess Carbon Dioxide Transportation Options in the Illinois Basin

Topical Report

Douglas J. Nyman
D.J. Nyman & Associates

J. Steve Dracos
Universal Ensco, Inc.

Optimization of Geological Sequestration of Carbon Dioxide in the Illinois Basin

Shiaoguo Chen, Yongqi Lu, and Massoud Rostam-Abadi

Abstract

The Midwest Geological Sequestration Consortium (MGSC) is one of seven regional partnerships funded by the United States Department of Energy (DOE). The MGSC partnership is investigating the geological sequestration options for carbon dioxide (CO_2) in the 60,000-mi^2 Illinois Basin. The Basin covers most of Illinois, western Indiana, and western Kentucky.

Stationary sources in the Illinois Basin emitted 283 million metric tonnes of CO_2 in 2002. About 261 millions tonnes of this amount were emitted by 122 power plants (emission sources), each emitting more than 10,000 tonnes annually. The potential geological structures (sinks) for CO_2 storage in the Basin include mature oil reservoirs, deep, unminable coal beds, and deep saline reservoirs. It has been estimated that the storage capacity of the 24 largest sinks within oil fields identified to date in the Basin is about 4,671 million tonnes. The power plants and storage fields are scattered throughout the Illinois Basin.

An integrated sequestration process includes capture, transportation, and injection of CO_2 into the geological fields. The links between different emission sources, sinks, and different transportation routes will impact the economic performance of the sequestration process. The objective of this study was to optimize the integrated CO_2 sequestration process by determining the most economical distribution of captured CO_2 among all of the identified storage fields in the Illinois Basin at CO_2 emission control levels of 10, 25, and 50%.

A commercial optimization software package, LINGO, was used to perform the optimization study. The costs of CO_2 capture from existing coal-fired power plants and pipeline transportation were obtained from an earlier techno-economic study completed by the MGSC in October 2004. The CO_2 capture costs ($53 to 59/tonne CO_2 avoided) were derived from a monoethanolamine (MEA)-based process. The loss of electricity capacity in the Basin due to the installation of MEA plants was not included in the optimization study. Sequestration costs were evaluated with and without by-product credits from enhanced oil recovery (EOR) and coalbed methane recovery (ECBM).

The results from this optimization study revealed that the average cost of the sequestration process with by-products recovery ranged from about $44 to $56/tonne of CO_2 sequestered, depending on the control

level. These costs included the cost of electricity loss due to the installation of MEA plants. The increase in the cost of electricity, shared by all utilities in the Basin, is about 3.72, 10.50, and 22.50 mills/kWh at 10, 25, and 50% of CO_2 emission reductions, respectively. Without by-product recovery, it costs about \$60/tonne of CO_2 sequestered, and electricity cost increases by 5.25, 11.74, and 23.77 mills/kWh for the respective control levels. The cost of capturing CO_2 from power plants contributed to >90% of the total sequestration costs. The average transportation and injection costs were <2% and 8%, respectively, of the total sequestration cost, depending on level of control. One of the reasons for the low cost of transportation is the location of the ubiquitous geological storage structures in the Illinois Basin. A sensitivity study was also performed to evaluate the impact of CO_2 capture cost on sequestration cost.

Executive Summary

The Midwest Geological Sequestration Consortium (MGSC) is one of seven regional partnerships funded by the United States Department of Energy (DOE). The MGSC partnership is investigating the geological sequestration options for carbon dioxide (CO_2) in the 60,000-mi^2 Illinois Basin. The Basin covers most of Illinois, western Indiana, and western Kentucky.

Stationary sources in the Illinois Basin emitted 283 million metric tonnes of CO_2 in 2002. About 261 million tonnes of this amount were emitted by 122 power plants (emission sources). The potential geological structures (sinks) for CO_2 storage in the Basin include mature oil reservoirs, the deepest (unminable) coal beds, and deep saline reservoirs. It has been estimated that the storage capacity of the 24 largest sinks identified to date in the Basin is about 4,671 million tonnes. The power plants and the storage fields are scattered in all areas of the Basin.

An integrated sequestration process includes capture, transportation, and injection of CO_2 into the geological fields. The links between different emission sources and sinks as well as different transportation routes impact the economic performance of the sequestration process. The objective of this study was to optimize the integrated CO_2 sequestration process in the Illinois Basin by determining the most economical distribution of captured CO_2, at control levels ranging from 10 to 50%, among all of the identified storage fields.

A commercial software package, LINGO, was used to optimize the integrated CO_2 sequestration system. The coal-fired power plants with emissions larger than 100,000 tonnes annually (about 98% of total power plant emissions) and the 24 largest storage fields within existing oil fields in the Basin were considered. The costs of CO_2 capture (90% reduction) from coal-fired power plants and pipeline transportation were obtained from an earlier techno-economic study completed by the MGSC in October 2004. The CO_2 capture costs ($53 to $59/tonne of CO_2 avoided) were derived from a monoethanolamine (MEA)-based process. The loss of electricity capacity in the Basin due to the installation of MEA plants was not included in the optimization study. Sequestration costs were evaluated with and without by-product credits from enhanced oil recovery (EOR) and coalbed methane (ECBM) recovery. A 30-year life span was considered for the pipeline and MEA process.

The initial results from the optimization study revealed that capturing CO_2 from the 20 largest coal power plants, which emit about 68% of the total CO_2 emissions in the Basin, is the most economical. Therefore, only these 20 power plants were included in the optimization study. Electricity losses due to installing an MEA plant were about 1,634, 3,873, and 7,746 MW at the 10%, 25%, and 50% control level, respectively. The average cost of the sequestration process with by-product recovery (assuming $20/tonne CO_2 credit for EOR and $15/tonne CO_2 credit for ECBM) ranged from $44 to $56/tonne CO_2

sequestered, depending on the control level. These costs included the cost of electricity loss due to the installation of MEA plants. The increase in the cost of electricity, shared by all utilities in the Basin, is about 3.72, 10.50, and 22.50 mills/kWh at 10, 25, and 50% of CO_2 reduction, respectively. Without by-product recovery, it costs almost $60/tonne of sequestered CO_2. Electricity losses are comparable to those when by-product credits are included, and the increase in electricity cost is about 5.25, 11.74, and 23.77 mills/kWh at 10, 25, and 50% of CO_2 reduction, respectively. The cost of capturing CO_2 from power plants contributes to >90% of the total sequestration costs. The average pipeline and injection costs were <2 and 8%, respectively, of the total sequestration cost. One of the reasons for the low cost of transportation is the location and abundance of geological storage structures in the Illinois Basin. Due to the low cost of the pipeline, the locations of power plants (with respect to sink locations) were found to be less important than the scale of the plants.

The results from a sensitivity analysis revealed that the CO_2 capture cost has the most impact on the overall cost of the of the sequestration process. Data show that sequestration cost is linearly related to capture cost at all levels. The impact of CO_2 capture cost is more pronounced as levels of CO_2 emission control increase, which indicates that future efforts to reduce sequestration cost should focus on developing more cost-effective capture technologies. For example, at the 50% emission control level with a 50% reduction in the current capture costs, the costs for sequestering 1 tonne of CO_2 decreases from $56.35 to $29.61, and the increase in electricity cost decreases from 22.50 to 11.82 mills/kWh.

Introduction

The Midwest Geological Sequestration Consortium (MGSC) is one of the seven regional partnerships funded by the United States Department of Energy (DOE). The MGSC partnership is investigating the geological sequestration options for carbon dioxide (CO_2) in the 60,000-mi^2 Illinois Basin. The Basin covers most of Illinois, western Indiana, and western Kentucky.

In 2002, stationary sources in the Illinois Basin emitted about 283 million tonnes of CO_2 (Chen et al., 2004). Electric generation facilities, which emit more than 10,000 tonnes annually, contribute about 261 million tonnes of the Basin's total emissions. The Basin is rich in different geological structures such as relatively deep coal beds, mature oil reservoirs, and deep saline reservoirs that are potentially suitable for CO_2 storage. The power plants (emission sources) and the storage fields (sinks) are scattered all over the Illinois Basin, but they are mostly concentrated in certain areas. In an integrated sequestration process, the optimal links between these emission sources and geological sinks have to be identified.

An integrated sequestration process includes capture, transportation, and injection of CO_2 into the geological field. The links between different emission sources, sinks, and transportation routes will

impact the economic performance of the sequestration process. In this report, the results from an optimization study of the integrated CO_2 sequestration process in the Illinois Basin are presented. The study determined the most economical distribution of captured CO_2 from coal-fired power plants among the 24 largest storage fields at 10, 25, and 50% CO_2 emission control levels.

Profiles of Emission Sources in the Illinois Basin

The Illinois Basin covers most of Illinois, western Indiana, and western Kentucky (Figure 1). Table 1 lists data for CO_2 emissions from the stationary sources for the United States and the Illinois Basin (Chen et al., 2004). In 2002, the total CO_2 emission from stationary sources in the Illinois Basin was 283 million tonnes, or about 11.7% of total U.S. emissions. The emissions from the manufacturing industry sector, which includes oil refineries, the steel industry, the cement industry, and other industries, were responsible for about 22 million tonnes, or 7.8% of the Illinois Basin emissions.

Table 1. Annual CO_2 emissions in the United States and the Illinois Basin.

Sources	U.S. total (tonnes)	Illinois Basin (tonnes)	Basin to U.S. (%)	Source (% of Basin)
Power generation	2,239,700,000[1]	261,310,000[2]	11.7	92.2
Coal	1,868,400,000[1]	256,256,000[2]	13.7	90.5
Natural gas	299,100,000[1]	5,006,000[2]	1.7	1.8
Oil	72,200,000[1]	48,000[2]	0.1	0.02
Industries	324,789,000	21,960,000	6.8	7.7
Refinery	184,918,000[3]	9,703,000[4]	5.2	3.4
Iron and steel	54,411,000[5]	3,857,000[6]	7.1	1.4
Cement	42,898,000[5]	3,245,000[6]	7.6	1.1
Ammonia	17,652,000[5]	214,000[6]	1.2	0.1
Aluminum	4,223,000[5]	820,000[6]	19.4	0.3
Lime	12,304,000[5]	273,000[6]	2.2	0.1
Ethanol	8,383,000[5]	3,848,000[7]	45.9	1.4
Total	2,564,489,000	283,270,000	11.0	100

[1] U.S. Environmental Protection Agency (2004) greenhouse gas inventory sector analysis.
[2] U.S. Environmental Protection Agency acid rain and EGRID data (classified by primary fuel type).
[3] Estimate from 2002 barrels per day totals (U.S. Department of Energy, 2004).
[4] Projected estimates from representative facilities.
[5] U.S. Environmental Protection Agency (2004) greenhouse gas inventory industrial process analysis.
[6] Source data from U.S. Geological Survey (2002).
[7] Source data from Iowa Department of Agriculture and Land Stewardship (2004): www.distillersgrains.com.

Table 2 lists the total CO_2 mass emitted and the number of emission sources (including both utility and manufacturing industries) in Illinois, Indiana, and Kentucky that are within the geological boundary of the Basin, including shaded areas in Figure 1 (Chen et al., 2004). Coal-fired electric power plants are the predominant stationary sources of emissions. In 2002, about 261 million tonnes of CO_2 were emitted in the Illinois Basin from 122 fossil fuel-fired power plants (only the power plants that emitted >10,000 tonnes of CO_2 annually were included). The geographical distribution of these power plants is shown in Figure 1.

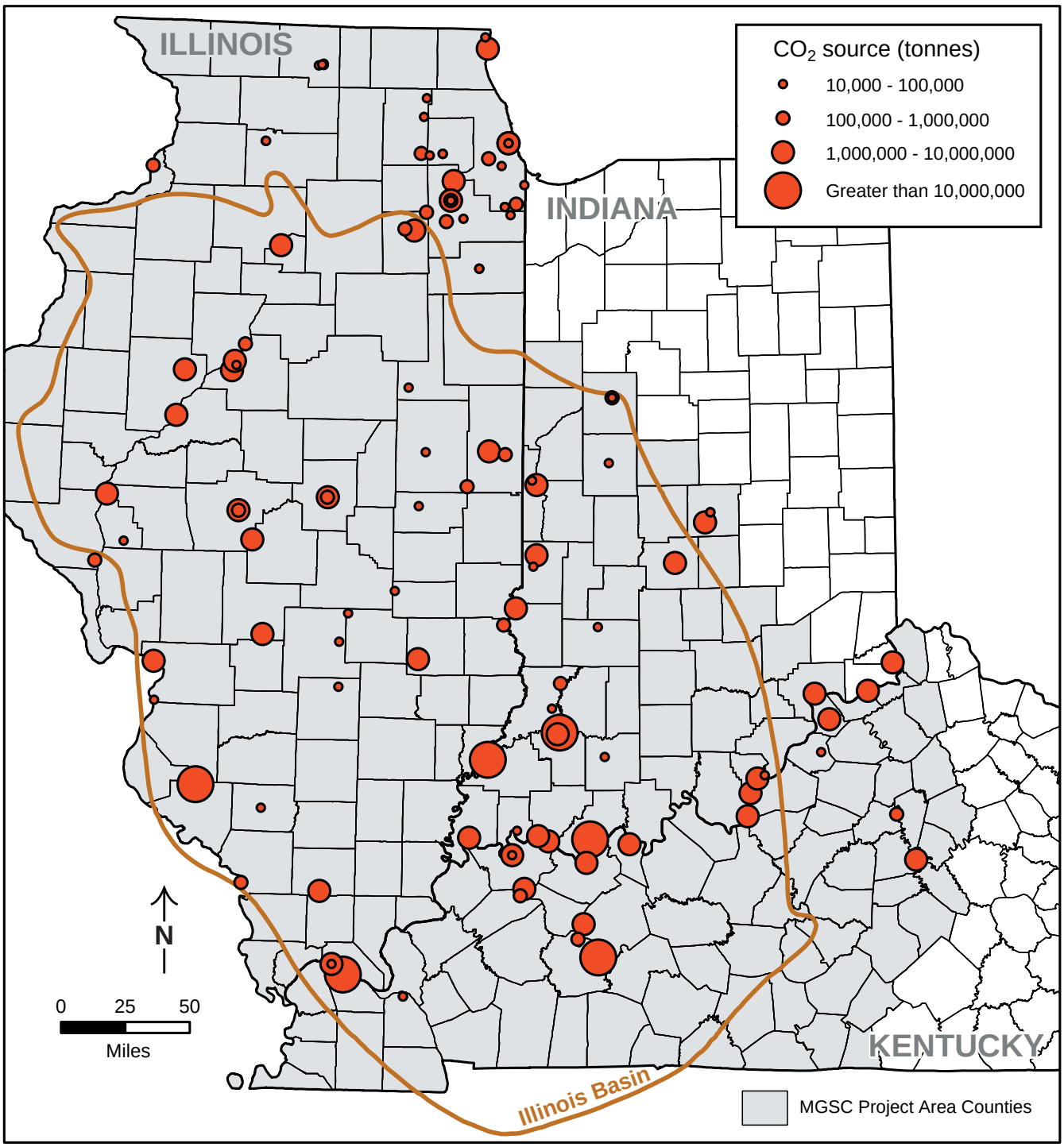

Figure 1 *Geographical distribution of power plants in the Illinois Basin (outline).*

Table 2. CO_2 emissions and emission sources in the Illinois Basin.

Sources	Illinois		Indiana		Kentucky		Total CO_2 emissions in basin (tonnes)	Total in basin (no.)
	CO_2 (tonnes)	Plants (no.)	CO_2 (tonnes)	Plants (no.)	CO_2 (tonnes)	Plants (no.)		
Power generation	94,088,000	75	92,176,000	26	75,045,000	21	261,309,000	122[1]
Coal	89,555,000		91,855,000		74,845,000		256,255,000	
Natural gas	4,485,000		321,000		200,000		5,006,000	
Oil	48,000		0		0		48,000	
Industries	18,593,000	33	2,322,000	11	1,046,000	5	21,961,000	49
Refinery	9,455,000	4	248,000	1	0	0	9,703,000	5
Iron and steel	3,685,000	17	142,000	5	30,000	1	3,857,000	23
Cement	1,301,000	4	1,353,000	3	591,000	1	3,245,000	8
Ammonia	214,000	1	0	0	0	0	214,000	1
Aluminum	0	0	464,000	1	356,000	1	820,000	2
Lime	273,000	1	0	0	0	0	273,000	1
Ethanol	3,665,000	6	115,000	1	69,000	2	3,849,000	9
Total	112,681,000	108	94,498,000	37	72,923,000	26	283,270,000	171

[1] Power plants emitting <10,000 tonnes of CO_2 currently are not included.

Figure 2 illustrates the mass of CO_2 emissions from individual plants in the Illinois Basin. The four largest power plants emitted about 23% of the total CO_2 emissions, the 12 largest power plants emitted more than 50% of total CO_2 emissions, and the 29 largest power plants emitted over 80% of total CO_2 emissions in the Illinois Basin (not shown). Considering their economies of scale, the larger power plants in the Basin are the most suitable sources for any CO_2 capture and sequestration retrofits.

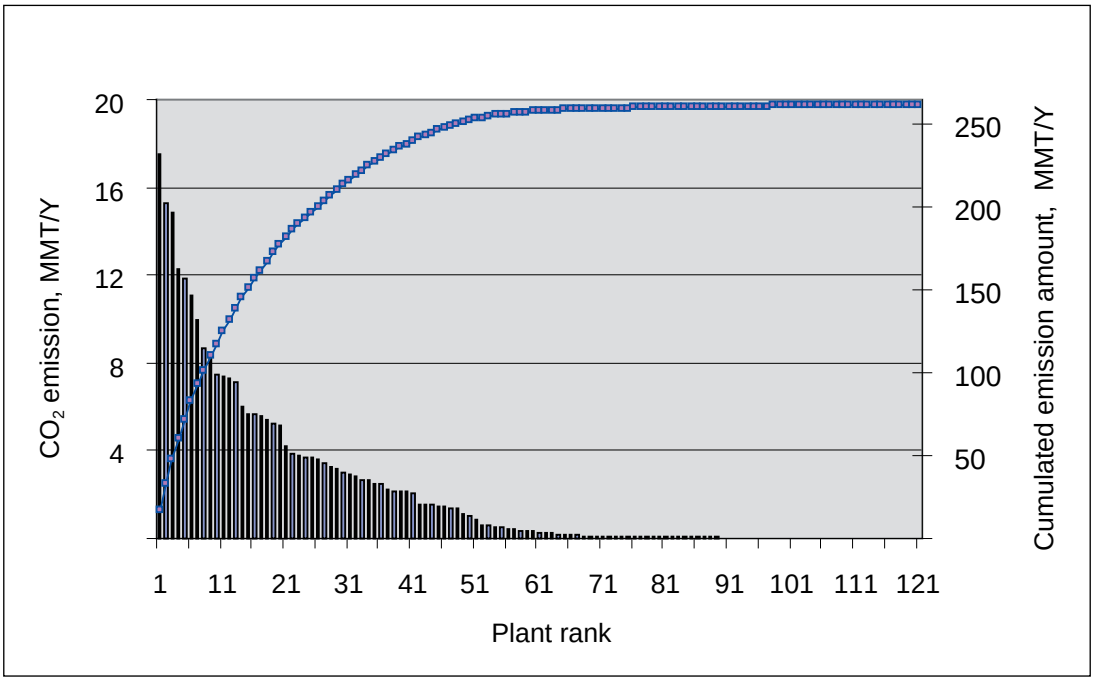

Figure 2 *CO_2 emission profile of the power plants in the Illinois Basin, ranked from largest to smallest.*

Most of the power plants in the Illinois Basin are equipped with pulverized coal boilers and use a simple steam cycle. The flue gas from these power plants contains about 14% CO_2. Other contaminants in the flue gas, such as nitrogen (NOx) and sulfur (SOx), may have to be removed before the gas enters a CO_2 capturing system. Power plants that burn high-sulfur bituminous coals are usually equipped with wet flue gas desulfurization (FGD) processes that are capable of removing >95% of SO_2 from combustion flue gas. As a result of the pre-existing FGD process, these plants may have an advantage over the power plants without the FGD process, which mostly burn western Powder River Basin (PRB) coal, because, if a chemical absorption process is used, SO_2 concentration has to be controlled to <30 ppm in order to reduce the loss of solvent due to reaction with SO_2.

The power plants that burn natural gas tend to be small and are mostly peak power plants. Total CO_2 emissions from these power plants are about 5 million tonnes annually, which is <2% of total emissions in the Illinois Basin. In addition, CO_2 concentration in flue gas from natural gas burning power plants (3 to 4 vol%) will be much lower than that from coal burning power plants (~14 vol%), which, in turn, increases the capture cost. In this optimization study, these small power plants were not considered.

Forty-nine non-utility industrial emission sources contributed about 22 million tonnes of CO_2 in 2002, which accounted for 7.8% of total emissions in the Basin. These energy-intensive manufacturing industries include petroleum refining, iron and steel manufacturing, and cement and lime production. However, these industrial emission sources are relatively small compared with those from typical power plants. The geographic distribution of these industrial sources in Illinois Basin is shown in Figure 3. Because of the economies of scale and lack of infrastructure required for CO_2 capture, these CO_2 emission sources were not considered in this optimization study.

In this optimization study, only 62 coal-fired power plants, each emitting >100,000 tonnes of CO_2 annually, were selected. There are several reasons for this decision. First, a preliminary assessment of the 24 largest sinks that have been identified to date in the Basin showed that their geological sequestration capacities are not sufficient for storage of CO_2 emissions from all of the power plants in the Basin. Second, the remaining power plants account only for about 2% of the total power plant emissions in the Basin, and the economy of scale favors CO_2 capture from larger power plants. Third, if all power plants are included in the optimization process, the number of variables tested exceeds the limits of the LINGO software package. Preliminary results from the optimization study confirmed that the inclusion of the 60 smaller plants did not impact the selection of power plants or storage fields at the control levels selected in this study.

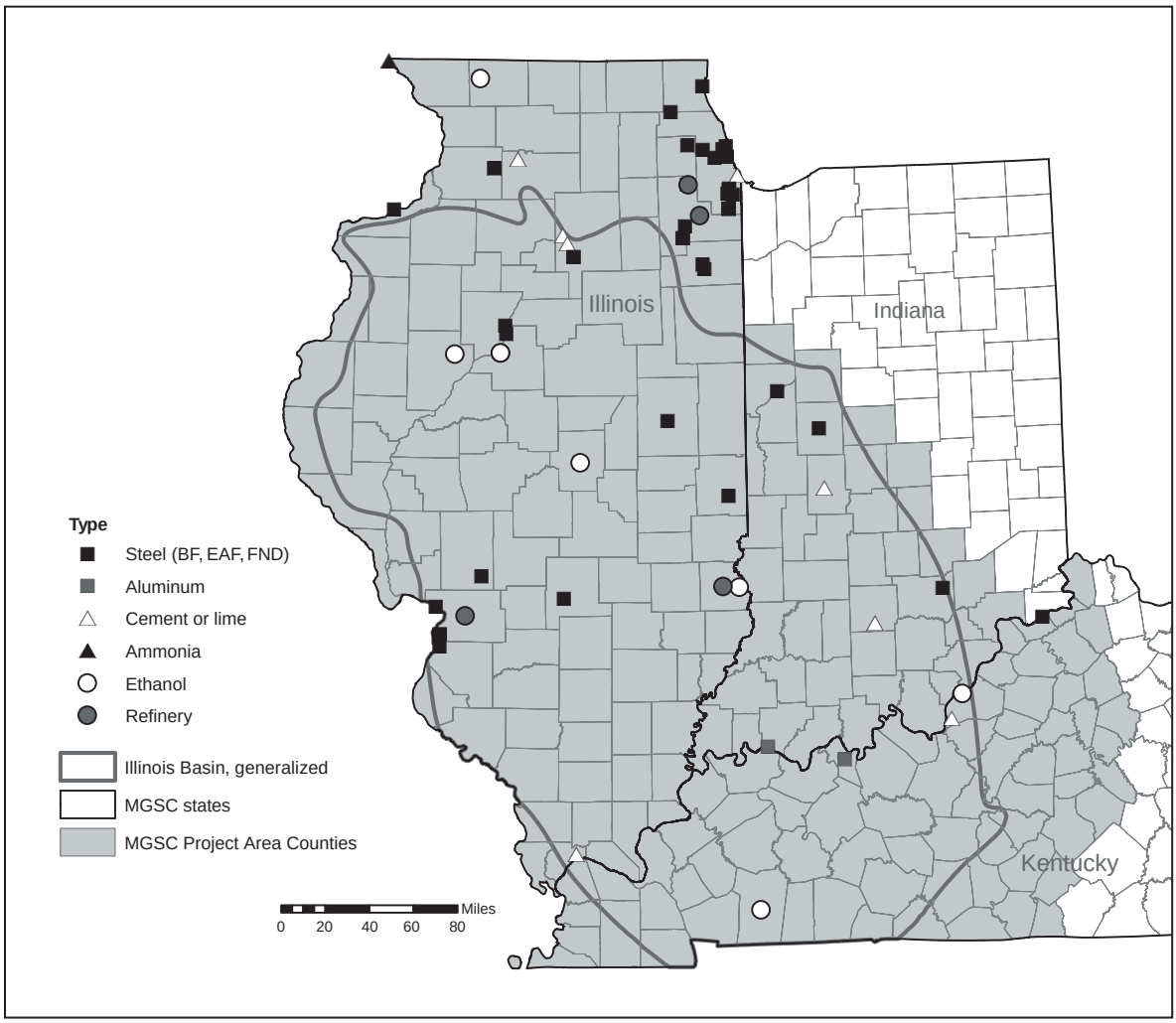

Figure 3 *Geographical distribution of industrial emission sources in the Basin (BF, blast furnace; EAF, electric arc furnace; FND, foundry).*

Profiles of Potential Storage Sinks in the Illinois Basin

The Illinois Basin is rich in geological structures that are potentially suitable for CO_2 sequestration. In this study, three types of storage structures were considered: mature oil field, the deepest coal bed, and deep saline reservoir. Figure 4 shows the geographic distribution of the 24 largest potential storage fields that have been identified to date by the MGSC partnership. Because of the geographical extent of the Clay City Consolidated oil field, the MGSC divided the CO_2 storage of this field into three subfields: Clay City SW (Clay and Wayne Counties), Clay City N (Clay County), and Clay City NE (Jasper County). It should be pointed out that the storage fields are scattered in large areas (some cover hundreds of square miles) across the Basin. In Figure 4, circles represent the centroids of storage fields (based on the total capacity of the field). Each storage field may include all three types of storage structures in a

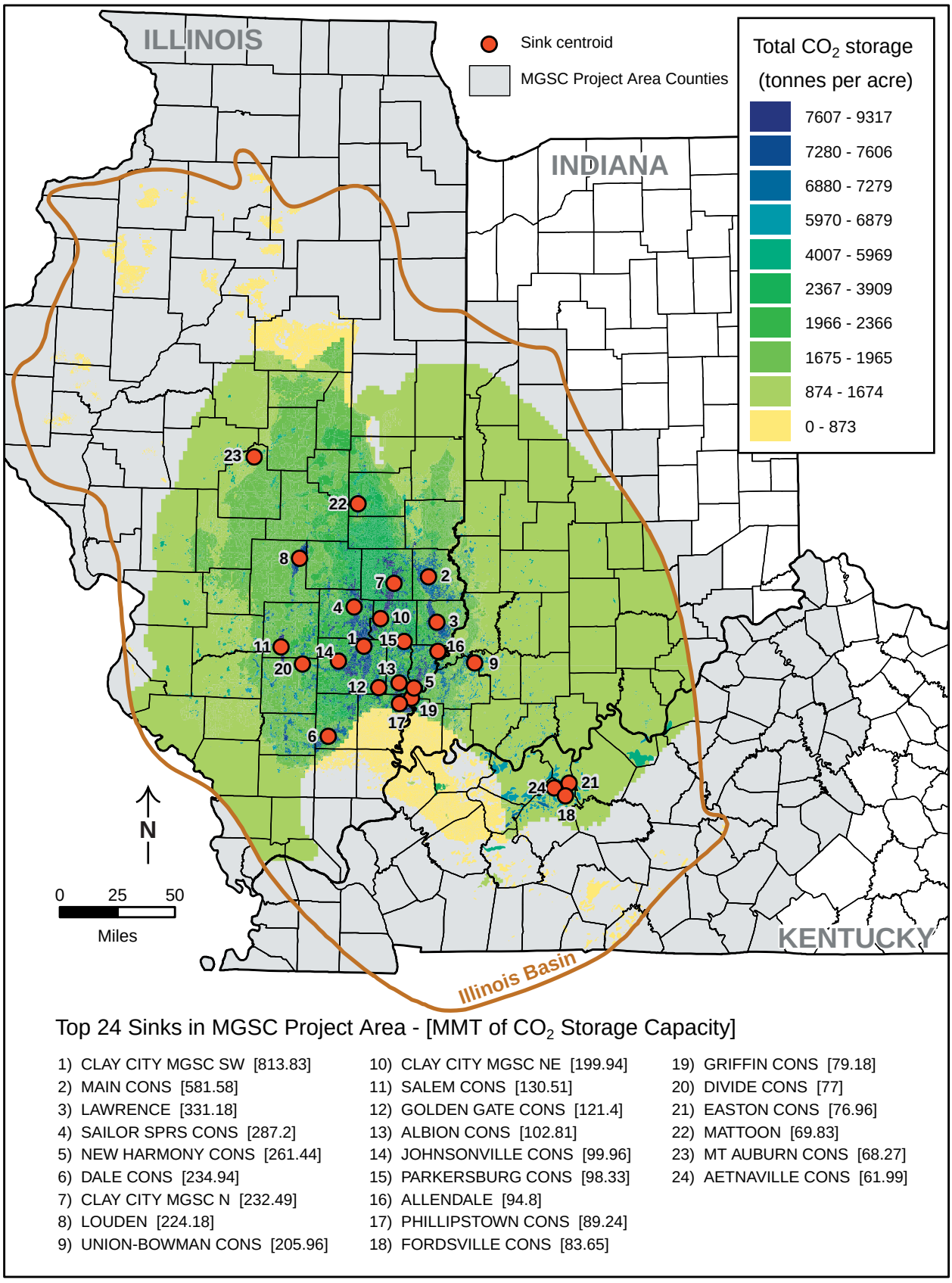

Figure 4 *Geographical distributions of the 24 largest storage sinks in the Illinois Basin.*

vertically stacked arrangem ent. Table 3 lists the CO_2 storage capacity of the 24 storage fields. The total capacity of each storage field consists of the three components.

The best current estimate of the total CO_2 storage capacity for the three types of structures in the Basin is about 4.7 billion tonnes. Oil fields, coal bed seams, and saline reservoirs account for 6%, 6%, and 88%

Table 3. Capacities and locations of the top 24 potential sinks in the Illinois Basin.

Rank	Field name	Field ID	State	Summary, oil CO_2 (MMT)	Summary, coal CO_2 (MMT)	Summary, saline CO_2 (MMT)	Total_CO_2 (MMT)	Longitude (DD_N83_X)	Latitude (DD_N83_Y)
1	CLAY CITY (MGSC SW)	171119	IL	39.38	70.39	709.95	819.72	–88.33	38.56
2	MAIN CONS.	171361	IL	39.01	17.32	533.12	589.46	–87.81	39.00
3	LAWRENCE	171336	IL	29.21	14.06	289.80	333.07	–87.74	38.71
4	SAILOR SPRS. CONS.	171530	IL	9.25	29.44	251.20	289.89	–88.41	38.80
5	NEW HARMONY CONS.	171415	IL	21.73	20.54	222.25	264.52	–87.92	38.30
6	DALE CONS.	171151	IL	15.70	9.86	211.09	236.65	–88.60	37.98
7	CLAY CITY (MGSC N)	171119	IL	10.89	27.06	196.55	234.49	–88.09	38.95
8	LOUDEN	171354	IL	21.93	8.44	195.33	225.71	–88.86	39.10
9	UNION-BOWMAN CONS.	181996	IN	8.99	1.32	199.42	209.73	–87.44	38.46
10	CLAY CITY (MGSC NE)	171119	IL	9.55	19.74	172.36	201.65	–88.20	38.73
11	SALEM CONS.	171533	IL	17.38	4.17	109.55	131.09	–88.99	38.54
12	GOLDEN GATE CONS.	171230	IL	4.24	8.80	109.90	122.94	–88.20	38.30
13	ALBION CONS.	171010	IL	4.86	7.72	91.76	104.33	–88.04	38.33
14	JOHNSONVILLE CONS.	171299	IL	3.78	7.57	89.47	100.83	–88.53	38.46
15	PARKERSBURG CONS.	171462	IL	2.72	7.83	88.91	99.47	–88.00	38.59
16	ALLENDALE	171015	IL	4.46	4.78	87.79	97.02	–87.73	38.53
17	PHILLIPSTOWN CONS.	171474	IL	3.99	7.86	77.87	89.72	–88.04	38.20
18	FORDSVILLE CONS	2112962	KY	1.88	0.00	82.08	83.97	–86.72	37.62
19	GRIFFIN CONSOL.	181787	IN	12.08	5.60	62.26	79.95	–87.94	38.23
20	DIVIDE CONS.	171160	IL	1.82	3.41	72.40	77.63	–88.82	38.44
21	EASTON CONS	21212261	KY	0.47	0.00	76.85	77.32	–86.69	37.70
22	MATTOON	171377	IL	2.08	5.35	62.82	70.24	–88.39	39.45
23	MT. AUBURN CONS.	171399	IL	1.69	0.93	66.63	69.25	–89.25	39.73
24	AETNAVILLE CONS.	214643	KY	0.87	0.00	61.54	62.41	–86.80	37.67
	Total			**267.96**	**282.21**	**4,120.91**	**4,671.08**		

of the total storage capacity, respectively. This capacity would be filled in about 18 years if 90% of the CO_2 emission mass at the 2002 level (283 million tonnes) is sequestered each year.

CO_2 Capture Options and Cost

Several options are available for the capture of CO_2 from electric power plants. Depending on the stage that CO_2 is removed from the power generation system, CO_2 capture can be classified as pre-combustion, post-combustion, or oxyfuel combustion.

In the post-combustion configuration, CO_2 is captured from the flue gas after the fuel is combusted. In the pre-combustion configuration, the original carbon-containing fuel is transformed into a non-carbon-containing fuel (usually hydrogen) prior to combustion. Carbon in the fuel is converted to CO_2 and separated. Hydrogen is then used to produce power in a gas turbine, fuel cell, or other power generation system. In oxyfuel combustion, pure oxygen instead of air is used for combustion in either a boiler or gas turbine. However, if fuel is combusted in very pure oxygen, the flame temperature will be excessively high; therefore, a CO_2-rich flue gas is usually recycled to the boiler to reduce the flame temperature. The advantages and disadvantages of each configuration were discussed in the 2004 MGSC topical report prepared for the DOE (Chen et al., 2004).

In each configuration, different capture technologies may be selected, depending on the power generation technology and the characteristics of the flue gases. The most important parameters are the CO_2 concentration and the total pressure in the flue gas stream. Other parameters include contaminants in the gas stream, transportation, and disposal methods. In the topical report, Chen et al. (2004) presented the results from a detailed engineering analysis of many separation technologies such as absorption (physical or chemical), adsorption (temperature swing adsorption and pressure swing adsorption), membrane, and cryogenic processes. Absorption-based processes were identified as having the best opportunities for post-combustion configuration, and membrane processes were identified as best for pre-combustion configuration for high temperature H_2 separation. Oxy-combustion may be an alternative to post-combustion configuration, but this technology is still in pilot-scale development. Table 4 lists the characteristics of different CO_2 emission sources and recommended capture technologies. Currently, most of the existing power plants in the Illinois Basin use conventional pulverized coal (PC) combustion technologies. For these existing power plants, a post-combustion configuration is the most suitable, and absorption-based processes are the best options.

Solvent is the key to the performance of an absorption-based process. Currently, commercially available solvents for absorption-based processes are amines. Among them, the monoethanolamine amine (MEA)

process is the most widely used. In this study, the MEA absorption process was considered as the technology of choice for capturing CO_2 from the existing power plants in the Illinois Basin.

A techno-economic analysis of the PC plant retrofitted with the MEA system (PC+MEA) was performed using the CHEMCAD software package. A summary of the cost analysis results for retrofitting Illinois

Table 4. Capture technologies for power plants and industrial facilities.

Emission source	Pressure (bar)	CO_2 (%)	Impurities	Capture technology[1]
Power plants				
PC	1.2	14	SO_x, NO_x	CA
IGCC post-combustion	1.2	8	NO_x	CA
IGCC shifted syngas	30	40	H_2S	PA or H_2 membrane
NGCC post-combustion	1.2	4	NO_x	CA
NGCC shifted syngas				PA or H_2 membrane
PC + O_2/CO_2	1.2	>90	SO_x, NO_x, H_2O	Cryogenic
Industrial processes				
Iron and steel	1.2	20–27		CA or shift + PA
Refineries		8–15	SO_x, NO_x	CA
Cement	1.2	13–33		CA
Lime		13–33		CA
Ammonia	30	>95		Pure
Ethanol	1.0	85	VOCs, H_2O	Cryogenic

[1] CA, chemical absorption; PA, physical absorption; PC, pulverized coal; VOCs, volatile organic compounds.

Table 5. Cost analysis of the power plant retrofit with the MEA unit (Chen et al., 2004).

Net power plant output, MW	250	500	1,000
Net output (with MEA), MW	179	358	708
Capital cost, $1,000			
Total plant cost	89,252	147,331	240,095
Total plant investment	97,298	160,614	261,742
Total capital requirement	102,416	170,008	278,741
Annual carrying charge, $1,000/year	18,619	30,908	50,675
O & M[1] costs, $1,000/year			
Fixed O & M	3,410	5036	7,634
Variable O & M	7,673	15796	31,202
Electricity loss	39,083	78,339	154,940
Increase of electricity cost, mills/kWh	62.77	59.24	56.30
CO_2 avoided, 1,000 tonnes/year	1,157	2,320	4,572
Cost of CO_2 avoidance, $/tonnes of CO_2	59.47	56.07	53.47

[1]O & M, operating and maintenance.

coal-fired power plants is provided in Table 5. The power plant was assumed to be fully depreciated with a 30-year life remaining. A retrofit factor of 20% was assumed to account for the extra cost needed to retrofit older plants compared with that needed for new plants. The financial criteria were the same as in the previous techno-economic study presented in the 2004 MSGS topical report (Chen et al., 2004).

The scale of a power plant can strongly influence its economics, especially when the plant size is small. In order to examine the economy of scale, the economic analysis was conducted for three plant capacities with net outputs of 250, 500, and 1,000 MW, respectively (Table 5 and Figure 5).

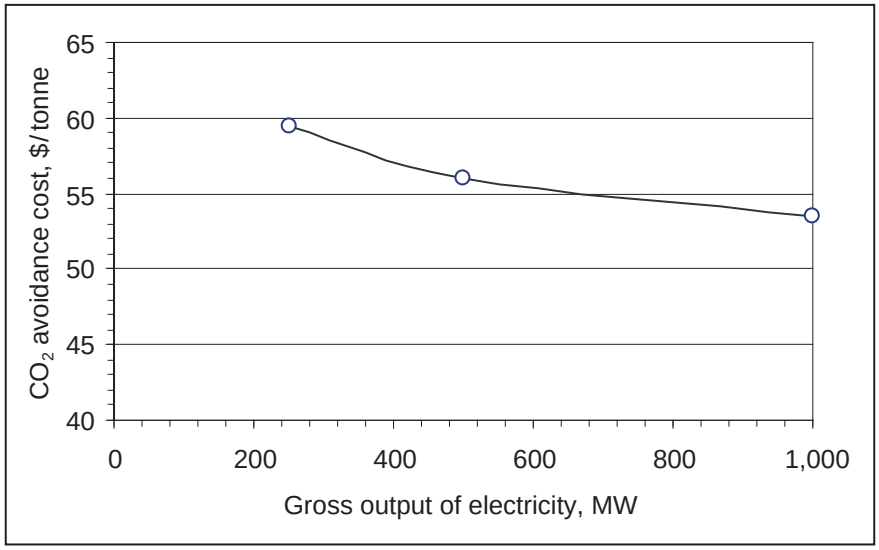

Figure 5 *Effect of plant size on CO_2 avoidance costs of the pulverized coal plus monoethylamine-based process.*

The economy of scale diminishes above a certain plant size, because more parallel trains are needed, and cost will be roughly proportional to the capacity. In this study, a 1,000-MW capacity was selected as the cut-off size. Above this capacity, CO_2 avoidance cost was assumed to remain constant.

Based on the results from the techno-economic analyses (Table 5), the correlation between the annual emission reduction of a power plant and the total CO2 avoidance cost was determined. The equation is

$$Avoidance\ cost\ (\$MM/Y) = 60.05 \times Q^{0.9226}$$

where Q is the amount of CO_2 captured, in million tonnes per year. This equation is suitable for plant capacities less than 1,000 MW. For power plants >1,000 MW, CO_2 avoidance cost was assumed to be constant ($53.47/tonne), and the total annual cost was proportional to CO_2 reductions. These avoidance costs include the cost of electricity loss due to the installation of MEA plants.

Pipeline Transportation and Cost

CO_2 can be transported by truck/motor carriers, railways, ships, and pipeline. Pipeline transportation of CO_2 captured from a power plant is the most economical transportation method because the sequestration process involves transportation of a large volume of CO_2 over long periods. In this study, only pipeline transportation was considered.

Pipeline diameter was calculated based on the flow rate of CO_2 (Table 6) (Chen et al., 2004). Table 6 also includes cases where long pipelines and, thus, a midpoint pressure boost, is required. In this study, no midpoint boosting was considered because all of the pipelines were <125 miles long.

Table 6. Flow capacity as a function of pipe diameter and pressure drop.

Pipe diameter (inches) (1)	Flow capacity with inlet pressure only, 1,000 psi pressure drop over 200 miles (MMSCFD)[1] (2)	Flow capacity with 100% boosting at mid-point, 1,000-psi pressure drop over 100 miles		
		Flow capacity (MMSCFD) (3)	Required BHP[2] for 100% boosting at 100-mile mid-point	
			BHP/mile (4)	BHP/ 100 miles (5)
12	125	190	24	2,400
16	250	350	36	3,600
18	340	490	55	5,500
20	450	650	68	6,800
22	560	840	86	8,600
24	700	1,050	110	11,000

[1]MMSCFD, million standard cubic feet per day.

[2]BHP, brake horsepower.

The pipeline transportation cost analysis was conducted by D.J. Nyman and Associates and was described in the 2004 topical report (Chen et al., 2004). The cost includes right-of-way, materials, construction and services, and annual operating cost. Tables 7 and 8 summarize the pipeline costs for different pipeline sizes.

The pipeline cost (excluding the operating cost) on a per mile basis was depreciated over 30 years. The depreciation was based on 45% bonds at 9% nominal interest rate per year and 55% equity at a return rate of 12% per year. The income tax and inflation rate were assumed to be 38% and 0%, respectively. A correlation (Figure 6) between annual transportation cost (million dollars/mile) and million tonnes of CO_2 transported annually *(Q)* was developed:

$$Cost\ (\$MM/mile/Y) = 0.0494 \times Q^{0.4413}.$$

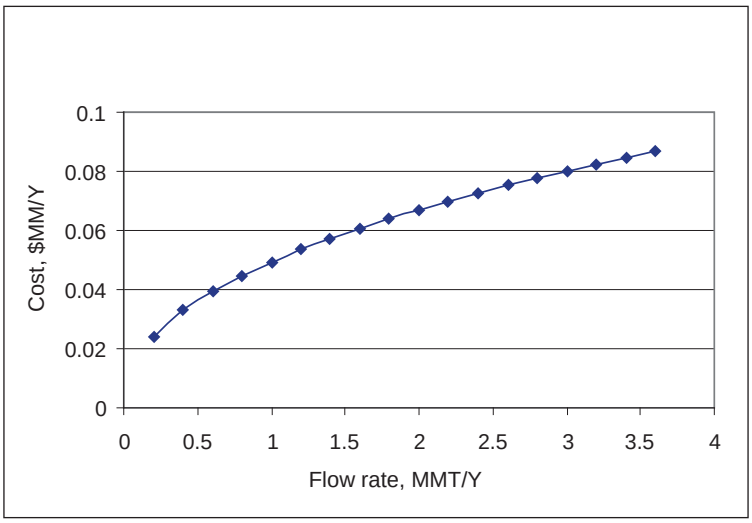

Figure 6 *Correlation between transportation cost and flow rate.*

Table 7. Summary of pipeline transportation cost.

Diameter (inches)	Right-of-way ($/mile)	Materials ($/mile)	Construction ($/mile)	Services ($/mile)	Total cost($/mile)[1]
4	36,713	24,303	85,071	29,217	175,304
6	36,713	47,630	115,915	38,049	238,307
8	44,500	79,370	141,753	47,812	313,435
10	44,500	115,424	173,476	56,678	390,078
12	51,731	159,084	210,730	67,447	488,992
16	66,750	247,199	275,533	88,422	677,905
18	66,750	310,766	306,206	95,721	779,444
20	66,750	381,893	336,354	102,050	887,047
22	66,750	460,465	365,978	107,183	1,000,375
24	66,750	546,136	395,601	121,018	1,129,505

[1]Some numbers have been rounded.

Table 8. Annual pipeline operating costs.

Diameter (inches)	($/mile)	($/200 miles)
4	2,667	533,333
6	4,000	800,000
8	5,333	1,066,667
10	6,667	1,333,333
12	8,000	1,600,000
16	10,667	2,133,333
18	12,000	2,400,000
20	13,333	2,666,667
22	14,667	2,933,333
24	16,000	3,200,000

Cost of CO_2 Injection into Storage Fields and By-product Credit

The permeability and depth of the geological structures impact the economics of CO_2 injection into storage fields. Injection of CO_2 into oil fields most likely will be least expensive (compared with coalbed and saline reservoirs) because mature oil fields have numerous existing wells and surface infrastructure. In addition, injection of CO_2 into oil fields and coal seams generates revenues from sales of oil and coalbed methane, respectively.

In this study, the variability in permeability, depth, and other characteristics of sinks was not considered, which is, of course, not realistic because permeability and depth impact the injectability of an injection well. However, these detailed data are not currently available for all of the selected injection sites. In this study, all of the selected sinks were assumed to have comparable permeability, depth, and other injectability characteristics.

An injection cost of $5/tonne CO_2 was assumed for storage in saline reservoirs. For mature oil fields, the sequestration process was considered as an EOR process. According to several research reports (Bergman et al., 1997; Holtz et al., 1999, 2001; Stevens, 1998), EOR is a break-even business if CO_2 can be purchased at about $20/tonne and the recovered oil can be sold at $25/barrel. Therefore, in this study, a $20/tonne CO_2 credit was allocated to the EOR sequestration process. Obviously, at the current price of $50 to 60 per barrel of oil, a higher CO_2 credit is possible. Only a few studies related to CBM recovery from CO_2 injection are available. Based on the review of several research reports (Gale and Fruend, 2001; Stevens et al., 2001; Reeves and Schoeling, 2001), a credit of $15/tonne of CO_2 was assigned to sequestering CO_2 into coal bed seams.

These cost data are preliminary estimates. For a more detailed economic analysis, updated cost data related to the specific fields should be used.

Mathematical Model for Optimization of Integrated Capture-transportation-storage

The large number of emission sources and sinks selected for this study (Figure 7) provides many different sequestration scenarios and different economic performances at a required CO_2 emission control level. The objective of the optimization study was to find the most economical integrated sequestration scenarios for the three emission control levels. A simple example is shown schematically in Figure 8. The most general mathematical model that can be used to describe the optimization of the integrated sequestration process is a distribution network that includes multiple emission sources,

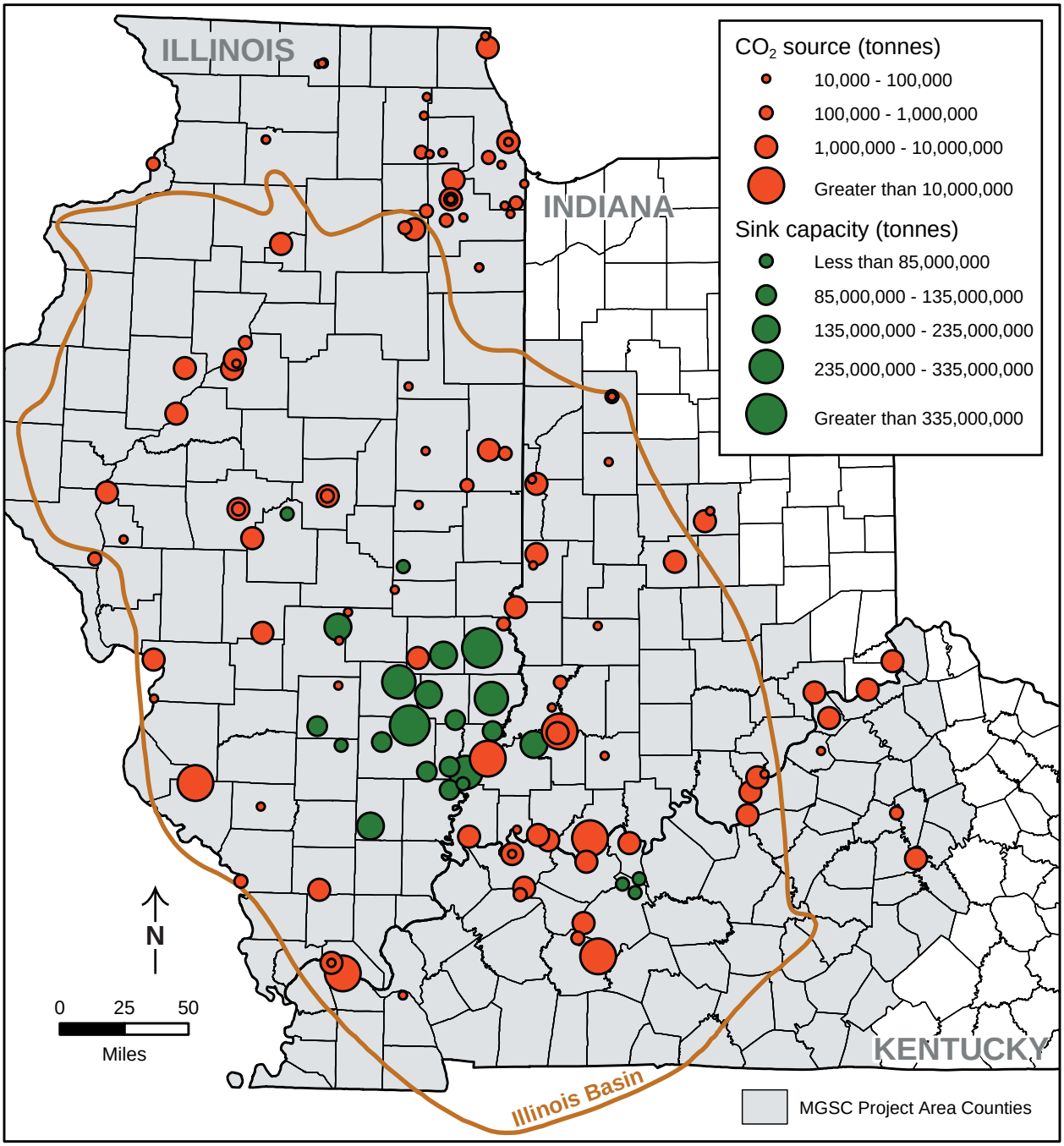

Figure 7 *The geographical distribution of selected CO_2 sources and sinks in the study area.*

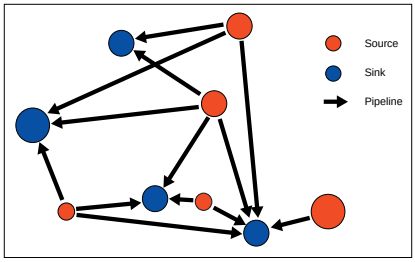

Figure 8 *Schematic diagram of the optimization problem.*

different transportation routes, multiple storage sinks, and different technologies or options available at each level.

The CO_2 sequestration cost is related to each node of the network and is a function of specific conditions such as the locations of the CO_2 sources, scales of the sources, separation technologies, transportation methods, and the sinks (type, location, and scale). For a specific CO_2 sequestration pathway, a minimum sequestration cost exists.

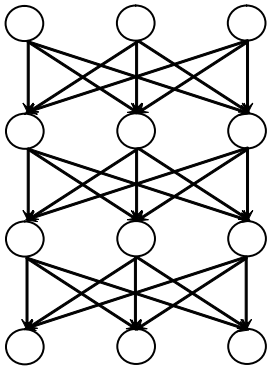

… level i = 1,2,3… CO_2 emission (e.g., power plants)

… level j = 1,2,3… separation (chemical adsorption technology option)

… level k = 1,2,3… transportation methods (pipeline route)

… level l = 1,2,3… geologic storage fields

The arrows in the diagram represent various contributions of options considered. Mathematically, this nonlinear optimization problem can be expressed as follows:

$$\min \sum_i \sum_j \sum_k \sum_l R_i X_i (S_{ij} C_{ij} + F_{il} T_{ikl} D_{il} C_{ikl} + F_{il} C_l)$$

$$\textit{subject to} \quad \begin{cases} \sum_i R_i X_i = R_{\text{target}} \\ X_i = \{0,1\}, \quad \forall i \\ \sum_j S_{ij} = 1, \quad \forall i \\ \sum_k T_{ikl} = 1, \quad \forall i,l \\ \sum_l F_{il} = 1, \quad \forall i \\ \sum_i R_i X_i F_{il} \le Cap_l, \quad \forall l \\ S_{ij}, T_{ik}, F_{il} \ge 0, \quad \forall i, j, k, l \end{cases}$$

where i is the source; j is the separation technology; k is the transportation option; l is the type of sink; R_i is the recoverable CO_2 emissions from ith source, million tonnes/year; X_i is the integer constant 0 or 1; R_{target} is the total CO_2 sequestration target in the region, million tonnes/year; S_{ij} is the share of jth separation technology to the ith source; T_{ikl} is the share of kth transportation option for the ith source to transport to the lth sink; F_{il} is the share of lth sink to the ith source; D_{il} is the distance from ith source to

the *l*th sink, miles; Cap_l is the total capacity of the *l*th sink, million tonnes/year; C_{ij} is the unit cost of the jth capture technology for the *i*th source, $/tonne; C_{ikl} is the unit cost of the *k*th transportation option for the *i*th source to the *l*th sink, $/tonne/mile, C_l is the CO_2 injection unit cost in the *l*th sink, $/tonne, and $\forall$ is for all. It should be pointed out that Cap is the annual available capacity of the geological sinks (data in Table 3 divided by 30 years).

In this study, the general model just described was simplified by considering several assumptions. First, only the PC power plants in the Basin were considered as emission sources. An MEA-based absorption process was selected for capturing CO_2 from the PC plants.
Second, whenever an emission source was selected, all of its flue gas volume was treated to capture 90% of its CO_2. This assumption makes the optimization an integer planning problem, which is more complicated mathematically.

Third, once a power plant has been selected, the CO_2 emissions can be transported to more than one sink. This assumption is based on the fact that splitting CO_2 emissions from one source into several sinks could be economically favorable when the transportation cost is only a small fraction of the total sequestration cost.

Fourth, to simplify the optimization further, a straight pipeline connected a source to a sink was assumed; however, this assumption may not be realistic in some cases. Pipeline diameter was selected based on the optimized flow rate between source and sink. For the case shown in Figure 9, the preferred pipeline route to sink 2 is from a side pipeline from the main pipeline connecting source 1 and sink 1, rather than installation of a separate pipeline (dashed line) to connect source 1 to sink 2. For simplicity, the shortest length between a source and a sink (i.e., straight line) was assumed for the estimate of the cost of the pipeline. For a more specific case study, the geological conditions of the area must be considered to determine the pipeline routes accurately.

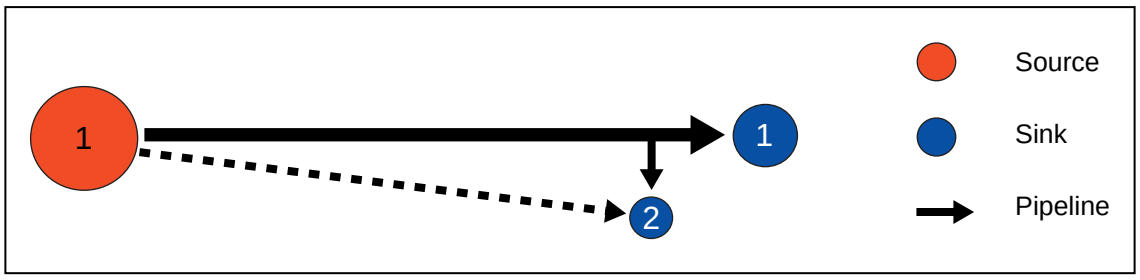

Figure 9 *An extreme example of the optimization problem.*

Fifth, CO_2 emissions from new power generation plants to compensate for the electricity loss due to the installation of the MEA plants were not considered. The power consumed by an MEA plant is typically about 30% of the net electricity output of a power plant.

Based on the above assumptions, the mathematical model is reduced to

$$\min \sum_i \sum_l R_i X_i (C_i + F_{il} D_{il} C_{il} + F_{il} C_l)$$

$$\textit{subject to} \quad \begin{cases} \sum_i R_i X_i = R_{\text{target}} \\ X_i = \{0, 1\}, \quad \forall i \\ \sum_l F_{il} = 1, \quad \forall i \\ \sum_i R_i X_i F_{il} \le Cap_l, \quad \forall l \\ F_{il} \ge 0, \quad \forall i, l \end{cases}$$

where i is the source; l is the type of sink; R_i is the recoverable CO_2 emissions from ith source (assuming 90% of capture efficiency), million tonnes/year; X is the integer 0 or 1; R_{target} is the total CO_2 sequestration target in the region, million tonnes/year; F_{il} is the share of lth sink to the ith source, D_{il} is the distance from ith source to lth sink, mile; Cap_l is the total capacity of the lth sink, million tonnes/year; C_i is the CO_2 capture unit cost, $/tonne; C_{il} is the CO_2 pipeline transportation unit cost, $/tonne/mile; C_l is the CO_2 injection unit cost, $/tonne; and $\forall$ is for all.

In the preceding model, the credits from the EOR and ECBM recovery were added into the CO_2 injection cost, C_l. This was achieved according to the following relationships:

$$\sum_i R_i X_i F_{il} \le Cap_{l1}, C_l = -C_{l1}$$

$$Cap_{l1} \le \sum_i R_i X_i F_{il} \le Cap_{l1} + Cap_{l2},$$

$$C_l = \frac{-C_{l1} Cap_{l1} - C_{l2} (\sum_i R_i X_i F_{il} - Cap_{l1})}{\sum_i R_i X_i F_{il}}$$

$$\sum_i R_i X_i F_{il} \ge Cap_{l1} + Cap_{l2},$$

$$C_l = \frac{-C_{l1} Cap_{l1} - C_{l2} Cap_{l2} + C_{l3} (\sum_i R_i X_i F_{il} - Cap_{l1} - Cap_{l2})}{\sum_i R_i X_i F_{il}}$$

where C_{l1} and C_{l2} are the unit benefits of the EOR and ECBM, respectively, and C_{l3} is the unit injection cost of the saline reservoir, $/tonne. Cap_{l1} and Cap_{l2} are the annual CO_2 storage capacities of the EOR and ECBM (million tonnes/year), respectively.

A commercial optimization software package, LINGO version 9.0, was used in this study (LINDO Systems Inc., 2004). CO_2 capture cost data, Geographic Information Systems (GIS) databases related to the location and scale of each source and sink in the region, and storage costs were the main inputs for the optimization study.

Scenario Analysis of the Integrated System

As described earlier, the preliminary CO_2 storage capacity of the 24 largest sinks identified to date in the Illinois Basin is about 4.7 billion tonnes. This capacity would be filled in about 18 years if 90% of the CO_2 emission mass at the 2002 level (283 million tonnes) is sequestered each year. Because infrastructure will last >30 years, and a 90% control level is unlikely, it was decided to use 50%, 25%, and 10% emission control levels rather than a 90% control level.

The initial optimization efforts focused on evaluating the impacts of the transportation and capture costs on the overall sequestration cost. It was concluded that sequestering CO_2 emissions from the 20 largest power plants in the Basin (about 68% of the total emissions from power plants) provides the most economical scenario. Transportation cost was found to be <$1.1/tonne CO_2 sequestered for the 50% control level (less for the 25% and 10% levels). The cost of capturing CO_2 from smaller power plants, even those that are located near a sink, increased the overall sequestration cost, mainly due to economies of scale. The 20 selected power plants are listed in Table 9.

Table 9. Power plants selected in optimization studies.

Plant name	ORIS code	Emitted (million tonnes)	Captured (million tonnes)	Plant name	ORIS code	Emitted (million tonnes)	Captured (million tonnes)
GIBSON	006113	17.46	15.71	NEWTON	006017	7.37	6.63
ROCKPORT	006166	15.27	13.75	POWERTON	000879	7.30	6.57
PARADISE	001378	14.83	13.35	MEROM	006213	7.12	6.41
AES	000994	12.23	11.01	KINCAID	000876	6.00	5.40
BALDWIN	000889	11.86	10.67	WARRICK	006705	5.67	5.10
GHENT	001356	11.09	9.98	WILL_COUNTY	000884	5.66	5.09
SHAWNEE	001379	9.95	8.96	JOLIET_29	000384	5.57	5.01
MILL_CREEK	001364	8.67	7.81	WABASH_RIVER	001010	5.38	4.85
JOPPA_STEAM	000887	8.35	7.52	COFFEEN	000861	5.22	4.70
CLIFTY_CREEK	000983	7.48	6.73	CAYUGA	001001	5.19	4.67

50% Basin Emission Control Level

At a 50% Basin emission control level, 128.4 million tonnes of CO_2 emissions/year from 15 power plants are sequestered. The selected power plants are listed in Table 10. The CO_2 emissions from these power plants range from 5.2 to 17.5 million tonnes/year with a total of 142.7 million tonnes/year. The efficiency of CO_2 capture at each selected power plant was assumed as 90%.

Table 10. Power plants selected at the 50% emission control level.

Plant name	ORIS code	Emitted (million tonnes)	Captured (million tonnes)	Capture cost ($ million)
GIBSON	006113	17.46	15.71	840.01
ROCKPORT	006166	15.27	13.75	735.21
PARADISE	001378	14.83	13.35	713.82
AES	000994	12.23	11.01	588.70
BALDWIN	000889	11.86	10.67	570.52
SHAWNEE	001379	9.95	8.96	479.09
MILL_CREEK	001364	8.67	7.81	417.60
JOPPA_STEAM	000887	8.35	7.52	402.09
NEWTON	006017	7.37	6.63	354.51
POWERTON	000879	7.30	6.57	351.30
MEROM	006213	7.12	6.41	342.74
KINCAID	000876	6.00	5.40	288.74
WARRICK	006705	5.67	5.10	272.70
WABASH_RIVER	001010	5.38	4.85	259.33
COFFEEN	000861	5.22	4.70	251.31
Total		**142.71**	**128.44**	**6,867.69**

The capacity usages of the 24 sinks are listed in Table 11. All of the capacity of mature oil fields and coal beds is utilized. This result is expected because CO_2 sequestration in these sinks produces revenue from selling valuable by-products and thus reduces the cost of the sequestration process. Overall, about 82% of the total geological storage capacity is projected to be filled in 30 years.

The geographical connections between the 15 emission sources and 24 sinks and the CO_2 flow rates in pipelines are listed in Table 12. The distances between various sources and sinks range from 9.9 to 122 miles. The flow-weighted average distance is 57.4 miles (Figure 10). This result is consistent with the assumption that no pressure boost is required in the middle point of a pipeline because pipeline distances were <200 miles.

At the 50% control level, the sequestration cost including capture, injection, and transportation is $7.24 billion/year ($56.35/tonne of CO_2). Contributions from capture, transportation, and injection are $6.87 billion/year ($53.47/tonne CO_2), $138.72 million/year ($1.08/tonne CO_2), and $230.75 million/year ($1.80/

tonne of CO_2), respectively, which account for 95%, 2%, and 3% of the total sequestration cost in the Basin. Note that the negative total injection costs in Table 11 indicate that the revenue from selling the by-products (oil and coalbed methane) exceeds the cost of injection. Finally, the loss of electricity due to installing MEA equipment is about 7,746 MW. CO_2 emissions from new power generation plants designed to compensate for the electricity loss were not included in this study.

Table 11. The capacity usage of all the sinks at the 50% emission control level.[1]

		Mature oil fields		Coal bed		Saline aquifer		Total	Injection
Field name	Field ID	Capacity (MMT/Y)	Used (MMT/Y)	Capacity (MMT/Y)	Used (MMT/Y)	Capacity (MMT/Y)	Used (MMT/Y)	Used (MMT/Y)	Cost ($MM/Y)
CLAY_CITY_SW	171119	1.31	1.31	2.35	2.35	23.67	22.14	25.79	49.22
MAIN_CONS	171361	1.30	1.30	0.58	0.58	17.77	17.18	19.06	51.25
LAWRENCE	171336	0.97	0.97	0.47	0.47	9.66	9.57	11.01	21.34
SAILOR_SPRS	171530	0.31	0.31	0.98	0.98	8.37	4.16	5.45	–0.06
NEW_HARMONY	171415	0.72	0.72	0.68	0.68	7.41	7.41	8.82	12.28
DALE_CONS_	171151	0.52	0.52	0.33	0.33	7.04	6.67	7.52	17.93
CLAY_CITY_N	171119	0.36	0.36	0.90	0.90	6.55	4.39	5.66	1.16
LOUDEN	171354	0.73	0.73	0.28	0.28	6.51	5.92	6.93	10.73
UNION	181996	0.30	0.30	0.04	0.04	6.65	6.65	6.99	26.58
CLAY_CITY_NE	171119	0.32	0.32	0.66	0.66	5.75	0.00	0.98	–16.23
SALEM_CONS_	171533	0.58	0.58	0.14	0.14	3.65	3.65	4.37	4.59
GOLDEN_GATE_CONS	171230	0.14	0.14	0.29	0.29	3.66	0.00	0.43	–7.23
ALBION_CONS_	171010	0.16	0.16	0.26	0.26	3.06	3.06	3.48	8.20
JOHNSONVILLE	171299	0.13	0.13	0.25	0.25	2.98	2.98	3.36	8.60
PARKERSBURG	171462	0.09	0.09	0.26	0.26	2.96	0.00	0.35	–5.73
ALLENDALE	171015	0.15	0.15	0.16	0.16	2.93	2.93	3.23	9.27
PHILLIPSTOWN	171474	0.13	0.13	0.26	0.26	2.60	0.00	0.39	–6.59
FORDSVILLE	2112962	0.06	0.06	0.00	0.00	2.74	2.74	2.80	12.42
GRIFFIN	181787	0.40	0.40	0.19	0.19	2.08	2.08	2.66	–0.48
DIVIDE	171160	0.06	0.06	0.11	0.11	2.41	2.41	2.59	9.15
EASTON_CONS	21212261	0.02	0.02	0.00	0.00	2.56	0.00	0.02	–0.31
MATTOON	171377	0.07	0.07	0.18	0.18	2.09	2.09	2.34	6.41
MT__AUBURN_CONS	171399	0.06	0.06	0.03	0.03	2.22	2.22	2.31	9.51
AETNAVILLE	214643	0.03	0.03	0.00	0.00	2.05	1.86	1.89	8.73
Total		**8.93**	**8.93**	**9.41**	**9.41**	**137.36**	**110.10**	**128.44**	**230.75**

[1]Some numbers are rounded.

25% Emission Control Level

At an emission control level of 25%, seven power plants were identified (Table 13). The total CO_2 emissions from the seven power plants is 71.1 million tonnes/year with 64.0 million tonnes/year captured (90% removal).

Table 12. Connections between emission sources and sinks at the 50% control level.

Sources	ID	Sinks	ID	Flow rate (MMT/Y)	Distance (mile)	Transportation cost ($MM/Y)
GIBSON	6113	CLAY_CITY_SW	171119	3.09	32.96	2.68
GIBSON	6113	NEW_HARMONY	171415	2.46	10.01	0.74
GIBSON	6113	GOLDEN_GATE_CONS	171230	0.43	24.26	0.83
GIBSON	6113	ALBION_CONS	171010	3.48	15.20	1.30
GIBSON	6113	PARKERSBURG	171462	0.35	19.67	0.61
GIBSON	6113	ALLENDALE	171015	3.23	11.00	0.91
GIBSON	6113	GRIFFIN	181787	2.66	13.68	1.04
ROCKPORT	6166	CLAY_CITY_SW	171119	13.75	82.72	12.99
PARADISE	1378	NEW_HARMONY	171415	6.36	88.30	9.87
PARADISE	1378	UNION	181996	2.29	86.45	6.15
PARADISE	1378	FORDSVILLE	2112962	2.80	28.78	2.24
PARADISE	1378	EASTON_CONS	21212261	0.02	34.33	0.27
PARADISE	1378	AETNAVILLE	214643	1.89	29.87	1.95
AES	994	LAWRENCE	171336	11.01	29.44	4.19
BALDWIN	889	LOUDEN	171354	0.36	82.19	2.57
BALDWIN	889	SALEM_CONS	171533	4.37	52.29	4.95
BALDWIN	889	JOHNSONVILLE	171299	3.36	74.05	6.25
BALDWIN	889	DIVIDE	171160	2.59	58.54	4.40
SHAWNEE	1379	CLAY_CITY_SW	171119	8.96	100.19	13.02
MILL_CREEK	1364	MAIN_CONS	171361	7.81	121.97	14.92
JOPPA_STEAM	887	DALE_CONS	171151	7.52	55.40	6.67
NEWTON	6017	CLAY_CITY_N	171119	5.66	9.94	1.06
NEWTON	6017	CLAY_CITY_NE	171119	0.98	14.86	0.73
POWERTON	879	LOUDEN	171354	6.57	108.64	12.32
MEROM	6213	MAIN_CONS	171361	6.41	20.51	2.30
KINCAID	876	SAILOR_SPRS	171530	0.75	79.77	3.48
KINCAID	876	MATTOON	171377	2.34	59.70	4.29
KINCAID	876	MT__AUBURN_CONS	171399	2.31	16.58	1.19
WARRICK	6705	UNION	181996	4.71	37.84	3.70
WARRICK	6705	PHILLIPSTOWN	171474	0.39	43.07	1.41
WABASH_RIVER	1010	MAIN_CONS	171361	4.85	42.30	4.19
COFFEEN	861	SAILOR_SPRS	171530	4.70	56.18	5.50
Total				**128.44**	**57.37 (avg.)**	**138.72**

The capacity usages of the 24 sinks are listed in Table 14. Similar to the 50% control level, all of the mature oil fields and coal beds are filled. In addition, 45.7 million tonnes/year of CO_2 are sequestered in saline reservoirs. About 41% of the total geological storage capacity is filled in 30 years.

The geographical connections between the seven power plants, the 24 sinks, and the CO_2 flow rates in pipelines are listed in Table 15. The pipeline distance between various sources and sinks ranged from 9.9 to 77.5 miles with a flow-weighted average distance of 26.7 miles (Figure 11).

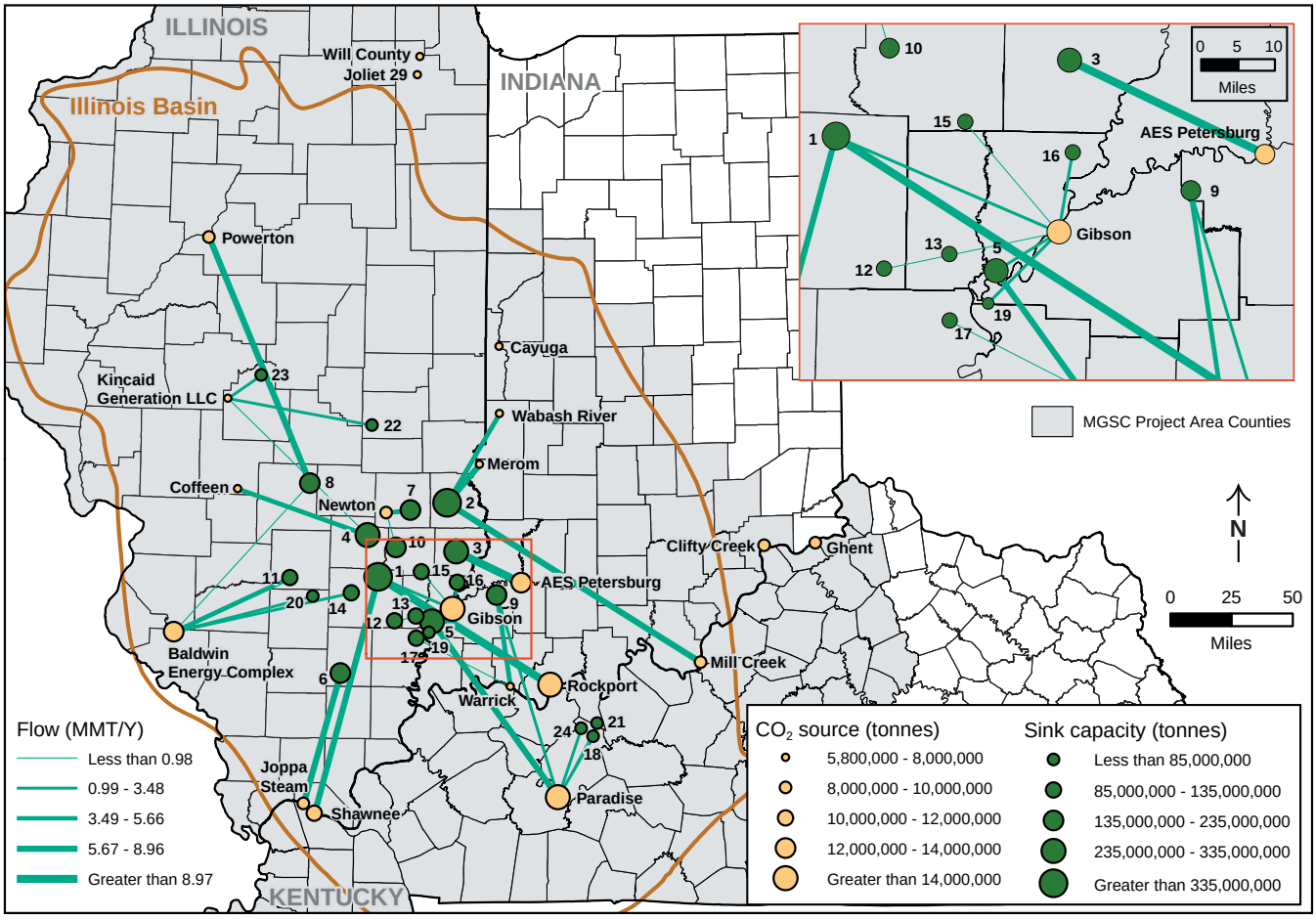

Figure 10 *Distribution of the captured CO_2 among the sinks at 50% emission control level.*

At a 25% control level, the total sequestration cost including capture, injection, and transportation is $3.38 billion/year ($52.77/tonne of CO_2). Contributions from capture, transportation, and injection are $3.42 billion/year ($53.46/tonne of CO_2), $47.27 million/year ($0.74/tonne of CO_2), and –$91.35 million/year (–$1.43/tonne of CO_2), respectively. Note that for the 25% control level, total transportation cost is about one third of the 50% control level. The negative injection cost indicates that the revenues from selling the by-products exceed the injection costs. The net benefit of the CO_2 injection to storage sinks is $91.35 million/year, compared with the injection expense of $230.75 million/year at the 50% control level. This is an absolute difference of $322.1 million/year. At the 25% control level, a smaller amount of CO_2 is stored in the higher cost saline reservoirs. The loss of electricity due to CO_2 capture is about 3,873 MW at the 25% control level.

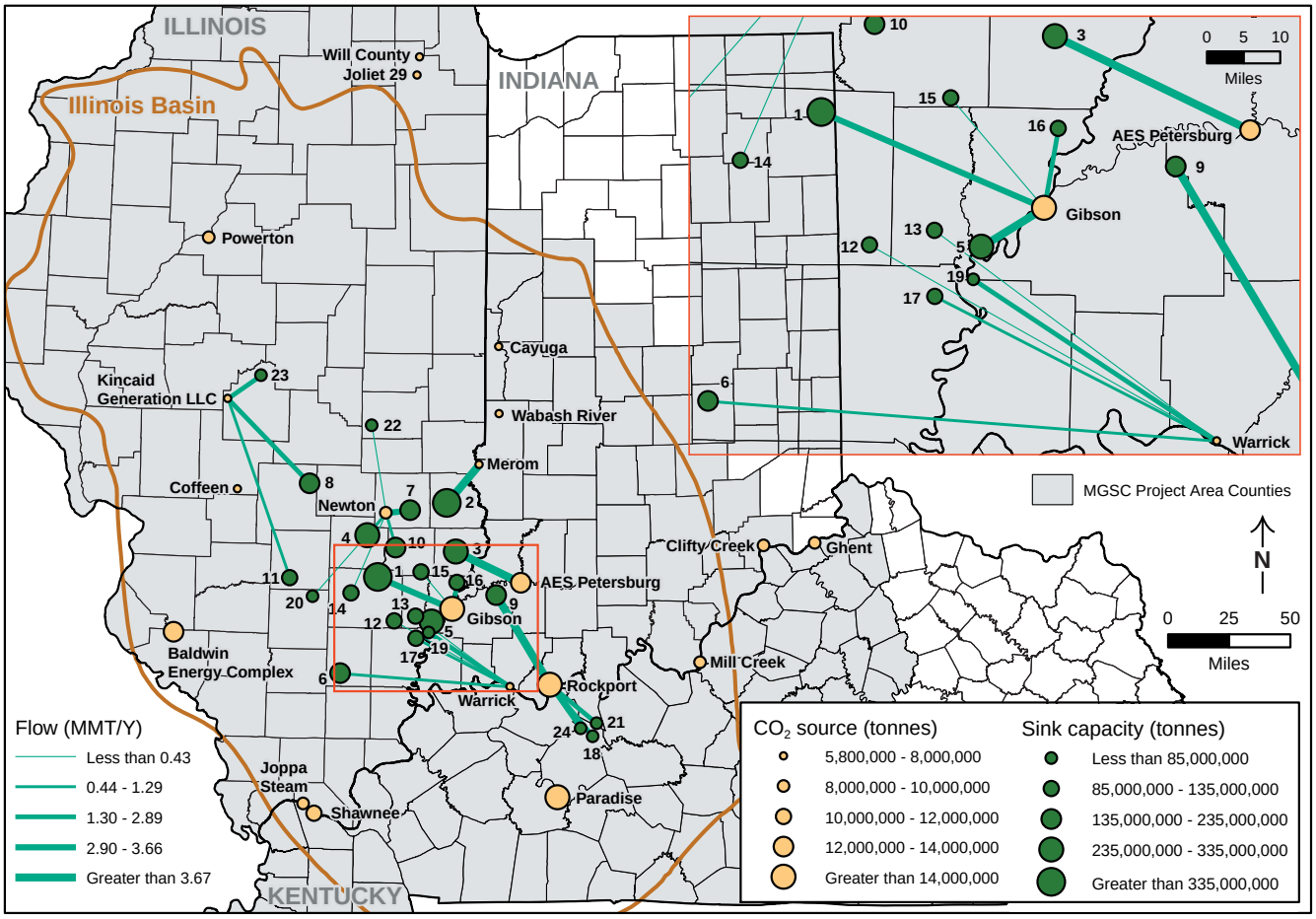

Figure 11 *Distribution of the captured CO_2 among the sinks at the 25% emission control level.*

10% Emission Control Level

At a 10% emission control level, only three power plants were identified (Table 16). The total CO_2 emissions from the three power plants are 30.05 million tonnes/year with 27.04 million tonnes/year captured (90% removal).

The capacity usages at the 10% emission control level are listed in Table 17. Again, as with the previous two cases, all of the capacities available in oil fields and coal beds are filled. In addition, 8.71 million tonnes/year of CO_2 is sequestered in saline reservoirs. About 17% of the total storage capacity would be filled in 30 years.

The geographical connections between the three power plants and the 24 sinks and the CO_2 flow rates in pipelines are listed in Table 18. The pipeline distance range from 10 to 77 miles with a flow-weighted average distance of 22.2 miles (Figure 12). This distance is shorter than the distances for the 50% (57.4 miles) and 25% (26.7 miles) control level cases, respectively.

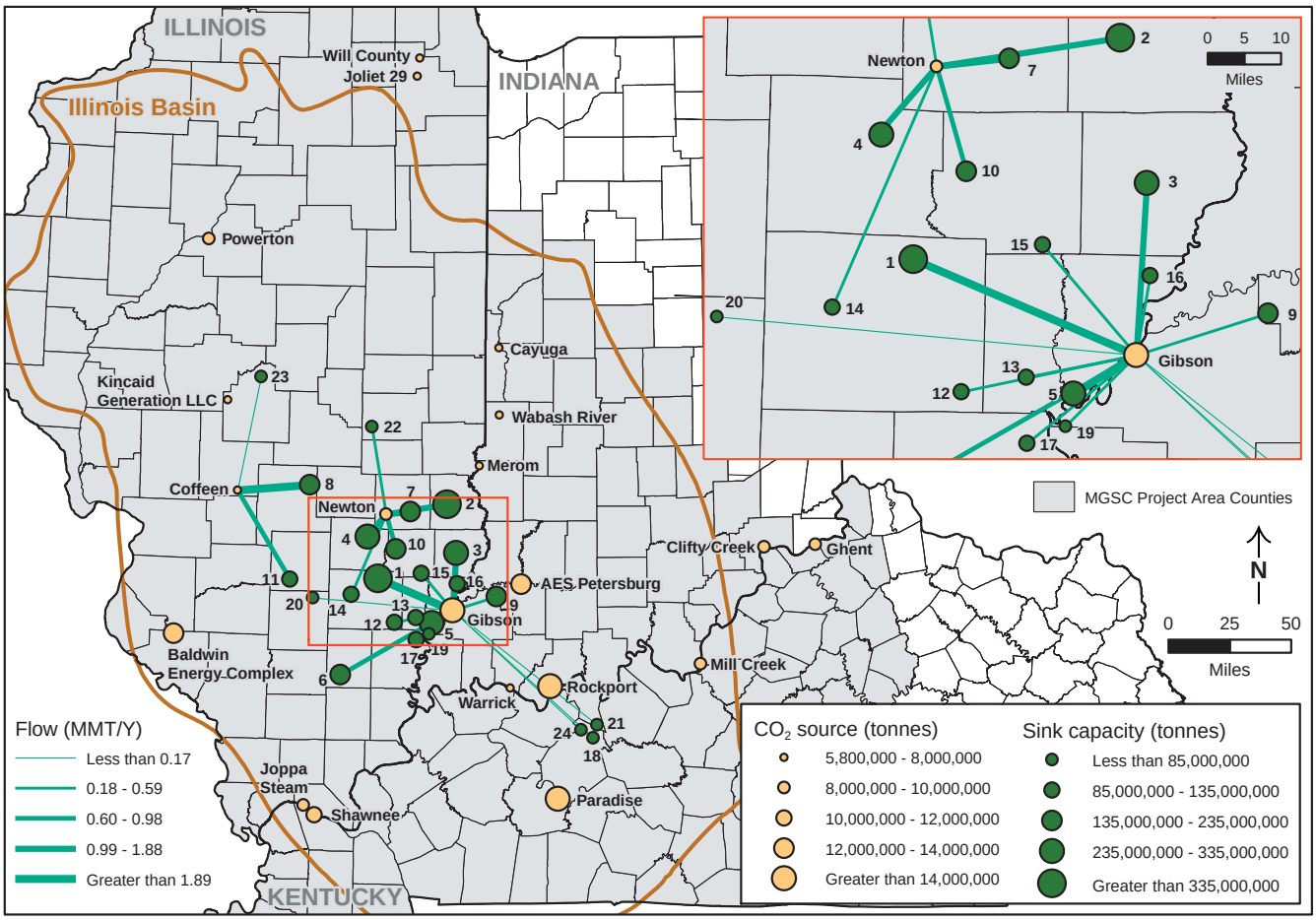

Figure 12 *Distribution of the capture CO_2 among the sinks at the 10% emission control level.*

Table 13. Power plants selected in 25% CO_2 emission control level.

Plant name	ORIS code	Emitted (million tonnes/year)	Captured (million tonnes/year)	Capture cost (million tonnes/year)
GIBSON	6113	17.46	15.71	840.01
ROCKPORT	6166	15.27	13.75	735.21
AES	994	12.23	11.01	588.70
NEWTON	6017	7.37	6.63	354.51
MEROM	6213	7.12	6.41	342.74
KINCAID	876	6.00	5.40	288.74
WARRICK	6705	5.67	5.10	272.70
Total		**71.12**	**64.02**	**3,422.61**

At a 10% emissions control level, the total sequestration cost—including capture, injection, and transportation—is $1.20 billion/year ($44.22/tonne of CO_2). Contributions from capture, transportation, and injection are $1.45 billion/year ($53.45/tonne of CO_2), $26.63 million/year ($0.98/tonne of CO_2), and

–$276.20 million/year (–$10.21/tonne of CO_2), respectively. Again, the negative injection cost indicates that the injection is profitable. The loss of electricity due to CO_2 capture is about 1,634 MW at the 10% control level.

Table 14. Capacity usage of all of the sinks at the 25% emission control level.[1]

Field name	Field ID	Mature oil fields		Coal beds		Saline aquifer		Total used (MMT/Y)	Injection cost ($MM/Y)
		Capacity (MMT/Y)	Used (MMT/Y)	Capacity (MMT/Y)	Used (MMT/Y)	Capacity (MMT/Y)	Used (MMT/Y)		
CLAY CITY (MGSC SW)	171119	1.31	1.31	2.35	2.35	23.67	0.00	3.66	–61.45
MAIN CONS.	171361	1.30	1.30	0.58	0.58	17.77	4.53	6.41	–12.01
LAWRENCE	171336	0.97	0.97	0.47	0.47	9.66	9.57	11.01	21.34
SAILOR SPRS. CONS.	171530	0.31	0.31	0.98	0.98	8.37	0.00	1.29	–20.89
NEW HARMONY CONS.	171415	0.72	0.72	0.68	0.68	7.41	7.41	8.82	12.28
DALE CONS.	171151	0.52	0.52	0.33	0.33	7.04	0.00	0.85	–15.40
CLAY CITY (MGSC N)	171119	0.36	0.36	0.90	0.90	6.55	2.72	3.99?	–7.18
LOUDEN	171354	0.73	0.73	0.28	0.28	6.51	1.36	2.38	–12.02
UNION-BOWMAN CONS.	181996	0.30	0.30	0.04	0.04	6.65	6.65	6.99	26.58
CLAY CITY (MGSC NE)	171119	0.32	0.32	0.66	0.66	5.75	0.00	0.98	–16.23
SALEM CONS.	171533	0.58	0.58	0.14	0.14	3.65	0.00	0.72	–13.67
GOLDEN GATE CONS.	171230	0.14	0.14	0.29	0.29	3.66	0.00	0.43	–.23
ALBION CONS.	171010	0.16	0.16	0.26	0.26	3.06	0.00	0.42	–7.10
JOHNSONVILLE CONS.	171299	0.13	0.13	0.25	0.25	2.98	0.00	0.38	–6.31
PARKERSBURG CONS.	171462	0.09	0.09	0.26	0.26	2.96	0.00	0.35	–.73
ALLENDALE	171015	0.15	0.15	0.16	0.16	2.93	2.16	2.46	5.42
PHILLIPSTOWN CONS.	171474	0.13	0.13	0.26	0.26	2.60	0.00	0.39	–6.59
FORDSVILLE CONS.	2112962	0.06	0.06	0.00	0.00	2.74	2.74	2.80	12.42
GRIFFIN CONS.	181787	0.40	0.40	0.19	0.19	2.08	2.08	2.66	–0.48
DIVIDE CONS.	171160	0.06	0.06	0.11	0.11	2.41	0.00	0.17	–2.92
Easton CONS	21212261	0.02	0.02	0.00	0.00	2.56	2.20	2.21	10.66
MATTOON	171377	0.07	0.07	0.18	0.18	2.09	0.00	0.25	–4.06
MT. AUBURN CONS.	171399	0.06	0.06	0.03	0.03	2.22	2.22	2.31	9.51
AETNAVILLE CONS.	214643	0.03	0.03	0.00	0.00	2.05	2.05	2.08	9.68
Total		**8.93**	**8.93**	**9.41**	**9.41**	**137.36**	**45.68**	**64.02**	**–91.35**

[1]Some numbers are rounded.

Comparison of Emission Control Levels

The total CO_2 sequestration costs for the three selected CO_2 control levels in the Basin are summarized in Table 19. These costs include the electricity loss due to the installation of MEA plants. The increase in the cost of electricity, shared by all utilities in the Basin, is about 3.72, 10.50, and 22.50 mills/kWh at 10, 25, and 50% of CO_2 reduction, respectively.

Table 15. Connections between emission sources and sinks at the 25% emission control level.

Sources	ID	Sinks	ID	Flow rate (MMT/Y)	Distance (miles)	Transportation cost ($MM/Y)
GIBSON	6113	CLAY_CITY_SW	171119	3.66	32.96	2.89
GIBSON	6113	NEW_HARMONY	171415	8.82	10.01	1.29
GIBSON	6113	PARKERSBURG	171462	0.35	19.67	0.61
GIBSON	6113	ALLENDALE	171015	2.89	11.00	0.87
ROCKPORT	6166	UNION	181996	6.66	42.71	4.87
ROCKPORT	6166	FORDSVILLE	2112962	2.80	27.43	2.13
ROCKPORT	6166	EASTON_CONS	21212261	2.21	24.68	1.73
ROCKPORT	6166	AETNAVILLE	214643	2.08	21.83	1.49
AES	994	LAWRENCE	171336	11.01	29.44	4.19
NEWTON	6017	DIVIDE	171160	0.17	45.27	1.03
NEWTON	6017	MATTOON	171377	0.25	36.12	0.96
NEWTON	6017	SAILOR_SPRS	171530	1.29	11.92	0.66
NEWTON	6017	CLAY_CITY_N	171119	3.57	9.94	0.86
NEWTON	6017	CLAY_CITY_NE	171119	0.98	14.86	0.73
NEWTON	6017	JOHNSONVILLE	171299	0.38	35.73	1.15
MEROM	6213	MAIN_CONS	171361	6.41	20.51	2.30
KINCAID	876	LOUDEN	171354	2.38	48.04	3.48
KINCAID	876	SALEM_CONS	171533	0.72	77.46	3.31
KINCAID	876	MT__AUBURN_CONS	171399	2.31	16.58	1.19
WARRICK	6705	DALE_CONS	171151	0.85	69.32	3.19
WARRICK	6705	GOLDEN_GATE_CONS	171230	0.43	54.24	1.86
WARRICK	6705	ALBION_CONS	171010	0.42	47.91	1.61
WARRICK	6705	PHILLIPSTOWN	171474	0.73	43.07	1.85
WARRICK	6705	GRIFFIN	181787	2.66	39.74	3.03
Total				**64.02**	**26.68 avg.**	**47.27**

Table 16. Power plants selected at the 10% CO_2 emission control level.

Plant name	ORIS code	Emissions (MMT/Y)	Captured (MMT/Y)	Capture cost ($MM/Y)
GIBSON	006113	17.46	15.71	840.01
NEWTON	006017	7.37	6.63	354.51
COFFEEN	000861	5.22	4.70	251.31
Total		**30.05**	**27.05**	**1,445.83**

Table 17. Capacity usage of all the sinks at the 10% emission control level.

Field name	Field ID	Mature oil fields		Coal beds		Saline aquifer		Total used (MMT/Y)	Injection cost ($MM/Y)
		Capacity (MMT/Y)	Used (MMT/Y)	Capacity (MMT/Y)	Used (MMT/Y)	Capacity (MMT/Y)	Used (MMT/Y)		
CLAY CITY (MGSC SW)	171119	1.31	1.31	2.35	2.35	23.67	0.00	3.66	–61.45
MAIN CONS.	171361	1.30	1.30	0.58	0.58	17.77	0.00	1.88	–34.67
LAWRENCE	171336	0.97	0.97	0.47	0.47	9.66	0.00	1.44	–26.50
SAILOR SPRS. CONS.	171530	0.31	0.31	0.98	0.98	8.37	0.00	1.29	–20.89
NEW HARMONY CONS.	171415	0.72	0.72	0.68	0.68	7.41	5.23	6.64	–1.09
DALE CONS.	171151	0.52	0.52	0.33	0.33	7.04	0.00	0.85	–15.40
CLAY CITY (MGSC N)	171119	0.36	0.36	0.90	0.90	6.55	0.60	1.86	–15.33
LOUDEN	171354	0.73	0.73	0.28	0.28	6.51	2.88	3.90	–4.43
UNION-BOWMAN CONS.	181996	0.30	0.30	0.04	0.04	6.65	0.00	0.34	–6.65
CLAY CITY (MGSC NE)	171119	0.32	0.32	0.66	0.66	5.75	0.00	0.98	–16.23
SALEM CONS.	171533	0.58	0.58	0.14	0.14	3.65	0.00	0.72	–13.67
GOLDEN GATE CONS.	171230	0.14	0.14	0.29	0.29	3.66	0.00	0.43	–7.23
ALBION CONS.	171010	0.16	0.16	0.26	0.26	3.06	0.00	0.42	–7.10
JOHNSONVILLE CONS.	171299	0.13	0.13	0.25	0.25	2.98	0.00	0.38	–6.31
PARKERSBURG CONS.	171462	0.09	0.09	0.26	0.26	2.96	0.00	0.35	–5.73
ALLENDALE	171015	0.15	0.15	0.16	0.16	2.93	0.00	0.31	–5.36
PHILLIPSTOWN CONS.	171474	0.13	0.13	0.26	0.26	2.60	0.00	0.39	–6.59
FORDSVILLE CONS.	2112962	0.06	0.06	0.00	0.00	2.74	0.00	0.06	–1.26
GRIFFIN CONSOL.	181787	0.40	0.40	0.19	0.19	2.08	0.00	0.59	–10.86
DIVIDE CONS.	171160	0.06	0.06	0.11	0.11	2.41	0.00	0.17	–2.92
Easton CONS.	21212261	0.02	0.02	0.00	0.00	2.56	0.00	0.02	–0.31
MATTOON	171377	0.07	0.07	0.18	0.18	2.09	0.00	0.25	–4.06
MT. AUBURN CONS.	171399	0.06	0.06	0.03	0.03	2.22	0.00	0.09	–1.59
AETNAVILLE CONS.	214643	0.03	0.03	0.00	0.00	2.05	0.00	0.03	–0.58
Total		**8.93**	**8.93**	**9.41**	**9.41**	**137.36**	**8.71**	**27.05**	**–276.20**

Sensitivity Analysis

The capture cost and EOR and ECBM by-product credits could change during the course of a sequestration period. The DOE has set a target cost of $10/tonne for CO_2 sequestration. This might be an ambitious goal; however, with advancement in various technologies employed in the sequestration process and an anticipated increase in the price of oil and natural gas, the net CO_2 sequestration cost will tend to decrease. This section presents the results from a sensitivity study to evaluate the impacts of costs of CO_2 capture and by-products recovered from CO_2 storage on the overall sequestration cost.

CO_2 Capture Cost

The sensitivity study was performed by assuming that the CO_2 capture cost of an MEA-based absorption process will be reduced by 80%, 50%, and 25% from the current estimate of $53.47/tonne for a new

1,000-MW power plant. The change in capture cost will not impact the selection of capture sources or transportation routes. Thus, transportation and injection costs remain the same. The results are shown in Figure 13 and Table 20.

The sequestration cost is linearly related to the capture cost at all levels. The impact of CO_2 capture cost is more pronounced with an increase in CO_2 emission control levels. This observation indicates that future efforts to reduce sequestration costs should focus on developing more cost-effective capture technologies.

Table 20 presents the impact of capture cost on the average costs of CO_2 sequestration per tonne, total sequestration costs, and the average increase in electricity cost at different control levels. For example, at the 50% control level and a 50% reduction in the current capture costs, the costs for sequestering 1 tonne of CO_2 decreases from $56.35 to $29.61, and the increase in electricity cost decreases from 22.50 to 11.82 mills/kWh.

Table 18. Connections between emission sources and sinks at the 10% control level.

Plant name	ID	Sink name	ID	Flow rate (MMT/Y)	Distance (miles)	Transportation cost ($MM/Y)
GIBSON	6113	CLAY_CITY_SW	171119	3.66	32.96	2.89
GIBSON	6113	LAWRENCE	171336	1.44	23.48	1.36
GIBSON	6113	NEW_HARMONY	171415	6.64	10.01	1.14
GIBSON	6113	DALE_CONS	171151	0.85	52.68	2.43
GIBSON	6113	UNION	181996	0.34	18.77	0.58
GIBSON	6113	GOLDEN_GATE_CONS	171230	0.43	24.26	0.83
GIBSON	6113	ALBION_CONS	171010	0.42	15.20	0.51
GIBSON	6113	PARKERSBURG	171462	0.35	19.67	0.61
GIBSON	6113	ALLENDALE	171015	0.31	11.00	0.32
GIBSON	6113	PHILLIPSTOWN	171474	0.39	19.12	0.63
GIBSON	6113	FORDSVILLE	2112962	0.06	77.43	1.13
GIBSON	6113	GRIFFIN	181787	0.59	13.68	0.54
GIBSON	6113	DIVIDE	171160	0.17	57.11	1.31
GIBSON	6113	EASTON_CONS	21212261	0.02	75.09	0.59
GIBSON6	6113	AETNAVILLE	214643	0.03	71.61	0.74
NEWTON	6017	MATTOON	171377	0.25	36.12	0.96
NEWTON	6017	MAIN_CONS	171361	1.88	25.25	1.65
NEWTON	6017	SAILOR_SPRS	171530	1.29	11.92	0.66
NEWTON	6017	CLAY_CITY_N	171119	1.86	9.94	0.65
NEWTON	6017	CLAY_CITY_NE	171119	0.98	14.86	0.73
NEWTON	6017	JOHNSONVILLE	171299	0.38	35.73	1.15
COFFEEN	861	LOUDEN	171354	3.90	29.37	2.64
COFFEEN	861	SALEM_CONS	171533	0.72	42.09	1.80
COFFEEN	861	MT__AUBURN_CONS	171399	0.09	47.37	0.80
Total				**27.05**	**22.19 (avg.)**	**26.63**

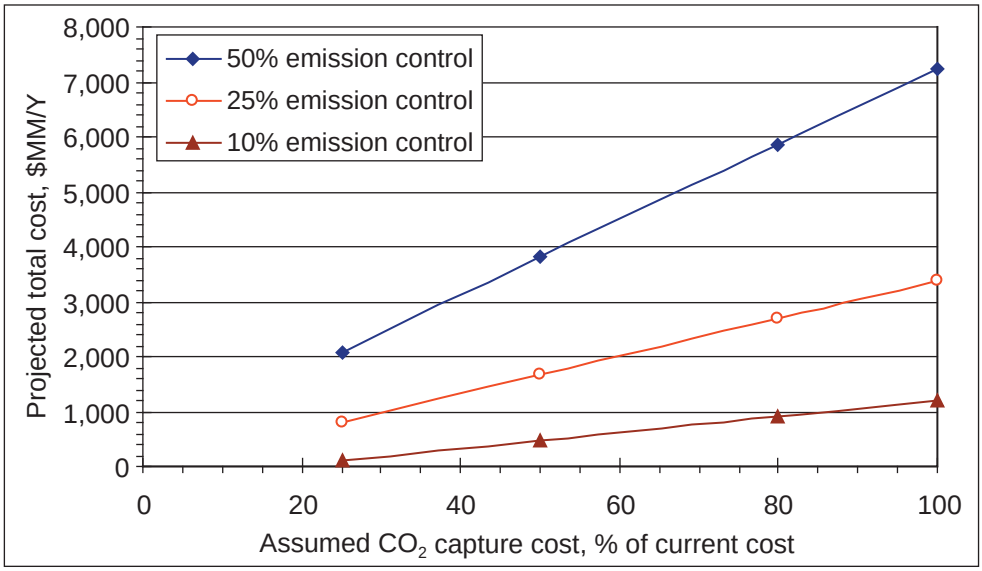

Figure 13 *Sensitivity of total CO_2 sequestration cost to the capture cost.*

Table 19. Summary of CO_2 sequestration costs with by-product credits.

Emission control level	50% (128.44MMT/Y)	25% (64.02MMT/Y)	10% (27.05MMT/Y)
Capture cost, $MM/Y	6,867.69	3,422.61	1,445.83
Transportation cost, $MM/Y	138.72	47.27	26.63
Injection cost, $MM/Y	230.75	–91.35	–276.20
Total cost, $MM/Y	7,237.16	3,378.53	1,196.26
Average cost, $/tonne of CO_2 sequestered	56.35	52.77	44.22
Electricity loss, MW	7,746	3,873	1,634
Average increase electricity cost, mills/kWh	22.50	10.50	3.72

Table 20. Sensitivity of CO_2 sequestration cost to capture cost.

Capture cost reduction, %	25%	50%	80%	100%
	50% emission control			
Total cost, $MM/Y	2,086.39	3,803.32	5,863.62	7,237.16
Average cost, $/tonne of CO_2 sequestered	16.24	29.61	45.65	56.35
Average increase of electricity cost, mills/kWh	6.49	11.82	18.23	22.50
	25% emission control			
Total cost, $MM/Y	811.57	1,667.23	2,694.01	3,378.53
Average cost, $/tonne of CO_2 sequestered	12.68	26.04	42.08	52.77
Average increase of electricity cost, mills/kWh	2.52	5.18	8.37	10.50
	10% emission control			
Total cost, $MM/Y	111.89	473.35	907.09	1,196.26
Average cost, $/tonne of CO_2 sequestered	4.14	17.50	33.53	44.22
Average increase of electricity cost, mills/kWh	0.35	1.47	2.82	3.72

CO_2 Sequestration Cost without EOR and ECBM Benefits

Without EOR and ECBM by-product credits, the distribution of captured CO_2 among the 24 sinks will be different from the scenarios described with by-product benefits. However, excluding the by-product credits in the optimization process has little impact on the selection of emission sources. The results from the optimization study confirmed this prediction. When by-product credits were not considered, the emission sources identified were identical to the cases in which the by-products were included for the 50% and 25% control levels, and only one emission source was different for the 10% control level.

The capacity usages at the three different emission control levels are listed in Table 21. For the 50%, 25%, and 10% control levels, 19, 15, and 5 sinks, respectively, were identified. These results are different from the scenarios when by-product credits were included. The total injection costs were proportional to the amount of CO_2 stored at a unit cost of $5/tonne of CO_2. Differences in the injectability characteristics of sinks are not considered.

The distribution of captured CO_2 among the sinks at different emission control levels is listed in Tables 22 to 24. Figures 14, 15, and 16 present the geographical distribution of the selected power plants and sinks for the 50%, 25%, and 10% emission control levels, respectively. The total transportation cost in this scenario is lower than when by-product credits were included. For example, at 50% emission control level, transportation cost is reduced from $138.7 million/year with by-product recovery to $137.8 million/year without by-product recovery. Trends for the 25% and 10% control levels are similar.

Table 25 provides a summary of the results. The total costs for transportation and injection are small compared with the capture cost with or without by-product credits. One reason for lower transportation cost is the relatively short distance between the emission sources and the available geological structures in the Illinois Basin. Also included in Table 25 are the increases in electricity costs, shared by all utilities in the Basin, for the sequestration process. They range from 5.25 to 23.77 mills/kWh, depending on the level of control.

Summary and Conclusions

Stationary sources in the Illinois Basin emitted 283 million tonnes of CO_2 in 2002, about 261 million tonnes of which were emitted by 122 power plants.

At the time this study was conducted, the 24 largest geological storage sites (outlined by the presence of oil fields) were identified in the Basin. These sites had a total CO_2 geological storage capacity of about 4.7 billion tonnes (6% in oil fields, 6% in coal bed seams, and 88% in saline reservoirs).

Table 21. Capacity usage of all the sinks at different emission control levels.

Field name	Field ID	50%			25%			10%		
		Total capacity (MMT/Y)	Used (MMT/Y)	Injection cost ($MM/Y)	Total capacity (MMT/Y)	Used (MMT/Y)	Injection cost ($MM/Y)	Total capacity (MMT/Y)	Used (MMT/Y)	Injection cost ($MM/Y)
CLAY_CITY_SW	171119	27.32	27.02	135.10	27.32	0	0	27.32	0	0
MAIN_CONS_	171361	19.65	19.06	95.30	19.65	6.41	32.05	19.65	6.41	32.05
LAWRENCE	171336	11.10	11.01	55.05	11.1	11.01	55.05	11.1	0	0
SAILOR_SPRS_	171530	9.66	5.45	27.25	9.66	0	0	9.66	0	0
NEW_HARMONY	171415	8.82	8.82	44.10	8.82	8.82	44.10	8.82	8.82	44.10
DALE_CONS_	171151	7.89	7.52	37.60	7.89	0	0	7.89	0	0
CLAY_CITY_N	171119	7.82	6.63	33.15	7.82	6.63	33.15	7.82	6.63	33.15
LOUDEN	171354	7.52	6.93	34.65	7.52	3.09	15.45	7.52	0	0
UNION	181996	6.99	6.99	34.95	6.99	6.99	34.95	6.99	3.66	18.3
CLAY_CITY_NE	171119	6.72	0	0	6.72	0	0	6.72	0	0
SALEM_CONS_	171533	4.37	4.37	21.85	4.37	0	0	4.37	0	0
GOLDEN_GATE_CONS	171230	4.10	0	0	4.10	0	0	4.1	0	0
ALBION_CONS_	171010	3.48	3.48	17.40	3.48	3.48	17.40	3.48	0	0
JOHNSONVILLE	171299	3.36	3.36	16.80	3.36	0	0	3.36	0	0
PARKERSBURG	171462	3.32	0	0	3.32	0.19	0.95	3.32	0	0
ALLENDALE	171015	3.23	3.23	16.15	3.23	3.23	16.15	3.23	3.23	16.15
PHILLIPSTOWN	171474	2.99	0	0	2.99	2.44	12.20	2.99	0	0
FORDSVILLE	2112962	2.80	0	0	2.80	2.10	10.50	2.8	0	0
GRIFFIN	181787	2.66	2.66	13.30	2.66	2.66	13.30	2.66	0	0
DIVIDE	171160	2.59	2.59	12.95	2.59	0	0	2.59	0	0
EASTON_CONS	21212261	2.58	2.58	12.90	2.58	2.58	12.90	2.58	0	0
MATTOON	171377	2.34	2.34	11.70	2.34	0	0	2.34	0	0
MT__AUBURN_CONS	171399	2.31	2.31	11.55	2.31	2.31	11.55	2.31	0	0
AETNAVILLE	214643	2.08	2.08	10.40	2.08	2.08	10.40	2.08	0	0
Total		**155.70**	**128.44**	**642.15**	**155.7**	**64.02**	**320.10**	**155.70**	**28.75**	**143.75**

Table 22. The connection between emission sources and sinks at 50% control level.

Sources	ID	Sinks	ID	Flow rate (MMT/Y)	Distance (miles)	Transportation cost ($MM/Y)
GIBSON	6113	CLAY_CITY_SW	171119	4.32	32.96	3.11
GIBSON	6113	NEW_HARMONY	171415	2.02	10.01	0.67
GIBSON	6113	ALBION_CONS	171010	3.48	15.20	1.30
GIBSON	6113	ALLENDALE	171015	3.23	11.00	0.91
GIBSON	6113	GRIFFIN	181787	2.66	13.68	1.04
ROCKPORT	006166	CLAY_CITY_SW	171119	13.75	82.72	12.99
PARADISE	1378	NEW_HARMONY	171415	6.80	88.30	10.16
PARADISE	1378	UNION	181996	6.55	86.45	9.79
AES	000994	LAWRENCE	171336	11.01	29.44	4.19
BALDWIN	889	LOUDEN	171354	0.36	82.19	2.57
BALDWIN	889	SALEM_CONS	171533	4.37	52.29	4.95
BALDWIN	889	JOHNSONVILLE	171299	3.36	74.05	6.25
BALDWIN	889	DIVIDE	171160	2.59	58.54	4.40
SHAWNEE	001379	CLAY_CITY_SW	171119	8.96	100.19	13.02
MILL_CREEK	001364	MAIN_CONS	171361	7.81	121.97	14.92
JOPPA_STEAM	000887	DALE_CONS	171151	7.52	55.40	6.67
NEWTON	6017	CLAY_CITY_N	171119	6.63	9.94	1.13
POWERTON	000879	LOUDEN	171354	6.57	108.64	12.32
MEROM	006213	MAIN_CONS	171361	6.41	20.51	2.30
KINCAID	876	SAILOR_SPRS	171530	0.75	79.77	3.48
KINCAID	876	MATTOON	171377	2.34	59.70	4.29
KINCAID	876	MT__AUBURN_CONS	171399	2.31	16.58	1.19
WARRICK	6705	UNION	181996	0.44	37.84	1.30
WARRICK	6705	EASTON_CONS	21212261	2.58	38.37	2.88
WARRICK	6705	AETNAVILLE	214643	2.08	33.59	2.29
WABASH_RIVER	001010	MAIN_CONS	171361	4.85	42.30	4.19
COFFEEN	000861	SAILOR_SPRS	171530	4.70	56.18	5.50
Total				**128.44**	**59.52 (avg.)**	**137.81**

The integrated CO_2 sequestration process in the Illinois Basin was optimized at control levels of 10%, 25%, and 50% using a commercial nonlinear optimization software tool, LINGO, for evaluating the most economical options for the integrated sequestration process.

The costs of CO_2 capture (90% reduction) from coal-fired power plants and pipeline transportation were obtained from a previous techno-economic study completed by the MGSC in October 2004. The CO_2 avoidance costs ($53 to $59/tonne) were based on an MEA process. An injection cost of $5/tonne of CO_2 for saline reservoirs and net revenues of $20/tonne of CO_2 for EOR and $15/tonne CO_2 for ECBM were assumed. The loss of electricity capacity in the Basin due to the installation of MEA plants was not included in the optimization study. Sequestration costs were evaluated with and without by-product credits from EOR and ECBM. A 30-year life span was considered for the pipeline and MEA process.

Table 23. Connections between emission sources and sinks at 25% control level.

Sources	ID	Sinks	ID	Flow rate (MMT/Y)	Distance (miles)	Transportation cost ($MM/Y)
GIBSON	6113	NEW_HARMONY	171415	8.82	10.01	1.29
GIBSON	6113	ALBION_CONS	171010	3.48	15.20	1.30
GIBSON	6113	PARKERSBURG	171462	0.19	19.67	0.46
GIBSON	6113	ALLENDALE	171015	3.23	11.00	0.91
ROCKPORT	006166	UNION	181996	6.99	42.71	4.98
ROCKPORT	006166	FORDSVILLE	2112962	2.10	27.43	1.88
ROCKPORT	006166	EASTON_CONS	21212261	2.58	24.68	1.85
ROCKPORT	006166	AETNAVILLE	214643	2.08	21.83	1.49
AES	000994	LAWRENCE	171336	11.01	29.44	4.19
NEWTON	6017	CLAY_CITY_N	171119	6.63	9.94	1.13
MEROM	006213	MAIN_CONS	171361	6.41	20.51	2.30
KINCAID	876	LOUDEN	171354	3.09	48.04	3.91
KINCAID	876	MT__AUBURN_CONS	171399	2.31	16.58	1.19
WARRICK	6705	PHILLIPSTOWN	171474	2.44	43.07	3.15
WARRICK	6705	GRIFFIN	181787	2.66	39.74	3.03
Total				**64.02**	**24.44 (avg.)**	**33.06**

Table 24. Connections between emission sources and sinks at 10% control level.

Sources	ID	Sinks	ID	Flow rate (MMT/Y)	Distance (miles)	Transportation cost ($MM/Y)
GIBSON	6113	NEW_HARMONY	171415	8.82	10.01	1.29
GIBSON	6113	UNION	181996	3.66	18.77	1.64
GIBSON	6113	ALLENDALE	171015	3.23	11.00	0.91
NEWTON	6017	CLAY_CITY_N	171119	6.63	9.94	1.13
MEROM	006213	MAIN_CONS	171361	6.41	20.51	2.30
Total				**28.75**	**13.56 (avg.)**	**7.27**

Table 25. Summary of CO_2 sequestration costs without by-product credits.

Sequestration cost	Emission control level		
	50% (128.44 MMT/Y)	25% (64.02 MMT/Y)	10% (28.75 MMT/Y)
Capture cost, $MM/Y	6,867.69	3,422.61	1,537.26
Transportation cost, $MM/Y	137.81	33.06	7.27
Injection cost, $MM/Y	642.20	320.10	143.75
Total cost, $MM/Y	7,647.70	3,775.77	1,688.28
Average cost, $/tonne CO_2 sequestered	59.54	58.98	58.72
Electricity loss, MW	7,746	3,873	1,634
Average increase of electricity cost, mills/kWh	23.77	11.74	5.25

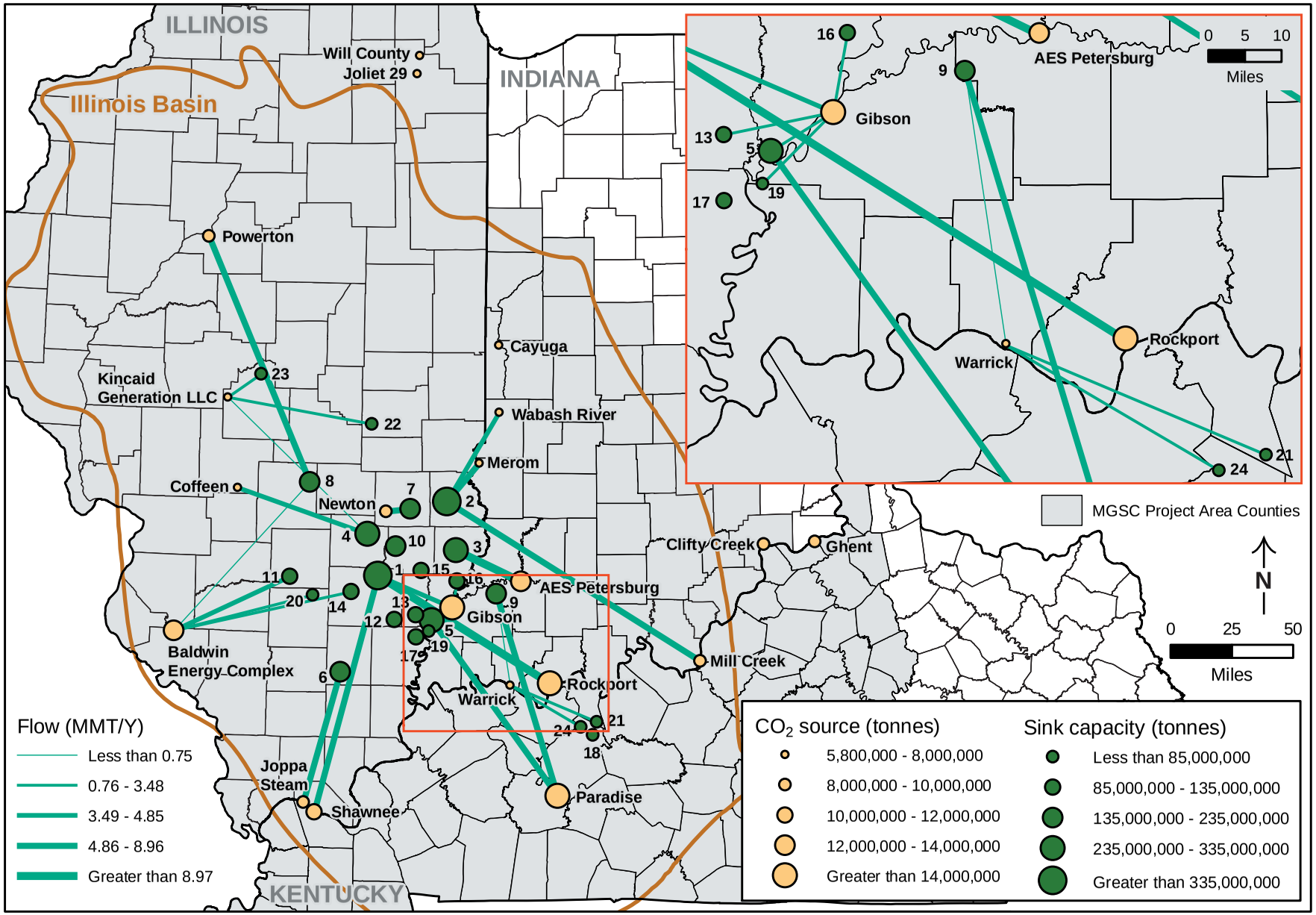

Figure 14 *Distribution of the captured CO_2 among the sinks at 50% emission control level, without EOR or ECBM benefit.*

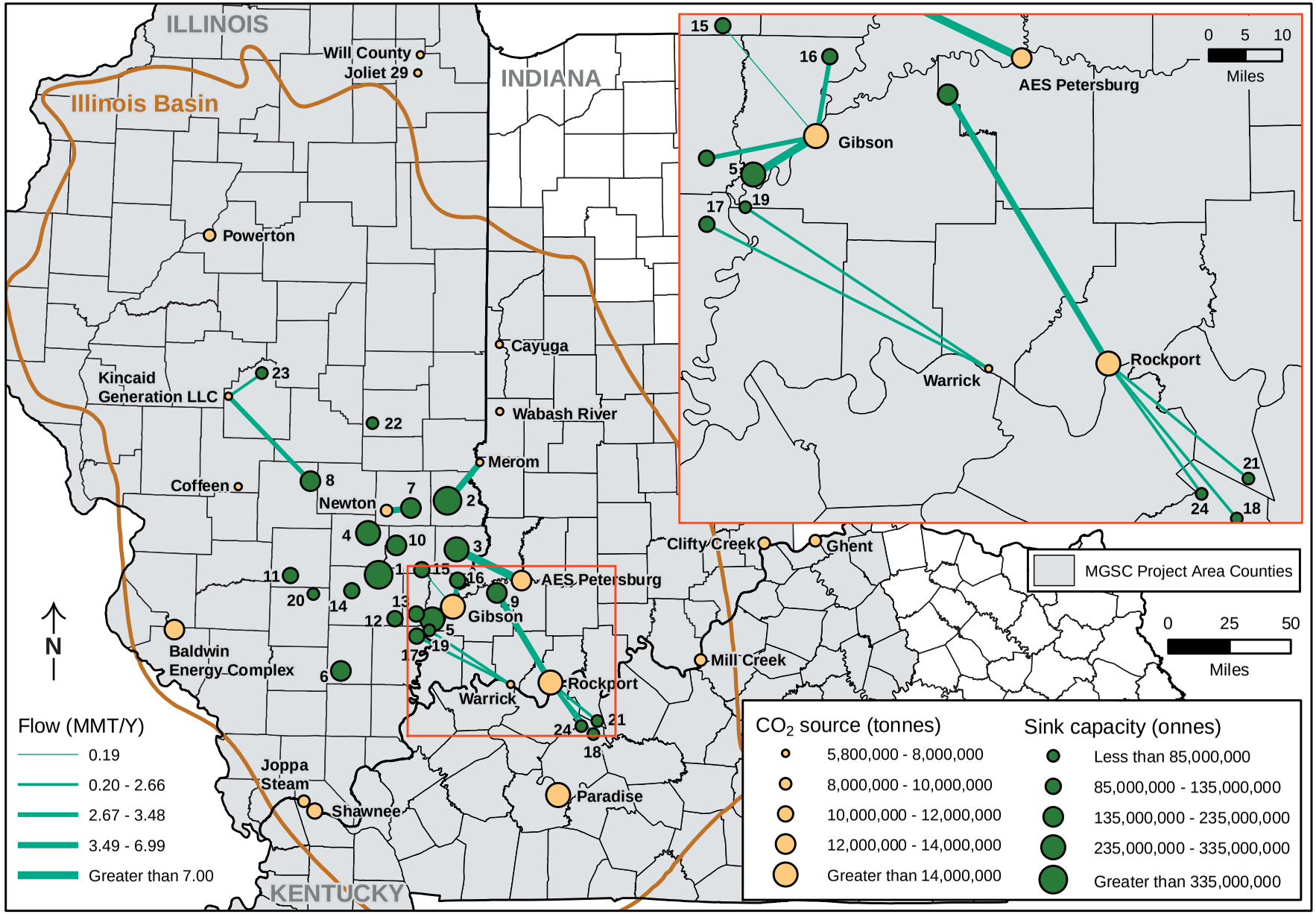

Figure 15 *Distribution of the captured CO_2 among the sinks at 25% emission control level, without EOR or ECBM benefits.*

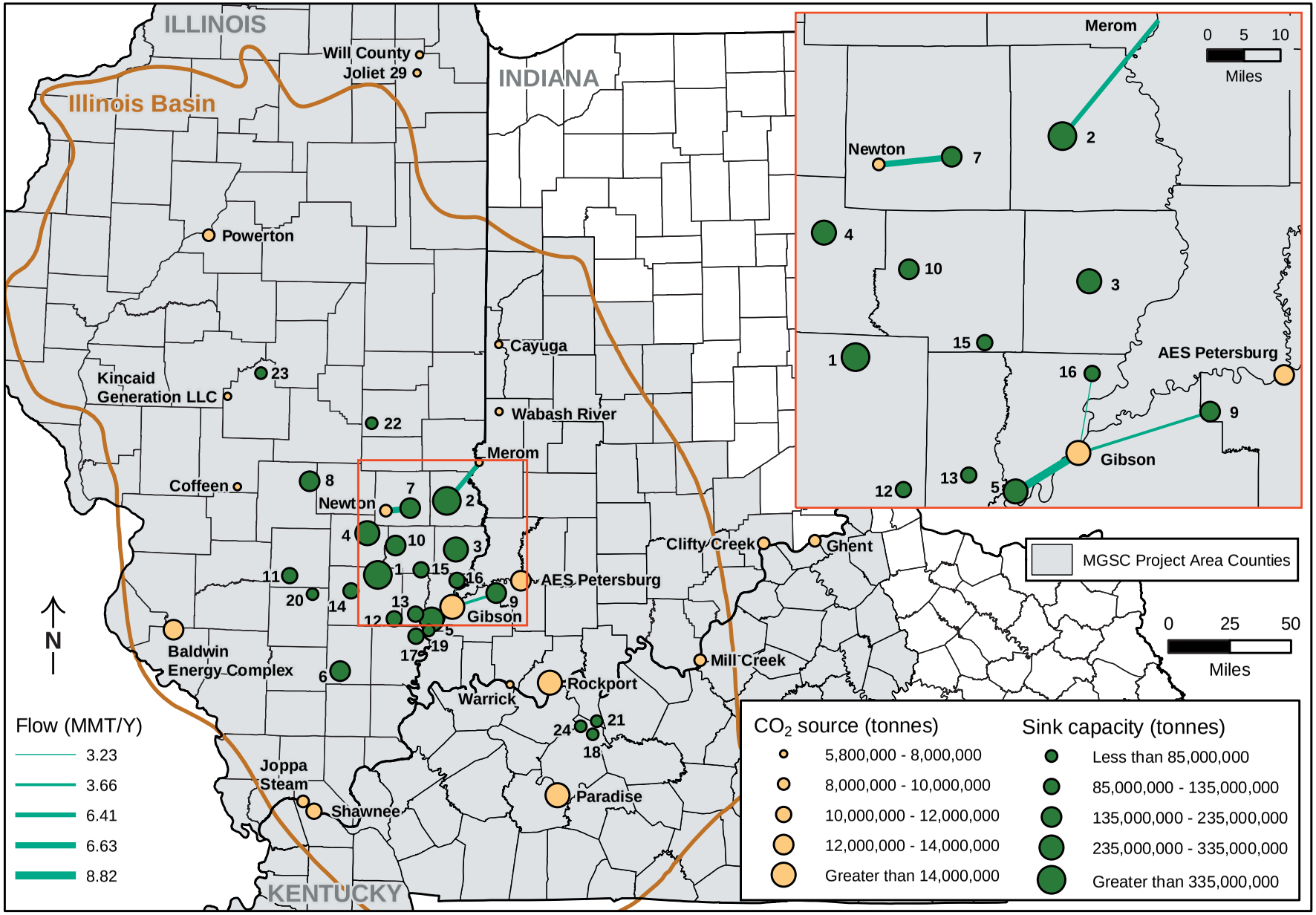

Figure 16 *Distribution of the captured CO_2 among the sinks at 10% emission control level, without EOR or ECBM benefits.*

The scale of a power plant impacted the overall sequestration cost more than its location did. Thus, CO_2 control from large power plants was more economical than that from small power plants. In addition, regardless of the locations of storage sinks, CO_2 storage in EOR and ECBM fields was economically preferable due to the potential income from by-products.

When the revenues from by-products recovery were included, the average cost of the sequestration process ranged from $44 to $56/tonne of CO_2 sequestered, depending on the control level. The cost for capturing CO_2 from power plants contributed to more than 95% of the total sequestration cost when the benefits from EOR and ECBM were included.
Electricity loss due to installing MEA plant was about 7,746, 3,873, and 1,634 MW at the 50%, 25%, and 10% emission control levels, respectively. The costs associated with the electricity loss were incorporated in the CO_2 avoidance costs. The total sequestration cost thus includes the cost of electricity loss.

With by-products recovery, the increase in electricity costs in the Basin were estimated to be 3.72, 10.50, and 22.50 mills/kWh at 10, 25, and 50% emission control levels, respectively. With a 50% reduction in capture cost, the increased electricity costs are 1.47, 5.18, and 11.82 mills/kWh.
Without EOR and ECBM by-product recovery, the cost of CO_2 sequestration was about $60/tonne of CO_2 sequestered. The average costs of CO_2 capture, transportation, and injection were about 90%, 2%, and 8%, respectively, of the total sequestration cost. The cost of sequestering each tonne of CO_2 significantly increased at a lower emission control level when the benefits from EOR and ECBM were not included.

Without by-product recovery, increased costs for electricity in the Basin were estimated to be 5.25, 11.74, and 23.77 mills/kWh at the 10, 25, and 50% emission control levels, respectively.

Sensitivity analysis confirmed that the most attractive approach to reduce the overall cost of the sequestration process was to develop more cost-effective technologies for capturing CO_2 from existing coal-fired power plants.

Recommendations

The following recommendations should be considered in future optimization studies of the integrated sequestration process in the Illinois Basin:

- Incorporate CO_2 emissions from auxiliary power plants that are needed to compensate electricity loss due to CO_2 capture from existing power plants.

- Include a projection of the future CO_2 emissions from new power plants according to the mid-term energy demand and supply analysis.

- Update the integrated sequestration costs, especially as improved and new capture technologies become available.

- Use updated capacities of the geological structures in the Basin including more detailed characterization of data that are specific to individual storage sinks, such as permeability, reservoir thickness, and reservoir depth.

- Perform a dynamic analysis accounting for CO_2 emissions, transportation, and storage over the lifetime of the sequestration process.

- Allow nodes in pipelines for optimizing network transportation.

References

Bergman, P.D., E.M. Winter, and Z.-Y. Chen, 1997, Disposal of power plant CO_2 in depleted oil and gas reservoirs in Texas: Energy Conversion and Management, v. 38, Suppl. 1, p. S211–S216.

Chen, S.G., Y. Lu, M. Rostam-Abadi, D. J. Nyman, J.S. Dracos, and R.Varagani, 2004, Assessment of geological carbon sequestration options in the Illinois Basin: Illinois State Geological Survey, Topical Report, DE-FC26-03NT41994, September 2004.

Gale, J., and P. Freund, 2001, Coal-bed methane enhancement with CO_2 sequestration worldwide potential: Environmental Geosciences, v. 8, p. 210–217.

Holtz, M. H., P. Nance, and R.J. Finley, 1999, Reduction of greenhouse gas emissions through underground CO_2 sequestration in Texas oil reservoirs; Final Contract Report prepared for EPRI through U.S. Department of Energy, under contract no. W04603-04.

Holtz, M.H., P. Nance, and R.J. Finley, 2001, Reduction of greenhouse gas emissions through underground CO_2 sequestration in Texas oil reservoirs: Environmental Geosciences, v. 8, p. 187–199.

Iowa Department of Agriculture and Land Stewardship, 2004, U.S. Fuel Ethanol Production Capacity. http://www.distillersgrains.com/plantlisting.asp Accessed March 31, 2006.

LINDO Systems Inc., 2002, Optimization Modeling with LINGO: Chicago, LINDO Systems Inc.

Reeves, S.R., and L. Schoeling, 2001, Geological sequestration of CO_2 in coal seams: Reservoir mechanisms, field performance and economics: Proceedings GHGT-5, Cairns, Australia, 2001, p. 593–596.

Stevens S., V.A. Kuuskraa, and J. O'Donnell, 1998, Enhanced oil recovery scoping study: EPRI Report TR-113836.

Stevens, S.H.,V.A. Kuuskraa, J. Gale, and D. Beecy, 2001, CO_2 injection and sequestration in depleted oil and gas fields and deep coal seams: Worldwide Potential and Costs: Environmental Geosciences, v. 8, p. 200–209.

U.S. Department of Energy, 2004, U.S. Refineries and Refining Capacities. http://www.eia.doe.gov/emeu/finance/usi&to/downstream/update/#tab4 Accessed July 10, 2004.

U.S. Environmental Protection Agency, 2004, U.S. EPA Greenhouse Gas Inventory. http://yosemite.epa.gov/oar/globalwarming.nsf/content/ResourceCenterPublicationsGHGEmissionsUSEmissionsInventory2004.html Accessed May 15, 2004.

U.S. Geological Survey, 2002, USGS Minerals Yearbook. http://minerals.usgs.gov/minerals/pubs/commodity/myb/ Accessed April 10, 2004.

Scenarios and Outcomes for a Specific Carbon Dioxide Transportation Option, Pekin to Edwards County, Illinois: 7,700,000 Tons of CO_2 per Year, Pipeline Route, Size Calculation, and Cost Based on Task 3 (M 4-12)

Introduction

The team of Dr. D.J. Nyman and Associates and Universal Ensco, Inc. (UEI) was commissioned to prepare this report on a specific carbon dioxide (CO_2) pipeline transportation option in support of the Midwest Geological Sequestration Consortium's (MGSC) assessment of opportunities for geological sequestration of CO_2 in the Illinois Basin.

This report was prepared by J. Steve Dracos of UEI, under the general direction of Douglas J. Nyman of D.J. Nyman & Associates. Mr. Dracos was assisted by UEI's engineering and Geographic Information Systems (GIS) staff in the assessment of pipeline hydraulics and routing of the pipeline. This report presents a specific pipeline route, a range of pipeline diameter, and cost for each diameter in response to a specific transportation scenario between a main CO_2 source and a storage site as defined by the Illinois State Geological Survey (ISGS). The presentation is based on the 2004 MGSC report to the U.S. Department of Energy (DOE) (Phase I, year 1) *Assessing CO_2 Pipeline Transportation Options in the Illinois Basin* by Nyman and Dracos. Initially, the ISGS provided two possible options but ultimately selected a scenario for transportation of 10.3 million m^3/day (362 million standard cubic feet (scf)/day) or 6,985,322 tonnes/year (7,700,000 tons/year) of CO_2 from the Pekin, Illinois, area (Pekin) to a terminal point in Edwards County, Illinois. The selected conceptual route originated in the Pekin area central to an existing power plant. The route runs generally southward to a point slightly east of Springfield and then turns south-southeasterly toward the Illinois-Indiana border. The terminal point in Edwards County was selected by ISGS as an approximate geographic central point for the MGSC's estimate for CO_2 storage in the Illinois Basin.

The 2004 report was based on a conceptual route with beginning and ending points that are very similar to the specific scenario requested for this study by ISGS. Because of this similarity, the data and discussions of the previous route are applicable to this report. As such, it is recommended that the reader review the previous report prior to reading this report.

Even though a specific route has been selected, this analysis remains in the conceptual stage. Sufficient data have been obtained and analyzed to provide a basis for making the key determinations necessary to move the project to the basic design stage.

Preliminary Route Selection

Route selection was based on origination and termination points provided by the ISGS. The origination point was a large power plant near Pekin, Illinois (Lat 40° 32’ 23.84” N, Long 89° 40’ 42.98” W). The termination point was the geographic central point of an oil production area in Edwards County, Illinois (Lat 38° 24’ 52.54” N, Long 88° 6’ 5.40” W), which potentially could use CO_2 for enhanced oil recovery operations in the future. The straight line distance between these points is 273.4 km (169.9 miles).

As discussed in the 2004 report, pipeline routes are selected in two stages, preliminary route selection and detailed route selection. The preliminary route is used as a basis for the planning and budgeting phases of the project. Once the project receives funding for permitting and right-of-way acquisition, detailed route selection and design are initiated. The work developed and presented in this report pertains to the preliminary route selection.

The objective of the preliminary route selection is to identify a viable pipeline route that will minimize impact to the public, landowners, and the environment pursuant to commercial constraints. This objective was accomplished based on UEI’s existing general knowledge of the area and also on information relative to land acquisition, environmental requirements, and construction methods compiled in the previous report. These data and knowledge were then applied to specific site data acquired by UEI’s GIS department. The GIS group obtained data from various Internet resources to support the “in-office” route selection process. Due to the abundance of detailed information relevant to routing a pipeline through Illinois, the preliminary route selection defined herein is thought to be valid and unlikely to change significantly during a subsequently detailed route selection phase. If the project receives further funding, ground or aerial reconnaissance should be used to confirm the route. In addition, high resolution aerial photography should be purchased and the route refined before the start of planning for survey, land acquisition, environmental review, permitting, construction, and detailed route selection.

Route Selection Process

Data Acquisition.

Land use data in GIS form were obtained from Web sites maintained by the U.S. Census Bureau, ESRI, the Illinois Department of Agriculture, ISGS, and the U.S. Department of Agriculture (Table 1).

GIS Data Compilation.

Land use data were imported into an ArcView GIS database.

Table 1. Illinois mapped data used for pipeline routing.

Source	Description	Review attributes
U.S. Census Bureau	Topologically Integrated Geographic Encoding and Referencing system (TIGER) Data. Web site - http://www.census.gov/geo/www/tiger/	• Roads • Railroads • Rivers • County lines • Water bodies • Urban areas • Population by zip code
Digital Chart of the World (DCW)	ESRI product developed for the US Defense Mapping Agency. Web site www.geocomm.com	• Power lines • Parks • Federal lands • Landmarks
Illinois Department of Agriculture	Web site http://www.agr.state.il.us/gis/landcover.html	• Land use
Illinois State Geological Survey	Web site http://www.isgs.uiuc.edu/nsdihome/browse/statewide/pipelineb.gif	• Pipelines
U.S. Department of Agriculture	Web site http://datagateway.nrcs.usda.gov/	• Land use a) 1:24,000 Digital Raster Graphics b) 1-m grayscale imagery

Route Review.

The general pipeline route was reviewed by reference to commonly available maps and general knowledge of the central Illinois landscape. The route passes through prime farmland, generally without major terrain or environmental features. Thus, the main parameters that governed route location reverted to avoidance of population centers, utilities, parks, and rivers. By including these factors, the route was optimized for land use by GIS data and GIS aerial photography.

1. ***Population*** The 273.4-km (169.9-mile) direct route was examined while viewing the urban areas and population by zip code data (Figure 1). The reviews indicated a direct route would pass through the following urban areas: Lincoln, West Decatur, and Shelbyville. The best possible routing to avoid these areas would be to the west. Therefore, the direct route was segmented by adding vertices or points of intersection (PI) midway between Springfield and Decatur.

2. ***Utility corridors*** The newly segmented route was reviewed against utility, pipeline, and railroad data (Figure 2). Most cross-country pipelines in Illinois are oriented in a southwest to northeast direction and, thus, are of little use as a possible corridor for the proposed CO_2 pipeline, which would run generally in a south-southeast orientation. The data also show that most utilities are east-to-west or north-to-south with no significant existing corridor near the proposed route. Therefore, existing utility corridors appear to be of limited use in the preliminary design. Existing utility corridors should be examined more carefully during the detailed route selection process, but it is doubtful that the prospects for using existing utility corridors would improve.

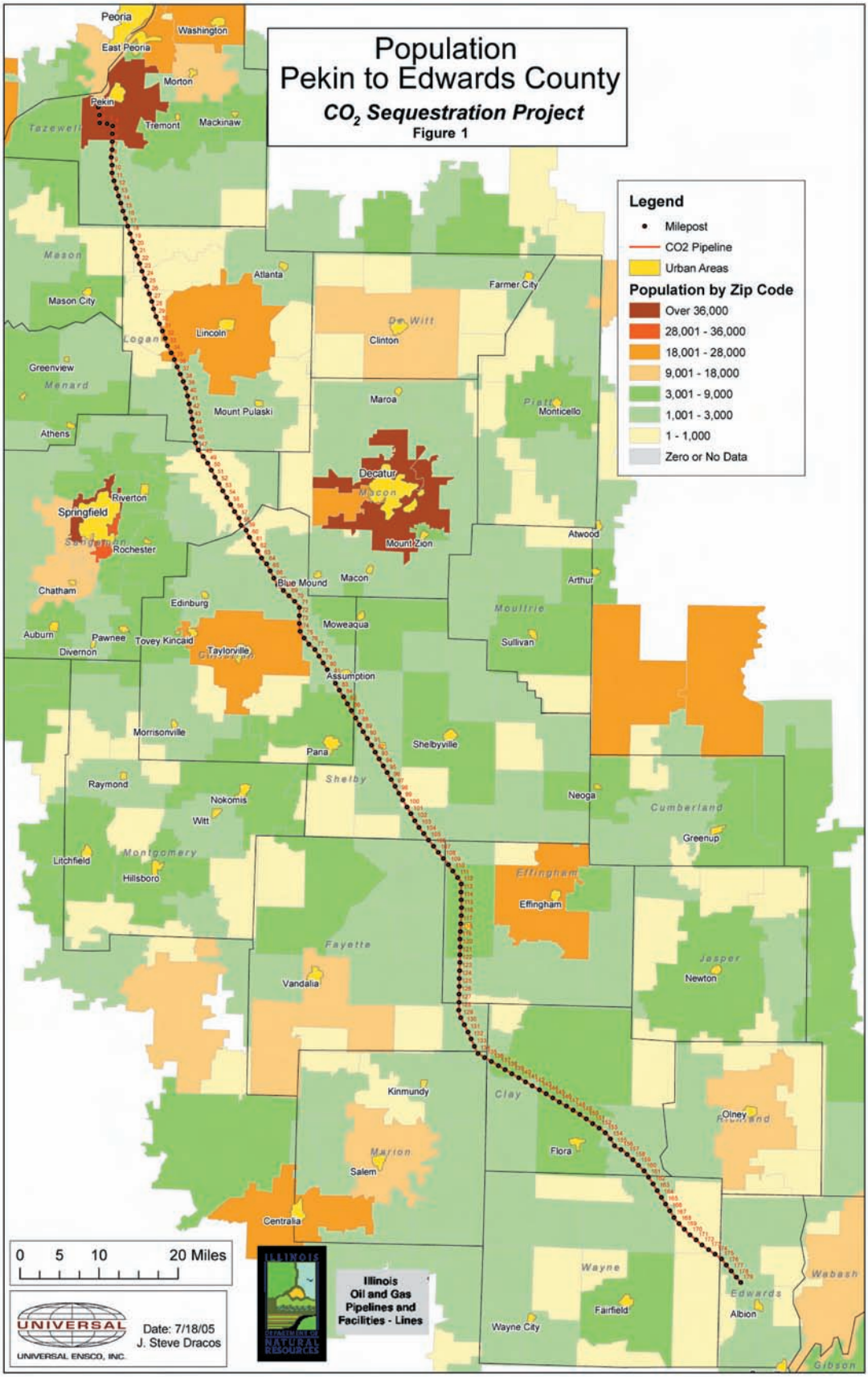
Population
Pekin to Edwards County
CO2 Sequestration Project
Figure 1
Legend
Milepost
CO2 Pipeline
Urban Areas
Population by Zip Code
Over 36,000
28,001 - 36,000
18,001 - 28,000
9,001 - 18,000
3,001 - 9,000
1,001 - 3,000
1 - 1,000
Zero or No Data
Peoria
Washington
East Peoria
Morton
Pekin
Tremont
Mackinaw
Tazewell
Mason
Mason City
Atlanta
Lincoln
Logan
Farmer City
De Witt
Clinton
Greenview
Menard
Mount Pulaski
Maroa
Piatt
Monticello
Athens
Decatur
Macon
Springfield
Riverton
Sangamon
Rochester
Mount Zion
Atwood
Chatham
Blue Mound
Macon
Arthur
Edinburg
Moultrie
Auburn
Pawnee
Tovey Kincaid
Moweaqua
Sullivan
Divernon
Taylorville
Christian
Assumption
Morrisonville
Pana
Shelbyville
Shelby
Raymond
Nokomis
Witt
Neoga
Cumberland
Greenup
Litchfield
Montgomery
Hillsboro
Effingham
Effingham
Fayette
Vandalia
Jasper
Newton
Kinmundy
Clay
Olney
Richland
Marion
Salem
Flora
Centralia
Wayne
Wabash
Edwards
Albion
Fairfield
Wayne City
Gibson
0 5 10 20 Miles
UNIVERSAL
UNIVERSAL ENSCO, INC.
Date: 7/18/05
J. Steve Dracos
ILLINOIS
DEPARTMENT OF NATURAL RESOURCES
Illinois Oil and Gas Pipelines and Facilities - Lines

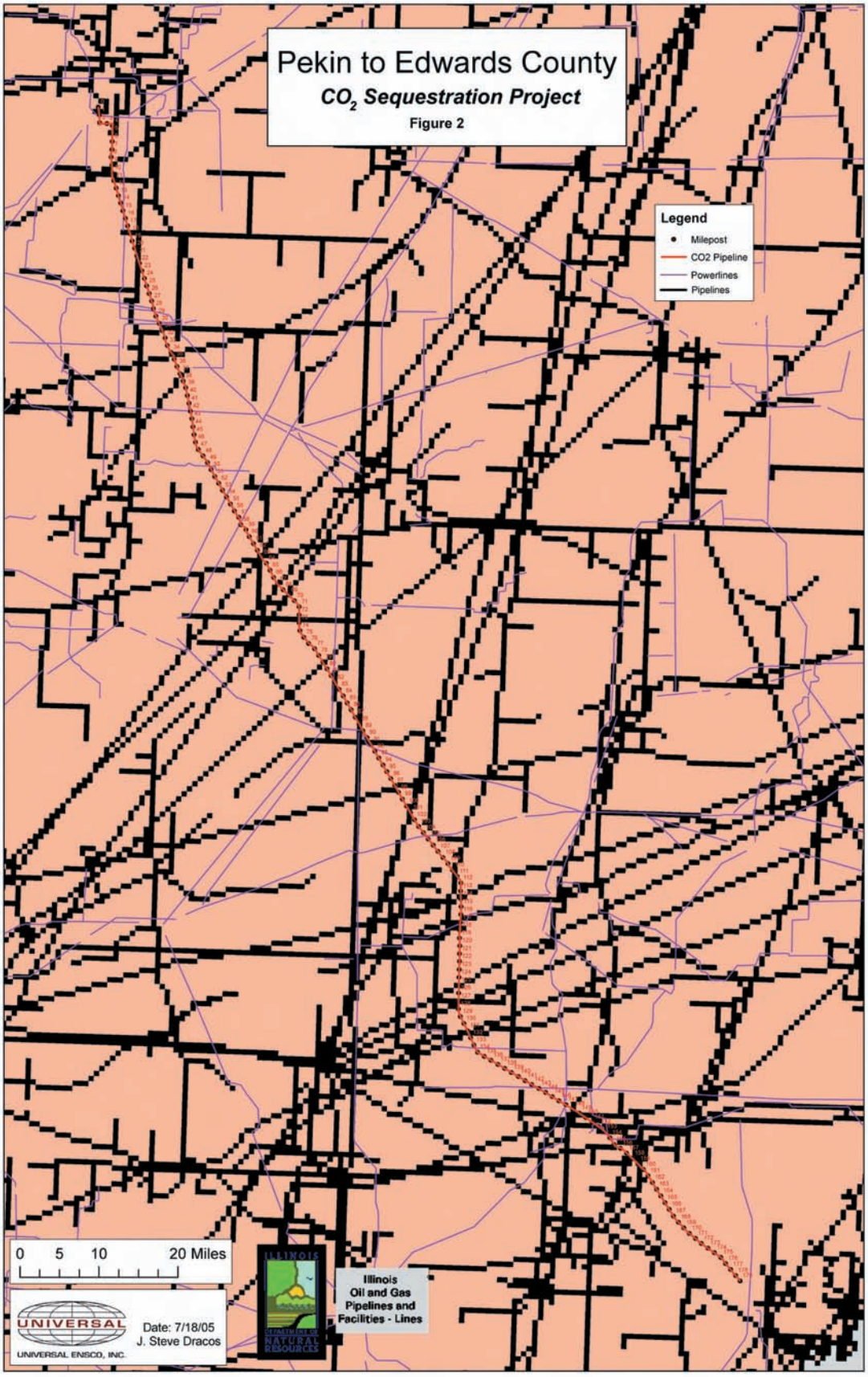
Pekin to Edwards County
CO_2 Sequestration Project
Figure 2
Legend
Milepost
CO2 Pipeline
Powerlines
Pipelines
0 5 10 20 Miles
UNIVERSAL
UNIVERSAL ENSCO, INC.
Date: 7/18/05
J. Steve Dracos
ILLINOIS
DEPARTMENT OF NATURAL RESOURCES
Illinois
Oil and Gas
Pipelines and
Facilities - Lines

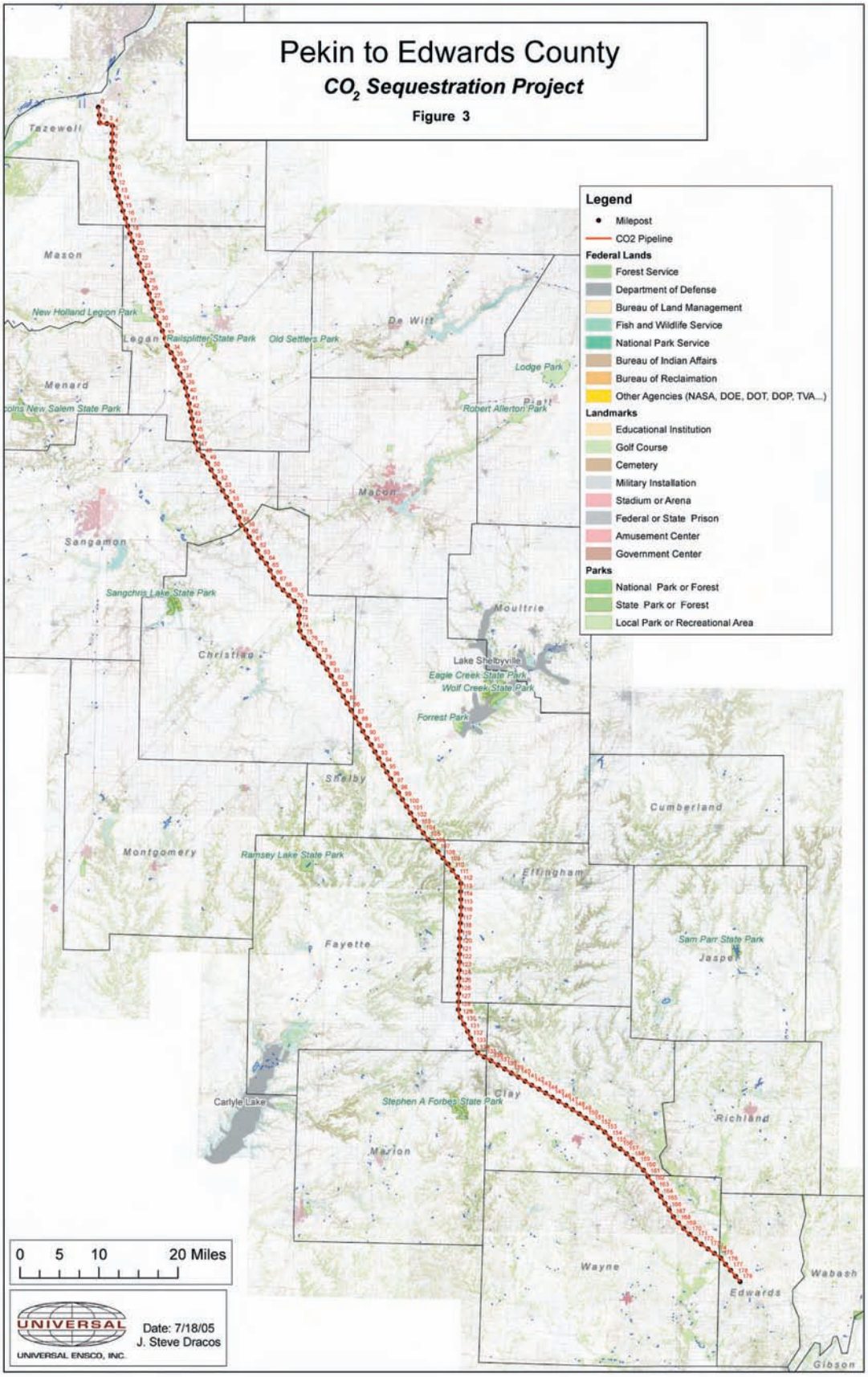
Pekin to Edwards County
CO2 Sequestration Project
Figure 3
Legend
Milepost
CO2 Pipeline
Federal Lands
Forest Service
Department of Defense
Bureau of Land Management
Fish and Wildlife Service
National Park Service
Bureau of Indian Affairs
Bureau of Reclaimation
Other Agencies (NASA, DOE, DOT, DOP, TVA...)
Landmarks
Educational Institution
Golf Course
Cemetery
Military Installation
Stadium or Arena
Federal or State Prison
Amusement Center
Government Center
Parks
National Park or Forest
State Park or Forest
Local Park or Recreational Area
Tazewell
Mason
New Holland Legion Park
Logan
Railsplitter State Park
Old Settlers Park
De Witt
Lodge Park
Piatt
Robert Allerton Park
Menard
Lincolns New Salem State Park
Macon
Sangamon
Sangchris Lake State Park
Moultrie
Christian
Lake Shelbyville
Eagle Creek State Park
Wolf Creek State Park
Forrest Park
Shelby
Cumberland
Montgomery
Ramsey Lake State Park
Effingham
Fayette
Sam Parr State Park
Jasper
Carlyle Lake
Stephen A Forbes State Park
Clay
Richland
Marion
Wayne
Edwards
Wabash
Gibson
0 5 10 20 Miles
UNIVERSAL
UNIVERSAL ENSCO, INC.
Date: 7/18/05
J. Steve Dracos

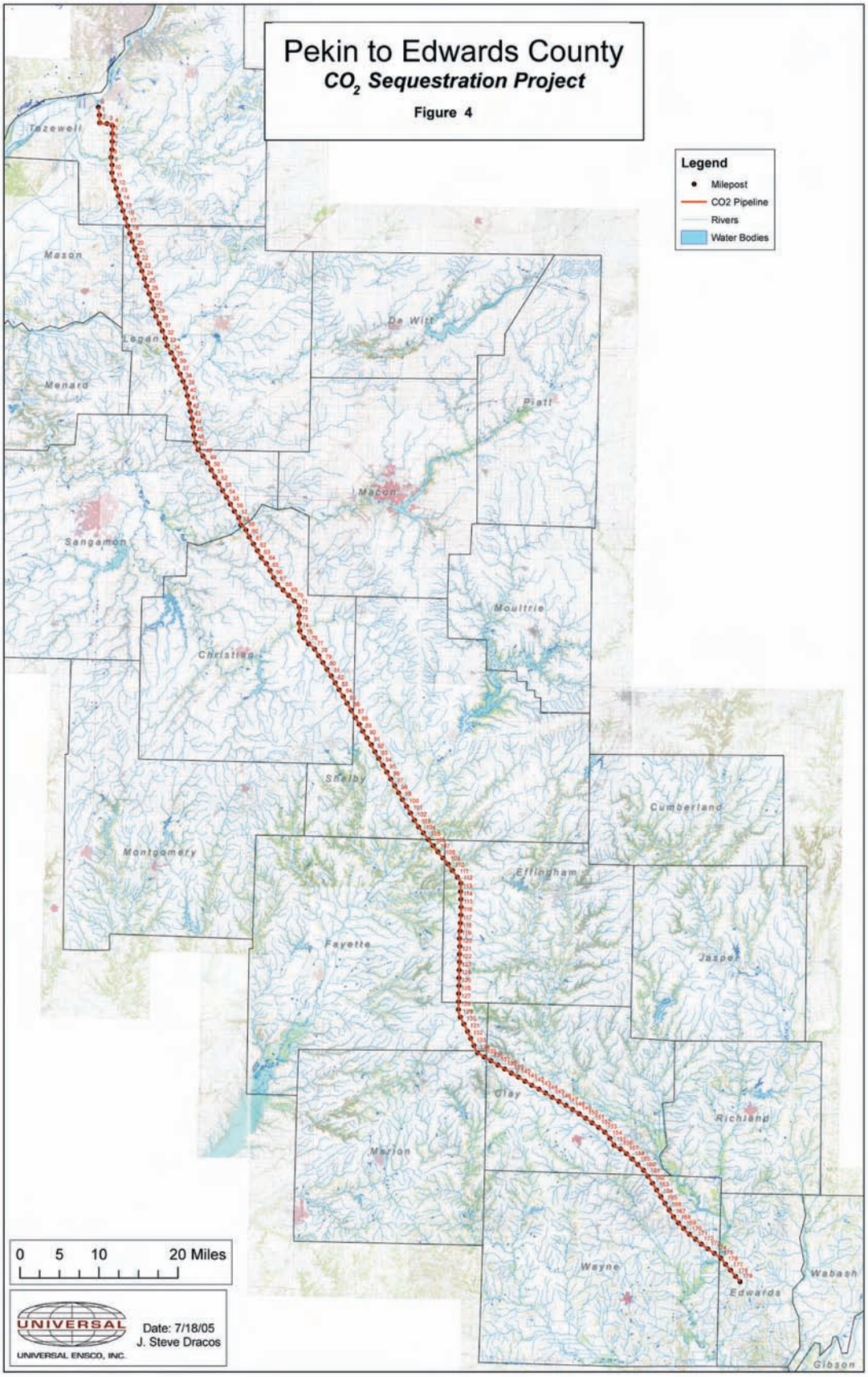
Pekin to Edwards County
CO2 Sequestration Project
Figure 4
Legend
Milepost
CO2 Pipeline
Rivers
Water Bodies
Tazewell
Mason
Logan
De Witt
Menard
Piatt
Macon
Sangamon
Moultrie
Christian
Shelby
Cumberland
Montgomery
Effingham
Fayette
Jasper
Clay
Richland
Marion
Wayne
Wabash
Edwards
Gibson
0 5 10 20 Miles
UNIVERSAL
UNIVERSAL ENSCO, INC.
Date: 7/18/05
J. Steve Dracos

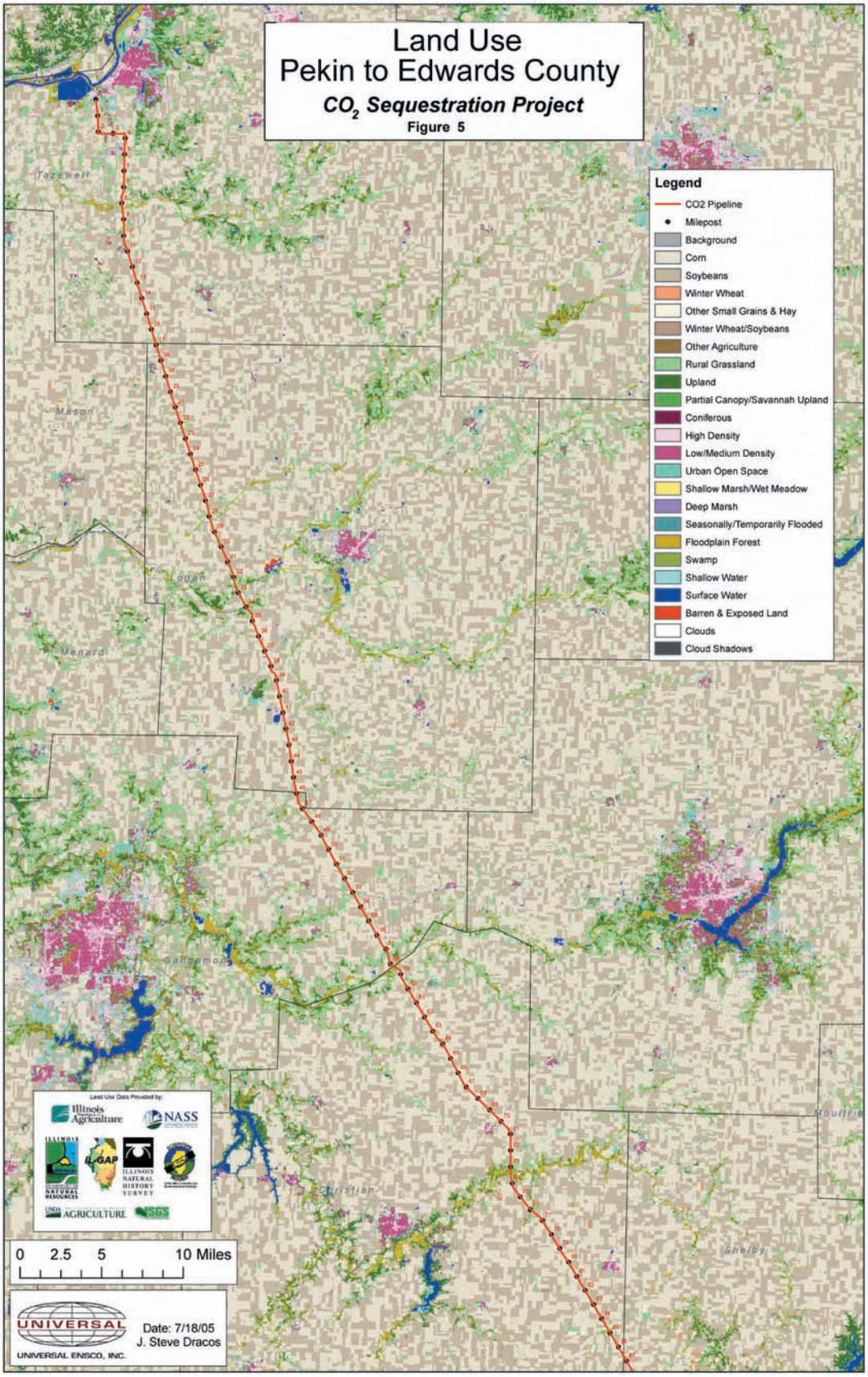
Land Use
Pekin to Edwards County
CO2 Sequestration Project
Figure 5
Legend
CO2 Pipeline
Milepost
Background
Corn
Soybeans
Winter Wheat
Other Small Grains & Hay
Winter Wheat/Soybeans
Other Agriculture
Rural Grassland
Upland
Partial Canopy/Savannah Upland
Coniferous
High Density
Low/Medium Density
Urban Open Space
Shallow Marsh/Wet Meadow
Deep Marsh
Seasonally/Temporarily Flooded
Floodplain Forest
Swamp
Shallow Water
Surface Water
Barren & Exposed Land
Clouds
Cloud Shadows
Tazewell
Mason
Logan
Menard
Sangamon
Christian
Shelby
Land Use Data Provided by:
Illinois Agriculture
NASS
IL-GAP
Illinois Natural History Survey
AGRICULTURE
0 2.5 5 10 Miles
UNIVERSAL
UNIVERSAL ENSCO, INC.
Date: 7/18/05
J. Steve Dracos

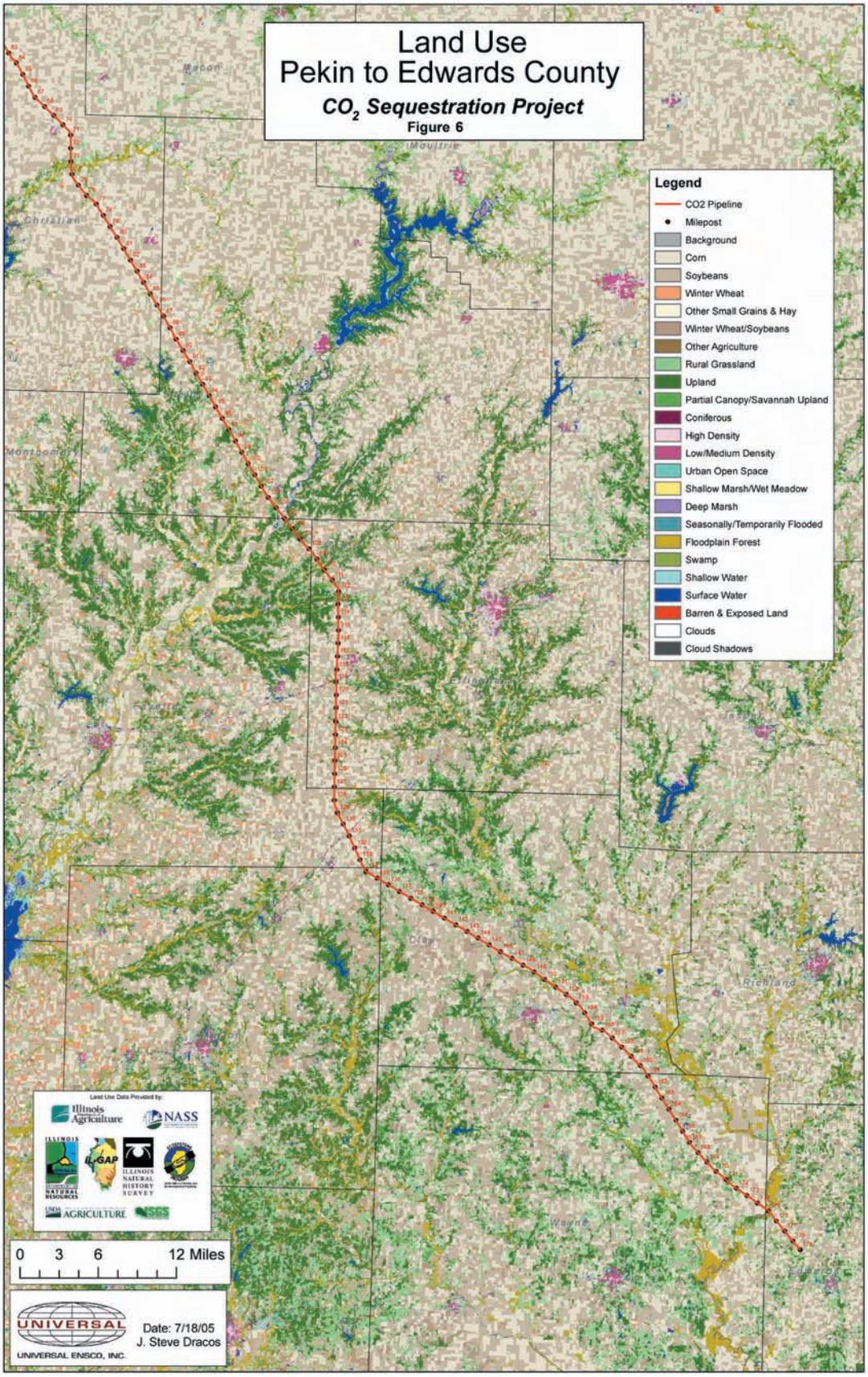
Land Use
Pekin to Edwards County
CO2 Sequestration Project
Figure 6
Legend
CO2 Pipeline
Milepost
Background
Corn
Soybeans
Winter Wheat
Other Small Grains & Hay
Winter Wheat/Soybeans
Other Agriculture
Rural Grassland
Upland
Partial Canopy/Savannah Upland
Coniferous
High Density
Low/Medium Density
Urban Open Space
Shallow Marsh/Wet Meadow
Deep Marsh
Seasonally/Temporarily Flooded
Floodplain Forest
Swamp
Shallow Water
Surface Water
Barren & Exposed Land
Clouds
Cloud Shadows
Land Use Data Provided by:
Illinois Agriculture
NASS
IL-GAP
Illinois Natural History Survey
AGRICULTURE
0 3 6 12 Miles
UNIVERSAL
UNIVERSAL ENSCO, INC.
Date: 7/18/05
J. Steve Dracos

3. ***Parks, preserves, and landmarks*** The route was reviewed with federal lands, landmarks, and park data (Figure 3). Only one area of interference was located at the New Holland Legion State Park. A few PIs were added to move the pipeline route to the east of the park.

4. ***Rivers, wetlands, and water bodies*** Route review with the river, wetlands and waterbodies (Figure 4) indicated a possible problem at the lower one-third of it where the route did not cross the watersheds but actually followed them. Using the GIS system, a count and listing of the water crossings were for the lower third of the route showed multiple crossings of the tributaries of the Little Wabash River. As a result, a more detailed view of the route was analyzed, and a significant number of PIs were added. The route at the lower end was moved to the west so that it crossed the Little Wabash River only once and did not run along the river valley. Using the more detailed view, PIs were also added on the rest of the pipeline route to cross streams in as short a deep burial segment as possible (essentially perpendicular to stream channels) and to avoid running parallel to streams.

5. ***Land use*** Land use data from the Illinois Department of Agriculture for 1999 through 2000 was reviewed relative to the pipeline route (Figures 5 and 6). These data indicated that additional rerouting (more PIs) was necessary in the lower third of the route to minimize impact on the floodplain forests. These were avoided due to the probability of encountering old growth forest, the Indiana bat habitat, and archeological sites.

6. ***Photography*** The route was viewed using 1-m pixel, orthorectified photography available from Terra-Server. The route was reviewed from south to north in an iterative process to minimize/optimize the crossing of other pipelines, roads, railroads and streams. Some effort was made to avoid routing the pipeline near farm residences. During the session, the route from the originating point near Pekin was revised to be southerly to a point where it turned east until encountering a railroad, which it could then follow to the south out of the Pekin area. A series of route maps (1 inch on the map represents 2,000 ft on the ground surface) are included in the Appendix.

After the route was set, the GIS system added the mileposts to each of the maps in the report. The route modifications increased the length of the preliminary route from a 273.4-km (169.9-mile) straight line distance to a total length of 287.9 km (178.9 miles).

A summary of land use along the pipeline route is provided by county in Table 2. The land use along the route is agricultural; the mix of crops is primarily corn and soybeans.

Table 2. Land use summary along pipline route.

	Land use by county (%)[1]											
Land use description	**Tazewell**	**Logan**	**Sangamon**	**Christian**	**Shelby**	**Fayette**	**Effingham**	**Marion**	**Clay**	**Wayne**	**Edwards**	**Total**
Agricultural	90.6	93.7	94.6	93.9	81.6	78.7	85.6	90.8	91.9	89.9	79.0	90
Pasture	7.3	5.2	4.4	3.9	6.8	2.9	5.2	2.2	5.2	4.6	9.0	5
Marsh and streams	0.0	0.1	0.0	0.2	1.1	1.4	0.8	0.4	0.0	0.0	0.7	0
Floodplain forest	0.0	0.2	0.0	1.0	1.1	0.8	0.3	0.0	0.3	0.0	5.1	1
Timber	0.0	0.0	0.1	0.5	1.5	0.3	1.1	4.0	1.0	3.9	4.5	1
Scrub	0.0	0.3	0.0	0.4	7.7	15.7	6.3	2.6	1.5	1.3	1.7	3
Light urban	2.1	0.6	0.9	0.2	0.1	0.2	0.5	0.0	0.1	0.3	0.0	0
	100	100	100	100	100	100	100	100	100	100	100	100
	Agricultural makeup by county (%)[1]											
Crop type	**Tazewell**	**Logan**	**Sangamon**	**Christian**	**Shelby**	**Fayette**	**Effingham**	**Marion**	**Clay**	**Wayne**	**Edwards**	**Total**
Corn	63.1	59.1	48.2	55.7	27.7	42.7	35.3	31.2	24.9	43.1	40.1	45.1
Soybeans	36.9	40.9	50.0	41.8	59.6	48.0	43.9	45.2	60.6	47.1	40.9	47.1
Winter wheat	0.0	0.0	1.8	0.3	7.6	0.8	7.0	5.8	0.0	1.8	0.0	1.8
Winter wheat/soybeans	0.0	0.0	0.0	0.4	2.6	5.0	11.6	17.8	13.5	5.6	14.8	4.6
Other small grains & hay	0.0	0.0	0.0	1.7	2.3	0.3	2.3	0.0	1.1	2.4	4.1	1.2
Other agriculture	0.0	0.0	0.0	0.1	0.3	3.1	0.0	0.0	0.0	0.0	0.0	0.2
	100	100	100	100	100	100	100	100	100	100	100	100

[1]Illinois Department of Agriculture (1999–2000).

Design Elements

A preliminary diameter or ranges of diameters were selected based on the planned flow rate and the route selected. The preliminary route indicates that 10.3 million m^3/day (362 million scf/day) of CO_2 will be transported over a distance of 287.9 km (178.9 miles) from Pekin, Illinois, to Edwards County, Illinois. Due to the conceptual status of the project and the limited scope of services for Task 9, the diameter selection process is limited to the methods for sizing described in Section 3 of the 2004 Task 3 report. Although these methods are approximate they will provide a valid range of diameters so that the costing phase of the scope of work can be accomplished.

If the project proceeds to the basic engineering phase, the hydraulics and costing will be developed with greater specificity and accuracy. During the basic engineering phase, the pipeline diameter should be optimized for multiple cases using hydraulic calculations for a range of diameters, wall thicknesses, pipe grades, pumping configurations, and delivery pressures. For each case, an accurate capital cost, power cost, and operating cost will be prepared. In addition, the economic impact of multiple phase flow pattern will be investigated. All of these variables will be assessed based on the owners' economic guidelines (such as the minimum acceptable internal rate of return for capital) to develop the pipeline diameter.

Because this is a conceptual report, attempting to optimize any single item from this list will not add value to the end results. Within a given range of diameters, however, some operational considerations are presented that demonstrate potential impact on flow rate and cost.

Pipeline Diameter

Referring to the discussion in Section 3 of the 2004 MGSC pipeline report, CO_2 pipelines normally operate in the supercritical region, which is above 7,433 kPa (1,078 psia). Most CO_2 pipelines operate with an upstream pressure of 17,237 kPa (2,500 psig) or higher and have a delivery pressure near 10,342 kPa (1,500 psig). The meter and regulator stations at each end require a pressure drop of approximately 345 kPa (50 psi) each, which gives a pipeline differential pressure of about 6,895 kPa (1,000 psi) to achieve the flow rate. For the purpose of this preliminary design, the maximum and minimum operating pressures in the pipeline are approximated as 17,237 kPa (2,500 psig) and 10,342 kPa (1,500 psig), respectively, in this report. Graphs from Section 3 of the 2004 report for pressure drop and horsepower versus flow rate for pipeline diameters ranging from 4.5 to 24 inches are duplicated as Figures 7 and 8 respectively. These figures were used to determine a range of diameters for further hydraulic analysis.

Three pipeline diameters, 40.64, 45.72, and 50.8 cm (16, 18, and 20 inches), were selected for hydraulic calculations using the formula in Section 3 of the 2004 report. The calculations were made using

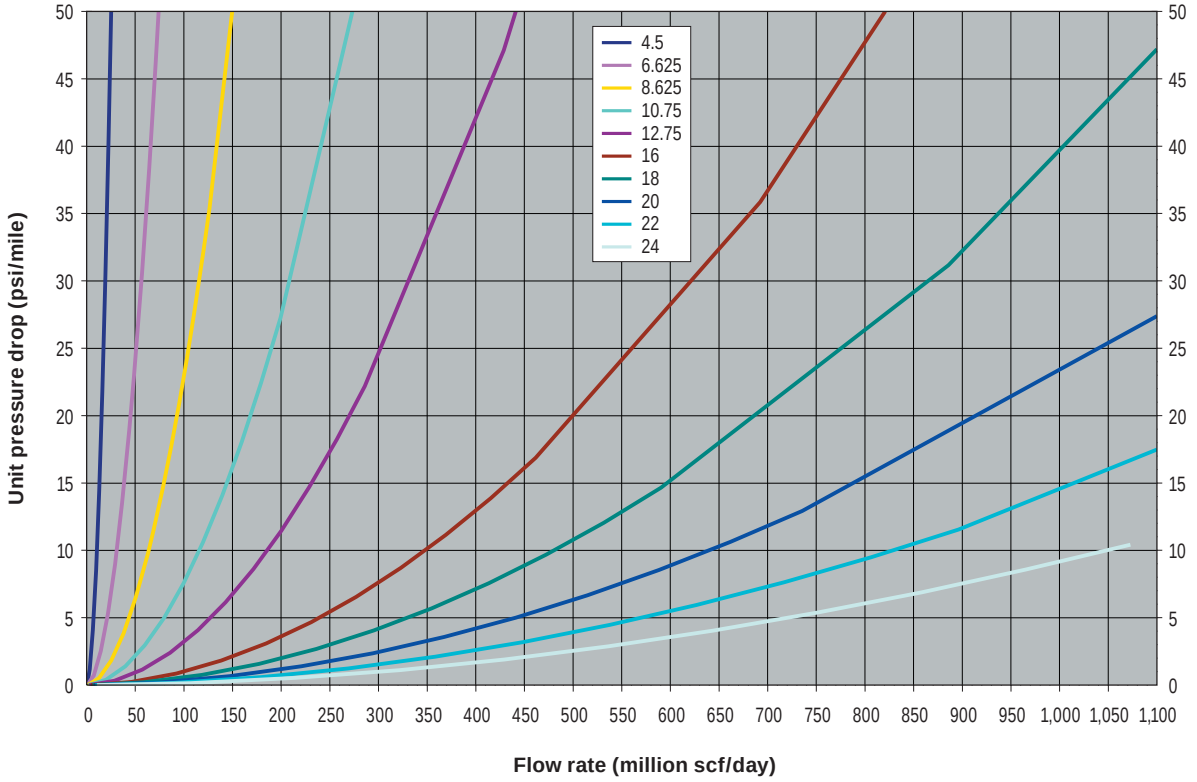

Figure 7 *Unit pressure drop versus flow rate as a function of pipe outside diameter.*

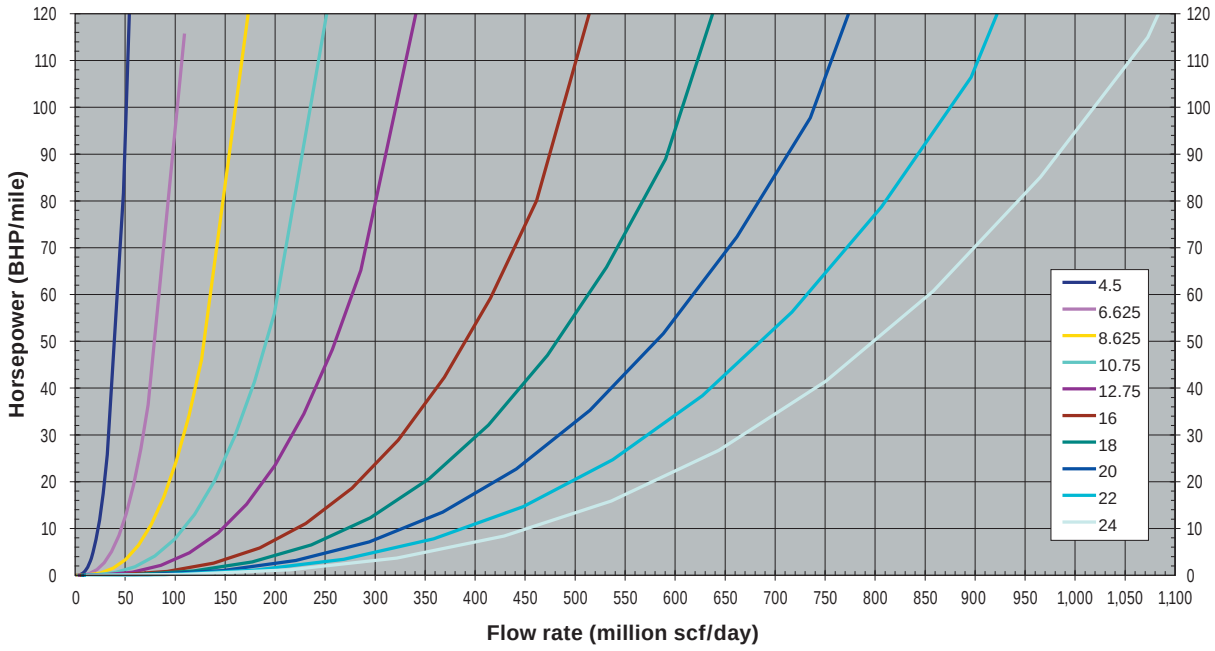

Figure 8 *Horsepower versus flow rate as a function of pipe outside diameter.*

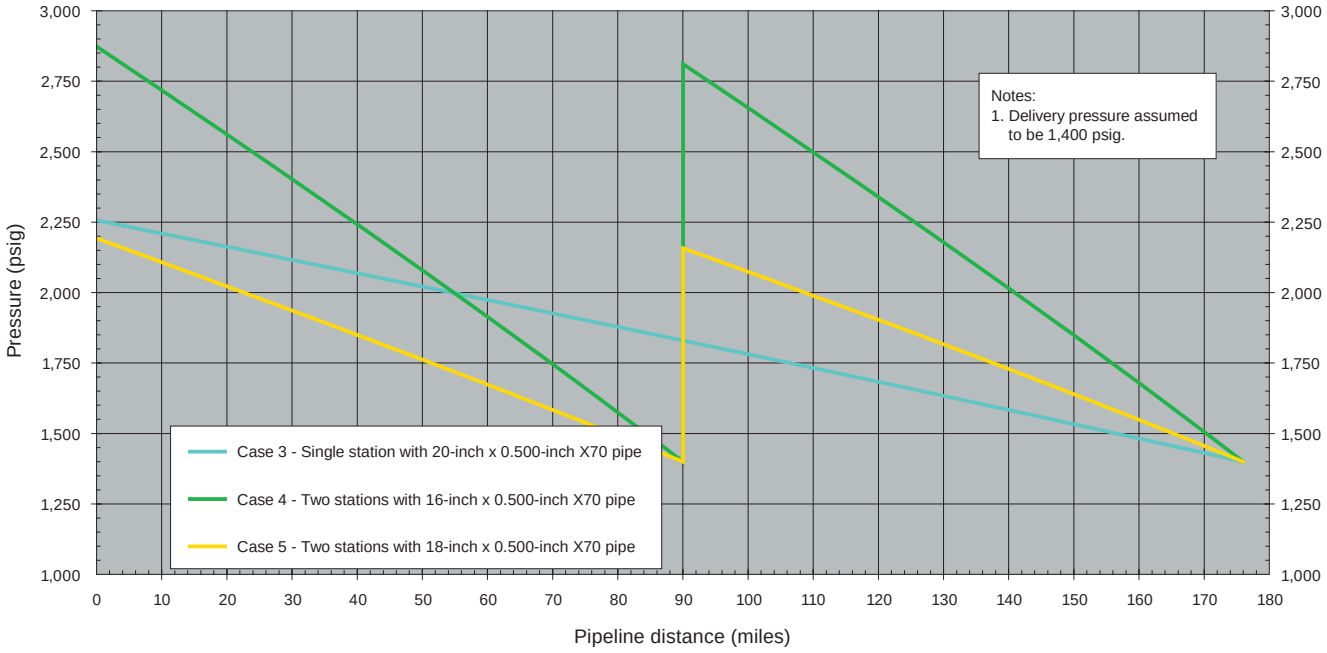

Figure 9 *Specific transportation option, Pekin to Edwards County, Illinois: 7.7 million tons per year, CO_2 sequestration pipeline.*

8.0-km (5-mile) segments to calculate the CO_2 properties, assuming no elevation change along the route, a booster station location (if required) at Milepost (MP) 90, and an assumed pipeline length of 287.9 km (178.9 miles) based on the route analysis. The cases calculated were for a 40.64-cm (16-inch) pipeline with origin station and booster station, an 45.72-cm (18-inch) pipeline with origin station and booster station, and a 50.8-cm (20-inch) pipeline with origin station only. After a number of calculations were made it was decided to use a lower delivery pressure from 10,342 to 9,653 kPa (1,500 psi to 1,400 psi). The results of the calculations are displayed for the three cases as a plot of pressure versus distance in Figure 9, and the specific pressure and horsepower are summarized in Table 3.

These three cases demonstrate the typical cases that are presented in the scoping phase of the basic engineering sizing of a pipeline. The first case is the smallest diameter pipeline with booster stations that meet the initial flow rate but lacks expansion capability. This case has the lowest construction cost but consumes the most power and for this report is represented by the 40.64-cm (16-inch) pipeline with origin and booster station. The second case is usually represented by the diameter that does not require booster stations. By definition, this case always has significant expansion capability augmented by the addition of booster stations (50.8-cm (20-inch) pipeline in this report). The final case that is usually presented is a diameter and boosting configuration that is a compromise between the first and second

case (45.72-cm (18-inch) pipeline in this report). Detailed costs are then prepared for each case to determine which should be optimized. The cost of the 16-, 18-, and 20-inch pipeline cases are presented next.

Table 3. CO_2 pipeline design for flow rate of 362 million scf/day and distance of 180 miles.[1]

Pipe diameter (inch)	Pressure (psi)		BHP required per mile (Figure 8)	BHP required (HP)		Required
	Origin station	Booster station MP 90		Origin station at Pekin	Two booster stations MP90	Station total (psi)
16	2,870	2,810	40	3,600	3,560	7,160
18	2,190	2,160	22	1,980	1,960	3,940
20	2,250		12.5	2,240	N/A	2,230

[1]Assumptions: pipeline length is 178.9 miles; flow rate is 362 million scf/day; minimum pressure is approximately 1,400 psi per Figure 8; maximum pressure is approximately vary psi as per the 2004 Task 3 report; single station operation is desired if maximum pressure will not exceed 2,500 psi; if two stations are required, assume section station at pipeline midpoint at Milepoint (MP) 90 and operate both stations at equal discharge pressure.

Operational Considerations

As discussed herein and in the previous report, many variables impact the design of the pipeline for each case and for the system in general. Considerations related to variations in operating pressure, the addition of booster station(s) and the reduction of delivery pressure are presented.

16-inch case

As shown in Figure 7, the 16-inch pipeline will require a booster station. At the stated capacity of 10.3 million m^3/day (362 million scf/day) of CO_2 over a distance of 287.9 km (178.9 miles), the 16-inch pipeline is at full capacity. The operation of a remote unmanned booster station at a pressure of 20,684 kPa (3,000 psig) at the design flow rate should be thoroughly investigated in the next stage of the project as the required pumps could be at or near the limit of practical design. Alternate designs using multiple smaller units operating in parallel could be a solution to the size limit, but they will increase the complexity of operation.

18-inch case

The 18-inch pipeline in the current hydraulic design also requires a booster station. However, the pump units are operating at 15,168 kPa (2,200 psig), which is well below the normal range (17,236 kPa (2,500 psi)) of CO_2 projects. If the operating pressure is increased to 17,236 kPa (2,500 psi), the capacity of the 18-inch pipeline could increase by 1.7 to 2.0 million m^3/day (60 to 70 million scf/day). The extra cost of pipe and construction would be approximately $2 million over the 18-inch pipeline with a single booster.

20-inch case

The 20-inch pipeline provides considerable spare capacity either by increasing the operating pressure or by adding a booster station. If the pressure increased to 17,236 kPa (2,500 psig), the capacity of the 20-inch would be increased by 2.83 to 3.40 million m^3/day (100 to 120 million scf/day). The cost of the additional pipe and construction would be around $2.5 million. Adding a booster station would increase the capacity by 5.66 to 6.23 million m^3/day (200 to 220 million scf/day) over the 20-inch pipeline.

Delivery Pressure Reduction

The delivery pressure for hydraulic analysis was reduced from 10,243 to 9,652 kPa (1,500 psig to 1,400 psig) because the 18-inch case and the 20-inch case were approaching an equipment pressure classification break point. By lowering the delivery pressure, the operating pressure of the 20- and 18-inch pipelines are within the limits for ANSI 900 fittings and valves. If the delivery pressure is not lowered, the next higher rating of ANSI 1500 would be required, which would result in significant cost increases for the valves and fittings at the diameters under consideration. In Phase II of the DOE project, the delivery pressure at Edwards County should be optimized, if feasible, to keep the pipeline operating pressure at a level that would not require the ANSI 1500 fittings.

Costs

The methods and data used for the development of the costing information in Section 8 of the 2004 Task 3 report were used for determining the conceptual cost of the proposed project. Based on the length of the route, the range of pipeline diameters, and pump station configuration, the tables and data from the previous report are used to calculate the approximate cost for the three cases presented in of this report. The summary of unit costs were originally presented in Table 8-7 of the 2004 Task 3 report.

Table 4. Unit costs for pipeline construction per mile.

Diameter (inches)	Cost per mile, U.S. Dollars				
	Right-of-way	Materials	Construction	Services	Total
4	36,713	24,303	85,071	29,217	175,304
6	36,713	47,630	115,915	38,049	238,307
8	44,500	79,370	141,753	47,812	313,435
10	44,500	115,424	173,476	56,678	390,078
12	51,731	159,084	210,730	67,447	488,992
16	66,750	247,199	275,533	88,422	677,905
18	66,750	310,766	306,206	95,721	779,444
20	66,750	381,893	336,354	102,050	887,047
22	66,750	460,465	365,978	107,183	1,000,375
24	66,750	546,136	395,601	121,018	1,129,505

For each of the three cases (40.64-cm (16-inch) pipeline origin and booster station, 45.72-cm (18-inch) pipeline origin and booster station, and 50.8-cm (20-inch) pipeline origin):

1. The pipeline cost was calculated extending the unit prices in Table 4 by length of the route. (The measured distance of 287.9 km (178.9 miles) was rounded to 290 km (180 miles) to allow for some minor reroutes.)
2. The cost of pumping facilities for each case was calculated by extending the horsepower amounts in Table 3 of this report by $1.34/W ($1,000/hp) as presented in Section 8 of the 2004 Task 3 report.
3. Pipeline operating costs were extended for the length and diameter using the $16.317/meter diameter/km/year ($667/inch diameter/miles/year) as presented in Section 8 of the 2004 Task 3 report.
4. Pump station operating costs were extended for the horsepower amounts shown in Table 3 of this report by $0.067/W/year ($50/horsepower/year) presented in Section 8 of the 2004 Task 3 report.
5. Power costs were extended for the horsepower amounts in Table 3 of this report by $0.48/W/year ($360/horsepower/year) presented in Section 8 of the 2004 Task 3 report.

These costs for the three cases are summarized in Table 5. As expected, the 16-inch case, which has no additional capacity, also has the least capital cost and highest operating cost. The 20-inch case, which has the greatest flexibility for expansion, has the highest capital cost and lowest operating cost. The 18-inch case is a compromise between the 16-inch and the 20-inch case.

Table 5. Comparison of costs for 16-, 18- and 20-inch diameter pipeline options, 180-mile pipeline from Pekin to Edwards County, Illinois.

Installation unit costs, pipeline, and stations (from Table 8-7 of 2004 Task 3 Report)			
Component cost	**16 inches**	**18 inches**	**20 inches**
	Unit costs per mile of pipeline, $		
Pipeline right-of-way	66,750	66,750	66,750
Pipeline materials	247,199	310,766	381,893
Pipeline construction	275,533	306,206	336,354
Support services	88,422	95,721	102,050
Midpoint station, $/HP	Station unit cost $/BHP		
	1,000	1,000	N/A
Total installation costs, pipeline and stations for a 180-mile pipeline			
Component cost	**16 inches**	**18 inches**	**20 inches**
Pipeline right-of-way	12	12	12
Pipeline materials	45	56	69
Pipeline construction	50	55	60
Support services	16	17	18
Midpoint station, 3,600 BHP	3.6	2.0	0.0
Total cost ($1,000,000)	127	142	159
Annual operating costs			
Component cost	**16 inches**	**18 inches**	**20 inches**
Pipeline operating cost ($667/inch-diameter/mile/year for 180 miles (2004 Task 3 report, Table 8-8)	1.9	2.2	2.4
Station operating costs ($50/hp/year for maintenance and $360/hp/year for power), $1,000,000	7,200 hp	3,960 hp	2,250 hp
	3.0	1.6	0.9

If the project implementation is delayed for several years or more, it would be advisable to update the conceptual cost estimate for inflation/deflation in pipe and land values and inflation in construction and service. The cost of steel is expected to be highly variable over the next few years, and construction costs are expected to increase due to the large number of planned oil and gas pipeline projects.

A more detailed cost estimate for the proposed pipeline can be prepared in a future project phase, once a final pipeline diameter and route have been selected. This detailed estimate would include material quantities and prices based on drawings and vendor prices; construction costs based on route review by

contractors and engineers, right-of-way costs based on detailed work space estimates combined with spot values appraised for the route; and a detailed estimate of all services required.

In the future, potential savings should be available through the use of higher tensile strength pipe. CO_2 pipelines have been limited to X70 grade pipe; however, X80 grade pipe was recently installed on a CO_2 pipeline project in Mississippi and Alabama. For the same pressure rating, the weight of the X80 pipe will be approximately 7/8 of the X70 pipe weight. It is reported that, even though the price per ton of the X80 pipe and the associated construction costs for X80 are higher, the net effect was a reduction in overall cost. Because X80 pipe requires welding procedures that are not well established, the construction contractor includes contingency into their commercial bids. As procedures for X80 pipe manufacture and construction become standard practice, it should be possible to achieve the full 1/8 savings in pipe costs. Until that time, net cost savings are anticipated to be approximately 50% of the 1/8 weight savings.

Appendix

The digital version of this appendix contains 32 route aerial photograph maps at a detailed scale (1 inch on the map represents 2,000 ft on the ground surface). (The maps that follow in the printed version have been reduced to page size.) The maps together show the area of pipeline route selection, specific transportation option, Pekin to Edwards County, Illinois.

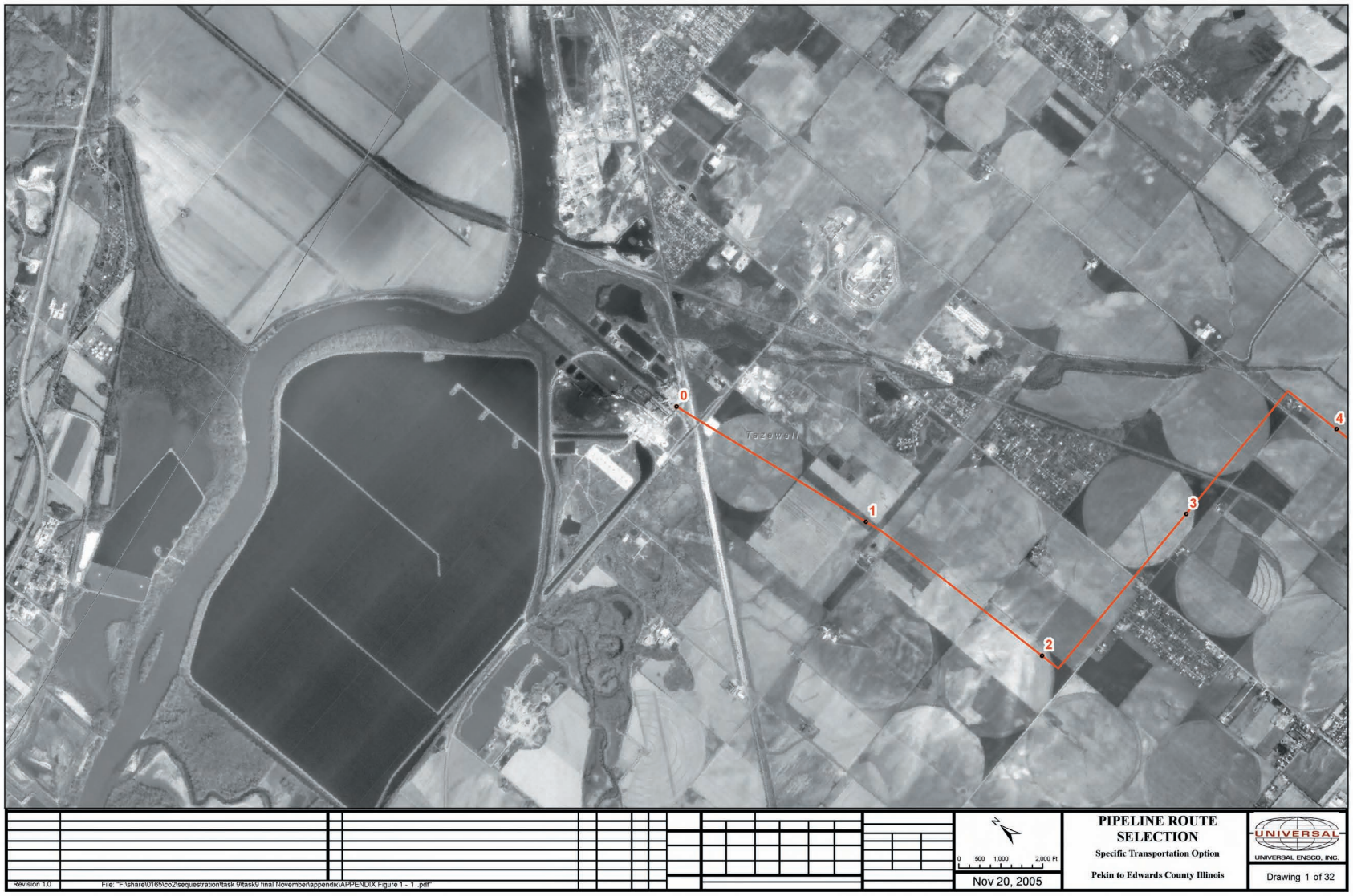
0
1
2
3
4
Tazewell
N
0 500 1,000 2,000 Ft
Nov 20, 2005
PIPELINE ROUTE SELECTION
Specific Transportation Option
Pekin to Edwards County Illinois
UNIVERSAL
UNIVERSAL ENSCO, INC.
Drawing 1 of 32
Revision 1.0
File: "F:\share\0165\co2\sequestration\task 9\task9 final November\appendix\APPENDIX Figure 1 - 1 .pdf"


Tazewell
2
3
4
5
6
7
8
9
N
0 500 1,000 2,000 Ft
Nov 20, 2005
PIPELINE ROUTE SELECTION
Specific Transportation Option
Pekin to Edwards County Illinois
UNIVERSAL
UNIVERSAL ENSCO, INC.
Drawing 2 of 32
Revision 1.0
File: "F:\share\0165\co2\sequestration\task 9\task9 final November\appendix\APPENDIX Figure 1 - 2 .pdf"

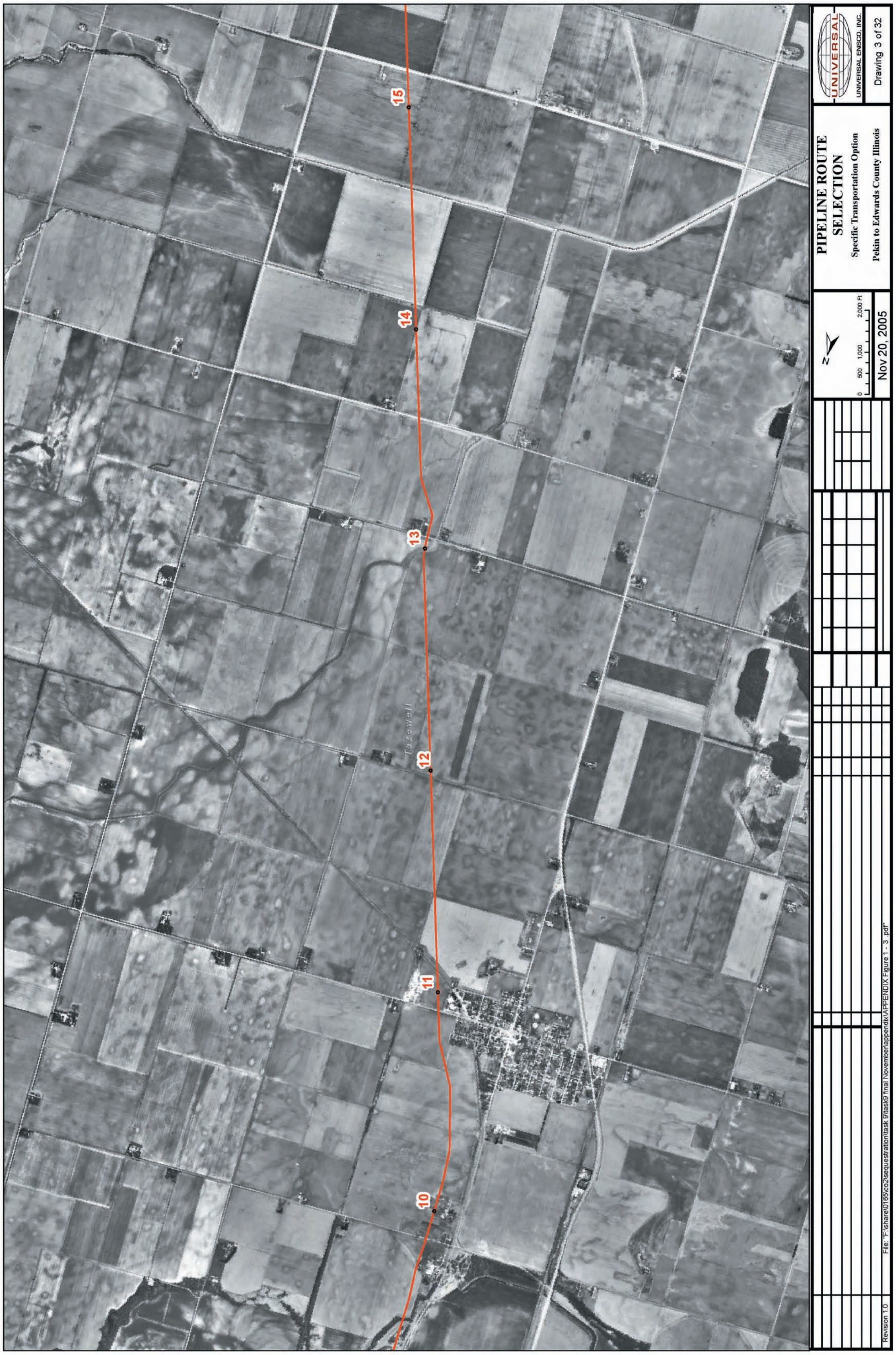
PIPELINE ROUTE
SELECTION
Specific Transportation Option
Pekin to Edwards County Illinois
UNIVERSAL
UNIVERSAL ENSCO, INC.
Drawing 3 of 32
N
0 500 1,000 2,000 Ft
Nov 20, 2005
Revision 1.0
Tazewell
10
11
12
13
14
15

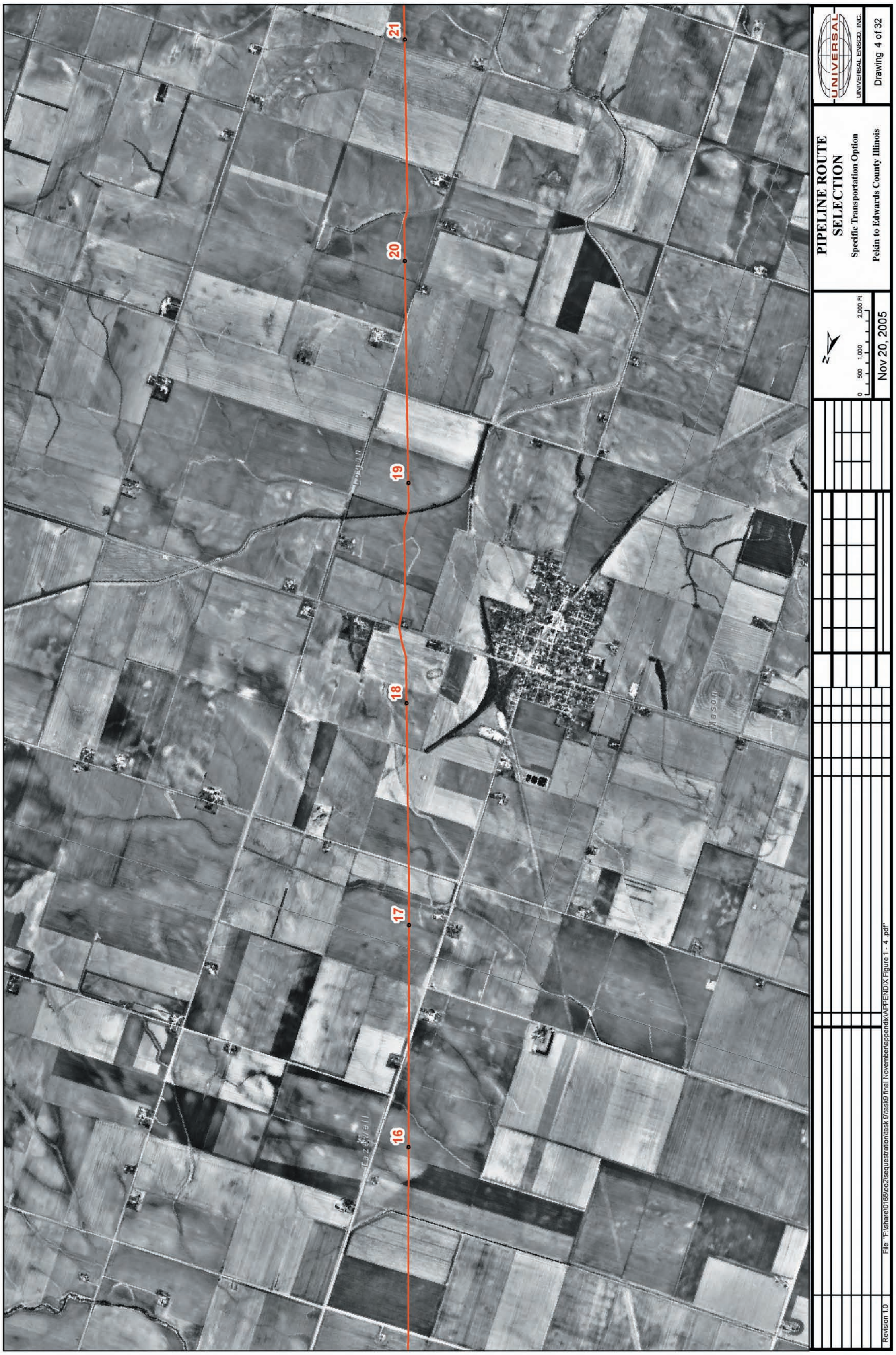
PIPELINE ROUTE SELECTION
Specific Transportation Option
Pekin to Edwards County Illinois
UNIVERSAL
UNIVERSAL ENSCO, INC.
Drawing 4 of 32
N
0 500 1,000 2,000 Ft
Nov 20, 2005
Revision 1.0
File: "F:\share\0165\co2\sequestration\task 9\task9 final November\appendix\APPENDIX Figure 1 - 4 .pdf"
16
17
18
19
20
21
Logan
Mason
Tazewell

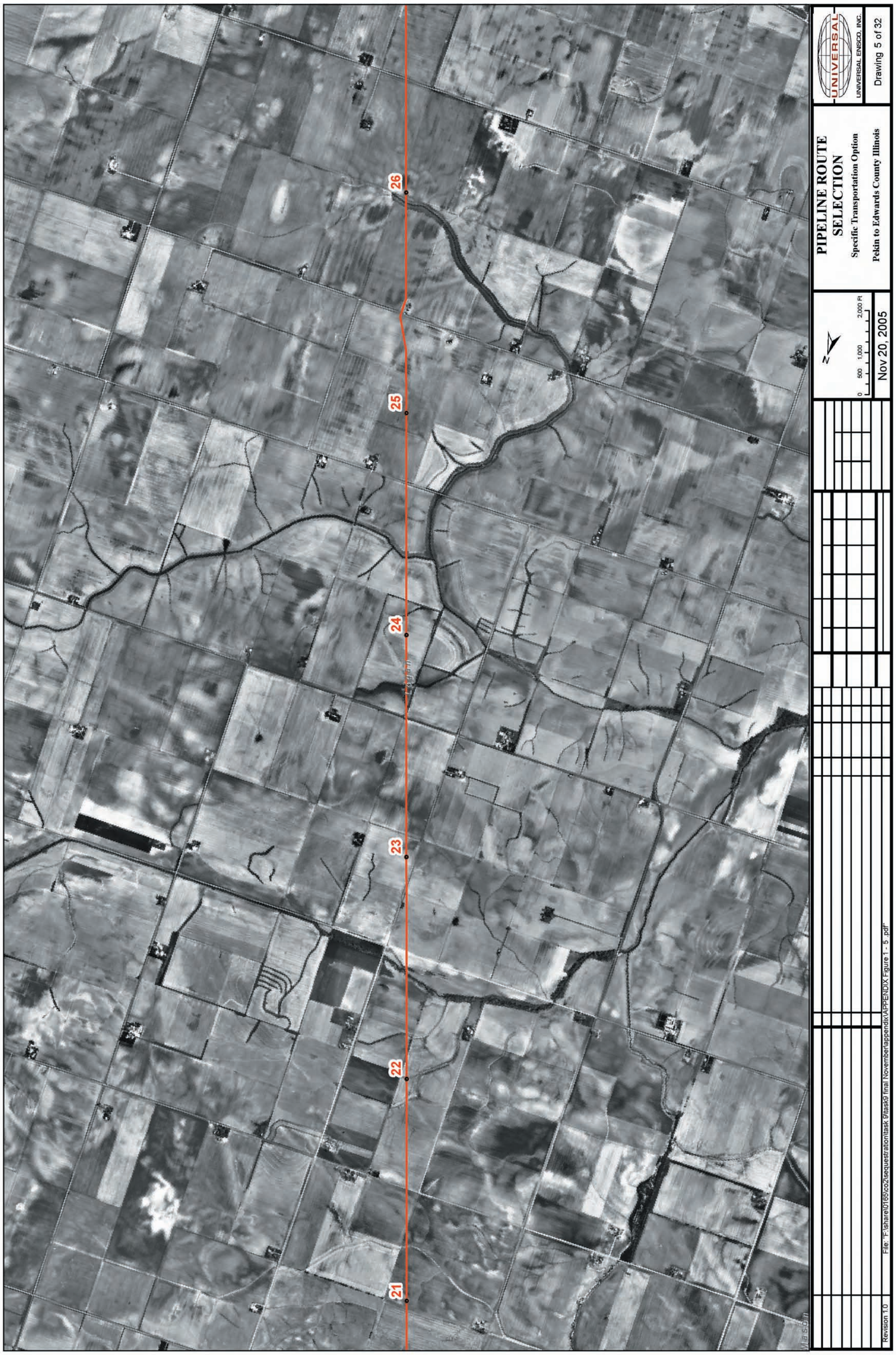

21
22
23
24
25
26
PIPELINE ROUTE SELECTION
Specific Transportation Option
Pekin to Edwards County Illinois
UNIVERSAL
UNIVERSAL ENSCO, INC.
Drawing 5 of 32
N
0 500 1,000 2,000 Ft
Nov 20, 2005
Revision 1.0

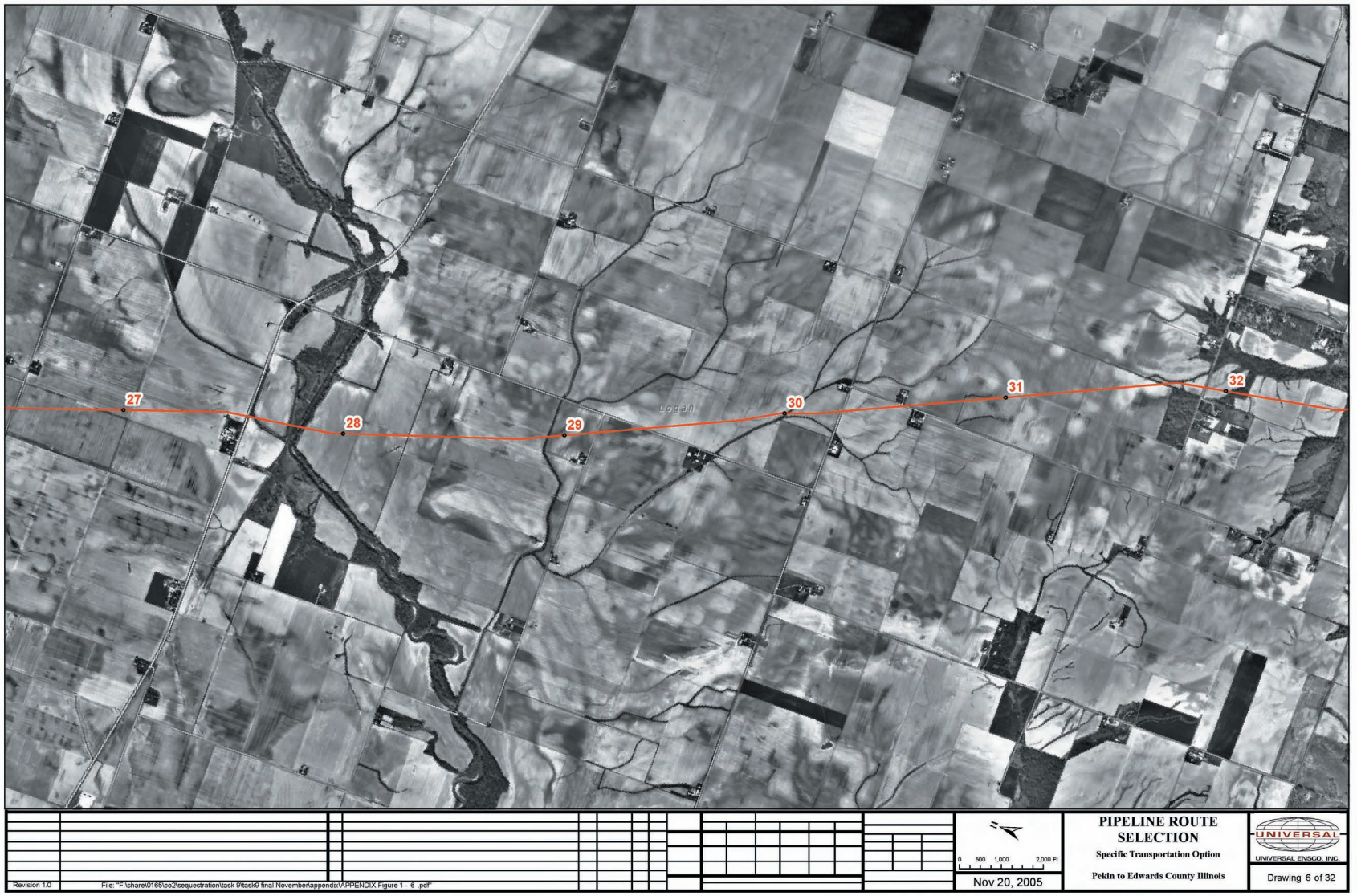
27
28
29
30
31
32
Logan
0 500 1,000 2,000 Ft
Nov 20, 2005
PIPELINE ROUTE SELECTION
Specific Transportation Option
Pekin to Edwards County Illinois
UNIVERSAL
UNIVERSAL ENSCO, INC.
Drawing 6 of 32
Revision 1.0
File: "F:\share\0165\co2\sequestration\task 9\task9 final November\appendix\APPENDIX Figure 1 - 6 .pdf"

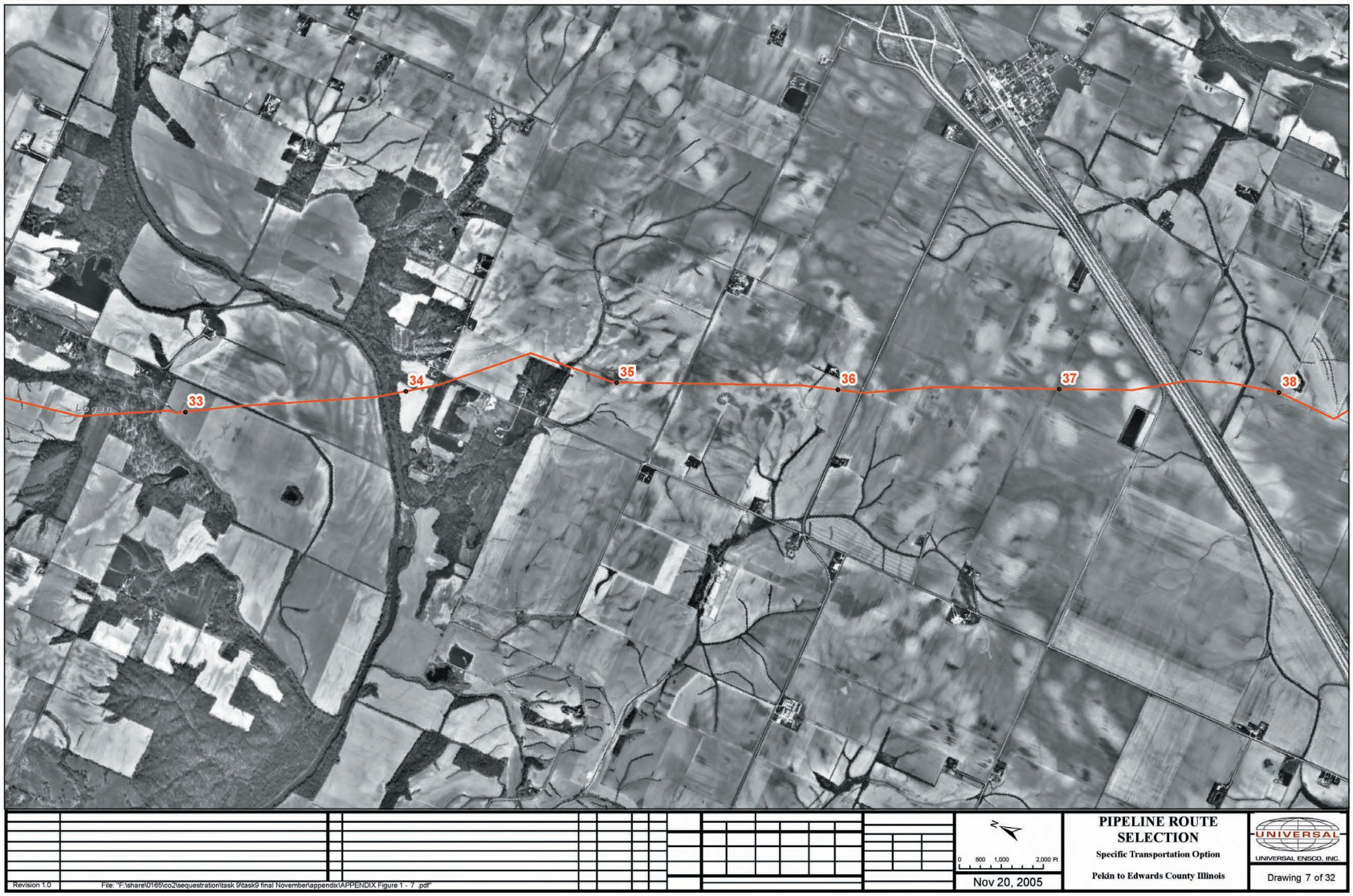
33
34
35
36
37
38
Logan
0 500 1,000 2,000 Ft
Nov 20, 2005
PIPELINE ROUTE SELECTION
Specific Transportation Option
Pekin to Edwards County Illinois
UNIVERSAL
UNIVERSAL ENSCO, INC.
Drawing 7 of 32
Revision 1.0
File: "F:\share\0165\co2\sequestration\task 9\task9 final November\appendix\APPENDIX Figure 1 - 7 .pdf"

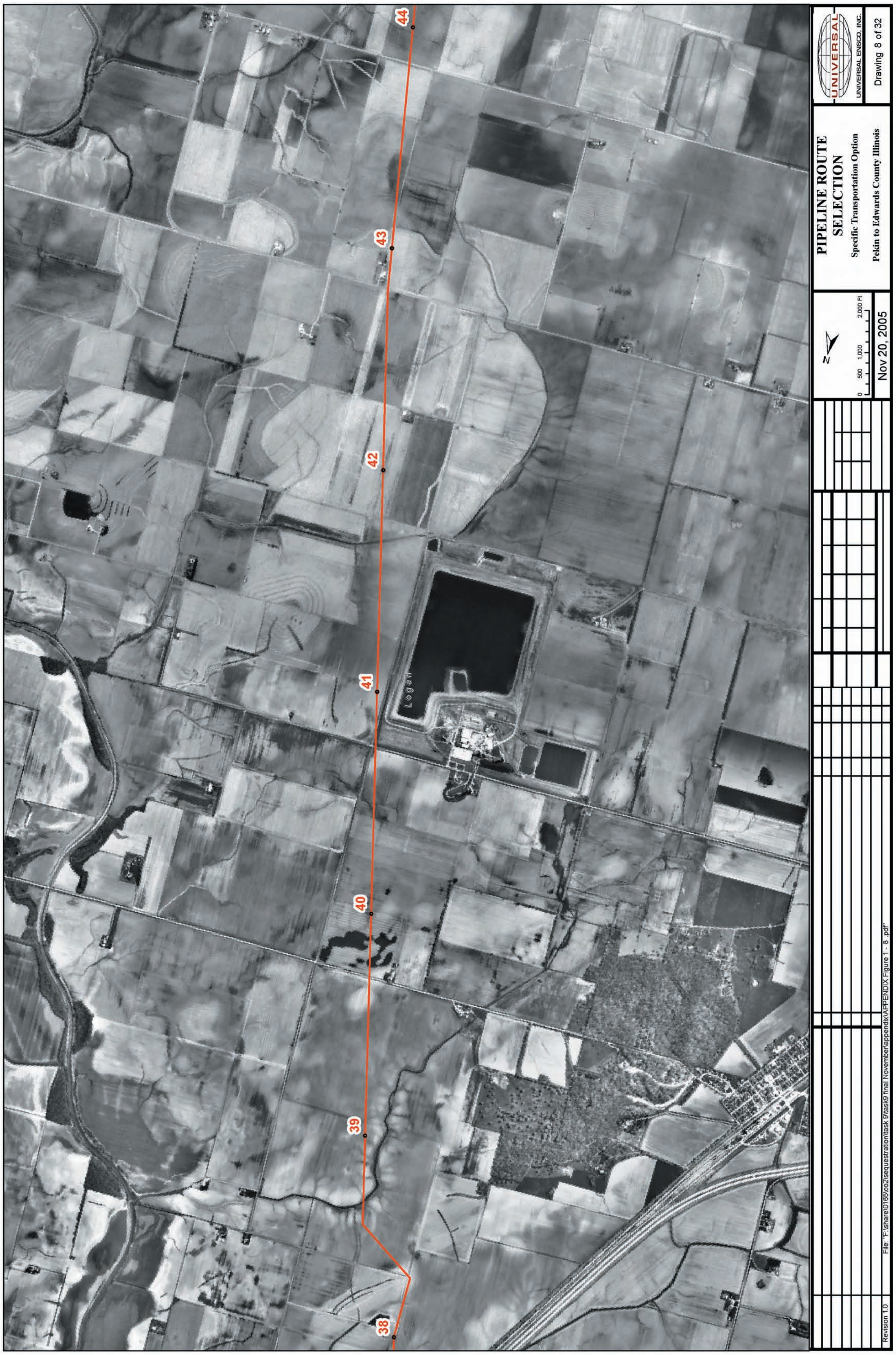
38
39
40
41
42
43
44
Logan
N
0 500 1,000 2,000 Ft
Nov 20, 2005
PIPELINE ROUTE SELECTION
Specific Transportation Option
Pekin to Edwards County Illinois
UNIVERSAL
UNIVERSAL ENSCO, INC.
Drawing 8 of 32
Revision 1.0
File: "F:\share\0165\co2\sequestration\task 9\task9 final November\appendix\APPENDIX Figure 1 - 8 .pdf"

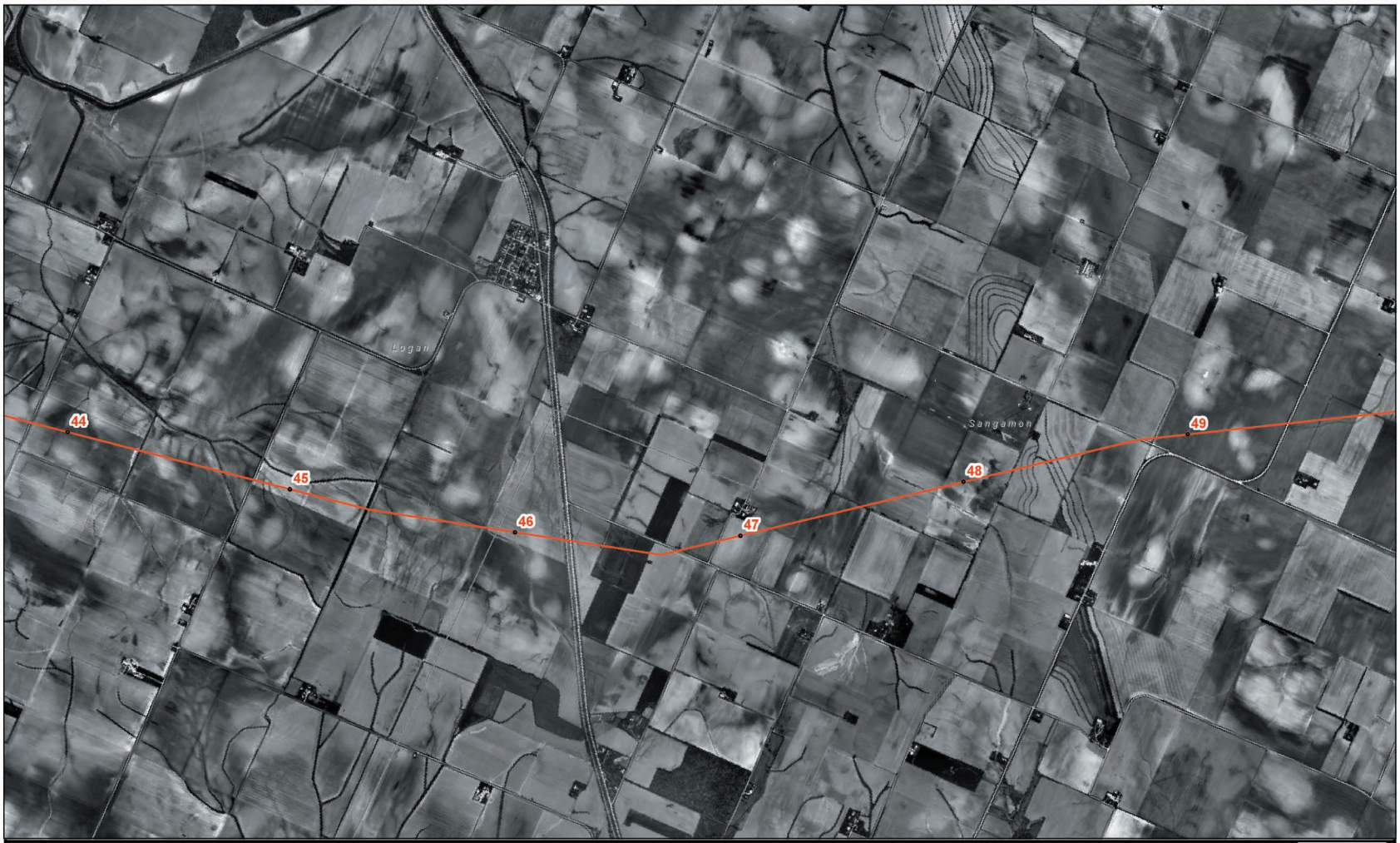

0 500 1,000 2,000 Ft

Nov 20, 2005

PIPELINE ROUTE SELECTION

Specific Transportation Option

Pekin to Edwards County Illinois

UNIVERSAL ENSCO, INC.

Drawing 9 of 32

Revision 1.0

File: "F:\share\0185\co2\sequestration\task 9\task9 final November\appendix\APPENDIX Figure 1 - 9 .pdf"

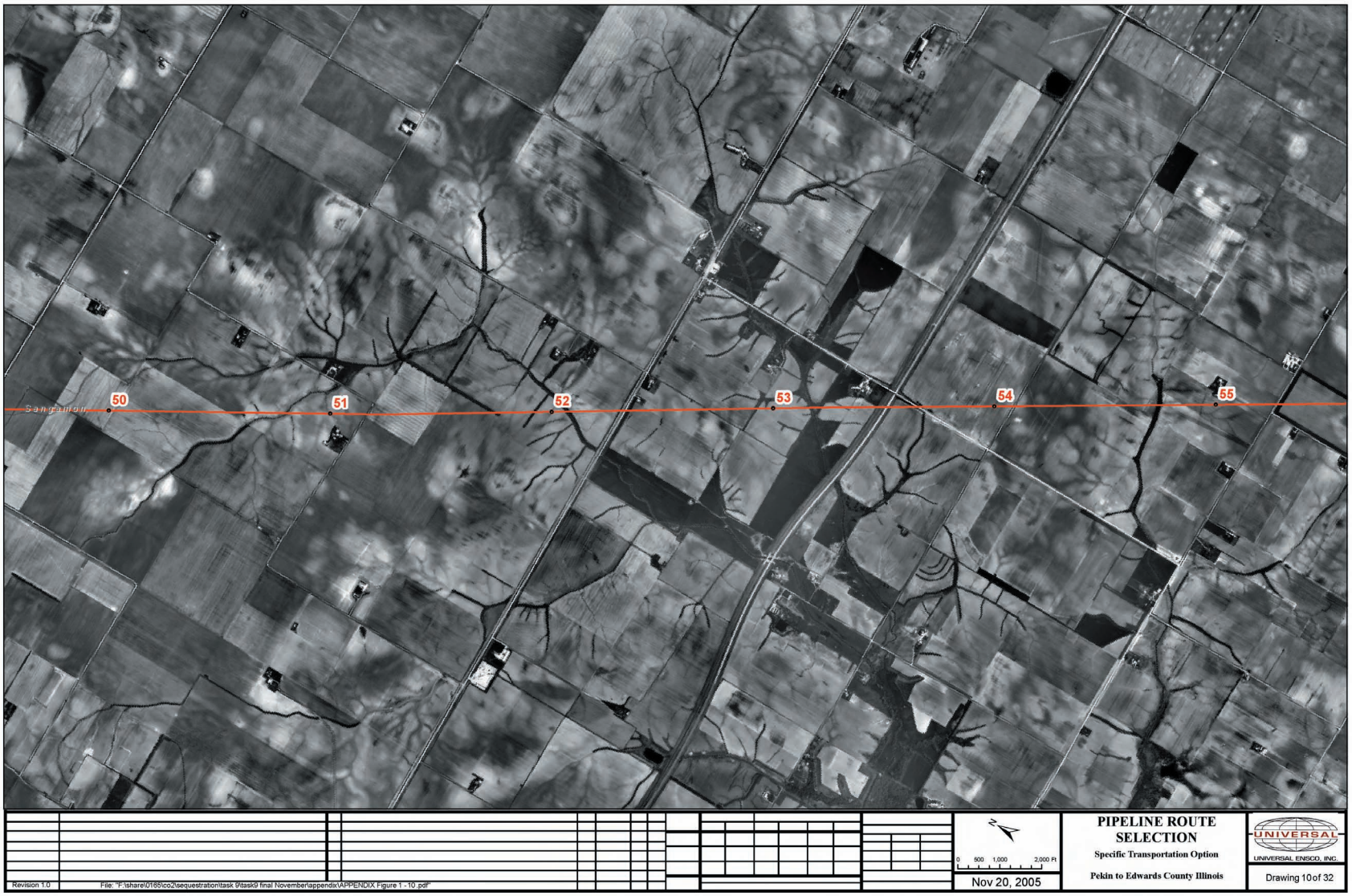
Sangamon
50
51
52
53
54
55
0 500 1,000 2,000 Ft
Nov 20, 2005
PIPELINE ROUTE SELECTION
Specific Transportation Option
Pekin to Edwards County Illinois
UNIVERSAL
UNIVERSAL ENSCO, INC.
Drawing 10 of 32
Revision 1.0
File: "F:\share\0185\co2\sequestration\task 9\task9 final November\appendix\APPENDIX Figure 1 - 10 .pdf"

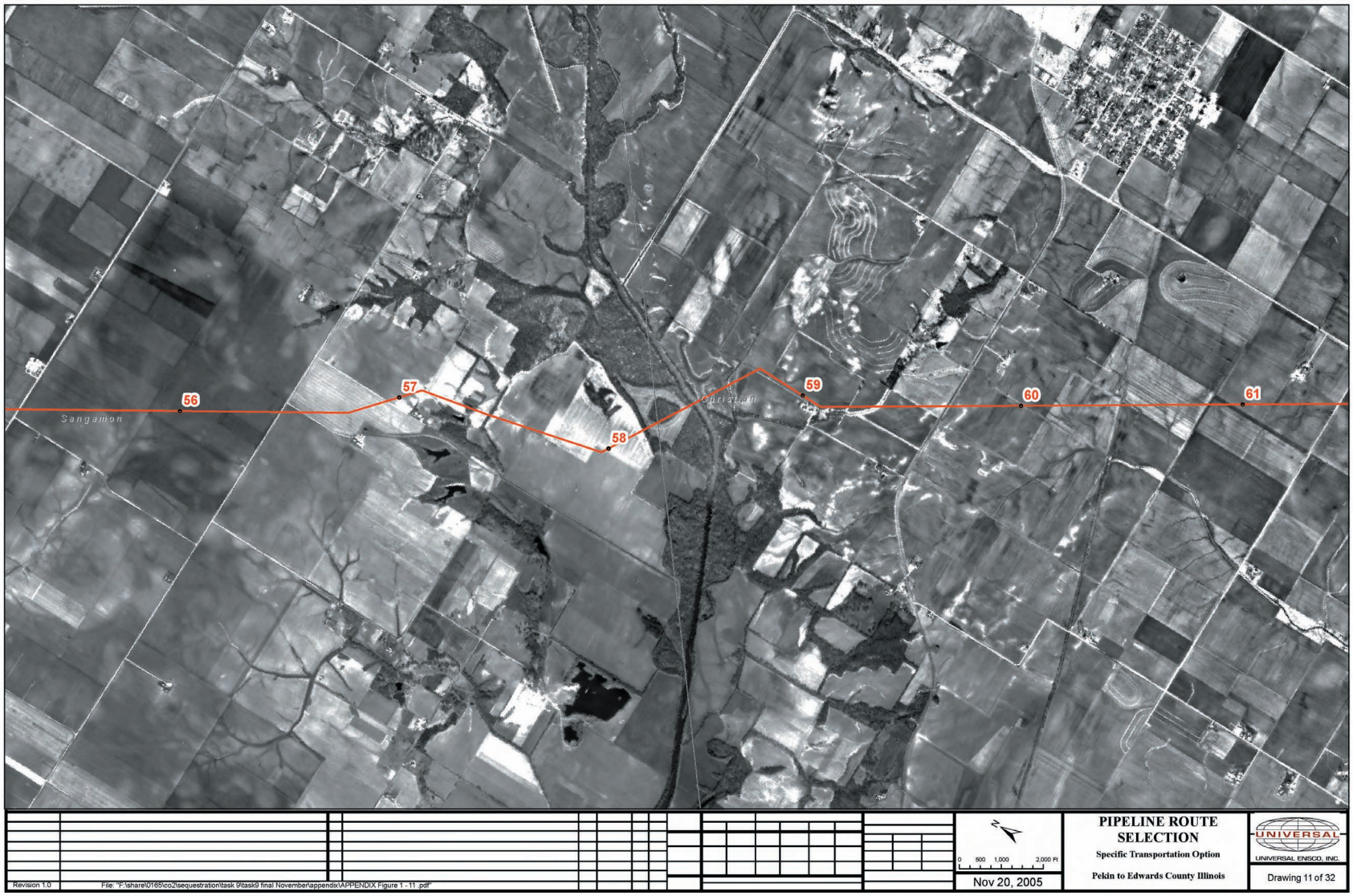
56
57
58
59
60
61
Sangamon
Christian
0 500 1,000 2,000 Ft
Nov 20, 2005
PIPELINE ROUTE SELECTION
Specific Transportation Option
Pekin to Edwards County Illinois
UNIVERSAL
UNIVERSAL ENSCO, INC.
Drawing 11 of 32
Revision 1.0
File: "F:\share\0165\co2\sequestration\task 9\task9 final November\appendix\APPENDIX Figure 1 - 11 .pdf"

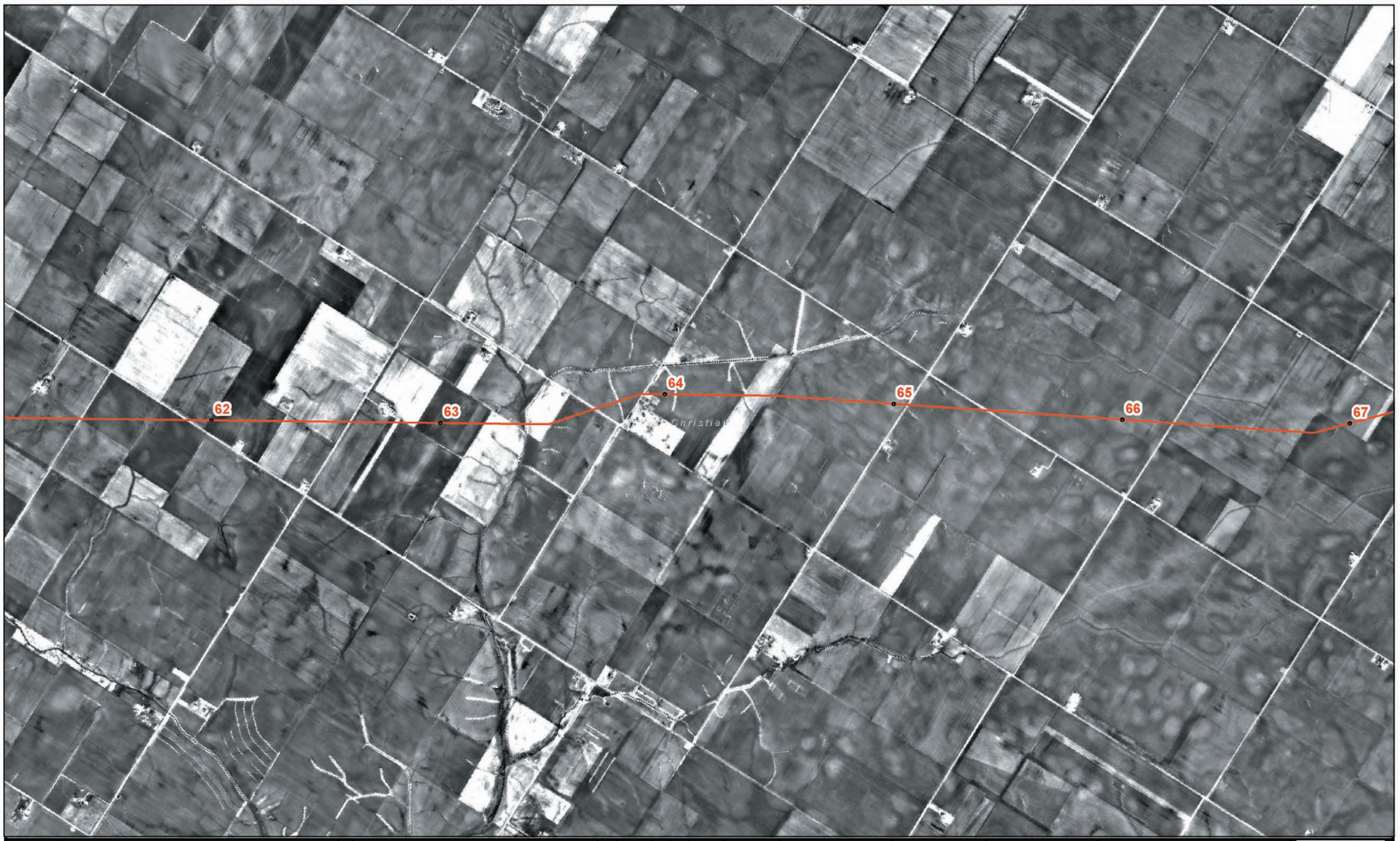

Revision 1.0

File: "F:\share\0165\co2\sequestration\task 9\task9 final November\appendix\APPENDIX Figure 1 - 12 .pdf"

0 500 1,000 2,000 Ft

Nov 20, 2005

PIPELINE ROUTE SELECTION

Specific Transportation Option

Pekin to Edwards County Illinois

UNIVERSAL

UNIVERSAL ENSCO, INC.

Drawing 12 of 32

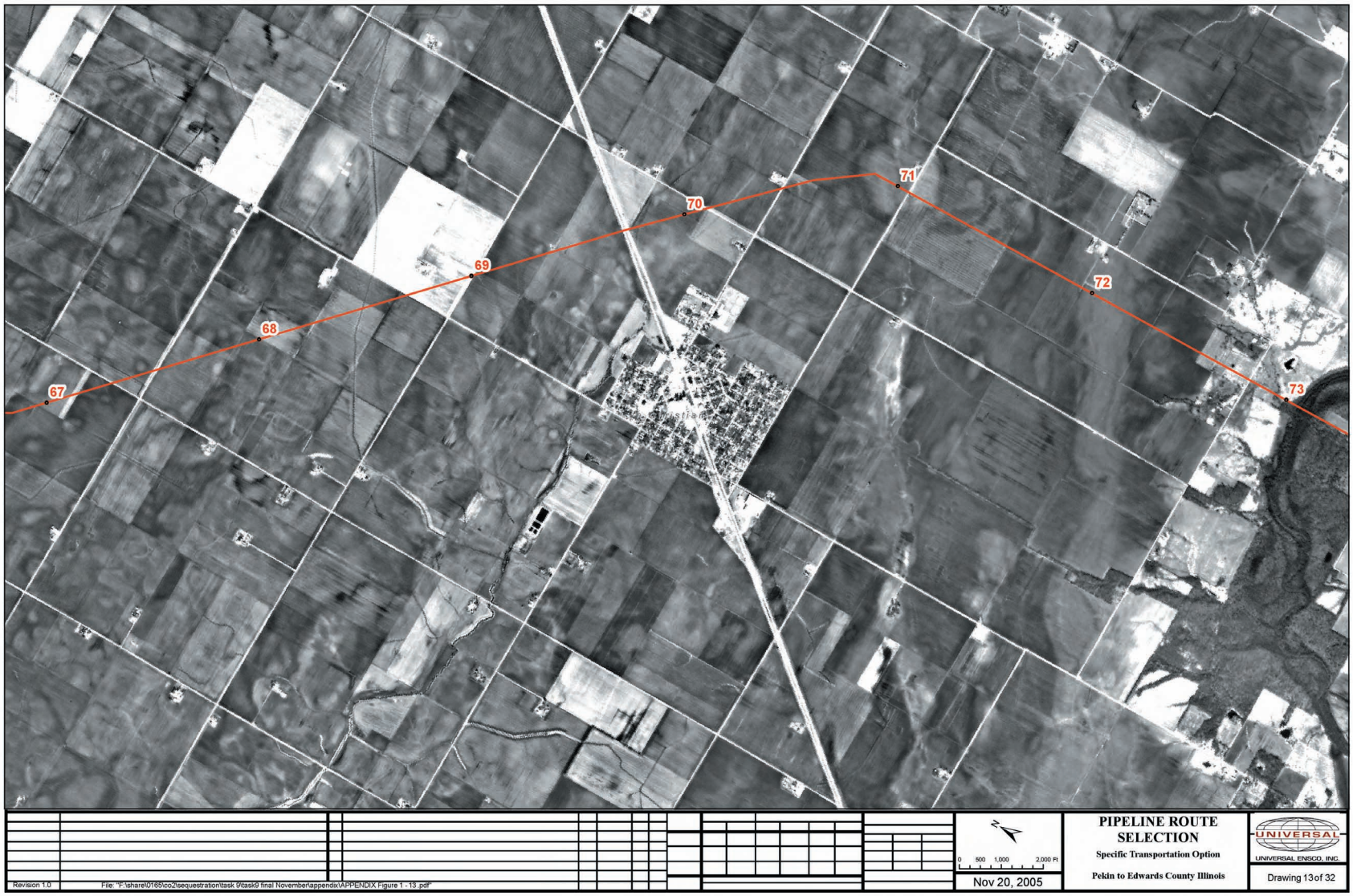
67
68
69
70
71
72
73
N
0 500 1,000 2,000 Ft
Nov 20, 2005
PIPELINE ROUTE SELECTION
Specific Transportation Option
Pekin to Edwards County Illinois
UNIVERSAL
UNIVERSAL ENSCO, INC.
Drawing 13 of 32
Revision 1.0
File: "F:\share\0165\co2\sequestration\task 9\task9 final November\appendix\APPENDIX Figure 1 - 13 .pdf"

79
78
77
76
75
74
73
Christian
PIPELINE ROUTE SELECTION
Specific Transportation Option
Pekin to Edwards County Illinois
UNIVERSAL
UNIVERSAL ENSCO, INC.
Drawing 14 of 32
0 500 1,000 2,000 Ft
Nov 20, 2005
Revision 1.0
File: "F:\share\0165\co2\sequestration\task 9\task9 final November\appendix\APPENDIX Figure 1 - 14.pdf"

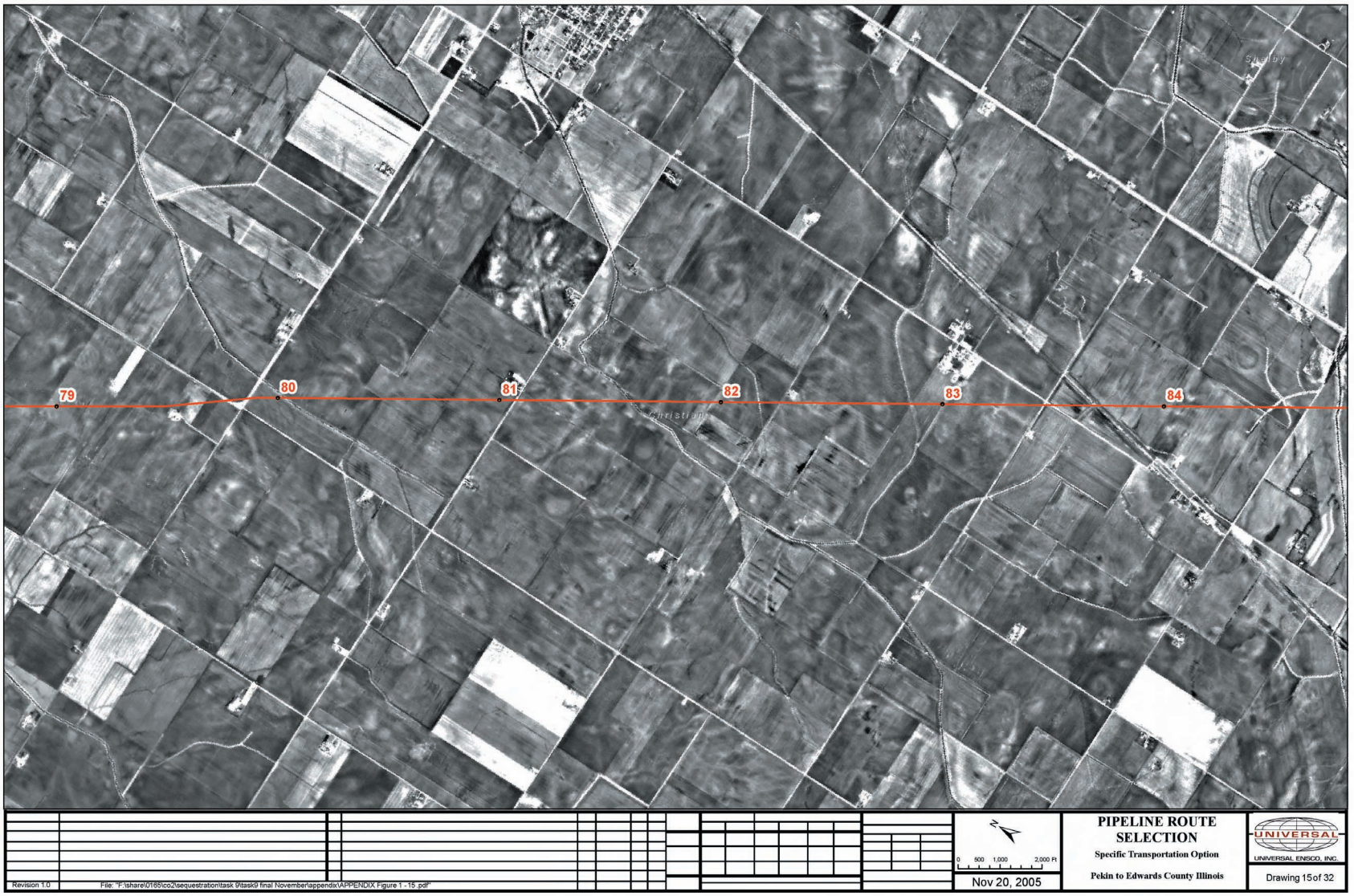
79
80
81
82
83
84
Christian
Shelby
0 500 1,000 2,000 Ft
Nov 20, 2005
PIPELINE ROUTE SELECTION
Specific Transportation Option
Pekin to Edwards County Illinois
UNIVERSAL
UNIVERSAL ENSCO, INC.
Drawing 15 of 32
Revision 1.0
File: "F:\share\0185\co2\sequestration\task 9\task9 final November\appendix\APPENDIX Figure 1 -15 .pdf"

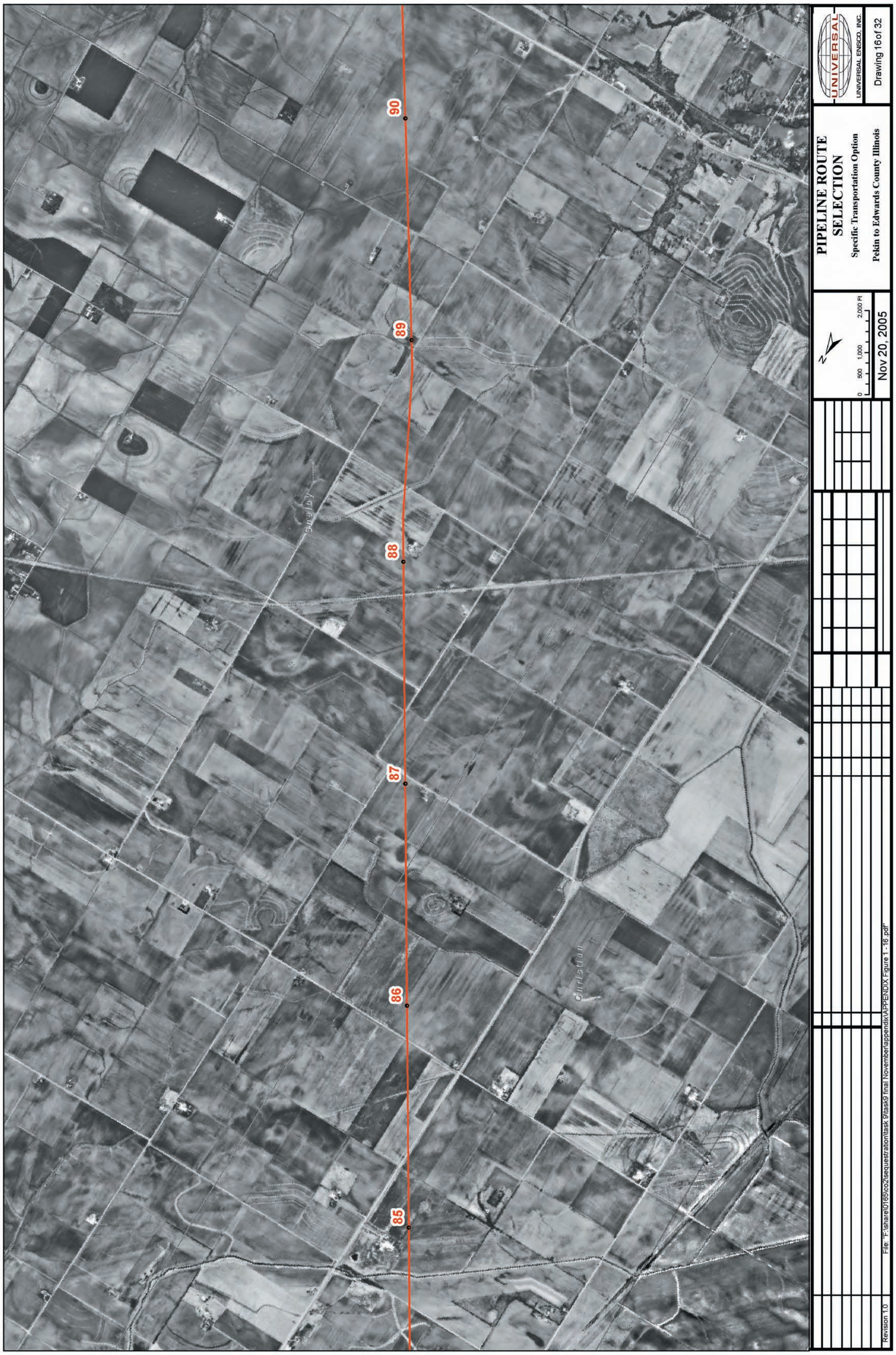
90
89
88
87
86
85
Shelby
Christian
PIPELINE ROUTE SELECTION
Specific Transportation Option
Pekin to Edwards County Illinois
UNIVERSAL
UNIVERSAL ENSCO, INC.
Drawing 16 of 32
N
0 500 1,000 2,000 Ft
Nov 20, 2005
Revision 1.0
File: "F:\share\0165\co2\sequestration\task 9\task9 final November\appendix\APPENDIX Figure 1 - 16.pdf"

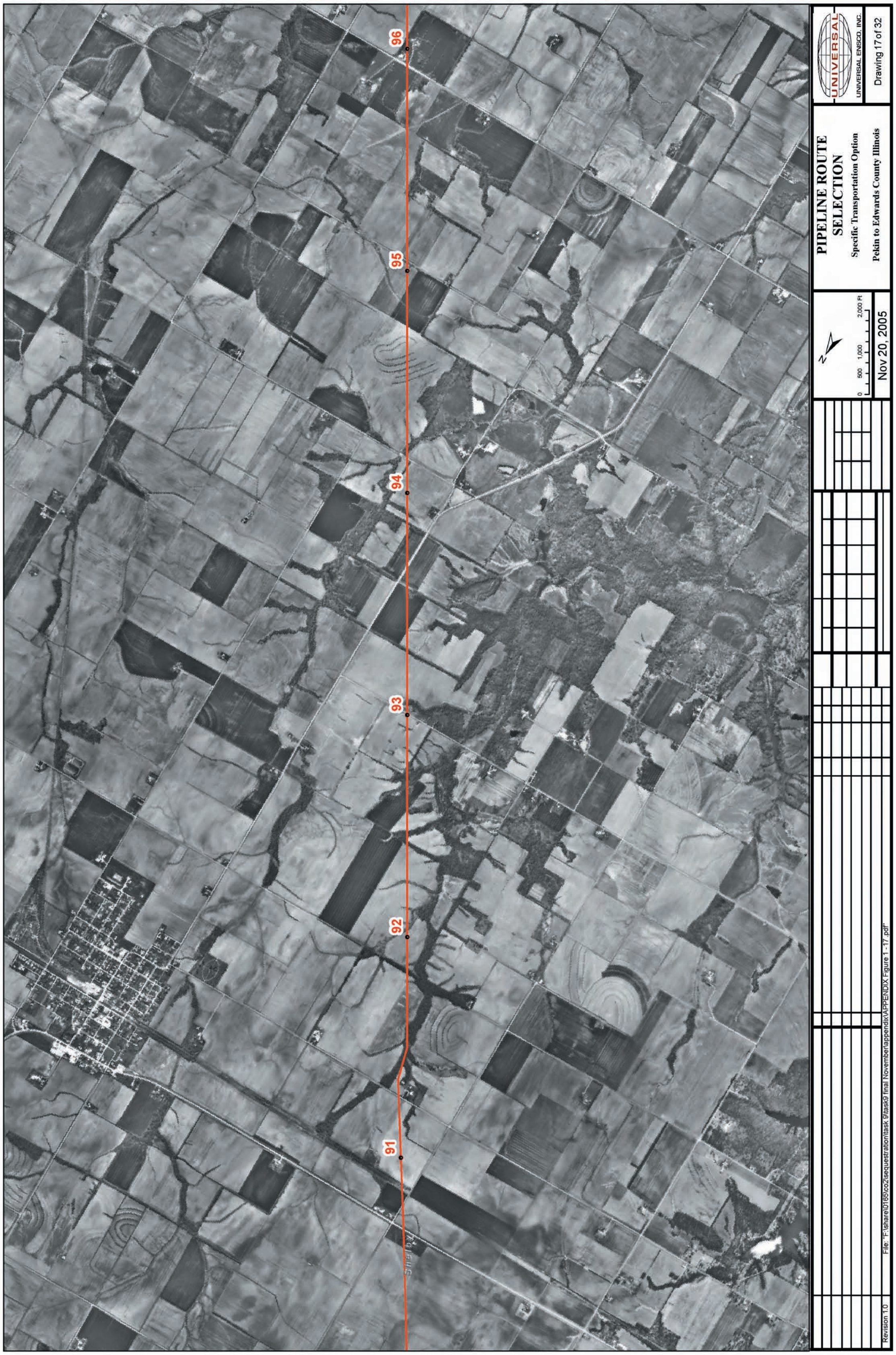
96
95
94
93
92
91
PIPELINE ROUTE SELECTION
Specific Transportation Option
Pekin to Edwards County Illinois
UNIVERSAL
UNIVERSAL ENSCO, INC.
Drawing 17 of 32
0 500 1,000 2,000 Ft
Nov 20, 2005
Revision 1.0
File: "F:\share\0165\co2\sequestration\task 9\task9 final November\appendix\APPENDIX Figure 1 - 17 .pdf"


96
97
98
99
100
101
PIPELINE ROUTE SELECTION
Specific Transportation Option
Pekin to Edwards County Illinois
UNIVERSAL
UNIVERSAL ENSCO, INC.
Drawing 18 of 32
0 500 1,000 2,000 Ft
Nov 20, 2005
Revision 1.0

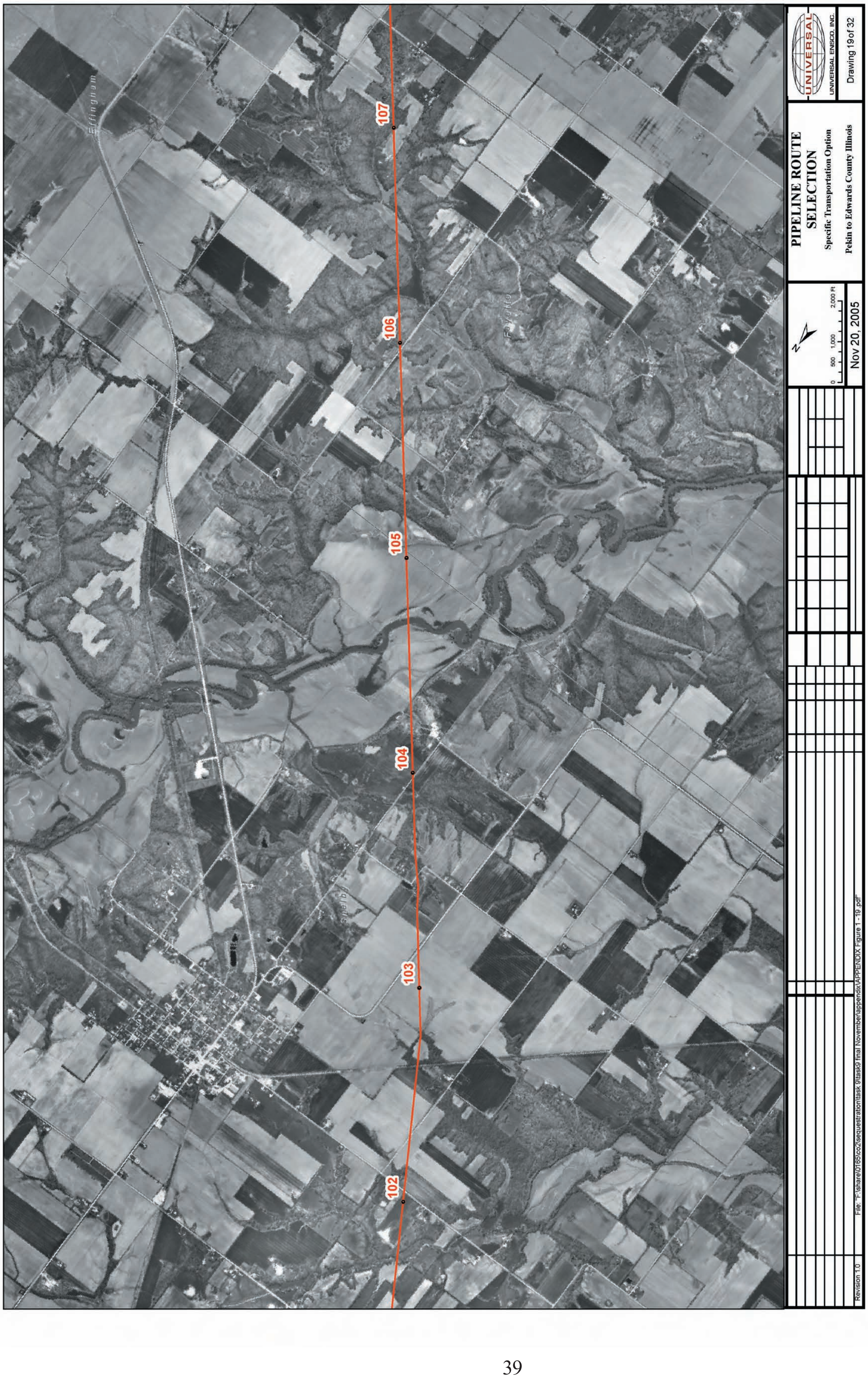
107
106
105
104
103
102
Effingham
PIPELINE ROUTE SELECTION
Specific Transportation Option
Pekin to Edwards County Illinois
UNIVERSAL
UNIVERSAL ENSCO, INC.
Drawing 19 of 32
0 500 1,000 2,000 Ft
Nov 20, 2005
Revision 1.0
File: "F:\share\0165\co2\sequestration\task 9\task9 final November\appendix\APPENDIX Figure 1 - 19.pdf"

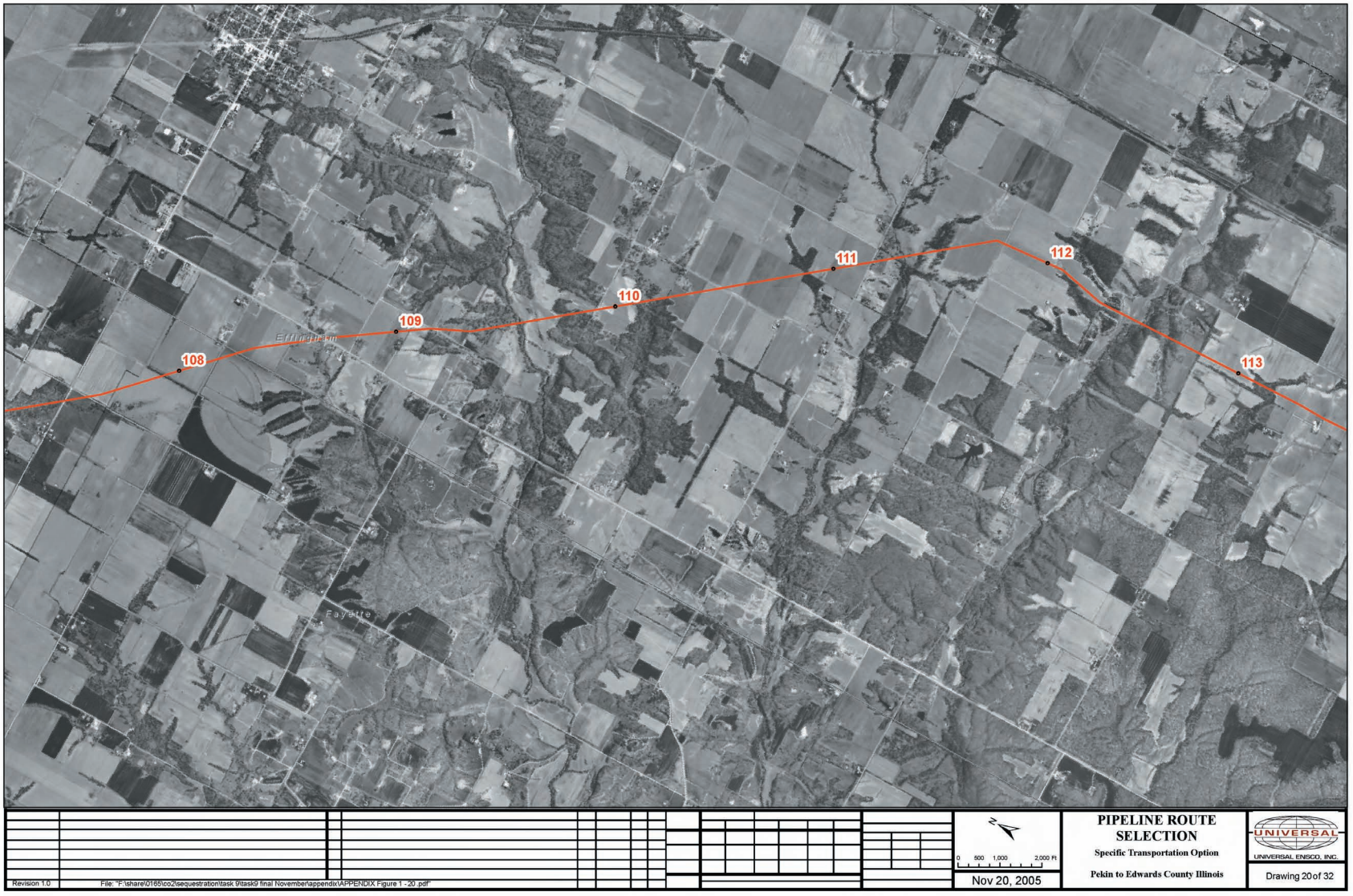
108
109
110
111
112
113
Effingham
Fayette
N
0 500 1,000 2,000 Ft
Nov 20, 2005
PIPELINE ROUTE SELECTION
Specific Transportation Option
Pekin to Edwards County Illinois
UNIVERSAL
UNIVERSAL ENSCO, INC.
Drawing 20 of 32
Revision 1.0
File: "F:\share\0185\co2\sequestration\task 9\task9 final November\appendix\APPENDIX Figure 1 - 20 .pdf"


114
115
116
117
118
119
Effingham
N
0 500 1,000 2,000 Ft
Nov 20, 2005
PIPELINE ROUTE SELECTION
Specific Transportation Option
Pekin to Edwards County Illinois
UNIVERSAL
UNIVERSAL ENSCO, INC.
Drawing 21 of 32
Revision 1.0
File: "F:\share\0185\co2\sequestration\task 9\task9 final November\appendix\APPENDIX Figure 1 -21 .pdf"

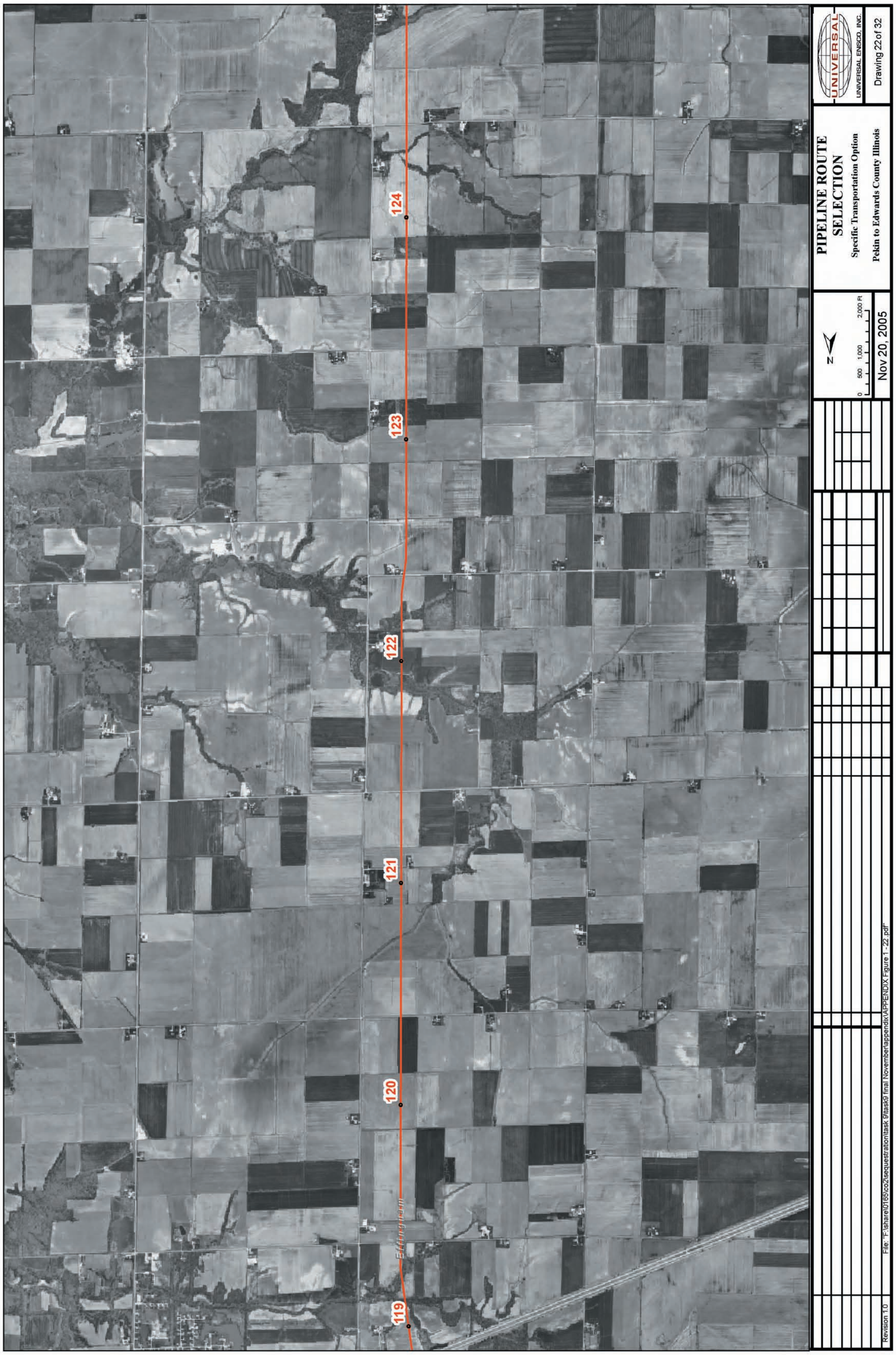

124
123
122
121
120
119
Effingham
N
0 500 1,000 2,000 Ft
Nov 20, 2005
PIPELINE ROUTE SELECTION
Specific Transportation Option
Pekin to Edwards County Illinois
UNIVERSAL
UNIVERSAL ENSCO, INC.
Drawing 22 of 32
Revision 1.0
File: "F:\share\0165\co2\sequestration\task 9\task9 final November\appendix\APPENDIX Figure 1 - 22.pdf"


125
126
127
128
129
130
Effingham
Fayette
0 500 1,000 2,000 Ft
Nov 20, 2005
PIPELINE ROUTE SELECTION
Specific Transportation Option
Pekin to Edwards County Illinois
UNIVERSAL
UNIVERSAL ENSCO, INC.
Drawing 23 of 32
Revision 1.0
File: "F:\share\0165\co2\sequestration\task 9\task9 final November\appendix\APPENDIX Figure 1 - 23 .pdf"


PIPELINE ROUTE SELECTION
Specific Transportation Option
Pekin to Edwards County Illinois
UNIVERSAL
UNIVERSAL ENSCO, INC.
Drawing 24of 32
Nov 20, 2005
0 500 1,000 2,000 Ft
Revision 1.0
131
132
133
134
135
136
Clay
Marion
Fayette

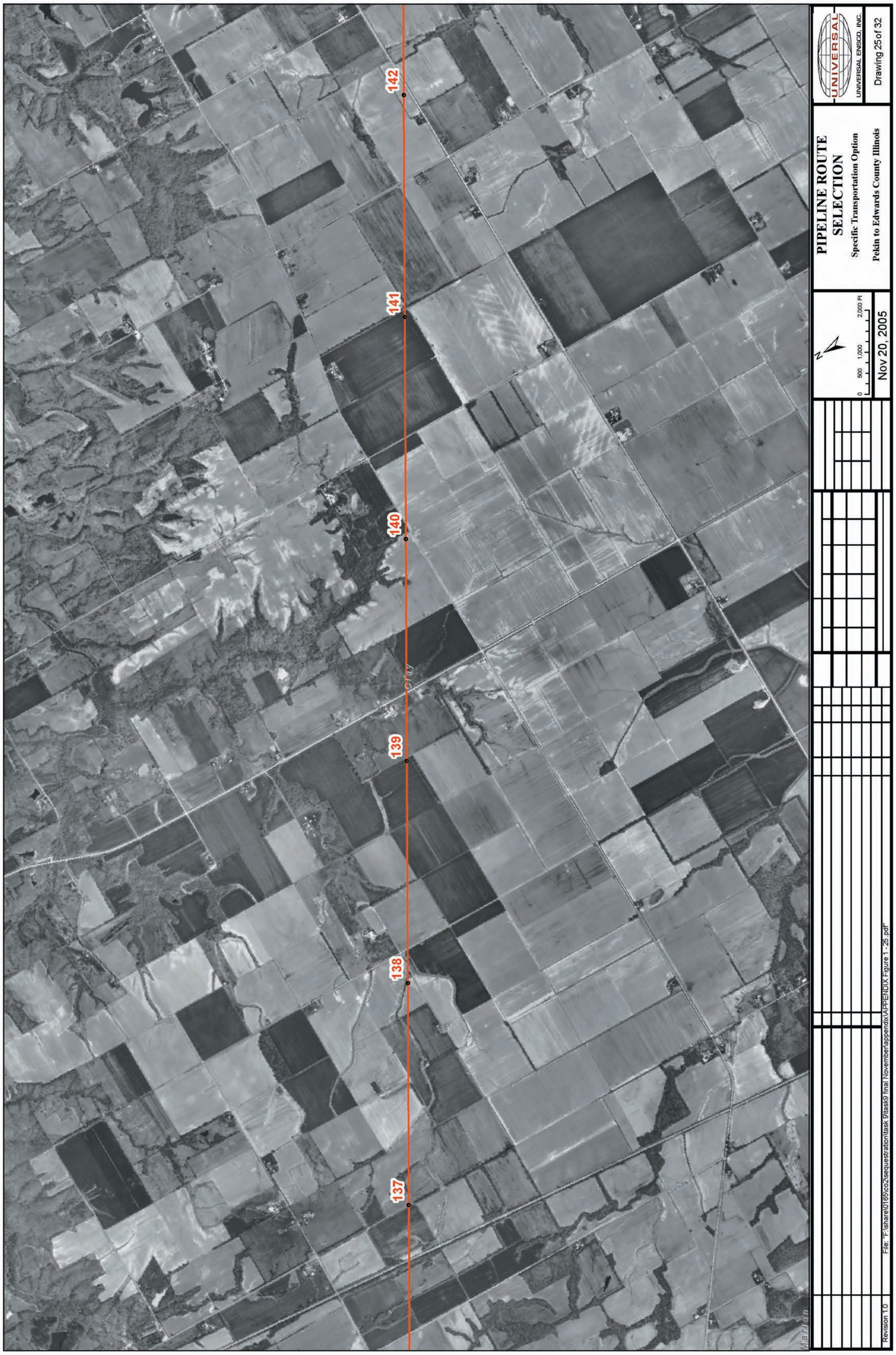
142
141
140
139
138
137
Clay
Marion
PIPELINE ROUTE SELECTION
Specific Transportation Option
Pekin to Edwards County Illinois
UNIVERSAL
UNIVERSAL ENSCO, INC.
Drawing 25 of 32
0 500 1,000 2,000 Ft
Nov 20, 2005
Revision 1.0

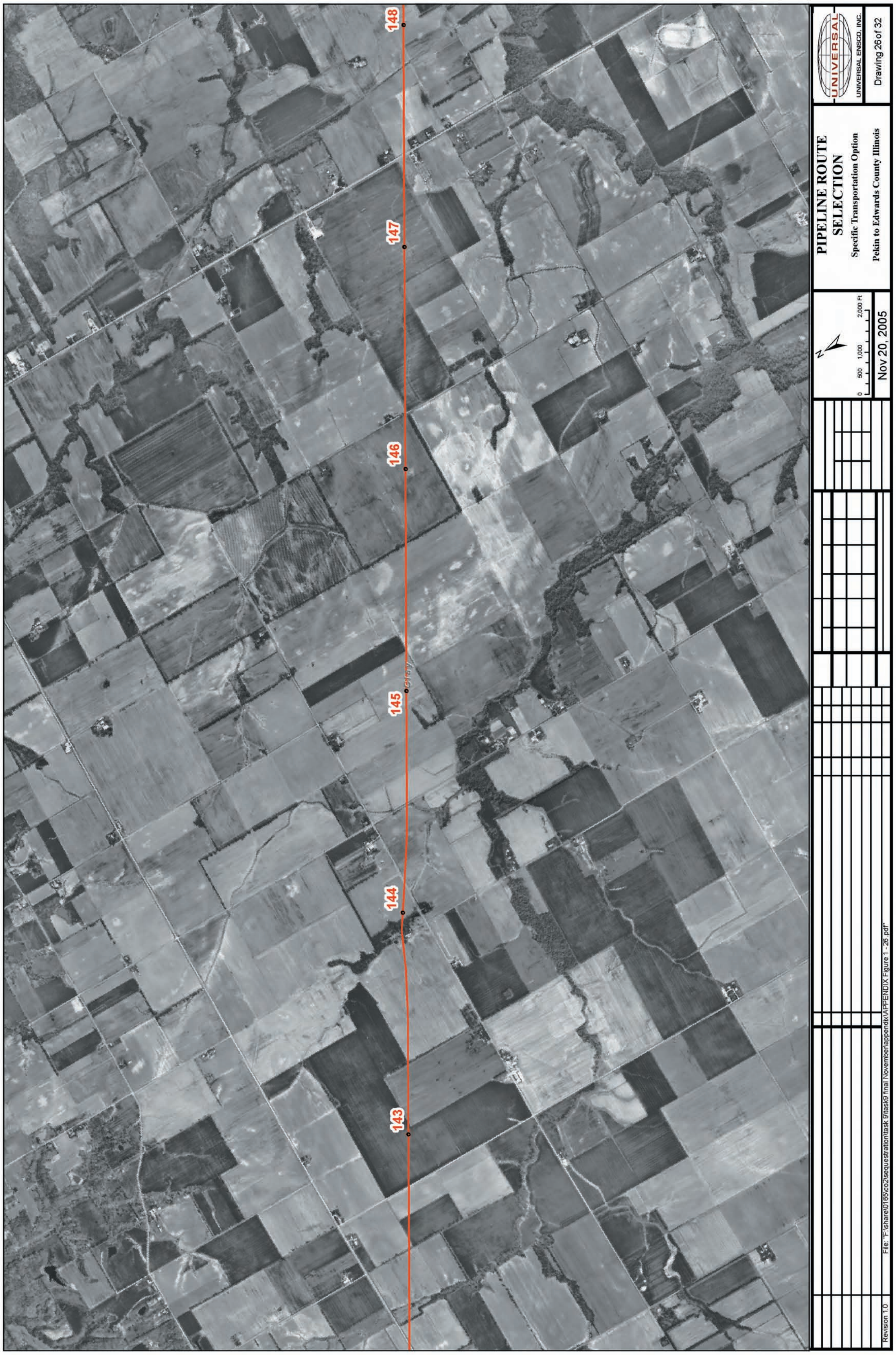
148
147
146
145
144
143
PIPELINE ROUTE SELECTION
Specific Transportation Option
Pekin to Edwards County Illinois
UNIVERSAL
UNIVERSAL ENSCO, INC.
Drawing 26 of 32
Nov 20, 2005
Revision 1.0

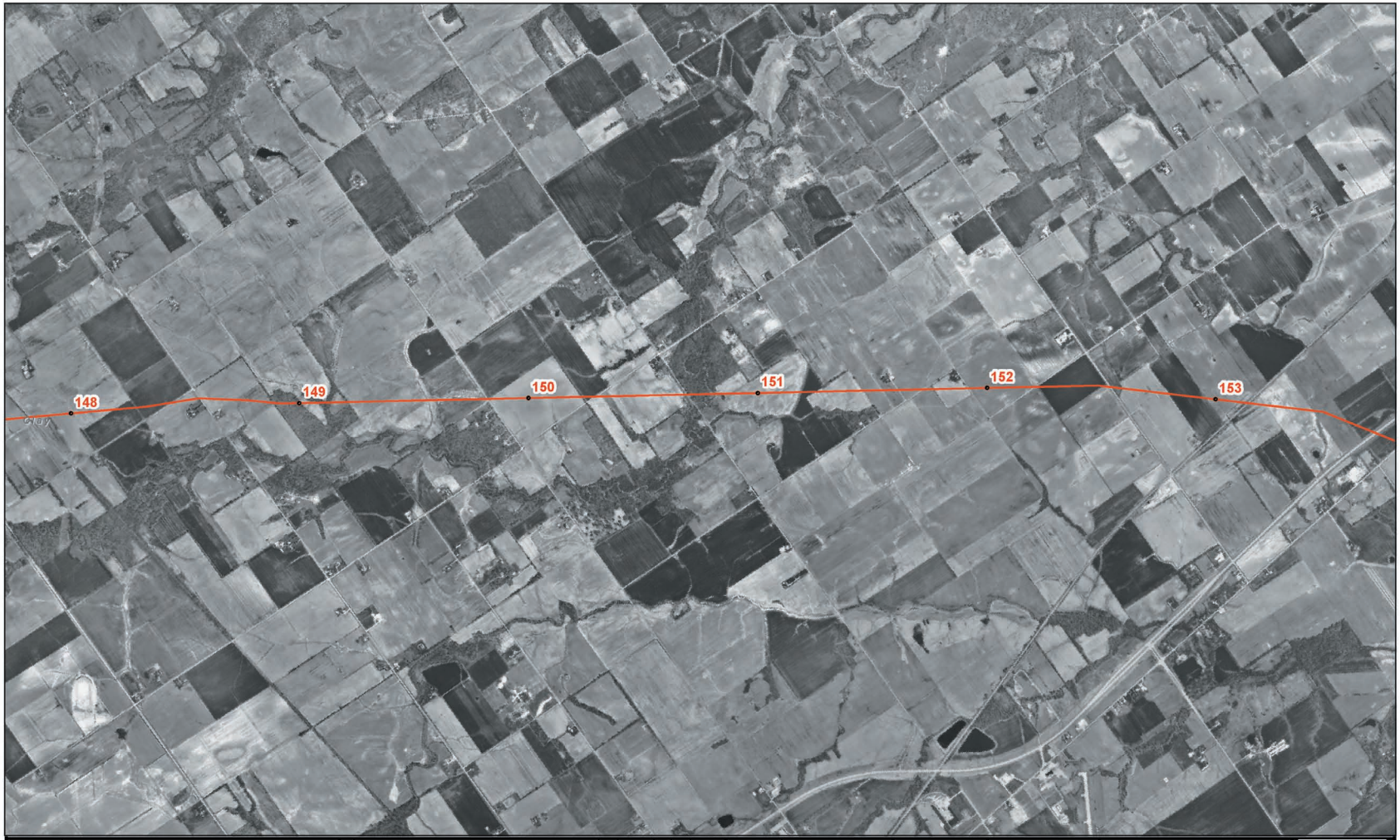
148
149
150
151
152
153
0 500 1,000 2,000 Ft
Nov 20, 2005
PIPELINE ROUTE SELECTION
Specific Transportation Option
Pekin to Edwards County Illinois
UNIVERSAL
UNIVERSAL ENSCO, INC.
Drawing 27 of 32
Revision 1.0
File: "F:\share\0165\co2\sequestration\task 9\task9 final November\appendix\APPENDIX Figure 1 - 27 .pdf"

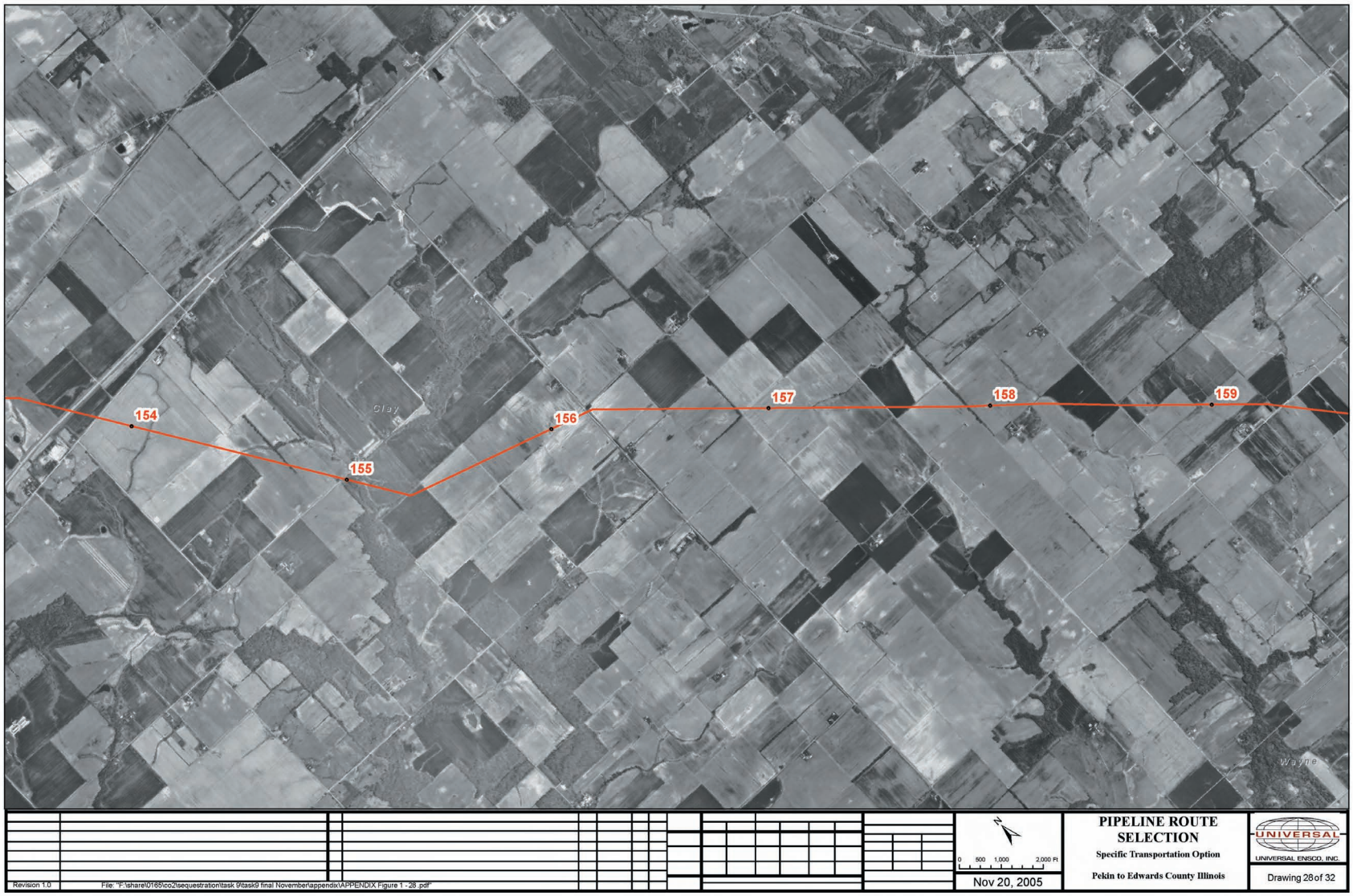
154
155
156
157
158
159
Clay
Wayne
0 500 1,000 2,000 Ft
Nov 20, 2005
PIPELINE ROUTE SELECTION
Specific Transportation Option
Pekin to Edwards County Illinois
UNIVERSAL
UNIVERSAL ENSCO, INC.
Drawing 28 of 32
Revision 1.0
File: "F:\share\0165\co2\sequestration\task 9\task9 final November\appendix\APPENDIX Figure 1 - 28 .pdf"

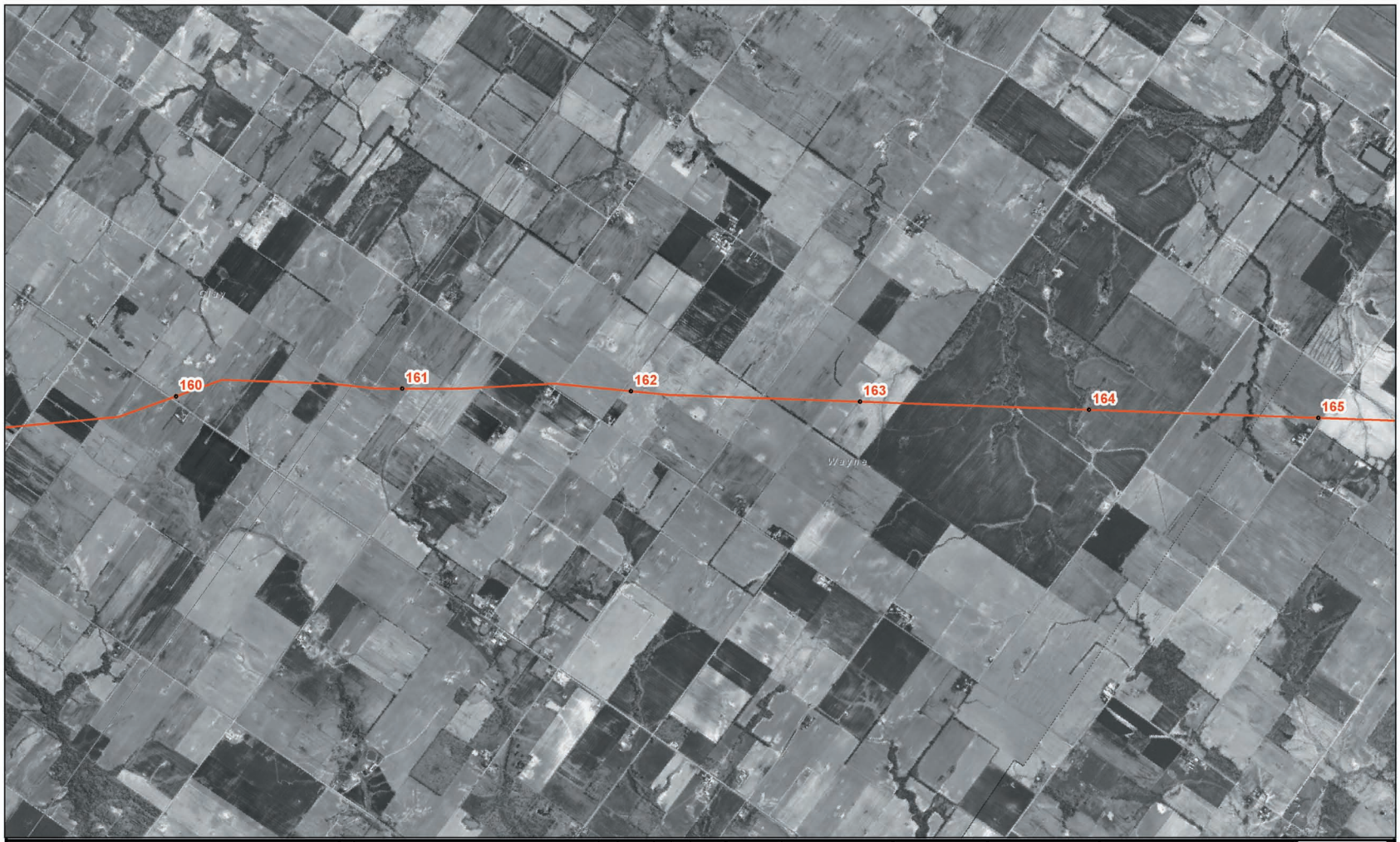
Clay
160
161
162
163
164
165
Wayne
Revision 1.0
File: "F:\share\0165\co2\sequestration\task 9\task9 final November\appendix\APPENDIX Figure 1 -29 .pdf"
0 500 1,000 2,000 Ft
Nov 20, 2005
PIPELINE ROUTE SELECTION
Specific Transportation Option
Pekin to Edwards County Illinois
UNIVERSAL
UNIVERSAL ENSCO, INC.
Drawing 29 of 32

165
166
167
168
169
170
171
PIPELINE ROUTE SELECTION
Specific Transportation Option
Pekin to Edwards County Illinois
UNIVERSAL
UNIVERSAL ENSCO, INC.
Drawing 30 of 32
0 500 1,000 2,000 Ft
N
Nov 20, 2005
Revision 1.0

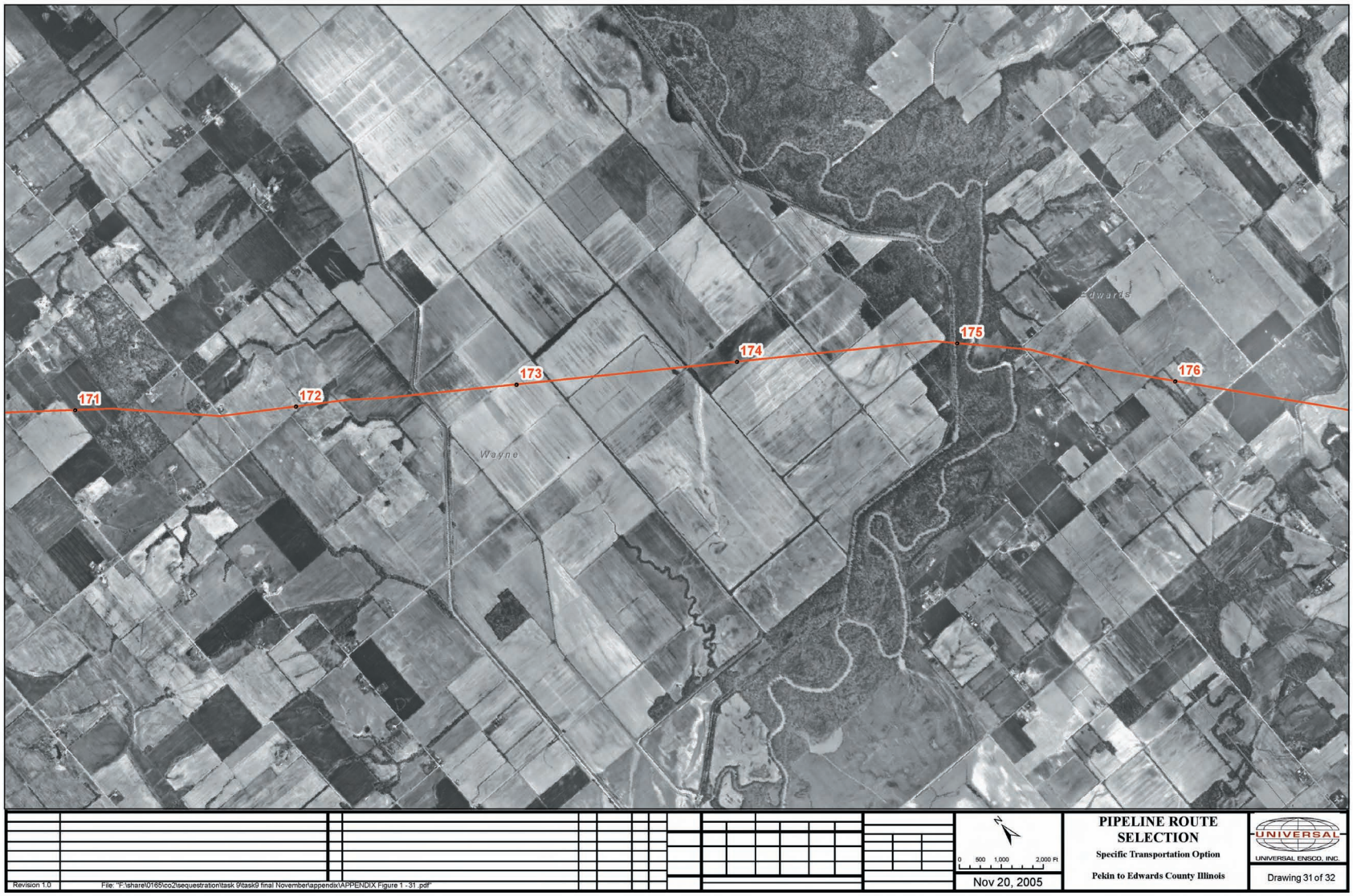
171
172
173
174
175
176
Wayne
Edwards
N
0 500 1,000 2,000 Ft
Nov 20, 2005
PIPELINE ROUTE SELECTION
Specific Transportation Option
Pekin to Edwards County Illinois
UNIVERSAL
UNIVERSAL ENSCO, INC.
Drawing 31 of 32
Revision 1.0
File: "F:\share\0165\co2\sequestration\task 9\task9 final November\appendix\APPENDIX Figure 1 - 31 .pdf"

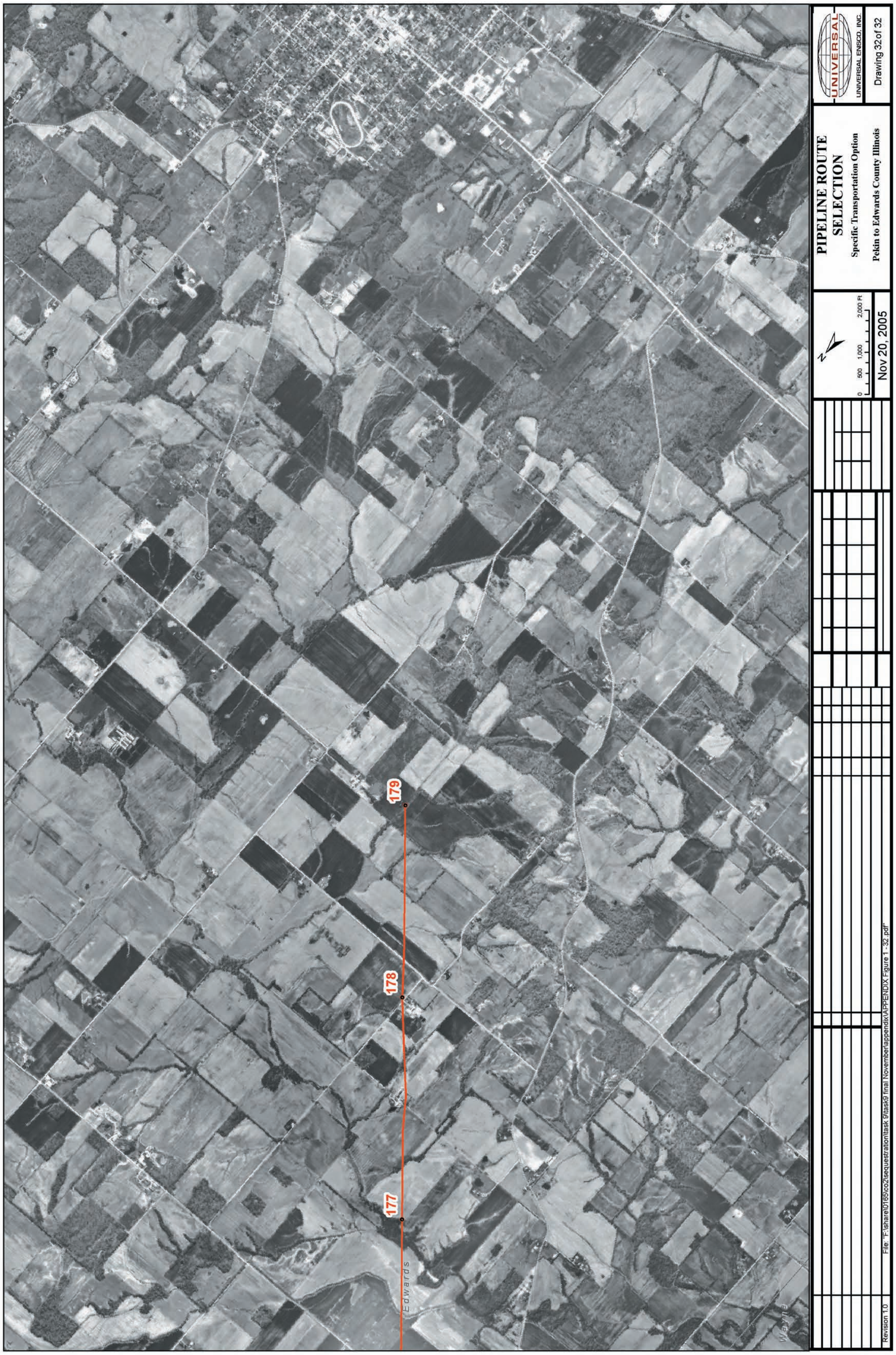
PIPELINE ROUTE SELECTION
Specific Transportation Option
Pekin to Edwards County Illinois
UNIVERSAL
UNIVERSAL ENSCO, INC.
Drawing 32 of 32
0 500 1,000 2,000 Ft
Nov 20, 2005
177
178
179
Edwards
Wayne
Revision 1.0
File: "F:\share\0165\co2\sequestration\task 9\task9 final November\appendix\APPENDIX Figure 1 - 32.pdf"